

REGULATOR INFORMATION DISTRIBUTION SYSTEM (RIDS)

ACCESSION NBR:8011070465 DOC.DATE: 80/10/31 NOTARIZED: NO DOCKET #
 FACIL:50-410 Nine Mile Point Nuclear Station, Unit 2, Niagara Moha 05000410
 AUTH.NAME AUTHOR AFFILIATION
 RHODE,G.K. Niagara Mohawk Power Corp.
 RECIP.NAME RECIPIENT AFFILIATION
 YOUNGBLOOD,B.J. Licensing Branch 1

SUBJECT: Forwards "Geologic Investigation - Radwaste Thurst Structure."

SEE REPORTS

DISTRIBUTION CODE: B001S COPIES RECEIVED:LTR 1 ENCL 25 SIZE: 1+800
 TITLE: PSAR/FSAR AMDTS and Related Correspondence

NOTES:

ACTION:	RECIPIENT ID CODE/NAME	COPIES		RECIPIENT ID CODE/NAME	COPIES	
		LTTR	ENCL		LTTR	ENCL
ACTION:	A/D LICENSNG	1	0	YOUNGBLOOD,B	1	0
	RUSHBROOK,M.	1	0	KIPER,K.	04	1
INTERNAL:	ACCID EVAL BR26	1	1	AUX SYS BR 07	1	1
	CHEM ENG BR 08	1	1	CONT SYS BR 09	1	1
	CORE PERF BR 10	1	1	EFF TR SYS BR12	1	1
	EMERG PREP 22	1	0	EQUIP QUAL BR13	1	1
	GEOSCIENCES 14	1	1	HUM FACT ENG BR	1	1
	HYD/GEO BR 15	2	2	I&C SYS BR 16	1	1
	I&E 06	3	3	LIC GUID BR	1	1
	LIC QUAL BR	1	1	MATL ENG BR 17	1	1
	MECH ENG BR 18	1	1	MPA	1	0
	NRC PDR 02	1	1	OELD	1	0
	OP LIC BR	1	1	POWER SYS BR 19	1	1
	PROC/TST REV 20	1	1	QA BR 21	1	1
	RAD ASSESS BR22	1	1	REAC SYS BR 23	1	1
	REG FILE 01	1	1	SIT ANAL BR 24	1	1
	STRUCT ENG BR25	1	1	SYS INTERAC BR	1	1
EXTERNAL:	ACRS 27	16	16	LPDR 03	1	1
	NSIC 05	1	1			

NOV 10 1980

TOTAL NUMBER OF COPIES REQUIRED: LTTR 55 ENCL 49

30374

25

1

41

1902. 2. 11

October 31, 1980

US NRC
DISTRIBUTION
SERVICES
BRANCH

1980 NOV 7 AM 9 19

DISTRIBUTION
SERVICES UNIT

Mr. B. J. Youngblood, Chief
Licensing Branch No. 1
Division of Licensing
Office of Nuclear Reactor Regulation
U. S. Nuclear Regulatory Commission
Washington, D. C. 20555

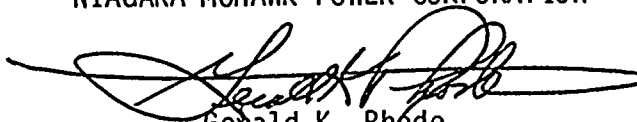
Dear Mr. Youngblood:

Re: Nine Mile Point Unit 2
Docket No. 50-410

Enclosed is a report regarding the geologic investigation of the Nine Mile Point Unit 2 Radwaste Thrust Structure. This report provides the data and analyses to confirm the conclusions made in response to the Nuclear Regulatory Commission's Request for Additional Information Q361.1.

Very truly yours,

NIAGARA MOHAWK POWER CORPORATION



Gerald K. Rhode
Vice President
System Project Management

PEF:ja
Enclosures (25)

LTR ONLY
B001 51/25

ENCL
B024 51/25
ADD: XEROX TO L E
ACRS 1616

8011070465

A

TABLE OF CONTENTS

INVESTIGATION

<u>Section</u>	<u>Page</u>
1.0 Introduction	1
1.1 General	1
1.2 History of "Thrust" Fault Investigations	2
1.3 Purpose and Approach	6
2.0 Results of Geologic Investigation	10
2.1 Mapping Program	10
2.1.1 Introduction	10
2.1.2 Purpose	11
2.1.3 Scope	11
2.1.4 Approach	12
2.1.5 Stratigraphy	13
2.1.6 Structure	14
2.1.6.1 Circulating Water Piping Trench	14
2.1.6.2 Relocated Cooling Tower Excavation	16
2.1.6.3 North Radwaste Trench	18
2.1.6.4 East Lake Water Tunnel	21
2.1.7 Summary and Interpretation	23
2.2 Exploration of the Extent of the Radwaste Fault	25
2.2.1 Introduction and Purpose	25
2.2.2 Scope of Work	26
2.2.3 Investigation Results	28
2.2.3.1 400-Series Boreholes	28
2.2.3.2 Photographs and Field Inspection	
Maps of Reactor Containment	29
2.2.3.3 800-Series Borings	30
2.2.4 Conclusions	32
2.3 Age of Deformation	33
2.3.1 Statement of the Problem	33
2.3.2 Technical Approach	34
2.3.3 Onsite Bedrock Topography	35
2.3.4 Calcite Mineralization	35
2.3.4.1 General	35
2.3.4.2 Results of Paragenetic Studies	37
2.3.4.3 Isotopic and Radiometric Analyses	43
2.3.5 Relation of Interstitial Sediment to the Radwaste Fault	46
2.3.5.1 General	46
2.3.5.2 Origin and Age of Interstitial Sediment	46
2.3.6 Deformation of Clays - A Question of Origin	56
2.3.7 Conclusions	59
3.0 Stress Determinations by Overcoring	61
3.1 Introduction	61
3.2 Purpose	61
3.3 Scope	61
3.4 Procedure	62
3.5 Results	63
3.6 Discussion	66
3.7 Conclusions	80

8011070465

<u>Section</u>	<u>Page</u>
4.0 Summary and Conclusions	82
4.1 Overview of Participation by Consultants	82
4.2 Conclusions	84
5.0 References	91

5

Jf

0

LIST OF TABLES

<u>Table</u>	<u>Title</u>
2.3-1	GA3 Series - Specimens of Calcite Mineralization Collected from Circulating Water Piping Trench Excavations
2.3-2	GA4 Series - Specimens of Calcite Mineralization Collected from North Radwaste Trench
2.3-3	GA5 Series - Specimens of Calcite Mineralization Collected from East Lake Water Tunnel
2.3-4	800 Series - Specimens of Calcite Mineralization Collected from Cores of Borings 801 and 806
2.3-5	Radiometric Dating of Low Temperature Calcite
2.3-6	Isotope Analyses of Low Temperature Calcite
2.3-7	Mineralogic Analyses
2.3-8	Correlation of Pollen Stratigraphy - Eastern New York and Southern Connecticut
2.3-9	Specimens of Interned Sediment from Trenches and Borings as Part of Radwaste Fault Study
3.3-1	Summary of Overcore Tests, Boring RS-1
3.3-2	Summary of Overcore Tests, Boring RS-2
3.3-3	Summary of Overcore Tests, Boring RS-3
3.3-4	Summary of Overcore Tests, Boring RS-4
3.3-5	Summary of Overcore Tests, Boring OC-4
3.3-6	Summary of Biaxial Tests, Boring RS-1
3.3-7	Summary of Biaxial Tests, Boring RS-2
3.3-8	Summary of Biaxial Tests, Boring RS-3
3.3-9	Summary of Biaxial Tests, Boring RS-4
3.3-10	Summary of Biaxial Tests, Boring OC-4

LIST OF PLATES

- 1-1 Site Location Map Showing General Configuration of Bedrock Surface and Geologic Structures in the Immediate vicinity of Nine Mile Point Nuclear Generating Station, Scriba, N.Y.
- 2.1-1 Approximate Stratigraphic Intervals wherein "Thrust" Faults were Mapped During this Investigation
- 2.1-2 Geologic Plan View Showing a Portion of the Circulating Water Piping Trench Excavation
- 2.1-3 Cross Section of Walls of Upper Sump Trench in Circulating Water Piping Excavation
- 2.1-4 Cross Section of Walls of Upper Sump Trench in Circulating Water Piping Excavation
- 2.1-5 Cross Section of Northeast Wall of Lower Sump Trench in Circulating Water Piping Excavation
- 2.1-6 Geologic Plan View of Portion of Relocated Cooling Tower Excavation
- 2.1-7 Cross Section of Portion of Bedrock Scarp in Relocated Cooling Tower Excavation
- 2.1-8 Cross Section of Portion of Bedrock Scarp in Relocated Cooling Tower Excavation
- 2.1-9 Generalized Cross Section of Northeast Wall of North Radwaste Trench
- 2.1-10 Generalized Cross Section of Southwest Wall of North Radwaste Trench
- 2.1-11 Detailed Cross Section of Northeast Wall, North Radwaste Trench
- 2.1-12 Detailed Cross Section of Southwest Wall, North Radwaste Trench
- 2.1-13 Geologic Plan View of Floor of Exploratory Excavation into South Wall of North Radwaste Trench
- 2.1-14 Detailed Cross Section of South Wall of Exploratory Excavation into Southwest Wall of North Radwaste Trench
- 2.1-15 Detailed Cross Section of East Wall of Exploratory Excavation into Southwest Wall of North Radwaste Trench

LIST OF PLATES (cont.)

- 2.1-16 Plan View of Radwaste Building Excavation showing Structure Contours on Base of Oswego Sandstone
- 2.1-17 Photograph of Portion of Northeast Wall of North Radwaste Trench
- 2.1-18 Cross Section of Right Rib of East Intake Tunnel Station 0+10 to 0+60
- 2.1-19 Cross Section of Left Rib of East Intake Tunnel Station 0+10 to 0+95
- 2.1-20 Cross Section Station 2+30 to 2+90
- 2.1-21 Cross Section Station 4+25 to 4+85
- 2.1-22 Cross Section Station 6+10 to 7+10
- 2.1-23 Cross Section Station 8+38 to 8+95
- 2.1-24 Cross Section Station 9+45 to 10+02
- 2.1-25 Three Dimensional Representation of Lake Water Intake Tunnels
- 2.1-26 Structural Elements from Areas of Investigation
- 2.1-27 Site Location Map Showing General Configuration of Bedrock Surface and Slip Directions of Thrust Faults

- 2.2-1 Borehole Location Map
- 2.2-2 Cross Section along Line of 800-Series Borings
- 2.2-3 Simplified Geologic Cross Section North and West Walls of Auxilliary Bay
- 2.2-4 Detailed Log of a Portion of Boring 801
- 2.2-5 Photograph of Rotated Beds in Boring 801, at Depth of 46.5 feet
- 2.2-6 Detailed Log of Portion of Boring 802

LIST OF PLATES (cont.)

- 2.2-7A Detailed Log of Portion of Boring 802
- 2.2-7B Detailed Log of Portion of Boring 802 Cont'd
- 2.2-8 Detailed Log of Portion of Boring 803
- 2.2-9 Detailed Log of Portion of Boring 804
- 2.2-10A Detailed Log of Portion of Boring 806
- 2.2-10B Detailed Log of Portion of Boring 806 Cont'd
- 2.2-11 Photographs of Laminated Clay in B-810 at Depth of 252.2 Feet
- 2.2-12 Photographs of Laminated Clay in B-805 at Depth of 121.55 Feet

- 2.3-1 Geologic Profile of Overburden from Old Borings Across Valley at Leading Edge of Radwaste Fault, Nine Mile Point Unit 2 Site
- 2.3-2 Paragenetic Relationships of Groundwater Calcite Mineralization at Nine Mile Point Unit 2 Site
- 2.3-3 Type 1 Calcite
- 2.3-4 Type 1 Calcite
- 2.3-5 Travertine
- 2.3-6 Type 3 Calcite
- 2.3-7 Specimen GA4-S8, South Wall of Slot, North Radwaste Trench
- 2.3-8 Specimen GA4-6, North Wall of Slot, North Radwaste Trench
- 2.3-9 Distribtuion of ^{13}C Ratios of Carbonates
- 2.3-10 Distribution of ^{13}C Ratios of Carbonates
- 2.3-11 Distribution of ^{18}C Ratios of Carbonates Showing Relationship to Site Specimens
- 2.3-12 Mixture of Breccia and Sediment as Shown by Sample GA4-S5 North Radwaste Trench

LIST OF PLATES (cont.)

- 2.3-13 Pollen Samples, West Wall Cooling Tower Trench, CTT-1
- 2.3-14 Grain Size Distribution Curve
- 2.3-15 Grain Size Distribution Curve
- 2.3-16 Grain Size Distribution Curve
- 2.3-17 Grain Size Distribution Curve
- 2.3-18 Grain Size Distribution Curve
- 2.3-19 Grain Size Distribution Curve
- 2.3-20 Grain Size Distribution Curve
- 2.3-21 Classification of Soil Specimens from Grain Size Analysis
- 2.3-22 Percent Mineral Content of Samples from Trench 4 and North Radwaste Trench
- 2.3-23 Relative Pollen Percentages, Spore and Miscellaneous Microfossil Abundance
- 2.3-24 Frequency Diagrams for Pollen Spectra Representing Total of Samples from North Radwaste and Circulating Water Piping Trenches
- 2.3-25 Photographs of Late Pleistocene Clay Showing Clay Laminae with 70° Dip Equal to that of Short Limb of Kink Fold Along Radwaste Fault Zone
- 2.3-26 Photographs of Deformation in Late Pleistocene Clays Showing A) Location of Folds, B) Fold in Clays
- 2.3-27 Photographs of Deformation Features in Late Pleistocene Clay North Radwaste Trench
- 3.3-1 Site Location Map
- 3.3-2 Boring RS-1 - Results of In Situ Stress Determinations
- 3.3-3 Boring RS-2 - Results of In Situ Stress Determinations
- 3.3-4 Boring RS-3 - Results of In Situ Stress Determinations
- 3.3-5 Boring RS-4 - Results of In Situ Stress Determinations
- 3.3-6 Boring OC-4 - Results of In Situ Stress Determinations

LIST OF PLATES (cont.)

- 3.3-7 Cross Section through Borings OC-4 and RS-4 showing
Horizontal Normal Displacements in Vertical Planes
Orientated N70°W in the North of the Fault Block
- 3.3-8 Cross Section through RS-3, RS-2, and RS-1 showing
Horizontal Normal Displacements in Vertical Planes
Oriented N70°W to the South of the Fault Block
- 3.3-9 Diagram Showing Stress Nomenclature

APPENDICES

A. Boring Logs - 800-Series Borings

B. Consultants' Reports - Analysis of Calcite Mineralization

B.1 Barnes, H.L.

- B.1-1 Report - Samples from Nine Mile Point Nuclear Station, Unit 2, Series GA3
- B.1-2 Report - Samples from Nine Mile Point Nuclear Station, Unit 2, North Radwaste Trench, Samples GA4-1A and 1B
- B.1-3 Report - Samples from Nine Mile Point Nuclear Station, North Radwaste Trench; Samples GA4-2 to GA4-9, GA4-11, GA4-BH, GA4-S8-A and GA4-X
- B.1-4 Letter dated 2/26/80 Concerning Samples HK-1 and HK-2
- B.1-5 Letter dated 3/28/80 concerning Samples HK-1 and HK-2
- B.1-6 Letter dated 5/12/80 Concerning Samples HK-3 and TU-1 Report - Samples GA5 and 800-Series
- B.1-7 Report - Characteristics of Mineralization in Fractures of Samples GA5-3, -4, -5, -6, and -7

B.2 Krueger, H.

- B.2-1 Report - Sample SL-10 (^{14}C Analysis)
- B.2-2 Report - Samples HK-1 and HK-2 (^{14}C Analysis)
- B.2-3 Report - Samples HK-1 and HK-2 (^{18}O Analysis)
- B.2-4 Report - Sample GA4-S31 (^{14}C Analysis)
- B.2-5 Report - Sample HK-3 (^{14}C Analysis Attempt)
- B.2-6 Report - Sample HK-3

B.3 Ku, T.L.

- B.3-1 Uranium-Series Age Dating of Calcite Material, Samples SW-1 and SW-2
- B.3-2 $^{230}\text{Th}/^{234}\text{U}$ Dating of Sample TU-1

APPENDICES (cont.)

C. Consultants' Reports - Compositional Analysis of Interned Sediments

C.1 Sirkin, L.

- C.1-1 Report - Pollen Analysis of Sample CWPT-1
- C.1-2 Report - Pollen Analysis of Samples GA3-S1 and GA3-S2
- C.1-3 Report - Additional Pollen Analysis of Samples CWPT-1 and GA3-S1
- C.1-4 Report - Pollen Analysis of Samples GA4-S1-A, S2-A, S4-A, S5-A, S6-B, and S8-B
- C.1-5 Report - Pollen Analysis of Samples GA4-20, 21, 21A, 22, 24, and 26
- C.1-6 Report - Pollen Analysis of Samples 806-S1, 806-S3, 810-1, 810-3, 810-4, and 805-1

C.2 Terasmae, J.

- C.2-1 Report on Palynological Analysis of Laminated Silty Clay

C.3 Vassiliou, A.H.

- C.3-1 Report - Mineralogic Analyses, Samples GA4-1, 2, 4, 5, 6, and 7 and SL-CWPT-1, 2, and 3
- C.3-2 Report - Mineralogic Analysis, Samples GA4-27, 28 and 29

D. Consultants' Reports - Configuration of Interned Sediment in North Radwaste Trench

D.1 Sirkin, L.

- D.1-1 Report - Concerning Observations made in North Radwaste Trench

D.2 Péwé, T.L.

- D.2-1 Report - Consideration of Origin and Age of Clay in Bedrock at Nine Mile Point

E. Stress Determinations by Overcoring

E.1 Table E-1

APPENDICES (cont.)

- E.2 RS-Series Boring Logs (Plates E-1 through E-4)
- E.3 Strain Relief Curves for Overcoring Tests
(Plates E-5 through E-113)
- F. Consultants' Reports - Significance of Observed
Geologic Structures
 - F.1 Price, N.J.
 - F.1-1 Assessment of Radwaste Structure at Nine
Mile Point Nuclear Station
 - F.1-2 Further Thoughts on the Stability of the
Nine Mile Point Site
 - F.1-3 Third Thoughts on the Stability of the
Radwaste Structure
 - F.2 Péwé, T.L.
 - F.2-1 Report - Consideration of the Effects of
Permafrost and Ground Ice Growth on Structures
at the Site
 - F.3 Fairhurst, C.
 - F.3-1 Potential for Differential Movement Along
the Radwaste Structure, Nine Mile Point,
New York, Over the Next 50 Years
 - F.4 Jahns, R.H. and Philbrick, S.S.
 - F.4-1 Notes on the Radwaste Fault Structure, Nine
Mile Point No. 2 Generating Station, Niagara
Mohawk Power Corporation

1.0 INTRODUCTION

1.1 GENERAL

This report presents the data collected and the conclusions drawn during the geologic investigations at the site of Niagara Mohawk's Nine Mile Point Nuclear Generating Station, Unit 2, during a period from June 1979 through July 1980. The main topic of the studies were "thrust" faults which have been exposed at several locations at the site. These faults were initially noted in the fall of 1976, in the general area of the heater bay. The faults were described previously in two reports submitted by Niagara Mohawk Power Corporation.

The collective data base and geologic evaluations presented in this report are derived from four lines of investigation and a review. Included are:

- ° detailed geologic mapping of selected exposures;
- ° exploration with borings;
- ° study of secondary materials (lacustrine clays and low temperature calcite mineralization) encountered within the zones of deformation;
- ° in situ stress determinations; and
- ° expert opinions by several prominent members of the scientific community.

The information in this report is intended for use in conjunction with the previously presented data in evaluating the significance of the "thrust" fault structures in relation to the nuclear

facilities at the site. This data has been utilized in addressing some concerns expressed by the U.S. Nuclear Regulatory Commission in their questions Q361.1 through Q361.35. These questions were transmitted in two letters dated October 1, 1979 and July 9, 1980.

1.2 HISTORY OF "THRUST" FAULT INVESTIGATIONS

The types of geologic structures, such as in the heater bay and the radwaste building excavations, shall be referred to throughout the remainder of this report as the "thrust" or Radwaste Fault structures. These features were initially discovered in the autumn of 1976 in the following components of the power complex:

- ° the north and south radwaste trenches;
- ° the heater bay;
- ° the normal switchgear building;
- ° the circulating water intake building; and
- ° the north notch of the reactor containment.

In early spring of 1977, "thrust" faults were discovered in the cooling water intake shaft at a depth of approximately 120 feet. Similar faults were also encountered in the lake water intake tunnels upon their excavation in the spring of 1980. They are present throughout nearly the entire 1500 foot length of the east tunnel.

In late spring of 1979, excavations for the revised circulating water piping trench were completed. In the eastern half of this excavation, minor deformational features were encountered.

The style of deformation was very similar to that of the previously mapped "thrust" faults. However, the magnitudes of displacements were considerably smaller. Additional minor "thrust" fault structures were encountered during the spring of 1980, while completing excavations for the cooling tower.

Plate 1-1 presents the locations of all known occurrences of the "thrust" fault structures at the Nine Mile Point Site. Investigation of these faults was undertaken in the autumn of 1976. Dames & Moore and Stone & Webster Engineering Corporation were involved in the initial investigation. Three interpretations were advanced concerning the origin, age, and significance of the deformation. These are:

- ° the structures were developed prior to lithification of the sediments during early- to mid-Paleozoic time;
- ° the structures developed as a result of brittle failure after lithification of the sediments during late Paleozoic time;
- ° the structures developed as a result of brittle failure which occurred in relatively recent geological time, under conditions of shallow burial, and was considered to be a manifestation of high lateral stresses.

A thorough examination of these structures by Professor F.A. Donath of the University of Illinois at Urbana led to the elimination of the first interpretation stated above.

The features were thoroughly examined and an extensive effort was made to collect information to determine the age and cause of the deformation. The data obtained up to that time did not permit an unequivocal interpretation, but it was recognized that there were two possibilities. One was that the structures had formed in Paleozoic time, contemporaneously with the development of regional conjugate shear fractures. The alternative interpretation suggested that the Heater Bay structure developed after the youngest structures associated with epigenetic mineralization, probably of Late Paleozoic to Cretaceous age. The principal basis for this interpretation was the apparent absence of mineralization along the structure. This mineralization typically occurs along the Paleozoic age shear fractures.

The early investigation (1976) revealed the occurrence of laminated glaciolacustrine clay, subsequently determined to be of Late Wisconsinan Age, along the Heater Bay discontinuity. The clay laminae were seen to be contorted, and this was interpreted to indicate that the discontinuity might have experienced movements in postglacial time.

The observations and interpretations of the Heater Bay structure investigation were presented by Niagara Mohawk Power Corporation in two reports. These reports are:

- ° "Geologic Investigation of Nine Mile Unit 2; An Interim Report", 1977, Niagara Mohawk Power Corporation, Scriba, N.Y.; and

° "Nine Mile Point Nuclear Station Unit 2: Geologic Investigation Vols. I, II and III"; 1978, Niagara Mohawk Power Corporation, Syracuse, N.Y.

During a telephone conversation on March 14, 1979, between representatives of Niagara Mohawk Power Corporation, Dames & Moore, and the U.S. Nuclear Regulatory Commission, the Commission expressed concern regarding the contortions in the clay infillings, as well as the absence of a definite statement in the 1978 report precluding movements along the discontinuity during the operational life of the facilities. This concern was formally expressed by the U.S. Nuclear Regulatory Commission in both preliminary and finalized questions addressed to Niagara Mohawk Power Corporation. The questions included requests for information regarding the design of the Unit 2 power complex to account for the potential movements along the geologic discontinuities.

In May, 1979, it was decided that the design for the radwaste building should involve deepening of the radwaste trench to a level at which the discontinuity would only intersect the vertical walls of the excavation. It was also decided that a gap be left between the walls of the radwaste building and the rock face. The gap would be filled with a suitable material, to prevent the transfer of strain from the bedrock to the walls of the radwaste building. The planned excavation commenced on August 14, 1979, and was conducted under the supervision of Dames & Moore personnel. The structure was found to be more

extensive than expected. Further investigation of the structure was initiated and additional data were obtained concerning the age of the structure, its extent, and the age of last movement.

1.3 PURPOSE AND APPROACH

The purpose of the investigation reported herein was to collect and analyze data to evaluate the significance of the "thrust" fault structures with regard to the onsite facilities. Specifically, the study was directed toward acquiring information to address the following two points:

- ° to determine if future movements along the "thrust" fault structures could be ruled out; and
- ° if not, then to deduce the nature, distribution, and likely magnitude of cumulative displacements along the structures during the operational life of the facilities.

During the early stages of the investigation (September, October 1979) it was decided that the bases of the assessment of the future behavior of the "thrust" faults would include:

- ° the geometry and areal extent of the structures, described in Sections 2.1 and 2.2 below;
- ° the age of formation, genesis and age of displacements along the faults, described in Section 2.3 below; and
- ° their boundary and equilibrium conditions; and factors controlling the present equilibrium

conditions and future changes affecting these factors, described in Section 3.0 below.

As the investigation developed and the complexity and relative uniqueness of the geologic structures were made evident, it was decided that the interpretations would be greatly enhanced if the consultation of the leading practitioners in the field were obtained. Drs. F.A. Donath, D.R. Coates and S.S. Alexander continued their review of the geologic activities at the Nine Mile Point site as consultants to Niagara Mohawk Power Corporation. These individuals have served as consultants since 1977 during investigations of the Cooling Tower Fault. Their reviews of proposed studies and suggestions regarding additional analytical procedures proved helpful in completing this investigation.

Dr. N.J. Price initially was associated with the geologic investigations of the Cooling Tower Fault (1978). Dr. Price visited the Nine Mile Point site in the fall of 1979 and again in the spring of 1980 to examine the "thrust" fault, as exposed in the north radwaste trench. As a result of his initial visit, Dr. Price provided Dames & Moore with his assessment of various aspects of the structure. He concluded that this fault is a near-surface, aseismic structure and postulated several models to be utilized in assessing the possible range of future movements. Dr. Price discussed the role of the high-angle faults (Cooling Tower and Drainage Ditch Faults) as boundaries to the "thrust" sheet and recommended field investigations. In December of

1979, Dr. Price focused the action of the investigation on the future stability of the structure and the importance of shear strains.

In keeping with the decision to involve eminent practitioners, in January of 1980, Dames & Moore established a panel of consultants to review the investigations to date and provide an independent assessment of the data. The panel was empowered to recommend additional investigations and/or analyses. Drs. S.S. Philbrick, R.H. Jahns, and Mr. W.W. Moore comprised this panel. During the course of their review, they utilized the specialized services of Drs. T.L. Péwé and C. Fairhurst.

In early February 1980, Dr. Jahns, Dr. Philbrick and Mr. Moore visited the site and inspected the deformation exposed in the north radwaste trench. A summary of the work performed at the site was provided to the panel. Based on this visit, the panel recommended that a series of borings be drilled to investigate the down-dip extent of the structure (Section 2.2) and that in situ strain relief measurements be performed (Section 3.0). At that time it was recommended that Dr. Fairhurst be retained as a consultant to the review panel regarding the rock mechanics aspects of the project. Additionally, the panel recommended that Dr. Péwé visit the site to comment on (1) the possible role of ice in the formation of the Radwaste Structure and Cooling Tower Fault; and (2) the origin and age of the clay deposited in the voids in the bedrock.

Dr. Fairhurst's involvement with the review panel commenced in March 1980. His primary participation concerned the overcoring program (Section 3.0). Dr. Fairhurst assisted in planning the scope of this program, as well as analyzing the results with respect to assessing the possibility of future movement along the thrust structures. Dr. Fairhurst's report is included in Appendix F.

Other consultants whose expertise in related aspects of the study is widely recognized and who had previous experience working on the project actively participated in the investigation of the "thrust" structures, they are listed below with their area of expertise. The results of the analyses by the various consultants are provided in the referenced appendices.

Dr. H. Barnes - Pennsylvania State University Paragenetic and geothermometric analysis mineralization	Appendix B.1
Dr. H. Krueger - Geochron Laboratories - Isotopic and Radiometric Analyses	Appendix B.2
Dr. T.L. Ku - University of Southern California - Th/U Dating	Appendix B.3
Dr. L. Sirkin - Adelphi University - Palynological Analyses	Appendix C.1
Dr. J. Terasmae - Brock University - Palynological Analyses	Appendix C.2
Dr. A. Vassiliou - Rutgers University - Newark - Mineralogical Analyses	Appendix C.3

Further specific details concerning the purpose, scope and approach of individual facets of the investigation are presented with the corresponding sections.

2.0 RESULTS OF GEOLOGIC INVESTIGATIONS

2.1 MAPPING PROGRAM

2.1.1 INTRODUCTION

This section of the report presents results of the geologic mapping program undertaken to investigate the "thrust" structures. Early, it became apparent that these structures were similar to each other in terms of structural style and age. The locations of the "thrust" structures are presented on Plate 1-1. This plate shows that both the locations of the bedrock discontinuities and the excavations for the facility coincide with a north trending valley in the bedrock.

The structures can best be described as small, gently dipping to nearly horizontal shear planes across which the upper strata have been transported to the west. In a geometric sense they would be classified as thrust faults. These "thrusts" appear to be confined to specific stratigraphic units. They generally occur as planes of slip parallel to bedding with short intervals where the discontinuity transects the layering at a low angle and then merges with bedding at a higher stratigraphic level. Small brittle asymmetric folds and monoclines, reflecting the direction of bedrock transport, commonly occur within the zones of deformation. The observed displacements across the faults differ considerably, both along individual structures, and from exposure to exposure, ranging from less than an inch to several feet.

2.1.2 PURPOSE

The purpose of the mapping program was dual:

- ° to document the occurrence and location of "thrust" structures exposed in bedrock excavations at the site;
- ° to identify and define pertinent structural relationships which could provide information concerning the determination of the age of development, the age of last movement, and, the mechanism of deformation.

2.1.3 SCOPE

Geologic mapping was conducted in four separate areas of the site: the circulating water piping trench, the relocated cooling tower excavation, the north radwaste trench, and the east lake water tunnel (Plate 1-1).

In the circulating water piping trench a geologic plan view was made, at a scale of 1:36, of an area of approximately 10,000 square feet. Within this area detailed cross sections were drawn, at a scale of 1:12, of the walls of the upper and lower sump trenches.

A plan view of an area of approximately 7500 square feet was made of the floor of the relocated cooling tower excavation. Additionally, two cross sections were drawn, at scales of 1:30 and 1:12, of bedrock faces within this area.

Six cross sections and a plan view were prepared of the exposures in the north radwaste trench. Cross sections of the exposure were drawn, at scales of 1:60 and 1:12. Two cross sections and a plan view were made, at a scale of 1:12, of a small auxiliary excavation in the southwest wall of the main exposure.

Seven cross sections were drawn, at a scale of 1:60, of the exposures of "thrust" faults in the east lake water tunnel. However, with the exception of the exposure nearest the tunnel portal, exposures in the left rib of the tunnel were mapped.

The sampling of secondary materials (calcite and clay) associated with the structures and the collection of structural measurements for geometric analysis were included within the scope of this program. Photographic documentation of the exposures and sample locations was conducted in conjunction with all mapping.

2.1.4 APPROACH

All drawings represent in detail, the configuration and geometric relationships in the exposures. Stratigraphic correlations were necessary to define the sense and amount of displacement across the faults. It was important to identify structural relationships pertaining to the secondary materials occurring within the structures. At each location a sufficient number of structural measurements were collected to define accurately the geometry of the structure and the direction of slip.

2.1.5 STRATIGRAPHY

Plate 2.1-1 shows the stratigraphic units within which the "thrust" structures occur at the site. An extensive description of the stratigraphic sequence at the site is presented in the April 1978 report.

The cooling tower and circulating water piping trench excavations are situated within the lower portion of the Oswego Sandstone. The deepest portions of these excavations extend into the Transition Zone. The bedrock exposed at these locations consists of gray, fine-to-medium grained, massive and commonly cross bedded siliceous sandstone. It contains numerous well-developed sedimentary channels commonly filled with argillaceous and thinly bedded strata.

Approximately 25 feet of stratigraphic section is exposed in the north radwaste trench. The excavation extends from the lower Oswego Sandstone, through the Transition Zone, and a few feet into the upper portion of Unit "A" of the Pulaski Formation. The lithologic character of the Oswego Sandstone at this location is essentially identical to that described above. The Transition Zone consists of thin-to-medium bedded sandstone, graywacke, and siltstone. Occasional black shale layers generally less than one-half inch thick are also present. Unit "A" consists of medium-to-thickly bedded sandstone and graywacke.

The east lake water tunnel exposes about 15 feet of the stratigraphic sequence which comprises the upper portion of Unit "C" of the Pulaski Formation. This sequence consists of medium-to-thick bedded and commonly fossiliferous sandstone strata separated by medium bedded shaly siltstone beds.

2.1.6 STRUCTURE

Structural observations made at exposures of "thrust" faults on the site are discussed in order of their occurrence, from the circulating water piping trench in the south to the lake water intake tunnels in the north (Plate 1-1).

2.1.6.1 Circulating Water Piping Trench

Plate 2.1-2 is a plan view of the area investigated in the circulating water piping trench, illustrating various geologic structures and sample locations. Plates 2.1-3 through 2.1-5 are geologic cross sections representing the bedrock discontinuities encountered at this location.

The "thrust" structures consist of tenuously interconnected breccia zones parallel to bedding or sedimentary channel surfaces. Small folds produced by rigid body rotation of bedrock slabs are associated with the main discontinuities, in the upper and lower sump trenches (Plate 2.1-2).

The structure in the upper trench consists of a breccia zone up to 6 inches thick. As shown on Plates 2.1-3 and 2.1-4, the

breccia zone is situated at the base of a northwest trending sedimentary channel. The axes of small folds, developed in response to slip across the zone, trend from S05E to S38E, plunging from 5 to 16 degrees (Plate 2.1-26). The movement of the strata above the zone was to the east or northeast as reflected by the geometry of the folds. The amount of translation across the structure could not be determined. However, sedimentary relationships suggest that a displacement of approximately one foot is a reasonable estimate.

The principal discontinuity in the lower sump trench is a westward dipping breccia zone depicted on Plate 2.1-5. Stratigraphic separation and the rotation sense of a small monoclinial fold indicate that the hanging wall strata were translated to the east relative to the footwall strata. The axis of the monocline in the south end of this trench trends approximately S03W and plunges 12 degrees. This fold consists of a series of rotated bedrock slabs separated by voids. The displacement across the breccia zone (Plate 2.1-5) could not be determined with certainty; however, stratigraphic correlations indicate the horizontal translation may be as much as 4 to 4.5 feet.

Bedrock dilations are common in the circulating water piping trench, but secondary infilling materials were identified only within the structure exposed in the upper sump trench. There, unconsolidated sediments occur along the breccia zone for a distance of several feet (Plate 2.1-3). Two types of material

were identified, a light gray plastic clay, and a tan to gray laminated silty clay. The laminae of the latter were contorted by diapiric structures. Plate 2.1-3 shows the locations of samples representing both soils for palynological analysis (Samples GA3-S1 and GA3-S2). In addition, slickensided and brecciated calcite mineralization was identified on the sole of the breccia zone. To obtain information concerning the age of deformation, samples of this calcite were collected for fluid inclusion analysis (Samples GA3-17, 18, and 19; Plate 2.1-2). The results of the laboratory analysis of these secondary materials are presented in Section 2.3.

Several observations and conclusions concerning the deformational character of these "thrust" faults can be made:

- ° the structures result from slip along bedding planes;
- ° the sedimentary configuration of the bedrock has influenced the mode of deformation (that is, brecciation or folding);
- ° dilation occurred in association with the deformation; and,
- ° the slickensided and brecciated calcite indicates that the faults might have undergone repeated movements.

2.1.6.2 Relocated Cooling Tower Excavation

Plate 2.1-6 is a plan view of the area investigated in the cooling tower excavation. Plates 2.1-7 and 2.1-8 are cross

sections representing bedrock discontinuities at this location.

The "thrust" faults exposed in this excavation were similar to the bedrock discontinuities in the circulating water piping trench. Several small brittle folds have resulted from bedding plane slip along these discontinuities. The zones contain breccia, as well as unconsolidated sediments. The presence of till within the bedrock at this location distinguishes these structures from the faults in the circulating water piping trench.

The eastern "thrust" structure is presented in cross section on Plate 2.1-7. From this plate and the geologic plan view, (Plate 2.1-6), it is apparent that at least part of the bedrock is surrounded by till. This suggests that the deformation could be attributed to glacial processes.

The other structures mapped in the cooling tower excavation are shown in cross section on Plate 2.1-8. The dislocations in the bedrock have occurred along bedding planes, which are now filled, in most cases, with till and breccia. A small monocline, the axis of which trends approximately N77W, has been developed in association with the slip. The sense of rotation of this monocline indicates that the hanging wall block moved to the southwest relative to the footwall block. In addition to the till, calcite mineralization occurs at the

base of the breccia zones, and cements breccia clasts and displays southwest trending slickensides.

2.1.6.3 North Radwaste Trench

The exposure in the north radwaste trench is the most prominent of all the "thrust" faults at the site. Plates 2.1-11 and 2.1-12 are cross sections representing the structure in this exposure. An auxiliary excavation was made into the southwest wall of the trench to examine the structural relationships of secondary materials found within the "thrust" structure. Plate 2.1-13 is a plan view and Plates 2.1-14 and 2.1-15 are cross sections representing this excavation.

As illustrated on the generalized cross sections (Plates 2.1-9 and 2.1-10) the "thrust" fault consists of a broad zone of deformation. This zone is developed within the Transition Zone and displays a dip of 20 to 30 degrees to the east. From Plates 2.1-11 and 2.1-12, it is apparent that the structure is composed of a stack of bedrock elements displaced to the west along bedding planes. The most intense deformation is culminated along the inclined portion of the discontinuity. There is no continuous shear dislocation of the beds along the footwall of this structure. The displacements observed are accomplished in a variety of modes, including:

- ° discontinuous shear dislocation of individual beds or groups of beds;
- ° rigid body rotation of beds to form small folds;

- ° broad arching of the hanging wall strata; and
- ° dilation of the bedrock along bedding planes and variously oriented fractures.

The displacement is greatest across the nearly horizontal zone of brecciation which is effectively the upper limit of the ramp portion of the structure (Plate 2.1-17). The apparent separation across this zone was established to range from 5 to 7 feet (Plates 2.1-11 and 2.1-12). This is based on the correlation of a fossiliferous sandstone bed. The magnitude of overall shortening is not easily established. In the deepest part of the excavation the apparent dip separation across the fault was determined to be 4.5 feet. This displacement was established by correlating a fossiliferous horizon across the structure.

Plate 2.1-16 is a structure contour map showing the configuration of the top of the Transition Zone in the vicinity of the north radwaste trench. It shows that the displacements across the "thrust" have resulted in an arching of this horizon. This broad warp displays a northward trend, and an amplitude of about 2.5 feet.

The overall direction of structural transport of the hanging wall of the radwaste structure is to the west. However, the direction of slip of individual stratigraphic elements within the "thrust" structure varies from S80W to N60W. These slip

directions were determined on the basis of fold axis orientations and the directions of slickensides (Plate 2.1-26).

Possibly the most significant characteristic of the structure was the presence of numerous indicators of dilation within the bedrock mass, such as voids, open fractures of various attitudes, and zones of loose bedrock rubble. In addition, calcite mineralization and unlithified sediments occur within the structure.

Calcite, cementing breccia clasts, was found at a number of locations and was commonly slickensided (for example, sample locations GA4-1, -2, and -3; Plates 2.1-11 and 2.1-12). In one case, this calcite occurred on a randomly oriented bedrock fragment within the breccia zone (sample location GA4-8; Plate 2.1-11) indicating that the dislocation of the fragment followed mineralization (Section 2.3.4). Calcite mineralization cemented laminated clay within bedding planes at sample location GA4-7 (Plate 2.1-12).

Two types of unlithified sediments infilled openings within the structure: a gray to tan laminated silty clay, and a gray massive plastic clay. The latter type was most commonly present in zones of intensely shattered bedrock along the ramp of the fault. At several locations laminated clay was mixed with the breccia (sample locations GA4-S5, -S6 and S27; Plates 2.1-11, -12, and -13). Laminated clay was also found along

bedding planes, where it appeared to be contorted (sample location GA4-S1, Plate 2.1-12). Examples of deformation of the laminated clays occur in the exposures of a small monocline at elevation 223 feet (Plates 2.1-12 and 2.1-14). At this location clay layers 1/4 to 1 inch thick dip from 20 to 70 degrees, parallel to the limb of the monocline (Plate 2.1-12, -13, and -14).

The configuration and general appearance of the radwaste "thrust" fault lead to the following conclusions concerning the mechanism of deformation:

- ° the deformation resulted from the shear displacement to the west of the strata along bedding planes in the hanging wall;
- ° the deformation occurred under conditions of low vertical confinement as indicated by the dilation of the strata in this exposure;
- ° the cumulative displacement on this "thrust" has been achieved by incremental displacements as indicated by the structural relationships within this exposure.

Further discussion concerning the age of the structure is provided in Section 2.3.

2.1.6.4 East Lake Water Tunnel

The locations of exposures of "thrust" faults along the lake water tunnels are shown on Plate 1-1. Cross sections representing

these exposures are presented on Plates 2.1-18 through 2.1-24. Plate 2.1-25 is a three-dimensional representation showing the configuration of the structures relative to both tunnels.

As shown on Plate 2.1-25, the five fault exposures in the east tunnel probably do not represent separate discontinuities. Rather, it appears that the shear planes at either extremity of the zone of faulting represent the same structure. The three intermediate faults are splays from this main structure. This is consistent with the magnitudes of the displacements at the individual exposures, which are greatest at the extremities.

The "thrust" faults in the east tunnel consist of a series of discrete, intimately related, gently southeastward dipping to nearly horizontal shear planes, ranging in strike from N10E to N35E. A similar shear plane occurs in the north tunnel (Plate 2.1-25). The cumulative displacements across the faults are small, approximately one foot, and the hanging wall strata are consistently displaced to the west. The slip direction along individual shear planes was inferred from the rake of slickensides and the axial trends of small folds (Plate 2.1-26). In the tunnel exposures these directions range from N40W to N85W, with the majority of slip trending N55W to N60W.

The individual shear planes are generally sinuous and contain small amounts of breccia. The faults characteristically

emerge from bedding planes and cross the strata at a gentle angle, re-entering bedding planes at a higher stratigraphic level (Plates 2.1-18, -19, -22, and -23).

Rotation of the layering occurs only in the vicinity of shear plane bifurcations (Plates 2.1-18 and 2.1-20). Dilation of the stratigraphic section, expressed as voids and open fractures, occurs in association with these faults (Plate 2.1-18, -19, -23 and -24); however, this dilation appeared to be developed to a lesser degree than the dilation at "thrust" fault exposures closer to the bedrock surface.

Secondary materials were also found within these "thrust" structures. The most prevalent is calcite mineralization, which occurs within dilated bedding planes and along shear surfaces. Calcite on fault planes commonly cements breccia fragments, and displays dip slip slickensides. Samples of calcite mineralization were collected from ten locations (Plates 2.1-19, -20, -22, and -24). A discussion of this mineralization is presented in Section 2.3.4. In one location, soft gray, massive, plastic clay was present within a zone of dilation (Plate 2.1-22).

2.1.7 SUMMARY AND INTERPRETATION

The "thrust" structures mapped during this investigation appear to be integrally related, because of their similarities in structural style, mechanism of deformation, and apparent relative age.

Spatially, the structures appear to be confined to the area in proximity to the bedrock valley and between the high angle faults, namely the Cooling Tower and Drainage Ditch Faults (Plate 1-1). The "thrust" faults are distributed throughout the strata exposed by excavation. However, the individual structures are confined to particular stratigraphic intervals in the vicinity of prominent lithologic interfaces (Plate 2.1-2).

The "thrust" faults are all similar in terms of their overall appearance, and display the following common structural characteristics:

- ° intense brecciation;
- ° small scale brittle folding and bending;
- ° dilation;
- ° indications of repeated movements; and,
- ° generally westward sense of structural transport.

Plate 2.1-26 summarizes structural information pertaining to the slip directions along the "thrust" faults. The data from the circulating water piping trench and cooling tower exposures have been grouped together because of their proximity and their occurrence within the same stratigraphic unit. At each location where "thrust" structures were exposed a range for the slip direction was developed. This range varies from west-south-west to west-north-west progressively from the cooling tower area to the tunnel exposures. It is apparent that the slip direction varies, depending either on the location of a

particular exposure and/or depth of development (effectively stratigraphic position of the fault exposures).

Variation in the slip direction of the faults attests to the heterogeneous nature of the strain along these structures. It is possible that this has resulted from a progressive change in the stress trajectories either laterally or with depth.

In terms of relative geologic age, the "thrust" faults display marked similarities. At each location secondary materials which are mesoscopically identical in appearance, occur within the structures. These materials are low temperature calcites and glaciolacustrine sediments containing pollen (Section 2.3.5). In addition, the presence of unfilled bedrock dilations indicates that the "thrust" faults developed under conditions of low vertical confinement.

In view of the overall similarities of the faults, it is apparent that they have developed as a result of similar deformational mechanisms operating at essentially the same time. The structural relationships suggest that the cumulative displacements resulted from either repeated or continuous releases of strain energy.

2.2 EXPLORATION OF THE EXTENT OF THE RADWASTE FAULT

2.2.1 INTRODUCTION AND PURPOSE

In addition to the mapping of the Radwaste Fault, presented in

the previous section, knowledge pertaining to the extent of the fault was desired. Specifically, it was thought that the style of deformation displayed by the fault is such that it must eventually change from an east-dipping "thrust" to a layer-parallel zone of slip.

Two methods of tracing the fault were pursued: exploration boreholes and strain-relief measurements. Additionally, it was thought that a review of all previous boring and excavation records could contribute information about the extent of the fault. The strain-relief measurement program was conducted as part of the overall rock mechanics investigation of the Radwaste Fault and is presented in Section 3.0 of this report.

2.2.2 SCOPE OF WORK

In 1972, the 400-series of boreholes was drilled as part of onsite exploration for the Preliminary Safety Analysis Report for Unit 2. Twelve boreholes from this series were selected and re-examined. New lithologic logs were prepared, at a scale of 1:60, utilizing the lithologic convention developed during the investigation of the Cooling Tower Fault. Moreover, occurrences of shear fractures, slickensides, breccia, bedding dips, clay seams, and mineralization were recorded. Cross sections were prepared to evaluate vertical stratigraphic displacements.

The excavations for the reactor containment had been photographed and mapped by Stone and Webster Engineering Corporation as part of the geological inspection program. These photographs and maps were re-examined to recognize radwaste-type deformation which had not previously been identified.

Nine vertical boreholes designated the 800-series were drilled along a line trending eastward and roughly perpendicular to the strike of the Radwaste Fault (Plate 2.2-1). The boreholes were PQ-size (3.28 inch core diameter), and were continuously cored to depths ranging from 90 feet, near the radwaste trench, to 300 feet, farther east. The samples from each borehole were photographed and logged, at a scale of 1:60, for lithology, fractures, mineralization, seams of unlithified sediment, attitude of layering, etc. Furthermore, detailed reconstructions of the core were analyzed and drawn, at a scale of 1:6, for portions of Borings 801, 802, 803, and 804.

Calcite mineralization and unlithified sediment (clay) were found in the cores. Specimens were documented with photographs and detailed drawings (scale 1:1) and then collected for laboratory analysis. The calcite was analyzed by Dr. H.L. Barnes of the Pennsylvania State University as part of the concurrent program of mineral studies reported in Section 2.3. The samples of clay were sent to Dr. L.A. Sirkin of Adelphi University for palynologic (pollen) analysis, as part of a similar program also presented in Section 2.3.

Two types of downhole surveys were made of each boring. Natural gamma-radiation logs were completed using a Mount Sopris Model 1000-C portable borehole logging unit. Moreover, downhole, wide-angle videotapes for each boring were recorded by Deep Venture Surveys of Perryville, Florida using a truck-mounted borehole television camera.

Appendix A contains the geologic and gamma radiation logs for the 800-series borings.

2.2.3 INVESTIGATION RESULTS

2.2.3.1 400-Series Boreholes

The locations of selected 400-series boreholes are presented on Plate 2.2-1. Upon re-examination of the cores from these borings, evidence of bedding plane slip deformation was recognized at two stratigraphic levels. One level occurs within Unit A of the Pulaski Formation; the other is near the interface of Unit B and Unit C of the Pulaski Formation. A comparison of these data with information obtained from the 800-series boreholes (Section 2.2.3.3) reveals that the upper zone can be related to the Radwaste "thrust" fault. The lower zone is characterized by a similar style of deformation, namely bedding plane breccias and gently dipping shear fractures. However, this zone remains confined within or immediately beneath the base of the Pulaski Formation Unit B.

The upper zone of Radwaste deformation is inferred to be present on the basis of structures recognized in the cores

from Borings 403, 404, 407, 408, and 411. However, similar deformation in Unit A could not be identified with certainty in the boreholes located south of Boring 411. In all but two borings (408 and 412), there is evidence of bedding plane slip deformation near the base of Unit B of the Pulaski Formation.

2.2.3.2 Photographs and Field Inspection Maps of the Reactor Containment Excavation

To define further the overall configuration of the Radwaste Fault, the photographs and field inspection maps of the walls of the north auxiliary bay excavation were examined. Photographs taken in 1976 were compared to the original field maps of the excavations. In this manner, it was determined that zones of bedding plane slip deformation at two stratigraphic levels were also recognizable within these excavations (Plate 2.2-3).

The upper zone of deformation coincides with that inferred from the 400-series borings. This zone (north wall) exhibited beds which appear to have been rotated up to approximately 10 degrees. This rotation apparently resulted from westward slip of the upper beds relative to the lower beds. On the west wall, the zone can be traced parallel to bedding as far as the north reactor notch (Plate 2.2-3).

The lower zone of deformation on Plate 2.2-3, occurs between the thick sandstone beds of Unit B near the base of the excavation. This may represent the same zone of deformation recognized at

this stratigraphic level in the cores from the 400- and 800-series boreholes (Plate 2.2-2).

2.2.3.3 800-Series Borings

Plate 2.2-2 presents a geologic cross section prepared from the borehole logs (Appendix A), as well as the television camera survey. Two principal zones of deformation have been recognized, as described above. These are the Radwaste Fault Zone and the Unit B slip zone. In addition, numerous thin clay seams were detected through the stratigraphic section penetrated by the borings.

The Radwaste Fault Zone - The deformation within the Radwaste Fault Zone is intense and is associated with a 16 inch vertical stratigraphic displacement, identified between Borings 407 and 804. There are three members of the upper zone which are depicted in the cross section shown on Plate 2.2-2. The upper member represents a continuation of the fault in the north radwaste trench (corresponding to Boring 407) where the inclined "thrust" fault passed into a bedding plane at elevation 214. A few feet beneath it, the middle member which was detected only in Borings 407, 801, 802, and 803 occurs. The lower member (between elevations 190 to 210) exhibits the most intense deformation. Detailed logs of this zone in Borings 801, 802, and 803 are shown on Plates 2.2-4, -6, -7, and -8. Gamma logs were used to identify lithologic contacts in areas of low core recovery. Folding within this zone was evidenced

by bedding which dips up to 50 degrees, as shown on Plates 2.2-4, -5, and -7B. It was not possible to determine the dip direction from the cores; however, from the north auxiliary bay exposures it can be inferred that westward slip of the upper layer relative to the lower layer caused the rotation of the beds.

Several other aspects of the Radwaste Fault Zone bear mentioning. First, at the base of the lower member, an olive-green illite rich layer was identified (Plate 2.2-2). This layer was recognized during mapping in the north auxiliary bay (Plate 2.2-3). The illite, in some locations, is concentrated and the layer may be several inches thick. It is characteristically unctuous. Where it is concentrated, slickensides are pronounced, indicating slip along this layer. Secondly, calcite mineralization similar to that observed in the radwaste trench occurs along the members of this fault zone. Three samples were collected for analysis from Boring 801, and the details are presented in Section 2.3. Thirdly, measurements of the groundwater level in the 800-series borings indicate that the third member of the fault zone has a much greater permeability than the surrounding bedrock, indicating dilation.

The Unit B Slip Zone - In eight of the nine boreholes, a zone of brecciation accompanied with gently dipping slickensided fractures is present, principally at the base of Unit B. Other intensely deformed but less continuous zones were identified

within Unit B (Plates 2.2-2, -7, and -9). The most continuous zone occurs at the base of the reactor excavation (Plate 2.2-3).

Interstitial Clay - At various depths in six of the 800-series borings, clay was noted to fill dilated bedding planes. In more than one instance, this clay exhibits laminations (Plates 2.2-10, -11, and -12).

There are two significant factors regarding this clay:

- ° the laminated clay occurs at depths as great as 270 feet (Plate 2.2-2);
- ° pollen analysis of clay samples yielded minor amounts of pollen and spores in each specimen (Section 2.3 and Appendix C.1).

2.2.4 CONCLUSIONS

On the basis of the foregoing discussion, several principal conclusions can be drawn:

- (1) The gently dipping "thrust" fault in the north radwaste trench is the upper member of a stack of several similar structural features. These features dip eastward and pass into bedding planes. The sense of displacement on these features is the hanging wall to the west. Laterally, the zone has been traced with borings a minimum distance of 500 feet.

- (2) Individual members of the stack of "thrusts" display a common style of deformation including dilation, brecciation, and local rotation of bedding. Low-temperature groundwater calcite commonly occurs in association with these structures.
- (3) The lowermost continuous zone of deformation occurs near the base of Unit B of the Pulaski Formation. Below this zone there are occurrences of bedding plane breccia and gently dipping shear fractures, but they do not appear to be discrete, continuous zones.
- (4) Laminated clays indicate that dilation across bedding planes occurred at depths as great as 270 feet.

2.3 AGE OF DEFORMATION

2.3.1 STATEMENT OF THE PROBLEM

The foregoing sections presented data pertaining to a series of gently dipping "thrust" and bedding plane faults. Knowledge of the age of deformation is important in judging the probability of future deformation. Toward this end, there are three questions which must be answered:

- ° what is the geologic age of initial "thrust" fault development;
- ° has there been recurrent movement; and, if so
- ° what is the age of latest displacement?

A major purpose of the effort to evaluate the "thrust" fault was to obtain data regarding the above three questions.

2.3.2 TECHNICAL APPROACH

The age of development of the "thrust" fault was sought considering their relationship to:

- ° other geologic structures whose ages are fairly well known, namely the Cooling Tower and Drainage Ditch Faults;
- ° the bedrock topography on site, inasmuch as the present bedrock surface is the result of glacial sculpturing of an older erosion surface;
- ° sediment interbedded in dilated openings in the bedrock; and
- ° calcite mineralization.

Utilizing the existing site excavations, there was no direct way to assess the relative age of the "thrust" faults with respect to the steeply dipping faults, by examining their cross-cutting relationships. Therefore, the relative ages of the structures could only be assessed indirectly through structural and rock mechanics analyses of the origin and mechanism of the "thrust" faults.

To assess the relationship of the radwaste type faults to the bedrock surface, a detailed contour map (Plate 1-1) was prepared utilizing data regarding the top of bedrock from site borings, outcrops, and excavation maps.

Evaluations of the origin and age of the interstitial sediment and the calcite mineralization, as well as their relationships to the "thrust" faults, were used to deduce the age(s) of deformation. This information, in conjunction with the mapping, also served to define whether movement along the "thrust" faults has been recurrent.

2.3.3 ONSITE BEDROCK TOPOGRAPHY

Plate 1-1 illustrates the site bedrock topography, which shows a buried valley incised in the rock. It is important to note that the "thrust" faults, occur on both banks of the valley and that the hanging wall strata are generally displaced toward the center of this feature. This suggests that the presence of the valley has contributed to the development of the "thrust" faults.

Data from foundation borings show that the valley contains Late Wisconsinan till, overlain by younger sediment, related to Lake Iroquois, and some peat (Plate 2.3-1). There is no evidence of weathering beneath the till. From these data, one can infer that the valley is of Wisconsinan age or older.

2.3.4 CALCITE MINERALIZATION

2.3.4.1 General

Mapping of the bedding plane faults (Section 2.1) revealed an association between fine-grained calcite mineralization and the shear planes. The calcite was found to occur in a variety

of forms such as "conglomerate", concretionary nodules, and patches of drusy euhedral crystals.

A number of samples were collected for mineralogical studies. The objective of these studies was to determine the origin of these minerals, to define their relationships to the radwaste-type of deformation and to the epigenetic calcite mineralization reported in the 1978 study (Niagara Mohawk Power Corporation, 1978, Volume 1, Section 6.0). It was anticipated that the studies would yield data useful in inferring the age(s) of deformational episodes on the "thrust" faults. The above objectives were accomplished employing three principal approaches:

- ° paragenetic and geothermometric analyses of calcite minerals;
- ° isotopic studies of calcite, utilizing ^{13}C and ^{18}O ratios; and
- ° radiometric dating of calcite by the ^{14}C and $^{230}\text{Th}/^{234}\text{U}$ methods.

Dr. H.L. Barnes of the Pennsylvania State University directed the laboratory analyses for the paragenetic studies. He also provided assistance in evaluating the results of isotopic and radiometric analyses. The determination of isotopic ratios and the ^{14}C dating of calcite were performed by Mr. H.W. Krueger of Krueger Enterprises, a division of Geochron Laboratories, Cambridge, Massachusetts. Dr. T.L. Ku, of the University of Southern California, performed the $^{230}\text{Th}/^{234}\text{U}$ disequilibrium

dating of calcite. The results of the above analyses are provided in Appendix B.

2.3.4.2 Results of Paragenetic Studies

General

Specimens of calcite mineralization were collected from four areas onsite. Samples collected from the circulating water piping trench are designated as the GA3 series (Table 2.3-1). The specimen locations are shown on Plate 2.1-2. Those from the north radwaste trench are designated the GA4 series, and are presented in Table 2.3-2 with their locations shown on Plates 2.1-9 through 14. Tables 2.3-3 and 2.3-4 present information concerning the specimens collected from the east lake water tunnel (GA5 series) and the 800-series boreholes, respectively. Locations of specimens from the tunnel are shown on Plates 2.1-19 through 2.1-24. Sample locations pertaining to the borings are shown on Plates 2.2-4 and 2.2-10. The paragenetic relationships are derived from analyses of each of the four sample series.

Paragenesis of Calcite Mineralization*

Plate 2.3-2 is a summary diagram illustrating the paragenetic relationships derived from this study. They are distinctively different from the paragenetic relationships defined in the 1978 Cooling Tower Fault report.

*The most recent data (Appendix B.1-7) obtained necessitate this modification of the paragenetic sequence compared to that presented in Q361.33 to the NRC submitted prior to this report.

Type 1 calcite (Plate 2.3-2 and Appendix B.1-3) was the term initially used to represent a very fine-grained (average of 15 μm) calcium carbonate which occurs as the matrix material enclosing breccia fragments of the host rock. Fragments of older milky calcite are also present in some samples. This calcite exhibits deformational twinning, healed fractures, and contains sulfide minerals as well as fluid inclusions. The liquid-to-vapor ratios of the fluid inclusions are similar to the milky calcite of the JT series samples of the Cooling Tower Fault study. Typically, the textures of Type 1 calcite are cataclastic (Plates 2.3-3 and 2.3-4). No fluid inclusions have been found in Type 1 calcite, possibly because cataclasis liberated any which may have formed within it. Type 1 calcite also exhibits post-deformational solutioning, which has created cavities that are commonly lined with younger Type 3 calcite (Appendix B.1-1).

Based on the use of ultraviolet fluorescence in the analysis of the GA5 sample series (Appendix B.1-7), it has been determined that Type 1 calcite breccia contains Type 3 calcite (see below) as a dominant cement around host rock clasts and fragments of milky calcite. This suggests that Types 1 and 3 are paragenetically equivalent, where at first they were suspected to be distinct (Plate 2.3-2).

Type 2 patchy calcite was only recognized in samples from the circulating water piping trench (GA3 series; Appendix

B.1-1), where it occurred on open subvertical tension cracks emanating upward from bedding plane breccia zones. Although not as intensely deformed as Type 1, open cleavages are present. In terms of paragenesis, Type 2 is equivalent to Type 1 (Plate 2.3-2).

A number of forms of very fine-grained travertine are present in the north radwaste trench and cooling tower area (Appendix B.1). This mineral group is paragenetically related and similar in occurrence to Type 1 calcite in that, although never found directly associated with Type 1, it always underlies or is infilled by later forms of calcite. The travertine deposits are typically deformed, but not as severely as Type 1 (Appendix B.1-3, p. 45, shows a small fault in banded travertine). Plates 2.3-5 and 2.3-6 show examples of the travertine recognized in the north radwaste trench.

Silty calcite was seen microscopically as thin laminae of very fine-grained calcareous material containing abundant siliceous and sulfidic detritus. This mineral was deposited on travertine and is placed later in the paragenetic scheme (Plate 2.2-3).

Dr. Barnes considers this to be a minor depositional stage, which apparently occurred before and after the deposition of Type 3 calcite, perhaps "as products of either in situ settling soon after...deformation, or a transported material washed in from other areas while the fractures were still relatively open" (Appendix B.1-3).

Type 3 calcite, or sparry calcite, occurs in a variety of habits filling fractures and voids or other openings in Type 1 calcite and travertine. Examples of Type 3 calcite are shown on Plate 2.3-6. The stubby, euhedral crystals are characteristic, and differ in size from 50 μm in diameter to radiating crystals more than 1 mm long. Deformation of Type 3 calcite is mild, such as twinning, small fractures, or chipping into platelets. The fractures in Type 3 commonly are healed by later calcite. Primary and secondary fluid inclusions are commonly present in Type 3 calcite. As described in Appendix B.1-1 and B.1-3, these inclusions have different aspects from those of the JT series. Specifically:

- ° Inclusions in Type 3 calcite either contain no vapor phase or display high liquid-to-vapor ratios.
- ° In Type 3 calcite, it was not possible to measure homogenization temperatures employing the usual techniques, because of the single-phase nature of most of the inclusions. Two other methods were used instead. Decrepitation temperatures of the inclusions were determined. This is the temperature at which the inclusion leaked or ruptured upon heating. Theoretically, because the trapped fluid is incompressible, the fluid transfers a critical stress to the crystal which ruptures when heated above its original entrapment temperature. Thus, the lowest temperature recorded should represent the maximum filling temperature for a given population

of inclusions. This method yielded a maximum filling temperature of 40°C for the sample from the radwaste trench. A maximum filling temperature of 30°C was also determined by cooling the inclusions until a vapor phase formed, and reheating it until the liquid filled the inclusion. Dr. Barnes (oral communication, 1980) indicated that the latter method is preferable, but the agreement between the methods in this instance is very satisfactory.

- ° Freezing tests on inclusions in Type 3 calcite revealed that the fluid in the inclusions is dilute with concentrations equivalent to 5-6 weight percent of NaCl.

The above characteristics indicate that the Type 3 calcite formed very near the ground surface at temperatures similar to present ambient temperatures. Dr. Barnes has further reasoned (Appendices B.1-5 and B.1-7) that low salinities of fresh waters are uncommon even at depths of 0.5 kilometers. Therefore, the implicit depth of burial at the time of formation of Type 3 calcite was less than 0.5 km.

The latest calcite of the paragenetic sequence is brown calcite which occurs overlying Type 3 calcite. This calcite is discontinuous and of varied thickness. It was recognized only by microscopic analysis, and was apparently not deformed.

The sequence of crystallization of Types 1, 2, 3, travertine, and silty calcite presented on Plate 2.3-2 is not unequivocal. However, each type, except silty calcite, shows very similar fluorescence (that is, trace element contents), associated minerals, and fluid inclusion characteristics (Appendix B.1-7, Table 1). This suggests that the four varieties may be different facies of the same depositional stage.

D₅ and D₆ stages of deformation of the calcite minerals, are defined in the paragenetic sequence (Plate 2.3-2). These stages pertain to the deformation of two groups of minerals: Type 1 calcite and travertine, and Type 3 calcite. Both stages occur later than stage D₄ determined in previous studies (Niagara Mohawk Power Corporation, 1978, Vol. I).

Another variety of calcite, observed in specimen GA4-S8-A, was analyzed, but could not be correlated with the paragenetic sequence. This calcite cements a laminated silty layer; an occurrence observed in more than one location in the radwaste trench. Part of this specimen (GA4-S8-B) was sent to Dr. L.A. Sirkin for pollen analysis (Plate 2.3-12 and Table 2.3-9). Fractures, healed by calcite, were found in the cemented silt layer (Appendix B.1-3, p. 50). The healing calcite was analyzed by Dr. Barnes who related it, to the Type 1 calcite on the basis of its association with brecciation.

Specimen GA4-6 provides some insight into the relationship of calcite mineralization to Radwaste Fault deformation. As shown on Plates 2.1-11 and 2.3-8, the calcite occurred on the overturned side of a bedrock slab within the fault breccia. Plate 2.3-8 shows the position of the rock fragment prior to sampling. Analysis of the minerals revealed that Type 1 calcite is present, and solution cavities in this calcite are filled with Type 3 calcite (Appendix B.1-3, p. 24). It is apparent that at least two stages of fault slip were required to position the sample as observed. The brecciated, cataclastic nature of the Type 1 calcite indicates one stage. Later, Type 3 calcite crystallized in solution cavities within Type 1. A second stage of slip then rotated the bedrock slab into its present position (keeping in mind that Type 1 is always found on the sole of the shear surface). Reconstruction of this specimen to its pre-deformational state would suggest a minimum transport distance of 3 inches to the west.

2.3.4.3 Isotopic and Radiometric Analyses

^{13}C and ^{18}O ratios of samples of Type 1, Type 3, and travertine were analyzed to determine if these minerals were derived from a common source, and to help evaluate the meaning of the radiometric analyses. Furthermore, radiocarbon (^{14}C) dating was attempted using these minerals. The results are provided in Tables 2.3-5 and 2.3-6.

It is apparent that Type 1 calcite formed below the groundwater table. Its texture and grain size suggest a low-temperature

origin. Radiocarbon and uranium-series dates suggest that the age of Type 1 is younger than 300,000 years B.P. (Table 2.3-5). Additionally, re-examination of specimens JT-13, 43, and 44 taken from the Cooling Tower Fault breccia in Pit 1 (Niagara Mohawk Power Corporation, 1978, Vol. 1, Sections 4.0 and 6.0) by Dr. Barnes (Appendix B.1-7) reveals that these specimens are predominantly Type 1 calcite for the following reasons:

- ° They contain fluid inclusions, with either a single phase or a high liquid/vapor ratio.
- ° The sulfides (pyrite and marcasite) in JT-44 closely correspond to sulfides seen in Type 1 calcite.
- ° Uranium-series analyses of Type 1 by Dr. Ku in samples TU-1 (analyzed recently) and SW-1 and SW-2 (analyzed in 1977) both yielded an excess of ^{230}Th . Thus, the absolute ages for SW-1 and SW-2 (Table 2.3-5) are not at variance with the result from sample TU-1. The true age of crystallization for Type 1 is equivocal. ^{13}C analysis for sample HK-1 which yielded a ^{14}C age of greater than 36,000 years B.P. shows that the carbon is actually older marine carbon (Plates 2.3-9 and 2.3-10) leached from the Pulaski Formation. The ^{18}O isotope ratio for HK-1 (Table 2.3-6 and Plate 2.3-11) indicates a fresh water origin for the oxygen. This further indicates that Type 1 calcite formed at low temperatures, near the ground surface, by precipitation from fresh water below the groundwater table. The time of formation was either sometime during the Sangamonian

interglacial stage, or during the Wisconsin stage.

The travertine yielded a ^{14}C age of $14,180 \pm 550$ years B.P. (Table 2.3-5). The paragenetic and isotopic studies indicate that the travertine precipitated from fresh water in the vadose zone (Plates 2.3-9, 10, and 11 and Table 2.3-6), as implied by the ^{13}C and ^{18}O ratios. The ^{14}C age is compatible with the age of mollusc shells (sample SL-10, Table 2.3-5 and Plate 2.3-13). These shells occur in sediment deposited during the late stages of glacial Lake Iroquois. An insufficient quantity of Type 3 calcite was collected for a successful ^{14}C date, but the ^{13}C ratio implies that the carbon is also derived from fresh water (Plate 2.3-9 and 2.3-10). Accordingly, it is reasonable to interpret that Type 3 calcite is a low temperature mineral crystallized at or near the present ground surface at approximately the same time or later than the travertine.

In summary, the available evidence indicates that the six calcite varieties studied as part of the Radwaste Fault investigation are:

- ° younger than the epigenetic mineralization of probably Mesozoic age (Niagara Mohawk Power Corporation, 1978, Vol. 1); and
- ° Quaternary in age, probably no older than Sangamonian or Wisconsinan.

2.3.5 RELATION OF INTERSTITIAL SEDIMENT TO THE RADWASTE FAULT

2.3.5.1 General

In Sections 2.1 and 2.2, it was reported that unlithified sediment occurs along bedding planes and within brecciated zones. Similar occurrences had been reported earlier (Niagara Mohawk Power Corporation, 1978, Volume 1, Sections 3.0 and 4.0). It seems obvious that dilation of the bedrock to form openings within which the sediment could be deposited occurred in proximity to the thrust faults, and at depths as great as 270 feet.

Two questions pertain to the unlithified sediments. The first concerns the origin and age of the sediment. The second is whether or not this sediment has been affected by slip along the "thrust" faults.

2.3.5.2 Origin and Age of Interstitial Sediment

General

As described in Section 2.1, the mapping effort established that there are three types of unlithified materials within the zones of deformation:

- ° gray to greenish-gray gouge (with breccia);
- ° non-laminated, plastic gray clay; and
- ° laminated tan to brown silty clay.

Locally, these materials are mixed together within the breccia zones (Plate 2.3-12). The investigation was undertaken to

determine the origin of the interstitial sediment. Three possibilities existed:

- ° The sediment is all, or in part, of glaciolacustrine origin;
- ° the sediment is all, or in part, a form of gouge; and
- ° the sediment is a combination of gouge and weathered shale.

It was suspected that the laminated, tan clay is glaciolacustrine in origin because of its similar appearance to the Lake Iroquois deposits. Also, in the heater bay and in the trenches across the Cooling Tower Fault, similar laminated clay was pollenated with species similar to those found in the Pleistocene overburden.

Specimens were collected for grain-size distribution analysis to help distinguish depositional environments of the sediment. Specimens were also collected for compositional and heavy mineral analyses. Additional pollen analysis was performed to define the depositional climates of the clays. The samples collected consisted of the tan clay, the gray clay, the breccia and gouge, as well as the bedrock in contact with the gouge. Three "control" samples from the overburden for which the pollen spectra and the geologic ages are known (Plate 2.3-13) were analyzed. One specimen of lignitic peat was collected and a radiocarbon date was obtained. Table 2.3-9 lists all specimens of sediment which were analyzed.

The grain-size analyses were performed in the Soil Mechanics Laboratory of Dames & Moore in Cranford, New Jersey. The compositional and heavy mineral analyses were performed by Dr. A.H. Vassiliou of Rutgers, the State University, Newark, New Jersey. The procedures employed are described in his reports in Appendix C.3.

The pollen analyses were performed by Dr. L.A. Sirkin, Professor of Palynology and Pleistocene Geology, Adelphi University, Long Island, New York. The procedures used are described and results provided in Appendix C.1. At the recommendation of the consultants to Niagara Mohawk Power Corporation, samples of the clays were sent to Dr. J. Terasmae, Professor of Palynology and Pleistocene Geology at Brock University in St. Catherines's, Ontario, Canada to provide an independent evaluation of Dr. Sirkin's findings and interpretations. Dr. Terasmae's report is provided in Appendix C.2.

Mr. H.W. Krueger, of Krueger Enterprises, performed the radio-carbon analysis of the peat. His report is provided in Appendix B.2.

Grain-Size Distributions

Five samples of clay were collected for sieve/hydrometer analysis. Two specimens were collected from the tan, laminated silty clay in the north radwaste trench. Three control samples from the circulating water piping trench (Plate 2.3-13) were

also tested. Samples of the gray clay were not tested because it was not possible to properly process a sufficient amount of representative material. The test results are presented on Plates 2.3-14 through 2.3-18. From these diagrams, the relative ratios of sand-silt-clay were computed and plotted on a ternary diagram (Plate 2.3-21) according to the classification defined in Krumbein and Sloss (1963, p. 159). For comparison, the ratios for two specimens collected from the bedrock in Trench 4 and whose test results were reported in 1978 (Niagara Mohawk Power Corporation, 1978, Vol. II, Section 1.0) are also plotted on Plate 2.3-21. One of the specimens (AS-43) consisted of tan laminated clayey silt, very similar to the type seen in the bedrock of the north radwaste trench. The other (AS-44) was sand infilling a vertical fracture which emanated upward from the sediment filled layer where sample AS-43 was collected.

Inspection of the ternary plot shows that the laminated sediment from the radwaste trench (GA4-S1 and GA4-S4) is similar in composition to the varved clay of glacial Lake Iroquois (SL-CWPT-1; 12,500 years B.P.). The silts (SL-CWPT-2 and SL-CWPT-3) were collected from the fossiliferous marl of the Sandy Creek stage of Lake Iroquois (12,000 to 10,000 years B.P.). The mollusc shells from this unit yielded a date of $12,545 \pm 330$ ^{14}C years B.P. (SL-10; Appendix B.2-5).

The grain size distribution curves for the laminated clays (GA4-S1, GA4-S4, and AS-43) are remarkably similar (Plates

2.3-14, -15, and -19). The curves for these specimens are also very similar to the control sample SL-CWPT-1. The shapes of the curves for the two control samples of Sandy Creek sediment (Plates 2.3-17 and 2.3-18) are more similar to the curve representing AS-44 (Plate 2.3-20), although the sand/silt/clay ratios are very different.

The test results seemingly suggest a textural correspondence between the laminated clay in the north radwaste trench and the Lake Iroquois sediments.

Compositional and Heavy Mineral Analyses

Sixteen specimens of various materials were analyzed for their mineralogic compositions by Dr. A.H. Vassiliou (Appendix C.3-1). These specimens include the three control specimens collected from the overburden in the circulating water piping trench.

Additionally, Dr. Vassiliou tested three specimens of laminated clay by performing heavy mineral separations as described in Appendix C.3-2. Investigators (Connally, 1964; Gwyn and Dreimanis, 1979) have used the heavy mineral assemblages of tills to distinguish deposits of various Wisconsinan glacial lobes. The possibility was considered that the laminated clay from the radwaste trench might bear recognizable heavy mineral assemblages linking their origin to a particular Wisconsinan glacial stage. The results, however, were inconclusive

(Appendix C.3-2) because the assemblages were atypical of those required for a correlation.

The data from mineralogic analysis by Dr. Vassiliou are summarized in Table 2.3-7. Specimens of groups I through IV were all collected from the north radwaste trench, whereas Group V specimens were collected from the circulating water piping trench. Each group contains specimens of similar texture and apparent origin. Examination of these data allow five principal observations to be made and several conclusions follow.

- (1) The data suggest that the material comprising some samples is heterogenous. For example, the modes of samples GA4-S7-A and GA4-S2-M of gray clay are similar. Also, GA4-S7-A bears some resemblance to GA4-S5-C (breccia) based upon the relative proportions of the qtz/fsp, % kaol/%chl, and kaol + chl. From this observation, it is concluded that mixing of the materials has occurred within the breccia zones (Plate 2.3-12).
- (2) The compositions of the gray, plastic clay and the tan, laminated clay are distinctly different from the compositions of the breccia, gouge, and the bedrock in contact with the breccia zones. This is demonstrated by (a) the much greater qtz-fsp/carbonate in breccia, (b) the higher ratio of calcite/dolomite

in clay, (c) consistently higher qtz/fsp in breccia and bedrock, and (d) the total percentage of kaol + chl is more erratic in the breccias than in the clays. These observations suggest that the clays are not a product of cataclasis.

- (3) The gray clay is not compositionally identical to the tan clay; however, the compositional differences are not very pronounced. This statement is supported by (a) the lower carbonate content of the gray clay as expressed in the ratio, qtz + fsp/carbonate; (b) gray clay seemingly has higher percentage of total clays, as well as higher kaol/chl ratio than the tan clay. These observations suggest, although tenuously, either different sources or different depositional environments for each.

- (4) There is an obvious compositional similarity between the breccia and gouge and the bedrock in terms of their mineral constituents.

- (5) The gray and tan clay from the radwaste trench (in contrast to the breccia and gouge) are compositionally similar to samples SL-CWPT-1 and SL-CWPT-2. The marl in the circulating water piping trench (SL-CWPT-3) is more calcareous and does not resemble any of the sediments in the radwaste trench. These

relationships are illustrated by the relative ratios of calcite/ dolomite and qtz + fsp/carbonate. The observations lead to the conclusion that the clays in the radwaste trench resemble Lake Iroquois sediment more closely than they resemble the breccia or bedrock.

To further test conclusion (5) above, the mineral contents of the laminated clays from the north radwaste trench were compared to that from earlier analyses of interstitial sediment from Trench 4 (Niagara Mohawk Power Corporation, 1978, Vol. II, Plate 1-4). This comparison is illustrated on Plate 2.3-22. With the exception of the relative silica content, the carbonate, clay and feldspar contents are similar. The studies in 1978 determined that AS-43 and AS-44 were derived from the overburden.

On the basis of the results of the compositional analysis, one may conclude that the tan and gray clays are neither products of cataclasis nor weathering of the bedrock. Rather, these clays are derived from a source similar to that of the overburden.

Pollen Analysis and Absolute Dating

Twenty-two samples were analyzed for their pollen spectra. Two samples were taken from the circulating water piping trench, fourteen from the north radwaste trench, and six from some of the 800-series boreholes (Section 2.2; Table 2.2-9).

Dr. Sirkin found various amounts of pollen in all specimens analyzed (Appendix C.1-1 and 6). Four samples yielded enough pollen that their relative percentages could be plotted, thus permitting a tenuous interpretation of which pollen zone they might represent (Table 2.3-8).

The Gray Clay

The specimens of gray clay contained too little pollen to evaluate in terms of established pollen stratigraphy. Nevertheless, the pollen forms present in the gray clay are Pleistocene in age (Appendix C.1-4). Dr. Sirkin suggested that the pollen identified could be representative of the Spruce Pollen Zone (Table 2.3-8). They represent a vegetational setting of a conifer parkland, with areas of wet ground marginal to a proglacial lake, such as Lake Iroquois. The results are very consistent with the pollen data obtained from the Lake Iroquois varved clay of the overburden at the site (Niagara Mohawk Power Corporation, 1978, Vol. II).

The Tan Clay

The specimens of tan clay yielded a more diverse spectrum of pollen than the gray clay. These spectra for samples from the north radwaste and circulating water piping trenches are shown on Plate 2.3-23. The assemblage of pollen and spores for specimen GA4-S1A suggest an arboreal, spruce parkland or shrub tundra vegetation with scattered trees which is characteristic of the early Spruce Pollen Zone, namely subzone A1

(Table 2.3-8). Specimen GA4-S4A yielded a pollen assemblage, including hardwood, suggesting somewhat warmer climatic conditions, such as those represented by later Spruce subzones, namely subzone A4. The age of the A zone is 12,000 to 10,400 years B.P. (Niagara Mohawk Power Corporation, 1978, Vol. 2, Section 1.0). Specimen GA4-S8B represents a cemented layer of laminated silty clay (Plate 2.1-12 and Table 2.3-9). This specimen yielded a few pollen grains interpreted to be characteristic of subzone A4 of the Spruce Pollen Zone. This specimen was also analyzed by Dr. Barnes (Section 2.3.4.2). Calcite within fractures in fragments of this layer (Plate 2.1-11) is probably similar to Type 1, Type 3, and travertine (Section 2.3.4.2). The pollen were cemented by this calcite, hence cementation and brecciation seem to have occurred later than pollen emplacement.

Within the auxiliary excavation into the south wall of the north radwaste trench, a clay layer containing patches of lignite-rich peat was discovered. Sample GA4-S31 from this layer was radiocarbon dated, yielding an age of $11,060 \pm 360$ ^{14}C years B.P. (Appendix B.2-5).

In summary, the conclusions which can be drawn from these studies are:

- (1) The origin of the gray clay is uncertain, but it is probably derived from a source similar to

overburden, based on its composition, pollen content, which is similar to the overburden. Possibly, it was deposited during Lake Iroquois.

- (2) The tan, laminated clay is a glaciolacustrine sediment deposited in Lake Iroquois, and likely, during the Sandy Creek Stage. This is demonstrated by the pollen content, as well as the $11,060 \pm 360$ year B.P. ^{14}C date.
- (3) The laminated clay from the deeper levels penetrated by the 800-series borings is likely of glaciolacustrine origin. The age of this clay cannot be firmly established with the evidence available because the pollen therein are insufficient in number. However, the species of pollen identified, and their state of preservation, suggest a Late Quaternary age.

2.3.6 DEFORMATION OF CLAYS - A QUESTION OF ORIGIN

During the mapping of the radwaste trench, attention was paid to the relation of the interstitial clays to the bedrock deformation. If deformation of the clays could be attributed, at least in part, to slip along the fault, this would indicate that the age of latest fault displacement post-dates the time of clay deposition. Consideration was also given to the possibility that the configuration of these clays might demonstrate

that the rock deformation pre-dates their deposition thereby placing an upper bound to the time of the latest fault displacement.

Initially, the deformed clay was discovered in the south wall of the north radwaste trench (Plate 5.1-12). At approximately elevation 221, a pronounced anticlinal fold in the bedrock is exposed. This fold had a somewhat different appearance on the south wall from that on the north wall. The fold on the south side was expressed as bending with minor-scale kink-like folds, whereas on the north side, a concentric anticline was apparent. This anticline was truncated near its crest by a nearly horizontal bedding plane breccia (Plate 2.1-11) which exhibits nearly 7 feet of displacement (Plate 2.1-11). Clay was preserved within the dilated kink fold on the south wall. Plate 2.3-25 presents photographs of this exposure. The pencil tip in these pictures point to the exposure of laminated, tan-colored, clay between bedding slabs which dip 65 to 70 degrees to the west on the short limb of the fold. The base of the fold is bounded by a bedding plane shear zone.

The meaning of the attitude of the clay was uncertain. One could conceive of a situation where groundwater flow through the dilated openings in the fold permitted emplacement of clay following the completion of folding.

Excavation southward along the fold axis was extended to obtain additional data. Plates 2.1-13 and 2.1-14 illustrate the extent of the excavation and the configuration of the bedrock structure therein. Additional layers of laminated clay were discovered (as well as the lignitic peat that yielded the ^{14}C date of $11,060 \pm 360$ years B.P.). It was also discovered that the clay exhibited abundant contortions, folds, small internal shear displacements, and fluidization structures. Plates 2.3-26 presents photographs of a layer of clay within the kink fold, which exhibits folded laminae. Plate 2.3-27 depicts clay deformation on the upper side of the short limb of the fold.

To aid in the interpretation of the deformational features in the clay, and their relationship to the kink fold in the bedrock, several consultants examined the exposure. These consultants were Dr. D.R. Coates of the State University of New York at Binghamton; Dr. L.A. Sirkin of Adelphi University; and, Dr. T.L. Péwé of Arizona State University. Drs. Sirkin and Péwé provided written discussions based upon their examinations of the exposure (Appendix D).

One can summarize the conclusions drawn from the examinations of the exposure by the various professional geologists as belonging to two categories in terms of the origin of the deformational features in the clay.

One explanation is that some, or all, of the deformational features were induced concomitant with the bedrock folding. The other is that the deformational features are penecontemporaneous with deposition of the clay. This argument implies that all bedrock deformation had occurred prior to the time of clay deposition. Consequently, the attitudes of the clay layers would be, in essence, inherited from the highly irregular surfaces that developed from the older bedrock deformation.

2.3.7 CONCLUSIONS

On the basis of the previous discussions, the following conclusions can be drawn:

- (1) The initial development of the Radwaste Fault is known, on the basis of studies and radiometric dates of calcite mineralization, to be less than 300,000 years B.P. and to have occurred at (a) shallow levels in the crust, and (b) at ambient temperatures less than 30°C. A Late Sangamonian or younger age is conceivable.
- (2) Movements along the Radwaste Fault have been recurrent as evidenced by the different stages of deformation recorded in the mineralization (D₅ and D₆, Plate 2.3-2).
- (3) The age of latest displacement is equivocal. Nevertheless, evidence has been obtained documenting

deformation of travertine minerals which formed approximately 12,000 years ago, and Type 3 calcite known to be the same age or younger than the travertine.

TABLE 2.3-1

GA3 SERIES

SPECIMENS OF CALCITE MINERALIZATION COLLECTED FROM CIRCULATING WATER PIPING TRENCH EXCAVATIONS

Sample No.	Location	Elevation Approximate Plant Coordinates	Structural Setting
GA3-1	Floor of excavation near south end of zone of closely spaced conjugate fractures	<u>237</u> S847, W313.5	Calcite collected from surface oriented N45E, 25°S.
GA3-2	Floor of excavation near south end of zone of closely spaced conjugate fractures	<u>237</u> S847.5, W313.5	Calcite collected from surface oriented E-W, 09S not parallel to bedding; calcite contains small sandstone clasts.
GA3-3	do.	<u>236.5</u> S945, W315	Calcite on bedding plane oriented N10W, 09E.
GA3-4	Floor of excavation within zone of closely spaced conjugate fractures.	<u>238</u> S816, W316.5	Calcite on surface oriented N05W, 09°S; not parallel to bedding, cements small sandstone clasts.
GA3-5	Floor of excavation within zone of closely spaced conjugate fractures	<u>238</u> S817, W316.5	Calcite on surface oriented N75W, 04S; not parallel to bedding.
GA3-6	Floor of excavation on east side of zone of closely spaced conjugate fractures	<u>237.5</u> S813, W307	Calcite on bedding plane oriented N30W, 08N brecciation along this plane at other locations.
GA3-7	Floor of excavation at south end of hot water trench	<u>236</u> S784, W236	Calcite on bedding plane oriented N60W, 04N.
GA3-7A	do.	do.	Calcite with small sandstone clasts on subhorizontal surface equivalent to base of bedding plane breccia zone.
GA3-8	do.	<u>236</u> S784, W238	do.
GA3-9	Floor of excavation, hot water trench	<u>237</u> S774, W248	Calcite coating on fracture oriented N53W, 90°.
GA3-10	Floor of excavation, hot water trench	<u>236.5</u> S765, W254	Calcite and sulfide mineralization on fracture oriented N47W, 90°.
GA3-10A	do.	do.	Calcite and sulfide mineralization on fracture oriented N72E, 87°S.
GA3-11	Floor of excavation, hot water trench; central part of northwest trending zone of fractures	<u>235.5</u> S775, W253	Calcite coating fracture oriented N50W, 40°N.
GA3-12	Floor of excavation within zone of closely spaced conjugate fractures	<u>238</u> S814, W312	Calcite coating fracture oriented N46W, 88°S.
GA3-13	do.	<u>238</u> S817.5, W317.5	Calcite coating on fracture oriented N70E, 85°S.
GA3-14	do.	<u>238</u> S803, W311	Calcite coating fracture oriented N53W, 88°N.
GA3-15	do.	<u>238</u> S801, W317	Calcite coating on fracture oriented N70E, 87°N.

TABLE 2.3-1 (cont.)

Sample No.	Location	Elevation Approximate Plant Coordinates	Structural Setting
GA3-16	Floor of excavation, upper sump trench	234 Samples Collected On A Line Extending From	Calcite containing sandstone clasts on surface oriented N-S; 20°W - base of breccia zone.
GA3-17	do.	S777, W326	Calcite on surface oriented N05W, 13°W - base of breccia zone.
GA3-18	do.	to S770, W324	Calcite on subhorizontal surface nearly parallel to bedding - contains sandstone clasts - located at base of breccia zone.
GA3-19	do.	233 S733, W323	Calcite containing sandstone clasts on surface oriented N05E, 20°W - not parallel to bedding - base of breccia zone.

TABLE 2.3-2

GA4 SERIES
SPECIMENS OF CALCITE MINERALIZATION COLLECTED FROM NORTH RADWASTE TRENCH

Sample No.	Location	Elevation Approximate Plant Coordinates	Structural Setting
GA4-1	On floor, near west end of north wall (N60W)	<u>228</u> N267, W132.5	Very thin (less than or equal to 1 mm) coating of calcite on Oswego Sandstone; surface strikes N07W to N19E, dips 05° to 20° E. Dip-slip slickensides present at base of bedding plane breccia. West over east displacement sense.
GA4-S3	North wall of slot in N.R.W.T.	<u>224</u> N254, W122	N62E, approximately 90° mineralized joint fracture - contains two patches of nodular calcareous mineral - possibly limestone "concretion." Sample of concretions only.
GA4-2	On floor of slot near base of south wall of N.R.W.T.	<u>222</u> N242, W131.5	Two patches of calcite on siltstone or graywacke bed at base of brecciated zone with faint striae, 0-10°. Fold axis above breccia is N35W, 04° N.
GA4-3	On floor of slot of N.R.W.T. near south wall	<u>218.5</u> N236, W115.5	Base of breccia zone on sandstone bed. Locally on low angle shear across bed. Local striae - dip slip. Calcite with breccia clasts, lineated calcite.
GA4-4	On floor of slot in N.R.W.T. at base of north wall	<u>217.5</u> N242.5, W109.5	Calcareous concretion on N10W, 35NE surface which is striated near GA4-3.
GA4-5	On north wall of slot of N.R.W.T.	<u>220</u> N240, W108	Calcite on 2 nearly orthogonal fractures. Both have rough surfaces: N65W, 50SW; N10E, 90°.
GA4-6	North wall of slot of N.R.W.T.	<u>217</u> N233, W101	Brecciated calcite with clasts of host rock occurs on fragment of bedrock, randomly oriented and contained within breccia/gouge at base of slot.
GA4-7	South wall of slot in N.R.W.T.	<u>220</u> N234.5, W112.5	Sandstone bedding plane contains dark gray amorphous calcareous patches resembling limestone. Bed is tilted because of folding within deformed zone exposed in trench.
GA4-8	On floor of slot at base of south wall	<u>222.5</u> N259, W128	Striated calcite on horizontal, siltstone layer which is bounded above by breccia/gouge (with soil) along bedding, and below by dilated bedding fracture filled with soil.
GA4-9	At bottom of south end of slot in N.R.W.T.	<u>214</u> N225, W97	On sheared fossil layer dipping 25° to 30° toward east. Both striated calcite (dip-slip) and brecciated calcite with rock clasts occur on shear surface.
GA4-10	Top of south wall of N.R.W.T.	<u>228.75</u> N235, W109	Zoned patches of calcite and/or concretions on irreg. N70E vertical joint.
GA4-11	Top of south wall of N.R.W.T. slot (2 to 3 ft south of GA4-10) on approx. N45W, 90° fracture in same sandstone bed containing GA4-10	<u>228.75</u> N233, W110	Similar to GA4-10. Also contains radial sprays of dark gray euhedral crystals, probably calcite. Several generations may be present.
GA4-S8	South wall of N.R.W.T. slot	<u>218.5</u> N230.5, W109	Pocket of brecciated zone of gray massive plastic clay and fragments of cemented tan, laminated silt containing healed fractures. Sampled for analysis of healing agent in fractures.
GA4-BH	Top of north wall of N.R.W.T.	<u>238.9</u> N241, W97	Grout from Boring 407 - control specimen for GA4-X.
GA4-X	North wall of N.R.W.T.	<u>219</u> N240, W100	Occurs in zone of folded and dilated rock within voids and cementing rock fragments. Substance unknown.
GA4-12	South wall of N.R.W.T. slot	<u>223</u> N240, W122	Dripstone on NW vertical joint.
GA4-13	2 feet south of GA4-11	<u>228.75</u> N231, W111	Same sandstone layer as GA4-11.

TABLE 2.3-2 (cont.)

Sample No.	Location	Elevation Approximate Plant Coordinates	Structural Setting
GA4-14	No specimen taken	—	—
GA4-15	South wall of N.R.W.T. slot	230 N233, W112	Patches of gray euhedral calcite crystals on joint (N85E, 90) in sandstone bed. Fracture surface is irregular.
GA4-16	Same as GA4-13	230 N231, W111	See GA4-13.
GA4-17	South wall of N.R.W.T. slot	230 N227, W110	Patch of gray euhedral calcite crystals on fracture (N05W, 90) Fracture surface is irregular.

TABLE 2.3-3

GA5 SERIES
SPECIMENS OF CALCITE MINERALIZATION COLLECTED FROM EAST LAKE WATER TUNNEL

Sample No.	Location	Elevation	Structural Setting
GA5-1A	North Wall (left rib) Stations 0+47 to 0+50	137	Calcite on footwall of fault N45E, 55SE
GA5-1B	do.	do.	N42E, 52SE, Slickensides rake 45°NE
GA5-1C	do.	do.	N47E, 45SE, Slickensides rake 45°NE
GA5-1D	do.	do.	N30E, 47SE, Slickensides rake 80°NE
GA5-2A	North Wall (left rib)	134	Calcite on footwall plane of thrust: N40E, 32SE
GA5-2B	do.	do.	Brecciated calcite (Type 1) on footwall of thrust N45E, 38SE, Slickensides rake 40°NE
GA5-3, 3A-3E	Shear surface - floor 6+32 to 6+44 footwall	138	Bulk Type I breccia and white (grayish) calcite coatings, some displaying dip slip slicks
GA5-4	Shear surface - floor, 6+44 footwall	138	Type I breccia, minor secondary calcite coating
GA5-5	Shear surface - 9+82.5 Left rib footwall	152.5	Type I breccia with stubby euhedral calcite crystals and white patchy calcite coating
GA5-6	Shear surface, 9+59 Left rib footwall	143	White (grayish) calcite coating
GA5-7	Shear surface, 8+51	145.5	Type I breccia
GA5-8	Shear surface, 6+46 Left rib footwall	143	Type I breccia, white calcite coating with oblique slip slicks
GA5-9, 9A	Shear surface at 2+62.5 and 2+69 Left rib (2+62.5 - footwall)	139.5	9 - Grayish white calcite coatings
		143	9A - Fragments of white calcite and Type I breccia on loose fragments of rock in open work breccia
GA5-10	Shear surface, 4+59 Left rib footwall	143.5	Minor grayish white calcite coatings

TABLE 2.3-4

800 SERIES
SPECIMENS OF CALCITE MINERALIZATION COLLECTED FROM CORES OF BORINGS 801 AND 806

Sample No.	Location	Elevation	Structural Setting
801-M1	Boring 801, N227.7, W75.3	197.8	Depth 43.6'; calcite breccia on beds dipping 30°.
801-M2	do.	196.4	Depth 45.0'; patches of calcite on bedding planes with breccia.
801-M3	do.	194.9	Depth 46.5'; calcite breccia a low-angle fracture.
806-M1	Boring 806, N73.1, E468.4	111.7	Depth 148.9'; slickensided calcite on 15° dipping shear fracture. Beds 0°.

TABLE 2.3-5
RADIOMETRIC DATING OF LOW TEMPERATURE CALCITE

Sample No.	Specimen Material	^{14}C (years)	$^{230}\text{Th}/^{234}\text{U}$ (years)
HK-1	Type 1 Calcite	Greater than 36,000	—
HK-2	Travertine	$14,180 \pm 550$	—
TU-1	Type 1 Calcite	—	Less than 300,000
SL-10*	Mollusc shells	$12,545 \pm 330$	—
SW-1 ⁺	Drusy calcite	—	$170,000 \pm 2,000$
SW-2 ⁺	Drusy calcite	—	$81,000 \pm 1,000$

TABLE 2.3-6
ISOTOPE ANALYSES OF LOW TEMPERATURE CALCITE

Sample No.	Specimen Material	^{13}C (o/oo)	^{18}O (o/oo)
HK-1	Type 1 Calcite	+3.1	$+21.1 \pm 0.2$
HK-2	Travertine	-7.5	$+22.6 \pm 0.2$
HK-3	Type 3 calcite	-4.7	—
SL-10*	Mollusc shells	-6.9	—

*Sample from marl in circulating water piping trench, reported in NMPC, 1978, Geologic Investigation, Vol. 2, Section 1.0.

⁺Sample from Pit 1 near old Cooling Tower excavation; equivalent to specimens JT-13, 43, and 44: NMPC, 1978, Geologic Investigation: Vol. 1, Section 4.0 and 6.0. See Plate 5.3-13 of this report.

TABLE 2.3-7
MINERALOGIC ANALYSES

SPECIMENS		WET CHEMICAL ANALYSIS WEIGHT PERCENT			XRD AND THIN SECTION ANALYSIS										RATIOS, ETC.				
		Carb. Range	Average Carbonate	Access Min.	VOLUME PERCENT														
					Granular Minerals					Clay Minerals									
Group	GA4 No.	Description			Qtz	Fsp	Cal	Dol	Sid	Acc*	Chl	Ill	Kaol	Clay	Kaol+Chl (%)	Kaol* Chl	Qtz Fsp	Cal Dol	Qtz+Fsp Cal+Dol+Sid
I	S1-B	Tan, laminated silty clay	-	15.0	-	32	11	11	3	1	9	27	6	42	35	0.59	2.9	3.7	3.1
	S4-B		24.8-25.1	24.9	-	30	9	11	5	-	11	31	3	45	30	0.25	3.3	2.2	2.4
	S6-D1		2.0-5.0	3.5	-	18	4	29	-	1,2	12	33	3	48	32	0.23	4.5	-	0.76
	S5-B+		12.0-26.1	19.1	-	34	13	24	6	1	7	15	-	22	32	-	2.6	4.0	1.6
II	S2-M	Gray, soft clay (non-laminated)	-	9.7	Pyrite, hornblende	24	10	2	5	1,2,3	13	40	5	58	30	0.36	2.4	0.4	4.9
	S5-B+		12.0-26.1	19.1	-	34	13	24	6	1	7	15	-	22	32	-	2.6	4.0	1.6
	S6-D2		15.6-15.9	15.7	-	37	38	20	7	1,2	5	18	4	27	32	0.68	4.6	2.9	2.8
	S7-A		-	14.2	Pyrite, hornblende	22	7	-	7	1,2	8	43	12	63	32	1.50	3.1	-	4.1
III	S5-C	Breccia and gouge	12.2-22.3	17.2	Hornblende	29	9	-	3	1,4	10	39	9	58	32	0.88	3.2	-	12.7
	S6-A		5.0-5.1	5.1	-	65	12	10	-	1	7	4	1	12	65	0.18	5.4	-	7.7
	S7-B		35.4-45.1	40.2	Pyrite, hornblende	26	5	-	17	1,2	8	38	5	51	25	0.67	5.2	-	1.8
IV	S5-D	Bedrock in contact with breccia zone specimen	-	4.7	-	37	7	-	-	1,2	15	39	1	55	29	0.07	5.3	-	-
	S6-C		-	4.7	Hornblende	68	11	2	-	1,2	5	12	1	18	33	0.14	6.2	-	39.5
	S7-C		-	22.0	-	40	11	-	16	1,2	12	20	-	32	39	-	3.6	-	3.2
V	CWPT-1	Lake Iroquois and Sandy Creek overburden sediment	-	14.1	Magnetite, zircon rutile	37	16	8	10	1,2	10	18	-	28	39	-	2.3	0.8	2.9
	CWPT-2		-	13.9	Magnetite, zircon rutile	42	18	11	10	1	6	11	-	18	37	-	2.3	1.1	2.9
	CWPT-3		31.6-31.8	31.7	-	25	4	41	5	1,5	8	15	-	24	36	-	6.3	8.2	0.63

*Ratio of % KAOL to % CHL with respect to total clay content.

+Sample is mixture of groups I & II.

**For explanation of terminology, see Appendix B.

1. Hematite
2. Hornblende
3. Pyrite
4. Pyroxene
5. Apatite

TABLE 2.3-8

CORRELATION OF POLLEN STRATIGRAPHY — EASTERN NEW YORK AND SOUTHERN CONNECTICUT*

Pollen Zones	Stages	Northern Hudson Valley	Southern Wallkill Valley	Southern New England	Western Long Island
<u>OAK</u>	C3a	Spruce Rise	Oak, Hemlock	Spruce Rise	Oak, Chestnut,
	C3b	Pine, Birch, Hemlock		Oak, Hemlock	Holly
	C2	Beach, Pine, Hemlock	Oak, Hickory	Oak, Hickory	Oak, Hickory
	C1	Hemlock, Birch	Oak, Hemlock	Oak, Hemlock	Oak, Hemlock
POST -		Pine, Oak			
<u>PINE</u>	B2	Pine, Oak	Pine, Oak	Pine, Oak	Pine, Oak
	B1	Pine, Birch	Pine	Pine	Pine
<u>SPRUCE</u>	A4	Spruce Maximum	Spruce Returns	Spruce Returns	Spruce Returns
	A3	Alder, Pine (A3-4)	Pine, Spruce, Oak (12,850 \pm 250)	Pine Spruce, Oak	Pine, Spruce
	A1,2	Spruce, Pine, Grass (Spruce Park)	Pine, Spruce	Birch, Spruce	Pine Spruce
<u>HERB</u>	T3	Pine, Birch, Spruce, NAP, Park-Tundra (12,400 \pm 200)	Pine, Spruce, Birch	Birch Park-Tundra	Pine, Spruce, NAP
	T2		Spruce, Pine, Fir	Spruce Park-Tundra	Spruce
	T1	Glaciated	Pine, Birch Shrub-Tundra	Tundra	Park-Tundra
	W		Glaciated	Glaciated	Park-Tundra Near Tundra

*From Connally and Sirkin, 1969

TABLE 2.3-9

SPECIMENS OF INTERNED SEDIMENT FROM TRENCHES AND BORINGS AS PART OF RADWASTE FAULT STUDY

Specimen Number	Location	Description	Testing (H,M,P,R)
1. GA4-S1	North Rad Trench (N.R.T.) So. Wall, el. 223.6	Tan laminated silty clay on bedding plane.	H, M, P
2. GA4-S2	N.R.T., No Wall, el. 219	Gray plastic, massive clay, within breccia of fold. With embedded rock fragments.	M, P
3. GA4-S3	See Table 5.3-2	NA	—
4. GA4-S4	N.R.T., West end of No. Wall, el. 233	Tan, laminated silty clay along dilated bed.	H, M, P
5. GA4-S5	N.R.T., No. Wall, el. 226	Mined gray and tan clay and gouge in brecciated zone. Also bedrock sample.	M, P
6. GA4-S6	N.R.T., So. Wall, el. 222.5	Mixed gray, tan clay, gouge, breccia.	M, P
7. GA4-S7	N.R.T., base of No. Wall, east end, el. 215	Gray clay in breccia/gouge on 20° dipping shear. Bedrock sample also.	M
8. GA4-S8	N.R.T., So. Wall, el. 218.5 to 219.5 Near east end	1 mm of cemented, laminated silt in breccia and with other non-cemented clay.	M, P, F
9. GA4-S9	N.R.T., So. Wall, el. 219.5 West of GA4-S8	Cemented silt at top of non-cemented clay.	—
10. GA4-S10 to S19	No Specimens Collected	NA	—
11. GA4-S20	N.R.T., So. Wall extension, West end, el. 220-222	Tan to grayish laminated clay in kink fold; on tilted bed.	P
12. GA4-S21	do.	Mottled, tan laminated clay within folded and brecciated zone.	P
13. GA4-S21A	do.	do.	P
14. GA4-S22	do.	do.	P
15. GA4-S23	do.	Laminated tan clay with contortions.	P
16. GA4-S24	do.	Laminated clay with contortions on tilted sandstone bed.	P
17. GA4-S25	do.	do.	P
18. GA4-S26	do.	Laminated clay with contortions.	P
19. GA4-S27	do.	Tan silt and clay, contorted with rock fragments underlying breccia on tilted rock bed.	—
20. GA4-S28	do.	Tan laminated clayey silt adhered to vertical joint at east end of extension excavation.	—
21. GA4-S29	do.	Tan, mottled laminated clay on 26° bed of sandstone (GA4-S25).	—
22. GA4-S30	do.	1/2 to 3/4 inch thick tan to gray laminated clay or bed dipping 35°.	—
23. GA4-S30A	do.	Same as S30, some small clay dikes.	—
24. GA4-S31	N.R.T., So. Wall extension, el. 221	Patchy thin layer of dark brown lignitic peat in laminated silty clay	R
25. GA4-S31A	do.	Same as GA4-S31.	—

TABLE 2.3-9 (cont.)

Specimen Number	Location	Description	Testing (H,M,P,R)
26. SL-CWPT-1	West Wall, Circul. Water Piping Trench, 800' So. of Reactor Center, el. 224.5	Varved clay from Lake Iroquois deposits in overburden, 1.4 ft. above bedrock.	H, M, P*
27. SL-CWPT-2	do., el. 249	Upper part of laminated clayey silt of Sandy Creek sands, 3.75 ft. above rock.	H, M, P*
28. SL-CWPT-3	do., el. 250	Yellow brown marl with mollusc shells 5.2 ft. above rock.	H, M, P*, R*
29. 806-S1	N 73.1, E 468.4, Depth 151 ft.	Grayish laminated, clay on parting parallel to beds.	P
30. 806-S2	do., Depth 149.8 ft.	Same as 806-S2.	—
31. 806-S3	do., Depth 144.7 ft.	Breccia and laminated clay on parting parallel to beds.	P
32. 805-1	N 55.7, E 318.7, Depth 121.6 ft.	Tan to gray laminated clay on bedding plane.	P
33. 810-1	S 87.3, E 707.7, Depth 207.3 ft.	Fat, mottled greenish gray clay on bedding. contact dipping 20°.	P
34. 810-2	do., Depth 213.3 ft.	Laminated brownish gray clay on bedding	—
35. 810-3	do., Depth 251.4 ft.	Clay with rock fragments. Gray to brown. Parallel to bedding	P
36. 810-4	do., Depth 252.3 ft.	Brownish-gray, lamianted clay, contorted. On bedding plane.	P
37. 810-5	do., Depth 124.3 ft.	Brownish-gray laminated clay on bedding.	—

H Grain-size
 M Mineralogy
 P Pollen
 R Radiocarbon
 F Fluid Inclusion

*Testing performed and reported in 1978 Cooling Tower Fault Study.

3.0 STRESS DETERMINATIONS BY OVERCORING

3.1 INTRODUCTION

Strain relief measurements were conducted in four vertical boreholes (the RS series) from April through July 1980. These measurements were required to assist in the evaluation of the "thrust" fault structures exposed on the site. This report presents the results of the overcoring program and an interpretation of their significance.

3.2 PURPOSE

Strain relief observations in the RS series of vertical borings were conducted to explore the geometry of the Radwaste Structure, the related stress distribution and the mechanism of deformation.

3.3 SCOPE

Strain relief measurements were conducted by overcoring the U.S. Bureau of Mines (USBM) deformation gauge in vertical borings extending to 120 feet below the surface. The combination of the method used and the orientation of the borings permitted determination of maximum and minimum normal stresses in the plane of bedding. (The method does not allow determination of whether or not these values represent the principal stresses.) All four borings were sited within the fault block bounded by the Drainage Ditch Fault and the Cooling Tower Fault. Between 20 and 32 successful stress determinations were achieved in each boring. Testing was commenced near the base of the

Oswego Sandstone. Two borings were terminated in Unit B of the Pulaski Formation and two borings in Unit C.

3.4 PROCEDURE

Both field and analytical procedures were identical* to those previously employed at the site (Niagara Mohawk Power Corporation, 1978). The essence of the method adopted is as follows:

1. Drill an Ex boring (1.5 inches diameter) in the base of the 6 inch boring.
2. Scribe inside of Ex boring with oriented scriber.
3. Orient and insert USBM deformation gauge in Ex boring.
4. Overcore the gauge with 6 inch O.D. bit and monitor deformation of Ex boring while overcoring.
5. Retrieve oriented overcore, load in a biaxial pressure cell, observe changes of diameter of Ex boring and compute elastic modulus.
6. Calculate stresses assuming plane stress theory applicable to deformation of a circular hole in an infinite plate.

*The only exception to this statement concerns the range of the unloading curve obtained during biaxial pressure testing of overcores, for which pressure/displacement relations were used to calculate Young's modulus. For the RS series of determinations a range corresponding in each case to the observed deformation in the field in each individual test was selected. During previous testing in the OC series of borings (NMPC, 1978), an upper limit of 2000 psi was selected as standard. For this reason, and because the results obtained in Boring OC-4 are re-interpreted in the light of the Radwaste Structure, the results previously obtained in this boring are presented again in this report incorporating the recalculated values of stress.

Test results were classified according to the character and quality of the observed deformation curves obtained in situ and the quality of the biaxial load/deformation curves.

3.5 RESULTS

Plate 3-1 shows the location of the RS borings. Borings RS-1, RS-2, and RS-3 were located along a line subparallel to the Cooling Tower Fault. These borings were located in the southern section of the fault block, 500 to 700 feet north of the Cooling Tower Fault. Boring RS-4 was located less than 300 feet east of the reactor excavation. Apart from near-surface measurements in Boring OC-9, strain relief within the fault block was previously measured in Boring OC-4. Plates 3-2 through 3-6 show the information obtained from Borings RS-1 through RS-4, and Boring OC-4, as follows:

1. Lithology
2. Stratigraphy
3. Bedding plane fractures
4. Maximum and minimum normal displacement observed during overcoring (P and Q, microinches)
5. Orientation of the axis of maximum displacement (P)
6. Displacement difference (P-Q, microinches)
7. Modulus of elasticity determined by biaxial loading of the overcore (psi)
8. Maximum and minimum stress (psi)
9. Stress difference

Results of stress determinations are tabulated in Tables 3-1 through 3-5. Biaxial tests for the RS-series of stress determinations are summarized in Tables 3-6 through 3-9, and in Table 3-10 for tests from Boring OC-4. Boring logs, calibration records, and strain relief curves are presented in Appendix E.

Results of stress determinations from Boring RS-1 are characterized by:

- a) stresses ranging between approximately zero and 1000 psi;
- b) a generally consistent E-W orientation of maximum normal stress;
- c) essentially constant stress difference of about 200-300 psi.

Results from Boring RS-2 are characterized by:

- a) stresses ranging from about -100 psi to 1000 psi (highly variable over a short vertical distance);
- b) an approximately consistent N50E to N60E oriented maximum normal stress;
- c) a zone of maximum normal stresses which are relatively low (even zero) in the Oswego Sandstone;
- d) an approximately consistent stress difference of 100 to 200 psi in the upper section, with a progressive increase from the middle of Unit A of the Pulaski Formation downwards to a magnitude of approximately 500 psi.

Results from Boring RS-3 are characterized by:

- a) stresses varying generally from -200 psi to 800 psi, the higher values occurring only below the Oswego Sandstone;
- b) fairly variable orientation of maximum normal stress, but with a recurring orientation of about N60°E throughout the boring;
- c) stress difference of about 200 psi, increasing steadily with depth below the Oswego Sandstone Formation to about 600 psi (locally higher).

Results from Boring RS-4 are characterized by:

- a) maximum normal stresses of about zero or slightly less to 400 psi in the Oswego Sandstone Formation and the upper part of Unit A, being more variable at greater depth where the results range from approximately zero to greater than 1000 psi. Almost one-third of the determinations of minimum normal stress ranged from -150 psi to -300 psi;
- b) apart from measurements above the Transition Zone, the orientation of maximum normal stress is remarkably constant, oriented N60°E-N70°E throughout the penetrated section;
- c) stress difference appears to increase with depth throughout much of the borehole, ranging from about 50 psi near-surface to about 600 psi at greater depth.

3.6 DISCUSSION

To interpret the results of stress determinations, it is important to note the location of the RS-series boreholes (Plates 3-1) considering:

- ° location with respect to the sites of previous stress determinations (the OC-series boreholes);
- ° location with respect to geological structures;
- ° location with respect to the bedrock valley.

Plates 1-1 and 3-1 show that the RS-series of stress determinations were conducted in a bedrock block bounded by the Cooling Tower Fault and Drainage Ditch Fault, situated east of the north-trending bedrock depression. Plate 3-1 also shows the location of a northeast striking synclinal axis in the vicinity of Boring RS-1 (New York State Electric and Gas, 1979). The syncline has been proposed on the basis of subsurface data; however, the precise location of the axis with respect to Boring RS-1 is uncertain.

As shown on Plate 3-1, only two of the OC-series borings (OC-4 and OC-9) were drilled within the block. Borings OC-5, -7 (horizontal), and -8 (vertical), were drilled from the base of the cooling water intake shaft approximately 100 feet below ground surface. All these measurements were made near the bedrock valley, in the vicinity of the exposures of the "thrust" fault structures (Plate 1-1). Borings OC-1, -2 and -3 were drilled at locations outside the fault block.

Based on the results of geological studies at the site, it is clear that the fault block within which the RS-series of measurements were conducted, has experienced extensional relief in two directions. These directions are parallel and perpendicular to the strike of the bounding faults. The degree of extensional relief resulting from displacement on these structures diminishes to zero with depth in both directions. The relief is negligible at a depth of approximately 200 feet for the Cooling Tower Fault buckling, and at a depth of approximately 100 feet for the "thrust" fault structures.

The degree of strain relief diminishes progressively with distance from the front of the structure; that is, parallel to the slip vector or extension direction. This non-homogenous deformation should express itself in terms of gradients of remanant strain energy both perpendicular and parallel to the faults. The identification of these gradients was the principal objective of this program, in the context of defining the extent of the "thrust" fault structures.

Horizontal translation resulting from buckling on the Cooling Tower Fault, as well as "thrust" fault related translations, were heterogeneous in terms of magnitude and direction. This non-homogenous translation can, as in the case of other geological structures, result in changes of distortional strain patterns in addition to extensional strains. The differences in slip vectors will be reflected in different

quantities of shear stresses acting in vertical planes oriented parallel and normal to the boundary faults. In terms of stress determination, these shear stresses would be manifested as a systematic change in orientation of normal stresses acting in a horizontal plane (Plate 3-9).

The deformation resulting from the heterogeneous relief, therefore, can be expected to be expressed by changes in both orientation and magnitude of stresses relative to the pre-deformation state of stress. Accordingly, the first step in the interpretation of results should be the definition of the pre-deformation stress conditions. By defining the departures from these conditions at each test location, estimates can be made of the boundaries of the relieved block (the extent of the "thrust" fault structures), as well as the stress states pertaining to these boundaries.

The magnitude and orientation of the pre-deformation stress within the block can be obtained on the basis of information from Borings OC-8, -5, -7, and RS-4. The results from these borings can be taken to represent the state of stress throughout the entire 200 feet penetrated. That is, throughout the zone within which the degree of extension diminishes progressively. At a depth of about 200 feet the influences of the "thrust" sheet and the buckling across the Cooling Tower Fault should be minimal. It is apparent that these results show depth dependent changes in the orientation and magnitude of normal

stresses in the horizontal plane. The magnitude of the maximum normal stress increases from a very low value, near the bedrock surface, to as much as 2500-3000 psi, at a depth of approximately 200 feet. The value of the maximum normal stress is approximately 1100 psi at 100 feet. It is interesting to note, that the change in the stress magnitudes is accompanied with a change in the stress orientation, to a certain degree. In the upper portion of the explored section the maximum normal stress is oriented about northeast. At a depth of approximately 100 feet, where the stress magnitude attains a value of 1100 psi, the orientation of the maximum normal stress shifts to east-west, and remains relatively constant despite the increase in magnitude below this depth. From these observations the following values of the pre-deformational stress within the block are evident:

- ° the orientation of the maximum stress was east-west, and,
- ° the magnitude of the maximum stress was approximately 2500 to 3000 psi.

Furthermore, the data indicate the development of the "thrust" structure exposed in the radwaste trench manifests itself as a change in stress values in the hanging wall block, relative to the footwall block. The orientation of the maximum stress in the hanging wall block is northeast and the magnitude is low, whereas in the footwall block the orientation is east-west and the magnitude is 1200 to 1300 psi. Therefore, the maximum

stress reduction (stress drop) attributable to the development of the "thrust" structure is 1200 to 1300 psi.

Comparison of the strain relief data from Borings RS-1, -2, -3, and OC-4 (Plates 3-2 through 3-6) with the postulated pre-deformational state of stress reveals notable differences. Only at the bases of Borings OC-4 and RS-1, is the maximum normal stress oriented east-west. Elsewhere, departure from this orientation is apparent and is accompanied with a reduction in the stress magnitude. The changes in stress magnitude indicate definite stress gradients parallel and normal to the Cooling Tower Fault. The development of these gradients is readily attributable to the lateral relief of the bedrock along both directions.

Comparison of the stress states determined in the OC-series borings and the RS-series borings can be used to evaluate the southern and western boundaries of the relieved block ("thrust" sheet). Comparison of stresses parallel to the Cooling Tower Fault in Borings OC-2 and RS-1 clearly indicate that this fault represents the southern boundary of the block. Comparison of stresses (differences of magnitude and orientation) in Borings OC-3 and RS-3 indicates that the bedrock depression through the site represents the western boundary of the block (Plates 1-1 and 3-1).

The results of strain relief measurements do not permit identification of the northern boundary. This boundary can be expected to offer very low frictional resistance which could result either from low normal stress or low overall shear strength. This supposition is in agreement with the rotation of stresses observed in Borings OC-4 and RS-4. There are two reasonable possibilities satisfying these requirements, that is the Drainage Ditch Fault or the free boundary where the strata outcrop in Lake Ontario.

Definition of the base, as well as the eastern boundary of the relieved block, remains to complete the evaluation of the boundary conditions. There are two interpretations.

Data obtained from the subsurface exploration of the extent of the Radwaste Structure were used to prepare the geological cross section shown on Plate 2.2-2. From this cross section it can be inferred that the down dip continuation of the "thrust" fault in the radwaste trench occurs in the immediate vicinity of the illite rich layer in Unit A of the Pulaski Formation. This layer has been identified in Borings RS-4 and OC-4 at a depth of approximately 70 feet. In these borings (Plates 3-5 and 3-6) the occurrence of the layer corresponds to a significant change in the magnitude of the displacements recorded during overcoring, being low in the upper section relative to the lower section. However, the orientation of the maximum horizontal stress is different in these two borings.

In RS-4, this orientation is relatively constant throughout the tested section, averaging approximately N70E. In Boring OC-4 it changes from N60E-N70E to approximately east-west across the illite layer. Although the slip surface developed along this layer is present in both borings, the zone of deeper thrust relief (for example, the deformation at the base of Unit B shown on Plate 2.2-2) is present in Boring RS-4 but not in Boring OC-4 and thus may account for the observed differences. This suggests that the lower boundary of the relieved block may dip to the west between Borings OC-4 and RS-4. However, the base of the "thrust" structure exposed in the radwaste trench is horizontal, at least in this section of the fault block. Considering the differences in the magnitude and orientation of the stresses above and below the illite zone in Boring OC-4, it can be concluded that the eastern boundary of the "thrust" sheet is located east of this boring.

Further information pertaining to both the depth of development of the "thrust" sheet as well as the eastern boundary can be obtained considering the strain relief measurements in Borings RS-1, -2, and -3. Comparing the results from Borings OC-4 and RS-1 some similarities are evident. Apart from notable differences in the magnitude of horizontal stress which represents a stress gradient normal to the Cooling Tower Fault, the similarities are:

- ° comparable reduction in the magnitude of maximum normal stress of the sections in the borehole above and below the illite layer; and,

° recognizable changes in the orientation of the maximum stress across the illite layer.

The sense of rotation of the maximum stress in Borehole RS-1 across the illite layer is counterclockwise. This is opposite to the sense of rotation observed in Boring OC-4. This must indicate that the sense of shear stress acting in vertical planes which are parallel to the Cooling Tower Fault (Plate 3-9) and located above the illite layer is opposite in each of the borings. An explanation of this is apparent considering the location of Boring RS-1 with respect to the axis of the syncline (Plate 3-1). In order for this explanation to be plausible, the axis of the syncline (and accompanying reversal of sense of shear stress in horizontal planes) must be located west of Boring RS-1 and not to the east as shown on Plate 3-1 (plotted location from: New York State Electric and Gas, 1979). If this is true these borings are located on opposing limbs of the syncline. This situation would result in a tendency toward a westward translation of the upper parts of the section in Boring OC-4 and eastward translation of the corresponding section in Boring RS-1. This would result in an opposite sense of rotation of the maximum stress in the two boreholes above the illite layer. This interpretation requires that the magnitude of displacements related to the "thrust" sheets diminish southward. Accordingly, the lower boundary of the "thrust" sheet in Borings OC-4 and RS-1 correspond to the slip surface localized along the illite-rich layer. Also, the eastern boundary of the "thrust" sheet exposed in the excavations

must be situated between Borings OC-4 and RS-1, most likely along the axis of the syncline. Following this interpretation further, it is necessary to place the base of the thrust structure exposed in the radwaste trench along the illite layer, in Borings RS-2 and RS-3. This layer was encountered at depths of 76 and 64 feet, respectively.

Data from all three borings in the south of the fault block show departures from the postulated pre-deformation east-west orientation of the maximum stress. The departure is counter-clockwise in Boring RS-2 and RS-3, but clockwise in Boring RS-1. Furthermore, the maximum normal stresses below the illite layer in Borings RS-1 and -2 increase from west to east, and reflect a reversal in the stress gradient observed above the layer and between Borings RS-4 and OC-4. This reversal may reflect the effect of strain redistribution related to buckling on the Cooling Tower Fault. In this case, Boring RS-1 would be located east of the centerline of this buckling (line of maximum fault-normal slip) whereas Borings RS-3 and -2 would be located west of this line. This difference of location with respect to the centerline of the buckle would result in differences of sense of shear stress acting in vertical planes, parallel and normal to the fault. Hence, this could account for the different senses of rotation of the maximum horizontal stress observed at various test locations. The larger magnitude of the maximum stress in Boring RS-2 than in Boring RS-1 could be accounted for assuming that Boring RS-2 is located near the

western termination of the Cooling Tower Fault buckle where distortion is dominant.

In summary, the presented observations and analysis imply the following:

- ° the distribution of strain relief in plan was characterized by translations parallel to the fault and along bedding planes which occurred on either side and away from a synclinal axis located between Borings RS-1 and OC-4. The magnitudes of fault-parallel dislocations are maximum near the Drainage Ditch Fault and decrease in magnitude southward within the fault block. The magnitude of bedding plane translations normal to the Cooling Tower Fault and related to buckling diminishes away from the centerline of buckling toward the extremities of the fault.
- ° The distribution of strain relief in a vertical plane parallel to the bounding faults can be characterized as a zone in which layer parallel differential extensional relief occurred. This zone is contained between two planes; one is nearly vertical and is located near the bedrock depression on the site; the other plane can be envisaged as a curved surface dipping westward. This latter surface intersects the relatively shallow illite layer encountered in Boring OC-4 and extends beneath the main site

excavations. It is the base of the "thrust" sheet. The degree of strain relief of individual strata or groups of strata, comprising the "thrust" sheet diminishes eastward and with depth.

A second alternative to the interpretation of the present strain distribution that is consistent with the known facts is possible. This alternative interpretation also concludes that the illite layer represents the base of the Radwaste Structure but only in the northern portions of the fault block. The eastern boundary of the structure is situated east of Boring OC-4 in this case as well. In contrast to the first interpretation, this alternative explains the northeasterly re-orientation of the maximum stress in the upper portions of Boring OC-4 (above the illite layer) by a uniform layer-parallel strain relief parallel to the boundary faults. This relief has been superimposed upon the pre-deformational east-west oriented maximum stress. The eastern boundary is assumed to be the synclinal axis positioned east of Boring RS-1 as shown on Plate 3-1. The presence of a second "thrust" sheet to the east of the synclinal axis, with accompanying easterly translation, is not required.

The re-orientation of maximum stress observed in Borings RS-1, RS-2, and RS-3 are attributed primarily to buckling on the Cooling Tower Fault. The centerline of buckling (line of maximum southerly translation) is positioned just east of

Boring RS-2. Rather than a uniform southerly translation of beds in the central portions of the Cooling Tower Fault, with distortional strain development restricted to sections near the ends of the fault, a generally curved pattern defined by these southerly displacements is envisaged. This would lead to uniformly distributed distortional strains derived by progressively changing magnitudes of southerly displacement along the length of the buckle.

This alternative also incorporates an increase in the depth of the base of the Radwaste Structure, from the north to the south within the fault block, in response to the greater pre-existing strain relief in proximity to the Cooling Tower Fault Buckle. This buckle-related strain relief included modification of shear stresses in the plane of bedding and re-orientation of the maximum stress such that fault-parallel translation required for Radwaste Structure formation was not a suitable mode of subsequent deformation in the upper sections of Boreholes RS-1, RS-2, and RS-3. According to this interpretation, none of the three boreholes located in the south of the fault block has penetrated to the base of the Radwaste Structure.

In the cross section presenting results from Boreholes RS-4 and OC-4 (Plate 3-7), the Radwaste Structure appears to be composed of two layers: an upper layer largely confined to the Oswego Sandstone which shows a clear gradient of layer-parallel N70W oriented strain; and second, a deeper layer showing

extraordinarily low N70W trending stresses (a very low gradient). A similar double-layer distribution is apparent in the cross section containing Borings RS-1, RS-2, and RS-3 (Plate 3-8), but in this case the upper relatively high gradient layer extends much deeper and is inclined toward the east. In Boring RS-3 the base of this layer extends to elevation 200 feet. At Boring RS-1 this layer extends to elevation 160-170 feet, and coincides with the marked change in orientation of maximum horizontal stress noted earlier in this discussion.

Below this level in the south of the fault block, a relative increase of the degree of bedding plane fracturing can be observed in Borings RS-1 and RS-2. This zone is interpreted to represent a predominance of the radwaste mode of deformation. The relatively minor change of orientation from a pre-deformational east-west to N80E trend observed in Boring RS-1, is attributed to the superimposition of fault-parallel normal strain relief by Radwaste Structure development, upon the N80W orientation developed predominantly by buckling. This interpretation envisages a passive extension of overlying beds, strongly influenced by buckling on the Cooling Tower Fault, with an underlying zone having fault-parallel strain-relief components less influenced by buckling at the greater depths where the Radwaste Structure developed. This interpretation does not require the development of large fault-parallel shear strains on vertical planes as the hanging wall of the "thrust" structure was uniformly displaced westwards. This displacement was

relatively uniform in plan, but occurred at deeper levels in proximity to the Cooling Tower Fault. In contrast to the observations in Borings RS-2 and RS-1, no increase of the frequency of bedding fracturing in the deep zone of Boring RS-3 is observed. However, the strain relief measurements reflect antiformal bending associated with a N70W strain superimposed on a strain state in which the maximum stress is oriented N60E. This is interpreted to represent a fault-parallel translation and buckling of strata against asperities on an inclined basal plane similar to that observed in the radwaste trench. Thus, the base of the structure is interpreted to lie very close to the base of Boring RS-2, progressively deepening at a gentle angle in an eastward direction.

In view of the changing sense of shear stress associated with the axis of the syncline, it is assumed that the eastern boundary of the Radwaste Structure coincides with the axis of the syncline, positioned as shown on Plate 3-1.

In terms of the overall evaluation of the Radwaste Structure, it is the common aspects of the preceding alternatives which are most relevant. Both interpretations include the presence of a synclinal axis, representing the eastern boundary of the Radwaste Structure. This implies that stresses acting at the eastern boundary of the structure do not include layer-parallel shear stress because the axial plane of the syncline represents a plane across which a reversal of the sense of bedding-parallel

shear stress occurs. The magnitude of normal stress at the eastern boundary of the structure is inferred to range from 700 to 1100 psi.

3.7 CONCLUSIONS

The existence of stress gradients, normal and parallel to the Cooling Tower Fault, demonstrates that deformation involving internal extensional relief has occurred in both these directions within the fault block. That is, deformation has not occurred as rigid body translation. Abundant geological evidence has revealed planes of slip parallel to the bedding, thus indicating shear strain in the plane of bedding. In plan view, the observed strain pattern must have resulted principally from two factors: buckling in the vicinity of the Cooling Tower Fault with predominantly fault-normal layer-parallel translation; and predominantly fault-parallel translation associated with "thrusting" to the west.

The Cooling Tower Fault represents the southern boundary of the "thrust" sheet. The northern boundary is inferred to be either the Drainage Ditch Fault or the outcrop of the strata in the lake. In any case, the fault-normal stresses are relatively low, such that frictional restraint is very limited. The western boundary of the "thrust" sheet coincides with the bedrock depression where near-zero normal stresses pertain. The base of the Radwaste "thrust" Structure lies approximately coincident with the illite layer in Unit A of the Pulaski

Formation at least in the northern portion of the fault block. Two alternative interpretations have been advanced to account for the depth of the base of the structure in the southern portion of the fault block. One interpretation requires that the base of the structure be confined to the illite layer. The other interpretation is that base of the structure is considerably deeper because of the influences of buckling on the Cooling Tower Fault. Regardless of the interpretation, the eastern boundary of the structure is assumed to be coincident with the axial plane of a syncline, inferred to be positioned in the vicinity of Boring RS-1. This boundary is free of bedding parallel shear stress.



TABLE 3-1
SUMMARY OF OVERCORE TESTS
BORING RS-1¹

TEST NO.	DEPTH (Ft)	ROCK TYPE	MAXIMUM DISPLACEMENT (1/4 In.)	MINIMUM DISPLACEMENT (1/4 In.)	MODULUS $\times 10^6$ PSI	MAXIMUM NORMAL STRESS (PSI)	MINIMUM NORMAL STRESS (PSI)	ORIENTATION MAXIMUM NORMAL STRESS
1	41'2 1/2"	Siliceous Sandstone	384	- 17	2.8	265	77	N79W
2	43'10"	Siliceous Sandstone	441	144	3.5	427	253	N81E
3	46'5"	Siliceous Sandstone to Argillaceous Sandstone	1385	1100	2.6 (?)	1135 (?)	1012 (?)	N88E
4	47'9"	Siliceous Sandstone with Occasional Shale Interbed	338	-152	5.3 (?)	381 (?)	-52 (?)	N84E
8	53'9"	Siliceous Sandstone	428	- 64	5.7	581	112	N84W
9	55'	Siliceous Sandstone with Occasional Shale Clasts	374	70	4.5	448	218	N75W
12	58'3"	Siliceous Sandstone to Slightly Argillaceous Sandstone	333	-185	5.4	368	-101	N73W
14	61'	Graywacke	366	110	3.8	383	221	N72W
15 ⁽²⁾	63'4"	Siliceous Sandstone with Shale Interbeds	317 (?)	- 50 (?)	3.8 (?)	286 (?)	52 (?)	N82W (?)
16 ⁽³⁾	64'8 1/2"	Argillaceous Sandstone with Shale Interlamination	1266 (?)	719 (?)	3.8 (?)	1430 (?)	1083 (?)	N82W (?)
17	66'1"	Argillaceous Sandstone with Siliceous Sandstone Interbeds	326	46	8.0	683	308	N81W
18 ⁽⁴⁾	68'4"	Interbedded Argillaceous Sandstone and Siliceous Sandstone	597 (?)	194 (?)	5.3	876 (?)	519 (?)	N83W (?)
20	71'	Argillaceous Sandstone	603	282	6.0	1046	723	N67W
22	73'1 1/2"	Siliceous Sandstone Grading to Argillaceous Sandstone	648	436	5.3	1052	864	N71W

TABLE 3-1
SUMMARY OF OVERCORE TESTS
BORING RS-1¹

TEST NO.	DEPTH (Ft)	ROCK TYPE	MAXIMUM DISPLACEMENT (1/4 In.)	MINIMUM DISPLACEMENT (1/4 In.)	MODULUS $\times 10^6$ PSI	MAXIMUM NORMAL STRESS (PSI)	MINIMUM NORMAL STRESS (PSI)	ORIENTATION MAXIMUM NORMAL STRESS
24	74'9 1/2"	Argillaceous Sandstone	318	- 13	6.0	471	139	N70W
25	76'1"	Argillaceous Sandstone	303	142	7.2 (?)	630 (?)	436 (?)	N50E
26	78'4"	Siliceous Sandstone	378	0	4.8	454	151	N67W
27	81'8"	Argillaceous Sandstone	562	241	3.5	563	374	N71W
28 ⁽⁵⁾	83'10"	Argillaceous Sandstone	851 (?)	486 (?)	3.9 (?)	987 (?)	749 (?)	N70W (?)
29	87'1/2"	Interbedded Siliceous Sandstone and Argillaceous Sandstone	402	56	6.2 (?)	653 (?)	294 (?)	N86W
30	88'2"	Argillaceous Sandstone	796	441	4.3	1015	760	N56W
34	92'9"	Argillaceous Sandstone	563	182	4.9	764	452	N82W
35 ⁽⁶⁾	96'10"	Siliceous Sandstone to Argillaceous Sandstone	540 (?)	242 (?)	4.2	652 (?)	443 (?)	N75W (?)
36	98'2"	Siliceous Sandstone Grading to Argillaceous Sandstone	584	266	5.2	875	598	N89W
38	100'9"	Argillaceous Sandstone	537	162	4.5	666	383	N88E
40 ⁽⁷⁾	103'3"	Argillaceous Sandstone Grading to Siliceous Sandstone	511 (?)	137 (?)	4.9	682 (?)	375 (?)	N80E (?)
44 ⁽⁸⁾	120'6"	Siliceous Sandstone	553 (?)	-123 (?)	7.1	911 (?)	107 (?)	N80E (?)
48 ⁽⁹⁾	123'11"	Argillaceous Sandstone and Shale Interbedded	391 (?)	-155 (?)	3.8 (?)	323 (?)	- 24 (?)	N81E (?)

TABLE 3-1
SUMMARY OF OVERCORE TESTS
BORING RS-1¹

TEST NO.	DEPTH (Ft)	ROCK TYPE	MAXIMUM	MINIMUM	MODULUS x10 ⁶ PSI	MAXIMUM	MINIMUM	ORIENTATION MAXIMUM NORMAL STRESS
			DISPLACEMENT (μ In.)	DISPLACEMENT (μ In.)		NORMAL STRESS (PSI)	NORMAL STRESS (PSI)	

- NOTES:
- 1) Data calculated assuming plane-stress and isotropy in the plane of bedding.
 - 2) Axis I uncertain, Axis II drift
 - 3) Drift on Axis III
 - 4) Axes I, II, and III slightly unstable
 - 5) Axes I, II and III failed to stabilize at the end of overcoring test.
 - 6) Axes I, II and III failed to stabilize at the end of overcoring test
 - 7) Axes II and III failed to stabilize at the end of overcoring test
 - 8) Axis I uncertain
 - 9) Axes I, II and III uncertain

TABLE 3- 2
SUMMARY OF OVERCORE TESTS
BORING RS-2¹

TEST NO.	DEPTH (Ft)	ROCK TYPE	MAXIMUM DISPLACEMENT (in.)	MINIMUM DISPLACEMENT (in.)	MODULUS $\times 10^6$ PSI	MAXIMUM NORMAL STRESS (PSI)	MINIMUM NORMAL STRESS (PSI)	ORIENTATION MAXIMUM NORMAL STRESS
2	22'8"	Siliceous Sandstone	200	- 16	4.5	220	57	N05W
3	25'8 1/2"	Siliceous Sandstone	20	- 99	3.7	- 12	- 85	N45E
4	29'7"	Siliceous Sandstone	-14	- 76	2.4	- 24	- 48	N15E
5	30'10"	Siliceous Sandstone	327	-335	4.5	243	-256	N20E
6	32'11"	Siliceous Sandstone	70	-163	1.9	8	- 67	N57E
7	35'2"	Siliceous Sandstone	197	-112	1.6	64	- 19	N51E
8	38'8"	Argillaceous Sandstone with Shale Laminations Grading to Medium to Light Gray Sandstone	629	390	3.6 (?)	684 (?)	540 (?)	N49E
9 ⁽²⁾	41'1"	Sandstone with Shale Interbeds	177 (?)	-219 (?)	2.6 (?)	68 (?)	-104 (?)	N49E (?)
10	43'8"	Graywacke Grading to Siliceous Sandstone	131	-101	7.3	179	-104	N42E
14	47'4"	Siliceous Sandstone with Argillaceous Sandstone Interbeds	232	-150	3.1 (?)	142 (?)	- 57 (?)	N71E
15	49'1/2"	Siliceous Sandstone	39	- 72	7.9	30	-117	N10W
17	51'6"	Silty Shale to Siltstone Grading to Argillaceous Sandstone	323	- 54	3.6 (?)	275 (?)	48 (?)	N56E
18	53'	Graywacke	565	475	2.2 (?)	398 (?)	365 (?)	N82E
19	55'2"	Argillaceous Sandstone	163	- 11	3.8 (?)	152 (?)	41 (?)	N49E

TABLE 3-2
SUMMARY OF OVERCORE TESTS
BORING RS-2¹

TEST NO.	DEPTH (Ft)	ROCK TYPE	MAXIMUM DISPLACEMENT (In.)	MINIMUM DISPLACEMENT (In.)	MODULUS x10 ⁶ PSI	MAXIMUM NORMAL STRESS (PSI)	MINIMUM NORMAL STRESS (PSI)	ORIENTATION MAXIMUM NORMAL STRESS
20	56'9"	Siliceous Sandstone with Argillaceous Sandstone Interbeds	70	- 98	2.9 (?)	27 (?)	- 54 (?)	N36E
21 ⁽³⁾	58'	Siliceous Sandstone with Argillaceous Sandstone Interbeds with Shale Laminations	542 (?)	394 (?)	2.9 (?)	488 (?)	416 (?)	N29E (?)
23	60'1 1/2"	Siliceous Sandstone with Argillaceous Sandstone Interbeds	7	-142	4.3	- 43	-151	N46E
24	61'10"	Argillaceous Sandstone	302	206	4.2	389	322	N11W
25	63'2"	Argillaceous Sandstone	552	442	3.7	647	574	N21E
27	65'7"	Argillaceous Sandstone Grading to Siliceous Sandstone	703	603	3.6	814	754	N41E
28	66'10"	Argillaceous Sandstone Grading to Siliceous Sandstone	180	76	4.0	205	136	N50E
30	69'5"	Siliceous Sandstone Grading to Argillaceous Sandstone	477	257	4.8	676	499	N66E
31	71'8"	Siliceous Sandstone	199	-128	4.4	173	- 69	N59E
32	73'1"	Argillaceous Sandstone	459	319	4.2 (?)	594 (?)	497 (?)	N80E
33	74'5"	Siliceous Sandstone, Occasional Shale Clasts	150	- 91	3.8	114	- 40	N68E
34 ⁽⁴⁾	76'2"	Argillaceous Sandstone with Occasional Siliceous Sandstone Interbeds	413 (?)	16 (?)	3.9 (?)	408 (?)	149 (?)	E-W (?)
36 ⁽⁵⁾	79'6"	Argillaceous Sandstone Grading to Siliceous Sandstone with Shale Laminations	687 (?)	319 (?)	6.2 (?)	1231 (?)	850 (?)	N37E (?)

TABLE 3 - 2
SUMMARY OF OVERCORE TESTS
BORING RS-2¹

TEST NO.	DEPTH (Ft)	ROCK TYPE	MAXIMUM DISPLACEMENT (1/4 In.)	MINIMUM DISPLACEMENT (1/4 In.)	MODULUS $\times 10^6$ PSI	MAXIMUM NORMAL STRESS (PSI)	MINIMUM NORMAL STRESS (PSI)	ORIENTATION MAXIMUM NORMAL STRESS
38	82'1"	Siliceous Sandstone Grading to Argillaceous Sandstone	368	-149	6.8 (?)	543 (?)	- 46 (?)	N55E
40	84'7 1/2"	Argillaceous Sandstone	1025	487	3.4	1010	704	N52E
42 ⁽⁶⁾	87'5"	Siliceous Sandstone	750 (?)	-301 (?)	4.9 (?)	797 (?)	- 65 (?)	N51E (?)
44	90'4"	Argillaceous Sandstone	964	293	4.2 (?)	1117(?)	645 (?)	N41E
45	91'8"	Argillaceous Sandstone Grading to Siliceous Sandstone	538	-130	5.3 (?)	658 (?)	65 (?)	N51E

- NOTES: 1) Data calculated assuming isotropic plane stress analysis
 2) Axes I, II and III unstable
 3) Axes I, II and III uncertain because core fractured after 12.5 inches of overcoring
 4) Axis II uncertain
 5) Core broke at 12.5 inches during overcore test
 6) Axis I failed to stabilize at end of overcore test

TABLE 3-3
SUMMARY OF OVERCORE TESTS
BORING RS-3¹

TEST NO.	DEPTH (Ft)	ROCK TYPE	MAXIMUM DISPLACEMENT (1/4 In.)	MINIMUM DISPLACEMENT (1/4 In.)	MODULUS x10 ⁶ PSI	MAXIMUM NORMAL STRESS (PSI)	MINIMUM NORMAL STRESS (PSI)	ORIENTATION
								MAXIMUM NORMAL STRESS
1	6'8"	Argillaceous Sandstone	- 38	-312	4.8	-170	-390	N23E
2	7'11"	Siliceous Sandstone Grading Slightly Argillaceous	-135	-325	2.6	-158	-240	N64E
4	13'2"	Siliceous Sandstone	48	-170	3.4	- 7	-131	N45E
5	16'2"	Siliceous Sandstone	392	-168	2.6	219	- 25	N74E
7	18'4 1/2"	Siliceous Sandstone with Occasional Argillaceous Sandstone Interbeds	292	-116	2.9 (?)	184 (?)	- 14 (?)	N69E
10	25'8 1/2"	Argillaceous Sandstone with Occasional Siltstone Interbeds	986	424	1.9 (?)	536 (?)	357 (?)	N53E
11 ⁽²⁾	27'9"	Siliceous Sandstone with Interbeds of Argillaceous Sandstone and Shaley Siltstone	- 89 (?)	-265 (?)	2.9 (?)	-128 (?)	-214 (?)	N40E (?)
14	32'10 1/2"	Siliceous Sandstone Grading to Argillaceous Sandstone	198	- 8	3.7 (?)	181 (?)	54 (?)	N40W
16	35'11 1/2"	Slightly Argillaceous Sandstone to Argillaceous Sandstone	107	-166	2.9	38	- 95	N58E
19	39'7"	Argillaceous Sandstone	335	121	3.3 (?)	310 (?)	192 (?)	N40E
24	48'5"	Argillaceous Sandstone	957	535	2.9 (?)	824 (?)	619 (?)	N69W
28	54'4"	Argillaceous Sandstone with Occasional Siliceous Sandstone, Shale Interbeds	579	76	3.4 (?)	515 (?)	228 (?)	N60E
35	67'2"	Argillaceous Sandstone with Siliceous Sandstone Interbeds	783	-257	3.6 (?)	628 (?)	2 (?)	N20E

TABLE 3-3
SUMMARY OF OVERCORE TESTS
BORING RS-3¹

TEST NO.	DEPTH (Ft)	ROCK TYPE	MAXIMUM DISPLACEMENT (In.)	MINIMUM DISPLACEMENT (In.)	MODULUS $\times 10^6$ PSI	MAXIMUM NORMAL STRESS (PSI)	MINIMUM NORMAL STRESS (PSI)	ORIENTATION
								MAXIMUM NORMAL STRESS
36 ⁽³⁾	68'5 1/2"	Argillaceous Sandstone	1073 (?)	-373 (?)	3.4 (?)	809 (?)	- 14 (?)	N09E (?)
37	69'7 3/4"	Siliceous Sandstone with Occasional Shale Interbed	793	-438	4.9	796	-214	N34E
38	70'10"	Interbedded Siliceous Sandstone and Argillaceous Sandstone	659	-366	5.3 (?)	713 (?)	-196 (?)	N72E
39	72'1"	Siliceous Sandstone Grading to Argillaceous Sandstone with Shale Laminations	804	-435	4.0 (?)	661 (?)	-169 (?)	N88E
41	74'6"	Siliceous Sandstone with Occasional Interbed of Argillaceous Sandstone	415	-214	4.0	345	- 76	N63E
42	75'10 1/2"	Siliceous Sandstone with Occasional Argillaceous Sandstone Interbeds	286	- 99	6.5	411	- 7	N60E
43	77'1 1/2"	Argillaceous Sandstone with Occasional Siliceous Sandstone Interbeds	735	-178	4.0	676	65	N65E

NOTES: 1) Data calculated assuming isotropic plane stress analysis
 2) Axes I, II and III uncertain
 3) Axis I failed to stabilize at end of overcore test

TABLE 3-4
SUMMARY OF OVERCORE TESTS
BORING RS-4¹

TEST NO.	DEPTH (Ft)	ROCK TYPE	MAXIMUM DISPLACEMENT (In.)	MINIMUM DISPLACEMENT (In.)	MODULUS $\times 10^6$ PSI	MAXIMUM NORMAL STRESS (PSI)	MINIMUM NORMAL STRESS (PSI)	ORIENTATION
								MAXIMUM NORMAL STRESS
3	24'6"	Argillaceous Sandstone Grading to Siliceous Sandstone	292	70	2.5 (?)	197 (?)	104 (?)	N07E
4	27'1 1/2"	Siliceous Sandstone	1	-327	2.5 (?)	- 67 (?)	-205 (?)	N85E
5 ⁽²⁾	28'6"	Siliceous Sandstone	- 48 (?)	-204 (?)	2.3	- 67 (?)	127 (?)	N68E (?)
6	30'11 1/2"	Siliceous Sandstone	138	-210	4.1	70	-169	N15W
7 ⁽³⁾	36'1 1/2"	Silty Shale to Graywacke to Siliceous Sandstone	720 (?)	300 (?)	2.7	554 (?)	364 (?)	N64E (?)
8 ⁽⁴⁾	39'3"	Siliceous Sandstone with Occasional Shale Clasts	249 (?)	108 (?)	4.1 (?)	293 (?)	195 (?)	N70E
11 ⁽⁵⁾	58'8"	Argillaceous Sandstone	344 (?)	- 23 (?)	4.1 (?)	346 (?)	94 (?)	N68E (?)
12	60'7"	Graywacke	- 37	-228	4.1	-115	-247	N51E
13	62'	Argillaceous Sandstone with Occasional Siliceous Sandstone Interbeds	- 15	-280	5.0 (?)	-135 (?)	-357 (?)	N64E
14	63'8"	Argillaceous Sandstone with Occasional Siliceous Sandstone Interbeds and Shaley Laminations	710	132	4.2	793	382	N71E
15 ⁽⁶⁾	65'9 1/2"	Siliceous Sandstone with Shale Clasts Grading to Argillaceous Sandstone	896 (?)	18 (?)	4.2 (?)	948 (?)	331 (?)	N68E (?)
17 ⁽⁷⁾	68'7"	Argillaceous Sandstone with Occasional Siliceous Sandstone Interbeds, Grading to Siltstone	1151 (?)	382 (?)	4.2 (?)	1343 (?)	794 (?)	N68E (?)

TABLE 3-4
SUMMARY OF OVERCORE TESTS
BORING RS-4¹

TEST NO.	DEPTH (Ft)	ROCK TYPE	MAXIMUM DISPLACEMENT (1/4 In.)	MINIMUM DISPLACEMENT (1/4 In.)	MODULUS $\times 10^6$ PSI	MAXIMUM NORMAL STRESS (PSI)	MINIMUM NORMAL STRESS (PSI)	ORIENTATION: MAXIMUM NORMAL STRESS
19	71'3"	Interbedded Argillaceous Sandstone and Siliceous Sandstone with Occasional Shale Laminations	839	734	4.2 (?)	1138 (?)	1064 (?)	N27E
24 ⁽⁸⁾	80'10 1/2"	Siliceous Sandstone	148 (?)	3 (?)	3.8	142 (?)	49 (?)	N12E (?)
25	82'1 1/2"	Argillaceous Sandstone with Occasional Siliceous Sandstone Interbeds and Shale Laminations	1220	429	3.3	1126	689	N87W
27	83'11"	Argillaceous Sandstone with Shale with Interbeds	987	88	3.9	991	405	N77E
28 ⁽⁹⁾	85'3"	Argillaceous Sandstone with Siliceous Sandstone Interbeds	345 (?)	-274 (?)	3.6	229 (?)	-144 (?)	N87 W (?)
33	91'6"	Siliceous Sandstone	676	-664	3.2	366	-353	N70E
49 ⁽¹⁰⁾	115'9 3/4"	Interbedded Argillaceous Sandstone, Siliceous Sandstone and Shale	610 (?)	- 96 (?)	4.3 (?)	623 (?)	114 (?)	N66E (?)
50	116'10 1/2"	Siliceous Sandstone	223	- 60	5.2	273	20	N33E
51	119'9"	Siliceous Sandstone Grading to Argillaceous Sandstone	976	505	4.6	1317	954	N45E

TABLE 3-4
SUMMARY OF OVERCORE TESTS
BORING RS-4¹

TEST NO.	DEPTH (Ft)	ROCK TYPE	MAXIMUM	MINIMUM	MODULUS x10 ⁶ PSI	MAXIMUM	MINIMUM	ORIENTATION
			DISPLACEMENT ($\frac{1}{4}$ In.)	DISPLACEMENT ($\frac{1}{4}$ In.)		NORMAL STRESS (PSI)	NORMAL STRESS (PSI)	MAXIMUM NORMAL STRESS

- NOTES: 1) Data calculated assuming isotropic plane stress analysis
 2) Axes I, II and III uncertain
 3) Axes I, II and III failed to stabilize at the end of overcore test
 4) Axes I, II and III unstable
 5) Axis II uncertain
 6) Axis II uncertain, Axis III failed to stabilize at the end of the overcore test
 7) Axis III failed to stabilize at the end of the overcore test
 8) Axis II failed to stabilize at the end of the overcore test
 9) Axes I and II uncertain
 10) Axis II uncertain

TABLE 3-5
SUMMARY OF OVERCORE TESTS
BORING OG-4^{1,2}

TEST NO.	DEPTH (Ft)	ROCK TYPE	MAXIMUM DISPLACEMENT (In.)	MINIMUM DISPLACEMENT (In.)	MODULUS $\times 10^6$ PSI	MAXIMUM NORMAL STRESS (PSI)	MINIMUM NORMAL STRESS (PSI)	ORIENTATION MAXIMUM NORMAL STRESS
2	16'3 1/2"	Sandstone with Shale Interclasts (different rock type than biaxial test)	1138	467	3.9	1237	875	N68E
3 ⁽³⁾	19'2"	Cross bedded Sandstone with Shale Interclasts along Cross Bedding	232 (?)	-184 (?)	6.1 (?)	260 (?)	-164 (?)	N70E (?)
4	22'2"	Sandstone with Shale Intraclasts at 22'6"	775	-209	4.4	774	50	N74E
7	24'4 1/2"	Sandstone with Shale Interclasts at 24'2"	1006	114	4.6	1114	252	N78E
8 ⁽⁴⁾	28'2 1/2"	Graywacke/Sandstone/Shale (different rock type than biaxial test)	1527 (?)	393 (?)	4.0 (?)	1658 (?)	900 (?)	N72E (?)
12 ⁽⁵⁾	33'2"	Silty Sandstone	285	87	4.6	361	209	N90E
14	38'2"	Sandstone with Shaley Intraclast Layer at 38'5"	768	-382	4.5 (?)	722 (?)	-143 (?)	N73E
15	39'11"	Sandstone with Thin Bed of Graywacke at 39'11" - Numerous Shale Clasts	1131	324	4.5 (?)	1395 (?)	788 (?)	N72E
16 ⁽⁶⁾	42'0"	Subgraywacke	489 (?)	202 (?)	3.7	515 (?)	337 (?)	N22E (?)
17	43'4 1/2"	Fossiliferous Graywacke	318	- 86	3.8 (?)	276 (?)	37 (?)	N88E
18	45'2"	Graywacke/Sandstone/Graywacke Interbeds	527	- 27	3.9 (?)	505 (?)	143 (?)	N67E
19 ⁽⁷⁾	50'4 1/2"	Sandstone/Graywacke-buttons at Contact	528 (?)	-240 (?)	5.9	663 (?)	- 97 (?)	N63E (?)

TABLE 3-5
SUMMARY OF OVERCORE TESTS
BORING OC-4^{1,2}

TEST NO.	DEPTH (Ft)	ROCK TYPE	MAXIMUM DISPLACEMENT (In.)	MINIMUM DISPLACEMENT (In.)	MODULUS $\times 10^6$ PSI	MAXIMUM NORMAL STRESS (PSI)	MINIMUM NORMAL STRESS (PSI)	ORIENTATION MAXIMUM NORMAL STRESS
20	56'3 1/2"	Graywacke	1162	342	3.8	1212	691	N72E
21	59'3"	Siltstone/Sandstone/Graywacke-fracture at Shale/Sandstone Contact (mechanical or natural?)	991	-373	4.3 (?)	922 (?)	- 48 (?)	N52E
22	63'11"	Graywacke/Sandstone (different rock type than biaxial test)	889	-579	4.7 (?)	821 (?)	-334 (?)	N67E
23	69'1 1/2"	Interbedded Graywacke and Sandstone with Large Sandstone Clasts	913	- 60	4.6	1002	280	N78E
24	72'1"	Graywacke/Sandstone/Graywacke - contacts at 71'10" and 72'2"	353	-216	8.2 (?)	572 (?)	-206 (?)	N89W
25	76'1/2"	Graywacke	919	-526	4.8 (?)	1314 (?)	998 (?)	N70W
26	77'2 1/2"	Sandstone	1031	178	4.5	1229	586	N84E
27	81'9"	Sandstone/Graywacke/Sandstone	973	429	3.7	1032	696	N68W
28	86'0"	Sandstone	1131	-179	4.3	1162	214	N88W
31	106'7"	Graywacke with Shale layer at 106'5"	934	- 494	4.6 (?)	1266 (?)	926 (?)	N78W

- NOTES: 1) Modified to incorporate revised modulus calculations (see Table H-10)
 2) Data calculated employing an isotropic plane-stress analysis.
 3) Data termed uncertain because of the possible overload to transducers of Axes I and II
 4) Data termed uncertain because core fractured at 10 inches
 5) Core fractures at 14 1/2 inches. This did not affect data results because the final point to determine the deformation range was considered before the fracture occurred
 6) Data termed uncertain because the core fractured at 12 1/2 inches
 7) Gauge vibration noted at 7 1/2 inches along Axes I and II

TABLE 3-6
SUMMARY OF BIAxIAL TESTS^(1,2)
BORING RS-1

TEST NO.	ROCK TYPE	DEPTH (ft)	E ₁ (x10 ⁶ psi)	E ₂ (x10 ⁶ psi)	E ₃ (x10 ⁶ psi)	E _{AVG} (x10 ⁶ psi)
1 ⁽³⁾	Siliceous Sandstone	41'2 1/2"	2.7	3.2	2.6	2.8
2 ⁽⁴⁾	Siliceous Sandstone	43'2"	3.6	3.4	3.4	3.5
3 ^(5,6)	Siliceous Sandstone to Argillaceous Sandstone	46'5 1/2"	2.8	2.5	2.6	2.6 (?)
4 ^(7,8)	Siliceous Sandstone with occasional Shale interbed	47'9"	5.7	4.8	5.3	5.3 (?)
8	Siliceous Sandstone	53'9"	5.3	5.9	5.8	5.7
9	Siliceous Sandstone, occasional Shale Clasts	55'	4.5	4.6	4.5	4.5
12	Siliceous Sandstone to Slightly Argillaceous Sandstone	58'3"	5.5	5.5	5.2	5.4
14 ⁽⁹⁾	Graywacke	61'2"	3.6	4.1	3.8	3.8
15 ⁽¹⁰⁾	Siliceous Sandstone with Shale interbeds	63'4"				3.8 (?)
16 ⁽¹¹⁾	Argillaceous Sandstone with Shale Interlamination	64'8 1/2"	3.8	3.8	3.8	3.8 (?)
17	Argillaceous Sandstone with Siliceous Sandstone interbeds	66'1"	7.2	8.8	8.3	8.0
18	Interbedded Argillaceous Sandstone and Siliceous Sandstone	68'4"	5.0	5.5	5.4	5.3

TABLE 3-6

SUMMARY OF BIAXIAL TESTS
BORING RS-1

TEST NO.	ROCK TYPE	DEPTH (ft)	E ₁ (x10 ⁶ psi)	E ₂ (x10 ⁶ psi)	E ₃ (x10 ⁶ psi)	E _{AVG} (x10 ⁶ psi)
20	Argillaceous Sandstone	71'	6.3	6.4	5.3	6.0
22	Siliceous Sandstone grading to Argillaceous Sandstone	73'1 1/2"	5.7	5.4	4.7	5.3
24	Argillaceous Sandstone	74'9 1/2"	5.6	6.2	6.5	6.0
25 ⁽¹²⁾	Argillaceous Sandstone	76'1"	7.0	7.3	9.6	7.2 (?)
26	Siliceous Sandstone	78'4"	4.6	5.0	4.9	4.8
27	Argillaceous Sandstone	81'8"	3.7	3.3	3.4	3.5
28 ⁽¹³⁾	Argillaceous Sandstone	83'10"	3.6	4.1	4.0	3.9 (?)
29 ⁽¹⁴⁾	Interbedded Siliceous Sandstone and Argillaceous Sandstone	87' 1/2"	6.0	6.3	9.2	6.2 (?)
30	Argillaceous Sandstone	88'2"	4.2	4.4	4.4	4.3
34	Argillaceous Sandstone	92'9"	4.9	5.0	4.9	4.9
35	Siliceous Sandstone Grading to Argillaceous Sandstone	96'10"	4.4	4.0	4.2	4.2
36	Siliceous Sandstone grading to Argillaceous Sandstone	98'2"	5.3	5.3	5.0	5.2
38	Argillaceous Sandstone	100'9"	4.5	4.6	4.3	4.5
40	Argillaceous Sandstone Grading to Siliceous Sandstone	103'3"	5.1	4.9	4.7	4.9

TABLE 3-6

SUMMARY OF BIAXIAL TESTS
BORING RS-1

TEST NO.	ROCK TYPE	DEPTH (ft)	E ₁ (x10 ⁶ psi)	E ₂ (x10 ⁶ psi)	E ₃ (x10 ⁶ psi)	E _{AVG} (x10 ⁶ psi)
44	Siliceous Sandstone	120'6"	6.7	7.2	7.5	7.1
48 (15)	Argillaceous Sandstone and Shale Interbedded	123'11"				3.8

- NOTES:
- 1) For analytical procedures see Volume III, Rock Stresses, Dames & Moore, 1978.
 - 2) All original plots and calculations are available for reference in the Nine Mile II project file at Dames & Moore, Baldwinsville, N.Y.
 - 3) Biaxial test at 41'
 - 4) Biaxial test at 43'2"
 - 5) Core failed at 1000 pounds per square inch during first loading cycle. Modulus based on second unload cycle after core failed,
 - 6) Biaxial test at 46'5 1/2"
 - 7) Core failed at 1000 pounds per square inch during first loading cycle. Modulus based on second unload cycle after core failed
 - 8) Biaxial test at 47'7"
 - 9) Biaxial test at 61'2"
 - 10) Assumed modulus (Test 16, RS-1)
 - 11) Core failed after 800 pounds per square inch during first loading cycle. Modulus based on second unload cycle after core failed
 - 12) E_{AVG} based on E₁ and E₂ only
 - 13) Core failed at 981 pounds per square inch during first loading cycle. Modulus based on second unload cycle after core failed
 - 14) E_{AVG} based on E₁ and E₃ only
 - 15) Assumed Modulus (Test 16, RS-1)
 - 16) U₁θ oriented N08E.

TABLE 3-7

SUMMARY OF BIAXIAL TESTS (1,2)
BORING RS-2

TEST NO.	ROCK TYPE	DEPTH (ft)	E ₁ (x10 ⁶ psi)	E ₂ (x10 ⁶ psi)	E ₃ (x10 ⁶ psi)	E _{AVG} (x10 ⁶ psi)
2	Siliceous Sandstone	22'8"	4.4	4.7	4.3	4.5
3	Siliceous Sandstone	25'8 1/2"	3.7	3.8	3.6	3.7
4	Siliceous Sandstone	29'7"	2.4	2.5	2.4	2.4
5 ⁽³⁾	Siliceous Sandstone	30'10"	4.3	4.4	4.8	4.5
6	Siliceous Sandstone	32'11"	1.8	1.9	1.9	1.9
7	Siliceous Sandstone	35'2"	1.5	1.7	1.6	1.6
8 ^(4,5)	Argillaceous Sandstone with Shale laminations grading to medium to light gray sandstone	38'8"	3.6	3.7	3.5	3.6 (?)
9 ^(6,7)	Sandstone with Shale interbeds	41'4"	2.3	2.7	2.7	2.6 (?)
10	Graywacke grading to Siliceous Sandstone	43'8"	8.2	6.8	6.9	7.3
14 ⁽⁸⁾	Siliceous Sandstone with Argillaceous Sandstone interbeds	47'4"			3.1	3.1 (?)
15	Siliceous Sandstone	49' 1/2"	8.9	7.3	7.5	7.9
17 ⁽⁹⁾	Silty Shale to Siltstone grading to Argillaceous Sandstone	51'6"				3.6 (?)

TABLE 3-7

SUMMARY OF BIAXIAL TESTS
BORING RS-2

TEST NO.	ROCK TYPE	DEPTH (ft)	E ₁ (x10 ⁶ psi)	E ₂ (x10 ⁶ psi)	E ₃ (x10 ⁶ psi)	E _{AVG} (x10 ⁶ psi)
18 ⁽¹⁰⁾	Graywacke	53'	2.1	2.1	2.5	2.2 (?)
19 ⁽¹¹⁾	Argillaceous Sandstone	55'2"	3.8	4.1	3.6	3.8 (?)
20 ⁽¹²⁾	Siliceous Sandstone with Argillaceous Sandstone interbeds	56'9"	3.2	2.4	3.0	2.9 (?)
21 ⁽¹³⁾	Siliceous Sandstone with Argillaceous Sandstone interbeds with Shale laminations	58'				2.9 (?)
23	Siliceous Sandstone with Argillaceous Sandstone interbeds	60' 1 1/2"	4.2	4.1	4.6	4.3
24	Argillaceous Sandstone	61'10"	4.0	3.9	4.6	4.2
25	Argillaceous Sandstone	63'2"	3.8	3.4	3.8	3.7
27	Argillaceous Sandstone Grading to Siliceous Sandstone	65'7"	3.7	3.5	3.5	3.6
28	Argillaceous Sandstone Grading to Siliceous Sandstone	66'10"	4.2	3.9	3.8	4.0
30	Siliceous Sandstone grading to Argillaceous Sandstone	69'5"	5.4	4.4	4.7	4.8
31	Siliceous Sandstone	71'8"	4.7	4.3	4.3	4.4
32 ⁽¹⁴⁾	Argillaceous Sandstone	73'1"	4.4	4.2	4.1	4.2 (?)

TABLE 3-7

SUMMARY OF BIAXIAL TESTS
BORING RS-2

TEST NO.	ROCK TYPE	DEPTH (ft)	E ₁ (x10 ⁶ psi)	E ₂ (x10 ⁶ psi)	E ₃ (x10 ⁶ psi)	E _{AVG} (x10 ⁶ psi)
33	Siliceous Sandstone, Occasional Shale Clasts	74'5"	3.5	3.6	4.3	3.8
34 (15)	Argillaceous Sandstone with Occasional Siliceous Sand- Stone Interbeds	76'2"	3.5	4.2	4.1	3.9 (?)
36 (16)	Argillaceous Sandstone grading to Siliceous Sandstone with Shale laminations	79'6"	6.2	6.0	6.3	6.2 (?)
38 (17)	Siliceous Sandstone grading to Argillaceous Sandstone	82'1"	6.7	6.8	7.6	6.8 (?)
40 (18)	Argillaceous Sandstone	84'7 1/2"	3.4	3.2	3.6	3.4 (?)
42 (19)	Siliceous Sandstone	87'5"	4.9	4.9	5.9	4.9 (?)
44 (20)	Argillaceous Sandstone	90'4"				4.2 (?)
45 (21)	Argillaceous Sandstone grading to Siliceous Sandstone	91'8"	5.2	5.2	5.6	5.3 (?)

TABLE 3-7

SUMMARY OF BIAXIAL TESTS
BORING RS-2

TEST NO.	ROCK TYPE	DEPTH (ft)	E ₁ (x10 ⁶ psi)	E ₂ (x10 ⁶ psi)	E ₃ (x10 ⁶ psi)	E _{AVG} (x10 ⁶ psi)
-------------	-----------	---------------	--	--	--	--

- NOTES:
- 1) For analytical procedures, see Volume III, Rock Stresses, Dames & Moore, 1978
 - 2) All original plots and calculations are available for reference in the Nine Mile II project file at Dames & Moore, Baldwinsville, N.Y.
 - 3) Biaxial test at 30'8"
 - 4) Core failed at 1080 pounds per square inch during second unload cycle. Modulus based on second unload cycle after core failed.
 - 5) Biaxial test at 38'4"
 - 6) Core broke at 1120 pounds per square inch during first load cycle. Modulus based on first unload cycle after core failed.
 - 7) Biaxial test at 40'10"
 - 8) Modulus based on E₃ only
 - 9) Assumed modulus (Test 8, RS-2)
 - 10) Core failed at 1100 pounds per square inch during first load cycle. Modulus based on second unload cycle after core failed.
 - 11) Core failed at 1620 pounds per square inch during second loading cycle. Modulus based on second unloading cycle after core failed.
 - 12) Core failed after 600 pounds per square inch during first loading cycle. Modulus based on second unload cycle after core failed.
 - 13) Assumed Modulus (Test 20, RS-2)
 - 14) Core failed at 1200 pounds per square inch during first load cycle. Modulus based on second unload cycle after core failed.
 - 15) Core failed at 380 pounds per square inch during first loading cycle. Modulus based on second unload cycle after core failed.
 - 16) Core failed at 320 pounds per square inch during first loading cycle. Modulus based on second unload cycle after core failed.
 - 17) Modulus based on E₁ and E₂ only.
 - 18) Core failed at 800 pounds per square inch during first loading cycle. Modulus based on second unload cycle after core failed.
 - 19) Modulus based on E₁ and E₂ only.
 - 20) Assumed Modulus (Test 24, RS-2)
 - 21) Core failed at 1400 pounds per square inch during first loading cycle. Modulus based on second unload cycle after core failed.
 - 22) U₁θ oriented N57E.

TABLE 3-8

SUMMARY OF BIAXIAL TESTS (1,2)
BORING RS-3

TEST NO.	ROCK TYPE	DEPTH (ft)	E ₁ (x10 ⁶ psi)	E ₂ (x10 ⁶ psi)	E ₃ (x10 ⁶ psi)	E _{AVG} (x10 ⁶ psi)
1	Argillaceous Sandstone	6'8"	5.4	4.2	4.7	4.8
2 ⁽³⁾	Siliceous Sandstone grading slightly Argillaceous	7'11"	2.6	2.6	2.7	2.6
4	Siliceous Sandstone	13'2"	3.3	3.5	3.5	3.4
5	Siliceous Sandstone	16'2"	2.8	2.4	2.7	2.6
7 ⁽⁴⁾	Siliceous Sandstone with occasional Argillaceous Sandstone interbeds	18'4 1/2"	2.9	4.1	2.8	2.9 (?)
10 ^(5,6)	Argillaceous Sandstone, occasional Siltstone interbeds	25'8 1/2"	1.9	2.4	1.9	1.9 (?)
11 ⁽⁷⁾	Siliceous Sandstone with interbeds of Argillaceous Sandstone and Shaley Siltstone interbeds	27'9"				2.9 (?)
14 ⁽⁸⁾	Siliceous Sandstone grading to Argillaceous Sandstone	32'10 1/2"	3.4	4.1	4.0	3.7 (?)
16	Slightly Argillaceous Sandstone to Argillaceous Sandstone	35'11 1/2"	2.8	2.7	3.3	2.9
19 ⁽⁹⁾	Argillaceous Sandstone	39'7"				3.3 (?)
24 ⁽¹⁰⁾	Argillaceous Sandstone	48'5"	2.1	3.4	3.1	2.9 (?)
28 ⁽¹¹⁾	Argillaceous Sandstone with occasional Silceous Sandstone, Shale interbedded	54'4"				3.4 (?)

TABLE 3-8
SUMMARY OF BIAXIAL TESTS
BORING RS-3

TEST NO.	ROCK TYPE	DEPTH (ft)	E ₁ (x10 ⁶ psi)	E ₂ (x10 ⁶ psi)	E ₃ (x10 ⁶ psi)	E _{AVG} (x10 ⁶ psi)
35 ⁽¹²⁾	Argillaceous Sandstone with Siliceous Sandstone interbeds	67'2"	3.5	3.7	3.5	3.6 (?)
36 ^(13,14)	Argillaceous Sandstone	58 5 1/2"	3.7	3.1	3.3	3.4 (?)
37 ⁽¹⁵⁾	Siliceous Sandstone with occasional Shale interbed	69'7 3/4"	5.0	4.9	4.9	4.9
38 ⁽¹⁶⁾	Interbedded Siliceous Sandstone and Argillaceous Sandstone	70'10"	5.6	5.0	6.6	5.3 (?)
39 ⁽¹⁷⁾	Siliceous Sandstone grad- ing to Argillaceous Sand- stone with Shale Laminations	72'				4.0 (?)
41	Siliceous Sandstone, occasional interbed of Argillaceous Sandstone	74'6"	3.9	3.9	4.1	4.0
42	Siliceous Sandstone, occasional Argillaceous Sand- stone interbeds	75'10 1/2"	6.3	6.4	6.7	6.5
43 ⁽¹⁸⁾	Argillaceous Sandstone, occasional Siliceous Sand- stone interbeds	77' 1 1/2"	4.0	4.1	3.8	4.0

TABLE 3-8

SUMMARY OF BIAXIAL TESTS
BORING RS-3

TEST NO.	ROCK TYPE	DEPTH (ft)	E_1 ($\times 10^6$ psi)	E_2 ($\times 10^6$ psi)	E_3 ($\times 10^6$ psi)	E_{AVG} ($\times 10^6$ psi)
-------------	-----------	---------------	-------------------------------	-------------------------------	-------------------------------	-----------------------------------

- NOTES:
- 1) For Analytical Procedures see Volume III, Rock Stresses, Dames & Moore, 1978
 - 2) All original plots and calculations are available for reference in the Nine Mile II project file at Dames & Moore, Baldwinsville, N.Y.
 - 3) Biaxial test at 7'10"
 - 4) Core failed at 1000 pounds per square inch during first loading cycle. Modulus based on first unload cycle after core failed. E_{AVG} based on E_1 and E_3 only
 - 5) Core failed at 1350 pounds per square inch during second loading cycle. Modulus based on second unload cycle after core failed. E_{AVG} based on E_1 and E_2 only
 - 6) Biaxial test at 25'6"
 - 7) Assumed modulus (Test 7, RS-3)
 - 8) Core failed at 1700 pounds per square inch during second loading cycle. Modulus based on first unload cycle before core failed.
 - 9) Assumed modulus (test 25, RS-24)
 - 10) Core failed at 1000 pounds per square inch during first loading cycle. Modulus based on second unload cycle after core failed.
 - 11) Assumed Modulus (Test 36, RS-3)
 - 12) Core failed at 600 pounds per square inch during first loading cycle. Modulus based on second unload cycle after core failed
 - 13) Core failed at 1000 pounds per square inch during first loading cycle. Modulus based on second unload after core failed.
 - 14) Biaxial test at 68'4 1/2"
 - 15) Biaxial test at 69'3"
 - 16) E_{AVG} based on E_1 and E_2 only
 - 17) Assumed modulus (Test 41, RS-3)
 - 18) Biaxial test at 77' 2 1/2"
 - 19) Test 1 and 2, U_1 oriented N25E.
 - 20) Tests 3 through 43, U_1 oriented N40E.

TABLE 3-9
SUMMARY OF BIAXIAL TESTS (1,2)
BORING RS-4

TEST NO.	ROCK TYPE	DEPTH (ft)	E ₁ (x10 ⁶ psi)	E ₂ (x10 ⁶ psi)	E ₃ (x10 ⁶ psi)	E _{AVG} (x10 ⁶ psi)
3 ⁽³⁾	Argillaceous Sandstone grading to Siliceous Sandstone	24'6"				2.5 (?)
4 ^(4,5)	Siliceous Sandstone	27'1 1/2"	2.3	2.6	2.5	2.5 (?)
5	Siliceous Sandstone	28'6"	2.1	2.4	2.4	2.3
6	Siliceous Sandstone	30'11 1/2"	4.1	4.2	4.1	4.1
7 ⁽⁶⁾	Silty Shale to gray-wacke to Siliceous Sandstone	36'1 1/2"	2.7	2.6	2.7	2.7
8 ⁽⁷⁾	Siliceous Sandstone, occasional Shale clasts	39'3"				4.1 (?)
11 ⁽⁸⁾	Argillaceous Sandstone	58'8"				4.1 (?)
12	Graywacke	60'7"	3.9	4.2	4.2	4.1
13 ⁽⁹⁾	Argillaceous Sandstone with Occasional Siliceous Sandstone interbeds	62'	5.0	5.0	6.6	5.0 (?)
14	Argillaceous Sandstone with occasional Siliceous Sandstone interbeds and Shaley laminations	63'8"	4.9	3.8	3.8	4.2
15 ⁽¹⁰⁾	Siliceous Sandstone with Shale Clasts grading to Argillaceous Sandstone	65'9 1/2"				4.2 (?)

TABLE 3-9

SUMMARY OF BIAxIAL TESTS (1,2)
BORING RS-4

TEST NO.	ROCK TYPE	DEPTH (ft)	E ₁ (x10 ⁶ psi)	E ₂ (x10 ⁶ psi)	E ₃ (x10 ⁶ psi)	E _{AVG} (x10 ⁶ psi)
17 ⁽¹⁰⁾	Argillaceous Sandstone, occasional Siliceous Sandstone interbeds, grading to Siltstone	68'7"				4.2 (?)
19 ⁽¹⁰⁾	Interbedded Argillaceous Sandstone and Siliceous Sandstone with occasional Shale laminations	71'3"				4.2 (?)
24	Siliceous Sandstone	80'10 1/2"	3.9	3.6	4.0	3.8
25	Argillaceous Sandstone with occasional Siliceous Sandstone Interbeds and Shale Laminations	82'1 1/2"	3.4	3.0	3.4	3.3
27	Argillaceous Sandstone with Shale interbeds	83'11"	3.9	3.8	4.1	3.9
28 ⁽¹¹⁾	Interbedded Siliceous Sandstone and Argillaceous Sandstone	85'3"	3.6	3.7	3.5	3.6
33	Siliceous Sandstone	91'6"	3.2	3.6	2.9	3.2
49 ⁽¹²⁾	Interbedded Argillaceous Sandstone, Siliceous Sandstone and Shale	115'9 3/4"	4.1	4.4	4.5	4.3 (?)
50	Siliceous Sandstone	116'10 1/2"	5.2	5.4	5.0	5.2
51 ⁽¹³⁾	Siliceous Sandstone grading to Argillaceous Sandstone	119'9"	5.0	4.4	4.5	4.6

TABLE 3-9
SUMMARY OF BIAXIAL TESTS (1,2)
BORING RS-4

TEST NO.	ROCK TYPE	DEPTH (ft)	E ₁ (x10 ⁶ psi)	E ₂ (x10 ⁶ psi)	E ₃ (x10 ⁶ psi)	E _{AVG} (x10 ⁶ psi)
-------------	-----------	---------------	--	--	--	--

- NOTES:
- 1) For analytical procedures see Volume III, Rock Stresses, Dames & Moore, 1978
 - 2) All original plots and calculations are available for reference in the Nine Mile II project file at Dames & Moore, Baldwinsville, N.Y.
 - 3) Assumed Modulus (Test 4, RS-4)
 - 4) Core failed at 1800 pounds per square inch during first loading cycle. Modulus based on first loading cycle after core failed
 - 5) Biaxial test at 26'10 1/2"
 - 6) Biaxial test at 35'10 1/2"
 - 7) Assumed Modulus (Test 6, RS-3)
 - 8) Assumed Modulus (Test 12, RS-3)
 - 9) E_{AVG} based on E₁ and E₂ only
 - 10) Assumed modulus (Test 14, RS-4)
 - 11) Biaxial test at 85'5 1/2"
 - 12) Core failed at 1000 pounds per square inch during first loading cycle. Modulus based on first unload cycle after core failed.
 - 13) Biaxial test at 119'4 1/2"
 - 14) Tests 3 through 8 and 19 through 51, U₁θ oriented N28E.
 - 15) Tests 4 through 17, U₁θ oriented N23E.

TABLE 3-10

SUMMARY OF BIAXIAL TESTS¹
BORING OC-4

TEST NO.	ROCK TYPE	DEPTH (ft)	E ₁ (x10 ⁶ psi)	E ₂ (x10 ⁶ psi)	E ₃ (x10 ⁶ psi)	E _{AVG} (x10 ⁶ psi)
2	Massive Sandstone (different rock type than overcore test) (plane of measurement of biaxial test was 9 inches below plane of measurement of overcore test)	17'1/2"	3.8	4.2	3.8	3.9
3 ⁽²⁾	Cross bedded Sandstone with Shale intraclasts along cross bedding	19'2"	6.0	6.6	5.9	6.1 (?)
4	Sandstone with Shale intraclasts at 22'6"	22'2"	4.4	4.5	4.2	4.4
7	Sandstone with Shale intraclasts (plane of measurement of biaxial test was 8 1/2 inches above plane of measurement of overcore test)	23'8"	4.3	4.7	4.7	4.6
8 ⁽³⁾	Interbedded Graywacke and Sandstone (different rock type than overcore test) (plane of measurement of biaxial test was 4 1/2 inches above plane of measurement of overcore test)	27'10"	3.8	4.6	3.6	4.0 (?)
12 ⁽⁴⁾	Massive Silty Sandstone (plane of measurement of biaxial test was 2 inches above plane of measurement of overcore test)	33'0"	4.3	5.1	4.5	4.6 (?)

TABLE 3-10
SUMMARY OF BIAXIAL TESTS
BORING

TEST NO.	ROCK TYPE	DEPTH (ft)	E ₁ (x10 ⁶ psi)	E ₂ (x10 ⁶ psi)	E ₃ (x10 ⁶ psi)	E _{AVG} (x10 ⁶ psi)
15 ⁽⁵⁾	Sandstone with thin bed of Graywacke at 39'11" - numerous Shale Clasts	39'11"	4.8	4.3	4.5	4.5 (?)
16	Subgraywacke (plane of measurement of biaxial test was one inch below plane of measurement of overcore test)	42'1"	3.4	3.7	3.9	3.7
17 ^(6,13)	Fossiliferous Graywacke (plane of measurement of biaxial test was 3 inches above plane of measurement of overcore test)	43'1 1/2"	3.8	3.7	3.8	3.8 (?)
18 ^(7,13)	Graywacke/Sandstone/ Graywacke interbedded	45'2"	4.0	3.9	3.9	3.9 (?)
19 ⁽¹³⁾	Sandstone/Graywacke- buttons at contact	50'4 1/2"	5.8	5.9	5.9	5.9
20	Graywacke (plane of mea- surement of biaxial test was 3 inches above plane of measurement of overcore tests.	56'1/2"	3.9	3.8	3.6	3.8
21 ⁽⁸⁾	Siltstone/Sandstone/Gray- wacke - fracture at Shale/ Sandstone contact (mechanical or natural?)	59'3"				4.3 (?)

TABLE 3-10
SUMMARY OF BIAXIAL TESTS
BORING

TEST NO.	ROCK TYPE	DEPTH (ft)	E ₁ (x10 ⁶ psi)	E ₂ (x10 ⁶ psi)	E ₃ (x10 ⁶ psi)	E _{AVG} (x10 ⁶ psi)
22 ⁽⁹⁾	Massive Sandstone (different rock type than overcore test (plane of measurement of biaxial test was one inch below plane of measurement of overcore test))	64'0"	4.2	5.0	4.9	4.7 (?)
23 ⁽¹³⁾	Interbedded Graywacke and Sandstone with large Silt-Stone Clasts	69'1 1/2"	4.6	4.3	4.8	4.6
24 ⁽¹⁰⁾	Graywacke/Sandstone/Graywacke - contacts at 71'10" and 72'2"	72'1"	7.9	8.0	8.7	8.2 (?)
25 ⁽¹¹⁾	Graywacke (plane of measurement of biaxial test was 1 1/2 inches below plane of measurement of overcore test)	75'11"	4.4	5.0	4.9	4.8 (?)
26	Sandstone (plane of measurement of biaxial test was 1/2 inch below plane of measurement of overcore test)	77'3"	4.5	5.0	4.1	4.5
27	Sandstone/Graywacke/Sandstone (plane of measurement of biaxial test was one inch below plane of measurement of overcore test)	81'10"	3.7	3.7	3.6	3.7

TABLE 3-10
SUMMARY OF BIAXIAL TESTS
BORING

TEST NO.	ROCK TYPE	DEPTH (ft)	E ₁ (x10 ⁶ psi)	E ₂ (x10 ⁶ psi)	E ₃ (x10 ⁶ psi)	E _{AVG} (x10 ⁶ psi)
28	Sandstone	86'0"	4.2	4.4	4.4	4.3
31 ⁽¹²⁾	Graywacke with Shale layer at 106'5" (plane of measurement of biaxial test was 2 inches below plane of measurement of overcore test)	106'9"	4.3	4.5	4.9	4.6 (?)

- NOTES:
- 1) Revised modulus calculations utilizing ΔP within a comparable range to ΔR of the overcore test
 - 2) The core noticeably failed at 1800 psi of the second unloading cycle (at 18'11"). The first unloading cycle curve was used in the calculation of the modulus.
 - 3) The core noticeably failed at greater than 900 psi of the first loading cycle (at 27'8" and 28'0"). The second unloading cycle curve was used in the calculation of the modulus
 - 4) The core noticeably failed at greater than 1000 psi of the first loading cycle (at 33'4"). The second unloading cycle curve was used in the calculation of the modulus
 - 5) The core noticeably failed at greater than 1200 psi of the first loading cycle (at 40'0"). The second unloading cycle curve was used in the calculation of the modulus.
 - 6) The core noticeably failed at 2000 psi of the first loading cycle (at 43'1"). Testing was terminated at this point. This loading cycle curve was used in the calculation of the modulus.
 - 7) The core noticeably failed at greater than 1600 psi of the first loading cycle (at 45'4"). The second unloading cycle curve was used in the calculation of the modulus.

TABLE 3-10

SUMMARY OF BIAXIAL TESTS
BORING

TEST NO.	ROCK TYPE	DEPTH (ft)	E ₁ (x10 ⁶ psi)	E ₂ (x10 ⁶ psi)	E ₃ (x10 ⁶ psi)	E _{AVG} (x10 ⁶ psi)
-------------	-----------	---------------	--	--	--	--

- 8) Assumed modulus
- 9) The core noticeably failed at greater than 1400 psi of the first loading cycle (at 63'8"). The second unloading cycle curve was used in the calculation of the modulus
- 10) The core noticeably failed at greater than 1000 psi of the first loading cycle (at 71'10"). Testing was terminated at this point. This loading curve was used in the calculation of the modulus.
- 11) The core noticeably failed at greater than 1800 psi of the first loading cycle (at 76'0" and 76'4"). The second unloading cycle curve was used in the calculation of the modulus.
- 12) The core noticeably failed at 1570 psi of the first loading cycle (at 107'0"). The first unloading cycle curve was used in the calculation of the modulus
- 13) Core determined heterogeneous based on Schmidt Hammer test results.
- 14) U₁θ oriented N08E.

4.0 SUMMARY AND CONCLUSIONS

4.1 OVERVIEW OF CONSULTANTS' PARTICIPATION

A preliminary assessment of the Radwaste Structure was completed in mid-November, 1979. Tentative proposals for additional work were developed. It was during this period that Dames & Moore created a review panel consisting of Dr. Richard Jahns and Dr. Shailer Philbrick under the chairmanship of William D. Moore, Sr., founding partner of Dames & Moore. They were charged with the responsibility of formulating the scope of the investigative program, reviewing the analysis and interpretation, and obtaining the services of other experts, if required. Based on the analyses developed and their own experience, they were to develop conclusions.

Dr. N.J. Price of the Imperial College, London, had acted as consultant during previous investigations. Based on initial results of the investigation, he tentatively concluded that a majority of the displacement along the "thrust" fault had already occurred, but the possibility of new movements (up to 3 inches horizontally) could not be precluded.

In December of 1979, Dr. Price submitted a second analysis of the structure, focusing upon its future stability and the importance of shear strains and the possible influence of vibratory ground motion on the equilibrium conditions of the bedrock onsite. Dr. Price refined his previously postulated model and theorized about the possible stress drop associated

with the basal slip on the "thrust" sheet. The postulated model proved useful in predicting the extent of the structure as well as the stress distribution within it.

Based on the results of the overcoring program, Dr. Price further refined and appraised his model parameters. Dr. Price concluded that "the radwaste structure as a whole is unlikely to move as a result of bedding parallel shear stress changes which may take place in the next 40 years." However, Dr. Price recommended monitoring to define the magnitude of movements resulting from rock swell. Based on an independent review of the stress determinations, Dr. Fairhurst also concluded that most of the movement along the thrust structure should have already occurred and any future movements (within the life of the facility) would be negligibly small (Appendix F).

Dr. T.L. Péwé was asked by the review panel to intervene on two occasions, the first to comment on the possible effect of ice on the geologic structure, and the second to comment on the clays encountered in the voids in the bedrock.

Dr. Péwé visited the Nine Mile Point site on February 28, 1980. He examined the Drainage Ditch Fault, the deformation exposed in the north radwaste trench and the cooling tower excavation and photographs and maps prepared during the Cooling Tower Fault investigations. Based on his site visit and subsequent review of the data provided him, Dr. Péwé

concluded that ground ice did not cause the asymmetric folds in the bedrock at the site.

Dr. Péwé visited the site again on April 4, 1980. The purpose of this visit was to comment on the origin and age of the clay deposited in the voids in the bedrock. Specifically, there had been much debate regarding the relationship of the clay to bedrock movements along the Radwaste Structure. Because laminated clays had been noted in the dilated bedrock mass to be inclined up to 70 degrees, there was some speculation that the clays had been rotated by the bedrock movements. This was particularly significant because clays had been determined to be Late Wisconsinan in age (10,000 to 13,500 years B.P.).

Dr. Péwé concluded that the clays originated from glacial Lake Iroquois and were therefore Late Wisconsinan in age. Based on examination of the clays, particularly two occurrences of the clay layers overlying deformed bedrock structures (without disturbance), Dr. Péwé stated that he believes the clay post dates the bedrock deformation. His reports, dated March 10, 1980 and April 10, 1980, are included in Appendix D.

4.2 CONCLUSIONS

The geologic investigations of the "thrust" structures at Nine Mile Point have continued intermittently since the fall of 1976. Deformation characteristic of these "thrust" structures was encountered at several locations including the north radwaste

trench, heater bay excavation, normal switchgear excavation, circulating water piping trench, and lake water intake tunnels. These exposures roughly define a north-northeast trend that delineates the western edge of the "thrust" sheet. Investigatory procedures utilized to evaluate the geometry, age, and significance of the "thrust" structures consisted of detailed geologic mapping and structural analysis, subsurface exploration, in situ stress determinations, as well as analysis of calcite mineralization and lacustrine sediments encountered within the zones of deformation. The data collected, although extensive, did not always allow for an unequivocal interpretation. The experience of Drs. S.S. Philbrick and R.H. Jahns with similar and comparable features proved to be particularly important. The conclusions reached regarding the future stability of the "thrust" structures are based on their knowledge of the performance of analogous features in quarries and along valley-bottoms.

The conclusions reached as part of this investigation can be grouped into four categories: geometry and extent of the structure, age of deformation, equilibrium conditions, and future performance. The following summarizes the conclusions derived from the investigations and consultations regarding the "thrust" structures.

1. Geometry and Extent of Thrust Structures

- ° The Radwaste Structure is a member of a stack of "thrust" sheets. Displacement and deformation are more evident along the frontal edge of these sheets. Toward the east the deformation tends to be confined to bedding planes.
- ° The trend of the front of the "thrust" sheet is roughly coincident with a north-northeast trending bedrock valley. The sense of structural transport is generally into the valley.
- ° Dilation along bedding planes is evident to depths as great as 270 feet.
- ° Results of in situ stress determinations indicate that the Radwaste Structure extends at least 1700 feet to the east of the north radwaste trench.
- ° Radwaste-type deformation is not apparent outside of the block defined by the west-northwest trending Cooling Tower and Drainage Ditch Faults. These faults are assumed to act as lateral boundaries to the "thrust" sheets. In situ stress determinations indicate that the normal stresses acting perpendicular to the boundary faults are negligible.

2. Age of Deformation

- ° Movements along the Radwaste Structure have been recurrent. This is evident from the different stages of deformation recorded in the mineralization.

- ° As pointed out by Drs. Jahns, and Philbrick in their report (Appendix F), the initial development of the structure is believed to be associated with crustal loading and unloading during episodes of glaciation. This suggests that the "thrust" was initiated at sometime between 12,000 and 2,000,000 years ago. Based on experience with similar structures, Dr. Jahns and Philbrick believe that the age of initial formation can be refined to range from 150,000 and 400,000 years before present.
- ° The exact age of the latest deformation is equivocal. Laminated clays encountered within the zone of deformation have been dated as being approximately 11,000 years old. Clearly, there had to be some dilation of the bedrock prior to emplacement of the clays.

Dr. L. Sirkin (Appendix D.1), based on his observations in the north radwaste trench, states that the lacustrine sediments were deposited in the bedrock openings and were subsequently deformed. On the other hand

Dr. T.L. Péwé (Appendix F), states that the deformation in the bedrock occurred prior to the deposition of the clays on the basis of observations of the clay overlying the hinge of a fold. Drs. Jahns and Philbrick agree with Dr. Péwé's conclusions.

- ° From spatial associations it seems clear that the deformation occurred as a result of the relief of bedrock stress facilitated by the erosion of the north-northeast trending bedrock valley, as well as the reduction of vertical confining pressure.

3. Equilibrium Conditions

- ° The "thrust" faulting reflects the relief of stored strain energy. This relief is a result of the reduction in vertical confining pressure possibly caused by the removal of bedrock and/or overburden by erosion. The faulting occurs on the flanks of the small bedrock valley. Consequently, it is reasonable to postulate that further disturbance of equilibrium conditions occurred as a result of the removal of bedrock, concomitant with the formation of the valley. This bedrock had provided lateral restraint preventing the expansion of the strata on either side of the valley.

Furthermore, the development of buckling across the lateral boundaries of the "thrust" sheet (Cooling Tower and Drainage Ditch Faults) resulted in a significant reduction of the normal stress acting perpendicular to these boundaries. This reduction of normal stress must have affected the resistance to frictional sliding of the "thrust" sheet relative to the bedrock outside the boundaries.

- ° "The faulting is not related to current tectonic processes that could introduce additional amounts of strain energy" (Philbrick/Jahns, Appendix F). Thus, as stated in their report (Appendix F), "it can be concluded that no increase in the amount of stored strain energy will occur during the coming centuries".
- ° Dr. Price postulated that the stresses acting normal to the boundary faults act as clamping stresses restraining the movement of the "thrust" sheet. Rebound or crustal tilting could reduce these stresses and allow the "thrust" sheet to move. However, as a result of the in situ stress program, it was demonstrated that the clamping stresses are negligible and, therefore, not a significant factor in the overall equilibrium.

4. Future Movement of the Radwaste Structure

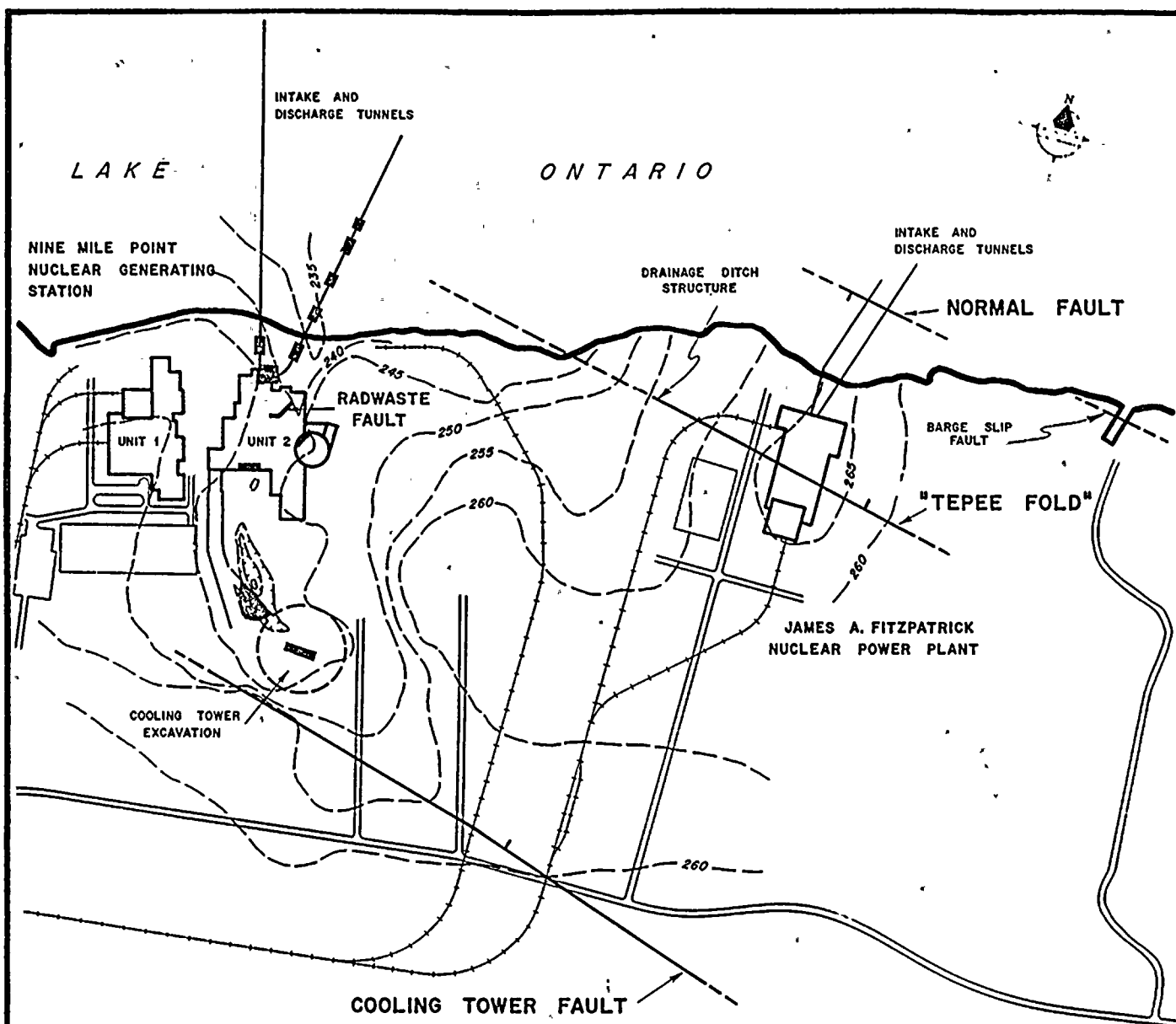
- ° It was not possible to demonstrate with certainty that no Holocene movements have occurred. The relationship of the lacustrine clays which are approximately 11,000 years old to the bedrock deformation is debatable and does not provide unequivocal resolution of the age of latest deformation.
- ° The possible future displacements on the "thrust" faults cannot be ruled out. Drs. Jahns and Philbrick concluded that "future movements along the structure

are not likely to occur". However, should they occur it is expected that further relief will involve "dilation and small movements along fractures and bedding surfaces". Because of the inability of the structure to build up significant amounts of strain energy, Drs. Philbrick and Jahns further concluded that "the radwaste structure is so nearly dead at present levels of exposure that its participation in such future movements would amount to no more than a small fraction of an inch".

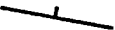
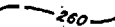

- ° Based on observations of analogous geologic structures, by Dr. Jahns in Maine, Vermont, New Hampshire, Massachusetts and New York and by Dr. Philbrick in Pennsylvania, West Virginia and Tennessee, it has been concluded that any future movements should not exceed 1/4 inch.

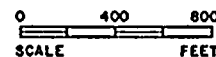
5.0 REFERENCES

- Connally, G.G., 1964, Garnet ratios and provenance in the glacial drift of western New York: Science, Vol. 144, p. 1452-1453.
- Connally, G.G., and Sirkin, L.A., 1969, Deglacial History of the Lake Champlain-Lake George Lowland, New York State Geol. Assoc. Guidebook to Field Excursions, 41st Ann. Mtg., Trip I, p. I-1 to I-20.
- Gwyn, Q.H. and A. Dreimanis, 1979, Heavy mineral assemblages in tills and their use in distinguishing glacial lobes in the Great Lakes region: Can. J. of Earth Sci., Vol. 16, p. 2219-2235.
- Krumbein, W.C., and L.L. Sloss, 1963, Stratigraphy and Sedimentation; W.H. Freeman and Company, San Francisco, 660 p.
- New York State Electric and Gas Corporation, 1979, Geologic Investigation, Demster Structural Zone; Appendix 2.5I, of Preliminary Safety Analysis Report, New Haven Units 1 and -2, Docket Nos. STN50-596 and STN50-597.
- Niagara Mohawk Power Corporation, April 14, 1978, Nine Mile Point Nuclear Station Unit 2: Geologic Investigation, Vols. I, II, and III.



EXPLANATION:

-  TRACE OF MODERATELY TO STEEPLY DIPPING STRUCTURE
-  BEDROCK SURFACE CONTOUR (EL. IN FEET)
-  LOCATIONS OF OBSERVED OCCURENCES OF STRUCTURES SIMILAR IN CHARACTER TO RADWASTE STRUCTURE

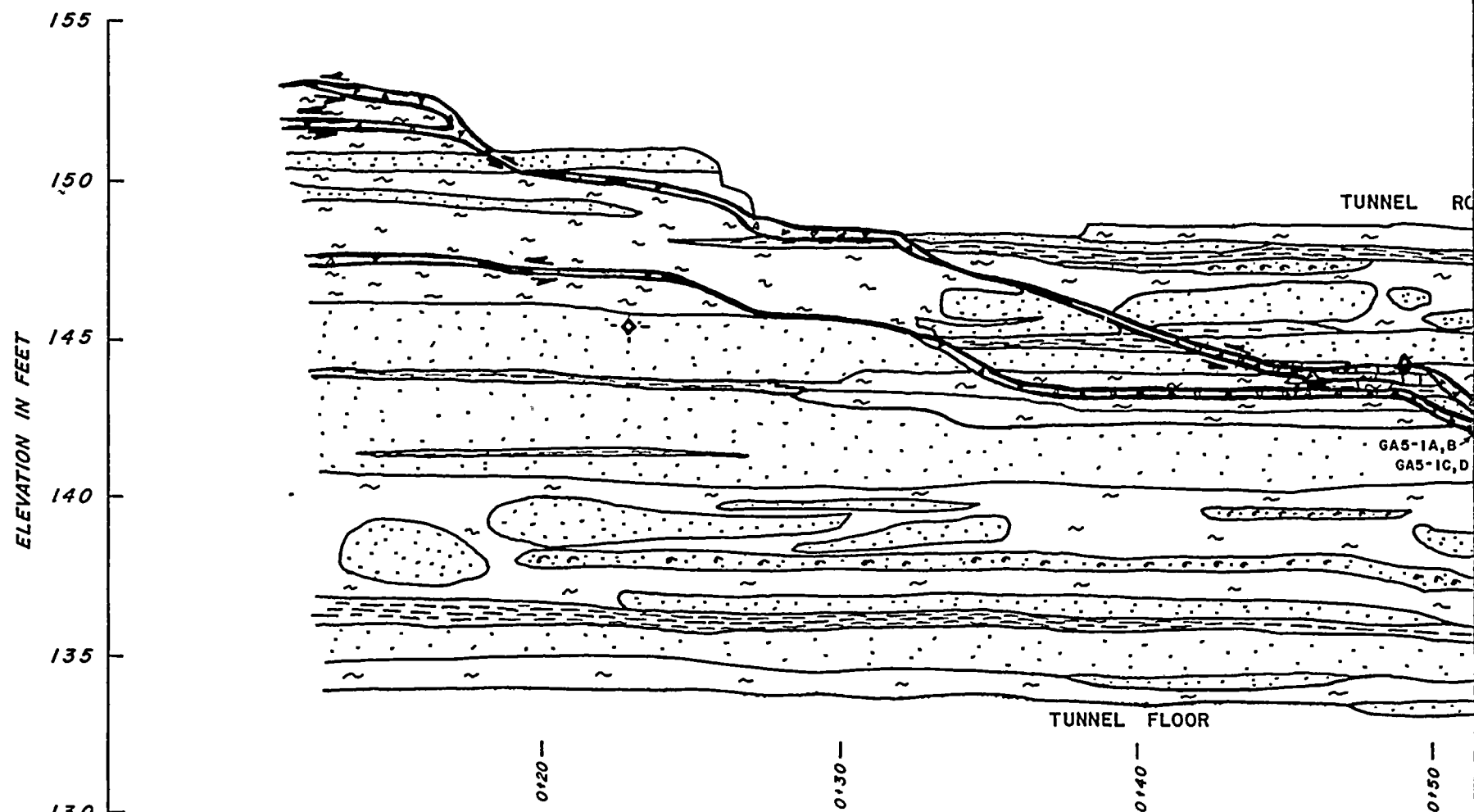


SITE LOCATION MAP

SHOWING GENERAL CONFIGURATION OF BEDROCK SURFACE
AND LOCATIONS OF KNOWN GEOLOGIC STRUCTURES



SECTION TREND N 65 E



EXPLANATION:

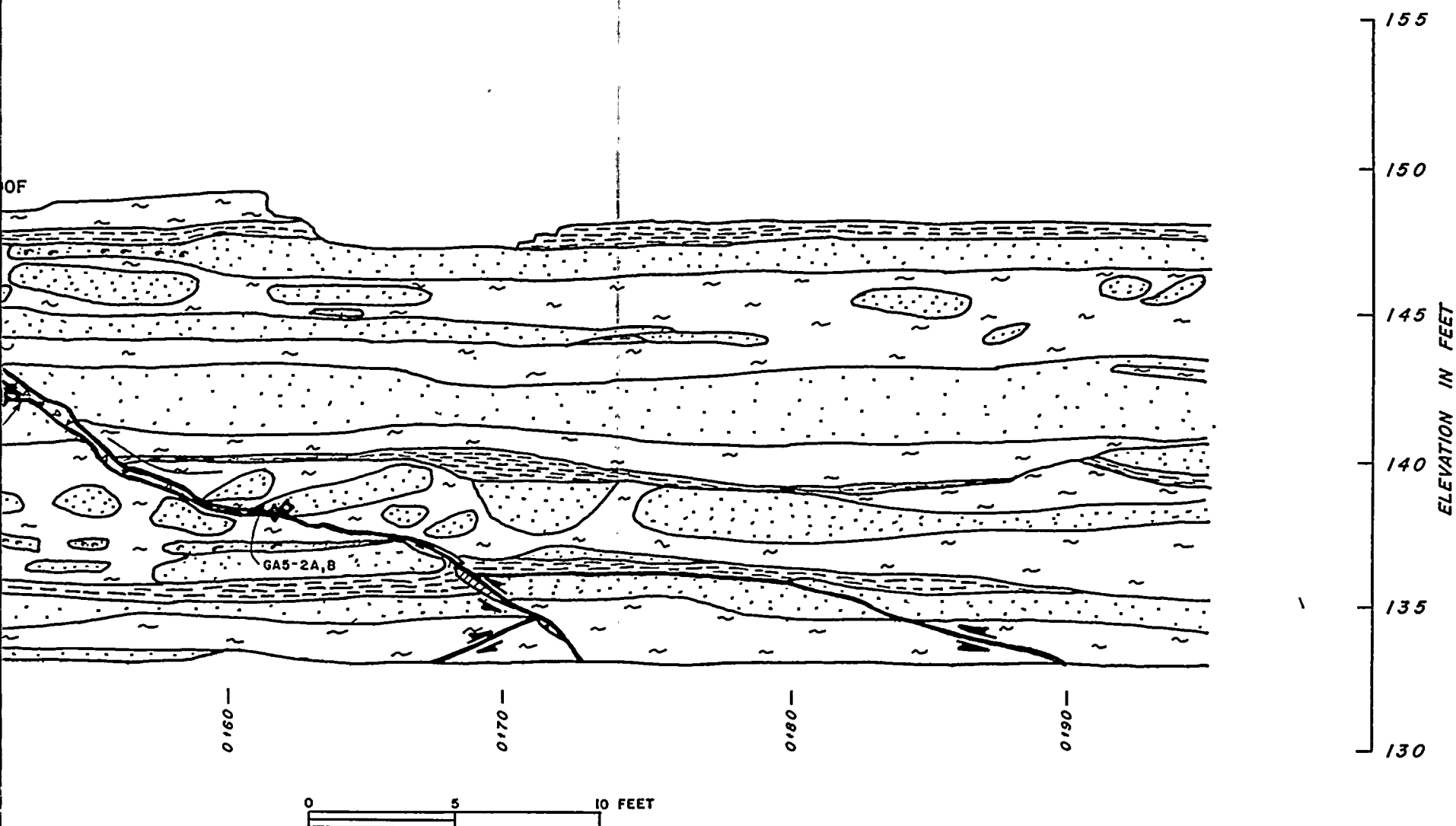


Light gray fine to medium grained siliceous sandstone
Fossiliferous sandstone
Sandstone with shaly interclasts
Medium dark gray fine to medium grained argillaceous sandstone or graywacke
Dark gray to black very fine grained argillaceous sandstone or siltstone
Black shale
Breccia - generally angular fragments of rock in soft light gray sandy silt matrix



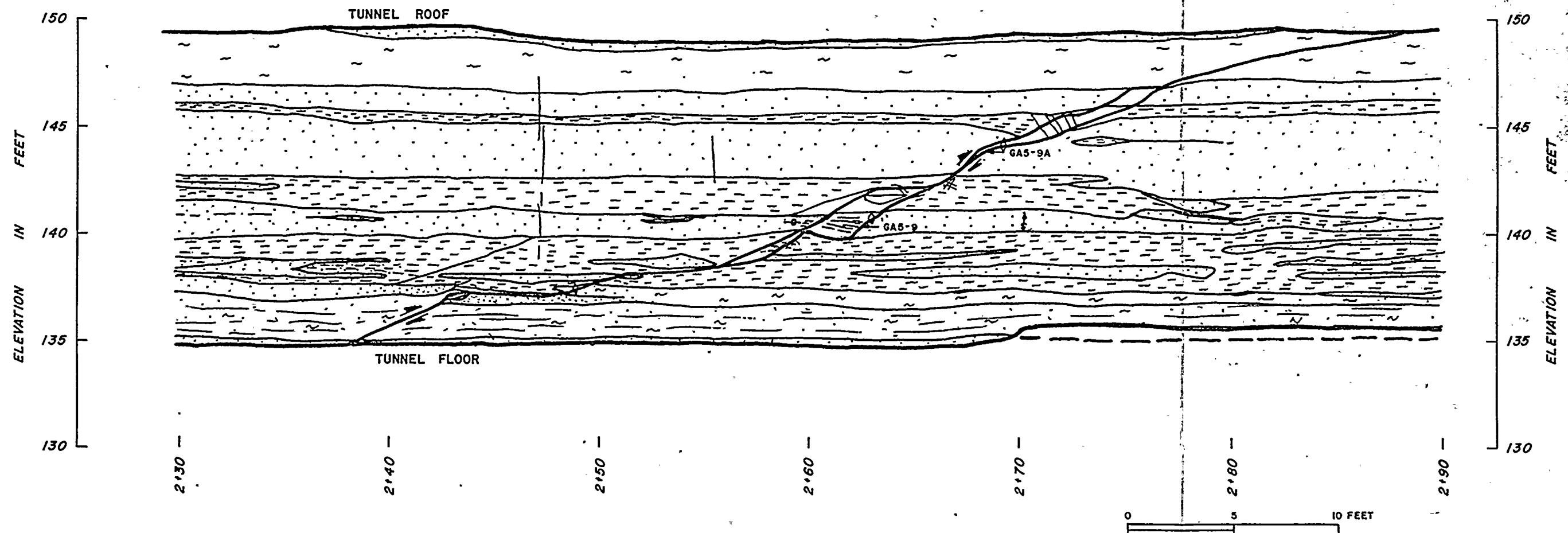
Joint or fracture
Joint or fracture filled with calcite or sulfides, respectively
Open joint or fracture
Calcite or sulfide coatings on surfaces parallel to cross section
Arrows indicate relative sense of movement; open where inferred
Sample Location

GA5-1A,B



CROSS SECTION - LEFT RIB , EAST INTAKE TUNNEL
STATION 0+10 TO 0+95

SECTION TREND N 06 W



EXPLANATION:



Light gray fine to medium grained siliceous sandstone
Fossiliferous sandstone
Sandstone with shaly interclasts
Medium dark gray fine to medium grained argillaceous sandstone or graywacke
Dark gray to black very fine grained argillaceous sandstone or siltstone
Black shale
Breccia - generally angular fragments of rock in soft light gray sandy silt matrix



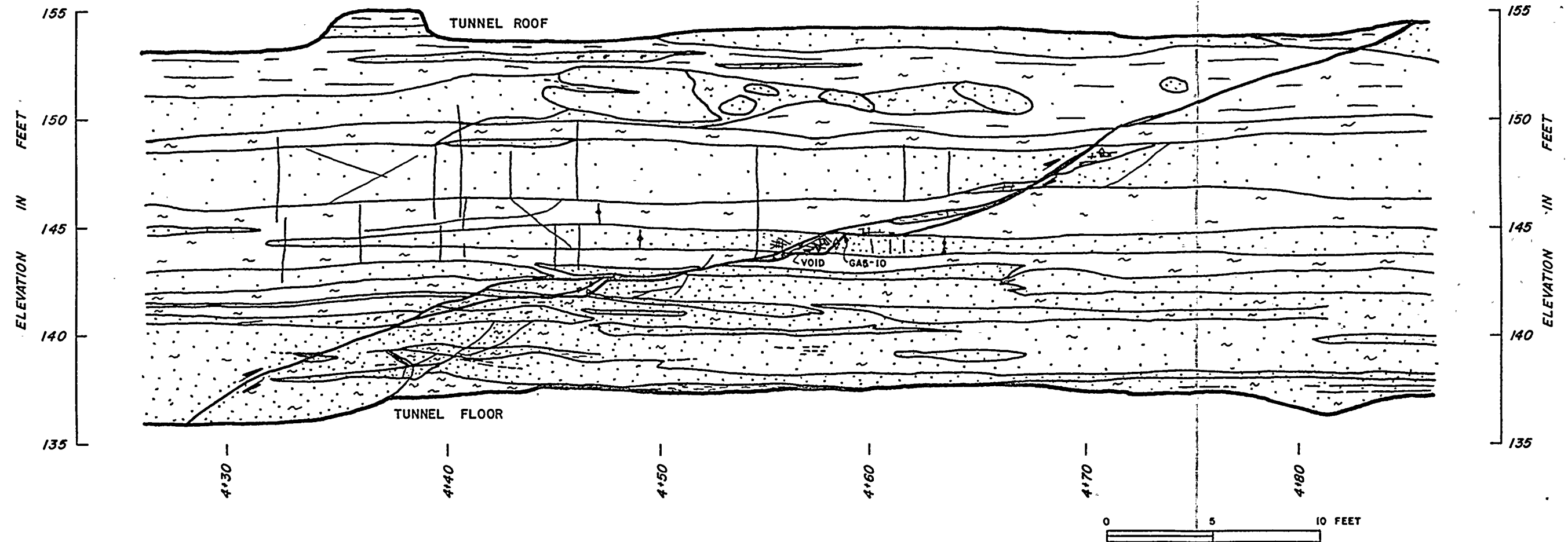
Joint or fracture
Joint or fracture filled with calcite or sulfides, respectively
Open joint or fracture
Calcite or sulfide coatings on surfaces parallel to cross section
Arrows indicate relative sense of movement; open where inferred

GA5-9

Sample location

CROSS SECTION - LEFT RIB,
EAST INTAKE TUNNEL

STATION 2+30 TO 2+90

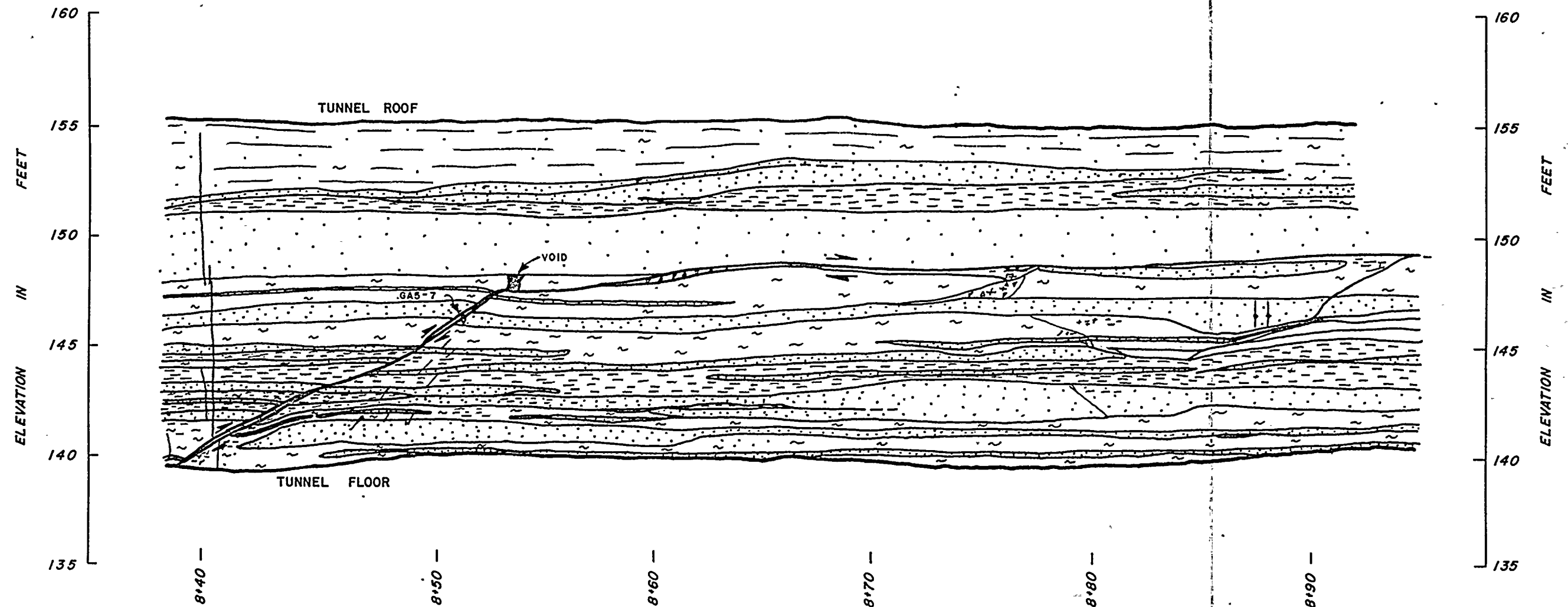


EXPLANATION:



- Light gray fine to medium grained siliceous sandstone
 Fossiliferous sandstone
 Sandstone with shaly interclasts
 Medium dark gray fine to medium grained argillaceous sandstone or graywacke
 Dark gray to black very fine grained argillaceous sandstone or siltstone
 Black shale
 Breccia - generally angular fragments of rock in soft light gray sandy silt matrix
 Joint or fracture
 Joint or fracture filled with calcite or sulfides, respectively
 Open joint or fracture
 Calcite or sulfide coatings on surfaces parallel to cross section
 Arrows indicate relative sense of movement; open where inferred
 Sample location

CROSS SECTION - LEFT RIB,
 EAST INTAKE TUNNEL
 STATION 4+25 TO 4+85



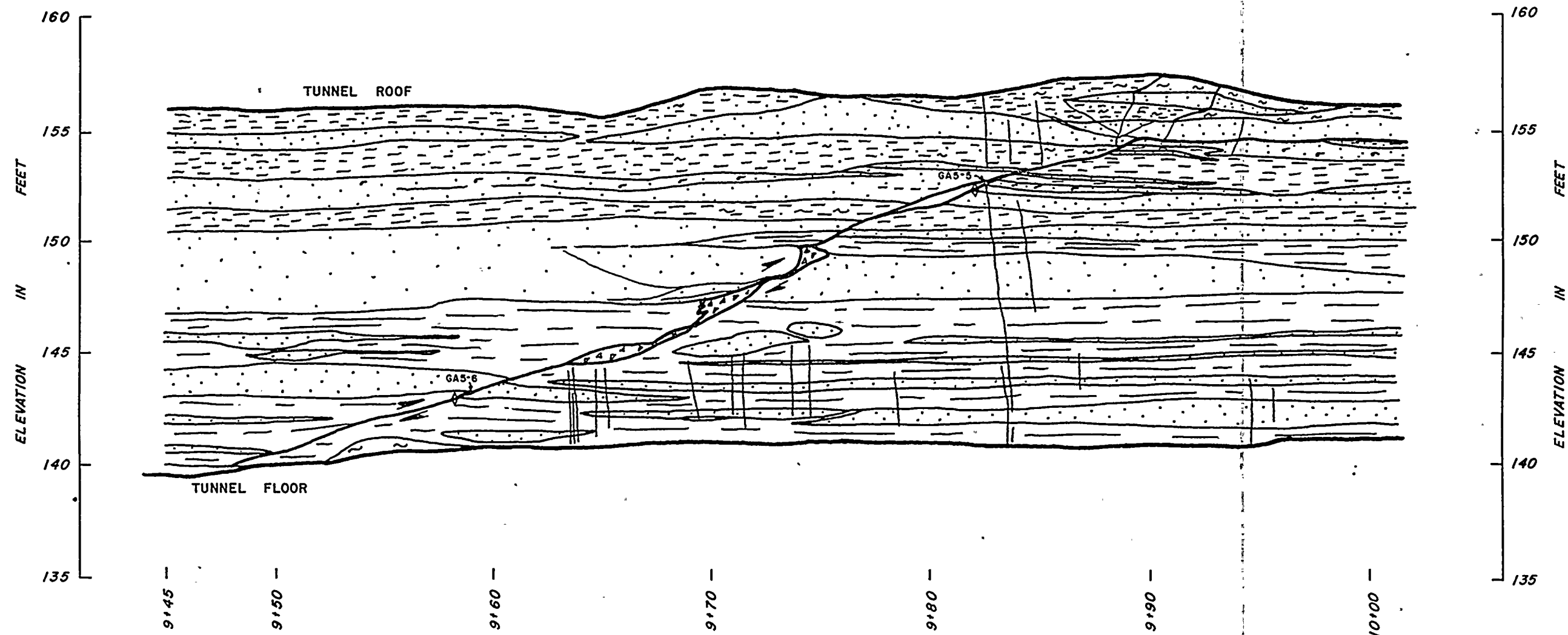
EXPLANATION:



- Light gray fine to medium grained siliceous sandstone
- Fossiliferous sandstone
- Sandstone with shaly interclasts
- Medium dark gray fine to medium grained argillaceous sandstone or graywacke
- Dark gray to black very fine grained argillaceous sandstone or siltstone
- Black shale
- Breccia - generally angular fragments of rock in soft light gray sandy silt matrix
- Joint or fracture
- Joint or fracture filled with calcite or sulfides, respectively
- Open joint or fracture
- Calcite or sulfide coatings on surfaces parallel to cross section
- Arrows indicate relative sense of movement; open where inferred
- Sample Location

0 5 10 FEET

**CROSS SECTION - LEFT RIB,
EAST INTAKE TUNNEL
STATION 8+38 TO 8+95**



EXPLANATION:

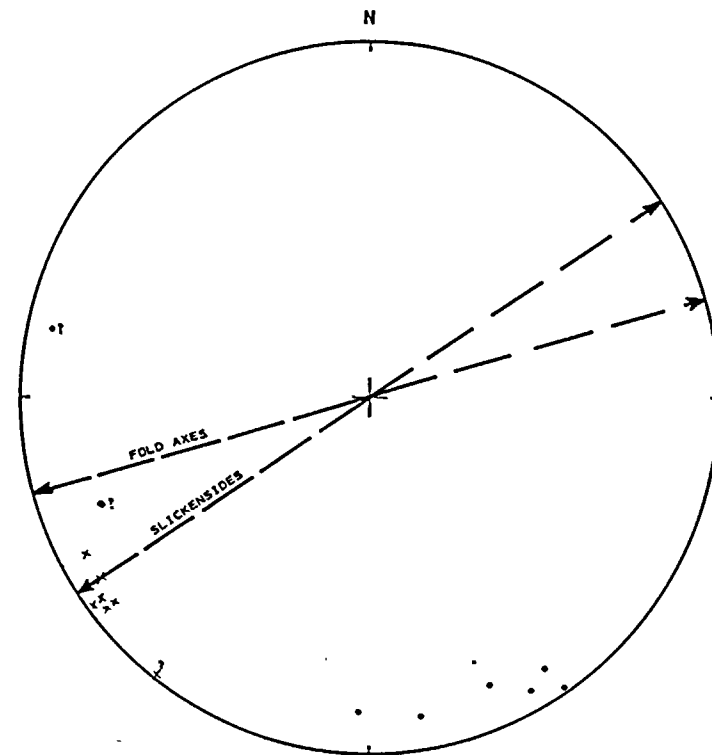


Light gray fine to medium grained siliceous sandstone
 Fossiliferous sandstone
 Sandstone with shaly intercalations
 Medium dark gray fine to medium grained argillaceous sandstone or graywacke
 Dark gray to black very fine grained argillaceous sandstone or siltstone
 Black shale
 Breccia - generally angular fragments of rock in soft light gray sandy silt matrix



Joint or fracture
 Joint or fracture filled with calcite or sulfides, respectively
 Open joint or fracture
 Calcite or sulfide coatings on surfaces parallel to cross section
 Arrows indicate relative sense of movement; open where inferred
 Sample location

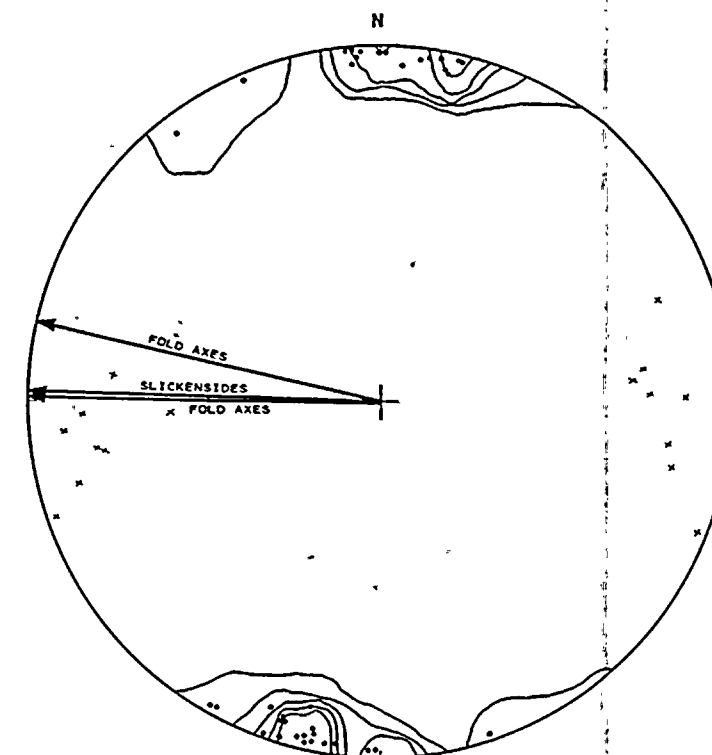
CROSS SECTION - LEFT RIB
 EAST INTAKE TUNNEL
 STATION 9+45 TO 10+02



• TREND AND PLUNGE OF FOLD AXES
X RAKE OF SLICKENSIDES

ARROWS REPRESENT DIRECTION OF SLIP
INDICATED BY MEDIAN ORIENTATIONS OF
FOLD AXES AND SLICKENSIDES

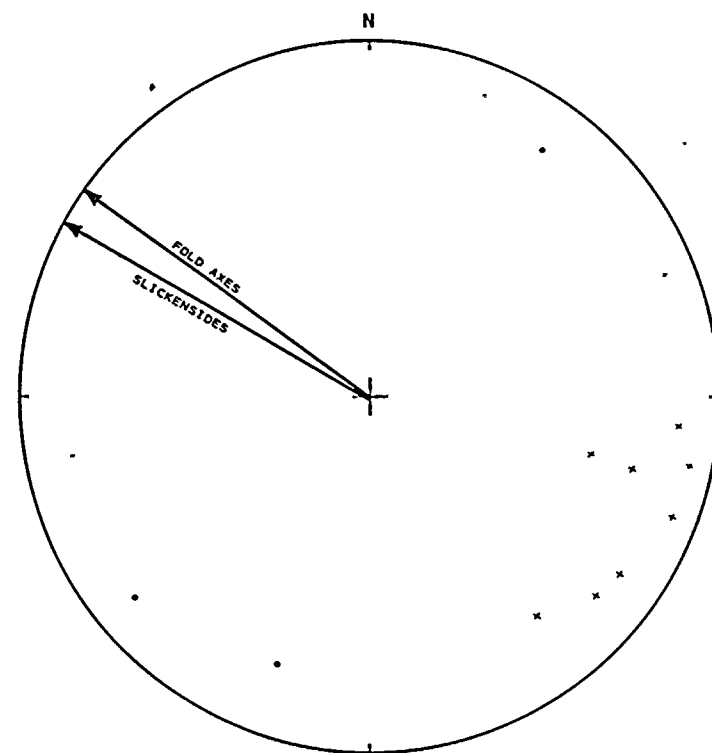
A. STRUCTURAL ELEMENTS FROM COOLING TOWER EXCAVATION
AND CIRCULATING WATER PIPING TRENCH



• TREND AND PLUNGE OF FOLD AXES
X RAKE OF SLICKENSIDES
CONTOUR INTERVAL = 10° WITH ONLY
FOLD AXIS DATA CONTOURED

ARROWS REPRESENT THE DIRECTION OF
SLIP AS INDICATED BY FOLD AXIS MAXIMA
AND MEDIAN DIRECTION OF SLICKENSIDES

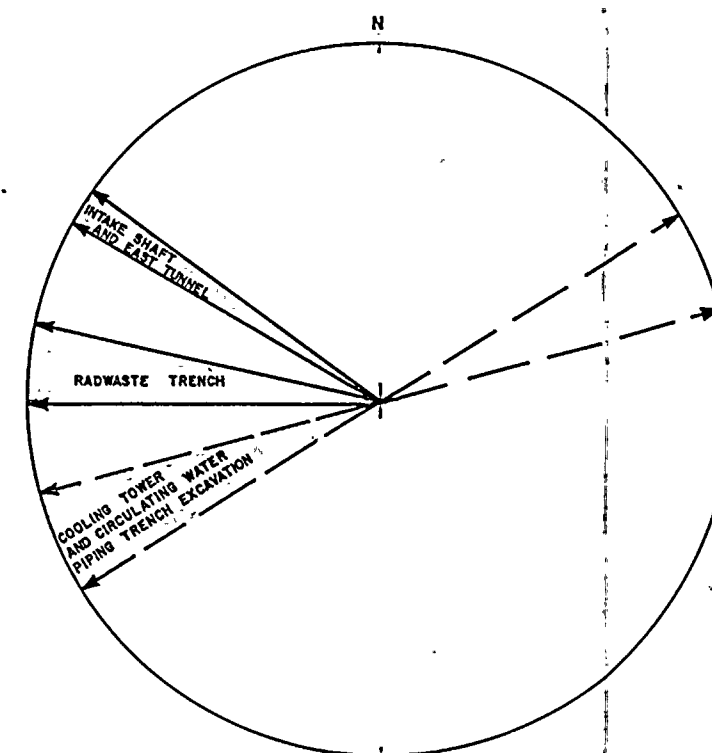
B. STRUCTURAL ELEMENTS NORTH RADWASTE TRENCH



• TREND AND PLUNGE OF FOLD AXIS
X RAKE OF SLICKENSIDES

ARROWS REPRESENT THE DIRECTION OF
SLIP INDICATED BY MEDIAN ORIENTATION
OF FOLD AXES AND SLICKENSIDES

C. STRUCTURAL ELEMENTS FROM INTAKE SHAFT
AND EAST TUNNEL

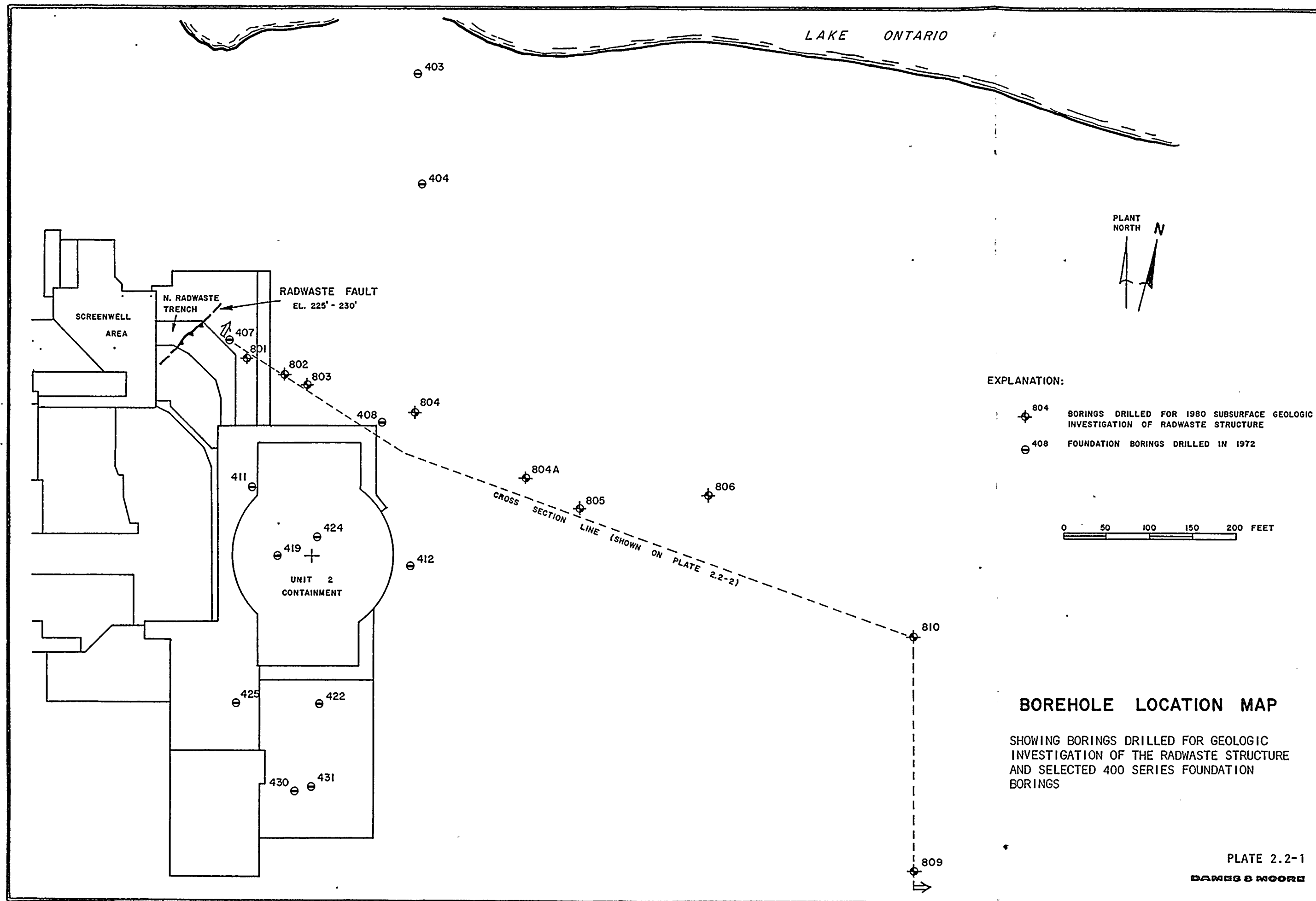


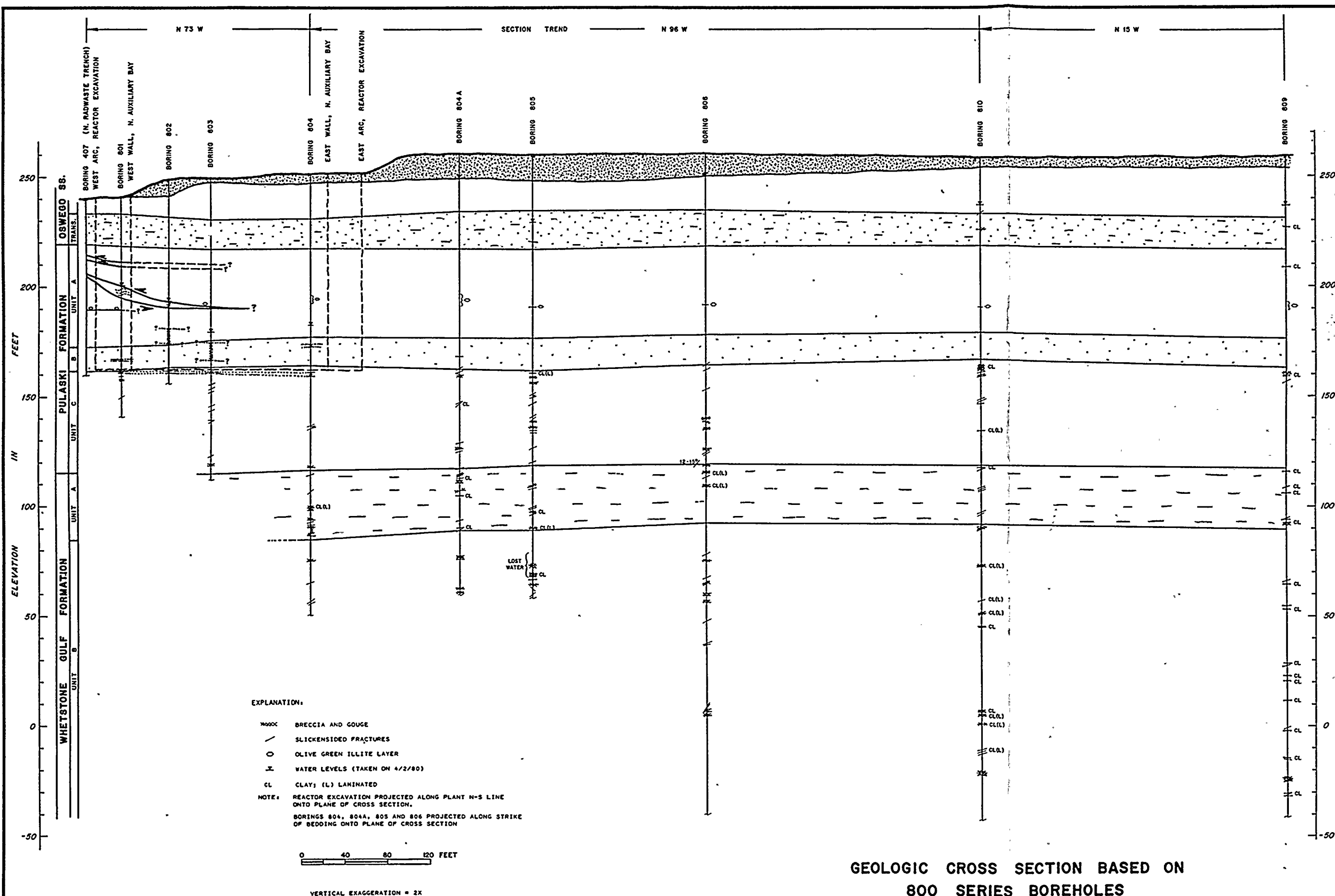
ARROWS REPRESENT RANGE OF SLIP DIRECTIONS
INDICATED BY THE ORIENTATION OF STRUCTURAL
ELEMENTS AT VARIOUS LOCATIONS ACROSS THE SITE

D. SLIP DIRECTION INDICATED BY RADWASTE-TYPE
STRUCTURES AT THE SITE

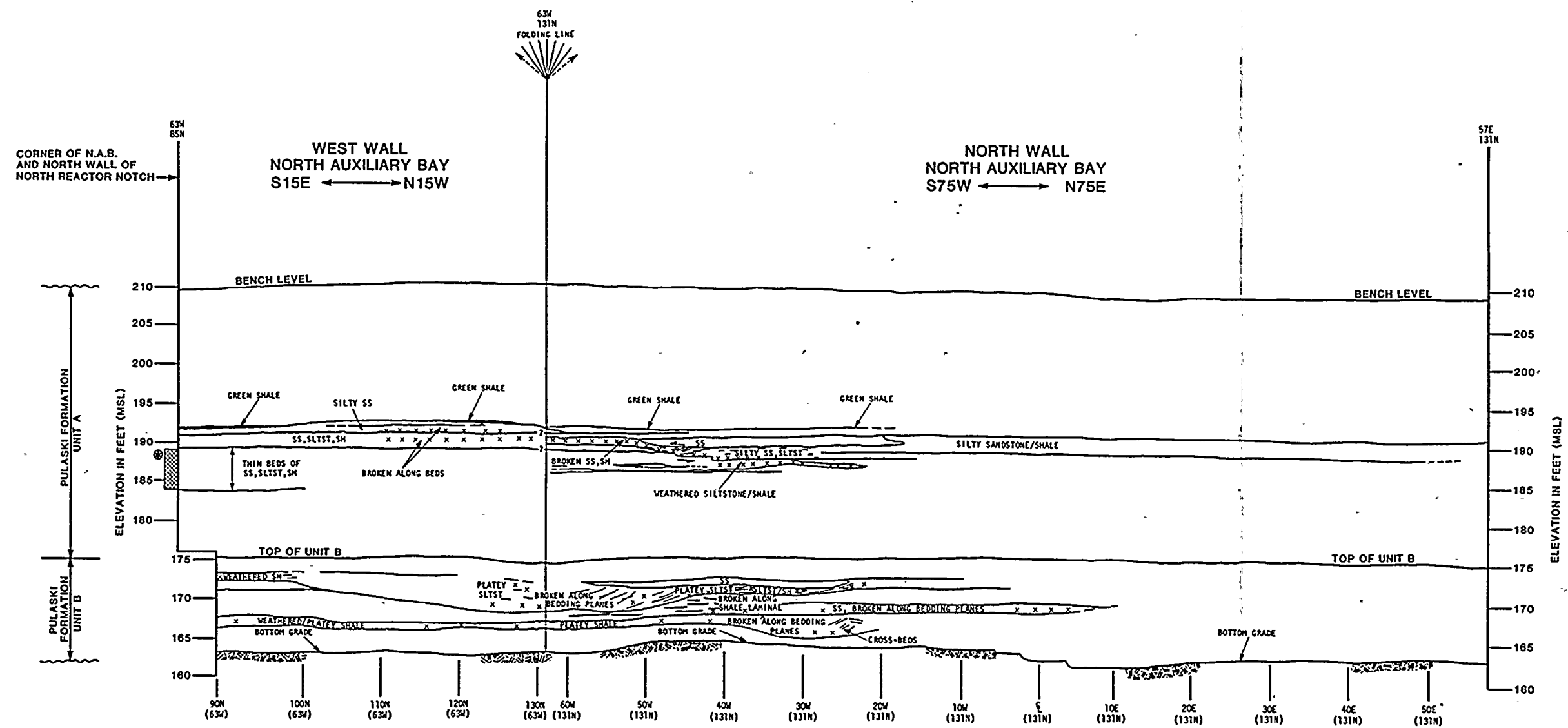
STRUCTURAL ELEMENTS FROM
AREAS OF INVESTIGATION

PLATE 2.1-26
DAMES & MOORE





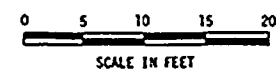
**GEOLOGIC CROSS SECTION BASED ON
800 SERIES BOREHOLES**



SIMPLIFIED GEOLOGIC CROSS-SECTION NORTH AND WEST WALLS OF NORTH AUXILIARY BAY

SHOWING OCCURRENCES OF BEDDING PLANE DEFORMATION ASSOCIATED
WITH THE RADWASTE SERIES OF FAULTS AS SHOWN ON PLATE 5.2-2

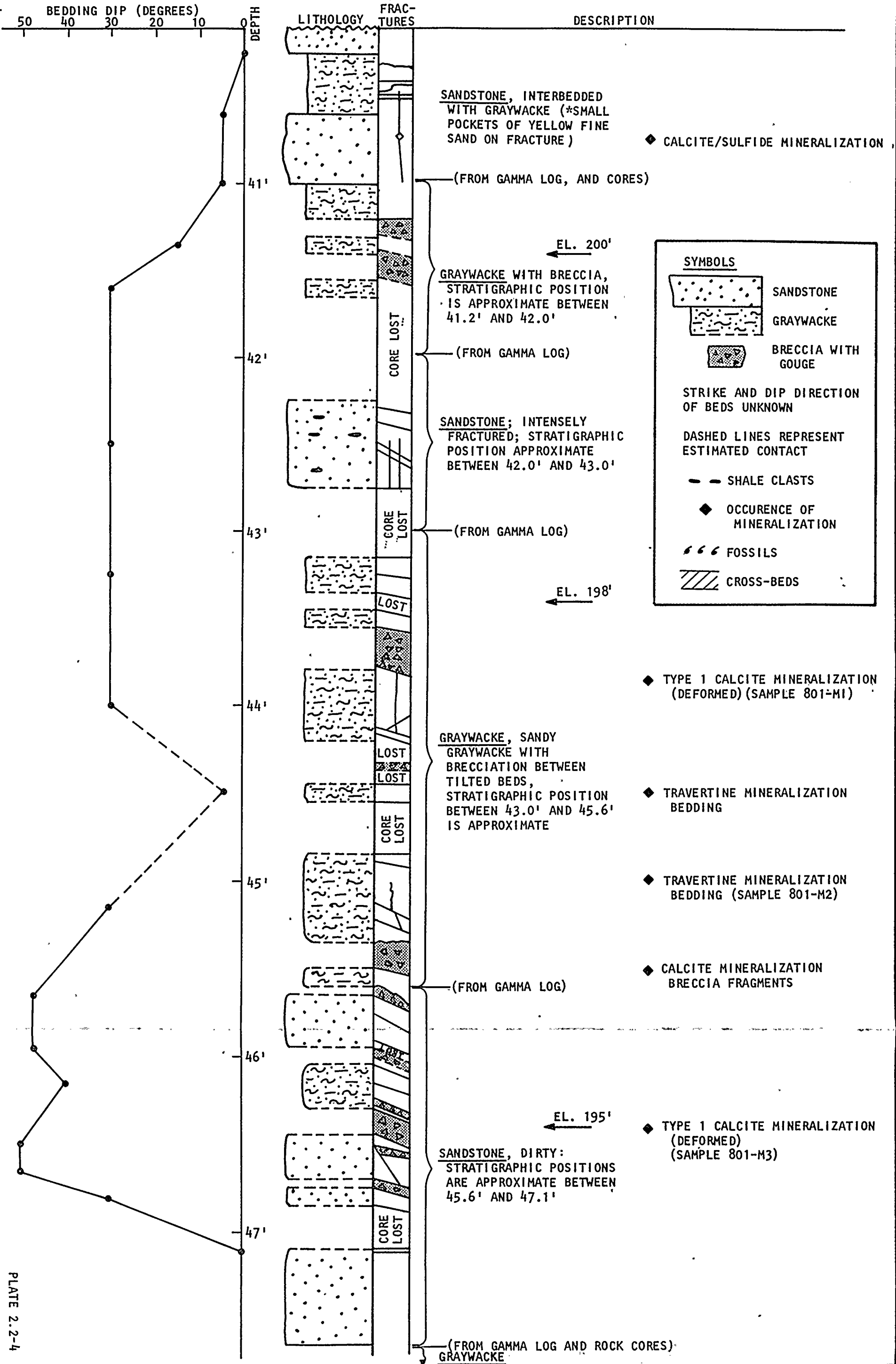
(DATA OBTAINED FROM FIELD INSPECTION DRAWINGS AND PHOTOGRAPHS)



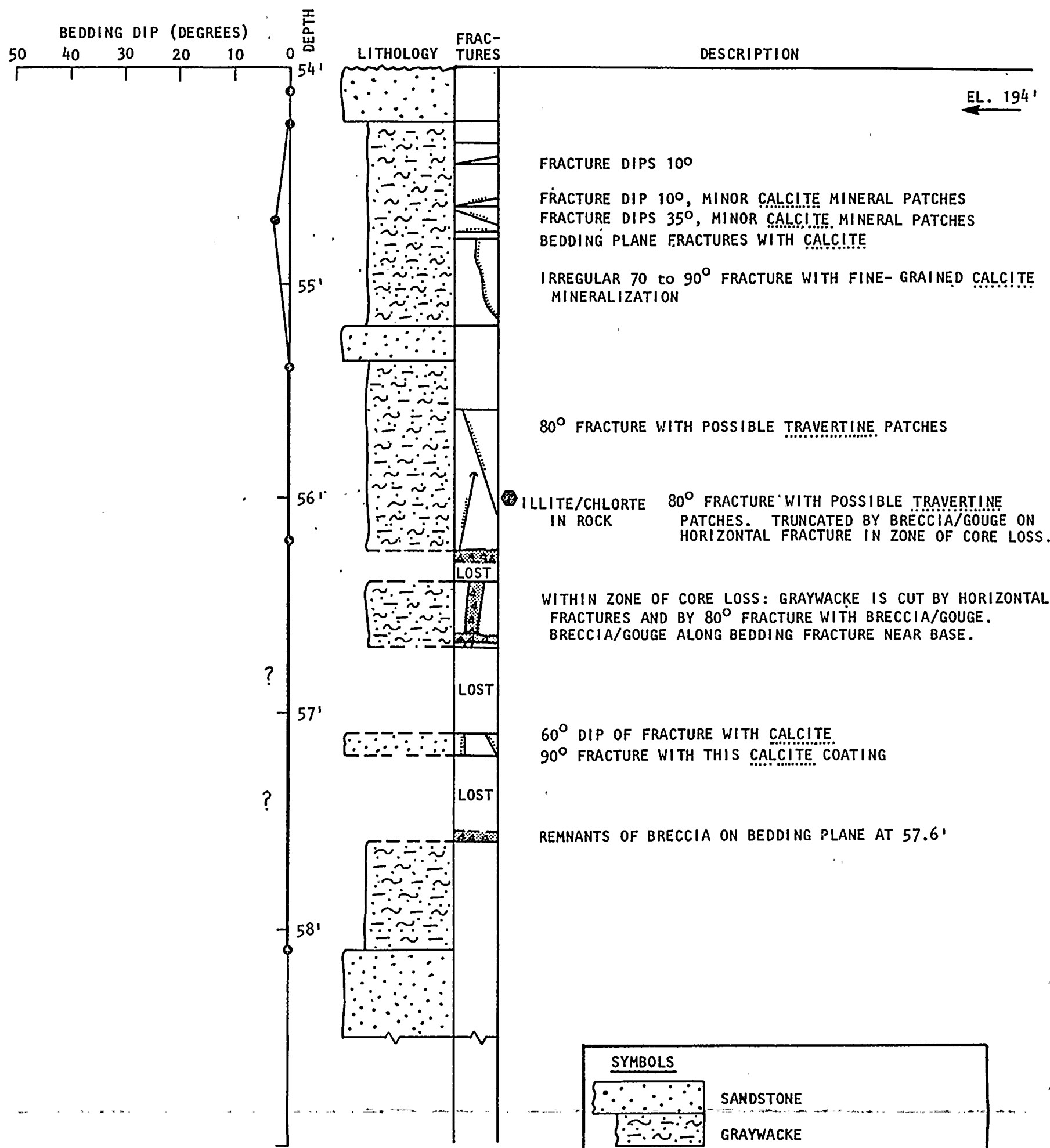
⊕ INTERVAL OF BEDS WHERE FOLD IN NORTH NOTCH SHOWS SLIP
TOWARD THE EAST. (NIAGARA MOHAWK POWER CORPORATION, 1978,
GEOLOGIC INVESTIGATION: VOLUME 1, SECTION 3.0, PLATE 3-41)

DETAILED LOG OF PORTION OF BORING 801

(EL. 241.4')



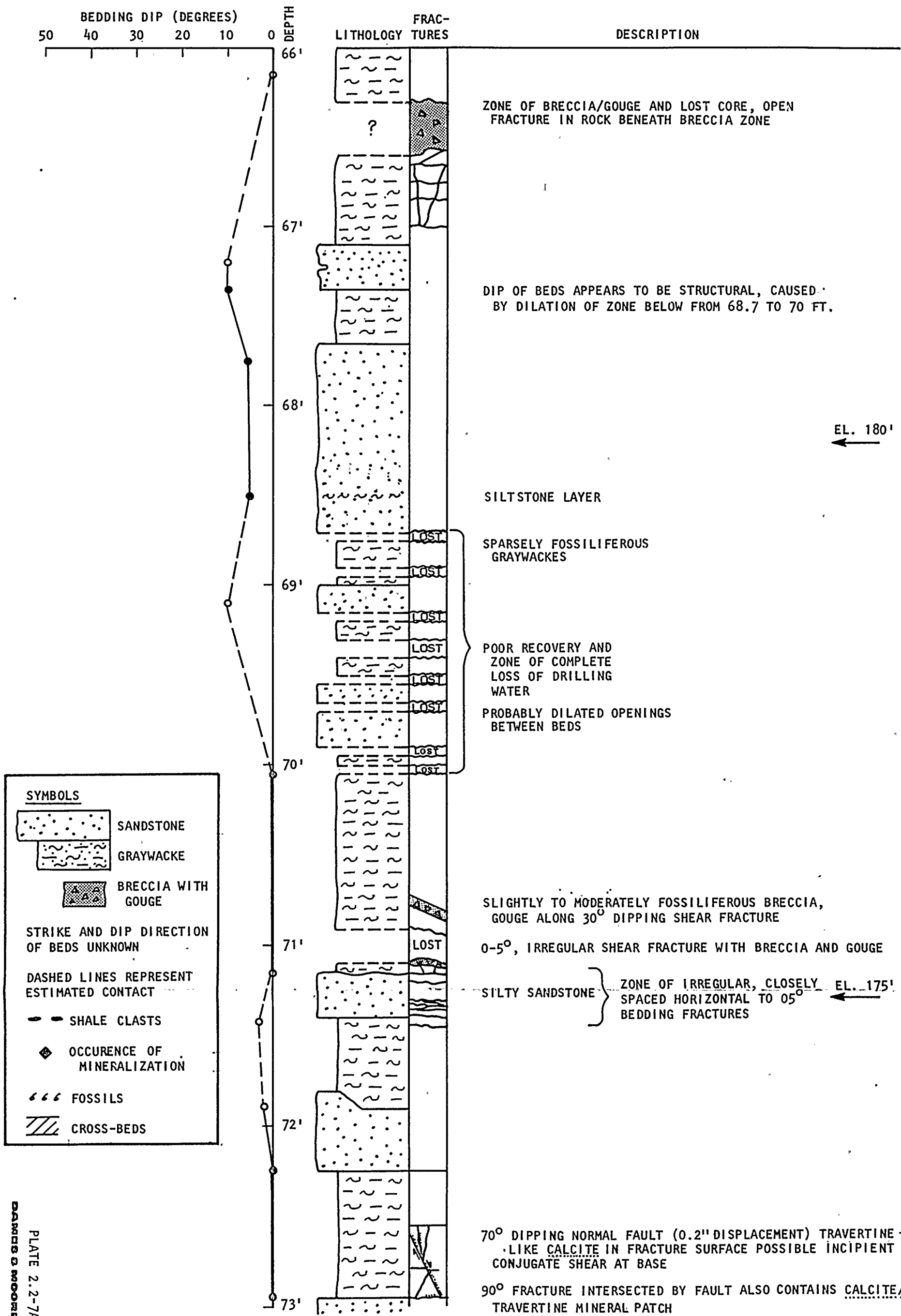
DETAILED LOG OF PORTION OF BORING 802
(EL. 248.2')



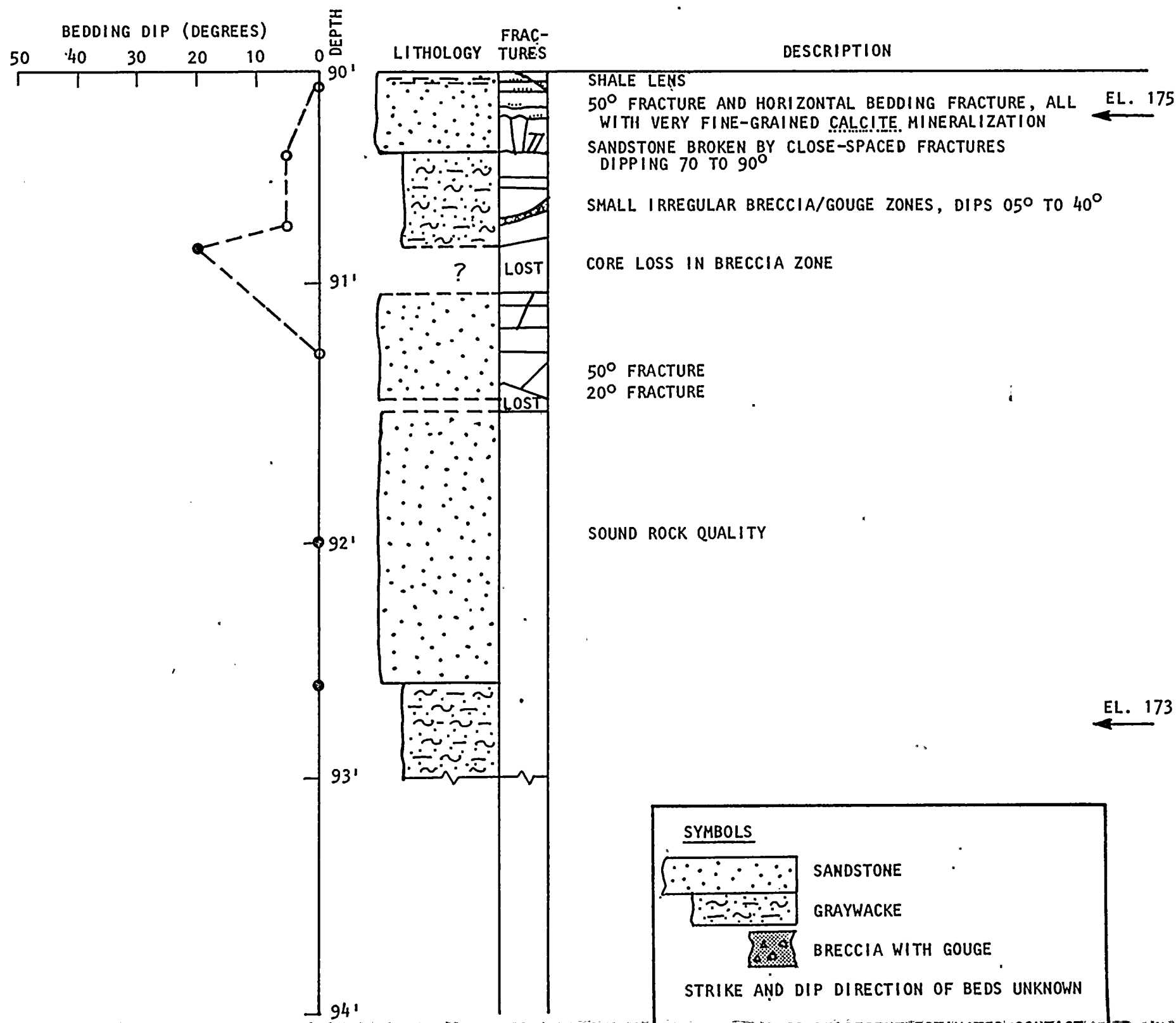
SYMBOLS

- SANDSTONE
- GRAYWACKE
- BRECCIA WITH GOUGE
- STRIKE AND DIP DIRECTION OF BEDS UNKNOWN
- DASHED LINES REPRESENT ESTIMATED CONTACT
- SHALE CLASTS
- OCCURENCE OF MINERALIZATION
- FOSSILS
- CROSS-BEDS

DETAILED LOG OF PORTION OF BORING 802
(EL. 248.8')



DETAILED LOG OF PORTION OF BORING 802 (CONT'D)



SYMBOLS

SANDSTONE

GRAYWACKE

BRECCIA WITH GOUGE

STRIKE AND DIP DIRECTION OF BEDS UNKNOWN

DASHED LINES REPRESENT ESTIMATED CONTACT

SHALE CLASTS

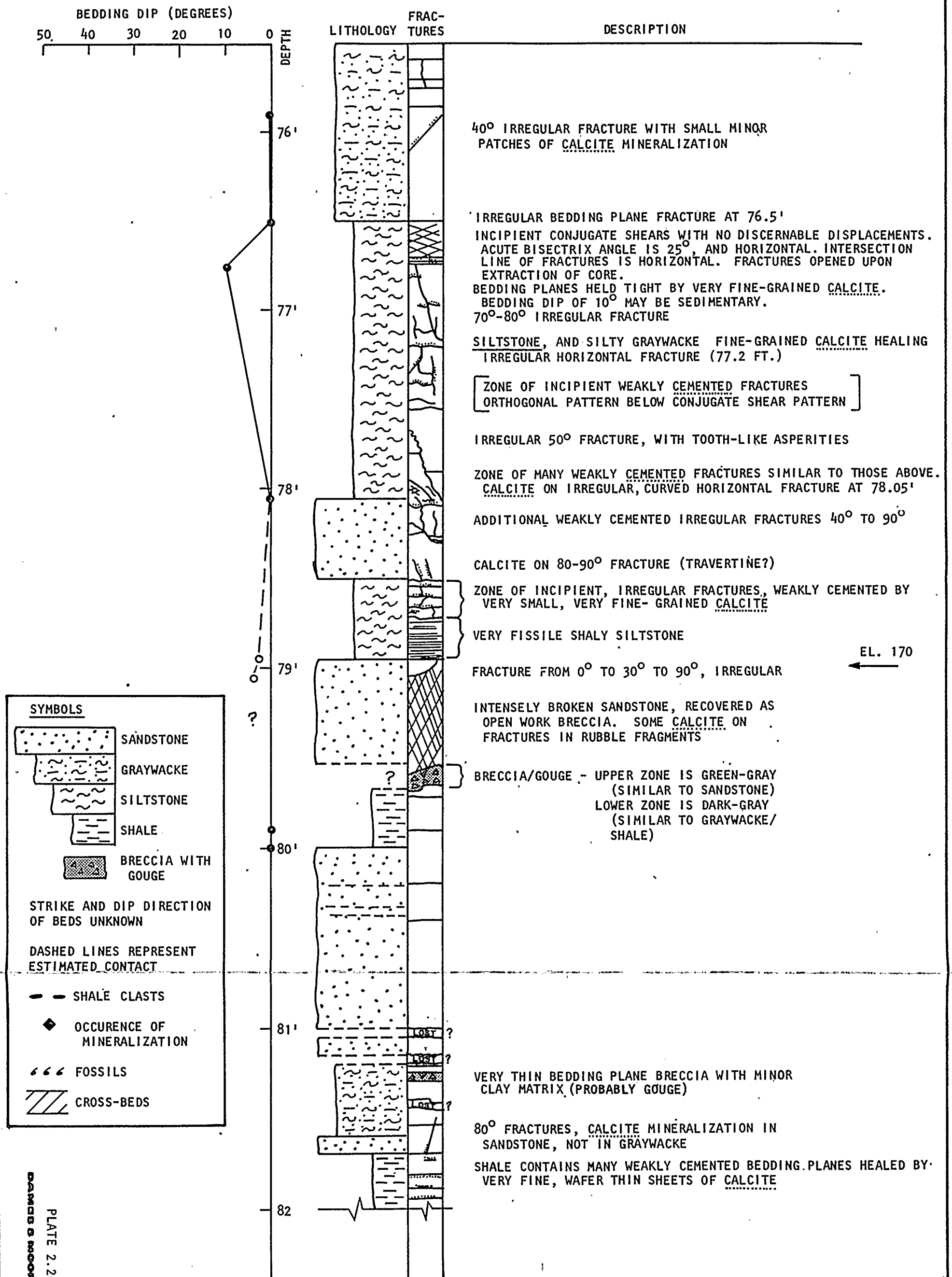
OCCURENCE OF MINERALIZATION

FOSSILS

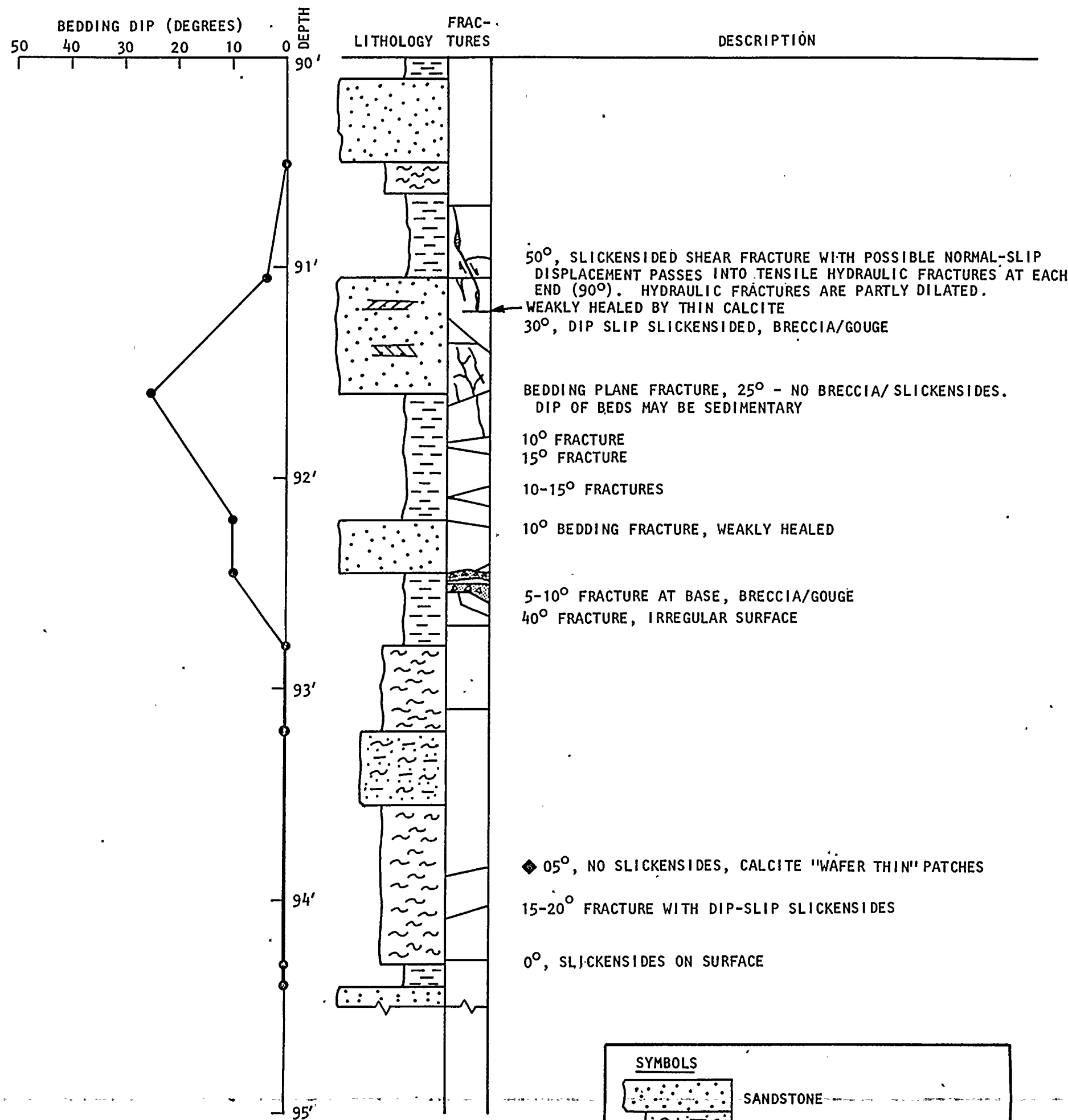
CROSS-BEDS

DETAILED LOG OF PORTION OF BORING 803

(EL. 249.0')



DETAILED LOG OF PORTION OF BORING 804 (EL. 251.7')



SYMBOLS

SANDSTONE

GRAYWACKE

SILTSTONE

SHALE

BRECCIA WITH GOUGE

STRIKE AND DIP DIRECTION OF BEDS UNKNOWN

DASHED LINES REPRESENT ESTIMATED CONTACT

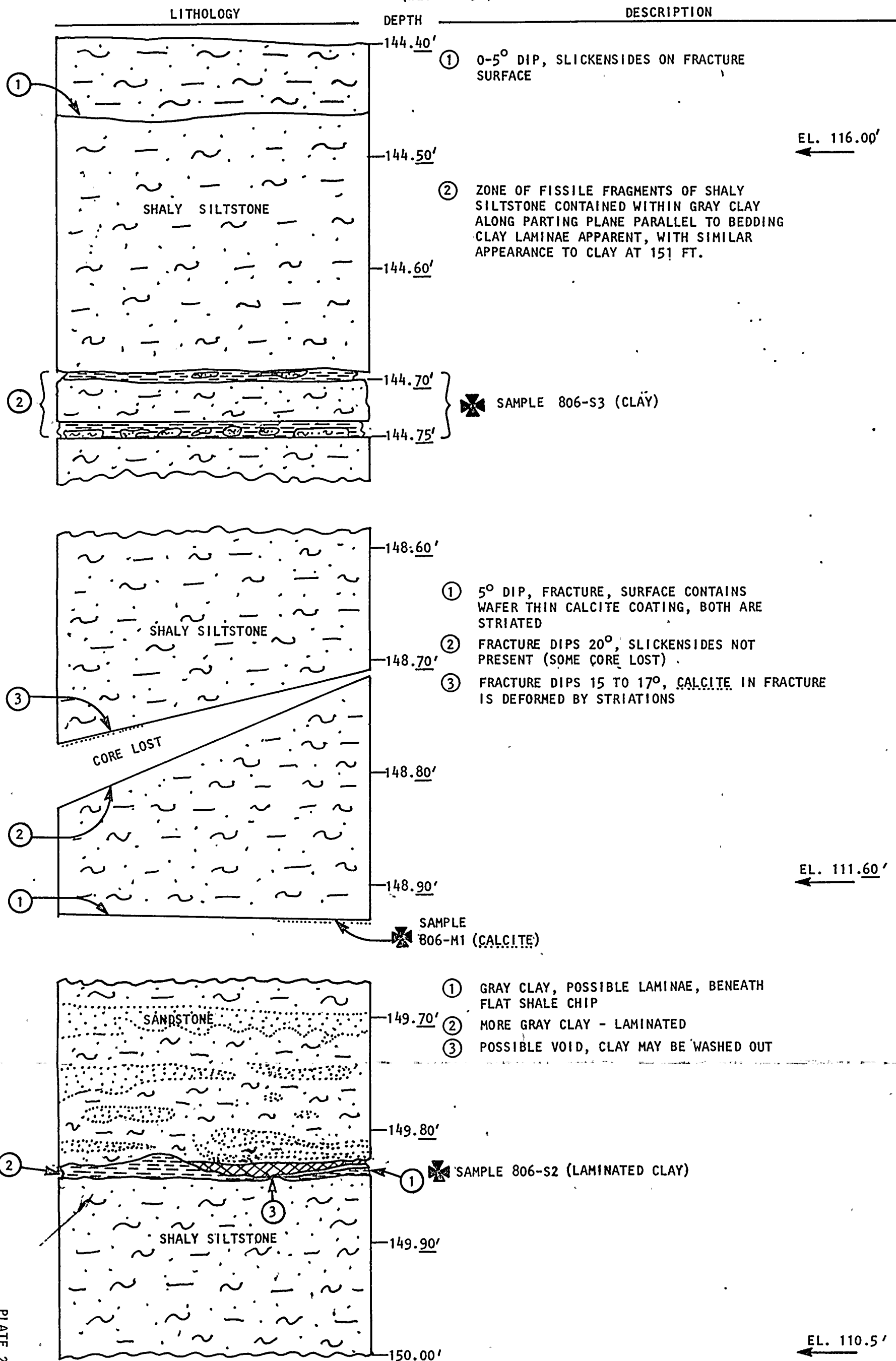
SHALE CLASTS

OCCURENCE OF MINERALIZATION

FOSSILS

CROSS-BEDS

DETAILED LOG OF PORTION OF BORING 806 (EL. 260.5')

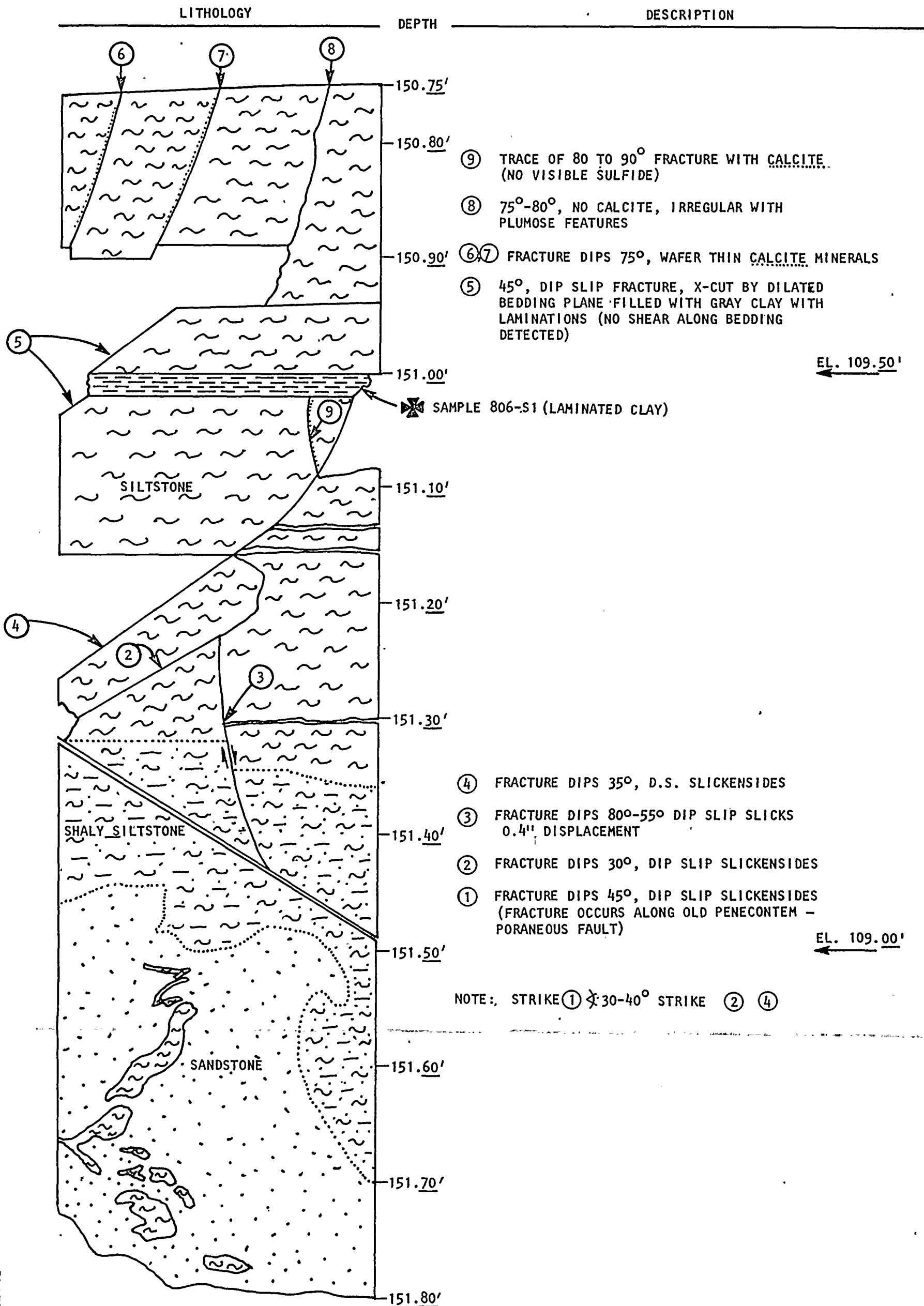


EL. 116.00'

EL. 111.60'

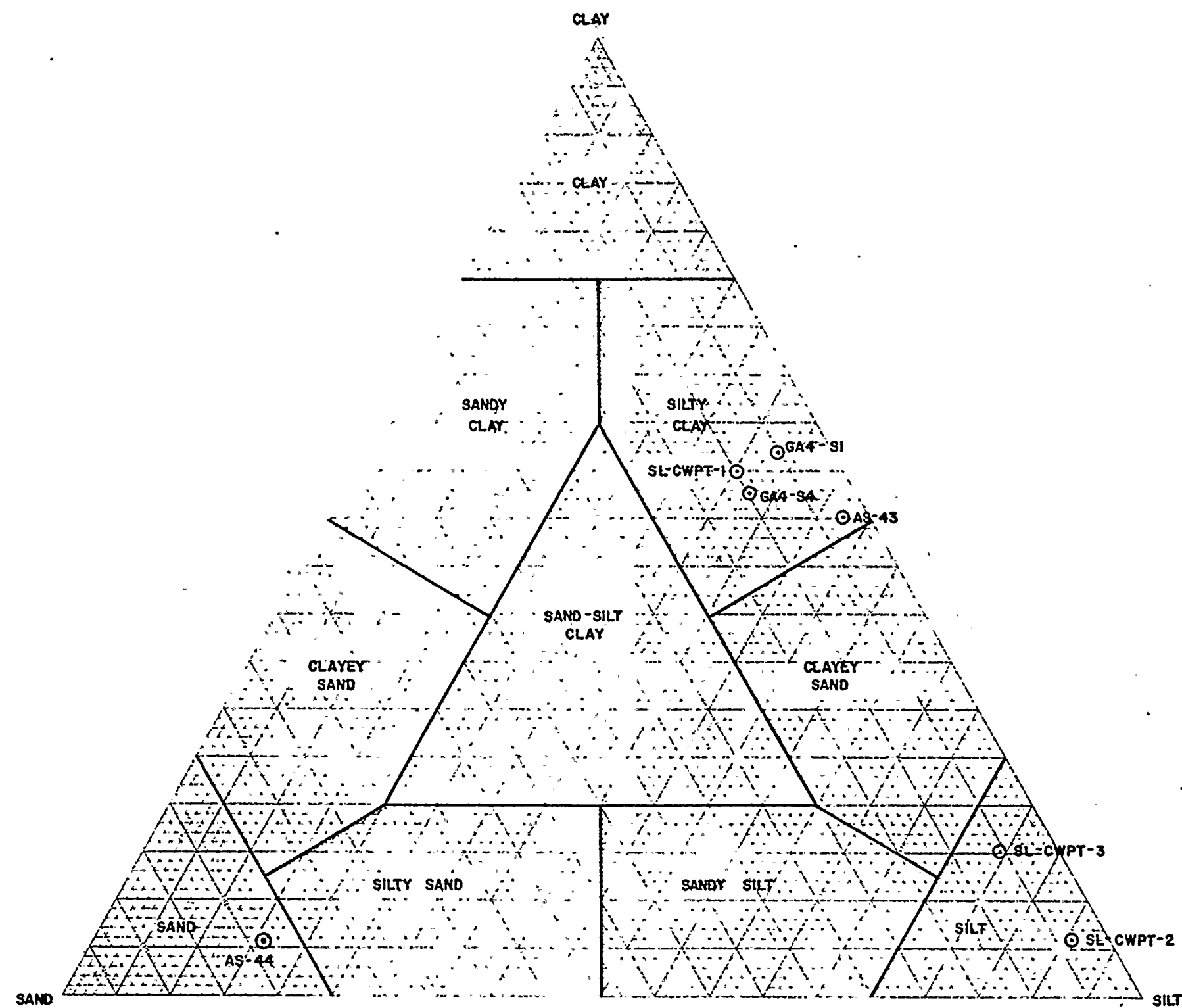
EL. 110.5'

DETAILED LOG OF PORTION OF BORING 806 (CONT'D) (EL. 260.5')



EL. 109.50'

EL. 109.00'



KEY:

- GA4 - NORTH RADWASTE TRENCH
- CWPT - CIRCULATING WATER PIPING TRENCH
- AS - TRENCH 4 ROCK SLOT

CLASSIFICATION OF SOIL SPECIMENS
FROM GRAIN SIZE ANALYSES

NOTE: CLASSIFICATION AFTER KRUMBEIN & SLOSS (1963)

LAKE ONTARIO

NINE MILE POINT
NUCLEAR GENERATING STATION

TRENCH 1

UNIT 1

UNIT 2

COOLING WATER
INTAKE SHAFT
RADWASTE FAULT

RS-4

TRENCH 2

RS-3

PIT 1

COOLING TOWER
EXCAVATION

COOLING TOWER FAULT

AXIS OF INFERRED SYNCLINE *

EXPLANATION:

— TRACE OF KNOWN STRUCTURE



TRENCH EXCAVATED TO INVESTIGATE THE COOLING TOWER FAULT



LOCATION OF OVERCORE BORING

* POSITION OF INFERRED SYNCLINE FROM N.Y.S. ELECTRIC
AND GAS CORP., 1979, NEW HAVEN UNITS 1 AND 2 PSAR,
AMENDMENT 1, FIG. 2.5-9.

INTAKE AND DISCHARGE TUNNELS

NORMAL FAULT

BARGE SLIP

"TEPEE FOLD"

JAMES A. FITZPATRICK
NUCLEAR POWER PLANT

RS-1

TRENCH 5

OC-2

OC-1

PLANT
NORTH



SCALE
0 200 400 600 800 FEET

SITE LOCATION MAP

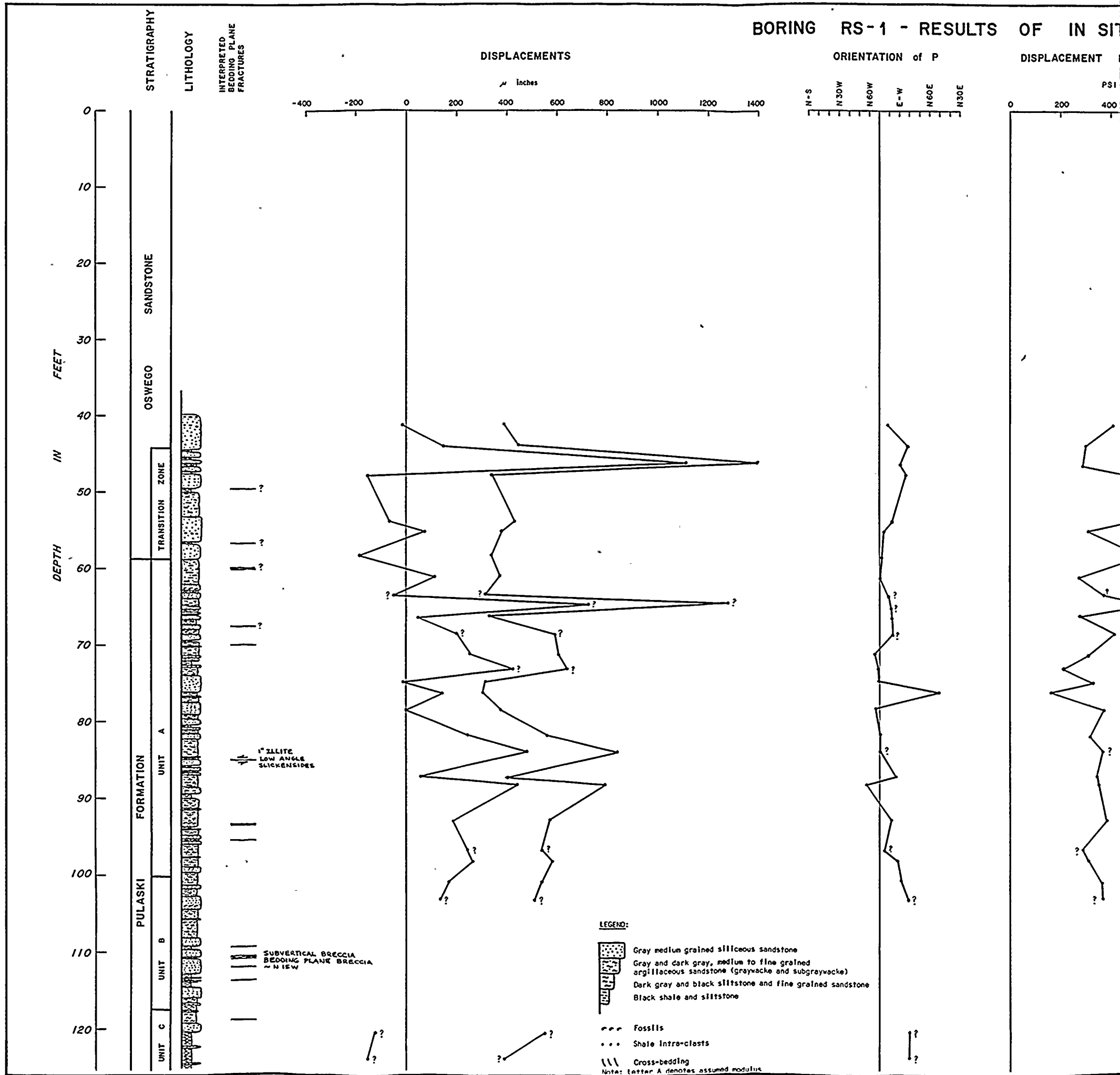
SHOWING LOCATIONS OF KNOWN WNW TRENDING STRUCTURES
AND RELATED TRENCHES, EXCAVATIONS AND DRILLING SITES
AT NINE MILE POINT NUCLEAR GENERATING STATION
SCRIBA, NEW YORK

PLATE 3-1

DAMES & MOORE

NOTE:
Final Safety Analysis Report for James A. Fitzpatrick
Nuclear Generating Station was the property of the
State of New York, 1979, 2nd edition, section 2.4.

BORING RS-1 - RESULTS OF IN SITU



STRESS DETERMINATIONS

DIFFERENCE

MODULUS

STRESS

STRESS DIFFERENCE

$\times 10^6$ PSI

PSI

PSI

600 800

0 1 2 3 4 5 6 7 8

-400 -200 0 200 400 600 800 1000

0 200 400 600

270

260

250

240

230

220

210

200

190

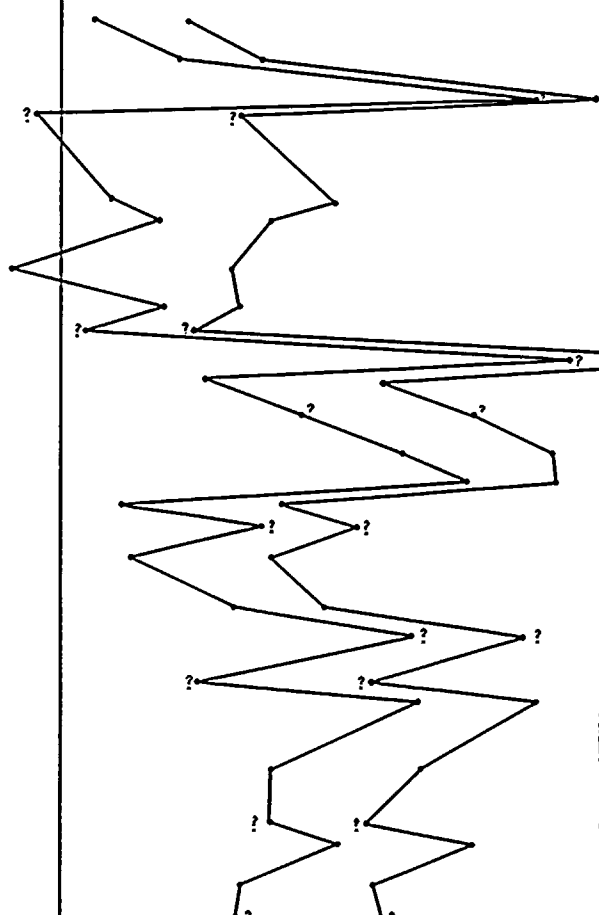
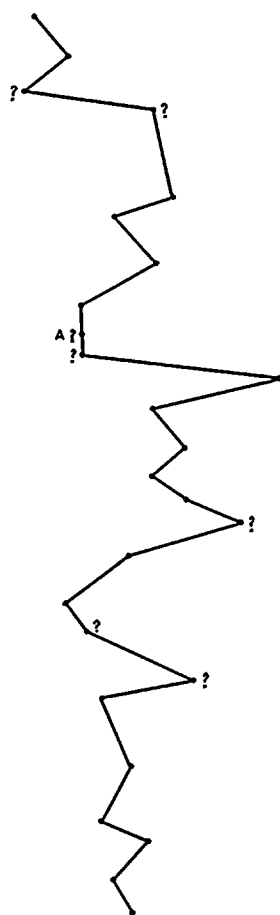
180

170

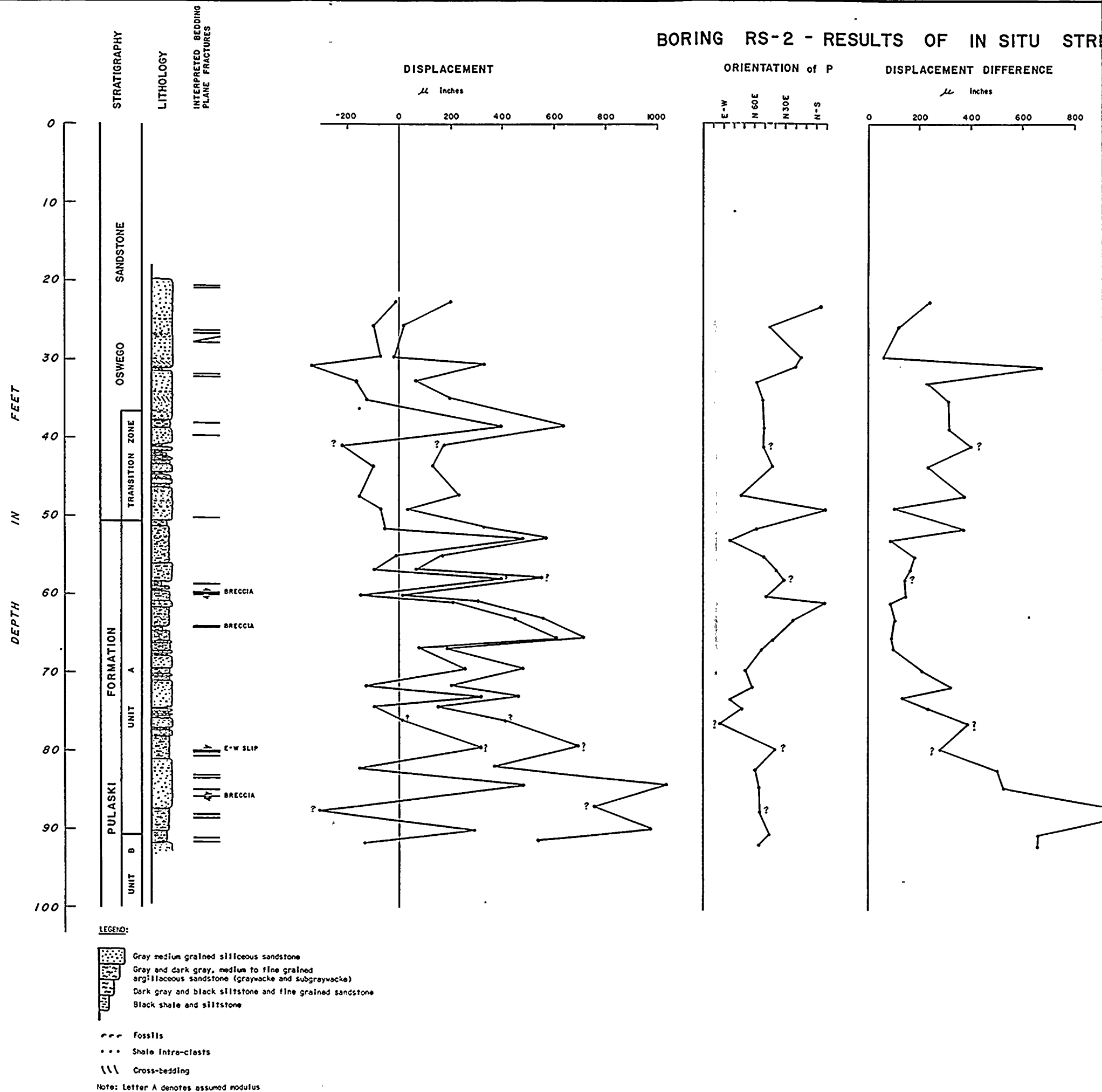
160

150

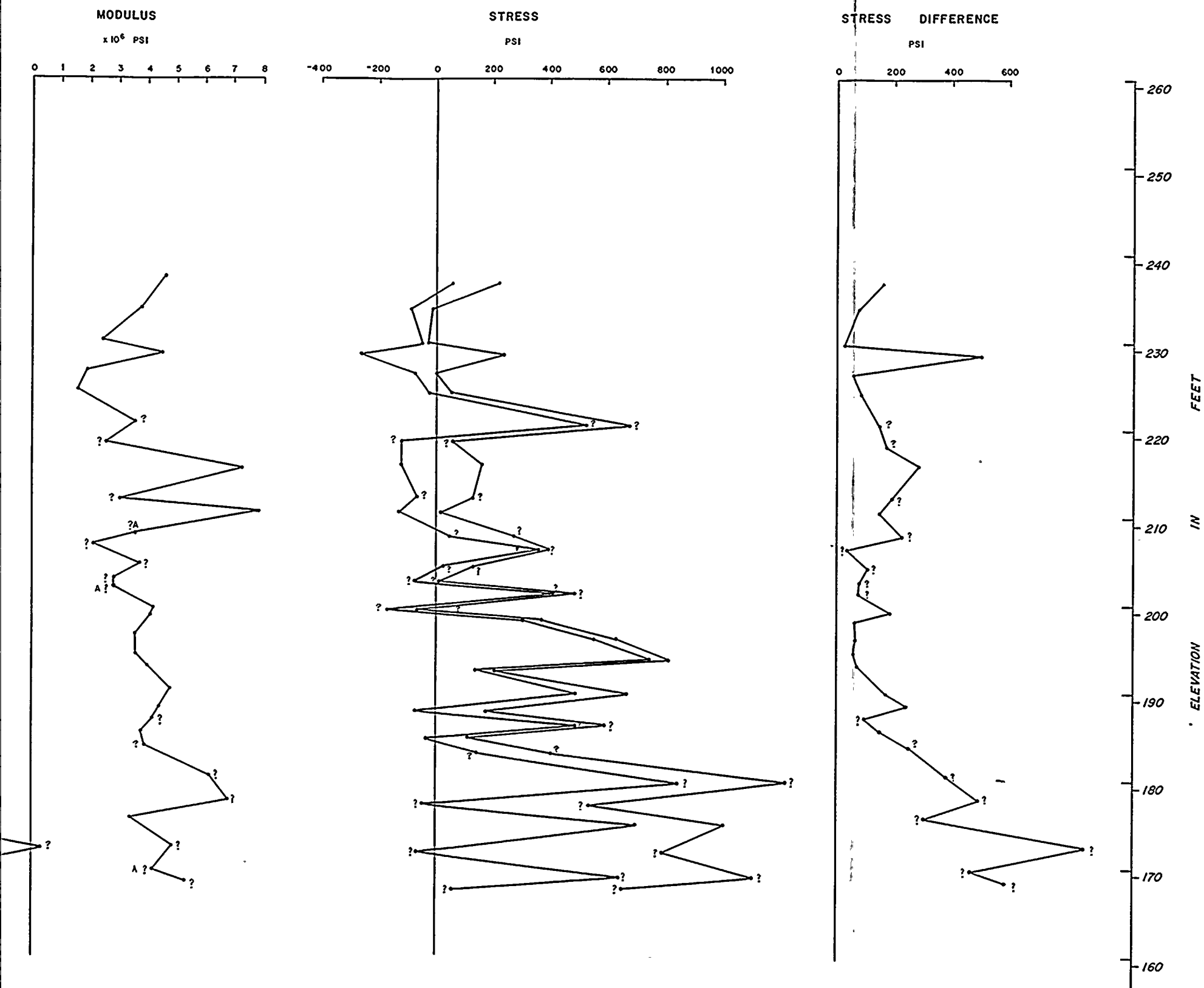
ELEVATION
IN
FEET

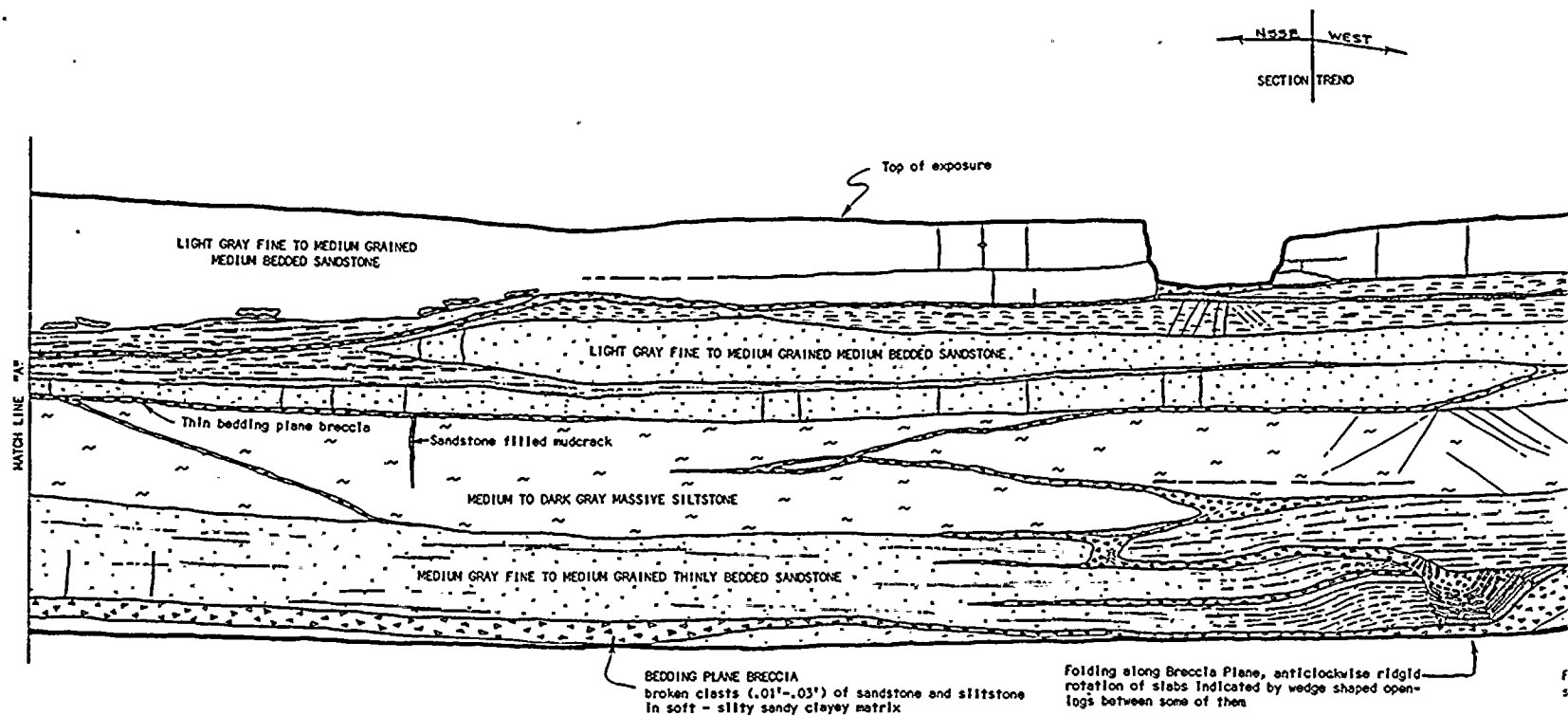
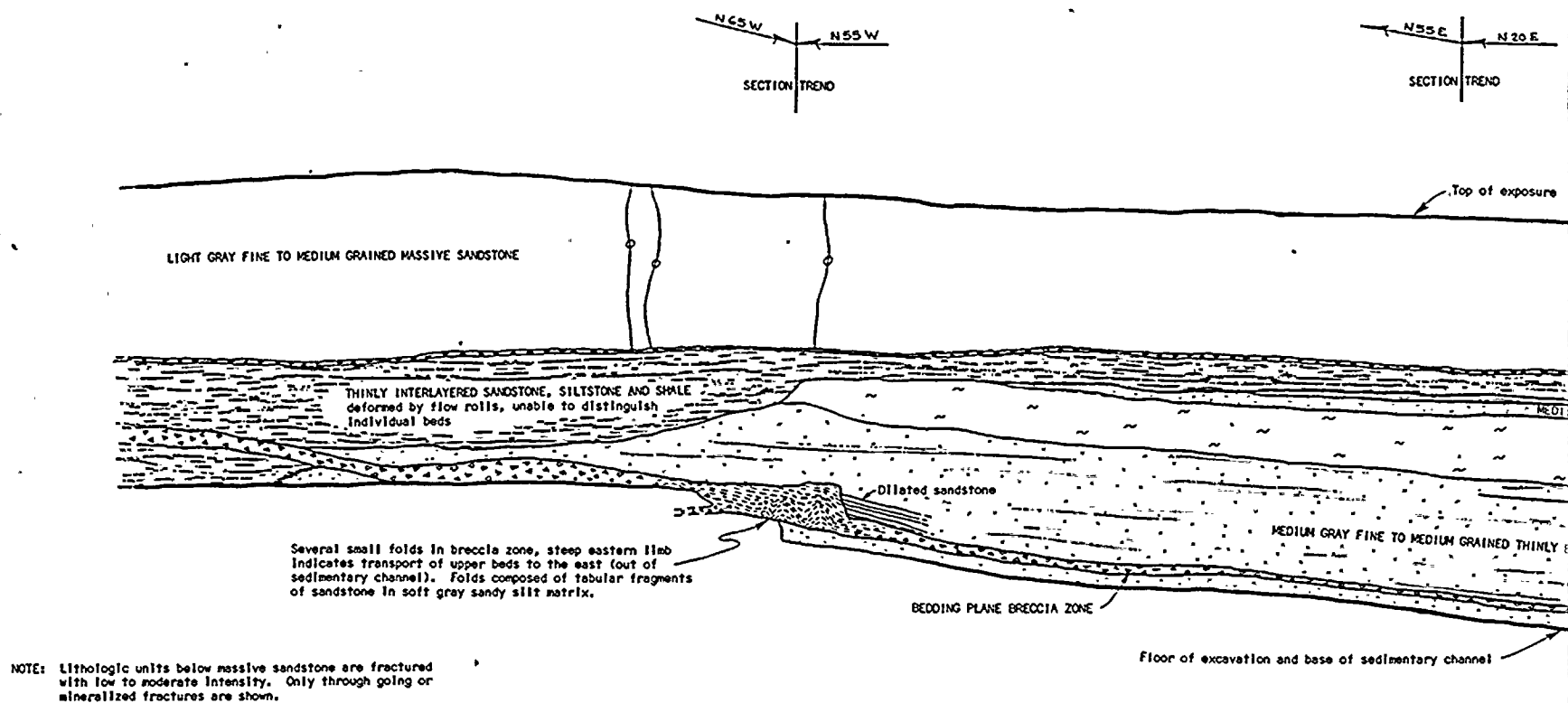


BORING RS-2 - RESULTS OF IN SITU STR



ESS DETERMINATIONS

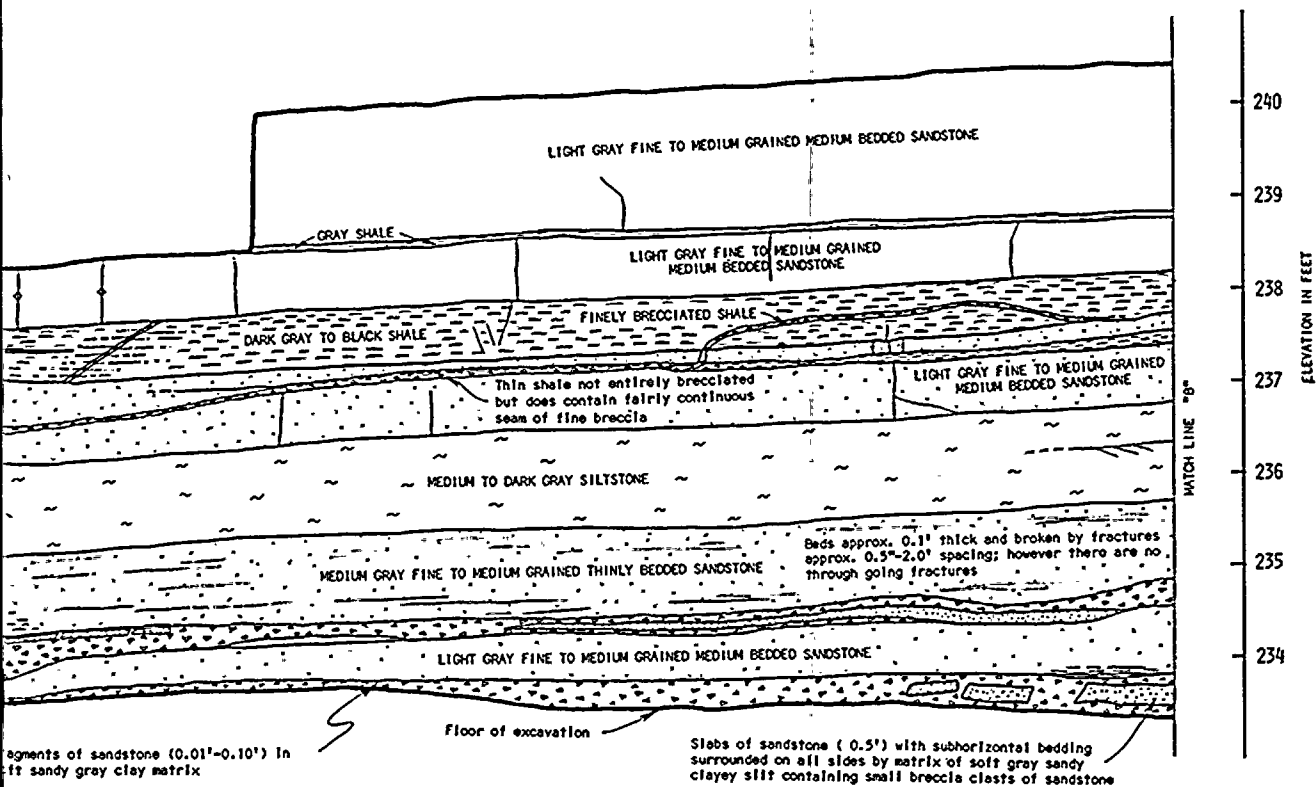
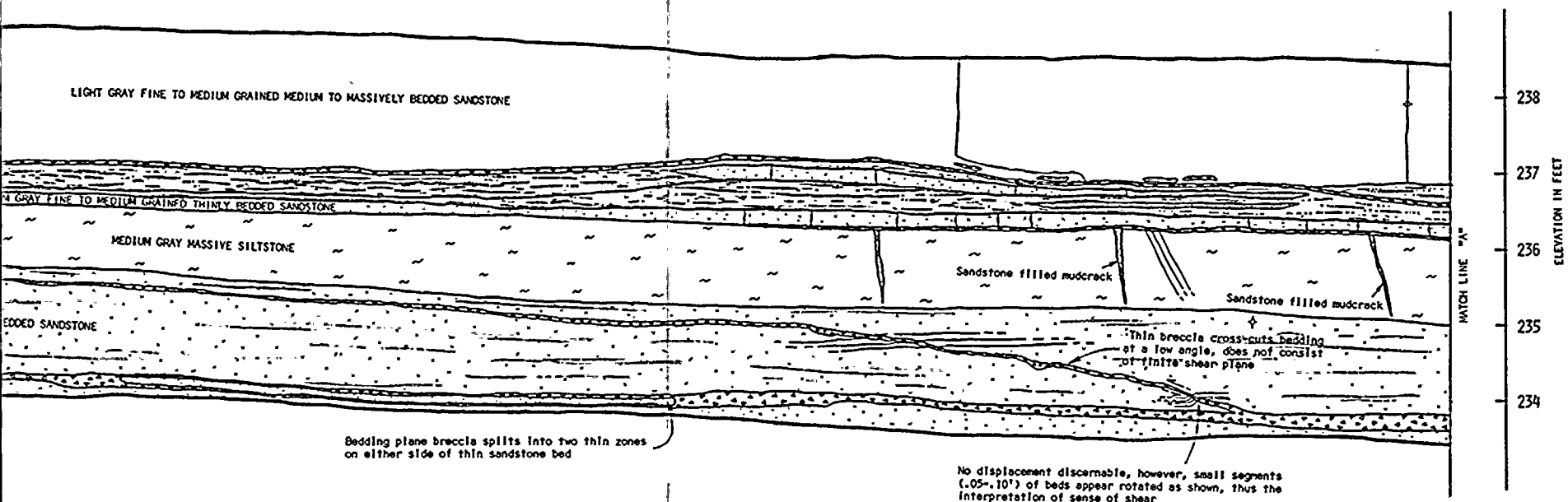




N 20 E
SECTION TREND

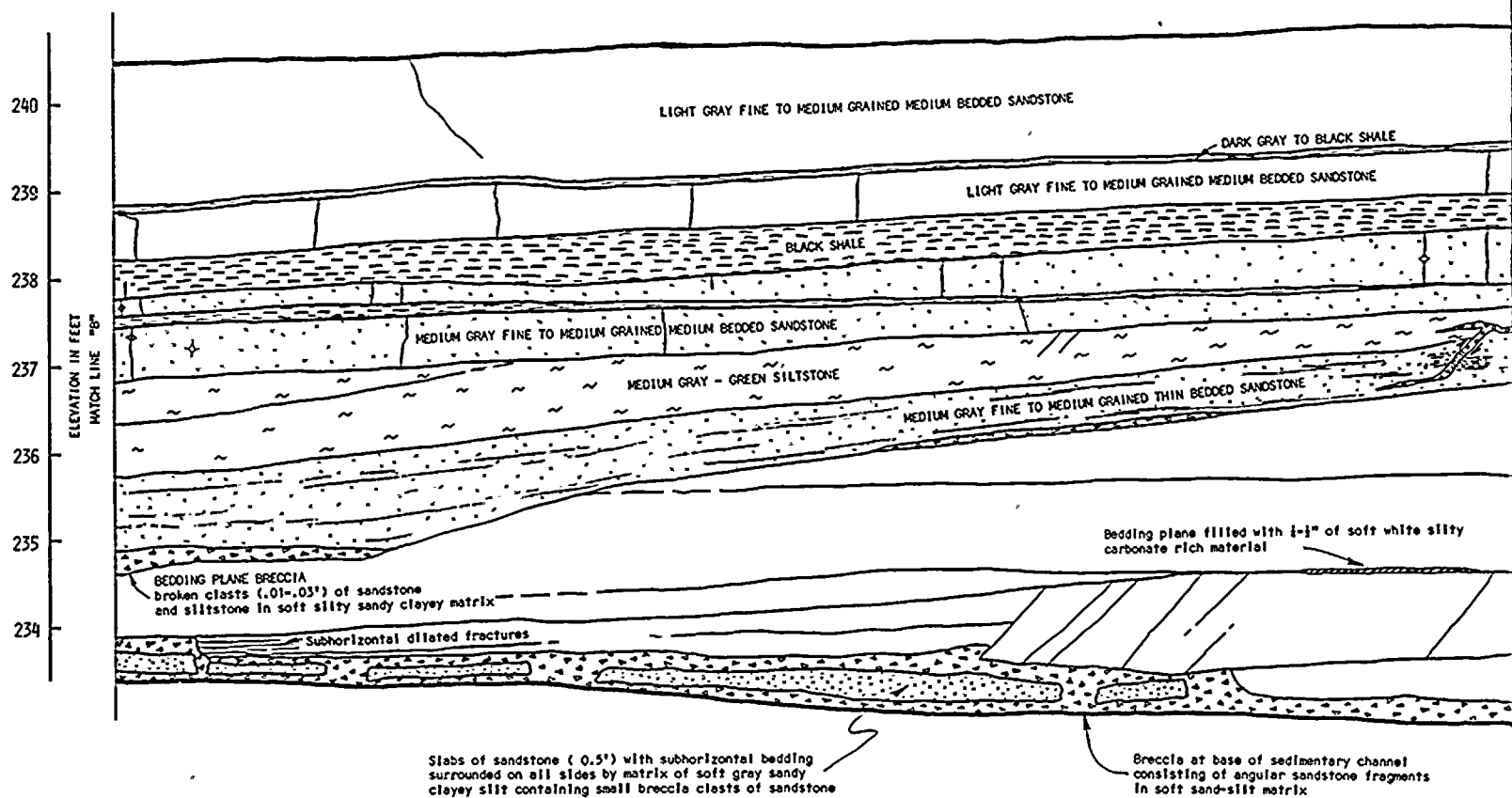
N 10 W
SECTION TREND

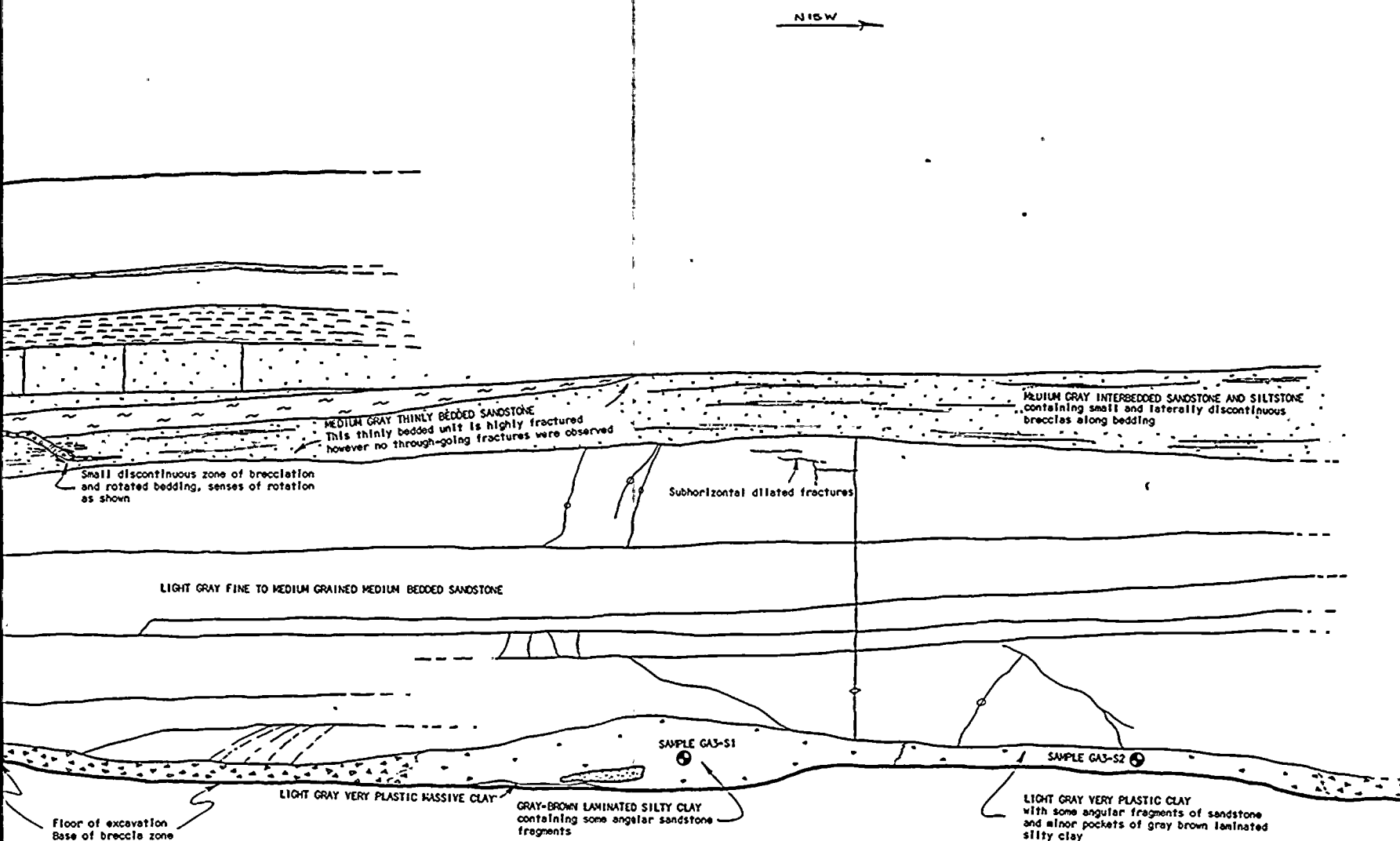
N 35 W
SECTION TREND



CROSS SECTION OF WALLS OF UPPER SUMP TRENCH IN CIRCULATING WATER PIPING TRENCH EXCAVATION

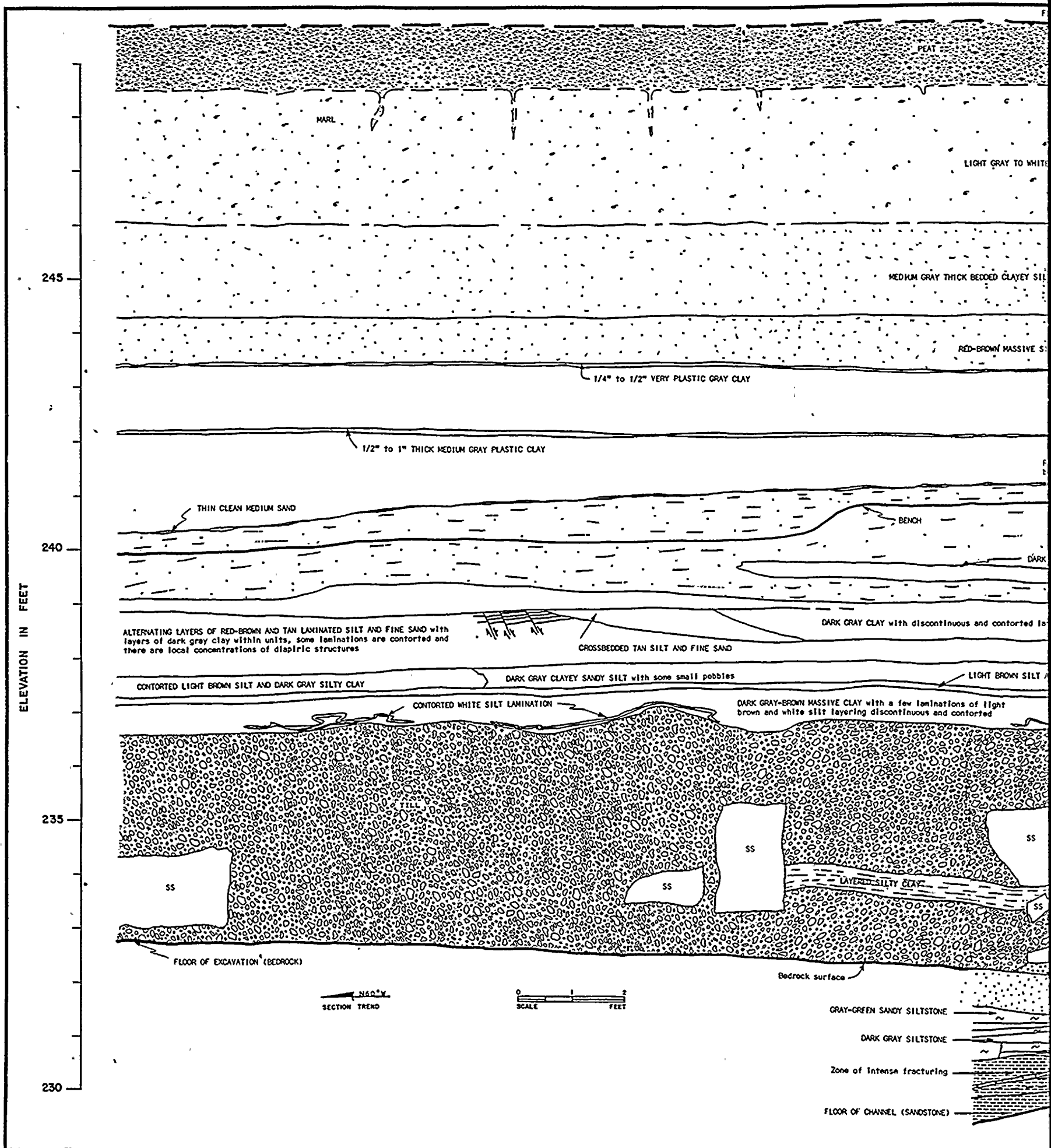
NOTE: Location of cross section shown on plate 2.1-2

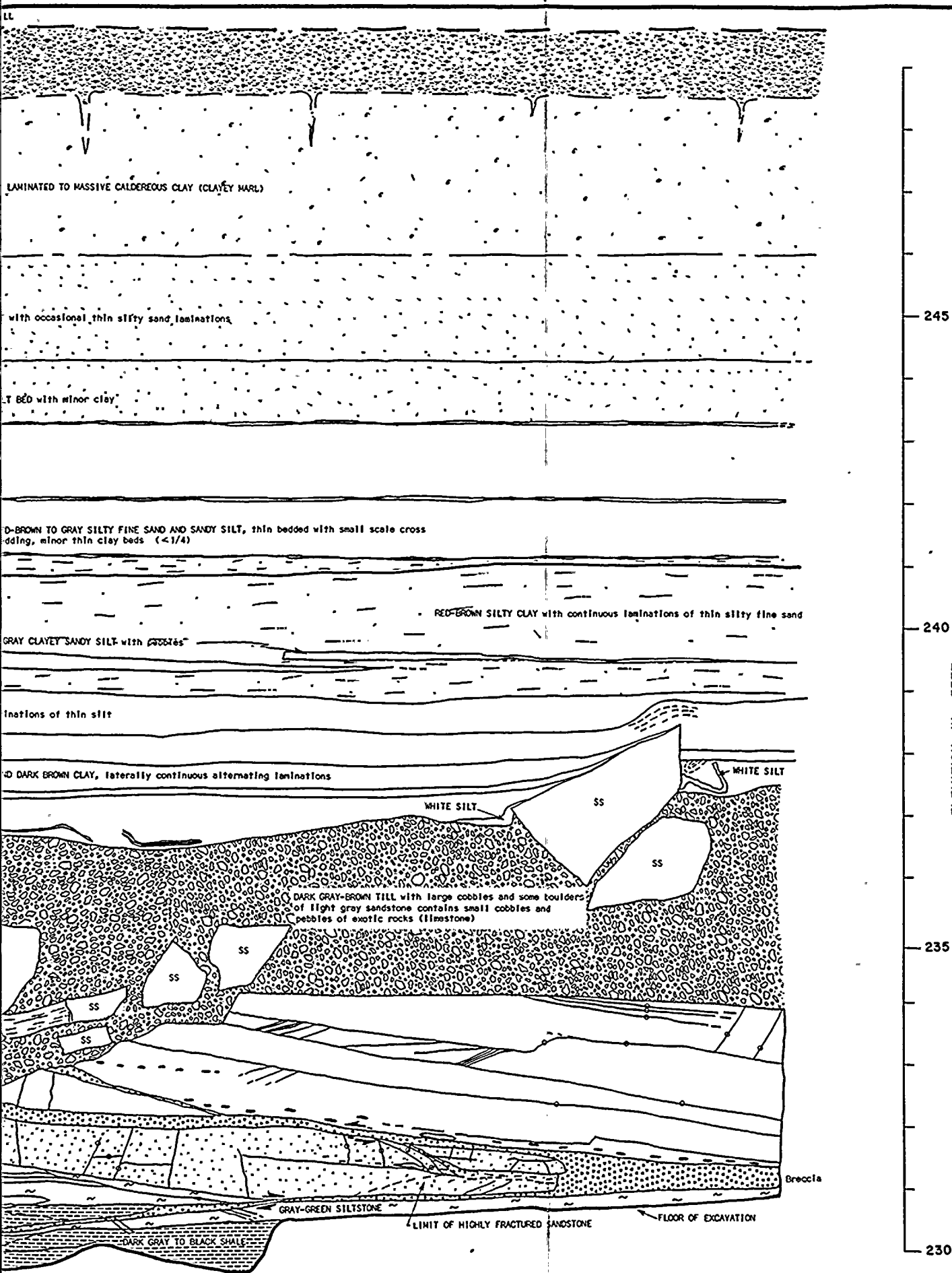




**CROSS SECTION OF WALL OF UPPER SUMP TRENCH
IN CIRCULATING WATER PIPING TRENCH EXCAVATION**

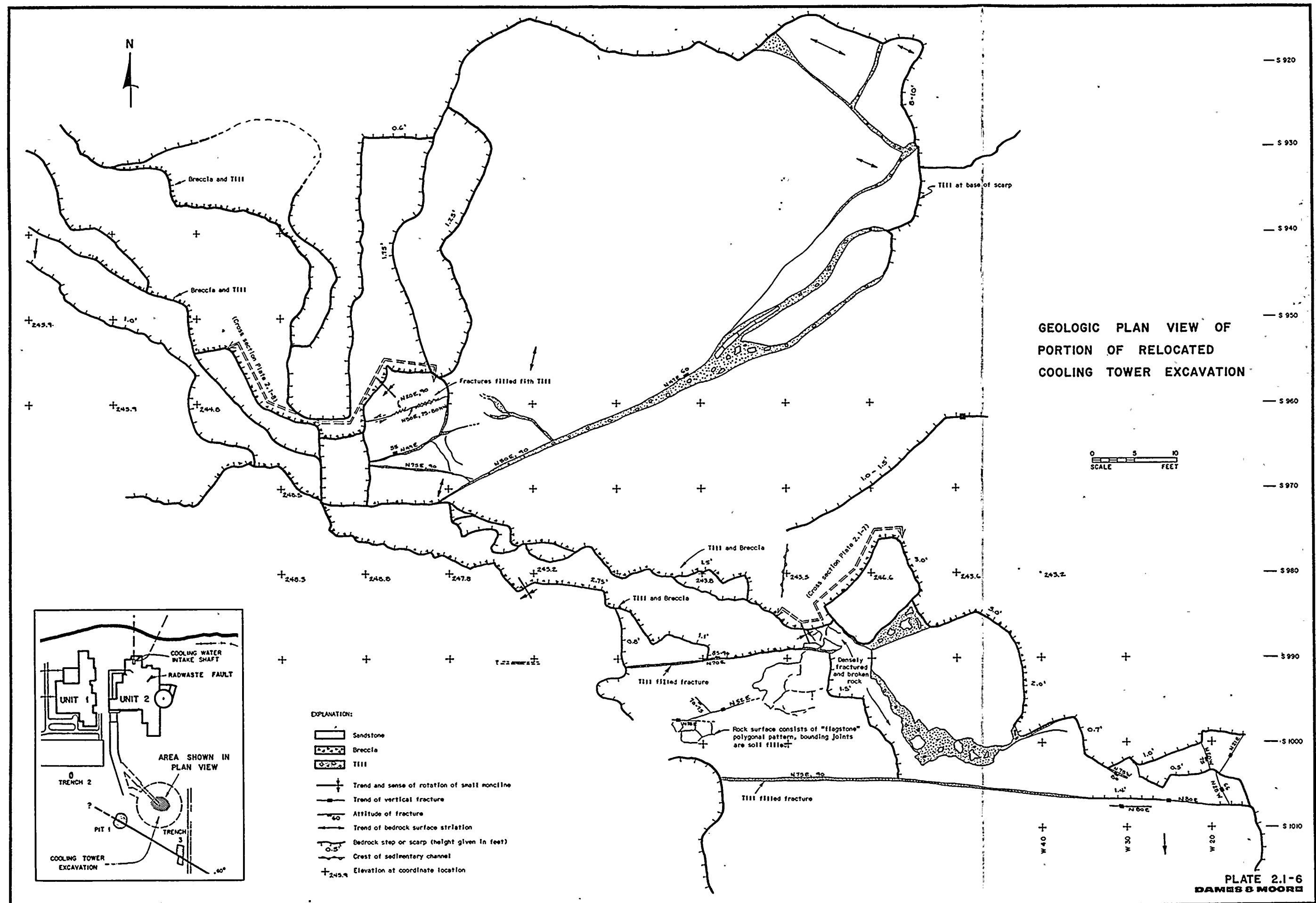
NOTE: Location of cross section shown on plate 2.1-2

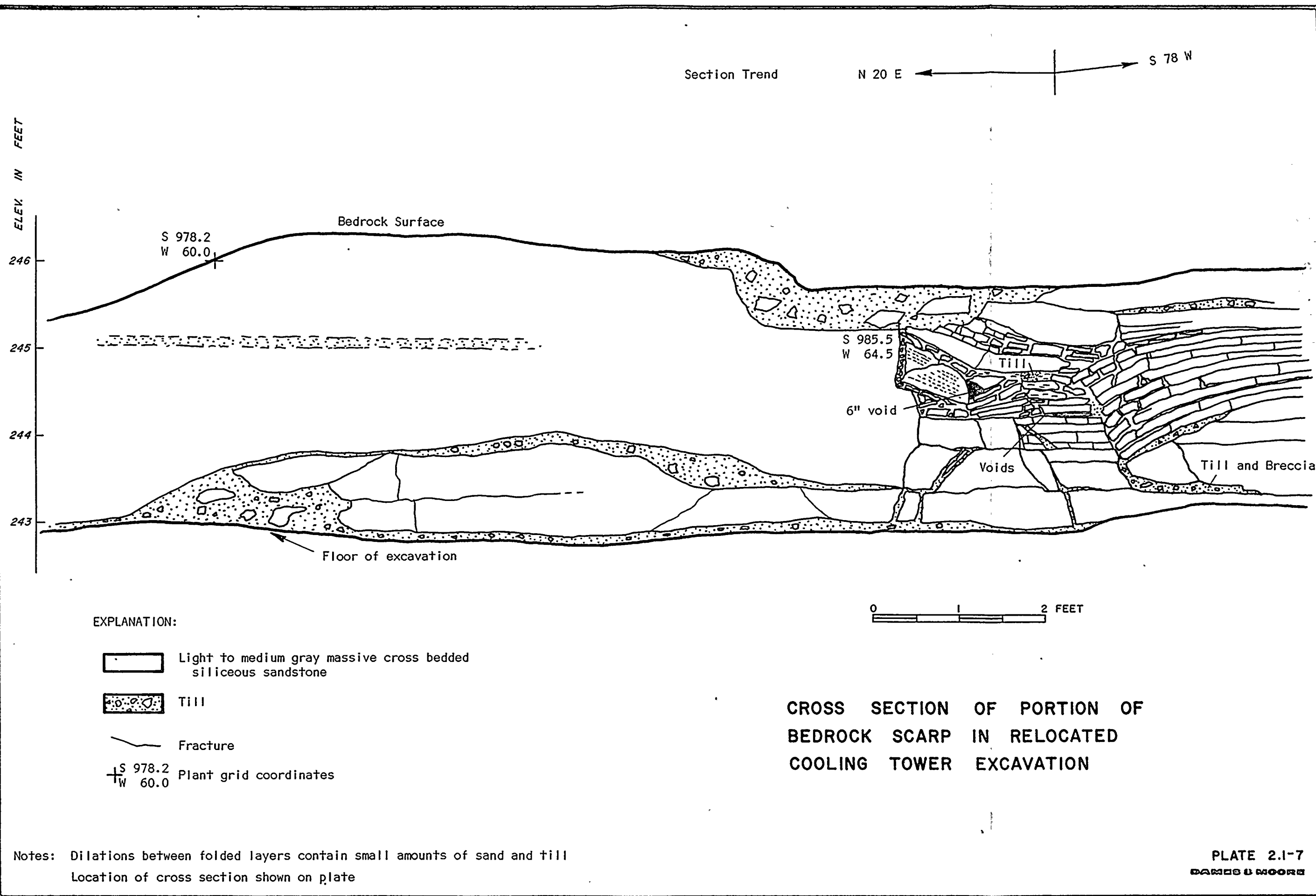


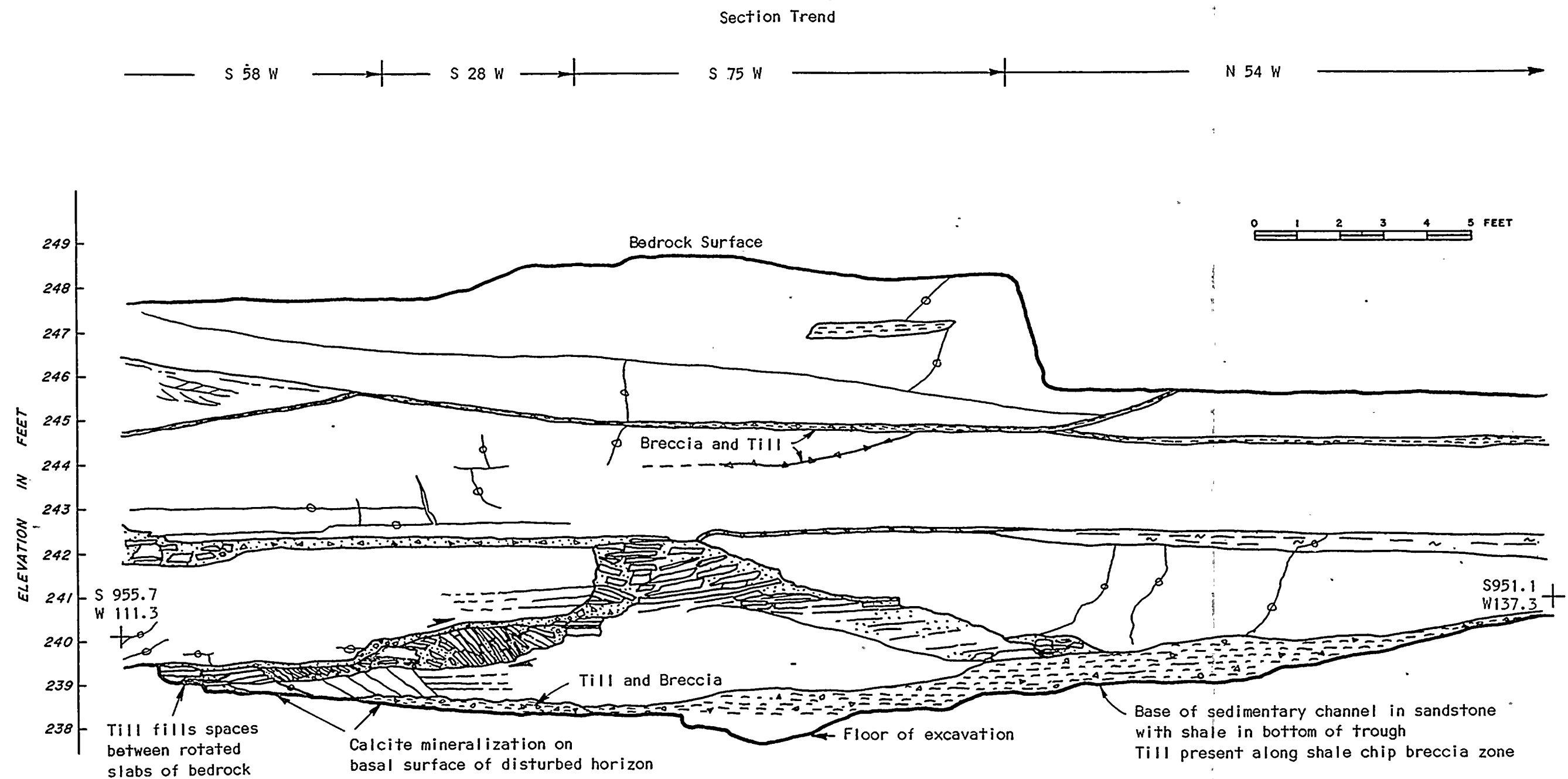


CROSS SECTION
OF NORTHEAST WALL
OF LOWER SUMP TRENCH
IN CIRCULATING WATER
PIPING TRENCH EXCAVATION

NOTE: Location of cross section shown on plate 2.1-2



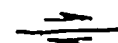




EXPLANATION:

- Light to medium gray massive siliceous sandstone
- Black shale
- Breccia
- Till

- Fracture
- Open Fracture



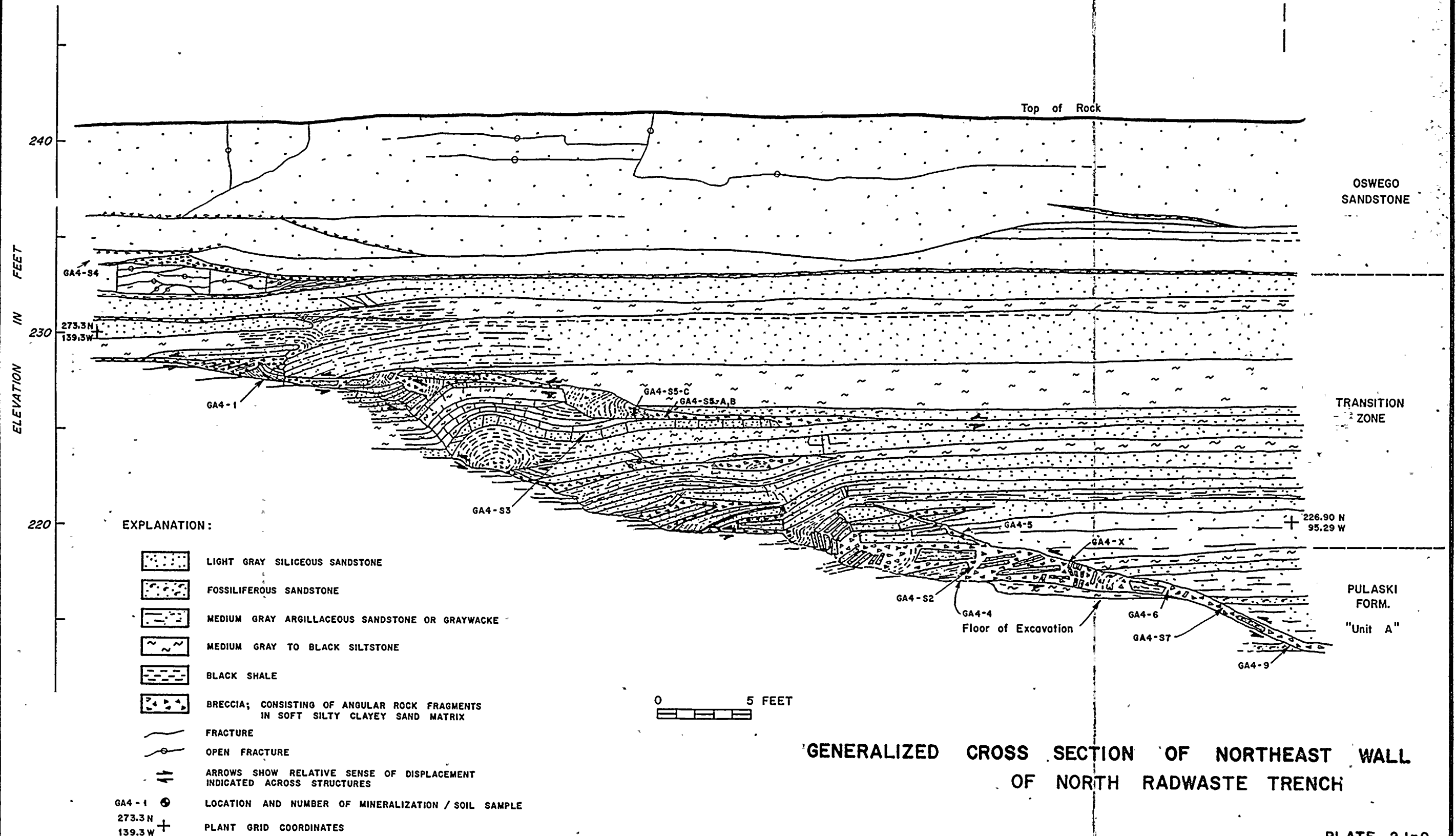
Arrows indicate relative sense of displacement

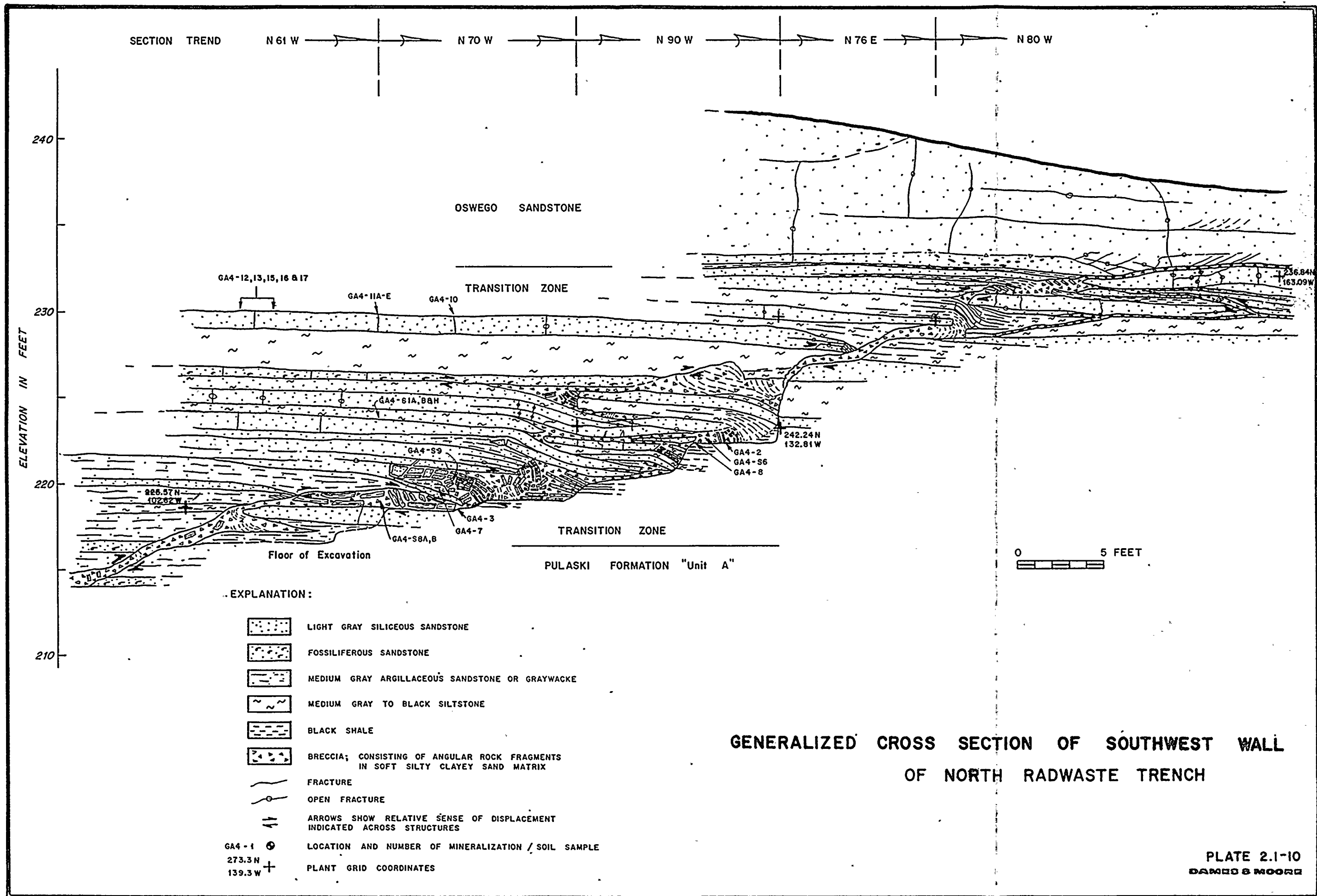
S 955.7
W 111.3 +

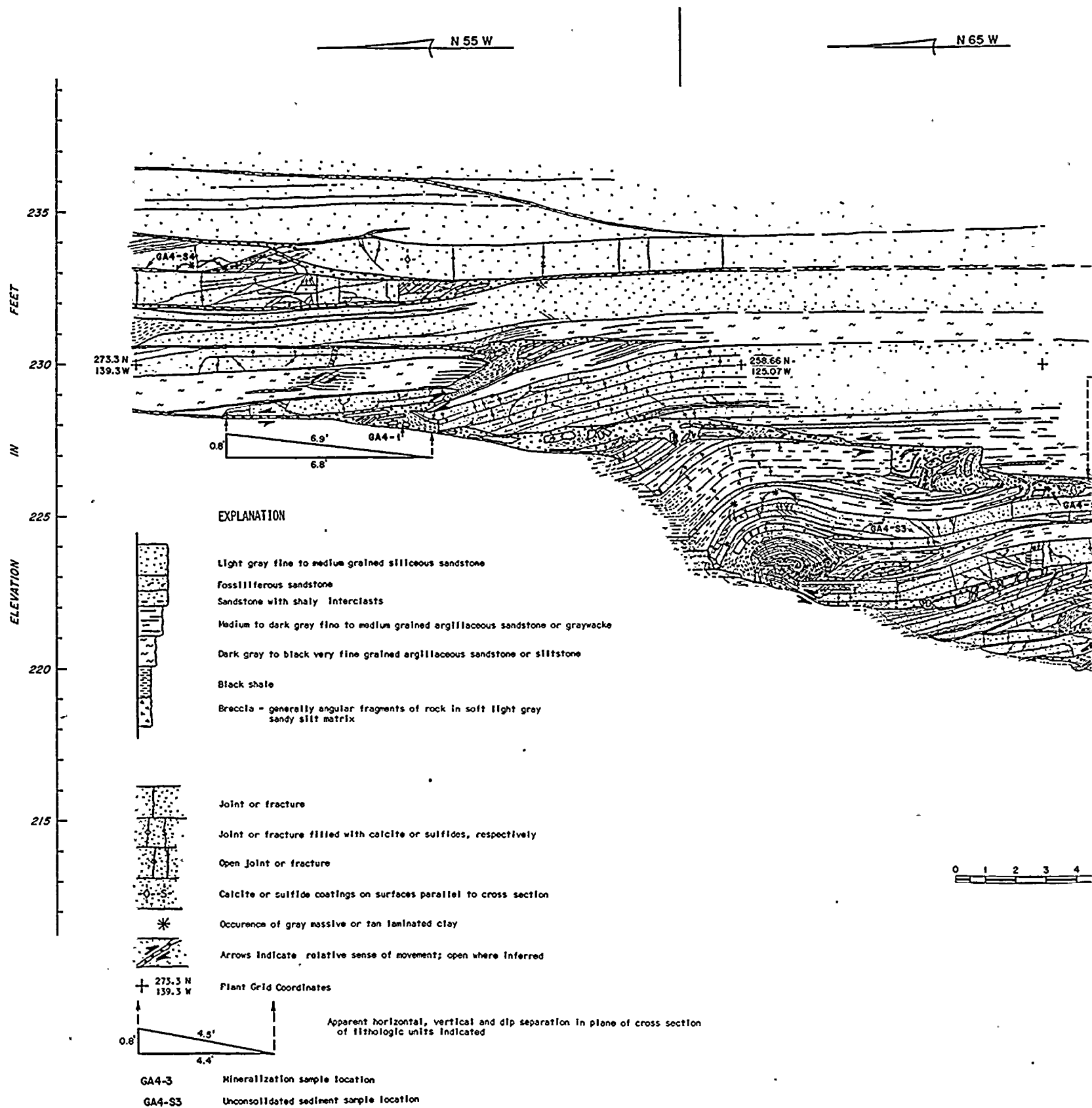
Plant grid coordinates

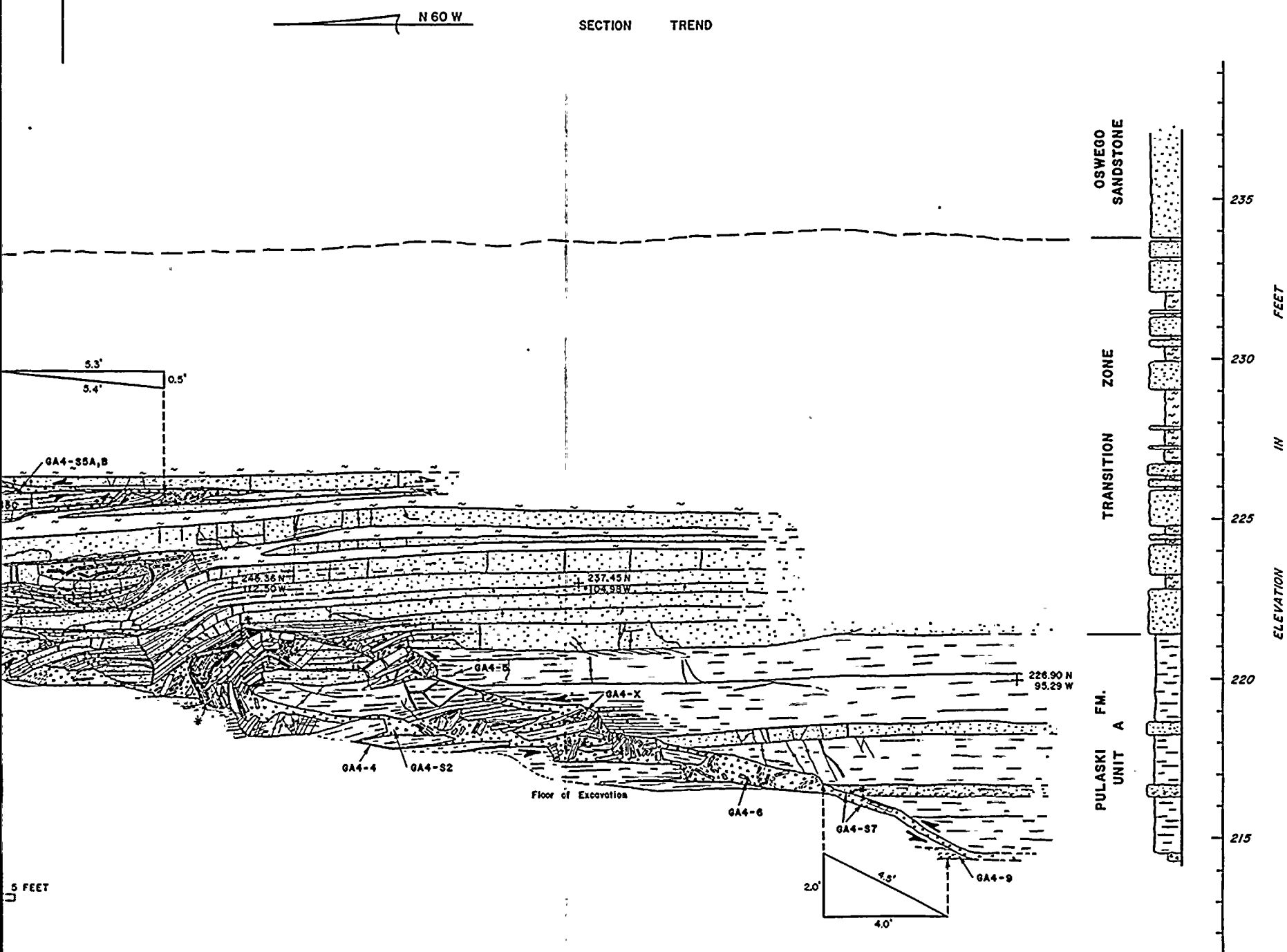
**CROSS SECTION OF PORTION OF BEDROCK
SCARP IN RELOCATED COOLING TOWER
EXCAVATION**

N 60 W SECTION TREND

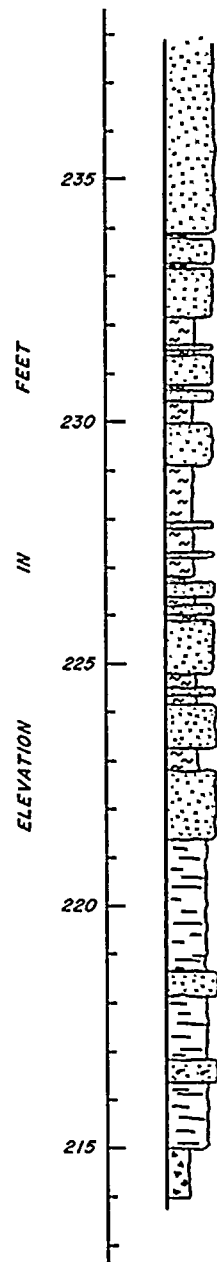








DETAILED CROSS SECTION - NORTHEAST WALL, NORTH RADWASTE TRENCH



OSWEGO
SANDSTONE

TRANSITION
ZONE

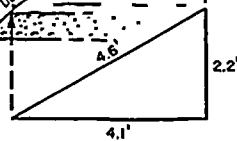
PULASKI FM.
UNIT A

N 88 W

N 60 W

N 72 W

Floor of Excavation



0 1 2 3 4 5 FEET

GA4-S1, A, B, H

235-15 N
111, 28 W

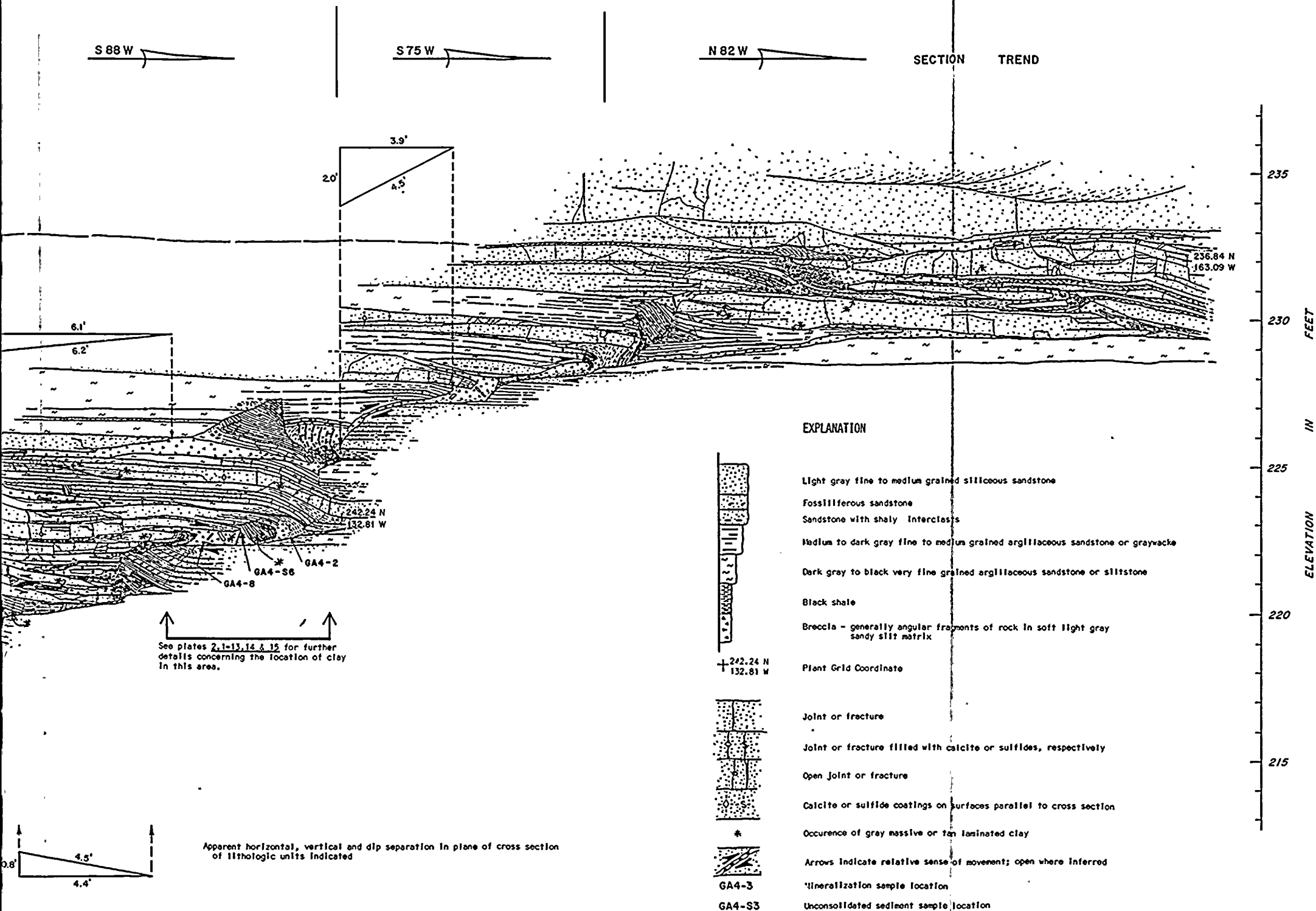
GA4-SBB

GA4-SBA

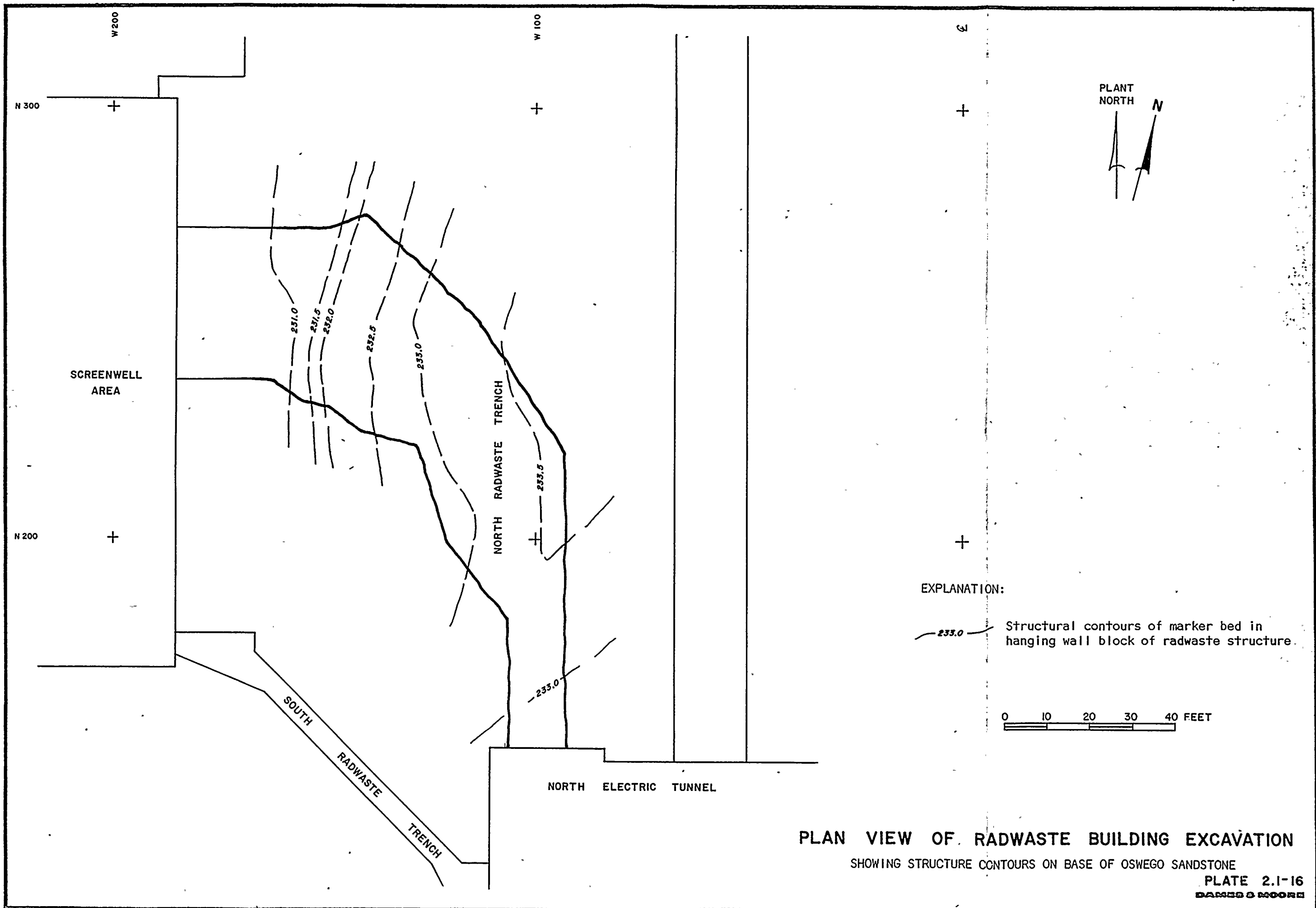
GA4-7

GA4-3

0.6'

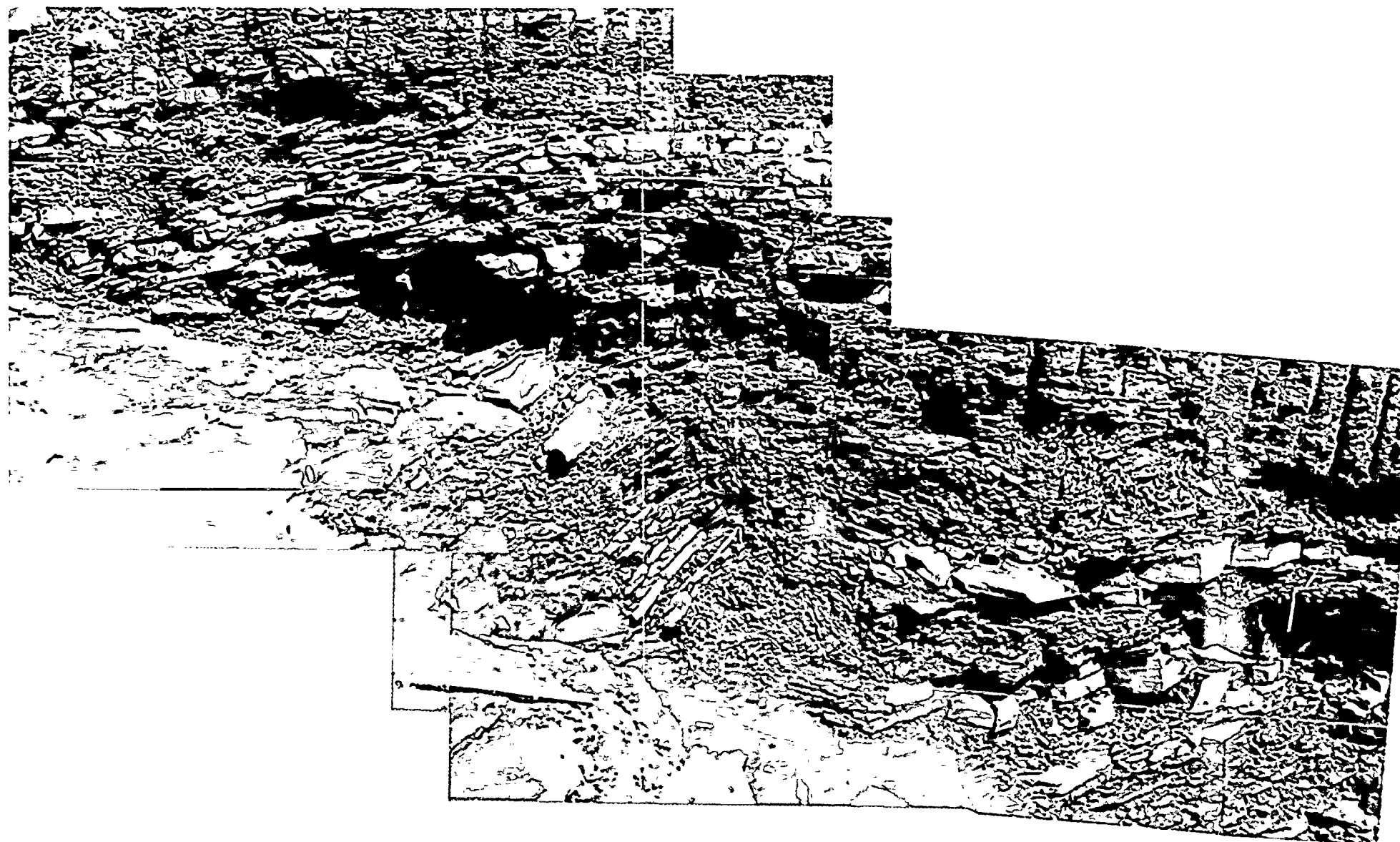


DETAILED CROSS SECTION - SOUTHWEST WALL, NORTH RADWASTE TRENCH

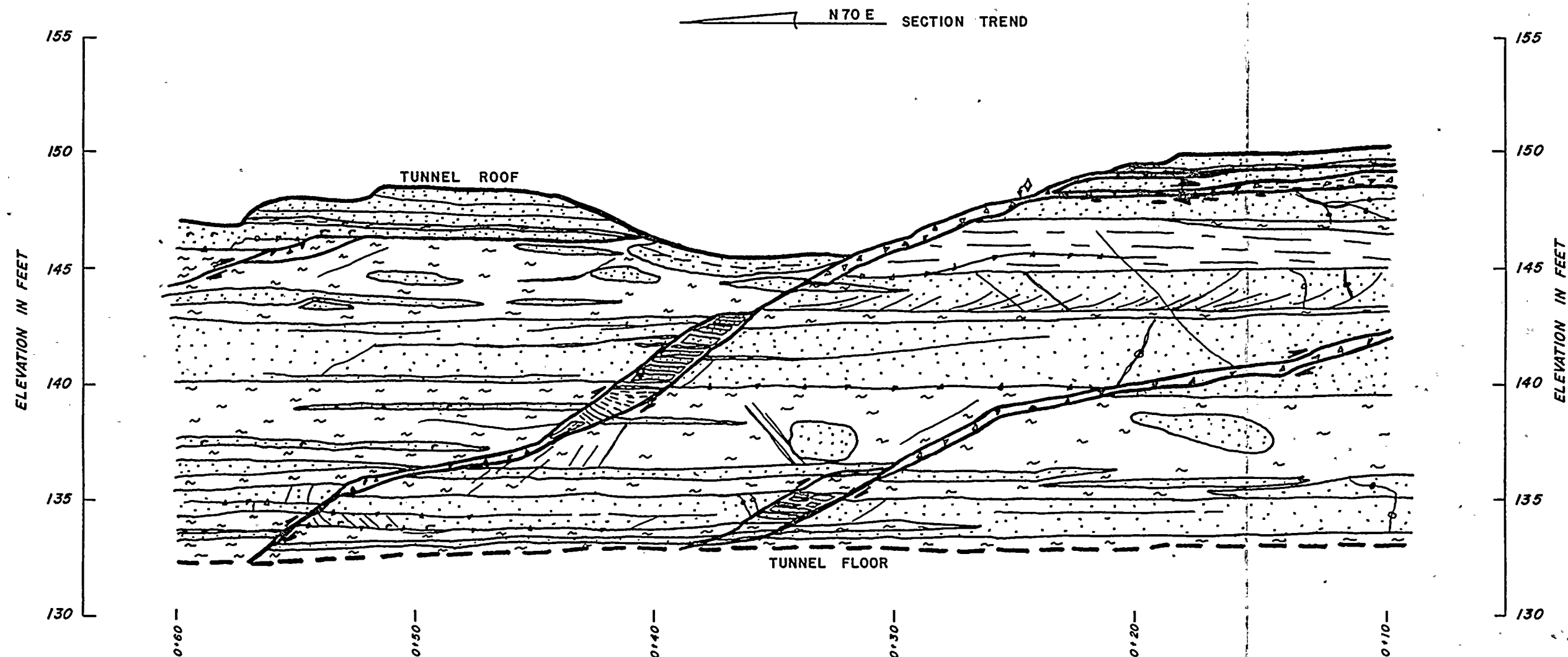


PLAN VIEW OF RADWASTE BUILDING EXCAVATION

SHOWING STRUCTURE CONTOURS ON BASE OF OSWEGO SANDSTONE



PHOTOGRAPH OF PORTION OF NORTHEAST WALL,
NORTH RADWASTE TRENCH



EXPLANATION:



Light gray fine to medium grained siliceous sandstone
 Fossiliferous sandstone
 Sandstone with shaly interclasts
 Medium dark gray fine to medium grained argillaceous sandstone or graywacke
 Dark gray to black very fine grained argillaceous sandstone or siltstone
 Black shale
 Breccia - generally angular fragments of rock in soft light gray sandy silt matrix



Joint or fracture
 Joint or fracture filled with calcite or sulfides, respectively
 Open joint or fracture
 Calcite or sulfide coatings on surfaces parallel to cross section
 Arrows indicate relative sense of movement; open where inferred

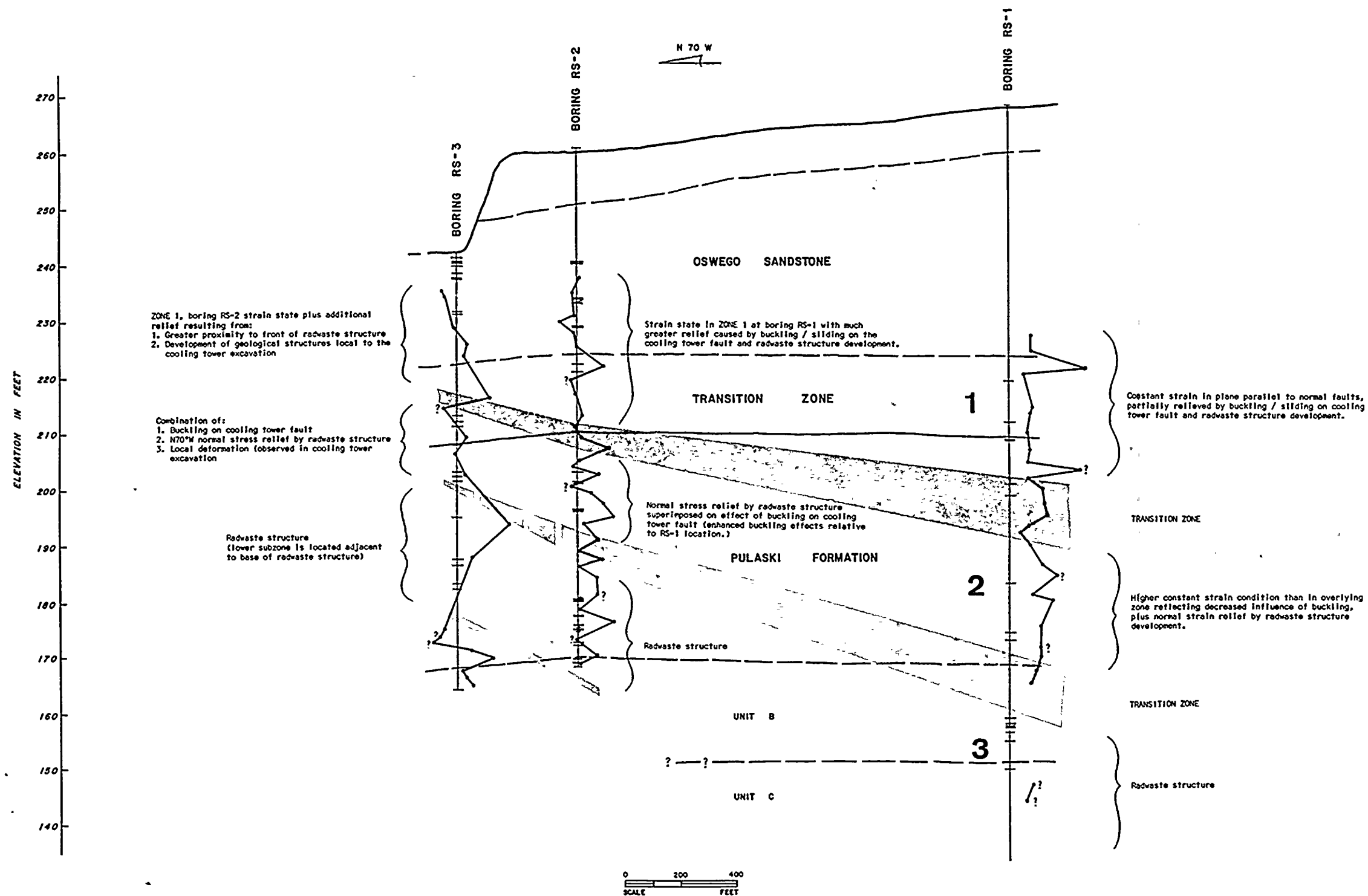
0 5 10 FEET

CROSS SECTION - RIGHT RIB,

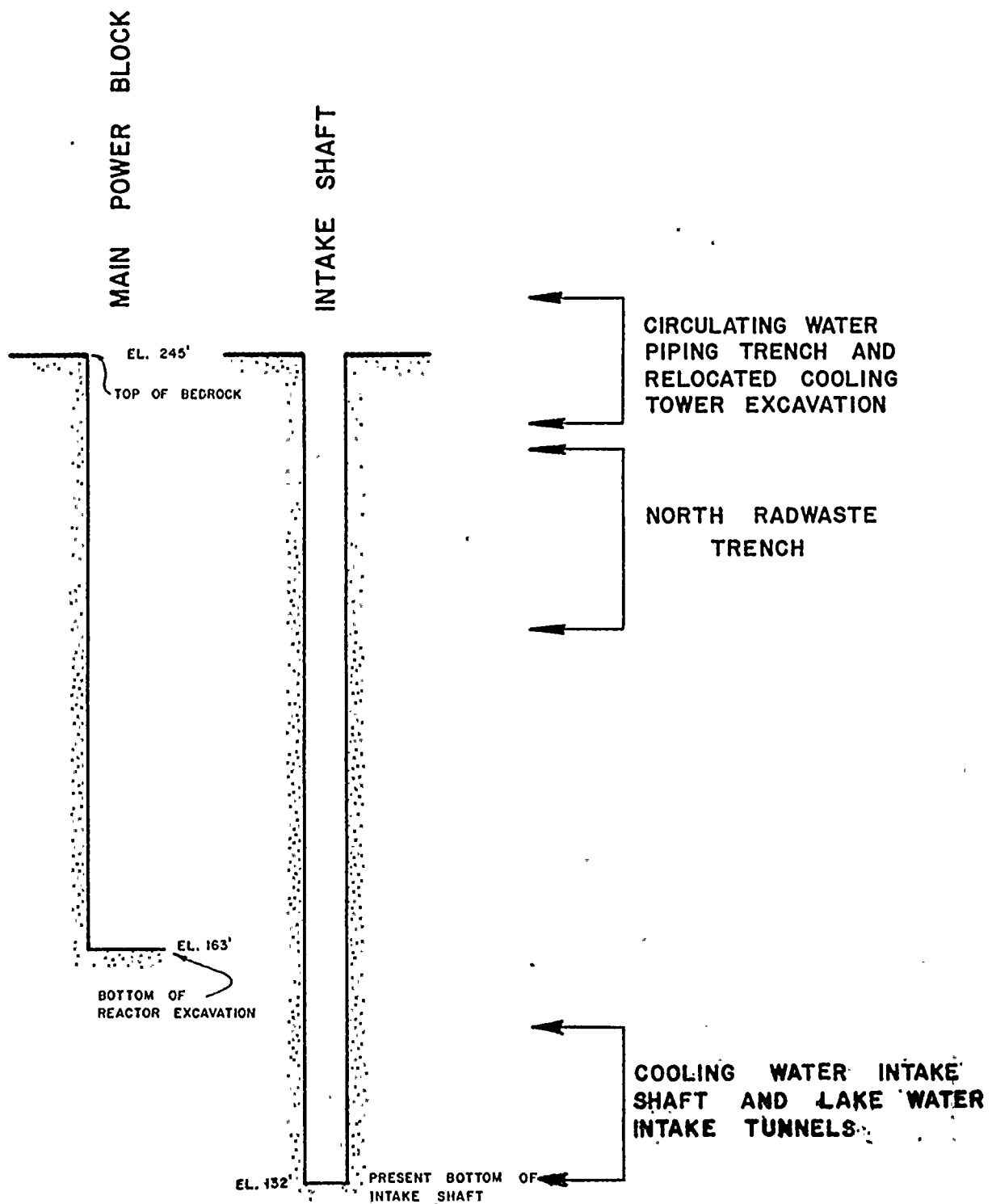
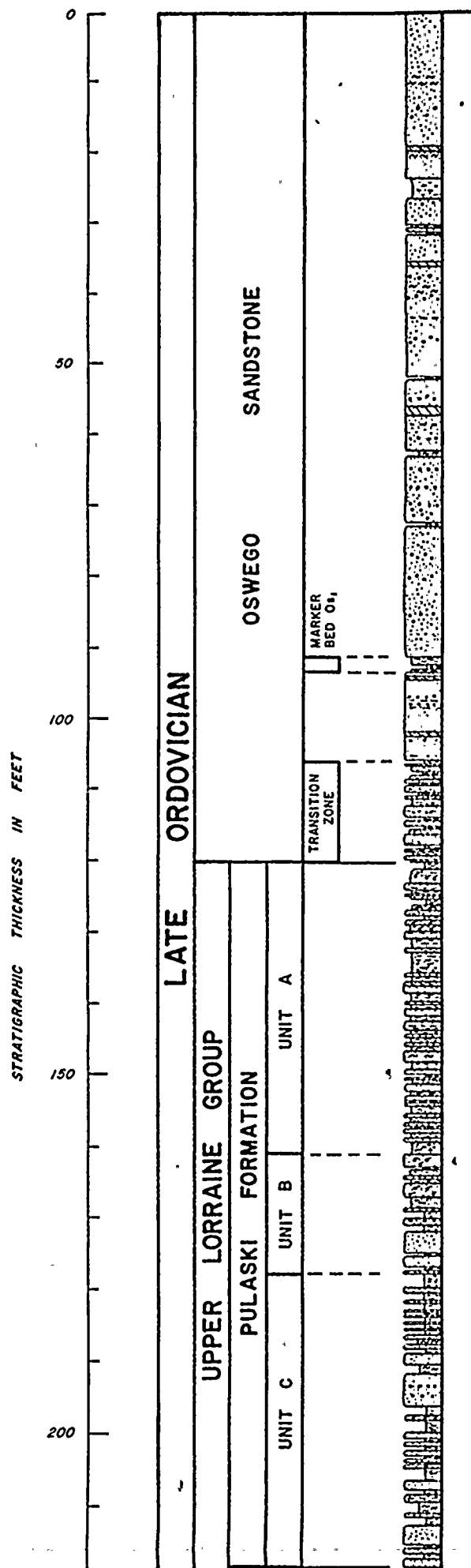
EAST INTAKE TUNNEL

STATION 0+10 TO 0+60

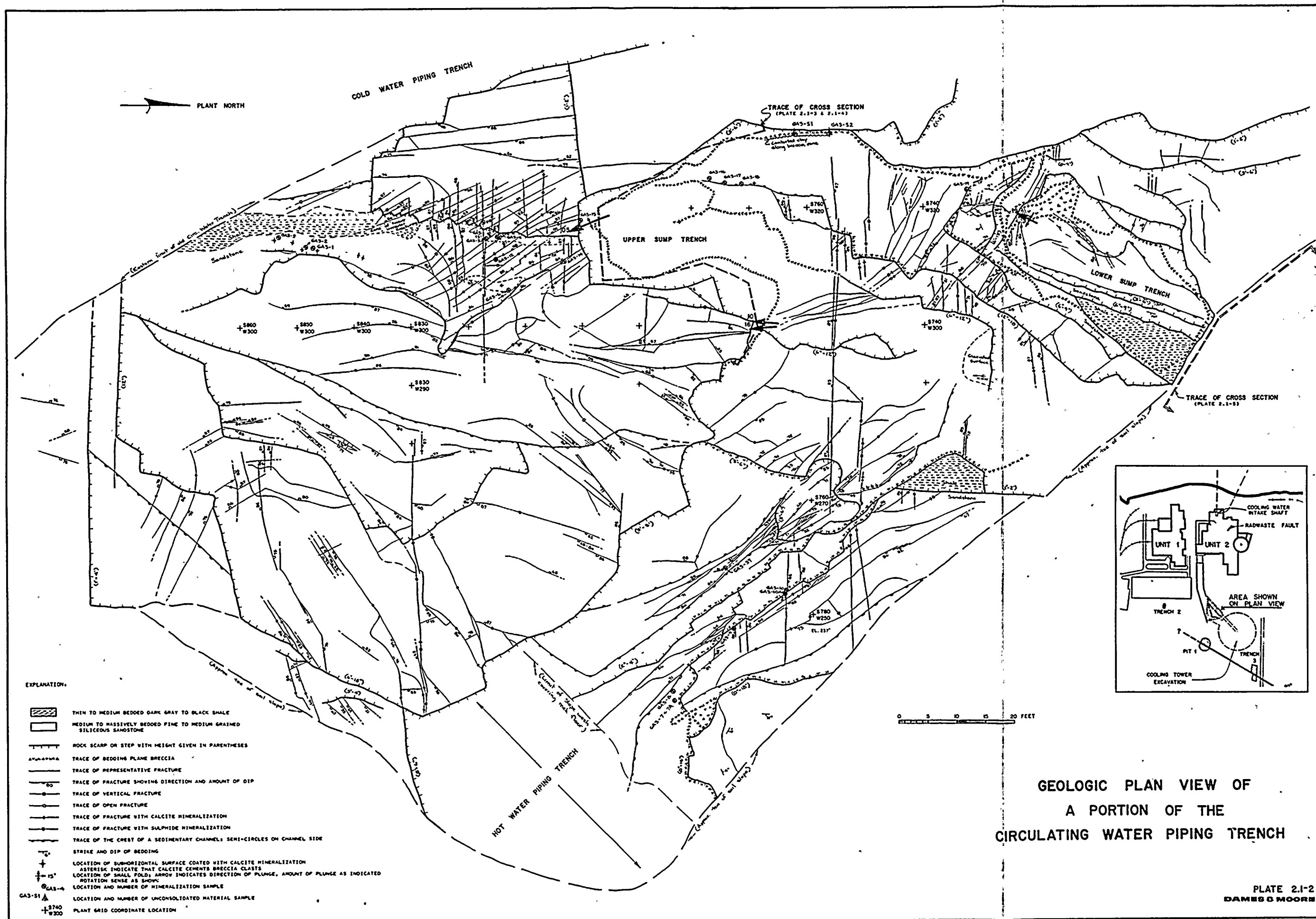
PLATE 2.1-18
 DAMES & MOORE



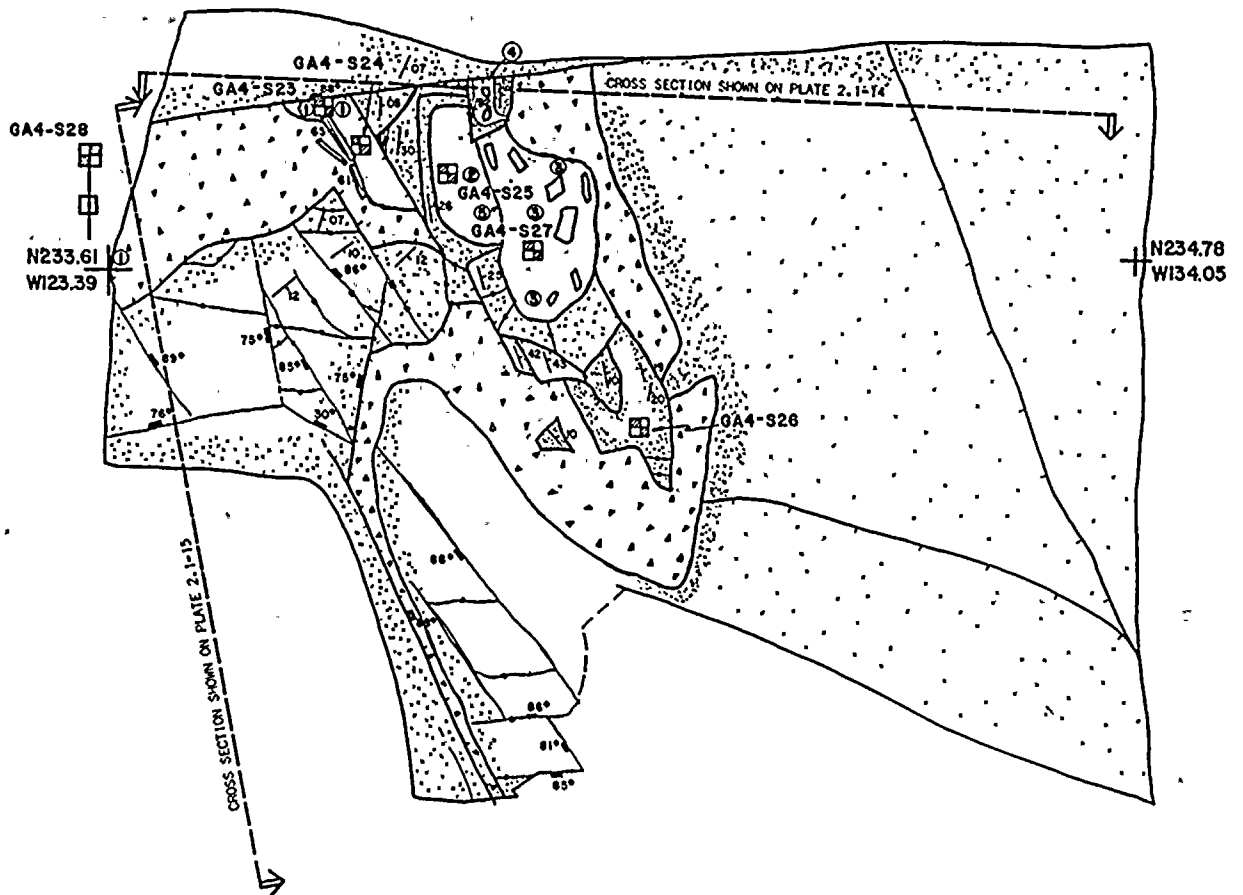
CROSS SECTION THROUGH RS-3, RS-2, AND RS-1 SHOWING HORIZONTAL NORMAL DISPLACEMENTS IN VERTICAL PLANES ORIENTED N70° W TO THE SOUTH OF THE FAULT BLOCK



APPROXIMATE STRATIGRAPHIC INTERVALS WHEREIN "THRUST" FAULTS WERE MAPPED DURING THIS INVESTIGATION



S80W



EXPLANATION:



Light gray fine - medium grained sandstone



Breccia - angular fragments of rock in soft silty sand matrix



Attitude of bedrock slab



Open Fracture



Attitude of fracture



Orientation of vortical fracture



Location of sample of unlithified sediment



Plant Grid Coordinates

NOTES:

1. Dark gray-brown laminated silty clay laminae show distortion by folding E-W shear sense.
2. Light tan laminated clayey silt laminae somewhat distorted but generally parallel to rotated bedrock slab.
3. Light tan laminated clayey silt, laminae extremely contorted, sediment contains subangular to angular fragments of sandstone, contortion of laminae and mixing with breccia clasts probably associated with fault movement.
4. Moderately dipping sandstone slab with light tan clayey silt and some sandstone clasts on upper surface silt laminae folded as follows:
5. Sample GA4-S29 - same as GA4-S25 but occurred beneath material shown as 1 on this plan.

GEOLOGIC PLAN VIEW

FLOOR OF EXPLORATORY EXCAVATION INTO SOUTHWEST WALL OF NORTH RADWASTE TRENCH

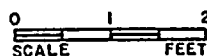
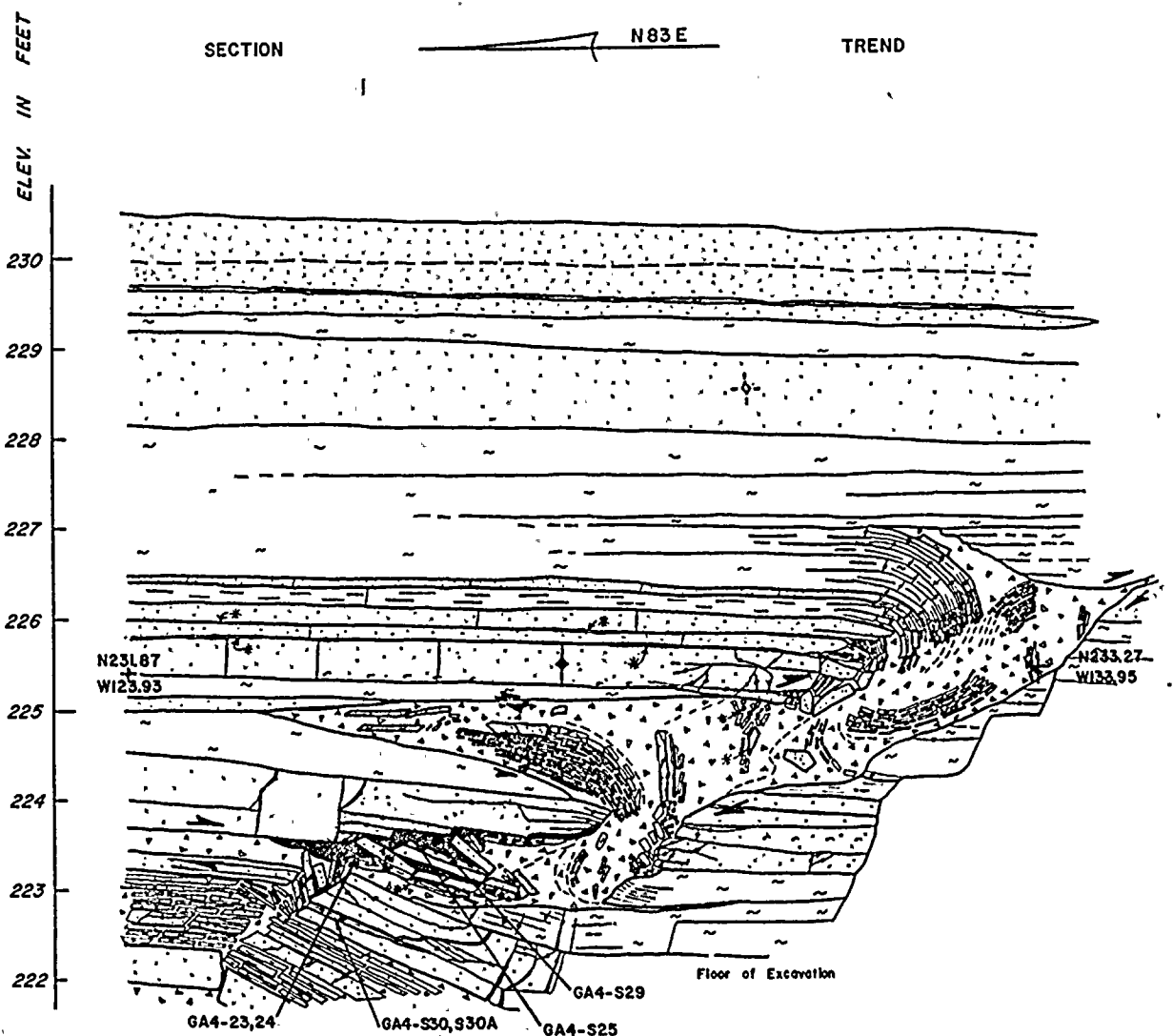


PLATE 2.1-13

DAMES & MOORE

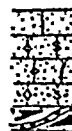




EXPLANATION:



Light gray fine to medium grained siliceous sandstone
 Fossiliferous sandstone
 Sandstone with shaley interclasts
 Medium dark gray fine to medium grained argillaceous sandstone or graywacke
 Dark gray to black very fine grained argillaceous sandstone or siltstone
 Black shale
 Breccia - generally angular fragments of rock in soft light gray sandy silt matrix



Joint or fracture
 Joint or fracture filled with calcite or sulfides, respectively
 Open joint or fracture
 Calcite or sulfide coatings on surfaces parallel to cross section
 Arrows indicate relative sense of movement

GA4-23

Sample location

N23L87
WI23.93

Void

*

Tan to gray clayey silt - often displaying distinct laminations

N23L87
WI23.93

Plant Grid Coordinates

0 1 2 FEET

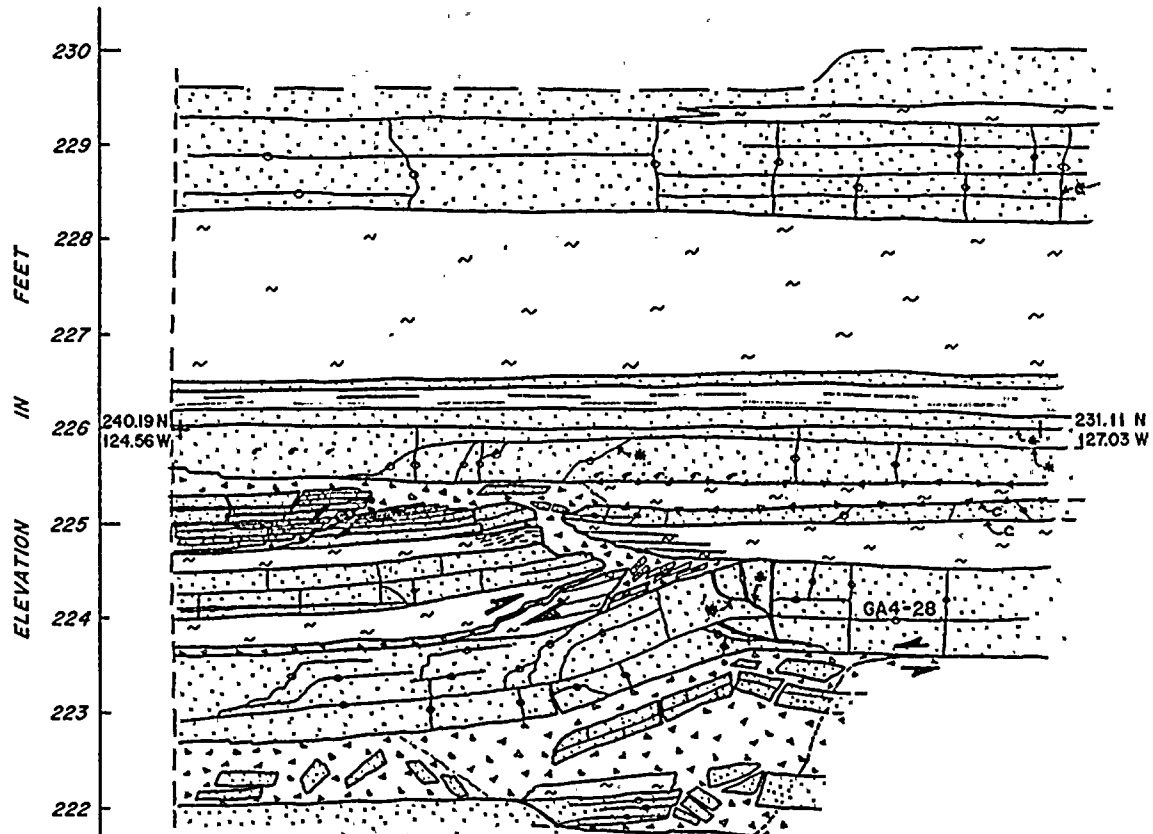
DETAILED CROSS SECTION OF EXPLORATORY EXCAVATION INTO SOUTH
 WALL OF NORTH RADWASTE TRENCH
 (SOUTH WALL)



SECTION

N 26 W

TREND



EXPLANATION:



Light gray fine to medium grained siltaceous sandstone
 Fossiliferous sandstone
 Sandstone with shaley interclasts
 Medium dark gray fine to medium grained argillaceous sandstone or graywacke
 Dark gray to black very fine grained argillaceous sandstone or siltstone
 Black shale
 Breccia - generally angular fragments of rock in soft light gray sandy silt matrix



Joint or fracture
 Joint or fracture filled with calcite or sulfides, respectively
 Open joint or fracture
 Calcite or sulfide coatings on surfaces parallel to cross section
 Arrows indicate relative sense of movement
 Tan to gray clayey silt

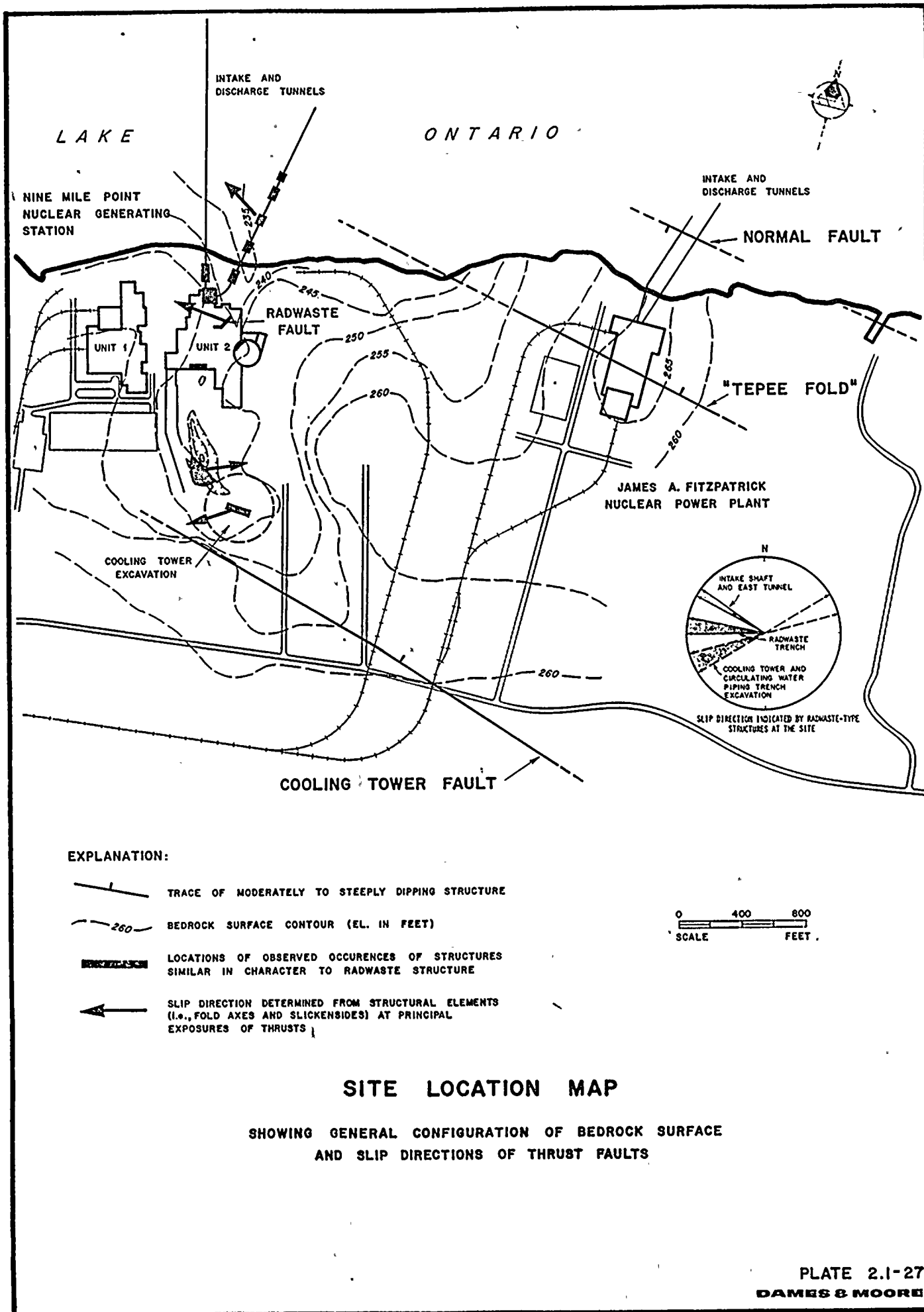
N240.19
 W124.56
 GA4-28

Plant Grid Coordinates
 Sample location

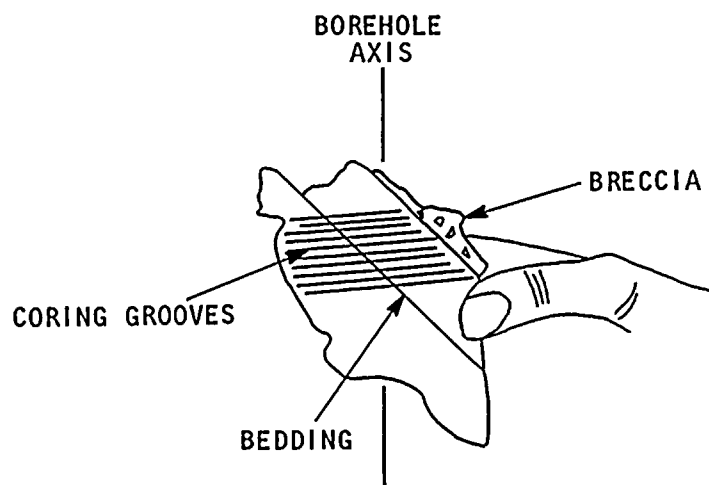
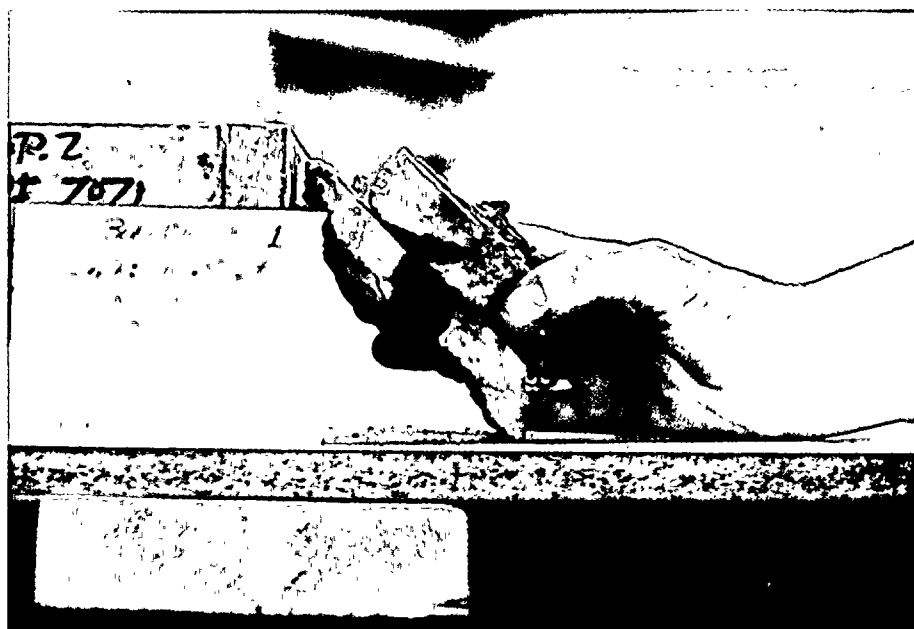
0 1 2 FEET

DETAIL CROSS SECTION OF EXPLORATORY EXCAVATION INTO SOUTH
 WALL OF NORTH RADWASTE TRENCH
 (EAST WALL)



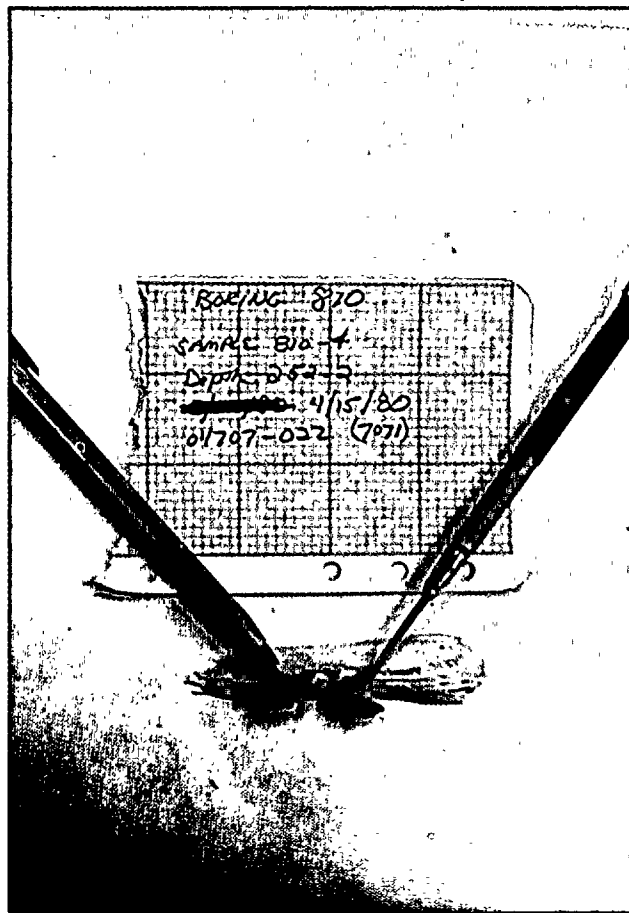




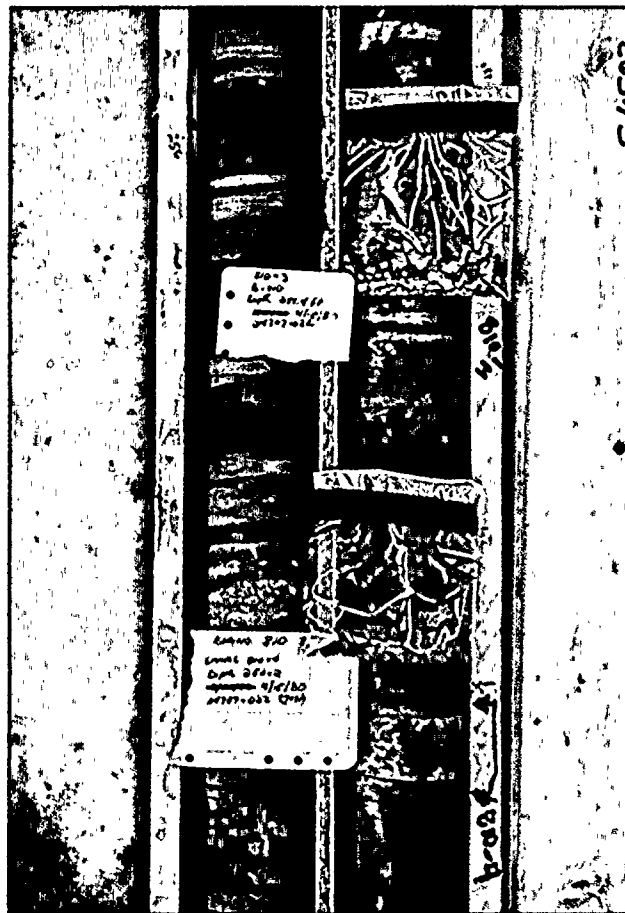


PHOTOGRAPH OF ROTATED BEDS
IN BORING 801, AT DEPTH OF 46.5 FEET

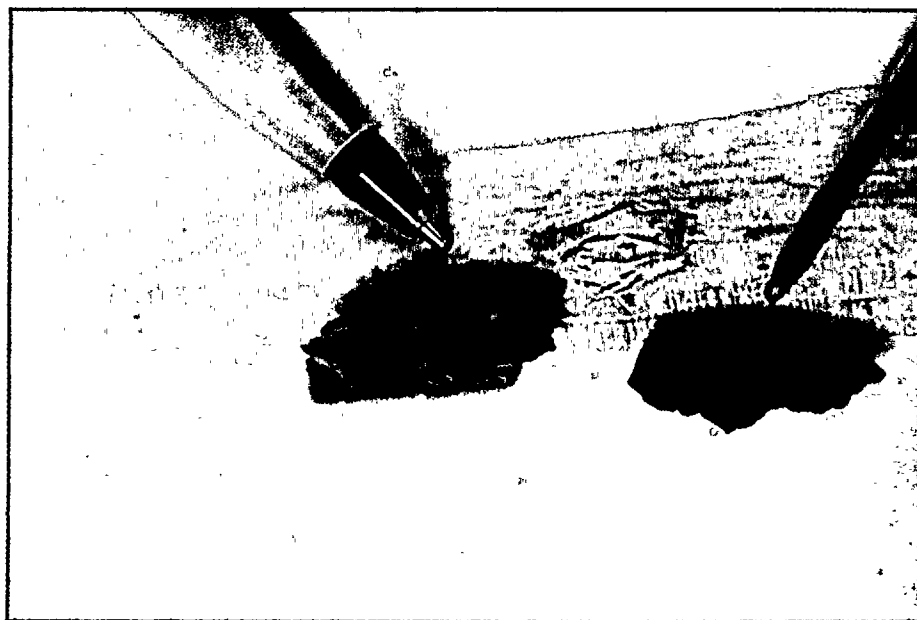




A



B

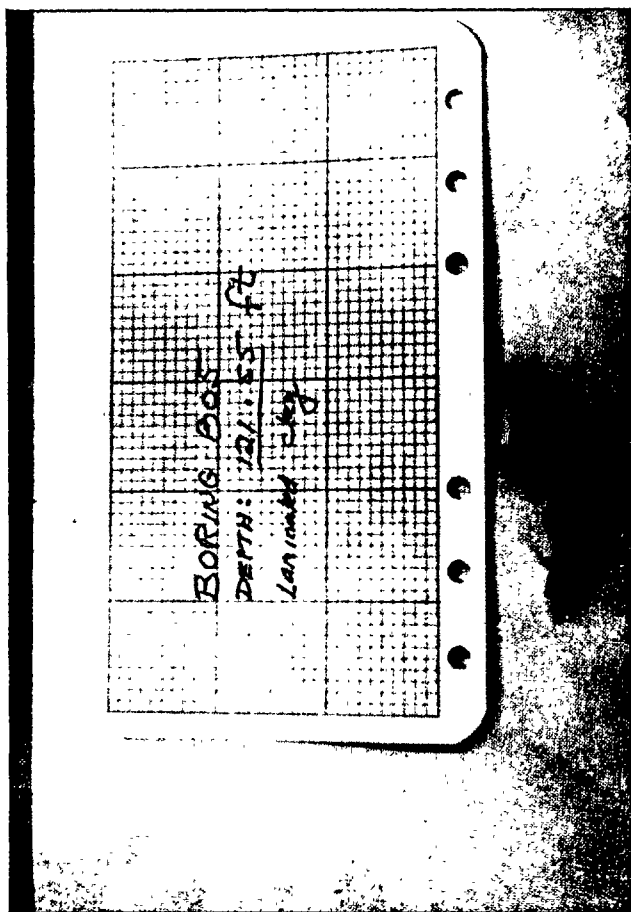


C

PHOTOGRAPHS OF LAMINATED CLAY
IN B-810 AT DEPTH OF 252.2 FEET

PLATE 2.2-11

DAMES & MOORE



A

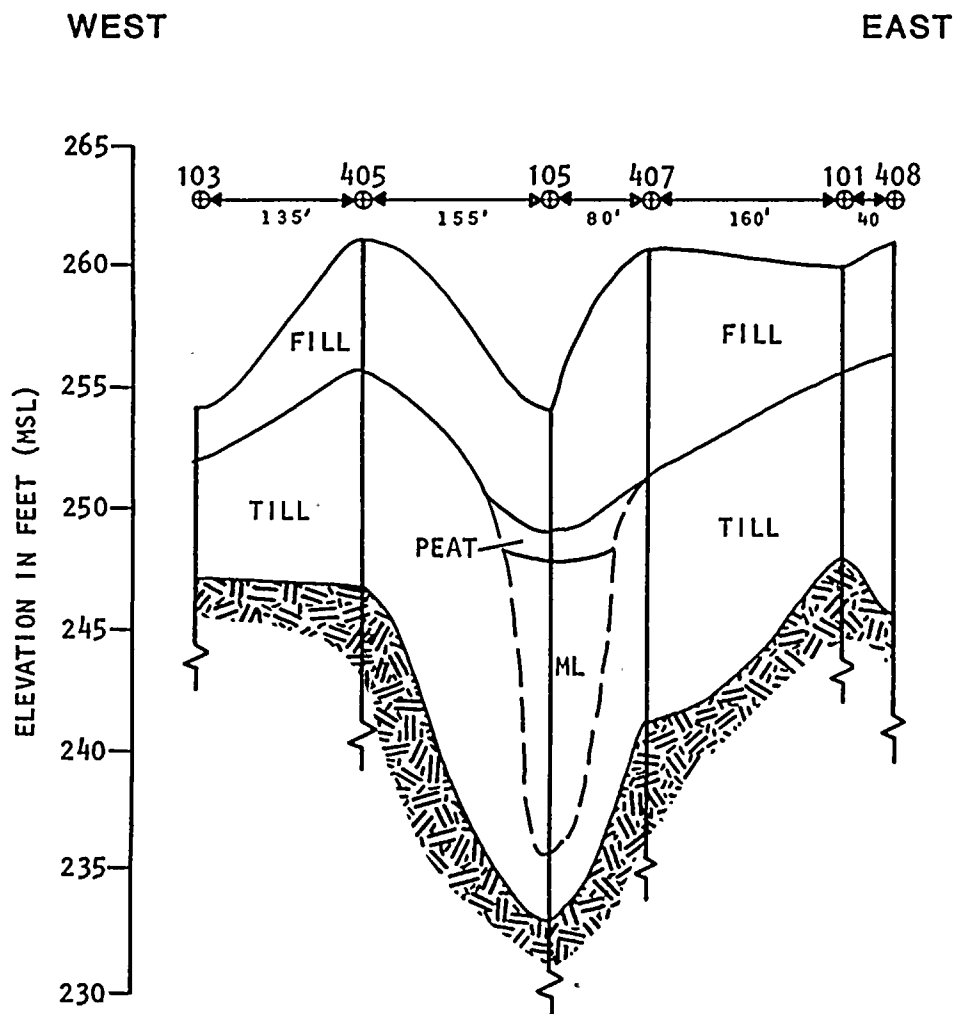


B



C

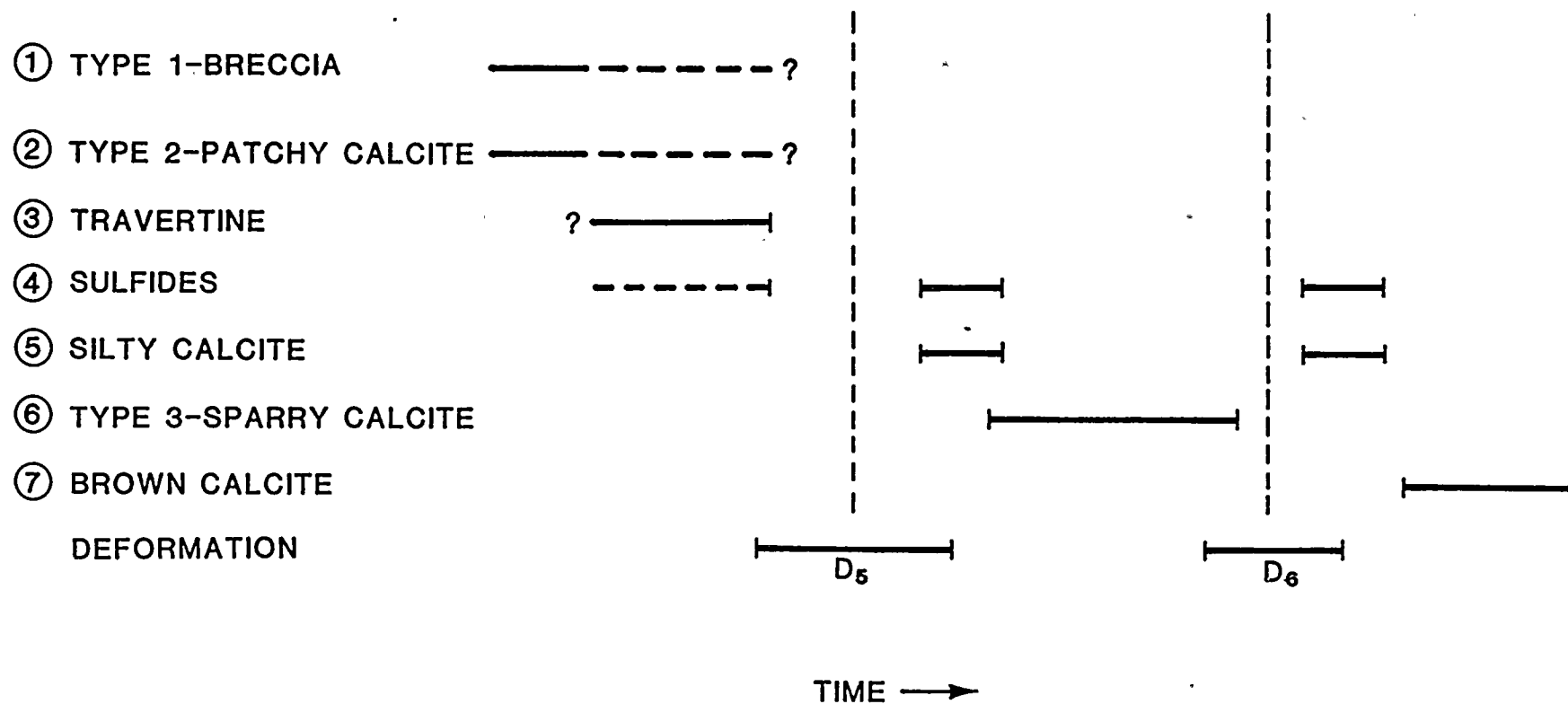
PHOTOGRAPHS OF LAMINATED CLAY
IN B-805 AT DEPTH OF 121.55 FEET

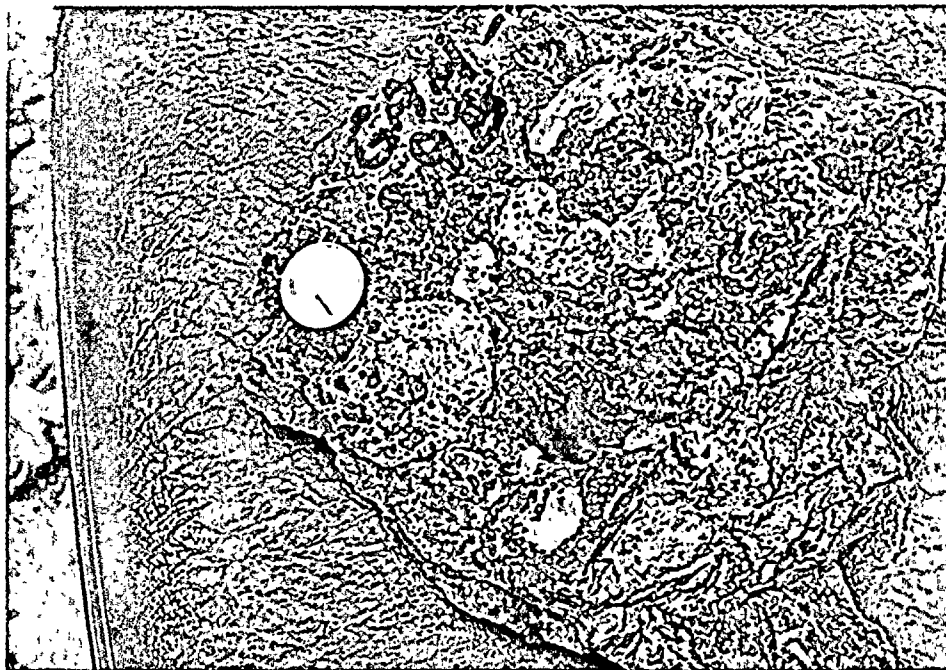


GEOLOGIC PROFILE OF OVERBURDEN FROM
OLD BORINGS ACROSS VALLEY AT LEADING EDGE
OF RADWASTE FAULT, NINE MILE POINT
UNIT 2 SITE



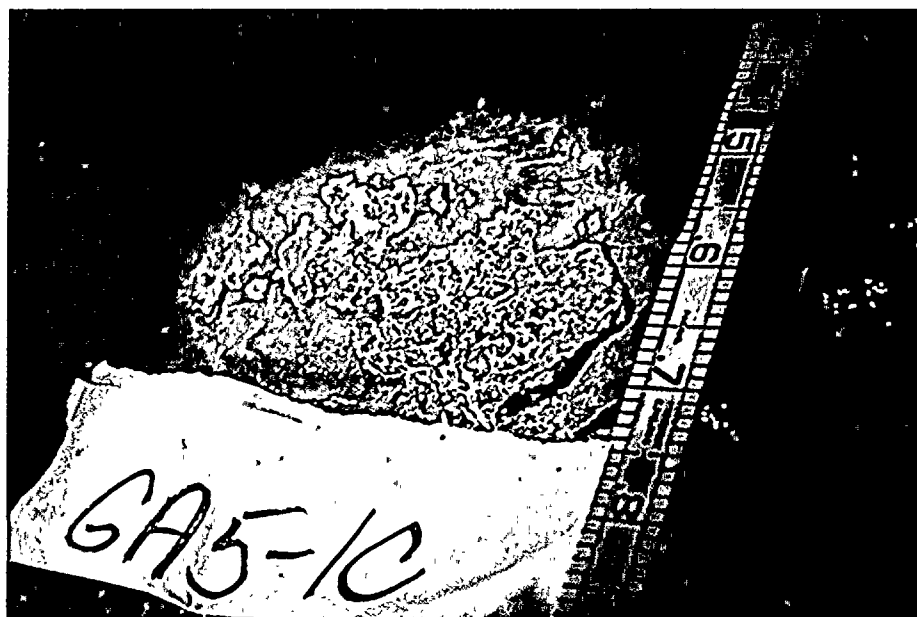
PARAGENETIC RELATIONSHIPS OF GROUNDWATER CALCITE MINERALIZATION AT NINE POINT UNIT 2 SITE





A

SPECIMEN (GA4-9B) SHOWING TYPE 1 CALCITE BRECCIA FROM RADWASTE FAULT. NOTICE SILICEOUS CLASTS CEMENTED AS INCLUSIONS.



B

SPECIMEN (GA5-1C) SHOWING TYPE 1 CALCITE BRECCIA FROM THRUST FAULT IN EAST LAKE WATER TUNNEL

TYPE 1 CALCITE

PLATE 2.3-3

DAMES & MOORE





A



B

DISTANT (A) AND CLOSE-UP (B) VIEWS OF SLICKENSIDED
TYPE 1 CALCITE BRECCIA FROM EAST TUNNEL THRUST FAULT

TYPE 1 CALCITE

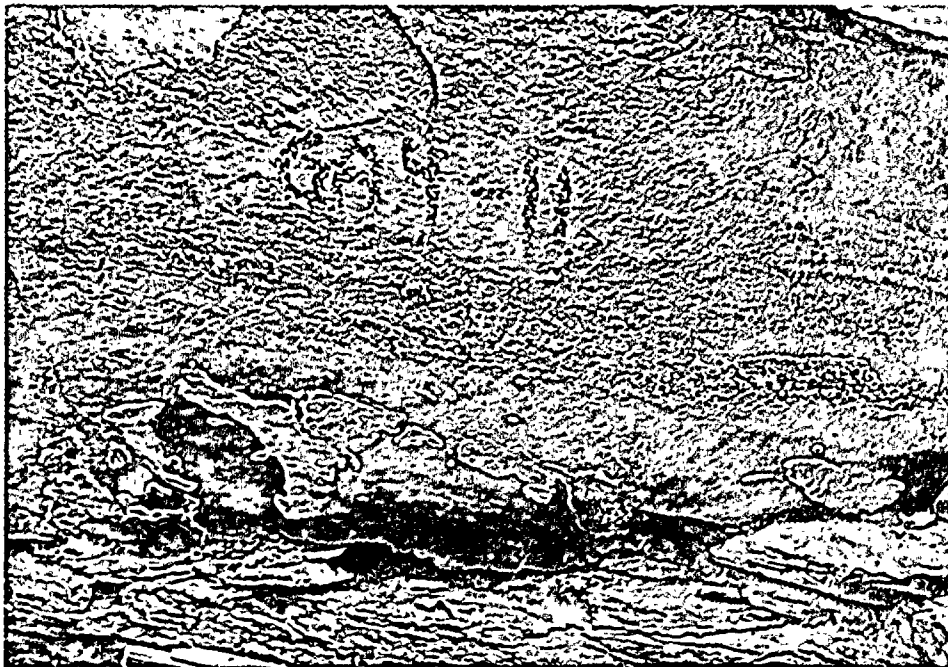
PLATE 2.3-4

DAMES & MOORE



A

SPECIMEN (GA4-7) SHOWING DRIPSTONE ON TILTED LAYER
OF FOLD WITHIN RADWASTE FAULT

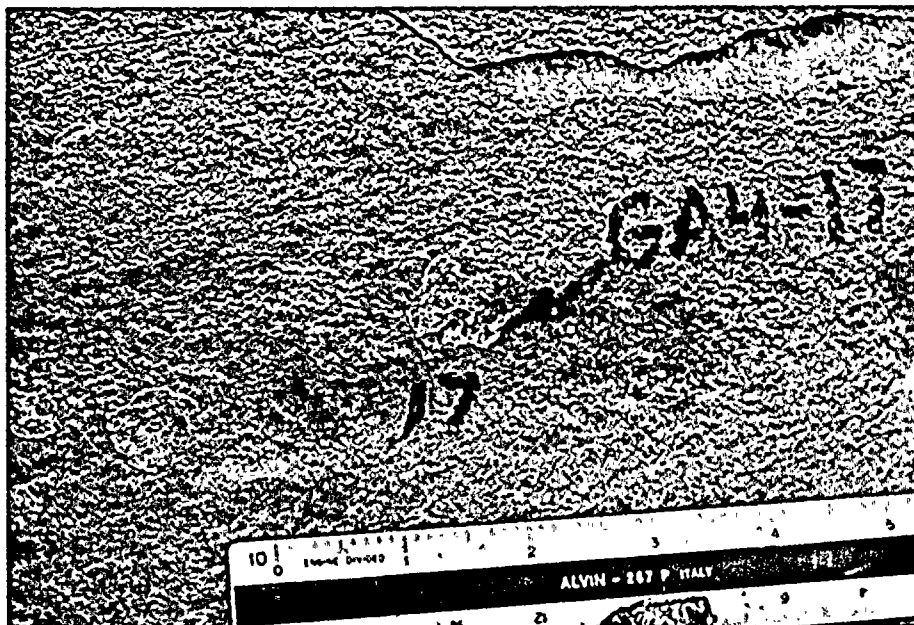


B

SPECIMEN (GA4-11) SHOWING BANDED TRAVERTINE
ON VERTICAL JOINT ABOVE RADWASTE FAULT ZONE

TRAVERTINE





A

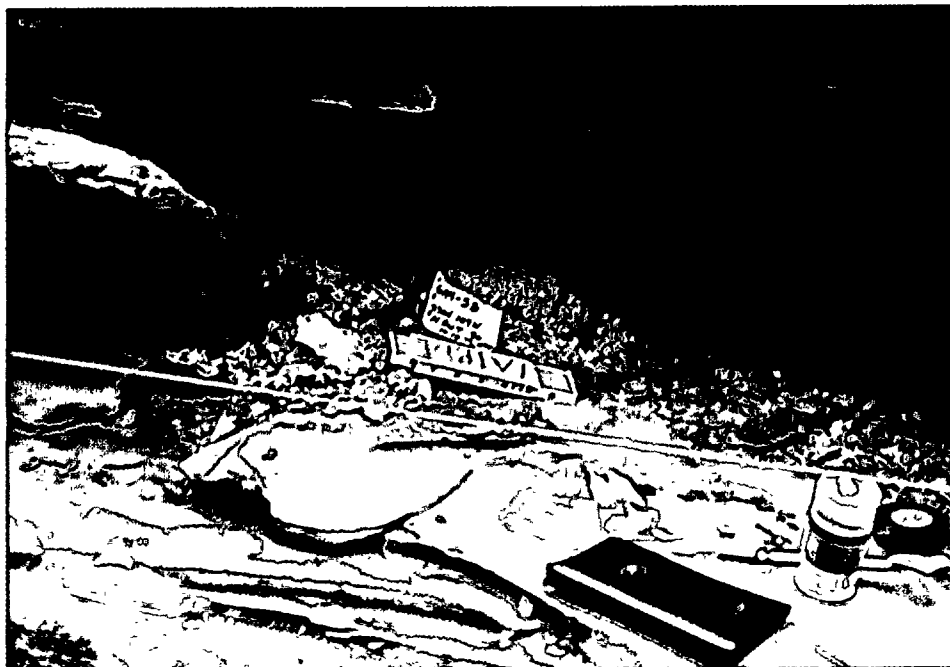


B

DISTANT (A) AND CLOSE-UP (B) VIEWS OF EUHEDRAL,
SPARRY CALCITE CRYSTALS OVER TRAVERTINE

(TYPE 3 CALCITE)





A



B

PHOTOGRAPHS SHOWING A
DISTANT AND B CLOSE-UP
VIEWS OF SPECIMEN GA4-S8
IN UNDISTURBED POSITION.
TWO TAN-COLORED, THIN
PLATES OF LAMINATION OF
CEMENTED SILT OCCUR AS
CLASTS WITHIN BRECCIA
ZONE OF RADWASTE FAULT

SPECIMEN GA4-S8

SOUTH WALL OF SLOT, NORTH RADWASTE TRENCH

PLATE 2.3-7

DAMES & MOORE



A



B

SPECIMEN GA4-6 SHOWING
DISTANT A AND CLOSE-UP B
VIEWS OF OVERTURNED
FRAGMENT WITHIN RADWASTE
FAULT BRECCIA IN UNDISTURBED
POSITION, WHERE TYPES 1
AND 3 CALCITE OCCUR ON
OVERTURNED SIDE. MINIMUM
TRANSPORT DISTANCE WOULD
BE APPROXIMATELY 3 INCHES.

SPECIMEN GA4-6

NORTH WALL OF SLOT, NORTH RADWASTE TRENCH

PLATE 2.3-8

DAMES & MOORE

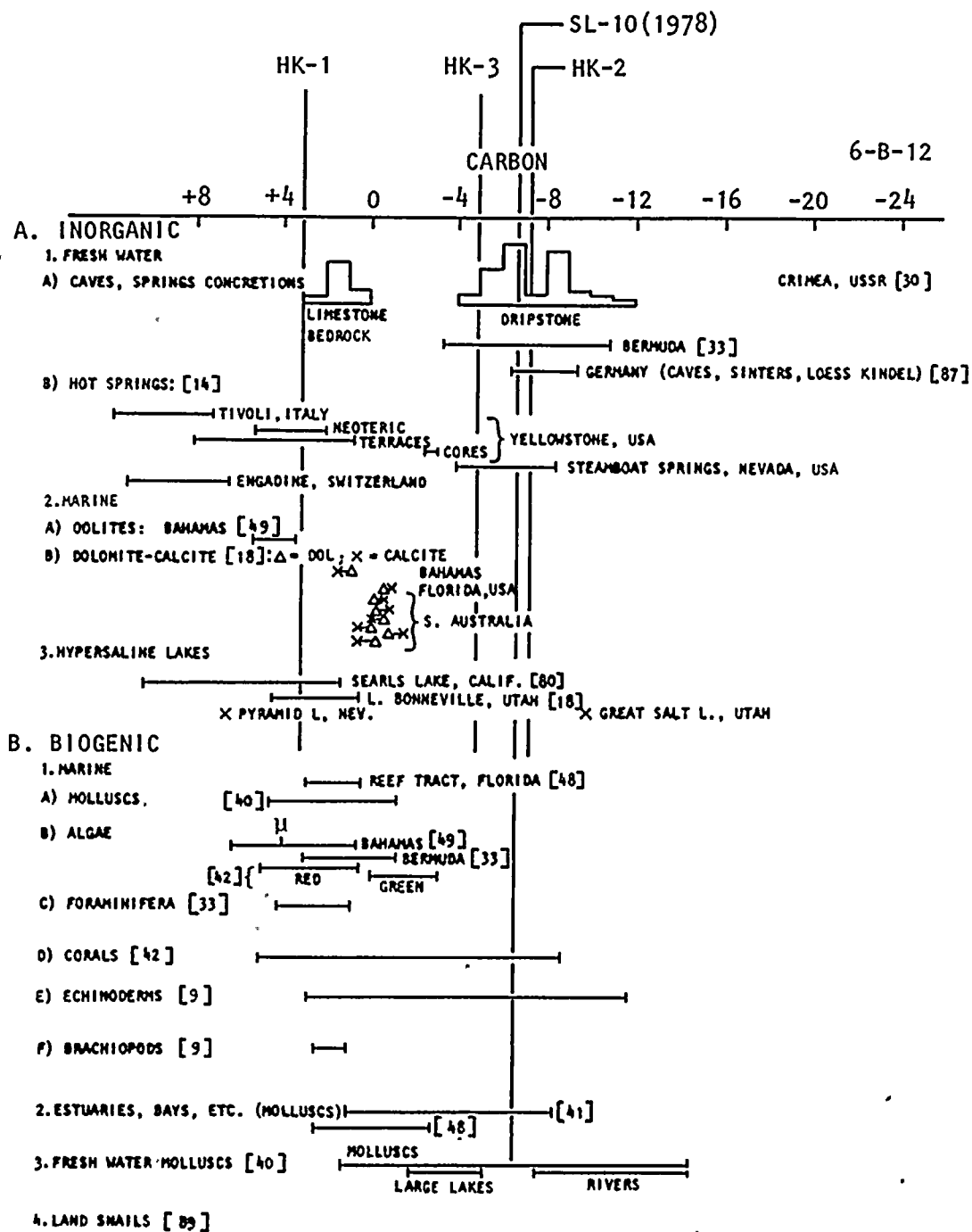


FIG. 6-B-7. DISTRIBUTION OF δ VALUES IN RECENT CARBONATE SEDIMENTS RELATIVE TO PDB STANDARD. (NUMBERS IN SQUARE BRACKETS SEE ADDENDUM ON REFERENCES 6-A TO 6-O p. 18.)

(TAKEN FROM APPENDIX B.1-5)

DISTRIBUTION OF ^{13}C RATIOS OF CARBONATES SHOWING RELATIONSHIP TO SITE SPECIMENS



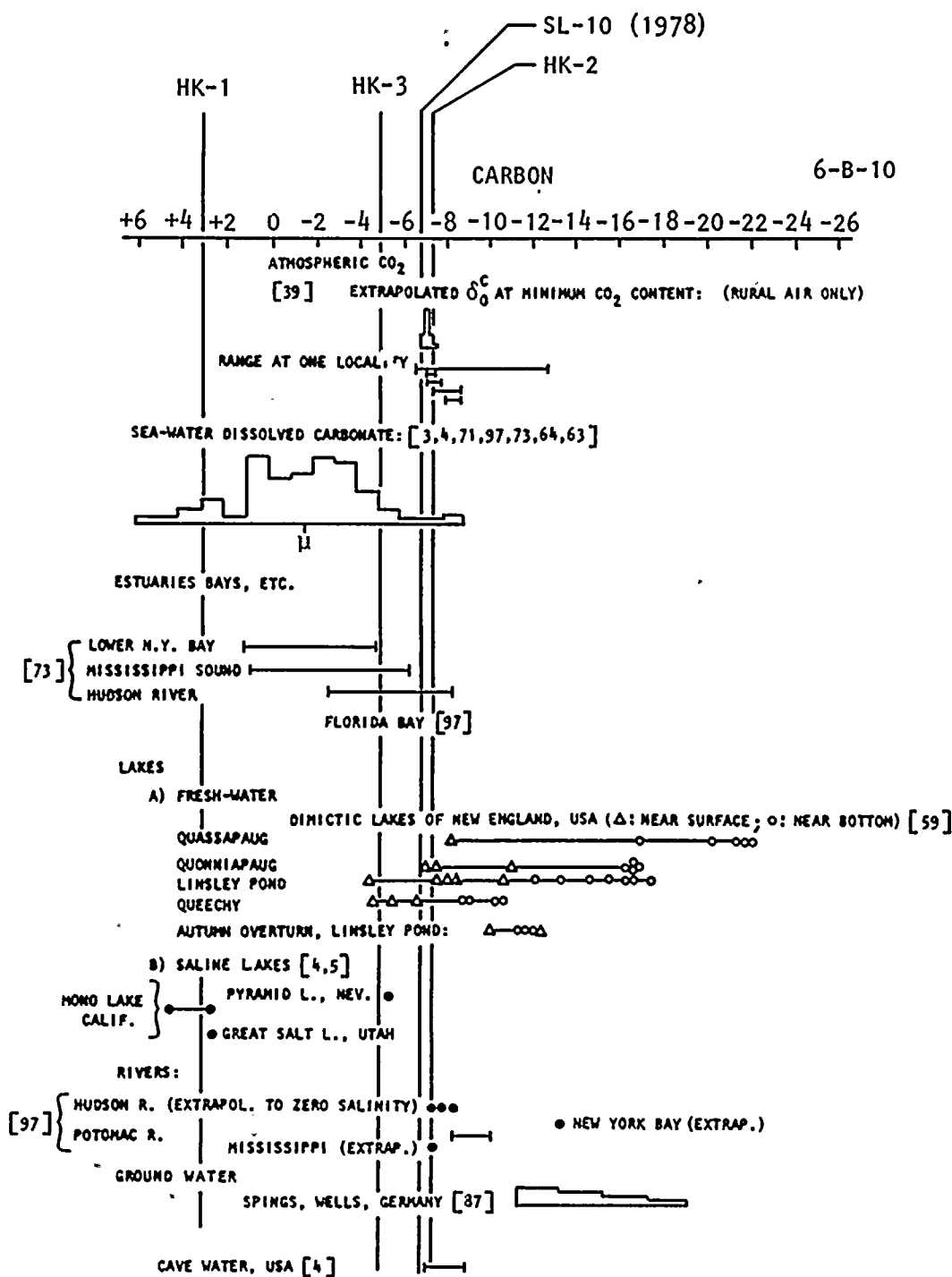


FIG. 6-B-6. DISTRIBUTION OF δ VALUES IN THE ATMOSPHERE AND HYDROSPHERE RELATIVE TO PDB STANDARD. (NUMBERS IN SQUARE BRACKETS SEE ADDENDUM ON REFERENCES 6-A TO 6-O p. 18.)

(TAKEN FROM APPENDIX B.1-5)

DISTRIBUTION OF ^{13}C RATIOS OF CARBONATES SHOWING RELATIONSHIP TO SITE SPECIMENS

PLATE 2.3-10

DAMES & MOORE



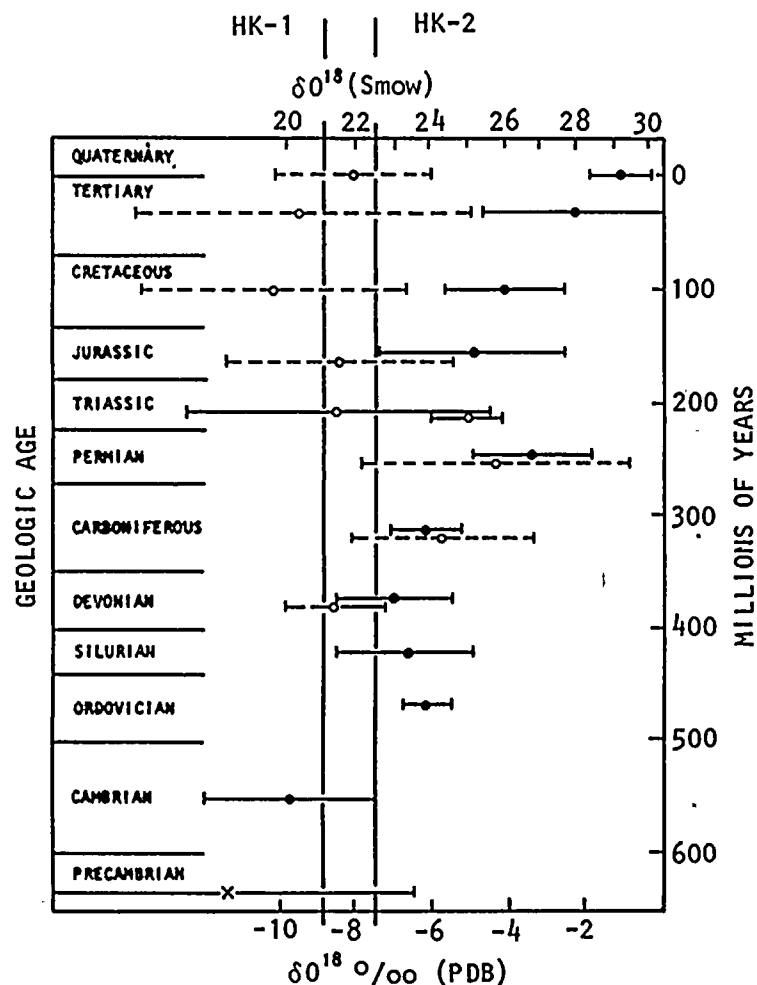


FIG. 8-B-25. AVERAGE ISOTOPIC COMPOSITIONS OF MARINE AND FRESHWATER LIMESTONES, BY GEOLOGIC AGE GROUPS. THE LINES REPRESENT PLUS OR MINUS ONE STANDARD DEVIATION. KEITH AND WEBER (1964). DASHED LINES REPRESENT FRESHWATER LIMESTONES.

(TAKEN FROM APPENDIX B.1-5)

DISTRIBUTION OF ^{18}O RATIOS IN CARBONATES SHOWING RELATIONSHIP TO SITE SPECIMENS





A



B

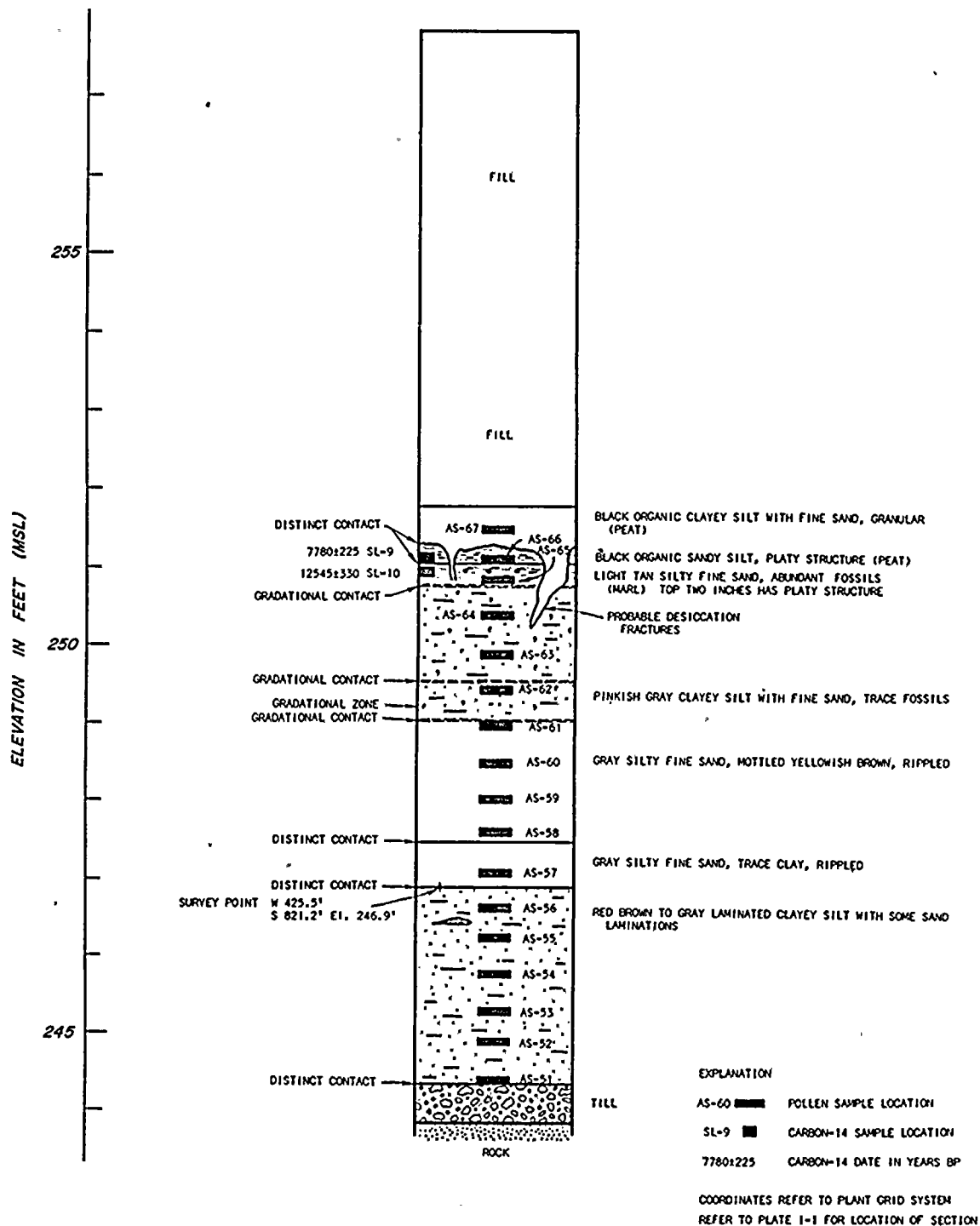
PHOTOGRAPHS SHOWING
DISTANT A AND CLOSE-UP B
VIEWS OF MIXTURE OF TAN
AND GRAY CLAY WITHIN
BRECCIA RADWASTE FAULT.

REFERENCE: PLATE 5.1-11
FOR SAMPLE LOCATION.

MIXTURE OF BRECCIA AND SEDIMENT
AS SHOWN BY SAMPLE GA4-S5 NORTH RADWASTE TRENCH

PLATE 2.3-12

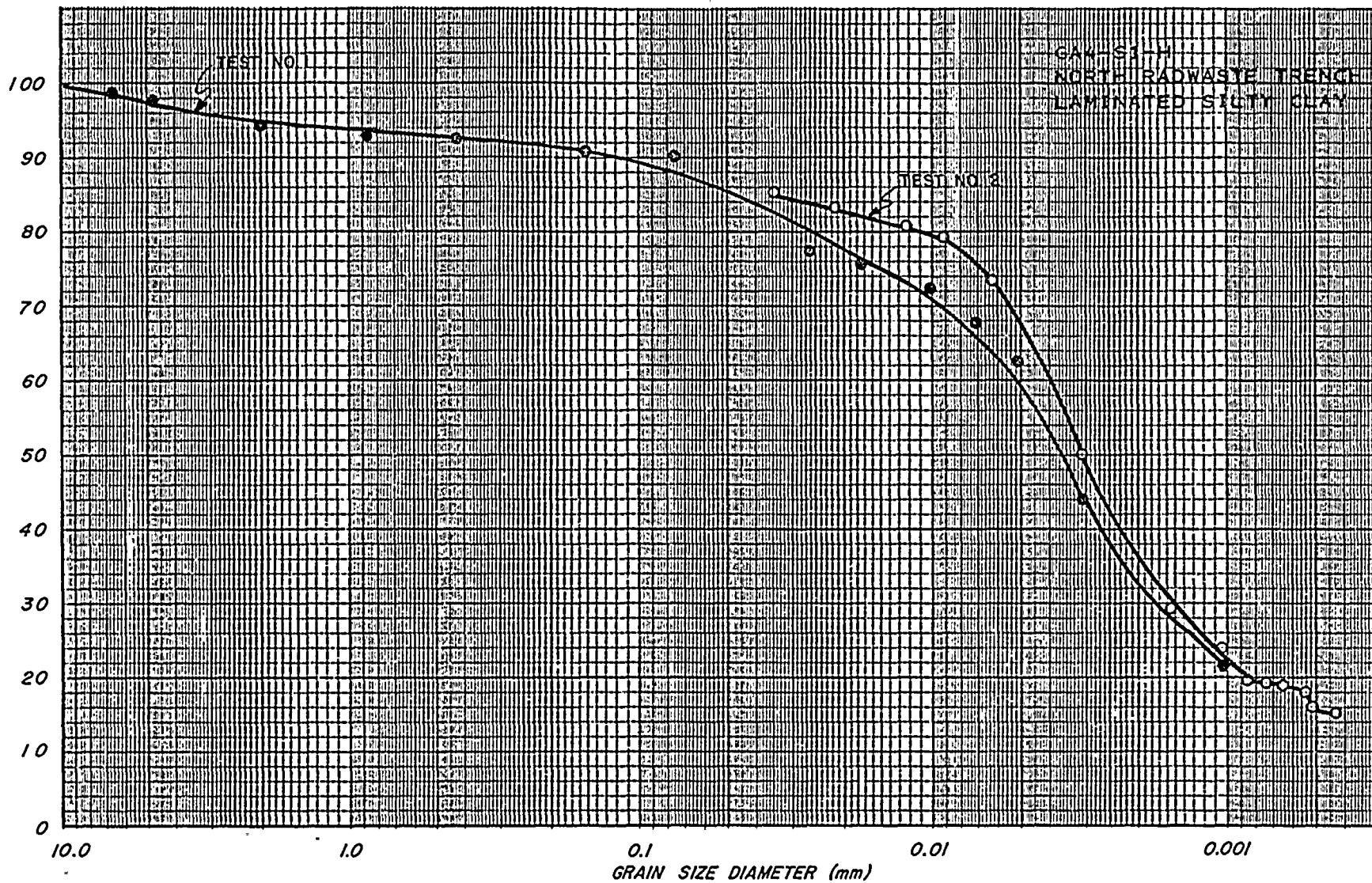
DAMES & MOORE



POLLEN SAMPLES
WEST WALL - COOLING TOWER TRENCH
CTT - I

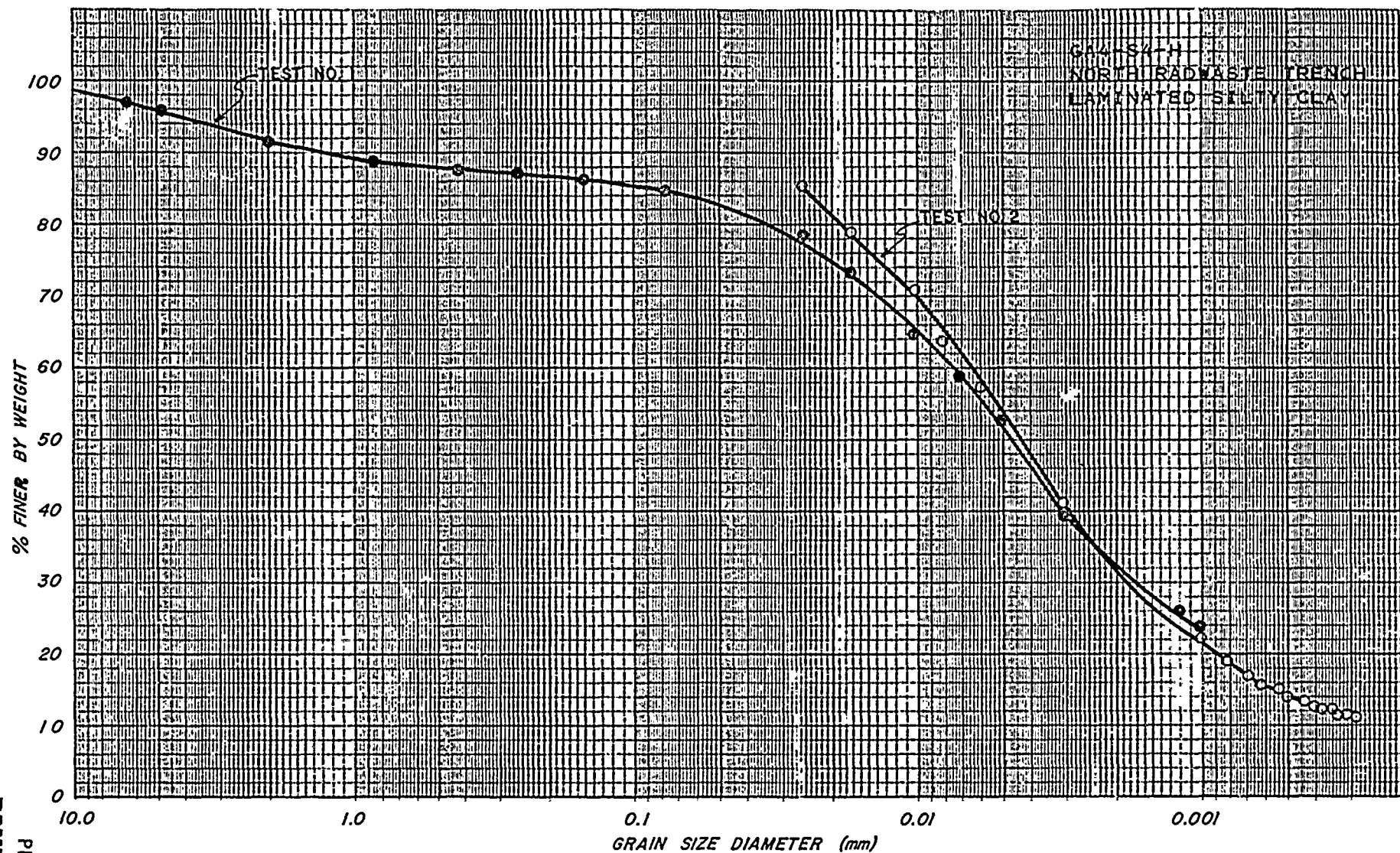


% FINER BY WEIGHT

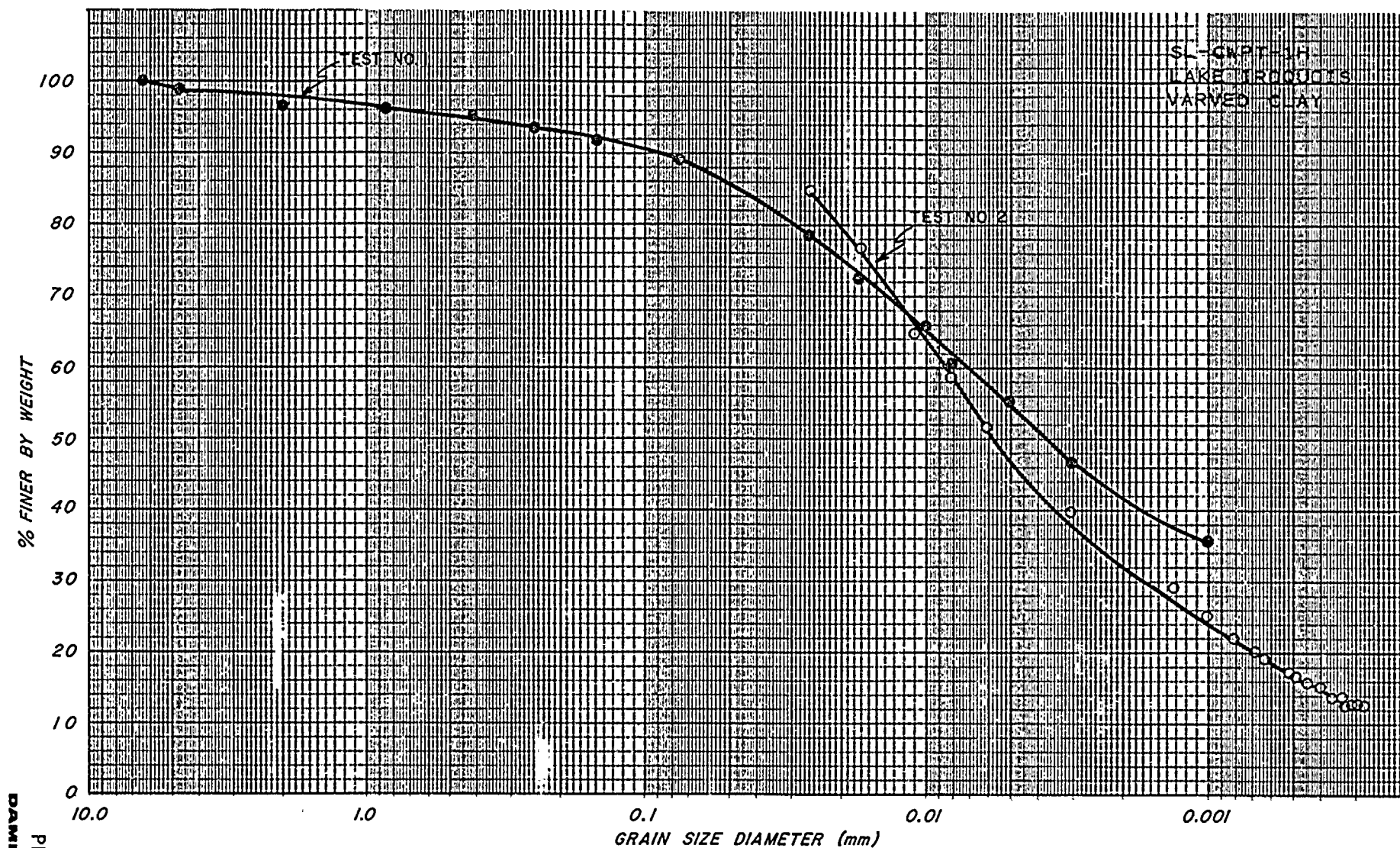


GRAIN SIZE DISTRIBUTION CURVE



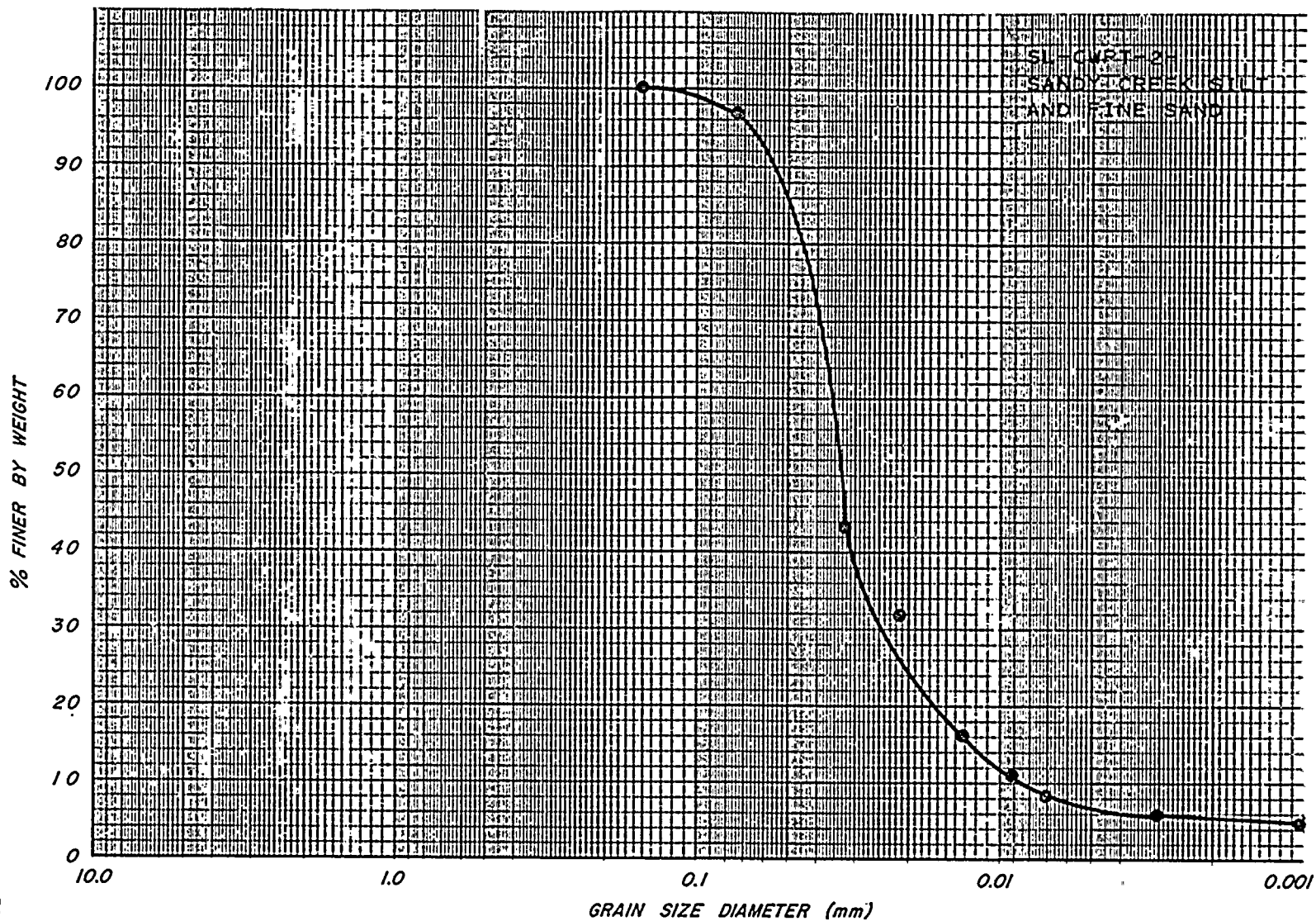






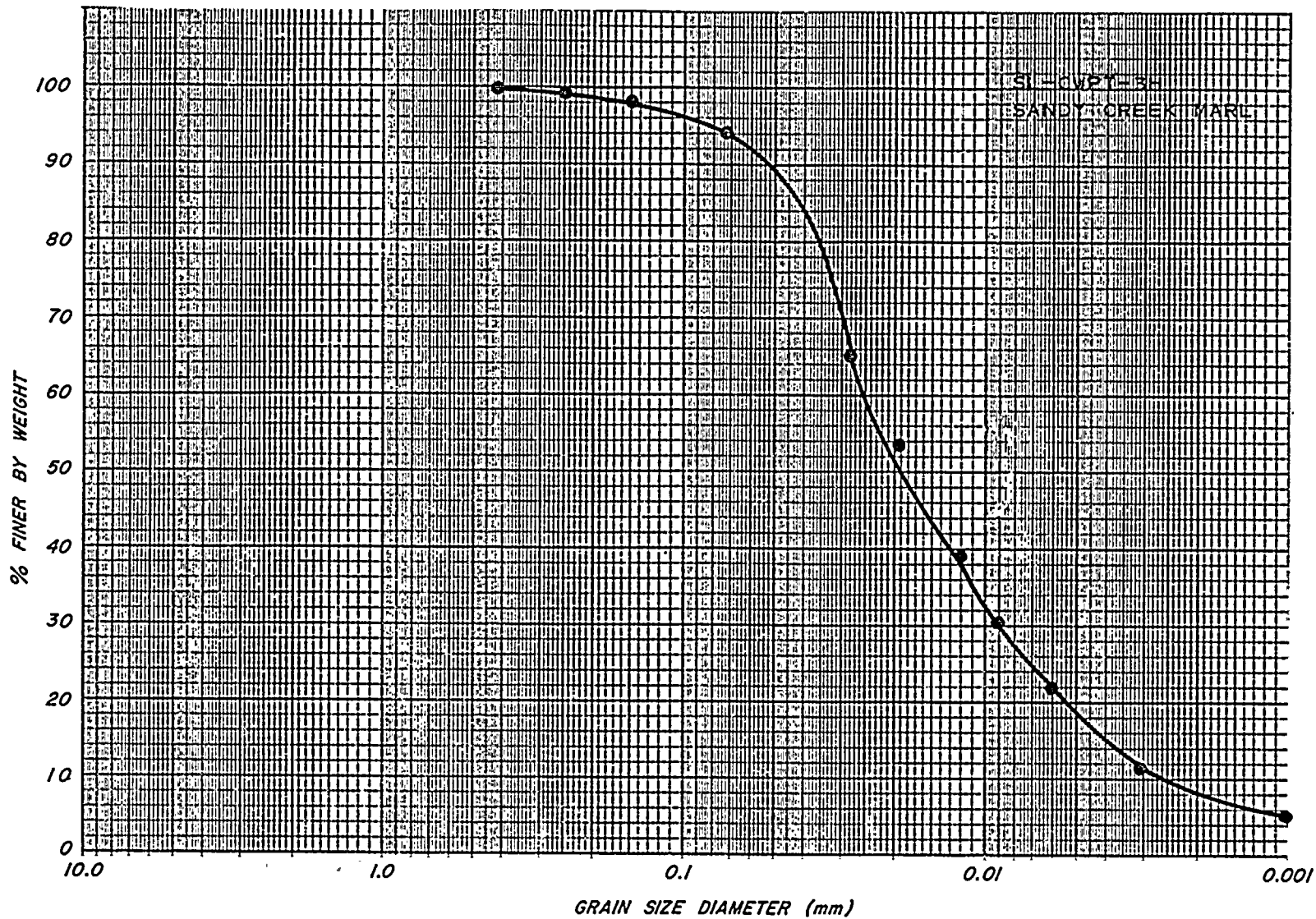
GRAIN SIZE DISTRIBUTION CURVE





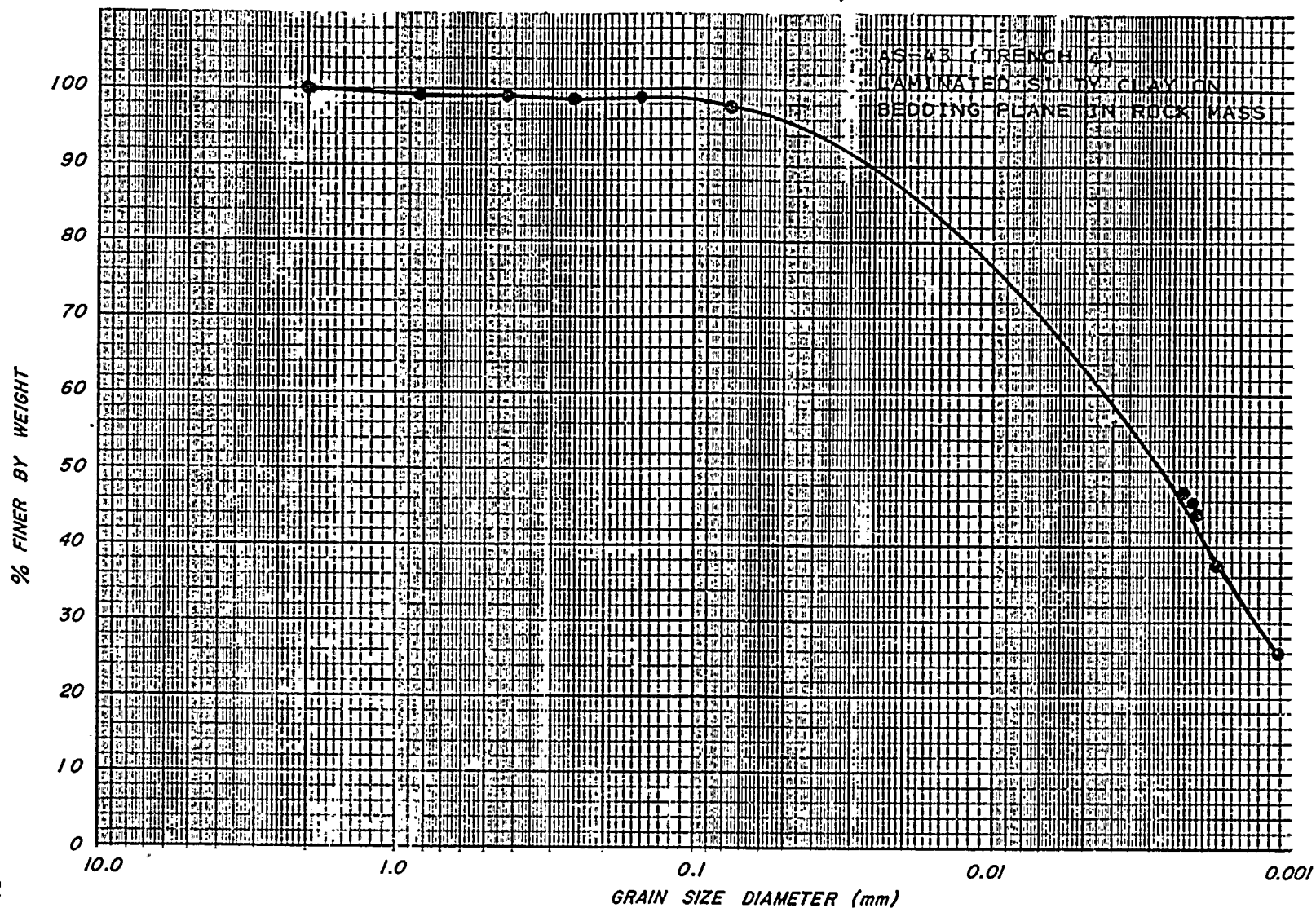
GRAIN SIZE DISTRIBUTION CURVE





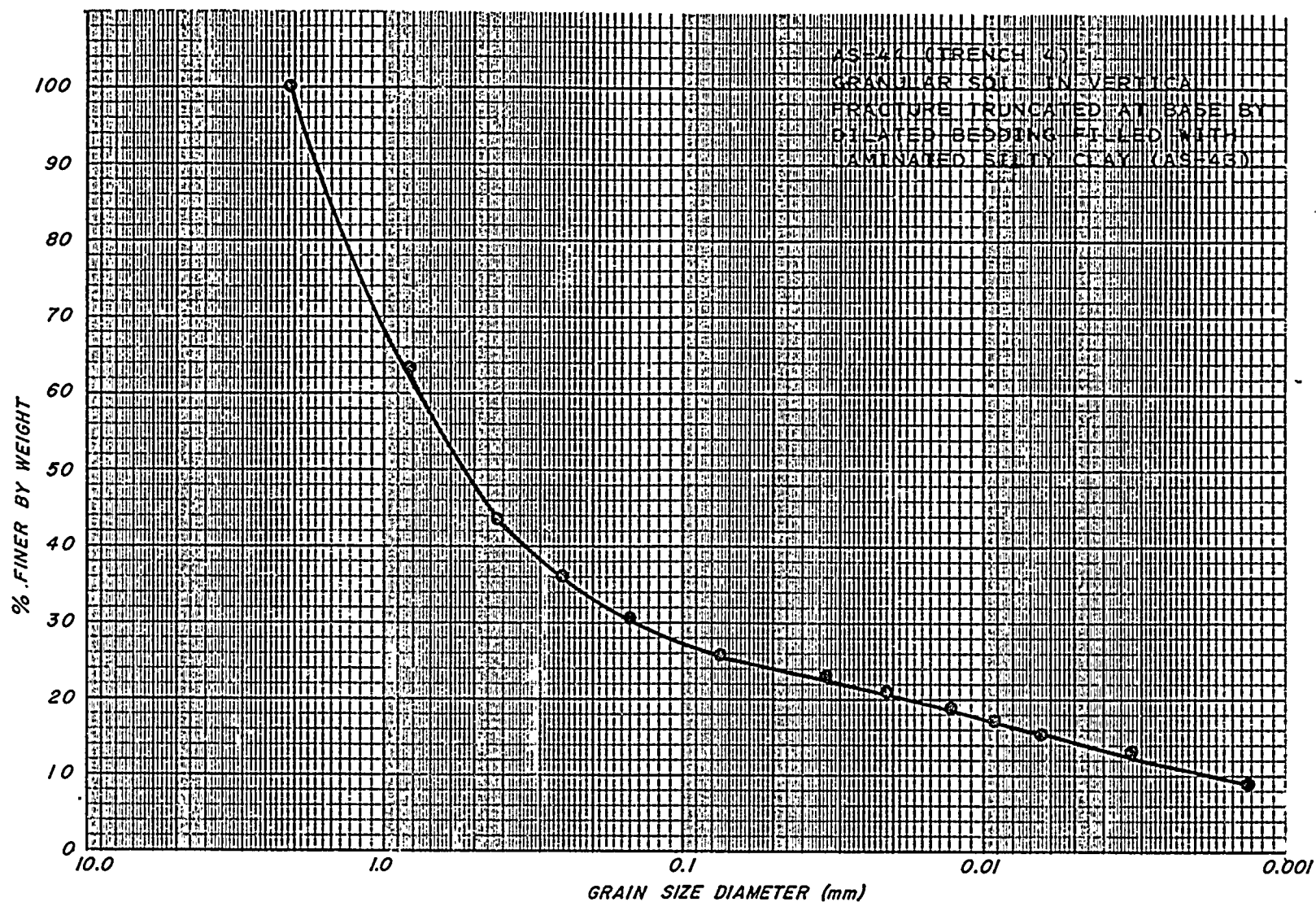
GRAIN SIZE DISTRIBUTION CURVE





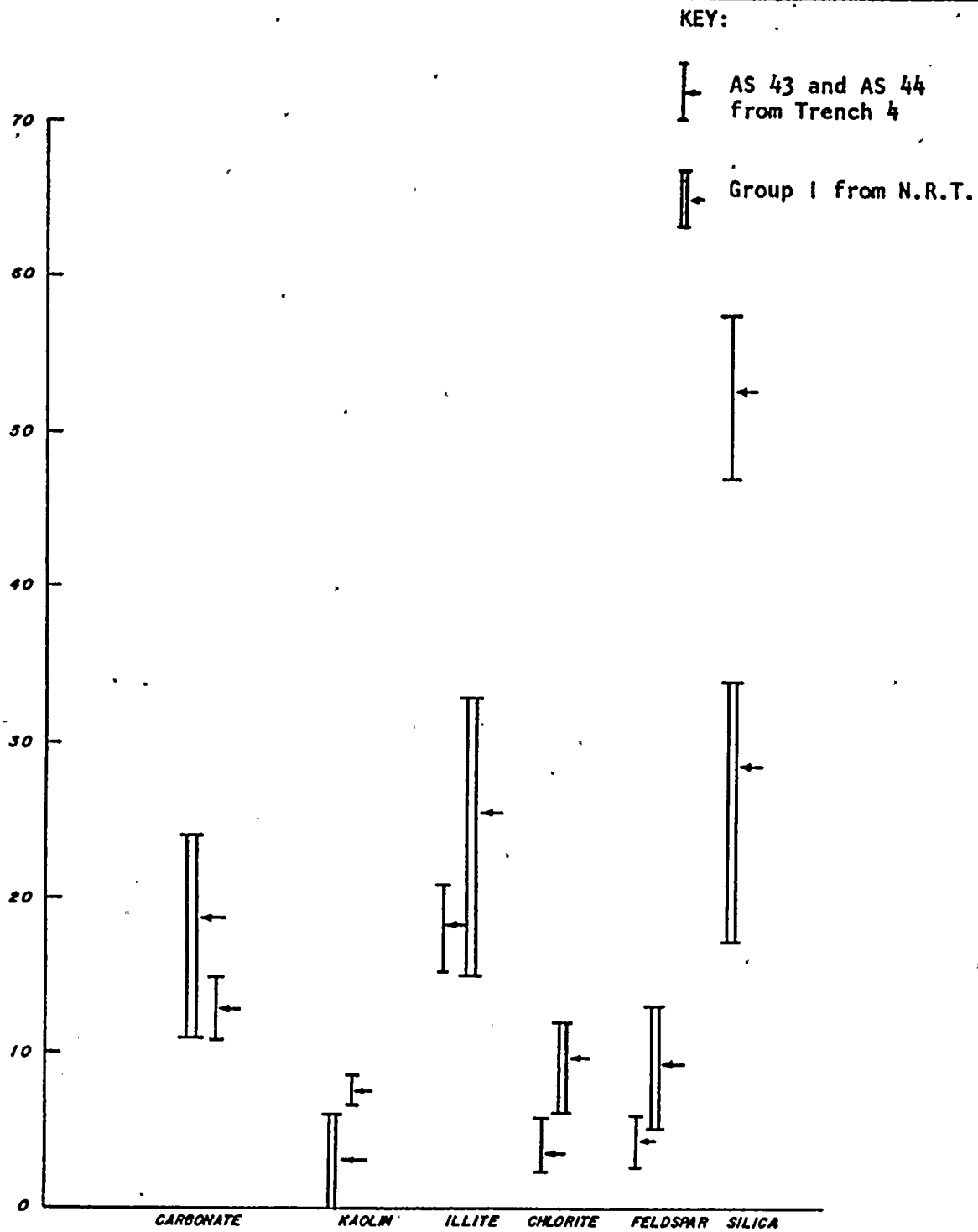
GRAIN SIZE DISTRIBUTION CURVE





GRAIN SIZE DISTRIBUTION CURVE

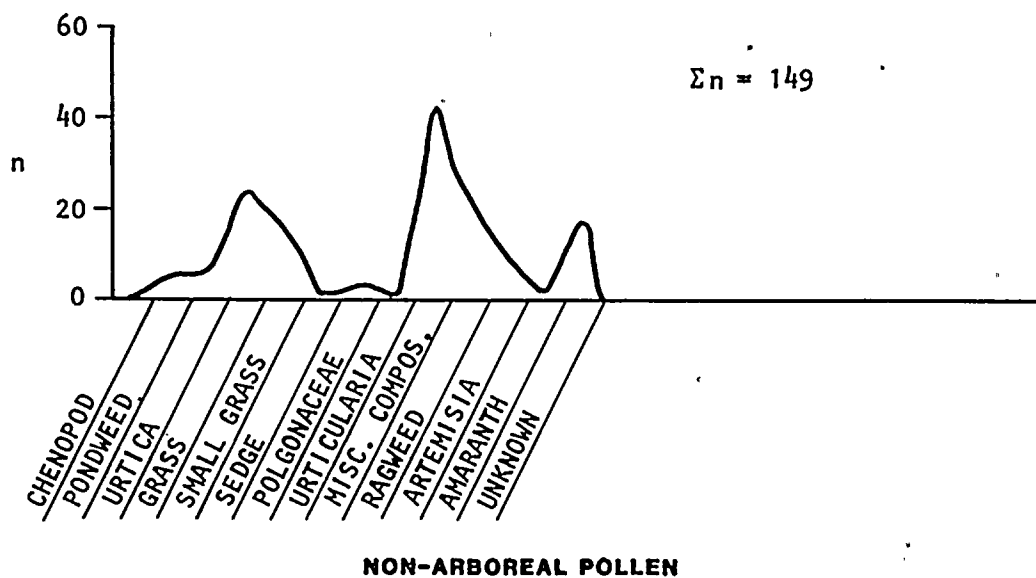
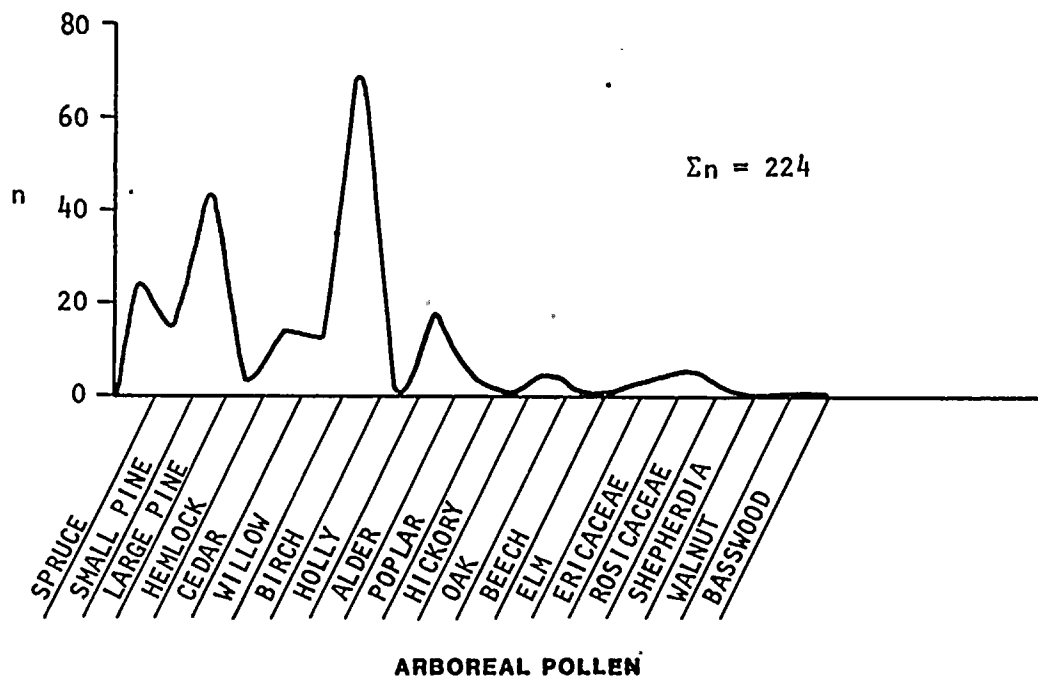




PERCENT MINERAL CONTENT OF SAMPLES
FROM TRENCH 4 AND NORTH RADWASTE TRENCH

Note:
Bar graph shows range.
Arrow shows arithmetic mean.

Reference: Plate 1-4 of Vol. II,
Niagara Mohawk Power Corp., 1978



FREQUENCY DIAGRAMS FOR POLLEN SPECTRA*

REPRESENTING TOTAL OF SAMPLES FROM
NORTH RADWASTE AND CIRCULATING WATER PIPING TRENCHES

* DOES NOT INCLUDE SPORE FREQUENCIES





A



B

PHOTOGRAPHS OF
LATE PLEISTOCENE CLAY
SHOWING CLAY LAMINAE WITH 70° DIP EQUAL TO THAT
OF SHORT LIMB OF KINK FOLD ALONG RADWASTE FAULT ZONE

REFERENCE: 2.1-12

PLATE 2.3-25
DAMES & MOORE

PLATE



11



A



B

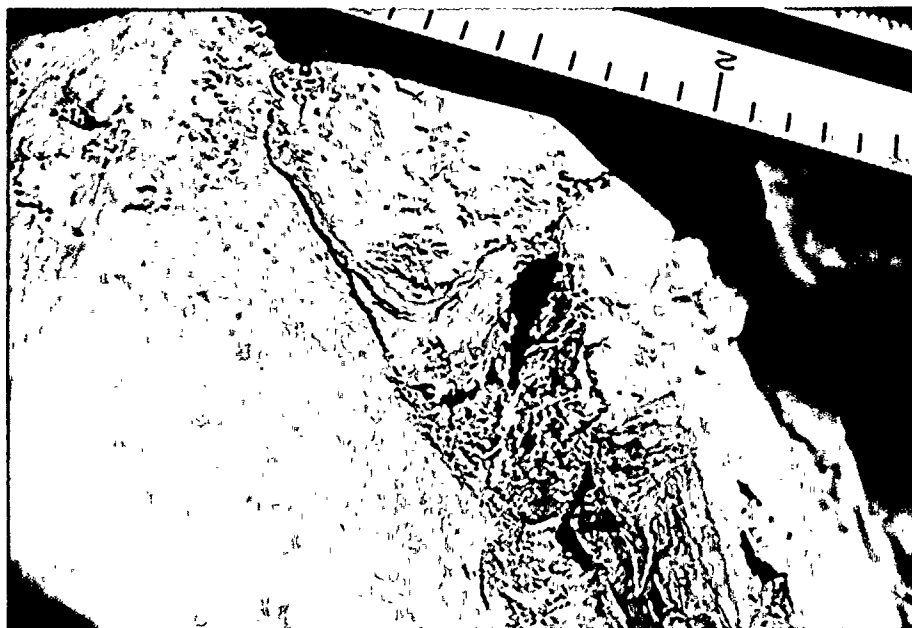
PHOTOGRAPHS OF DEFORMATION
IN LATE PLEISTOCENE CLAYS
SHOWING A) LOCATION OF FOLDS B) FOLD IN CLAYS

REFERENCES:

1. PLATES 2.1-13,14
2. PHOTOS COURTESY OF STONE & WEBSTER ENG. CORP.

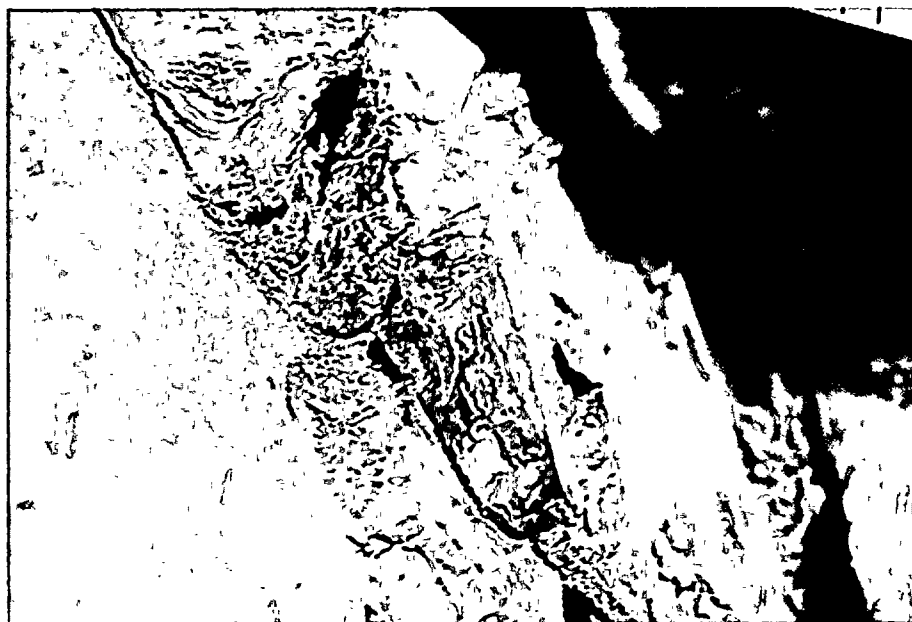
PLATE 2.3-26
DAMES & MOORE





A

LAMINATED CLAY IN CONTACT WITH SHORT LIMB OF KINK FOLD DIPPING 50° WEST
 CONTORTIONS IN CLAY INDICATE DOWN-DIP TRANSLATION OF CLAYS
 SCALE: TENTHS OF ONE INCH



B

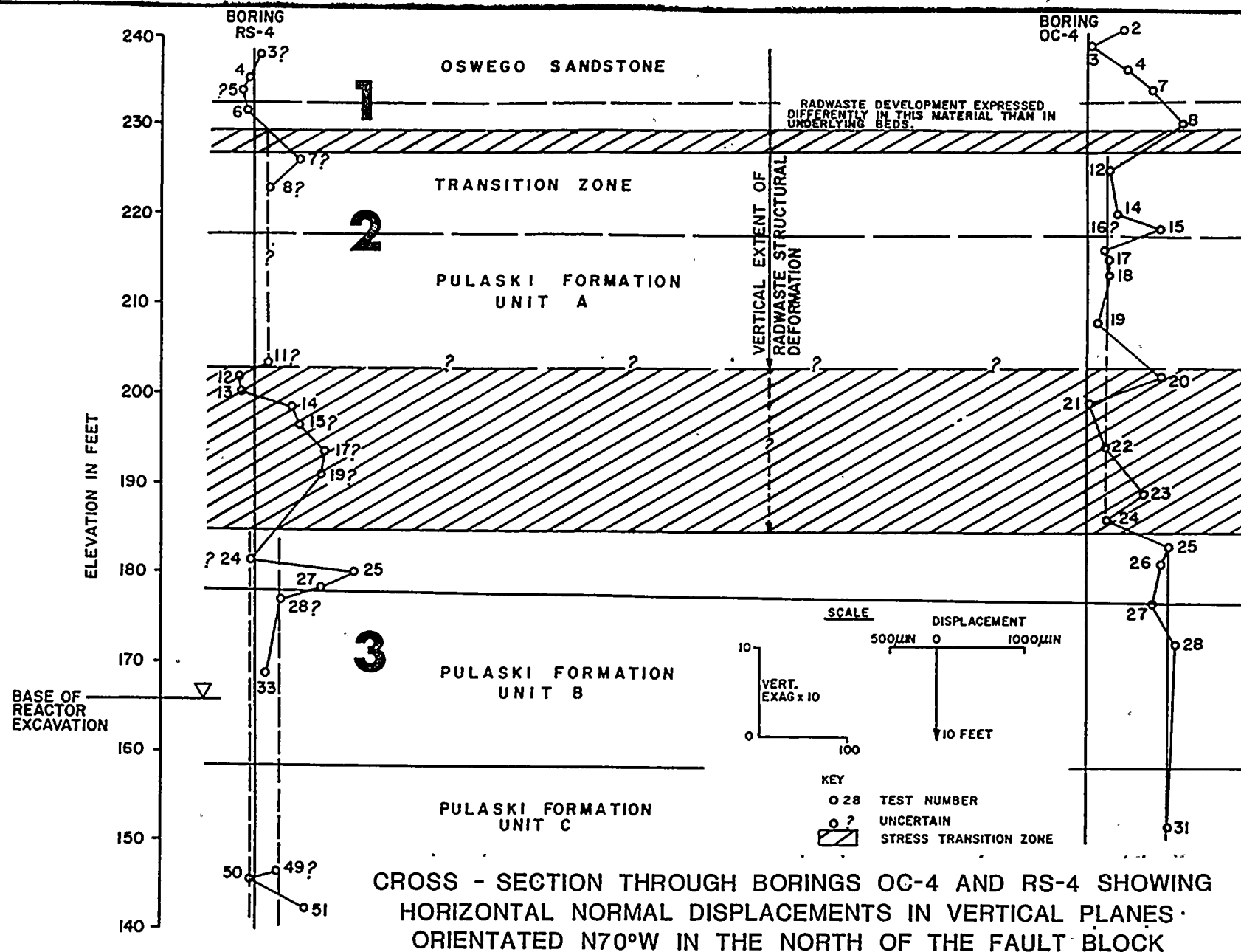
SIMILAR VIEW AS A

PHOTOGRAPHS OF DEFORMATION FEATURES IN LATE PLEISTOCENE CLAY

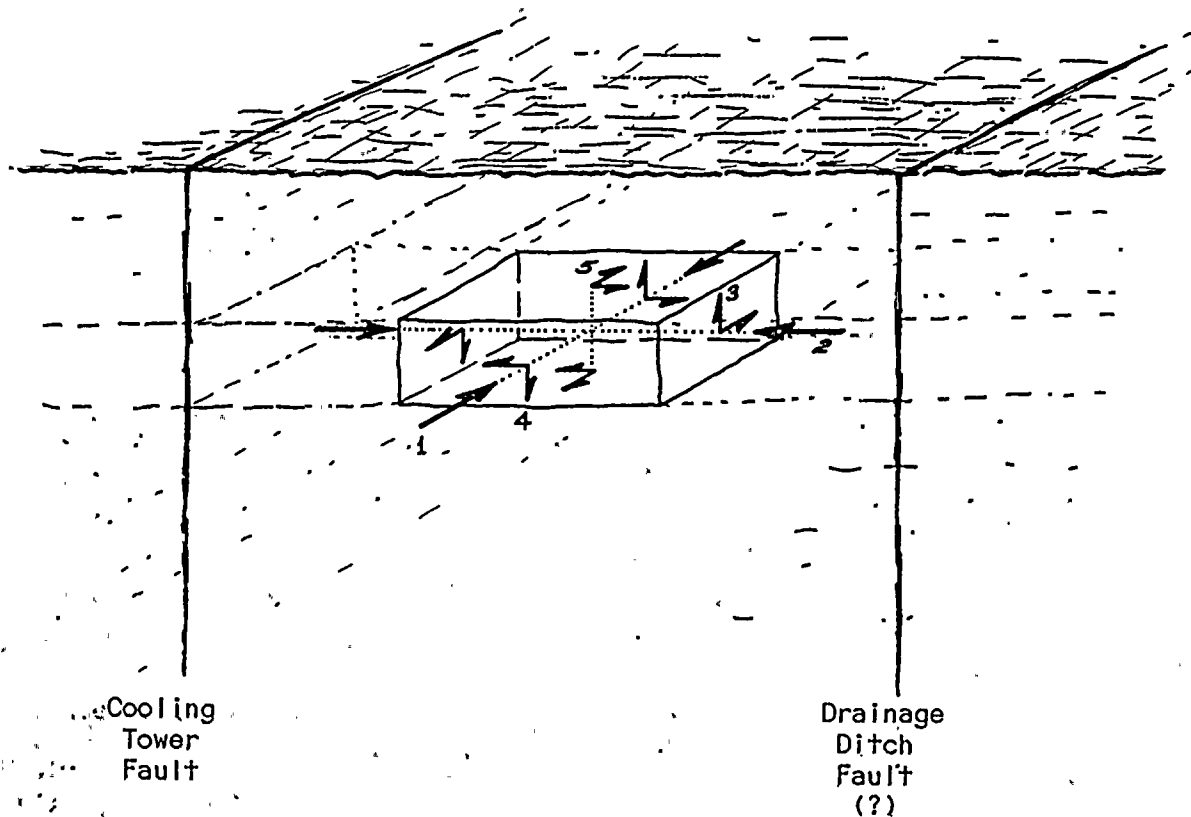
NORTH RADWASTE TRENCH

PLATE 2.3-27
 DAMES & MOORE









EXPLANATION:

1. Fault - parallel, layer - parallel normal stress
2. Fault - normal, layer - parallel normal stress
3. Shear stress in fault parallel vertical planes
4. Shear stress in fault normal vertical planes
5. Fault - parallel and fault - normal shear stresses in horizontal planes

· DIAGRAM SHOWING STRESS NOMENCLATURE



BORING 801

SURFACE ELEVATION 241.4'

COORDINATES N 227.7
W 75.3

DESCRIPTIVE GEOLOGIC NOTES

TOP OF ROCK ELEVATION 241.3'

LIGHT GRAY MEDIUM GRAINED THICKLY BEDDED SILICEOUS SANDSTONE WITH THIN BEDS OF SILTSTONE, HARD AND UNWEATHERED

OSWEGO SANDSTONE

TRANSITION ZONE

GRAY MEDIUM TO COARSE GRAINED, MEDIUM TO THICKLY BEDDED GRAYWACKE WITH ABUNDANT CLASTIC MASH, INTERBEDDED WITH DARK GRAY LAMINATED TO THINLY BEDDED SILTY SHALE AND LIGHT GRAY MEDIUM GRAINED THIN TO THICKLY BEDDED SILICEOUS SANDSTONE, FOSSILIFEROUS, MODERATELY HARD AND UNWEATHERED

PULASKI FORMATION

WATER LEVEL ELEVATION 201.2' (4-2-80)

UNIT A

SAMPLE 801-M1, CALCITE, 43.6'

SAMPLE 801-M2, CALCITE, 45.0'

SAMPLE 801-M3, CALCITE, 46.5'

0.03' THICK GREEN ILLITIC LAYER

UNIT B

LIGHT TO MEDIUM GRAY MEDIUM GRAINED ARGILLACEOUS SANDSTONE, OCCASIONAL DARK GRAY TO BLACK SILTY SHALE AND SILTSTONE, INTERBEDDED THIN SHALE STRINGERS, FOSSILIFEROUS, MODERATELY HARD AND UNWEATHERED

RUN NO.	BEDDING DIPS	FRACTURES
1		
2		0.15' THICK SUBHORIZONTAL BRECCIA WITH CLAY
3		f _c
4		
5		1 f _c
6		
7		
8		SUBHORIZONTAL OPEN FRACTURE SUBHORIZONTAL OPEN FRACTURE
9		f _c
10		f _c
11	30°	SEVERAL BRECCIA ZONES AND ASSOCIATED CORE LOSSES (SEE PLATE S.2-4)
12	30° 47° 50° 0°	f _c
13		170° SLICKENSIDES INDICATE SHEARING OF ILLITIC LAYER
14		f _c
15		
16		

SAMPLING AND CORING INFORMATION

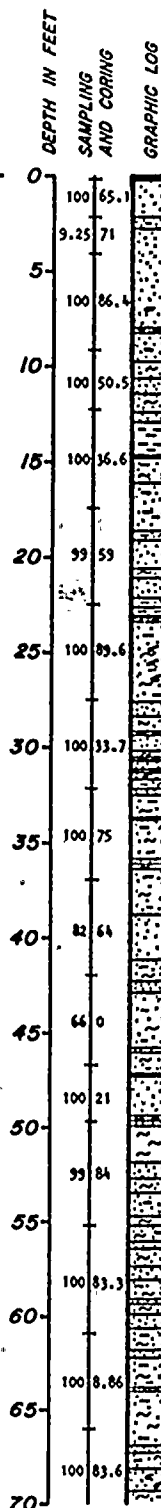
Core run
100/95 R.O.D.
Percent recovery

BEDDING DIPS

03° Bedding dips measured on selective bedding planes. An attempt was made to avoid all obvious cross bedding or other primary structures.

FRACTURES

Breccia zone
 Dip-slip slickensides
 Fractures-shown at approximate angle to core axis
 Mineralized fracture c = calcite s = sulfide
 Fractured zone

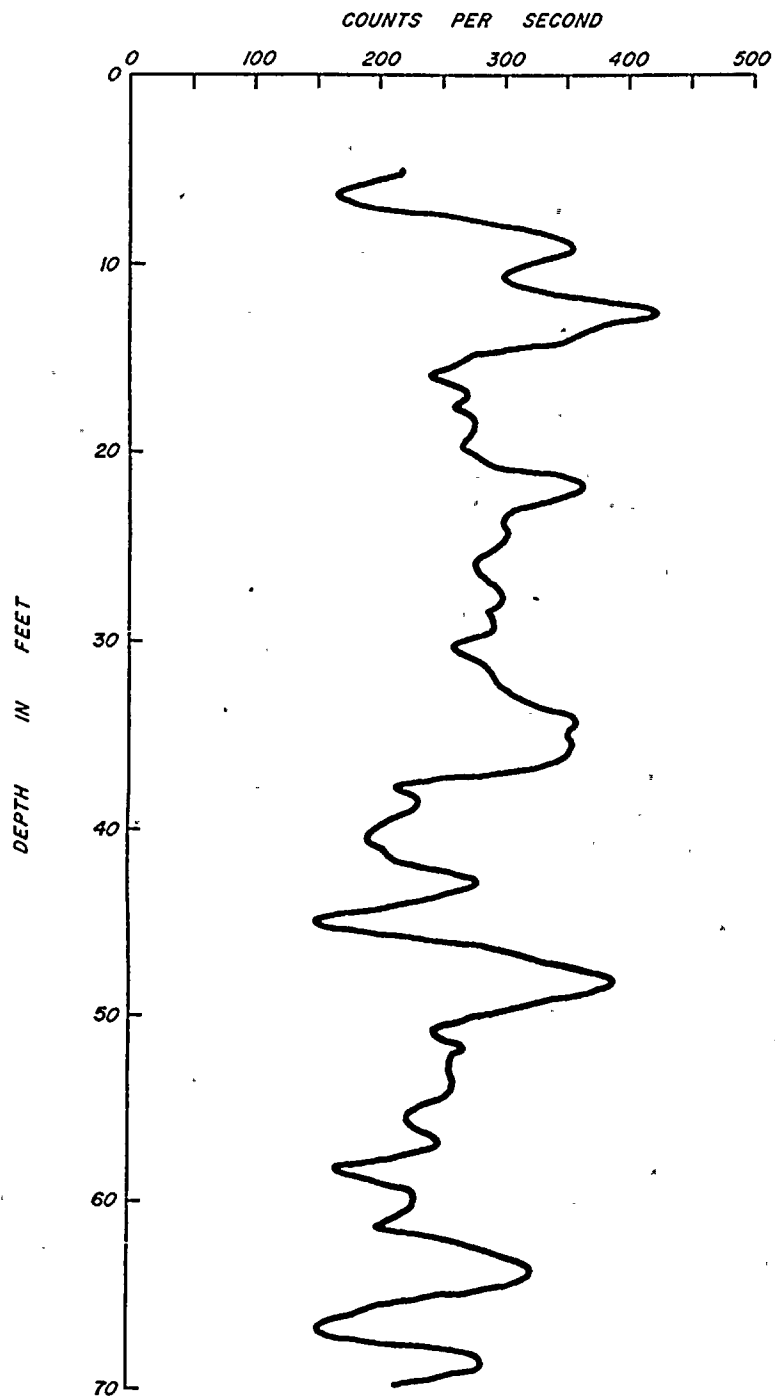


KEY TO SYMBOLS

Sandstone
 Graywacke
 Siltstone
 Shale
 Fossils
 Shale intra-clasts
 Cross-bedding
 Shale laminar

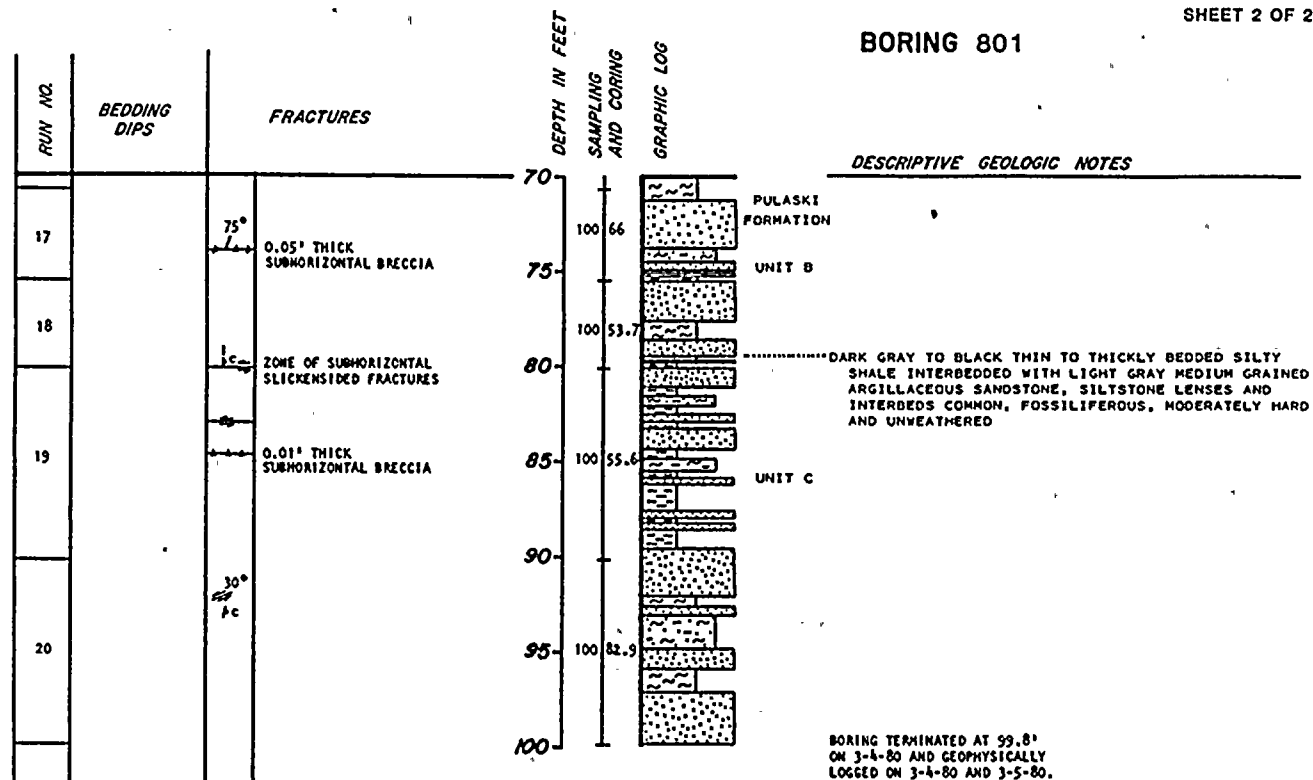


BORING B-801



GAMMA RAY LOG

BORING 801



SAMPLING AND CORING INFORMATION

Core run
100 95 R.Q.D.
Percent recovery

BEDDING DIPS

03° Bedding dips measured on selective bedding planes. An attempt was made to avoid all obvious cross bedding or other primary structures.

FRACTURES

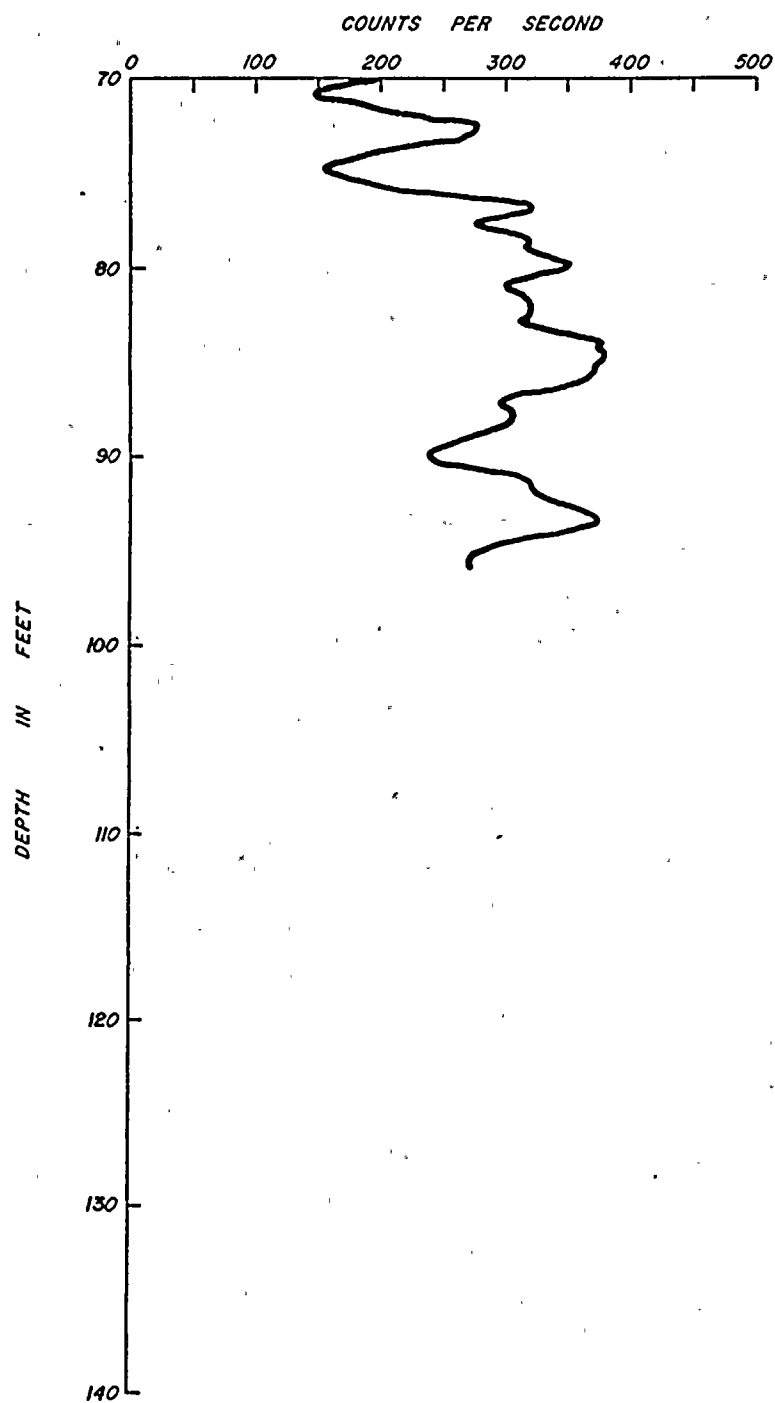
Breccia zone
 Dip-slip slickensides
 Fractures shown at approximate angle to core axis
 Mineralized fracture c = calcite s = sulfide
 Fractured zone

KEY TO SYMBOLS

Sandstone
 Graywacke
 Siltstone
 Shale
 Fossils
 Shale intra-clasts
 Cross-bedding
 Shale lamination

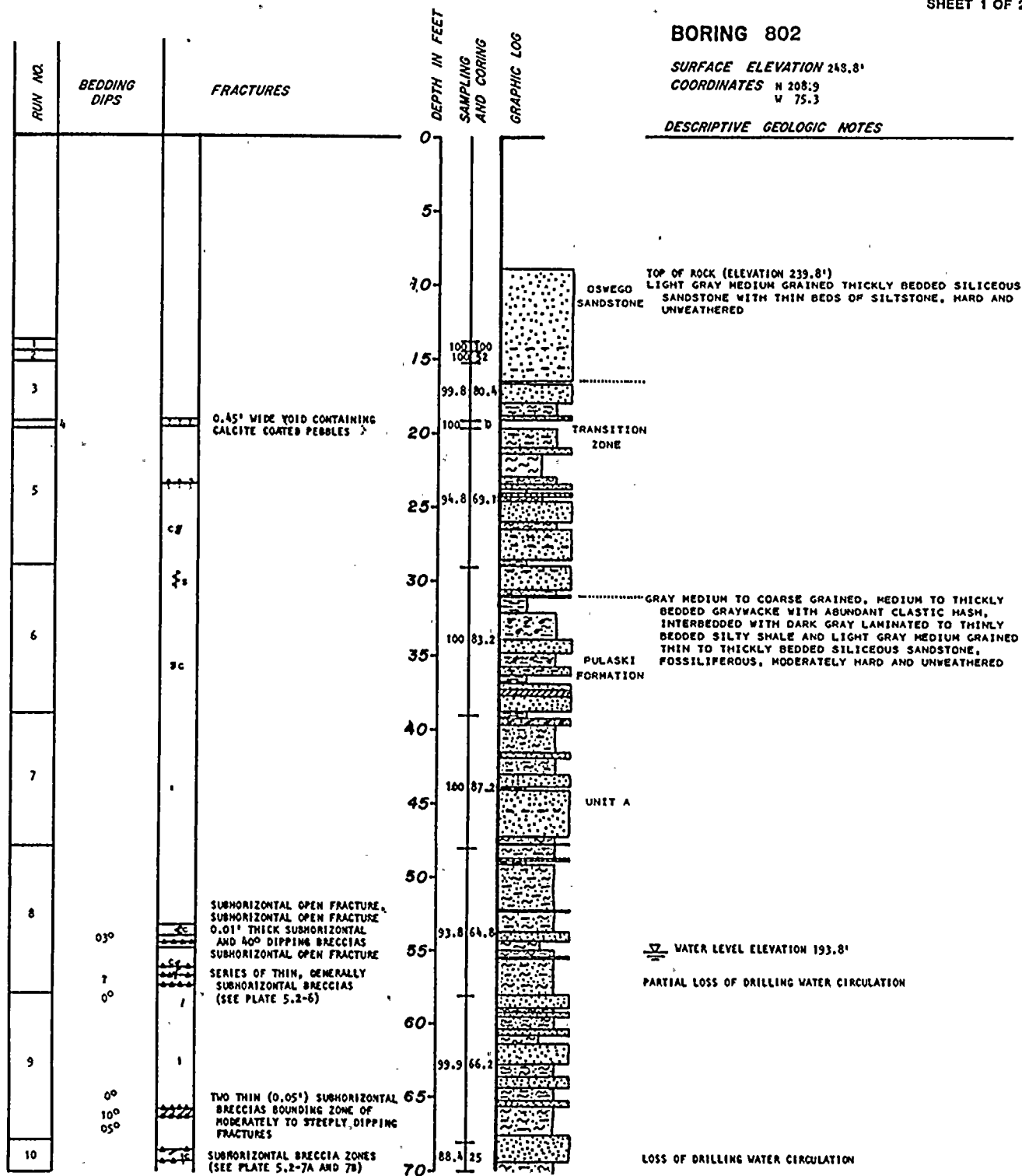


BORING B-801



GAMMA RAY LOG

SURFACE ELEVATION 243.8'
COORDINATES N 208.9
W 75.3

DESCRIPTIVE GEOLOGIC NOTES






SAMPLING AND CORING INFORMATION

Core run
100 95 R.Q.D.
Percent recovery

BEDDING DIPS

03* Bedding dips measured on selective bedding planes. An attempt was made to avoid all obvious cross bedding or other primary structures.

FRACTURES

-  Breccia zone
 Dip-slip slickensides
 Fractures-shown at approximate angle to core axis
 Mineralized fracture c = calcite s = sulfide
 Fractured zone

KEY TO SYMBOLS




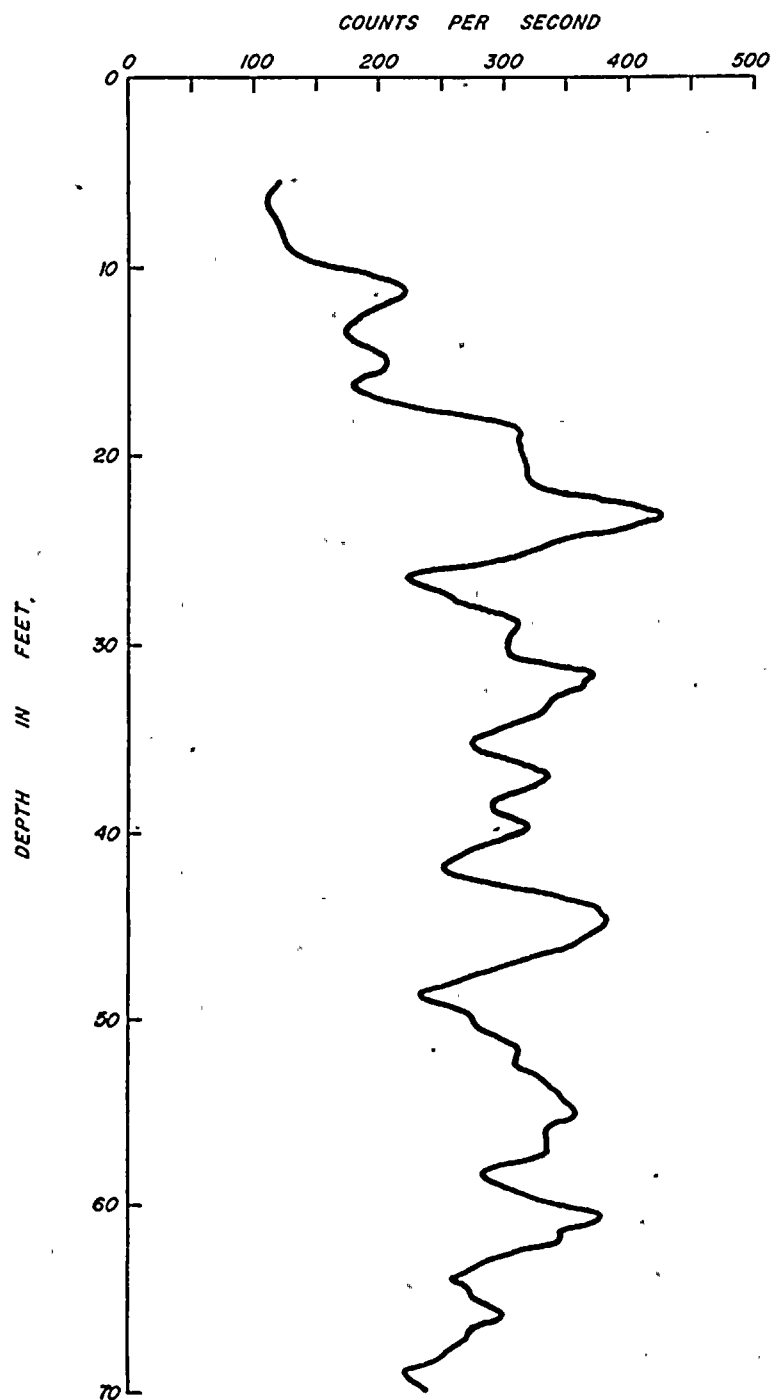
- | | |
|---|--------------------|
|  | Sandstone |
|  | Graywacke |
|  | Siltstone |
|  | Shale |
|  | Fossils |
|  | Shale intra-clasts |
|  | Cross-bedding |
|  | Shale laminae |

PLATE A-2.1
DAMES & MOORE

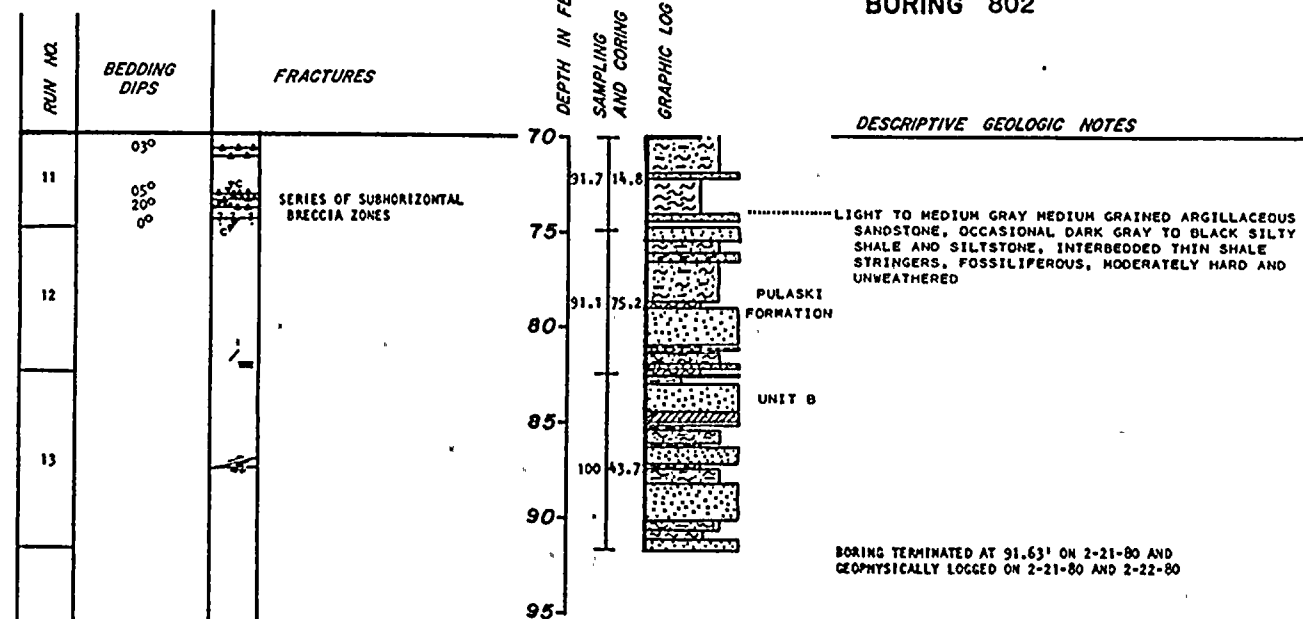


BORING B-802



GAMMA RAY LOG

BORING 802



SAMPLING AND CORING INFORMATION

Core run
 100 95 R.O.D.
 Percent recovery

BEDDING DIPS

03° Bedding dips measured on selective bedding planes. An attempt was made to avoid all obvious cross bedding or other primary structures.

FRACTURES

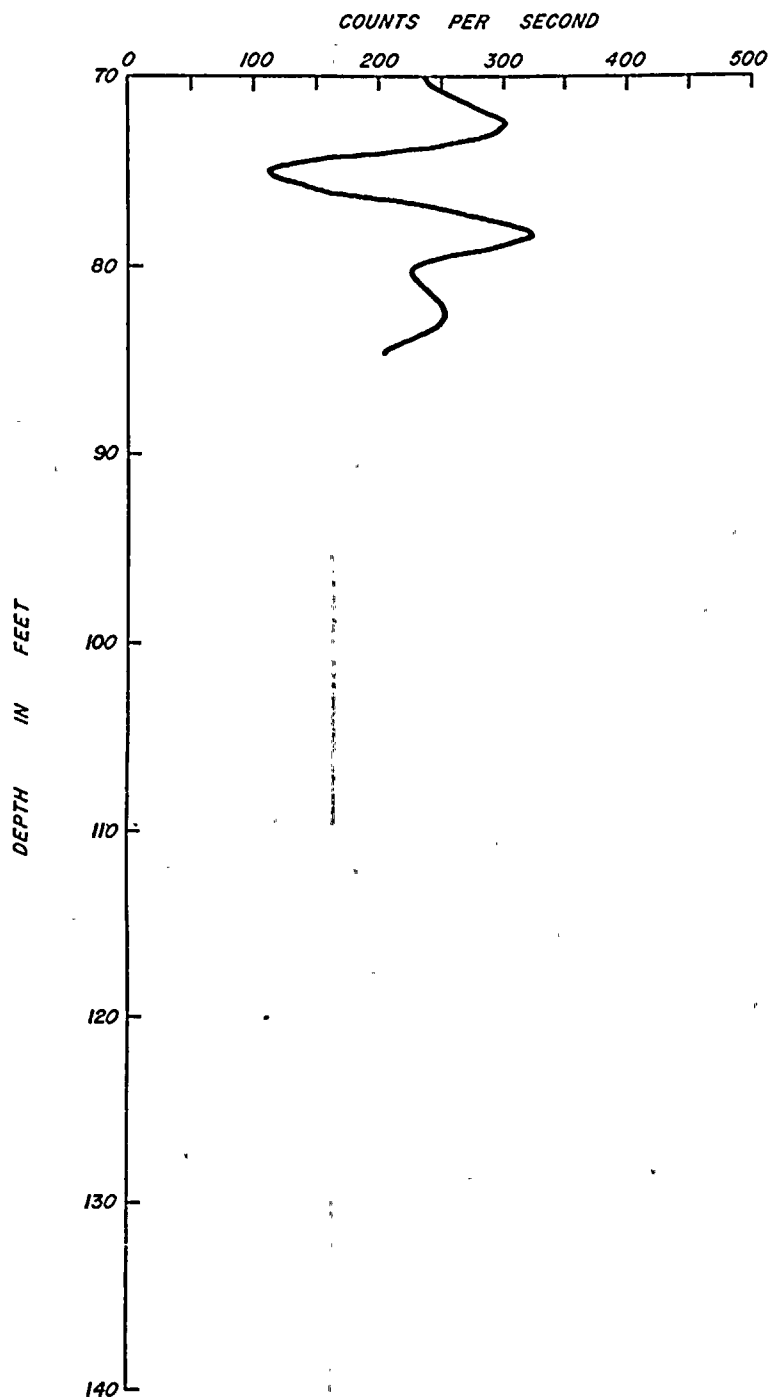
Breccia zone
 Dip-slip slickensides
 Fractures shown at approximate angle to core axis
 Mineralized fracture c = calcite s = sulfide
 Fractured zone

KEY TO SYMBOLS

Sandstone
 Graywacke
 Siltstone
 Shale
 Fossils
 Shale intra-clastic
 Cross-bedding
 Shale lamination



BORING B-802



GAMMA RAY LOG



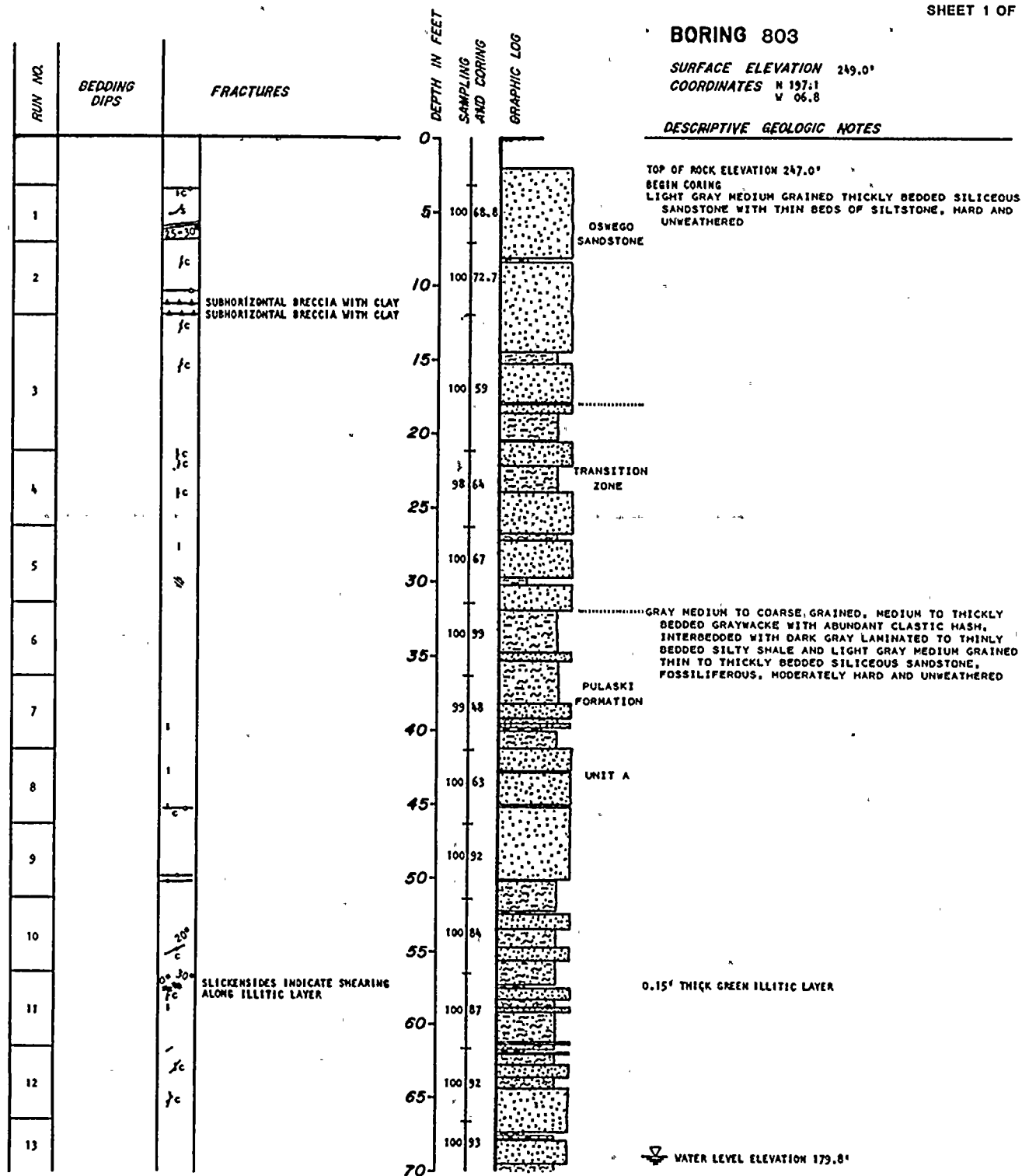
BORING 803

SURFACE ELEVATION 249.0'

COORDINATES N 197.1
W 06.8

DESCRIPTIVE GEOLOGIC NOTES

TOP OF ROCK ELEVATION 247.0'
 BEGIN CORING
 LIGHT GRAY MEDIUM GRAINED THICKLY BEDDED SILICEOUS
 SANDSTONE WITH THIN BEDS OF SILTSTONE, HARD AND
 UNWEATHERED



SAMPLING AND CORING INFORMATION

Core run
 100 95 R.O.D.
 Percent recovery

BEDDING DIPS

03° Bedding dips measured on selective bedding planes. An attempt was made to avoid all obvious cross bedding or other primary structures.

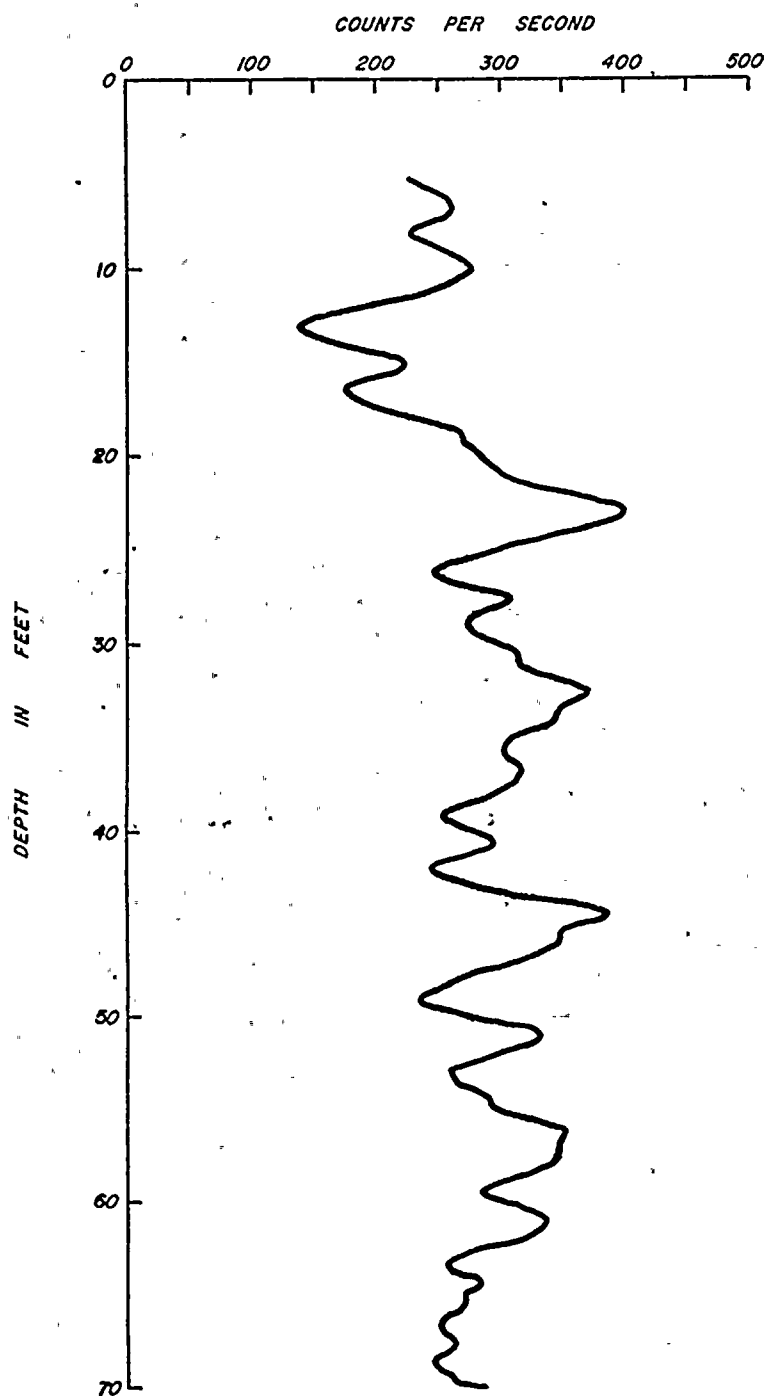
FRACTURES

- Brecchia zone
- Dip-slip slickensides
- Fractures-shown at approximate angle to core axis
- Mineralized fracture c = calcite s = sulfide
- Fractured zone

KEY TO SYMBOLS

- Sandstone
- Graywacke
- Siltstone
- Shale
- Fossils
- Shale intra-clasts
- Cross-bedding
- Shale laminae

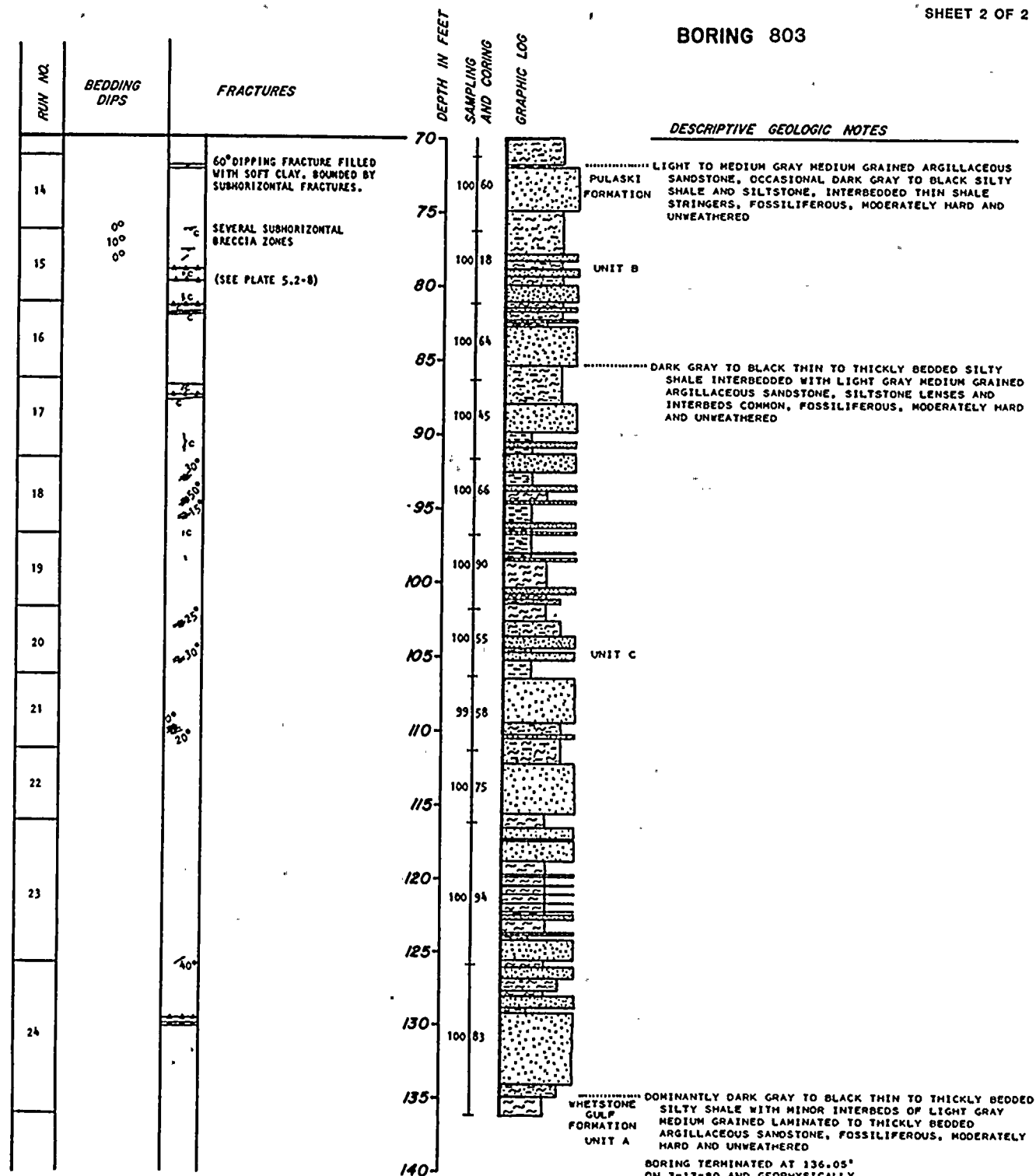
BORING B-803



GAMMA RAY LOG



BORING 803



SAMPLING AND CORING INFORMATION

Core run
100 95 R.O.D.
Percent recovery

BEDDING DIPS

03° Bedding dips measured on selective bedding planes. An attempt was made to avoid all obvious cross bedding or other primary structures.

FRACTURES

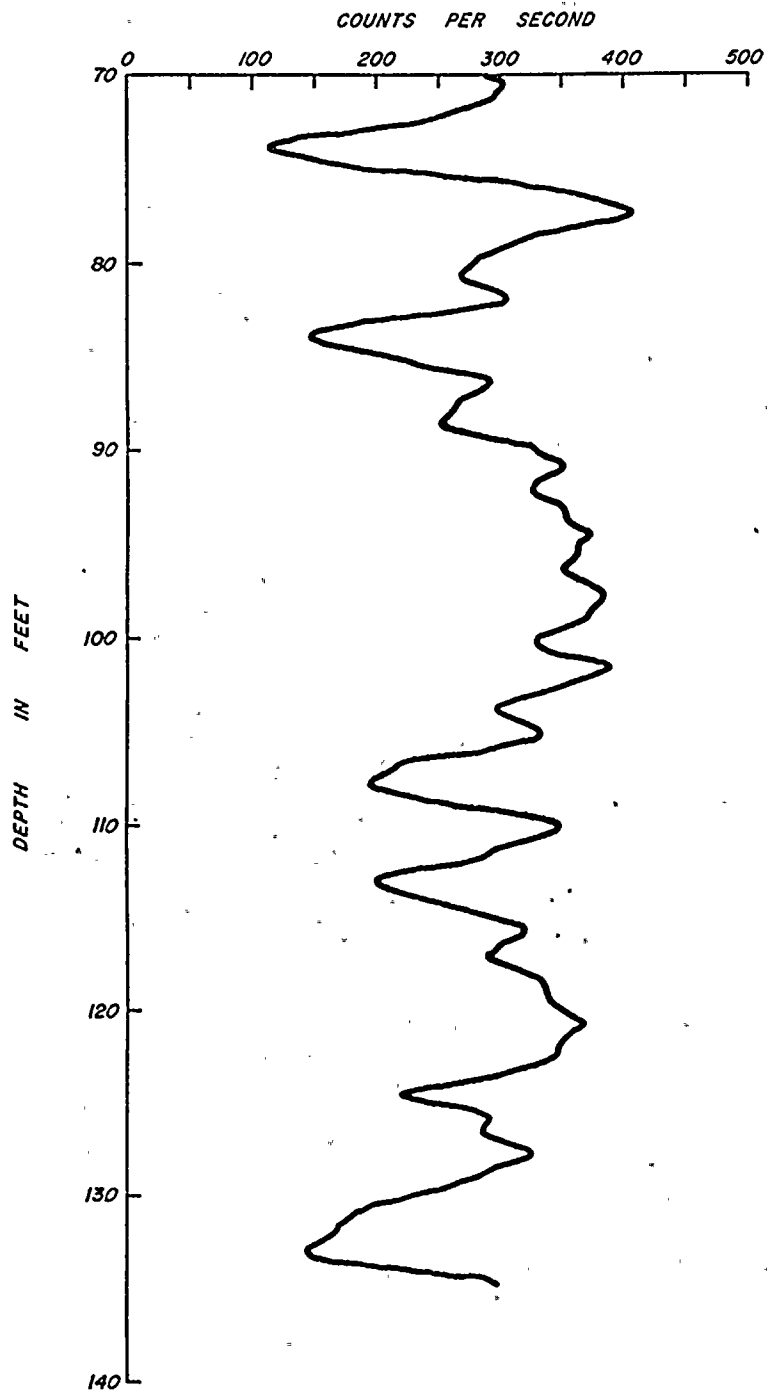
Breccia zone
Dip-slip slickensides
Fractures-shown at approximate angle to core axis
Mineralized fracture c = calcite s = sulfide
Fractured zone

KEY TO SYMBOLS

Sandstone
Graywacke
Siltstone
Shale
Fossils
Shale Intra-clasts
Cross-bedding
Shale laminae



BORING B-803



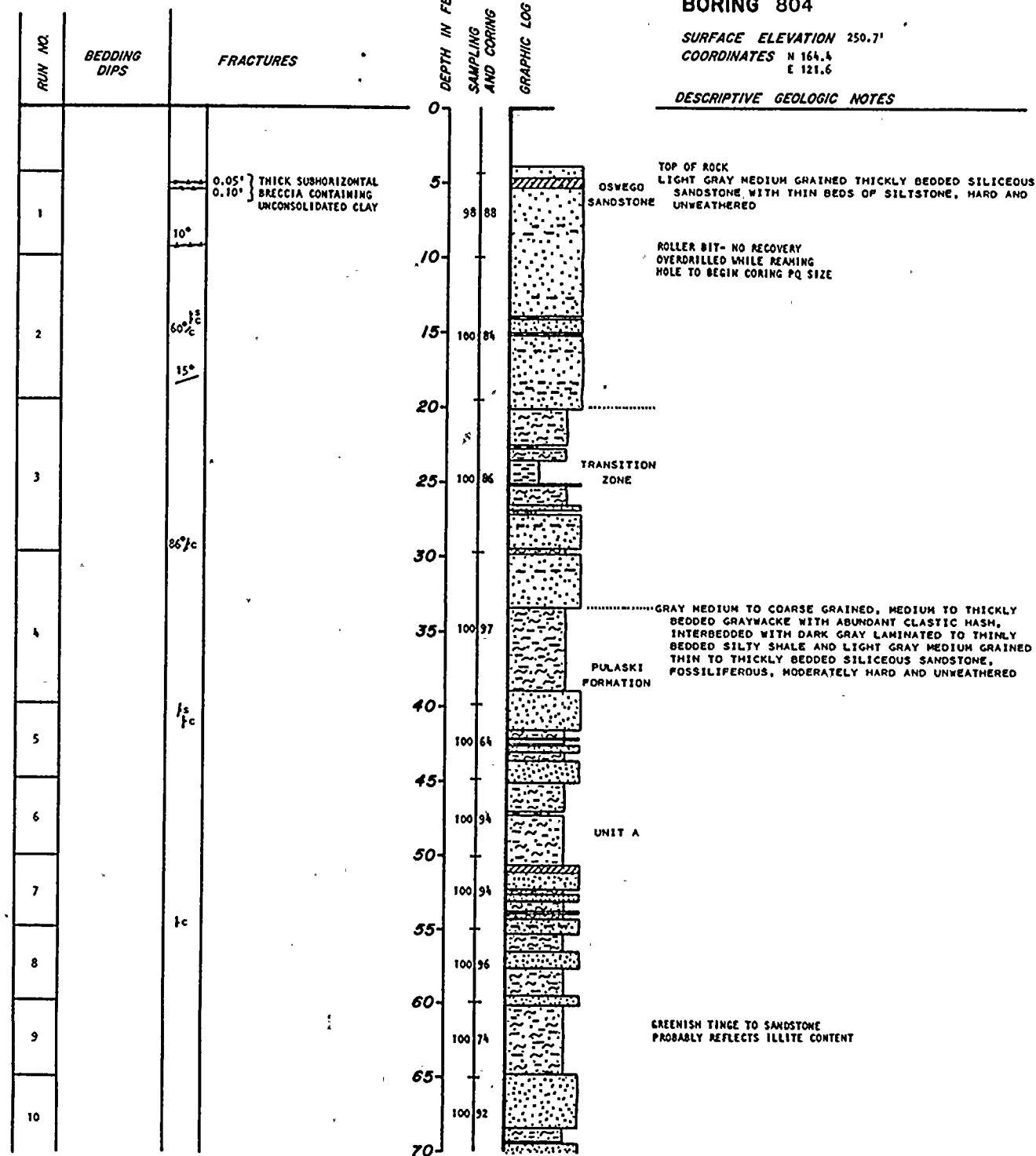
GAMMA RAY LOG

BORING 804

SURFACE ELEVATION 250.7'

COORDINATES N 164.4
E 121.6

DESCRIPTIVE GEOLOGIC NOTES



SAMPLING AND CORING INFORMATION

Core run
100 95 R.Q.D.
Percent recovery

BEDDING DIPS

03° Bedding dips measured on selective bedding planes. An attempt was made to avoid all obvious cross bedding or other primary structures.

FRACTURES

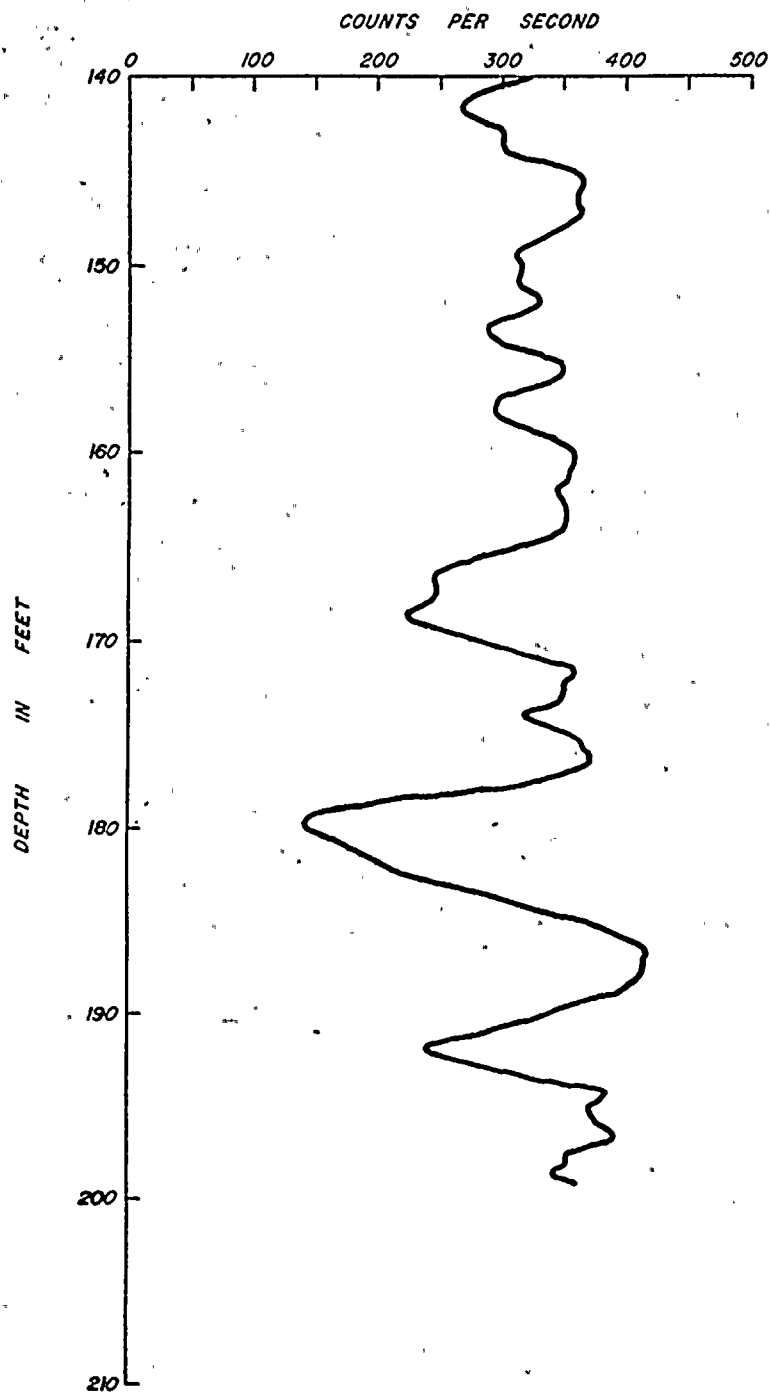
Breccia zone
Dip-slip slickensides
Fractures shown at approximate angle to core axis
Mineralized fracture c = calcite s = sulfide
Fractured zone

KEY TO SYMBOLS

Sandstone
Graywacke
Siltstone
Shale
Fossils
Shale intra-clasts
Cross-bedding
Shale lamination

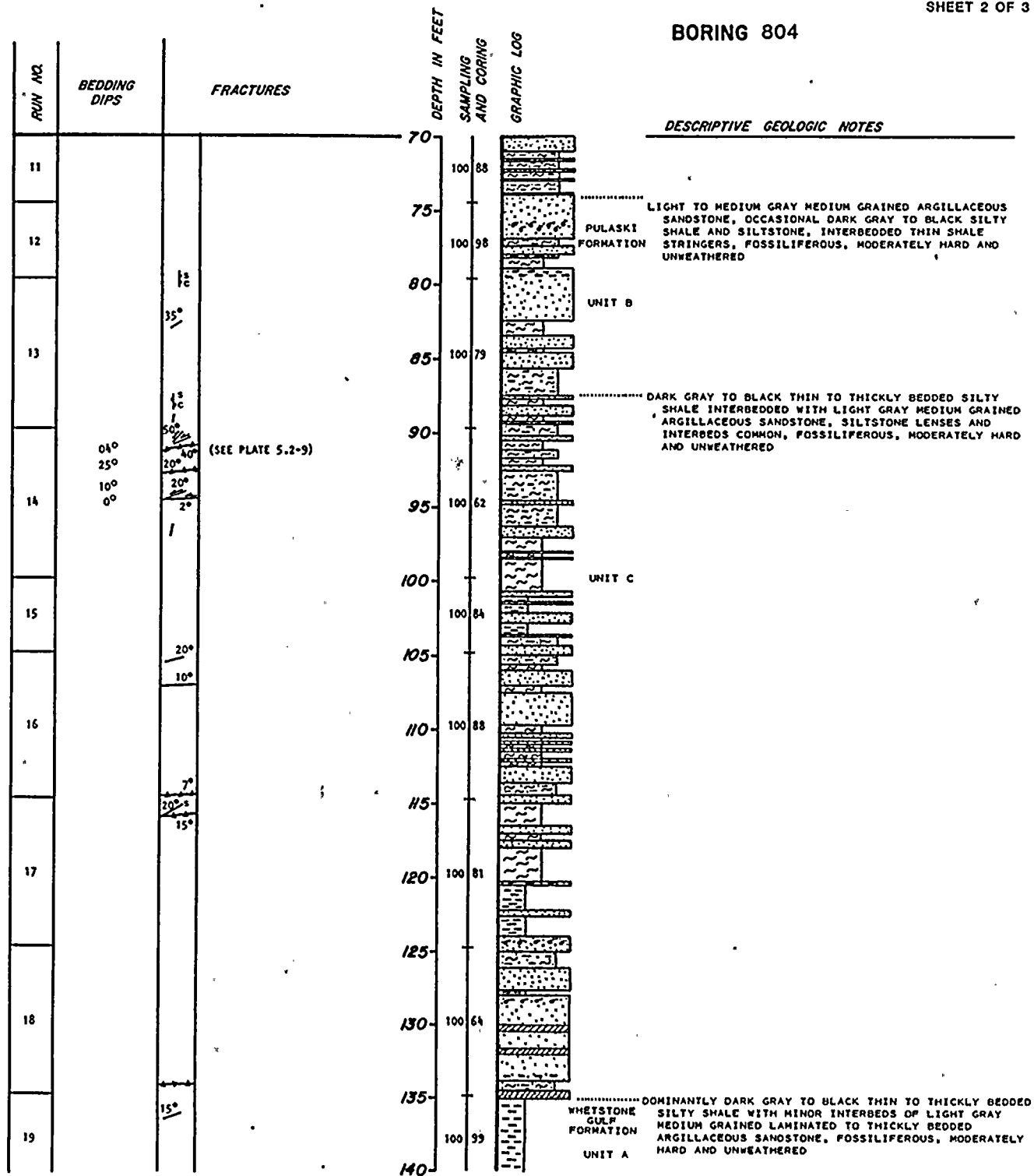


BORING B-804



GAMMA RAY LOG

BORING 804



SAMPLING AND CORING INFORMATION

Core run
100 95 R.Q.D.
Percent recovery

BEDDING DIPS

03° Bedding dips measured on selective bedding planes. An attempt was made to avoid all obvious cross bedding or other primary structures.

FRACTURES

Brachia zone
Dip-slip slickensides
Fractures shown at approximate angle to core axis
Mineralized fracture c = calcite s = sulfide
Fractured zone

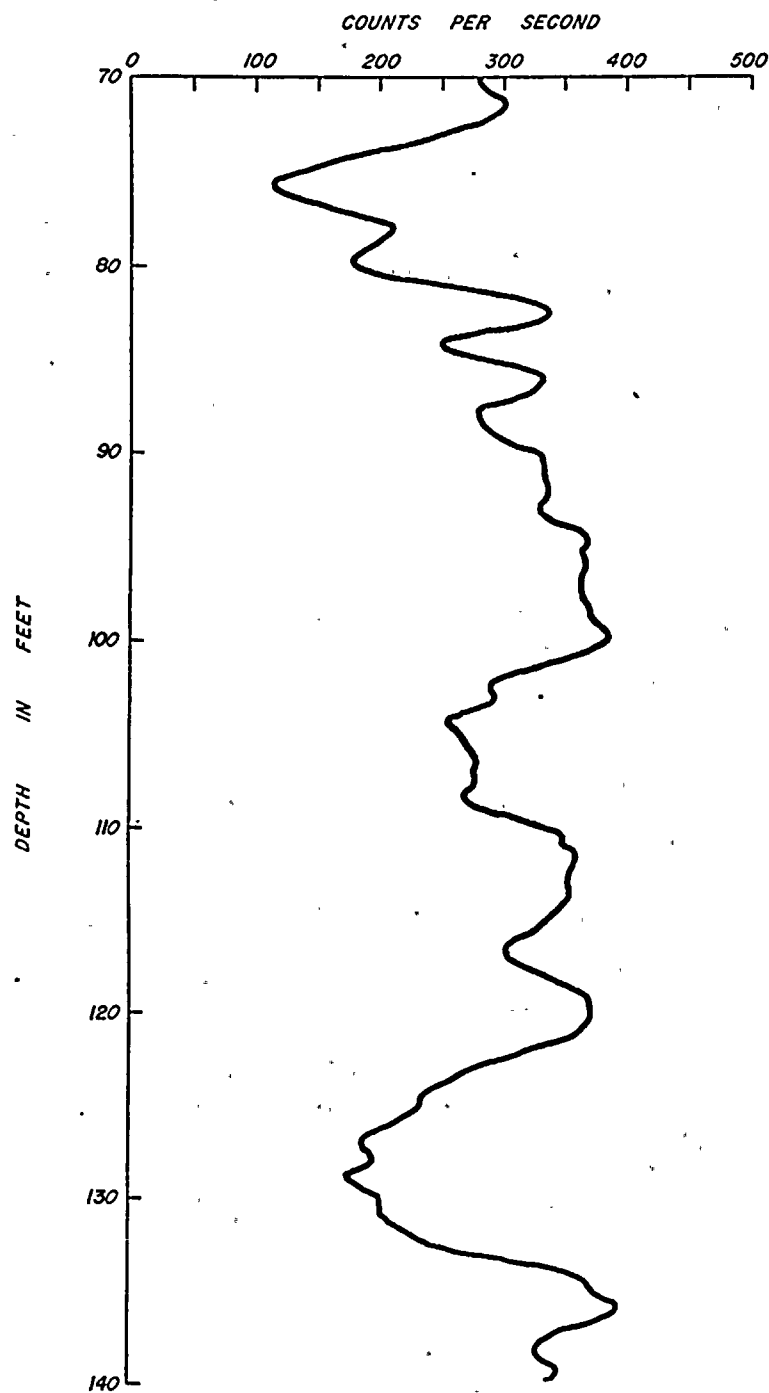
KEY TO SYMBOLS

Sandstone
Graywacke
Siltstone
Shale
Fossils
Shale intra-clasts
Cross-bedding
Shale laminae



)

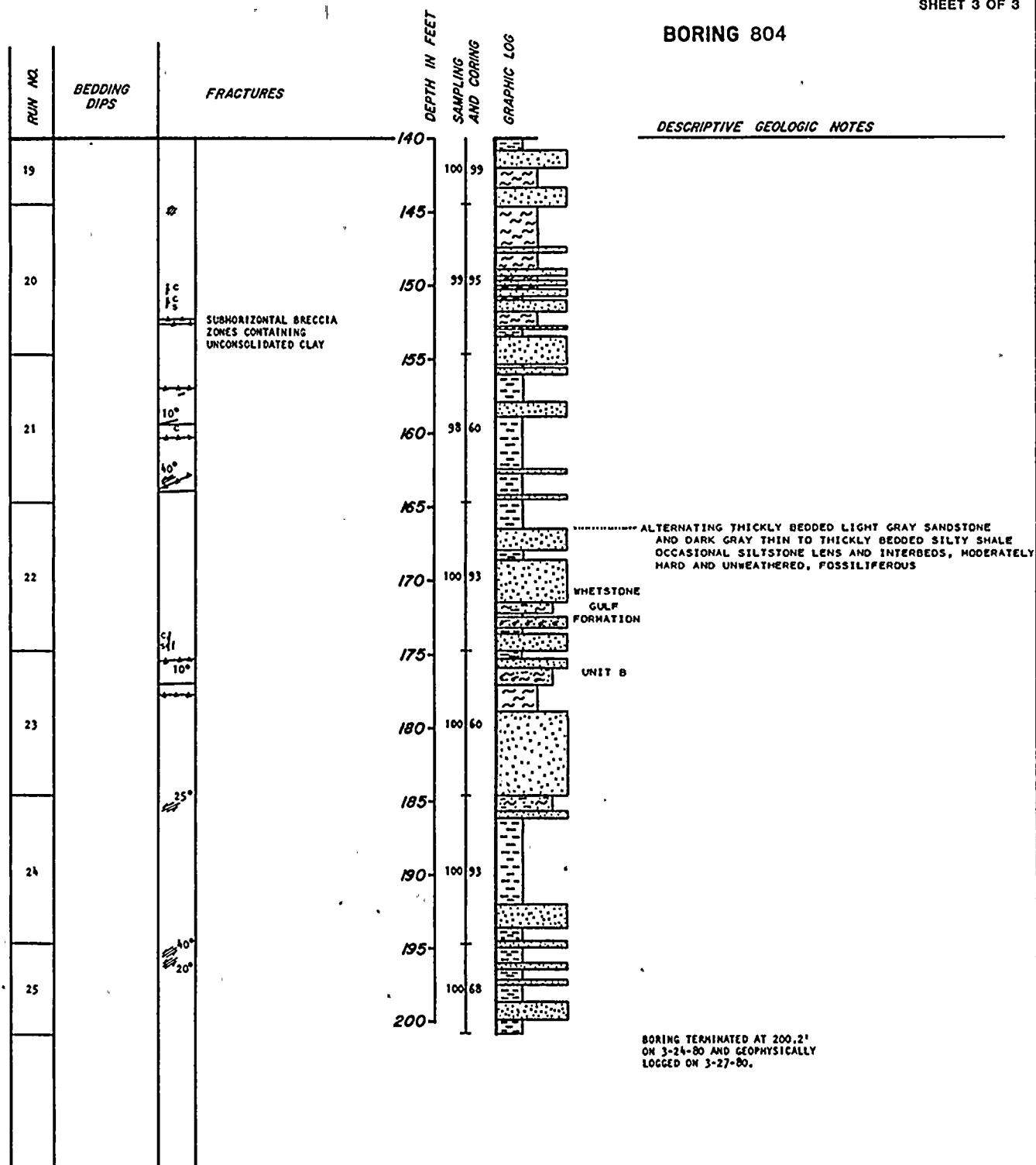
BORING B-804



GAMMA RAY LOG



BORING 804



SAMPLING AND CORING INFORMATION

Core run
100 95 R.O.D.
Percent recovery

BEDDING DIPS

03° Bedding dips measured on selective bedding planes. An attempt was made to avoid all obvious cross bedding or other primary structures.

FRACTURES

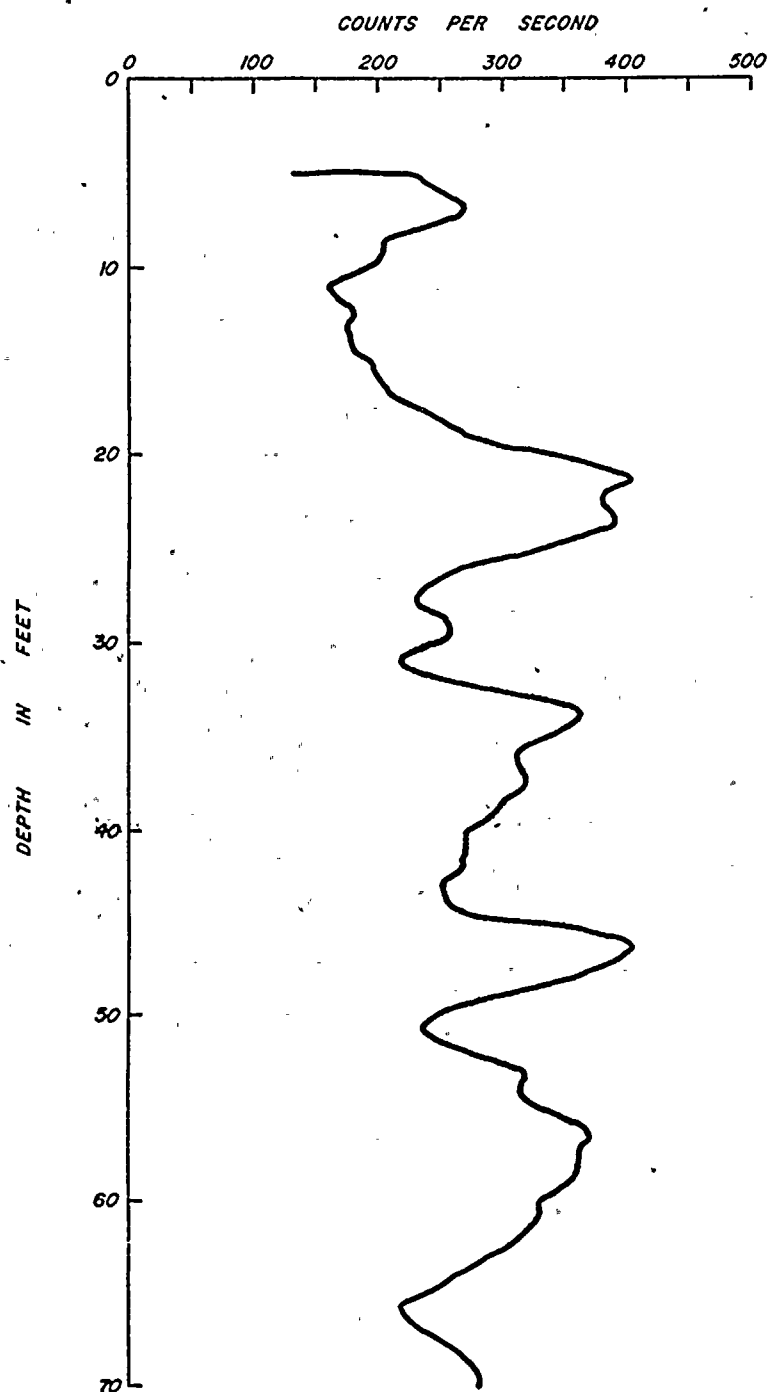
Breccia zone
Dip-slip slickensides
Fractures shown at approximate angle to core axis
Mineralized fracture c = calcite s = sulfide
Fractured zone

KEY TO SYMBOLS

Sandstone
Graywacke
Siltstone
Shale
Fossils
Shale intra-clasts
Cross-bedding
Shale laminae



BORING B-804



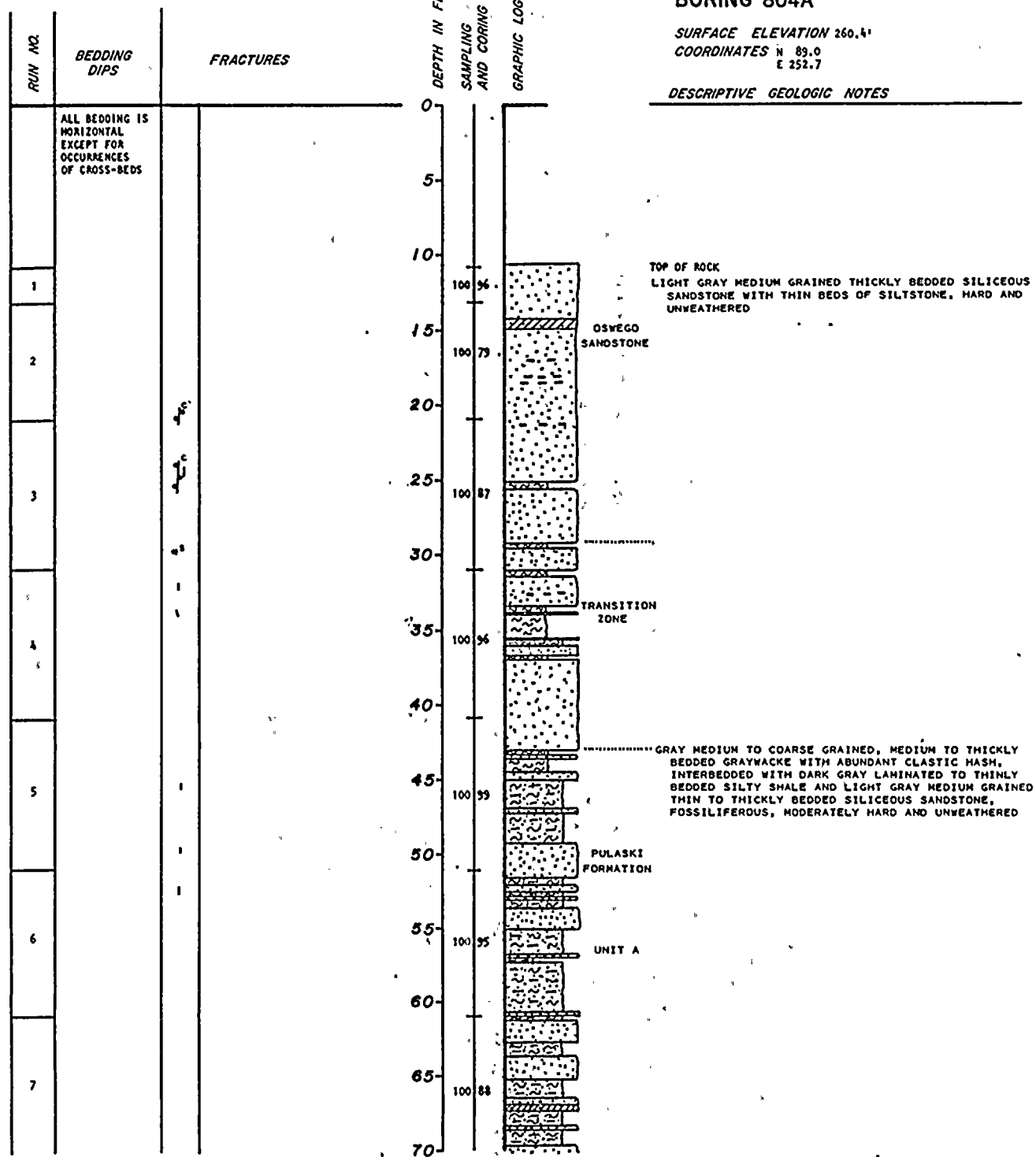
GAMMA RAY LOG



BORING 804A

SURFACE ELEVATION 260.4'
 COORDINATES N 89.0
 E 252.7

DESCRIPTIVE GEOLOGIC NOTES



SAMPLING AND CORING INFORMATION

Core run
 100 95 R.Q.D.
 Percent recovery

BEDDING DIPS

03° Bedding dips measured on selective bedding planes. An attempt was made to avoid all obvious cross bedding or other primary structures.

FRACTURES

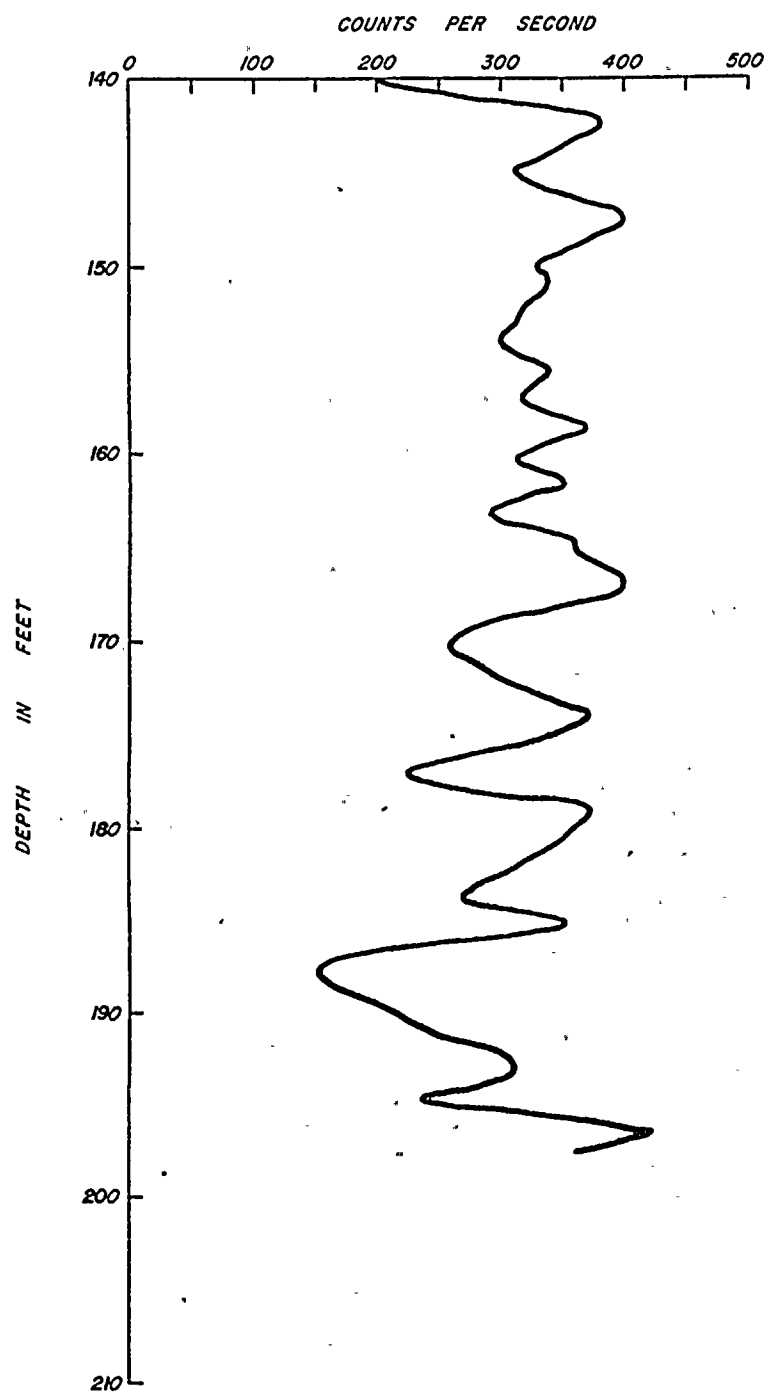
Breccia zone
 Dip-slip slickensides
 Fractures-shown at approximate angle to core axis
 Mineralized fracture c = calcite s = sulfide
 Fractured zone

KEY TO SYMBOLS

Sandstone
 Graywacke
 Siltstone
 Shale
 Fossils
 Shale intra-clasts
 Cross-bedding
 Shale laminar



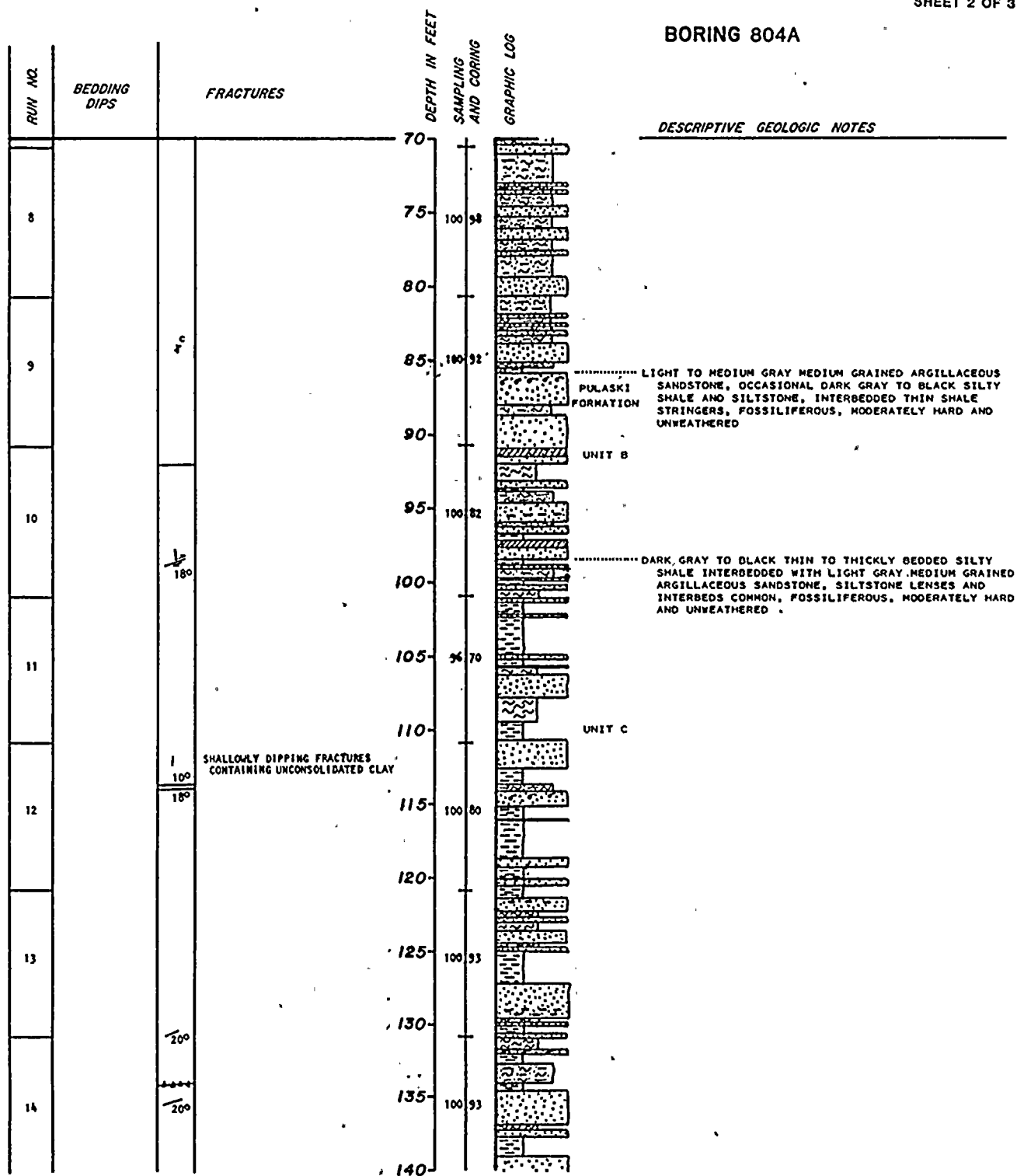
BORING B-804A



GAMMA RAY LOG



BORING 804A



SAMPLING AND CORING INFORMATION

Core run
100 99 R.O.D.
Percent recovery

BEDDING DIPS

03° Bedding dips measured on selective bedding planes. An attempt was made to avoid all obvious cross bedding or other primary structures.

FRACTURES

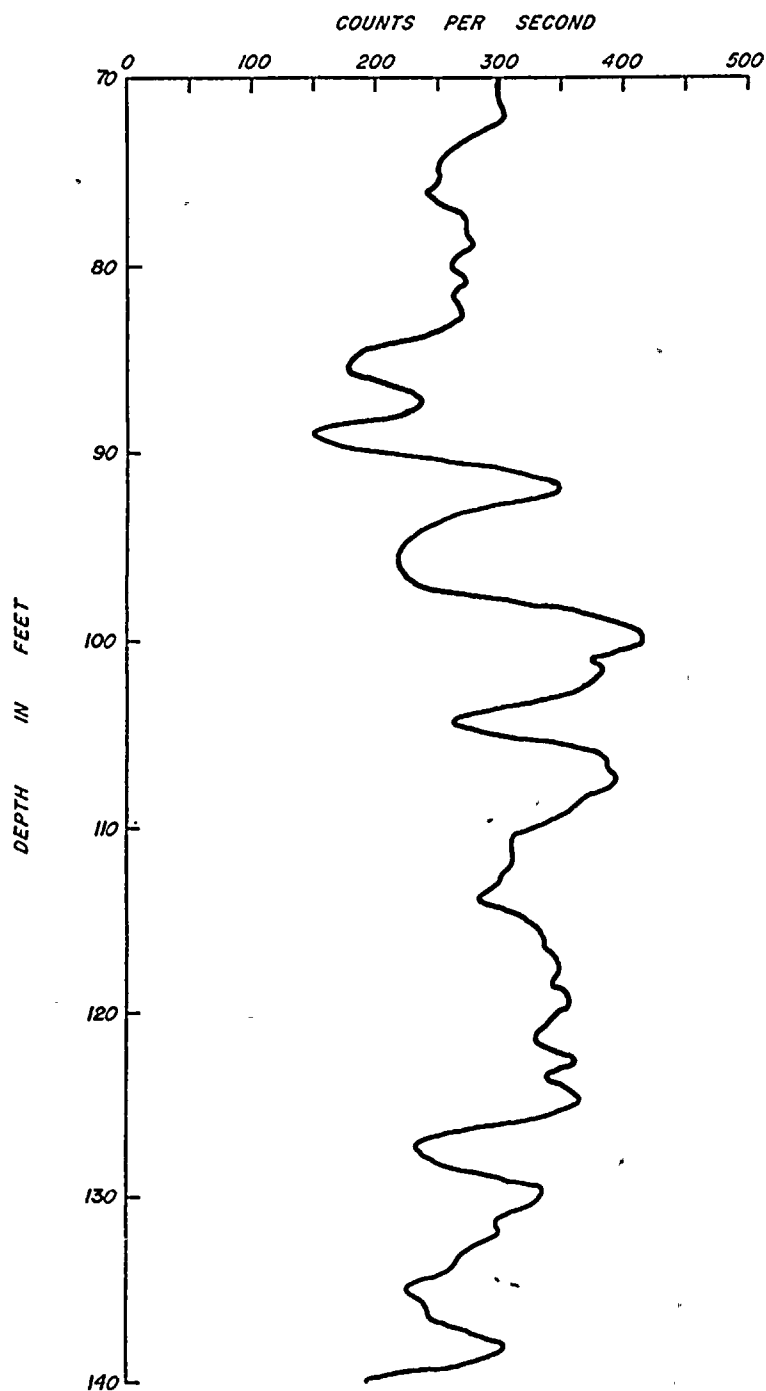
Brachiola zone
Dip-slip slickensides
Fractures shown at approximate angle to core axis
Mineralized fracture c = calcite s = sulfide
Fractured zone

KEY TO SYMBOLS

Sandstone
Graywacke
Siltstone
Shale
Fossils
Shale intra-clasts
Cross-bedding
Shale laminae



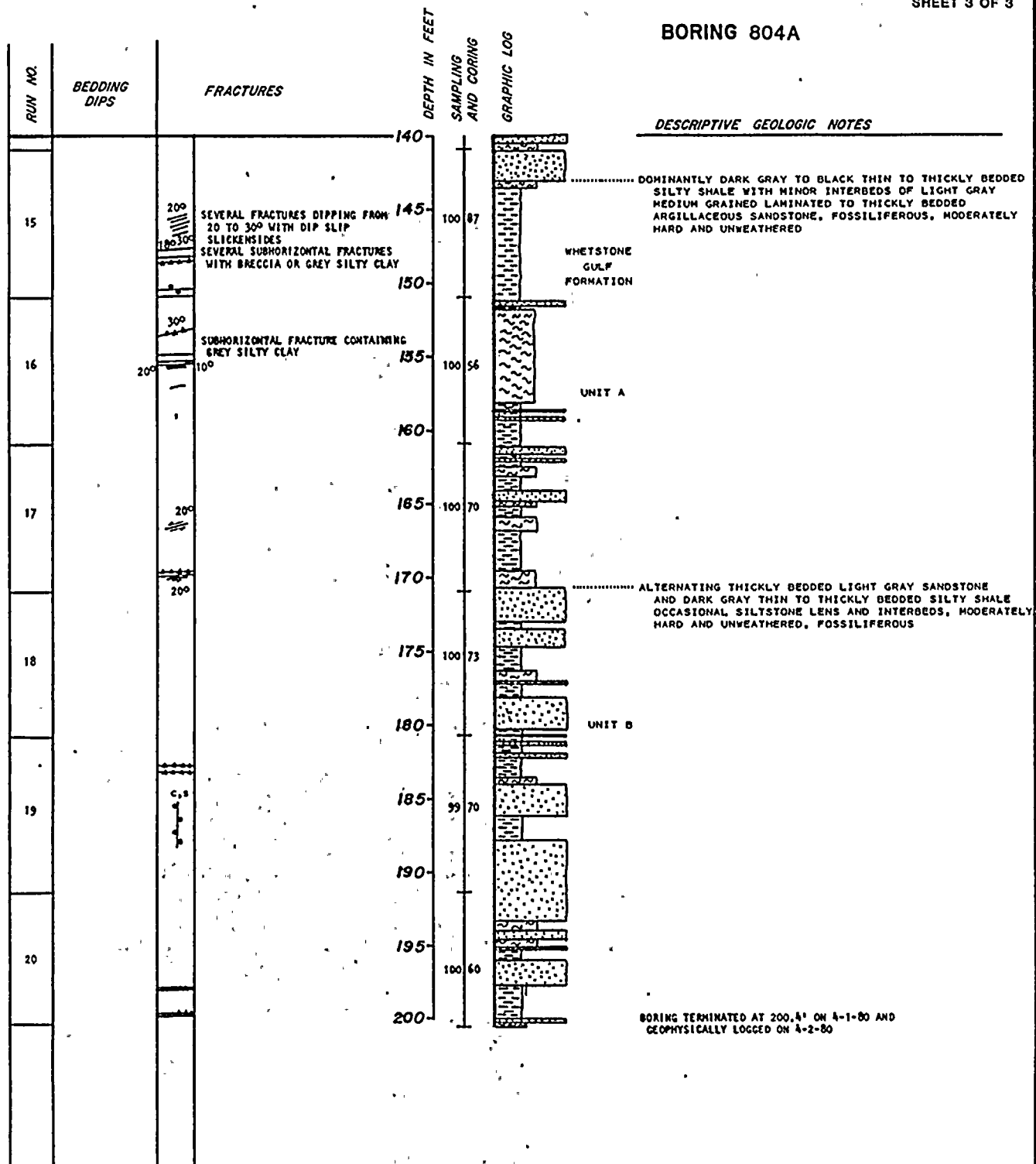
BORING B-804A



GAMMA RAY LOG



BORING 804A



SAMPLING AND CORING INFORMATION

Core run
100% R.O.D.
Percent recovery

BEDDING DIPS

03° Bedding dips measured on selective bedding planes. An attempt was made to avoid all obvious cross bedding or other primary structures.

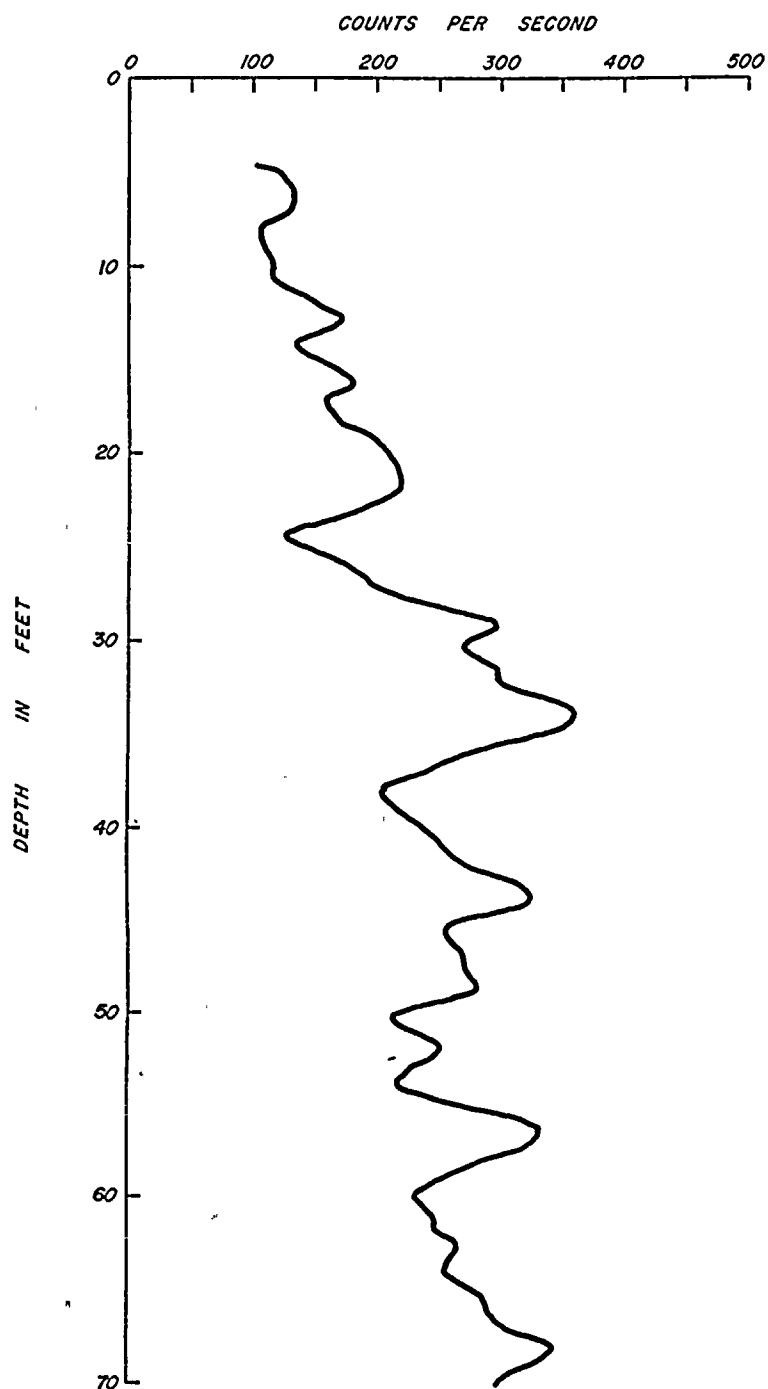
FRACTURES

Breccia zone
Dip-slip slickensides
Fractures shown at approximate angle to core axis
Mineralized fracture c = calcite s = sulfide
Fractured zone

KEY TO SYMBOLS

Sandstone
Graywacke
Siltstone
Shale
Fossils
Shale Intra-clasts
Cross-bedding
Shale lamination

BORING B-804A



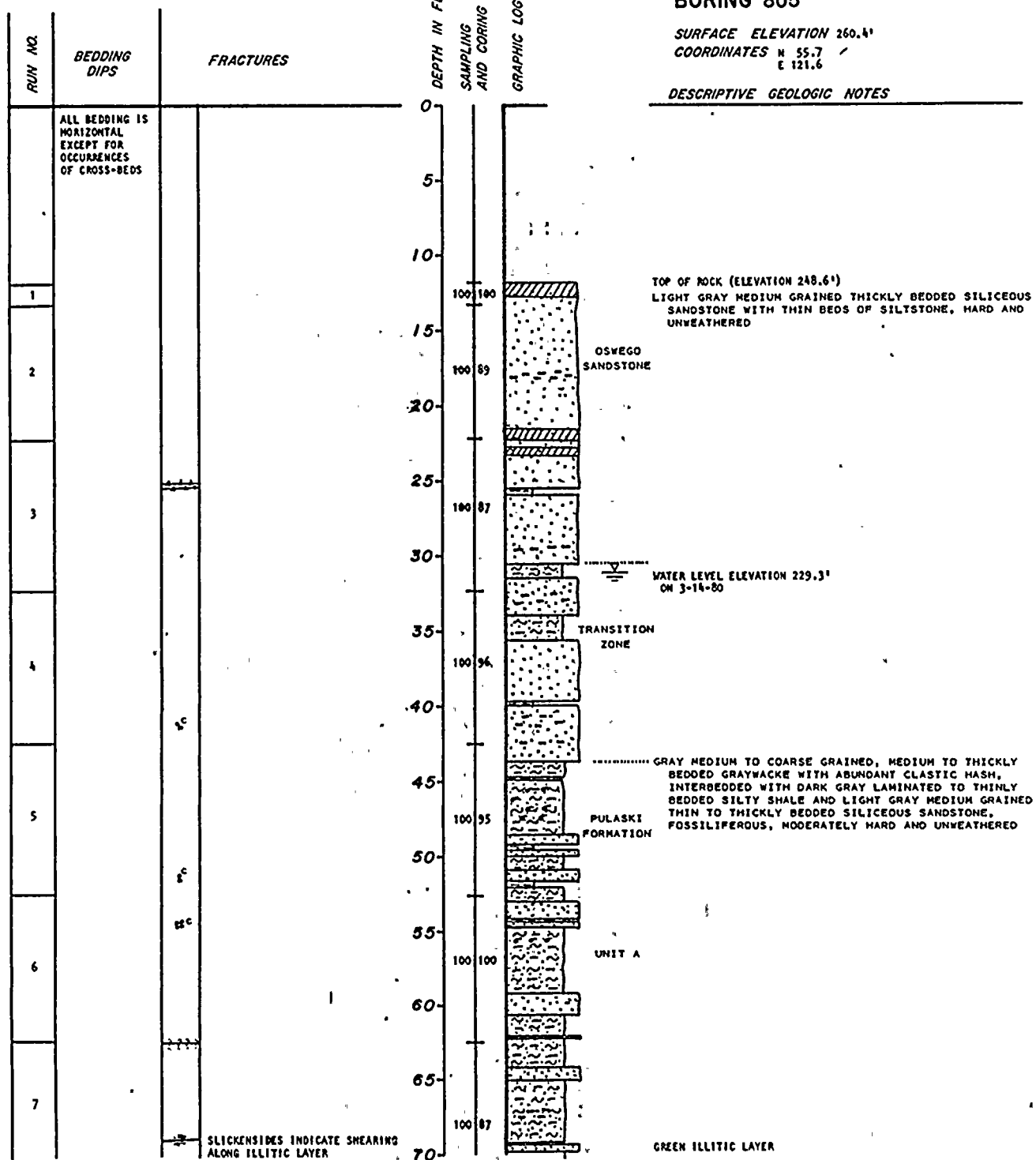
GAMMA RAY LOG



BORING 805

SURFACE ELEVATION 260.4'
 COORDINATES N 55.7 /
 E 121.6

DESCRIPTIVE GEOLOGIC NOTES



SAMPLING AND CORING INFORMATION

Core run
 100/95 R.Q.D.
 Percent recovery

BEDDING DIPS

03° Bedding dips measured on selective bedding planes. An attempt was made to avoid all obvious cross bedding or other primary structures.

FRACTURES

Breccia zone
 Dip-slip slickensides
 Fractures shown at approximate angle to core axis
 Mineralized fracture c = calcite s = sulfide
 Fractured zone

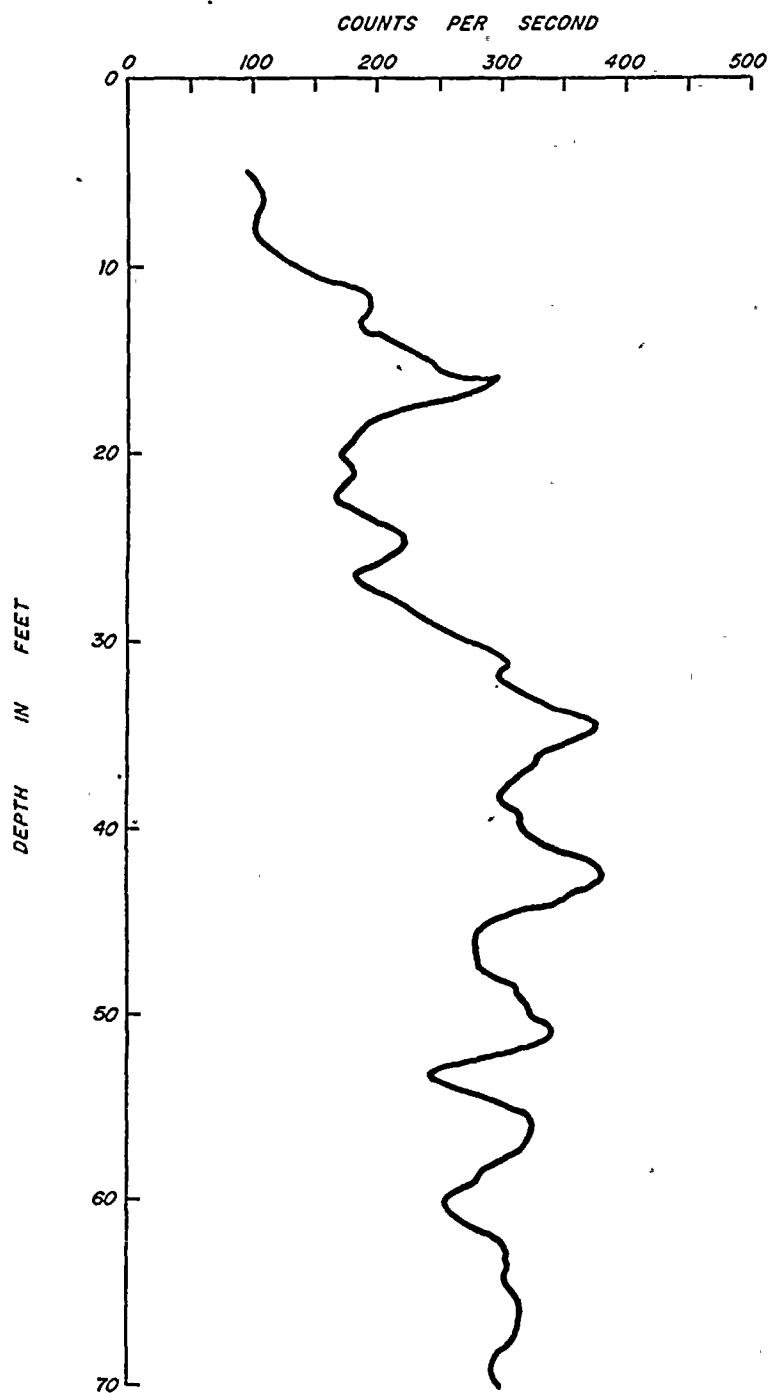
KEY TO SYMBOLS

Sandstone
 Graywacke
 Siltstone
 Shale
 Fossils
 Shale intra-clasts
 Cross-bedding
 Shale laminae

PLATE A-6.1

DAMES & MOORE

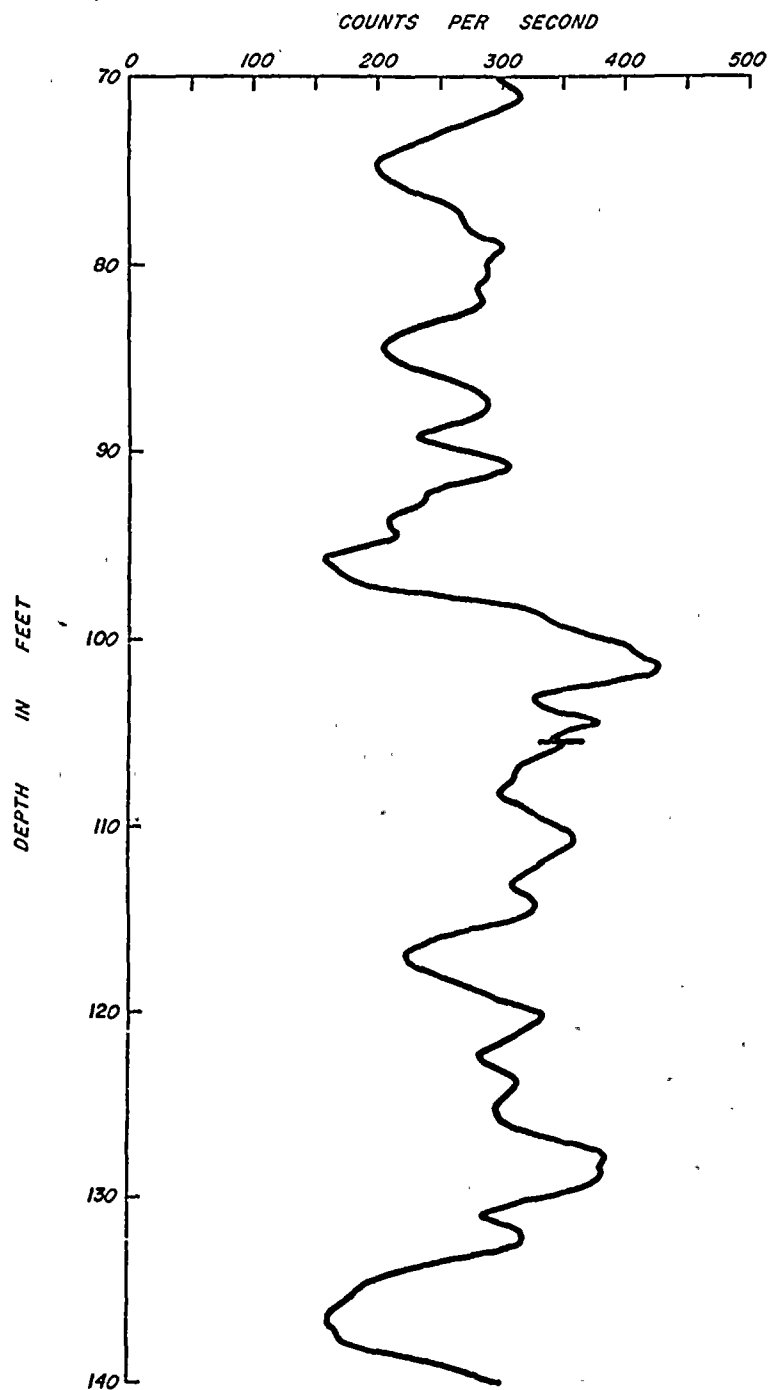
BORING B-805



GAMMA RAY LOG



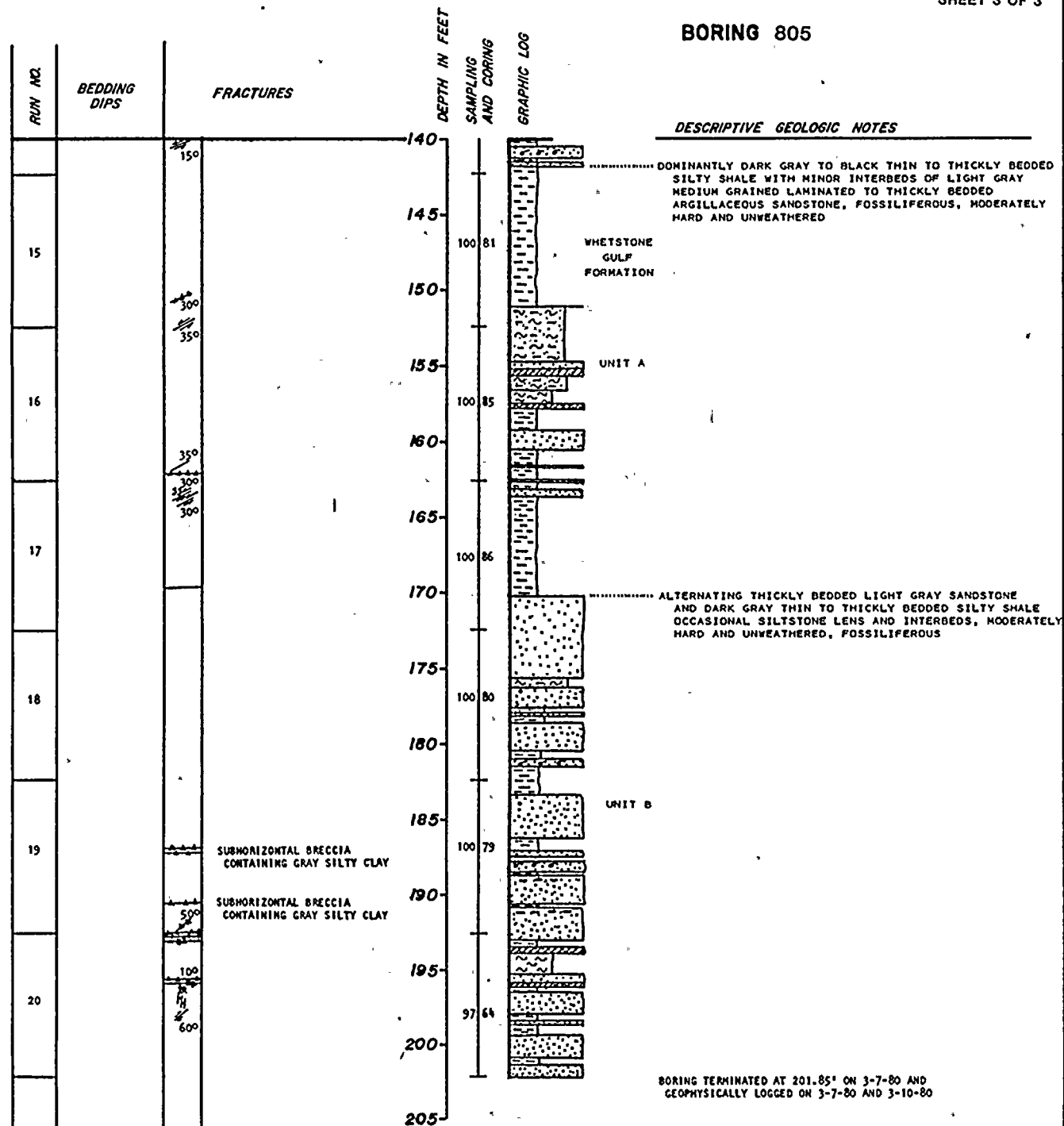
BORING B-805



GAMMA RAY LOG



BORING 805



SAMPLING AND CORING INFORMATION

Core run
100 95 R.Q.D.
Percent recovery

BEDDING DIPS

03° Bedding dips measured on selective bedding planes. An attempt was made to avoid all obvious cross bedding or other primary structures.

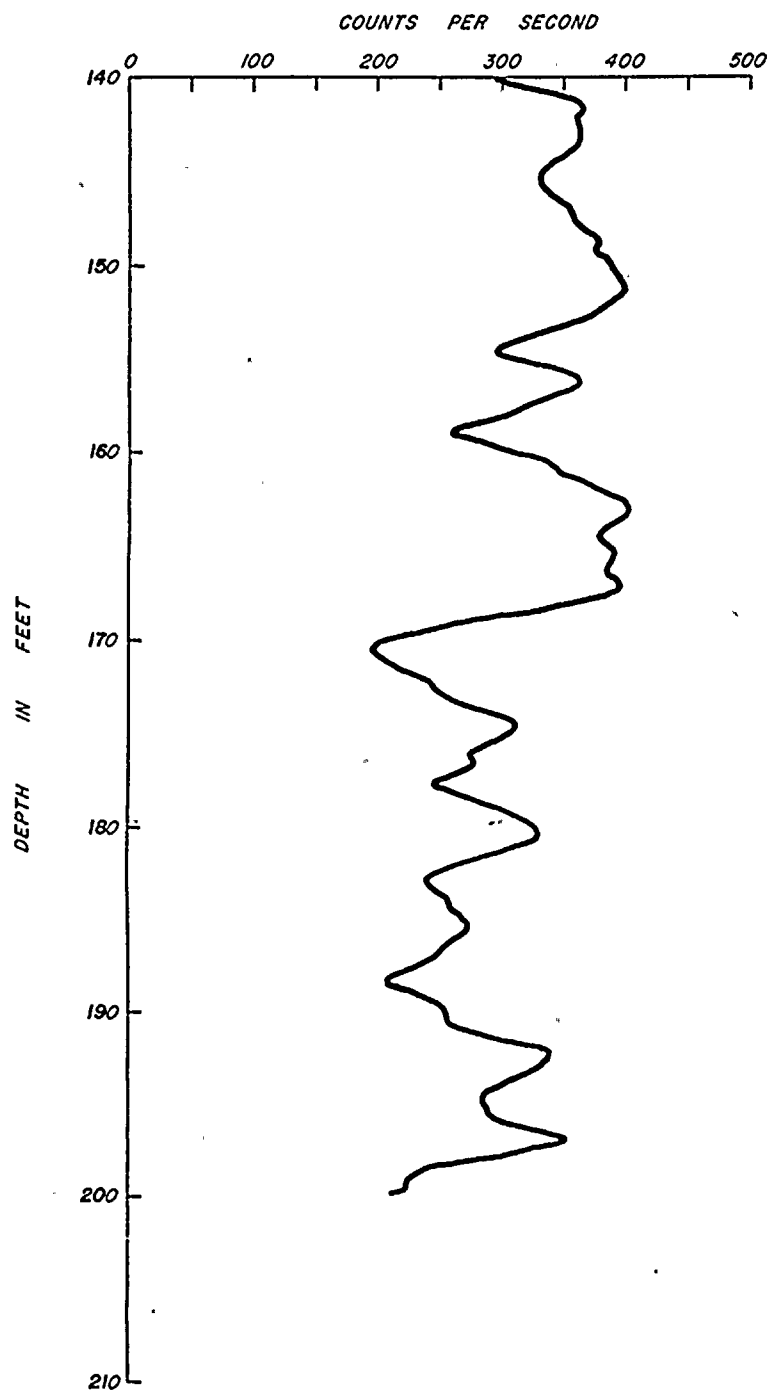
FRACTURES

Breccia zone
Dip-slip slickensides
Fractures-shown at approximate angle to core axis
Mineralized fracture c - calcite s - sulfide
Fractured zone

KEY TO SYMBOLS

Sandstone
Graywacke
Siltstone
Shale
Fossils
Shale intra-clasts
Cross-bedding
Shale laminae

BORING B-805



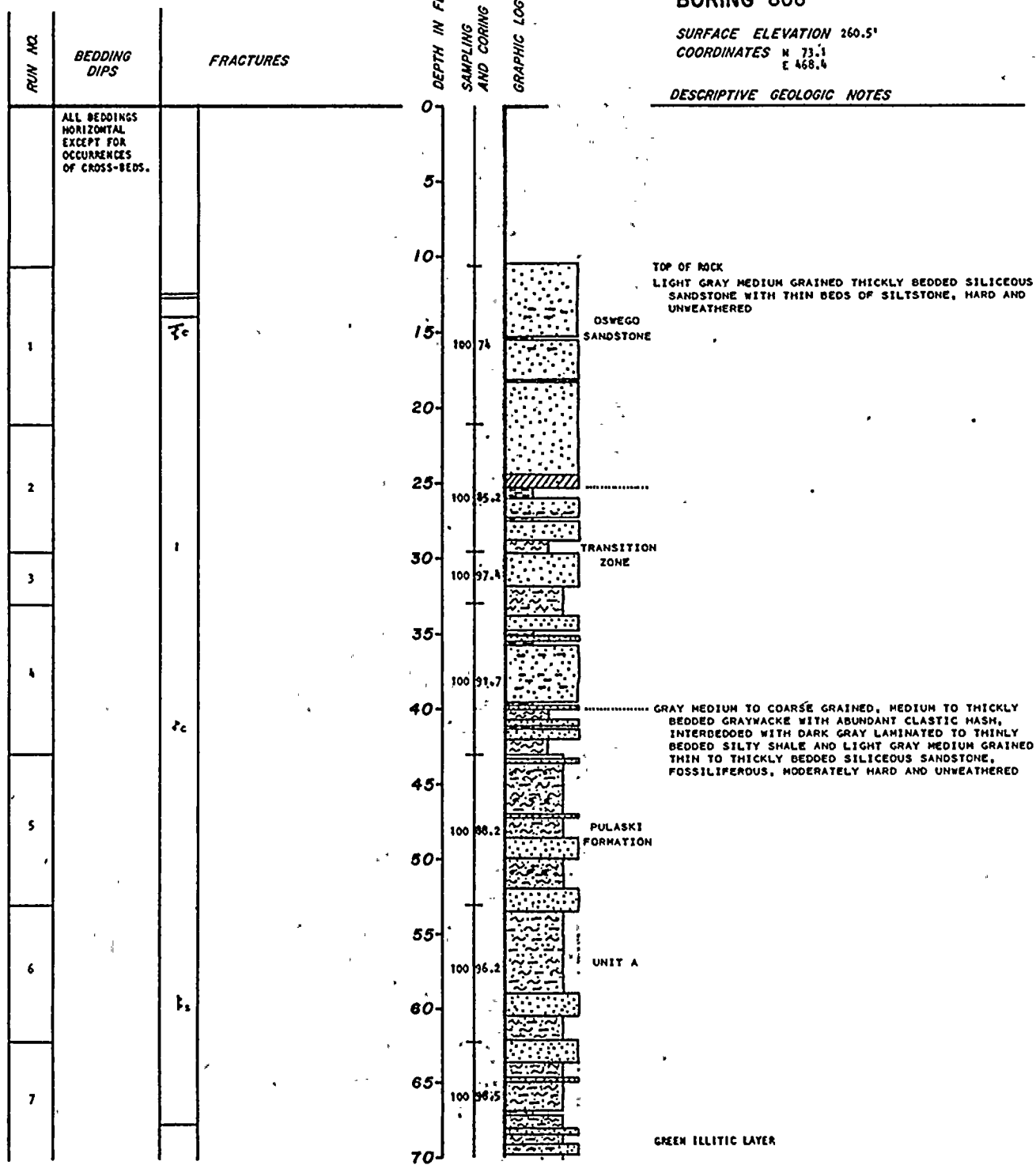
GAMMA RAY LOG

BORING 806

SURFACE ELEVATION 260.5'

COORDINATES N 73.1
E 468.6

DESCRIPTIVE GEOLOGIC NOTES



SAMPLING AND CORING INFORMATION

Core run
100 95 R.O.D.
Percent recovery

BEDDING DIPS

03° Bedding dips measured on selective bedding planes. An attempt was made to avoid all obvious cross bedding or other primary structures.

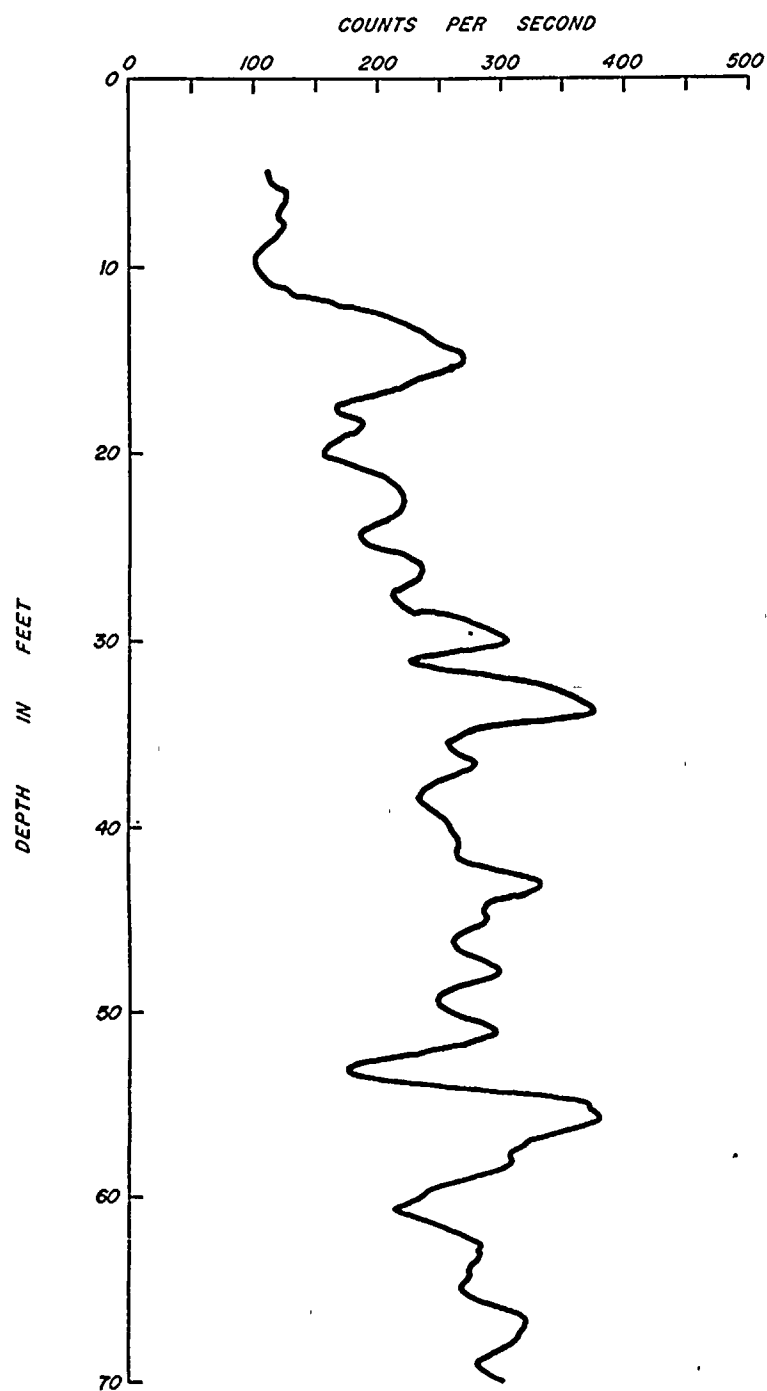
FRACTURES

\mathcal{F}_c Breccia zone
 \mathcal{F}_s Dip-slip slickensides
 Fractures shown at approximate angle to core axis
 Mineralized fracture c = calcite s = sulfide
 Fractured zone

KEY TO SYMBOLS

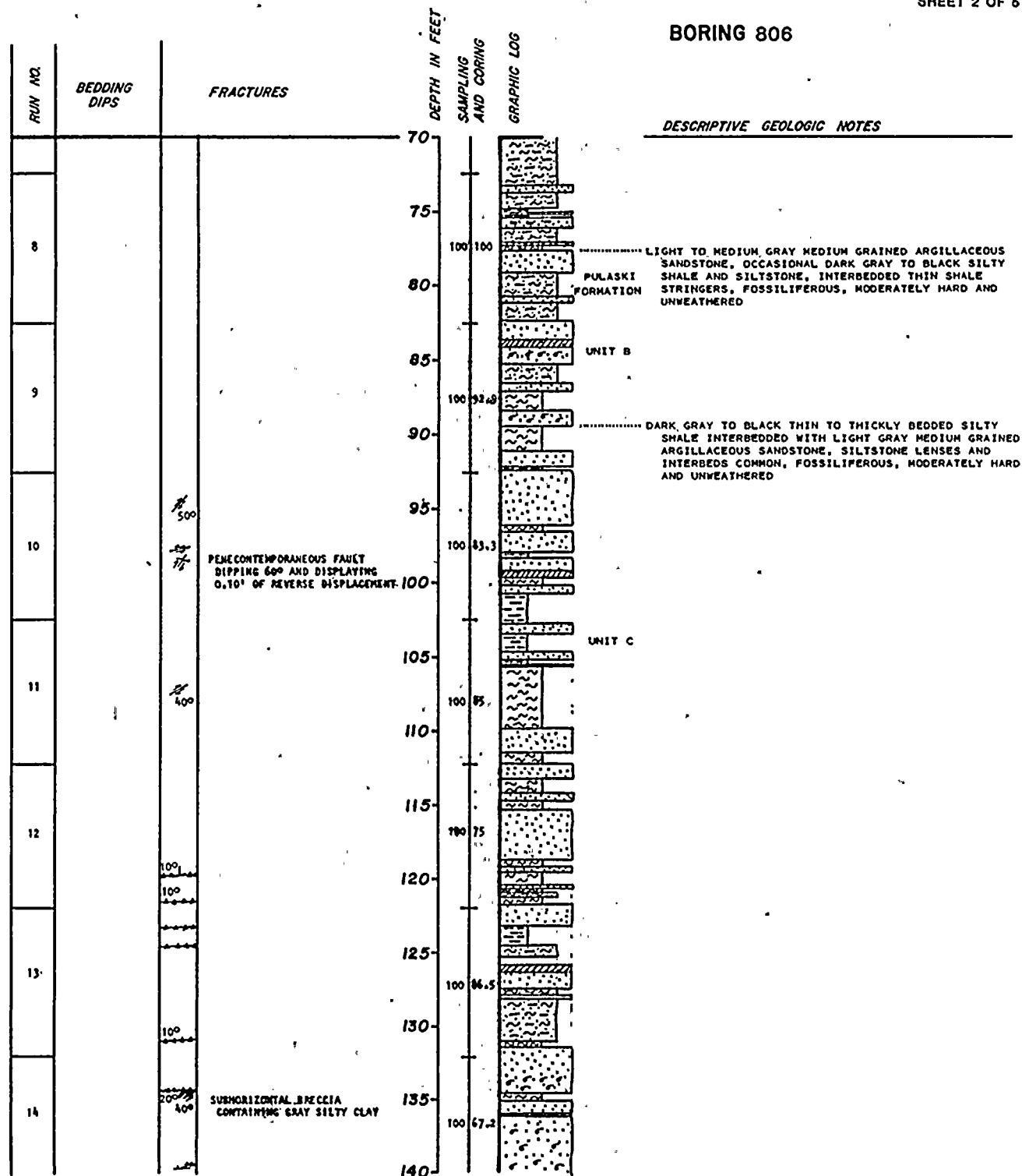
Sandstone
 Graywacke
 Siltstone
 Shale
 Fossils
 Shale intra-clasts
 Cross-bedding
 Shale laminae

BORING B-806



GAMMA RAY LOG

BORING 806



SAMPLING AND CORING INFORMATION

Core run
100 95 R.Q.D.
Percent recovery

BEDDING DIPS

03° Bedding dips measured on selective bedding planes. An attempt was made to avoid all obvious cross bedding or other primary structures.

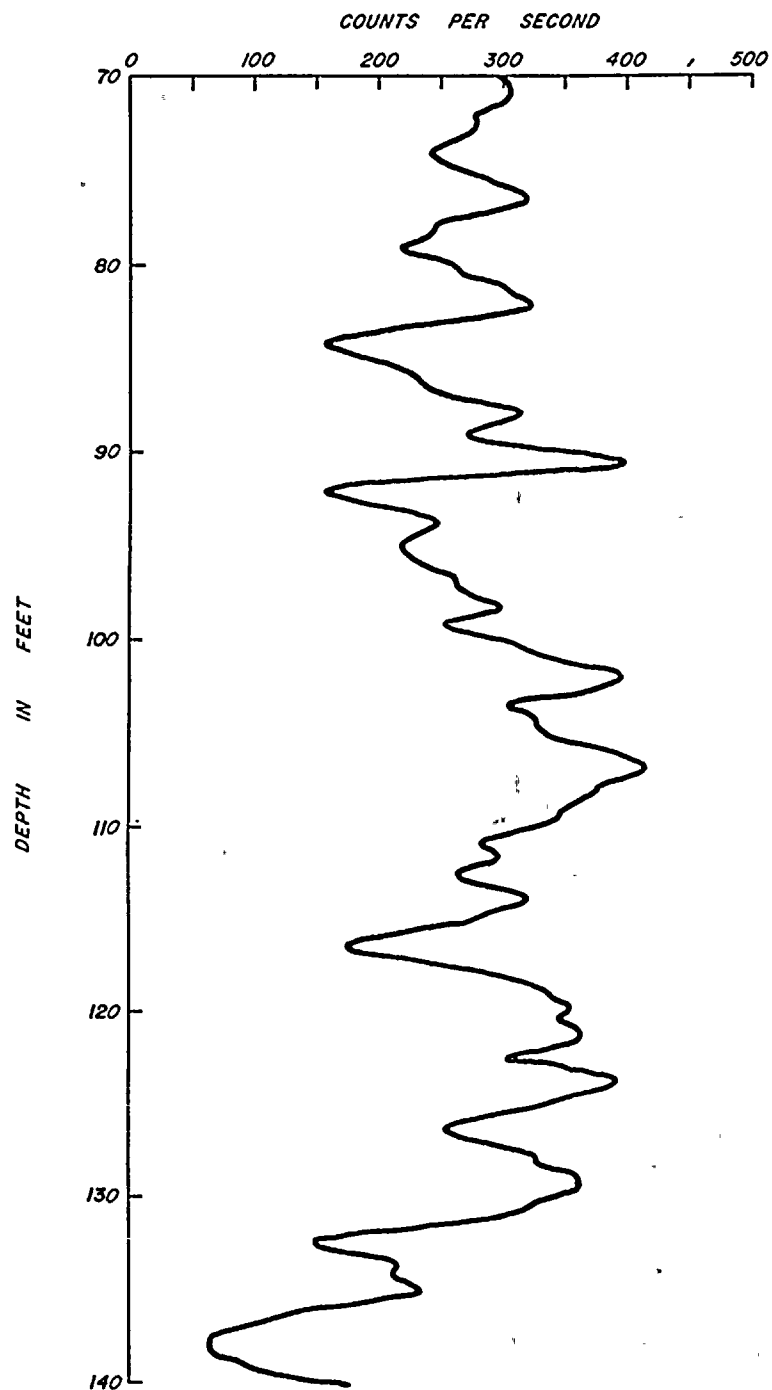
FRACTURES

FAULT Breccia zone
Dip-slip slickensides
Fractures shown at approximate angle to core axis
Mineralized fracture c = calcite s = sulfide
Fractured zone

KEY TO SYMBOLS

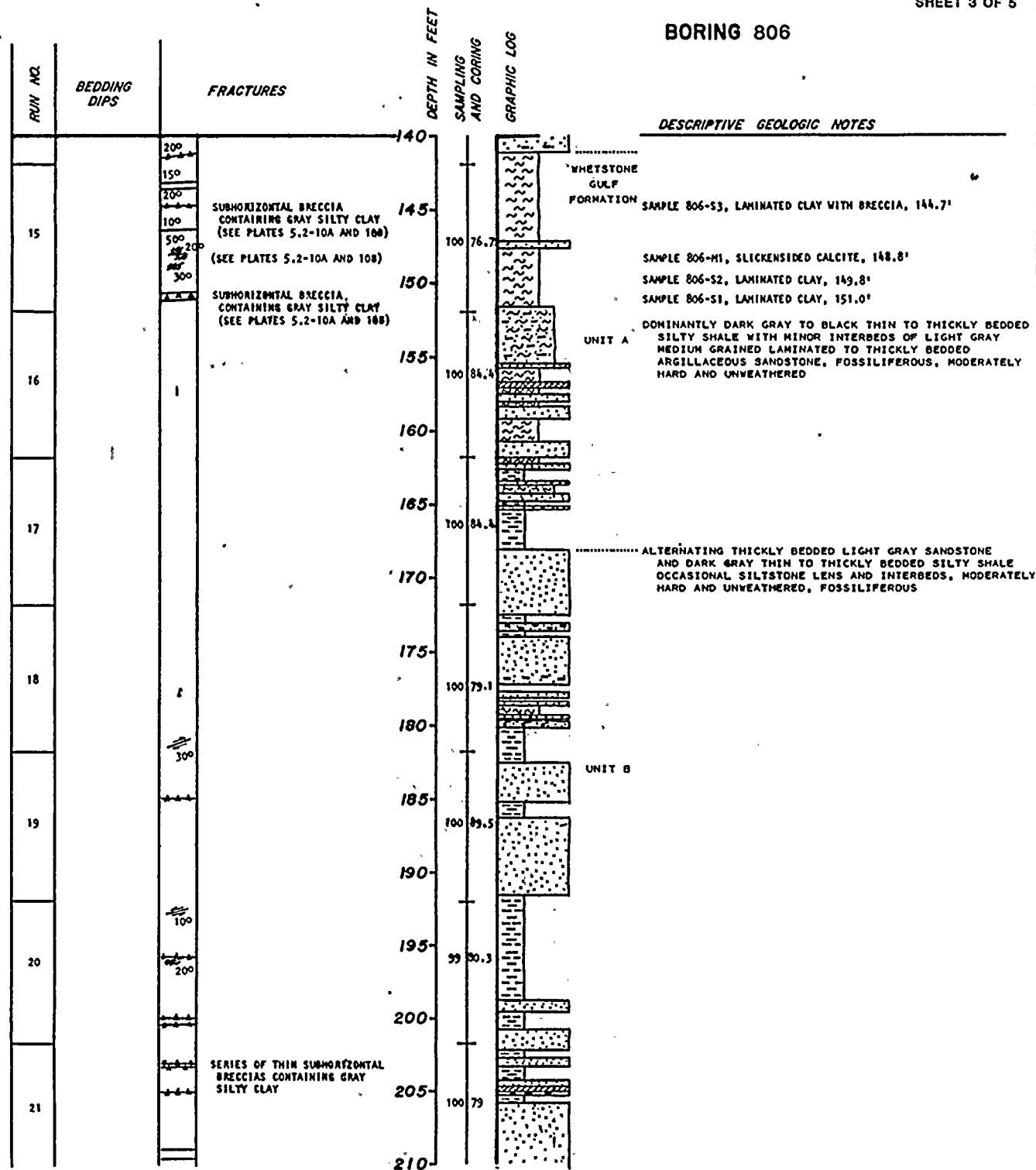
Sandstone
Graywacke
Siltstone
Shale
Fossils
Shale intra-clasts
Cross-bedding
Shale laminae

BORING B-806



GAMMA RAY LOG

BORING 806



SAMPLING AND CORING INFORMATION

Core run
100 95 R.Q.D.
Percent recovery

BEDDING DIPS

03° Bedding dips measured on selective bedding planes. An attempt was made to avoid all obvious cross bedding or other primary structures.

FRACTURES

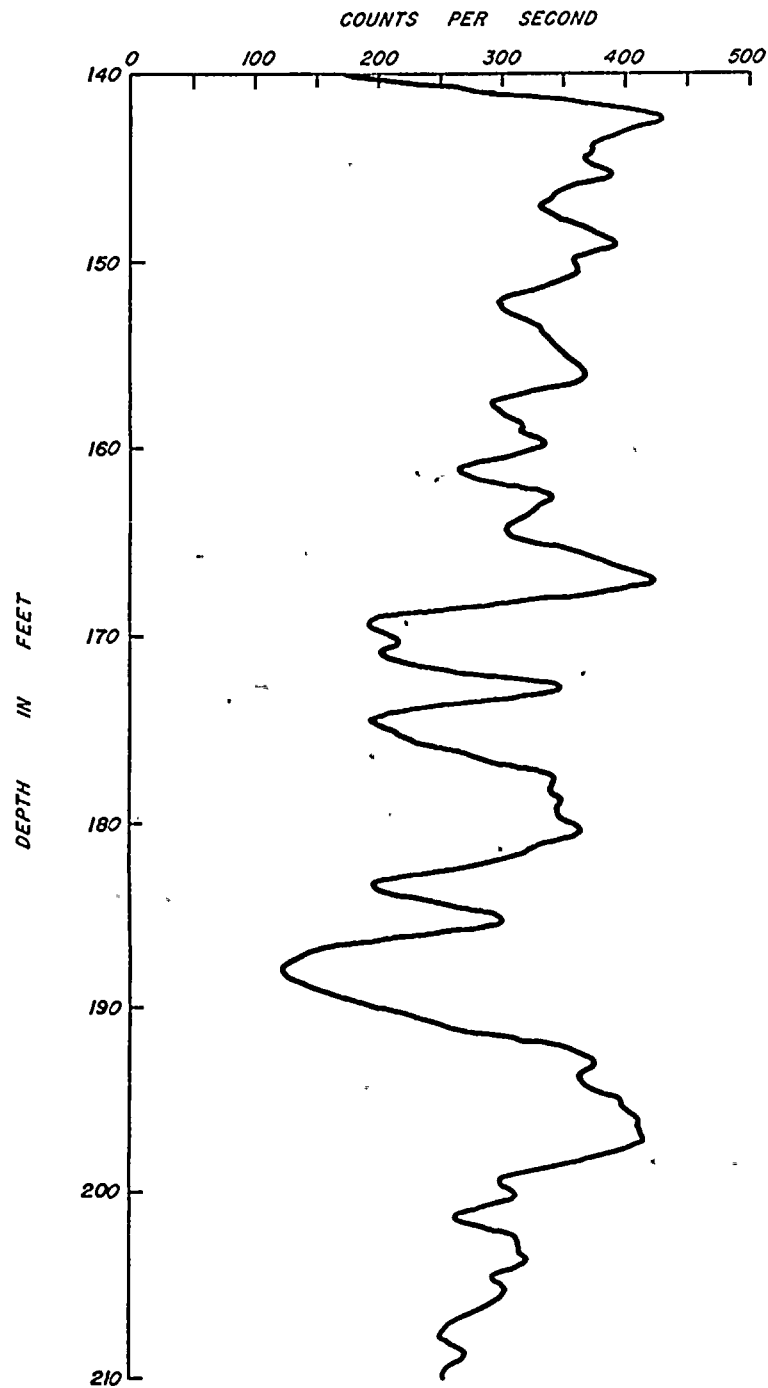
Breccia zone
Dip-slip slickensides
Fractures-shown at approximate angle to core axis
Mineralized fracture c = calcite s = sulfide
Fractured zone

KEY TO SYMBOLS

Sandstone
Graywacke
Siltstone
Shale
Fossils
Shale intra-clasts
Cross-bedding
Shale laminae



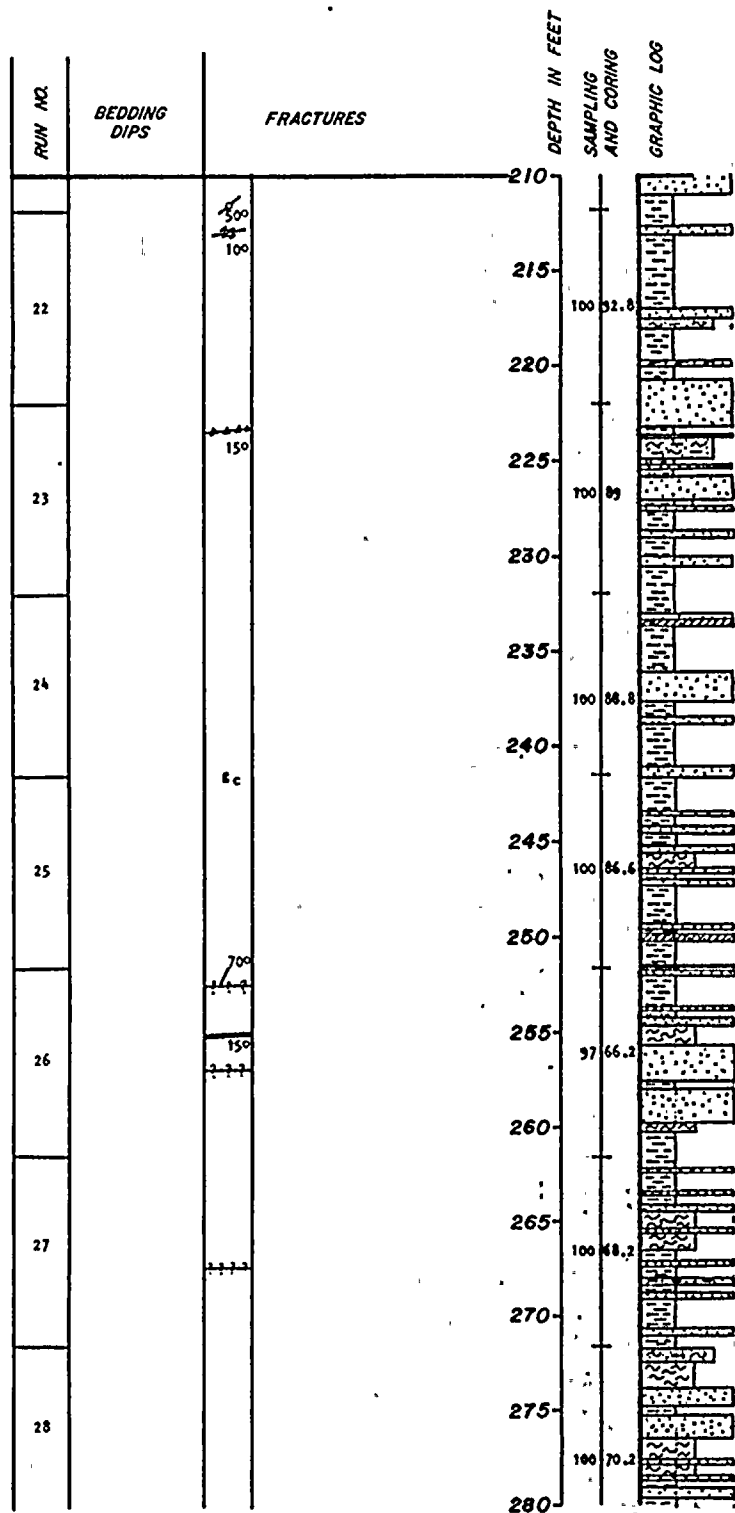
BORING B-806



GAMMA RAY LOG



BORING 806



DESCRIPTIVE GEOLOGIC NOTES

SAMPLING AND CORING INFORMATION

Core run
100 95 R.O.D.
Percent recovery

BEDDING DIPS

03° Bedding dips measured on selective bedding planes. An attempt was made to avoid all obvious cross bedding or other primary structures.

FRACTURES

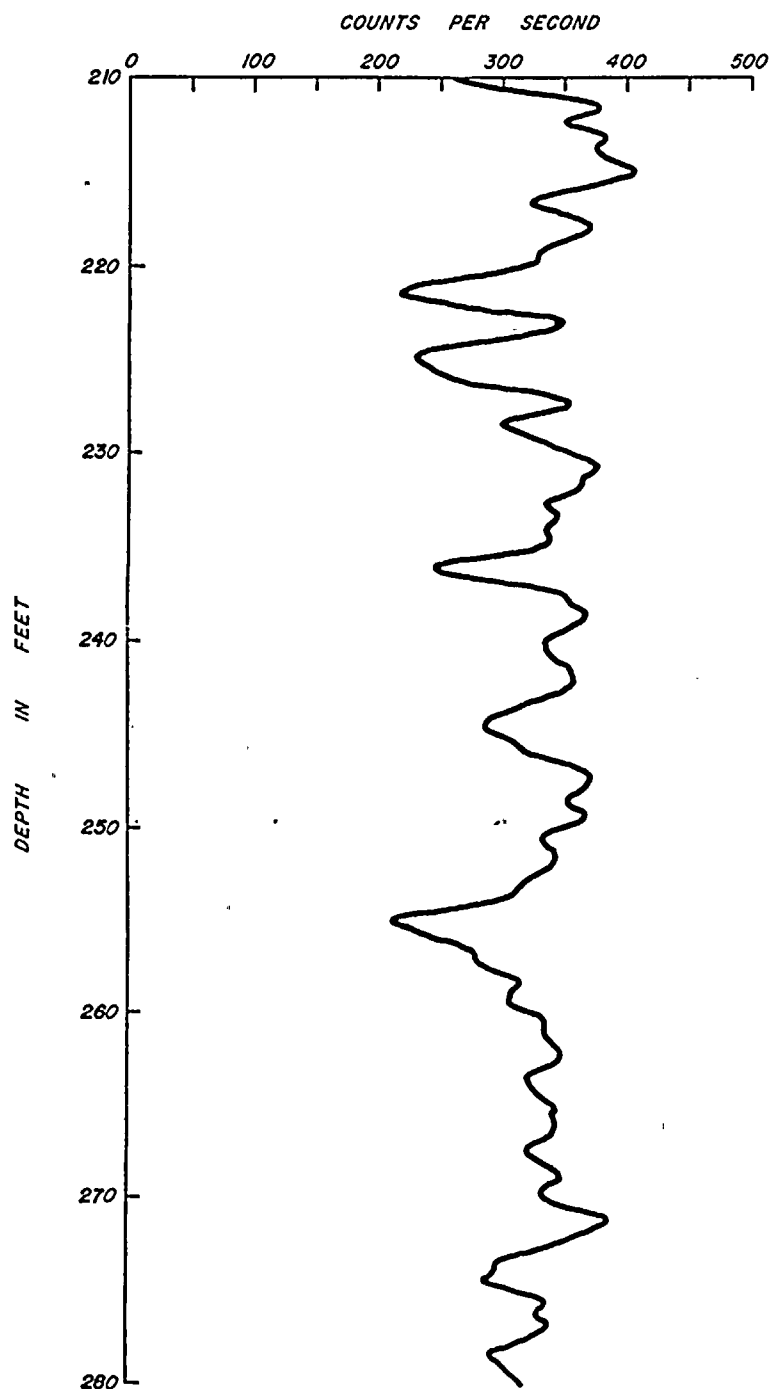
Breccia zone
Dip-slip slickensides
Fractures shown at approximate angle to core axis
Mineralized fracture c = calcite s = sulfide
Fractured zone

KEY TO SYMBOLS

Sandstone
Graywacke
Siltstone
Shale
Fossils
Shale intra-clasts
Cross-bedding
Shale laminae

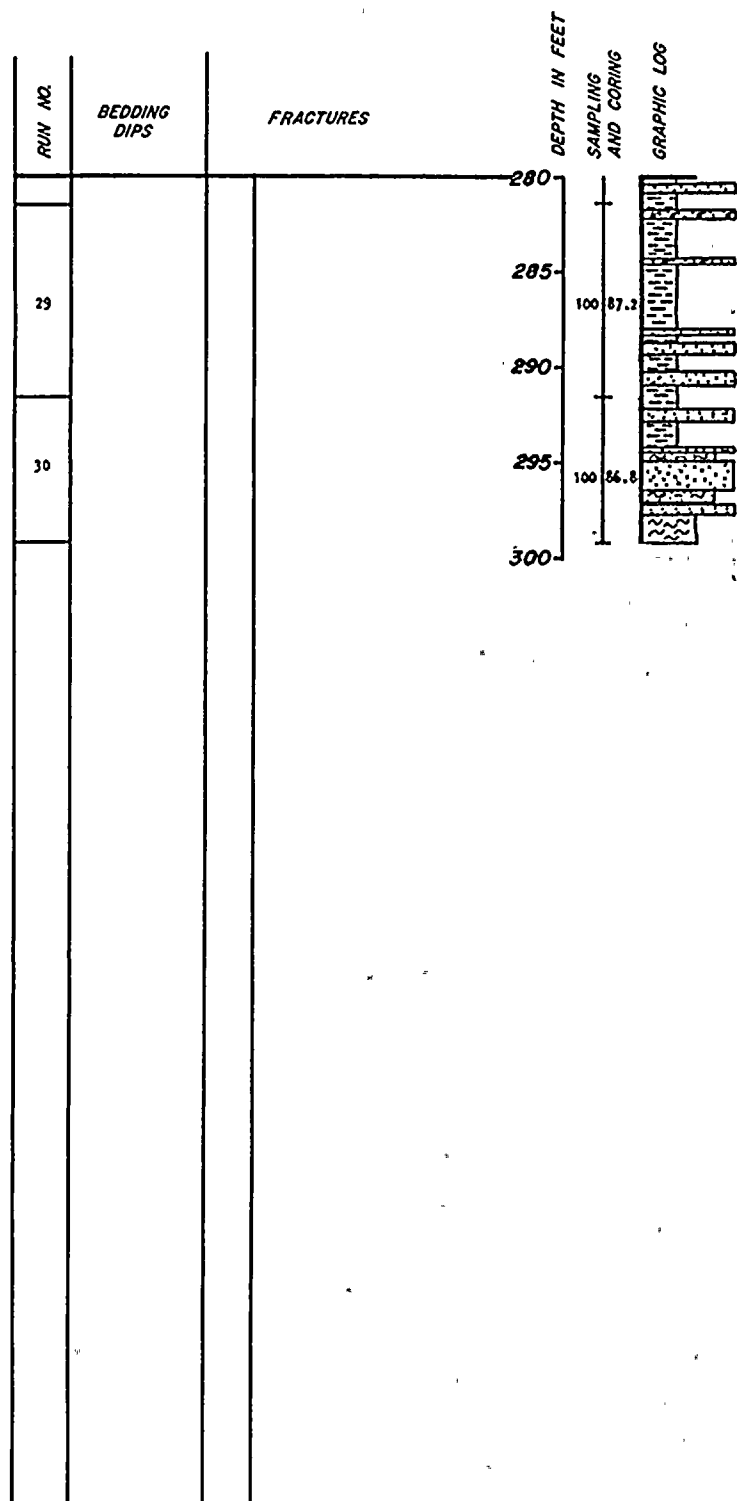


BORING B-806



GAMMA RAY LOG

BORING 806



DESCRIPTIVE GEOLOGIC NOTES

BORING TERMINATED AT 299.15' ON 2-29-80
AND GEOPHYSICALLY LOGGED ON 2-29-80

SAMPLING AND CORING INFORMATION

Core run
100/95 R.O.D.
Percent recovery

BEDDING DIPS

03° Bedding dips measured on selective bedding planes. An attempt was made to avoid all obvious cross bedding or other primary structures.

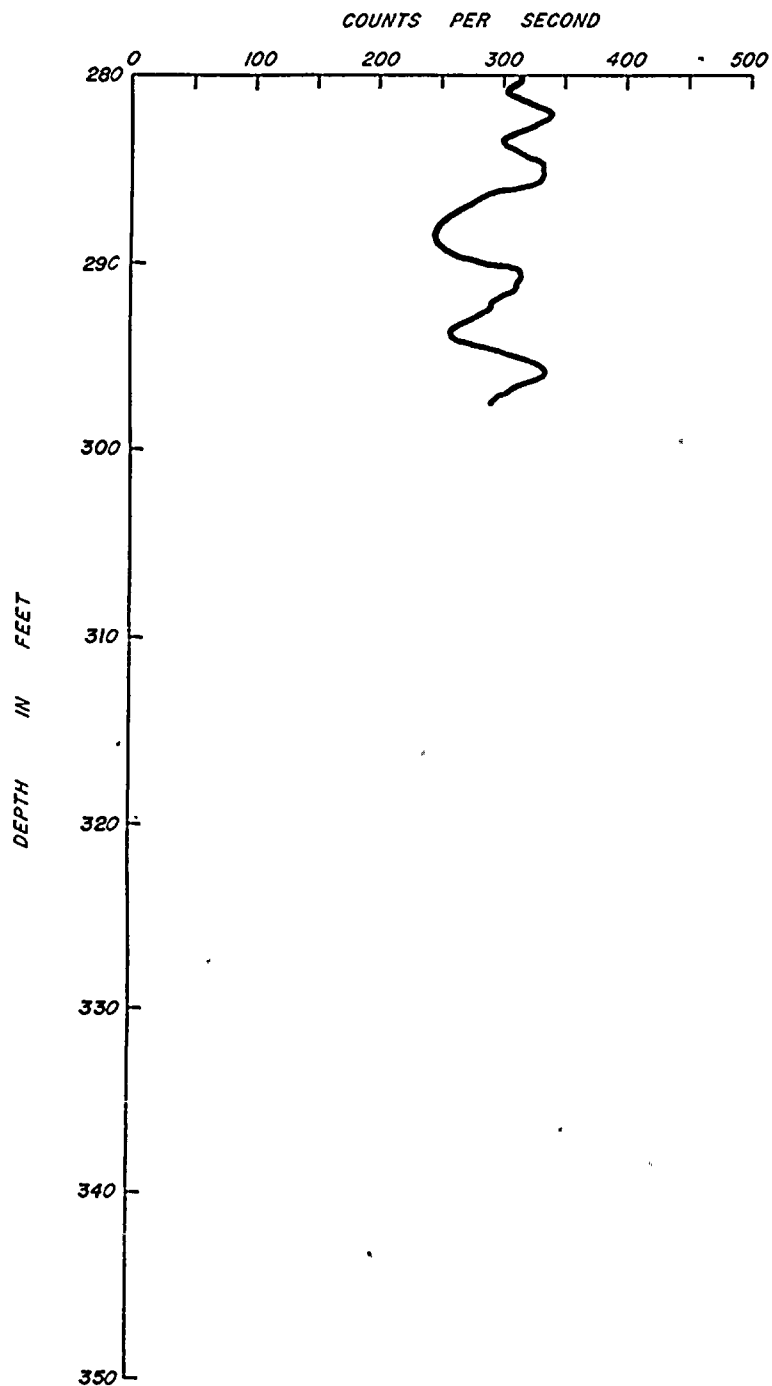
FRACTURES

Breccia zone
 Dip-slip slickensides
 Fractures shown at approximate angle to core axis
 Mineralized fracture c = calcite s = sulfide
 Fractured zone

KEY TO SYMBOLS

Sandstone
 Graywacke
 Siltstone
 Shale
 Fossils
 Shale intra-clasts
 Cross-bedding
 Shale laminae

BORING B-806



GAMMA RAY LOG

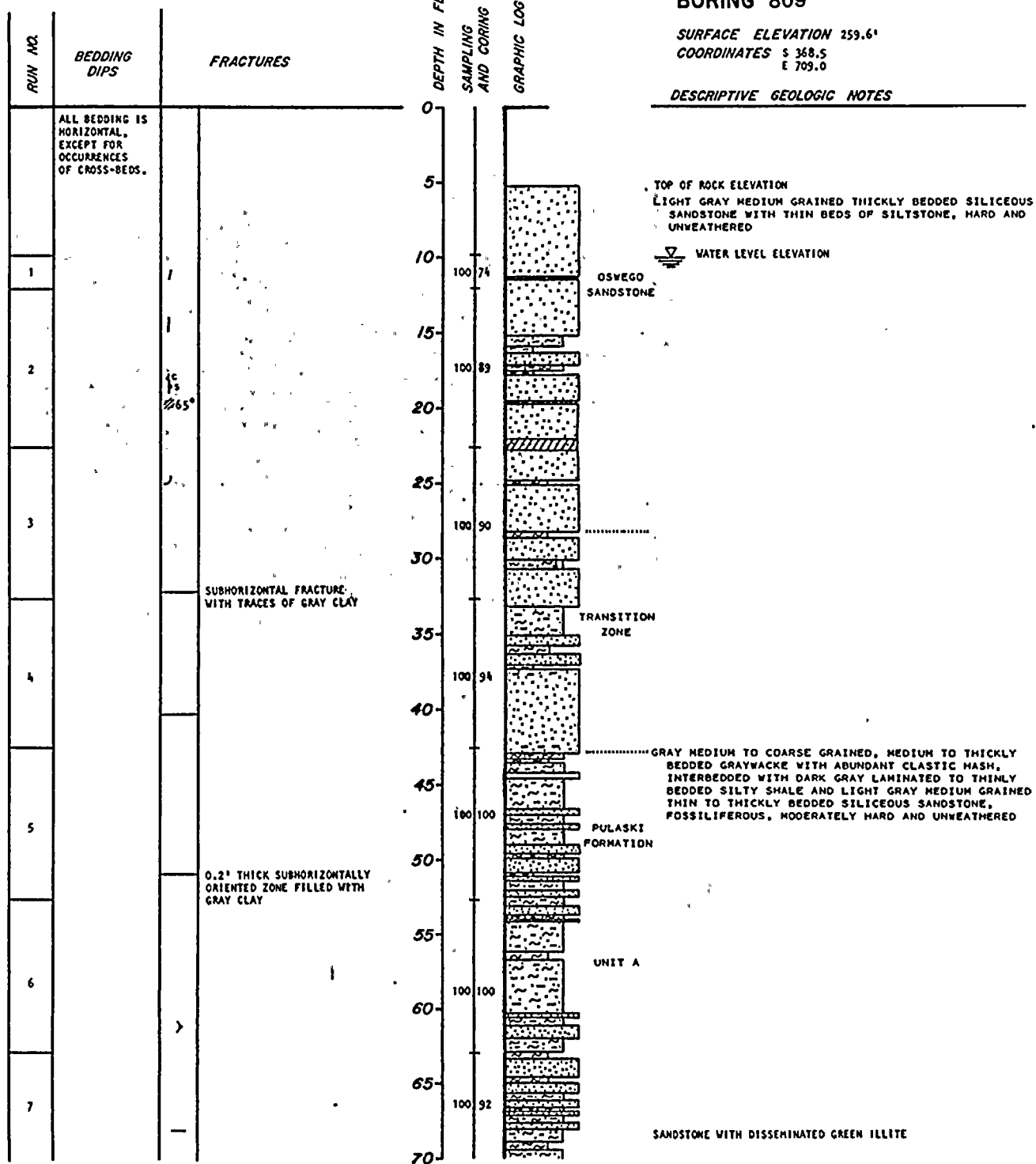


BORING 809

SURFACE ELEVATION 259.6'

COORDINATES S 368.5
E 709.0

DESCRIPTIVE GEOLOGIC NOTES



SAMPLING AND CORING INFORMATION

Core run
100 95 R.Q.D.
Percent recovery

BEDDING DIPS

03° Bedding dips measured on selective bedding planes. An attempt was made to avoid all obvious cross bedding or other primary structures.

FRACTURES

Breccia zone
 Dip-slip slickensides
 Fractures-shown at approximate angle to core axis
 Mineralized fracture c = calcite s = sulfide
 Fractured zone

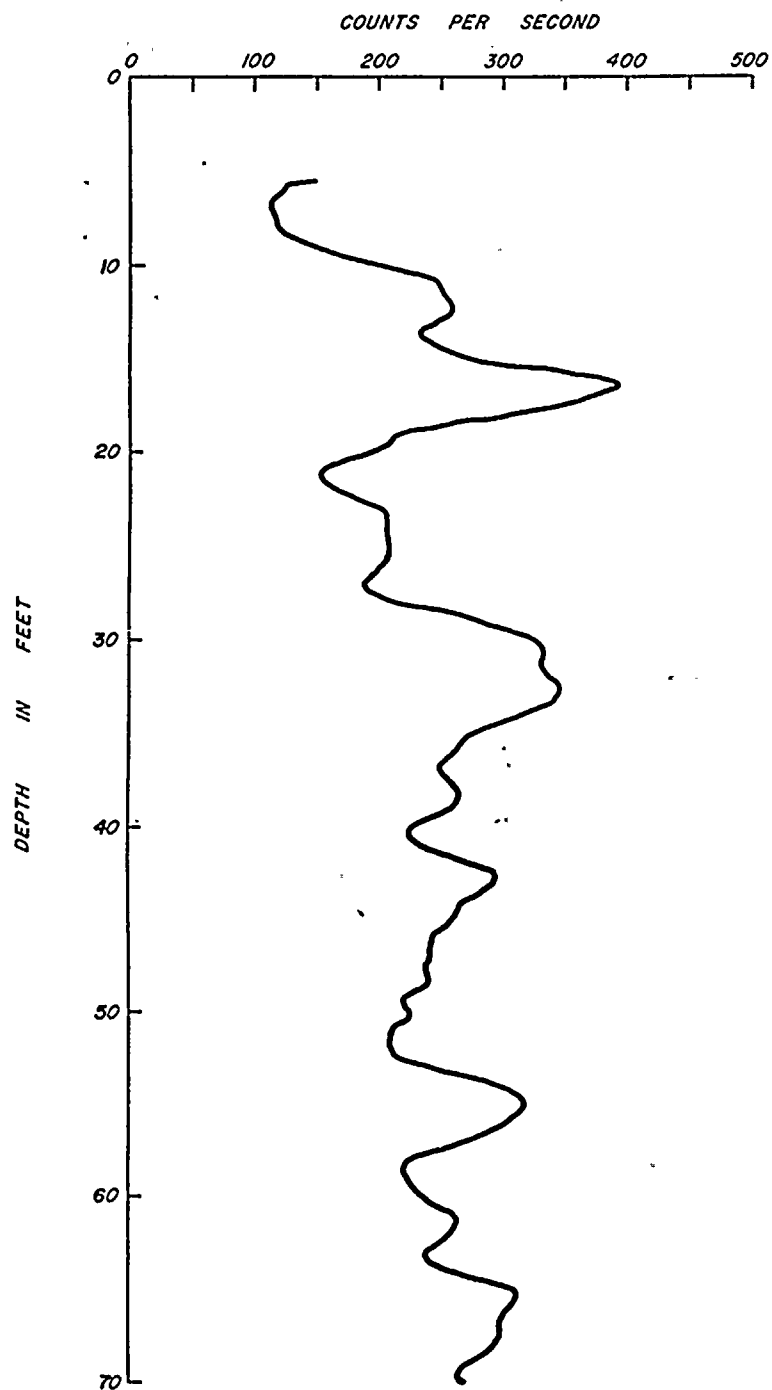
KEY TO SYMBOLS

Sandstone
 Graywacke
 Siltstone
 Shale
 Fossils
 Shale intra-clasts
 Cross-bedding
 Shale laminae

PLATE A-8.1

DAMES & MOORE

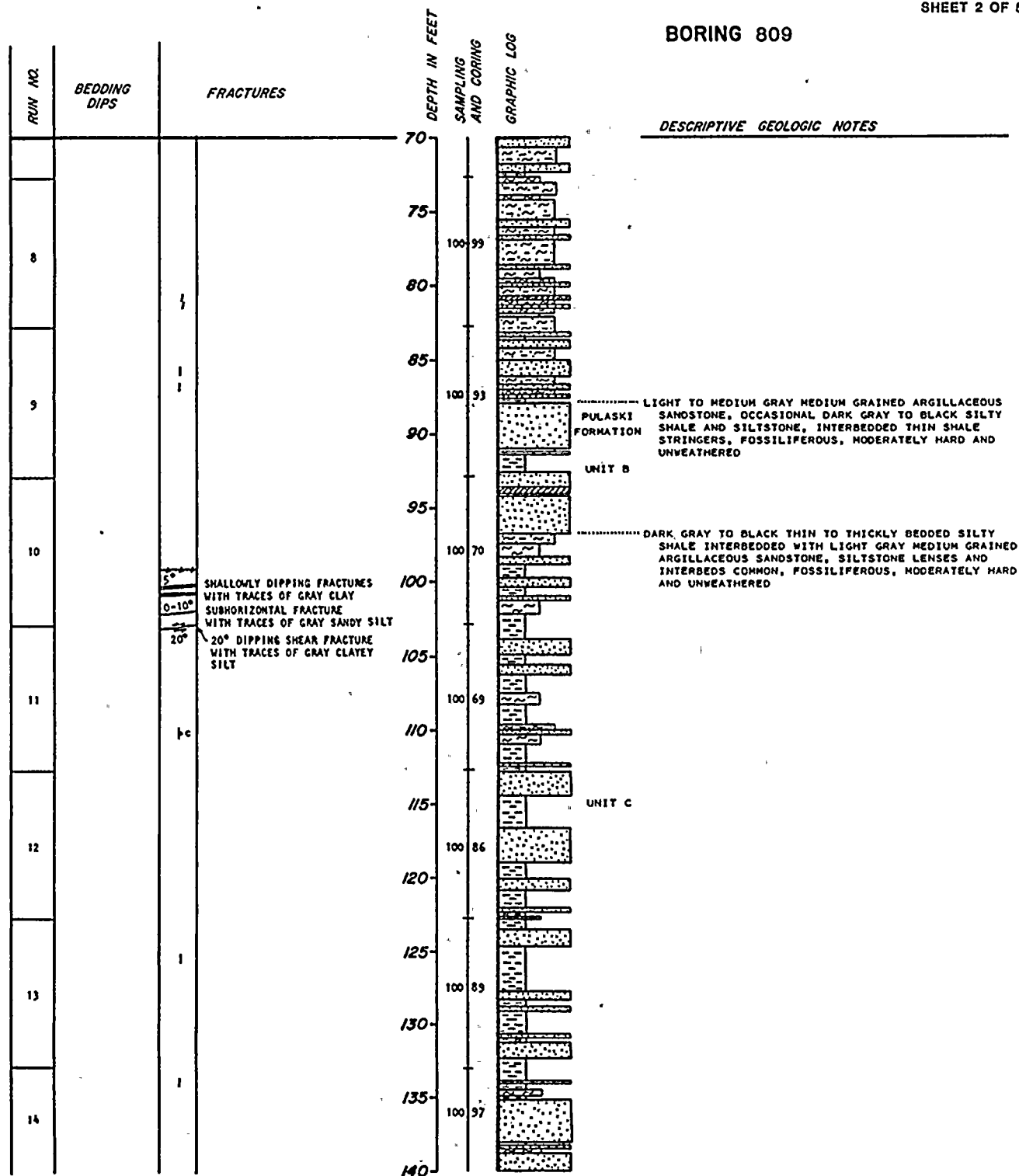
BORING B-809



GAMMA RAY LOG



BORING 809



SAMPLING AND CORING INFORMATION

Core run
100 95 R.O.D.
Percent recovery

BEDDING DIPS

03° Bedding dips measured on selective bedding planes. An attempt was made to avoid all obvious cross bedding or other primary structures.

FRACTURES

Breccia zone
Dip-slip slickensides
Fractures shown at approximate angle to core axis
Mineralized fracture c = calcite s = sulfide
Fractured zone

KEY TO SYMBOLS

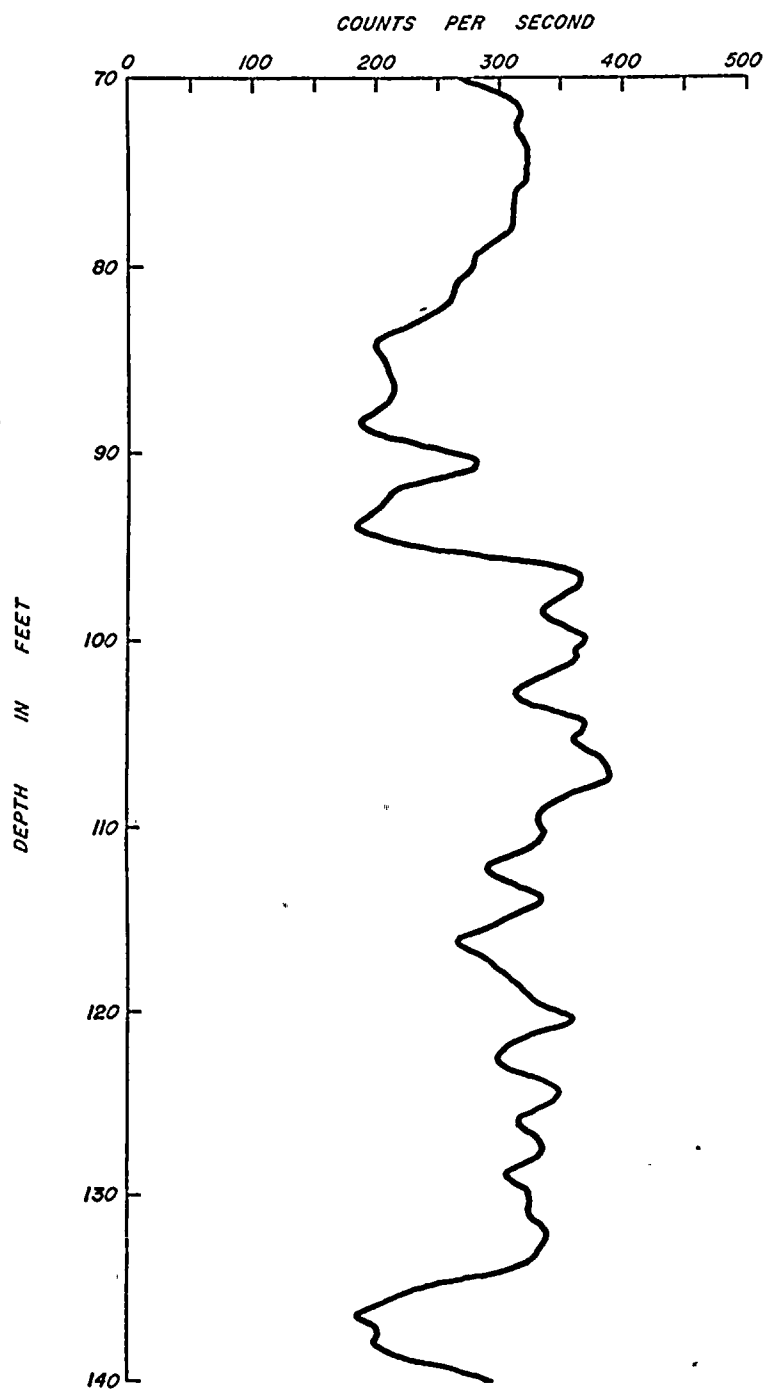
Sandstone
Graywacke
Siltstone
Shale
Fossils
Shale intra-clasts
Cross-bedding
Shale laminar

PLATE A-8.2

DAMES & MOORE



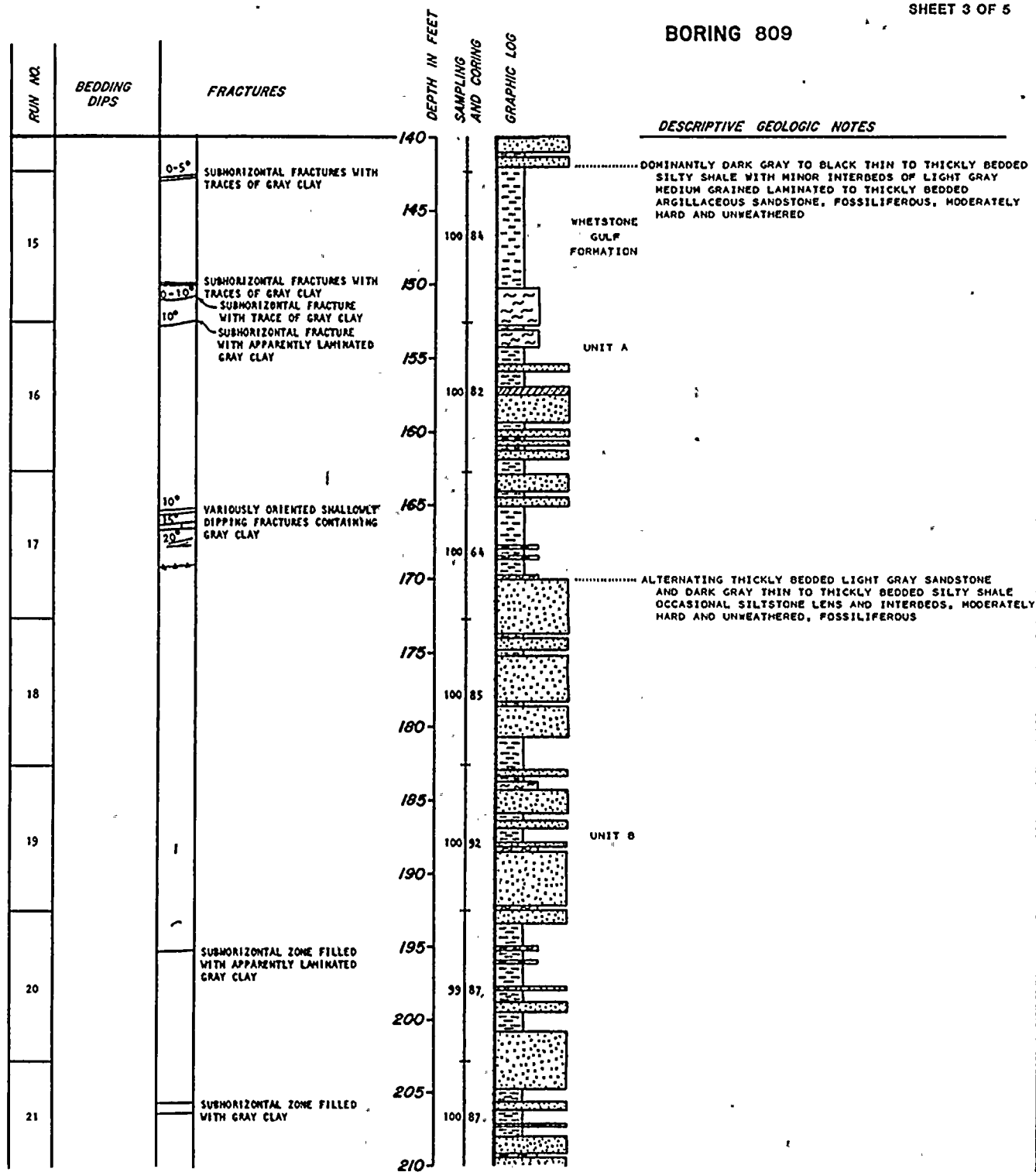
BORING B-809



GAMMA RAY LOG



BORING 809



SAMPLING AND CORING INFORMATION

Core run
100% R.Q.D.
Percent recovery

BEDDING DIPS

03° Bedding dips measured on selective bedding planes. An attempt was made to avoid all obvious cross bedding or other primary structures.

FRACTURES

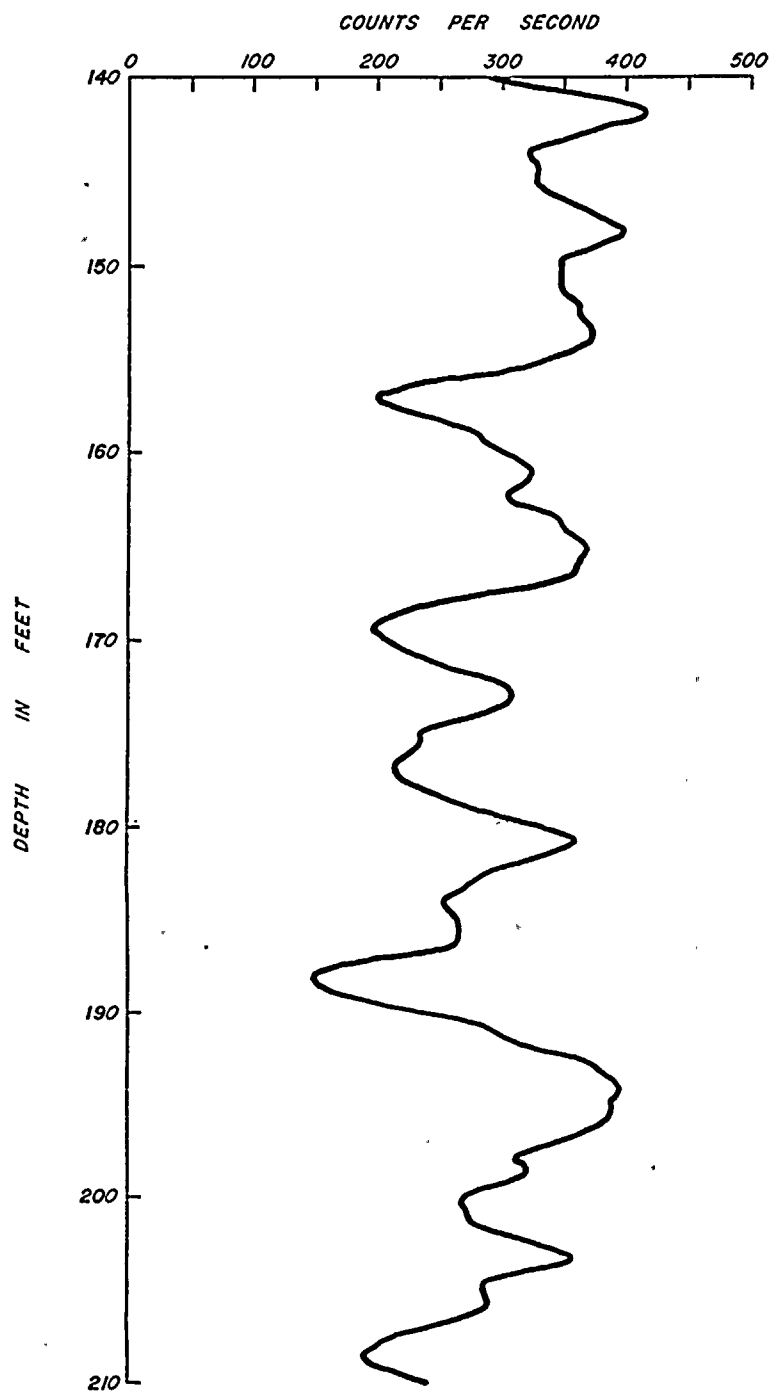
Breccia zone
Dip-slip slickensides
Fractures shown at approximate angle to core axis
Mineralized fracture c = calcite s = sulfide
Fractured zone

KEY TO SYMBOLS

Sandstone
Graywacke
Siltstone
Shale
Fossils
Shale intra-clasts
Cross-bedding
Shale laminae



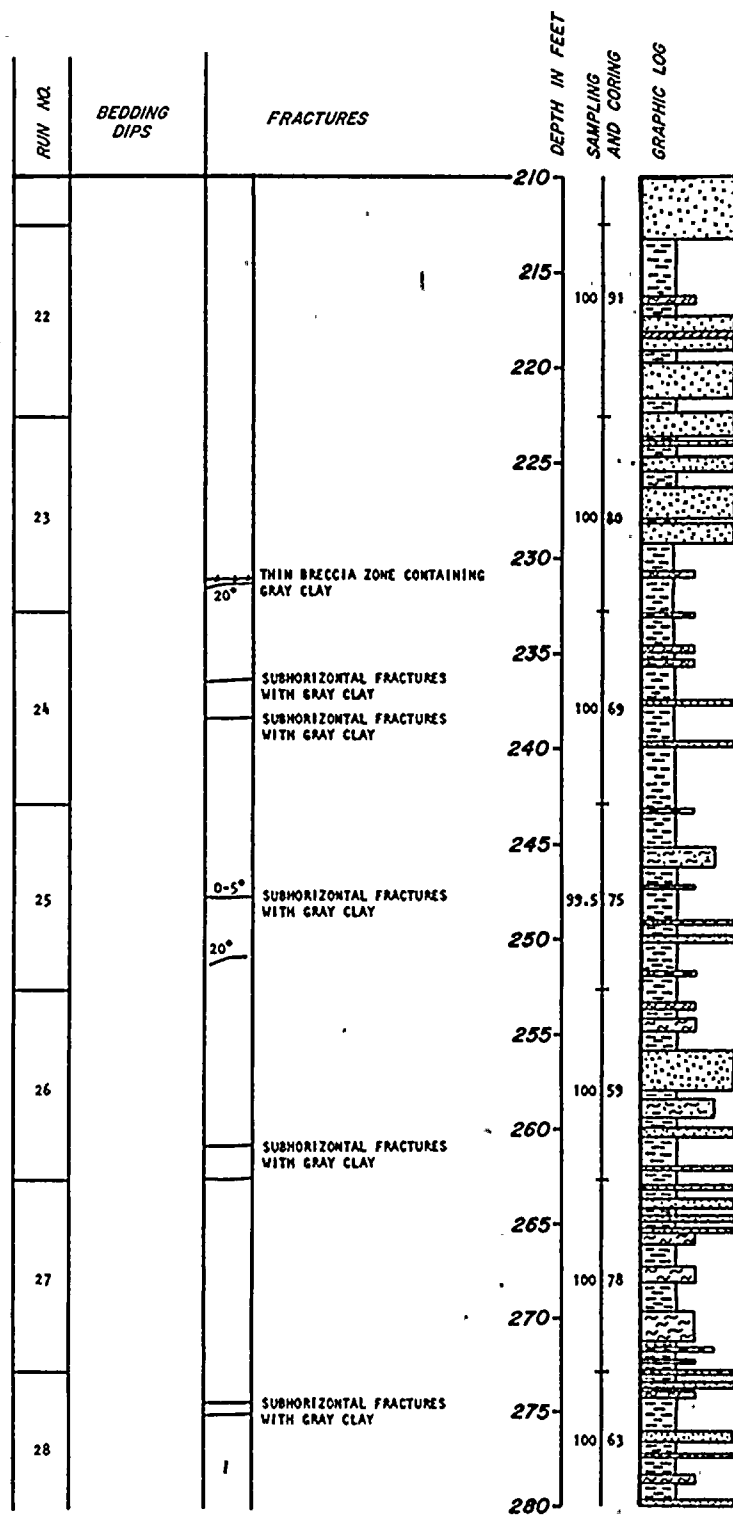
BORING B-809



GAMMA RAY LOG



BORING 809



DESCRIPTIVE GEOLOGIC NOTES

SAMPLING AND CORING INFORMATION

Core run
100 95 R.Q.D.
Percent recovery

BEDDING DIPS

03° Bedding dips measured on selective bedding planes. An attempt was made to avoid all obvious cross bedding or other primary structures.

FRACTURES

1-2-3 Breccia zone
Dip-slip slickensides
Fractures shown at approximate angle to core axis
Mineralized fracture c = calcite s = sulfide
Fractured zone

KEY TO SYMBOLS




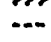
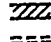



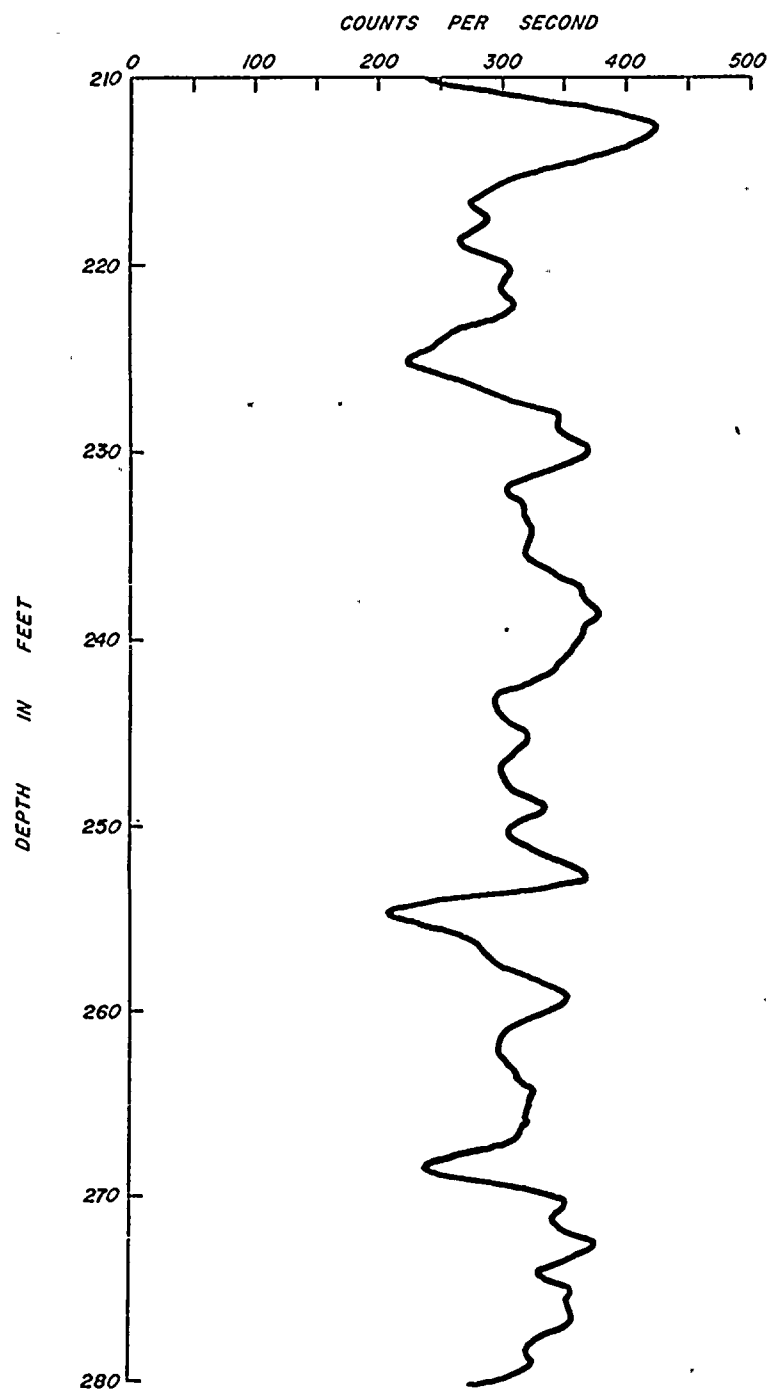
 Sandstone
 Graywacke
 Siltstone
 Shale
 Fossils
 Shale intra-clasts
 Cross-bedding
 Shale laminar

PLATE A-8.4

DAMES & MOORE



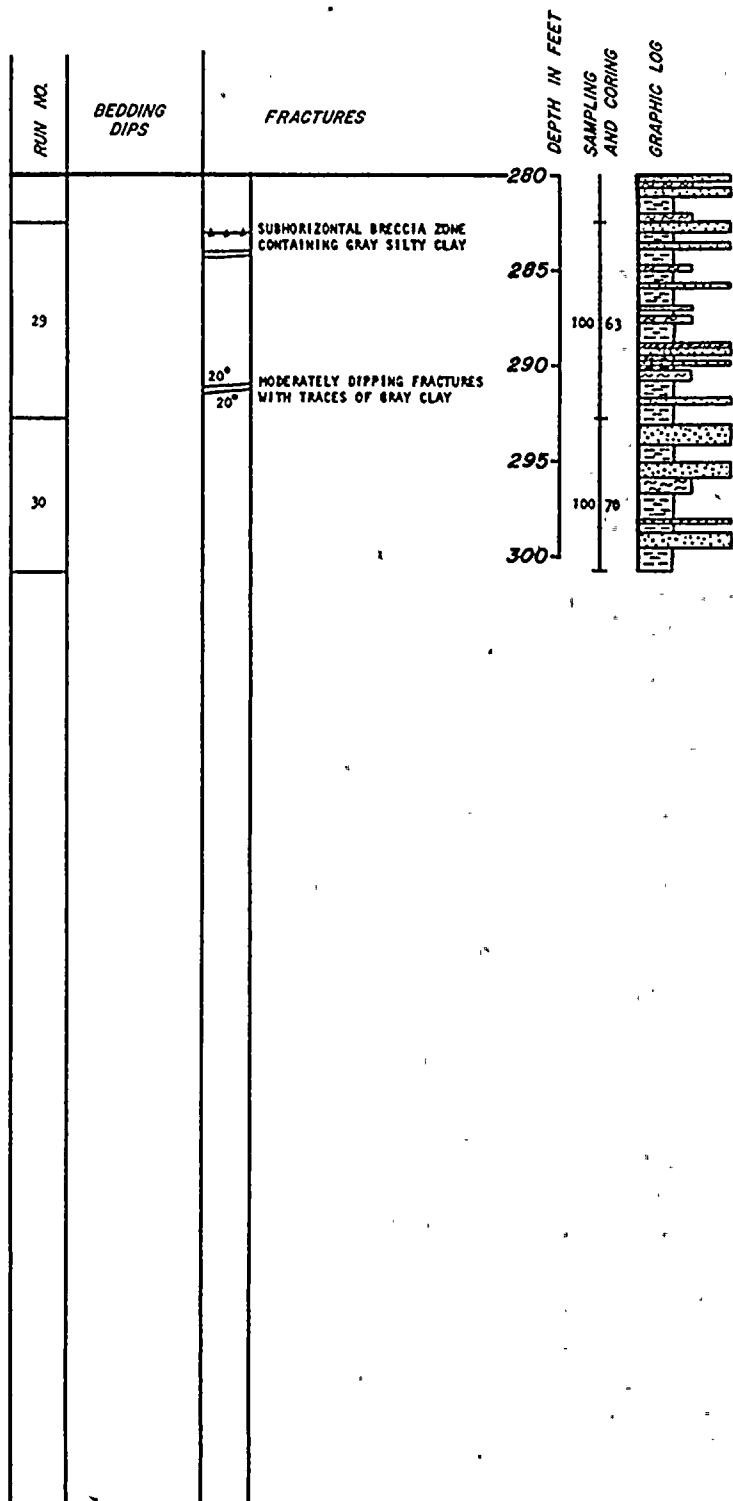
BORING B-809



GAMMA RAY LOG



BORING 809



DESCRIPTIVE GEOLOGIC NOTES

BORING TERMINATED AT 300.35'
ON 3-3-80 AND GEOPHYSICALLY
LOGGED ON 4-1-80.

SAMPLING AND CORING INFORMATION

Core run
100 95 R.O.D.
Percent recovery

BEDDING DIPS

03° Bedding dips measured on selective bedding planes. An attempt was made to avoid all obvious cross bedding or other primary structures.

FRACTURES

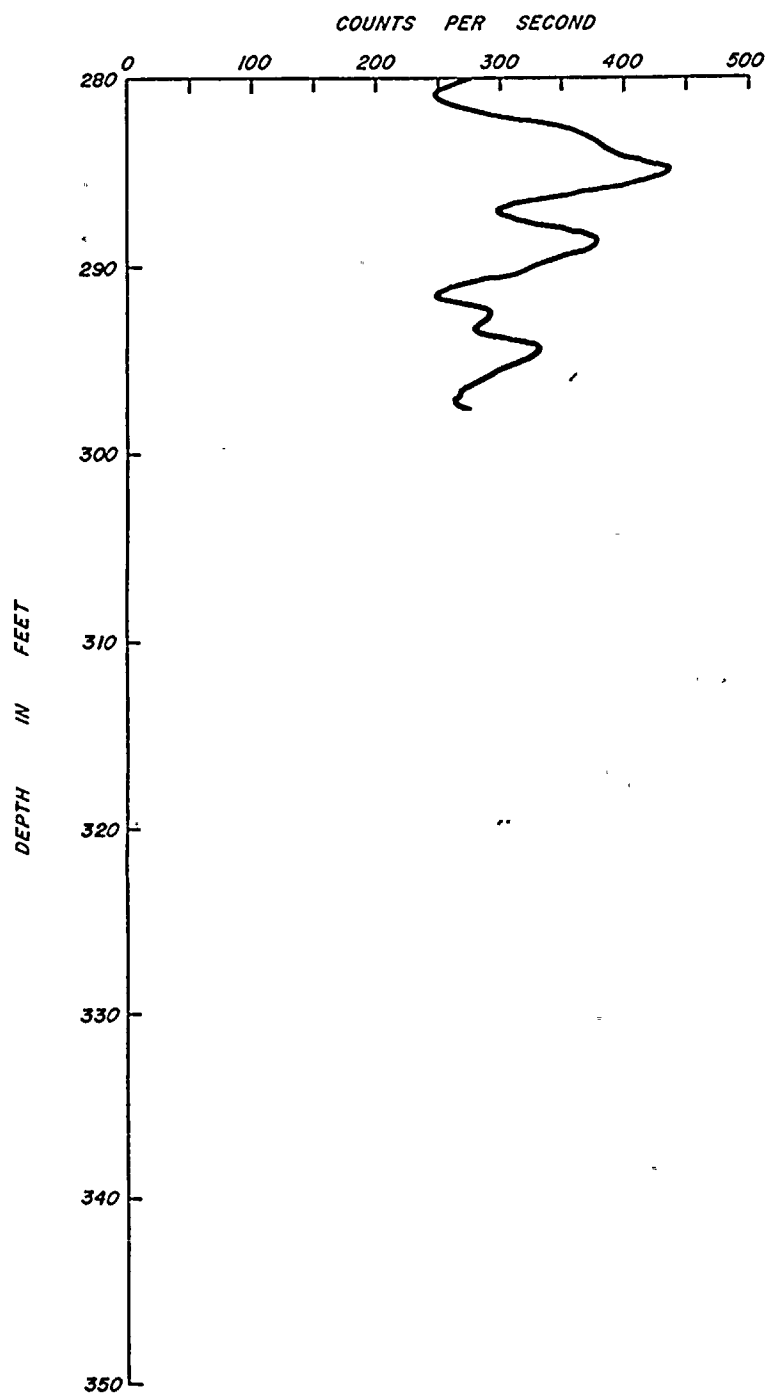
Breccia zone
 Dip-slip slickensides
 Fractures shown at approximate angle to core axis
 Mineralized fracture c = calcite s = sulfide
 Fractured zone

KEY TO SYMBOLS

Sandstone
 Graywacke
 Siltstone
 Shale
 Fossils
 Shale intra-clasts
 Cross-bedding
 Shale laminae



BORING B-809



GAMMA RAY LOG



BORING 810

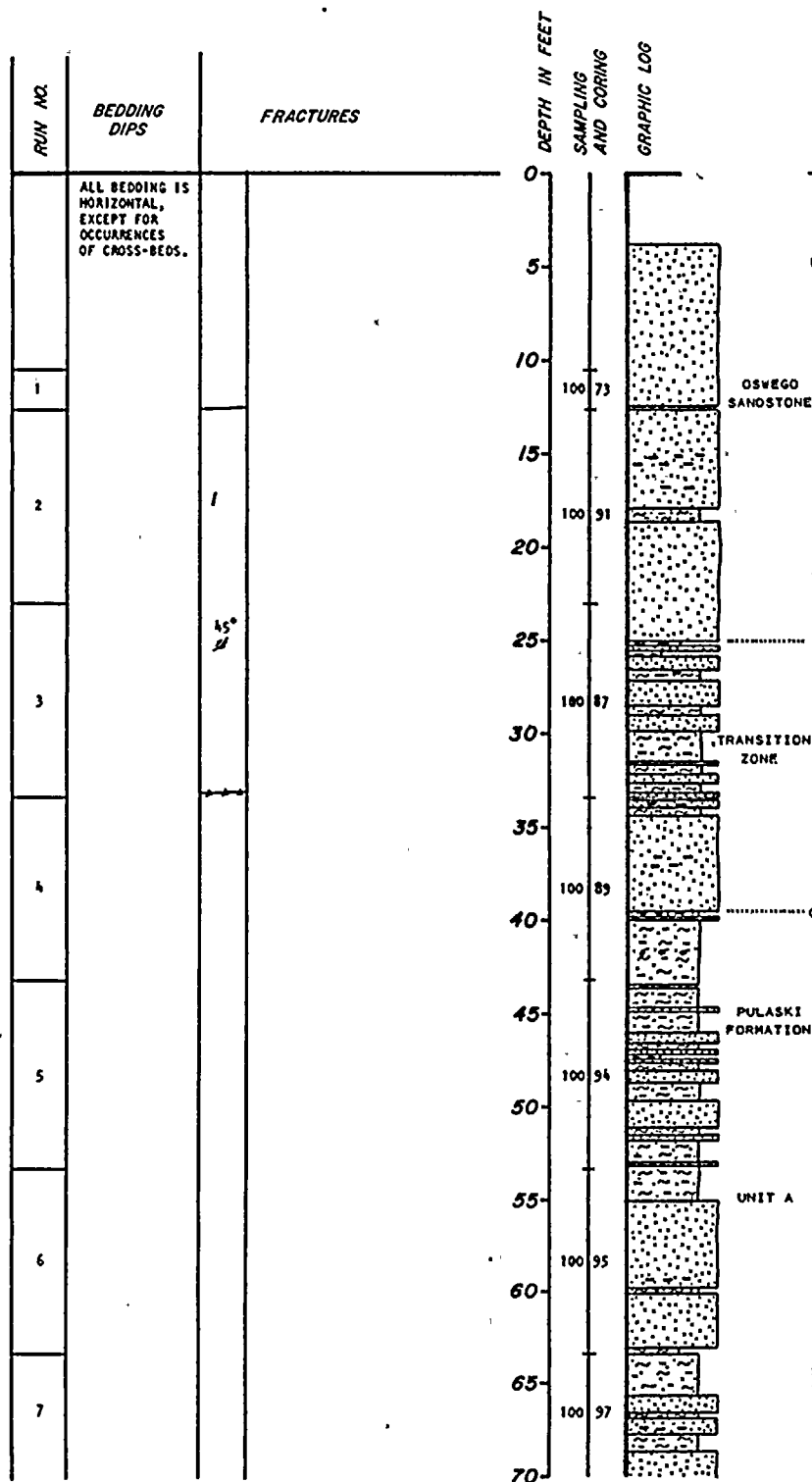
SURFACE ELEVATION 258.7'

COORDINATES S 87.3
E 707.7

DESCRIPTIVE GEOLOGIC NOTES

TOP OF ROCK (ELEVATION 254.6')
 LIGHT GRAY MEDIUM GRAINED THICKLY BEDDED SILICEOUS
 SANDSTONE WITH THIN BEDS OF SILTSTONE, HARD AND
 UNWEATHERED

WATER LEVEL ELEVATION 237.1' (4-2-80)



SAMPLING AND CORING INFORMATION

Core run
 100 95 R.Q.D.
 Percent recovery

BEDDING DIPS

03° Bedding dips measured on selective bedding planes. An attempt was made to avoid all obvious cross bedding or other primary structures.

FRACTURES

Braccia zone
 Dip-slip slickensides
 Fractures-shown at approximate angle to core axis
 Mineralized fracture c - calcite s - sulfide
 Fractured zone

KEY TO SYMBOLS

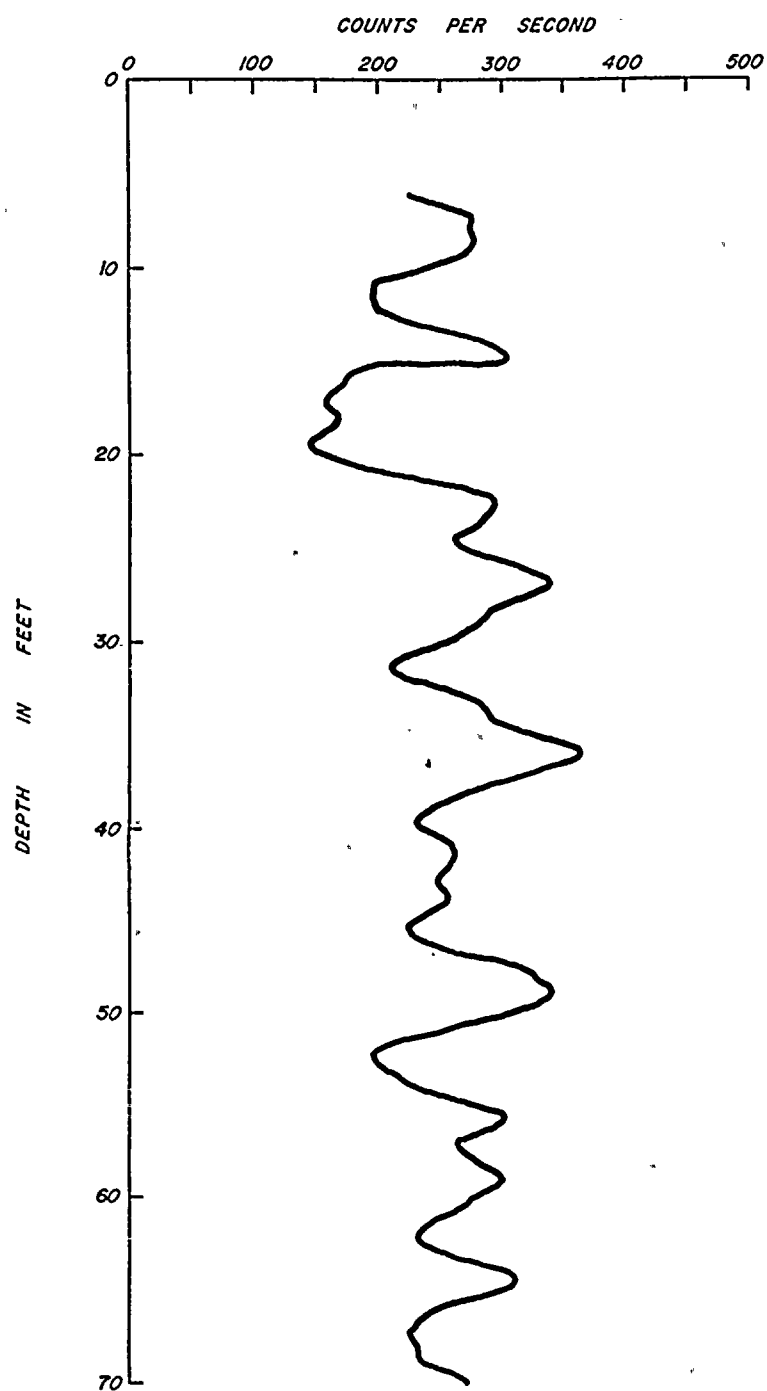
Sandstone
 Graywacke
 Siltstone
 Shale
 Fossils
 Shale Intra-clasts
 Cross-bedding
 Shale laminae

PLATE A-9.1

DAMES & MOORE

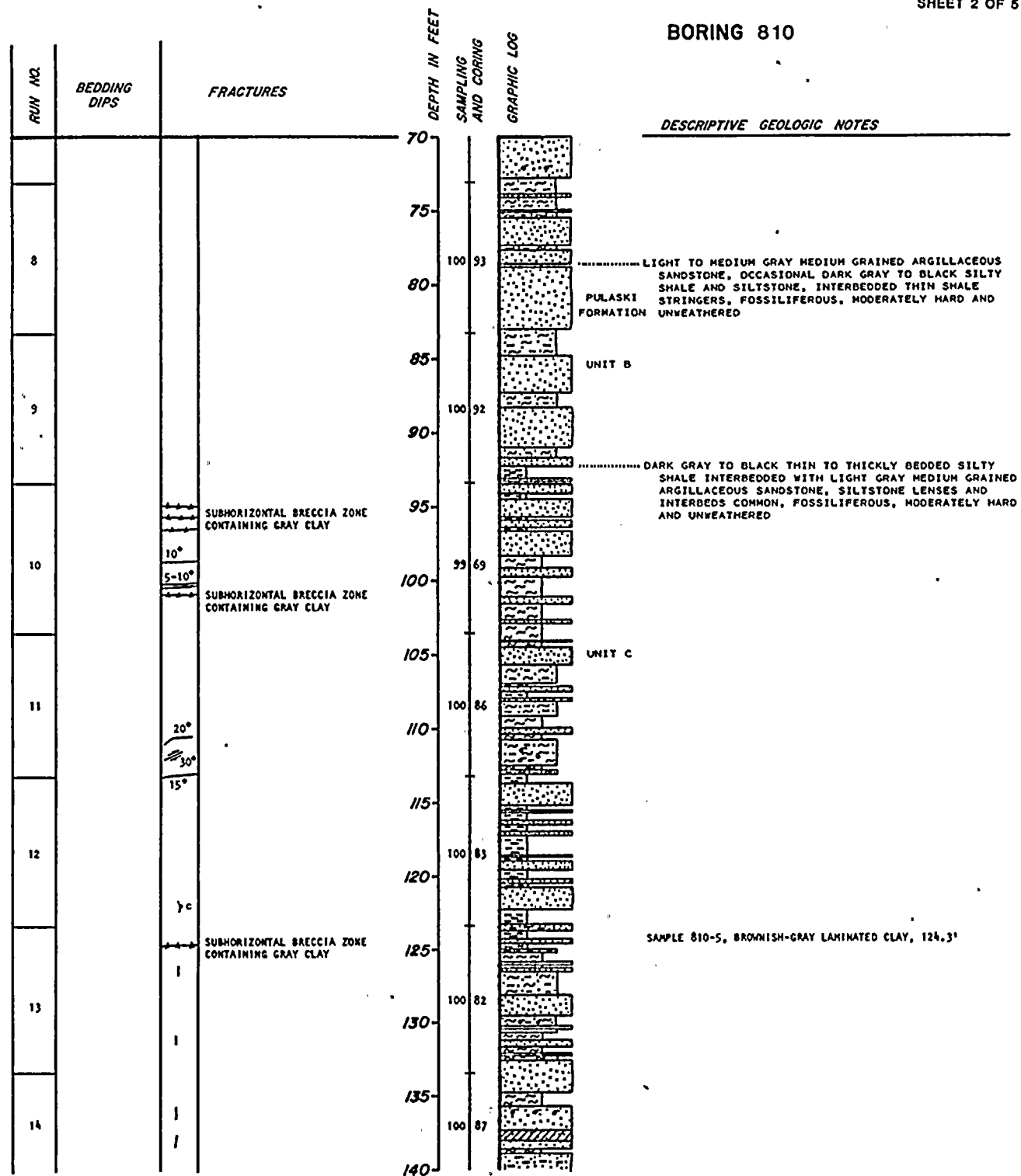


BORING B-810



GAMMA RAY LOG

BORING 810



SAMPLING AND CORING INFORMATION

Core run
100 95 R.O.D.
Percent recovery

BEDDING DIPS

03° Bedding dips measured on selective bedding planes. An attempt was made to avoid all obvious cross bedding or other primary structures.

FRACTURES

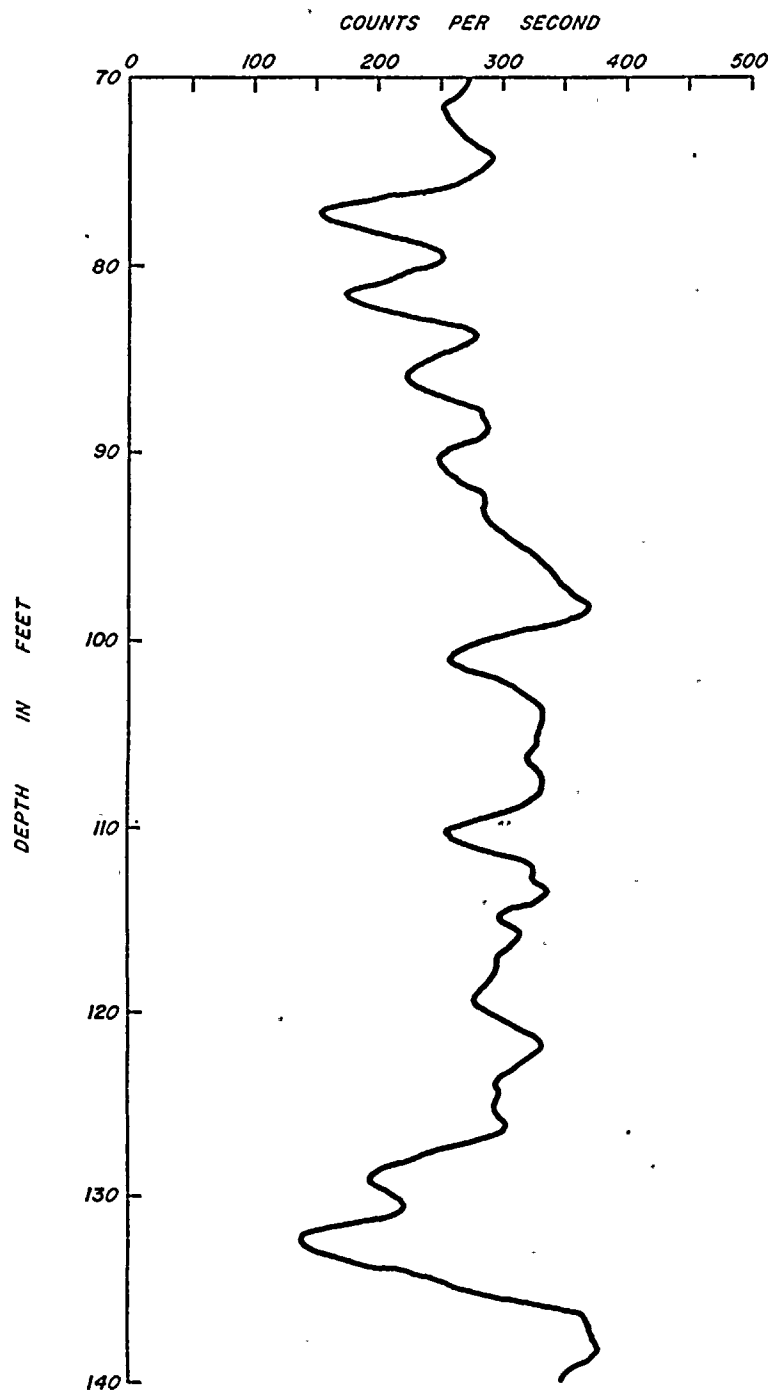
Breccia zone
Dip-slip slickensides
Fractures-shown at approximate angle to core axis
Mineralized fracture c = calcite s = sulfide
Fractured zone

KEY TO SYMBOLS

Sandstone
Graywacke
Siltstone
Shale
Fossils
Shale intra-clasts
Cross-bedding
Shale laminae

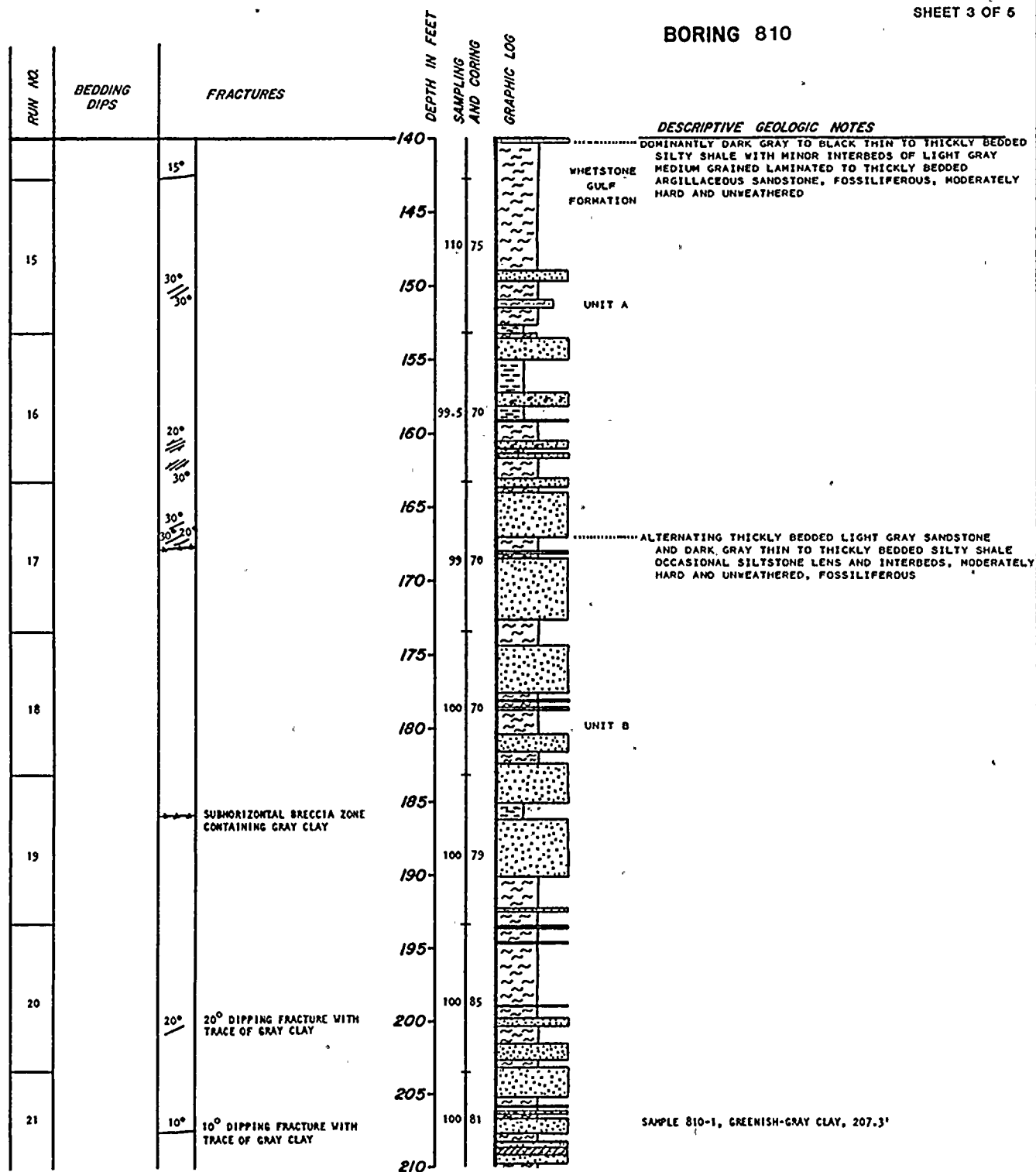


BORING B-810



GAMMA RAY LOG

BORING 810



SAMPLING AND CORING INFORMATION

Core run
100 95 R.O.D.
Percent recovery

BEDDING DIPS

03° Bedding dips measured on selective bedding planes. An attempt was made to avoid all obvious cross bedding or other primary structures.

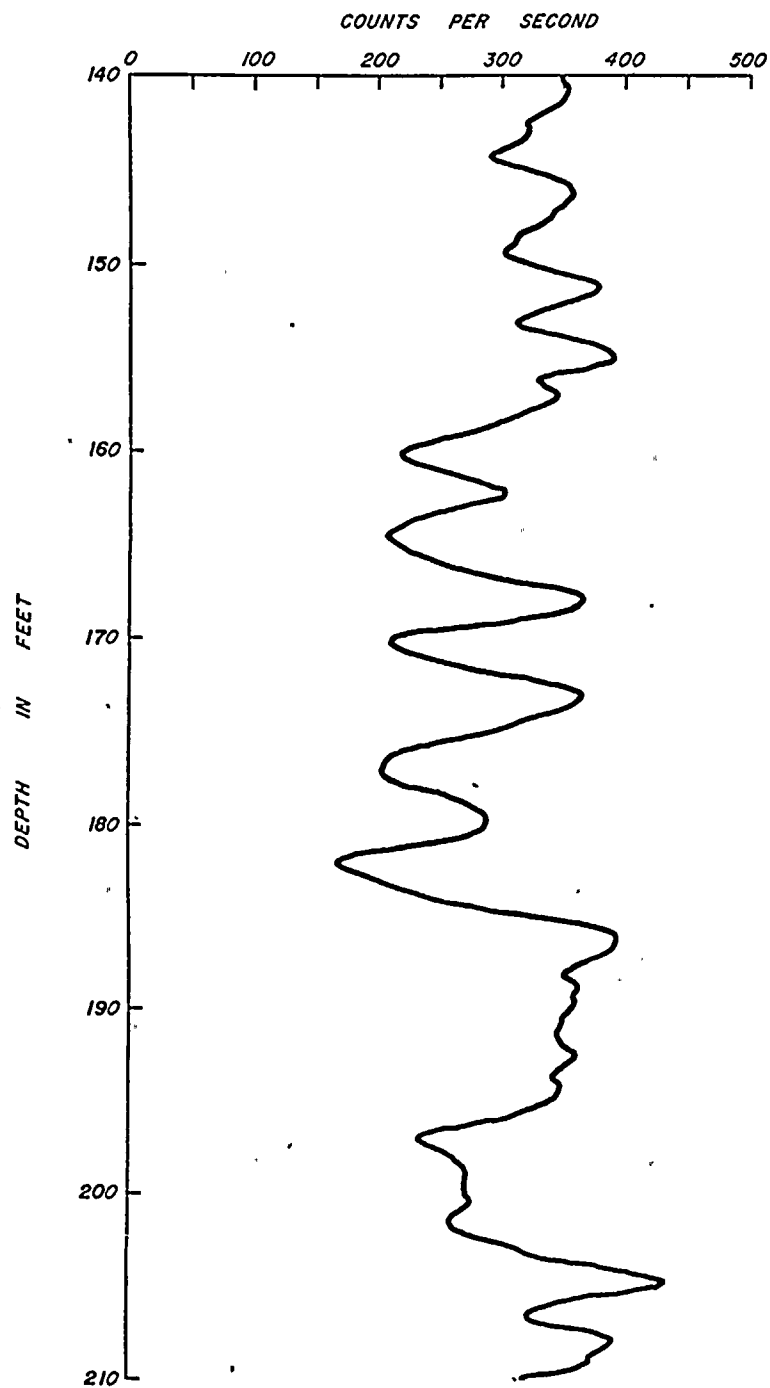
FRACTURES

Breccia zone
Dip-slip slickensides
Fractures-shown at approximate angle to core axis
Mineralized fracture c - calcite s - sulfide
Fractured zone

KEY TO SYMBOLS

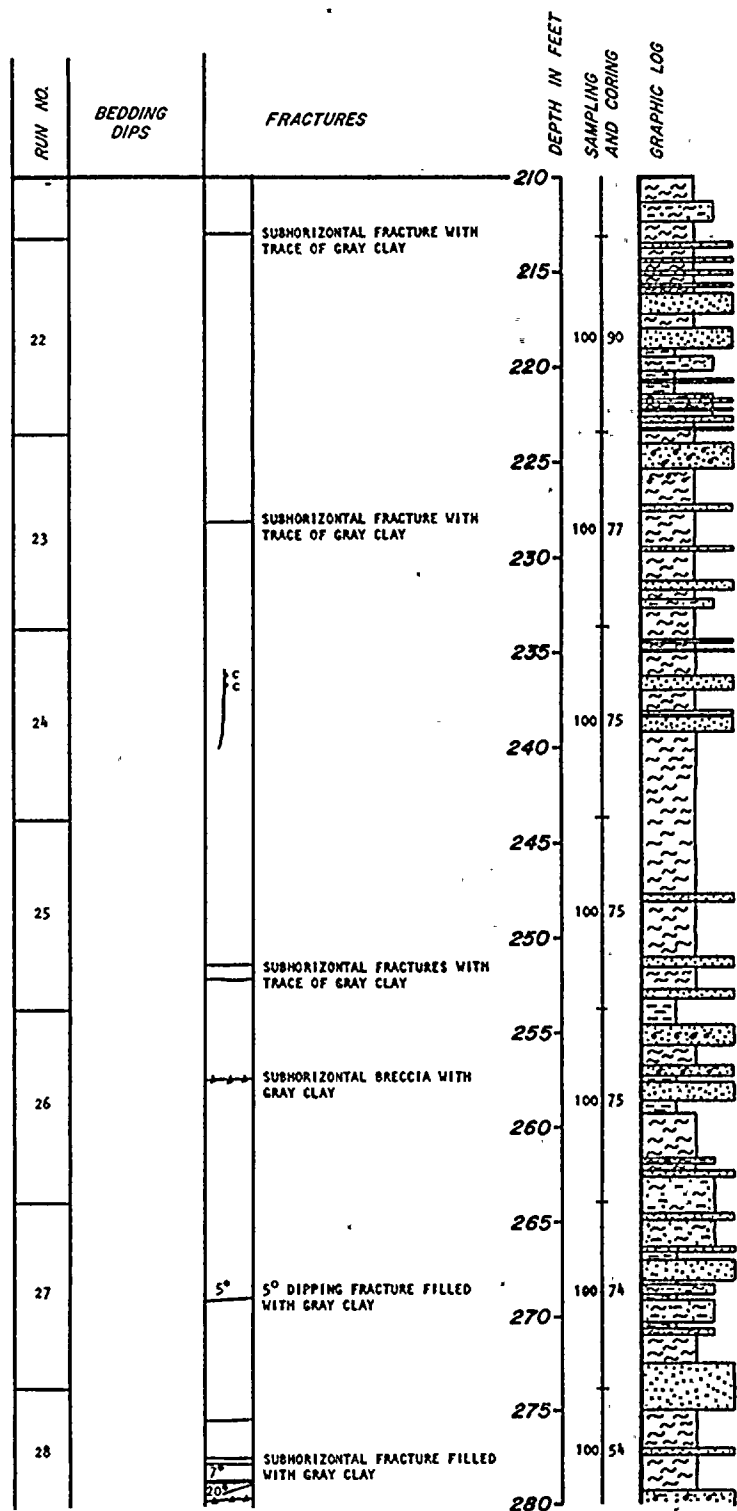
Sandstone
Graywacke
Siltstone
Shale
Fossils
Shale intra-clasts
Cross-bedding
Shale laminae

BORING B-810



GAMMA RAY LOG

BORING 810



DESCRIPTIVE GEOLOGIC NOTES

SAMPLE 810-2, LAMINATED BROWNISH-GRAY CLAY, 213.3'

SAMPLE 810-3, CLAY WITH ROCK FRAGMENTS, 251.4'
 SAMPLE 810-4, LAMINATED BROWNISH-GRAY CLAY, 252.3'

SAMPLING AND CORING INFORMATION

Core run
 100 95 R.Q.D.
 Percent recovery

BEDDING DIPS

03° Bedding dips measured on selective bedding planes. An attempt was made to avoid all obvious cross bedding or other primary structures.

FRACTURES

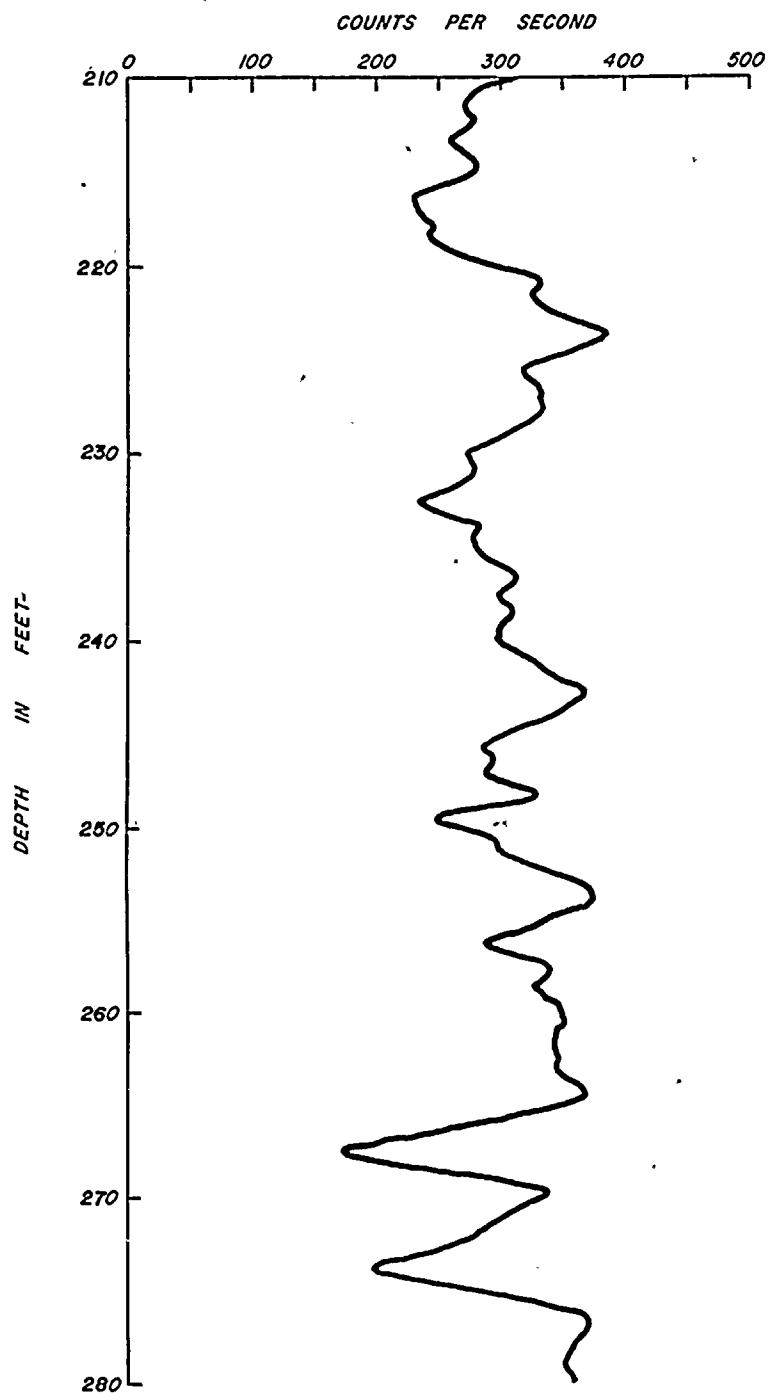
Breccia zone
 Dip-slip slickensides
 Fractures shown at approximate angle to core axis
 Mineralized fracture c = calcite s = sulfide
 Fractured zone

KEY TO SYMBOLS

Sandstone
 Graywacke
 Siltstone
 Shale
 Fossils
 Shale intra-clasts
 Cross-bedding
 Shale laminae

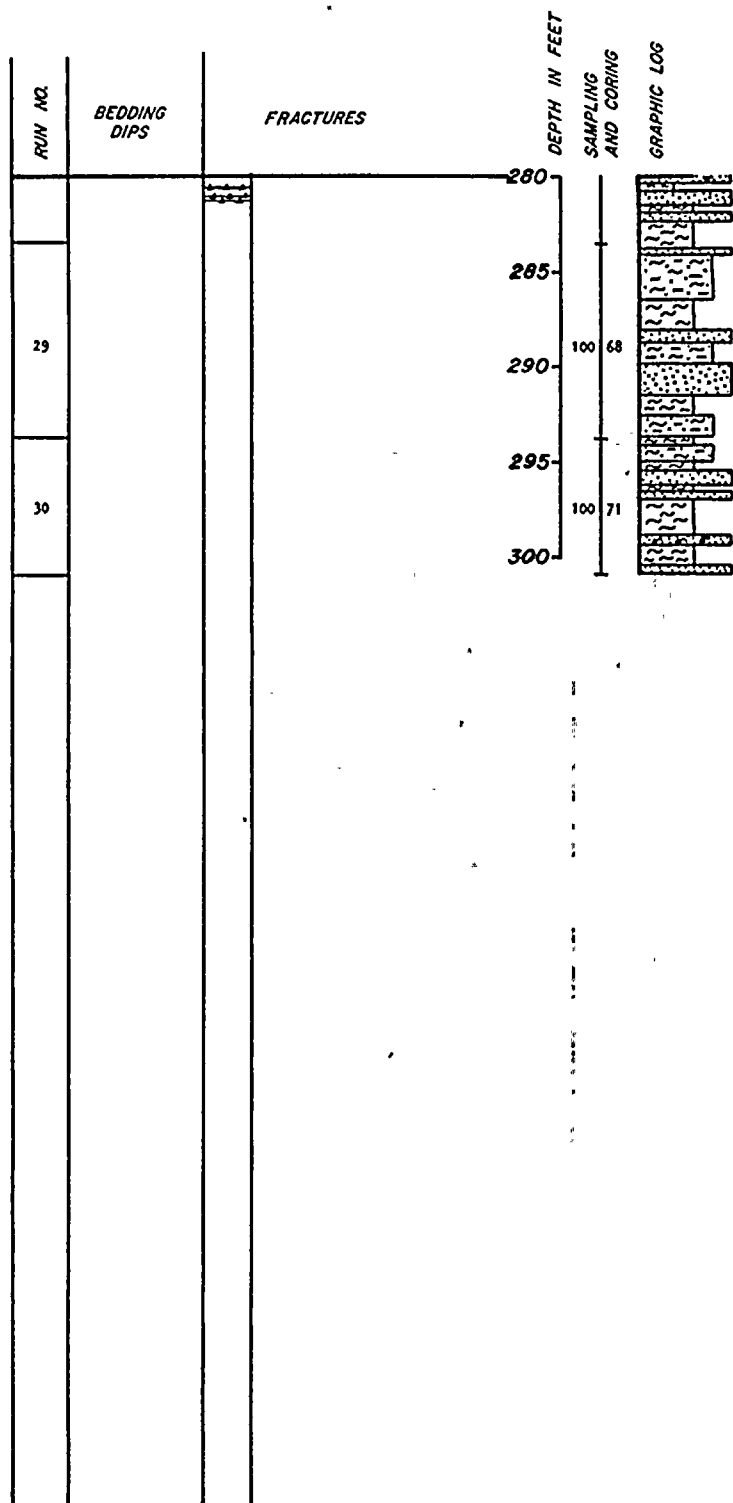


BORING B-810



GAMMA RAY LOG

BORING 810



DESCRIPTIVE GEOLOGIC NOTES

BORING TERMINATED AT 300.95'
ON 3-19-80 AND GEOPHYSICALLY
LOGGED ON 4-1-80

SAMPLING AND CORING INFORMATION

Core run
100% R.O.D.
Percent recovery

BEDDING DIPS

03° Bedding dips measured on selective bedding planes. An attempt was made to avoid all obvious cross bedding or other primary structures.

FRACTURES

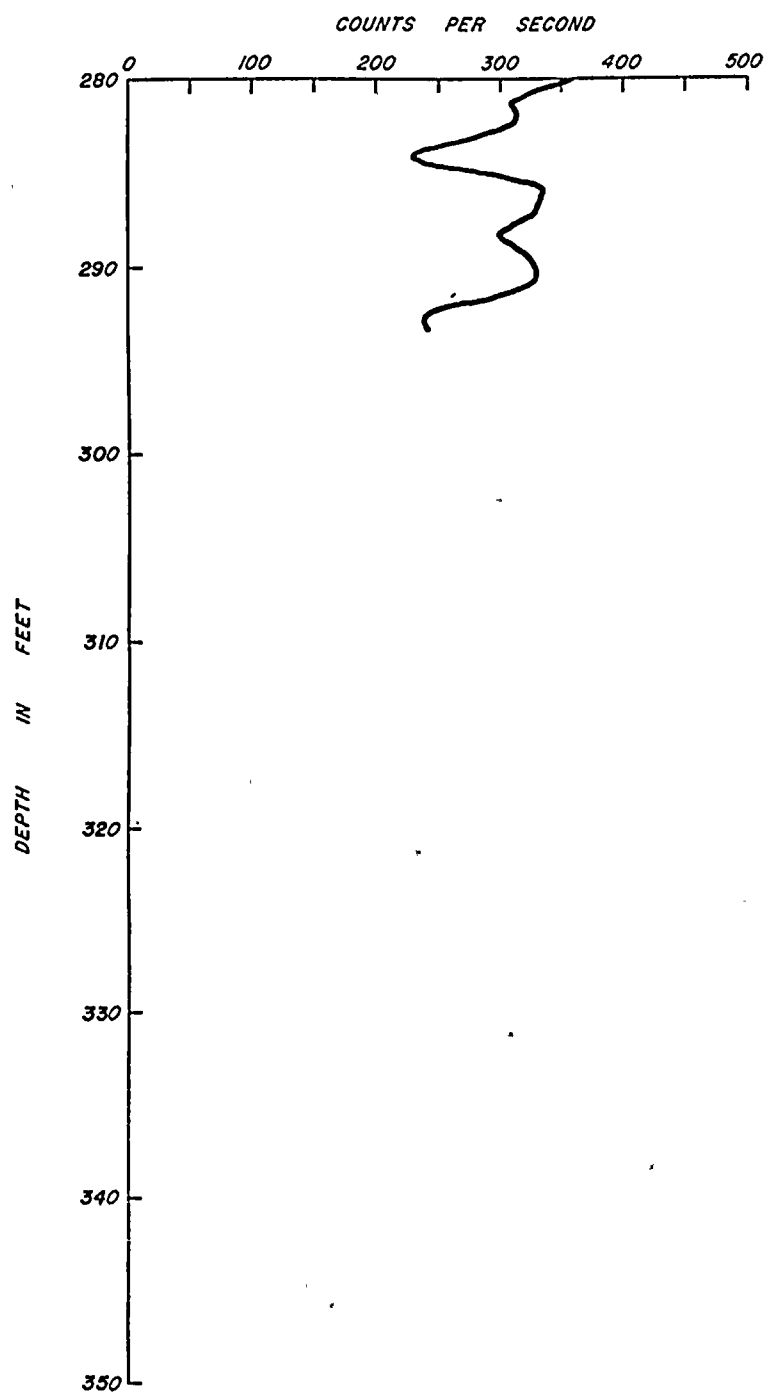
Breccia zone
Dip-slip slickensides
Fractures shown at approximate angle to core axis
Mineralized fracture c = calcite s = sulfide
Fractured zone

KEY TO SYMBOLS

Sandstone
Graywacke
Siltstone
Shale
Fossils
Shale intra-clasts
Cross-bedding
Shale laminae



BORING B-810



GAMMA RAY LOG

Fluid Inclusion Analyses

for

Dames and Moore, Inc.

Samples from Nine Mile Point Nuclear Station,
Unit 2, Series GA3
Job #4707-022-19
Transmittal Letter 04707B-DB-T0489



H. L. Barnes
Consulting Geochemist
September 4, 1979

Discussion of Results

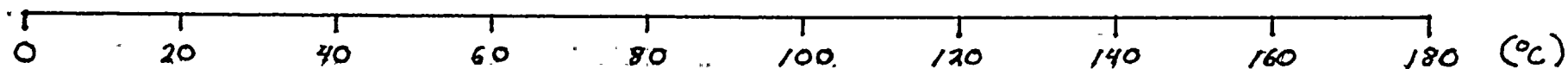
The textures of the calcites filling the fractures in these samples indicate a clear cut sequence of events. This sequence is best seen by classifying the calcites into three different types. Type 1 is associated with the sub-horizintal breccias and is intensely deformed often to become granulated. Type 2 is found on sub-vertical fractures and is mildy deformed. Type 3 is euhedral, small, undeformed crystals infilling open fractures and voids.

Temperatures

Fluid inclusions were not detected in either types 1 or 2 very probably because of deformation. The occurrence of marcasite associated with type 2 indicates temperatures below about 157°C.

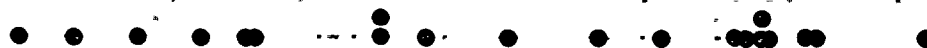
Inclusions in type 3 calcite were present but difficult to identify because bubbles were absent in their fluids. Consequently, this calcite and its inclusions formed at very low temperatures. These inclusions were heated to determine decrepitation temperatures because they represent maximum filling temperatures and to test by this distribution of temperature whether this type included more than one population. Figure 1 shows the distribution for primary and secondary inclusions and Figure 2 by sample number. Both indicate a single population and the lowest temperatures of 40°C indicate that they were formed at or below this temperature.

FLUID INCLUSION TEMPERATURE DISTRIBUTION



PRIMARY INCLUSIONS

CLEAR CALCITE



SECONDARY INCLUSIONS

CLEAR CALCITE

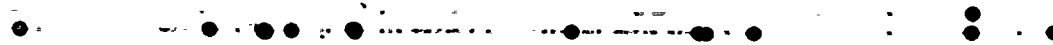


Figure 1



FLUID INCLUSION TEMPERATURES

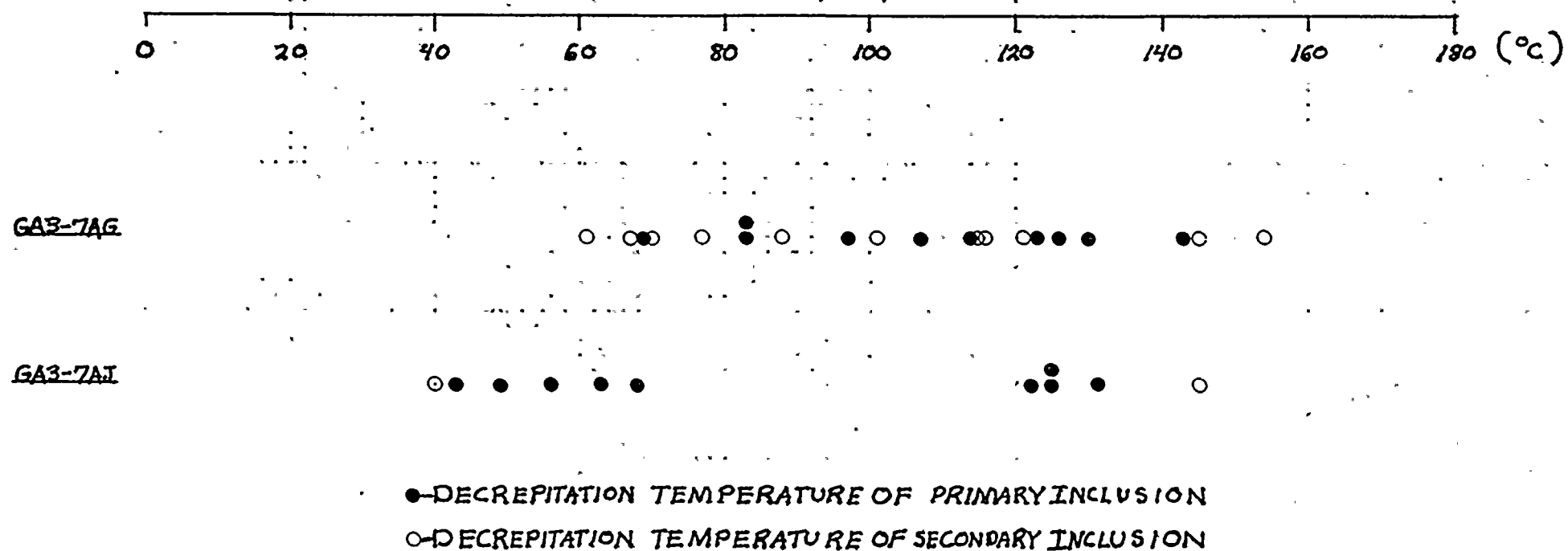


Figure 2.

Two inclusions were also cooled to test for separation of a vapor bubble to better define the filling temperatures. No bubbles formed but the inclusions froze at -3 and -4°C which show the fluid to be dilute with concentrations equivalent to 5-6 wt. % NaCl.

The cooling evidence and the low decrepitation temperatures demonstrate that type 3 calcite formed at temperatures indistinguishable from present ambient temperatures. Implicitly, the requirements of even shallow geothermal gradients prove that calcite precipitation occurred at or near the present surface. The low salinity is compatible with this observation.

Paragenesis

The paragenetic sequence, as indicated by the textures and temperature data from the samples is shown in Figure 3.

The textural relationship between marcasite, pyrite, and sphalerite indicates that the pyrite and sphalerite were deformed by D_2 of our report of October, 1977. The upper stability limit of 157°C for marcasite, as well as its weaker deformation, indicates that it was deposited after D_2 , but probably before D_3 , which was a pervasive deformation.

None of the three types of calcite observed in the GA3 series of samples is similar in textures, color, and inclusions to the lowest temperature calcites described in our earlier report. The lower temperature limit of $\sim 85^{\circ}\text{C}$ during D_4 is higher than the temperatures found for the calcites in the GA3 series. In the absence of



PARAGENETIC RELATIONSHIPS

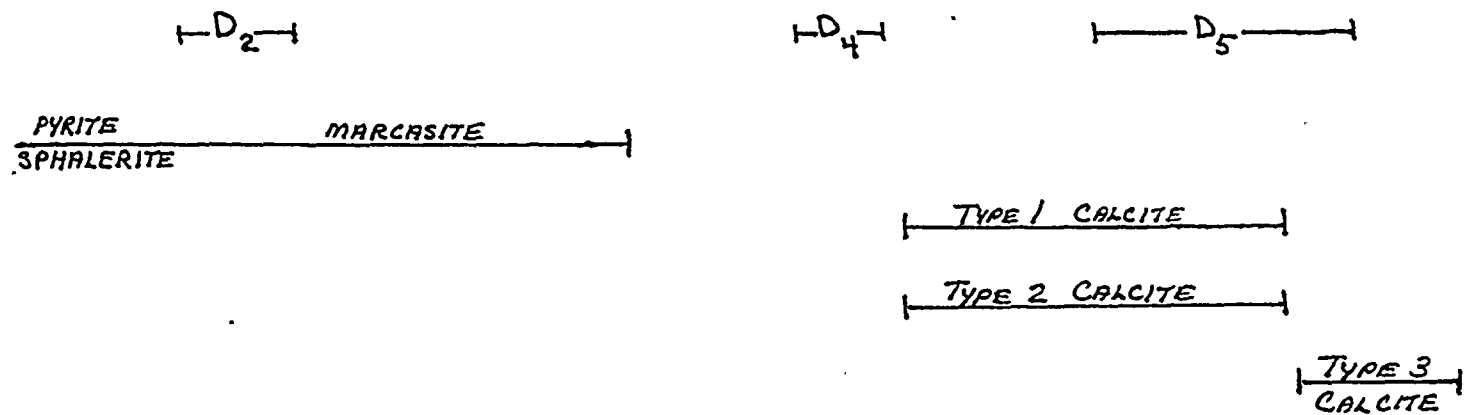


FIGURE 3

of temperature data for Types 1 and 2 calcites, they may have been deposited during or after D_4 . However, both are deformed, indicating a fifth period of deformation, D_5 .

The opening of fractures during D_5 allowed very low temperature fluids to circulate, precipitating Type 3 calcite. This evidence fits best with very low temperatures D_5 . Temperatures for single-phase primary and secondary fluid inclusions indicate that temperatures were well below 100°C by this time and probably were also below 40°C . The undeformed crystals of Type 3 calcite prove that deposition continued after D_5 and may still be taking place.



Descriptions of Samples

Ten samples (GA3) of a fine-grained orthoquartzite containing calcite coatings on fracture surfaces were examined for fluid inclusions mineralogy, and textures. These properties are illustrated for hand samples in the next section by photographs numbered consecutively 1 through 17 and for thin sections in the last section by figures numbered between 1-1 and 2-10. After examination, the calcites were divided into three types on the basis of texture and mode of occurrence as described below.

Type 1 Calcite

Occurrence: Type 1 calcite occurs as the matrix material in bedding-plane breccias and microbreccias in samples GA3-1, -4, -7A, -16, -18, and possible -17. (Sample GA3-17 was examined in hand specimen only). Examples are shown in Photos 3, 4, and 7 where the bedding-plane breccia is well-developed (samples GA3-4 and -7A).

Deformation and Texture: Type 1 calcite is intensely deformed as shown by the fine-grained cataclastic textures illustrated in Photos 2-3, 2-9, and 2-20. The average grain size of the calcite fragments is about 15 μ m. Photos 2-18 to 2-20 also show evidence of post-deformational solution to Type 1 calcite forming voids lined with Type 3 calcite.

Associations: Type 1 calcite is associated with angular fragments of the quartzite host rock up to 1 cm in length (Photo 4)



and angular fragments of individual quartz grains up to 75 μ m in length (Photos 2-3 and 2-20). In sample GA3-16, Type 3 calcite (sparry calcite) occurs filling fractures or voids in the breccia of which part is Type 1 calcite.

Inclusions: No fluid inclusions were found in any of the Type 1 calcite samples. The deformation has liberated the fluid inclusions and the small grain size makes improbable the discovery of any preserved inclusions.

Paragenesis

Type 1 calcite	_____
Type 3 calcite	_____
Deformation	D
	Time →



Type 2 Calcite

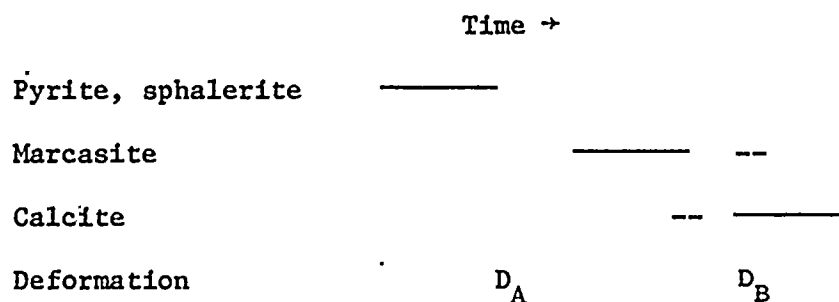
Occurrence: Type 2 calcite occurs as thin, patchy coatings on sub-vertical fracture surfaces on samples GA3-12, -13, and -14, (Photos 8 through 12). The fracture surfaces are very irregular, making sample preparation extremely difficult.

Deformation and Texture: Type 2 calcite is deformed but not as intensely as Type 1. The deformation is expressed as abundant open cleavages in the calcite but the individual cleavage fragments are not always separated from one another. Pyrite, marcasite, and sphalerite grains are also fractured (Photos 2-4, and 2-6). The deformation does not extend into the host rock (i.e. there is no observed brecciation on the vertical fractures.)

Associations: Marcasite, pyrite, and sphalerite are associated with the Type 2 calcite. All three sulfides were identified optically and pyrite and marcasite were confirmed by X-ray diffraction. All three are fractured, the pyrite and sphalerite more so than the marcasite (Photos 2-4, and 2-6). Close examination of Photo 2-4 shows that the sulfide grain is actually a microbreccia of pyrite and sphalerite clasts in a marcasite matrix. Photo 2-6 shows a grain of fractured marcasite alone.

Low magnification examination of the surfaces revealed that most of the sulfides were deposited on the walls of the fracture, rather than on or in the calcite. A few undeformed hemispherical rosettes of marcasite are preserved in depressions on the surfaces.



Paragenesis

This paragenesis is consistent with that developed in our report of October 20, 1977. The pyrite and sphalerite have undergone more deformation than the marcasite as shown by the separation and rotation of pyrite and sphalerite clasts (Photo 2-4) as opposed to the minor fracturing of the marcasite (Photo 2-6). Furthermore, the calcite on the fracture surfaces appears to be younger than the marcasite and is also deformed. Comparison of the above paragenesis with the paragenesis from the October, 1977 report suggests that D_A might well be D_2 of our earlier report and D_B could be either D_3 or D_4 .



Type 3 Calcite

Occurrence: Type 3 calcite occurs as sugary white coatings on subhorizontal surfaces and associated vertical fractures on samples GA3-1, GA3-7 and possibly GA3-18. On sample GA3-16 it occurs filling small solution fissures and holes within Type 1 calcite and along the boundaries separating Type 1 calcite from quartzite fragments (Photo 2-18). Type 1 calcite from sample GA3-7A has in places been truncated by fractures containing type 3 calcite (Sample #GA3-7AG.)

Deformation and Texture: Occurs as stubby euhedral crystals up to 1 mm in diameter. In GA3 -18 this type of calcite coats and cements several fragments of quartzite on the surface of a fracture (Photo #17). Type 3 calcite appears to be generally undeformed exhibiting closely interlocking grain boundaries and no evidence of frosting. Small fractures occur in some type 3 grains, occasionally passing through the crystal but rarely showing much separation. Some twinning was observed in the calcite near the edges of polished sections.

Associations: Usually very clean of other solids and not associated with any other minerals.

Inclusions: Inclusions are fairly common in samples GA3-7AG and GA3-7AJ but were difficult to detect owing to the absence of bubbles. Primary and secondary inclusions were observed in these samples.



No inclusions were observed in samples GA3-16, GA3-18 or GA3-1. Only decrepitation temperatures were measured in the 32 inclusions found in samples GA3-7A(G) and -7A(J) (Figure 1). These show a considerable range and are not separable into on the basis of decrepitation temperatures into populations of primary and secondary inclusions (Figure 2). Two inclusions in sample GA3-7AJ froze at temperatures of -3°C to -4°C , equivalent to a 5 to 6 wt % NaCl solution filling the inclusions. When heated, this same inclusion leaked about 17°C , probably due to rupturing of the walls of the inclusion during freezing.

The inclusions occur isolated within crystals (Figure 2-12) or, as secondary inclusions, when they are usually associated with other inclusions oriented along surface fractures (Figure 1-1) or grain boundaries. In several instances, the inclusions were not visible until their decrepitation temperature was reached and they suddenly become opaque. Occasionally fluids could be seen leaking from the inclusions when they would decrepitate. The inclusions generally had very irregular outlines and, depending on their orientations graded from transparent to nearly opaque.

Paragenesis

Type 1 calcite

Type 3 calcite

Deformation

D



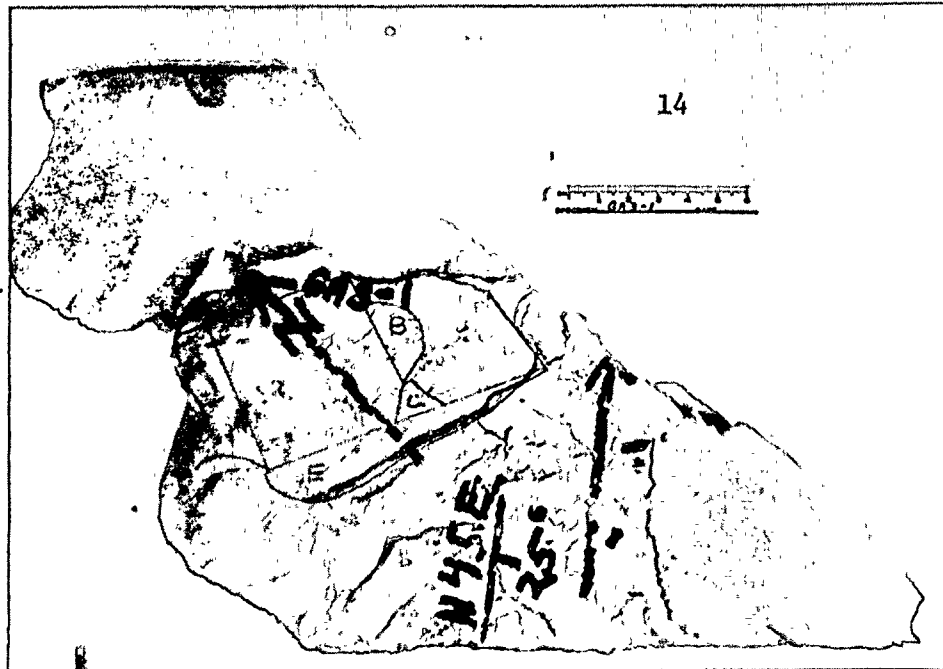
Photographs of Hand Samples

Overlays show locations of chips referred to in the text and photo captions. The photographs are numbered 1 through 17 consecutively.



15

Photo 1
Sample GA3-1
Small white calcite
crusts on surface



14

Photo 2
Sample GA3-1
Upper pieces
removed showing
lower surface
coated with
calcite

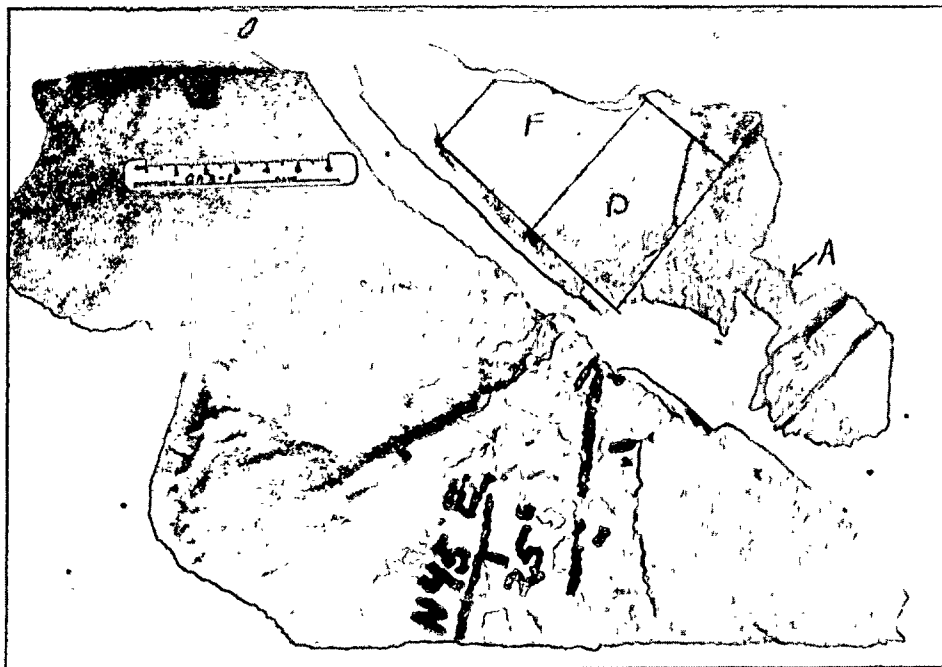


Photo 3
Sample GA3-4
Calcite coating
breccia fragments

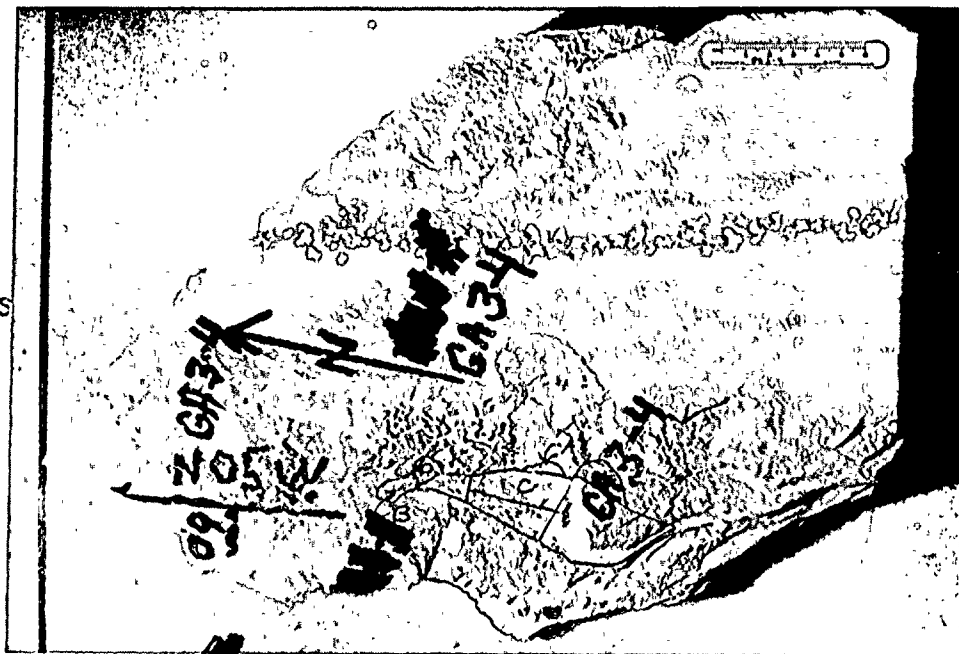




Photo 4
Sample GA3-4
Close-up of breccia
clasts cemented by
fine grained
calcite

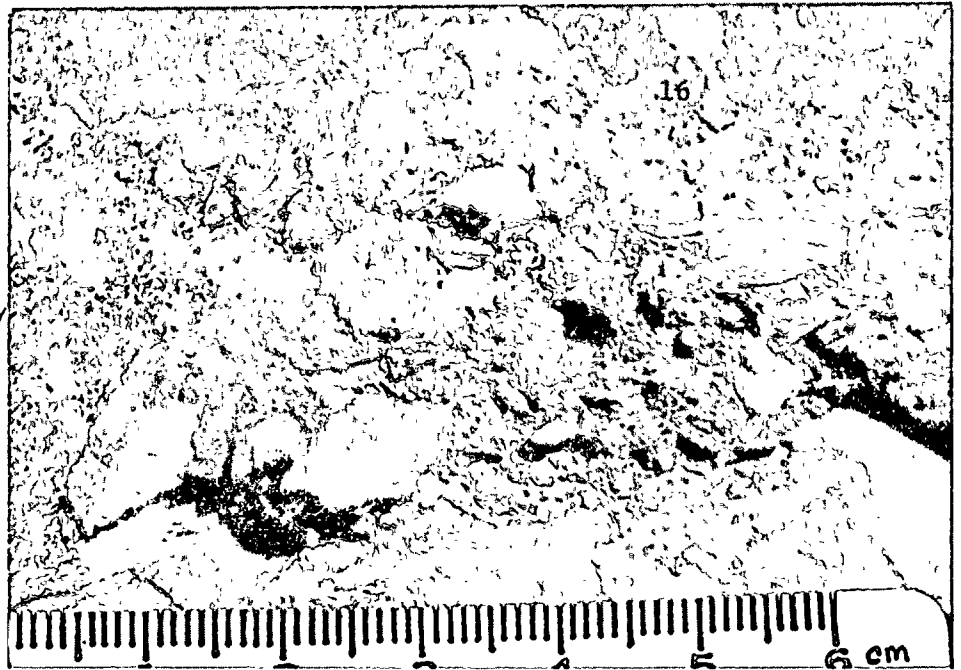


Photo 5
Sample GA3-7, 7A
Samples GA3-7(A,B,C,D)
taken below GA3-7A
on GA3-7 surface.
Samples GA3-7A(G-Q)
are from fractures
within 3 cm. below
the breccia surface.

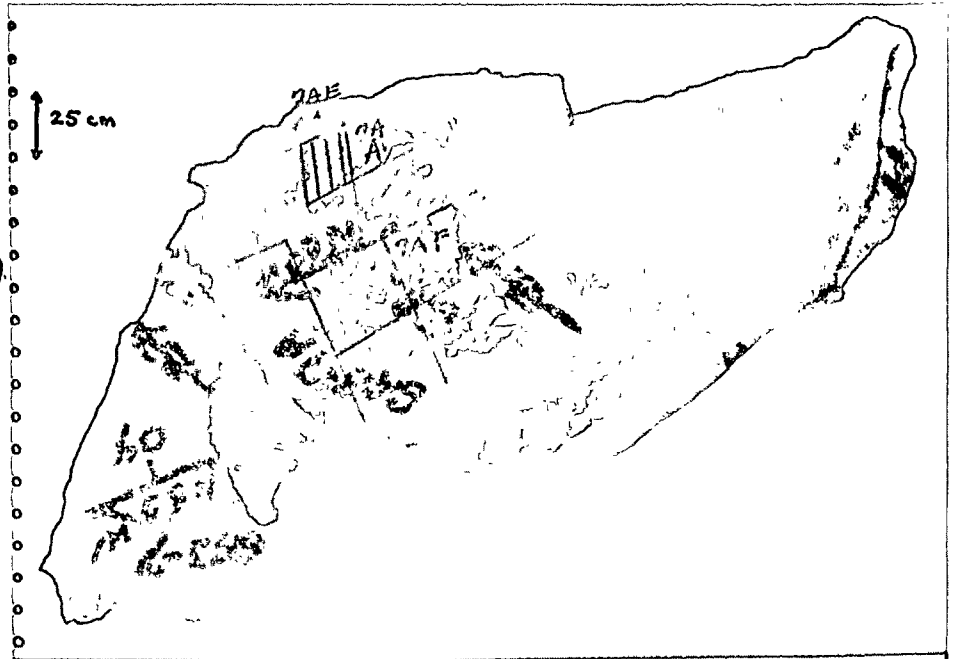
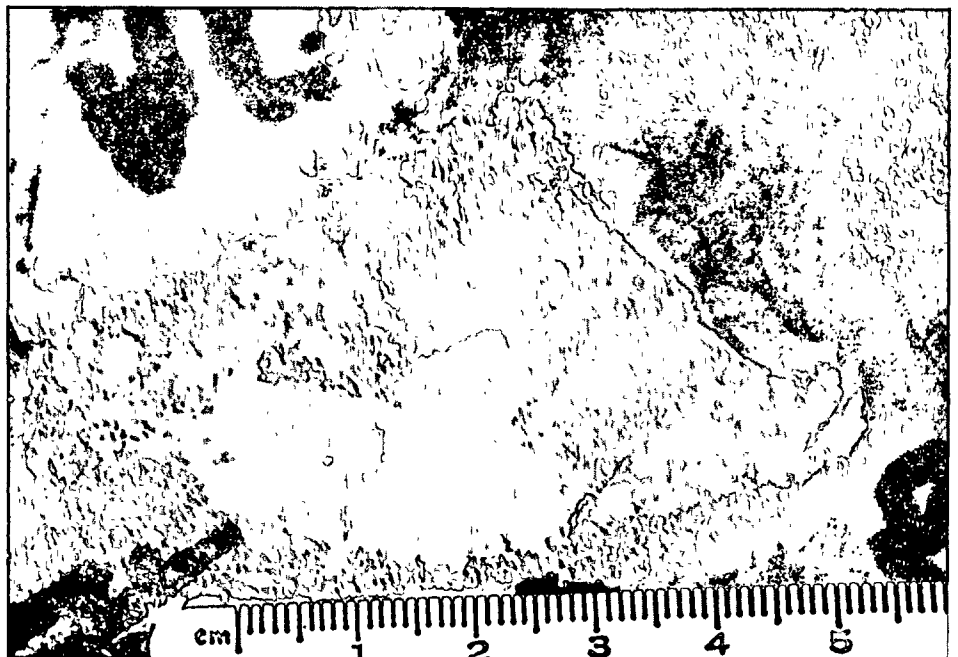


Photo 6
Sample GA3-7
Close-up of clear
calcite on bedding
surface





19

Photo 7
Sample GA3-7A
Close-up of micro
crystalline calcite
cementing breccia
fragments.

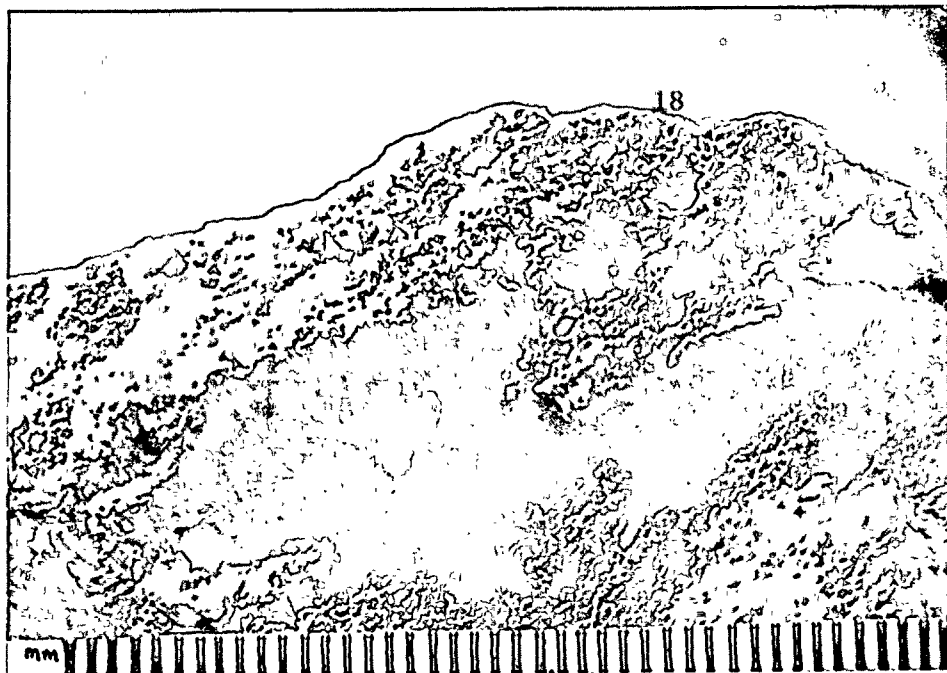


Photo 8
Sample GA3-12

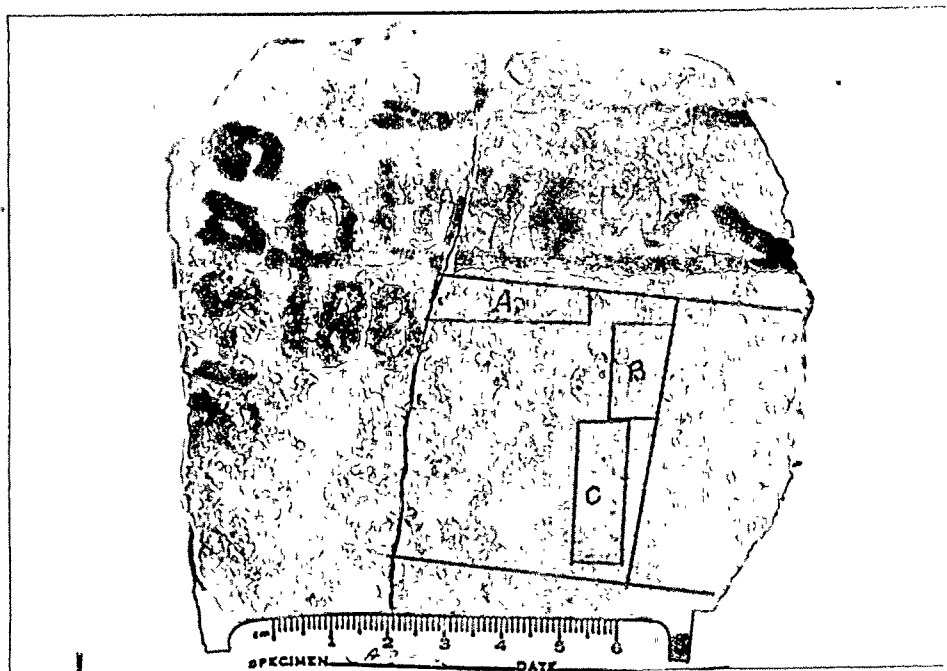


Photo 9
Sample GA3-12
Close-up showing
small white calcite
crusts

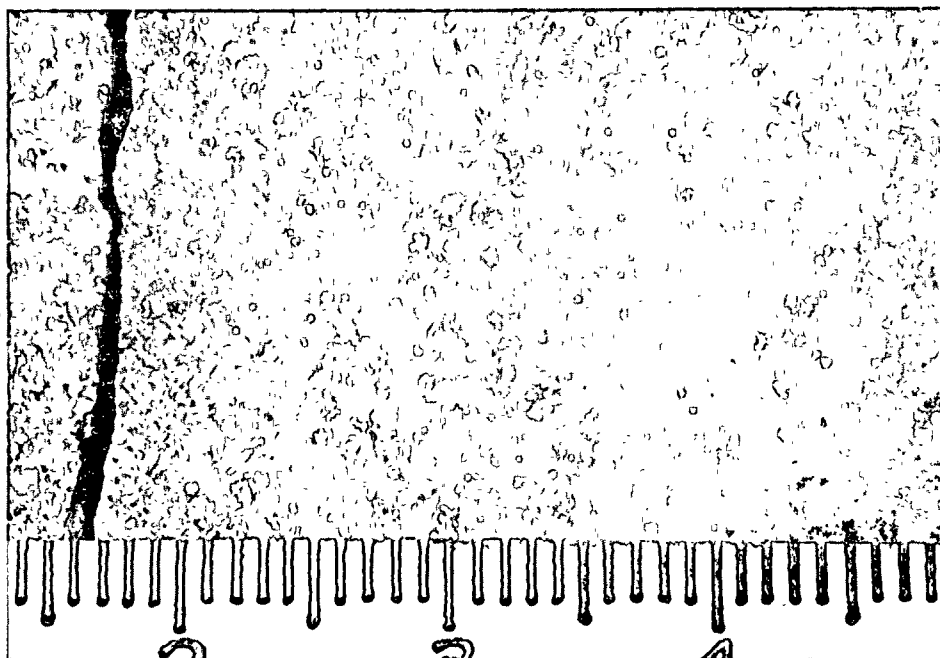


Photo 10
Sample GA3-13
Small white calcite
crusts on surface

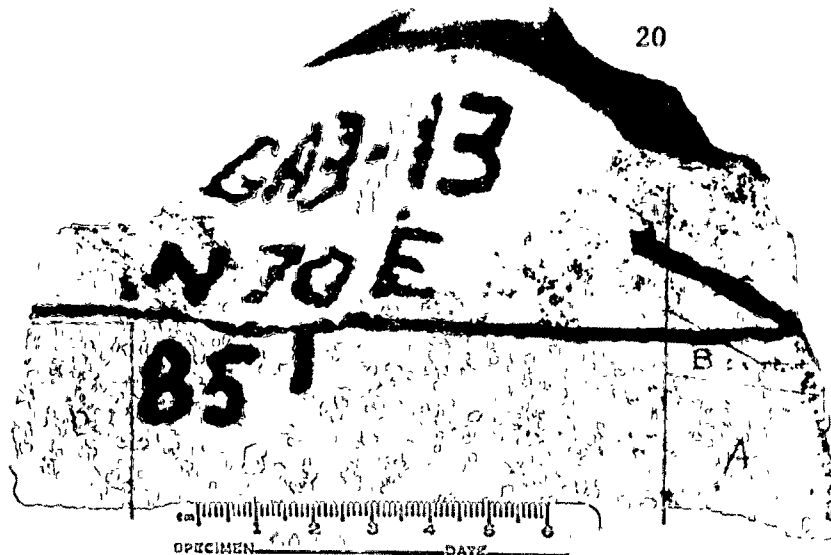


Photo 11
Sample GA3-14
Calcite crusts on
subvertical fracture
surface

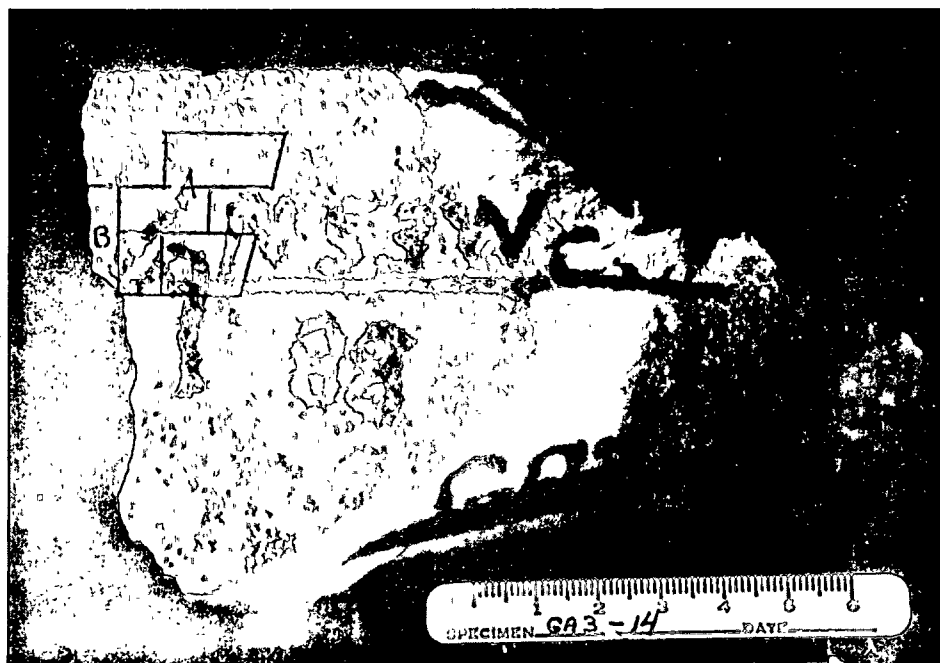


Photo 12
Sample GA3-14
Conjugate shear
surface showing
calcite mineralization.
Lower left of photo
shows an area
bearing secondary
iron oxides.

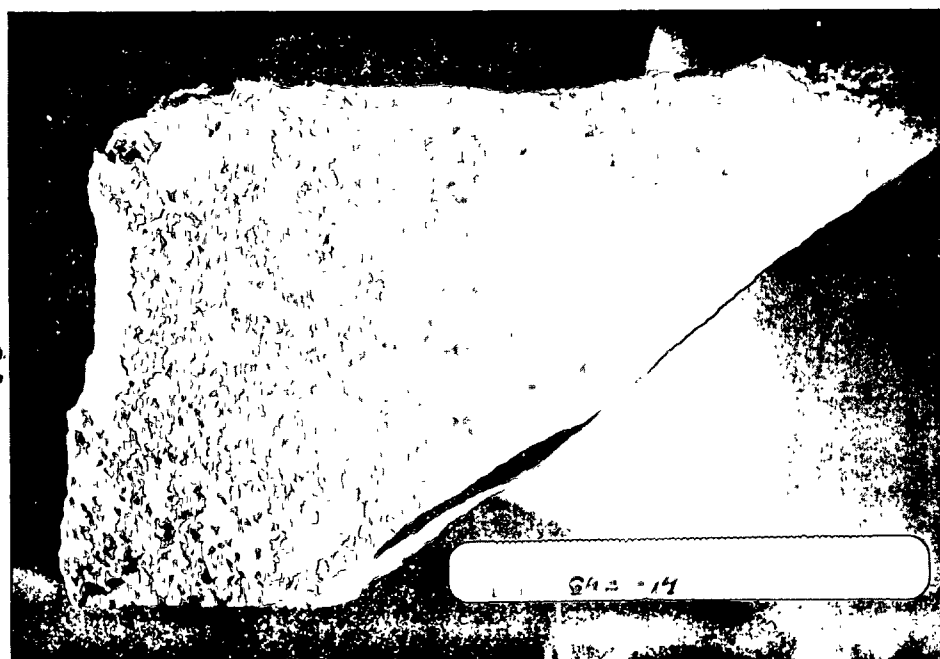




Photo 13
Sample GA3-16
Arrows represent
perpendiculars to
surfaces as mounted
on slides. Samples
GA3-16 (C, D, E) were
recut from those
shown.

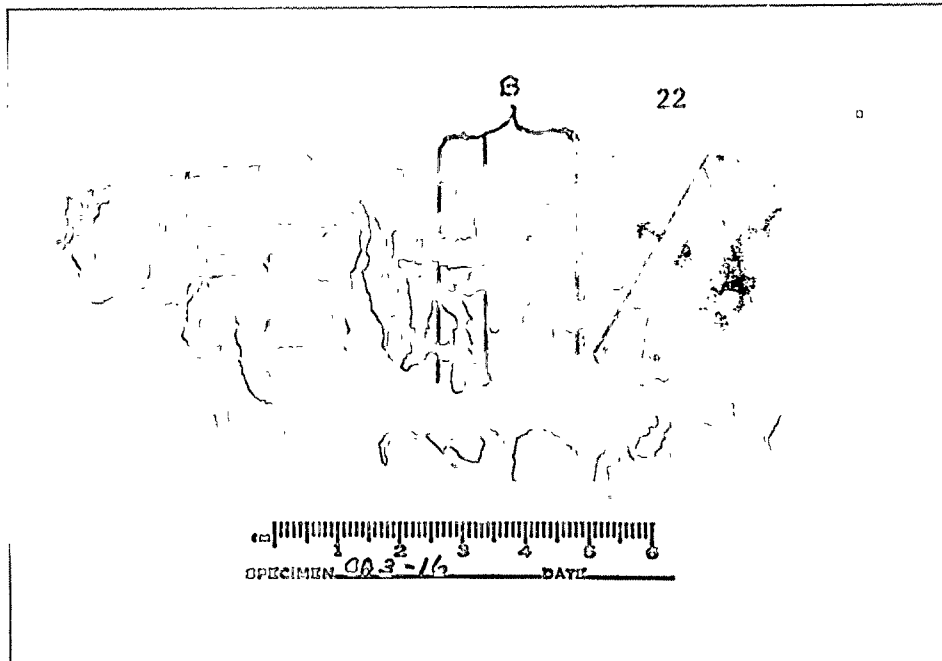


Photo 14
Sample GA3-16
Close-up of breccia
fragments cemented
by Calcite.

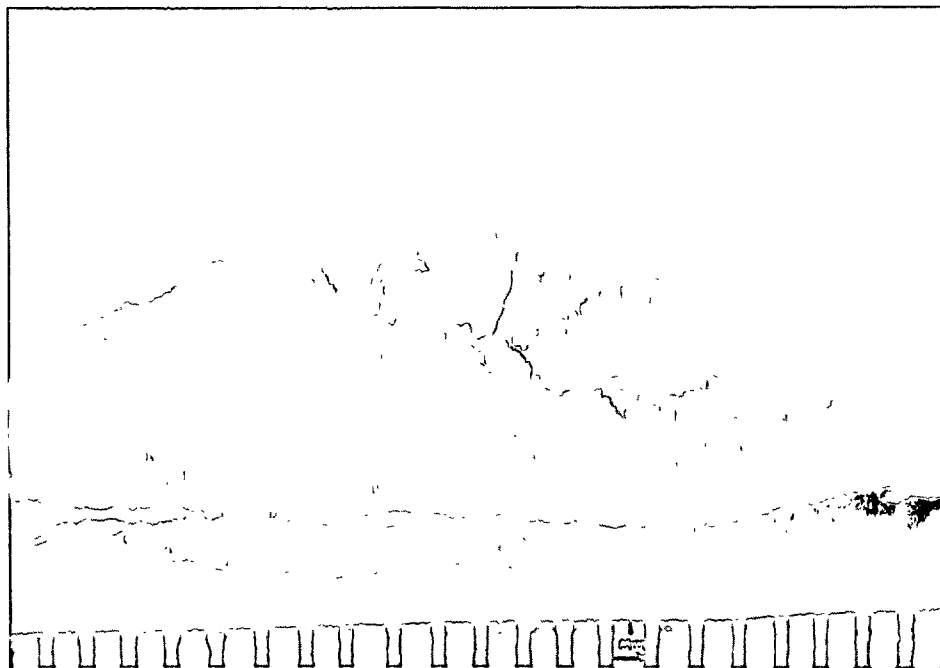


Photo 15
Sample GA3-17
Small white patches
of clear Calcite





Photo 16
Sample GA3-18

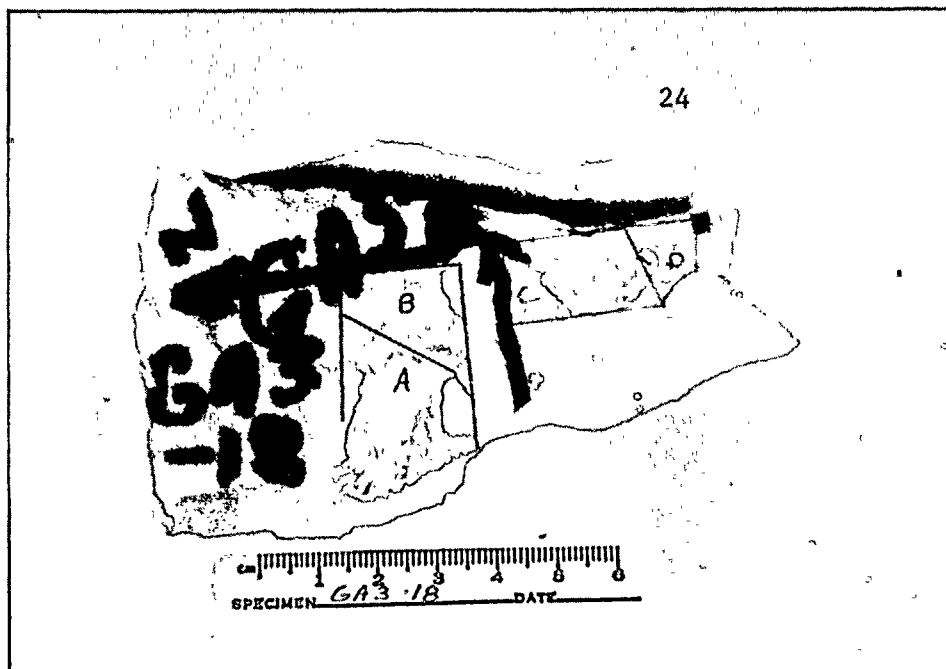


Photo 17
Sample GA3-18
Close-up of
sandstone clasts
cemented by
calcite





Microphotographs and Diagrams
of Representative Thin Sections.

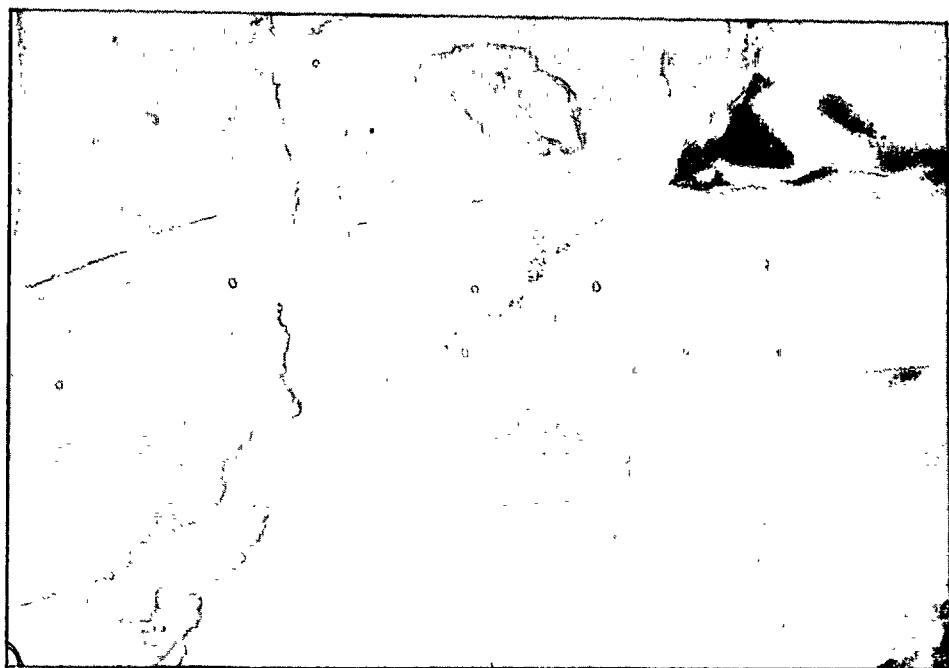
These illustrations are numbered
1-1 through 2-10.



Photo 1-1
Sample GA3-7A (G)
Secondary inclusion in
Type 3 calcite
Field of View = $575 \times 400 \mu\text{m}$



Photo 1-22
GA3-7A (G) Inclusion 12
Secondary inclusion in
Type 3 calcite
Field of View = $160 \times 110 \mu\text{m}$





ANALYST: RCA

8/79

FLUID INCLUSION SKETCHES

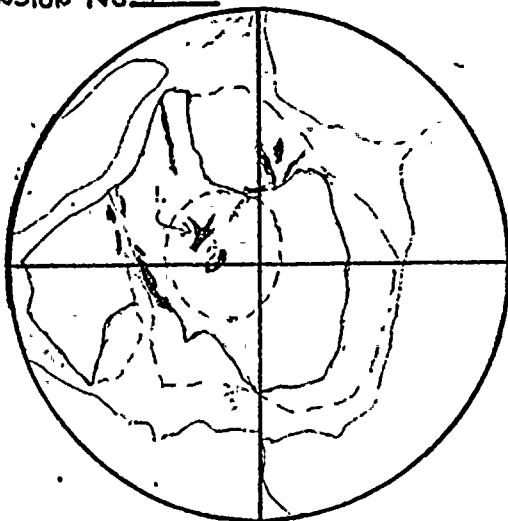
SAMPLE NO. 643-2AG

CHIP NO.

MINERAL: Calcite

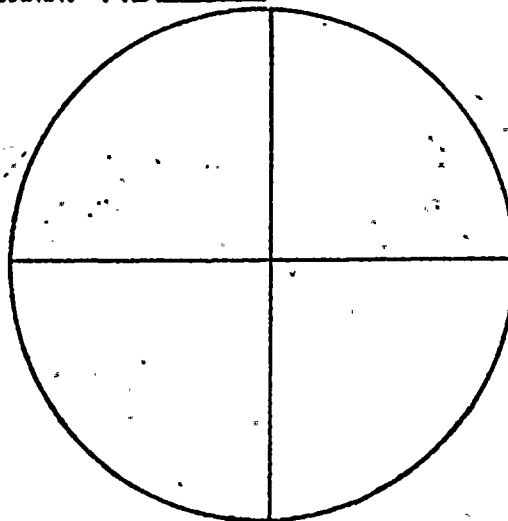
Inclusion No. 1

165X

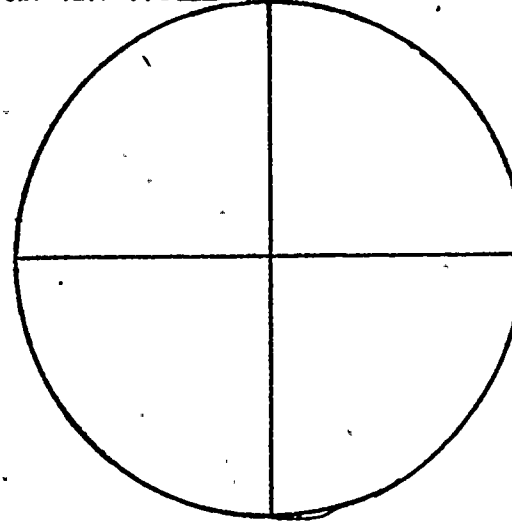


No change in inclusions shown.

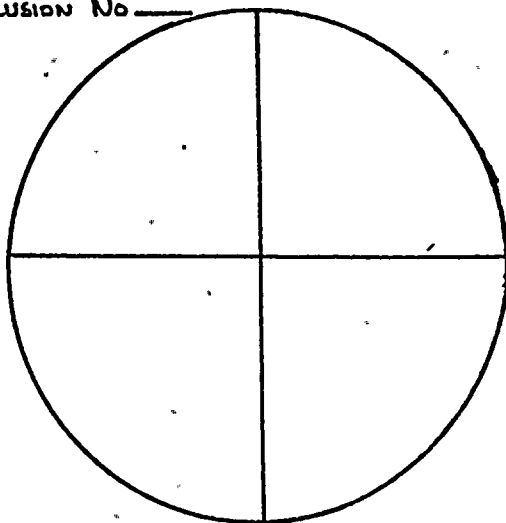
Inclusion No. _____



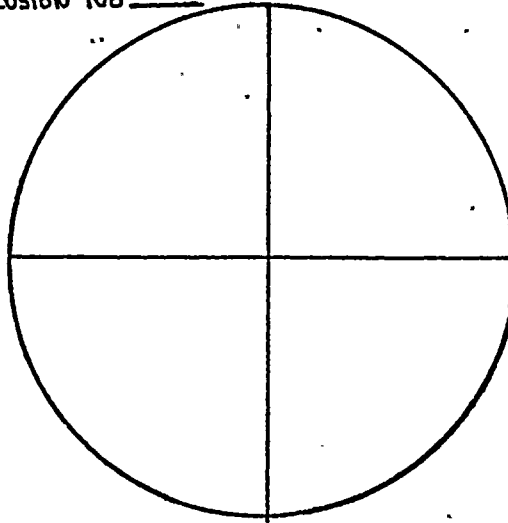
Inclusion No. _____



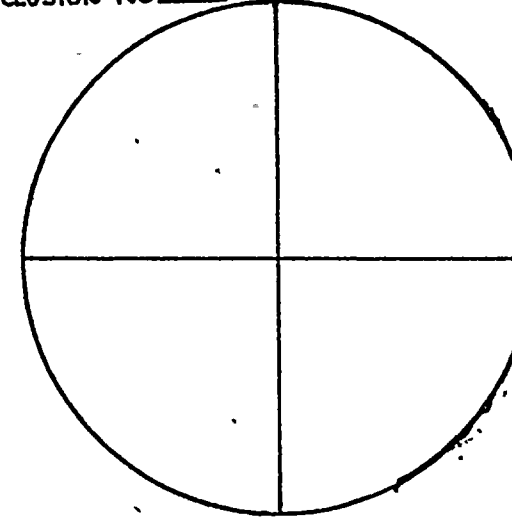
Inclusion No. _____



Inclusion No. _____



Inclusion No. _____





ANALYST: RCA & JBM 8/79

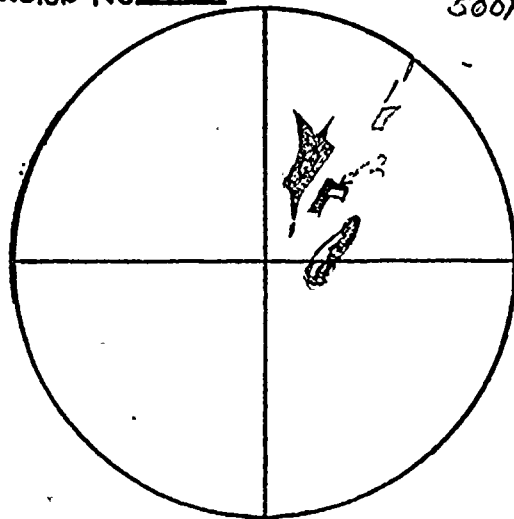
FLUID INCLUSION SKETCHES

SAMPLE No. C-13-A

CHIP No. 6

MINERAL: CALCITE

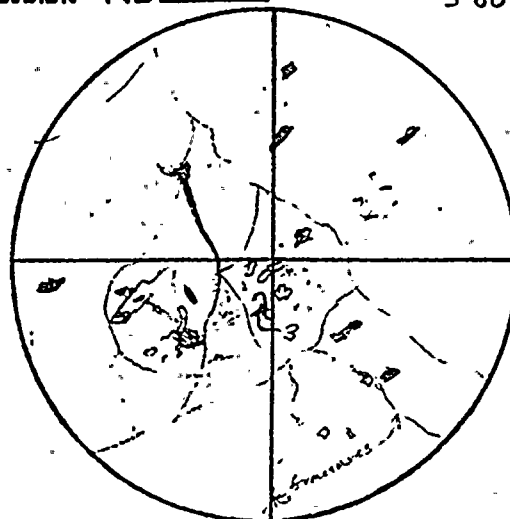
Inclusion No. 2 500X



[Close-up of area shown in sketch
of inclusion #1 by dashed circle]

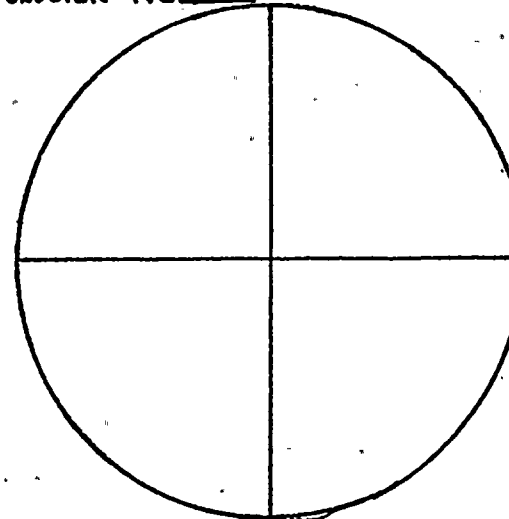
2) Decrepitation at 83°

Inclusion No. 3 500X

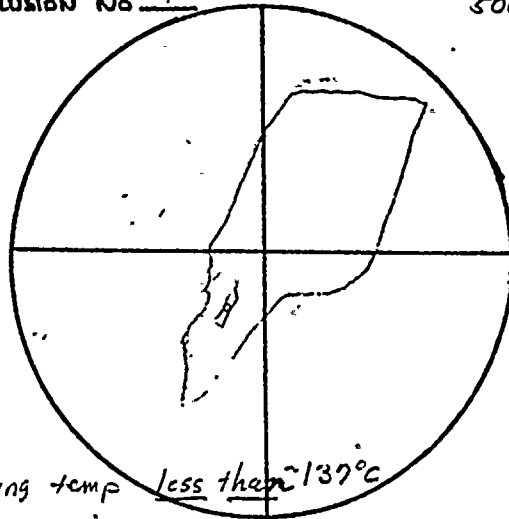


3) decrepitation 88°

Inclusion No. 4 500X



Inclusion No. 4 500X



Filling temp less than 137°

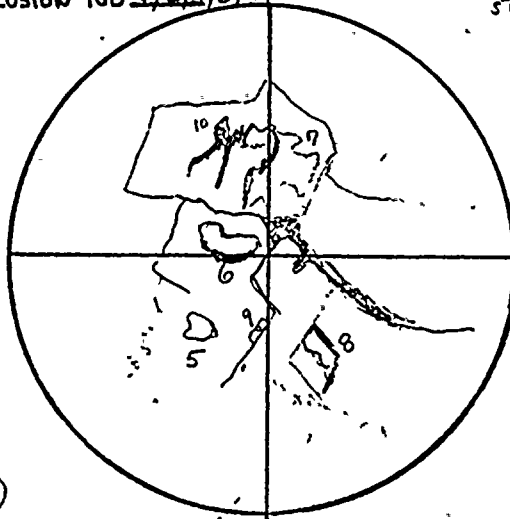
a) ... 132°

b) ... 137°

c) ... 136° (120°)

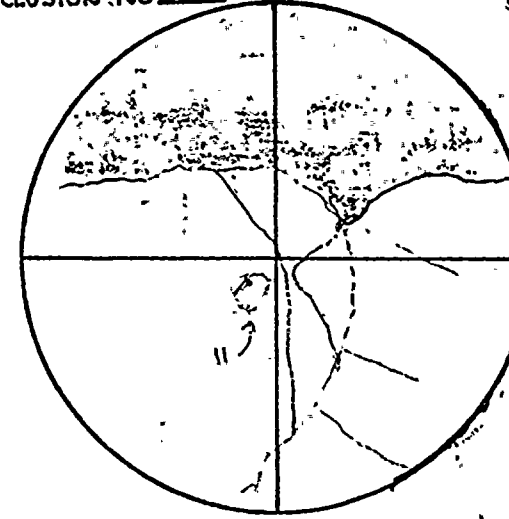
d) ... 139° held @ 200° for 15 min

Inclusion No. 5, 6, 7, 8, 9, 10 500X



5
6
7
8
9
10
No changes at all
up to 230°

Inclusion No. 11 500X



114° decrep. could see leakage into
fractures grain indy



51
51

51
51

ANALYST: RCA & JEM 8/79 FLUID INCLUSION SKETCHES

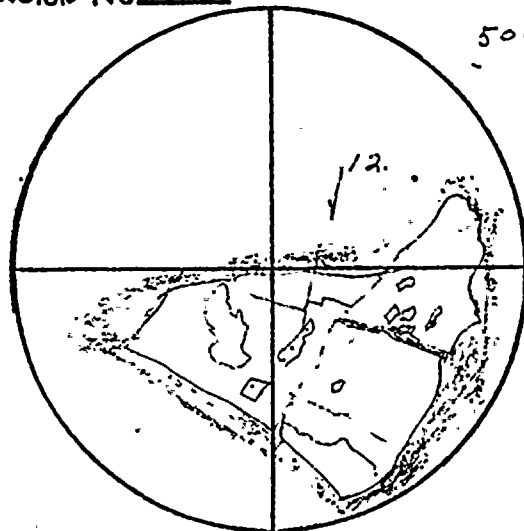
SAMPLE NO. GA3-7A

CHIP NO. G

MINERAL: Calcite

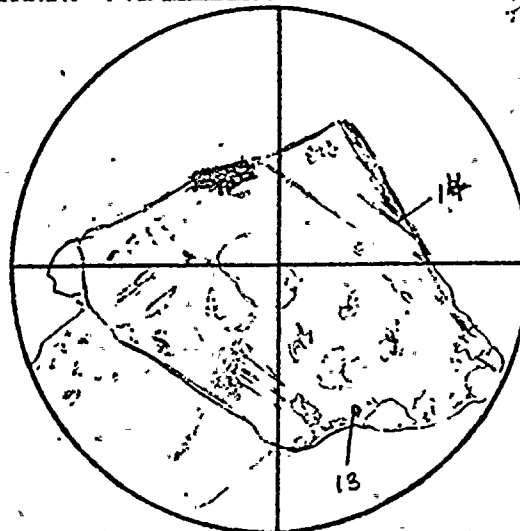
Inclusion No. 12

500X



12) 123°

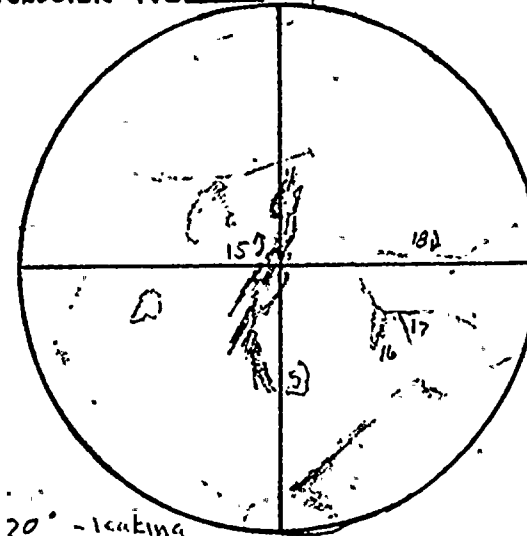
Inclusion No. 13, 14



13) 68.5°
14) 116°

Inclusions not visible but leakage in marked areas was recorded

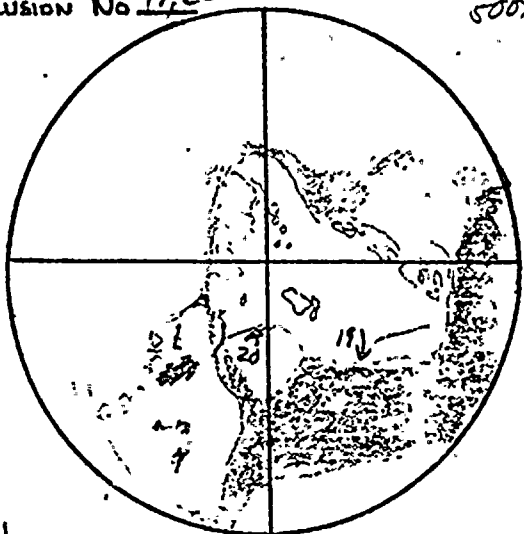
Inclusion No. 15, 16, 17, 18



15) 20° - leaking
16) 77°
17) 83°
18) 101° } wetting of fractures seen

Inclusion No. 19, 20

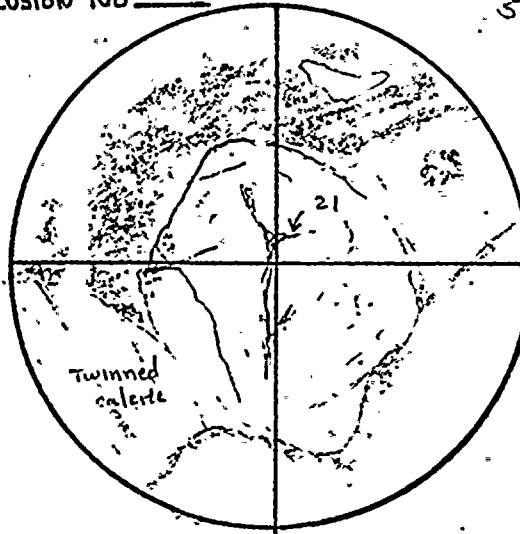
500X



19) 97°
20) 143° } leakage along fractures on grain boundaries

Inclusion No. 21

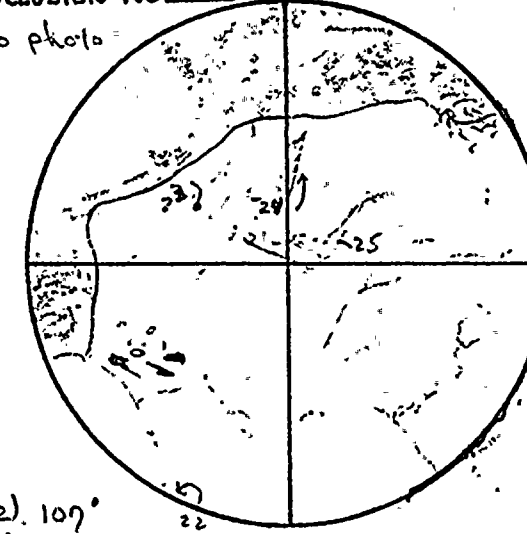
500X



21) 130° more flow at 145°

Inclusion No. 22, 23, 24, 25

No photo



22) 107°
23) 115°
24) 121°
25) 126°



ANALYST: RCA, JBM

SAMPLE NO. GA3-72

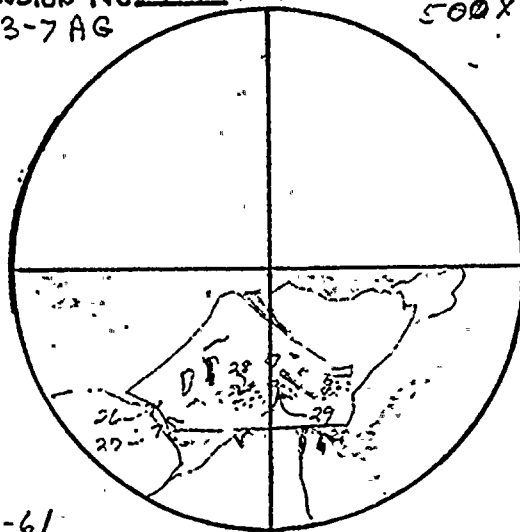
FLUID INCLUSION SKETCHES

CHIP NO. G, J

MINERAL: Calcite

Inclusion No. 26, 27, 28, 29
GA3-7A J

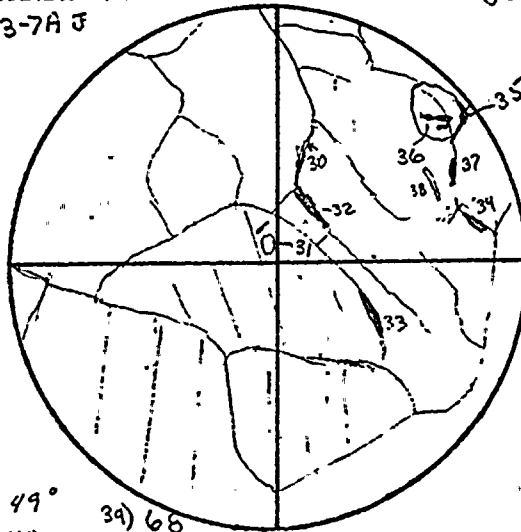
500X



26-61
27-67
28-145
29-154

Inclusion No. 30-39
GA3-7A J

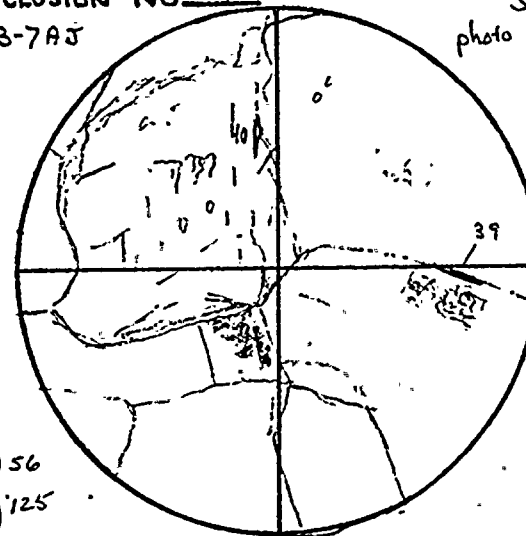
500X



30) 49°
31) 40
32) 43
33) 63
34) 66
35) 122
36) 125
37) 131
38) 145

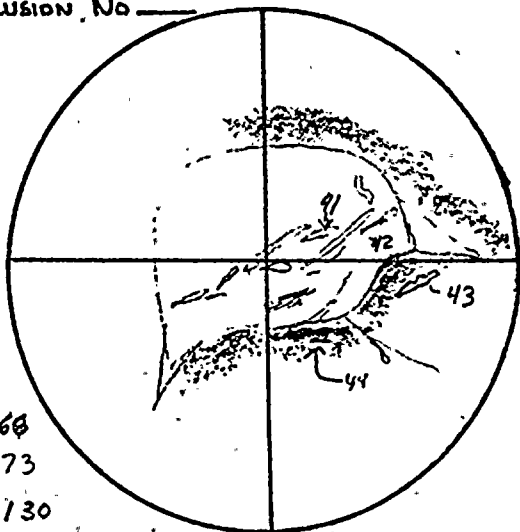
Inclusion No. 39, 40
GA3-7A J

500X
photo 163X



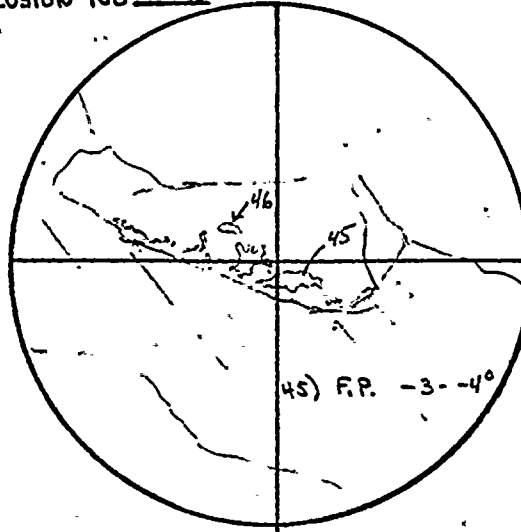
39) 56
40) 125

Inclusion No. _____



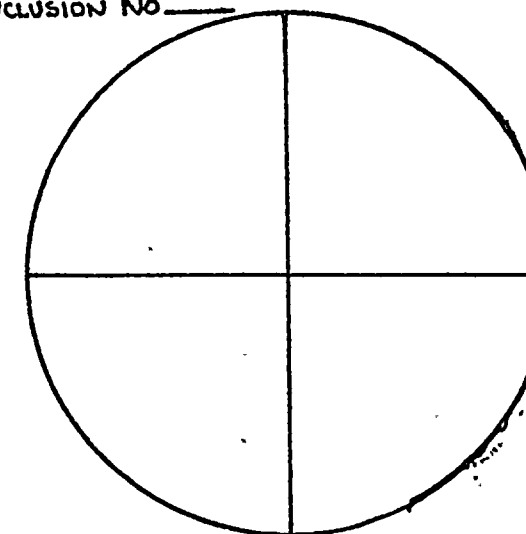
41) 60
42) 73
43) 130
44) 168

Inclusion No. _____



45) 15° - leaked after freezing
46) 19° - " " "

Inclusion No. _____





Type I
Calcite

Photo 2-3
Sample GA3-16 (A)
Type I calcite and quartz
fragments
Reflected light, crossed nicols
Field of View = $450 \times 300 \mu\text{m}$

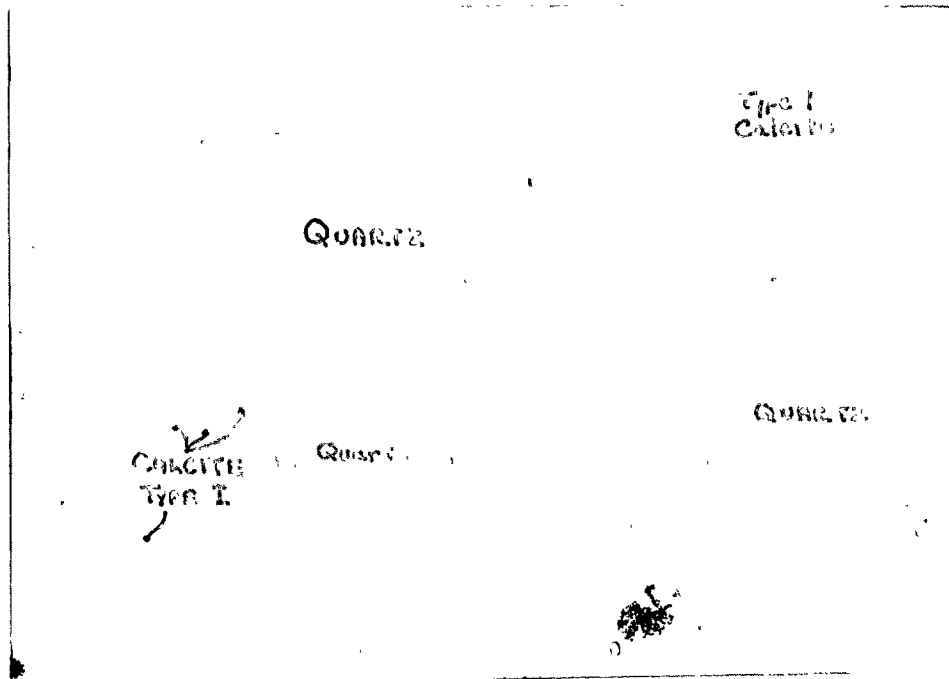


Photo 2-4
Sample GA3-12 (C)
Brecciated pyrite (py) and
sphalerite (sl) in marcasite
(mc). Reflected light.
Field of View = $460 \times 310 \mu\text{m}$

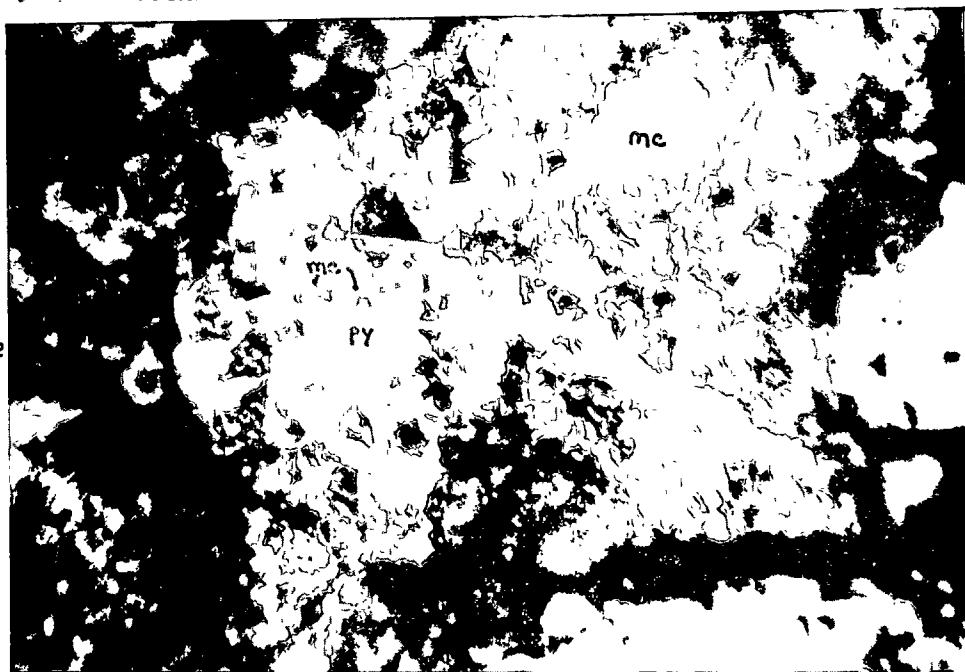


Photo 2-6
Sample GA3-12 (A)
Fractured marcasite
(Arrows indicate fractured
zones). Reflected light.
Field of View = $460 \times 310 \mu\text{m}$

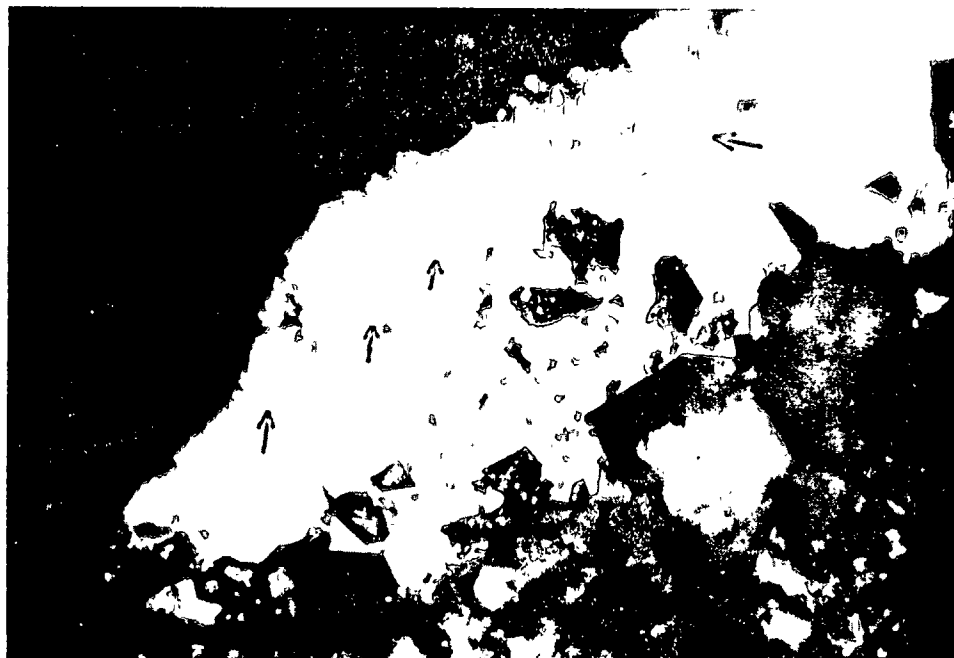




Photo 2-9
 Sample GA3-16(D)
 Type 1 calcite with quartz
 fragments (Q)
 Field of View = $275 \times 180 \mu\text{m}$

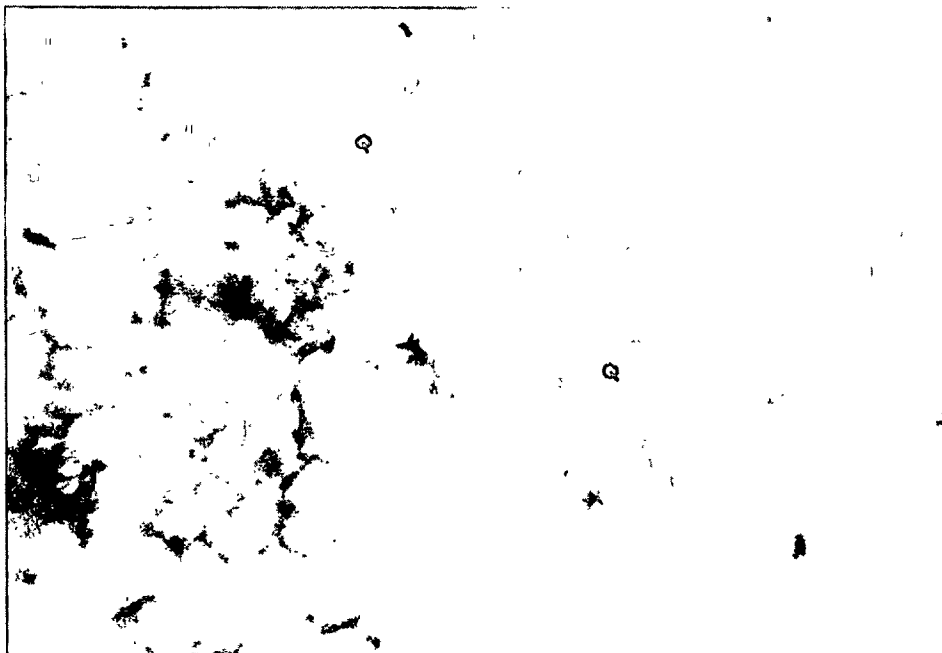


Photo 2-12
 Sample GA3-1 (D)
 Pseudosecondary single
 phase fluid inclusion in
 Type 3 calcite
 Field of View = $240 \times 160 \mu\text{m}$

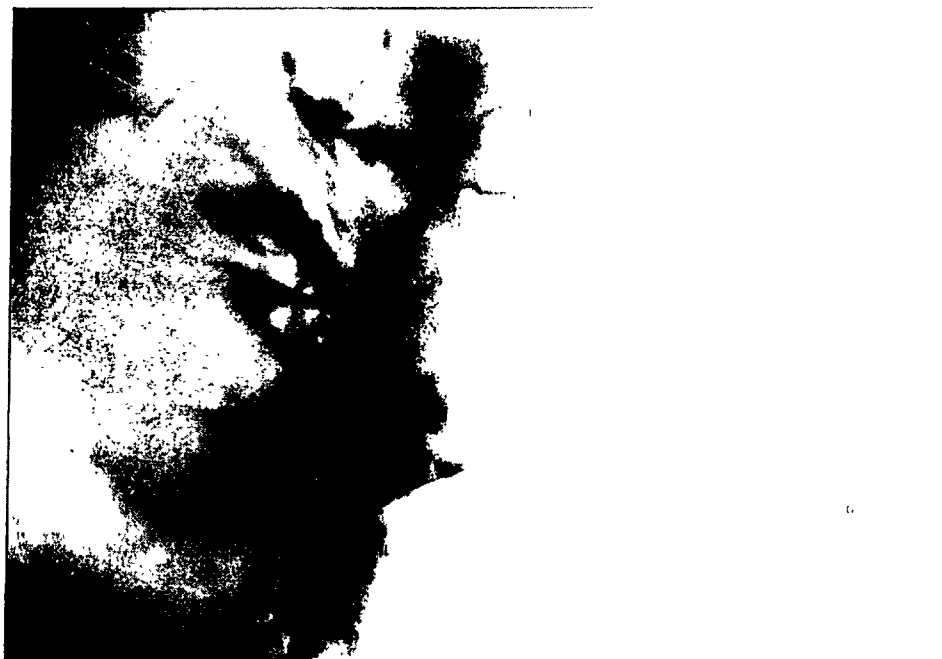


Photo 2-18
 GA3-16 (E)
 Type 3 calcite lining
 fracture-like opening in
 breccia. Crossed nicols.
 Field of View = $1.5 \times 1.0 \text{ mm}$

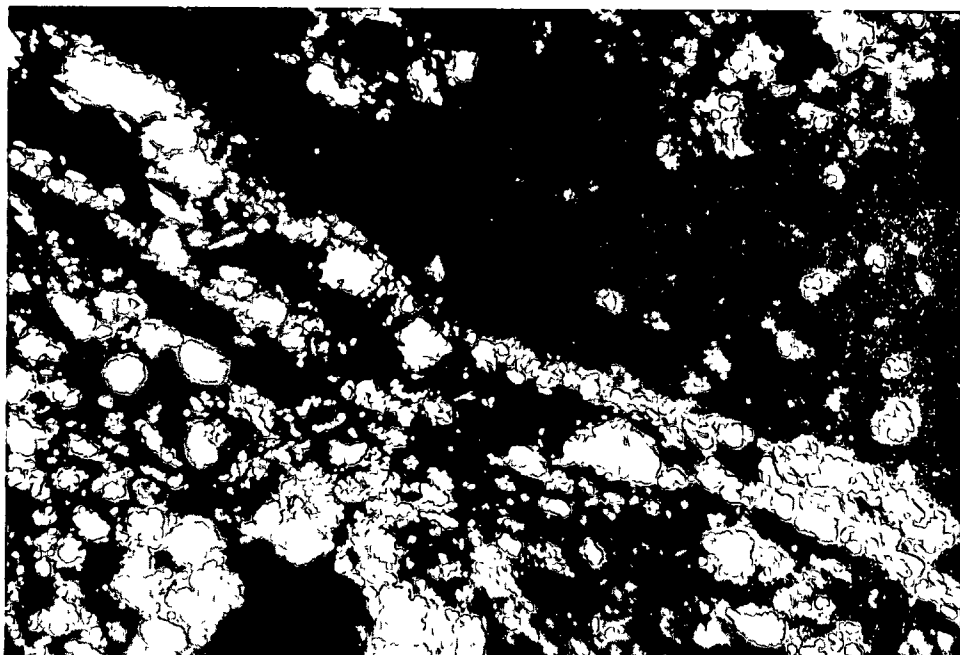


Photo 2-19
 Sample GA3-16 (E)
 Type 3 calcite lining opening
 in breccia
 Field of View 1.5 x 1.0mm

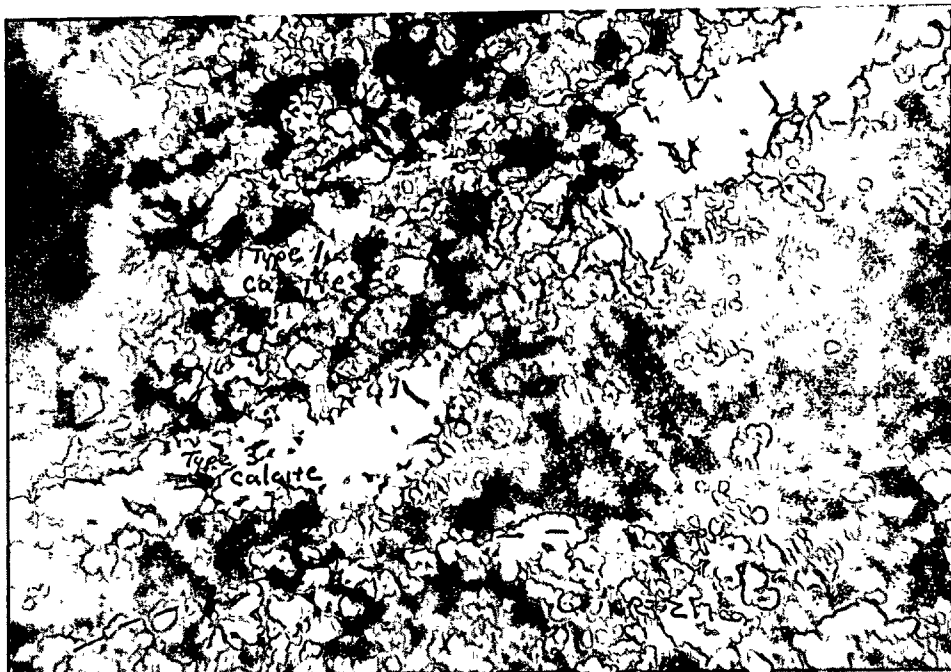
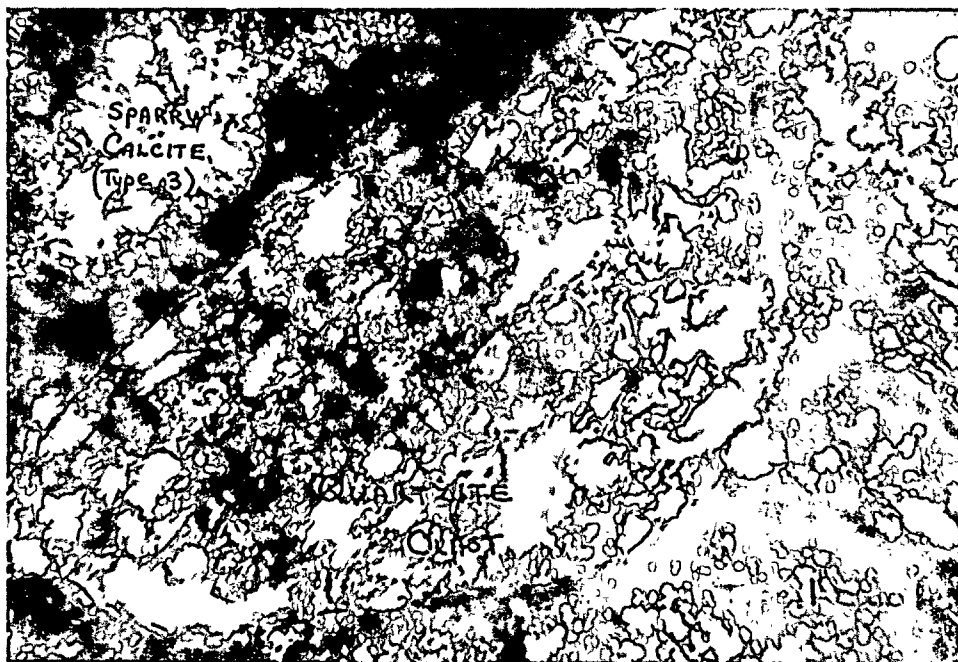


Photo 2-20
 Sample GA3-16 (E)
 Quartzite clast and void
 filled with Type 3 calcite
 in Type 1 calcite
 Field of View 1.5 x 1.0mm



Fluid Inclusion Analyses

for

Dames and Moore, Inc.

Samples from Nine Mile Point Nuclear Station,
Unit 2, North Radwaste Trench
Job No. 04707-022-19, W.I. 7070
Samples GA4-1A and 1B



H. L. Barnes
Consulting Geochemist
October 29, 1979



Discussion of Results

These two samples were examined to determine the textures and the inclusion filling temperatures of the calcite grains coating surfaces within fractures. These characteristics were also compared with those of the GA-3 series of samples for possible identity with one of the types found in this series.

The calcites forming the matrix of the breccia patches of sample GA4-1B are highly deformed and free of inclusions. Their characteristics appear to be identical to those of Type 1 calcites of the GA-3 series.

A slickensided white calcite was found on the surfaces of portions of both samples GA4-1A and GA4-1B. This calcite occurs on the topographic high areas along the fractures where contact between the walls caused abrasion and cataclastic textures. Because these calcites are closely related to the Type 1 calcites found in the shadow zones between the areas of contact along the fractures, this new type of calcite has been classified as Type 1 a. Both types probably represent the same periods of fracturing, crystal growth, and repeated fracturing.



Descriptions of Samples

Two samples, GA4-1A and B, of a fine-grained gray (Oswego) sandstone with thin coatings of slickensided or brecciated calcite were examined. Two textures of calcites were observed. One occurs on GA4-1B only and forms the matrix within patches of breccia. The second, which occurs on both samples, is a thin, white, slickensided coating of calcite. They are described in detail in this order below.

Matrix Calcites

Occurrence: These calcites occur as the matrix of the small patches of breccia found in the topographic "shadows" on the upper surface of GA4-1B. Examples are shown in Photos 3, 4, 5, and 6.

Deformation and Texture: Type 1 calcite is intensely deformed as shown in the photographs. The average grain diameter of the calcite clasts is about 15 μm whereas the sandstone clasts in the breccia may range from 90 μm (single quartz grains) to several millimeters. This breccia is poorly consolidated and friable.

Associations: The Type 1 calcite in GA4-1B is associated only with the sandstone clasts.

Inclusions: No fluid inclusions were found in these calcites. The deformation could have destroyed any inclusions that might have

been present initially and the small grain size precludes the preservation of any intact inclusions.

In all major aspects, the calcites of the breccia on sample GA4-1B are apparently identical to those of the GA3 series of samples that have been classified as "Type 1".

Slickensided Calcites

Occurrence: These calcites occur as thin, white, slickensided coatings on the surfaces of both GA4-1A and B as illustrated in Photos 1, 2, 7, and 8.

Deformation and Texture: The calcite samples are macroscopically slickensided and show a cataclastic texture in thin section (Photos 9, 10, 11, and 12). The average grain size is 5 to 10 μm , about half that of the matrix calcites. Deformation has been intense, but has not separated these calcite grains from the surface of the host rock.

Associations: A few small ($< 5 \mu\text{m}$) crystals of pyrite occur in this calcite (Photos 13 and 14). Some of the crystals are euhedral (such as the octahedra in the photos) while others are spherical to subspherical grains without any visible internal structure. The latter appear to be rounded single crystals rather than framboids and may have been dislodged and abraded grains from the host rock. A few grains of quartz can also be found intermixed with the calcite.

Inclusions: No fluid inclusions were found in this calcite due to its intense deformation.



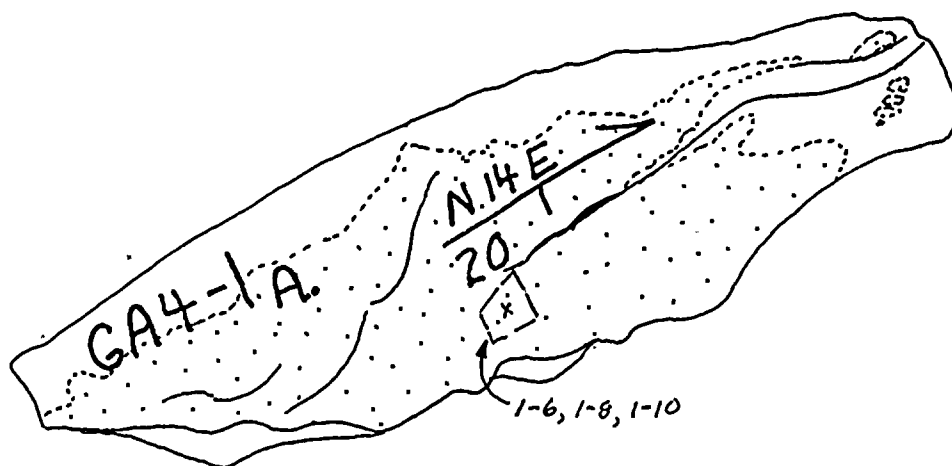
These calcites are classified as Type 1A because they occupy the contacting surfaces of the same fractures within which Type I calcites are found in the shadow zones.



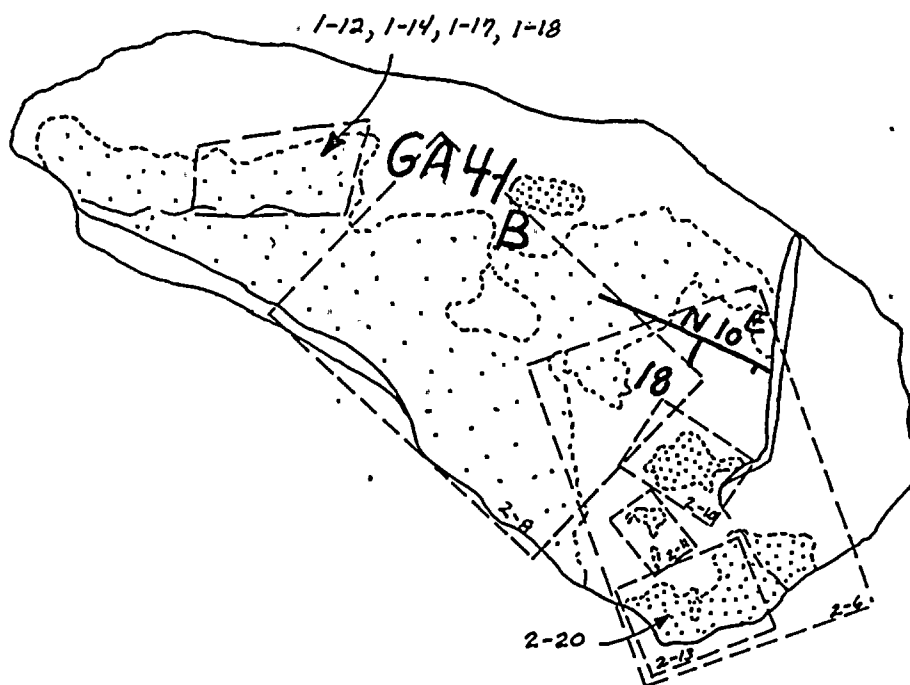
Photographs and Diagrams of Hand Samples

The photographs are numbered consecutively with the number of the film roll and the picture number on that roll being shown in parentheses. The megascopic characteristics of the samples are shown by photos numbered 1 through 5 and the photomicrographs are numbered 6 through 14. The locations of the photomicrographs are shown on the following two diagrams.





Sample GA4-1A. Sketch showing location of photomicrographs 1-6, -8, and -10. Light stippled area is Type Ia calcite. Compare with Photo 2-0.



Sample GA4-1B. Sketch showing locations of photographs and photomicrographs. Light stippled area is Type Ia calcite and heavy stippled area is Type I calcite. Compare with Photo 2-3

100

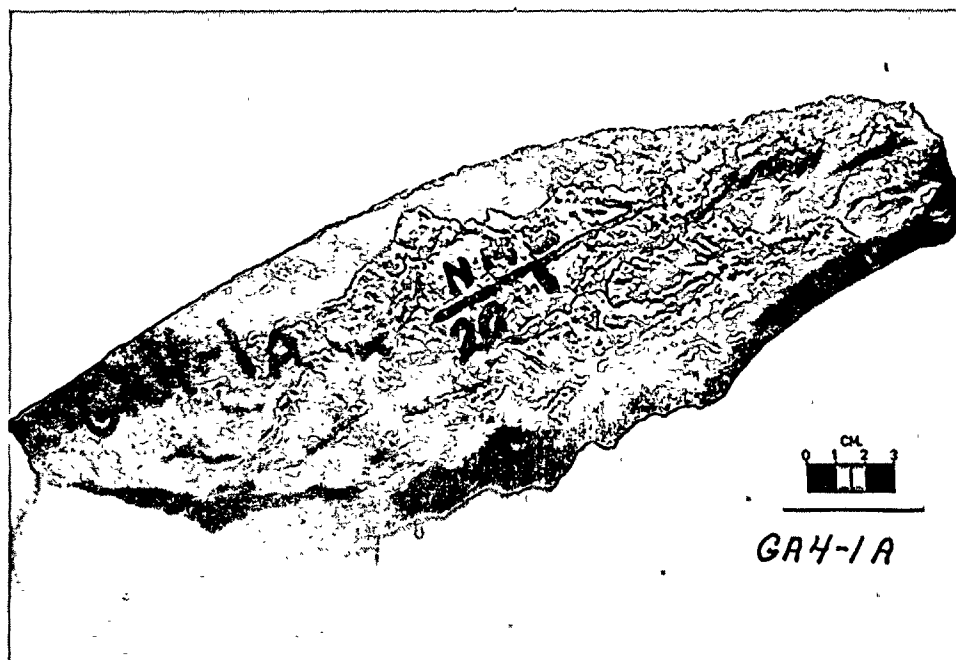


Photo 1 (2-0): Sample GA4-1A. All of the light-colored calcite on this sample is Type 1A.

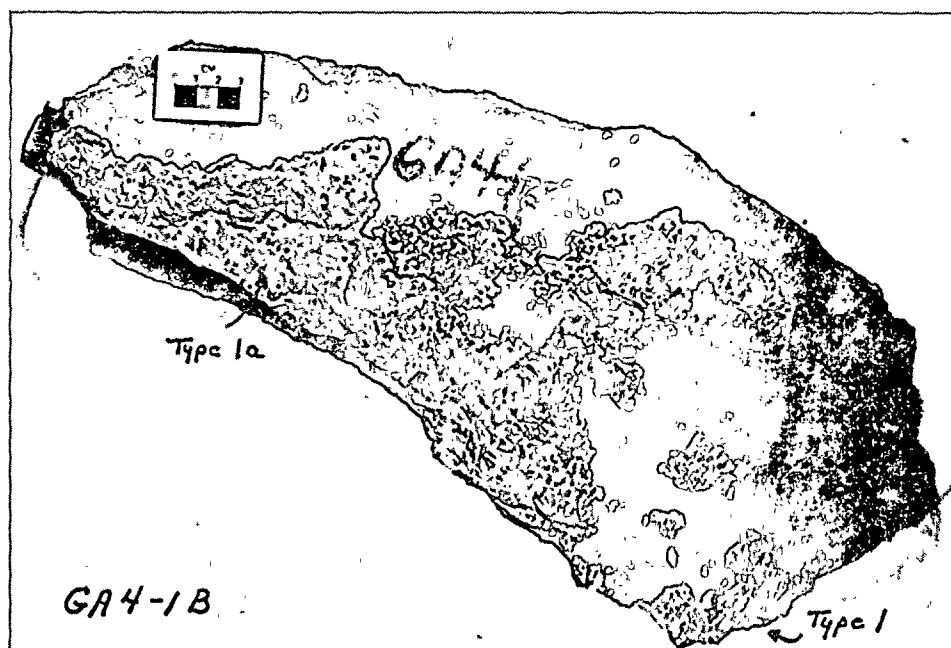


Photo 2 (2-3): Sample GA4-1B. Both Types 1 and 1A calcite are visible.

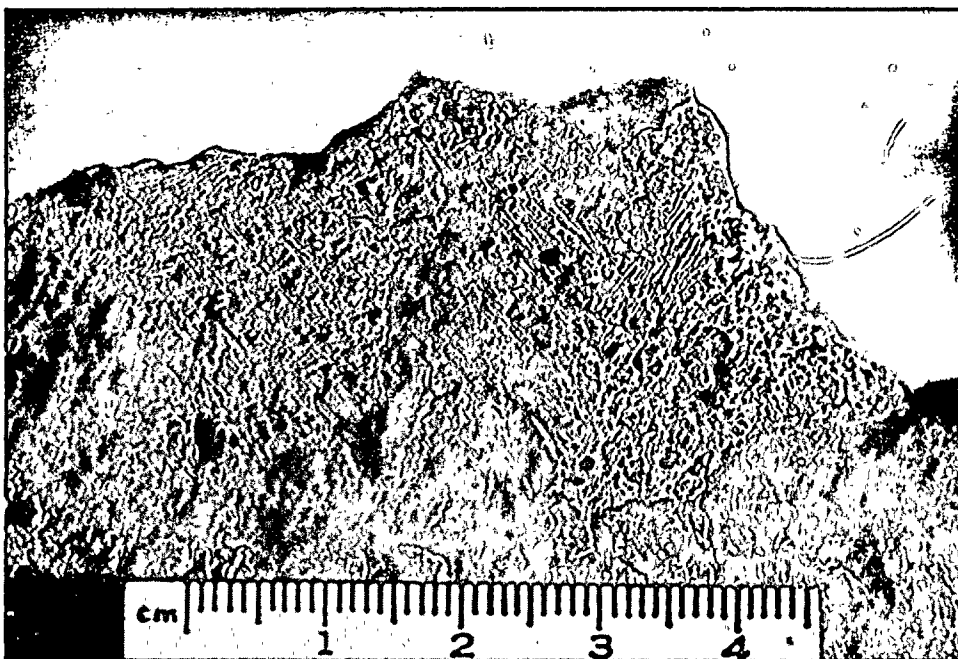
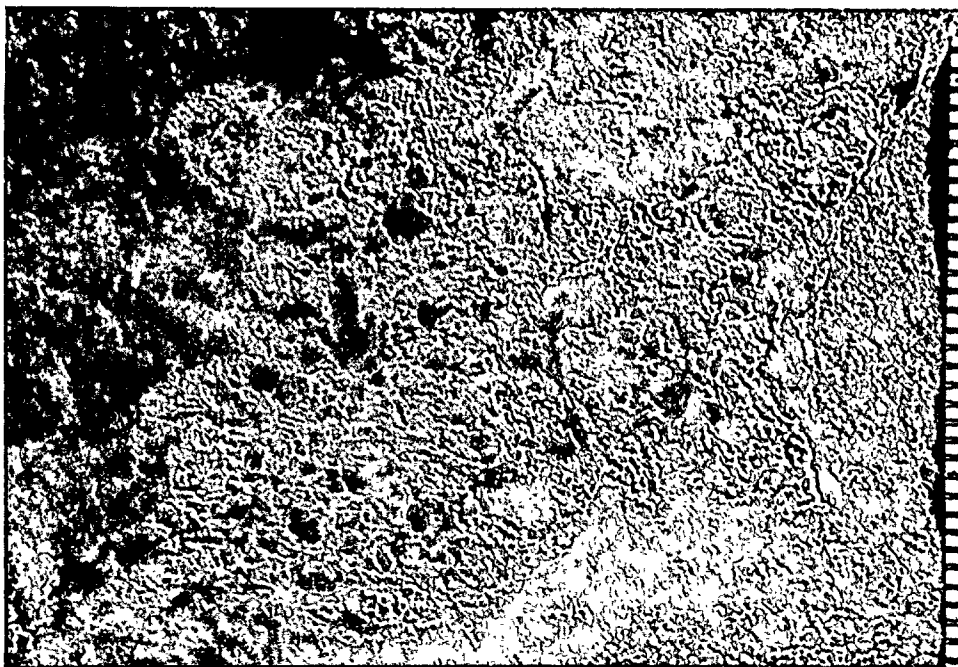
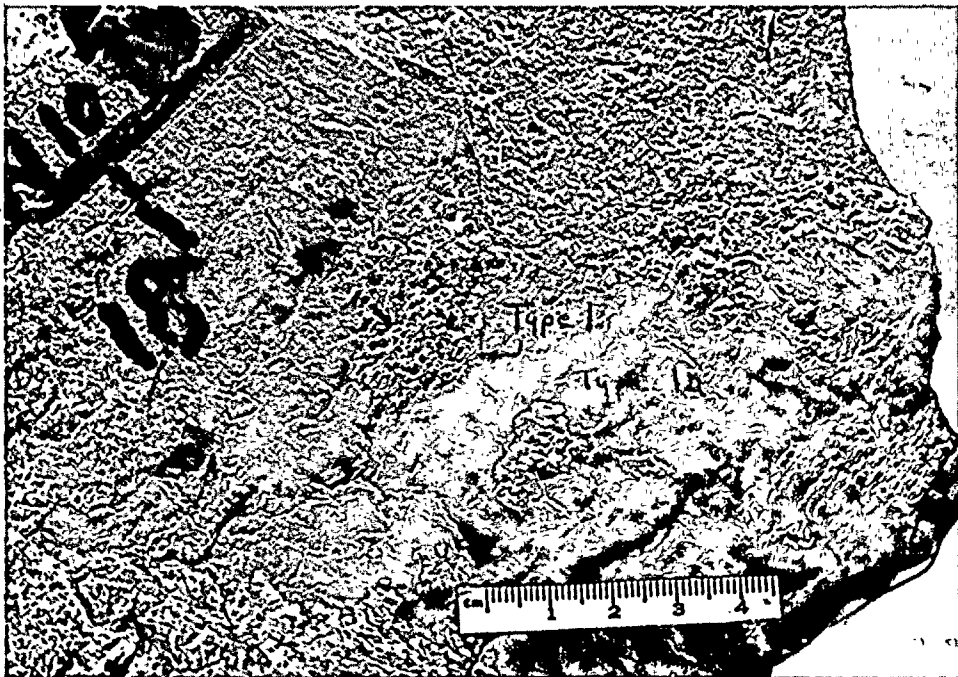


Photo 3 (2-6): Sample GA4-1B. A close-up showing breccia patches adhering to the down-slip side of raised surface features and slickensided calcite (Type 1A) on the up-slip side of the surface.

Photo 4 (2-10): Sample GA4-1B. A close-up of Type 1 calcite breccia patch from the center of Photo 2-6.

Photo 5 (2-13): Sample GA4-1B. A close-up of Type 1 calcite breccia at right side of Photo 2-6. The fine striations are probably due to small-scale movements of rock chips against the friable breccia during movement along the fracture surface.







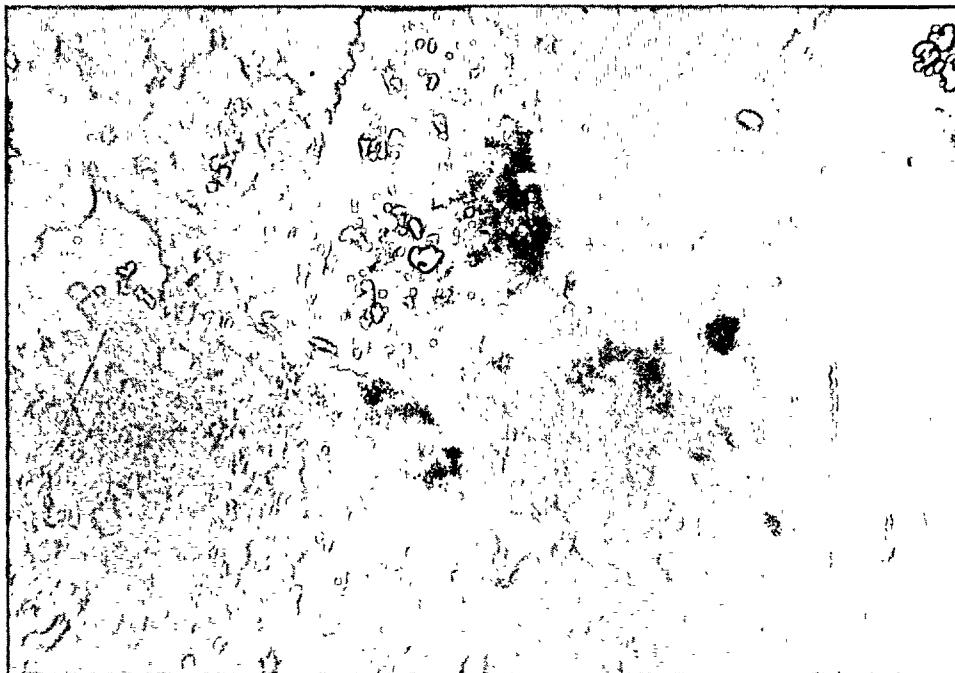


Photo 6 (1-20): Sample GA4-1B. A low magnification, incident light photomicrograph of Type 1 calcite from the breccia patch shown in Photo 5. The dark fragments are sandstone chips, the gray matrix is Type 1 calcite, and the white patches in the sandstone are small polished surfaces. The sample as a whole could not be polished. The field of view is 1.56 mm x 1.05 m.



Photo 7 (2-8): Sample GA4-1B. Slickensided Type 1A calcite. Note striations running from upper left to lower right.

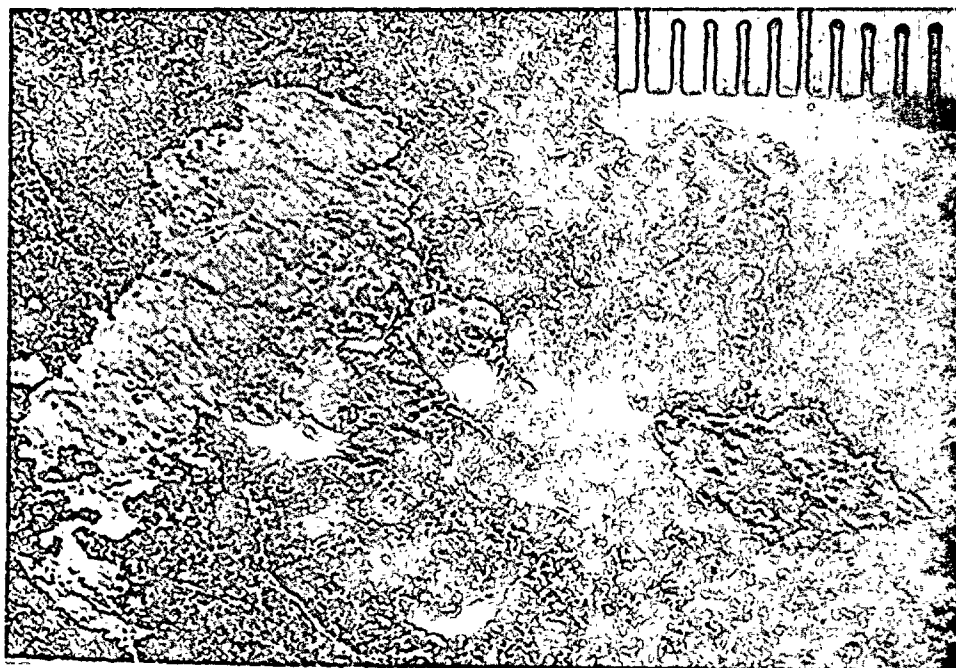


Photo 8 (2-11): Sample GA4-1B. A close-up of Type 1A calcite from the lower right center of Photo 3 (2-6). 1 division = 1 mm on scale.



Photo 9 (1-6): Sample GA4-1A. The typical texture of Type 1A calcite. Black objects to left of center are pyrite crystals. Circles in the lower left quarter are bubbles in the immersion oil. Field of view: 270 μm x 180 μm ; transmitted light, oil immersion.

Photo 10 (1-16): Sample GA4-1A. The boundary between sandstone and Type 1A calcite boundary. Compare with Photo 12 (1-14) for the same texture in sample GA4-1B. Field of view: 270 μm x 180 μm ; transmitted light, oil immersion.

Photo 11 (1-12): Sample GA4-1B. The typical texture of Type 1A calcite. Field of view: 270 μm x 180 μm ; transmitted light, oil immersion.

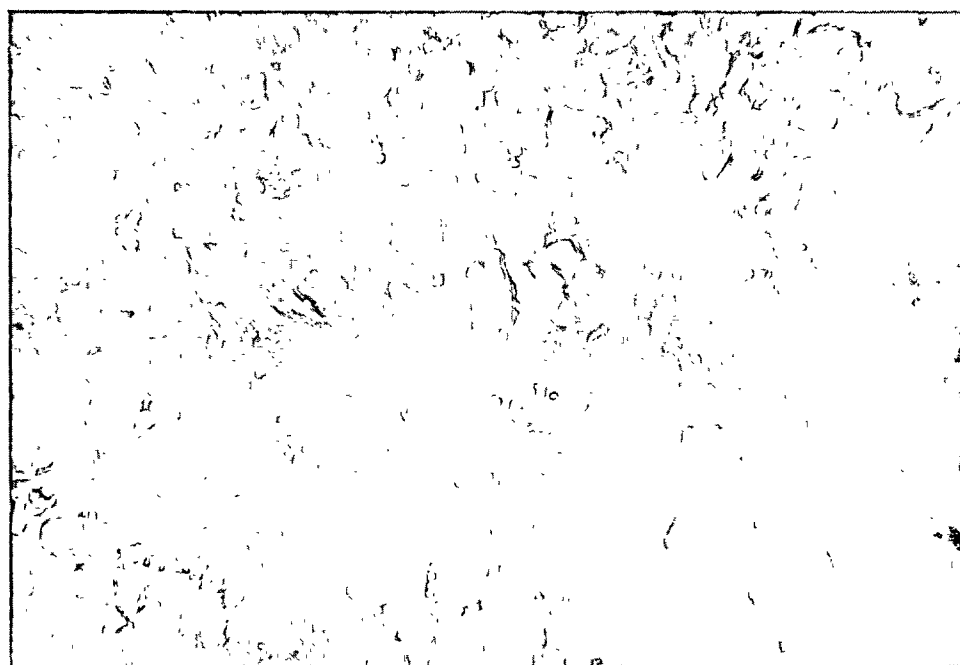
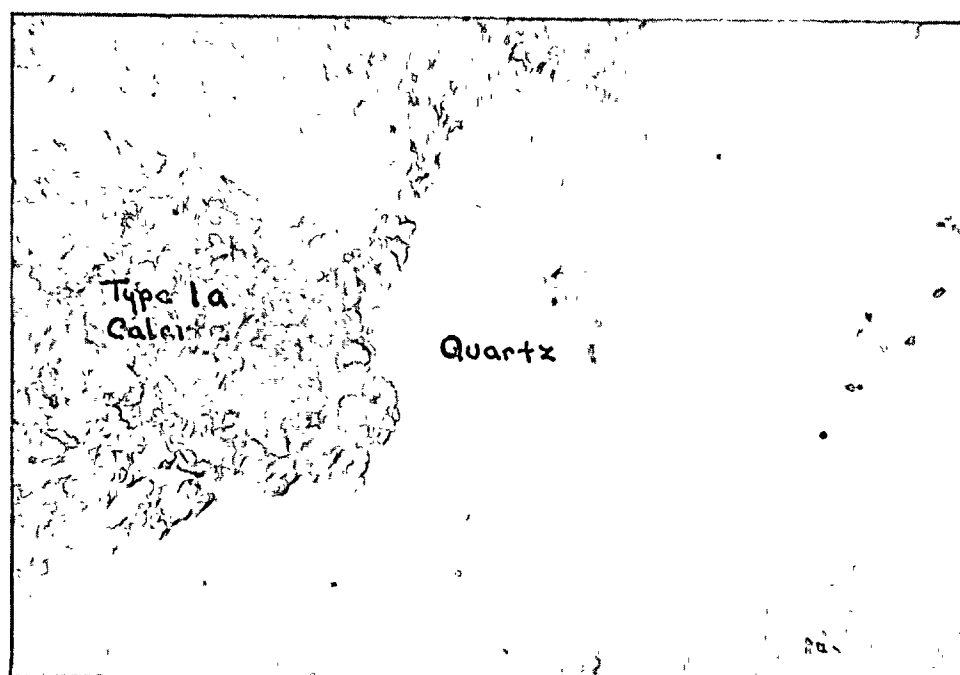
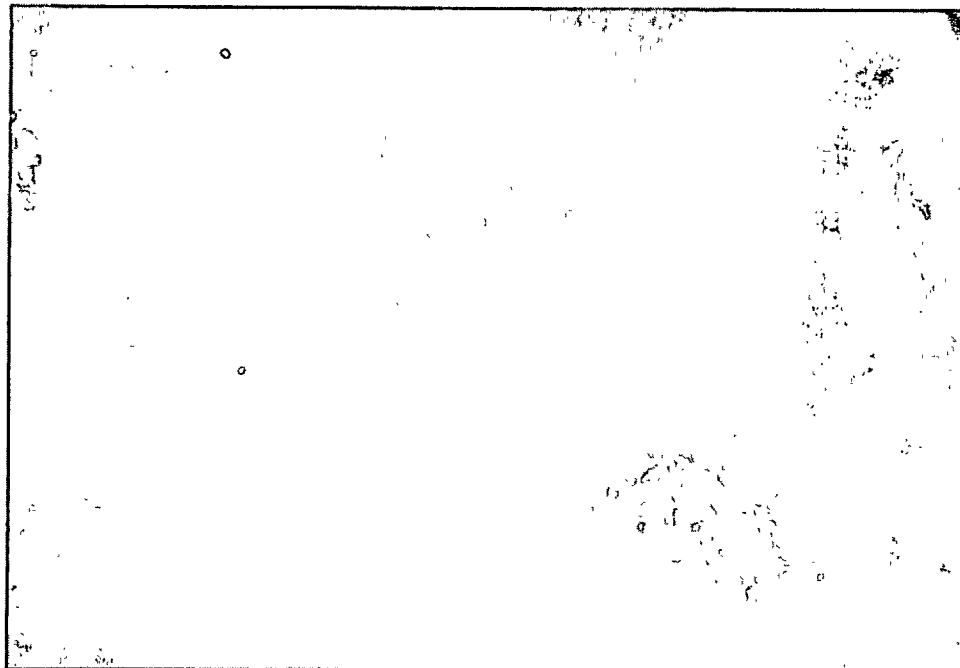


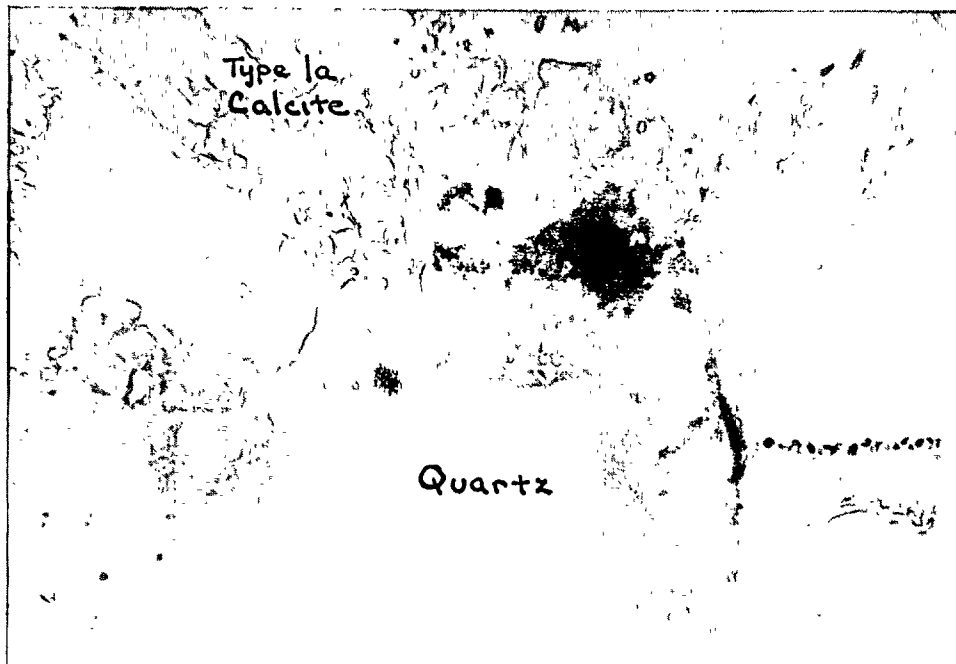


Photo 12 (1-14): Sample GA4-1B. The boundary between sandstone and Type 1A calcites. Compare with Photo 10 (1-16) of the same texture on sample GA4-1A. Field of view: 270 μm x 180 μm ; transmitted light, oil immersion.

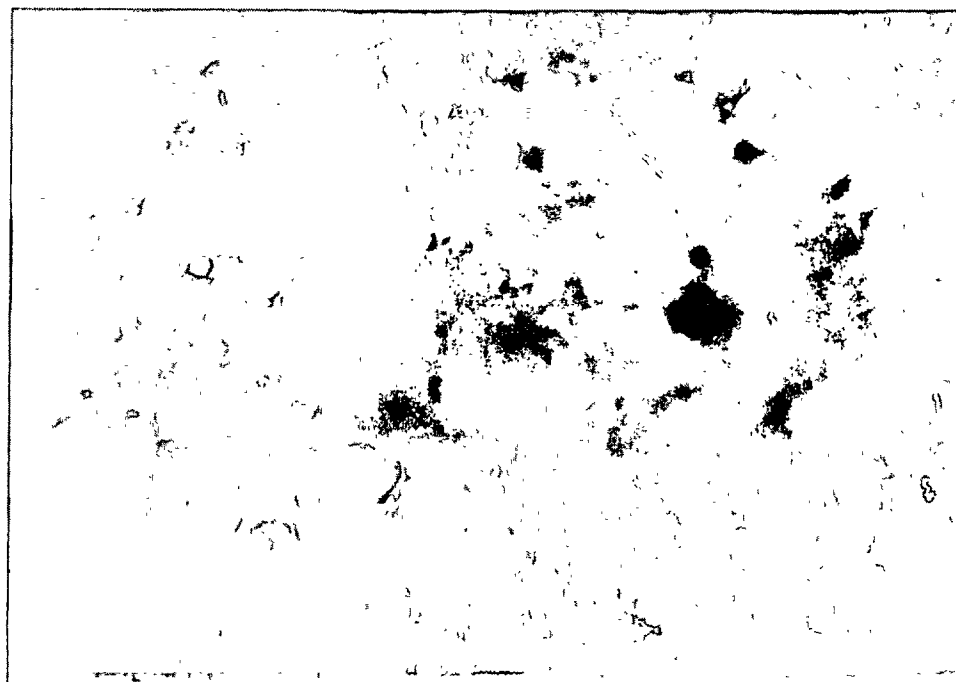
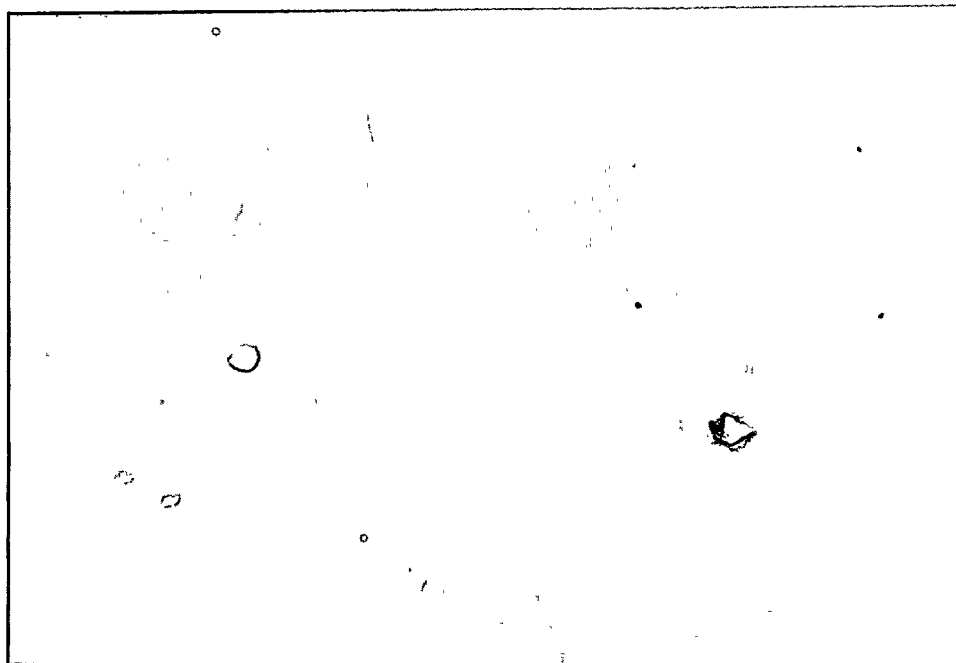
Photo 13 (1-17): Sample GA4-1B. Subspherical and octahedral pyrite crystals in Type 1A calcite. Field of view: 270 μm x 180 μm ; reflected light, oil immersion.

Photo 14 (1-18): Sample GA4-1B. The same view as Photo 13 (1-17) but with transmitted light.





15





Fluid Inclusion and Compositional Analyses

for

Dames and Moore, Inc.

Samples from Nine Mile Point Nuclear Station,
North Radwaste Trench
Job No. 04707-022-19, W.I. 7070
Samples GA4-2 to GA4-9, GA4-11, GA4-BH,
GA4-S8-A, and GA4-X



H. L. Barnes
Consulting Geochemist
December 14, 1979

Discussion of Results

The carbonates deposited in the fractures represented by this series of samples fall into three categories based on their sequence of deposition. The first of these is the oldest and includes brecciated and slickensided Type 1 calcite identical to that of the GA-3 series plus various travertine nodules and dripstones. The second category contains a variety of sparry calcites similar to Type 3 of the GA-3 series, and the youngest, third category is represented only by a brown calcite.

The type 1 breccia and the travertine deposits are paragenetically related by directly underlying the other calcites. This textural position implies that these two calcites may well be contemporaneous although they are apparently never contiguous. They are not found together because their modes of occurrence are different. Type 1 calcite infills fractures in the host rock and was deposited below the water table, whereas the travertine, if typical in origin, was a superficial deposit from ground waters on, or near, the surface. Both the Type 1 calcites and the travertine are deformed but Type 1 is more severely crushed as expected for the more susceptible vein fillings. The severe deformation of Type 1 has obliterated any additional textural evidence that might have served to paragenetically link Type 1 with the travertine deposits.

The sparry, Type 3 calcite is found in a variety of habits ranging from small, stubby crystals 50 μ m in diameter to large, radiating crystals more than 1 mm in length. Type 3 calcite occurs in fractures and openings in the breccias and travertine, showing it



to be younger than the deformation of Type 1, D_5 of the paragenesis. Some of the Type 3 calcite has been mildly fractured in a younger deformation, D_6 , as shown by some healed fractures in the Type 3 calcite of sample GA4-2 and by broken chips of platy Type 3 calcite in sample GA4-7.

The youngest mineral, the brown calcite lies on top of Type 3, sparry calcite. It is only irregularly present being both discontinuous and of variable thickness. This brown calcite is undeformed and coats and cements broken chips of the platy Type 3 calcite. Consequently, it has been placed after D_6 in the paragenetic sequence.

The calcite veins of sample GA4-S8-A could not be reliably correlated with the paragenetic sequence of the other samples. This sample was associated with breccias and its calcites were deformed; therefore, they appear to be older than D_5 in the paragenetic sequence.

Only indirect evidence of deposition temperatures was found in these samples. Fluid inclusions were absent in both Type 1 calcite and the travertine. Nevertheless, the fine grain size of the travertine implies a low temperature because calcite is easily recrystallized even at temperatures below 100°C . Single-phase liquid inclusions, both secondary and primary, are common in some specimens of the Type 3 sparry calcite. Again these inclusions indicate low depositional temperatures, below about 30°C . No inclusions were observed in the brown calcite.

In the paragenetic sequence of Figure 1, shown are depositional stages for minor silty calcite and pyrite as well as for the dominant calcite types all with respect to the more severe stage of deformation,

1. The first part of the document is a list of the names of the persons who were present at the meeting.

2. The second part of the document is a list of the names of the persons who were absent from the meeting.

3. The third part of the document is a list of the names of the persons who were present at the meeting.

4. The fourth part of the document is a list of the names of the persons who were absent from the meeting.

5. The fifth part of the document is a list of the names of the persons who were present at the meeting.

6. The sixth part of the document is a list of the names of the persons who were absent from the meeting.

7. The seventh part of the document is a list of the names of the persons who were present at the meeting.

8. The eighth part of the document is a list of the names of the persons who were absent from the meeting.

9. The ninth part of the document is a list of the names of the persons who were present at the meeting.

10. The tenth part of the document is a list of the names of the persons who were absent from the meeting.

PARAGENETIC RELATIONSHIPS

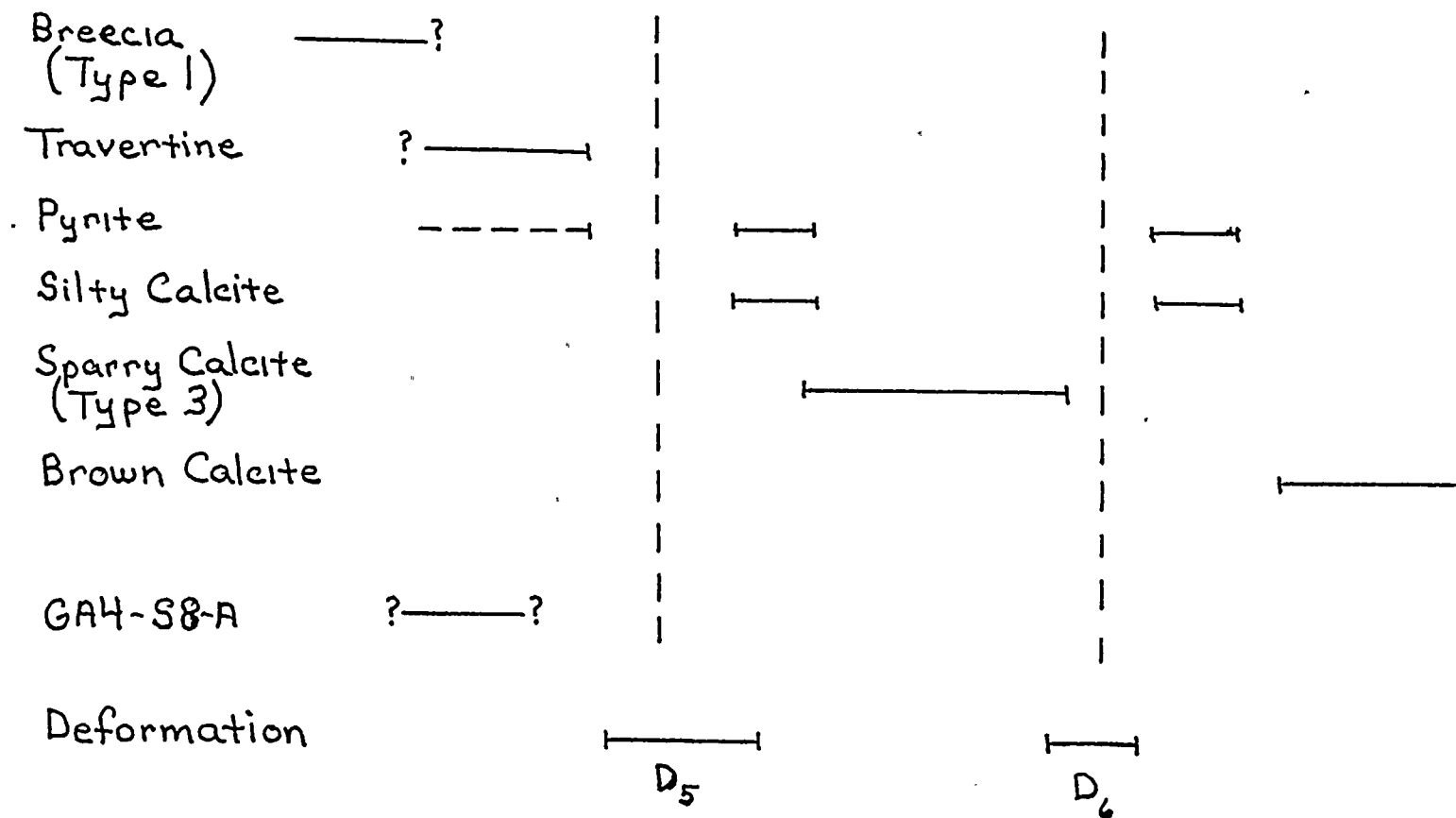


Figure 1



D₅, and the mild deformation, D₆. The two stages of silty, pyritic calcite may be the products of either in situ settling soon after each period of deformation or of transported material washed in from other areas while the fractures were still relatively open. Both stages of pyrite are very similar in that both contain fine-grained euhedral and spherical crystals as shown in Photo 26 of sample GA4-7. The parageneses of the vein filling for each sample are shown on the detailed paragenetic diagram, Figure 2. This figure provides documentation of the summary diagram, Figure 1.

Three samples were examined by X-ray powder diffraction methods to determine their mineralogical compositions as shown in Table 1. Sample GA4-X is not a natural material, but is a man-made cement composed of portlandite ($\text{Ca}(\text{OH})_2$), vaterite (CaCO_3), minor calcite (CaCO_3), and very small amounts of quartz and feldspar (probably plagioclase). Sample GA4-BH is known to be a grout and was used for comparison with GA4-X. The quartz, feldspar, and pyroxene are present in GA4-BH as sand-sized clasts bound by a portlandite, vaterite, and calcite cement. Sample GA4-S8-A is dominantly calcite with minor amounts of quartz and clay.



Figure 2

Individual Sample Parageneses

GA4-2		<u>Sparry calcite</u>	<u>Brown Calcite</u>
		<u>Radiating Calcite</u>	<u>Pyrite</u>
			<u>D6</u>
GA4-3	? <u>Breccia</u> ?	<u>D5</u>	<u>Sparry calcite</u>
GA4-4	? <u>Travertine</u>	<u>Sparry Calcite</u>	
	<u>Pyrite</u>	<u>D5</u>	
GA4-5	? <u>Travertine fragments</u> <u>matrix</u>	<u>Sparry Calcite</u>	
	<u>Pyrite</u>	<u>D5</u>	
GA4-6	<u>Breccia</u> ?	<u>Sparry Calcite</u>	
GA4-7	? <u>Travertine light gray</u> <u>dark gray</u>	<u>Silty Calcite</u>	<u>Silty Calcite</u>
	<u>Pyrite</u>	<u>Pyrite</u>	<u>Brown Calcite</u>
	<u>D5</u>	<u>Columnar Sparry Calcite</u>	<u>D6</u>
GA4-8	<u>Breccia</u> ?	<u>D5</u>	
	<u>Pyrite</u>		
GA4-9	<u>Breccia</u> ?	<u>D5</u>	
GA4-11	? <u>Travertine</u>	<u>Silty Calcite</u>	
	<u>Pyrite</u>	<u>Pyrite</u>	<u>Columnar Sparry Calcite</u>
		<u>D5</u>	
GA4-S8-A	? <u>Fine-grained tan Calcite</u> ?	<u>D5</u>	

Time →



Table 1. X-Ray Analyses of Selected Samples

Condition ¹	Sample	Phases present ²
Untreated	GA4-BH	Quartz, calcite, pyroxene, (feldspar), (vaterite), (portlandite)
	GA4-X	Portlandite, vaterite, calcite, (quartz), (?feldspar)
	GA4-S8-A	Calcite, quartz, (clays)
Treated with HCl	GA4-BH	Quartz, pyroxene, feldspar
	GA4-X	Quartz, (?feldspar)
	GA4-S8-A	Quartz, (clays)

¹Minor phases that are insoluble in dilute HCl were concentrated for analysis by removing soluble phases with 10% HCl.

²Phases present are listed in decreasing order of abundance. Parentheses indicate very minor amounts present and a question mark indicates the possibility, but not certainty of the presence of that phase.



Characteristics of Individual Samples

Detailed descriptions are given in the following sections for each sample in numerical order from GA4-2 to GA4-9, GA4-11, and GA4-S8-A. Photographs of the entire rock samples and associated fracture-filling minerals are found in similar order (except as noted in the captions) in the last section.



GA4-2

Occurrence: Calcite mineralization occurs on a siltstone layer at the base of a breccia zone sub-parallel to the bedding (Photo 1).

Deformation and Texture: GA4-2 calcite is dominantly a sparry colorless, clear calcite with an equant texture (Photo 2). This calcite shows evidence of minor deformation in healed fractures (Photo 3) and deformation twinning (Photo 4). Twinning is uncommon, though present in only about 2% of the ^{grains} grams. Grain size ranges from 100 μ m up to 1 mm. The colorless, coarse calcite at the edges of the coating are radiating fan-shaped sheaves of calcite (Photo 5). It contains numerous air-filled secondary inclusion trains and shows wavy extinction. Pyrite is associated with the outermost calcite, whether sparry or radiating. Brown calcite occurs in contact with the sparry and radiating calcite (Photo 6). In other prepared chips, the outer portions of the sparry calcite is silty, contains streaks of extremely fine grained material and, in some spots, quartz shards and euhedral pyrite as well (Photo 7).

Associations: Anhedral pyrite with sparry calcite, radiating calcite; euhedral pyrite, quartz shards and silt with sparry calcite; others as described above.

Fluid Inclusions: Secondary inclusion trains are common, but the inclusions are gas-filled, single phase inclusions, and are not suitable for geothermometry. Primary inclusions are very common along grain boundaries. All are very irregular in shape and contain only



liquid. A bubble occupying 1% of the volume of the inclusion if present would easily be observed; one can show that a temperature decrease of less than 10°C from 25°C would cause sufficient contraction of the liquid phase to produce such a bubble. The fact that all of the inclusions contain only a single phase does not, however, indicate that the inclusions formed between 15° and 25°C (although this is possible), only that the inclusions formed at a temperature of less than 25°C.

Several other inclusions (Photo 8) were observed to contain inordinantly large bubbles. The proximity of these inclusions to fractures (or the polished surface) leads one to suspect that they have leaked.

Paragenesis

Sparry calcite ($T < 25^{\circ}\text{C}$)	_____	-----
Radiating calcite	_____	
Pyrite	_____	
Brown calcite		_____
Deformation	_____	

GA4-3C, D

Occurrence: Calcite patches on a sandstone layer at the base of a bedding plane breccia zone. Patches exhibit slickensides, and are elongated parallel to slip direction. (Photo 9)



Photo 1: Sample GA4-2. Scale
is 10 mm long.

Photo 2: GA4-2. Polished section under
oblique transmitted illumination.
The coarse core is clear, sparry
calcite. The fine grained mate-
rial at the left end is brown
calcite. The chip is approximately
7 mm long.

Photo 3: GA4-2. Secondary inclusion
train (healed fracture) in
sparry calcite. Field of
view (FOV) = $460 \times 310 \mu\text{m}$.

Photo 4: GA4-2. Twin lamellae in sparry
calcite. Reflected light. FOV =
 $580 \times 390 \mu\text{m}$.

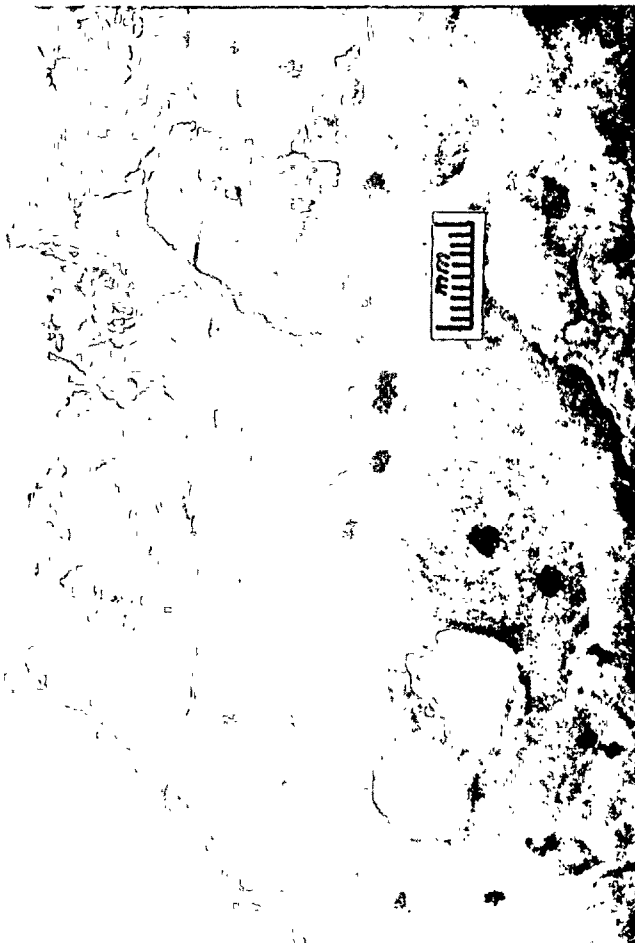




2



4



1



3

Photo 5: GA4-2. Fan-shaped calcite
with secondary inclusions.
FOV = 1.3 x 0.9 mm.

Photo 6: GA4-2. Sparry calcite/brown
calcite contact. FOV = 1.6 x
1.1 mm.

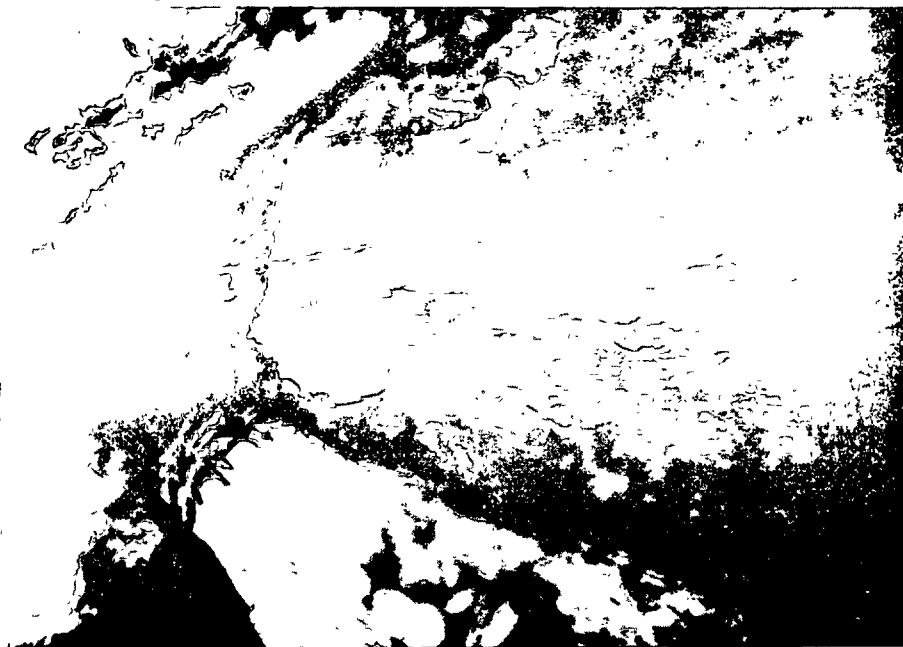
Photo 7: GA4-2. Quartz (high relief)
and pyrite (white) in sparry
calcite.

Photo 8: GA4-2. Inclusions in sparry
calcite. The secondary inclusion
trains occur at lower center and
lower right. An arrow indicates
an inclusion with a vapor bubble,
probably due to leakage.
FOV = 160 x 110 μ m.

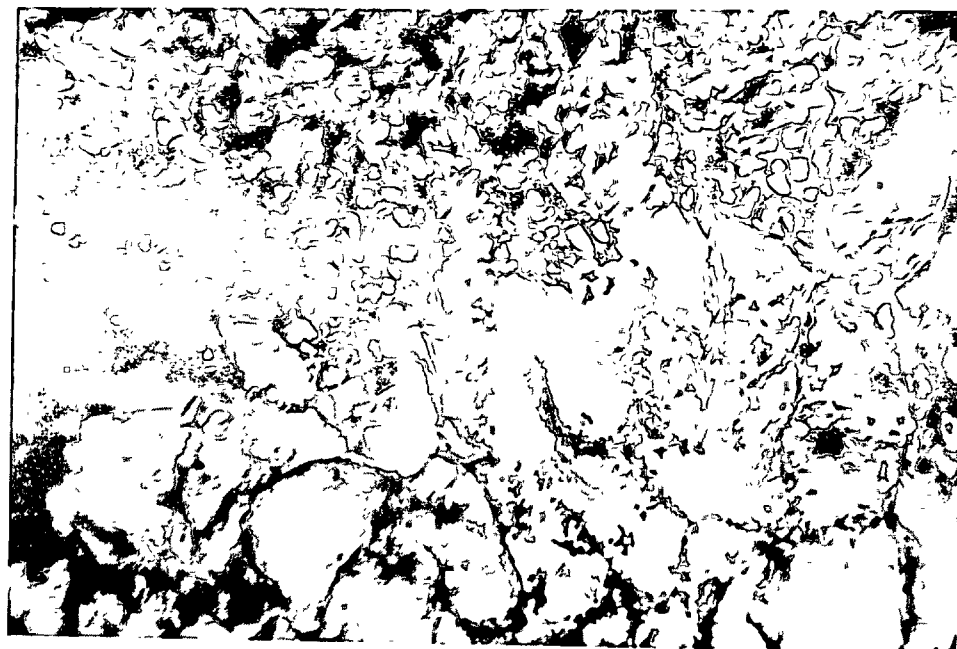


100

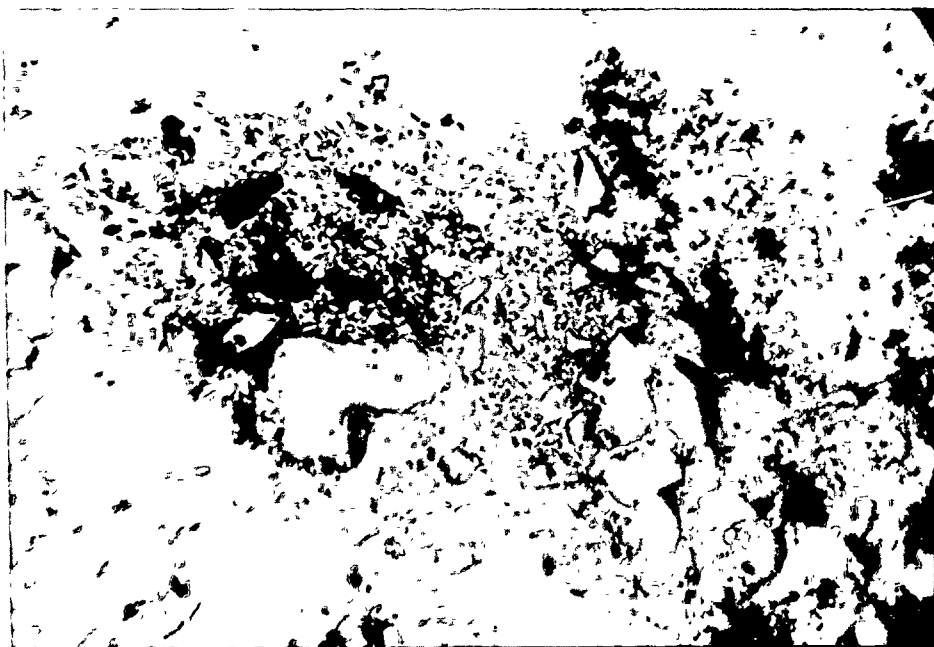




5



6



7



8

Texture and Deformation: Identical to samples GA4-3D, GA4-6 and GA4-8: fine-grained cataclastic calcite matrix (Type 1) surrounding angular grains of quartz and quartzite (Photo 10). Some healed fractures are evident as irregular, patchy networks of coarser-grained calcite (up to 150 μm) (Photo 11). The average grain-size of the matrix is 10-30 μm . The average grain-size of quartz and quartzite fragments is 30 μm and 250 μm , respectively. Minor scattered sulfides (pyrite, sphalerite) are found throughout the samples, and appear to be associated with quartz and quartzite grains.

Fluid Inclusions: None observed.

Paragenesis

Type 1 calcite

Deformation

Healed fracture calcite

Sulfides (in host)

GA4-3D

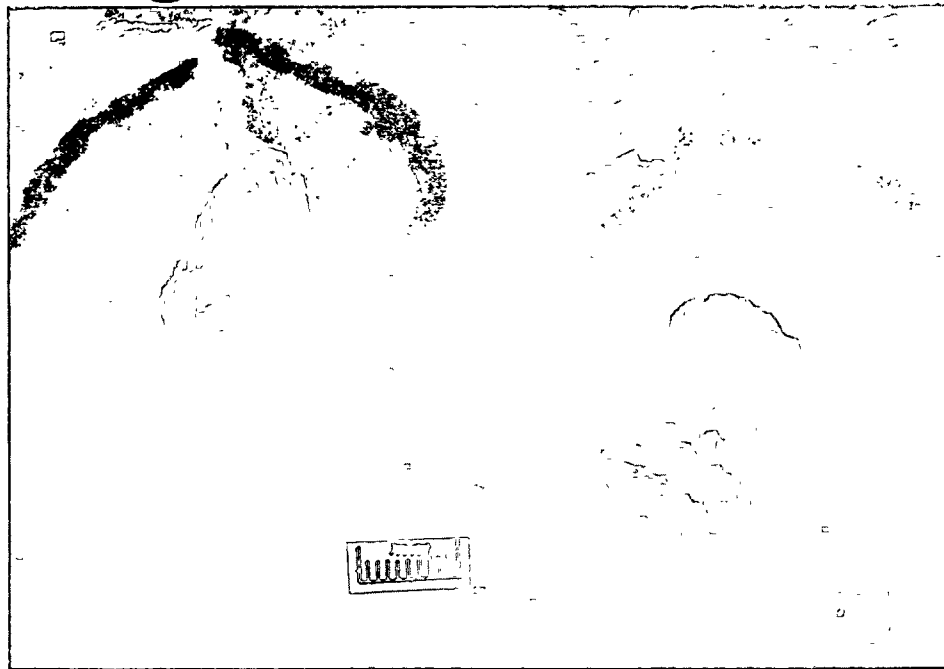
Occurrence: Microbreccia patches on sandstone. Basically, this sample is similar to GA4-6 and GA4-8. A matrix of cataclastic Type 1 calcite surrounds angular scattered quartz grains and fragments of quartzite bedrock. Minor sulfides are scattered throughout the samples.

Photo 9: GA4-3D. Isolated patches of Type 1 calcite (breccia and slickensides).

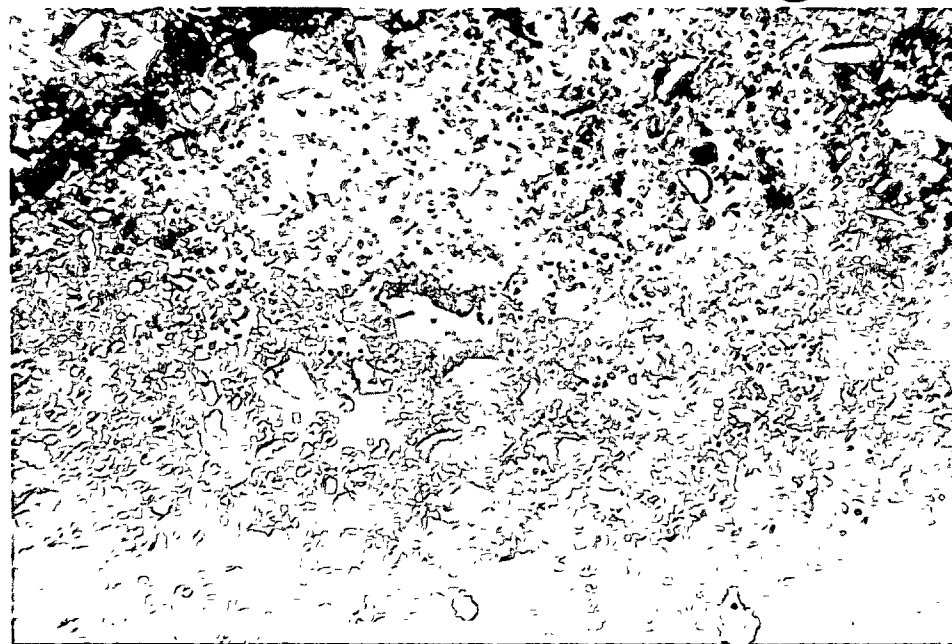
Photo 10: GA4-3C. Slickensided Type 1 calcite (fine-grained matrix) containing angular quartz shards and sandstone fragments (high relief). White grains are pyrite (subhedral) and skeletal detrital ilmenite. FOV = 1.6 x 1.1 mm in reflected light.

Photo 11: GA4-3C. Healed fractures in breccia. The calcite in the fractures is more coarsely crystalline than Type 1 and may be Type 3 calcite. FOV = 1.3 x 0.9 mm.





9



10



11



GA4-4

Occurrence: Small calcareous "concretions" on 35° east-dipping shear fracture at the base of a breccia zone.

Deformation and Texture: The deposits consist of very fine-grained (5-10 μm) argillaceous calcite containing a few quartz shards and abundant, extremely fine-grained pyrite ($< 1 \mu\text{m}$). The material is banded, in various shades of tan and gray, but the texture is fairly uniform across the bands. Some bands contain vugs lined with sparry calcite. Pyrite is concentrated along the bands.

The specimens are fractured by compression normal to the fracture surface. The fractures show as topographic features on the surface of the specimens (Photo 12) and as calcite filled cracks in thin section (Photo 13).

Associations: See above.

Fluid Inclusions: None because the grain size is too small.

Paragenesis

"Nodular" calcite _____

Pyrite _____

Sparry calcite in fractures _____

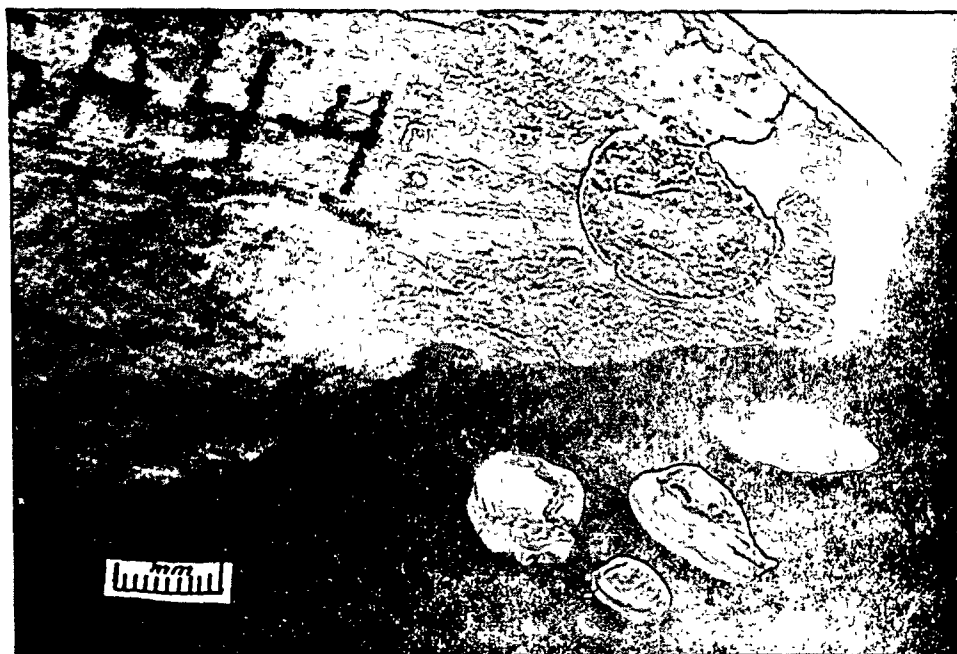
Deformation _____



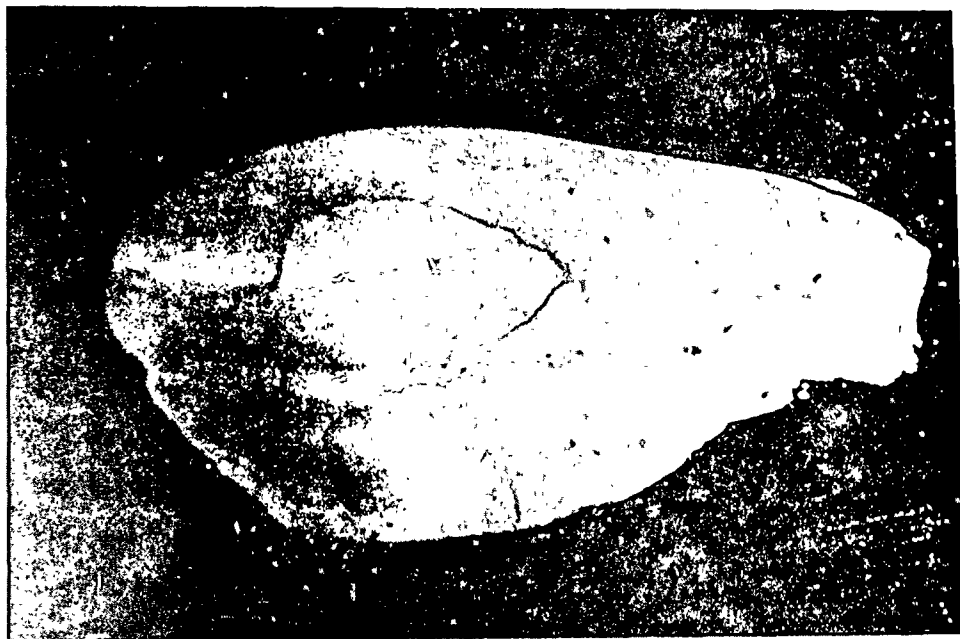
Photo 12: GA4-4. "Nodules" of argillaceous calcite. Note the surface expression of fractures in individual pieces.

Photo 13: GA4-4. A polished thin section of a "nodule," under oblique incident illumination. Note the semi-circular, sparry calcite-filled fracture and distinct banding (nonconcentric). The chip is about 15 mm long.





12



13



GA4-5

Occurrence: Sparry and microcrystalline calcite patches on fracture surfaces in the north wall of the slot (Photo 14).

Deformation and Texture: This sample is a texturally complex deposit of several types of calcite (Photo 15). The earliest calcite is very fine-grained ($< 10 \mu\text{m}$), brownish in color, and banded. It occurs as angular, well defined fragments (Photo 16) as well as poorly-defined patches (Photo 17). A second type of calcite occurs predominantly as a matrix to the earliest type. The grain size is generally 20 to 40 μm and the texture and color (tan) are fairly uniform. Contacts with the earlier calcite is gradational, possibly due to recrystallization or crystal enlargement along the contacts. The third type of calcite occurs as cross-cutting veins of clear, colorless calcite crystals about 40-70 μm in diameter. All three types of calcite can be seen in Photo 16. Euhedral to subhedral pyrite is unevenly dispersed through the first two types of calcite, but does not occur in the fracture fillings.

Associations: See above.

Fluid Inclusions: None observed because the grain size is too fine.



Paragenesis

Calcite in fragments _____

Calcite in matrix _____

Pyrite _____ ? - - - - -

Calcite in fractures _____

Deformation _____

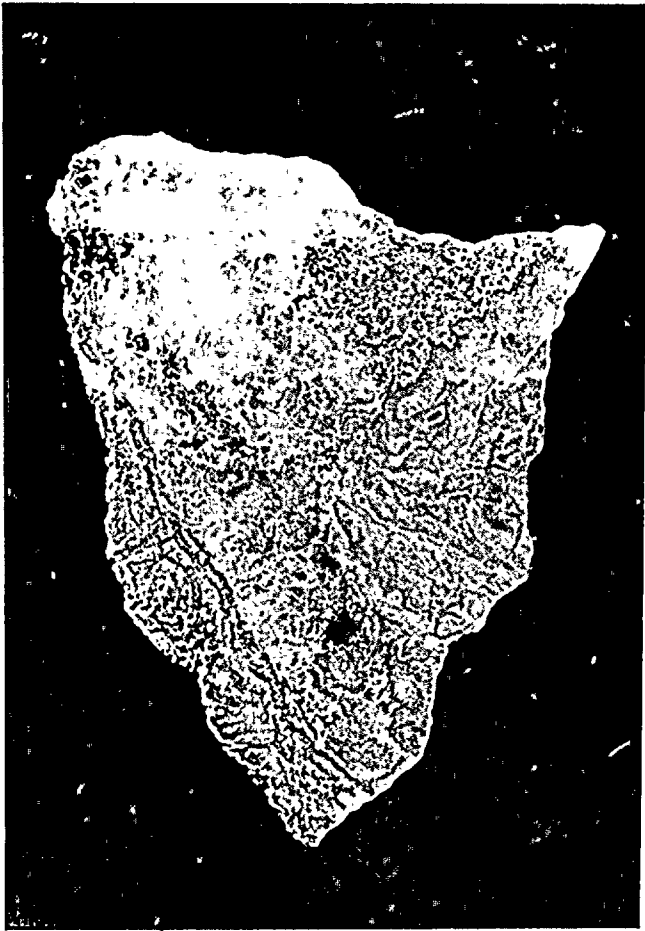
Photo 14: GA4-5

Photo 15: GA4-5. Travertine. Note the variety of textures. The black specks are pyrite grains. The chip is about 10 mm long and was photographed under oblique incident lighting.

Photo 16: GA4-5. Fragments, matrix (upper left and right), and fracture filling calcite. FOV = 1.6 x 1.1 mm.

Photo 17: GA4-5. Indistinct fragments and matrix calcite. Black grains are pyrite. FOV = 1.6 x 1.1 mm.





15



14



17



16

23

GA4-6

Occurrence: Small patches of microbreccia are located on the surfaces of a piece of bedrock (Photo 18). Several of the patches show slickensides associated with finer-grained microbreccia.

Deformation and Texture: The sample consists of angular, scattered quartz grains (up to 300 μm) and fragments of sandstone bedrock surrounded by a matrix of mosaic, irregular, fine-grained calcite up to 60 μm (Photo 19). This cataclastic calcite matrix is identical to the Type 1 calcite described in earlier reports (Sept. 1979, p. 7). The Type 1 calcite occasionally grades into a coarser, cleaner, non-deformed, idiomorphic calcite which coats solution cavities in the Type 1 calcite (Photo 20). This later calcite is identical to the Type 3 calcite described in earlier reports (Sept. 1979, p. 7 and p. 11, sample GA3-16), and is non-deformed and generally free of quartz grains. Scattered sulfides are frequently associated both with scattered quartz grains and with quartz grains within bedrock fragments. The quartz is occasionally surrounded by chalcopyrite, which is in turn surrounded by pyrite. Other instances show scattered, isolated grains of chalcopyrite, sphalerite, and pyrite; the latter infrequently surrounds detrital heavy minerals. None of the material observed microscopically could be correlated with the slickensided calcite noted in hand sample.

Associations: As noted under Deformation and Texture.



Inclusions: None were observed in Type 1 calcite because it is too fine-grained. The type 3, sparry calcite lining vugs in sample GA4-6 contains very few optically recognizable fluid inclusions. The inclusions that are present are very small (on the order of a few micrometers in diameter) and generally single-phase. The relatively rare, two-phase inclusions contain only a small vapor bubble in constant, random motion. The inclusions are typically found in three-dimensional patches within the crystals, suggesting that the inclusions are primary. A few inclusions were observed along the interface between two crystals. Such inclusions may not be primary.

The small size of the inclusions in the Type 3 calcite precludes any heating or freezing tests due to the limitations of magnification and resolution of the lenses used with the heating/freezing stage. However, the single-phase nature of the majority of the inclusions and the small size of the vapor bubble in the two-phase inclusions are consistent with a low temperature origin for this calcite. Based on the observed fluid inclusions and textural relationships, the sparry calcite lining vugs in sample GA4-6 clearly appears to be Type 3 calcite as previously defined and used here.

Paragenesis

Identical to that noted in earlier reports (Sept. 1979, p. 7-8).

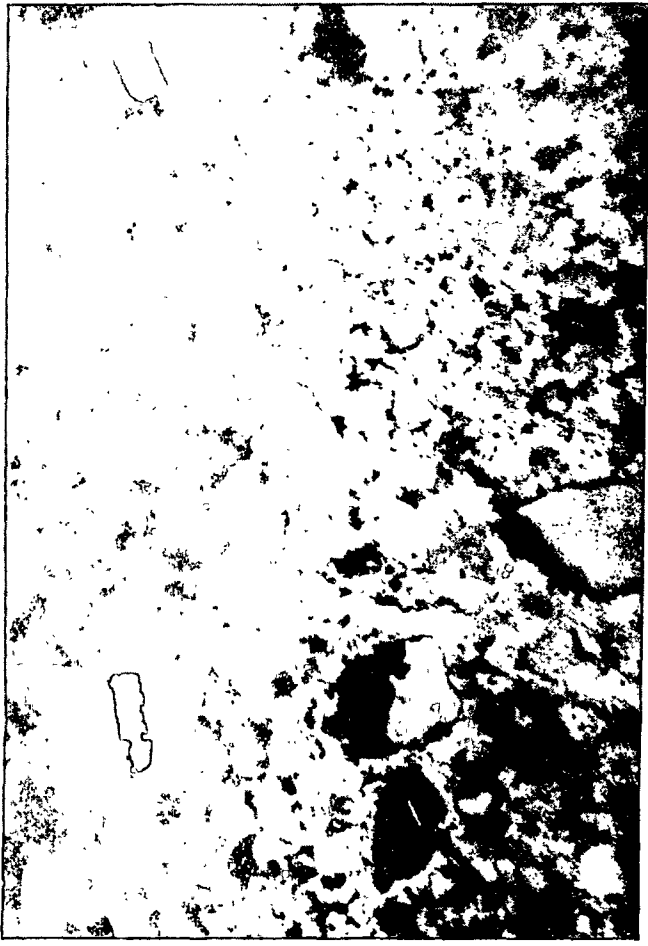


Photo 18: GA4-6. Breccia patches.

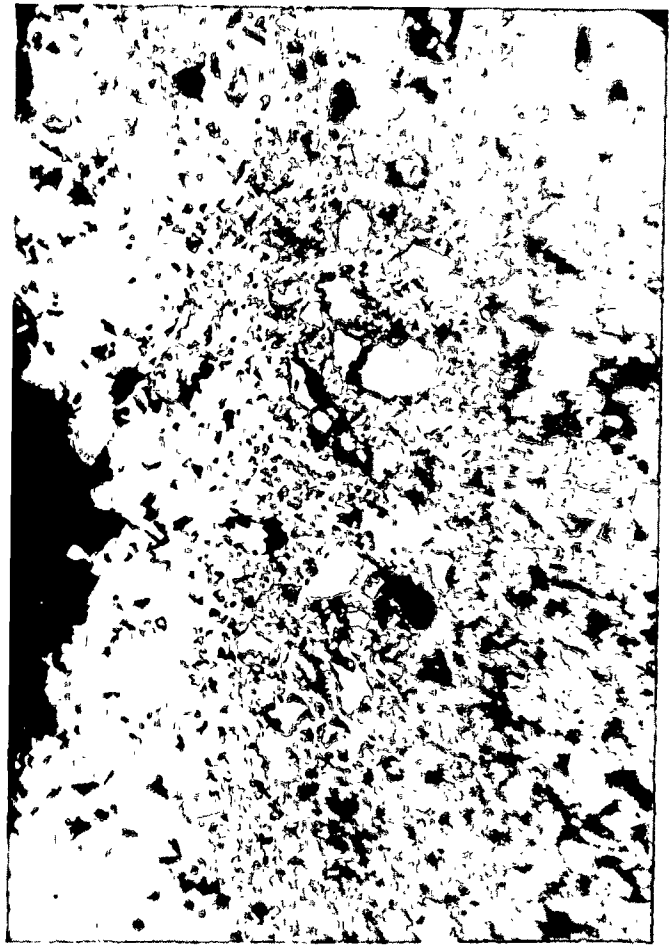
Photo 19: GA4-6. Type 3 calcite (breccia) containing quartz grains (gray, high relief), pyrite and chalcopyrite (white grain) and sphalerite (light gray rectangular grain). FOV = $580 \times 390 \mu\text{m}$. Reflected light.

Photo 20: GA4-6. Type 3 calcite (bottom) and quartz with Type 1 calcite around vug (top). FOV = $1.3 \times 0.9 \text{ mm}$ in reflected light.

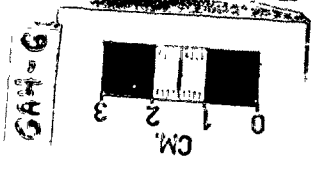




19



20



18



GA4-7

Occurrence: A calcareous, dripstone-like deposit on a sandstone bed in a zone of broad folding of the hanging-wall block of the discontinuity. A breccia zone, sub-parallel to bedding, is located approximately one foot below the specimen location. The sample consists of several types of calcite (Photo 21). One type forms semi-cylindrical rods of dripstone, some of which are still intact, but more are collapsed, having been hollow tubes at one time. One piece (Photo 22) is badly brecciated, while others (GA4-7) are collapsed tubes filled with a slightly coarser calcite (Photo 23). The dripstone tubes are deposited on a thin, laminated, platy substrate (Photo 21). This platy calcite also occurs as broken chips which have been cemented to each other and to the dripstone. The cementing calcite is distinct from either the platy or dripstone carbonate and occurs as a sparry coating on some of the dripstone, and as a cement between broken dripstone fragments.

Deformation and Texture: The platy calcite is composed of at least three distinct layers (Photo 24). From oldest to youngest, these are as follows: the oldest layer is composed of clear, sparry calcite in columns oriented perpendicular to the growth surface. The lower two-thirds of the layer contains many smaller, anhedral calcite grains showing high relief among the prismatic crystals, whereas the upper third of the columnar layer shows fine growth-layering made visible by a pale brownish coloration. The calcite prisms are terminated by crystal faces. This columnar calcite layer



is occasionally very thin or absent in which case, brown calcite (below) may be deposited directly on the dripstone.

The columnar calcite layer is overlain by a thin layer of dark, very fine-grained calcareous material. Pyrite is abundant in this layer and displays octahedral, cubic, and spherical habits. Quartz fragments are sometimes present, indicating that this material is, in part, clastic and may represent fine detritus washed from breccia patches (see the description of sample GA4-6). The pyrite, however, does not appear to have been transported or deformed. The dark, pyrite-rich layer is usually present, although in some chips it is discontinuous or entirely absent. Positive identification of this layer can be difficult because other pyrite-rich silty layers also occur elsewhere in the paragenetic textures.

Above the fine grained, silty layer is a frosting of undeformed, euhedral, brown calcite. The color and unusual habit are distinctive and can be used to positively identify this material throughout the sample. The crystals are elongated, with slightly rounded edges and faces, and are terminated by rhombohedral faces. The cross section is triangular and is preserved even when the crystals are closely grown, leaving open spaces between the crystals (Photo 25). These interstices are filled with fine-grained, pyrite-rich material from the layer described above. The dripstone rods are dominantly composed of laminated, very fine-grained calcite. These calcite grains are equant and the average grain size is about 7 μm . Pyrite is present as very irregular, anhedral grains widely scattered through



the dripstone core (Photo 26). The core of the dripstone is often fractured and, in one fragment, (Photo 22) partially brecciated. A dark, fine-grained layer coats the fractured material, but the fractures do not extend into the darker material.

Sparry, sometimes columnar, calcite is deposited on the outer surface of the dripstone. The layer varies in thickness and may be absent or represented by only a few, scattered, single crystals. Silty streaks splay away from the dripstone into the sparry calcite (Photo 27), but do not disrupt the growth of the crystals. On the opposite edge of the section is a layer of brown sparry calcite containing a large amount of fine-grained impurities. Similar relationships in other chips indicate that the brown calcite is the same as that observed in the platy calcite chips.

The fracturing of the dripstone indicates that a period of deformation occurred after the deposition of the dripstone, but before deposition of the dark gray layer. The platy calcite has also been broken and recemented by brown calcite to the dripstone rods (Photo 21). This evidence of a second deformation is visible macroscopically.

Associations: As described in Deformation and Textures.

Inclusions: The dripstone calcite is too fine grained to preserve useful inclusions. The coarser brown and colorless sparry calcites are coarse enough to contain inclusions but none were observed in either type.



Paragenesis

Dripstone	_____	_____	
Silty calcite (clastic?)		_____	_____
Pyrite	_____		_____
Columnar calcite		_____	
Brown calcite			_____
Deformation		D ₅	(D) ₆

The fine-grained texture of the dripstone indicates that temperatures have remained low enough to prevent recrystallization of the calcite.



Photo 21: GA4-7. "Dripstone" and platy travertine. Note brecciated piece at right and collapsed tube at center.

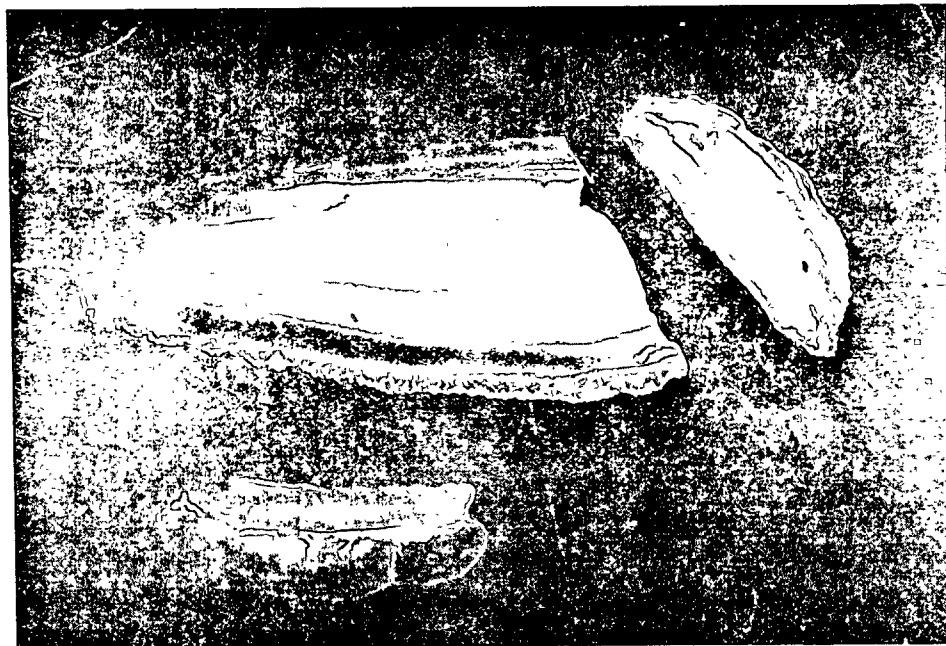
Photo 22: GA4-7. Thin section of brecciated piece in Photo 21. Only the dark core is fractured. The chip is about 2 cm long in oblique transmitted light.

Photo 23: GA4-7. Cross sections of "dripstone." The longitudinal section shows a faulted core rimmed by sparry calcite (top) and brown calcite (bottom). The other two sections show fracture fillings of sparry calcite. These two sections are from collapsed tubes. The large piece is about 15 mm long, in oblique transmitted light.

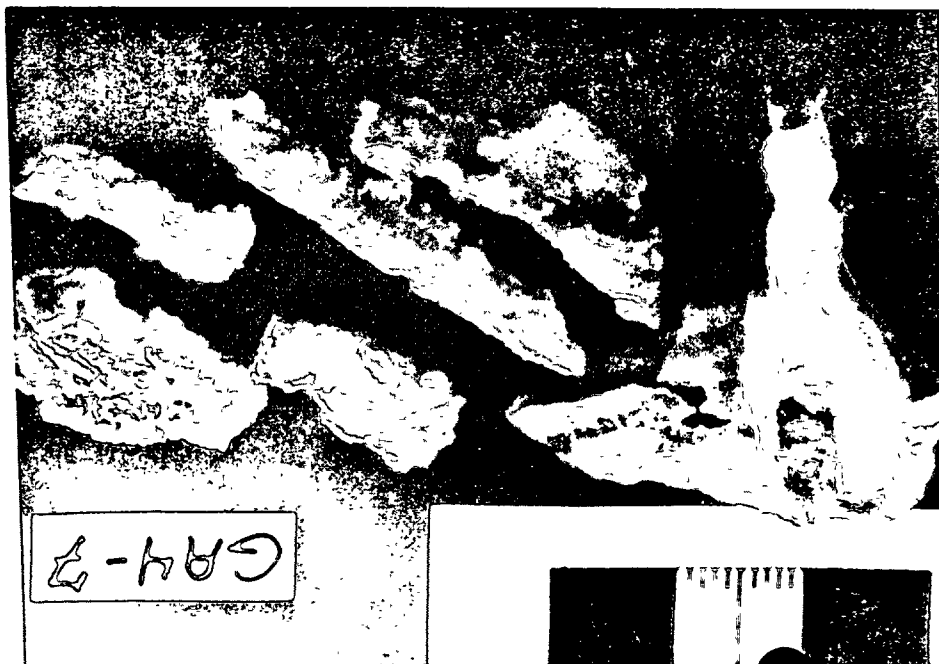
Photo 24: GA4-7. Cross section of platy calcite. From left to right: silty layer, columnar calcite, silty layer (dark), brown calcite (gray and dark layers at right). FOV = 1.3 x 0.9 mm.



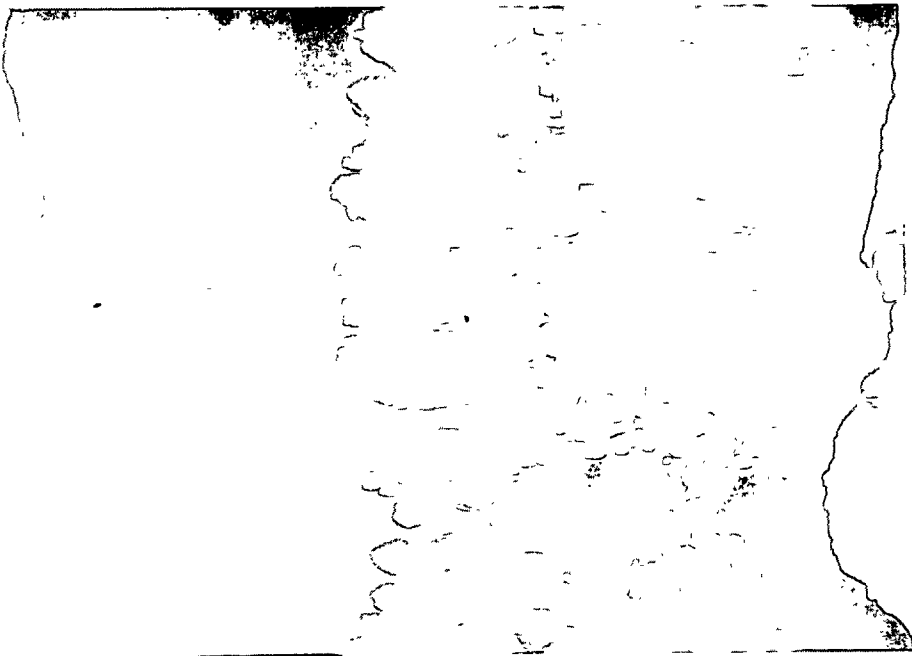
23



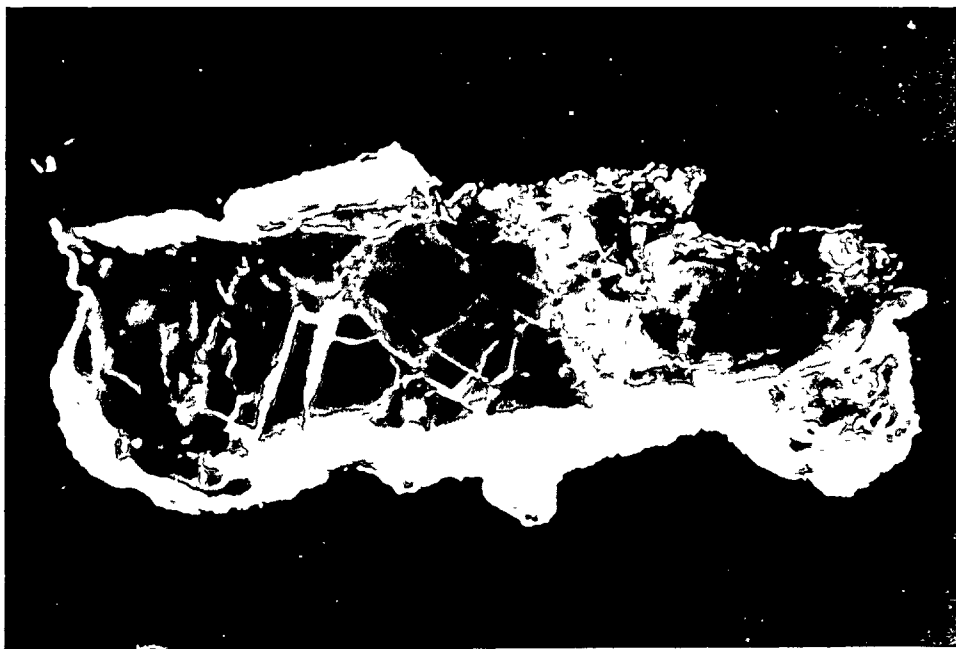
12



24



22



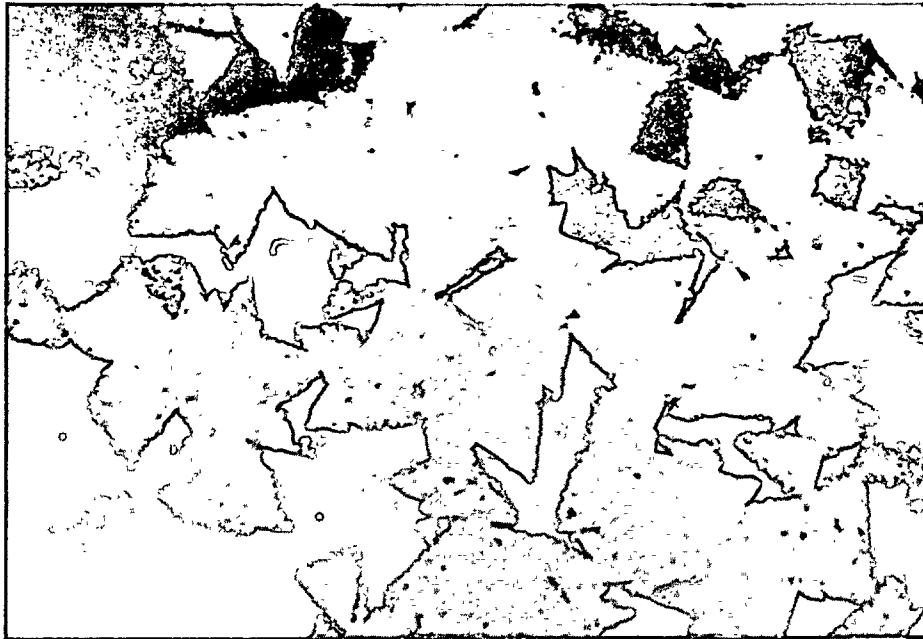
33



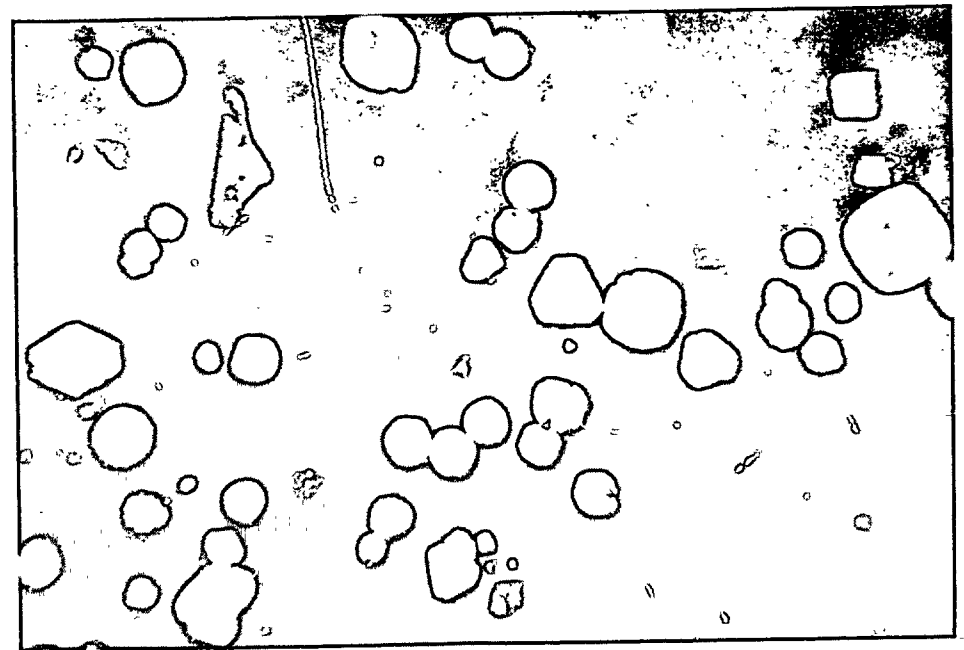
Photo 25: GA4-7. Brown calcite/pyritic silt contact. Section is cut parallel to contact surface.
FOV = 580 x 390 μm .

Photo 26: GA4-7. Pyrite in silty layer under brown calcite. All are euhedral in variety of habits. FOV = 160 x 110 μm .
Reflected light.

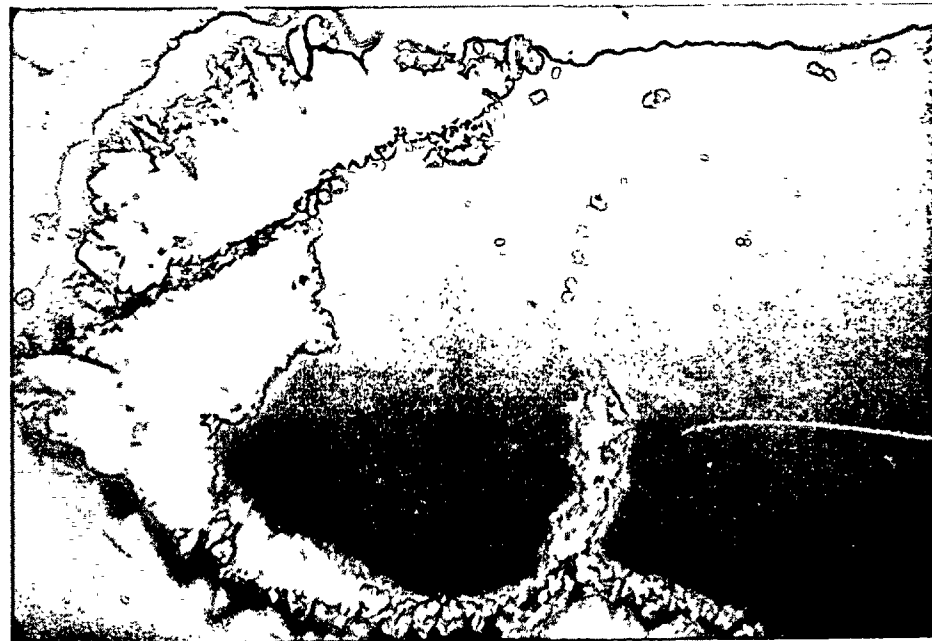
Photo 27: GA4-7. Sparry calcite filling fracture in "dripstone" core and coating end of the chip. Note argillaceous streak in sparry calcite. FOV = 1.3 x 0.9 mm.



25



26



27



GA4-8

Occurrence: Slickensided microbreccia patches located on siltstone (Photo 28).

Deformation and Texture: Samples consist of a fine-grained cataclastic calcite matrix (up to 60 μm grains surrounding scattered angular quartz grains (up to 300 μm grains and angular to subrounded fragments of quartzite. This calcite is identical to Type 1 calcite described in earlier reports (Sept. 1979) and is identical to that found in GA4-6. Scattered grains (up to 50 μm) of sulfides, chalcopryrite, sphalerite, and pyrite, occur throughout the samples. They are frequently, though not always, intergrown with quartz grains. The cataclastic texture of the calcite matrix is the only texture indicating deformation, and there are no solution cavities lined with Type 3 calcite as these were in sample GA4-6.

Fluid Inclusions: None were observed due to the cataclastic texture.

Paragenesis

Type 1 calcite	—————
Sulfides	- - - - -
Deformation	—————

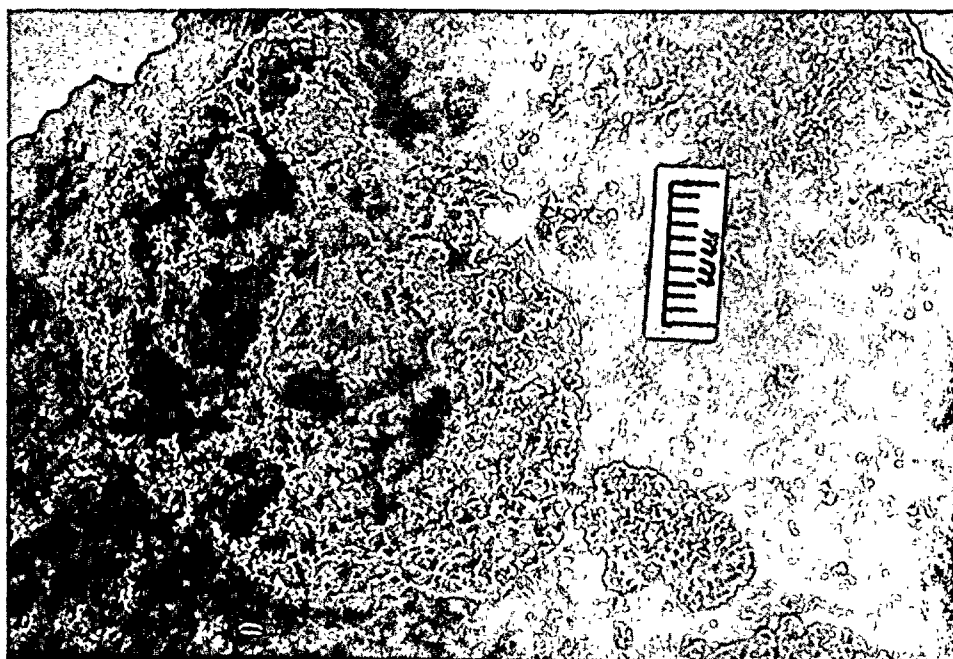


Photo 28: GA4-8. Type 1 calcite with slickensides.

Photo 29: GA4-9B. A patch of breccia on a substrate of dark gray sandstone.



28



29



GA4-9

Occurrence: Breccia patches occur on a 25° E-dipping shear surface at the south end of the slot. The host rock is a dark gray fossiliferous graywacké (Pulaski Fm.).

Texture and Deformation: All of the calcite deposits on these samples are patches of brecciated material containing Type 1 calcite and sandstone fragments (Photo 29), as described for samples GA4-3, -6, and -8.

Fluid Inclusions: None (not preserved).

Paragenesis

Type 1 calcite _____

Deformation _____



GA4-11 A and C

Occurrence: Several types of calcareous deposits occur on vertical fracture surfaces of the samples of GA4-11 including light gray "nodules" (see GA4-11 B), dark gray sparry calcite (brown calcite in thin section), and coarse, radiating calcite crystals (Photo 30).

Deformation and Texture: The colorless, radiating calcite crystals range in size from 2.5 mm in length down to less than 100 μm . The basal portions of the crystals contain abundant argillaceous patches that extend from a silty, calcareous substrate (Photo 31). The crystals are clear and free of both inclusions and any evidence of deformation.

The silty substrate has a calcite matrix (grain size of 5-10 μm), common very fine pyrite (1-10 μm) and uncommon quartz shards (< 75 μm).

Associations: Fine grained calcite is found with pyrite and quartz and clear, radiating calcite.

Fluid Inclusions: None found.

Paragenesis

Fine ground silty calcite _____

Pyrite _____

Coarse, clear calcite _____

Deformation _____



Photo 30: GA4-11A. Radiating crystals of sparry calcite on silty, banded travertine. The label is approximately 3 cm long.

Photo 31: GA4-11C. A polished thin section of a portion of the above sample. The chip is about 1 cm in diameter, in oblique incident illumination.





30



31



GA4-11B

Occurrence: This chip was taken from an irregular, vertical fracture surface (Photo 32). Several types of calcareous deposits occur on the same surface of which one is described here and the others are under other sections under GA4-11. The deposits are 1-2 mm thick and include light gray "nodular" deposits and dripstone, as well as dark gray, sparry calcite (brown calcite in thin section).

Deformation and Texture: The "nodular" vein filling is a laminated, fine-grained travertine (5-10 μ m) containing abundant clay-sized grains, probably of quartz and pyrite. Pyrite is abundant as anhedral to euhedral grains (< 1 μ m to 20 μ m) and is concentrated parallel to the laminations.

The infilling is faulted (Photo 33), indicating deformation after deposition.

Associations: See above.

Fluid Inclusions: None. The material is too fine-grained.

Paragenesis

Fine grained calcite - - - - -

Pyrite _____

Deformation _____

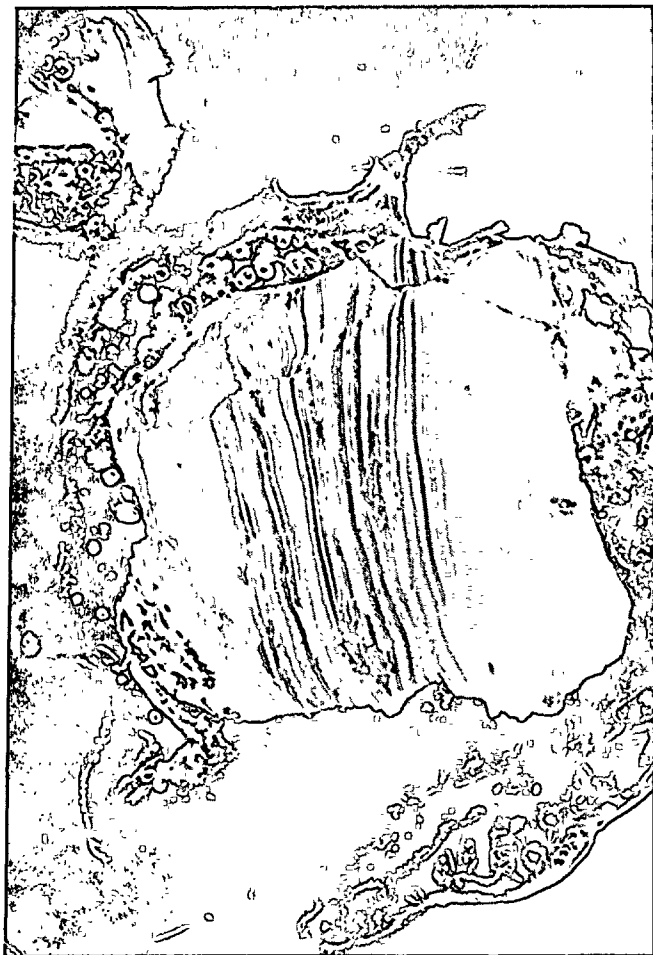
D₅

Photo 32: GA4-11B. Several types of calcareous crusts on a fracture surface: light gray "nodular" deposits at right, "dripstone" (right center), and brown calcite (dark gray at extreme left).

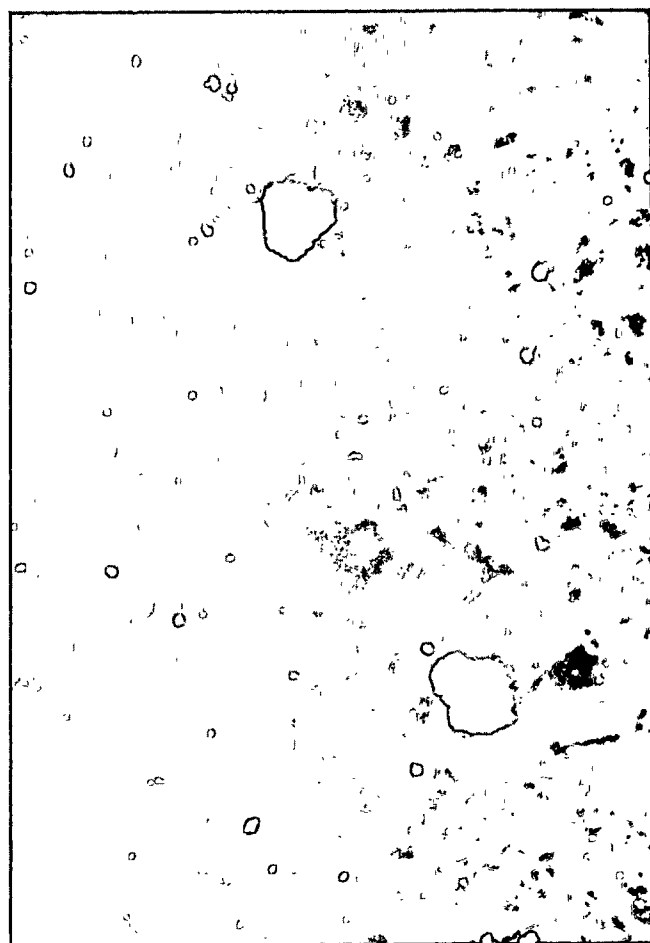
Photo 33: GA4-11B. A polished thin section of light gray deposits similar to those in Photo 32. Note the fault at the right. Dark areas are pyritic. This chip is about 1 cm across, in oblique incident illumination.

Photo 34: GA4-11E. Banded and mottled travertine. Dark areas are pyritic. This large chip is about 12 mm long, in oblique transmitted illumination.

Photo 35: GA4-11E. Pyrite (zoning present but not visible in photo) and quartz fragments in fine-grained calcite of the travertine chip shown in Photo 34. FOV = 460 x 310 μ m, in reflected light.

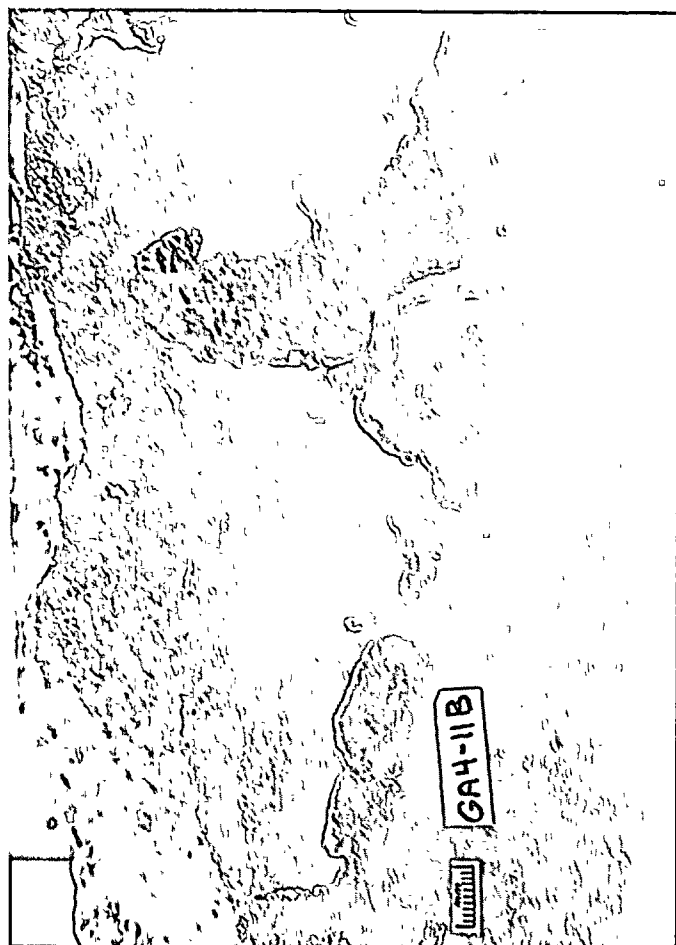


33



45

35



32



34



GA4-11E

Occurrence: Several forms of calcareous deposits occur on a near-vertical fracture surface, including a light and dark gray dripstone or nodular encrustations, dark gray sparry calcite, and colorless, clear, euhedral calcite crystals radiating from the surface of the dark gray calcite. The deposits are 1-2 mm thick, and vary in area from 2 mm diameter to several centimeters across.

Deformation and Texture: The dark gray dripstone-like crust is composed of very silty, horizontally laminated calcareous material (Photo 34). Quartz is abundant as angular shards and, rarely, as rounded grains.

These are cemented together in an impure, very fine-grained calcite matrix (average grain size about 10 μ m) (Photo 35). Pyrite is very common and displays a wide range of grain sizes and shapes. The pyrite also shows at least 2 zones--an inner, brighter zone and an outer, darker zone not visible in Photograph 35. The zoning mimics the present habits, indicating that habit changes have not occurred. En echelon wisps of extremely fine, dark minerals occur in some of the layers.

There is no evidence of deformation in this sample, but the material itself may have been deposited as a result of a period of deformation. The broken, angular quartz shards and sedimentary textures support the idea that silty material released or formed during deformation was deposited and cemented, forming the patches of calcareous crust.



Associations: Quartz shards with calcite and zoned pyrite as described above.

Fluid Inclusions: None; the material is too fine grained.

Paragenesis

Calcite (f.g., silty) _____

Pyrite _____

Deformation _____ -- --?



GA4-S8-A

Occurrence: Cemented, laminated, silty "clay" is present on bedding planes and in breccia of the south wall of the slot. The samples examined are unattached plates with rounded edges and angular, broken edges (Photo 36).

Deformation and Texture: The sample consists of very fine-grained calcite (5-10 μm) with less than 5% quartz (10-25 μm) and a trace of anhedral to subhedral pyrite ($\sim 4 \mu\text{m}$). No clay minerals were observed in thin sections or detected by X-ray diffraction. The texture is uniform and quartz and pyrite are evenly dispersed through the sample.

The surfaces of the samples are striated (Photo 37) and both pieces show evidence of fracturing and compression. The broken pieces have been recemented although the cementing calcite is not distinctly different from that in the sample itself. Deformation is not evident on a microscopic scale, presumably due to the homogeneity and fine grain size of the sample.

Associations: Sub-rounded quartz and small pyrite crystals are associated with the calcite.

Inclusions: The very fine grain size of the calcite in this sample precludes the preservation of fluid inclusions.

Paragenesis

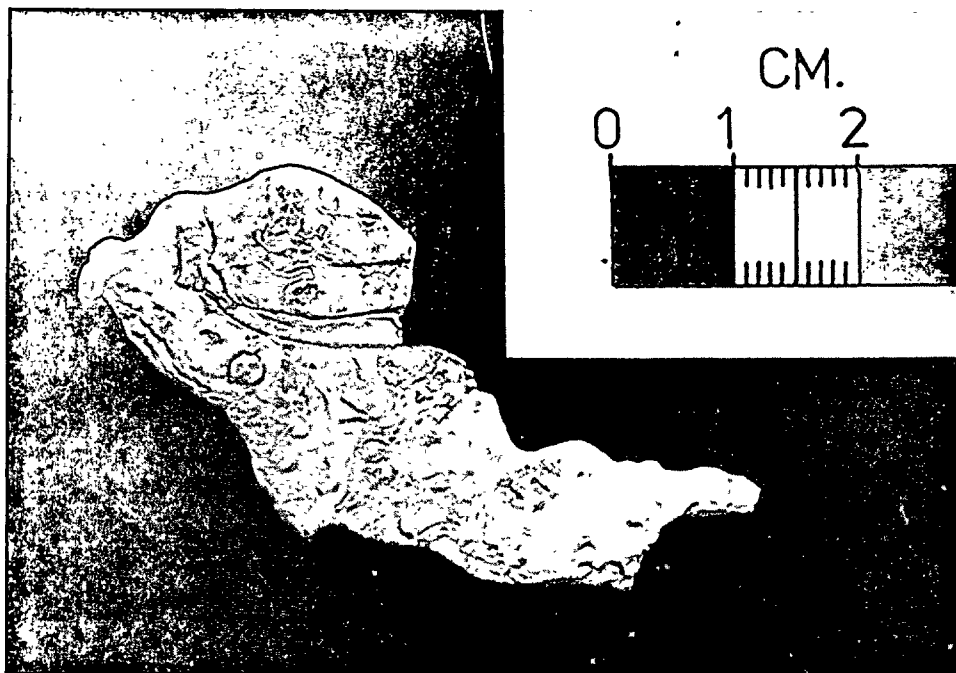
Calcite _____

Deformation _____

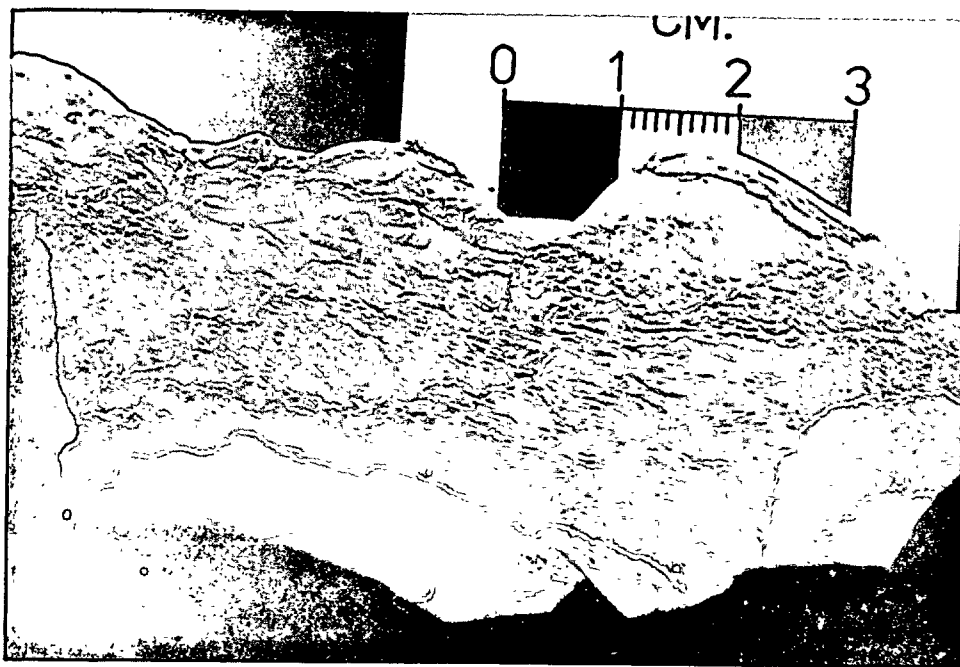
Photo 36: GA4-S8-A. Very fine-grained, tan calcite from a breccia zone. Note healed fractures and rounded edges.

Photo 37: GA4-S8-A. Same as above. Note the striated surface and compressed areas along the upper edge.





36



37



GA4-X

Occurrence: A very fine-grained grout-like substance occurring within openings in the breccia (Photo 38). X-ray analysis indicates portlandite and vaterite are major components.

Deformation and Texture: An extremely fine-grained material, containing scattered grains of fine-grained, nearly opaque solids. The fine-grained matrix is green in color, but too fine-grained to resolve mineralogically. The relatively high reflectivity (about 15%) of the granular, opaque matter suggests that it may be heavy minerals or organic material. Fractures occur near the margins of individual grains, but are apparently due to sample preparation rather than deformation. Several scattered, angular grains of quartz and feldspar (up to 0.6 mm) occur in a few sample grains.

The X-ray data and unusual textures suggest that this sample is artificial. The fine-grained matrix in this sample is similar in color and appearance to the grout matrix in GA4-BH. However, the latter lacks the granular opaque material.

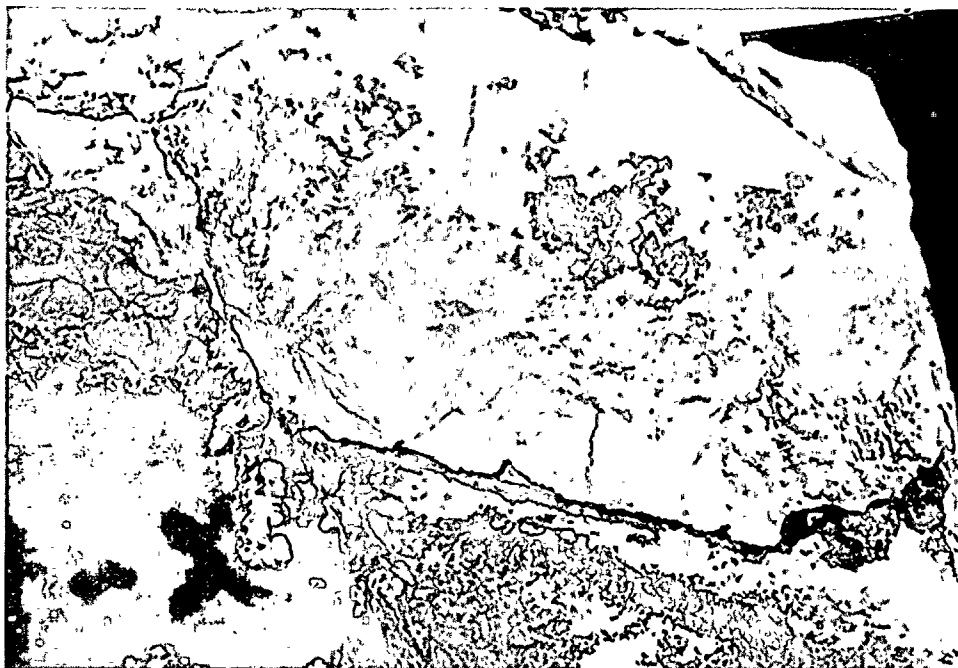


Photo 38: GA4-X. Chalky white, grout-like material.

Photographs of Rock Samples
Showing Locations and
Textures of Fracture-Filling
Minerals.



Photo 39: GA4-2.

Photo 40: GA4-3C.

Photo 41: GA4-3D.

Photo 42: GA4-3G.

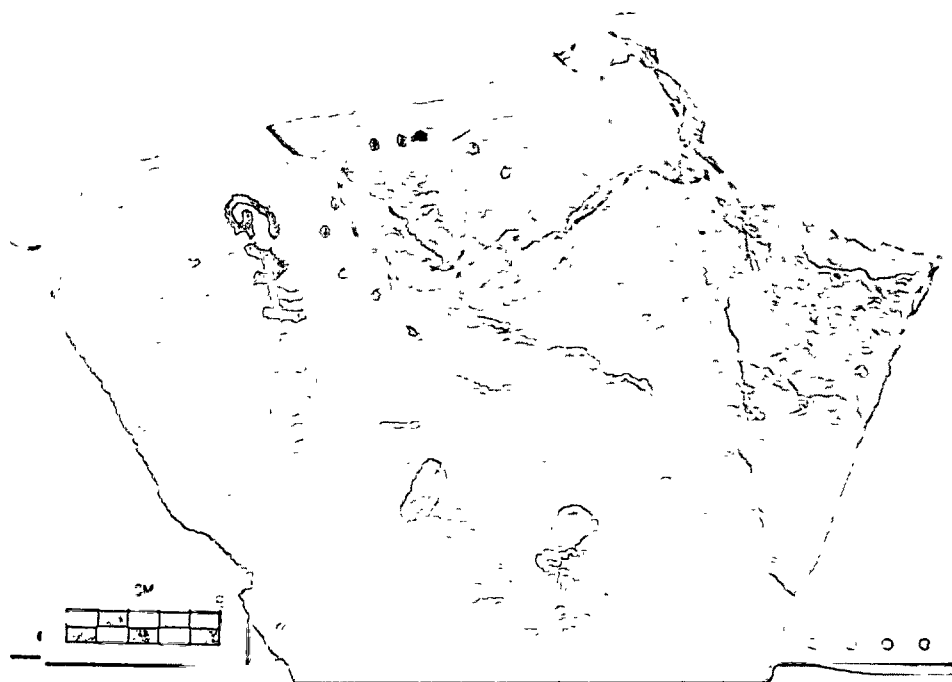




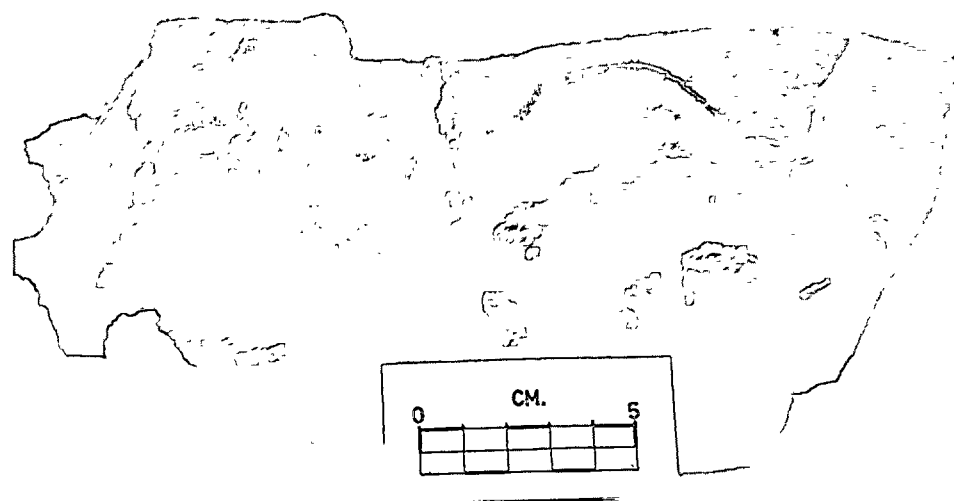
39



40



41



42

55



Photo 43: GA4-4.

Photo 44: GA4-5.

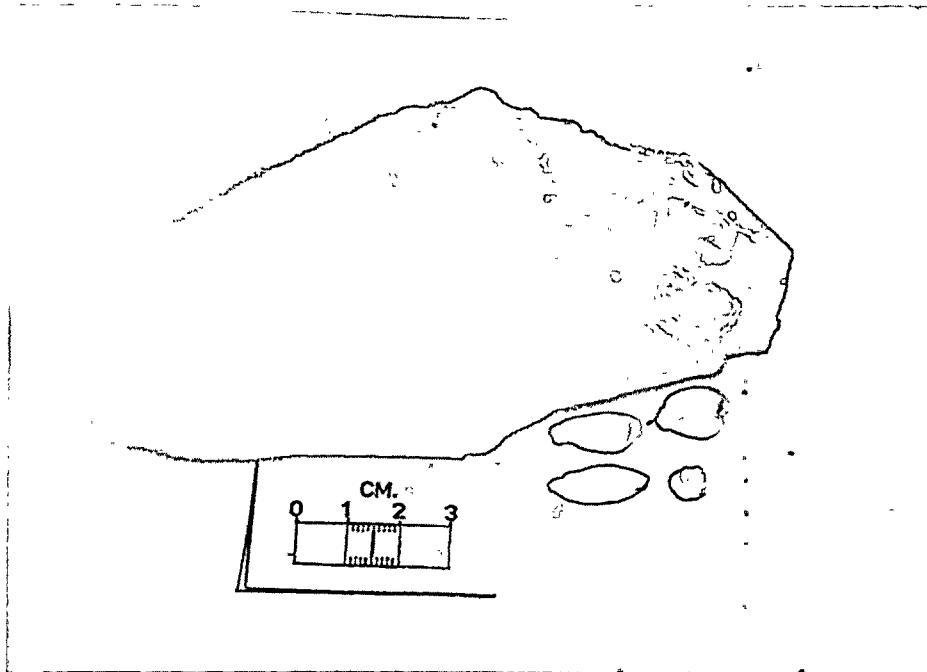
Photo 45: GA4-8.

Photo 46: GA4-9A.

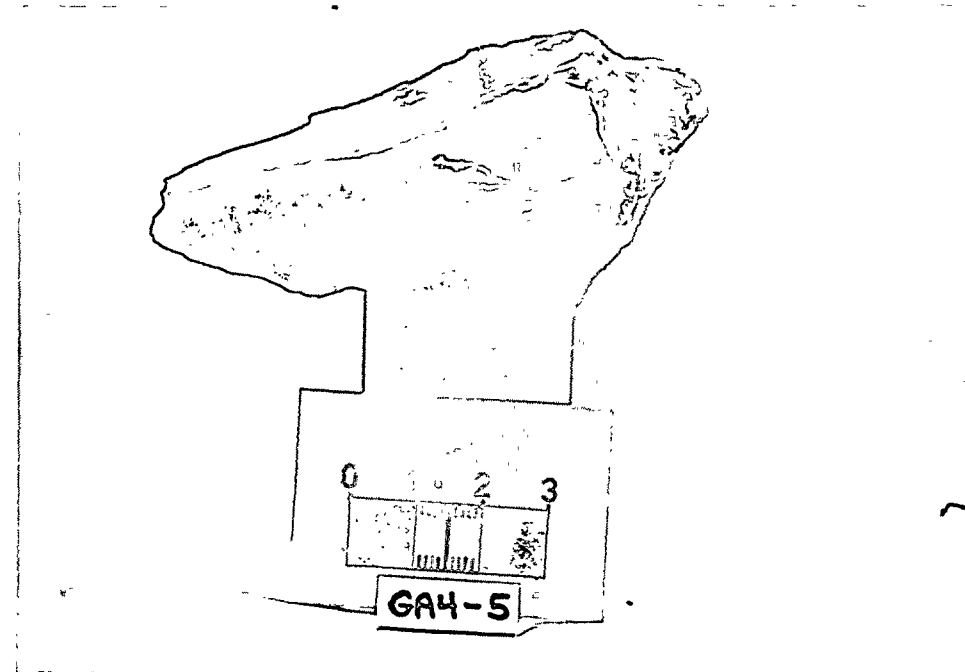
Note: GA4-6 -- See Photo 18.

GA4-7 -- See Photo 21.

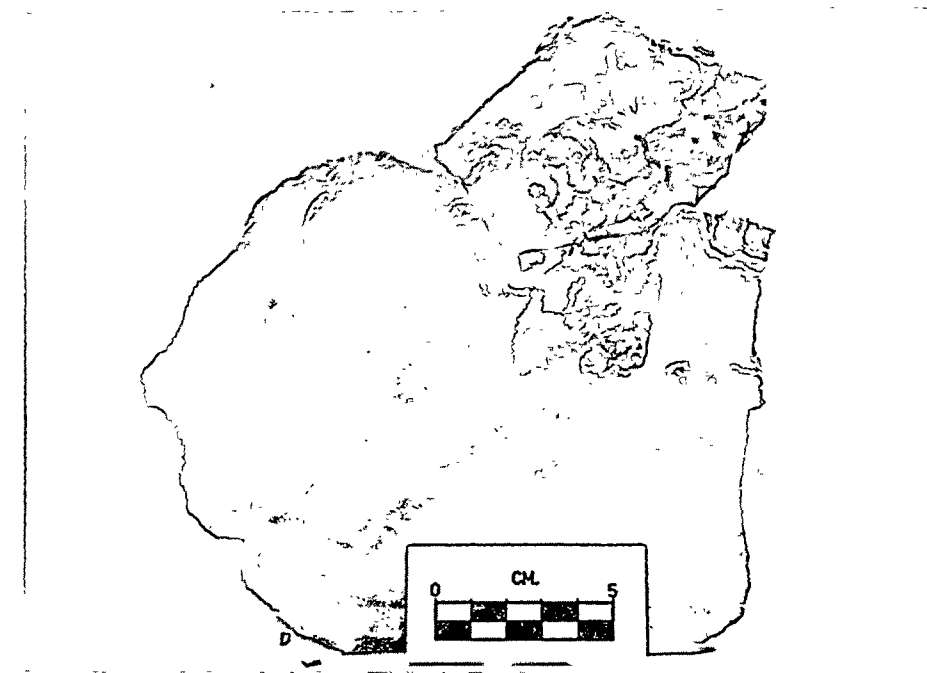




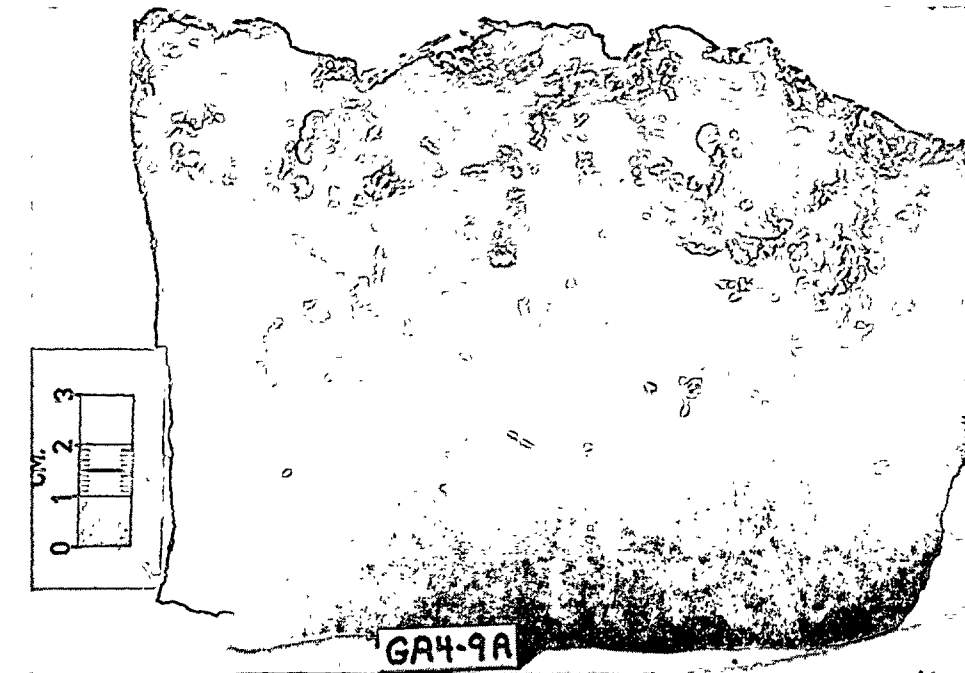
43



44



45



46



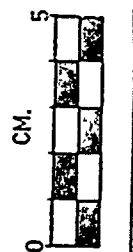
Photo 47: GA4-9B.

Photo 48: GA4-9C.

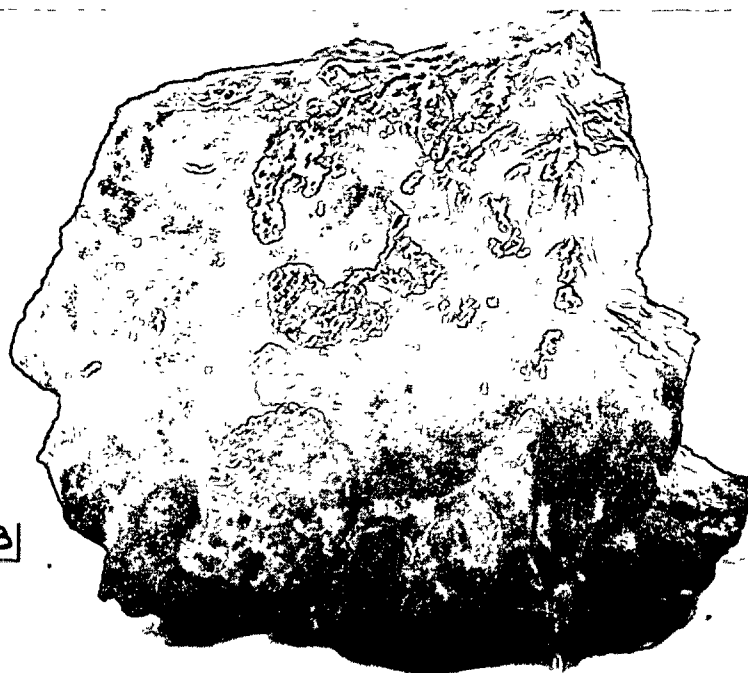
Photo 49: GA4-9G.

Photo 50: GA4-9H.

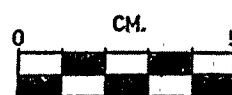




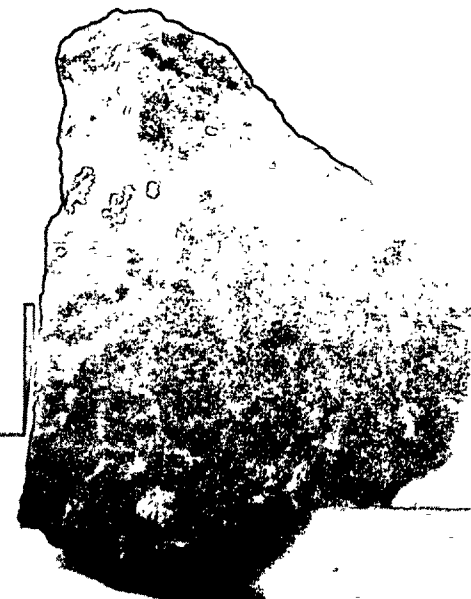
GA4-9B



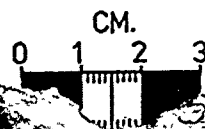
47



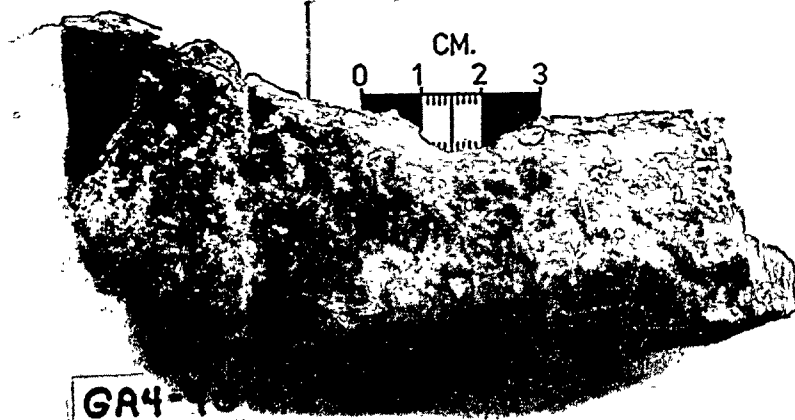
GA4-9C



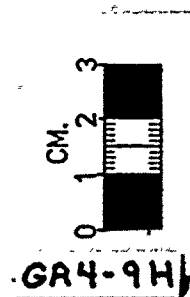
48



GA4-9D



49



GA4-9H



50

59

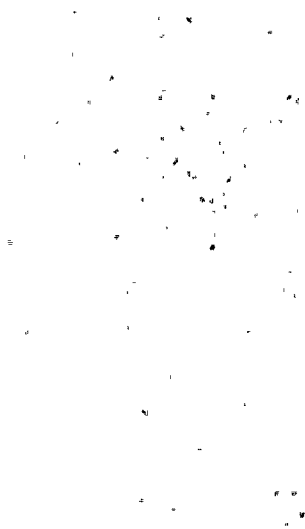


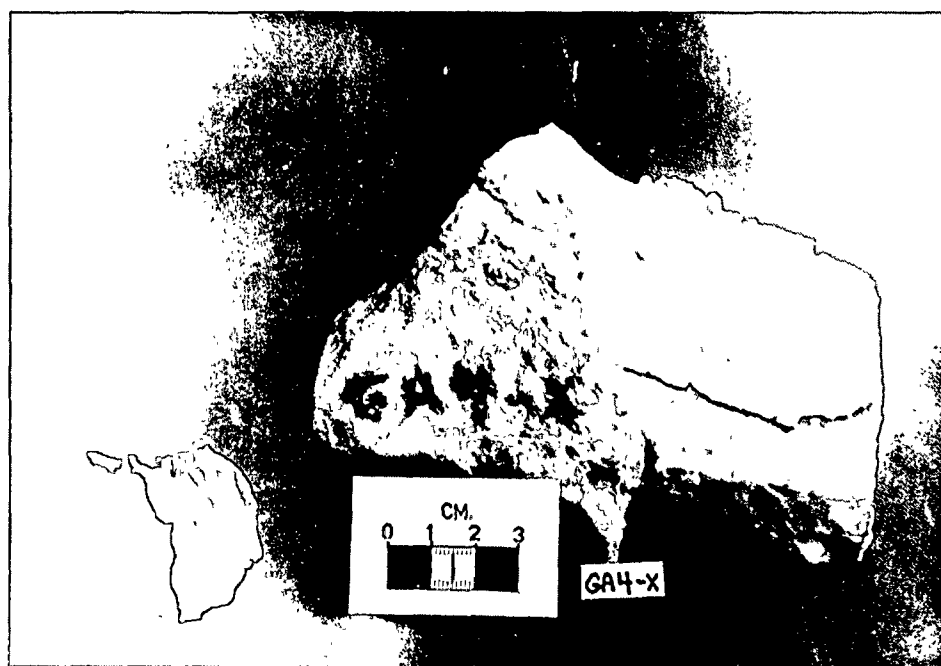
Photo 51: GA4-9J.

Photo 52: GA4-X.

Note: GA4-S8-A -- See Photos
36 and 37.



51



52



H. L. BARNES, *Consulting Geochemist*

213 EAST MITCHELL AVENUE
STATE COLLEGE, PENNSYLVANIA 16801

814-865-7573
814-238-2695

February 26, 1980

Mr. H. Scott Laird
Dames and Moore, Inc.
2996 Belgium Road
Baldwinsville, New York 13027

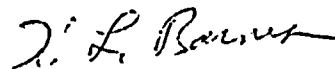
Dear Mr. Laird:

As we discussed by phone, five samples of individual generations of calcite coatings from the Nine Mile Point site have been separated as cleanly as possible for dating by ^{14}C and for ^{18}O measurements. Enclosed are detailed descriptions of the samples and the original of the Dames and Moore "Sample Shipment and Test Instruction Form" which was sent with samples HK-1 and HK-2 to Krueger Enterprises on February 26, 1980. The remaining three samples are now held in reserve.

The samples were prepared in the following manner. Generally the calcite coatings were easily pried from the sandstone substrate with a steel spatula. Sometimes it was necessary to use a hammer and sharp chisel to loosen the calcite coating. The separated calcite chips were collected on clean paper. Impurities were separated first by hand sorting and then during examination under a stereo microscope where necessary. In each sample, a virtually complete separation of an individual paragenetic stage of calcite was found to be possible as noted in the enclosed descriptions. Note that any spray paint, often used to label specimens, must be scrupulously avoided when sampling for radiocarbon dating.

The quality of the isotopic samples could be further improved by two easy procedures. Possible contamination by sweat during the collecting and handling of the samples could be removed by a dilute acid wash prior to digestion for CO_2 separation and isotopic measurements. Secondly, the ^{18}O measurements should be made only on the CO_2 liberated after the sample cleaning, and not the gases produced by digestion with BrF_5 . The pentafluoride attacks the silicates from the host rock and from silts but only the carbonate ^{18}O is important in an attempt to identify the source of the calcite-forming solutes.

Sincerely,



H. L. Barnes

HLB:lic

Enclosures



Calcite Samples Separated For Isotopic Analysis

<u>D + M No.</u>	<u>Weight (gm)</u>	<u>Source Rock</u>	<u>Sample Description</u>
HK-1	17.35	GA4-9	Type 1 calcite breccia free of travertine or other calcites. Individual pieces contain 15-50% sandstone and quartz fragments.
HK-2	8.49	GA4-11E	Travertine with less than 5% total of quartz plus pyrite silt.
	7.86	GA4-10	Travertine with less than 5% total of quartz plus pyrite silt. There is also a total of less than 1 vol. % of either Type 3 or brown calcite stages (undetermined) found on some chips.
	1.56	GA4-11F	Travertine with less than 5% total of quartz plus pyrite silt.
HK-3	0.89	GA4-11C, -11G, -11H	Type 3 sparry calcite with 5-10% impurities of quartz silt, sandstone host, and a few fragments of travertine. The small sample size precludes the elimination of all fragments also containing some of the (older) travertine.



H. L. BARNES, *Consulting Geochemist*

213 EAST MITCHELL AVENUE
STATE COLLEGE, PENNSYLVANIA 16801

814-865-7573
814-238-2695

March 28, 1980

Mr. H. Scott Laird
Dames and Moore, Inc.
2996 Belgium Road
Baldwinsville, New York 13027

Dear Mr. Laird:

The isotopic analyses of the Type 1 calcite breccia (sample HK-1) and of the travertine (sample HK-2) from the Nine Mile Point site provide useful indications of both the conditions and times of deposition of these carbonates in fractures. The reasoning by which these factors can be evaluated is described below assuming, of course, that the enclosed table of isotopic results are as accurate as one might expect.

The high ^{13}C ratio of HK-1 is common for marine carbonates, or springs from such rocks, and is comparatively rare among fresh water carbonates, as shown by figures 6-B-6 and 6-B-7. In contrast, the same figures show that the low ratio of HK-2 is characteristic of both fresh waters (including the Hudson River and some New England lakes) and fresh water carbonates.

The ^{18}O ratios of both HK-1 and HK-2 are shown by figure 8-B-25 to be normal for fresh water carbonates if younger than Triassic. However, even if as old as Triassic, a marine origin of the carbonate oxygen is also unlikely because paleogeographic reconstruction shows that the rocks of this region were emergent and eroding throughout the Mesozoic. Consequently, a fresh water origin of the oxygen in both carbonate samples is probable.

Circulation through the stratigraphic section of this region by fresh water (with isotopically heavy oxygen) could leach heavy marine carbon from the organics or carbonates of these sediments. Where decreased carbon dioxide pressures were encountered during solution flow into or along fractures, a common phenomenon, this saturated solution must then precipitate carbonates of the isotopic characteristics of HK-1. Deposition of HK-2 requires a superficial source of both carbon and oxygen in fresh waters of relatively shallow circulation.

The probable origin of the oxygen from fresh water limits the feasible depths of circulation of the waters through the stratigraphic section in the following manner. The maximum salinity for such waters is roughly equivalent to a brackish 5,000-10,000 p.p.m. of total dissolved solids. (T.D.S. of 5,000 p.p.m. is barely tolerable to livestock and is described as

Mr. H. Scott Laird

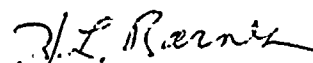
- 2 -

March 28, 1980

"moderately saline" by Hem.) Both the compilation of water analyses by White, Hem, and Waring and the discussion of formation waters of sedimentary basins by Hunt (illustrated by figure 6-3) show that such low salinity waters are unexpected in sedimentary sections at depths even as great as one-half kilometer. Hunt states that very many formation waters increase in total dissolved solids by 15,000-100,000 p.p.m. per 1,000 ft (0.30 Km) in depth. This proportion indicates that 0.5 Km is apparently an unusual depth for the circulation of the relatively "fresh" waters of the type responsible for the deposition of HK-1. Implicitly, the depth of burial during deformation D₄, about 3 Km based on geothermal gradients, must have decreased significantly prior to the deposition of Type 1 calcite at less than 0.5 Km.

In arguments concerning the thermal and chemical evolution of the geosyncline found in the region of the site during the early to mid-Paleozoic, comparisons have been made to the present Gulf Coast. Such a comparison is valid only if the site were also located in a warm climate during the infilling of the geosyncline. Examination of the paleolatitudes for this region in Silurian time, based on paleomagnetic reconstructions, was found to be about 15° south. Consequently, the two climates are sufficiently similar to warrant comparison of the two geosynclines.

Sincerely,



H. L. Barnes

HLB:lic

Enclosures

Isotopic Analyses

Number:	HK-1	HK-2
Sample:	<u>Type 1 Calcite Breccia</u>	<u>Travertine</u>
Source Rock:	GA4-9	GA4-11E
^{14}C Age (yrs.)	> 36,000	14,180 \pm 550
$\delta^{13}\text{C}$ (‰)	+ 3.1	- 7.5
$\delta^{18}\text{O}$ (‰)	+ 21.1 \pm 0.2	+ 22.6 \pm 0.2



Sources

- Wedepohl, K. H., editor (1978) Handbook of Geochemistry. Springer-Verlag, New York. Vol. II-1. Figures 6-B-6, 6-B-7, and 8-B-25.
- Hunt, J. M. (1979) Petroleum Geochemistry and Geology. Freeman, San Francisco. Figure 6-3.
- White, D. E., Hem, J. D., and Waring, G. A. (1963) Chemical composition of subsurface waters: U. S. Geol. Surv. Prof. Paper 440-F, Table 1 to Table II.
- Hem, J. D. (1970) Study and interpretation of the chemical characteristics of natural water: Sec. Edit., U. S. Geol. Surv. Water Supply Paper No. 1473.

HK-1

HK-2

6-B-10

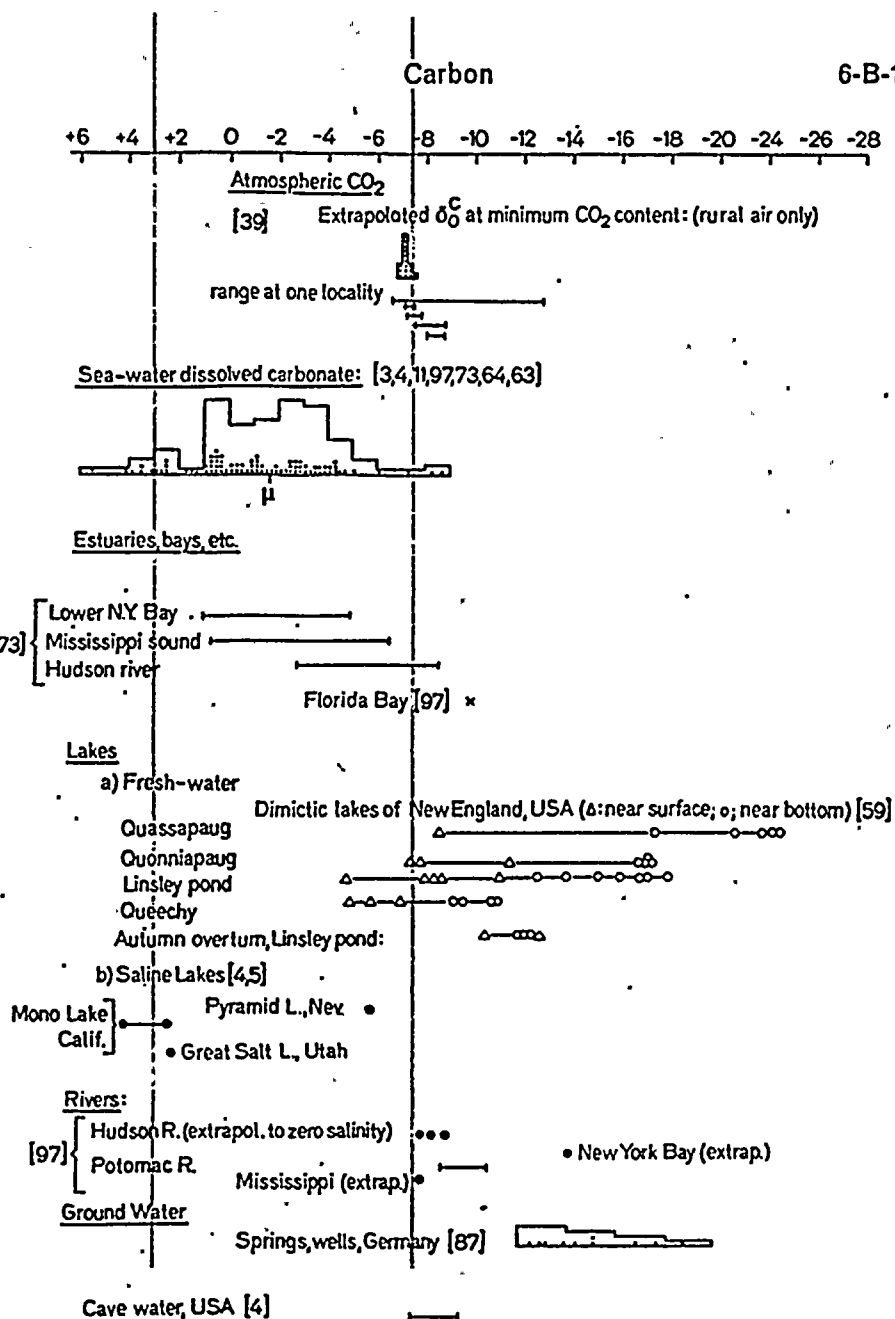


Fig. 6-B-6. Distribution of δ^{C} values in the atmosphere and hydrosphere relative to PDB standard. (Numbers in square brackets see Addendum on References 6-A to 6-O p. 18)

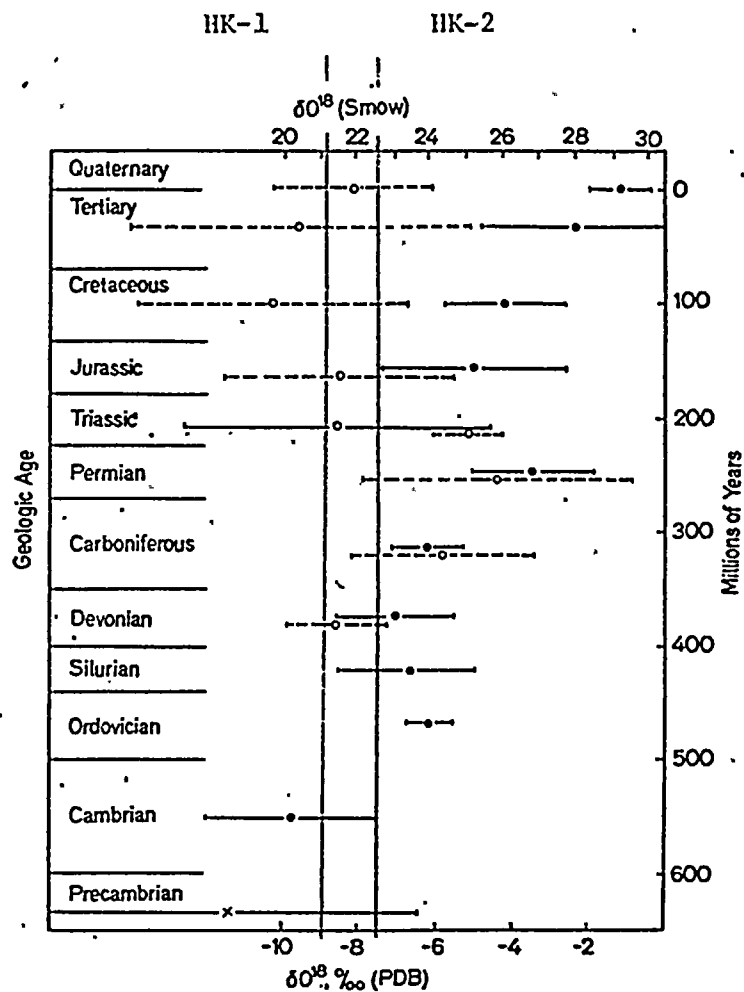


Fig. 8-B-25. Average isotopic compositions of marine and freshwater limestones, by geologic age groups. The lines represent plus or minus one standard deviation. KERR and WEBER (1964). Dashed lines represent freshwater limestones

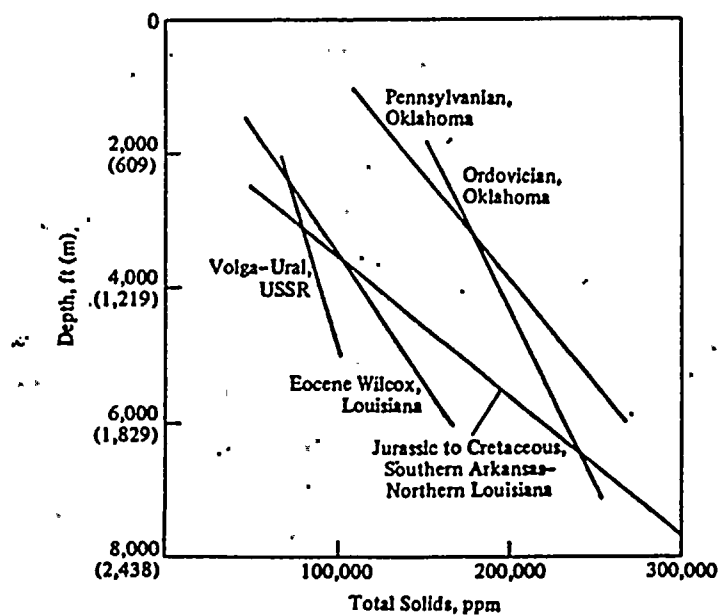


Figure 6-3
Change in salinity of reservoir waters with depth. [Dickey 1969]

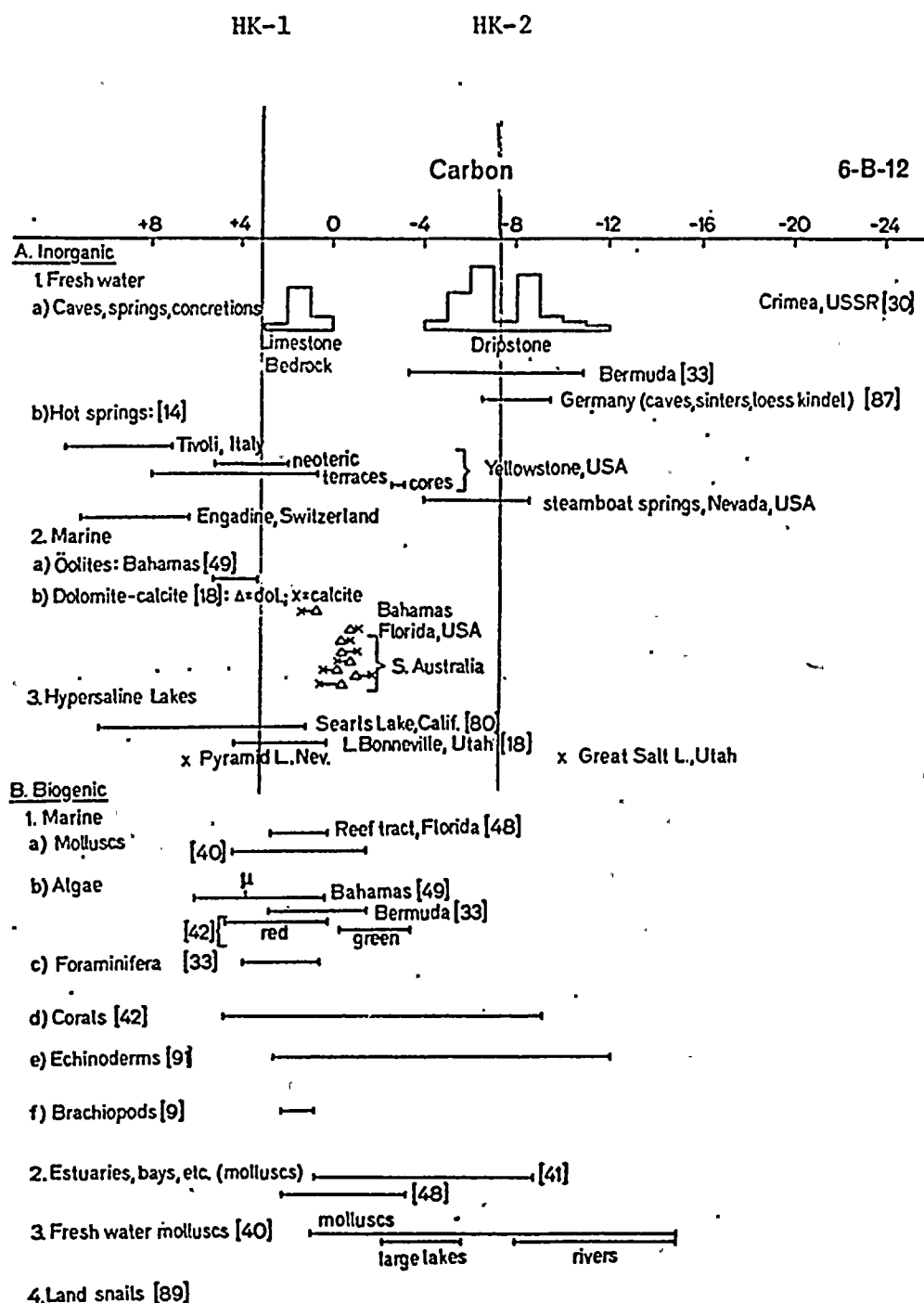


Fig. 6-B-7. Distribution of $\delta^{13}\text{C}$ values in Recent carbonate sediments relative to PDB standard.
(Numbers in square brackets see Addendum on References 6-A to 6-O p. 18)



H. L. BARNES, *Consulting Geochemist*

213 EAST MITCHELL AVENUE
STATE COLLEGE, PENNSYLVANIA 16801

814-865-7573
814-238-2695

May 12, 1980

Mr. H. Scott Laird
Dames and Moore, Inc.
2996 Belgium Road
Baldwinsville, New York 13027

Dear Mr. Laird:

The methods used to separate samples HK-3 and TU-I from their host rocks, and to prepare them for isotopic dating, were very similar to those used for samples HK-1 and HK-2 as described in my letter of February 26, 1980.

Sample HK-3 was separated from rock samples GA4-3A, E, F, and H, GA4-9D, E, F, and K, and GA4-11A, B, C, D, and E. All of the relatively sparse coating of type 3, sparry calcite was removed from the rock surfaces either by prying with a stainless steel spatula or by chipping with a small chisel and hammer. Fragments of the host sandstone were removed as completely as possible by hand picking under a low power microscope. The product, 1.07 grams total, was estimated to be 90-95% type 3 calcite with the remainder being quartz sand and silt grains. This sample was sent by registered mail on April 24 to Krueger Enterprises for ^{14}C dating.

Sample TU-1 was separated from rock samples GA4-3B, C, D, E, F, G, H, and J, GA4-6, GA4-8, and GA4-9A, C, D, E, F, H, and K. Again the calcite coating was separated using a hammer and small chisel. The firmly adhering coating of type 1, calcite breccia required more force for separation from the sandstone host than was necessary for type 3 calcite. The chips with larger proportions of sandstone were removed by hand picking under a microscope. The remaining chips contained variable ratios of calcite and quartz grains. In the total of 16.49 grams of product, the estimated contents were 50-60% of calcite and 40-50% of quartz. The sample is believed to be free of any calcite younger than type 1. This sample was sent by registered mail on April 26 to Dr. T. L. Ku for dating by the uranium-thorium decay series.

A report is enclosed summarizing the results of the examination of samples from series GA5 and 801 carried out by J. B. Murowchick and R. J. Bodnar under my direction.

Sincerely,



H. L. Barnes

HLB:lic
Enclosure



Characteristics of Mineralization in Fractures of
Samples GA5-1A, B, C, D, and 801-M2, -M3

Summary: The paragenetic sequence revealed by the textures of the calcite fracture coatings and their inclusions are virtually identical to those of types 1 and 3 calcites found in other samples from this area. The principal difference is that some clasts in the type 1 breccia of this GA5 series have been identified as fragments of the earlier milky calcite of the previous paragenetic sequence.

The carbonate mineralization in samples GA5-1A, B, C, and D, GA5-2A and B, and 801-M2 and -M3 is composed of the previously described type 1 and type 3 calcites. No new calcite types were found although the source material for the type 1 calcite has now been identified based upon the following evidence. Samples GA5-1A through D and GA5-2A and B each contain type 1 calcite as a matrix enclosing breccia fragments of the sandstone host rock and also of another calcite. This second calcite has deformation twinning, healed fractures, contains sulfide minerals and fluid inclusions, and is milky (photographs 1-6). Furthermore, the liquid-to-vapor ratio is apparently the same as that observed in the milky calcites of the JT-23 to JT-51 series of samples. Consequently, these calcite clasts are taken to be fragments of the milky calcite from earlier in the paragenetic sequence. These clasts have not been found in the GA3 and GA4 series. One large clast in GA5-2B was about 5 mm across. The detailed characteristics of samples GA5-2A and -2B are identical to those of the GA5-1 samples shown in photographs 1-5.



Type 3 calcite is also present and exhibits textures similar to those seen in GA3 series samples (photographs 7 and 8). Drusy type 3 calcite coats the surfaces of the samples.

Samples 801-M2 and -M3 both show the same detailed paragenetic calcite sequence beginning with type 1 calcite (without milky calcite clasts), an overgrowth of columnar type 3 calcite, and finally a brown calcite. The textures and sequence are identical to that observed in sample GA4-7. Zoning in the later half of the columnar type 3 calcite, and a thin, pyritic silty layer between the columnar type 3 and brown calcites are also present, as in GA4-7.

The pyrite in 801-M2 and -M3 is identical in shape and texture to that observed in GA4-7, even containing the same single, thin darker zone in the core that was observed previously (photograph 7) but marcasite is more abundant in these two samples. Marcasite occurs as rosettes, sometimes with a core of sphalerite, and as rims on the pyrite spherules (photograph 8).

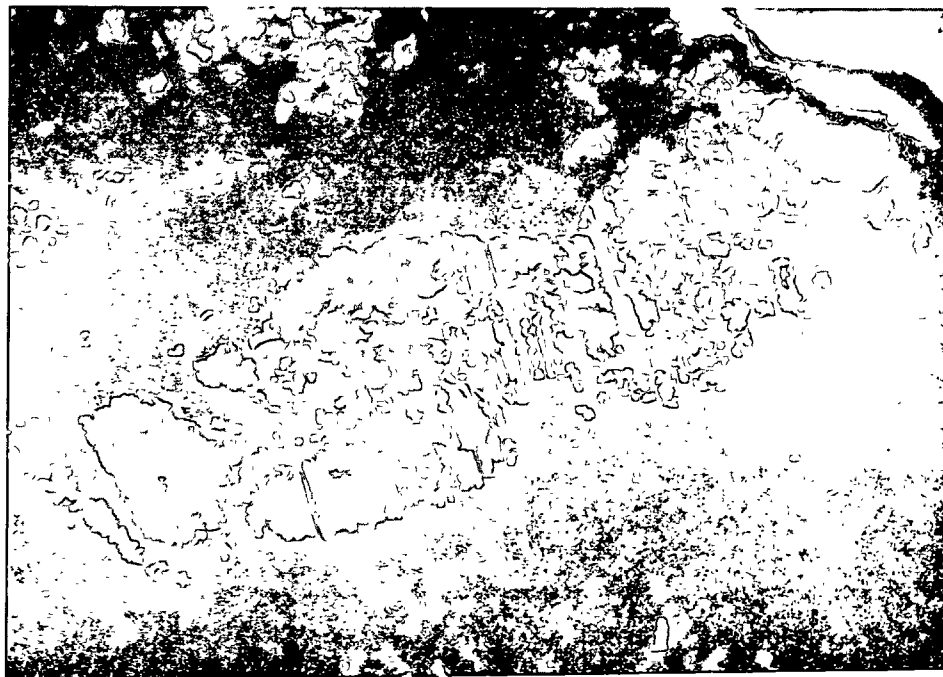


Photo 1: GA5-1A. Clast of milky calcite in type 1, calcite breccia. Note the numerous dark inclusions, deformation twinning, and healed fractures (lower left). Also note the overgrowths of undeformed clear calcite (probably type 3) at each end of the clast. Field of view: 1.8 mm x 1.2 mm in transmitted light.

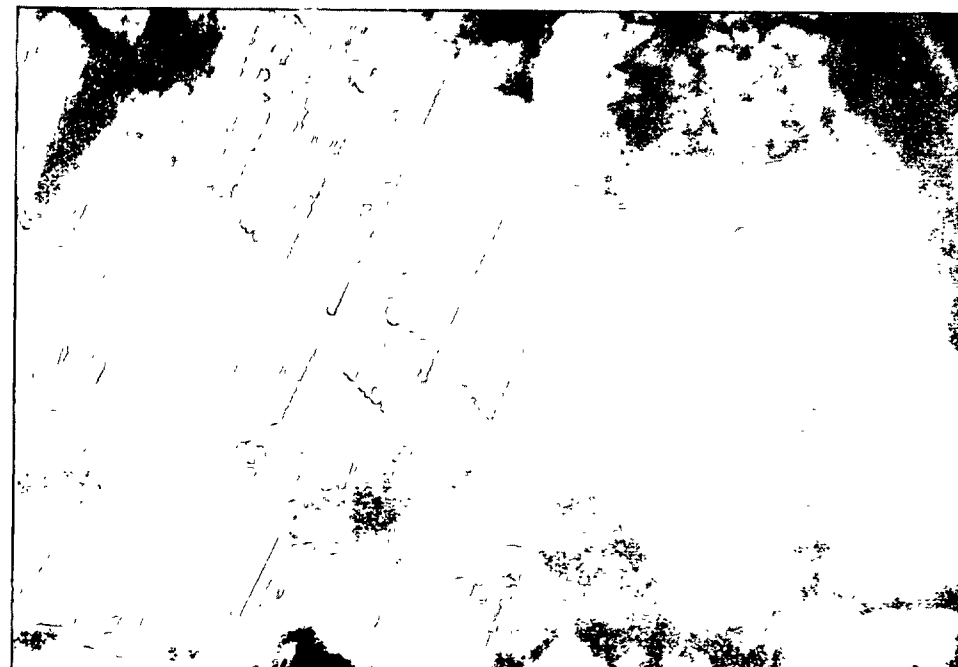
Photo 2: GA5-1A. Higher magnification view of area at the right end of the clast in Photo 1. Note twinning, inclusions, and undeformed overgrowth of type 3 calcite (right). Field of view: 463 μ m x 314 μ m.

Photo 3: GA5-1A. Type 1 calcite with quartz (breccia) and milky calcite clast showing deformation twins and growth twins in calcite overgrowth. The boundary between the milky calcite and the overgrowth is indicated by the change in the direction of each twin band. Field of view: 463 μ m x 314 μ m in reflected light.

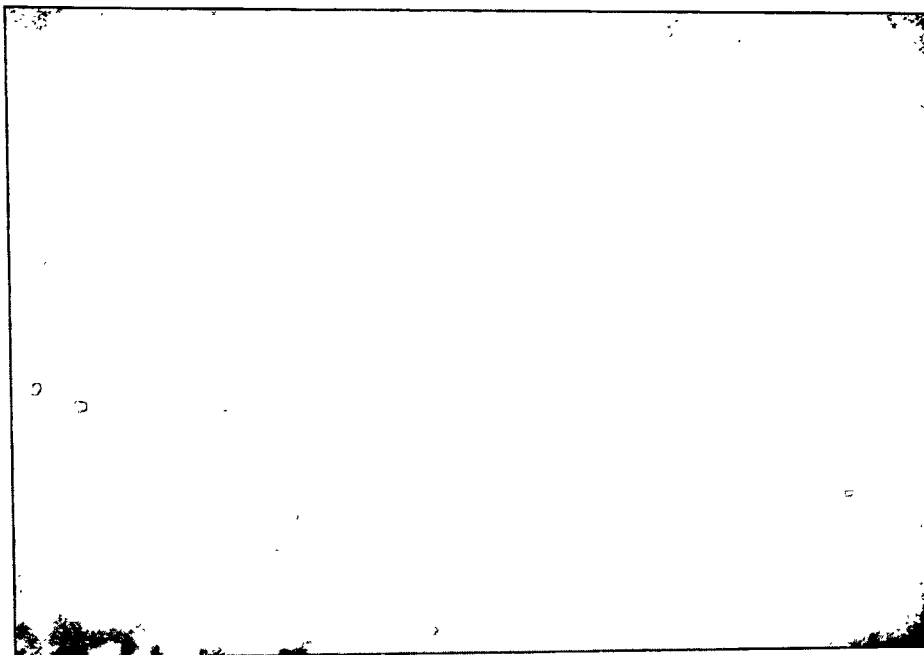
Photo 4: GA5-1B. Brecciated chalcopryrite in type 1 calcite breccia with quartz. The chalcopryrite is part of the pyrite-chalcopryrite-sphalerite-galena assemblage that is contemporaneous with the milky calcite. Field of view: 582 μ m x 394 μ m in reflected light.



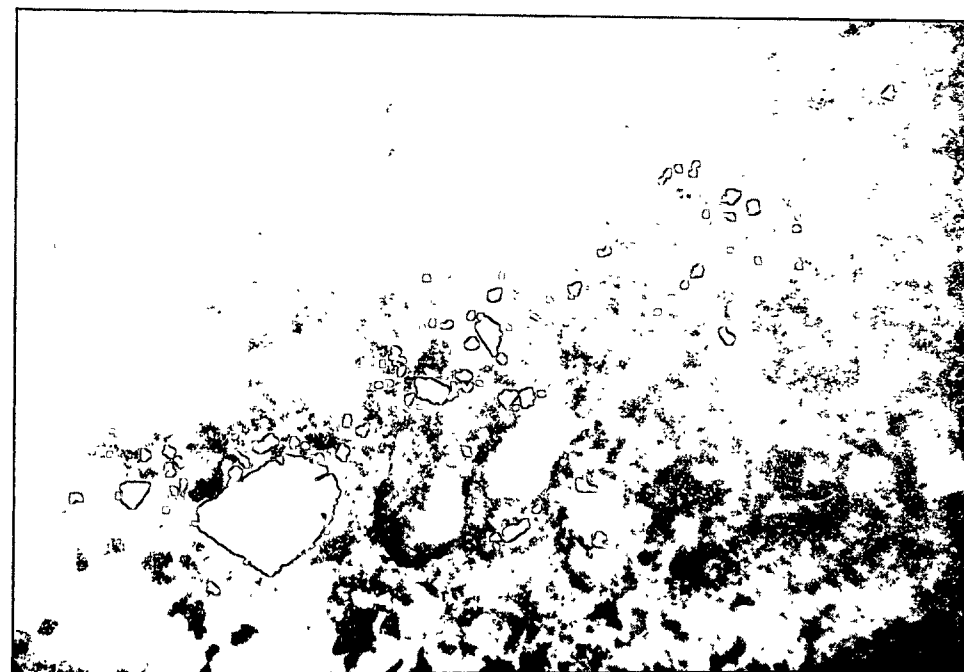
1



2



3



4



Photo 5: GA5-1A. Primary fluid inclusions in milky calcite. The bubbles are not visible due to constant motion during exposure. Field of view: 162 μm x 110 μm in transmitted light.

Photo 6: GA4-1D. Clusters of euhedral pyrite in type 1 calcite. The clusters apparently separated during brecciation, so the pyrite probably formed fairly late in the type 1 paragenesis, possibly at the expense of earlier sulfides. Field of view: 463 μm x 314 μm in reflected light.

Photo 7: 801-M2. Zoned pyrite rimmed by marcasite in type 3 calcite. The grain is 35 μm in diameter, in reflected light.

Photo 8: 801-M3. Marcasite rosettes, one with a sphalerite core. Type 1 calcite is to the left, brown calcite is to the right. Type 3 calcite is very thin in this particular view, but is represented by the grains immediately to the right of the marcasite with the sphalerite core. Field of view: 463 μm x 314 μm in reflected light.

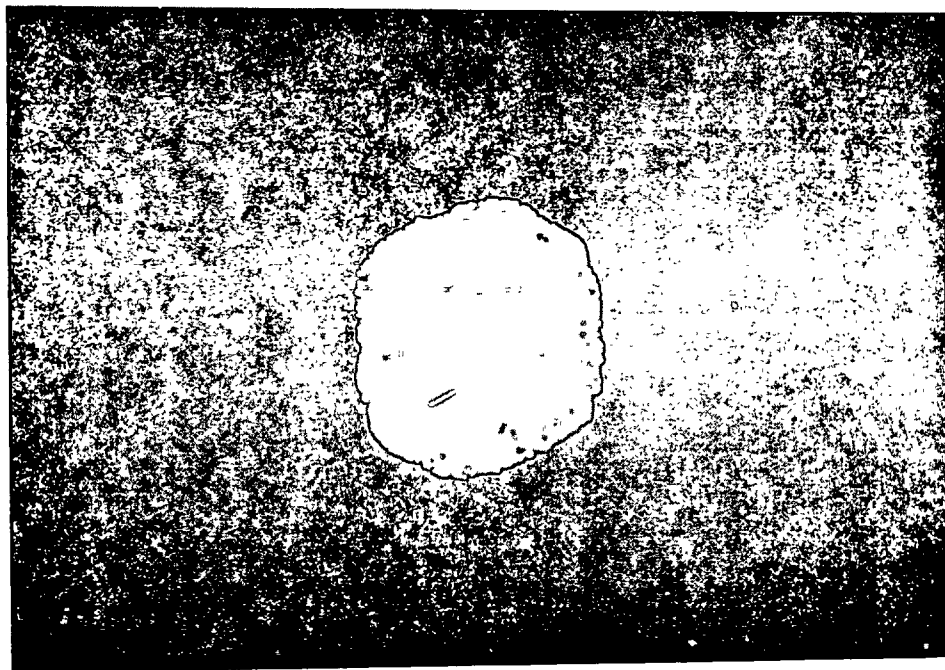




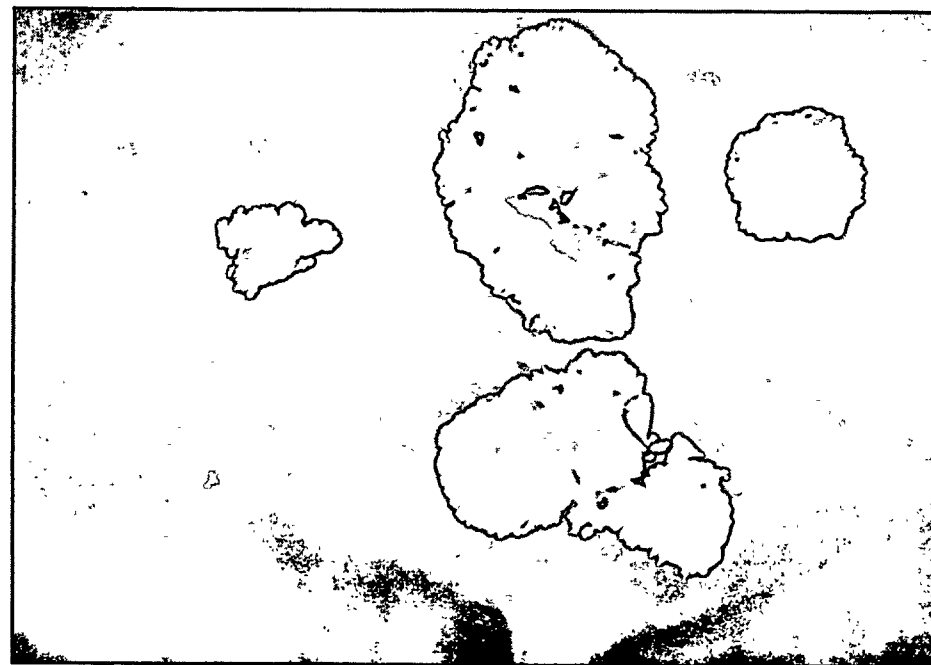
5



6



7



8

9



H. L. BARNES, *Consulting Geochemist*

213 EAST MITCHELL AVENUE
STATE COLLEGE, PENNSYLVANIA 16801

814-865-7573

814-238-2695

September 29, 1980

Mr. H. Scott Laird
Dames and Moore, Inc.
6 Commerce Drive
Cranford, New Jersey 07016

Dear Mr. Laird:

Six samples of the GA-5 series, from the East Lake Water Tunnel at the Nine Mile II location, were examined for comparison of their fluid inclusions and paragenetic characteristics with those found in previous samples from the region. The treatment is that specified under purchase order number SR-0402, dated July 31, 1980. Note that the use of ultra-violet illumination with our new Nikon microscope has made possible resolution of the ancestry of the younger calcites, thereby considerably simplifying the later stages of the paragenetic sequence.

The compilation of characteristics of the younger calcites in this report and their simpler paragenesis make useful a reappraisal of the classification of the calcites found in samples examined some time ago. As a result, the calcites of samples JT-13, -43, and -44 can now be identified as very probably type 1 because of the following shared characteristics. Each contain single-phase fluid inclusions. Marcasite occurs in JT-44 and pyrite in all three samples as in most other type 1 calcites. In addition, JT-13 and JT-43 are described as breccias.

Two samples dated by Dr. T-L. Ku may also be type 1 calcites. Samples SW-1 and SW-2 were both found to contain excess ^{230}Th described by him as of "extraneous origin." Sample TU-1 also has the same isotopic nature and is known to be type 1 calcite where the anomalous isotopic content is attributable to mixing from the old calcite breccia clasts with the young cementing calcite. Consequently, the nominal ages of SW-1 and SW-2, 170,000 and 20,000 years B.P., are of doubtful validity because of the probable contamination from older calcite clasts indicated, as in TU-1, by the excess ^{230}Th .

The preparation of samples and microscopic examinations were carried out principally by J. B. Murowchick, R. J. Bodnar, and A. P. Gize under my direction.

Sincerely,

H. L. Barnes
H. L. Barnes

HLB:lic
Enclosure: report, 7 color slides



Characteristics of Mineralization in Fractures of
Samples GA5-3, -3A, -4, -5, -6, and -7.

Summary: These samples were separated into two groups, one to provide material for possible isotopic dating and the second to be used for examination for paragenetic characteristics.

Initially, calcite patches and vein fillings were examined from samples GA5-4, -6, and -7 to determine the types of calcite present and their relative paragenetic sequence. The types found appeared identical with those previously described and showed no deviation from the earlier reported paragenesis. The use of fluorescent illumination has both verified the sequence of later stages of the paragenesis and has provided clues that type 1 calcite includes recognizable clasts of earlier calcites. Type 1 calcite breccia, because it contains type 3 as a cement, is paragenetically equivalent to type 3 calcite. Because of several striking similarities, types 1, 2, and 3 calcites and the travertine are very probably of the same paragenetic stage best dated near 13,600 years ago.

All exposed type 3 calcite was separated from samples GA5-3, -3A, and -5 for dating. However, the amount available and collected, 0.15 g total, is insufficient for this purpose. In addition, the complex origins of the components of this type of calcite are not ideally suited to dating by techniques based on radioactive isotopes. Alternative methods seem necessary.

The nature of the microscopic data is discussed below and the compiled data are given in Part I, Descriptions of Samples and in Part II Fluorescence of Calcites.

Discussion: The types of calcite found in samples GA5-4, -6, and -7 are described in sequence as follows beginning with the paragenetically oldest type.

A type of calcite, apparently equivalent to the clear calcite plus goethite of the JT series of samples, was found to be common in the coarse calcite clasts of GA5-4 and -7. Fluid inclusion temperatures (uncorrected for pressure) for this calcite, about 152°C, are within the range previously found for the clear calcite with goethite, about 150° to 175°C. A few higher homogenization temperatures, e.g. 241°C, were also found, but are suspect because these temperatures are from leaky inclusions. Consequently, both textures and filling temperatures indicate that these clasts are fragments of the paragenetically earlier goethite-containing calcite.

The type 1 calcite breccia in various locations is now known to contain sandstone host rock fragments as well as clasts of milky calcite, clear calcite, or clear calcite with goethite (also equivalent to clasts referred to as calcite with elongate inclusions). The clastic material is cemented by type 3 sparry calcite. Therefore, type 1 and 3 calcites are paragenetically identical and differ only texturally. Type 1 is a calcite breccia cemented by type 3 calcite; where free of clasts, it is simply identified as type 3 calcite.

The type 3 calcite cement was deposited from low temperature phreatic solutions and, based on the evidence in Table 1, apparently derives at least part of its carbon, oxygen and trace element contents from the brecciated calcites. Evidence for this inheritance is given by the dark red UV fluorescence seen in both the type 3 calcite cement and the clear calcite



Table 1: Characteristics of the types of calcites deposited below 50°C.

Type of Calcite	Texture	Isotopic Data	Other Features
Type 1	Intensely deformed (breccia) Cement is undeformed	U/Th age: <300,000 yrs ⁽¹⁾ ¹⁴ C age: >36,000 yrs ⁽¹⁾ C source: marine ⁽²⁾ O source: fresh water	Occurrence: Sub-horizontal fractures Fluid inclusions: All single-phase Assoc. minerals: mc, mk, py, po Fluorescence: pale blue becomes dark red near clasts of older calcites Contains clasts of three older types of calcite (milky, clear, or clear with goethite)
Type 2	Mildly deformed	no analyses	Occurrence: Sub-vertical fractures Fluid inclusions: no data Assoc. minerals: mc, py, sl Fluorescence: no data
Type 3	Undeformed small euhedral crystals in druses or radiating groups	¹⁴ C age: not possible due to high sulfide content C source: fresh water O source: fresh water	Occurrence: Open space filling in fractures and in breccia Fluid inclusions: All single-phase; 5-6 wt. % NaCl Assoc. minerals: mc, py, sl Fluorescence: pale blue
Travertine	Mildly deformed very fine grained, layered	¹⁴ C age: 13,600 yrs C source: fresh water O source: fresh water	Occurrence: in fractures probably only above the water table Fluid inclusions: none Assoc. minerals: py Fluorescence: weak pale blue
Brown	Undeformed euhedral drusy crystals	no data	Occurrence: Incomplete, thin druses on travertine and fracture surfaces Fluid inclusions: none Assoc. minerals: none Fluorescence: does not fluoresce

(1) These "ages" are inaccurate because they depend on the isotopic proportions inherited from the mixture of old calcite clasts and young calcite cement.

(2) Marine C is very probably derived from the calcite clasts in the breccia. The ultimate source is marine carbonate rocks in the stratigraphic sections of the region.

(3) mc = marcasite; mk = mackinawite (a metastable low temperature mineral); py = pyrite; po = pyrrhotite; sl = sphalerite.

in contrast to the type 3 calcite free of the earlier calcites (such as that coating the travertine deposits described in our December 14, 1979 report) which fluoresces a weak blue-white color rather than red (See Part II of this report, photo A-13). Very fine-grained clastic calcite is absent from the breccias, presumably because its high solubility would favor its dissolution and incorporation into the type 3 calcite cement.

The identification of type 3 calcite as the dominant cement of the clasts in the type 1 calcite breccia, found largely due to the use of fluorescence, provides a key correlation to improve the detailed paragenetic sequence of the low-temperature calcites. The five types of calcite in Table 1 were initially classified on the basis of texture and occurrence. Except for the brown calcite, which was unequivocally deposited last, the sequence for the other four calcites was not well defined. However, types 1, 2, and 3 calcites and the travertine show very similar fluorescence (i.e., trace element contents), associated minerals, and fluid inclusion characteristics (See Table 1). Consistent with these data is the possibility that these four carbonates are different facies of the same depositional stage in the paragenesis. Their differences in textures are attributable to the sites of deposition: the travertine was deposited above the water table, types 2 and 3 formed, respectively, near vertical fractures or in open cavities below the water table, and type 1 filled near horizontal fractures with breccia plus calcite cement.

Isotopic evidence indicates that both the carbon and oxygen of type 3 calcite and the travertine have freshwater origins. The apparent marine origin of the carbon in type 1 calcite could easily be inherited isotopically

from the compositions of the older calcite clasts in the breccia while the oxygen is derived from circulating ground water and both are the isotopic product of mixing of young "fresh water" calcite cement with older clastic calcite. Fluid inclusion data, where available, indicate low temperatures of deposition for these calcites. The associated sulfide mineral assemblages are similar among the four calcites, and are distinct from both the brown calcite and the older calcites. If the effects of impurities from the calcite clasts in type 1 is taken into account, type 1 cement, type 3 calcite, and the travertine show identical light blue fluorescence in contrast to the red, brown, yellow, or very dark blue of the older calcites shown in the photographs of Part II of this report. Because of these striking similarities, it is probable types 1, 2, and 3 calcites and the travertine do not represent genetically or temporally distinct types of calcite, but are instead different facies of the same depositional event.

The isotopic data on ages of deposition can now be examined for these four types of calcite. The ^{14}C age of 13,600 years for the travertine, based on the above discussion, applies to the deposition of types 1, 2, and 3 calcites as well and also to deformation, D_5 , whereby the type 1 breccia was formed. Although this represents only a single paragenetic stage, there is no direct evidence concerning its duration. Although there is no apparent reason for doubting the reliability of this isotopic date, the ages found for type 1 calcite are indeed open to question. Mixing of the isotopic compositions of the older clasts and the younger cement precludes dating by U-Pb, Pb-Pb, ^{14}C , U-Th decay series, and fission track



methods. The excess ^{230}Th found in sample TU-1, type 1 calcite, is compatible with contamination from the older calcite clasts as are also the compromised ages of less than 300,000 years by U/Th decay series and of greater than 36,000 years by ^{14}C measurements. A young age for these low temperature calcites is indicated by the shallow depth of burial, less than about 0.5 km, implicit in deposition by fresh waters and is in conformity with their preferred age of 13,600 years.



Sample GA5-4

A thick patch of breccia on the N35E-trending face of the sample (photos 1 and 2) provided material for examination. The breccia contains large clasts of coarse calcite (up to 2 cm across) as well as sandstone fragments and quartz grains. Sparry type 3 calcite cements the breccia and coats the N70E face of the sample as shown in photos 3 and 4.

Petrographic examination of a polished thin section of the breccia shows that the large clasts are composed of clear calcite (photos 5 and 6) (first described from samples JT-23 to JT-51 in our October, 1977 report) and a calcite equivalent to the clear calcite with goethite described in the same report (photos 7 and 8). Identification was confirmed by visual appearance based primarily on textures, fluid inclusion temperatures, and UV fluorescence. The calcite containing many elongated, tapering fluid inclusions on growth surfaces is in the same stratigraphic position, and has identical textures to those of previously described clear calcite with goethite. It is, therefore, taken to be an equivalent calcite that was deposited under conditions where goethite was unstable. The arrangement of the fluid inclusions and goethite needles suggests that impurities were deposited on the surfaces of the calcite during growth providing points of nucleation for the goethite or inhibiting growth to form fluid inclusions.

The breccia fragments are cemented with type 3 calcite (photo 9). This calcite fluoresces dark red, like the clasts of older calcite, instead of its usual pale blue-white fluorescence (photo A-13). This is probably due to the incorporation of trace elements from finely crushed clear calcite during cementation.

Fluid inclusions are numerous in the calcite clasts but absent in the sparry calcite cement. Several generations of inclusions are represented in the clear calcite (photos 5-8). Inclusions 1-11 (photos 10-19) are all secondary inclusions giving low homogenization temperatures of about 40-50°C. Inclusion 12 (photo 20) homogenized at 92.5° but may also be secondary. Inclusions 15 and 16 (photo 21) are primary, but inclusion 15 leaked. Inclusion 16 homogenized at 152°C and many of the other small inclusions in the field decrepitated at 150 to 200°, indicating homogenization temperatures toward the lower end of that range. These temperatures are consistent with those recorded for the clear calcite with goethite, but due to the range of temperatures found for the clear calcite with goethite, these temperatures do not, by themselves, confirm the identification of this calcite.

Paragenesis:

Clear calcite	_____	
Clear calcite with elongate inclusions	-----	
Type 3 calcite		_____
Deformation		$\overline{D_4}$ $\overline{D_5}$



Part I

Description of Samples



Photo 1: GA5-4. Whole sample, N35E-trending face with breccia patches.

Photo 2: Close-up of breccia patch in photo 1. The large clasts are clear calcite.

Photo 3: GA5-4. Whole sample, N70E-trending face with type 3 calcite coating.

Photo 4: Close-up of type 3 calcite at the left end of the sample in photo 3.



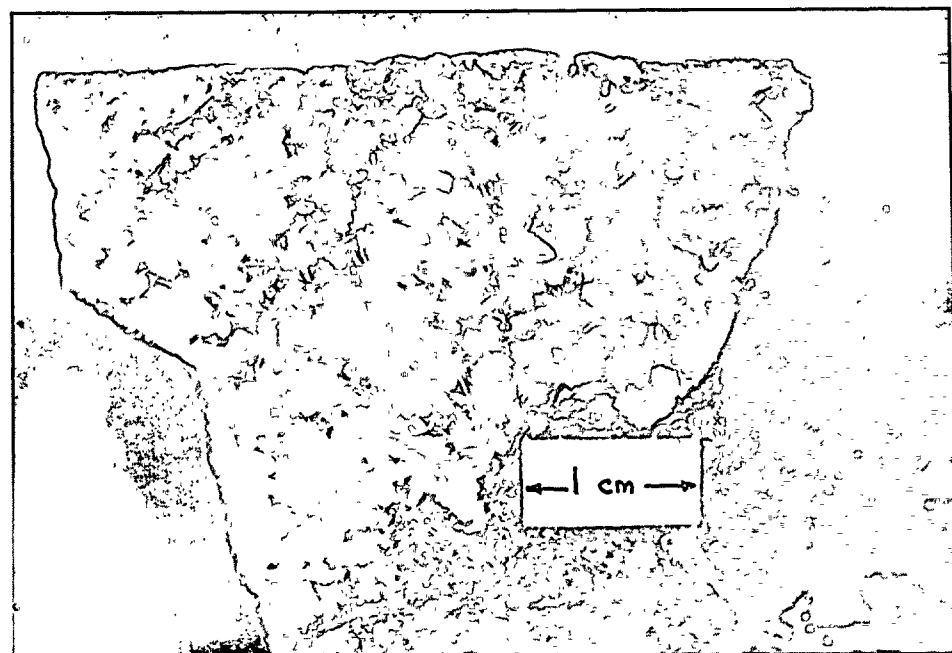
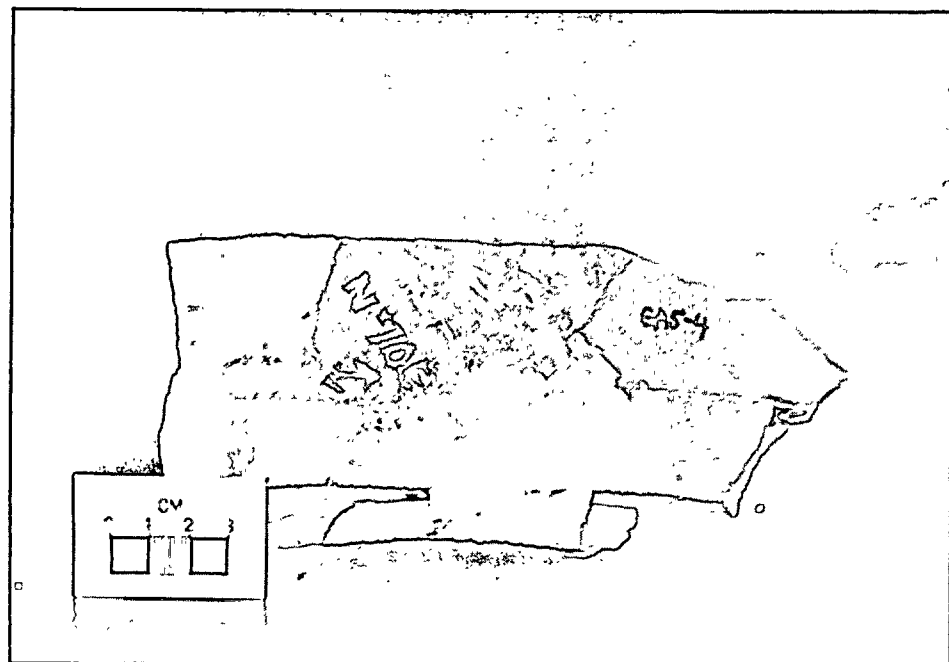
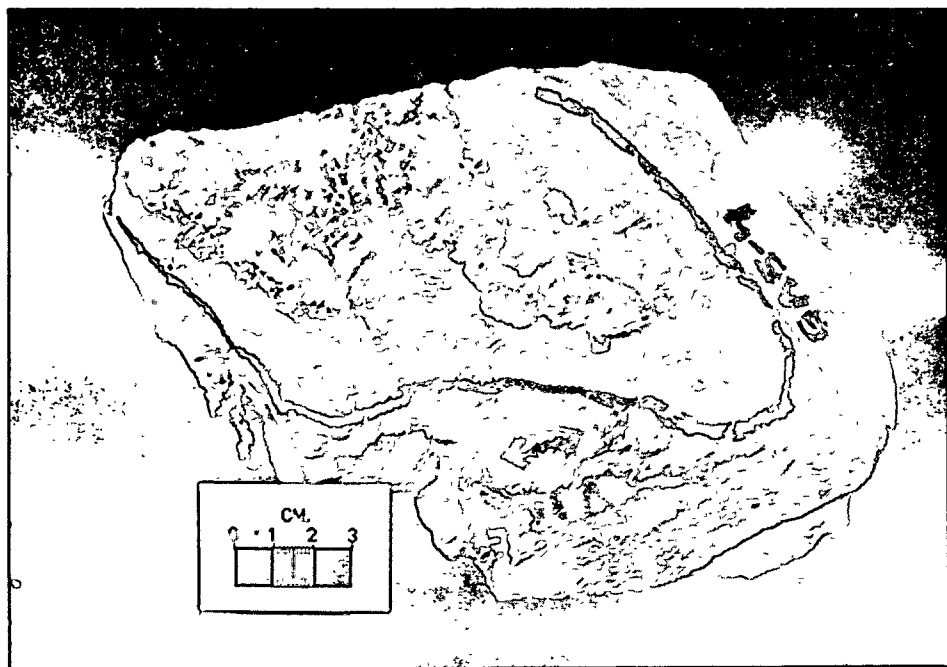




Photo 5: GA5-4. Clear calcite containing several sets of low temperature fluid inclusions. Field of view = $683 \times 461 \mu\text{m}$, in transmitted light.

Photo 6: GA5-4. Typical clear calcite displaying numerous sets of fluid inclusions along healed fractures and cleavage planes. Field of view = $1.37 \text{ mm} \times 0.93 \text{ mm}$, in transmitted light.

Photo 7: GA5-4. Boundary between clear calcite (bottom) and clear calcite with elongate inclusions (top). The latter is equivalent to the clear calcite with goethite found in other areas. Field of view = $1.37 \text{ mm} \times 0.93 \text{ mm}$, in transmitted light.

Photo 8: GA5-4. Close-up of clear calcite with elongate inclusions. The direction of calcite growth is from the upper right to lower left. Many of the inclusions in this calcite have a solid particle at their oldest end (arrows) which probably caused the formation of the inclusions. Field of view = $683 \times 461 \mu\text{m}$, in transmitted light.

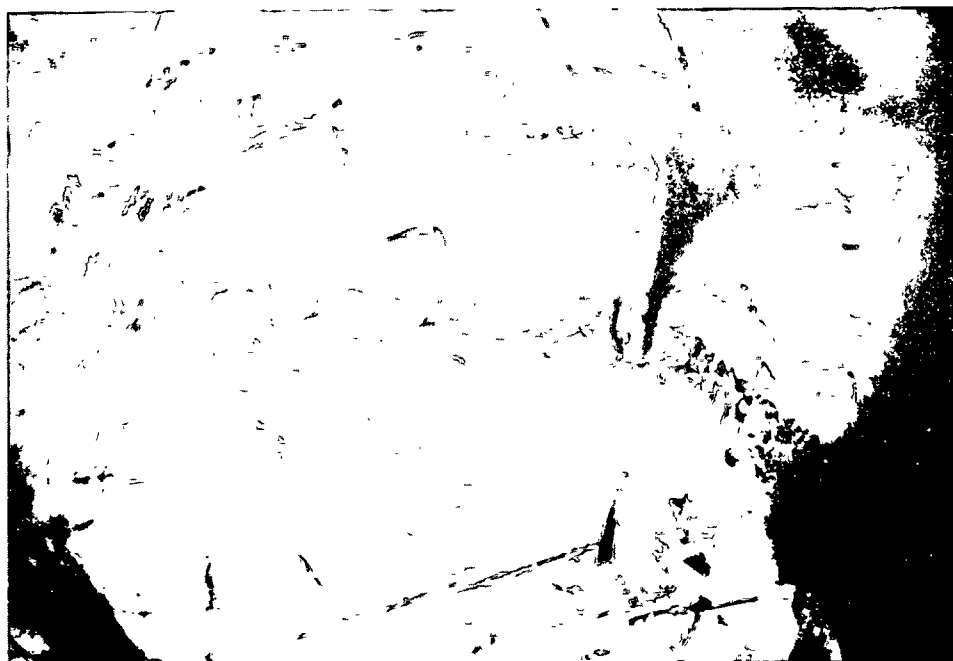




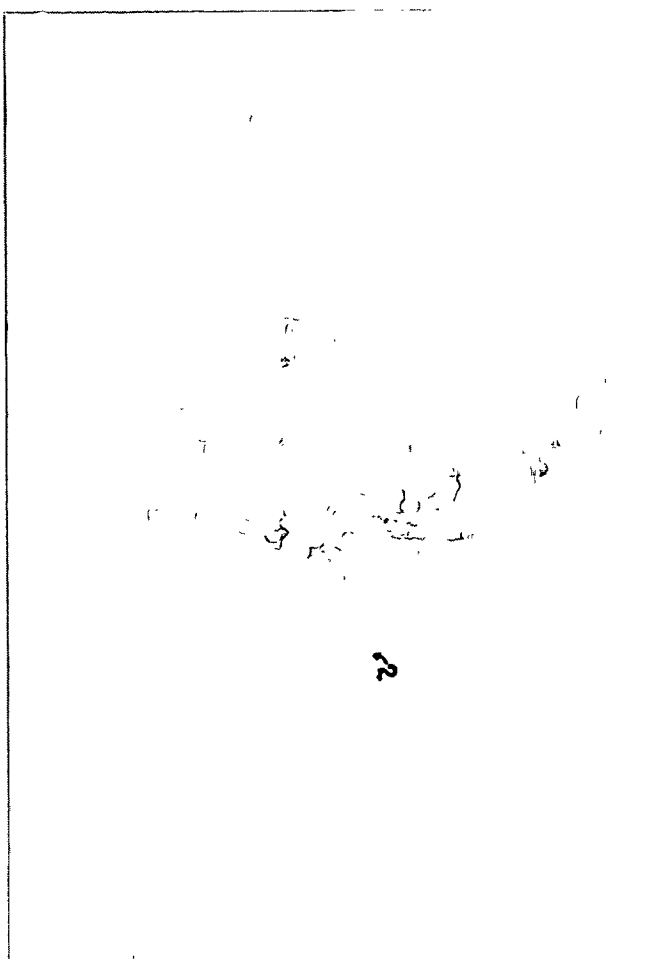
Photo 9: GA5-4. Type 3 calcite filling open space between sandstone breccia fragments. Field of view = 1.37 mm x 0.93 mm, in transmitted light.

Photo 10: GA5-4. Overview of fluid inclusions in clear calcite. The numbered inclusions are shown in the following photographs and were heated to obtain filling temperatures. Field of view = 683 x 461 μ m, in transmitted light.

Photo 11: GA5-4. Inclusion 1. Field of view = 170 x 116 μ m, in transmitted light.

Photo 12: GA5-4. Inclusion 2. Field of view = 170 x 116 μ m, in transmitted light.





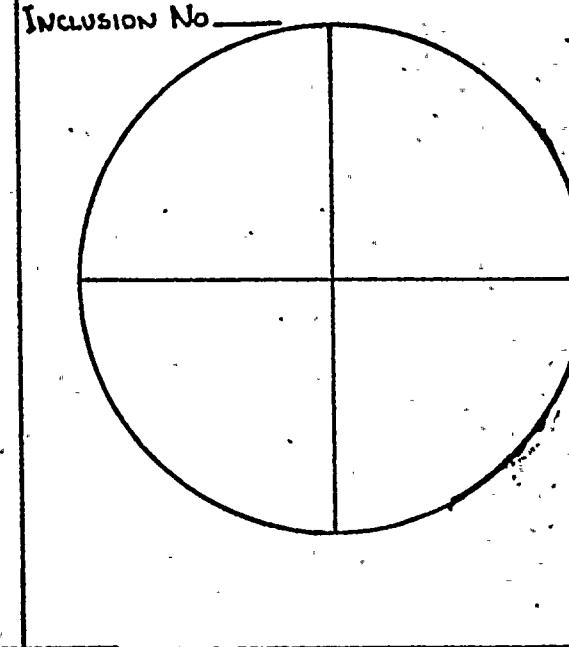
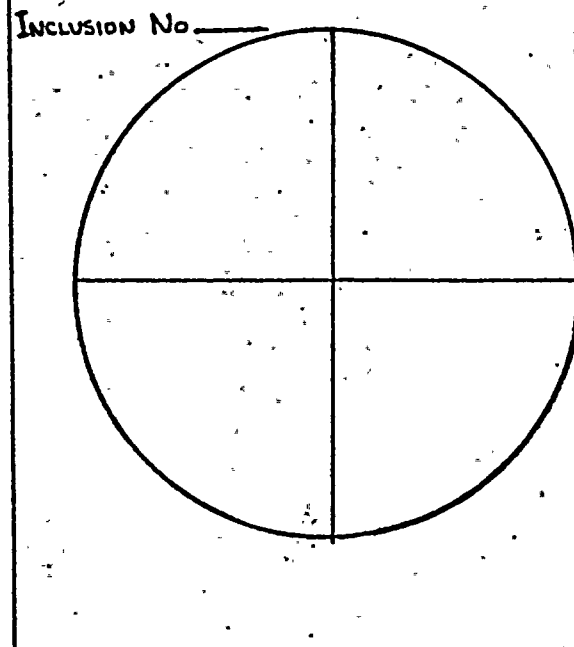
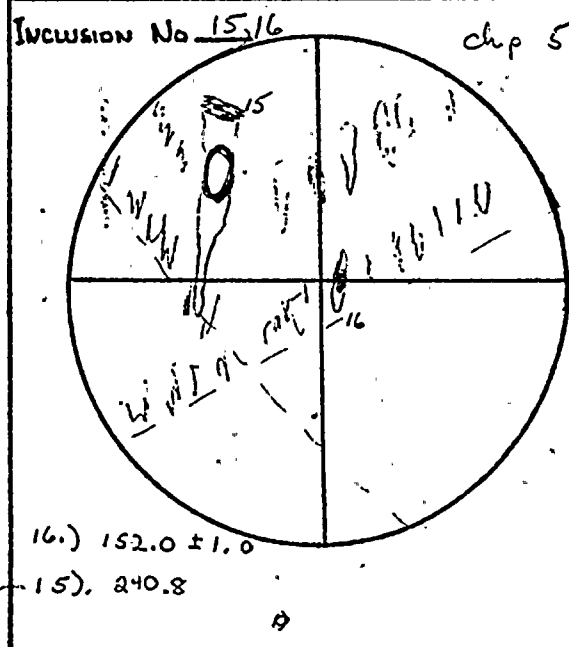
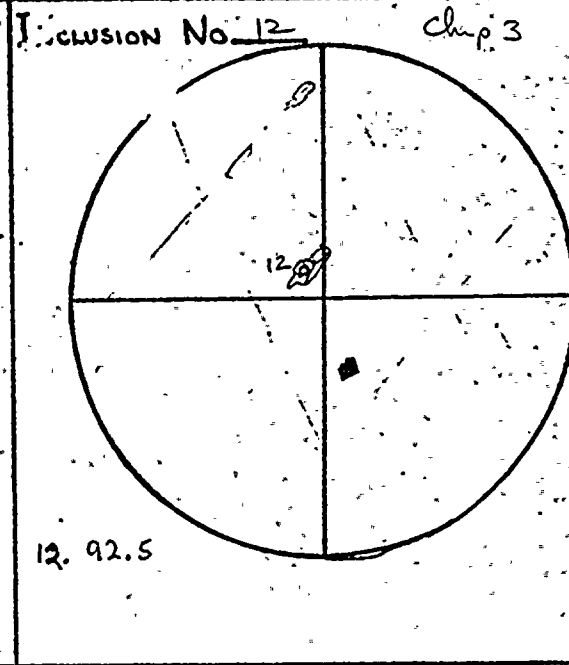
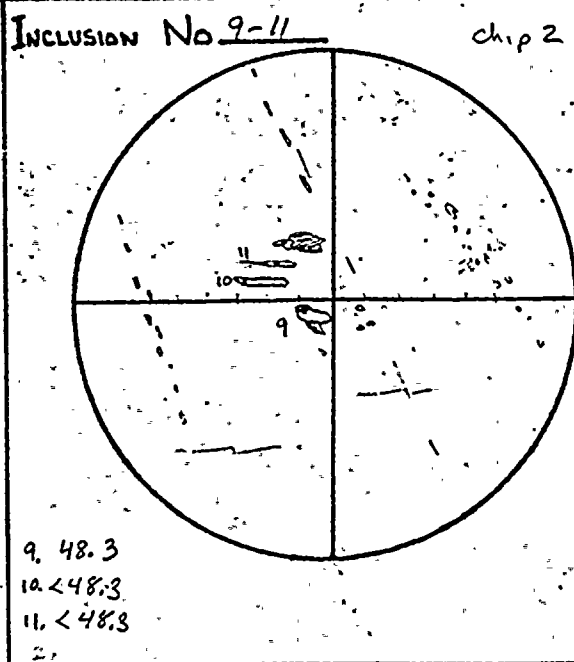
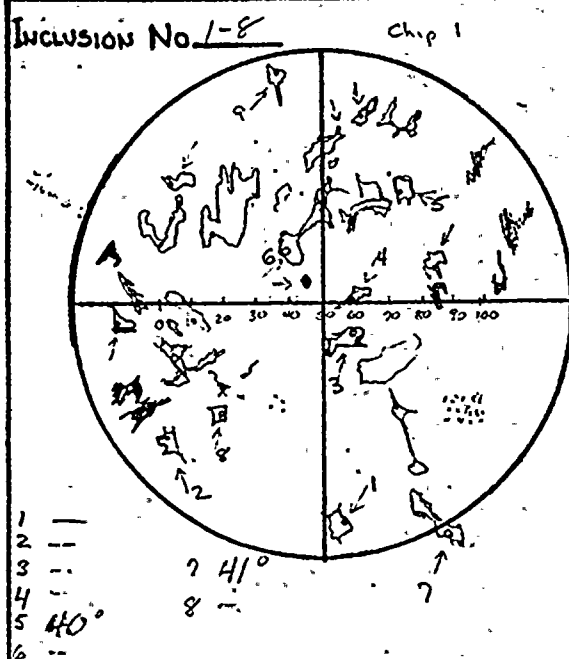


ANALYST: R J Bodnar
J B MURROWCHICK
SAMPLE NO. GAS-4

FLUID INCLUSION SKETCHES

CHIP NO.

MINERAL: Calcite (clear) clast
Clear Calcite w/ Elongate Inclusions



All others around this inclusion leaked at ~150-200°C. This temperature is probably too high.

Photo 13: GA5-4. Inclusion 3. Field of view =
170 x 116 μm , in transmitted light.

Photo 14: GA5-4. Inclusions 4 and 6. Field of
view = 170 x 116 μm , in transmitted
light.

Photo 15: GA5-4. Inclusion 5. Field of view =
170 x 116 μm , in transmitted light.

Photo 16: GA5-4. Inclusion 7. Field of view =
170 x 116 μm , in transmitted light.



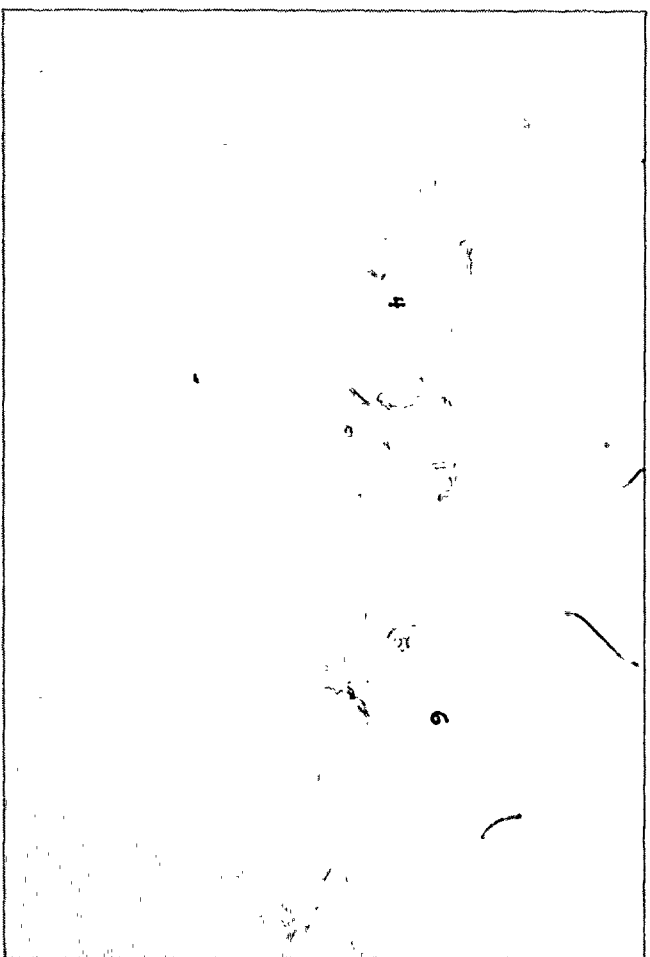
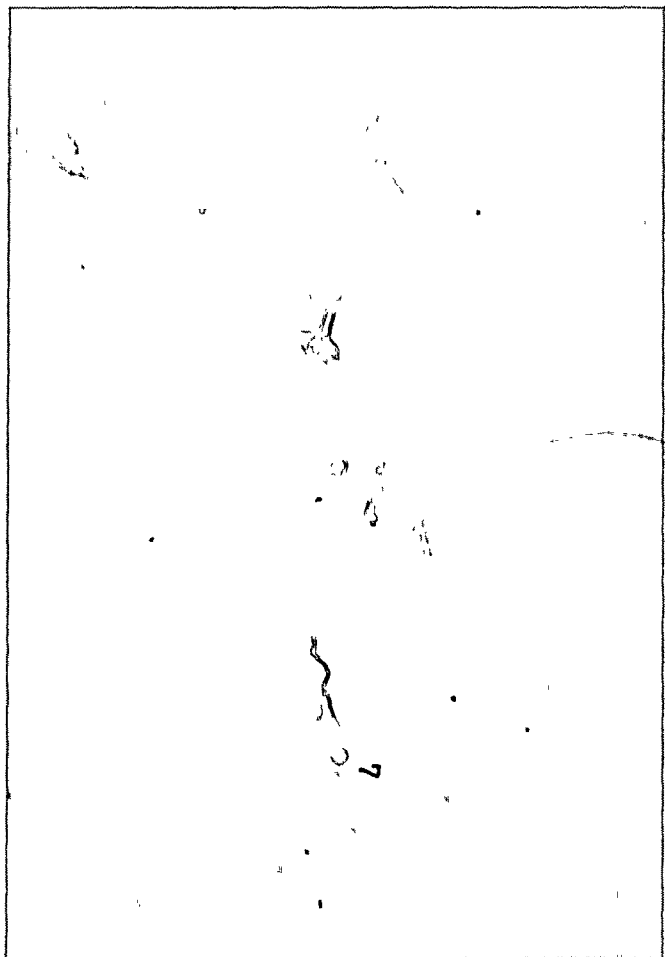
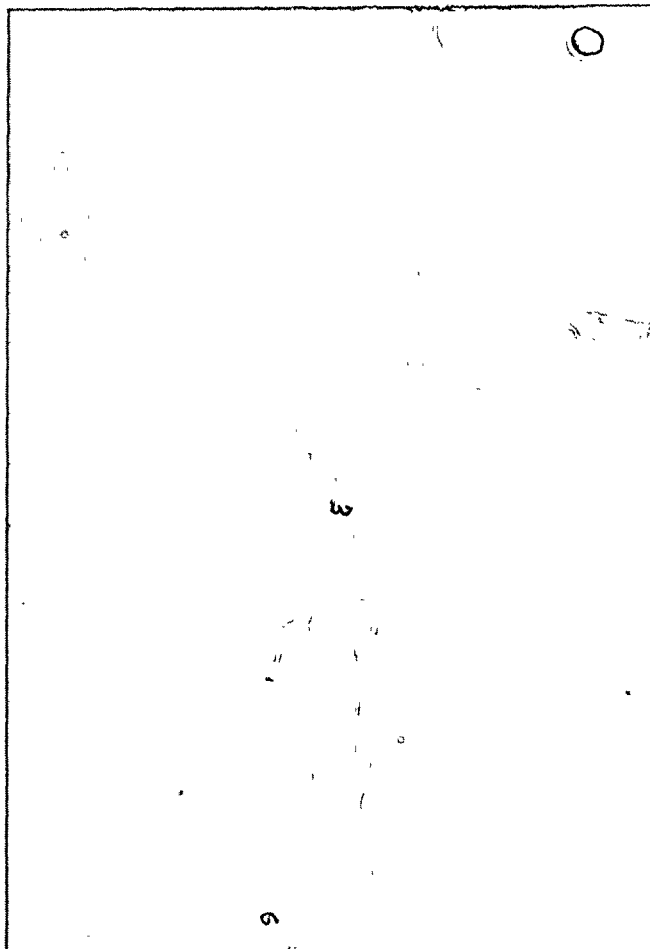
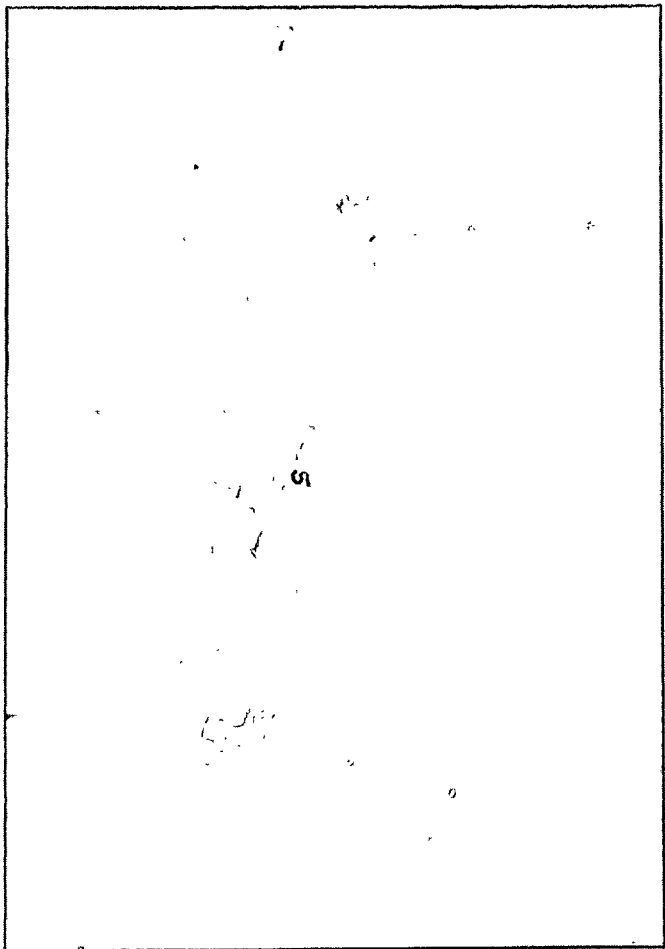




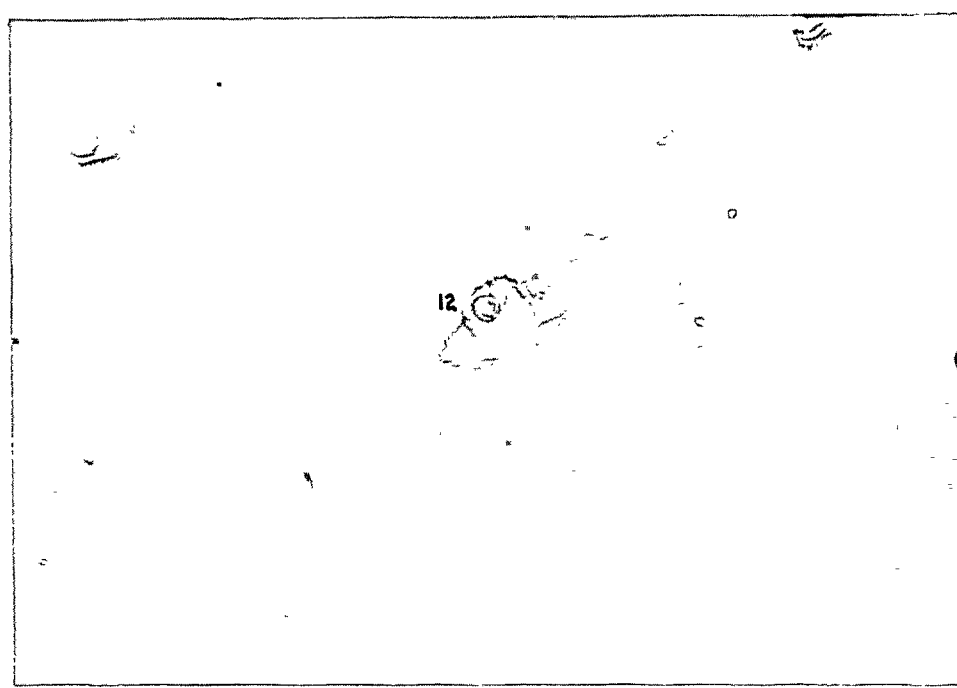
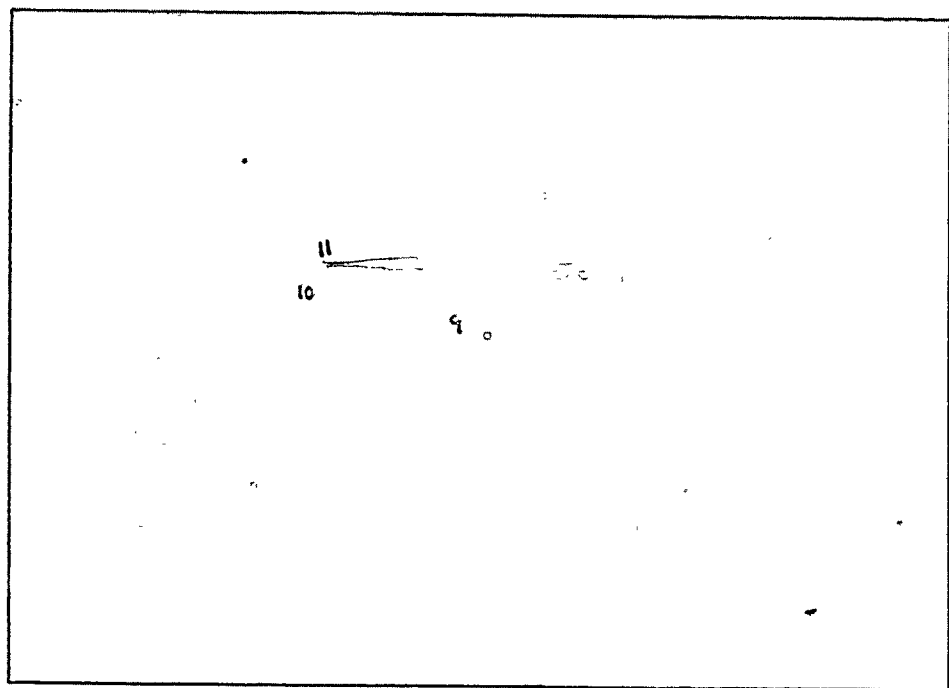
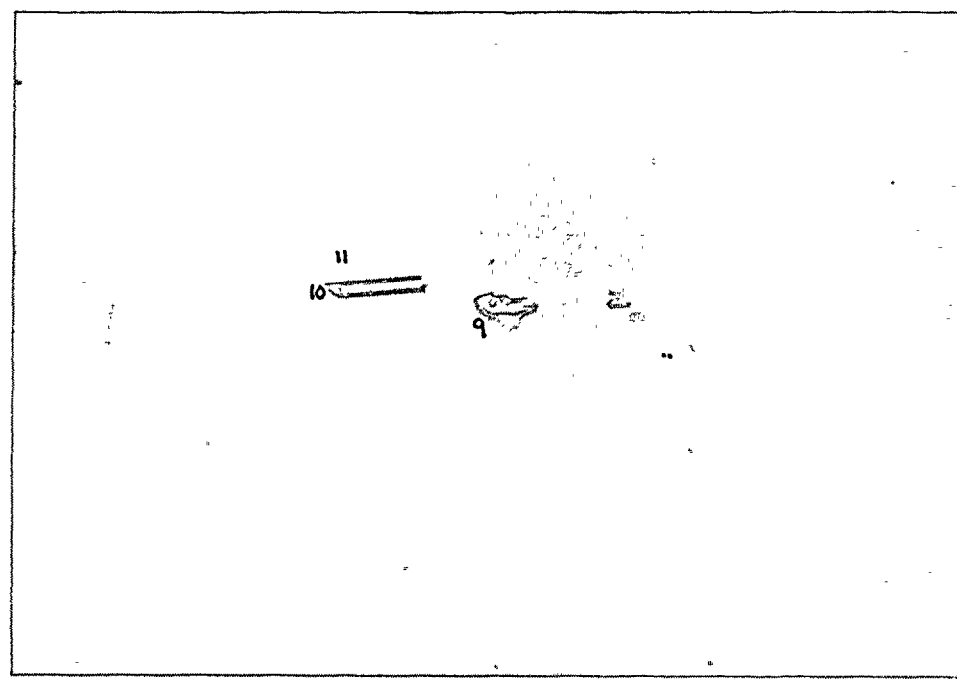
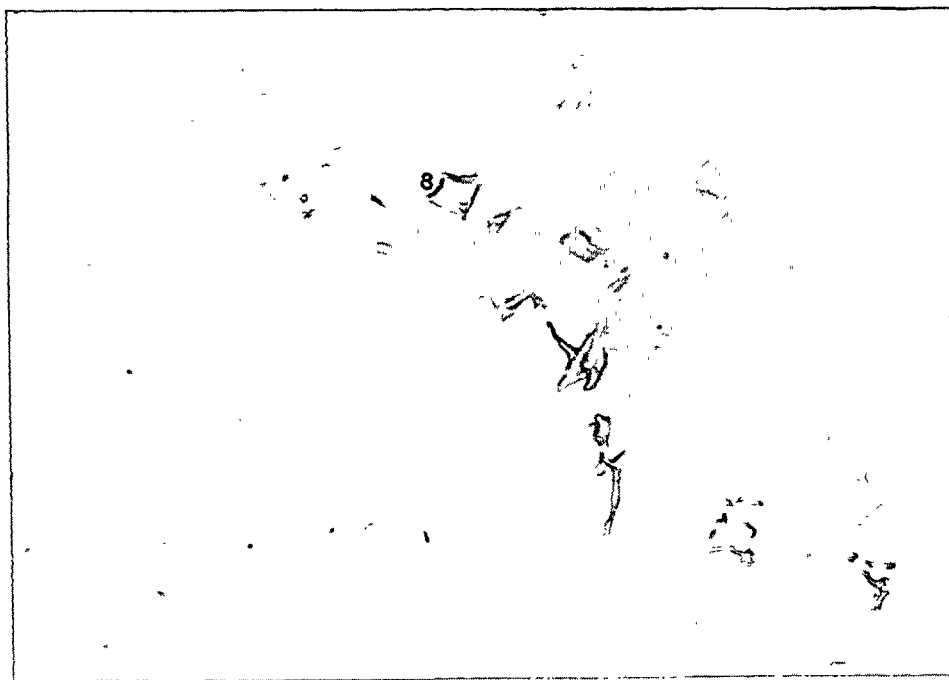
Photo 17: GA5-4. Inclusion 8. Field of view =
170 x 116 μm , in transmitted light.

Photo 18: GA5-4. Inclusions 9 and 10.
Field of view = 170 x 116 μm ,
in transmitted light.

Photo 19: GA5-4. Inclusion 11. Field of
view = 170 x 116 μm , in trans-
mitted light.

Photo 20: GA5-4. Inclusion 12. Field of
view = 170 x 116 μm , in transmitted
light.







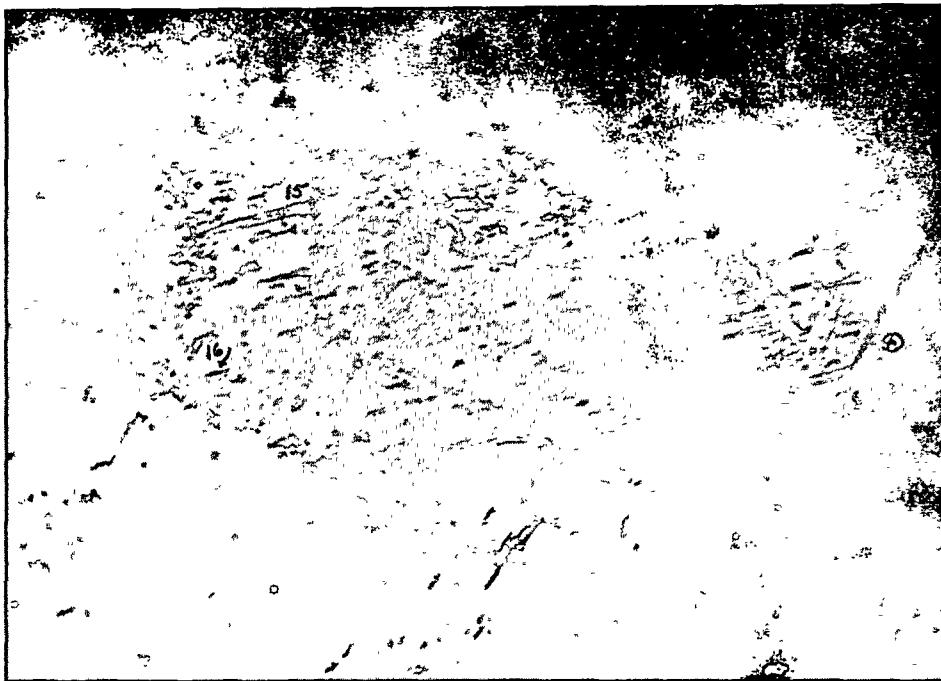


Photo 21: GA5-4. Inclusions 15 and 16. Note that many of these inclusions have a foreign object at their broad end. Field of view = $683 \times 461 \mu\text{m}$, in transmitted light.



Sample GA5-6

Calcite in sample GA5-6 occurs as irregular patches up to 1 x 2 cm on the surface of the sandstone block (photo 22). These patches are composed of nearly equant crystals less than one millimeter in diameter (visible at the lower end of the patch in photo 23 and in photo 24). The calcite shows twinning (D_4) and open cleavage (D_5) and the patches often are slickensided (D_5). The calcite contains various types of fluid inclusions typical of the clear calcite. Temperatures were not obtained because most of the inclusions were unsuitable for observation due to poor visibility, size, or leakage. Under UV, the fluorescence is dark red typical of the clear calcite. On the basis of these characteristics, we have identified this calcite as clear calcite.

It may be useful to point out that the clear calcite has been identified in three modes: coarse, clean, unbrecciated vein fillings in their original positions; clean, crushed calcite in place (such as on this sample); and clasts of clear calcite incorporated into a breccia.

Paragenesis:

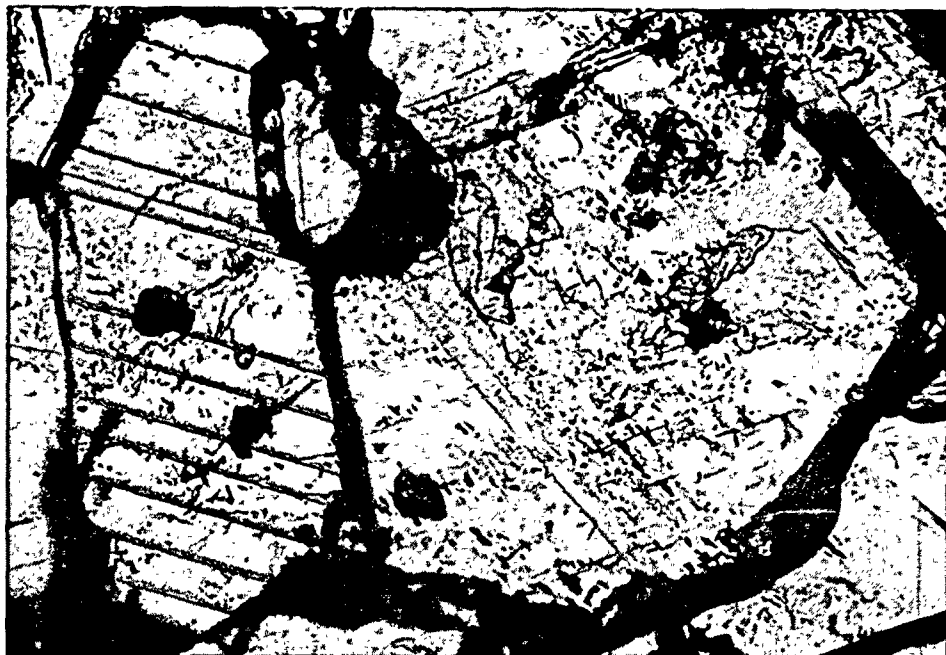
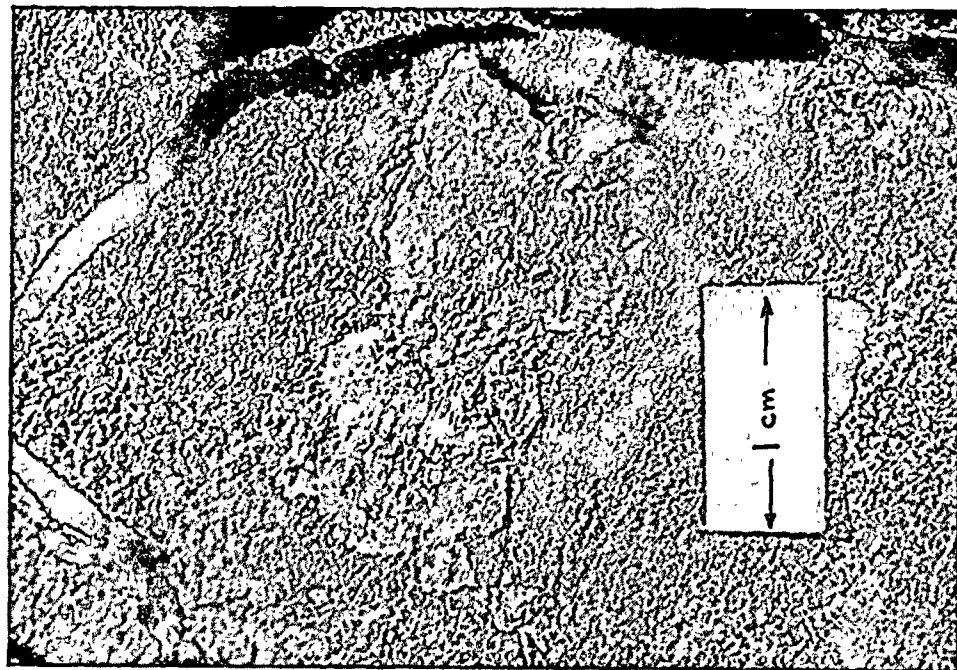
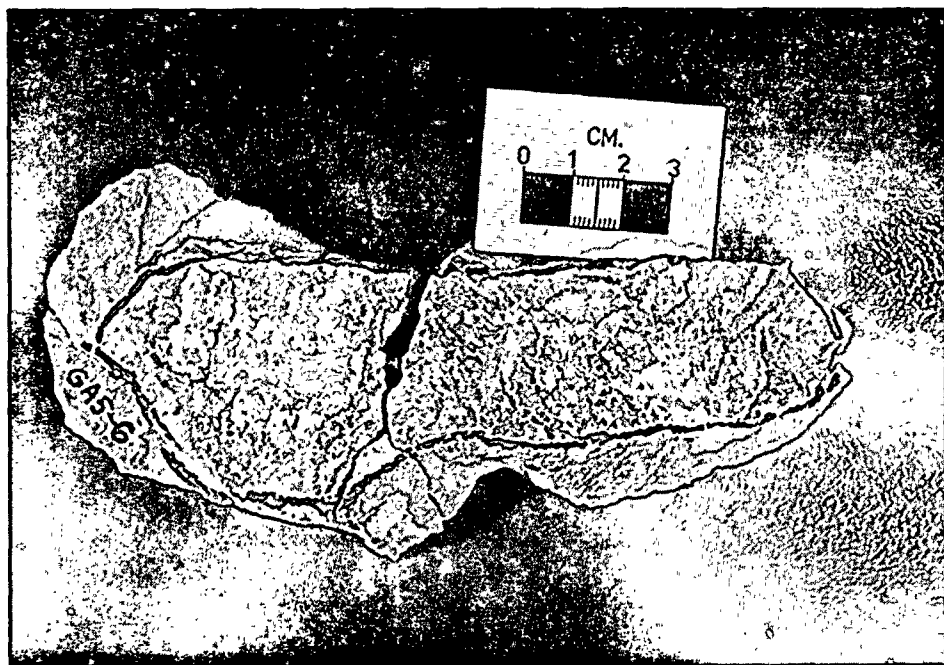
Clear calcite	_____	
Deformation	$\overline{D_4}$	$\overline{D_5}$



Photo 22: GA5-6. Whole sample with patches of deformed, but in place clear calcite.

Photo 23: GA5-6. Close-up of deformed clear calcite. Individual crystals can be seen at the lower end of the patch.

Photo 24: GA5-6. Twinned clear calcite from the patch in photo 23. Field of view = 1.37 mm x 0.93 mm, in transmitted light.





Sample GA5-7

A thick patch of breccia on the N53E trending face of this sample (photo 25) provided ample material for polished sections. This breccia is typical of the breccias examined in other samples but it also contains fragments of a dark gray siltstone (visible on the upper surface in photo 25) in addition to the sandstone and calcite clasts.

As in the other samples, the calcite clasts are composed of clear calcite (photo 26) and clear calcite with elongate inclusions (photo 27). Most of the inclusions are secondary single phase inclusions, but inclusions 13 and 14 (photos 28 and 29) appear to be parts of a large primary inclusion that was cut by a fracture during one of the earlier periods of deformation and was "reset" to the temperature at that time. Inclusion 13 homogenized at 118°C but inclusion 14 homogenized at 252°C. Either inclusion 14 leaked or it contained a bubble when the original inclusion was fractured then resealed, resulting in a high homogenization temperature. The 118°C for inclusion 13 (the temperature at which it was fractured) is near the 105°C temperature assigned to D₄ (October, 1977 report on JT series of samples).

The breccia also contains several iron sulfide minerals. Euhedral mackinawite (photos 30 and 31) and pyrrhotite (photo 32) appear to have grown soon after brecciation but before type 3 calcite cementation. Both the mackinawite and pyrrhotite can be found with rims of pyrite (photos 30 and 33, respectively), and in several instances, the pyrite is replacing the mackinawite (photo 34). Mackinawite's upper thermal stability limit



is not precisely known, but is in the range of 145-155°C (pressure corrected), indicating that brecciation occurred at or below these temperatures.

Paragenesis:

Clear calcite

Clear cal. with elong. inclusions

Pyrrhotite

Mackinawite

Pyrite

Type 3 calcite

Deformation

\overline{D}_4 \overline{D}_5



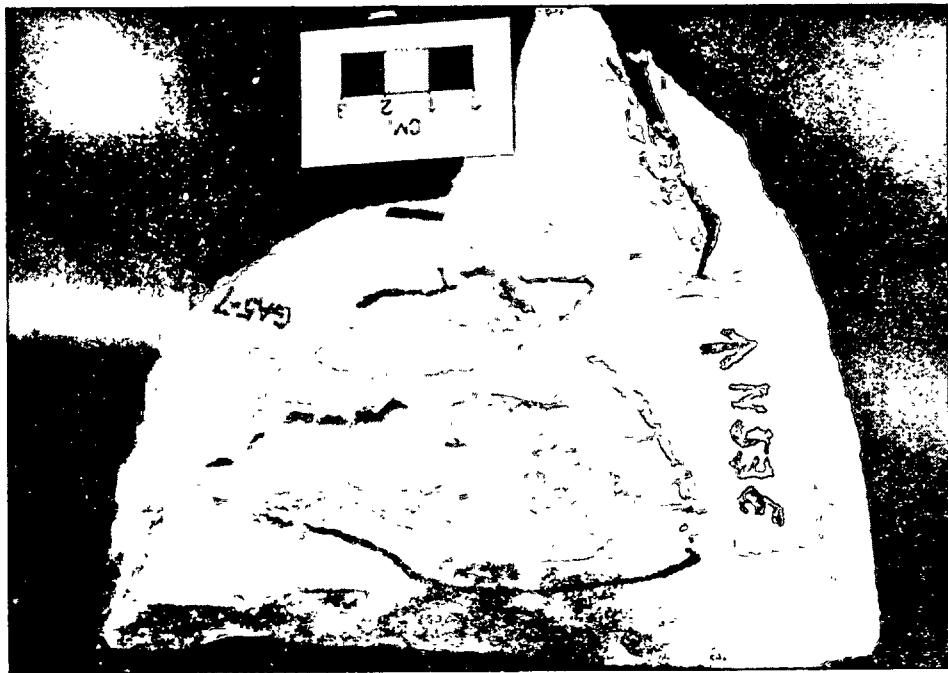
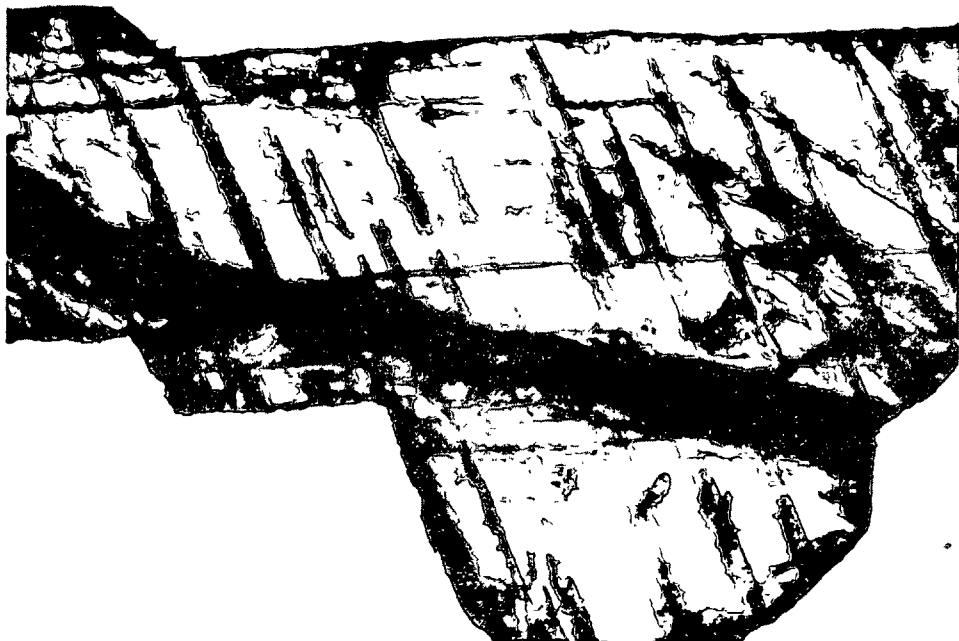
Photo 25: GA5-7. Whole sample showing N53E trending face with a breccia patch. The top surface of the sample is a dark gray siltstone while the rest of the sample is a fine-grained sandstone.

Photo 26: GA5-7. Breccia filling a fracture in previously deformed clear calcite. Inclusions 13 and 14 are from this chip. Field of view = 2.74×1.88 mm, in transmitted light.

Photo 27: GA5-7. Elongate inclusions originating on the surface of a clear calcite grain. Field of view = 340×230 μ m, in transmitted light.

Photo 28: GA5-7. Inclusion 13. The short arrow indicates a bubble. Long arrows indicate a healed fracture that split the original inclusion into two smaller inclusions. Field of view = 340×230 μ m, in transmitted light.





ANALYST: RJ Bodnar

FLUID INCLUSION SKETCHES

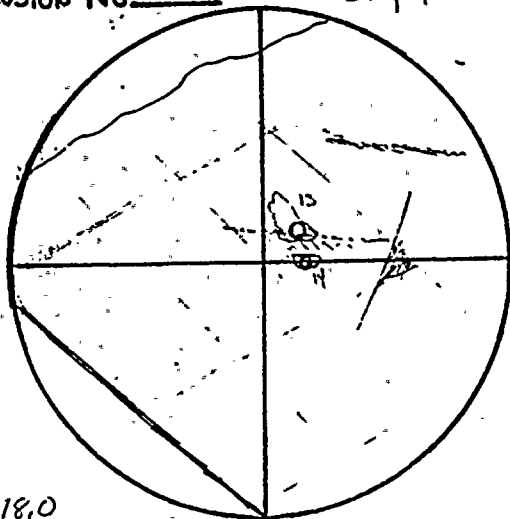
SAMPLE NO. GAS-7

CHIP NO. _____

MINERAL: clear calcite clast

Inclusion No. 13-14

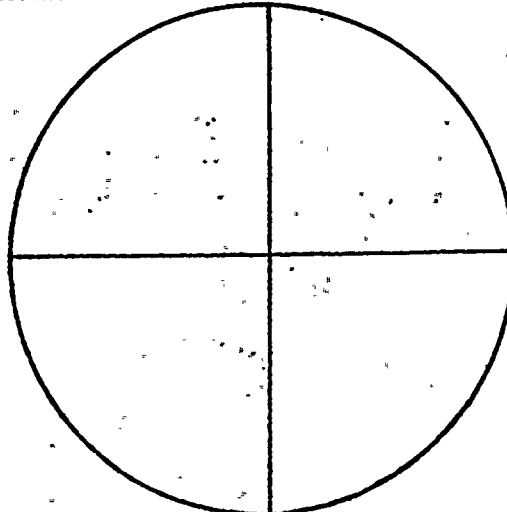
chip 4



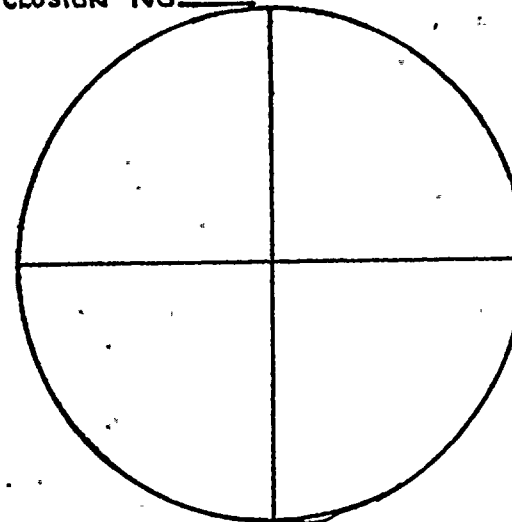
@ 118.0

14 | 252.1

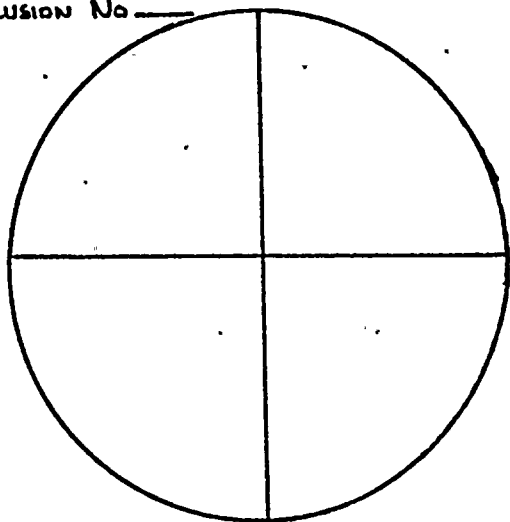
Inclusion No. _____



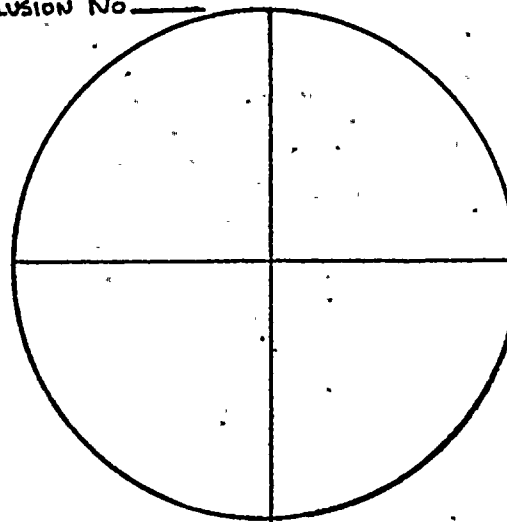
Inclusion No. _____



Inclusion No. _____



Inclusion No. _____



Inclusion No. _____

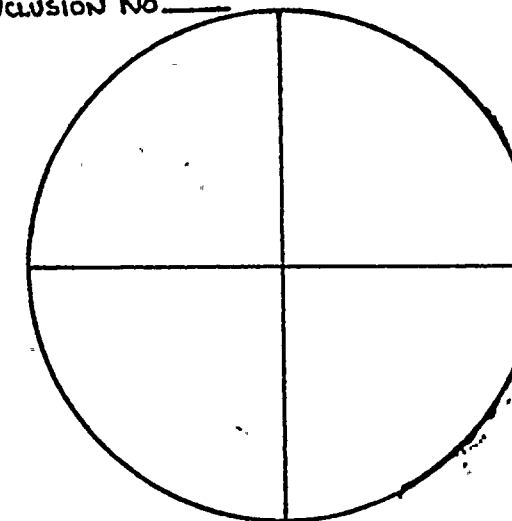


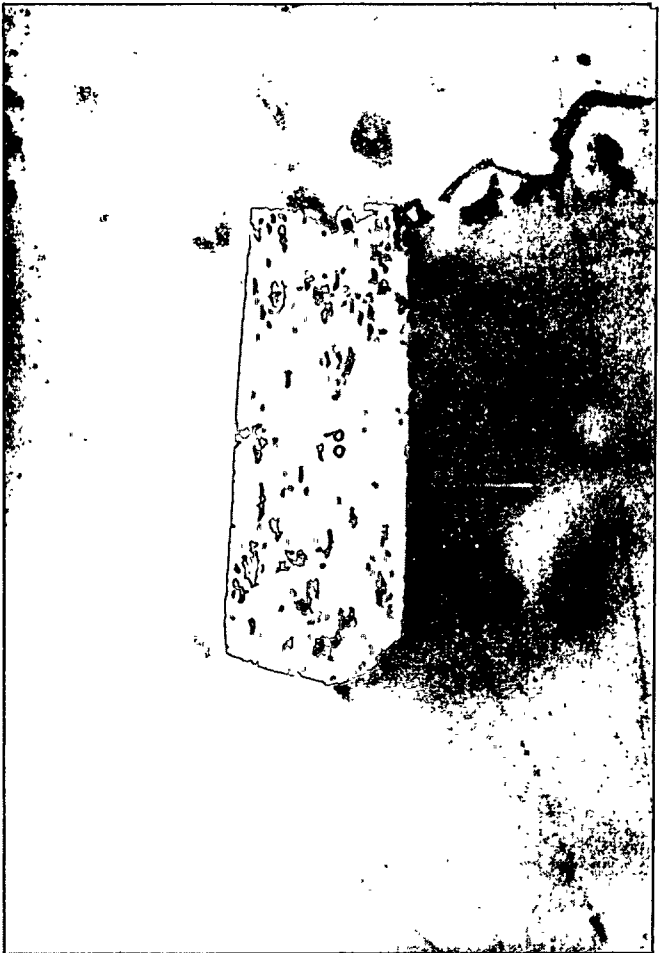
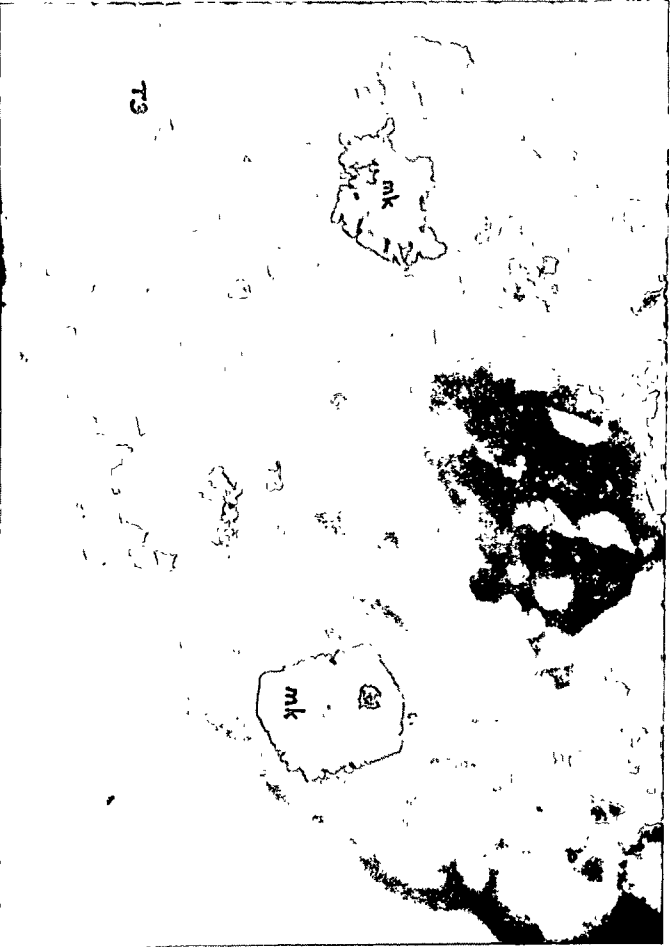
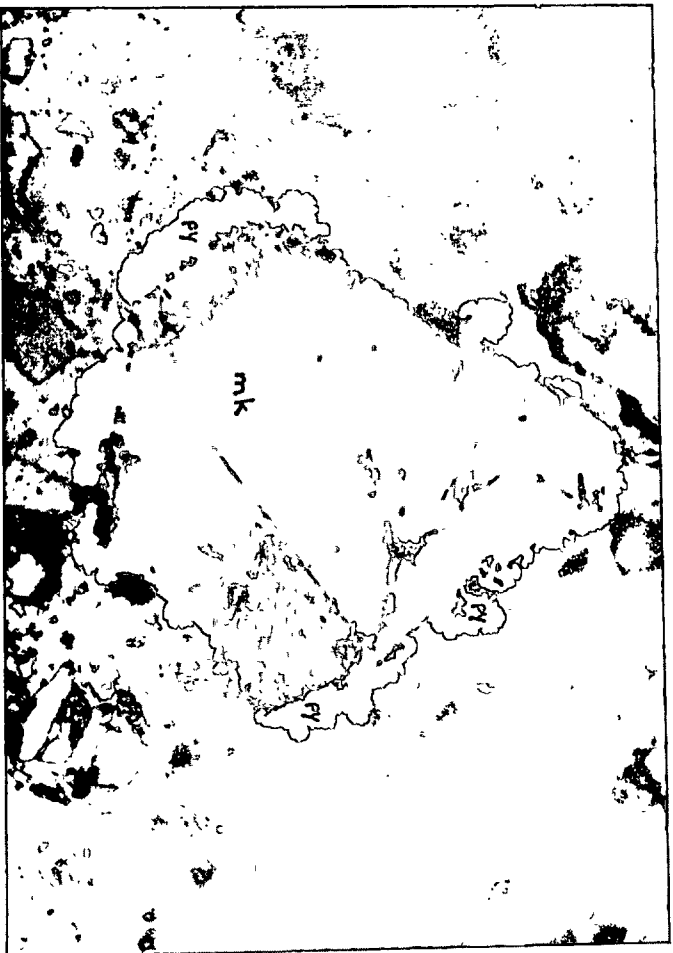
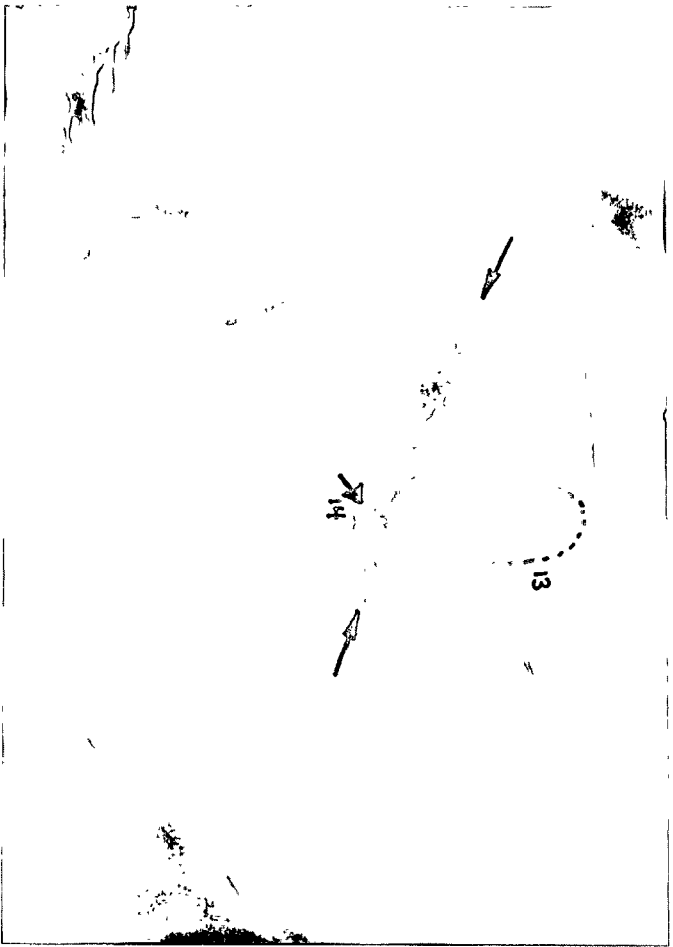
Photo 29: GA5-7. Inclusion 14. The short arrow indicates a bubble. Long arrows indicate a healed fracture. The outline of inclusion 13 is dotted. Field of view = $340 \times 230 \mu\text{m}$, in transmitted light.

Photo 30: GA5-7. Subhedral mackinawite (mk) crystal with an overgrowth of pyrite (py). The host material is a breccia containing quartz fragments (Q) in a type 3 calcite cement. Field of view = $340 \times 230 \mu\text{m}$, in reflected light.

Photo 31: GA5-7. Mackinawite crystals in a breccia containing quartz fragments (Q) in type 3 calcite (T3). Field of view = $683 \times 461 \mu\text{m}$, in reflected light.

Photo 32: GA5-7. An euhedral pyrrhotite crystal (po) in type 3 calcite. Note the low number of clastic fragments in the field even though this is in the breccia. Field of view = $340 \times 230 \mu\text{m}$, in reflected light.







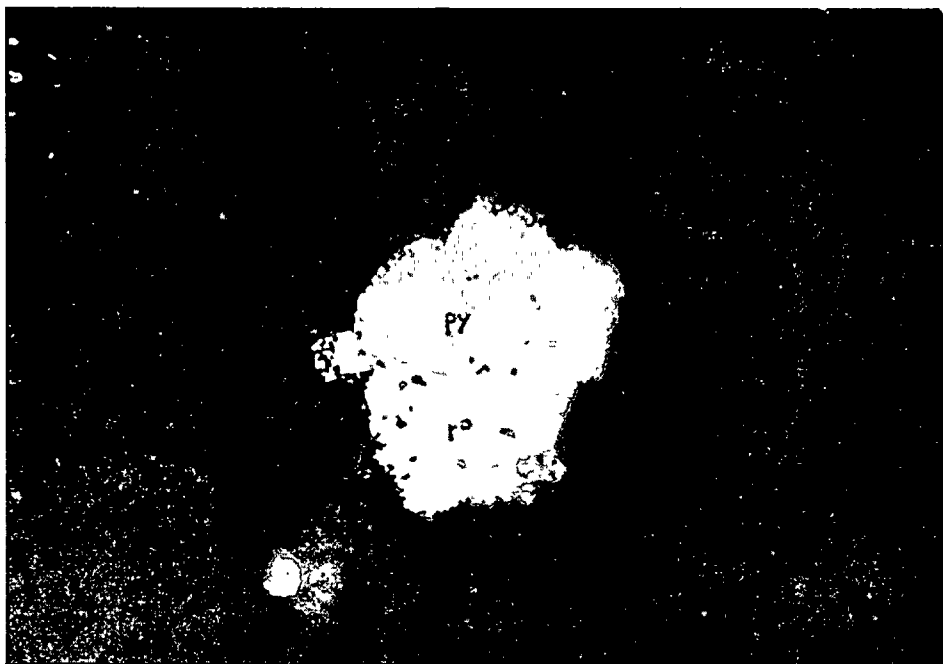


Photo 33: GA5-7. Pyrrhotite (po) surrounded by pyrite (py) in the breccia. Field of view = $137 \times 94 \mu\text{m}$, in reflected light.

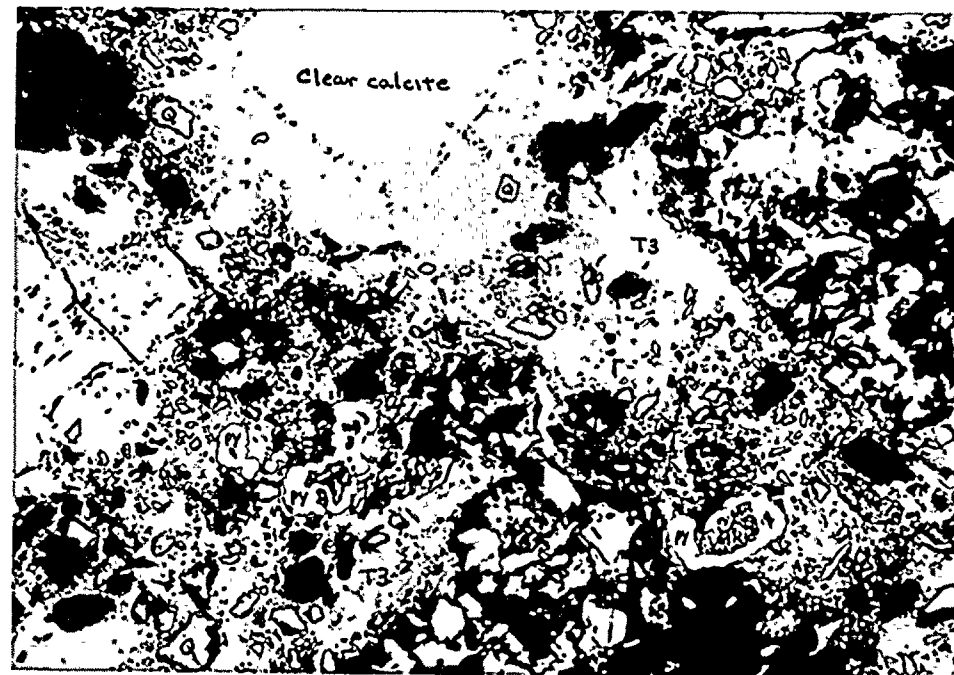


Photo 34: GA5-7. Irregular pyrite coatings (py) replacing mackinawite (mk) cores. Quartz grains (Q) are also present. Field of view = $1.37 \times 0.93 \text{ mm}$, in reflected light.

Part II

Fluorescence of Calcites

The following photographs illustrate the responses to ultraviolet light-induced fluorescence observed for six of the seven types of calcite identified from all samples examined from the Nine Mile Point region. The eighth type, the brown calcite, does not fluoresce. The photographs were taken using a Nikon epifluorescence unit with UV excitation filter and Nikon photomicrographic equipment. All exposure times were automatically controlled and ranged up to 12 minutes in length. Kodacolor II film (ASA 100) was used but due to the long exposure times, exposure corrections were made in accordance with the instructions enclosed with the film in order to approximate the observed, true colors.

The photographs are fairly accurate in color rendition but some color shifts have occurred due to the long exposure times and due to color biasing by the automated color printer. The shifts are not large, being most noticeable in photo A-2 which has an overall greenish cast making the actual red look brownish. Some of the fluorescence colors are very subtle and are more easily seen first-hand than recorded on film. The blues in photo A-8 and the red of the type 3 calcite in photo A-13 illustrate this observation.



Photo A-1: Milky calcite in transmitted light. The field of view is $685 \times 468 \mu\text{m}$. (PSU sample C-3C.)

Photo A-2: Milky calcite fluorescing. This is the same field of view as photo A-1. The entire field is filled with milky calcite which is fluorescing to various degrees (note calcite at the top and right sides). The light blue patches are impurities that were emplaced in cracks and holes during sample preparation.

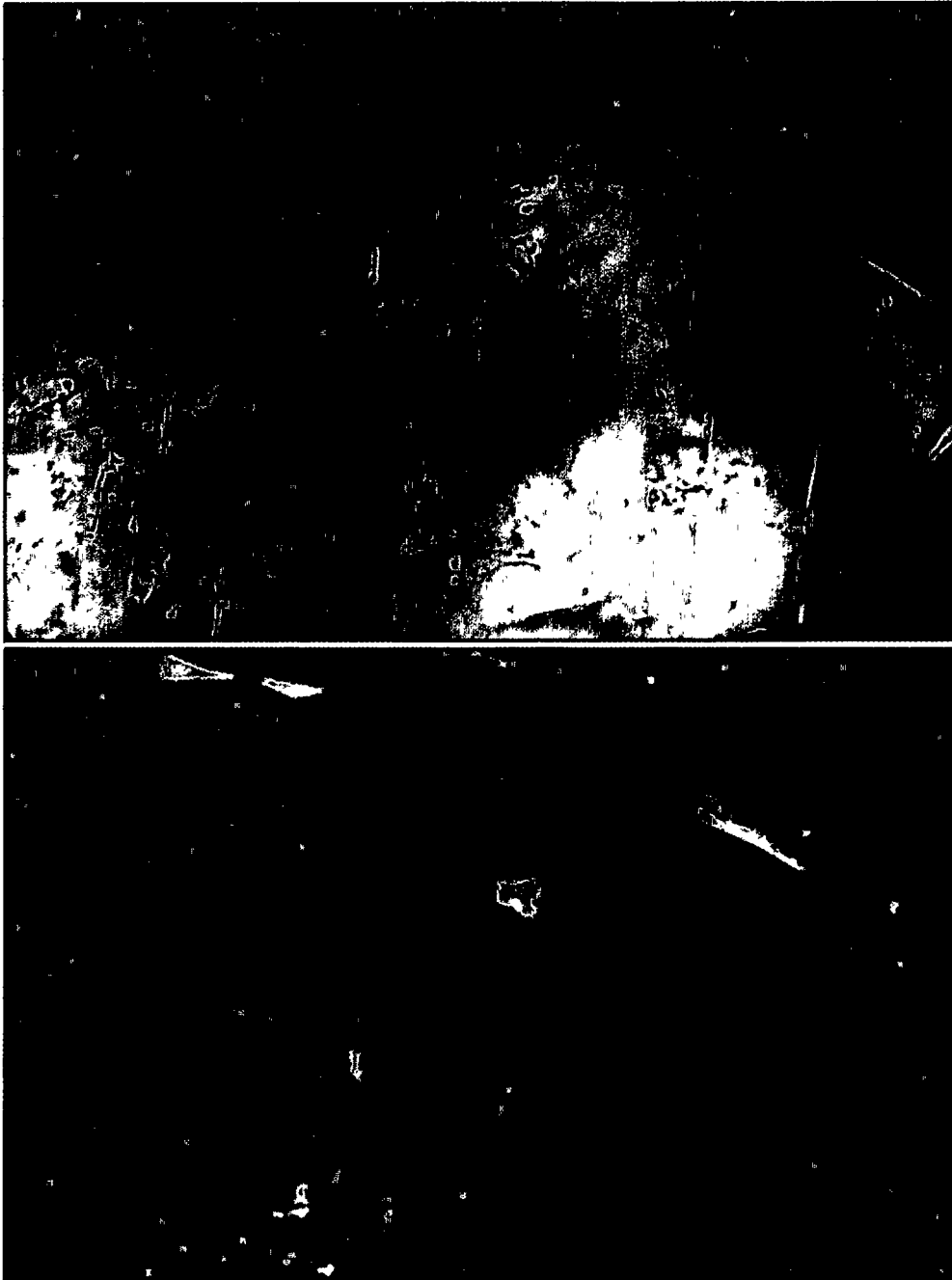


Photo A-3: Clear calcite and clear calcite with elongate inclusions in transmitted light. The field of view is 685 x 468 μm . (Dames and Moore sample GA5-4.)

Photo A-4: Clear calcite (red) and clear calcite with elongate inclusions (blue) fluorescing. The field of view is the same as above in photo A-3. The blue area at the center bottom of the photograph is caused by flare from a film of glue on the surface just below the field of view.

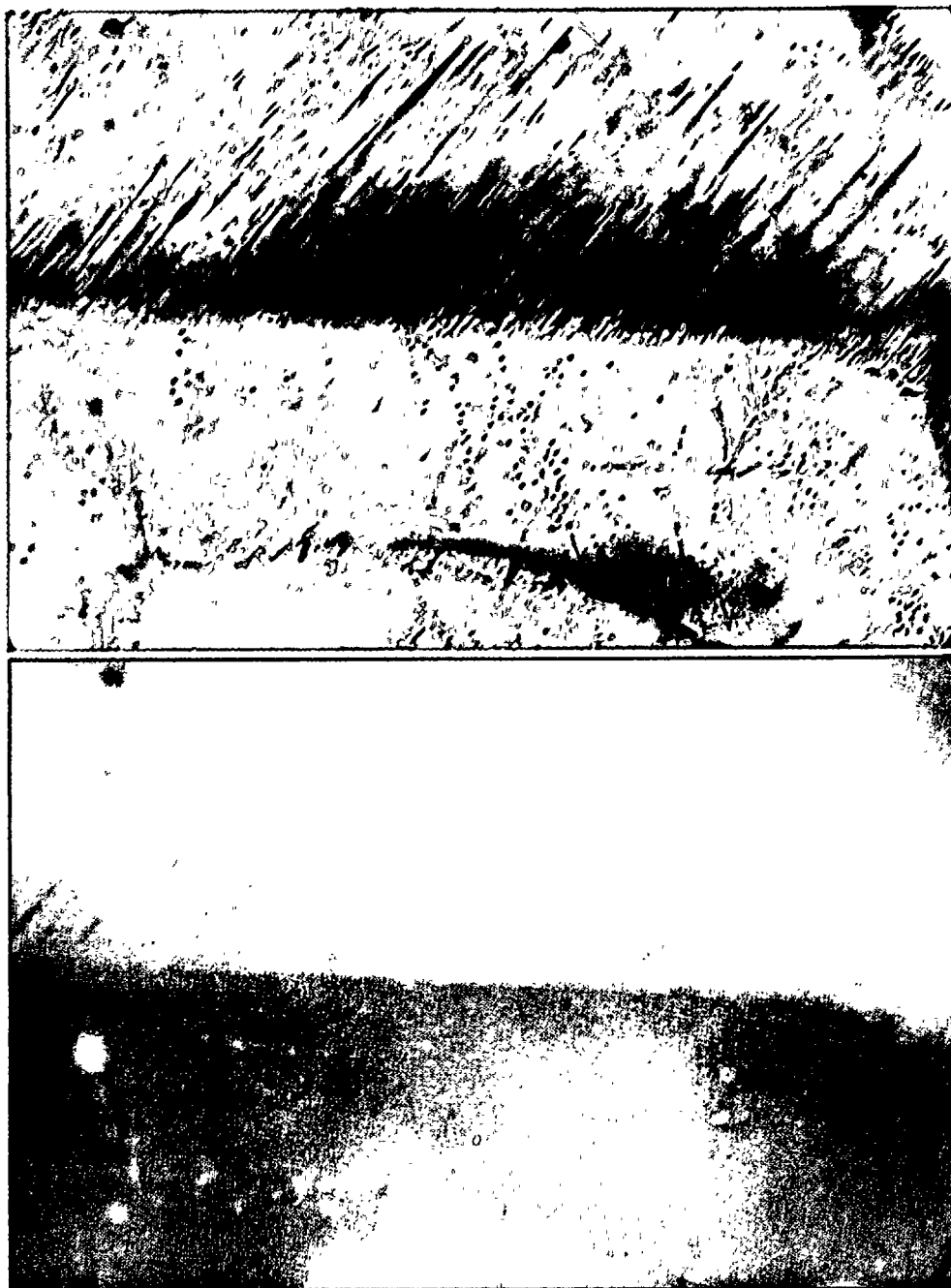




Photo A-5: Clear calcite with goethite in transmitted light. The brownish areas contain goethite needles. The field of view is 2.74 mm x 1.88 mm. (PSU sample C-3C.)

Photo A-6: Clear calcite with goethite-rich area fluorescing. Goethite does not fluoresce but the needles appear to be coated with a yellow-fluorescing organic material. The fluorescence of this material drowns out the blue fluorescence of the calcite, some of which is visible at the center bottom. (The light blue at the top is caused by glue on the surface.) The large yellow-fluorescing object may be a large piece of organic material. Similar objects have been found that appear to have a cellular structure. In transmitted light, these objects appear as thin brownish films and internal structures are not visible.

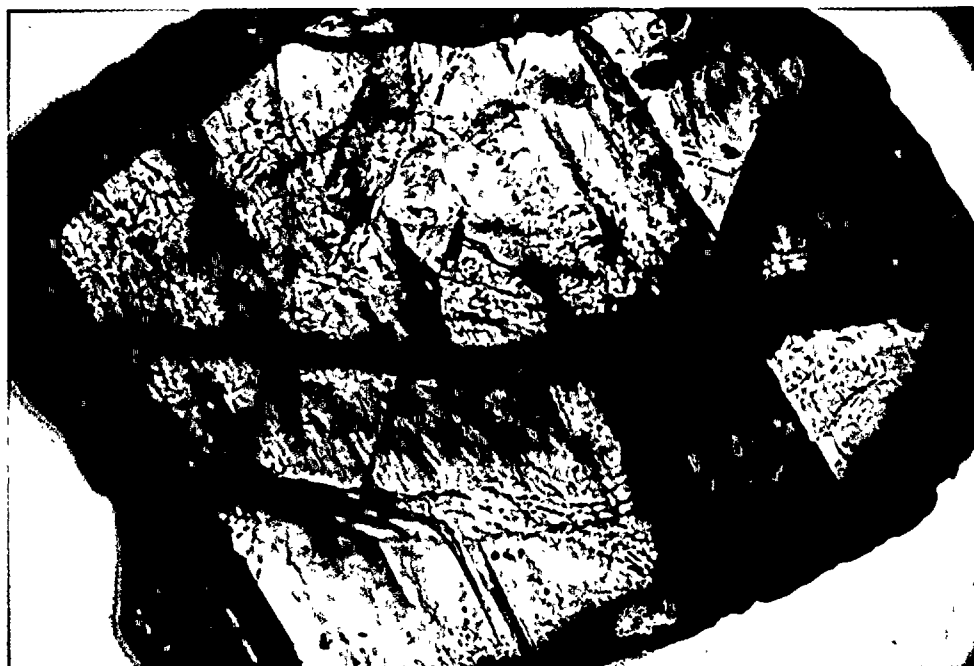




Photo A-7: Clear calcite with goethite in transmitted light. Field of view is 685 x 468 μm . (PSU sample C-3C.)

Photo A-8: Clear calcite with a goethite-rich area fluorescing. The characteristic fluorescence of the calcite is blue (upper left) but this is often invisible due to the strong yellow fluorescence of organic particles usually associated with the goethite. Note here that most of the goethite needles in this photograph are not fluorescing. Often, however, they are coated by a yellow-fluorescing substance. The field shown here is the same as above in photo A-7.

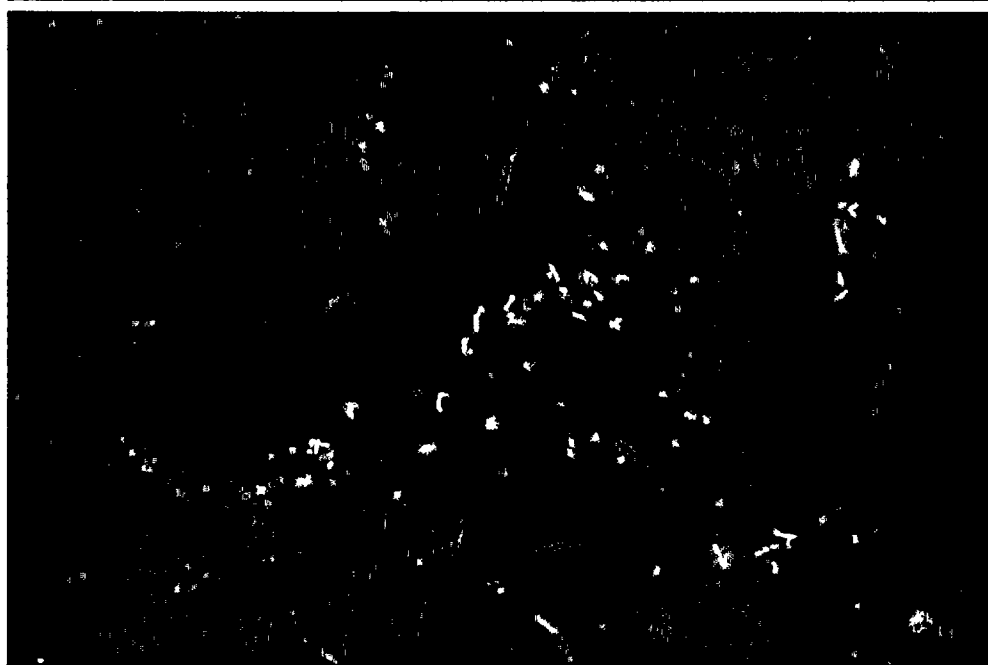
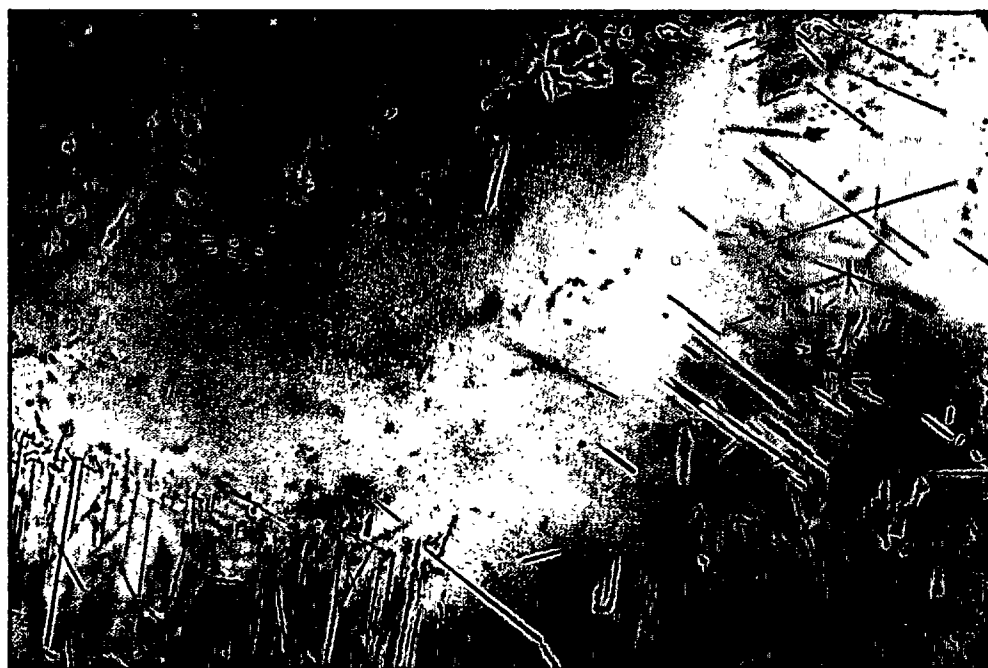


Photo A-9: Travertine with fracture-filling type 3 calcite in transmitted light. The field of view is 2.74 x 1.88 mm. (Dames and Moore sample GA4-4.)

Photo A-10: Travertine with type 3 calcite fluorescing. This is the same field as above in photo A-9. The travertine fluoresces a weak pale blue or not at all. The pale blue travertine fluorescence may be due to dispersion from the pale blue fluorescing type 3 calcite, which is filling fractures here.

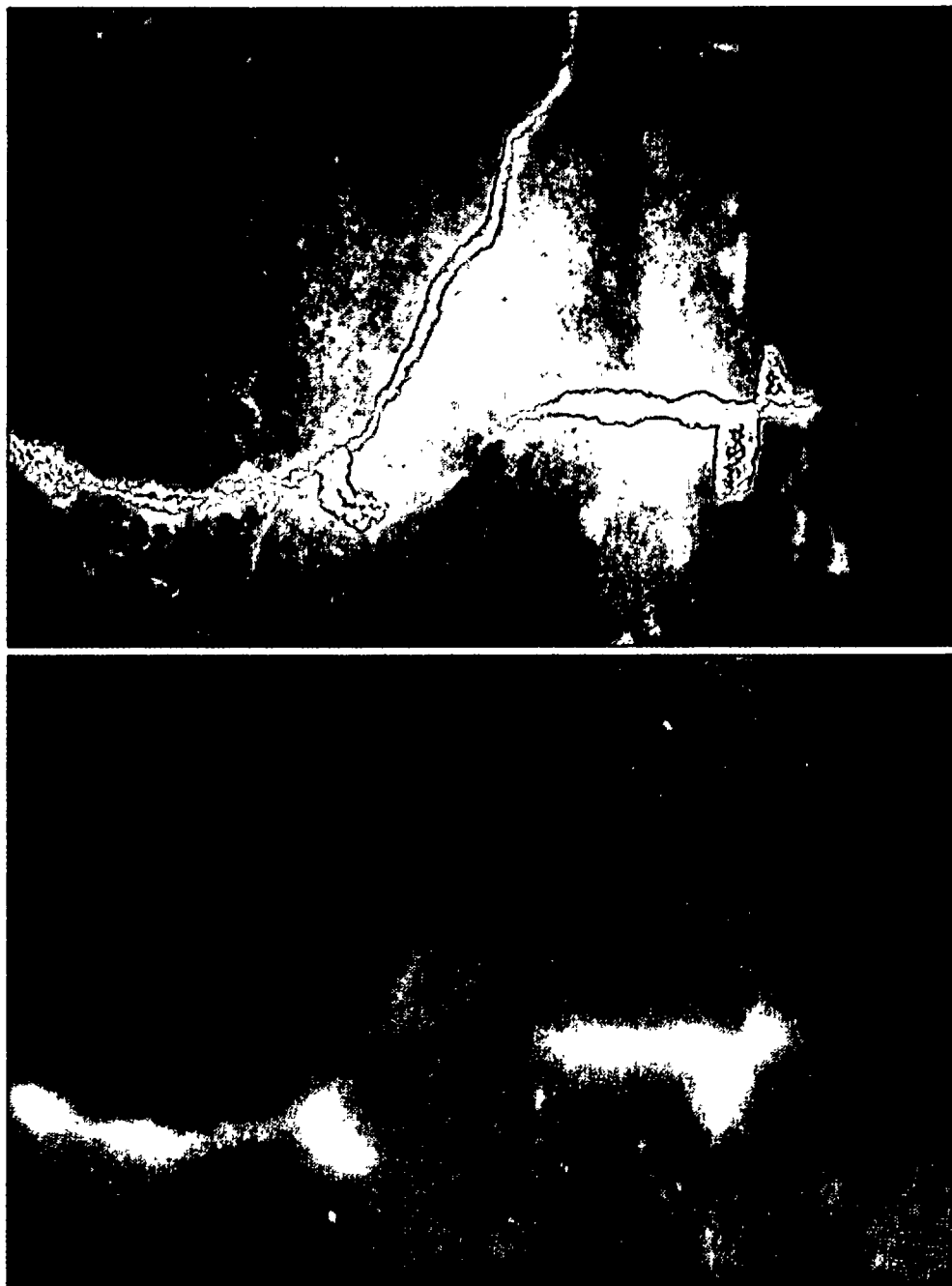
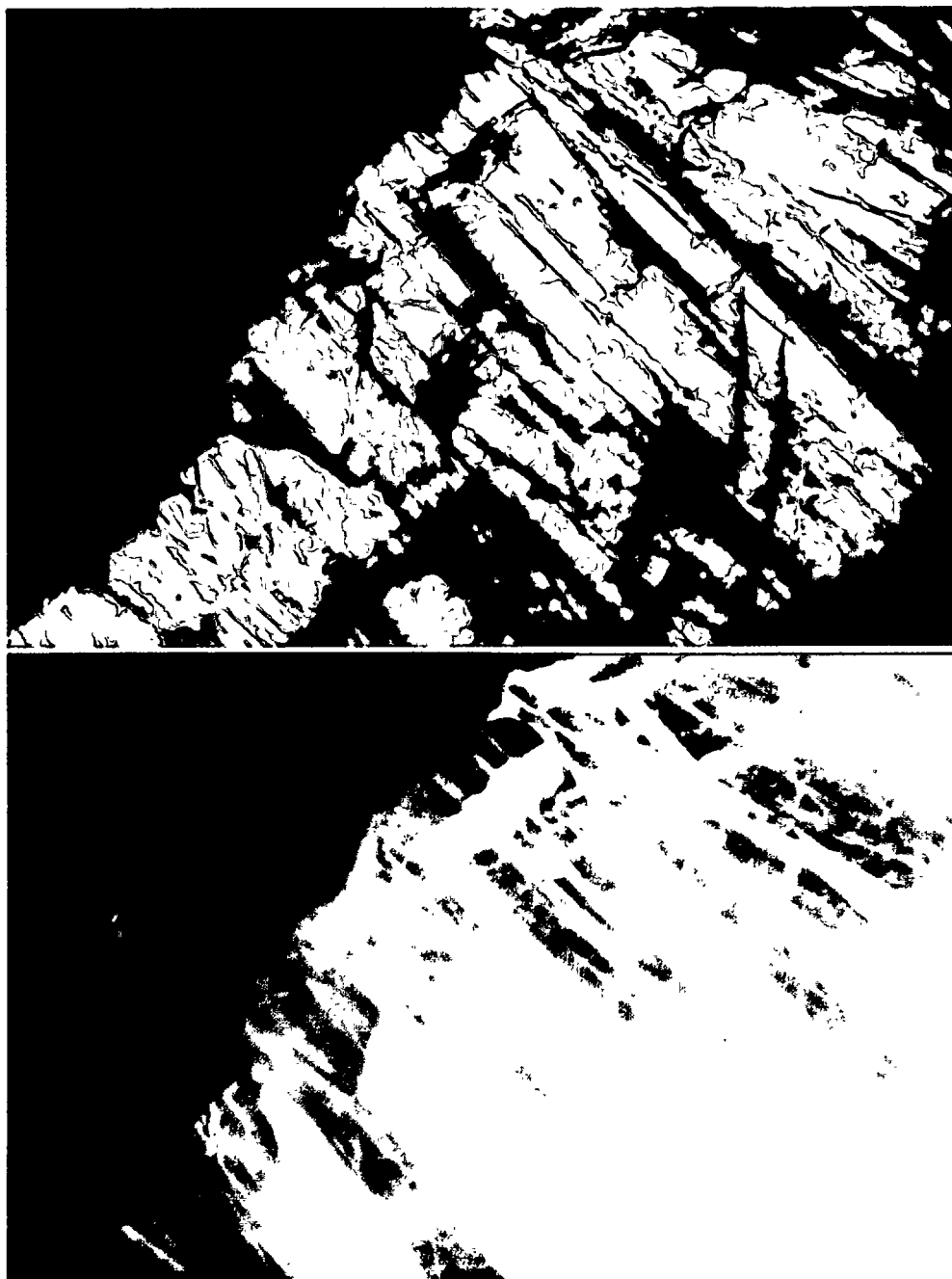




Photo A-11: Type 3 calcite in transmitted light. This is type 3 calcite free of foreign clasts. The field of view is 2.74 x 1.88 mm. (Dames and Moore sample GA4-11C.)

Photo A-12: Type 3 calcite fluorescing. This is the same field as photo A-11. This pale blue fluorescence is typical of type 3 calcite that has not been contaminated with fragments of milky calcites.



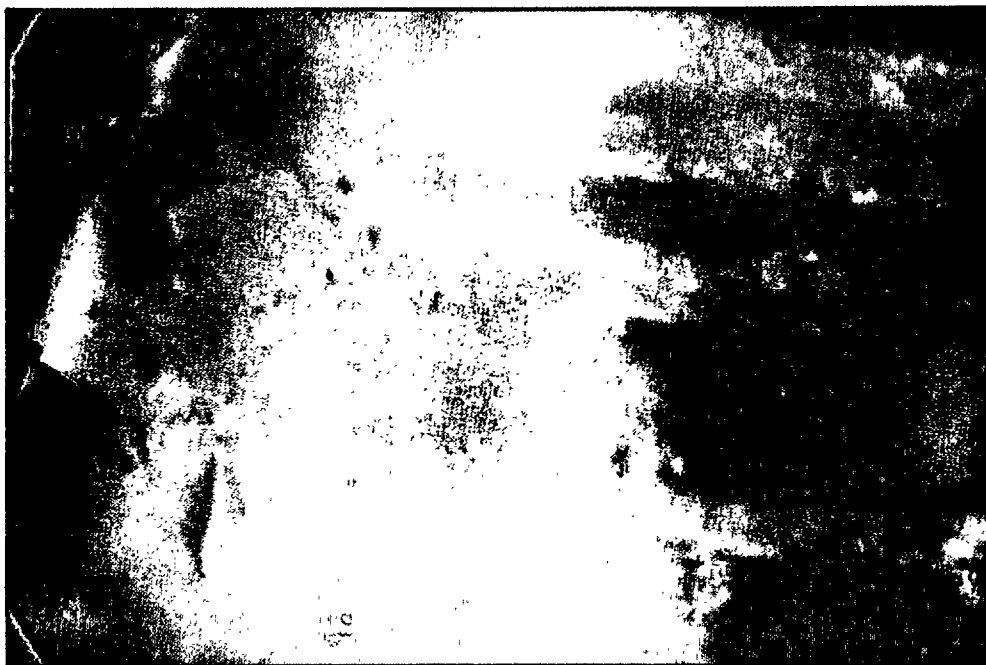
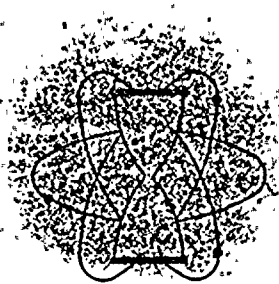


Photo A-13: Type 3 calcite with a clast of clear calcite. The type 3 calcite here has infiltrated along opened cleavage planes in the clear calcite clast and has been only slightly contaminated by the older material. The contaminated calcite has a slight reddish cast, visible in the center of the photograph. The field of view is $343 \times 232 \mu\text{m}$. (Dames and Moore sample GA5-4.)





KRUEGER ENTERPRISES, INC.

GEOCHRON LABORATORIES DIVISION

24 BLACKSTONE STREET • CAMBRIDGE, MASSACHUSETTS 02139 • (617) 876-3691

6 June 1977

Martha W. Pendleton
Dames & Moore
2996 Belgium Road
Baldwinsville, New York 11027

Dear Martha:

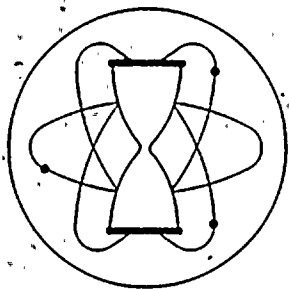
I am enclosing the final written reports and the invoice dealing with the two additional samples from the Niagara Mohawk Nine Mile II site which you sent us about 10 days ago, and the results of which I gave you on the phone last Friday.

I gathered from our discussion that the results would be of help in evaluating the chronology of the area. If you have further questions, please give me a call at your convenience. Meanwhile, I hope we can be of further service when you require this type of data again.

Sincerely,

Harold W. Krueger

HWK:hrn
encl.



KRUEGER ENTERPRISES, INC.

GEOCHRON LABORATORIES DIVISION

24 BLACKSTONE STREET • CAMBRIDGE, MA. 02139 • (617)-876-3691

RADIOCARBON AGE DETERMINATION

REPORT OF ANALYTICAL WORK

Our Sample No. **GX-4861**

Date Received: **31 May 1977**

Your Reference: **Telecom re Job 4707-025**

Date Reported: **3 June 1977**

Submitted by: **Martha W. Pendleton
Dames & Moore
2996 Belgium Road
Baldwinsville, New York 11027**

Sample Name: **Niagara Mohawk Nine Mile II site. Sample SL-10, marl from west wall of cooling tower trench. Shells.**

AGE = **12,545 \pm 330 C-14 years B.P. (C-13 corrected).**

Description: **Large sample of fresh water marl with dispersed small shells (at least 2 varieties of gastropods and 1 or more varieties of very small pelecypods).**

Pretreatment: **The marl was disaggregated in an ultrasonic cleaner and the gastropod and pelecypod shells were concentrated by sieving and hand sorting. The shells were then thoroughly washed in the ultrasonic cleaner to remove any residual marl fragments from their surfaces. They were then hydrolyzed with dilute HCl, under vacuum, to recover carbon dioxide for the analysis.**

Comment:

Uncorrected age was 12,260 C-14 years B.P.

The C-13 analysis indicates that the bog may have had significant contributions of old carbonate dissolving from local glacial tills. The age may thus be somewhat older than the true age of the marls.

$\delta C^{13}_{PDB} = -6.9$

‰

Notes: This date is based upon the Libby half life (5570 years) for C^{14} . The error stated is $\pm 1 \sigma$ as judged by the analytical data alone. Our modern standard is 95% of the activity of N.B.S. Oxalic Acid.

The age is referenced to the year A.D. 1950.





KRUEGER ENTERPRISES, INC.

GEOCHRON LABORATORIES DIVISION

24 BLACKSTONE STREET • CAMBRIDGE, MASSACHUSETTS 02139 • (617) 876-3691

14 March 1980

Scott Laird
Dames & Moore
2996 Belgium Road
Baldwinsville, NY 13027

Re: Job No. 04707-022(7070)

Dear Scott:

As I reported to your office by phone this afternoon, we have finished the radiocarbon dates on the two carbonates sent to us by Dr. Barnes. Our final reports are enclosed along with the appropriate invoice. The O-18 analyses should be done in a few more days and will be sent then.

The Type I calcite has no C-14 of significance and gave an age of 36,000 C-14 years or greater. Its C-13 suggests an origin from hydrothermal sources or from remobilized marine carbonates.

The travertine gave an age of 14,180 +/- 550 C-14 years B.P. and its C-13 suggests a source from descending meteoric waters.

I'm sure you may have questions, and I'll gladly discuss the matter in detail if you will give me a call at your convenience.

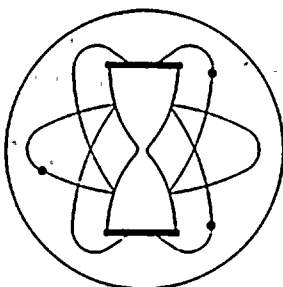
Sincerely,



Harold W. Krueger

HWK:hrn
encl.





KRUEGER ENTERPRISES, INC.
GEOCHRON LABORATORIES DIVISION

24 BLACKSTONE STREET • CAMBRIDGE, MA. 02139 • (617)-876-3691

PRIORITY BASIS
RADIOCARBON AGE DETERMINATION

REPORT OF ANALYTICAL WORK

Our Sample No. GX-7219

Date Received: 27 February 1980

Your Reference: Telecom per S. Laird

Date Reported: 14 March 1980

Submitted by: Scott Laird
Dames & Moore
2996 Belgium Road
Baldwinsville, NY 13027

Niagara Mohawk Power Co.
Nine Mile Point, N.Y.
Job No. 04707-022(7070)

Sample Name: Sample HK-1. Carbonate.

AGE = Greater than 36,000 C-14 years B.P.

Description: 17.35 grams of type I calcite breccia fragments.
Taken from field sample GA4-9.
Briefly rinsed in very dilute acetic acid prior to
analysis.

Pretreatment: The entire sample was powdered to -100 mesh and a small
split was taken for O-18 analysis. The remainder was
hydrolyzed, under vacuum, with HCl and the collected
carbon dioxide was used for the analysis.

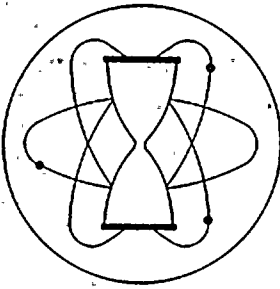
Comment: No significant C-14 activity was detected in this
sample. The sample size allows a limit age of
36,000 C-14 years B.P. but the sample could be much older.

$\delta C_{PDB}^{13} = +3.1 \text{ ‰}$

Notes: This date is based upon the Libby half life (5570 years) for C¹⁴. The error stated is $\pm 1 \sigma$
as judged by the analytical data alone. Our modern standard is 95% of the activity of
N.B.S. Oxalic Acid.

The age is referenced to the year A.D. 1950.





KRUEGER ENTERPRISES, INC.
GEOCHRON LABORATORIES DIVISION

24 BLACKSTONE STREET • CAMBRIDGE, MA. 02139 • (617)-876-3691

PRIORITY BASIS
RADIOCARBON AGE DETERMINATION

REPORT OF ANALYTICAL WORK

Our Sample No. GX-7220

Date Received: 27 February 1980

Your Reference: Telecom per S. Laird

Date Reported: 14 March 1980

Submitted by: Scott Laird
Dames & Moore
2996 Belgium Road
Baldwinsville, NY 13027

Niagara Mohawk Power Co.
Nine Mile Point, N.Y.
Job No. 04707-022(7070)

Sample Name: Sample HK-2. Carbonate.

AGE = 14,180 +/- 550 C-14 years B.P. (C-13 corrected)

Description: 8.49 grams of travertine.
Taken from field sample GA4-11E.
Briefly rinsed in very dilute acetic acid prior to analysis.

Pretreatment: The entire sample was powdered to -100 mesh and a small split was taken for O-18 analysis. The remainder was hydrolyzed, under vacuum, with HCl and the collected carbon dioxide was used for the analysis.

Comment: The sample was relatively small and was counted on each of two days with good agreement, the average being reported.

$\delta C_{PDB}^{13} = -7.5$ ‰.

Notes: This date is based upon the Libby half life (5570 years) for C¹⁴. The error stated is $\pm 1 \sigma$ as judged by the analytical data alone. Our modern standard is 95% of the activity of N.B.S. Oxalic Acid.

The age is referenced to the year A.D. 1950.



KRUEGER ENTERPRISES, INC.

GEOCHRON LABORATORIES DIVISION

24 BLACKSTONE STREET • CAMBRIDGE, MASSACHUSETTS 02139 • (617) 876-3691

19 March 1980

Scott Laird
Dames & Moore
2996 Belgium Road
Baldwinsville, NY 13027

Re: Job No. 04707-022(7070)

Dear Scott:

We have completed the O^{18} analyses on the two carbonate samples from Nine Mile Point. Our written report is enclosed along with the invoice for these analyses.

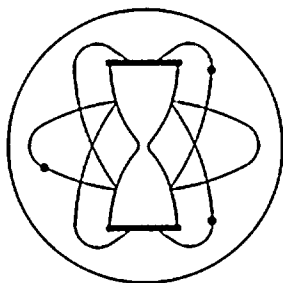
Both samples give O^{18} values between +21 and +23 o/oo and I'm not sure what, if anything they'll tell us about the carbonates, their origin, or their formation temperatures. I will try to review the literature to see if I can make anything out of the numbers. Meanwhile, you might call Dr. Barnes to see what he had in mind when he wanted to look at the O^{18} values.

Sincerely,

Harold W. Krueger

HWK:hrn
encl.





KRUEGER ENTERPRISES, INC.

GEOCHRON LABORATORIES DIVISION

24 BLACKSTONE STREET • CAMBRIDGE, MA, 02139 • (617)-876-3691

STABLE ISOTOPE RATIO ANALYSES.

REPORT OF ANALYTICAL WORK

Submitted by: Scott Laird
Dames & Moore
2996 Belgium Road
Baldwinsville, NY 13027

Date Received: 27 February 1980
Date Reported: 19 March 1980
Your Reference: Telecom per S. Laird
Niagara Mohawk Power Co.
Nine Mile Point, N.Y.

Job No. 04707-022(7070)

Our Lab. Number	Your Sample Number	Description	Analysis*
			δO^{18}
OR-13424	HK-1	Type I calcite (GX-7219)	+21.1
OR-13425	HK-2	Travertine (GX-7220)	+22.6

*Unless otherwise noted, all analyses are reported in ‰ notation and are computed as follows:

$$\delta R_{\text{sample}} \text{‰} = \left[\frac{R_{\text{sample}}}{R_{\text{standard}}} - 1 \right] \times 1000$$

Where:

D/H standard is SMOW
 C^{13}/C^{12} standard is PDB
 O^{18}/O^{16} standard is SMOW
 S^{34}/S^{32} standard is Cañon Diablo troilite

And:

$R_{\text{standard}} = 0.000316^{**}$
 $R_{\text{standard}} = 0.011237$
 $R_{\text{standard}} = 0.0039948^{**}$
 $R_{\text{standard}} = 0.0450045$

**Double atom ratio



KRUEGER ENTERPRISES, INC.

GEOCHRON LABORATORIES DIVISION

24 BLACKSTONE STREET • CAMBRIDGE, MASSACHUSETTS 02139 • (617) 876-3691

28 April 1980

H. Scott Laird
Dames & Moore
2996 Belgium Road
Baldwinsville, NY 13027

Re: Job No. 04707-022(7070)

Dear Scott:

We have completed the PRIORITY BASIS radiocarbon dating of your sample of lignitic material (GA4-S31). I have enclosed out written report and also the invoice for you to approve and forward for payment.

The sample proved adequate based upon the primary set of subsamples and the alternates were not required. They have been stored.

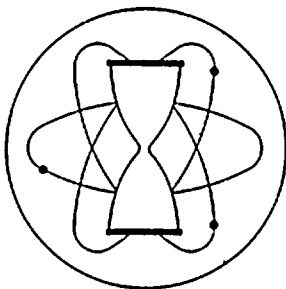
The age determined is 11,060 +/- 360 C-14 years B.P. If I recall our conversation correctly, you were anticipating a "last interglacial" (actually last interstadial) age and the result seems to agree with that. If you have any questions, please give me a call.

We have just now received the tiny carbonate sample from Dr. Barnes and I'll get in touch with Murthy to see if he wants to be around during the running of it. In any case, that results should appear in about 10 days to 2 weeks.

Sincerely,

Harold W. Krueger

HWK:hrn
encl.



KRUEGER ENTERPRISES, INC.

GEOCHRON LABORATORIES DIVISION

24 BLACKSTONE STREET • CAMBRIDGE, MA. 02139 • (617)-876-3691

PRIORITY BASIS RADIOCARBON AGE DETERMINATION

REPORT OF ANALYTICAL WORK

Our Sample No. GX-7257

Date Received: 11 April 1980

Your Reference: P.O. #SR-0355 (Change #1)

Date Reported: 28 April 1980

Submitted by: H. Scott Laird
Dames & Moore
2996 Belgium Road
Baldwinsville, NEW YORK 13027

Job No. 04707-022 (7070)

Sample Name: Sample GA4-S31. Organic matter.

AGE = 11,060 \pm 360 C-14 years B.P.

Description: Lignitic or peaty material in gray clay.

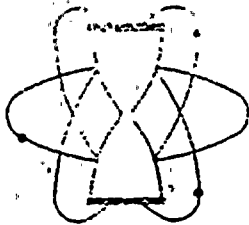
Pretreatment: The entire sample was dispersed in a large volume of water and the clays and organic matter were eluted away from any sand and silt by sedimentation and decantation. The clay/organic fraction was then treated with hot dilute HCl to remove any carbonates. It was then filtered, washed, dried, and roasted in oxygen to recover carbon dioxide from the organic matter for the analysis.

Comment:

δC_{PDB}^{13} = 0/00.

Notes: This date is based upon the Libby half life (5570 years) for C^{14} . The error stated is $\pm 1 \sigma$ as judged by the analytical data alone. Our modern standard is 95% of the activity of N.B.S. Oxalic Acid.

The age is referenced to the year A.D. 1950.



KRUEGER ENTERPRISES, INC.

GEOCHRON LABORATORIES DIVISION

24 BLACKSTONE STREET • CAMBRIDGE, MASSACHUSETTS 02139 • (617) 876-3691

13 May 1980

Scott Laird
Dames & Moore
14 Commerce Drive
Cranford, NJ 07016

Dear Scott:

I am enclosing the report on your sample HK-3 (Type 3 calcite) which we tried to analyze per your letter of 4/23/80 and Job No. 04707-022 (7070). I also enclose the invoice for the work completed although only the carbon isotopic composition could be measured.

The sample proved to be too small for any reliable C-14 age determination which is primarily what you wanted. We were able to obtain enough gas for a C-13/C-12 analysis as noted on the bottom of the report.

I am sorry that the effort that went into hand picking this material has not yielded all the data you desired, but there simply was not enough carbon present.

Please give me a call if you have any questions about the sample, or if we can be of further service.

Sincerely,



Harold W. Krueger

HWK:hrn
encl.





KRUEGER ENTERPRISES, INC.
GEOCHRON LABORATORIES DIVISION

24 BLACKSTONE STREET • CAMBRIDGE, MA. 02139 • (617)-876-3691

P R I O R I T Y B A S I S
RADIOCARBON AGE DETERMINATION

REPORT OF ANALYTICAL WORK

Our Sample No. GX-7272

Date Received: 28 April 1980

Your Reference: letter of 4/23/80
 from Dames & Moore

Date Reported: 12 May 1980

Submitted by: H.L. Barnes
 213 East Mitchell Avenue
 State College, PA 16801

Job No. 04707-022 (7070)

Sample Name: HK-3. Type 3 calcite.

AGE = Too small for analysis. (C-13 corrected)

Description: Very small sample of calcite fragments.

Pretreatment: The calcite was hydrolyzed, under vacuum, with HCl and
 the evolved CO₂ was used for the analysis.

Comment: Sample yielded less than 0.050 grams of carbon and was
 too small for reliable radiocarbon dating.

$\delta C_{PDB}^{13} = -4.7 \text{ } ^\circ/\text{oo.}$

Notes: This date is based upon the Libby half life (5570 years) for C¹⁴. The error stated is $\pm 1 \sigma$ as judged by the analytical data alone. Our modern standard is 95% of the activity of N.B.S. Oxalic Acid.

The age is referenced to the year A.D. 1950.

$^{230}\text{Th}/^{234}\text{U}$ Dating of TU-1

(Report #DM-3, 5/12/80)

Teh-Lung Ku

TU-1 is an impure carbonate sample received from Dr. H.L. Barnes through transmittal sheet 04707B-DK-T0666 dated April 26, 1980. It weighs 16.49 grams, in the form of small chips. About ten grams of handpicked, light-colored chips were pulverized in a ball-mill mixer, and leached with 0.5N HCl under gentle heating. The residue, consisting of 46.42% of the original weight, was totally dissolved with HF-HClO₄. Radiochemical analyses of uranium and thorium isotopes were performed on both the leachate and residue fractions, using isotope dilution (with ^{232}U and ^{228}Th "spikes") and alpha-spectrometric techniques.

The analytical results are listed below:

Fraction	^{238}U	^{234}U	^{232}Th	^{230}Th	$\frac{^{234}\text{U}}{^{238}\text{U}}$	$\frac{^{230}\text{Th}}{^{234}\text{U}}$
	dpm/g					
L	0.57±.02	0.93±.03	0.28±.01	3.99±.09	1.61±.07	4.32±.18
R	2.20±.16	2.12±.15	1.68±.10	3.98±.21	0.96±.07	1.88±.17
W	1.33±.08	1.48±.07	0.93±.05	3.98±.11	1.12±.05	2.69±.12

L: leachate; R: residue; W: whole sample (calculated from:
W = .5358L + .4642R).

The quoted uncertainties are one standard deviations derived from counting statistics.

As seen from the above data, the sample as a whole contains excess ^{230}Th unsupported by its ^{234}U parent, rendering the $^{230}\text{Th}/^{234}\text{U}$ dating technique inapplicable. There are two explanations for the excess ^{230}Th : (1) Open system: post-depositional loss of uranium has occurred. (2) Closed system: the excess ^{230}Th was initially present at the time of calcite precipitation. Explanation #1 would require extensive alteration of the calcite, which seems to be not supported by the stable isotopic data (as indicated on the transmittal sheet). Also, it would require an anomalously high uranium content of >5 ppm and $^{234}\text{U}/^{238}\text{U}$ activity ratio of >1.5 (^{234}U is generally more leachable than ^{238}U) for the calcite. We thus favor explanation #2, which is further suggested by the sample's containing a fair amount of Fe and possibly Mn as noted by us during analysis. The mineral phases containing these elements (e.g., hydroxides or 'clays') could scavenge ^{230}Th and form a part of the sample.

Accepting explanation #2, and assuming that the dilute acid leaching serves to separate ^{238}U in the calcite from that in detrital minerals (in which secular equilibrium among ^{238}U , ^{234}U and ^{230}Th is assumed to exist), one calculates (see Ku and Joshi: Dating terrestrial carbonate cementation with uranium-series isotopes. In: B. Patel, ed., Management of Environment, 551-557, Wiley Eastern Ltd., 1980) that the calcite contains: $^{230}\text{Th} = 5.60$ dpm/g, $^{234}\text{U} = 0.86$ dpm/g, and $^{238}\text{U} = 0.57$ dpm/g, or activity ratios $^{234}\text{U}/^{238}\text{U} =$



1.50 and $^{230}\text{Th} / ^{234}\text{U} = 6.51$. If the calcite were precipitated (together with, say, a Fe-Mn hydroxide phase) more than 300,000 years ago, it would initially have ratios of $^{234}\text{U} / ^{238}\text{U} > 2$ and $^{230}\text{Th} / ^{234}\text{U} > 90$. This is highly unlikely.

In summary, because of the excess ^{230}Th present in TU-1, the sample cannot be dated by the uranium-series method. However, from the available information and making appropriate geochemical assumptions, it is not unreasonable to assign a maximum age of 300,000 years as the time of calcite formation.

URANIUM-SERIES AGE DATING OF CALCITE MATERIAL

(J.O. No. 12177)

Teh-Lung Ku
USC Geochemical Report No. SW-1
Dec., 17, 1976

Results of the testing on the two samples provided by G. W. Page (letter dated November 10, 1976) are herein reported. The samples are designaged as SW-1 and SW-2. SW-1 is calcitic material from a rock (50± lbs.) face containing striations or slicken sides. SW-2 is "drusy" calcite coating on two smaller rock surfaces.

The accompanying table lists the analytical results and the estimated minimum ages for the specimens. The indicated uncertainties are based on one-sigma counting errors only. The testing procedures have been outlined in my October 22nd letter to Mr. J. H. Mullin.

Explanation of the results

For each sample, activities (expressed in disintegrations per minute, or dpm) of U^{238} , U^{234} , Th^{232} and Th^{230} were measured on two fractions. The leachate fraction is that portion soluble in 1 N HCl and comprises mostly $CaCO_3$. The other is the 1 N HCl insoluble residue fraction which consists mostly of alumino-silicate detrital minerals.

A distinct feature of the data is the excess Th^{230} over U^{234} in the leachate fractions of both samples. The magnitude of the excesses cannot be attributed to preferential

solution of Th^{230} from the detritals during the leaching procedure, as the amounts of residues are insignificant compared with those of acid-solubles. Therefore, the excess Th^{230} must be present in the total samples, which can be taken to indicate that either uranium has been leached out or Th^{230} has been added to the samples. We accept the latter as a better possibility based on the following considerations: firstly, in view of the observed excess U^{234} over U^{238} (i.e., $\text{U}^{234}/\text{U}^{238} > 1$) in the leachate phase, it is unlikely that U-leach was affected, as U^{234} is known to be more susceptible to leaching than U^{238} due to the former's recoil-produced origin; secondly, the presence of Th^{232} in the leachates indicates that parts of the Th^{230} in the same fractions could be of extraneous origin (Tatsumoto and Goldberg, 1959). This is particularly plausible as we note a significant quantity of iron present in the carbonates during dissolution (whose hydroxides may serve to scavenge Th), and the fact that, in the case of sample SW-2, were all the Th^{232} associated with the residue phase, the latter would have contained 45 ppm of thorium -- an inordinately high value ^{for} of silicate minerals.

A correction for this extraneous or common Th^{230} is in order. The correction should be $R + \text{Th}^{232} \exp(-\lambda t)$, in which R is the $\text{Th}^{230}/\text{Th}^{232}$ ratio entering the calcitic material, λ is the decay constant of Th^{230} and t is the time elapsed since addition of the common Th^{230} . We estimate the unknowns R and t as follows:

- (1) R may have a range of values as reflected by the $\text{Th}^{230}/\text{Th}^{232}$ data on natural waters and soils (Szabo, 1969; Cherdyntsev, 1971) commonly between 1 and 2 (Kaufman and Broecker, 1965). We choose the $\text{Th}^{230}/\text{Th}^{232}$ ratios found in the residues to be the values for R. They are respectively 0.98 and 1.11 for SW-1 and SW-2.
- (2) As the time of introduction of Th^{230} and Th^{232} is uncertain, we take $t=0$, meaning that the addition of the two isotopes occurred very recently. Such an approach enables us to derive minimum ages for the deposition of the calcites (as shown in the accompanying table), because in so doing we are maximizing the common- Th^{230} corrections. It should be noted that a "true" age of $\geq 300,000$ years for the two samples (approximate upper limit for the $\text{Th}^{230}/\text{U}^{234}$ dating method) is allowable by the data and interpretations presented above.

References Cited

- Cherdyntsev, V. V. (1971) Uranium-234. Jerusalem: Israel Program for Scientific Translation, 234 pp.
- Kaufman, A. and Broecker, W. S. (1965) Comparison of Th^{230} and C^{14} ages for carbonate materials from Lakes Lahontan and Bonneville. J. Geophys. Res. 70: 4039-54.
- Szabo, B. J. (1969) Uranium-series dating of Quaternary successions. Etudes sur le Quaternaire dans le Monde, pp. 941-49. Contress INQUA, Paris, 8th.
- Tatsumoto, M. and Goldberg, E. D. (1959) Some aspects of the marine geochemistry of uranium. Geochim. Cosmochim. Acta 17: 201-8.

Radiochemical and Age Data of the Samples

Sample* No.	% acid- solubles	U ²³⁸ (dpm/g)	U ²³⁴ (dpm/g)	Th ²³² (dpm/g)	Th ²³⁰ (dpm/g)	Th ^{230**} corr. (dpm/g)	Min. Age (10 ³ yrs)
SW-1 (L)	93.9	0.089±.005	0.154±.007	0.089±.004	0.221±.007	0.133±.008	170±20
SW-1 (R)		1.38±.05	1.30±.05	1.11±.06	1.09±.05	—	
SW-2 (L)	98.7	0.094±.003	0.133±.004	0.122±.004	0.207±.006	0.072±.007	81±10
SW-2 (R)		1.74±.08	1.78±.08	1.57±.08	1.75±.09	—	

*L and R refer to leachate fraction and residue fraction, respectively.

**Assuming recent addition of Th²³⁰ and corrected according to equation:

$$Th_{corr}^{230} = Th^{230} - R \cdot Th^{232}, \text{ where } R = Th^{230}/Th^{232} \text{ in the residue fraction}$$

***Calculated from equation:

$$Th_{corr}^{230}/U^{234} = (U^{238}/U^{234})_L [1 - \exp(-\lambda_o t)] + [1 - (U^{238}/U^{234})_L] [\lambda_o/(\lambda_o - \lambda_u)] [1 - \exp(\lambda_u - \lambda_o) t]$$

where λ_o and λ_u are respectively decay constants of Th²³⁰ and U²³⁴, subscript L denotes leachate fraction.

6/7/79

61 Kensington Rd
Garden City, NY 11530

Ronald P. Taylor
Project Geologist
Dames & Moore
2996 Belgium Road
Baldwinsville, New York 13027

RE: 04707B-DS-LO482

Dear Mr. Taylor:

I have completed the analysis of sample # CWT-1 for pollen and spore content. Visual inspection of the bag samples indicated that they can be separated into two groups based on color: bags A, B, and C range in color from 5Y 5/1 to 5Y 6/1, while E and G are 2.5Y 5/2, and A' is 2.5Y 7/2. Since the bags are all from the same horizon (#CWT-1) according to your determination, one bag from each color group was processed and analyzed in order to provide adequate coverage of the overall sample and to determine if the color change is significant. Consequently, approximately 25 gm of sediment were taken from bags B and G for processing and analysis.

Bag B. The sample is composed of very fine to coarse clastic sediment. The coarse fraction contains angular to subrounded fine sand to fine gravel, the latter comprised of sandstone fragments. No organic debris or microfossils were observed. The fine fraction yielded the following pollen and spores: pine (3 specimens), birch (12), cedar (1), willow (1), grass (4), ragweed (1), other composites (1), pondweed (1), Sphagnum (1).

Bag G. The coarse fraction revealed slightly more oxidation on the grains and fragments of sediment than that of bag B. Pollen and spores include pine (3), spruce (2), birch (3), alder (1), hickory (1), oak (1), cedar (3), grass (1), ragweed (2), other composites (1), unknowns (1), fernspores (3), and stellate leaf-hairs (1).

Discussion. Overall the microfloral population is sparse. The dominant forms are birch and pine with minor spruce and cedar and traces of other tree pollen. Nonarbooreal pollen representation is about one-third of the pollen sum. Furthermore, several of the specimens appear worn. In the absence of a statistically significant pollen sum, determination of the age of the sample is somewhat speculative. However, with larger amounts of pine, birch, and spruce, a scattering of other tree pollen and the absence of hemlock in the AP, and lower NAP values, the sample could represent the A4 subzone of the spruce pollen zone. In comparison with the pollen diagram developed for the SL and AS samples from this site, this correlation seems reasonable.

If you have any questions concerning this report please contact me. I will send my statement and representative microscope slides to you.

Yours truly,


Les Sirkin



7/17/79
61 Kensington Rd
Garden City NY 11530

Ronald P. Taylor
Project Geologist
Dames & Moore
2996 Belgium Road
Baldwinsville, NY 13027

Re: P.O. SR0316
04707-022-19

Dear Mr. Taylor:

I have completed the pollen analysis of samples GA3-S1 and GA3-S2 after processing approximately 25 gm of each sample. Of the two samples only GA3-S1 contained any microfloral specimens. Sample GA3-S2 was barren of microfossils.

Sample GA3-S1. This sample contains a sparse scattering of tree and herb pollen, and spores of late Pleistocene to modern age, and a trace of Paleozoic spores. Tree pollen include spruce (1 specimen), small-size pine (1), alder (2), Corylus (1), birch (1). Nonarboreal forms include a small-size grass (2), Artemisia (3), ragweed (5), and Urtica (2). The spores are Polypodiaceae (7), Lycopodium (1), and Sphagnum (1).

This sparse assemblage prohibits a definitive age determination, but compared with previous studies at this site, a 'spruce zone' age is possible. The late glacial or spruce zone age is suggested in the relatively high NAP representation along with a few cold environment indicators like spruce, small pine, and Lycopodium, and possible cold climate shrubs like birch, alder. There is also evidence to indicate an open vegetation, i. e. few trees and more abundant NAP, particularly grass and ragweed, and wet ground, i. e. alder, Corylus, Sphagnum, Lycopodium, and Urtica. Thus, the tentative correlation with CWT-1 and the AS and SL samples might be extended to include GA3-S1.

Yours truly,

Les Sirkin



encl: statement



8/7/79
61 Kensington Rd
Garden City, NY 11530

Gordon Appel
Project Geologist
Dames & Moore
2996 Belgium Road
Baldwinsville, New York 13027

Re: 04707B-DS-L0482 and 04707-022-19

Dear Gordon:

According to your instructions in our recent conversation, I have analyzed additional material from samples CWT-1 and GA3-S1. In doing so I have significantly increased the pollen sum for each sample and have determined relative pollen percentages for the combined sums for each sample (see accompanying pollen diagram). The additional data have provided more substantiation for the tentative conclusions stated in my prior reports on these samples, particularly in terms of the age and correlation of the sediments.

The percentages of the taxa show that birch, alder, and conifers, including spruce, two sizes of pine pollen, and cedar, are the most abundant arboreal forms. Pollen of deciduous hardwoods are rare and include only species characteristic of cooler climate trees. Shrubs, represented by Ericaceae, Rosaceae, including Dryas (?) in GA3-S1, and in part birch and alder, are common. The nonarboreal taxa are dominated by grass and composites, particularly ragweed in GA3-S1 where the NAP account for 56% of the pollen. In both samples, Polypodiaceae spores are abundant and Sphagnum is significant. Lycopodium is more abundant in GA3-S1.

As previously discussed, both samples contain pollen assemblages that indicate that deposition occurred during the Spruce Pollen Zone, with a minimum age of 10,000 years B. P., the youngest age determined for the A4 subzone of the Spruce Pollen Zone as indicated in the report for job # 04707-02S. The additional pollen data further demonstrate that a correlation in age can be made between the samples. It is also possible that these samples are somewhat older than the A4 subzone. The high shrub and NAP representation indicates a vegetational setting more like a conifer parkland than a coniferous forest, that is, a region with a more open aspect and more ground cover along with areas of wet ground or wetlands marginal to the postglacial lake.

If you have any questions concerning this report please contact me at your convenience. For the next week or so, I will be in Rhode Island where you may call me at 401 466 2174.

Best regards,


Les Sirkin

Encl: Statement.



SAMPLE
 SPRUCE
 SMALL PINE
 PINE
 HEMLOCK
 CEDAR
 WILLOW
 BIRCH
 ALDER
 POPLAR
 HICKORY
 OAK
 BEECH
 ELM
 ERICACEAE
 ROSACEAE
 % AP
 % NAP
 NAP:
 PONDWEED
 URTICA
 GRASS
 SMALL GRASS
 SEDGE
 POLYGONACEAE
 UTRICULARIA
 MISC COMPOSITAE
 RAGWEED
 ARTEMISIA
 AMARANTH
 UNKNOWN
 POLLEN SUM
 SPORES:
 SPHAGNUM
 LYCOPIDIUM
 POLYPODIACEAE
 PALEOZOIC

AP: SAMPLE
SPRUCE
SMALL PINE
PINE

HEMLOCK
CEDAR

WILLOW

BIRCH

ALDER

POPULAR

HICKORY

SAIK
BEFC

ELM

ERICACEAE

ROSACEAE

% AP

% NAP

POWDERED

URTICA

GRASS

SMALL GATSS

SEDOGE

POLYGONACEAE
TRICUL.

TRICULARIA
MISC

COMPOSITE

ARTEMISIA

AMARANTH

UNKNOWN

POLLEN SU.4

STOKES :

LYCOPEDIUM

DOLPODIACEAE

PALEOZOIC

11/12/79

61 Kensington Rd
Garden City, NY 11530

H. Scott Laird
Project Geologist
Danes & Moore
2996 Belgium Rd
Baldwinsville, NY 13027

Dear Mr. Laird:

I have processed and analyzed for pollen content the six samples in the GA4 series: S1-A, S2-A, S4-A, S5-A, S6-B, and S8-B. Based on prior studies relatively large amounts of each sample (approximately 25-30 gm) were processed in order to increase the pollen yield.

Furthermore, according to your instructions, sample S5-A was inspected for possible splitting into two different sediment fractions. Because the sample was small and the mixing of the sediments was complex, I did not feel confident that splitting of the sample into two distinctly different sediment types could be done without contamination. If a larger sample of each sediment type could be obtained and/or the two fractions could be split by you, I could attempt to evaluate the pollen content of the two samples.

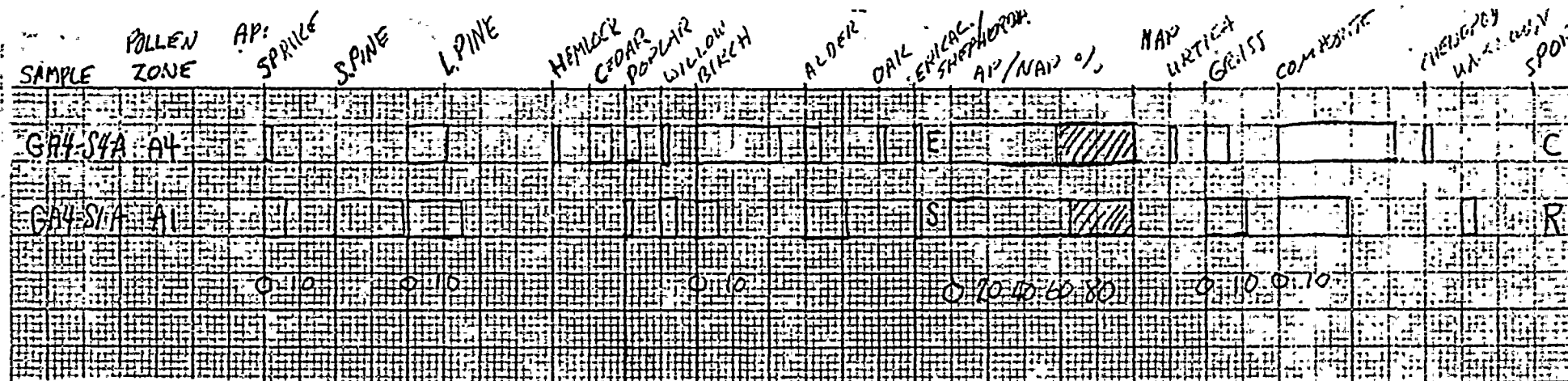
The results of pollen analysis of the GA4 samples is as follows, with the significant pollen data plotted on a pollen diagram that can be compared with the results of previous reports.

Sample GA4-S1A. This sample contains 47 specimens of pollen, plus several spores. About 66% of the microflora consists of tree and shrub pollen, predominantly pine, represented by both the large and small-sized forms, alder, birch, spruce, willow, poplar (?), and Shepherdia. The nonarboreal pollen include the composites, mainly ragweed, and grass. The overall pollen assemblage, although low in diversity probably represents the spruce pollen zone of the late-glacial following recession of the Woodfordian glacier. The presence of the small-sized pine pollen, generally associated with P. banksiana, along with several possible shrub varieties, spruce, and high NAP, suggests a boreal, spruce parkland or shrub tundra vegetation with scattered trees. This association is characteristic of the early spruce pollen zone, as for example subzone A1. The lack of tundra herbs restricts assigning an Herb Pollen zone age to the sample.

Sample GA4-S2A. This sample contains only 1 specimen of pine and 4 of ragweed, too little data to evaluate.

Sample GA4-S4A. This sample is similar in many respects to S1-A in pollen yield and content, but with some difference in diversity. About 4% of the pollen are in the NAP of which the composites are the most abundant. The AP consist of spruce (1), large-sized pine (5), hemlock (1), cedar (3), poplar (2), willow (1), birch (11), alder (2), oak (1), and Ericaceae (1). Of 12 spores found, 9 are in the Polypodiaceae. The main differences in the pollen assemblages are the higher NAP, lack of small-sized pine and spruce, and the appearance of cedar, hemlock, oak, and Ericaceae, all suggesting somewhat warmer climatic conditions. As such, this assemblage compares more favorably with the later spruce subzones, i. e. subzone A4.





Pollen Diagram for samples GA4-S4-A, GA4-S1-A.

L. SIKKIN REPORT 11/13/79
P.3

p 2. Sirkin report

Sample GA4-S5-A. While splitting of this sample was not feasible, the pollen yield proved to be extremely low: pine (4 specimens, 2 small, 2 large), birch (2), alder (1), grass (1), and spores (1). While the outcome may appear academic, the absence of Paleozoic forms may be significant. In fact none of the samples in this group contained Paleozoic forms. While the sample yield is not significant, the pine, birch representation may suggest a relationship to the other samples and hence the spruce pollen zone. The lack of Paleozoic forms may suggest that mixing of in situ and transported sediments has not occurred here.

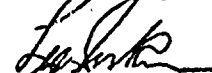
Sample GA4-S6-B. This sample also has a very low yield with pine (1), birch (2), grass (1), composites (1), and spores (3), represented; again, too few to assign a definite age.

Sample GA4-S8-B. Again the very few specimens retrieved from this sample can only provide a hint of the sample age: spruce (3), pine (3, 1 small, 2 large), hemlock (1), grass (1), ragweed (1). Possible age: spruce zone, subzone A4.

In summary, it appears that these samples were derived from sediments that contain pollen assemblages that are most readily assigned to the spruce pollen zone of the late-glacial.

If you have any questions concerning this information, please contact me at your convenience.

Sincerely yours,



Les Sirkin
Consultant

Encl.: Statement

Sent separately: one slide for each sample.



3/10/80
61 Kensington Road
Garden City, NY 11530

H. Scott Laird
Project Geologist
Dames & Moore
2996 Belgium Road
Baldwinsville, NY 13027

Re: P. O. SR 0316, Change orders #3, #4
04707B-DS-TO609

Dear Scott:

I have completed the palynologic analysis of samples GA4- 20, 21, 21A, 22, 24, & 26. Based on prior experience, relatively large (ca 30 gm) samples were processed and the residues were rerun in order to concentrate as many pollen and spores as possible. All of the samples, however, had a low yield. The pollen were mainly whole grains and well stained, although several fragments were also counted.

GA4-S20. Abundant lignitic particles were concentrated in the organic fraction, but only 8 pollen and 1 spore were retrieved. The pollen include pine, spruce, birch, alder, and holly and elm. The spore is Sphagnum.

GA4-S21. Only one pollen grain, an alder, was found.

GA4-S21A. This sample contains 12 pollen and 3 Polypodiaceae spores. The pollen include spruce, pine, birch, willow, cedar, oak, composite, grass, and Rosaceae (Dryas?).

GA4-S22. Ten pollen and 2 spores were found in this sample. The pollen include birch, Rosaceae, grass, and composites; the spores are Lycopodium and Polypodiaceae (one each).

GA4-S24. This sample yielded seven pollen and 6 spores. The pollen are of pine, Ericaceae, grass, composite, willow, and ?walnut; the spores include Sphagnum and Polypodiaceae. Three Paleozoic spores were also counted.

GA4-S26. Eight pollen, mainly birch, willow, cedar, Rosaceae, composite, and basswood, and 3 spores, one each of Lycopodium, Sphagnum, and Polypodiaceae, were counted.

Although sparse, the pollen are mainly those of the boreal assemblage, that is, pine, spruce, birch, willow, and Rosaceae. However, four of the samples contain at least one pollen grain of a cool temperate species of hardwood tree. The NAP are consistently represented by grass and composites. Sphagnum and Polypodiaceae



Sirkin, 3/10/80, p.2

spores confirm the origin of the sediments in a fresh water wetland, while the lycopod spores indicate cool or boreal conditions.

Even though the pollen yield is low, the spectra generally suggest an association with the late-glacial spruce pollen zone (Al₁) and were probably derived from sediments deposited at that time. The evidence favors an interpretation of cool or boreal conditions.

I will look forward to hearing from you, and please contact me if you have any questions concerning this report.

Yours truly,


Les Sirkin,
Consultant.

Encl: The statement attached includes the site visit, report, and expenses for that visit; and pollen analysis and report.

Representative slides for the GA₁ samples have been shipped to you, separately.

Encl: confidential reports, draft



4/28/80
61 Kensington Rd
Garden City, NY 11530

H. Scott Laird
Project Geologist
Dames & Moore
2996 Belgium Road
Baldwinsville, NY 13027

Re: P. O. SR 0316 Change order #5
(Acct 4707-022-19 7070)

Dear Scott:

I have completed the palynological analysis of samples 806-S1, 806-S3, 810-1, 810-3, 810-4, and 805-1. In each case, the entire sample was extensively processed in order to extract as much of the pollen as possible. However, only a few fossil pollen and spores were found. These microfossils were well stained, although several were broken and not readily identified. All of the samples contain considerable fine-grained, black opaque debris.

805-1, 121.55 ft. This sample yielded one ragweed pollen grain, and one trilete spore (Polypodiaceae?).

806-S1, 151.00 ft. One spore (polypodiaceae?) was found.

806-S3, 144.70 ft. One composite-type pollen (ragweed?) fragment and one Lycopodium spore were counted.

810-1, 207.3 ft. This sample contains one Chenopodiaceae pollen grain, one Rosaceae (?) pollen, and one spore (Polypodiaceae?).

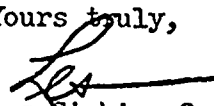
810-3, 251.4 ft. One tricolpate pollen grain (genus not determined).

810-4, 252.25 ft. Two Polypodiaceae-type spores were counted.

The microflora obtained from the samples provided for this study is insufficient for determination of the age of the sediment. The presence of rosaceous and chenopod pollen, and fern and lycopod spores might be an indication of cool and wet conditions at the surface source of the polleniferous sediment and would tend to confirm prior studies at the site. However, with such a small sample population, that point is only speculation.

If you have any questions concerning these results, please contact me.

Yours truly,


Les Sirkin, Consultant

Encl: Statement; representative slides - sent separately.



BROCK UNIVERSITY

REGION NIAGARA

Department of
Geological Sciences

416/684-7201
Ext. 273

St. Catharines,
Ontario L2S 3A1
Canada
March 17, 1980

REPORT ON PALYNOLOGICAL ANALYSES OF LAMINATED SILTY CLAY

Nine Mile Point Nuclear Station
Unit 2
Niagara Mohawk Power Corporation
04707B - DT - L0625

submitted by

J. TERASMAE

Enclosures:

1. Personal data re. the investigator
2. Analytical procedures
3. Report on results of analyses
4. Raw data

REPORT ON RESULTS

Both samples contained calcium carbonate (strong reaction with HCl). Pollen concentration in both samples was very low (about 300 - 400 per gram of sediment). All pollen was of Pleistocene age. No Paleozoic spores were present in the slides examined. Pollen preservation was poor and some pollen grains were broken. The undissolved matrix of the sample residue was found to be inorganic, with only a few plant tissue fragments.

In my view these samples indicate deposition in glacial environment, most likely a glacial lake. The low pollen concentration and poor preservation indicate to me the presence of glacial climate and absence of local vegetation. Atmospheric transport from sources to the south can account for the few spruce and pine pollen found in these samples. In contrast, postglacial sediments in the Great Lakes region commonly have a pollen concentration of tens of thousands of pollen grains per one gram of sediment, and over 100,000 per gram in some sediments (see for example, McAndrews and Power, 1973).

Although Paleozoic spores are quite frequently found in glacial lake sediments of the southern Great Lakes region, they are not necessarily present in every sample (as indicated by my personal experience over some 20 years).

In terms of age, these glacial lake sediments most likely belong in the Late-Wisconsinan episode (dated about 13,000 to 15,000 years before present). The geographical relationship of your site to known ice marginal positions of Late-Wisconsinan age may provide some helpful guidance. There is no absolutely sure way that an older Pleistocene age can be definitely excluded (at least on the basis of palynological data from only 2 samples). However, the presence of abundant carbonate (indicating no leaching) supports a Late-Wisconsinan age, rather than some earlier Pleistocene time. In my opinion the geological field evidence should be given priority in respect to the decision of whether or not the silty clay is most likely of Late-Wisconsinan age or older.

McAndrews, J.H. and Power, D.M., 1973. Palynology of the Great Lakes: the surface sediments of Lake Ontario. Canadian Journal of Earth Sciences, volume 10, no. 5, pp.777-792.



ANALYTICAL PROCEDURES

The following sequence of analytical procedures was used for preparation of the silty clay samples.

Note: some abbreviations used below:

- HCl - hydrochloric acid (dilute, 10%)
- HF - hydrofluoric acid (concentrated, 42%)
- C - centrifuge
- W - wash (distilled water)

1. Determine dry weight of sample:-
 - Weight of sample (oven dry) and container
 - Weight of container
 - Weight of sample used (in grams)
2. Add ca. 50 ml HCl to sample in beaker; stir; leave to react overnight
3. Add "spike" (*Lycopodium* tablets; each containing $12,500 \pm 500$ spores); 2 tablets added to each sample
4. Transfer sample to 15 ml centrifuge tube; C & W & C (repeat)
5. Transfer sample to 100 ml metal crucible
6. Add 30 ml HF; warm up on hot plate; leave to react overnight
7. Decant most of HF; add 30 ml water (distilled)
8. Transfer to 15 ml centrifuge tube; C & W & C (repeat)
9. Add 7 ml HCl, warm to 80°C; C & W & C
10. Add 3 ml glacial acetic acid; C and decant acid
11. Add 7 ml of acetolysis mix; heat to 100°C in water bath; C & W & C, decant water
12. Make slides of residue; corn syrup used as embedding medium

Note: the HCl, HF, and acetolysis steps are described in detail on attached pages (circled in red).

The prepared slides were examined under microscope, using 400 x magnification



RAW DATA

	Samples	
	GA4-S23	GA4-S25
Sample weight (in grams)	16.5510	13.2829
Pollen counted:		
Total surface of 3 slides scanned		
<u>Picea</u> (spruce)	6	4
<u>Pinus</u> (pine)	5	6
<u>Betula</u> (birch)	1	-
<u>Quercus</u> (oak)	-	1
Other pollen (unidentified because of poor preservation)	5	2
Total	17	13
"Spike" (<u>Lycopodium</u> spores) counted	69	83

$$\text{Pollen concentration} = \frac{\text{Spike added}}{\text{Spike counted}} \times \frac{\text{Pollen counted}}{\text{Dry weight of sample}}$$

Pollen concentration is expressed as number of pollen grains in one gram of dry sediment.

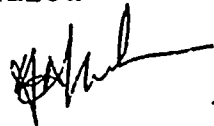
$$\text{Sample GA4-S23: } \frac{25,000}{69} \times \frac{17}{16.55} = 372 \text{ pollen per 1 g of sample}$$

$$\text{Sample GA4-S25: } \frac{25,000}{83} \times \frac{13}{13.28} = 295 \text{ pollen per 1 g of sample}$$



Dr. Andreas H. Vassiliou
Nov. 17, 1979

NEWARK COLLEGE OF ARTS AND SCIENCES • DEPARTMENT OF GEOLOGY • NEWARK • NEW JERSEY 07102



MINERALOGIC ANALYSIS REPORT

TO: Mr. H. Scott Laird
Dames & Moore
2996 Belgium Road
Baldwinsville, New York 13027

RE: Mineralogic analysis of soil and rock specimens as per SR 0334
Job No. 04707-022-19

PROCEDURES

(a) Sample Preparation

Bedrock specimens: representative portions ground and smeared on slides for XRD analysis as BULK specimens. Thin sections prepared for point counts. X-ray charts and thin sections enclosed.

Soil specimens: XRD samples were prepared by sedimenting clay-size particles onto glass slides (beaker method) All sedimented slides were classified and ran as untreated, glycolated, and heat treated (550°C for 1/hr).

All specimens: Ground portions used in bromoform separations for "heavies" content.

Representative portions acid treated for carbonate content, through calculation of weight loss (CO₂). Eight of the samples were tested twice for verification purposes.

(b) Standards Used

Chem. Carbonate content: Step procedures tested for quality control by using Fisher Scientific Reagent Grade CaCO₃. Difference between actual and analyzed values for the latter (using step procedures) determined to be in the 0.01 area.

X-ray diffraction: permaquartz standard used in every chart for alignment control and verification. This is shown on every X-ray chart enclosed.

X-ray Analysis (mineral identification) was done using three reference sources: (1) A.P.I. clay reference standards ran on our own machines for actual comparisons. (2) ASTM file cards for verification. (3) The reference

tables of Chen (1977).

Intensity factors: For non-clay and clay minerals determined experimentally (using 100% content for each mineral present in samples tested). Values (for scale of 500) compare well with values of Schultz (1964) and Johns et al (1954).

Quartz (21°): 850; Plag.(28°): 2800; Calcite(29.4°): 2600
Dolomite(31°): 3100; Clays(chl., ill., kaol.): 1500

Chlorite: 6.4° I; Illite: 8.9° I times factor 2;
kaolinite: 6.4° times 1.2 factor from 12.4° I.

RESULTS

(a) All analytic results are listed in Table 1 (attached)

(b) Comments on analytical results. (reference Table 1)

1. The range in weight percent content of carbonate (wet chemical) indicates that the samples are not homogeneous. Most of the clay/silt samples contain rock chips and fragments that most probably contribute to the inhomogeneity of the materials.
2. The inhomogeneity is also evident through the other analytical data (non-clay and clay mineral content) since there is no clear separation of samples according to origin groups (i.e. S5, S6, S7 groups).
3. The carbonate content through XRD, separated into calcite and dolomite (with some siderite), provides the simplest and most practical compositional distinctions between groups and individual samples, specifically in terms of the type of predominant carbonate present or in terms of the ratio between the two principal carbonates if both are present.
4. The accessory mineral content (heavies or accessories) does not provide any practical compositional distinction between the samples.
5. The total clay content and specific clay mineral content are often important compositional differentiates among clay/silt specimens, coupled with data on grain size distribution and the ratio of quartz to feldspar. Here these factors do not differentiate the samples into relatively simple compositional groups due to the apparent variation within sampling groups. However, if one disregards the classification according to sampling (i.e. S5, S6 etc.) and looks at the individual clay mineral content (in terms of 100 percent total clay), one can see certain compositional characters as evidenced from the following listing:



TABLE 1. MINERALOGY FROM ANALYTICAL DATA (XRD, wet chem., phys. sep.) A.H.Vassiliou 11/79
D&M SR0334 (4707-022-19)

SAMPLE Descriptions as provided	WEIGHT PERCENT			MINERAL CONTENT (percent) based on XRD ³										Comments ⁶
	Carbonate ¹		Heavies ²	Quar tz	Feld spar (plg)	Calc ite	Dolo mite+ (Sider)	Accesso- ries ⁴	C L A Y S					
	Range	Ave.							Tot al ⁵	Chlo rite	Illi te	Kaol in	Smec tite	
GA4-S1-B cl/slt		15.0	---	32	11	11	3	Hm	42	9	27	6	--	S
GA4-S2-M cl/fgmts		9.7	py;ho	24	10	2	5	Hm;Ho;Py	58	13	40	5	--	S
GA4-S4-B cl/slt	(24.8-25.1)	24.9	---	30	9	11	5	---	45	11	31	3	--	S
GA4-S5-B cl/slt	(12.0-26.2)	19.1	---	34	13	24	6	Hm	22	7	15	--	--	S
GA4-S5-C cl/slt/fgmts	(12.2-22.3)	17.2	ho	29	9	--	3	Hm;Px	58	10	39	9	--	S
GA4-S5-D bedrock		4.7	---	37	7	--	--	Hm;Ho	55	15	39	1	--	B+T
GA4-S6-A cl/slt/fgmts	(5.0- 5.1)	5.1	---	65	12	10	--	Hm	12	7	4	1	--	S
GA4-S6-C bedrock		4.7	ho	68	11	2	--	Hm;Ho	18	5	12	1	--	B+T
GA4-S6-D1 cl/slt	(2.0- 5.0)	3.5	---	18	4	29	--	Hm;Ho	48	12	33	3	--	S
GA4-S6-D2 cl	(15.6-15.9)	15.7	---	37	8	20	7	Hm;Ho	27	5	18	4	--	S
GA4-S7-A cl/fgmts		14.2	py;ho	22	7	--	7	Hm;Ho	63	8	43	12	--	S
GA4-S7-B cl/fgmts	(35.4-45.1)	40.2	py;ho	26	5	--	17	Hm;Ho	51	8	38	5	--	S
GA4-S7-C bedrock		22.0	---	40	11	--	16	Hm;Ho	32	12	20	--	--	B+T
SL-CWPT-1M cl/slt		14.1	mt;zr;rt	37	16	8	10	Hm;Ho	28	10	18	--	--	S
SL-CWPT-2M cl/slt		13.9	mt;zr;ho	42	18	11	10	Hm	18	6	11	--	1	S
SL-CWPT-3M marl	(31.6-31.8)	31.7	---	25	4	41	5	Hm;Ap	24	8	15	--	1	S

1. Percent CaCO_3 and $\text{CaMg}(\text{CO}_3)_2$ based on CO_2 weight loss through acid treatment (1:6 HCl). Step procedure control using reagent grade CaCO_3 . Recorded range in content illustrates inhomogeneity of the samples.
2. All samples tested with bromoform (2.85 SG). All found to contain less than 0.2 weight percent heavies. In some cases, heavies were specifically identified as shown.
py=pyrite; ho=hornblende; mt=magnetite; zr=ziroon; rt=rutile
3. Quantitative estimations based on intensity of X-ray diffraction spectra (see attached charts). Area of spectra according to method of Schultz (1964). Intensity factors determined experimentally for non-clay minerals. Clay content by difference as well as by calculated relative intensity factors. See text for more details.
4. Trace contents, generally a fraction of a percent but occasionally up to one percent.
Hm=hematite or iron oxide in general; Ho=hornblende; Py=pyrite; Px=pyroxene; Ap=apatite
5. The average of two determinations; by difference and through intensity factors for indiv. minerals.
6. S= sedimented slides (in beaker); B+T= Bulk samples (ground) plus information from thin sections.



Percent of Clay Content*

<u>Chlorite</u>	<u>Illite</u>	<u>Kaolin</u>	<u>Sample</u>
55	35	10	S6-A
39	61	--	S7-C
39	61	--	CWPT-2M
37	63	--	CWPT-1M
36	64	--	CWPT-3M
32	68	--	S5-B
29	67	4	S6-C
27	71	2	S5-D
26	68	6	S6-D1
24	70	6	S4-B
22	70	8	S2-M
22	65	13	S1-B
19	68	13	S6-D2
17	68	15	S5-C
15	75	10	S7-B
13	68	19	S7-A

* These figures can be obtained by recalculating the clay mineral content in total sample (see Table 1) to percent clay proportions


References:

1. Johns, Grim, & Bradley, 1954, Quantitative estimations of clay. J. Sed. Pet, V24, p. 242
2. Schultz, L.G., 1964, Quantitative interpretation of mineral. U.S.G.S Prof. Paper 391-C
3. Chen, Pei-Yuan, 1977, Table of Key Lines in X-ray Powder Diff. Patterns: ... in clays. - Indiana Geol. Survey Occasional Paper 21.





Dr. Andreas H. Vassiliou

March 17, 1980

NEWARK COLLEGE OF ARTS AND SCIENCES • DEPARTMENT OF GEOLOGY • NEWARK • NEW JERSEY 07102

MINERALOGIC ANALYSIS REPORT

TO: Mr. Scott Laird
Dames & Moore
2996 Belgium Road
Baldwinsville, New York 13027

RE: Heavy mineral separation and identification on clay
samples GA4-S27, GA4-S28, and GA4-S29 as per SR 0334
Change Order #1 and Job No. 04707-022 (7070).

PROCEDURES AND METHODS

Heavies from each of the three samples were separated and their weight percent calculated using two somewhat different procedures. The steps in each case together with pertinent observations are outlined below. The final results represent averages from the two procedures.

(A) Bromoform - Funnel Separation

1. Weigh sample before separating heavies (> 2.85 SG) in bromoform, using funnel with stopper and filter.
2. Microscopic observation of separates showed the presence of sulfide encrustations on clay surfaces.
3. After crushing of separates to free sulfides from the composite grains, heavies were again immersed in bromoform, and resulting separates were weighed to determine percent content of heavies.
4. Heavy fraction was passed through a Frantz Isodynamic Separator but no magnetic minerals were separated.
5. Identification of heavy fraction using physical and optical characteristics as well as X-ray diffraction analysis (representative X-ray chart enclosed).

The X-ray identification was based on standards (perma-quartz) and the JCPDS file.



#2 D&M 3/17/80

(B) Bromoform - Centrifuge Separation

Same steps as in (A) above except that the centrifuge was used in the separation process which produced slightly more separates in a shorter time.

RESULTS

Sample GA4-S27

It contains 0.5 weight percent heavies composed of marcasite and pyrite.

Sample GA4-S28

It contains 0.4 percent marcasite and pyrite.

Sample GA4-S29

It contains 0.8 percent marcasite and pyrite.

NOTES

- (a) In each of the three samples above, the marcasite is slightly more abundant than the pyrite. It also appears that some of the marcasite has altered to the more stable structure of the pyrite.
- (b) In spite of very careful microscopic examination (using a 250 X theoretical magnification), no garnet grains were observed. Only one isolated red grain, that could be garnet, was observed in sample GA4-S29. Besides the sulfides and the clay and quartz grains that form encrustations no other mineral grains were observed (microscopically or through XRD) in the heavy fractions.

W. L. Smith



2/20/80

61 Kensington Rd
Garden City, NY 11530

H. Scott Laird
Project Geologist
Dames & Moore
2996 Belgium Road
Baldwinsville, New York 13027

Dear Mr. Laird:

I am writing to you concerning my observations of the geology of the North Radwaste Trench exposure at the Nine Mile Point Nuclear Station Unit 2 site. I visited the site with you and the Dames & Moore geologists, accompanied by Dr. Coates on 2/15/80, in order to examine the bedrock exposure and investigate the source and setting pertaining to the origin of and the setting of the clay and silt samples that I have analyzed for pollen content.

The North Radwaste Trench exposure reveals a bedrock structure, a fault zone, in which fine-grained sediment has filled in openings in the bedrock between the beds, in the fault breccia, and in joints and other fractures. It is apparent that many openings exist in the bedrock and that the permeability created by these interconnected openings could allow for the passage of groundwater and fine sediment vertically and horizontally through the section. Furthermore, the clays and silts are deformed which indicates post depositional bedrock movements.

Samples of these sediments were obtained for palynological study from members of the Dames & Moore geological staff. These samples, which were taken prior to this visit and shipped to me, were carefully taken from fresh exposures by these geologists who packaged the samples directly at the exposure, according to my instructions, in order to eliminate contamination by airborne pollen. Pollen analysis indicates that contamination has not occurred.

Numerous samples of clay and silt from a variety of deposits in the bedrock openings consistently contain pollen assemblages that indicate a late-glacial age, based on comparison with the established pollen stratigraphy of New York for the late- and postglacial, that is, after 15,000 years before the present for the central New York region. The pollen assemblages from these samples generally include pollen of spruce, 2 pine species, birch, alder, willow, boreal shrubs, grass and composites, and spores of Sphagnum and ferns. These assemblages, which contain very few pollen of deciduous, hardwood trees, are best correlated with the spruce pollen or A zone that occurred in this region around 12,000 years ago, and indicate that spruce forests existed here at that time. The lack of hardwoods testifies both to the lack of contamination from the modern hardwood forest and therefore, the spruce (A) zone age for the sediments. Alternatively, in the surface exposure of proglacial lake sediments in the Cooling Tower Trench a sequence of



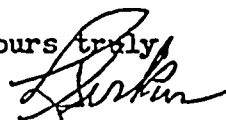
radiocarbon-dated pollen zones was encountered, the spruce zone at the base, succeeded by the pine (B) zone, and the oak (C) zone. In a qualitative sense, the pollen grains are all well stained (a stain is added in the processing of samples) which indicates a younger age for the pollen grains and relative freshness of the wall structure. Early Pleistocene, or Tertiary grains would only stain lightly, older grains would not accept the stain. The absence of pre-Pleistocene palynomorphs, except for those of bedrock age, rules out a pre-Pleistocene age for the infillings.

In comparison with the pollen stratigraphy of the overall Nine Mile Point site, based on sections from other exposures which I have previously studied, and with the ages of the sediments supported by pollen data and radiocarbon ages, the clays and silts in the bedrock openings are of late-glacial age. The presence of sediments of this age in proglacial lake deposits overlying the bedrock at this site provides a direct source of pollen bearing sediment for filling of the bedrock openings. There is no other source of such sediment in this area. It is, therefore, probable that the lacustrine sediments from the basal part of the lake section were remobilized and redeposited in the bedrock openings by groundwater and were subsequently deformed. Deformation, then, postdates the initial deposition of the clays, silts, and pollen during the late-glacial.

In summary, my recent inspection of the site reveals that deformed deposits of clay and silt extensively occur within equally extensive openings in the bedrock structure in this trench. Pollen analysis shows that spruce zone pollen assemblages are found in these sediments and also occur in nearby late-glacial lake deposits. An alternative source for such sediments and pollen has not been found.

I will look forward to hearing from you concerning these observations and will be available to comment on them if you have any questions.

Yours truly,



Les Sirkin,
Consultant.

538 E. Fairmont Drive
Tempe, AZ 85282

April 10, 1980

Mr. John J. Markham
Project Manager, Dames & Moore
2996 Belgium Road
Baldwinsville, NY 13207

Dear Mr. Markham:

The following is a letter report initiated at your request to consider the origin and age of the clay deposited in voids in the bedrock in and near the Radwaste Fault Zone in sedimentary bedrock at Nine Mile Point Nuclear Station-Unit 2, Scriba, New York and the relationship of this clay to bedrock movement along the fault. The report is based on discussions with geologists working at the site, reading of prepared reports, and two site investigations.

Introduction

Geologists of Dames & Moore and Stone & Webster have been studying the bedrock and overlying unconsolidated sediments at the Nine Mile Point site for several years for three power sites. My field inspection of the site was in the morning of February 29, 1980 and in the afternoon of April 4, 1980. Nine Mile Point Nuclear Station-Unit 2 is on the shore of Lake Ontario at Nine Mile Point, Scriba Township, Oswego County, New York.

Geology

General statement

Two thorough briefings were given by geologists of Dames & Moore and Stone and Webster. The first site visit dealt mainly with investigations of buckles in the sedimentary bedrock. Discussions with Stone & Webster geologists took place on the afternoon of February 28, 1980 in Boston, MA, and on the site in the morning of February 29, 1980. Discussions in detail with geologists of Dames & Moore occurred Friday afternoon at the site. In the morning of Friday, February 29, there was a field site visit in which we examined the geology in the Drainage Ditch, the Radwaste Trench, the Screen Well area, North Electric Cable "tunnel" and the Cooling Tower Excavation. In addition, it was possible to examine black and white and color photographs as well as many field sketches,



preliminary diagrams of geological exposures, and study geological reports. The second site visit was on April 4, 1980. At this time there were detailed discussions limited explicitly to the physical features of the clay in the Radwaste Trench. Discussions were with geologists of Dames & Moore and Stone & Webster. In the afternoon of April 4 it was possible for me to make about a 2 hour examination of the clay deposits in the bedrock in the Radwaste Trench in a special exposure that was prepared. I was accompanied by Mr. Scott Laird of Dames & Moore and Mr. Nick Drakulich of Stone & Webster.

Unconsolidated sediments

The area lies in the Erie-Ontario Lowland and has been overridden by glacier ice several times. Unconsolidated sediments include till of late Wisconsinan age. Unpublished data provided by site geologists indicate two tills, a dense basal till and the overlying upper till, interpreted to be an ablation till. Overlying the tills are various glaciofluvial deposits characteristic of stagnating glaciers and thawing ground, including melting glacial ice blocks. Also reported to be widespread in the site area are finely laminated clay-silts of former Lake Iroquois. Lake Iroquois formed with the withdrawal of the continental glacier; the lake is reported to have left the site about 13,500 years ago. It existed for hundreds if not thousands of years. In the bottom of the lake was deposited typical laminated clays and silts and clayey-silts, as well as silty clays. These deposits in some places directly overlie bedrock. In the site area and adjoining areas the clays and silts have been mapped and examined by geologists and consultants of Dames & Moore. Detailed mechanical analyses of the sediments, as well as mineralogical studies have been made. Also, pollen analyses have been performed. The pollen is characteristic of late Wisconsinan time.

Bedrock

The consolidated rocks at the site are of the Oswego formation of upper Ordovician age. The rocks consist of tabular, thin to medium beds of light grey to greenish-gray, fine-grained sandstone interlayered with thin beds of grey siltstone and dark grey shale. In the site area the top bed is a rather massive grey sandstone 3 to 5 feet thick. The beds dip very gently to the south or southwest less than one degree. Exposures in the Radwaste Trench permitted observation of bedrock faces totalling as much as 15 to 16 feet vertically and 40 feet horizontally.

Small faults in the bedrock of the Nine Mile Point area have been studied: Barge Slip Fault, Drainage Ditch Fault, (an extension of fault in the Fitzpatrick excavation) cooling Tower Fault, and the Radwaste Trench Fault. The latter is of interest in this investigation.

The Radwaste Trench Fault appears to be a bedding plane slip which also involves the rupturing of small, sharp, asymmetric anticlines that occur in the thin beds of the Oswego sandstone. Associated with the fracturing is a greenish grey to grey gouge or breccia with a fine-grained matrix. The thin ($\frac{1}{2}$ -1 inch) sandstone or siltstone layers have been deformed and, inasmuch as they were brittle,



have ruptured and some pieces of the rock are rotated. The rocks along the thrust fault are said to be displaced 1 to 7 feet.

The most important aspects of the structure is that the movement has created a dilation of the bedrock, especially near the fault zone, and there are numerous openings along bedding planes, and especially with the fractured and folded beds and rotated rock fragments. The voids observed are as much as 2 inches in diameter. In the openings in the bedrock is deposited locally a calcarous tan to grey slightly plastic clayey silt which shows very delicately preserved minute wavy laminations, and deformations of many types including folds, drapes and rather irregular convolutions. Close examination reveals that there is a grey clay and a tan or brownish clay, the later of which seems to preserve more of the laminations and deformation features. Clay deposits are up to 2 inches thick but generally are much thinner and form a coating on bedrock layers whether they are flat or tilted, even up to 30-40 degrees. It is the age, origin, and relationship of this clay to the bedrock which is central to this report.

Clayey silt filling voids in bedrock

Origin

The unconsolidated fine-grained sediments filling bedrock voids will be referred to as clay, although it has been shown to be a silty clay with some thin laminations, mostly silt, and in most places a clayey silt. Experts under contract with Dames & Moore and Dames & Moore personnel have carefully studied the size grade distribution, mineral composition, calcium carbonate concentration, and pollen content of the clay and its association with the gouge with fine grained matrix. The calcarous clay is almost totally different from the siliceous gouge matrix and therefore considered not to have been derived from the grinding of the bedrock during faulting or by weathering of the bedrock. The clay is remarkably similar in almost all details to the pollen, mineral, and calcium carbonate content and size grade distribution of the overlying clayey deposits of extinct Lake Iroquois. I concur with these workers that the clayey silt from the overlying Lake Iroquois filtered down with groundwater, especially when Lake Iroquois covered the region, and was carried by vertical and horizontal currents to be deposited in the voids of the bedrock underlying the lake.

Age

No C-14 dates have been obtained on organic material in the clay in the bedrock voids. However, pollen and analyses have been done on clay both in 1979 and 1980. These studies indicate that the silty clays were deposited during Pleistocene time in an environment abundant with spruce, most likely late glacial (i.e. late Wisconsinan time). This is essentially the same pollen spectra reported from the overlying lake sediment. Although it cannot be ruled out that the clay with pollen could be of an earlier Pleistocene spruce time, it would appear to me, based upon work of the pollen experts, that the age of the clay is indeed late Wisconsinan, 10,000-13,500 years BP.



Origin of structures in the clay

Scientists and engineers studying the clay have noted the deformation of the laminated clay, and various sketches and photographs of the material were available from Dames & Moore and Stone & Webster for my inspection. In addition, a few exposures of the deformed clay were seen in the Radwaste Trench on April 4, 1980.

The laminated clay is minutely deformed in places with folds and waves and distortions in the order of 1 millimeter up to folds and deformations up to 2 inches. The terms undulating laminations, wavy laminations, involutions, convolutions, drapes, rolls, folds, minute breaks, intricate deformation, and others have been used in the literature to describe these structures. The structures in the Radwaste Trench are in layers of clay $\frac{1}{2}$ to 2 inches thick on horizontal, and especially sloping, sandstone surfaces.

I have seen similar structures in Alaska and Europe in late Pleistocene glaciolacustrine silty clays and clays and they are commonly described in the literature in such sediments from Paleozoic to Holocene age, especially the later. Such structures are generally described as penecontemporaneous, meaning that they formed during the deposition or near the end of deposition, and formed by slumping, partial plastic deformation and perhaps some liquefaction of the water-saturated fine-grained material. Some deformation could be at the termination of the clay accumulation.

I believe that the silt and clay size particles were conducted downward and laterally by currents through minute to large openings in the rock when Lake Iroquois existed above providing a "high" water table (bedrock and lake clays completely saturated). The sediment-bearing currents (microturbidity currents) carried the fine grained particles through the openings where they settled out on horizontal or sloping surfaces. The soft, water-saturated clay layer could also have been disturbed by the sediment-laden water currents in what could be described as a small, or minute cave environment. Most of the deformation probably can be attributed to the effect of gravity on the sediments aided by water velocity and direction of currents. Any disturbance to the environment due to local shocks during glacial withdrawal, lake withdrawal and land rebounding would have been favorable for microdisturbances that might have caused or aided in the slumping or liquefaction of the sediments. Therefore, in summary, I believe that the deformation observed in the unconsolidated slightly plastic clayey silt is due to penecontemporaneous, or what could be called syndepositional and maybe some postdepositional, distortion and are not the result of the folding and faulting of the bedrock.

Relation of the clay to bedrock

It has been suggested that deformation of the clay took place during movement of the bedrock along the fault and that this movement produced some or much of the bedrock structure we see today. Two points should be mentioned here. First, I believe clay structures are syndepositional (contemporaneous deformation) and/or immediately post-depositional and do not require bedrock movement to form. Second, during field examinations on April 4, 1980 in the Radwaste Trench I found

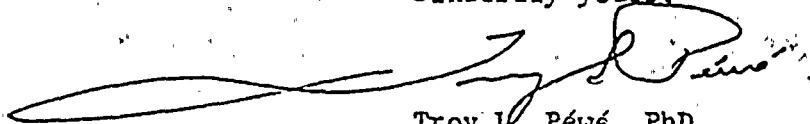


in two places where the clay was clearly post-depositional over small, sharp, asymmetric broken bedrock anticlines involving sandstone layers $\frac{1}{2}$ to $\frac{3}{4}$ inch thick. The clay clearly overlay the inclined sandstone layer and the broken edges of the sandstone slabs. In a report by geologists of Stone & Webster they state that on February 29, 1980 examination in the Radwaste Trench indicated that they clearly observed a clay layer deposited across the entire width of an anticlinal hinge which would indicate that the clay post-dates the bedrock deformation.

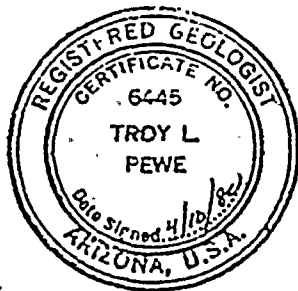
Conclusion

1. The grey and tan slightly plastic clayey silts fills voids in the bedrock associated with a low angle thrust fault exposed in Radwaste Trench.
2. The clayey silt originated from the overlying glaciolacustrine deposits of Lake Iroquois that formerly overlay the site.
3. The clayey silt is therefore late Wisconsinan in age, 10,000-13,500 years BP.
4. During deposition of the clay by small vertical and horizontal water currents in the bedrock, as well as settling from non-moving groundwater, the fine-grained sediment layers were minutely deformed by slumping and plastic deformation of the water-saturated sediments and perhaps by some liquefaction. These structures are syndepositional and post-depositional and are similar to those reported in glaciolacustrine sediments in many places in the world.
5. Because the deformed structures in the clay are syndepositional and because it can be shown that the clay layers in places overlie without disturbance the deformed broken bedrock structures and sharp broken edges of the sandstone layers, I believe the clay post dates the bedrock deformation.

Sincerely yours,



Troy L. Péwé, PhD.
Professor of Geology
Consulting Geologist



Registered Geologist
State of Arizona # 6445

Registered Geologist
State of California # 2834

Registered Engineering Geologist
State of California # 832





PHOTOGRAPH OF CLAY OVERLYING
BEDROCK SLAB IN NORTH RADWASTE TRENCH

TABLE E-1
U.S.B.M. GAUGE CALIBRATION RECORDS

<u>GAGE</u>	<u>DATE</u>	K_1 ($\times 10^{-6}$ In.)	K_2 ($\times 10^{-6}$ In.)	K_3 ($\times 10^{-6}$ In.)
W-33	4/03/80	0.98	1.01	0.99
W-33	4/07/80	0.99	1.01	1.00
T-32	4/07/80	1.01	1.00	1.02
W-54SS	4/08/80	0.91	0.89	0.91
T-39	4/09/80	1.04	1.08	1.05
W-33	4/11/80	0.97	1.01	1.00
T-32	4/11/80	1.02	0.99	1.00
W-54SS	4/11/80	0.90	0.90	0.93
W-54SS	4/15/80	0.89	0.91	0.92
T-39	4/16/80	1.07	1.09	1.07
W-33	4/17/80	0.98	1.00	0.98
T-39	4/17/80	1.08	1.08	1.05
T-32	4/17/80	1.04	1.00	1.03
T-39	4/21/80	1.03	1.08	1.08
W-54SS	4/21/80	0.87	0.89	0.90
T-32	4/22/80	1.02	1.00	1.02
W-33	4/22/80	1.01	0.97	1.01
W-54SS	4/22/80	0.88	0.92	0.90
T-39	4/24/80	1.07	1.09	1.04
T-32	4/24/80	1.00	0.98	1.00
T-39	4/25/80	1.04	1.08	1.08
W-54SS	4/25/80	0.88	0.92	0.92
T-32	4/29/80	1.01	0.96	1.01
T-39	4/28/80	1.14	1.20	1.17
W-54SS	4/30/80	0.89	0.92	0.92
T-32	4/30/80	1.05	0.98	1.02
T-39	4/30/80	1.03	1.10	1.09
W-53	5/01/80	1.06	1.09	1.08
T-38	5/02/80	1.04	1.05	1.12
W-54SS	5/03/80	0.84	0.92	0.89
W-54SS	5/04/80	0.91	0.90	0.89
W-53	5-05-80	1.10	1.10	1.06
T-38	5-06-80	1.04	1.06	1.12



1
2
3
4
5
6
7
8
9
10
11
12
13
14
15
16
17
18
19
20
21
22
23
24
25
26
27
28
29
30
31
32
33
34
35
36
37
38
39
40
41
42
43
44
45
46
47
48
49
50
51
52
53
54
55
56
57
58
59
60
61
62
63
64
65
66
67
68
69
70
71
72
73
74
75
76
77
78
79
80
81
82
83
84
85
86
87
88
89
90
91
92
93
94
95
96
97
98
99
100

TABLE E-1 CONTINUED

<u>GAGE</u>	<u>DATE</u>	K_1 ($\times 10^{-6}$ In.)	K_2 ($\times 10^{-6}$ In.)	K_3 ($\times 10^{-6}$ In.)
W-53	5/07/80	1.07	1.10	1.03
W-54SS	5/07/80	0.85	0.87	0.87
W-53	5/09/80	1.01	0.99	1.01
W-54SS	5/14/80	0.91	0.87	0.89
T-38	5/14/80	1.03	1.03	1.09
W-54SS	5/18/80	0.90	0.93	0.95
W-33	5/18/80	1.00	0.99	0.96
W-54SS	5/20/80	0.89	0.91	0.94
T-39	5/21/80	1.05	1.08	1.03
W-54SS	5/28/80	0.95	1.00	0.94
W-33	6/03/80	1.00	1.00	0.99
W-33	6/04/80	1.03	1.02	1.00
W-54SS	6/05/80	0.95	0.94	0.91
W-53	6/10/80	1.01	0.96	0.96
T-39	6/11/80	1.05	1.05	1.05
W-54SS	6/11/80	0.95	1.03	0.94
W-53	6/12/80	1.03	0.99	1.00
W-53	6/16/80	1.02	0.98	0.99
W-53	6/18/80	1.02	0.99	0.99
W-53	6/19/80	1.01	0.97	1.01
W-53	6/20/80	1.04	0.97	1.01
W-53	6/24/80	1.02	0.98	1.01
W-54SS	6/24/80	1.03	0.94	1.05
T-39	6/25/80	1.06	1.07	1.09



BORING RS-1

SURFACE ELEVATION
COORDINATES

DESCRIPTIVE GEOLOGIC NOTES

RUN NO.	BEDDING DIPS	FRACTURES	IN SITU STRESS MEASUREMENT		DEPTH IN FEET	SAMPLING REC. (%) AND CORING	GRAPHIC LOG
			TEST NUMBER	DEPTH IN FEET			
					0		
					5		
					10		
1					100		
2					100		
3					100		
4					100		
5					100		
6					100		
7					100		
8					100		
9			1	41°2'E	100		
10			2	43°10"	100		
11			3	46°5"	100		
12			4	47°9"	100		
13			5	48°11"	100		
14			6	50°0"	100		
15			7	50°11"	100		
16			8	53°9"	100		
17			9	55°	100		
18			10	56°2"	100		
19	20		11	56°8"	100		
20			12	58°3"	100		
21			13	59°5"	100		
22			14	61°	100		
23			15	63°4"	100		
24	25		16	64°8"	100		
25			17	66°1"	100		
26			18	68°4"	100		
27					100		
28					100		
29					100		
30					100		
31					100		

OVERBURDEN

LIGHT GRAY MEDIUM GRAINED THICKLY BEDDED SILICEOUS
SANDSTONE WITH THIN BEDS OF SILTSTONE, CROSS
BEDDING AND CLAY CLASTS COMMON, HARD AND
UNWEATHEREDOSWEGO
SANDSTONETRANSITION
ZONEPULASKI
FORMATION

UNIT A

GRAY MEDIUM TO COARSE GRAINED, MEDIUM TO THICKLY
BEDDED GRAYWACKE WITH ABUNDANT CLASTIC MASS,
INTERBEDDED WITH DARK GRAY LAMINATED TO THINLY
BEDDED SILTY SHALE AND LIGHT GRAY MEDIUM GRAINED
THIN TO THICKLY BEDDED SILICEOUS SANDSTONE,
FOSSILIFEROUS, MODERATELY HARD AND UNWEATHERED

SAMPLING AND CORING INFORMATION

Core run
R.Q.D.
Percent recovery

BEDDING DIPS

03° Bedding dips measured on selective bedding planes. An attempt
was made to avoid all obvious cross bedding or other primary
structures.

FRACTURES

Breccia zone
Dip-slip slickensides
Fractures-shown at approximate angle to core axis
Mineralized fracture c = calcite s = sulfide
Fractured zone

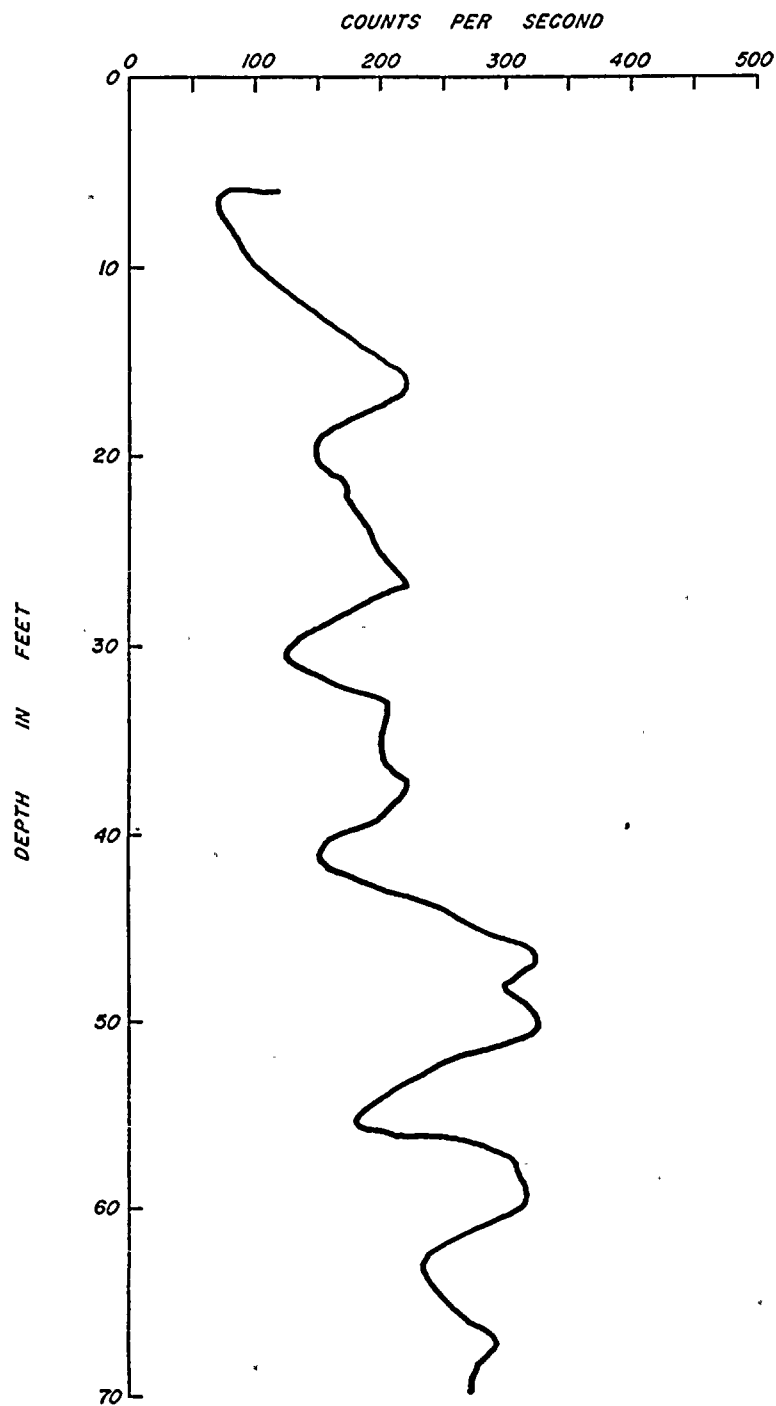
KEY TO SYMBOLS

Sandstone
Graywacke
Siltstone
Shale
Fossils
Shale intra-clasts
Cross-bedding
Shale laminae

PLATE E-1.1
DAMES & MOORE

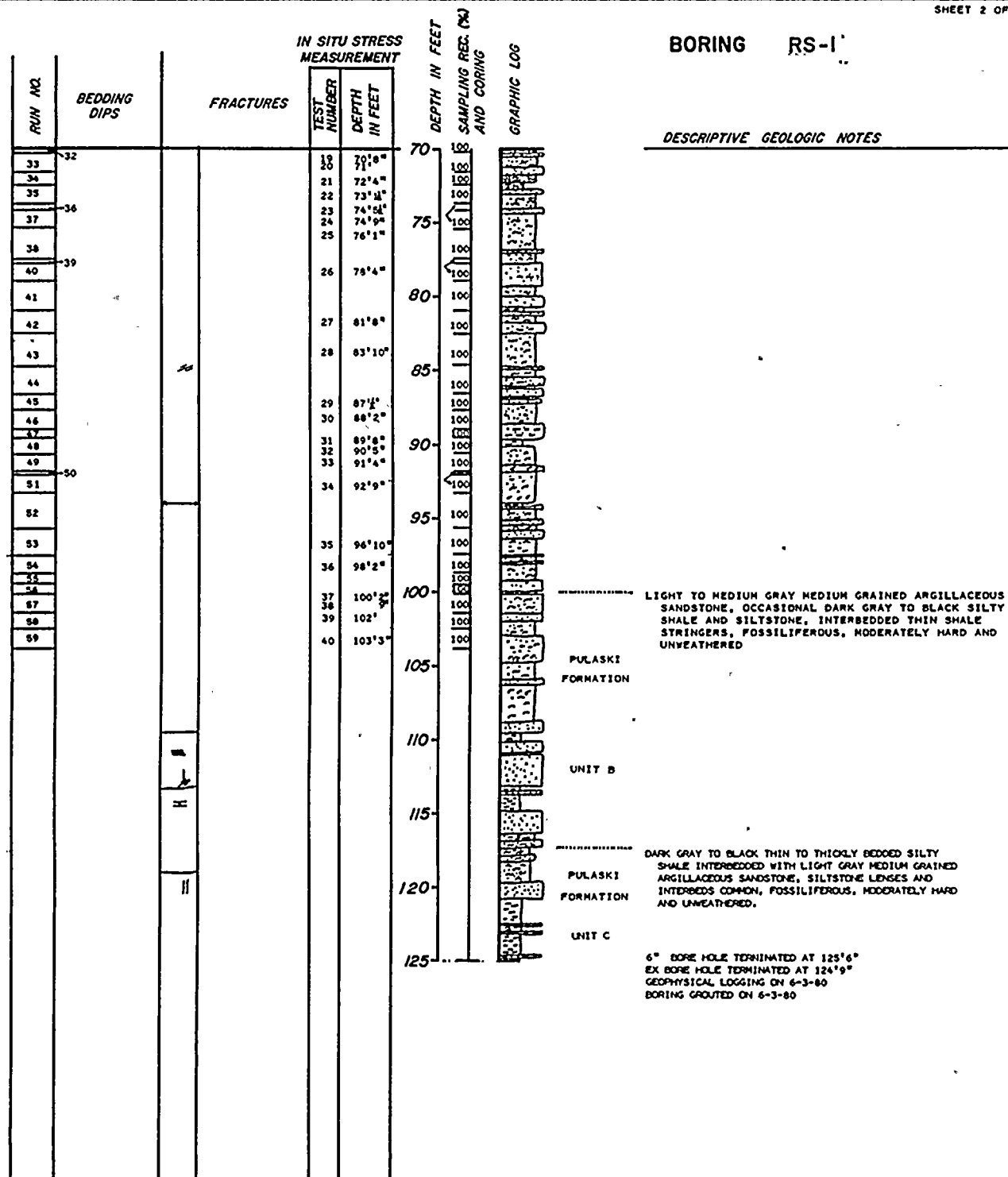


BORING RS-1



GAMMA RAY LOG

BORING RS-1



SAMPLING AND CORING INFORMATION

Core run
100% R.O.D.
Percent recovery

BEDDING DIPS

03° Bedding dips measured on selective bedding planes. An attempt was made to avoid all obvious cross bedding or other primary structures.

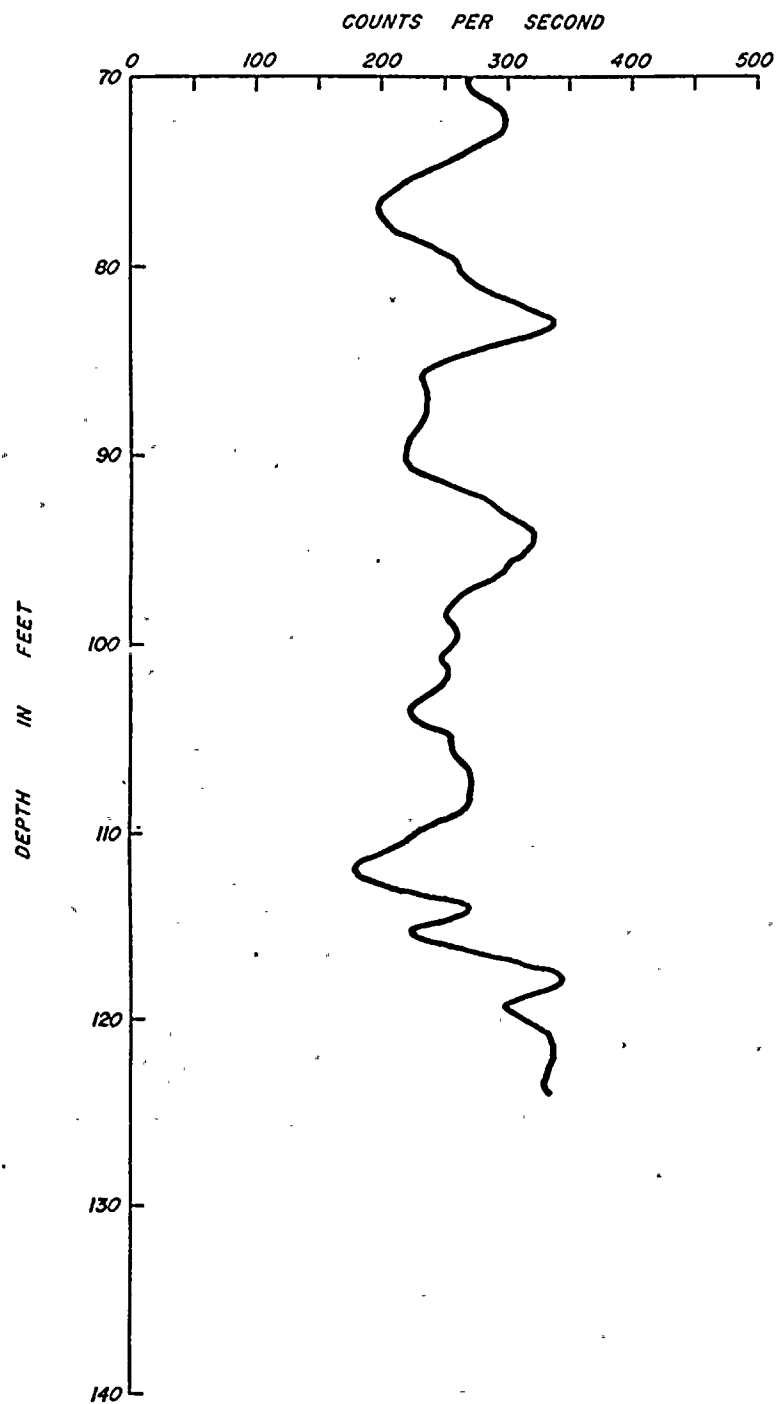
FRACTURES

--- Breccia zone
--- Dip-slip slickensides
--- Fractures-shown at approximate angle to core axis
--- Mineralized fracture c = calcite s = sulfide
--- Fractured zone

KEY TO SYMBOLS

--- Sandstone
--- Graywacke
--- Siltstone
--- Shale
--- Fossils
--- Shale intra-clasts
--- Cross-bedding
--- Shale laminae

BORING RS-1



GAMMA RAY LOG

BORING RS-2

SURFACE ELEVATION
COORDINATES

DESCRIPTIVE GEOLOGIC NOTES

FILL

LIGHT GRAY MEDIUM GRAINED THICKLY BEDDED SILICEOUS SANDSTONE WITH THIN BEDS OF SILTSTONE, CROSS-BEDDING AND CLAY CLASTS COMMON, HARD AND UNWEATHERED

OSWEGO
SANDSTONE

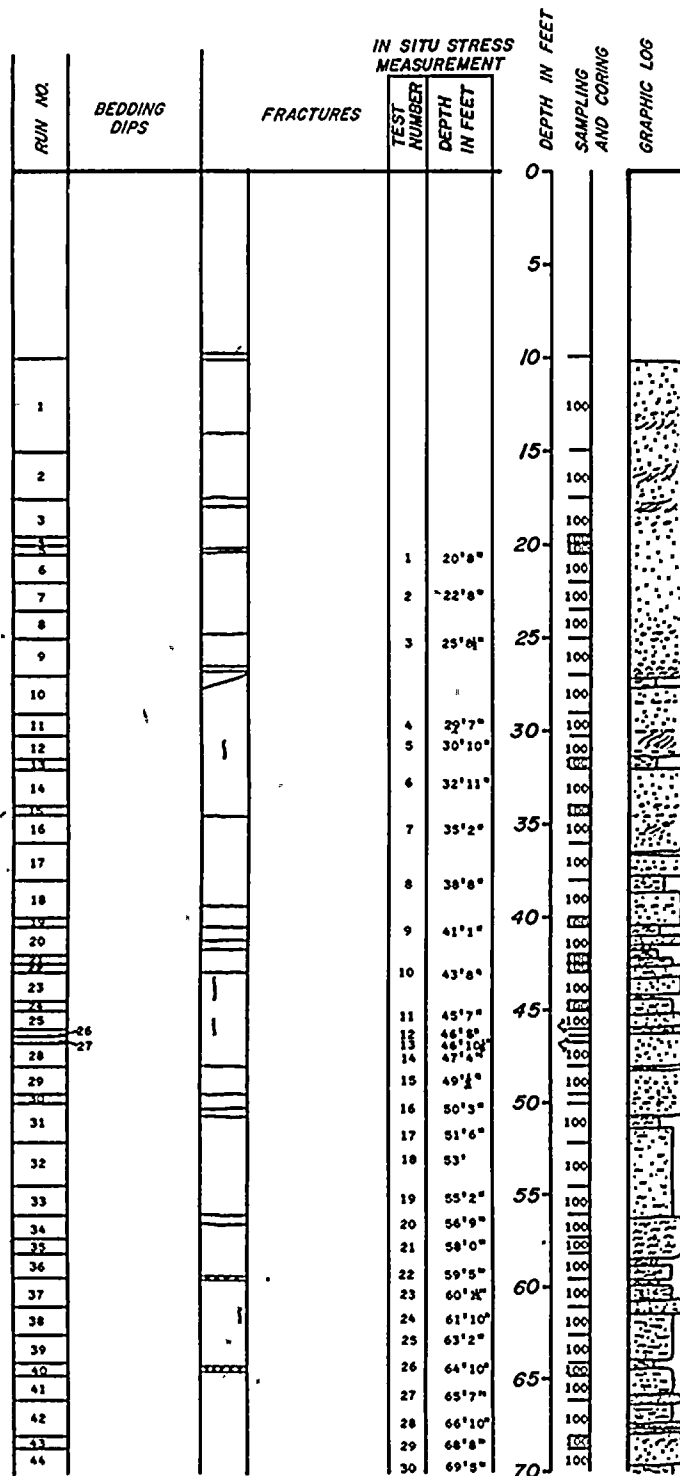
ILLITE

TRANSITION
ZONE

GRAY MEDIUM TO COARSE GRAINED, MEDIUM TO THICKLY BEDDED GRAYWACKE WITH ABUNDANT CLASTIC MASH, INTERBEDDED WITH DARK GRAY LAMINATED TO THINLY BEDDED SILTY SHALE AND LIGHT GRAY MEDIUM GRAINED THIN TO THICKLY BEDDED SILICEOUS SANDSTONE, FOSSILIFEROUS, MODERATELY HARD AND UNWEATHERED

PULASKI
FORMATION

UNIT A



SAMPLING AND CORING INFORMATION

Core run
100 95 R.Q.D.
Percent recovery

BEDDING DIPS

03° Bedding dips measured on selective bedding planes. An attempt was made to avoid all obvious cross bedding or other primary structures.

FRACTURES

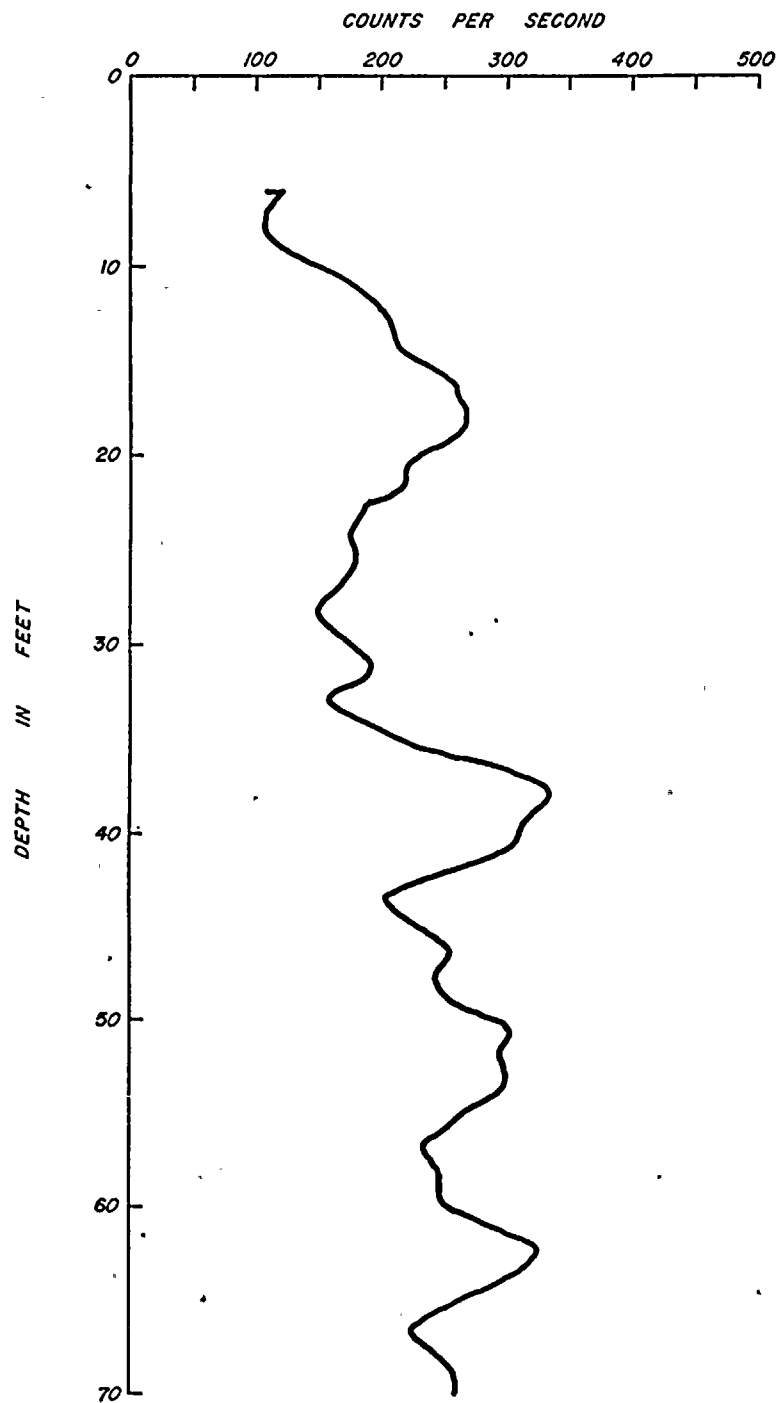
Breccia zone
Dip-slip slickensides
Fractures-shown at approximate angle to core axis
Mineralized fracture c - calcite s - sulfide
Fractured zone

KEY TO SYMBOLS

Sandstone
Graywacke
Siltstone
Shale
Fossils
Shale intra-clasts
Cross-bedding
Shale laminae

PLATE E-2.1
DAMES & MOORE

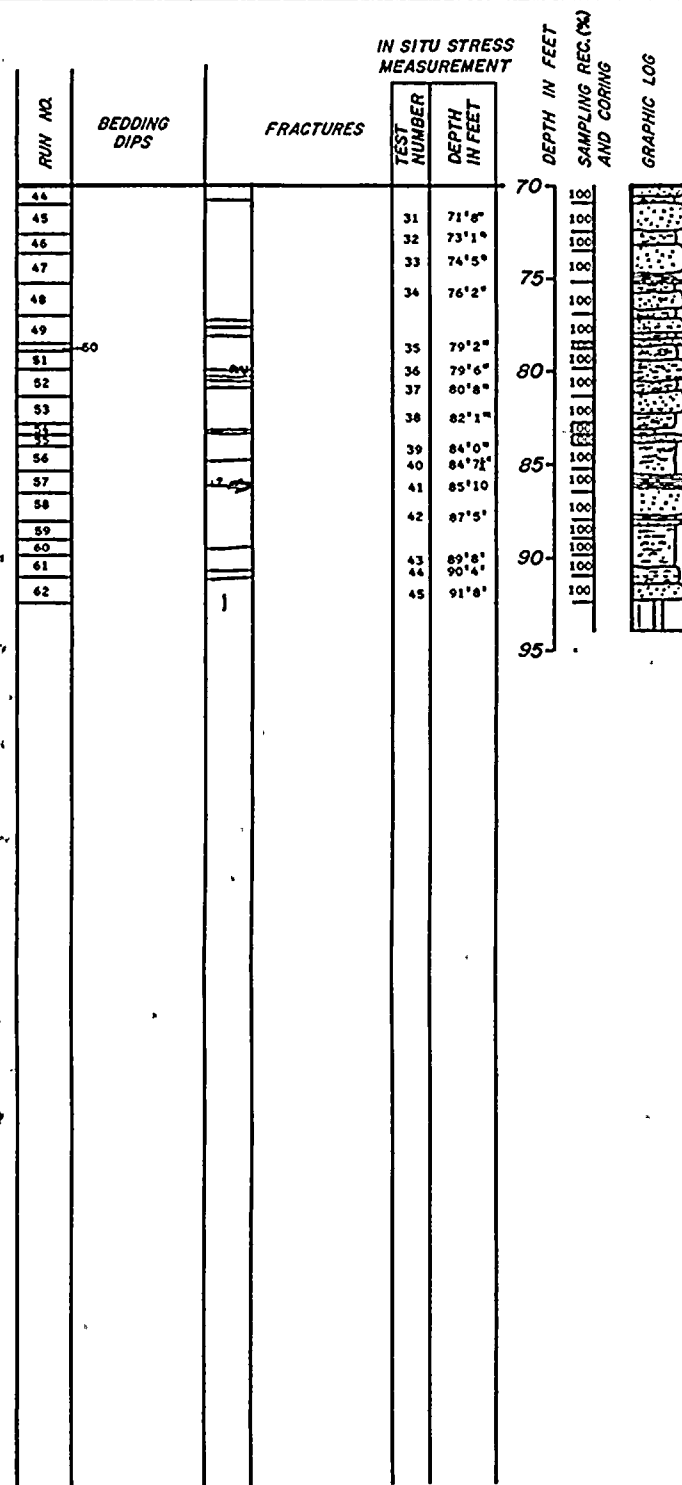
BORING RS-2



GAMMA RAY LOG



BORING RS-2



DESCRIPTIVE GEOLOGIC NOTES

BRIGHT GREEN ILLITE

PULASKI
FORMATION
UNIT B

LIGHT TO MEDIUM GRAY MEDIUM GRAINED ARGILLACEOUS SANDSTONE, OCCASIONAL DARK GRAY TO BLACK SILTY SHALE AND SILTSTONE, INTERBEDDED THIN SHALE STRINGERS, FOSSILIFEROUS, MODERATELY HARD AND UNWEATHERED

6" BORE HOLE TERMINATED AT 92'41" ON 5-6-80

EX BORE HOLE TERMINATED AT 94'

GEOPHYSICAL LOGGING ON 5-27-80

INSTALLED 92' OF INCLINOMETER CASING IN THE BORE HOLE ON 5-25-80

SAMPLING AND CORING INFORMATION

Core run
100/95 R.Q.D.
Percent recovery

BEDDING DIPS

03° Bedding dips measured on selective bedding planes. An attempt was made to avoid all obvious cross bedding or other primary structures.

FRACTURES

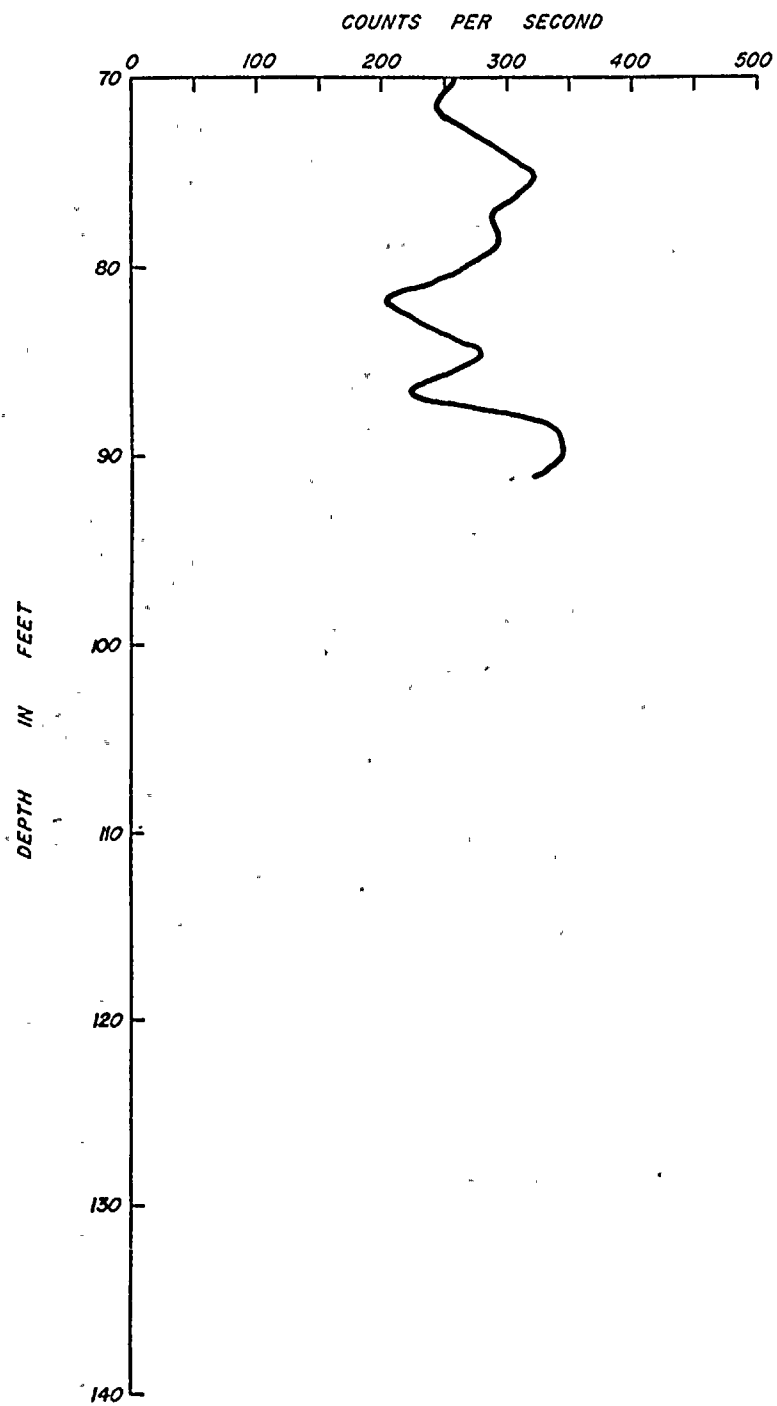
Breccia zone
 Dip-slip slickensides
 Fractures shown at approximate angle to core axis
 Mineralized fracture c = calcite s = sulfide
 Fractured zone

KEY TO SYMBOLS

Sandstone
 Graywacke
 Siltstone
 Shale
 Fossils
 Shale intra-clasts
 Cross-bedding
 Shale laminae



BORING RS-2



GAMMA RAY LOG

BORING RS-3

SURFACE ELEVATION
COORDINATES

DESCRIPTIVE GEOLOGIC NOTES

LIGHT GRAY MEDIUM GRAINED THICKLY BEDDED SILICEOUS SANDSTONE WITH THIN BEDS OF SILTSTONE, CROSS-BEDDING AND CLAY CLASTS COMMON, HARD AND UNWEATHERED

OSWEGO
SANDSTONETRANSITION
ZONE

GRAY MEDIUM TO COARSE GRAINED, MEDIUM TO THICKLY BEDDED GRAYWACKE WITH ABUNDANT CLASTIC MASH, INTERBEDDED WITH DARK GRAY LAMINATED TO THINLY BEDDED SILTY SHALE AND LIGHT GRAY MEDIUM GRAINED THIN TO THICKLY BEDDED SILICEOUS SANDSTONE, FOSSILIFEROUS, MODERATELY HARD AND UNWEATHERED

PLASKI
FORMATION

UNIT A

DISSEMINATED ILLITE

RUN NO.	BEDDING DIPS	FRACTURES	IN SITU STRESS MEASUREMENT		DEPTH IN FEET	SAMPLING REC. (%)	AND CORING	GRAPHIC LOG
			TEST NUMBER	DEPTH IN FEET				
1					0	100		
2					5	90		
3			1	6'8"	10	100		
4			2	7'11"	15	100		
5			3	11'1"	20	100		
6			4	13'2"	25	100		
7			5	16'2"	30	100		
8			6	17'6"	35	100		
9			7	18'4"	40	100		
10					45	100		
11			8	23'3"	50	100		
12			9	24'10"	55	100		
13			10	25'81"	60	100		
14			11	27'9"	65	100		
15			12	29'6"	70	100		
16			13	31'81"	75	100		
17			14	32'101"	80	100		
18			15	35'71"	85	100		
19			16	35'111"	90	100		
20			17	37'1"	95	100		
21			18	38'5"	100	100		
22			19	39'7"	105	100		
23			20	40'101"	110	100		
24			21	41'31"	115	100		
25			22	43'91"	120	100		
26			23	45'1"	125	100		
27			24	48'5"	130	100		
28			25	49'101"	135	100		
29			26	52'41"	140	100		
30			27	53'1"	145	100		
31			28	54'4"	150	100		
32			29	59'61"	155	100		
33			30	60'6"	160	100		
34			31	64'11"	165	100		
35			32	64'101"	170	100		
36			33	65'41"	175	100		
37			34	65'8"	180	100		
38			35	67'8"	185	100		
39			36	68'51"	190	100		
40			37	69'71"	195	100		
41					200	100		
42					205	100		
43					210	100		
44					215	100		
45					220	100		
46					225	100		
47					230	100		
48					235	100		
49					240	100		
50					245	100		
51					250	100		
52					255	100		

SAMPLING AND CORING INFORMATION

Core run
100 95 R.Q.D.
Percent recovery

BEDDING DIPS

03° Bedding dips measured on selective bedding planes. An attempt was made to avoid all obvious cross bedding or other primary structures.

FRACTURES

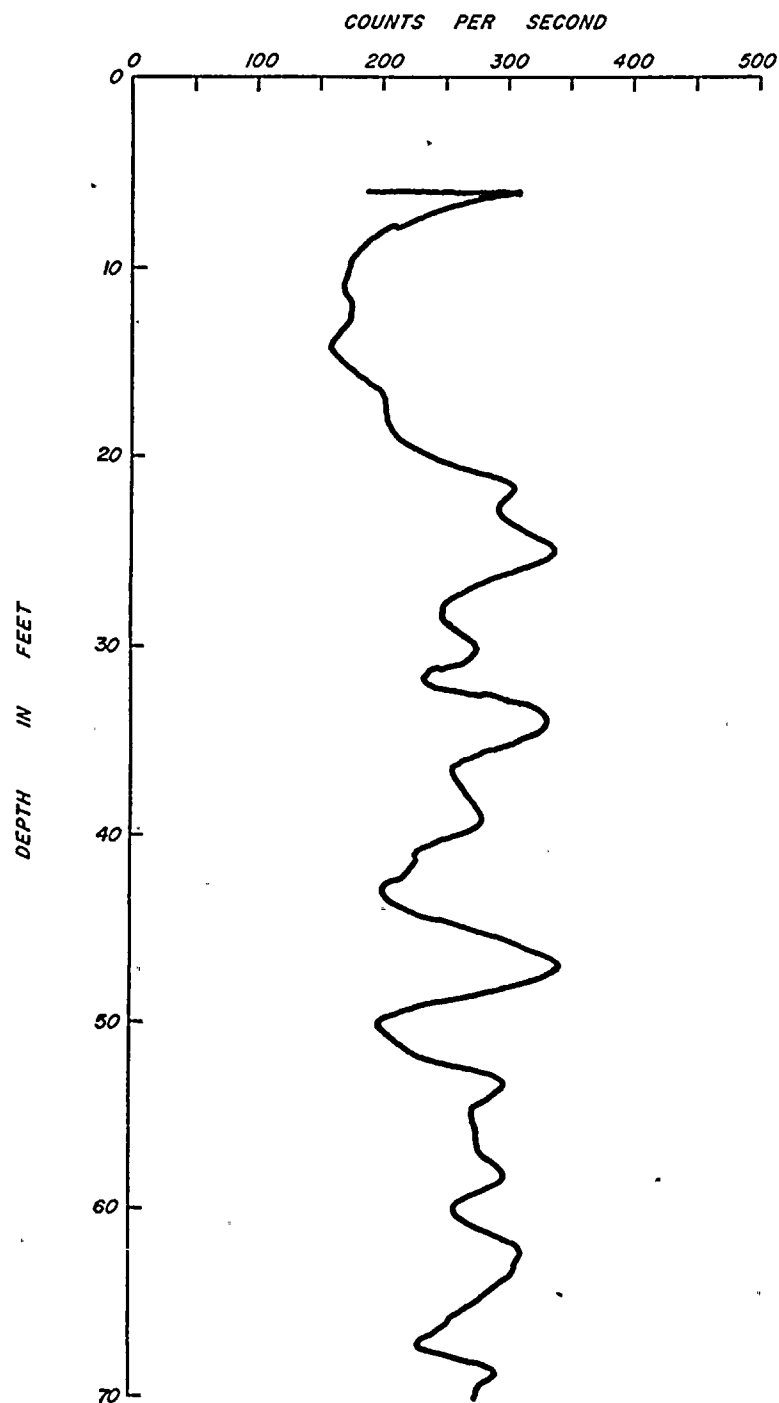
Breccia zone
Dip-slip slickensides
Fractures-shown at approximate angle to core axis
Mineralized fracture c - calcite s - sulfide
Fractured zone

KEY TO SYMBOLS

Sandstone
Graywacke
Siltstone
Shale
Fossils
Shale intra-clasts
Cross-bedding
Shale laminae




BORING RS-3



GAMMA RAY LOG



BORING RS-3

RUN NO.	BEDDING DIPS	FRACTURES	IN SITU STRESS MEASUREMENT		DEPTH IN FEET	SAMPLING REC. (%) AND CORING	GRAPHIC LOG
			TEST NUMBER	DEPTH IN FEET			
53		4	38	70' 10"	70	100	
54			39	72' 1"	72	100	
55			40	74'	74	100	
57			41	74' 6"	75	100	
58			42	75' 10 1/2"	76	100	
59			43	77' 1 1/2"	77	93	
					80		

DESCRIPTIVE GEOLOGIC NOTES

LIGHT TO MEDIUM GRAY MEDIUM GRAINED ARGILLACEOUS SANDSTONE, OCCASIONAL DARK GRAY TO BLACK SILTY SHALE AND SILTSTONE, INTERBEDDED THIN SHALE STRINGERS, FOSSILIFEROUS, MODERATELY HARD AND UNWEATHERED

6" BORE HOLE TERMINATED AT 77' 9" ON 5-9-80
EX BORE HOLE TERMINATED AT 79'
GEOPHYSICAL LOGGING (1/2) ON 5-27-80
BORE HOLE GROUTED ON 5-27-80






SAMPLING AND CORING INFORMATION

Core run
100% R.Q.D.
Percent recovery




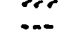
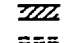



BEDDING DIPS

03° Bedding dips measured on selective bedding planes. An attempt was made to avoid all obvious cross bedding or other primary structures.

FRACTURES

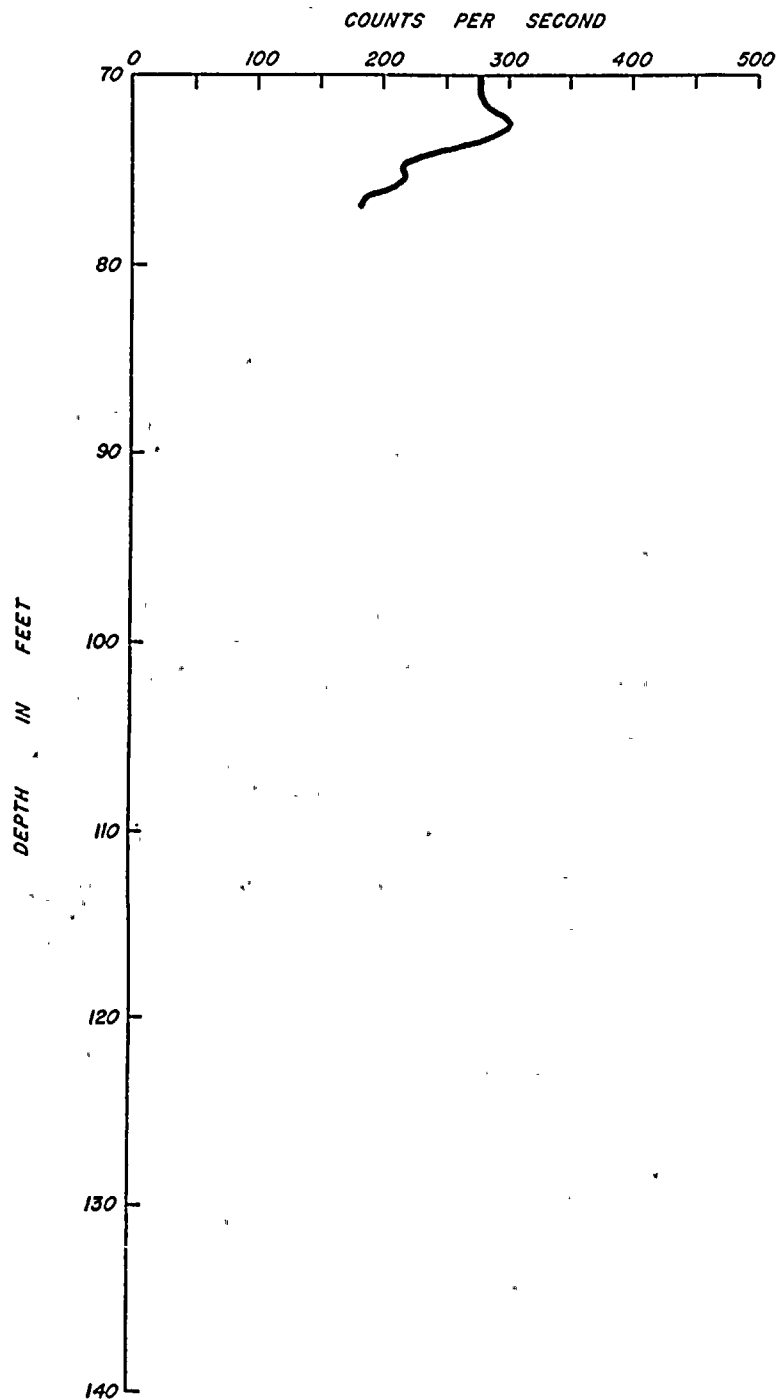
 Breccia zone
 Dip-slip slickensides
 Fractures-shown at approximate angle to core axis
 Mineralized fracture c = calcite s = sulfide
 Fractured zone

KEY TO SYMBOLS

 Sandstone
 Graywacke
 Siltstone
 Shale
 Fossils
 Shale intra-clasts
 Cross-bedding
 Shale laminae



BORING RS-3



GAMMA RAY LOG

BORING RS-4

SURFACE ELEVATION
COORDINATES

DESCRIPTIVE GEOLOGIC NOTES

FILL

LIGHT GRAY MEDIUM GRAINED THICKLY BEDDED SILICEOUS
SANDSTONE WITH THIN BEDS OF SILTSTONE, CROSS-
BEDDING AND CLAY CLASTS COMMON, HARD AND
UNWEATHEREDOSWEGO
SANDSTONETRANSITION
ZONEGRAY MEDIUM TO COARSE GRAINED, MEDIUM TO THICKLY
BEDDED GRAYWACKE WITH ABUNDANT CLASTIC MASH,
INTERBEDDED WITH DARK GRAY LAMINATED TO THINLY
BEDDED SILTY SHALE AND LIGHT GRAY MEDIUM GRAINED
THIN TO THICKLY BEDDED SILICEOUS SANDSTONE,
FOSSILIFEROUS, MODERATELY HARD AND UNWEATHEREDPULASKI
FORMATION

UNIT A

RUN NO.	BEDDING DIPS	FRACTURES	IN SITU STRESS MEASUREMENT		DEPTH IN FEET	SAMPLING REC. (%) AND CORING	GRAPHIC LOG
			TEST NUMBER	DEPTH IN FEET			
1					0		
2					5		
3					10		
4					15		
5					20		
6					25		
7					30		
8					35		
9					40		
10					45		
11					50		
12					55		
13					60		
14					65		
15					70		
16							
17							
18							
19							
20							
21							
22							
23							
24							
25							
26							
27							
28							
29							
30							
31							
32							
33							
34							
35							

SAMPLING AND CORING INFORMATION

Core run
100 95 R.Q.D.
Percent recovery

BEDDING DIPS

03° Bedding dips measured on selective bedding planes. An attempt was made to avoid all obvious cross bedding or other primary structures.

FRACTURES

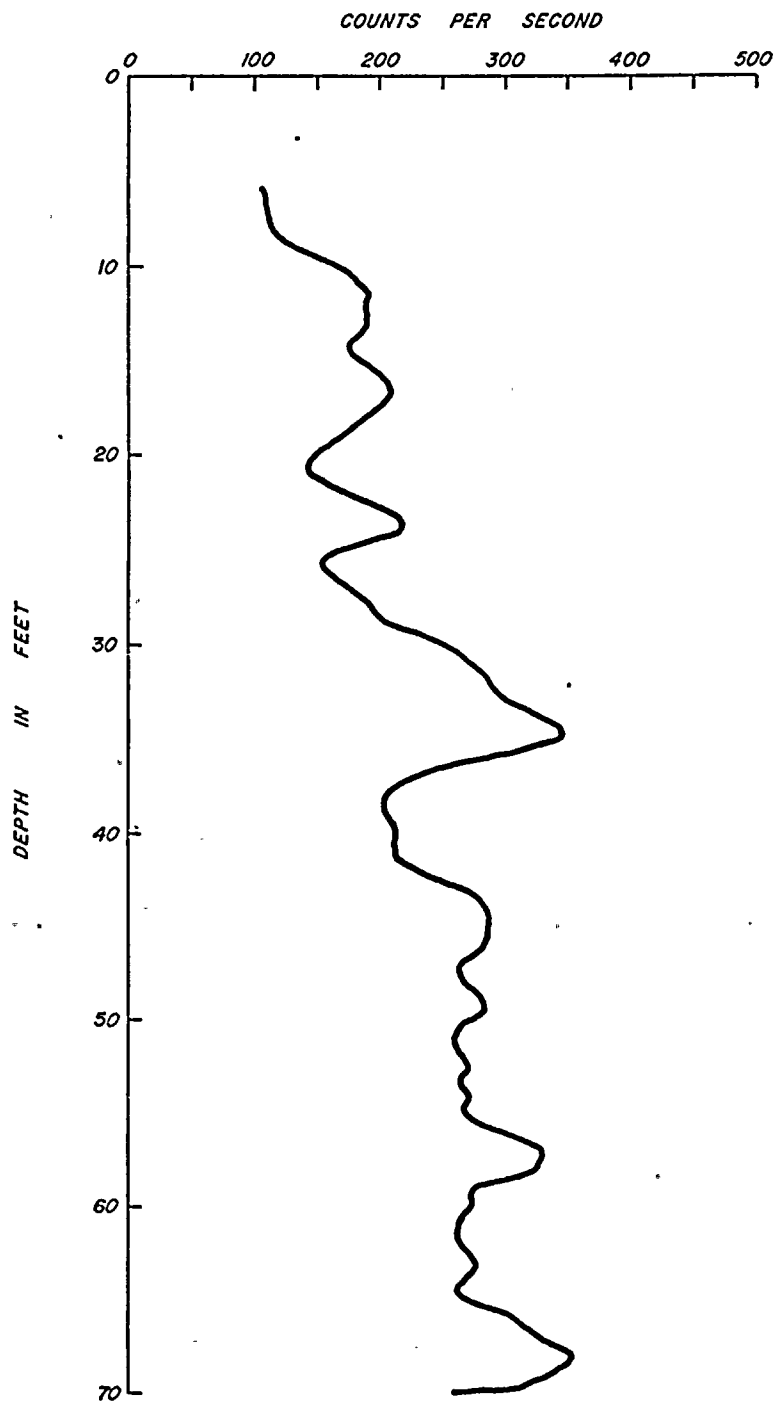
Breccia zone
Dip-slip slickensides
Fractures-shown at approximate angle to core axis
Mineralized fracture c - calcite s - sulfide
Fractured zone

KEY TO SYMBOLS

Sandstone
Graywacke
Siltstone
Shale
Fossils
Shale intra-clasts
Cross-bedding
Shale laminae

PLATE E-4.1
DAMES & MOORE

BORING RS-4



GAMMA RAY LOG



BORING RS-4

DESCRIPTIVE GEOLOGIC NOTES

RUN NO.	BEDDING DIPS	FRACTURES	IN SITU STRESS MEASUREMENT		DEPTH IN FEET	SAMPLING REC. (%) AND CORING	GRAPHIC LOG
			TEST NUMBER	DEPTH IN FEET			
37	36	I	18	70' 5"	70	100	PULASKI FORMATION
38			19	71' 5"	75	100	
39			20	76' 6"	80	100	UNIT B
40	41	I	21	78' 2"	85	100	
42		I	22/23	79' 2"	90	100	UNIT C
43		I	24	80' 10"	95	100	
44			25	82' 11"	100	100	PULASKI FORMATION
45			26	83' 4"	105	100	
47		I	27	83' 11"	110	100	UNIT C
48			28	85' 3"	115	100	
49			29	87' 1"	120	100	PULASKI FORMATION
50	81	I	30	88' 11"	125	100	
52		I	31	90'			
53			32	91' 24"			
54			33	91' 6"			
55			34	94' 5 1/2"			
56	57	I	35	98' 8 1/2"			
57		I	36	98' 1 1/2"			
58		I	37	98' 8"			
59			38	98' 10"			
60							
61			39	102' 8 1/2"			
62			40	104' 4"			
63			41	104' 8"			
64			42	104' 5 1/2"			
65							
66			43	107' 4 1/2"			
67			44	109' 1 1/2"			
68			45	109' 9 1/2"			
69							
70			46	116' 5 1/2"			
71			47	118' 5 1/2"			
72			48	118' 9 1/2"			
73			49	118' 9 1/2"			
74			50	116' 10 1/2"			
75							
76							
77							
78							
79							
80							
81							
82			51	119' 9"			

LIGHT TO MEDIUM GRAY MEDIUM GRAINED ARGILLACEOUS SANDSTONE, OCCASIONAL DARK GRAY TO BLACK SILTY SHALE AND SILTSTONE, INTERBEDDED THIN SHALE STRINGERS, FOSSILIFEROUS, MODERATELY HARD AND UNWEATHERED

PULASKI FORMATION

UNIT B

DARK GRAY TO BLACK THIN TO THICKLY BEDDED SILTY SHALE INTERBEDDED WITH LIGHT GRAY MEDIUM GRAINED ARGILLACEOUS SANDSTONE, SILTSTONE LENSES AND INTERBEDS COMMON, FOSSILIFEROUS, MODERATELY HARD AND UNWEATHERED

PULASKI FORMATION

UNIT C

6" BORE HOLE TERMINATED AT 120' 4" ON 6-25-80
EX BORE HOLE TERMINATED AT 124'
GEOPHYSICAL LOGGING (F) TO 102' 1" ON 6-17-80
BORE HOLE GROUTED ON 6-26-80

SAMPLING AND CORING INFORMATION

Core run
100% R.Q.D.
Percent recovery

BEDDING DIPS

03° Bedding dips measured on selective bedding planes. An attempt was made to avoid all obvious cross bedding or other primary structures.

FRACTURES

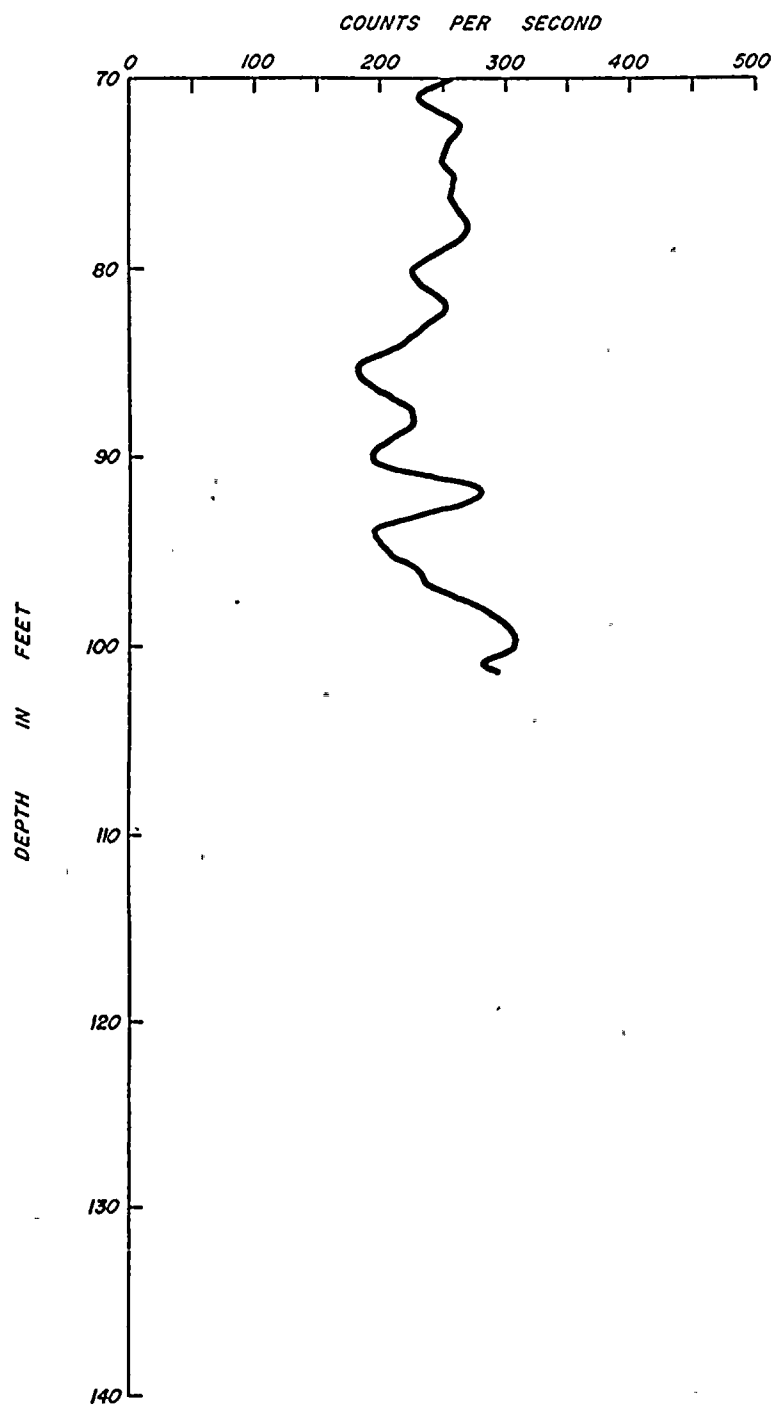
Breccia zone
Dip-slip slickensides
Fractures-shown at approximate angle to core axis
Mineralized fracture c - calcite s - sulfide
Fractured zone

KEY TO SYMBOLS

Sandstone
Graywacke
Siltstone
Shale
Fossils
Shale intra-clasts
Cross-bedding
Shale laminae

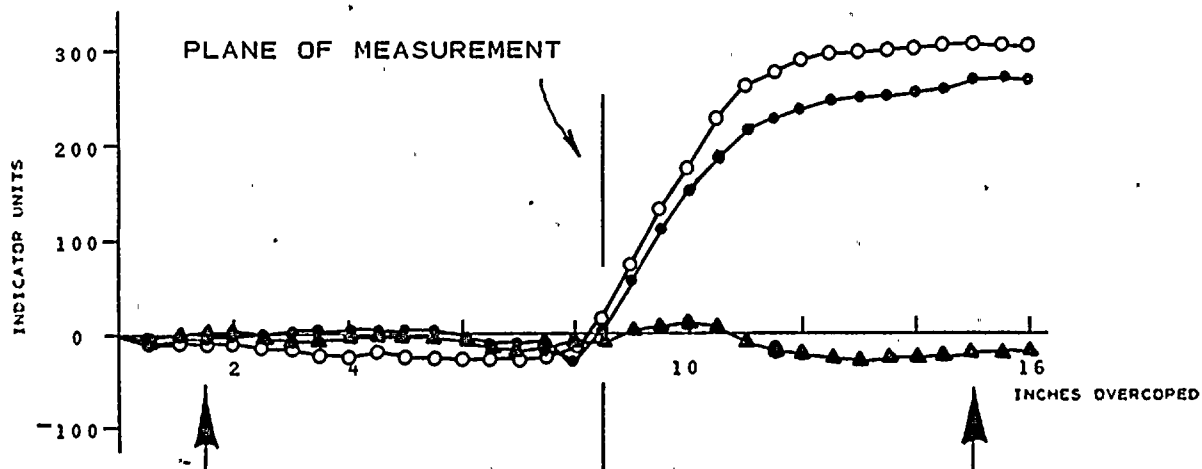


BORING RS-4



GAMMA RAY LOG





KEY:

- ▲ AXIS I
- AXIS II
- AXIS III

$$\begin{aligned}\Delta R_1 &= -22 - (-6) = -16 \\ \Delta R_2 &= 302 - (-10) = 312 \\ \Delta R_3 &= 264 - 1 = 263\end{aligned}$$

$$\begin{aligned}K_1 &= 1.01 \mu\text{IN.} & U_1 &= 1.01 \times -16 = -16 \\ K_2 &= 0.96 \mu\text{IN.} & U_2 &= 0.96 \times 312 = 300 \\ K_3 &= 1.01 \mu\text{IN.} & U_3 &= 1.01 \times 263 = 266\end{aligned}$$

ROCK TYPE: LIGHT GRAY SILICEOUS SANDSTONE

STRAIN RELIEF MEASUREMENTS

BORING NO. RS - 1

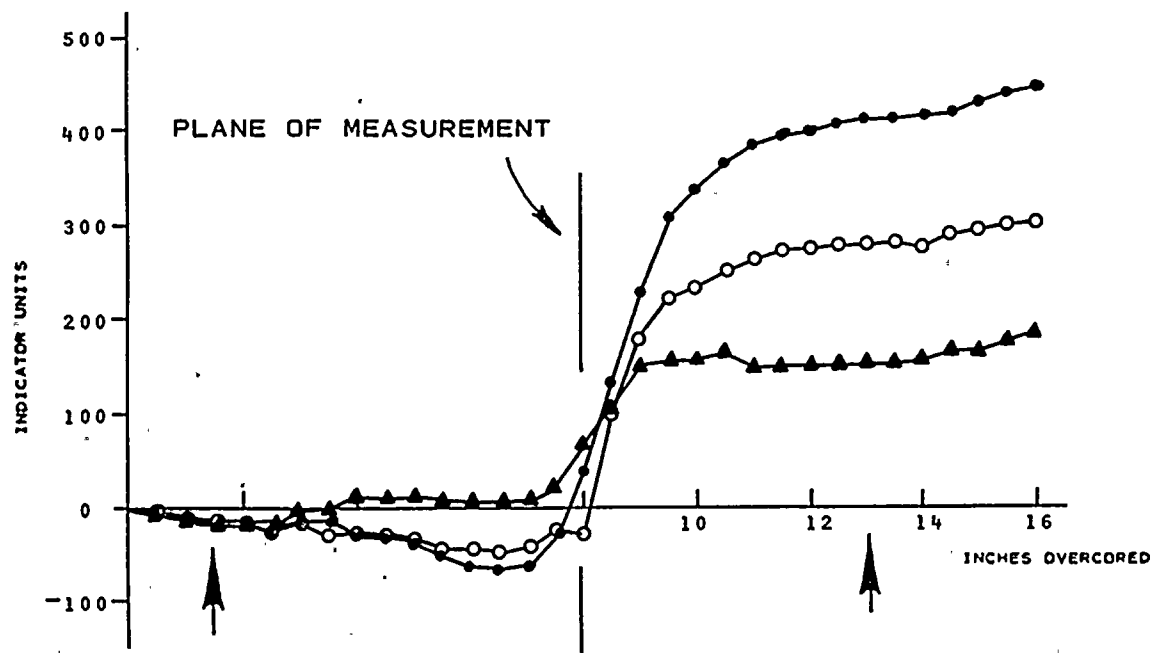
TEST NO. 1

DEPTH 41'2 1/2"

NOTE: A POSITIVE INCREASE IN INDICATOR UNITS
INDICATES EXPANSION OF THE EX HOLE
DURING OVERCORING

ARROWS (↑) INDICATE TOTAL DEFORMATION
USED TO CALCULATE STRESS

PLATE E-5
DAMES & MOORE



KEY:

- ▲ AXIS I
- AXIS II
- AXIS III

$$\begin{aligned}\Delta R_1 &= 154 - (-13) = 167 \\ \Delta R_2 &= 278 - (-16) = 294 \\ \Delta R_3 &= 411 - (-11) = 422\end{aligned}$$

$$\begin{aligned}K_1 &= 1.01 \mu\text{IN.} \\ K_2 &= 0.96 \mu\text{IN.} \\ K_3 &= 1.01 \mu\text{IN.}\end{aligned}$$

$$\begin{aligned}U_1 &= 1.01 \times 167 = 169 \\ U_2 &= 0.96 \times 294 = 282 \\ U_3 &= 1.01 \times 422 = 426\end{aligned}$$

ROCK TYPE: LIGHT TO MEDIUM GRAY
SILICEOUS SANDSTONE

STRAIN RELIEF MEASUREMENTS

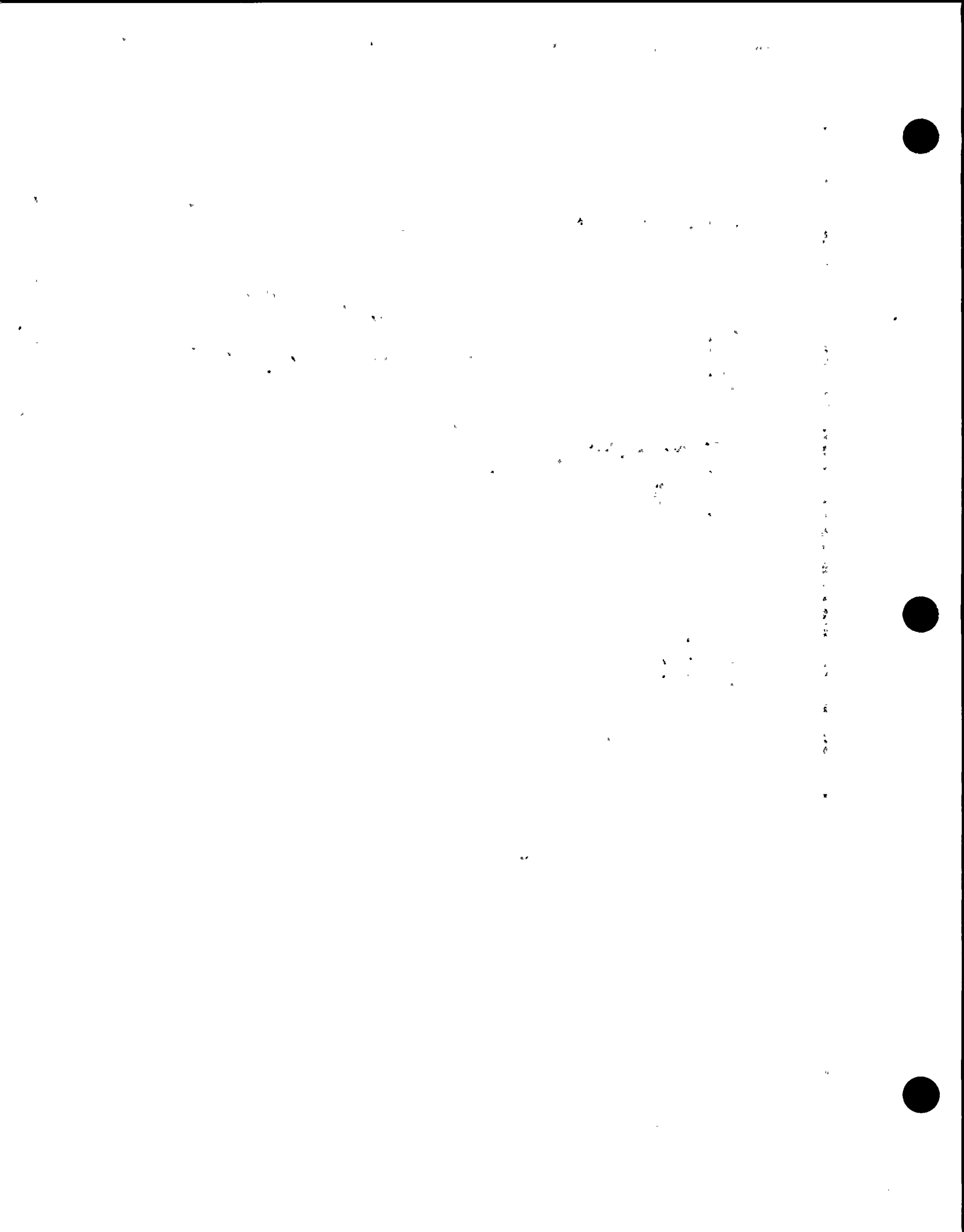
BORING NO. RS = 1

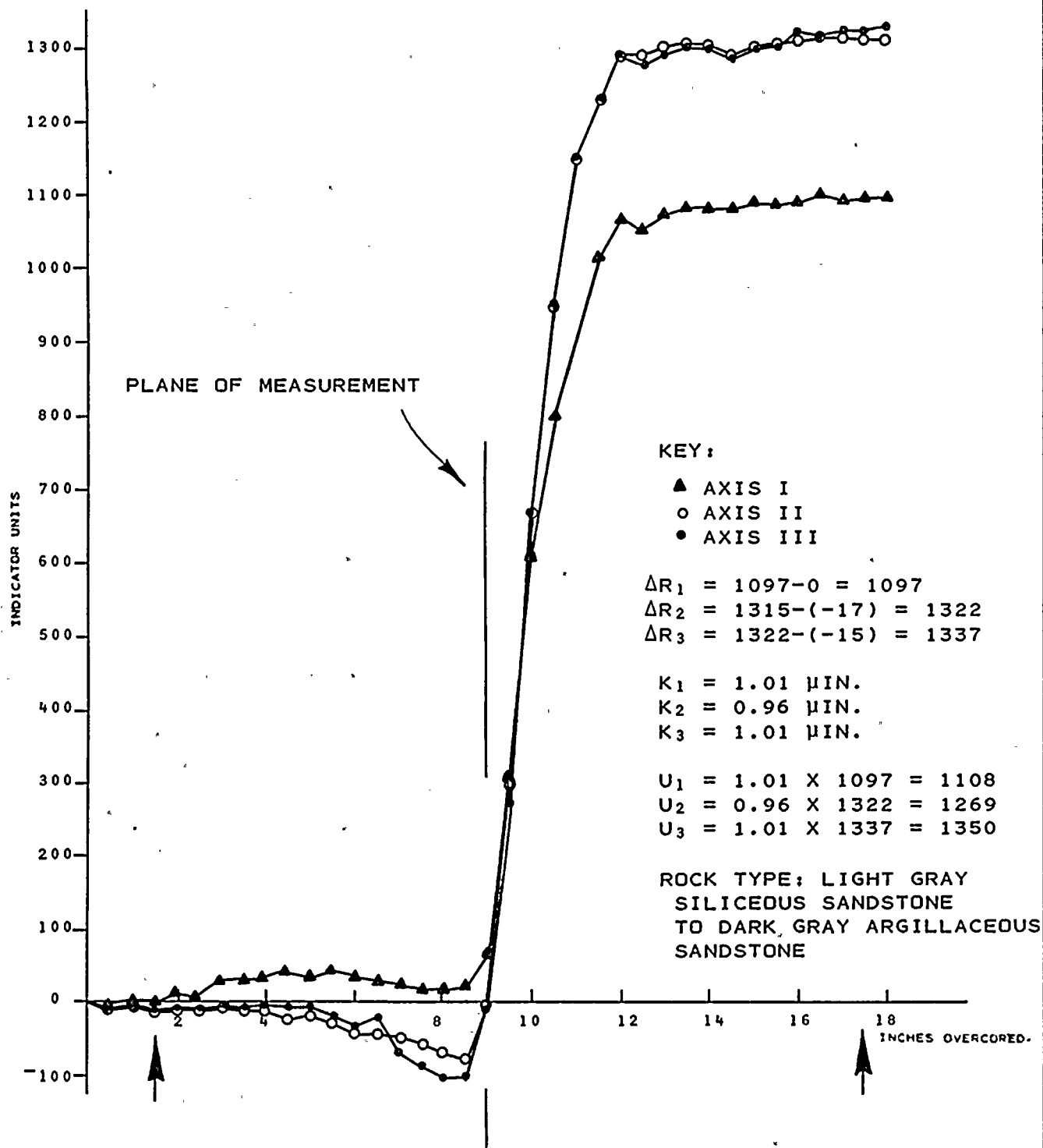
TEST NO. 2

DEPTH 43'10"

NOTE: A POSITIVE INCREASE IN INDICATOR UNITS
INDICATES EXPANSION OF THE EX HOLE
DURING OVERCORING

ARROWS (↓) INDICATE TOTAL DEFORMATION
USED TO CALCULATE STRESS

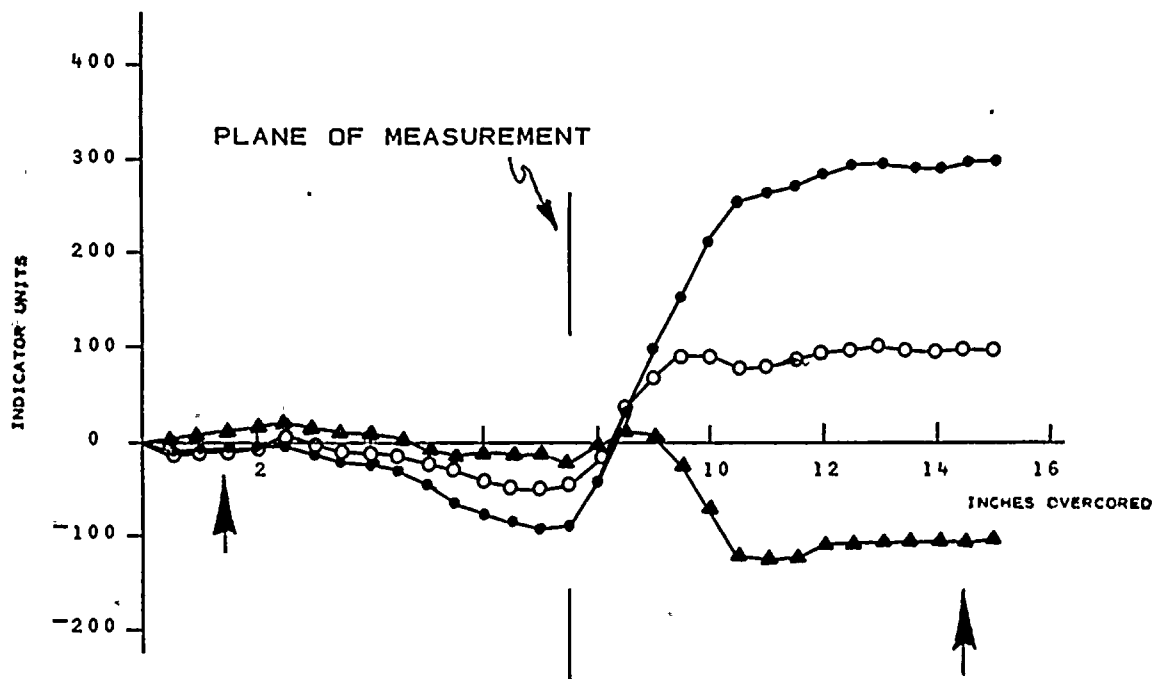




STRAIN RELIEF MEASUREMENTS
BORING RS - 1
TEST NO. 3
DEPTH 46'5"

NOTE: A POSITIVE INCREASE IN INDICATOR UNITS
INDICATES EXPANSION OF THE EX HOLE
DURING OVERCORING

ARROWS (↓) INDICATE TOTAL DEFORMATION
USED TO CALCULATE STRESS



KEY:

▲ AXIS I	$\Delta R_1 = -112 - 9 = -121$
○ AXIS II	$\Delta R_2 = 96 - (-8) = 104$
● AXIS III	$\Delta R_3 = 294 - (-5) = 299$

$K_1 = 1.01 \mu\text{IN.}$	$U_1 = 1.01 \times -121 = -122$
$K_2 = .096 \mu\text{IN.}$	$U_2 = 0.96 \times 104 = 100$
$K_3 = 1.01 \mu\text{IN.}$	$U_3 = 1.01 \times 299 = 302$

ROCK TYPE: LIGHT GRAY SILICEOUS SANDSTONE
WITH SHALE INTERBED

STRAIN RELIEF MEASUREMENTS

BORING RS - 1

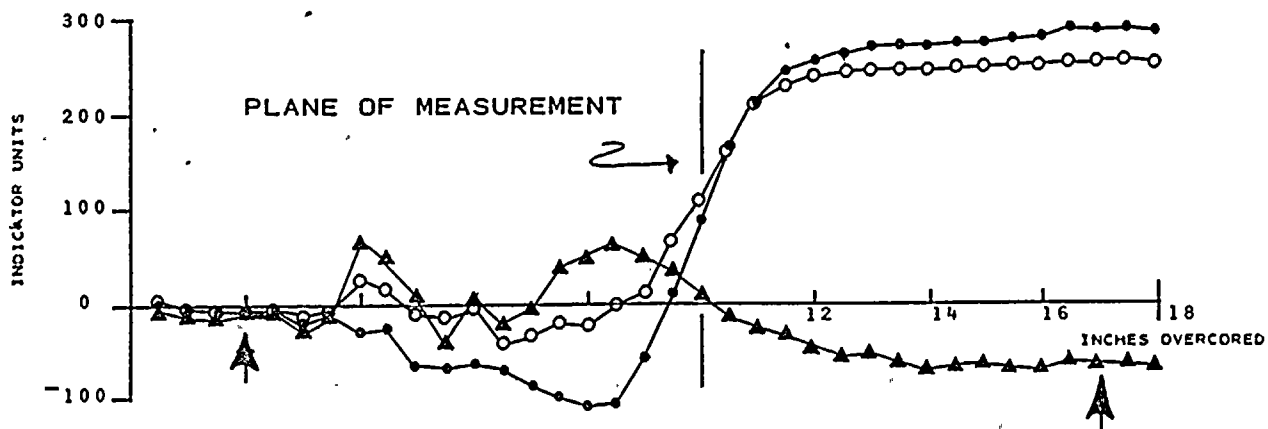
TEST NO. 4

DEPTH 47'9"

NOTE: A POSITIVE INCREASE IN INDICATOR UNITS
INDICATES EXPANSION OF THE EX HOLE
DURING OVERCORING

ARROWS (↑) INDICATE TOTAL DEFORMATION
USED TO CALCULATE STRESS





KEY:

- ▲ AXIS I
- AXIS II
- AXIS III

$$\begin{aligned}\Delta R_1 &= -68 - (-9) = -59 \\ \Delta R_2 &= 255 - (-9) = 264 \\ \Delta R_3 &= 287 - (-11) = 298\end{aligned}$$

$$\begin{aligned}K_1 &= 1.06 \mu\text{IN.} & U_1 &= 1.06 \times -59 = -63 \\ K_2 &= 1.09 \mu\text{IN.} & U_2 &= 1.09 \times 264 = 288 \\ K_3 &= 1.08 \mu\text{IN.} & U_3 &= 1.08 \times 298 = 322\end{aligned}$$

ROCK TYPE: LIGHT TO MEDIUM GRAY SANDSTONE

STRAIN RELIEF MEASUREMENTS

BORING RS - 1

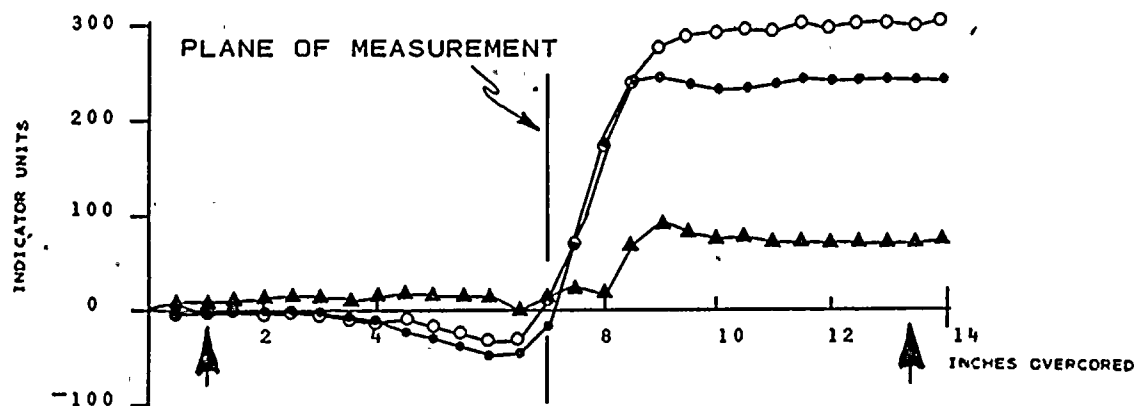
TEST NO. 8

DEPTH 53'9"

NOTE: A POSITIVE INCREASE IN INDICATOR UNITS
INDICATES EXPANSION OF THE EX HOLE
DURING OVERCORING

ARROWS (↑) INDICATE TOTAL DEFORMATION
USED TO CALCULATE STRESS





KEY:

▲ AXIS I	$\Delta R_1 = 72 - 2 = 70$
○ AXIS II	$\Delta R_2 = 299 - (-1) = 300$
● AXIS III	$\Delta R_3 = 241 - (-4) = 245$

$K_1 = 1.06 \mu\text{IN.}$	$U_1 = 1.06 \times 70 = 74$
$K_2 = 1.09 \mu\text{IN.}$	$U_2 = 1.09 \times 300 = 327$
$K_3 = 1.08 \mu\text{IN.}$	$U_3 = 1.08 \times 245 = 265$

ROCK TYPE: LIGHT GRAY SILICEOUS SANDSTONE,
OCCASIONAL SHALE CLASTS

STRAIN RELIEF MEASUREMENTS

BORING RS - 1

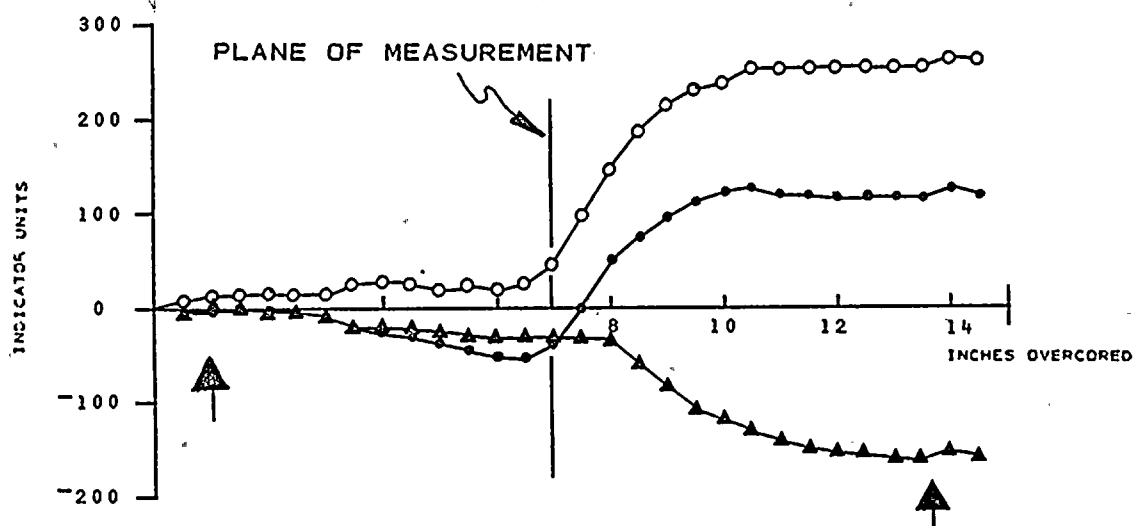
TEST NO. 9

DEPTH 55'0"

NOTE: A POSITIVE INCREASE IN INDICATOR UNITS
INDICATES EXPANSION OF THE EX HOLE
DURING OVERCORING

ARROWS (▲) INDICATE TOTAL DEFORMATION
USED TO CALCULATE STRESS





KEY:

▲ AXIS I	$\Delta R_1 = -162 - 0 = -162$
○ AXIS II	$\Delta R_2 = 254 - 8 = 246$
● AXIS III	$\Delta R_3 = 117 - 0 = 117$

$K_1 = 1.06 \mu\text{IN.}$	$U_1 = 1.06 \times -162 = -172$
$K_2 = 1.09 \mu\text{IN.}$	$U_2 = 1.09 \times 246 = 268$
$K_3 = 1.08 \mu\text{IN.}$	$U_3 = 1.08 \times 117 = 126$

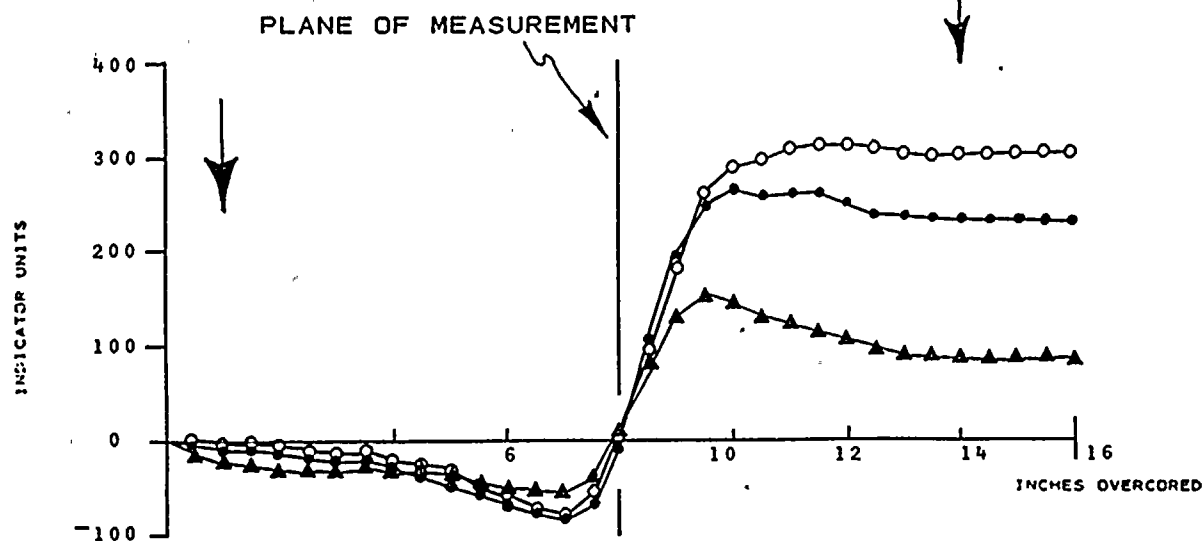
ROCK TYPE: LIGHT TO MEDIUM GRAY SILICEOUS
SANDSTONE TO SLIGHTLY ARGILLACEOUS.
SANDSTONE

STRAIN RELIEF MEASUREMENTS

BORING RS - 1
TEST NO. 12
DEPTH 58'3"

NOTE: A POSITIVE INCREASE IN INDICATOR UNITS
INDICATES EXPANSION OF THE EX HOLE
DURING OVERCORING

ARROWS (↑) INDICATE TOTAL DEFORMATION
USED TO CALCULATE STRESS



KEY:

▲ AXIS I	$\Delta R_1 = 90 - (-21) = 111$
○ AXIS II	$\Delta R_2 = 305 - (-2) = 307$
● AXIS III	$\Delta R_3 = 236 - (-7) = 243$

$K_1 = 1.06 \mu\text{IN.}$	$U_1 = 1.06 \times 111 = 118$
$K_2 = 1.09 \mu\text{IN.}$	$U_2 = 1.09 \times 307 = 335$
$K_3 = 1.08 \mu\text{IN.}$	$U_3 = 1.08 \times 243 = 262$

ROCK TYPE: MEDIUM GRAY GRAYWACKE

STRAIN RELIEF MEASUREMENTS

BORING RS - 1

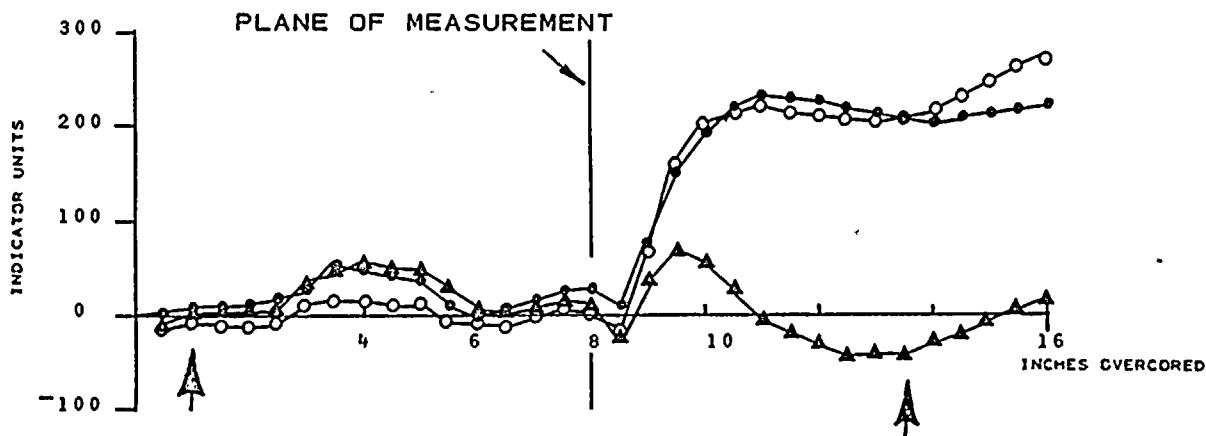
TEST NO. 14

DEPTH 61'0"

NOTE: A POSITIVE INCREASE IN INDICATOR UNITS
INDICATES EXPANSION OF THE EX HOLE
DURING OVERCORING

ARROWS (I) INDICATE TOTAL DEFORMATION
USED TO CALCULATE STRESS





KEY:

▲ AXIS I	$\Delta R_1 = -43 - (-2) = -45$
○ AXIS II	$\Delta R_2 = 208 - (-6) = 214$
• AXIS III	$\Delta R_3 = 208 - (-4) = 204$

$K_1 = 1.10 \mu\text{IN.}$	$U_1 = 1.10 \times -45 = -49.5$
$K_2 = 1.10 \mu\text{IN.}$	$U_2 = 1.10 \times 214 = 235$
$K_3 = 1.06 \mu\text{IN.}$	$U_3 = 1.06 \times 204 = 216$

ROCK TYPE: LIGHT GRAY SILICEOUS SANDSTONE
WITH BLACK SHALE INTERBEDS

STRAIN RELIEF MEASUREMENTS

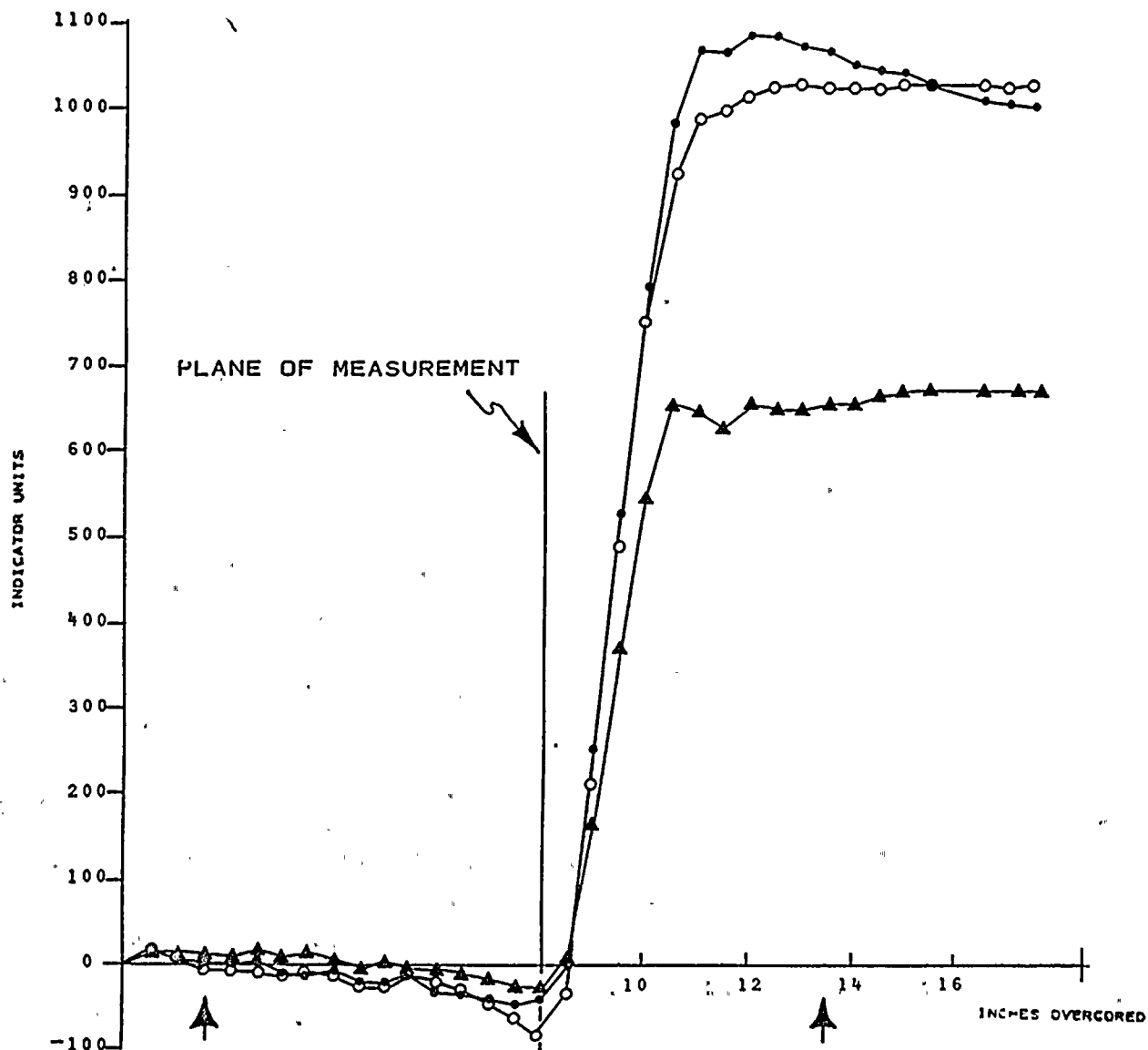
BORING RS - 1

TEST NO. 15

DEPTH 63'4"

NOTE: A POSITIVE INCREASE IN INDICATOR UNITS
INDICATES EXPANSION OF THE EX HOLE
DURING OVERCORING

ARROWS (↑) INDICATE TOTAL DEFORMATION
USED TO CALCULATE STRESS



KEY:

- ▲ AXIS I
- AXIS II
- AXIS III

$$\begin{aligned}\Delta R_1 &= 659 - 5 = 654 \\ \Delta R_2 &= 1024 - (-2) = 1026 \\ \Delta R_3 &= 1066 - 0 = 1066\end{aligned}$$

ROCK TYPE: MEDIUM DARK
GRAY ARGILLACEOUS
SANDSTONE WITH SHALE
INTERLAMINATIONS

$$K_1 = 1.10 \mu\text{IN.}$$

$$U_1 = 1.10 \times 654 = 719$$

$$K_2 = 1.10 \mu\text{IN.}$$

$$U_2 = 1.10 \times 1026 = 1129$$

$$K_3 = 1.06 \mu\text{IN.}$$

$$U_3 = 1.06 \times 1066 = 1130$$

STRAIN RELIEF MEASUREMENTS

BORING RS - 1

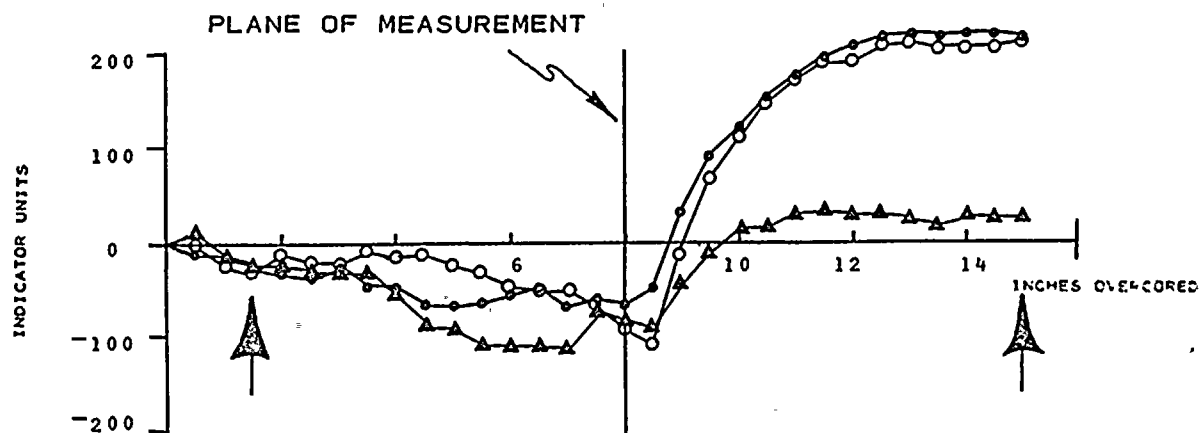
TEST NO. 16

DEPTH 64' 8 1/2"

NOTE: A POSITIVE INCREASE IN INDICATOR UNITS
INDICATES EXPANSION OF THE EX HOLE
DURING OVERCoring.

ARROWS (4) INDICATE TOTAL DEFORMATION
USED TO CALCULATE STRESS

PLATE E-14
DAMES & MOORE



KEY:

▲ AXIS I	$\Delta R_1 = 21 - (-21) = 42$
○ AXIS II	$\Delta R_2 = 210 - (-25) = 235$
• AXIS III	$\Delta R_3 = 217 - (-22) = 239$

$K_1 = 1.10 \mu\text{IN.}$	$U_1 = 1.10 \times 42 = 46$
$K_2 = 1.10 \mu\text{IN.}$	$U_2 = 1.10 \times 235 = 259$
$K_3 = 1.06 \mu\text{IN.}$	$U_3 = 1.06 \times 239 = 253$

ROCK TYPE: MEDIUM GRAY ARGILLACEOUS SANDSTONE
INTERBEDDED WITH LIGHT GRAY
SANDSTONE

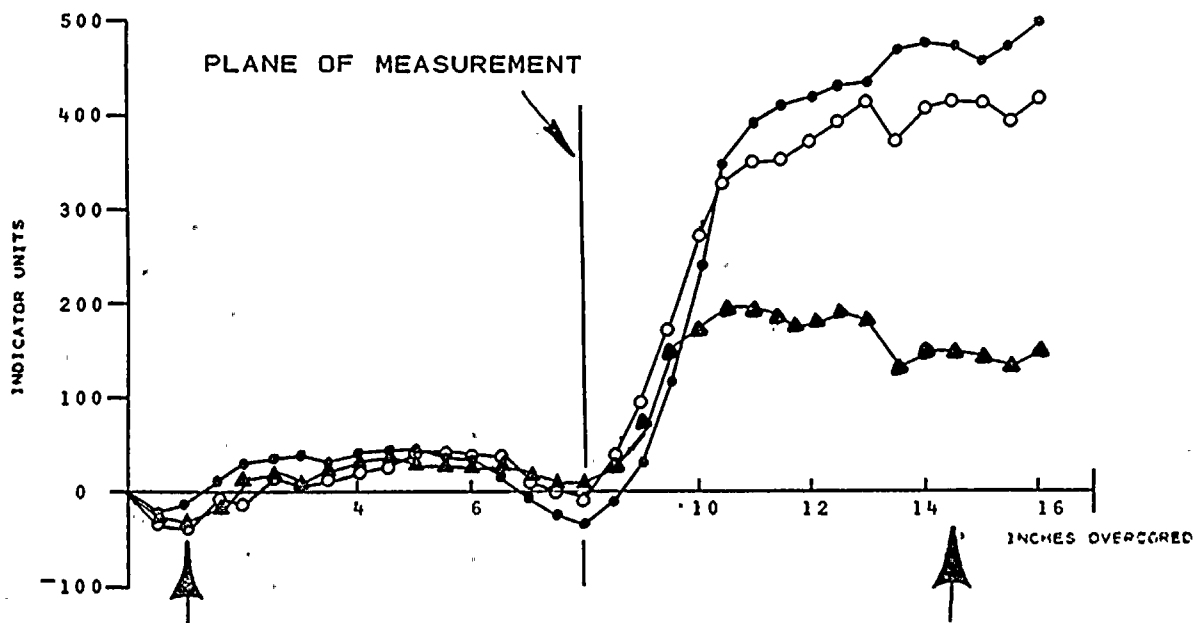
STRAIN RELIEF MEASUREMENTS
BORING RS - 1
TEST NO. 17
DEPTH 66'1"

NOTE: A POSITIVE INCREASE IN INDICATOR UNITS
INDICATES EXPANSION OF THE EX HOLE
DURING OVERCORING

ARROWS (↑) INDICATE TOTAL DEFORMATION
USED TO CALCULATE STRESS

PLATE E-15
DAMES & MOORE





KEY:

▲ AXIS I
○ AXIS II
◐ AXIS III

$$\Delta R_1 = 150 - (-31) = 181$$

$$\Delta R_2 = 409 - (-36) = 445$$

$$\Delta R_3 = 468 - (-19) = 487$$

$$K_1 = 1.07 \text{ } \mu\text{IN.}$$

$$U_1 = 1.07 \times 181 = 194$$

$$K_2 = 1.10 \text{ } \mu\text{IN.}$$

$$U_2 = 1.10 \times 445 = 490$$

$$K_3 = 1.03 \text{ } \mu\text{IN.}$$

$$U_3 = 1.03 \times 487 = 502$$

ROCK TYPE: LIGHT GRAY SILICEOUS SANDSTONE
TO MEDIUM ARGILLACEOUS SANDSTONE

STRAIN RELIEF MEASUREMENTS

BORING RS - 1

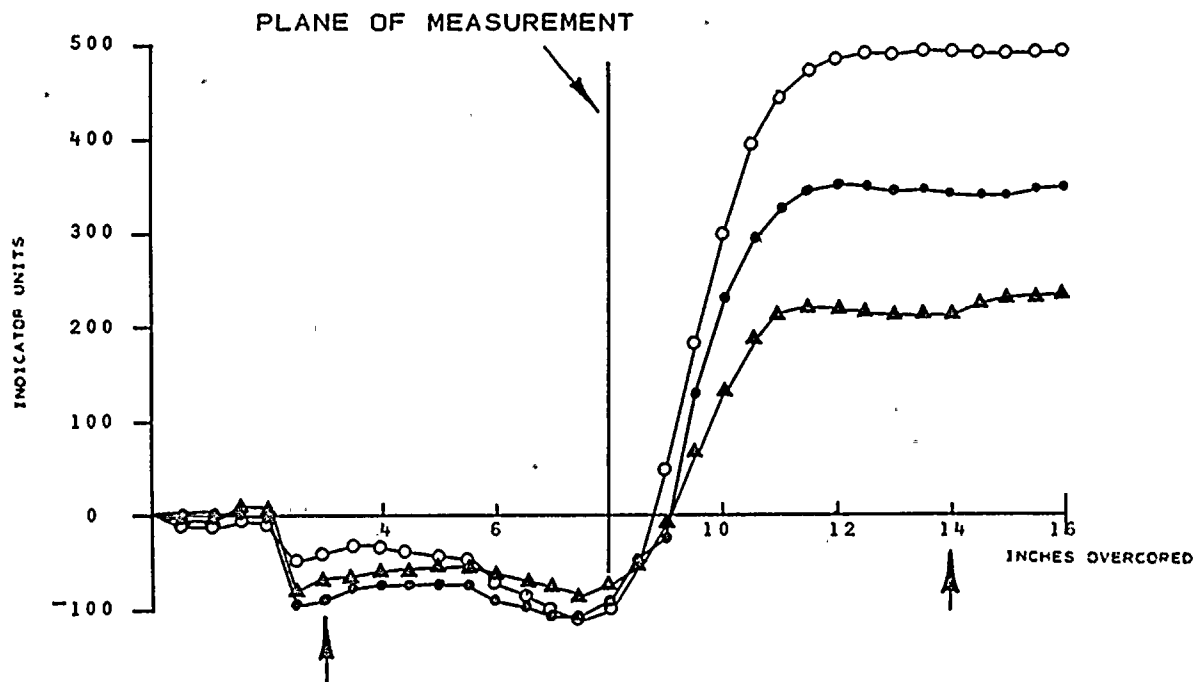
TEST NO. 18

DEPTH 68'4"

NOTE: A POSITIVE INCREASE IN INDICATOR UNITS
INDICATES EXPANSION OF THE EX HOLE
DURING OVERCORING

ARROWS (i) INDICATE TOTAL DEFORMATION
USED TO CALCULATE STRESS





KEY:

▲ AXIS I	$\Delta R_1 = 216 - (-68) = 284$
○ AXIS II	$\Delta R_2 = 489 - (-40) = 529$
● AXIS III	$\Delta R_3 = 340 - (-88) = 428$

$K_1 = 1.07 \mu\text{IN.}$	$U_1 = 1.07 \times 284 = 304$
$K_2 = 1.10 \mu\text{IN.}$	$U_2 = 1.10 \times 529 = 582$
$K_3 = 1.03 \mu\text{IN.}$	$U_3 = 1.03 \times 428 = 441$

ROCK TYPE: MEDIUM GRAY ARGILLACEOUS
SANDSTONE

STRAIN RELIEF MEASUREMENTS

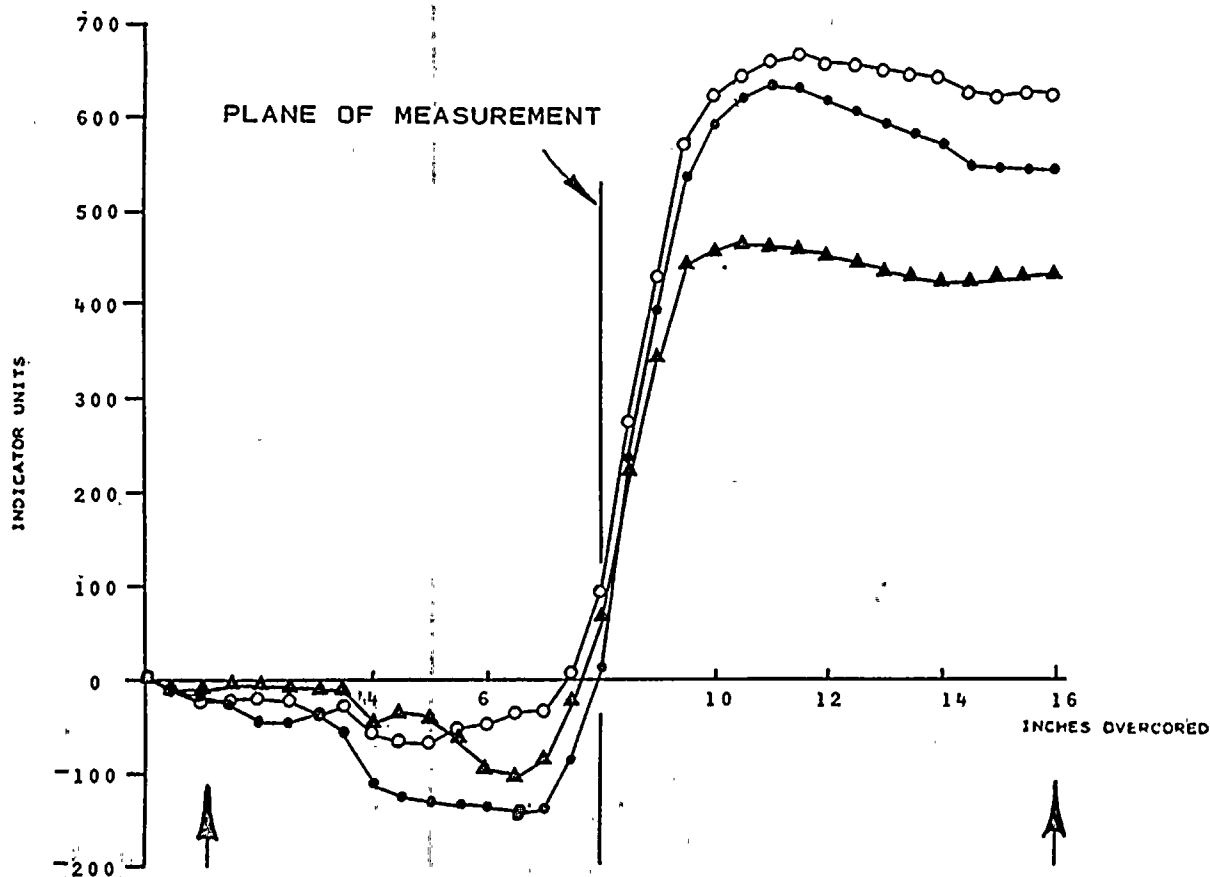
BORING RS - 1

TEST NO. 20

DEPTH 71'0"

NOTE: A POSITIVE INCREASE IN INDICATOR UNITS
INDICATES EXPANSION OF THE EX HOLE
DURING OVERCoring

ARROWS (♦) INDICATE TOTAL DEFORMATION
USED TO CALCULATE STRESS



KEY:

△ AXIS I	$\Delta R_1 = 431 - (-9) = 440$
○ AXIS II	$\Delta R_2 = 620 - (-12) = 632$
● AXIS III	$\Delta R_3 = 541 - (-10) = 551$

$K_1 = 1.01 \mu\text{IN.}$	$U_1 = 1.01 \times 440 = 444$
$K_2 = 0.99 \mu\text{IN.}$	$U_2 = 0.99 \times 632 = 626$
$K_3 = 1.01 \mu\text{IN.}$	$U_3 = 1.01 \times 551 = 557$

ROCK TYPE: LIGHT GRAY SANDSTONE TO MEDIUM
GRAY ARGILLACEOUS SANDSTONE

STRAIN RELIEF MEASUREMENTS

BORING RS - 1

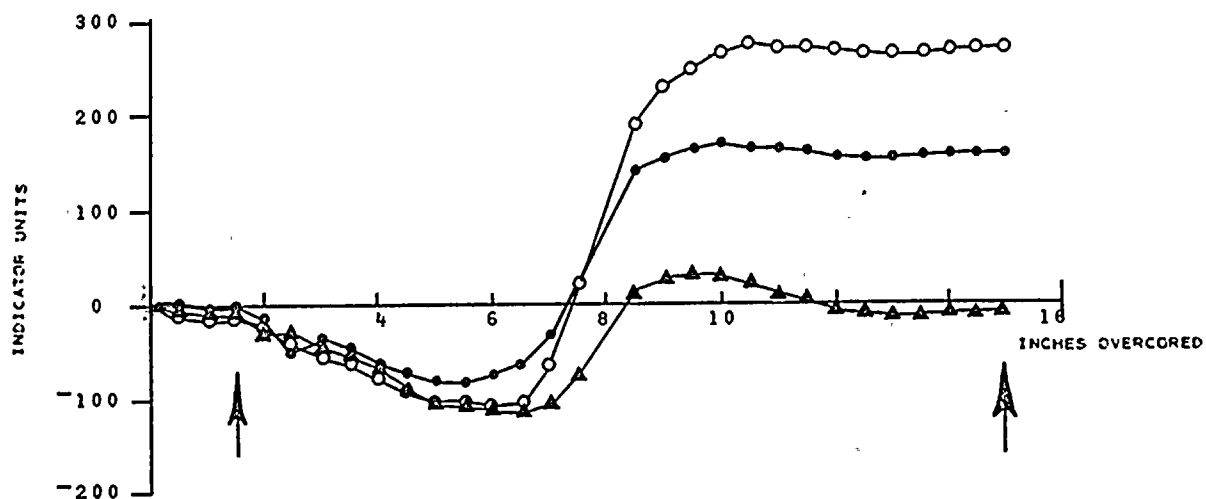
TEST NO. 22

DEPTH 73'1 1/2"

NOTE: A POSITIVE INCREASE IN INDICATOR UNITS
INDICATES EXPANSION OF THE EX HOLE
DURING OVERCoring

ARROWS (I) INDICATE TOTAL DEFORMATION
USED TO CALCULATE STRESS





KEY:

△ AXIS I
○ AXIS II
● AXIS III

$$\begin{aligned}\Delta R_1 &= -4 - (-6) = 2 \\ \Delta R_2 &= 276 - (-14) = 290 \\ \Delta R_3 &= 162 - (-4) = 166\end{aligned}$$

$$\begin{aligned}K_1 &= 1.01 \text{ } \mu\text{IN.} \\ K_2 &= 0.99 \text{ } \mu\text{IN.} \\ K_3 &= 1.01 \text{ } \mu\text{IN.}\end{aligned}$$

$$\begin{aligned}U_1 &= 1.01 \times 2 = 2 \\ U_2 &= 0.99 \times 290 = 287 \\ U_3 &= 1.01 \times 166 = 168\end{aligned}$$

ROCK TYPE: MEDIUM GRAY ARGILLACEOUS SANDSTONE

STRAIN RELIEF MEASUREMENTS

BORING RS - 1

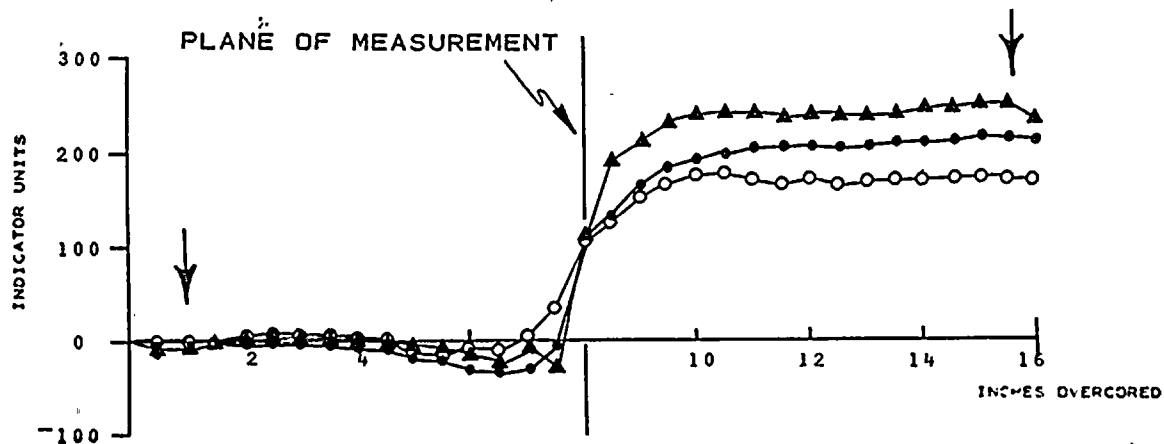
TEST NO. 24

DEPTH 74'9 1/2"

NOTE: A POSITIVE INCREASE IN INDICATOR UNITS
INDICATES EXPANSION OF THE EX HOLE
DURING OVERCORING

ARROWS (↑) INDICATE TOTAL DEFORMATION
USED TO CALCULATE STRESS





KEY:

▲ AXIS I $\Delta R_1 = 250 - (-4) = 254$
 ○ AXIS II $\Delta R_2 = 170 - 0 = 170$
 • AXIS III $\Delta R_3 = 316 - (-6) = 322$

$K_1 = 0.91 \mu\text{IN.}$ $U_1 = 0.91 \times 254 = 231$
 $K_2 = 0.87 \mu\text{IN.}$ $U_2 = 0.87 \times 170 = 148$
 $K_3 = 0.89 \mu\text{IN.}$ $U_3 = 0.89 \times 322 = 287$

ROCK TYPE: MEDIUM GRAY ARGILLACEOUS SANDSTONE

STRAIN RELIEF MEASUREMENTS

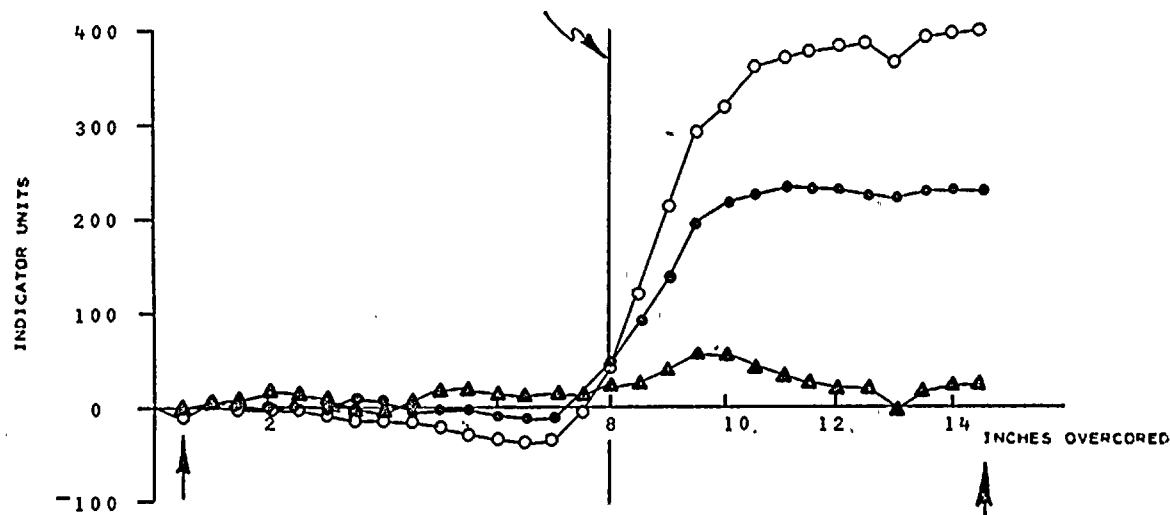
BORING RS - 1
 TEST NO. 25
 DEPTH 76'1"

NOTE: A POSITIVE INCREASE IN INDICATOR UNITS INDICATES EXPANSION OF THE EX HOLE DURING OVERCORING

ARROWS (4) INDICATE TOTAL DEFORMATION USED TO CALCULATE STRESS



PLANE OF MEASUREMENT



KEY:

- ▲ AXIS I
- AXIS II
- AXIS III

$$\Delta R_1 = 22 - (-4) = 26$$

$$\Delta R_2 = 398 - (-6) = 404$$

$$\Delta R_3 = 212 - (-4) = 216$$

$$K_1 = 0.91 \mu\text{IN.}$$

$$U_1 = 0.91 \times 26 = 24$$

$$K_2 = 0.87 \mu\text{IN.}$$

$$U_2 = 0.87 \times 404 = 351$$

$$K_3 = 0.89 \mu\text{IN.}$$

$$U_3 = 0.89 \times 216 = 192$$

ROCK TYPE: LIGHT GRAY SILICEOUS SANDSTONE

STRAIN RELIEF MEASUREMENTS

BORING RS - 1

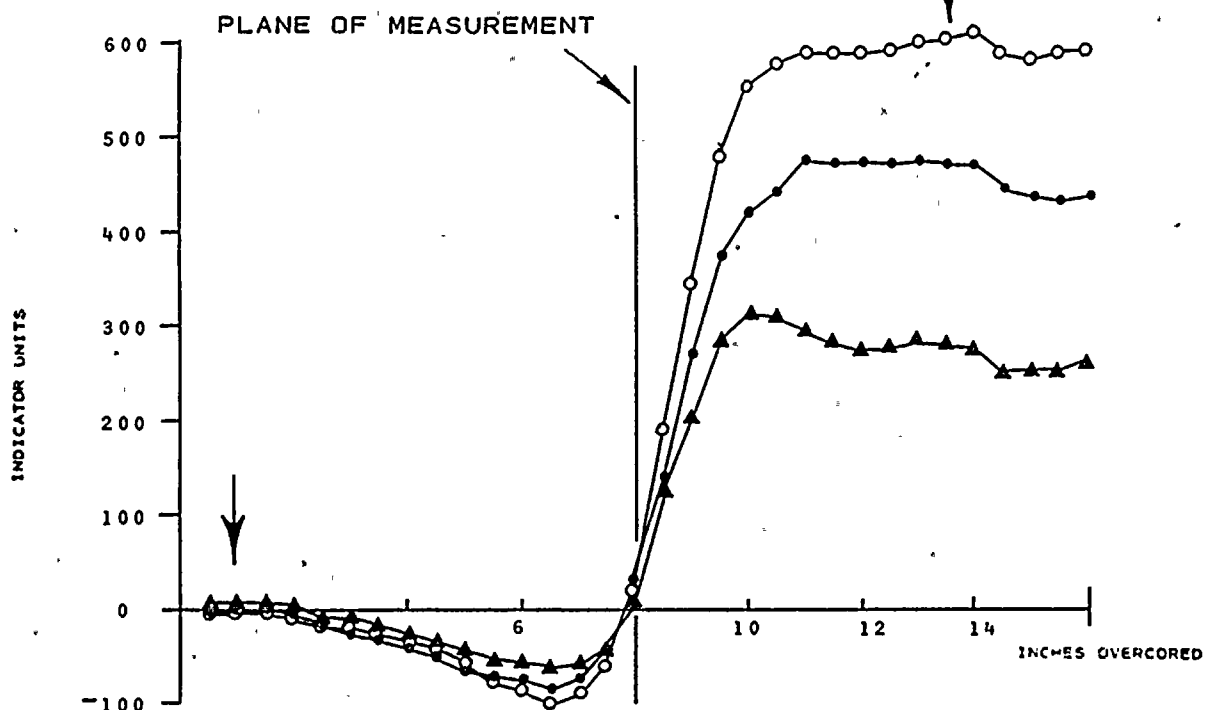
TEST NO. 26

DEPTH 78'4"

NOTE: A POSITIVE INCREASE IN INDICATOR UNITS INDICATES EXPANSION OF THE EX HOLE DURING OVERCORING

ARROWS (↔) INDICATE TOTAL DEFORMATION USED TO CALCULATE STRESS





KEY:

▲ AXIS I	$\Delta R_1 = 282 - (-4) = 278$
○ AXIS II	$\Delta R_2 = 602 - (-6) = 608$
● AXIS III	$\Delta R_3 = 472 - (-2) = 474$

$K_1 = 0.91 \mu\text{IN.}$	$U_1 = 0.91 \times 278 = 253$
$K_2 = 0.87 \mu\text{IN.}$	$U_2 = 0.87 \times 608 = 529$
$K_3 = 0.89 \mu\text{IN.}$	$U_3 = 0.89 \times 474 = 422$

ROCK TYPE: LIGHT TO MEDIUM GRAY ARGILLACEOUS SANDSTONE

STRAIN RELIEF MEASUREMENTS

BORING RS - 1

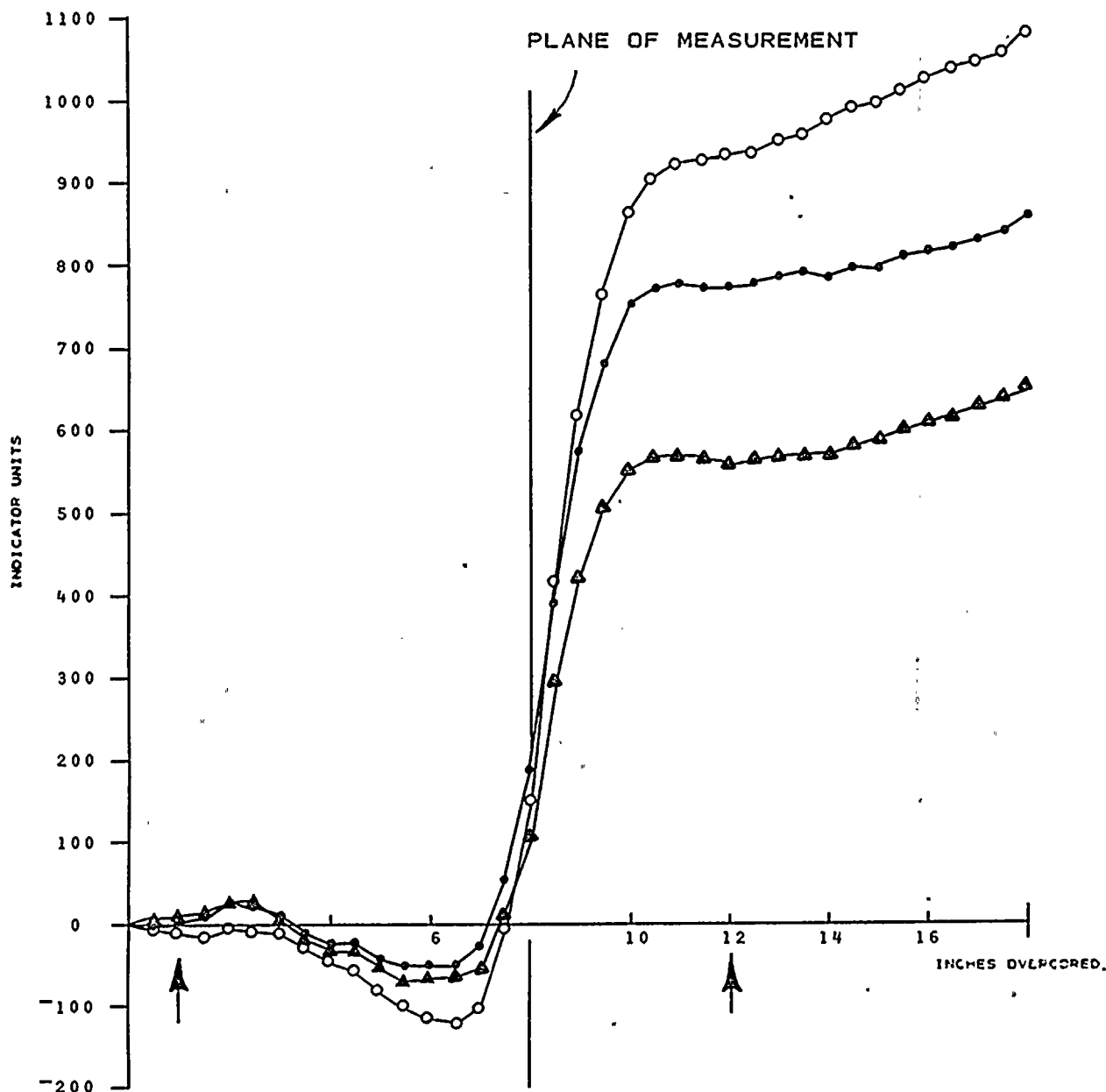
TEST NO. 27

DEPTH 81'8"

NOTE: A POSITIVE INCREASE IN INDICATOR UNITS INDICATES EXPANSION OF THE EX HOLE DURING OVERCORING.

ARROWS (↓) INDICATE TOTAL DEFORMATION USED TO CALCULATE STRESS





KEY:

- ▲ AXIS I
- AXIS II
- AXIS III

$$\Delta R_1 = 560 - 8 = 552$$

$$\Delta R_2 = 930 - (-8) = 938$$

$$\Delta R_3 = 774 - 2 = 772$$

ROCK TYPE: MEDIUM GRAY
ARGILLACEOUS SANDSTONE

$$K_1 = 0.91 \mu\text{IN.}$$

$$U_1 = 0.91 \times 552 = 502$$

$$K_2 = 0.87 \mu\text{IN.}$$

$$U_2 = 0.87 \times 938 = 816$$

$$K_3 = 0.89 \mu\text{IN.}$$

$$U_3 = 0.89 \times 772 = 687$$

STRAIN RELIEF MEASUREMENTS

BORING RS - 1

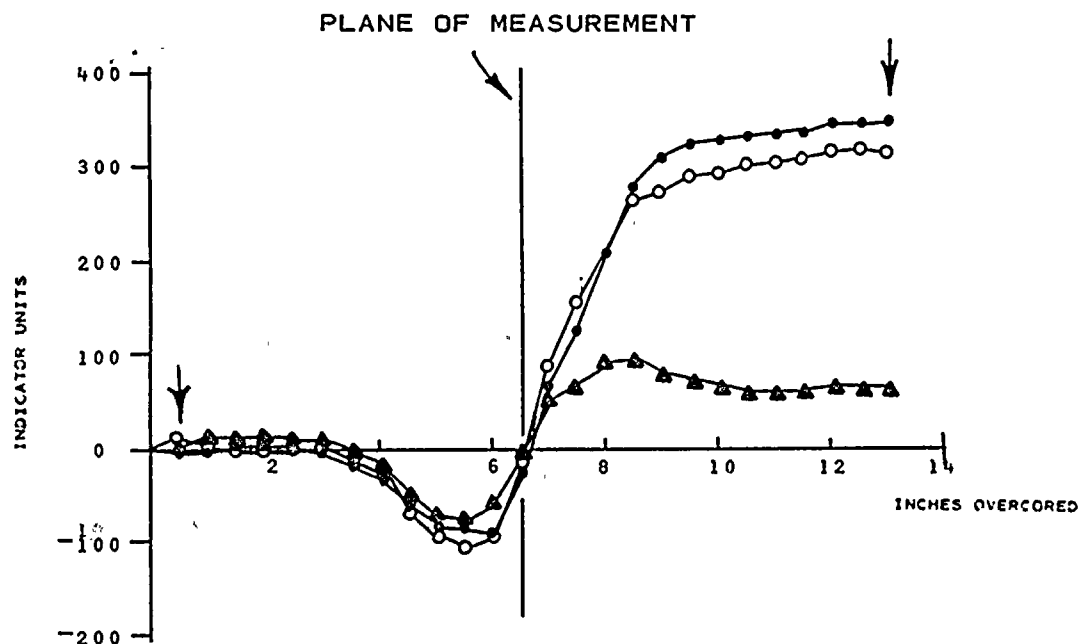
TEST NO. 28

DEPTH 83'10"

NOTE: A POSITIVE INCREASE IN INDICATOR UNITS
INDICATES EXPANSION OF THE EX HOLE
DURING OVERCoring

ARROWS (↓) INDICATE TOTAL DEFORMATION
USED TO CALCULATE STRESS





KEY:

△ AXIS I	$\Delta R_1 = 63 - (-1) = 64$
○ AXIS II	$\Delta R_2 = 318 - 1 = 317$
● AXIS III	$\Delta R_3 = 347 - (-6) = 353$

$K_1 = 0.90 \mu\text{IN.}$	$U_1 = 0.90 \times 64 = 58$
$K_2 = 0.93 \mu\text{IN.}$	$U_2 = 0.93 \times 317 = 295$
$K_3 = 0.95 \mu\text{IN.}$	$U_3 = 0.95 \times 353 = 335$

ROCK TYPE: LIGHT GRAY SILICEOUS SANDSTONE
TO DARK GRAY ARGILLACEOUS SANDSTONE

STRAIN RELIEF MEASUREMENTS

BORING RS - 1

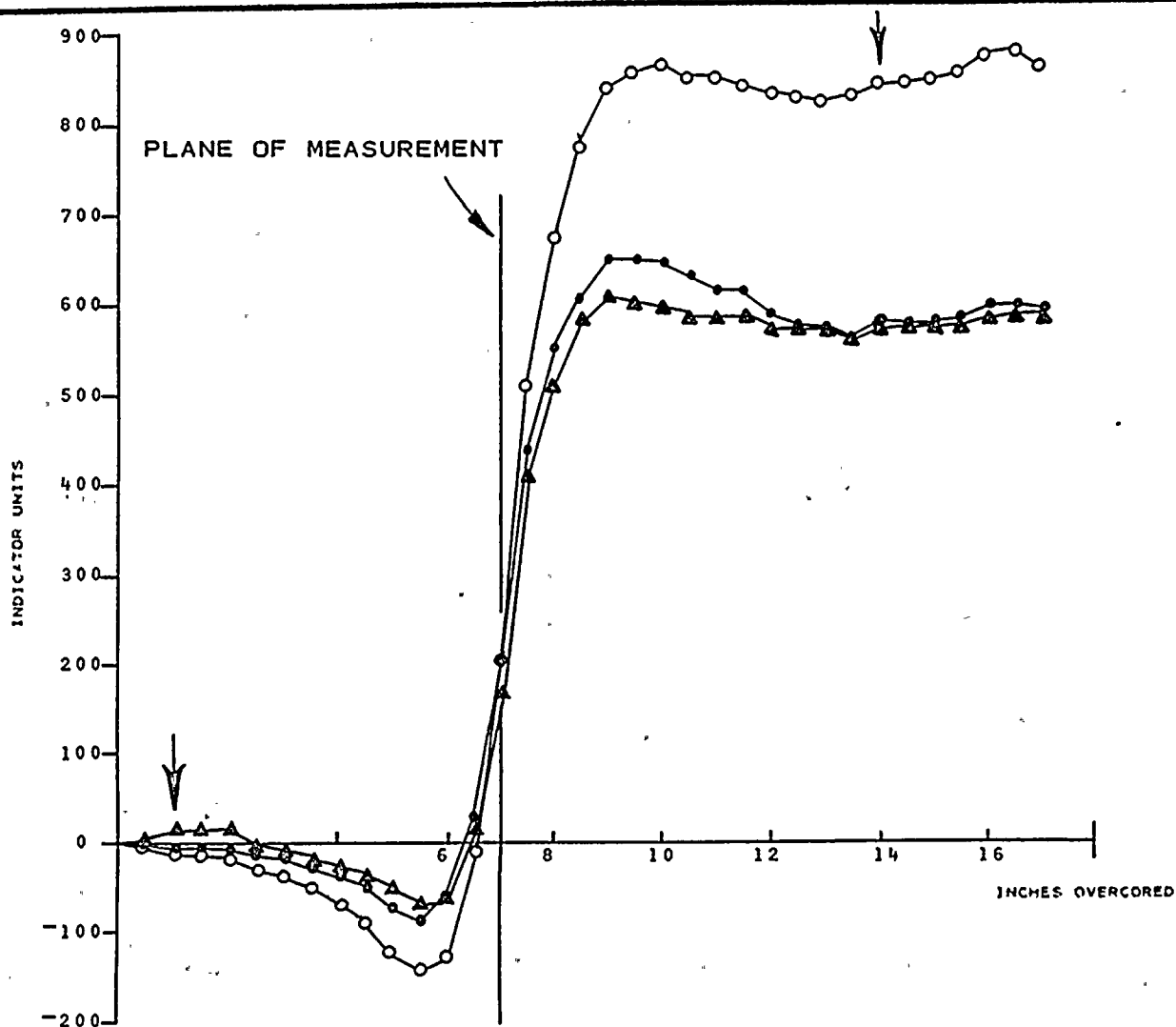
TEST NO. 29

DEPTH 87' 1/2"

NOTE: A POSITIVE INCREASE IN INDICATOR UNITS
INDICATES EXPANSION OF THE EX HOLE
DURING OVERCORING

ARROWS (↓) INDICATE TOTAL DEFORMATION
USED TO CALCULATE STRESS





KEY:

▲ AXIS I	$\Delta R_1 = 574 - 10 = 564$
○ AXIS II	$\Delta R_2 = 842 - (-12) = 854$
● AXIS III	$\Delta R_3 = 579 - (-4) = 583$
$K_1 = 0.90 \mu\text{IN.}$	$U_1 = 0.90 \times 564 = 508$
$K_2 = 0.93 \mu\text{IN.}$	$U_2 = 0.93 \times 854 = 794$
$K_3 = 0.95 \mu\text{IN.}$	$U_3 = 0.95 \times 583 = 554$

ROCK TYPE: DARK TO MEDIUM GRAY ARGILLACEOUS
SANDSTONE

STRAIN RELIEF MEASUREMENTS

BORING RS - 1

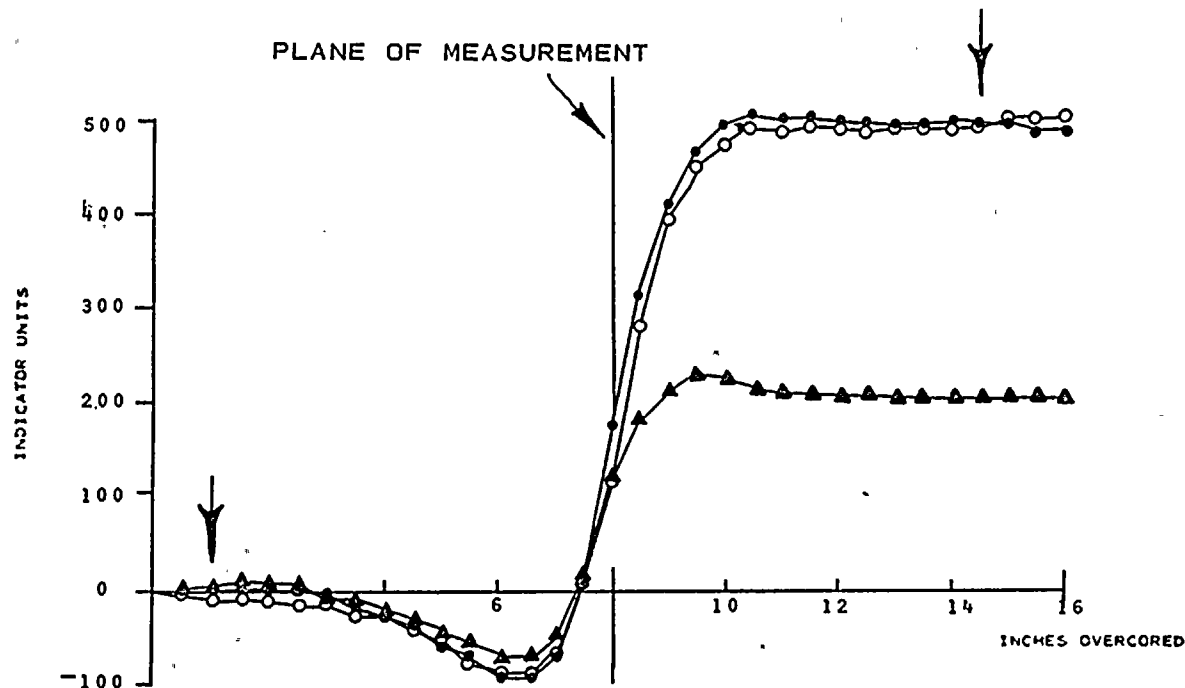
TEST NO. 30

DEPTH 88'2"

NOTE: A POSITIVE INCREASE IN INDICATOR UNITS
INDICATES EXPANSION OF THE EX HOLE
DURING OVERCORING

ARROWS (↓) INDICATE TOTAL DEFORMATION
USED TO CALCULATE STRESS





KEY:

▲ AXIS I	$\Delta R_1 = 207 - 5 = 202$
○ AXIS II	$\Delta R_2 = 496 - (-6) = 502$
● AXIS III	$\Delta R_3 = 494 - 1 = 493$

$K_1 = 0.90 \mu\text{IN.}$	$U_1 = 0.90 \times 202 = 182$
$K_2 = 0.93 \mu\text{IN.}$	$U_2 = 0.93 \times 502 = 467$
$K_3 = 0.95 \mu\text{IN.}$	$U_3 = 0.95 \times 493 = 468$

ROCK TYPE: MEDIUM GRAY ARGILLACEOUS SANDSTONE

STRAIN RELIEF MEASUREMENTS

BORING RS - 1

TEST NO. 34

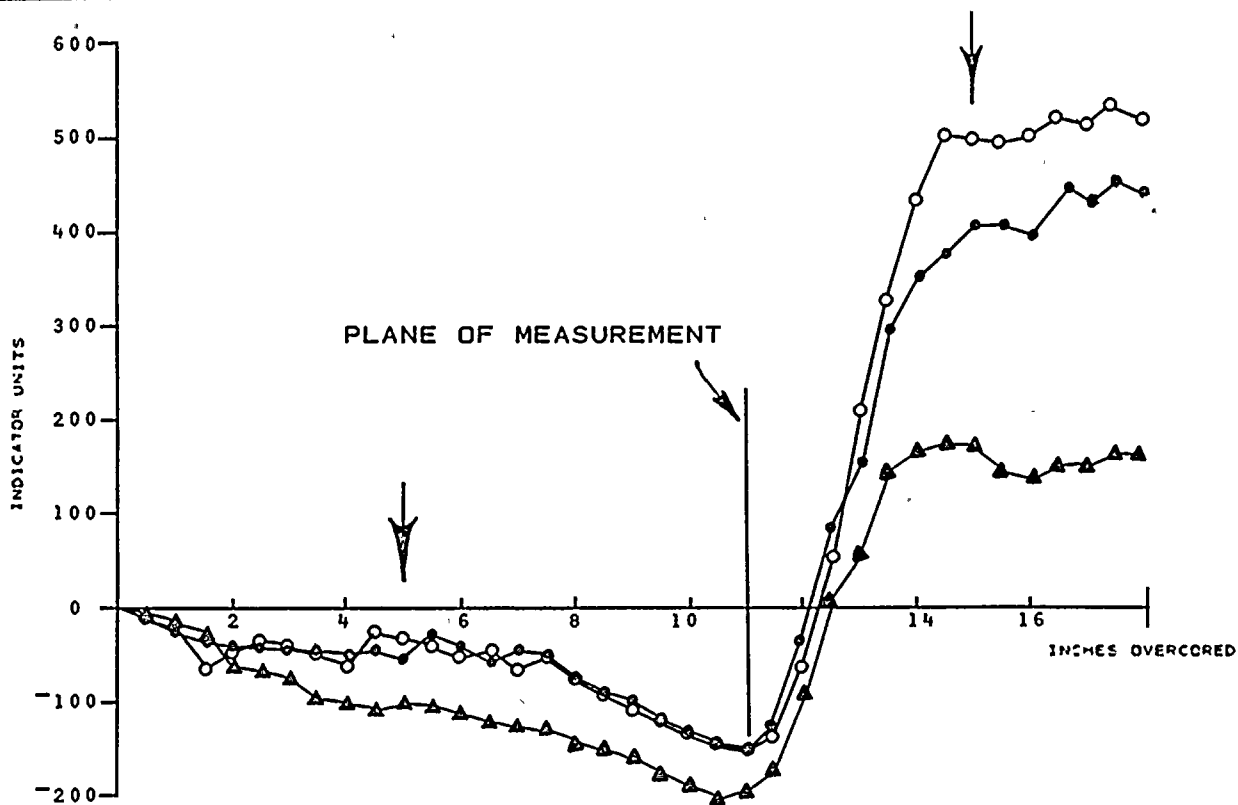
DEPTH 92'9"

NOTE: A POSITIVE INCREASE IN INDICATOR UNITS
INDICATES EXPANSION OF THE EX HOLE
DURING OVERCORING

ARROWS (f) INDICATE TOTAL DEFORMATION
USED TO CALCULATE STRESS

PLATE E-26
DAMES & MOORE





KEY:

△ AXIS I
○ AXIS II
◐ AXIS III

$$\begin{aligned}\Delta R_1 &= 170 - (-104) = 274 \\ \Delta R_2 &= 498 - (-34) = 532 \\ \Delta R_3 &= 403 - (-51) = 454\end{aligned}$$

$$K_1 = 0.90 \mu\text{IN.}$$

$$U_1 = 0.90 \times 274 = 247$$

$$K_2 = 0.93 \mu\text{IN.}$$

$$U_2 = 0.93 \times 532 = 495$$

$$K_3 = 0.95 \mu\text{IN.}$$

$$U_3 = 0.95 \times 454 = 431$$

ROCK TYPE: LIGHT GRAY SANDSTONE TO DARK
TO MEDIUM GRAY ARGILLACEOUS
SANDSTONE

STRAIN RELIEF MEASUREMENTS

BORING RS - 1

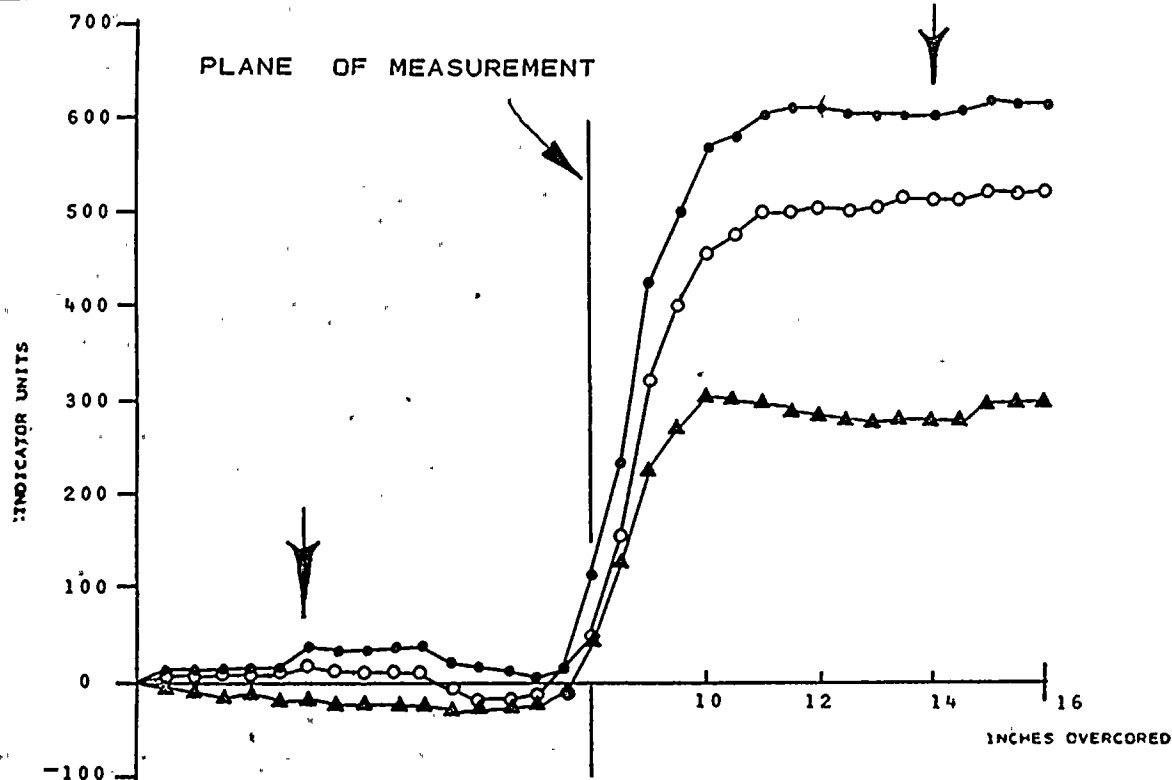
TEST NO. 35

DEPTH 96' 10"

NOTE: A POSITIVE INCREASE IN INDICATOR UNITS
INDICATES EXPANSION OF THE EX HOLE
DURING OVERCORING

ARROWS (†) INDICATE TOTAL DEFORMATION
USED TO CALCULATE STRESS





KEY:

- ▲ AXIS I
- AXIS II
- AXIS III

$$\Delta R_1 = 280 - (-21) = 301$$

$$\Delta R_2 = 516 - 15 = 501$$

$$\Delta R_3 = 605 - 40 = 565$$

$$K_1 = 0.90 \mu\text{IN.}$$

$$U_1 = 0.90 \times 301 = 271$$

$$K_2 = 0.93 \mu\text{IN.}$$

$$U_2 = 0.93 \times 501 = 466$$

$$K_3 = 0.95 \mu\text{IN.}$$

$$U_3 = 0.95 \times 565 = 537$$

ROCK TYPE: LIGHT GRAY SANDSTONE TO MEDIUM
GRAY ARGILLACEOUS SANDSTONE

STRAIN RELIEF MEASUREMENTS

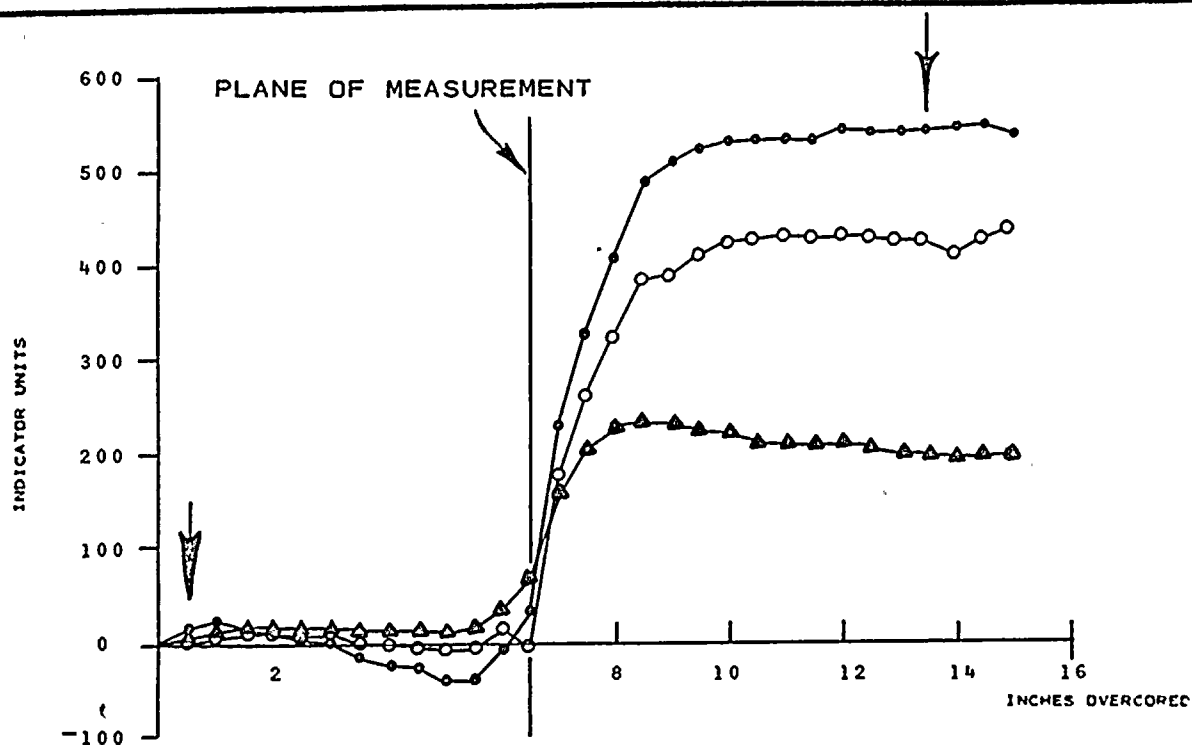
BORING RS - 1

TEST NO. 36

DEPTH 98'2"

NOTE: A POSITIVE INCREASE IN INDICATOR UNITS
INDICATES EXPANSION OF THE EX HOLE
DURING OVERCORING

ARROWS (A) INDICATE TOTAL DEFORMATION
USED TO CALCULATE STRESS



KEY:

Δ AXIS I	$\Delta R_1 = 200 - 5 = 195$
○ AXIS II	$\Delta R_2 = 422 - 3 = 419$
◐ AXIS III	$\Delta R_3 = 543 - 17 = 526$

$K_1 = 0.89 \mu\text{IN.}$	$U_1 = 0.89 \times 195 = 174$
$K_2 = 0.91 \mu\text{IN.}$	$U_2 = 0.91 \times 419 = 381$
$K_3 = 0.94 \mu\text{IN.}$	$U_3 = 0.94 \times 526 = 494$

ROCK TYPE: MEDIUM GRAY ARGILLACEOUS SANDSTONE

STRAIN RELIEF MEASUREMENTS

BORING RS - 1

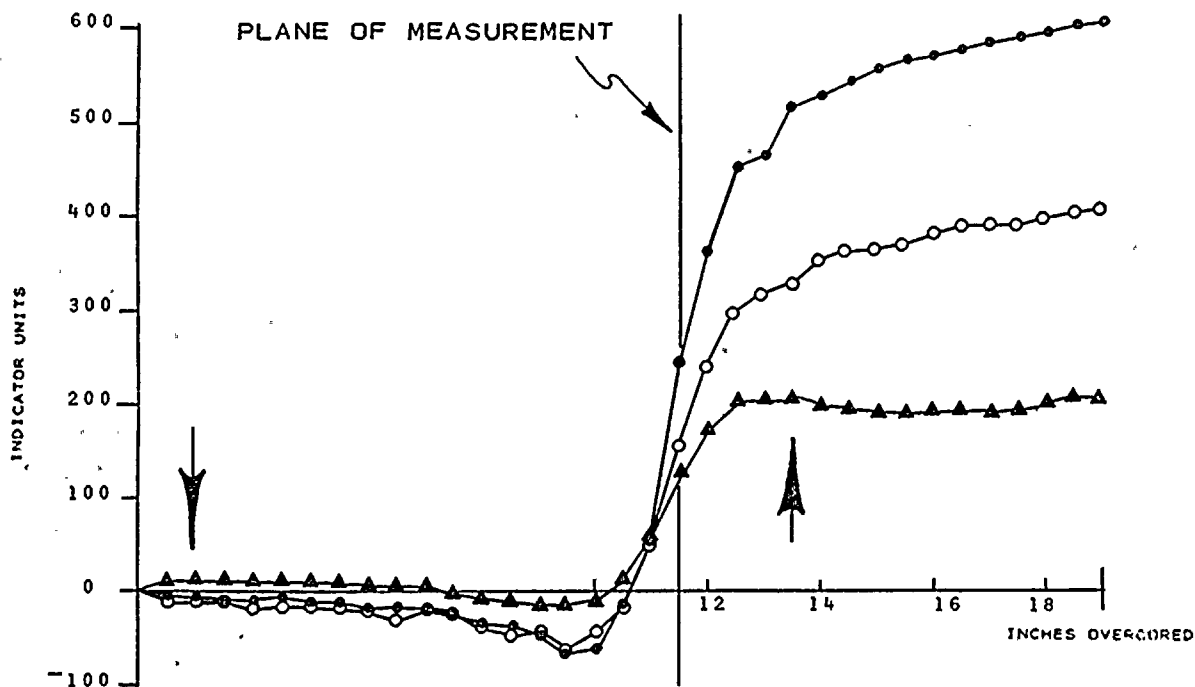
TEST NO. 38

DEPTH 100'9"

NOTE: A POSITIVE INCREASE IN INDICATOR UNITS
INDICATES EXPANSION OF THE EX HOLE
DURING OVERCORING

ARROWS (↓) INDICATE TOTAL DEFORMATION
USED TO CALCULATE STRESS





KEY:

▲ AXIS I
 ○ AXIS II
 • AXIS III

$\Delta R_1 = 203 - 10 = 193$
 $\Delta R_2 = 326 - (-10) = 336$
 $\Delta R_3 = 517 - (-9) = 526$

$K_1 = 0.89 \mu\text{IN.}$ $U_1 = 0.89 \times 193 = 172$
 $K_2 = 0.91 \mu\text{IN.}$ $U_2 = 0.91 \times 336 = 306$
 $K_3 = 0.94 \mu\text{IN.}$ $U_3 = 0.94 \times 526 = 494$

ROCK TYPE: MEDIUM GRAY ARGILLACEOUS SANDSTONE GRADING TO LIGHT GRAY SILICEOUS SANDSTONE

STRAIN RELIEF MEASUREMENTS

BORING RS - 1

TEST NO. 40

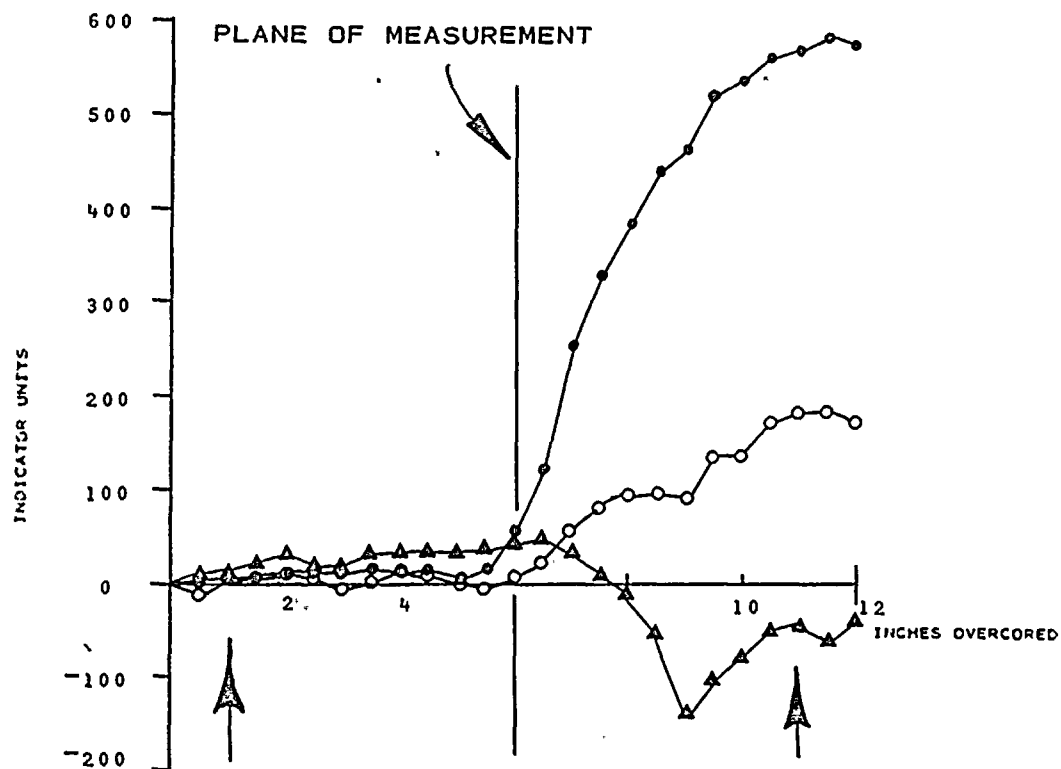
DEPTH 103'3"

NOTE: A POSITIVE INCREASE IN INDICATOR UNITS INDICATES EXPANSION OF THE EX HOLE DURING OVERCORING

ARROWS (4) INDICATE TOTAL DEFORMATION USED TO CALCULATE STRESS

PLATE E-30
DAMES & MOORE





KEY:

Δ AXIS I	$\Delta R_1 = -50 - 10 = -60$
○ AXIS II	$\Delta R_2 = 180 - 3 = 177$
• AXIS III	$\Delta R_3 = 565 - 7 = 558$

$K_1 = 0.95 \mu\text{IN.}$	$U_1 = 0.95 \times -60 = -57$
$K_2 = 1.00 \mu\text{IN.}$	$U_2 = 1.00 \times 177 = 177$
$K_3 = 0.94 \mu\text{IN.}$	$U_3 = 0.94 \times 558 = 525$

ROCK TYPE: LIGHT GRAY SILICEOUS SANDSTONE

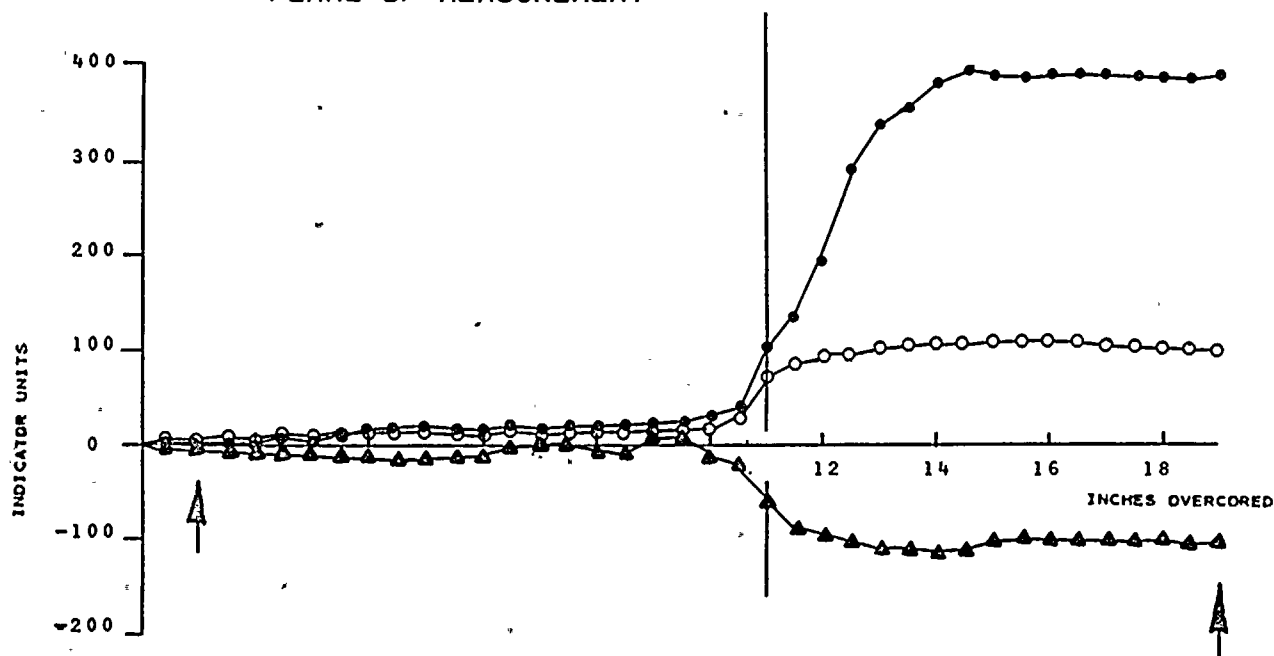
STRAIN RELIEF MEASUREMENTS
BORING RS - 1
TEST NO. 44
DEPTH 120'6"

NOTE: A POSITIVE INCREASE IN INDICATOR UNITS
INDICATES EXPANSION OF THE EX HOLE
DURING OVERCORING

ARROWS (↑) INDICATE TOTAL DEFORMATION
USED TO CALCULATE STRESS



PLANE OF MEASUREMENT



KEY:

AXIS I	$\Delta R_1 = -100 - 11 = -111$
AXIS II	$\Delta R_2 = 100 - 4 = 96$
AXIS III	$\Delta R_3 = 390 - 2 = 388$

$K_1 = 0.95 \mu\text{IN.}$	$U_1 = 0.95 \times -111 = -106$
$K_2 = 1.00 \mu\text{IN.}$	$U_2 = 1.00 \times 96 = 96$
$K_3 = 0.94 \mu\text{IN.}$	$U_3 = 0.94 \times 388 = 365$

ROCK TYPE: INTERBEDDED ARGILLACEOUS SANDSTONE
AND SHALE

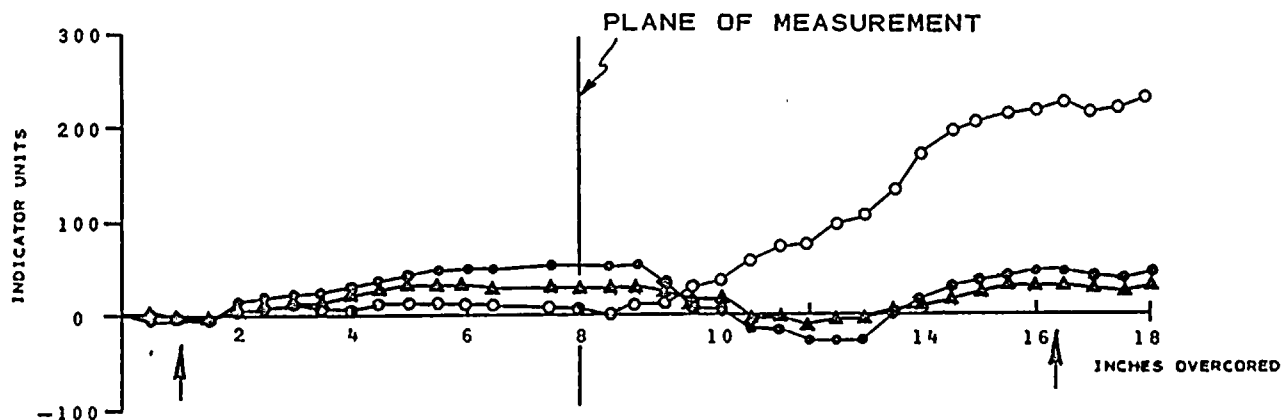
STRAIN RELIEF MEASUREMENTS

BORING RS - 1
TEST NO. 48
DEPTH 123' 11"

NOTE: A POSITIVE INCREASE IN INDICATOR UNITS
INDICATES EXPANSION OF THE EX HOLE
DURING OVERCORING

ARROWS (\uparrow) INDICATE TOTAL DEFORMATION
USED TO CALCULATE STRESS.





KEY:

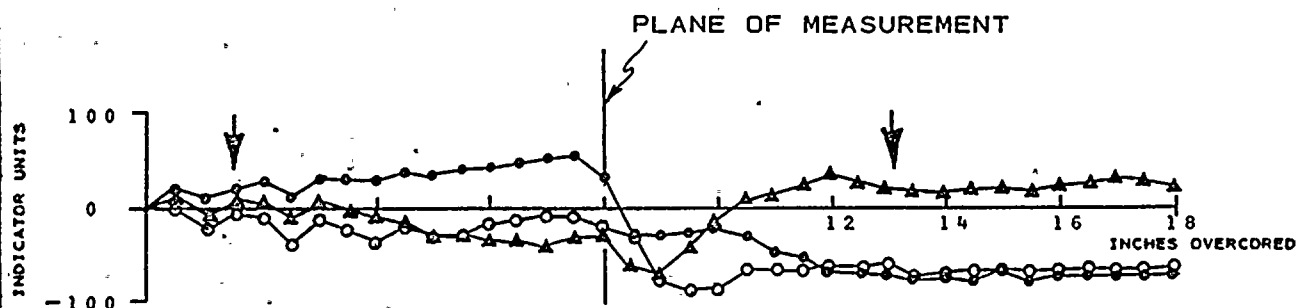
▲ AXIS I	$\Delta R_1 = 33 - (-2) = 35$
○ AXIS II	$\Delta R_2 = 222 - (-3) = 225$
• AXIS III	$\Delta R_3 = 45 - (-4) = 49$
$K_1 = .91 \mu\text{IN.}$	$U_1 = .91 \times 35 = 32$
$K_2 = .89 \mu\text{IN.}$	$U_2 = .89 \times 225 = 200$
$K_3 = .91 \mu\text{IN.}$	$U_3 = .91 \times 49 = 45$

ROCK TYPE: LIGHT GRAY SILICEOUS
SANDSTONE

STRAIN RELIEF MEASUREMENTS
BORING RS -2
TEST NO. 2
DEPTH 22'8"

NOTE: A POSITIVE INCREASE IN INDICATOR UNITS
INDICATES EXPANSION OF THE EX HOLE
DURING OVERCORING

ARROWS (†) INDICATE TOTAL DEFORMATION
USED TO CALCULATE STRESS



KEY:

▲ AXIS I	$\Delta R_1 = 20 - 3 = 17$
○ AXIS II	$\Delta R_2 = -64 - (-12) = -52$
● AXIS III	$\Delta R_3 = -76 - 20 = -96$

$K_1 = .91 \mu\text{IN.}$	$U_1 = .91 \times 17 = 15$
$K_2 = .89 \mu\text{IN.}$	$U_2 = .89 \times -52 = -46$
$K_3 = .91 \mu\text{IN.}$	$U_3 = .91 \times -96 = -87$

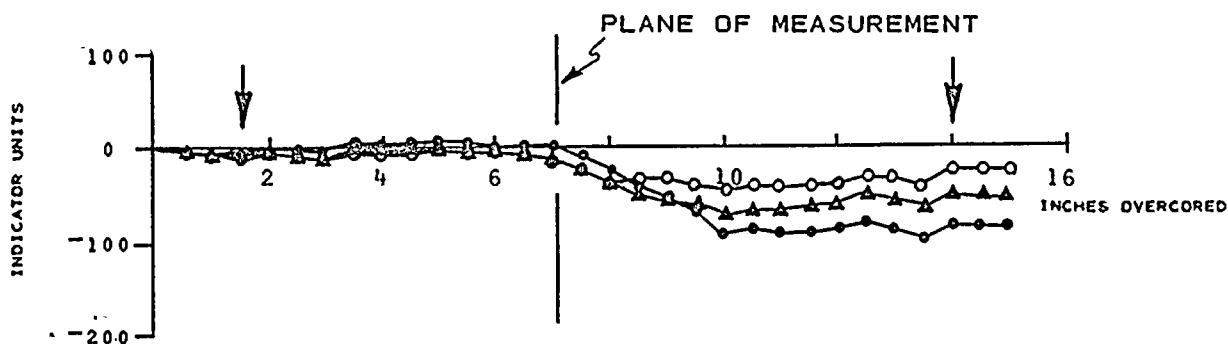
ROCK TYPE: LIGHT GRAY SILICEOUS
SANDSTONE

STRAIN RELIEF MEASUREMENTS
BORING RS - 2
TEST NO. 3
DEPTH 25'8 1/2"

NOTE: A POSITIVE INCREASE IN INDICATOR UNITS
INDICATES EXPANSION OF THE EX HOLE
DURING OVERCORING

ARROWS (A) INDICATE TOTAL DEFORMATION.
USED TO CALCULATE STRESS





KEY:

▲ AXIS I	$\Delta R_1 = -55 - (-8) = -47$
○ AXIS II	$\Delta R_2 = -33 - (-11) = -22$
• AXIS III	$\Delta R_3 = -86 - (-8) = -78$

$K_1 = .90 \mu\text{IN.}$	$U_1 = .90 \times -47 = -42$
$K_2 = .90 \mu\text{IN.}$	$U_2 = .90 \times -22 = -20$
$K_3 = .93 \mu\text{IN.}$	$U_3 = .93 \times -78 = -73$

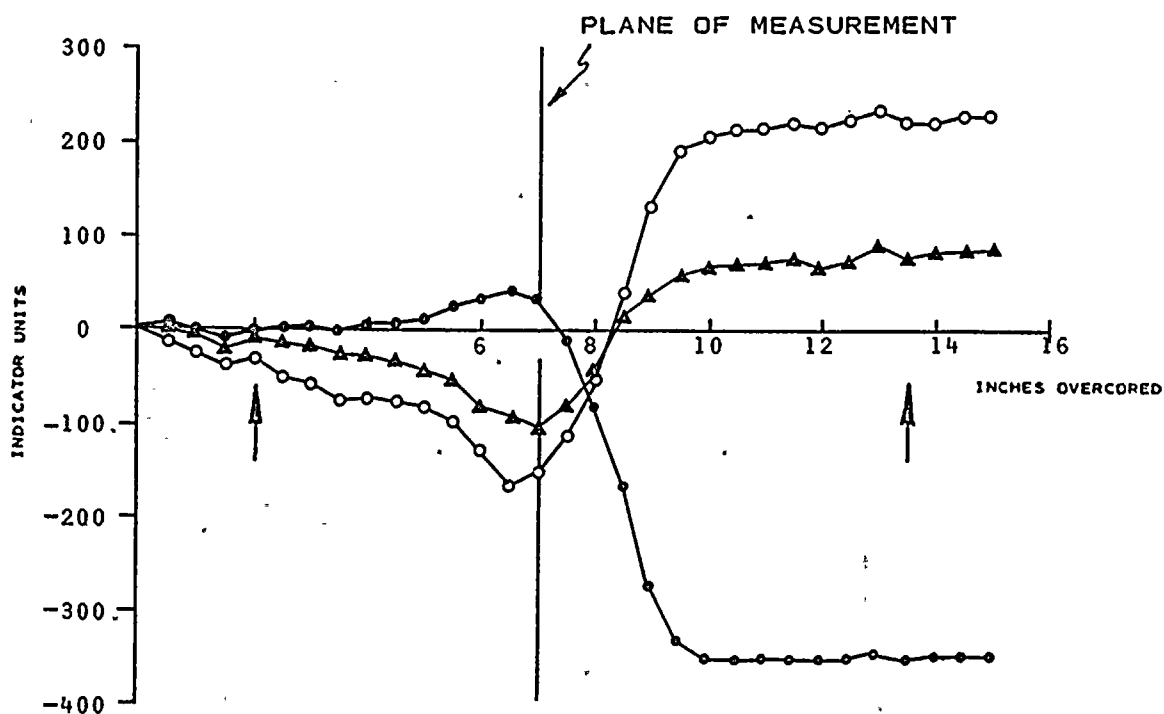
ROCK TYPE: LIGHT GRAY SILICEOUS
SANDSTONE

STRAIN RELIEF MEASUREMENTS
BORING RS - 2
TEST NO. 4
DEPTH 29'7"

NOTE: A POSITIVE INCREASE IN INDICATOR UNITS
INDICATES EXPANSION OF THE EX HOLE
DURING OVERCoring

ARROWS (↑) INDICATE TOTAL DEFORMATION
USED TO CALCULATE STRESS





KEY:

Δ AXIS I	$\Delta R_1 = 76 - (-14) = 90$
○ AXIS II	$\Delta R_2 = 221 - (-35) = 256$
• AXIS III	$\Delta R_3 = -352 - (-4) = -348$

$K_1 = .90 \mu\text{IN.}$	$U_1 = .90 \times 90 = 81$
$K_2 = .90 \mu\text{IN.}$	$U_2 = .90 \times 256 = 230$
$K_3 = .93 \mu\text{IN.}$	$U_3 = .93 \times -348 = -324$

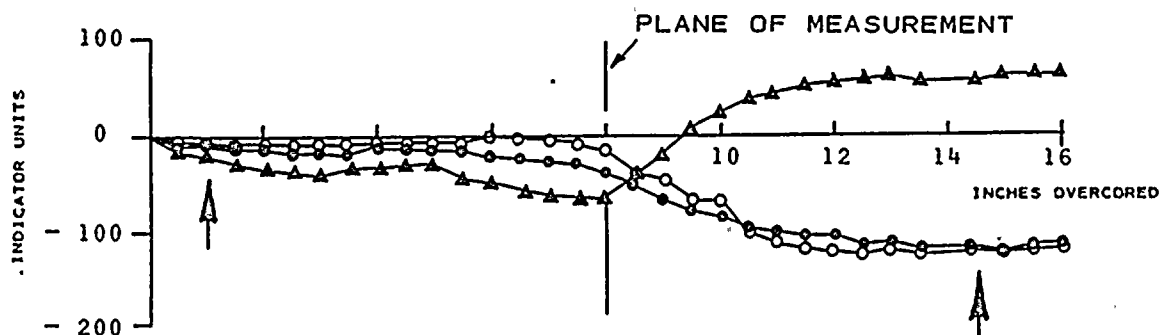
ROCK TYPE: LIGHT GRAY SILICEOUS
SANDSTONE

STRAIN RELIEF MEASUREMENTS
BORING RS - 2
TEST NO. 5
DEPTH 30'10"

NOTE: A POSITIVE INCREASE IN INDICATOR UNITS
INDICATES EXPANSION OF THE EX-HOLE
DURING OVERCORING

ARROWS (↑) INDICATE TOTAL DEFORMATION
USED TO CALCULATE STRESS





KEY:

▲ AXIS I	$\Delta R_1 = 59 - (-19) = 78$
○ AXIS II	$\Delta R_2 = -123 - (-6) = -117$
● AXIS III	$\Delta R_3 = -121 - (-8) = -113$
$K_1 = .90 \mu\text{IN.}$	$U_1 = .90 \times 78 = 70$
$K_2 = .90 \mu\text{IN.}$	$U_2 = .90 \times -117 = -105$
$K_3 = .93 \mu\text{IN.}$	$U_3 = .93 \times -113 = -105$

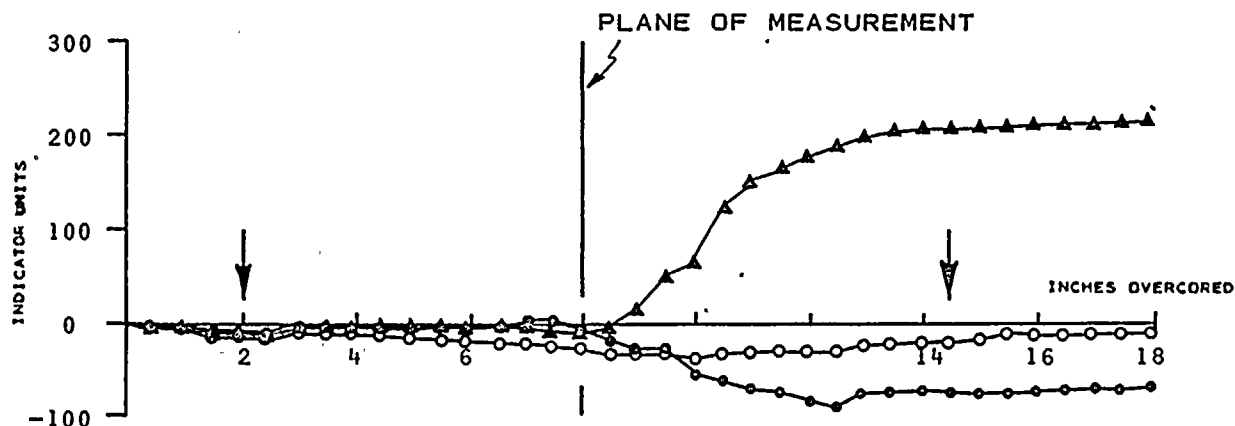
ROCK TYPE: LIGHT GRAY SILICEOUS
SANDSTONE

STRAIN RELIEF MEASUREMENTS
BORING RS - 2
TEST NO. 6
DEPTH 32'11"

NOTE: A POSITIVE INCREASE IN INDICATOR UNITS
INDICATES EXPANSION OF THE EX HOLE
DURING OVERCORING

ARROWS (†) INDICATE TOTAL DEFORMATION
USED TO CALCULATE STRESS





KEY:

▲ AXIS I	$\Delta R_1 = 205 - (-11) = 216$
○ AXIS II	$\Delta R_2 = -20 - (-15) = -5$
◊ AXIS III	$\Delta R_3 = -76 - (-10) = -66$

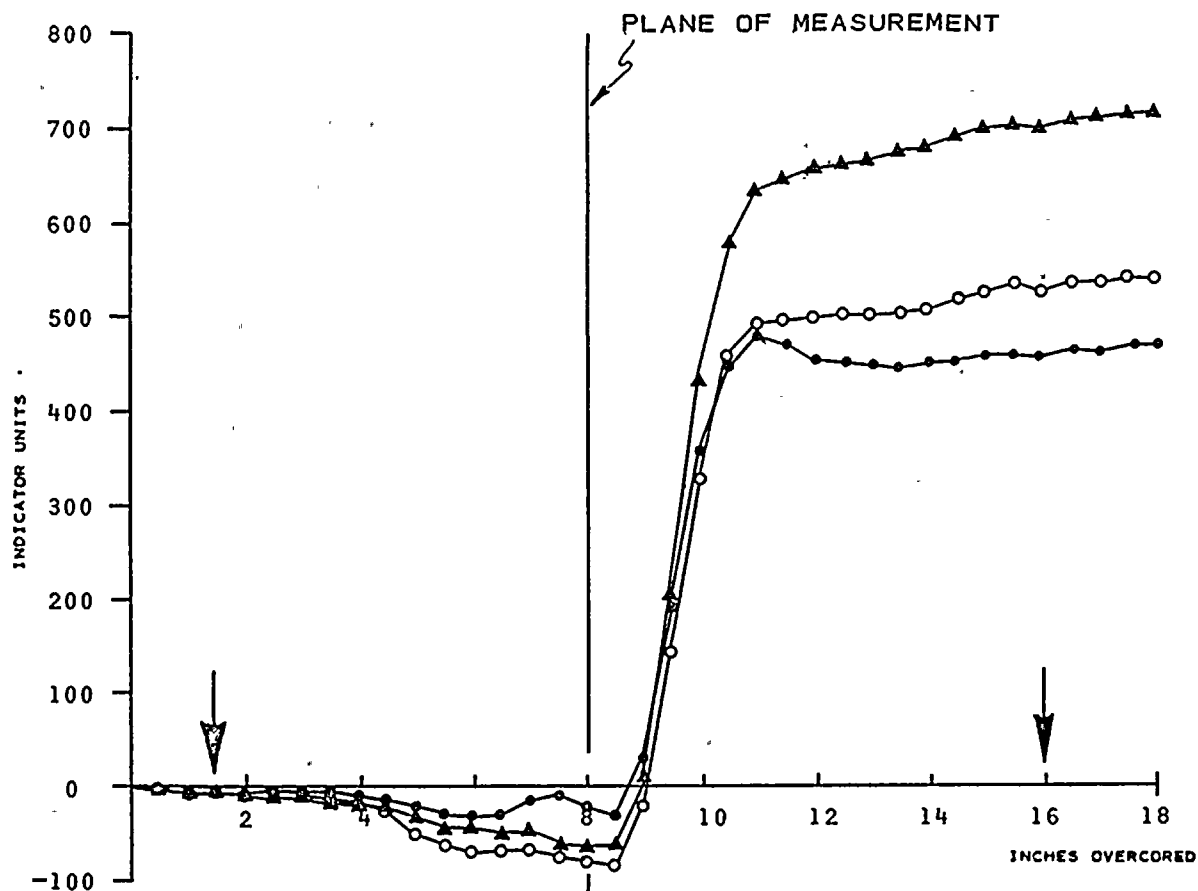
$K_1 = .90 \mu\text{IN.}$	$U_1 = .90 \times 216 = 194$
$K_2 = .90 \mu\text{IN.}$	$U_2 = .90 \times -5 = -5$
$K_3 = .93 \mu\text{IN.}$	$U_3 = .93 \times -66 = -61$

ROCK TYPE: LIGHT GRAY SILICEOUS
SANDSTONE

STRAIN RELIEF MEASUREMENTS
BORING RS - 2
TEST NO. 7
DEPTH 35'2"

NOTE: A POSITIVE INCREASE IN INDICATOR UNITS
INDICATES EXPANSION OF THE EX HOLE
DURING OVERCORING

ARROWS (†) INDICATE TOTAL DEFORMATION
USED TO CALCULATE STRESS



KEY:

▲ AXIS I	$R_1 = 698 - (-4) = 702$
○ AXIS II	$R_2 = 522 - (-4) = 526$
● AXIS III	$R_3 = 457 - (-5) = 462$

$K_1 = .89 \mu\text{IN.}$	$U_1 = .89 \times 702 = 625$
$K_2 = .91 \mu\text{IN.}$	$U_2 = .91 \times 526 = 479$
$K_3 = .92 \mu\text{IN.}$	$U_3 = .92 \times 462 = 425$

ROCK TYPE: DARK GRAY ARGILLACEOUS SANDSTONE
WITH SHALE INTERLAMINAE GRADING TO
MEDIUM TO LIGHT GRAY SANDSTONE

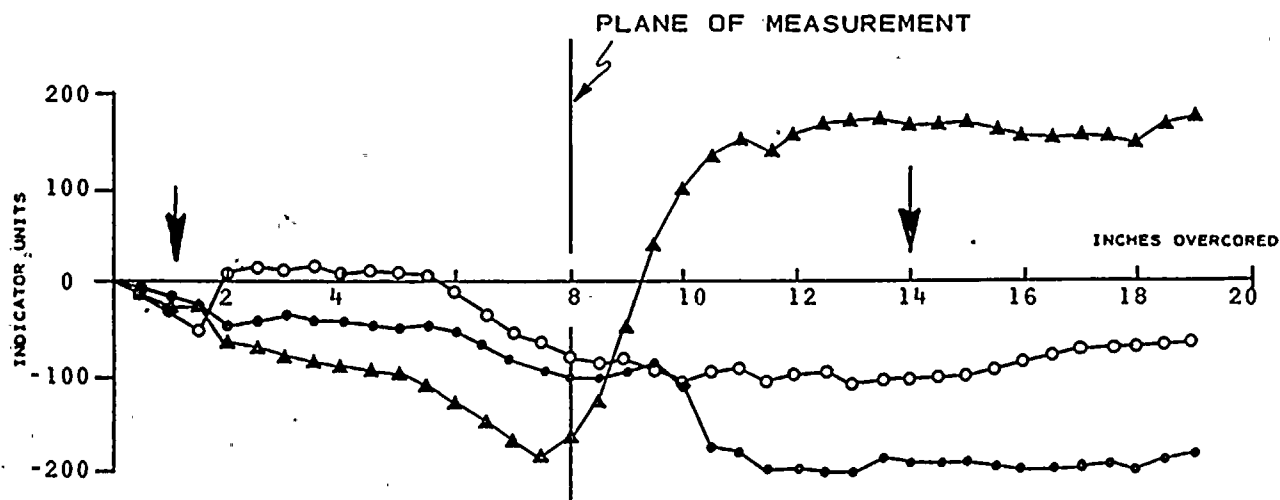
STRAIN RELIEF MEASUREMENTS BORING RS - 2 TEST NO. 8 DEPTH 38'8"

NOTE: A POSITIVE INCREASE IN INDICATOR UNITS
INDICATES EXPANSION OF THE EX HOLE
DURING OVERCORING

ARROWS (↓) INDICATE TOTAL DEFORMATION
USED TO CALCULATE STRESS

PLATE E-39
DAMES & MOORE





KEY:

▲ AXIS I	$\Delta R_1 = 190 - (-28) = 190$
○ AXIS II	$\Delta R_2 = -108 - (-36) = -72$
• AXIS III	$\Delta R_3 = -195 - (-16) = -179$

$K_1 = .89 \mu\text{IN.}$	$U_1 = .89 \times 190 = 169$
$K_2 = .91 \mu\text{IN.}$	$U_2 = .91 \times -72 = -66$
$K_3 = .92 \mu\text{IN.}$	$U_3 = .92 \times -179 = -165$

ROCK TYPE: SANDSTONE TO SHALE
TO SANDSTONE

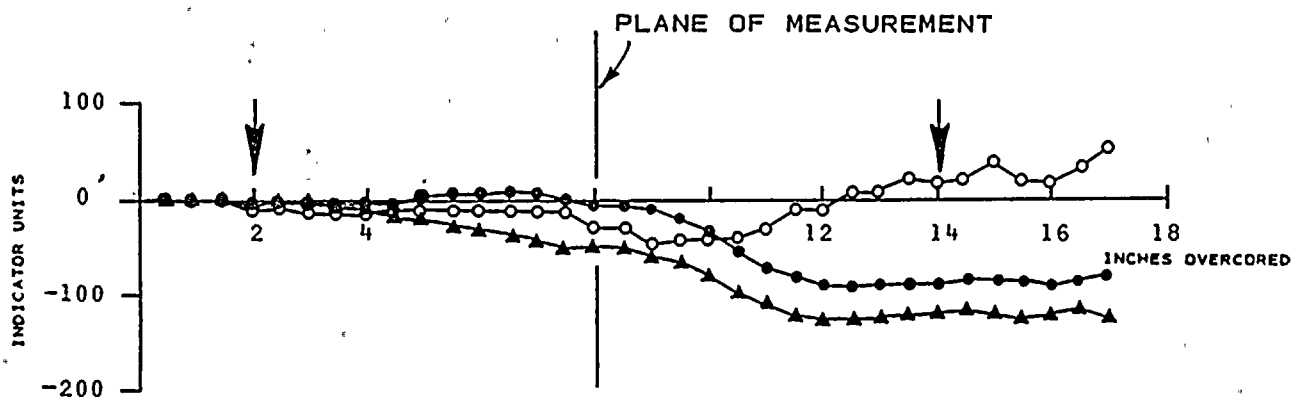
STRAIN RELIEF MEASUREMENTS
BORING RS - 2
TEST NO. 9
DEPTH 41'1"

NOTE: A POSITIVE INCREASE IN INDICATOR UNITS
INDICATES EXPANSION OF THE EX HOLE
DURING OVERCoring

ARROWS (†) INDICATE TOTAL DEFORMATION
USED TO CALCULATE STRESS

PLATE E-40
DAMES & MOORE





KEY:

▲ AXIS I $\Delta R_1 = -129 - 0 = -129$
 ○ AXIS II $\Delta R_2 = 19 - 0 = 19$
 • AXIS III $\Delta R_3 = -94 - 0 = -94$

$K_1 = .89 \mu\text{IN.}$ $U_1 = .89 \times -129 = -115$
 $K_2 = .91 \mu\text{IN.}$ $U_2 = .91 \times 19 = 17$
 $K_3 = .92 \mu\text{IN.}$ $U_3 = .92 \times -94 = -86$

ROCK TYPE: DARK GRAY GRAYWACKE TO LIGHT GRAY SILICEOUS SANDSTONE

STRAIN RELIEF MEASUREMENTS

BORING RS - 2

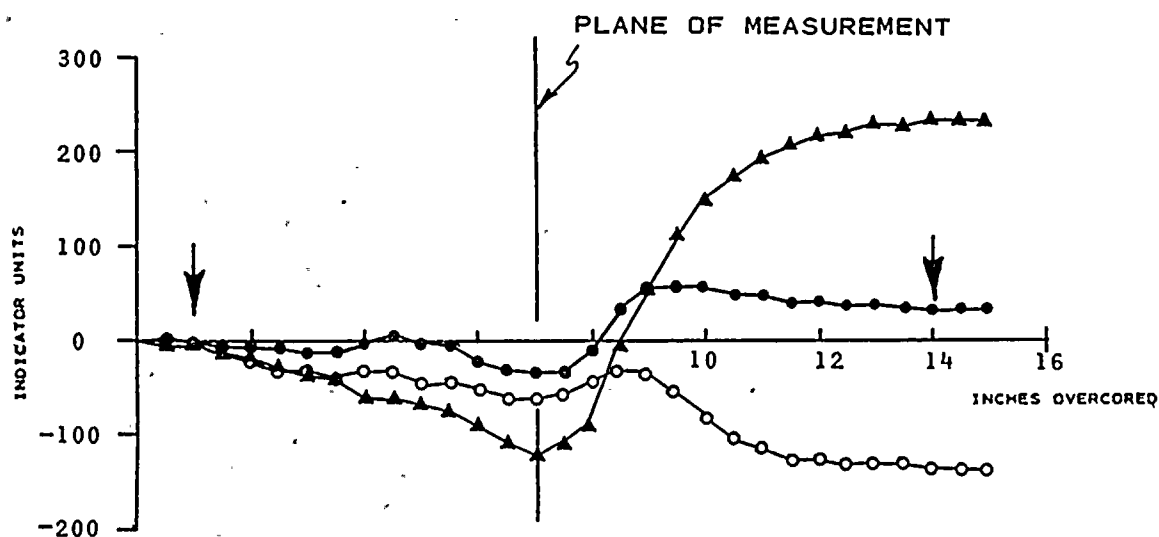
TEST NO. 10

DEPTH 43'10"

NOTE: A POSITIVE INCREASE IN INDICATOR UNITS INDICATES EXPANSION OF THE EX HOLE DURING OVERCoring

ARROWS (↑) INDICATE TOTAL DEFORMATION USED TO CALCULATE STRESS





KEY:

▲ AXIS I	$\Delta R_1 = 230 - (-6) = 236$
○ AXIS II	$\Delta R_2 = -140 - (-6) = -134$
• AXIS III	$\Delta R_3 = 31 - (-7) = 38$

$K_1 = .87 \mu\text{IN.}$	$U_1 = .87 \times 236 = 205$
$K_2 = .89 \mu\text{IN.}$	$U_2 = .89 \times -134 = -119$
$K_3 = .90 \mu\text{IN.}$	$U_3 = .90 \times 38 = 34$

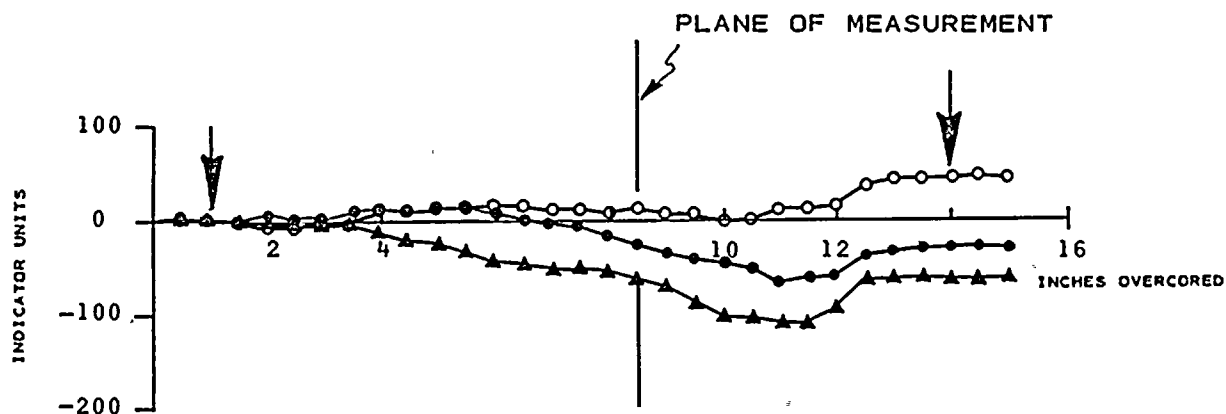
ROCK TYPE: LIGHT GRAY SILICEOUS SANDSTONE WITH MEDIUM
GRAY ARGILLACEOUS SANDSTONE INTERBEDS

STRAIN RELIEF MEASUREMENTS
BORING RS - 2
TEST NO. 14
DEPTH 47' 4"

NOTE: A POSITIVE INCREASE IN INDICATOR UNITS
INDICATES EXPANSION OF THE EX HOLE
DURING OVERCORING

ARROWS (↓) INDICATE TOTAL DEFORMATION
USED TO CALCULATE STRESS





KEY:

▲ AXIS I	$\Delta R_1 = -65 - (-2) = -63$
○ AXIS II	$\Delta R_2 = 42 - 0 = 42$
● AXIS III	$\Delta R_3 = -34 - 0 = -34$

$K_1 = .87 \mu\text{IN.}$	$U_1 = .87 \times -63 = -55$
$K_2 = .89 \mu\text{IN.}$	$U_2 = .89 \times 42 = 37$
$K_3 = .90 \mu\text{IN.}$	$U_3 = .90 \times -34 = -31$

ROCK TYPE: LIGHT GRAY SILICEOUS SANDSTONE

STRAIN RELIEF MEASUREMENTS

BORING RS - 2

TEST NO. 15

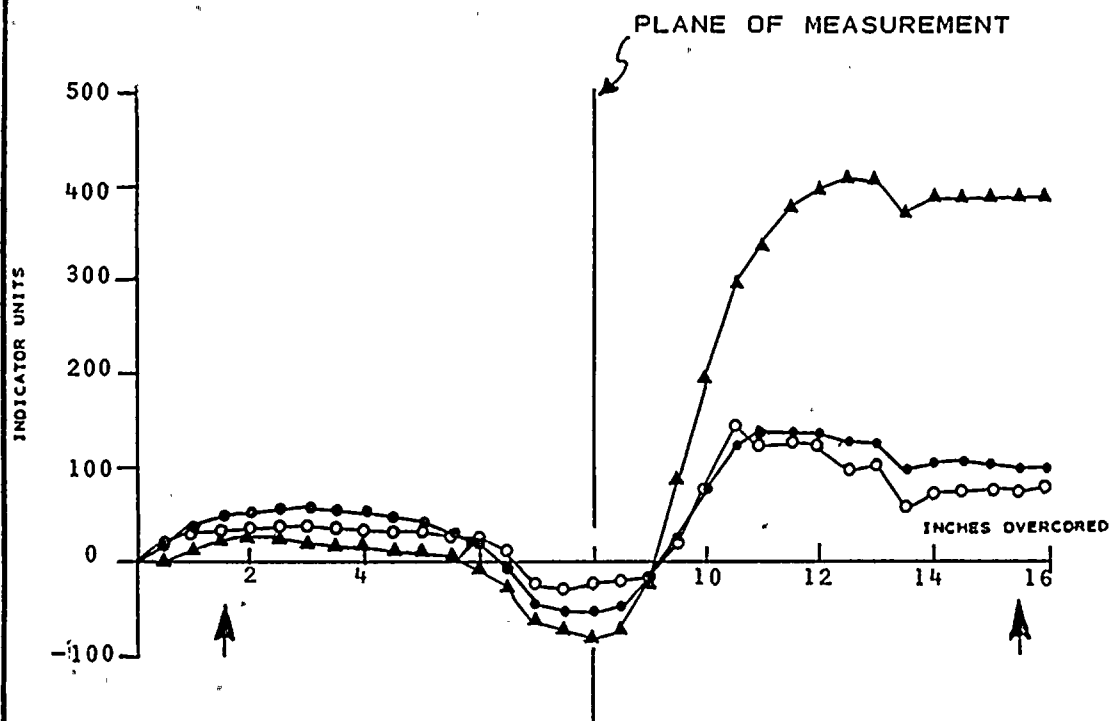
DEPTH 49' 1/2"

NOTE: A POSITIVE INCREASE IN INDICATOR UNITS
INDICATES EXPANSION OF THE EX' HOLE
DURING OVERCORING

ARROWS (↑) INDICATE TOTAL DEFORMATION
USED TO CALCULATE STRESS

PLATE E-43
DAMES & MOORE





KEY;

▲ AXIS I

○ AXIS II

● AXIS III

$$\Delta R_1 = 384 - 21 = 363$$

$$\Delta R_2 = 72 - 32 = 40$$

$$\Delta R_3 = 99 - 48 = 51$$

$$K_1 = .87 \mu\text{IN.}$$

$$K_2 = .89 \mu\text{IN.}$$

$$K_3 = .90 \mu\text{IN.}$$

$$U_1 = .87 \times 363 = 316$$

$$U_2 = .89 \times 40 = 36$$

$$U_3 = .90 \times 51 = 46$$

ROCK TYPE: DARK GRAY SILTSTONE AND SHALE GRADING TO,
ARGILLACEOUS SANDSTONE

STRAIN RELIEF MEASUREMENTS

BORING RS - 2

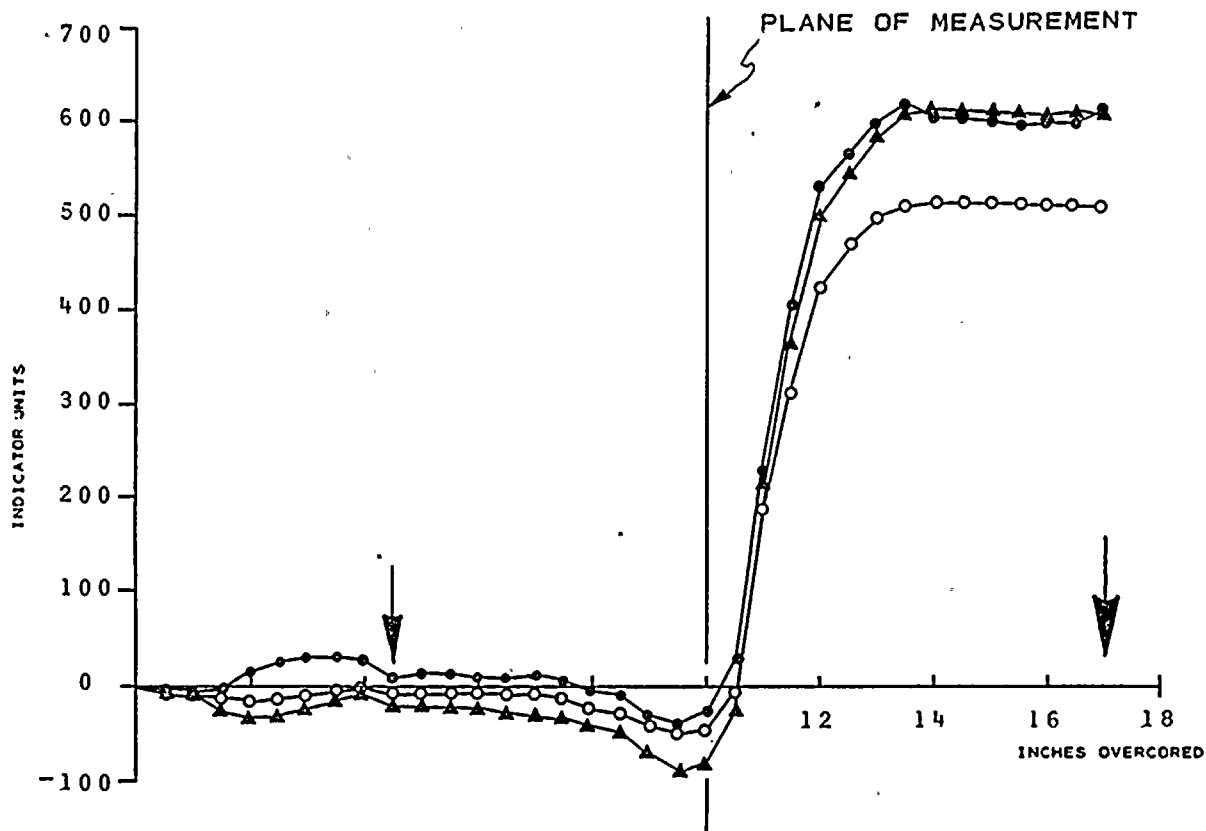
TEST NO. 17

DEPTH 51'6"

NOTE: A POSITIVE INCREASE IN INDICATOR UNITS
INDICATES EXPANSION OF THE EX HOLE
DURING OVERCORING

ARROWS (↑) INDICATE TOTAL DEFORMATION
USED TO CALCULATE STRESS





KEY:

▲ AXIS I	$\Delta R_1 = 601 - (-23) = 624$
○ AXIS II	$\Delta R_2 = 508 - (-9) = 517$
• AXIS III	$\Delta R_3 = 605 - (-11) = 594$

$K_1 = .88 \mu\text{IN.}$	$U_1 = .88 \times 624 = 549$
$K_2 = .92 \mu\text{IN.}$	$U_2 = .92 \times 517 = 476$
$K_3 = .90 \mu\text{IN.}$	$U_3 = .90 \times 594 = 535$

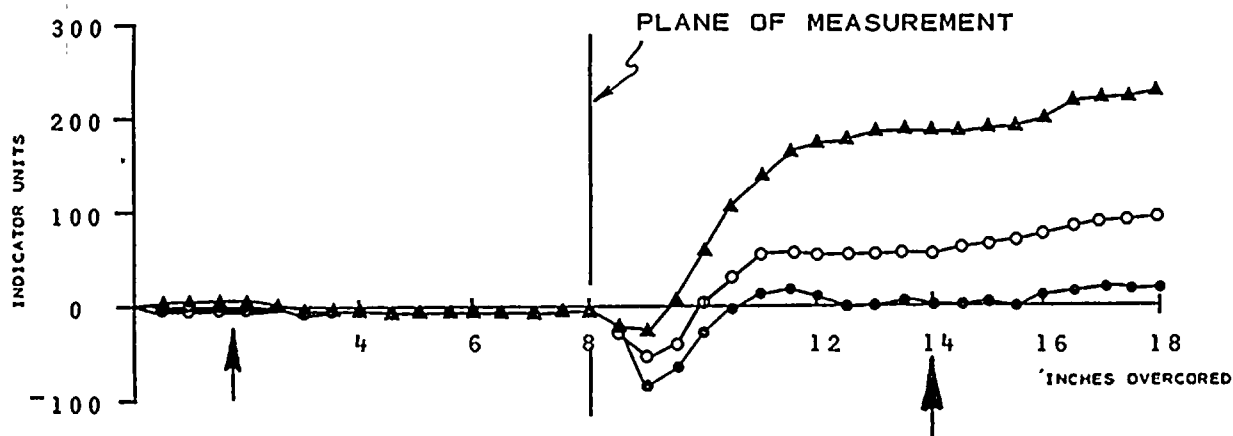
ROCK TYPE: MEDIUM GRAY GRAYWACKE

STRAIN RELIEF MEASUREMENTS
BORING RS - 2
TEST NO. 18
DEPTH 53'0"

NOTE: A POSITIVE INCREASE IN INDICATOR UNITS
INDICATES EXPANSION OF THE EX-HOLE
DURING OVERCORING

ARROWS (↓) INDICATE TOTAL DEFORMATION
USED TO CALCULATE STRESS

PLATE E-45
DAMES & MOORE



KEY:

△ AXIS I	$\Delta R_1 = 183 - 0 = 182$
○ AXIS II	$\Delta R_2 = 57 - (-3) = 60$
• AXIS III	$\Delta R_3 = -1 - (-7) = 6$

$K_1 = .88 \mu\text{IN.}$	$U_1 = .88 \times 182 = 160$
$K_2 = .92 \mu\text{IN.}$	$U_2 = .92 \times 60 = 55$
$K_3 = .90 \mu\text{IN.}$	$U_3 = .90 \times 6 = 5$

ROCK TYPE: MEDIUM GRAY ARGILLACEOUS SANDSTONE

STRAIN RELIEF MEASUREMENTS

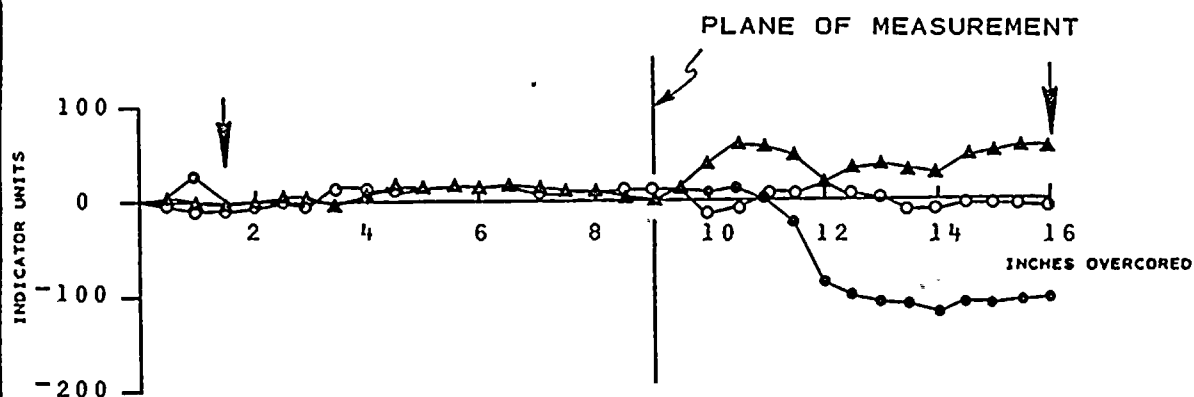
BORING RS - 2

TEST NO. 19

DEPTH 55'2"

NOTE: A POSITIVE INCREASE IN INDICATOR UNITS
INDICATES EXPANSION OF THE EX HOLE
DURING OVERCORING

ARROWS (↓) INDICATE TOTAL DEFORMATION
USED TO CALCULATE STRESS



KEY:

▲ AXIS I $R_1 = 50 - (-4) = 54$
 ○ AXIS II $R_2 = -4 - (-8) = 4$
 • AXIS III $R_3 = -108 - (4) = -104$

$K_1 = .88 \mu\text{IN.}$ $U_1 = .88 \times 54 = 48$
 $K_2 = .92 \mu\text{IN.}$ $U_2 = .92 \times 4 = 4$
 $K_3 = .90 \mu\text{IN.}$ $U_3 = .90 \times -104 = -94$

ROCK TYPE: LIGHT GRAY SILICEOUS SANDSTONE INTERBEDDED
WITH ARGILLACEOUS SANDSTONE

STRAIN RELIEF MEASUREMENTS

BORING RS - 2

TEST NO. 20

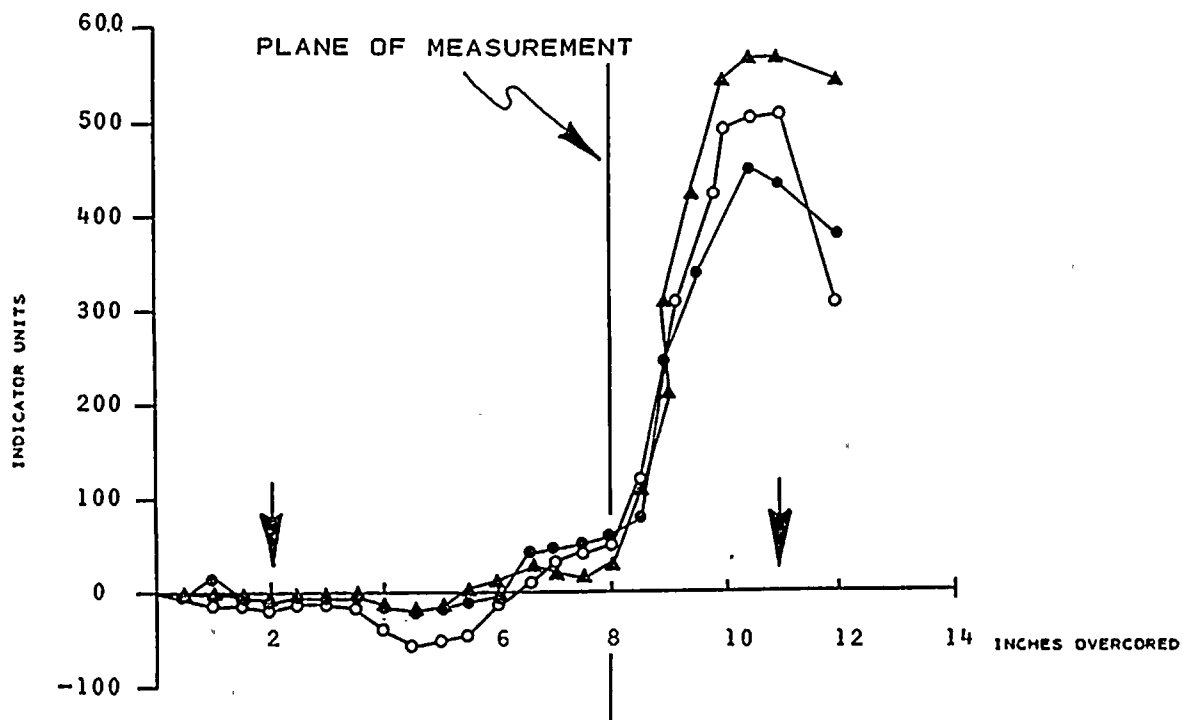
DEPTH 56'9"

NOTE: A POSITIVE INCREASE IN INDICATOR UNITS
INDICATES EXPANSION OF THE EX HOLE
DURING OVERCORING

ARROWS (↓) INDICATE TOTAL DEFORMATION
USED TO CALCULATE STRESS

PLATE E-47
DAMES & MOORE





KEY:

▲ AXIS I	$\Delta R_1 = 574 - (-4) = 578$
○ AXIS II	$\Delta R_2 = 524 - (-20) = 544$
● AXIS III	$\Delta R_3 = 434 - (-4) = 438$

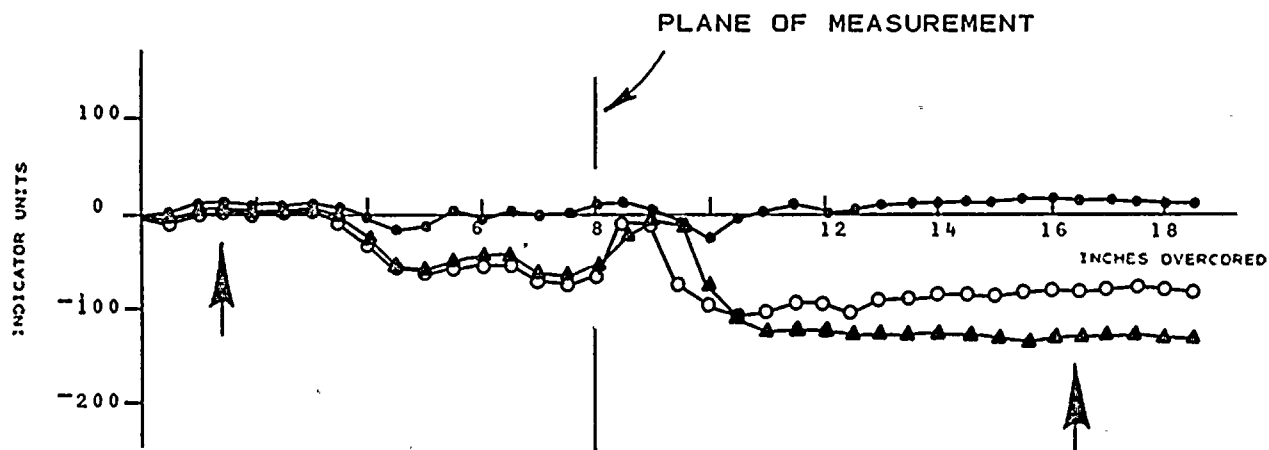
$K_1 = .88 \mu\text{IN}$	$U_1' = .88 \times 578 = 509$
$K_2 = .92 \mu\text{IN.}$	$U_2 = .92 \times 544 = 500$
$K_3 = .90 \mu\text{IN.}$	$U_3 = .90 \times 438 = 394$

ROCK TYPE: LIGHT GRAY SILICEOUS SANDSTONE INTERBEDDED WITH
DARK GRAY ARGILLACEOUS SANDSTONE WITH SHALE
LAMINATIONS

STRAIN RELIEF MEASUREMENTS
BORING RS - 2
TEST NO. 21
DEPTH 58'0"

NOTE: A POSITIVE INCREASE IN INDICATOR UNITS
INDICATES EXPANSION OF THE EX HOLE
DURING OVERCORING

ARROWS (↑) INDICATE TOTAL DEFORMATION
USED TO CALCULATE STRESS



KEY:

△ AXIS I	$\Delta R_1 = 16 - 14 = .2$
○ AXIS II	$\Delta R_2 = -81 - 5 = -86$
● AXIS III	$\Delta R_3 = -134 - 6 = -140$

$K_1 = 0.88 \mu\text{IN.}$	$U_1 = 0.88 \times 2 = 2$
$K_2 = 0.92 \mu\text{IN.}$	$U_2 = 0.92 \times -86 = -79$
$K_3 = 0.90 \mu\text{IN.}$	$U_3 = 0.90 \times -140 = -126$

ROCK TYPE: LIGHT GRAY SILICEOUS SANDSTONE INTERBEDDED WITH
MEDIUM TO DARK GRAY ARGILLACEOUS SANDSTONE

STRAIN RELIEF MEASUREMENTS

BORING RS - 2

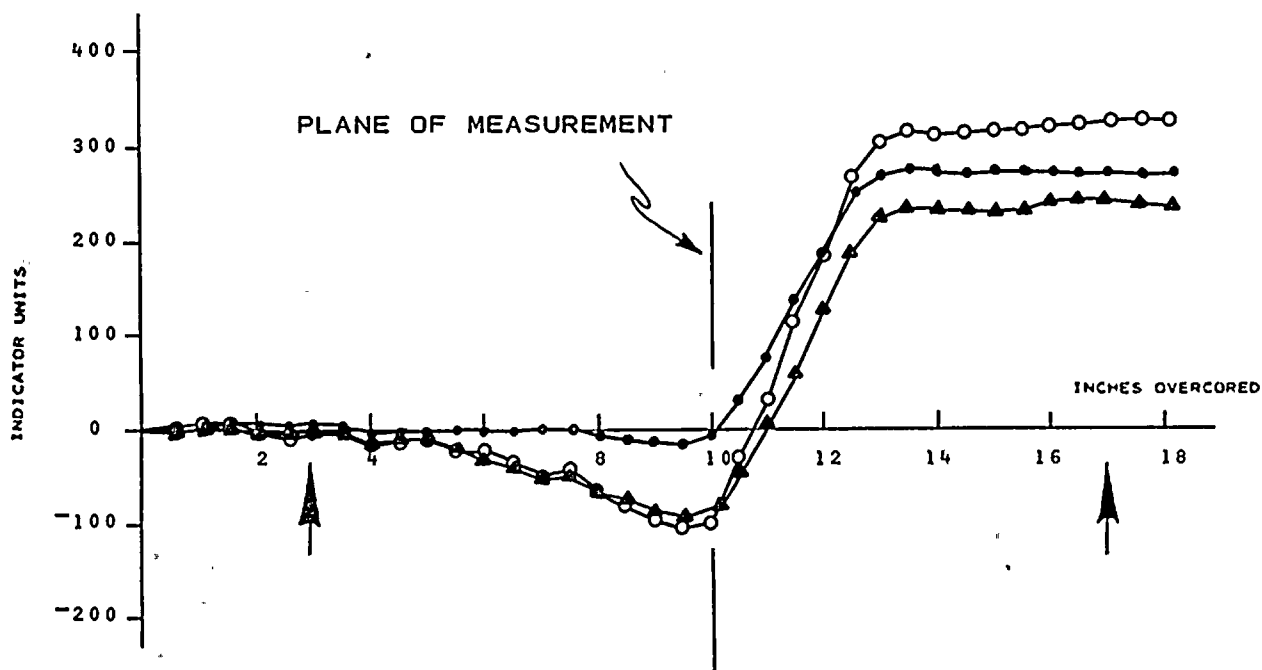
TEST NO. 23

DEPTH 60' 1 1/2"

NOTE: A POSITIVE INCREASE IN INDICATOR UNITS
INDICATES EXPANSION OF THE EX HOLE
DURING OVERCORING

ARROWS (↓) INDICATE TOTAL DEFORMATION
USED TO CALCULATE STRESS





KEY:

▲ AXIS I
○ AXIS II
● AXIS III

$$\begin{aligned}\Delta R_1 &= 241 - (-8) = 249 \\ \Delta R_2 &= 322 - (-4) = 326 \\ \Delta R_3 &= 266 - 2 = 264\end{aligned}$$

$$\begin{aligned}K_1 &= 0.88 \mu\text{IN.} & U_1 &= 0.88 \times 249 = 219 \\ K_2 &= 0.92 \mu\text{IN.} & U_2 &= 0.92 \times 326 = 300 \\ K_3 &= 0.92 \mu\text{IN.} & U_3 &= 0.92 \times 264 = 243\end{aligned}$$

ROCK TYPE: MEDIUM TO DARK GRAY ARGILLACEOUS SANDSTONE

STRAIN RELIEF MEASUREMENTS

BORING RS - 2

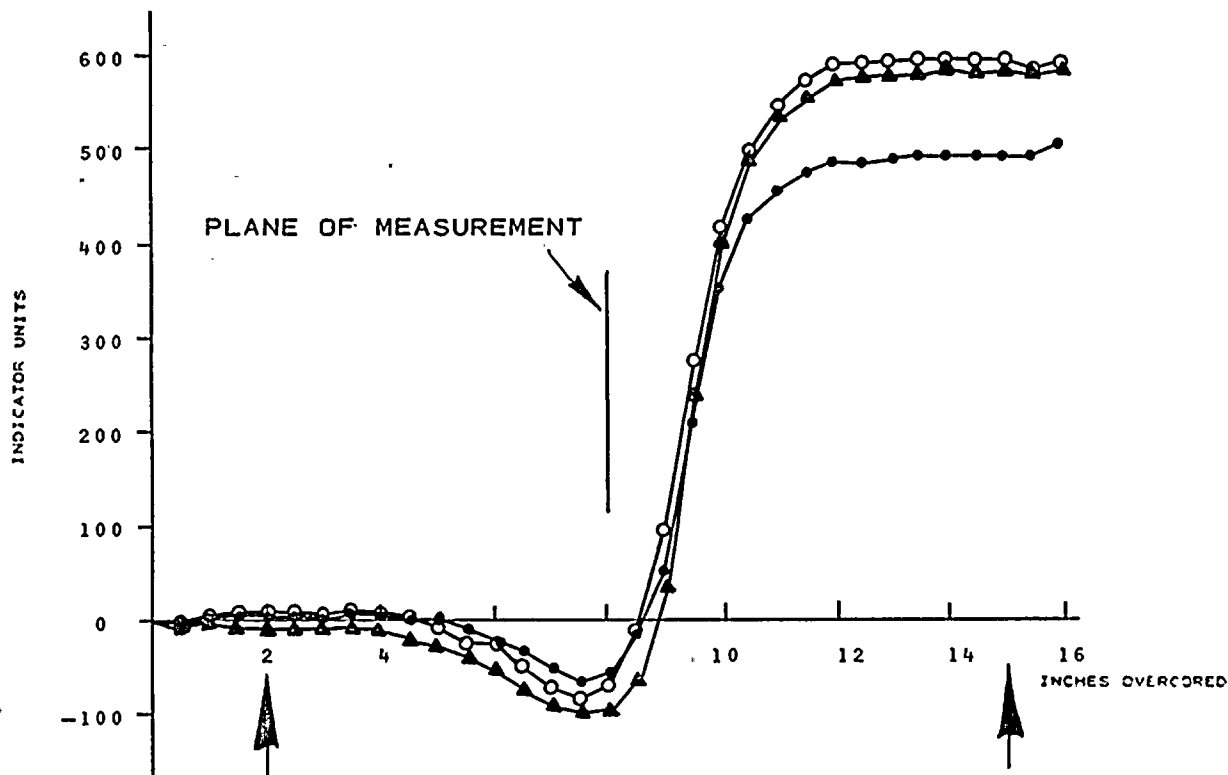
TEST NO. 24

DEPTH 61'0"

NOTE: A POSITIVE INCREASE IN INDICATOR UNITS INDICATES EXPANSION OF THE EX HOLE DURING OVERCoring

ARROWS (↑) INDICATE TOTAL DEFORMATION USED TO CALCULATE STRESS





KEY:

▲ AXIS I
○ AXIS II
• AXIS III

$\Delta R_1 = 580 - (-4) = 584$
 $\Delta R_2 = 590 - 10 = 580$
 $\Delta R_3 = 488 - 6 = 482$

$K_1 = 0.88 \mu\text{IN.}$ $U_1 = 0.88 \times 584 = 514$
 $K_2 = 0.92 \mu\text{IN.}$ $U_2 = 0.92 \times 580 = 534$
 $K_3 = 0.92 \mu\text{IN.}$ $U_3 = 0.92 \times 482 = 443$

ROCK TYPE: MEDIUM TO DARK GRAY ARGILLACEOUS
SANDSTONE

STRAIN RELIEF MEASUREMENTS

BORING RS - 2

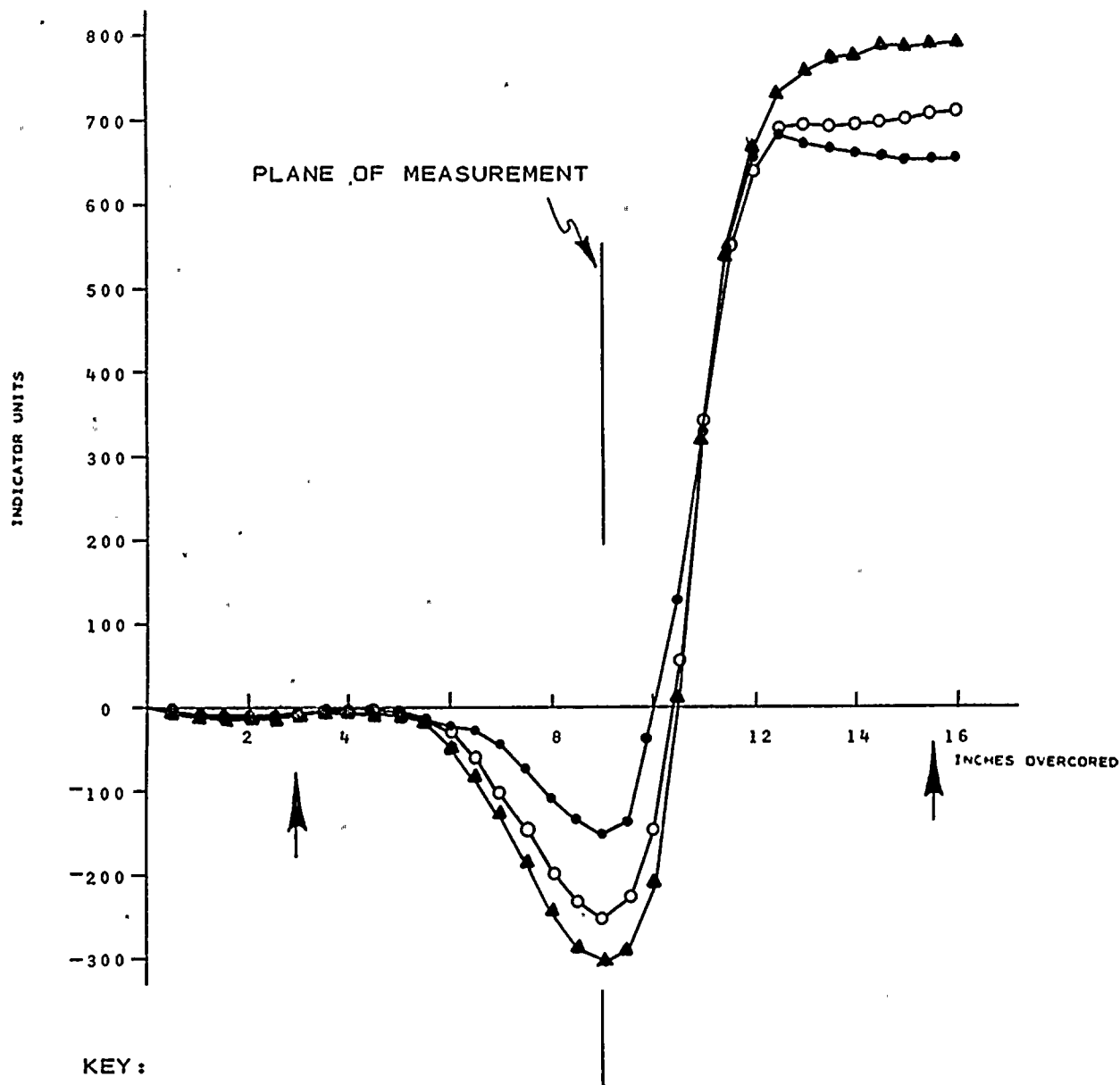
TEST NO. 25

DEPTH 63'2"

NOTE: A POSITIVE INCREASE IN INDICATOR UNITS
INDICATES EXPANSION OF THE EX HOLE
DURING OVERCORING

ARROWS (↑) INDICATE TOTAL DEFORMATION
USED TO CALCULATE STRESS

PLATE E-51
DAMES & MOORE



KEY:

▲ AXIS I $\Delta R_1 = 784 - (-6) = 790$
 ○ AXIS II $\Delta R_2 = 702 - (-10) = 712$
 • AXIS III $\Delta R_3 = 654 - (-8) = 662$

$K_1 = 0.88 \mu\text{IN.}$ $U_1 = 0.88 \times 790 = 695$
 $K_2 = 0.92 \mu\text{IN.}$ $U_2 = 0.92 \times 712 = 655$
 $K_3 = 0.92 \mu\text{IN.}$ $U_3 = 0.92 \times 662 = 609$

ROCK TYPE: MEDIUM GRAY ARGILLACEOUS SANDSTONE GRADING
 TO LIGHT GRAY SILICEOUS SANDSTONE

STRAIN RELIEF MEASUREMENTS

BORING RS - 2

TEST NO. 27

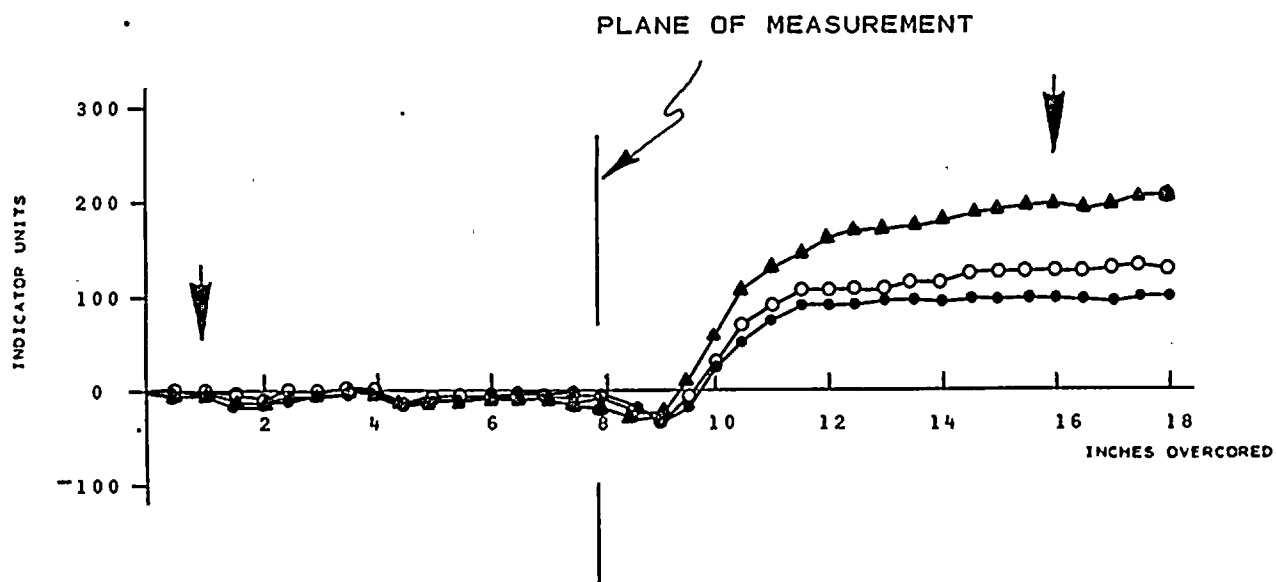
DEPTH 65'7"

NOTE: A POSITIVE INCREASE IN INDICATOR UNITS
 INDICATES EXPANSION OF THE EX HOLE
 DURING OVERCORING

ARROWS (↑) INDICATE TOTAL DEFORMATION
 USED TO CALCULATE STRESS

PLATE E-52
 DAMES & MOORE





KEY:

▲ AXIS I	$\Delta R_1 = 198 - (-4) = 202$
○ AXIS II	$\Delta R_2 = 124 - 0 = 124$
● AXIS III	$\Delta R_3 = 94 - (-6) = 100$

$K_1 = 0.88 \mu\text{IN.}$	$U_1 = 0.88 \times 202 = 178$
$K_2 = 0.92 \mu\text{IN.}$	$U_2 = 0.92 \times 124 = 114$
$K_3 = 0.92 \mu\text{IN.}$	$U_3 = 0.92 \times 100 = 92$

ROCK TYPE: LIGHT GRAY SILICEOUS SANDSTONE TO MEDIUM
GRAY SLIGHTLY ARGILLACEOUS SANDSTONE

STRAIN RELIEF MEASUREMENTS

BORING RS - 2

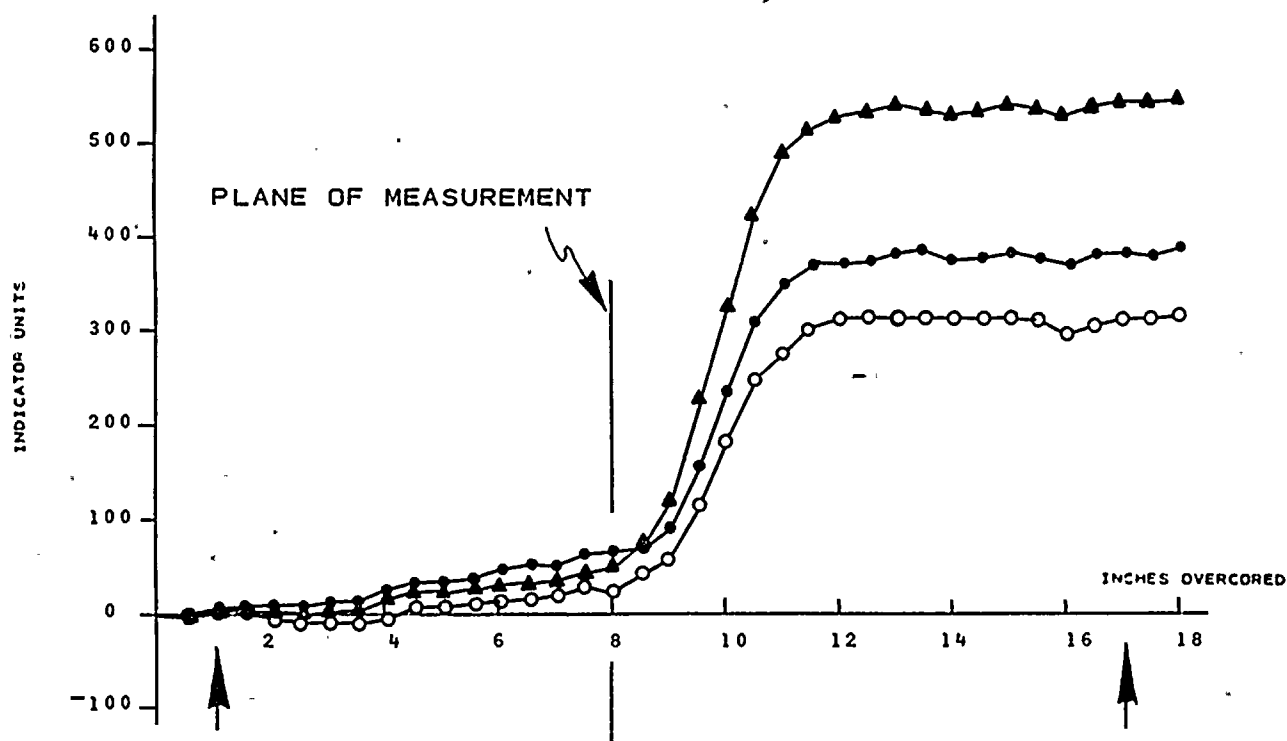
TEST NO. 28

DEPTH 66'10"

NOTE: A POSITIVE INCREASE IN INDICATOR UNITS
INDICATES EXPANSION OF THE EX HOLE
DURING OVERCORING

ARROWS (↑) INDICATE TOTAL DEFORMATION
USED TO CALCULATE STRESS





KEY:

▲ AXIS I
○ AXIS II
● AXIS III

$\Delta R_1 = 542 - 6 = 536$
 $\Delta R_2 = 310 - 0 = 310$
 $\Delta R_3 = 380 - 6 = 374$

$K_1 = 0.88 \mu\text{IN.}$

$U_1 = 0.88 \times 536 = 472$

$K_2 = 0.92 \mu\text{IN.}$

$U_2 = 0.92 \times 310 = 285$

$K_3 = 0.92 \mu\text{IN.}$

$U_3 = 0.92 \times 374 = 344$

ROCK TYPE: MEDIUM GRAY ARGILLACEOUS SANDSTONE GRADING
TO LIGHT GRAY SILICEOUS SANDSTONE

STRAIN RELIEF MEASUREMENTS

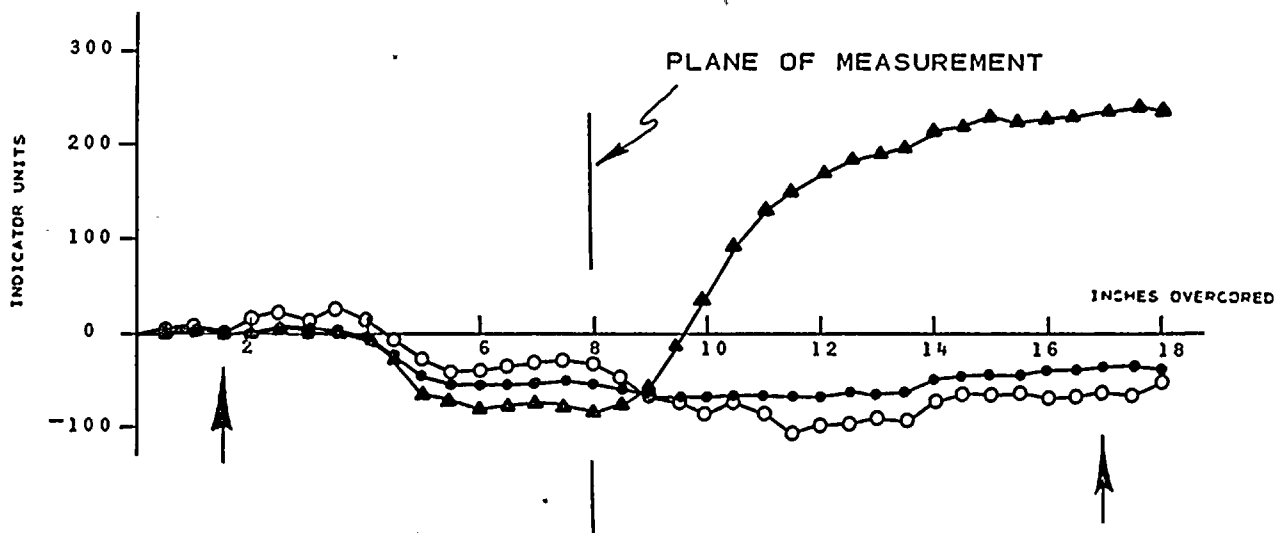
BORING RS - 2

TEST NO. 30

DEPTH 69'5"

NOTE: A POSITIVE INCREASE IN INDICATOR UNITS
INDICATES EXPANSION OF THE EX HOLE
DURING OVERCORING

ARROWS (↑) INDICATE TOTAL DEFORMATION
USED TO CALCULATE STRESS



KEY:

- ▲ AXIS I
- AXIS II
- AXIS III

$$\Delta R_1 = 226 - 0 = 226$$

$$\Delta R_2 = -62 - 0 = -62$$

$$\Delta R_3 = -38 - 0 = -38$$

$$K_1 = 0.88 \mu\text{IN.}$$

$$U_1 = 0.88 \times 226 = 199$$

$$K_2 = 0.92 \mu\text{IN.}$$

$$U_2 = 0.92 \times -62 = -57$$

$$K_3 = 0.92 \mu\text{IN.}$$

$$U_3 = 0.92 \times -38 = -35$$

ROCK TYPE: LIGHT GRAY SILICEOUS SANDSTONE

STRAIN RELIEF MEASUREMENTS

BORING RS - 2

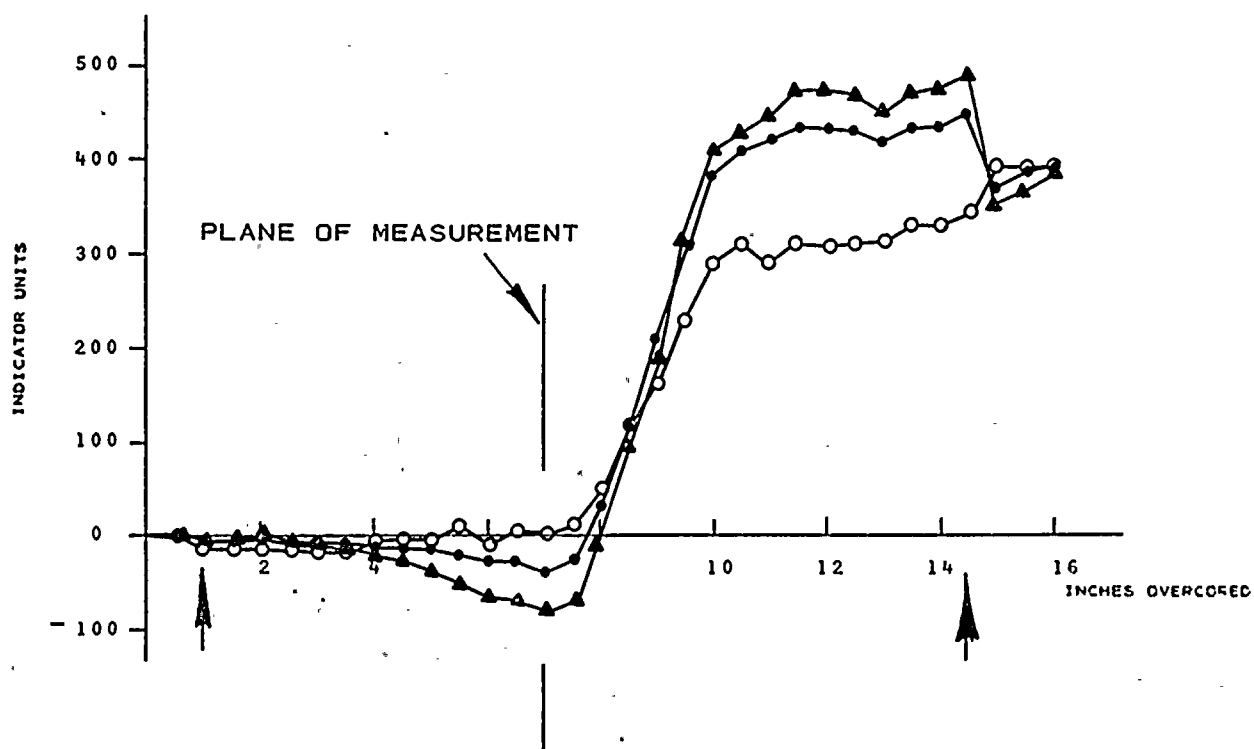
TEST NO. 31

DEPTH 71'8"

NOTE: A POSITIVE INCREASE IN INDICATOR UNITS INDICATES EXPANSION OF THE EX HOLE DURING OVERCORING

ARROWS (↑) INDICATE TOTAL DEFORMATION USED TO CALCULATE STRESS





KEY:

- ▲ AXIS I
- AXIS II
- AXIS III

$$\begin{aligned}\Delta R_1 &= 488 - (-4) = 492 \\ \Delta R_2 &= 340 - (-10) = 350 \\ \Delta R_3 &= 442 - (-2) = 444\end{aligned}$$

$$K_1 = 0.89 \mu\text{IN.}$$

$$U_1 = 0.89 \times 492 = 438$$

$$K_2 = 0.92 \mu\text{IN.}$$

$$U_2 = 0.92 \times 350 = 322$$

$$K_3 = 0.92 \mu\text{IN.}$$

$$U_3 = 0.92 \times 444 = 408$$

ROCK TYPE: MEDIUM GRAY ARGILLACEOUS SANDSTONE

STRAIN RELIEF MEASUREMENTS

BORING RS - 2

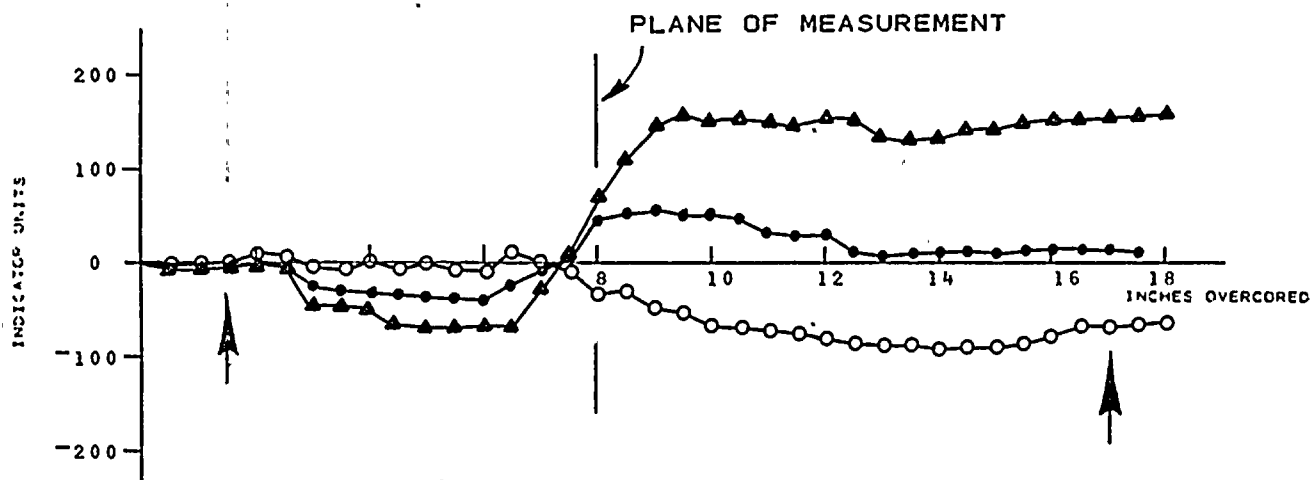
TEST NO. 32

DEPTH 73'1"

NOTE: A POSITIVE INCREASE IN INDICATOR UNITS INDICATES EXPANSION OF THE EX HOLE DURING OVERCoring.

ARROWS (†) INDICATE TOTAL DEFORMATION USED TO CALCULATE STRESS





KEY:

- ▲ AXIS I
- AXIS II
- AXIS III

$$\begin{aligned}\Delta R_1 &= 154 - (-4) = 158 \\ \Delta R_2 &= -72 - 0 = -72 \\ \Delta R_3 &= 16 - 2 = 14\end{aligned}$$

$$\begin{aligned}K_1 &= 0.89 \mu\text{IN.} & U_1 &= 0.89 \times 158 = 141 \\ K_2 &= 0.92 \mu\text{IN.} & U_2 &= 0.92 \times -72 = -66 \\ K_3 &= 0.92 \mu\text{IN.} & U_3 &= 0.92 \times 14 = 13\end{aligned}$$

ROCK TYPE: LIGHT GRAY SLIGHTLY SILICEOUS SANDSTONE, OCCASIONAL DARK GRAY SHALE CLASTS

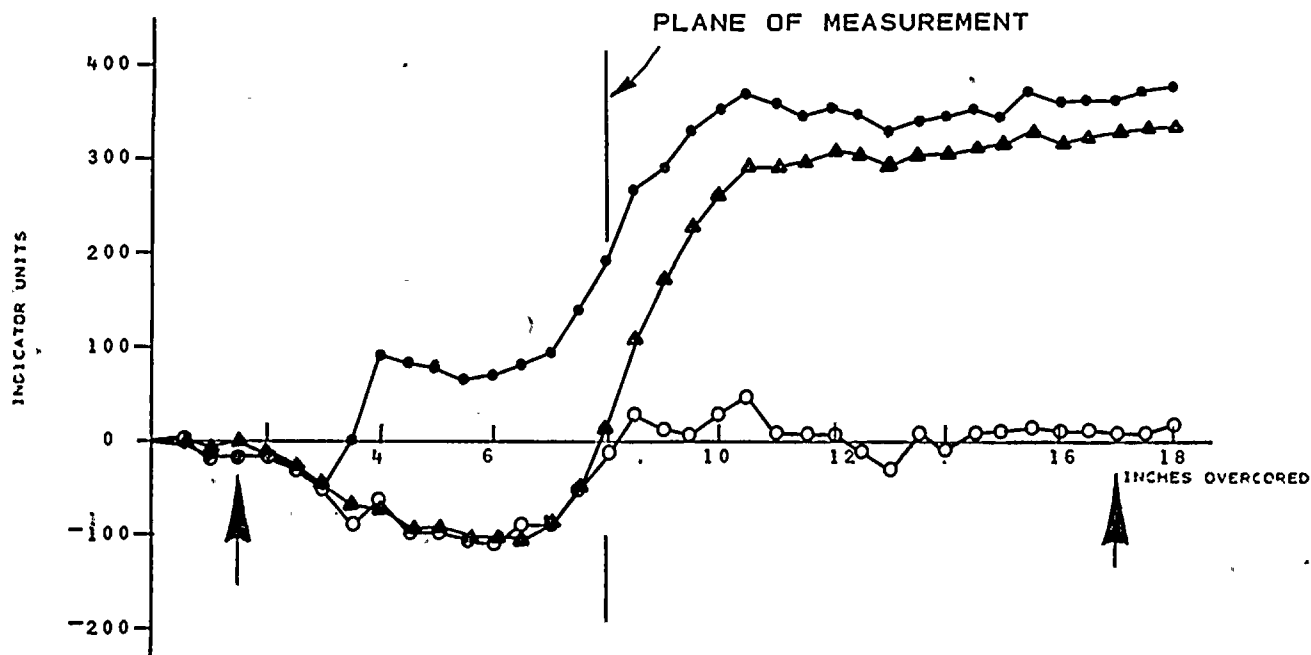
STRAIN RELIEF MEASUREMENTS

BORING RS - 2
TEST NO. 33
DEPTH 74'5"

NOTE: A POSITIVE INCREASE IN INDICATOR UNITS INDICATES EXPANSION OF THE EX. HOLE DURING OVERCORING

ARROWS (↓) INDICATE TOTAL DEFORMATION USED TO CALCULATE STRESS





KEY:

▲ AXIS I	$\Delta R_1 = 322 - (-10) = 332$
○ AXIS II	$\Delta R_2 = 6 - (-12) = 18$
● AXIS III	$\Delta R_3 = 360 - 0 = 360$

$K_1 = 0.89 \mu\text{IN.}$	$U_1 = 0.89 \times 332 = 295$
$K_2 = 0.92 \mu\text{IN.}$	$U_2 = 0.92 \times 18 = 17$
$K_3 = 0.92 \mu\text{IN.}$	$U_3 = 0.92 \times 360 = 331$

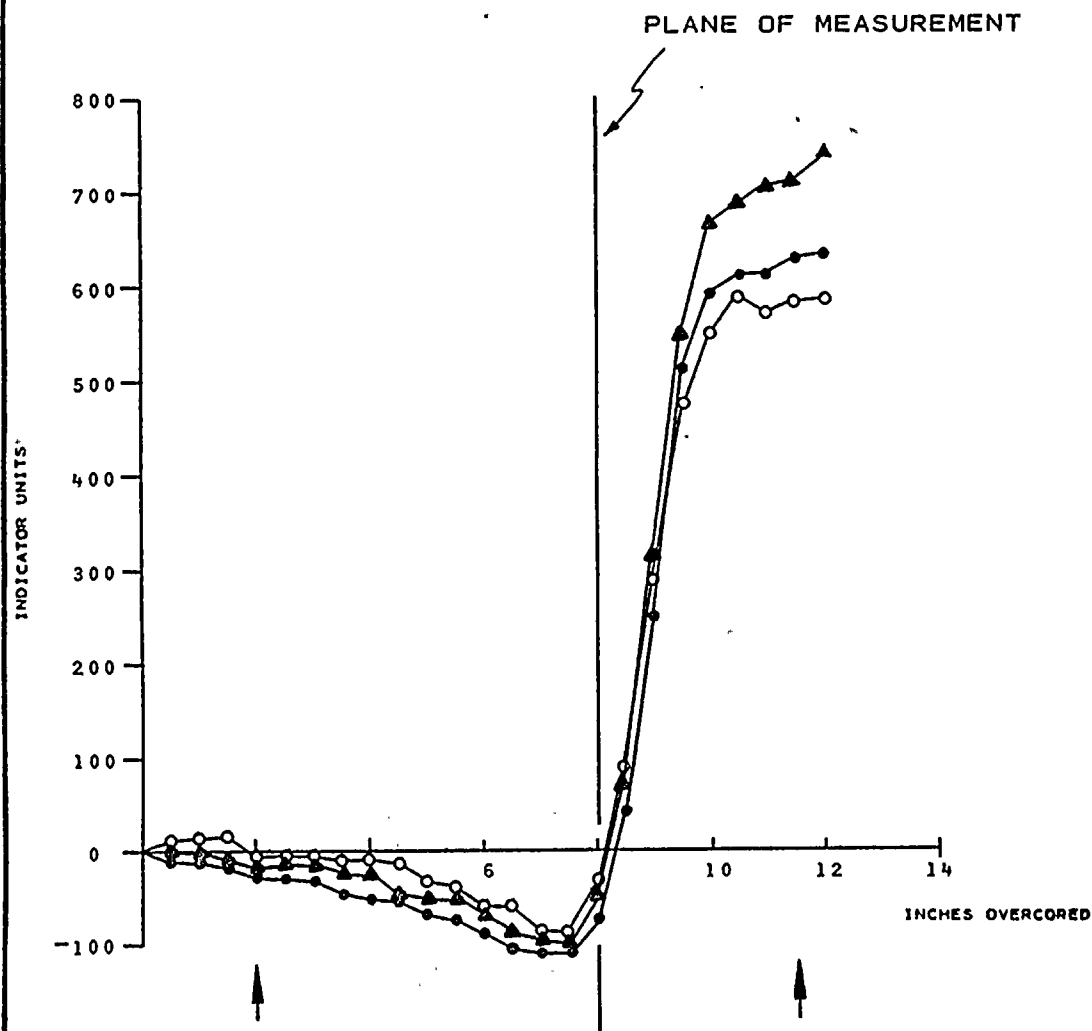
ROCK TYPE: ARGILLACEOUS SANDSTONE, OCCASIONAL LIGHT GRAY SILICEOUS SANDSTONE INTERBEDS

STRAIN RELIEF MEASUREMENTS
BORING RS - 2
TEST NO. 34
DEPTH 76'2"

NOTE: A POSITIVE INCREASE IN INDICATOR UNITS INDICATES EXPANSION OF THE EX HOLE DURING OVERCORING

ARROWS (↓) INDICATE TOTAL DEFORMATION USED TO CALCULATE STRESS





KEY:

- ▲ AXIS I
- AXIS II
- AXIS III

$$\Delta R_1 = 708 - (-16) = 724$$

$$\Delta R_2 = 580 - (-2) = 582$$

$$\Delta R_3 = 626 - (-22) = 648$$

$$K_1 = 0.89 \mu\text{IN.}$$

$$U_1 = 0.89 \times 724 = 644$$

$$K_2 = 0.92 \mu\text{IN.}$$

$$U_2 = 0.92 \times 582 = 535$$

$$K_3 = 0.92 \mu\text{IN.}$$

$$U_3 = 0.92 \times 360 = 331$$

ROCK TYPE: MEDIUM GRAY ARGILLACEOUS SANDSTONE TO
LIGHT GRAY SANDSTONE WITH SHALE LAMINATIONS

STRAIN RELIEF MEASUREMENTS

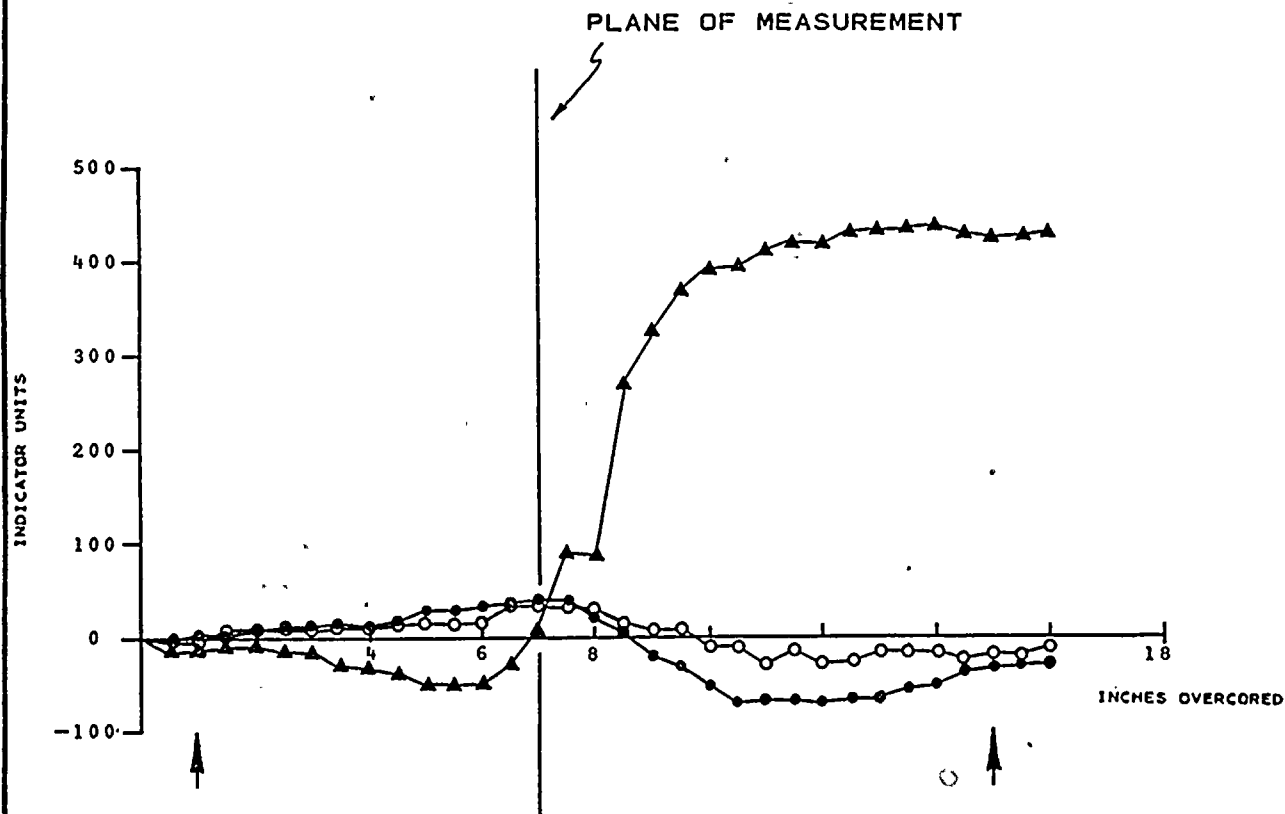
BORING RS - 2

TEST NO. 36

DEPTH 79'6"

NOTE: A POSITIVE INCREASE IN INDICATOR UNITS
INDICATES EXPANSION OF THE EX HOLE
DURING OVERCORING

ARROWS (↑) INDICATE TOTAL DEFORMATION
USED TO CALCULATE STRESS



KEY:

▲ AXIS I	$\Delta R_1 = 428 - (-10) = 438$
○ AXIS II	$\Delta R_2 = -10 - (-2) = -8$
● AXIS III	$\Delta R_3 = -36 - 0 = -36$

$K_1 = 0.84 \mu\text{IN.}$	$U_1 = 0.84 \times 438 = 368$
$K_2 = 0.92 \mu\text{IN.}$	$U_2 = 0.92 \times -8 = -7$
$K_3 = 0.89 \mu\text{IN.}$	$U_3 = 0.89 \times -36 = -32$

ROCK TYPE: LIGHT GRAY SILICEOUS SANDSTONE TO DARK GRAY ARGILLACEOUS SANDSTONE.

STRAIN RELIEF MEASUREMENTS

BORING RS - 2

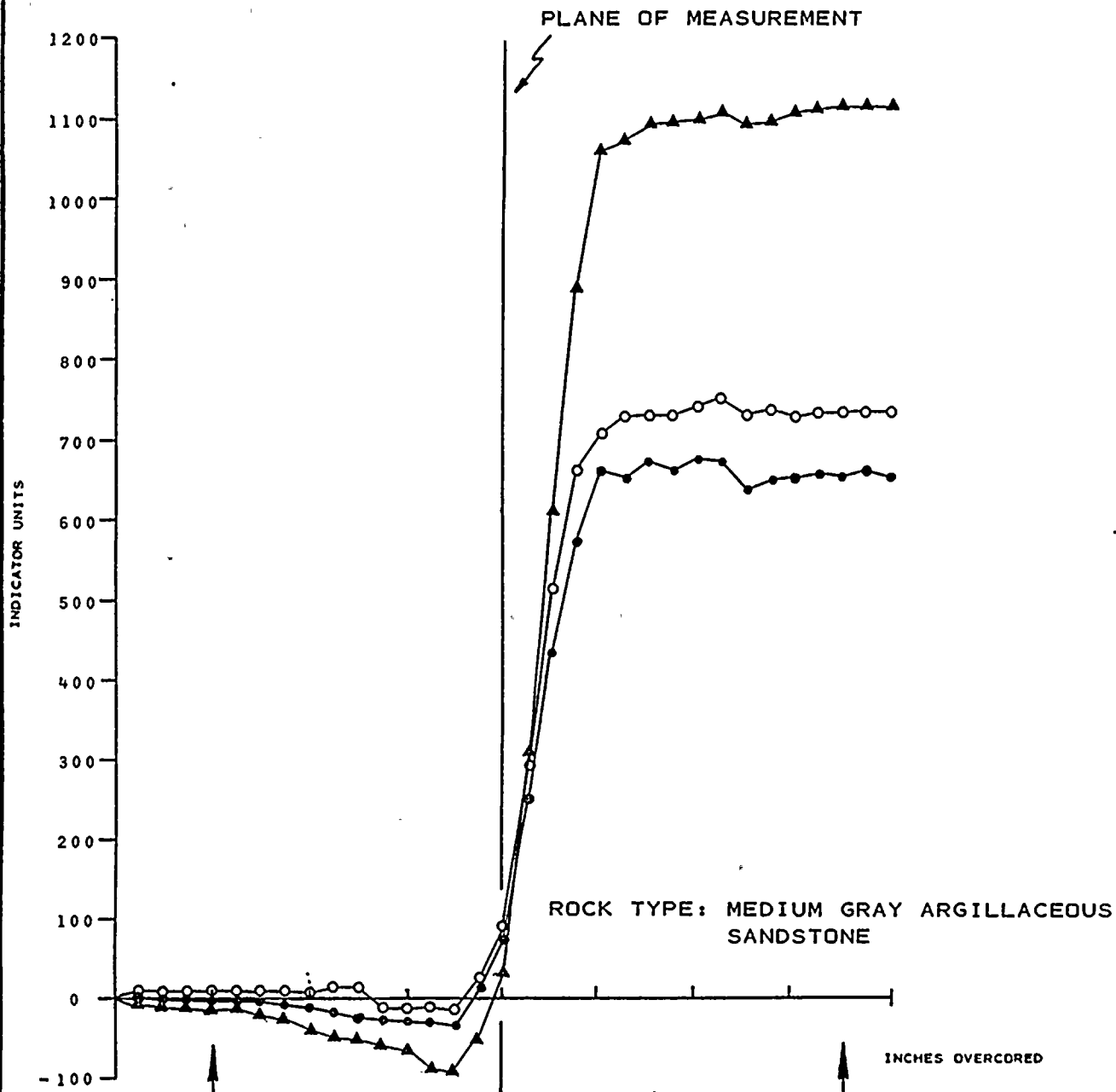
TEST NO. 38

DEPTH 82'1"

NOTE: A POSITIVE INCREASE IN INDICATOR UNITS INDICATES EXPANSION OF THE EX HOLE DURING OVERCORING

ARROWS (f) INDICATE TOTAL DEFORMATION USED TO CALCULATE STRESS

PLATE E-60
DAMES & MOORE



KEY:

- ▲ AXIS I
- AXIS II
- AXIS III

$$\Delta R_1 = 1112 - (-10) = 1122$$

$$\Delta R_2 = 736 - 2 = 734$$

$$\Delta R_3 = 654 - (-4) = 658$$

$$K_1 = 0.91 \mu\text{IN.}$$

$$U_1 = 0.91 \times 1122 = 1021$$

$$K_2 = 0.90 \mu\text{IN.}$$

$$U_2 = 0.90 \times 734 = 661$$

$$K_3 = 0.89 \mu\text{IN.}$$

$$U_3 = 0.89 \times 658 = 586$$

STRAIN RELIEF MEASUREMENTS

BORING RS = 2

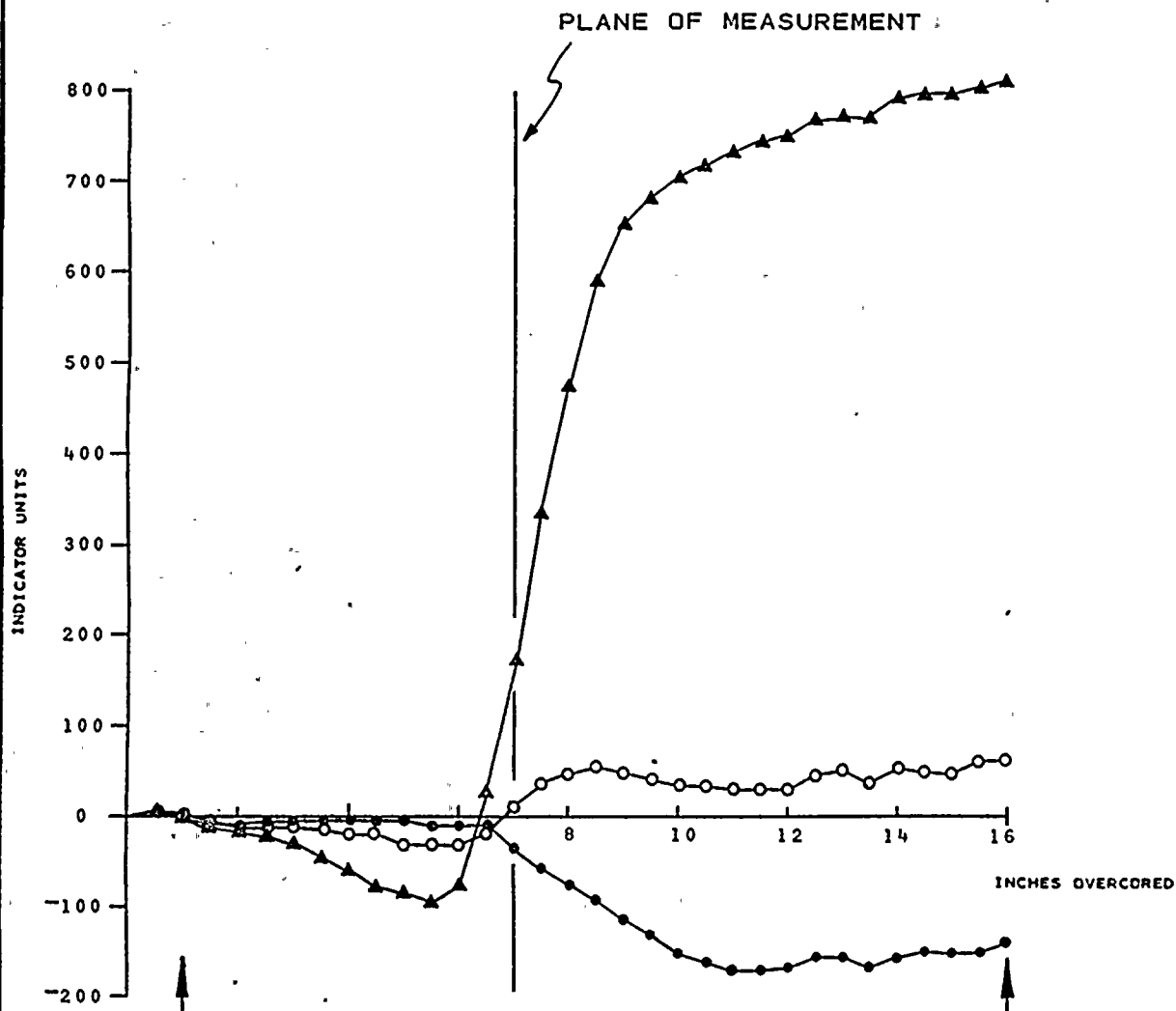
TEST NO. 40

DEPTH 84'7 1/2"

NOTE: A POSITIVE INCREASE IN INDICATOR UNITS INDICATES EXPANSION OF THE EX HOLE DURING OVERCORING

ARROWS (4) INDICATE TOTAL DEFORMATION USED TO CALCULATE STRESS





KEY:

- ▲ AXIS I
- AXIS II
- AXIS III

$$\Delta R_1 = 810 - (-2) = 812$$

$$\Delta R_2 = 66 - 0 = 66$$

$$\Delta R_3 = -140 - 0 = -140$$

$$K_1 = 0.91 \mu\text{IN.}$$

$$U_1 = 0.91 \times 812 = 739$$

$$K_2 = 0.90 \mu\text{IN.}$$

$$U_2 = 0.90 \times 66 = 59$$

$$K_3 = 0.89 \mu\text{IN.}$$

$$U_3 = 0.89 \times -140 = -125$$

ROCK TYPE: LIGHT GRAY SILICEOUS SANDSTONE

STRAIN RELIEF MEASUREMENTS

BORING RS - 2

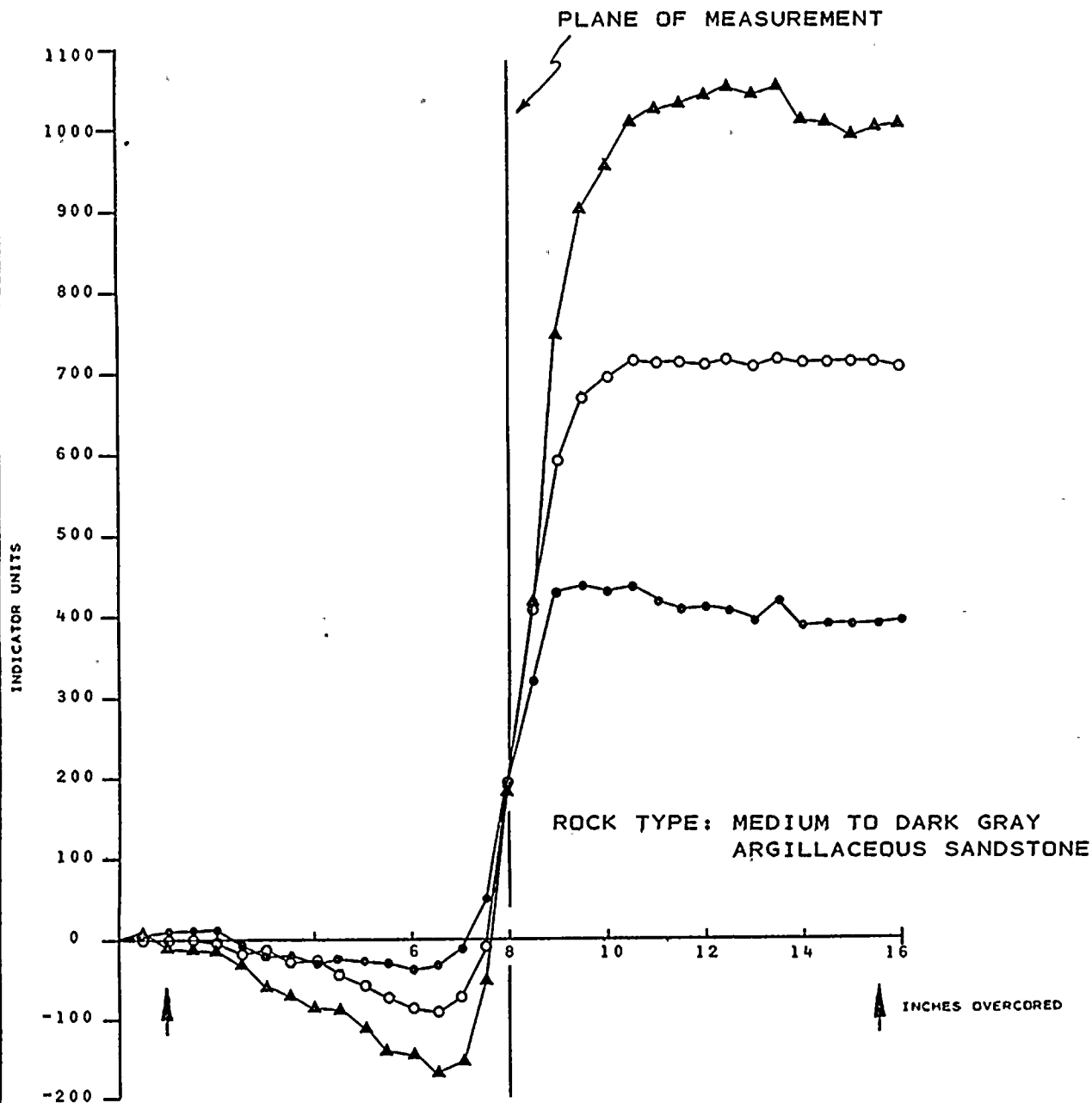
TEST NO. 42

DEPTH 87'5"

NOTE: A POSITIVE INCREASE IN INDICATOR UNITS
INDICATES EXPANSION OF THE EX HOLE
DURING OVERCORING

ARROWS (↑) INDICATE TOTAL DEFORMATION
USED TO CALCULATE STRESS





KEY:

- ▲ AXIS I
- AXIS II
- AXIS III

$$\Delta R_1 = 1000 - (-4) = 1004$$

$$\Delta R_2 = 710 - 0 = 710$$

$$\Delta R_3 = 378 - (-4) = 374$$

$$K_1 = 0.91 \mu\text{IN.}$$

$$U_1 = 0.91 \times 1004 = 914$$

$$K_2 = 0.90 \mu\text{IN.}$$

$$U_2 = 0.90 \times 710 = 639$$

$$K_3 = 0.89 \mu\text{IN.}$$

$$U_3 = 0.89 \times 374 = 333$$

STRAIN RELIEF MEASUREMENTS

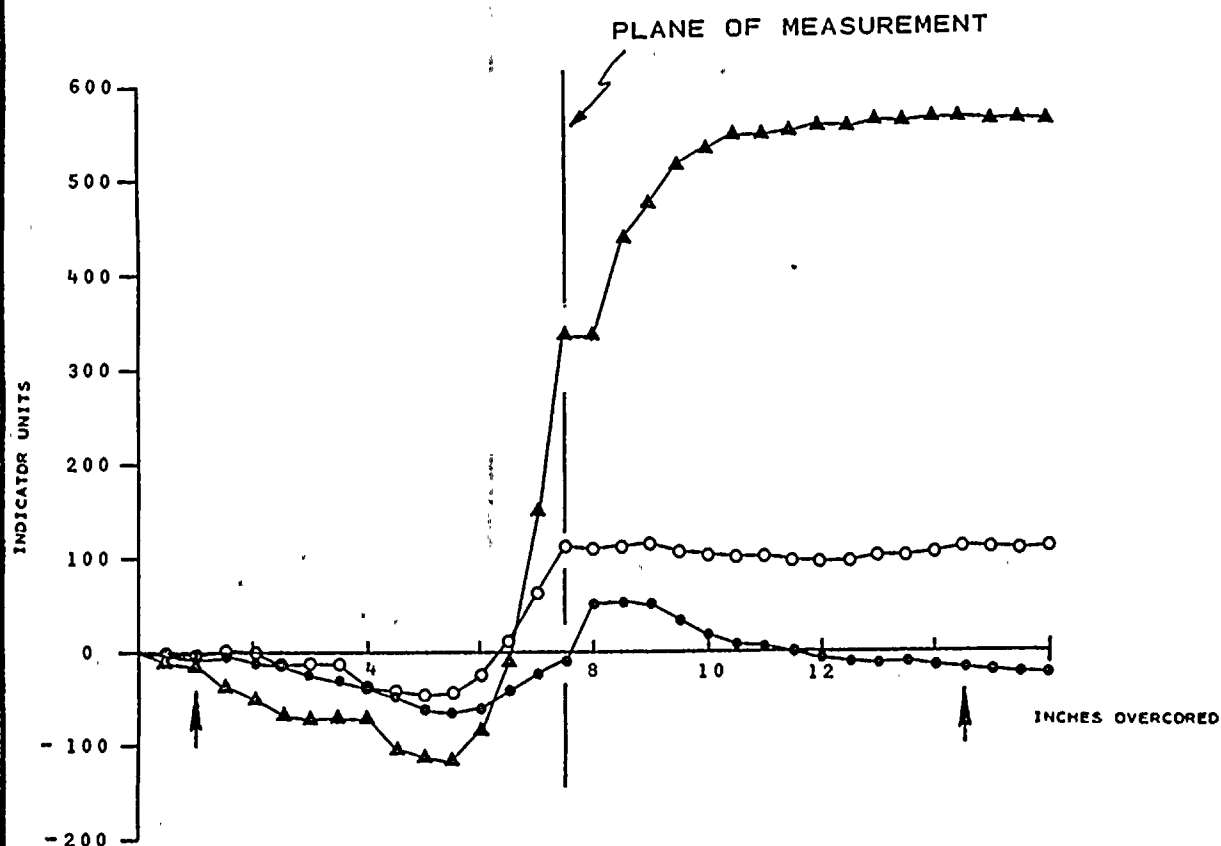
BORING RS - 2

TEST NO. 44

DEPTH 90'4"

NOTE: A POSITIVE INCREASE IN INDICATOR UNITS
INDICATES EXPANSION OF THE EX HOLE
DURING OVERCORING

ARROWS (↓) INDICATE TOTAL DEFORMATION
USED TO CALCULATE STRESS



KEY:

▲ AXIS I	$\Delta R_1 = 568 - (-17) = 585$
○ AXIS II	$\Delta R_2 = 108 - 0 = 108$
● AXIS III	$\Delta R_3 = -20 - (-2) = -18$

$K_1 = 0.91 \mu\text{IN.}$	$U_1 = 0.91 \times 585 = 532$
$K_2 = 0.90 \mu\text{IN.}$	$U_2 = 0.90 \times 108 = 97$
$K_3 = 0.89 \mu\text{IN.}$	$U_3 = 0.89 \times -18 = -16$

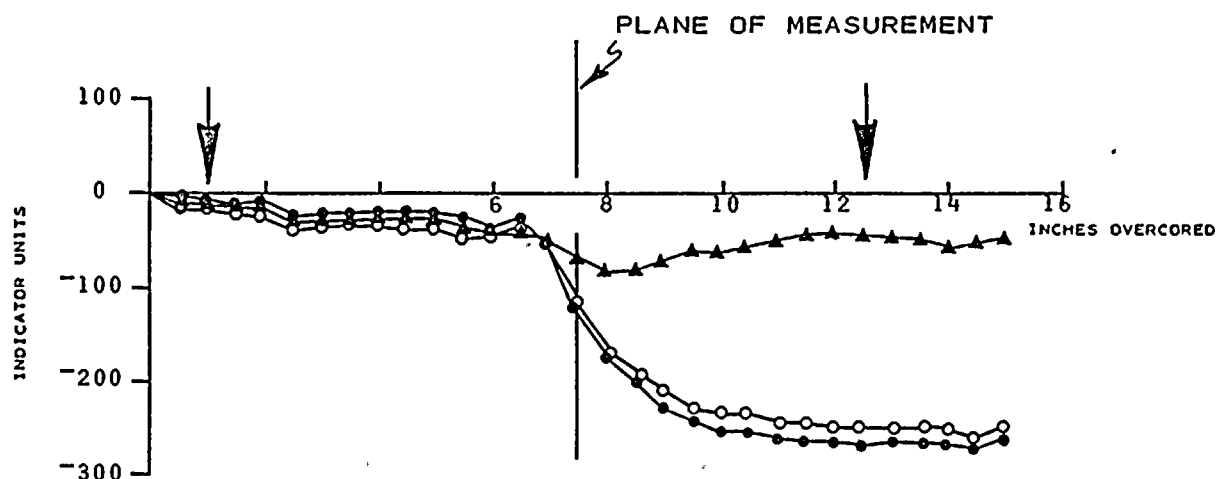
ROCK TYPE: DARK GRAY ARGILLACEOUS SANDSTONE TO
LIGHT GRAY SILICEOUS SANDSTONE

STRAIN RELIEF MEASUREMENTS
BORING RS - 2
TEST NO. 45
DEPTH 91'8"

NOTE: A POSITIVE INCREASE IN INDICATOR UNITS
INDICATES EXPANSION OF THE EX HOLE
DURING OVERCORING

ARROWS (↑) INDICATE TOTAL DEFORMATION
USED TO CALCULATE STRESS





KEY:

▲ AXIS I	$R_1 = -54 - (-15) = -39$
○ AXIS II	$R_2 = -251 - (-19) = -232$
● AXIS III	$R_3 = -266 - (-10) = -256$

$K_1 = 0.98 \mu\text{IN.}$	$U_1 = 0.98 \times -39 = -38$
$K_2 = 1.01 \mu\text{IN.}$	$U_2 = 1.01 \times -232 = -234$
$K_3 = 0.99 \mu\text{IN.}$	$U_3 = 0.99 \times -256 = -253$

ROCK TYPE: MEDIUM GRAY ARGILLACEOUS
SANDSTONE

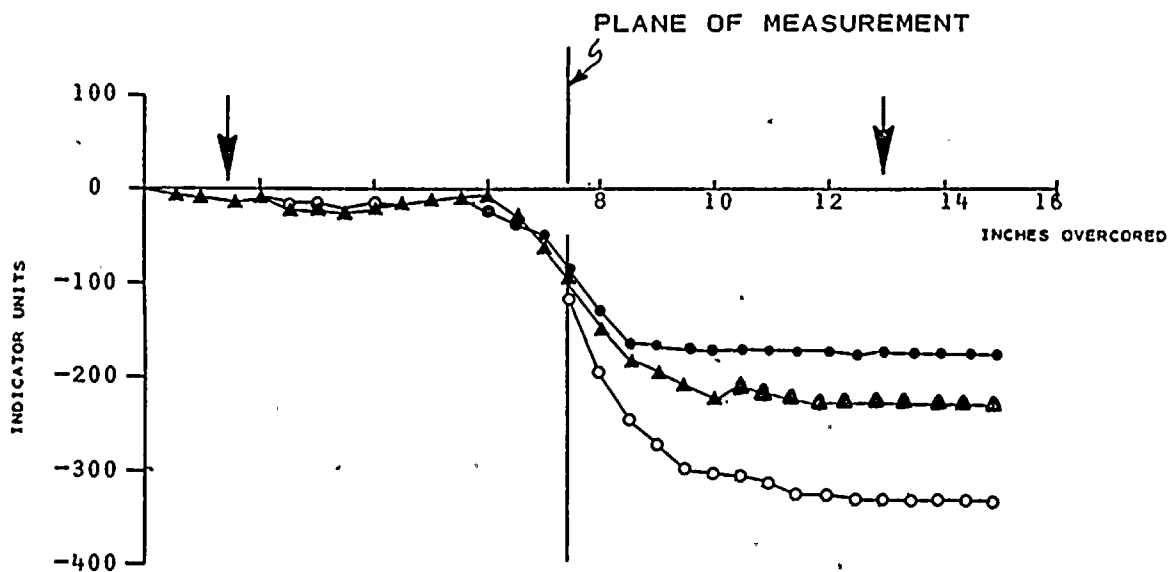
STRAIN RELIEF MEASUREMENTS
BORING RS - 3
TEST NO. 1
DEPTH 6'8"

NOTE: A POSITIVE INCREASE IN INDICATOR UNITS
INDICATES EXPANSION OF THE EX HOLE
DURING OVERCORING

ARROWS (↗) INDICATE TOTAL DEFORMATION
USED TO CALCULATE STRESS

PLATE E-65
DAMES & MOORE





KEY:

▲ AXIS I	$\Delta R_1 = -229 - (-15) = -214$
○ AXIS II	$\Delta R_2 = -330 - (-13) = -317$
● AXIS III	$\Delta R_3 = -176 - (-14) = -162$

$K_1 = 0.98 \mu\text{IN.}$	$U_1 = 0.98 \times -214 = -210$
$K_2 = 1.01 \mu\text{IN.}$	$U_2 = 1.01 \times -317 = -320$
$K_3 = 0.99 \mu\text{IN.}$	$U_3 = 0.99 \times -162 = -160$

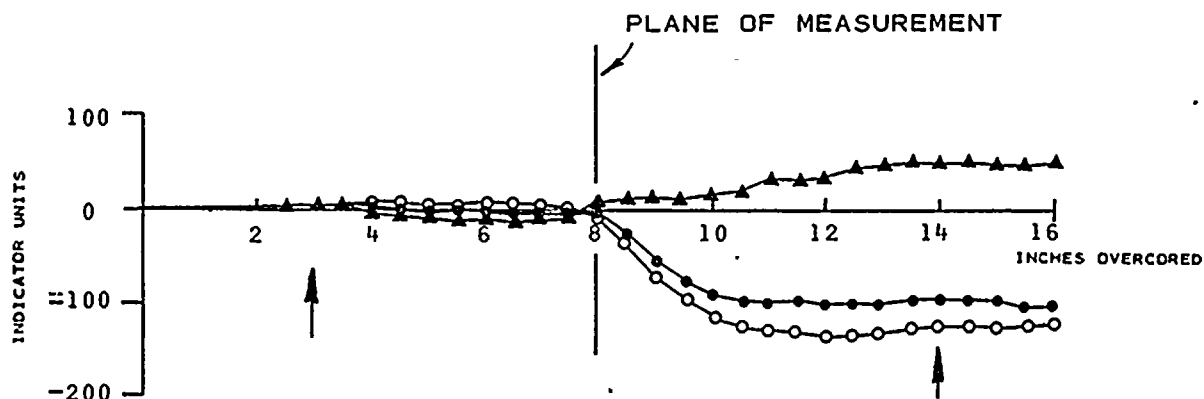
ROCK TYPE: LIGHT TO MEDIUM GRAY SILICEOUS SANDSTONE
GRADING TO MEDIUM GRAY ARGILLACEOUS SANDSTONE

STRAIN RELIEF MEASUREMENTS
BORING RS - 3
TEST NO. 2
DEPTH 7'11"

NOTE: A POSITIVE INCREASE IN INDICATOR UNITS
INDICATES EXPANSION OF THE EX HOLE
DURING OVERCORING

ARROWS (↓) INDICATE TOTAL DEFORMATION
USED TO CALCULATE STRESS





KEY:

- ▲ AXIS I
- AXIS II
- AXIS III

$$\begin{aligned}\Delta R_1 &= 49 - 3 = 46 \\ \Delta R_2 &= -124 - 6 = -130 \\ \Delta R_3 &= -94 - 4 = -98\end{aligned}$$

$$\begin{aligned}K_1 &= 0.99 \text{ MIN.} & U_1 &= 0.99 \times 46 = 46 \\ K_2 &= 1.01 \text{ MIN.} & U_2 &= 1.01 \times (-130) = -131 \\ K_3 &= 1.00 \text{ MIN.} & U_3 &= 1.00 \times (-98) = -98\end{aligned}$$

ROCK TYPE: LIGHT GRAY SILICEOUS SANDSTONE

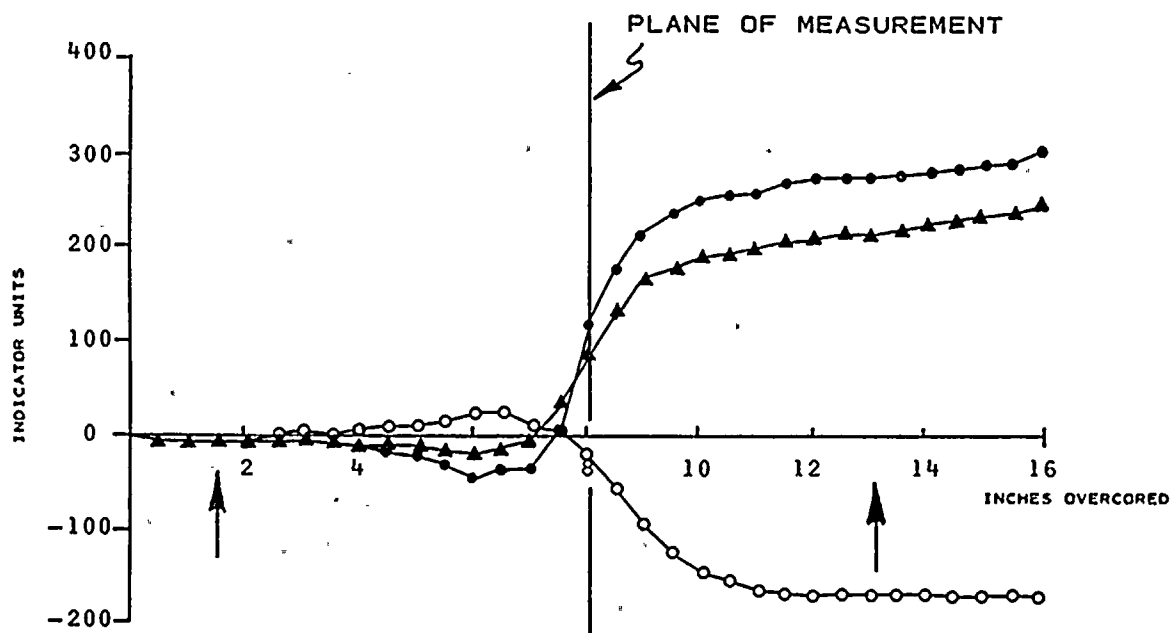
STRAIN RELIEF MEASUREMENTS
BORING RS - 3
TEST NO. 4
DEPTH 13'2"

NOTE: A POSITIVE INCREASE IN INDICATOR UNITS
INDICATES EXPANSION OF THE EX HOLE
DURING OVERCORING

ARROWS (↑) INDICATE TOTAL DEFORMATION
USED TO CALCULATE STRESS

PLATE E-67
DAMES & MOORE





KEY:

- ▲ AXIS I
- AXIS II
- AXIS III

$$\begin{aligned}\Delta R_1 &= 213 - (-8) = 221 \\ \Delta R_2 &= -173 - (-9) = -164 \\ \Delta R_3 &= 274 - (-8) = 282\end{aligned}$$

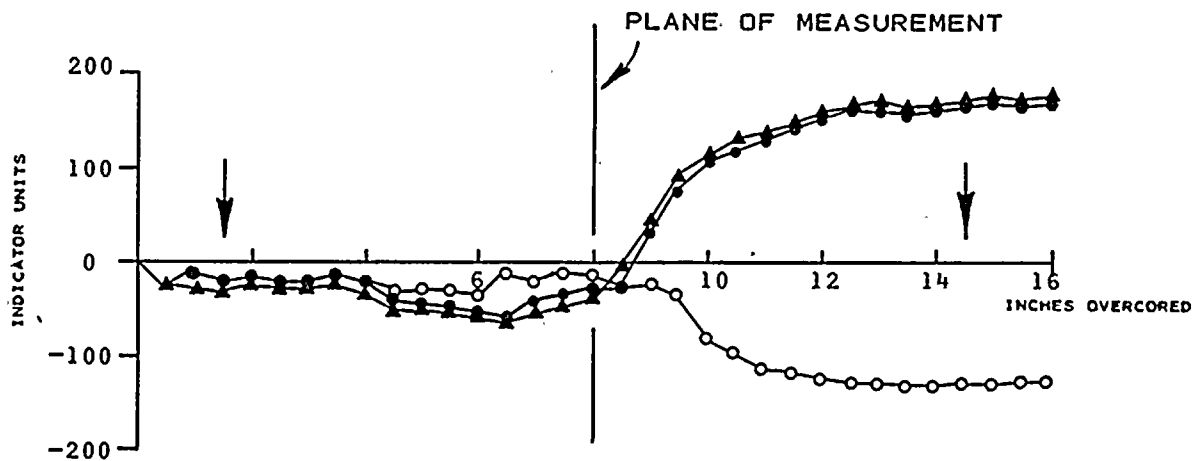
$$\begin{aligned}K_1 &= 0.99 \mu\text{IN.} & U_1 &= 0.99 \times 221 = 219 \\ K_2 &= 1.01 \mu\text{IN.} & U_2 &= 1.01 \times (-164) = -166 \\ K_3 &= 1.00 \mu\text{IN.} & U_3 &= 1.00 \times 282 = 282\end{aligned}$$

ROCK TYPE: LIGHT SILICEOUS SANDSTONE

STRAIN RELIEF MEASUREMENTS
BORING RS - 3
TEST NO. 5
DEPTH 16'2"

NOTE: A POSITIVE INCREASE IN INDICATOR UNITS
INDICATES EXPANSION OF THE EX HOLE
DURING OVERCORING

ARROWS (↓) INDICATE TOTAL DEFORMATION
USED TO CALCULATE STRESS



KEY:

- ▲ AXIS I
- AXIS II
- AXIS III

$$\begin{aligned}\Delta R_1 &= 170 - (-30) = 200 \\ \Delta R_2 &= -134 - (-19) = -115 \\ \Delta R_3 &= 162 - (-20) = 182\end{aligned}$$

$$\begin{aligned}K_1 &= 0.99 \mu\text{IN.} & U_1 &= 0.99 \times 200 = 198 \\ K_2 &= 1.01 \mu\text{IN.} & U_2 &= 1.01 \times (-115) = -116 \\ K_3 &= 1.00 \mu\text{IN.} & U_3 &= 1.00 \times 182 = 182\end{aligned}$$

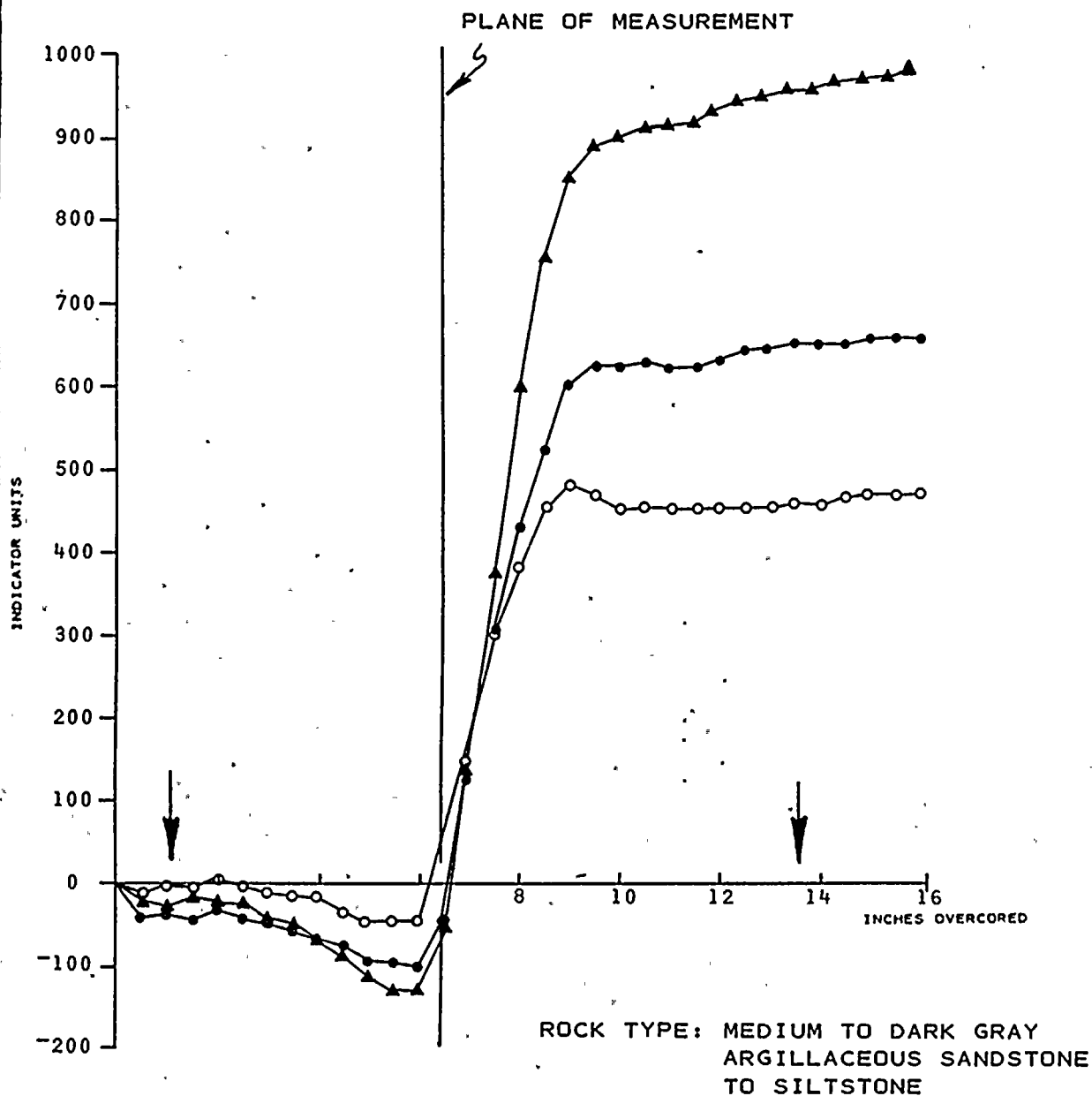
ROCK TYPE: LIGHT GRAY SILICEOUS SANDSTONE WITH OCCASIONAL
MEDIUM GRAY ARGILLACEOUS SANDSTONE INTERBEDS

STRAIN RELIEF MEASUREMENTS
BORING RS - 3
TEST NO. 7
DEPTH 18' 4 1/2"

NOTE: A POSITIVE INCREASE IN INDICATOR UNITS
INDICATES EXPANSION OF THE EX HOLE
DURING OVERCORING

ARROWS (↓) INDICATE TOTAL DEFORMATION
USED TO CALCULATE STRESS

PLATE E-69
DAMES & MOORE



KEY:

- ▲ AXIS I
- AXIS II
- AXIS III

$$\begin{aligned}\Delta R_1 &= 958 - (-28) = 986 \\ \Delta R_2 &= 459 - (-6) = 465 \\ \Delta R_3 &= 651 - (-37) = 688\end{aligned}$$

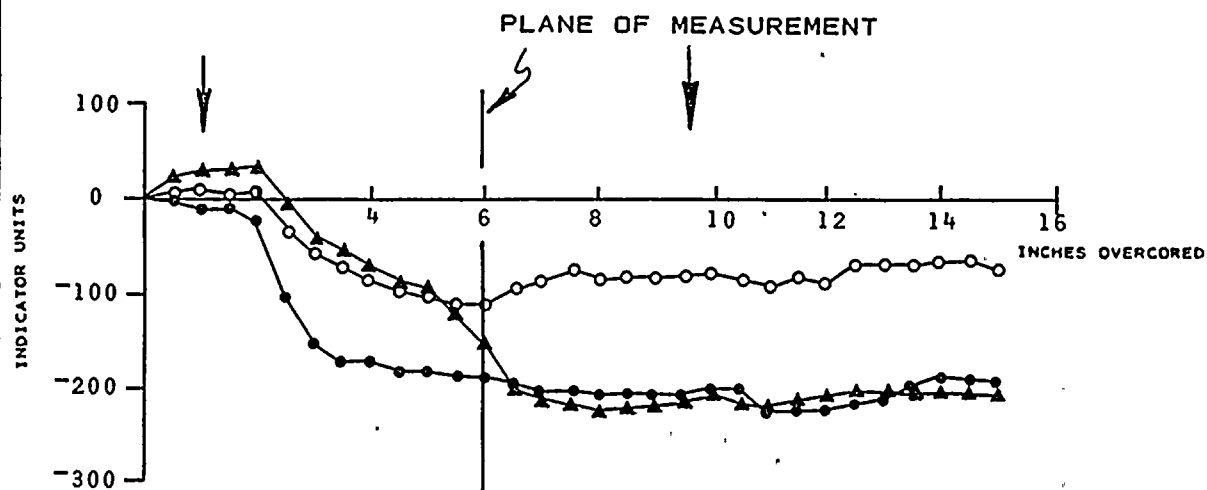
$$\begin{aligned}K_1 &= 0.97 \mu\text{IN.} \\ K_2 &= 1.01 \mu\text{IN.} \\ K_3 &= 1.00 \mu\text{IN.}\end{aligned}$$

$$\begin{aligned}U_1 &= 0.97 \times 986 = 939 \\ U_2 &= 1.01 \times 465 = 470 \\ U_3 &= 1.00 \times 688 = 688\end{aligned}$$

STRAIN RELIEF MEASUREMENTS
BORING RS - 3
TEST NO. 10
DEPTH 25' 8 1/2"

NOTE: A POSITIVE INCREASE IN INDICATOR UNITS
INDICATES EXPANSION OF THE EX HOLE
DURING OVERCORING

ARROWS (↑) INDICATE TOTAL DEFORMATION
USED TO CALCULATE STRESS



KEY:

- ▲ AXIS I
- AXIS II
- AXIS III

$$\begin{aligned}\Delta R_1 &= -218 - 28 = -246 \\ \Delta R_2 &= -81 - 10 = -91 \\ \Delta R_3 &= -209 - (-9) = -200\end{aligned}$$

$$\begin{aligned}K_1 &= 0.97 \text{ } \mu\text{IN.} & U_1 &= 0.97 \times -246 = -239 \\ K_2 &= 1.01 \text{ } \mu\text{IN.} & U_2 &= 1.01 \times -91 = -92 \\ K_3 &= 1.00 \text{ } \mu\text{IN.} & U_3 &= 1.00 \times -200 = -200\end{aligned}$$

ROCK TYPE: MEDIUM GRAY SANDSTONE WITH INTERBEDS OF
ARGILLACEOUS SANDSTONE AND SHALEY SILTSTONE

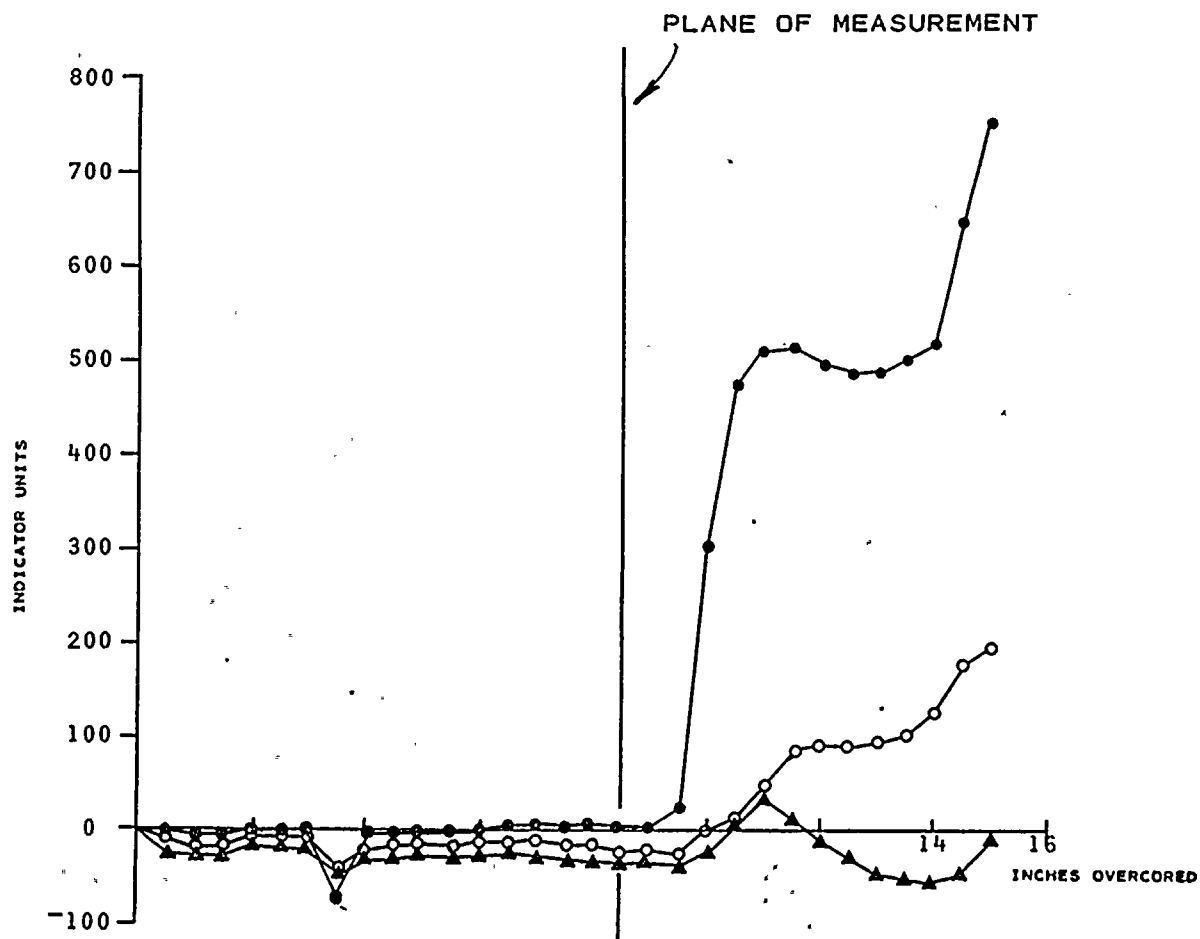
STRAIN RELIEF MEASUREMENTS
BORING RS - 3
TEST NO. 11
DEPTH 27'9"

NOTE: A POSITIVE INCREASE IN INDICATOR UNITS
INDICATES EXPANSION OF THE EX HOLE
DURING OVERCORING

ARROWS (↓) INDICATE TOTAL DEFORMATION
USED TO CALCULATE STRESS

PLATE E-71
DAMES & MOORE





KEY:

- ▲ AXIS I
- AXIS II
- AXIS III

ROCK TYPE: LIGHT GRAY SILICEOUS SANDSTONE,
OCCASIONAL SHALE CLASTS AND SHALE
INTERLAMINAE

STRAIN RELIEF MEASUREMENTS

BORING RS - 3

TEST NO. 13

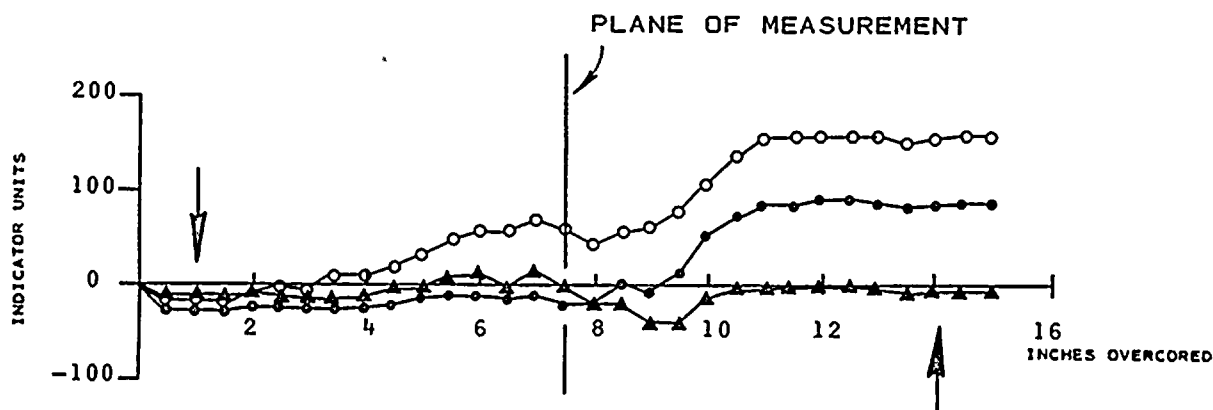
DEPTH 31'8 1/2"

NOTE: A POSITIVE INCREASE IN INDICATOR UNITS
INDICATES EXPANSION OF THE EX HOLE
DURING OVERCORING

TEST RESULTS NOT INCLUDED IN THE OVERALL
INTERPRETATION DUE TO THE IRREGULARITY
OF THE RESULTS

PLATE E-72
DAMES & MOORE





KEY:

▲ AXIS I	$\Delta R_1 = -12 - (-11) = -1$
○ AXIS II	$\Delta R_2 = 154 - (-19) = 173$
● AXIS III	$\Delta R_3 = 83 - (-29) = 112$

$K_1 = 0.97 \mu\text{IN.}$	$U_1 = 0.97 \times -1 = -1$
$K_2 = 1.01 \mu\text{IN.}$	$U_2 = 1.01 \times 173 = 175$
$K_3 = 1.00 \mu\text{IN.}$	$U_3 = 1.00 \times 112 = 112$

ROCK TYPE: LIGHT GRAY SILICEOUS SANDSTONE
TO MEDIUM GRAY ARGILLACEOUS SANDSTONE

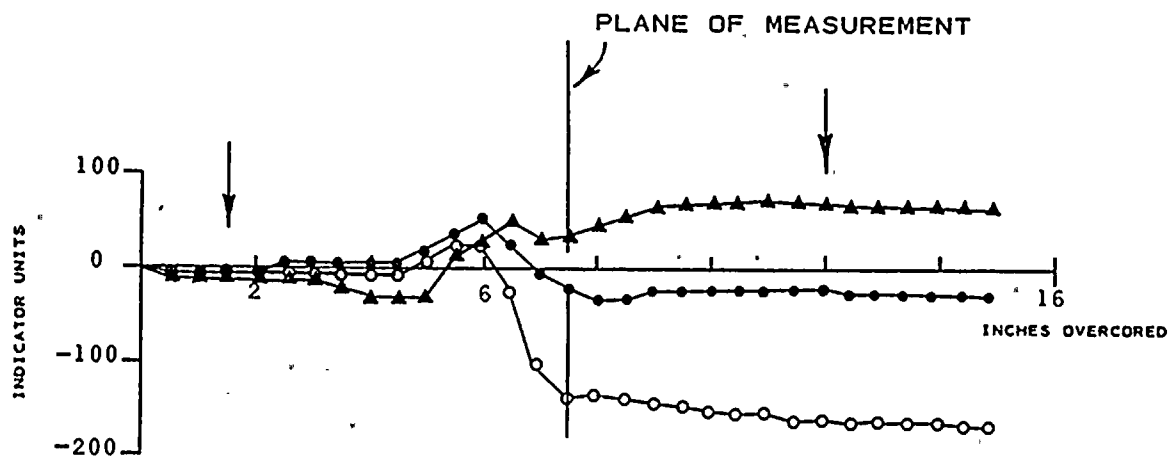
STRAIN RELIEF MEASUREMENTS
BORING RS - 3
TEST NO. 14
DEPTH 32'10 1/2"

NOTE: A POSITIVE INCREASE IN INDICATOR UNITS
INDICATES EXPANSION OF THE EX HOLE
DURING OVERCORING

ARROWS (↓) INDICATE TOTAL DEFORMATION
USED TO CALCULATE STRESS

PLATE E-73
DAMES & MOORE





KEY:

▲ AXIS I	$\Delta R_1 = 68 - (-15) = 83$
○ AXIS II	$\Delta R_2 = -161 - (-7) = -154$
● AXIS III	$\Delta R_3 = -23 - (-8) = -15$

$K_1 = 0.98 \mu\text{IN.}$	$U_1 = 0.98 \times 83 = 81$
$K_2 = 1.00 \mu\text{IN.}$	$U_2 = 1.00 \times -154 = -154$
$K_3 = 0.98 \mu\text{IN.}$	$U_3 = 0.98 \times -15 = -15$

ROCK TYPE: LIGHT TO MEDIUM GRAY SANDSTONE TO
MEDIUM GRAY ARGILLACEOUS SANDSTONE,
OCCASIONAL FOSSIL HASH.

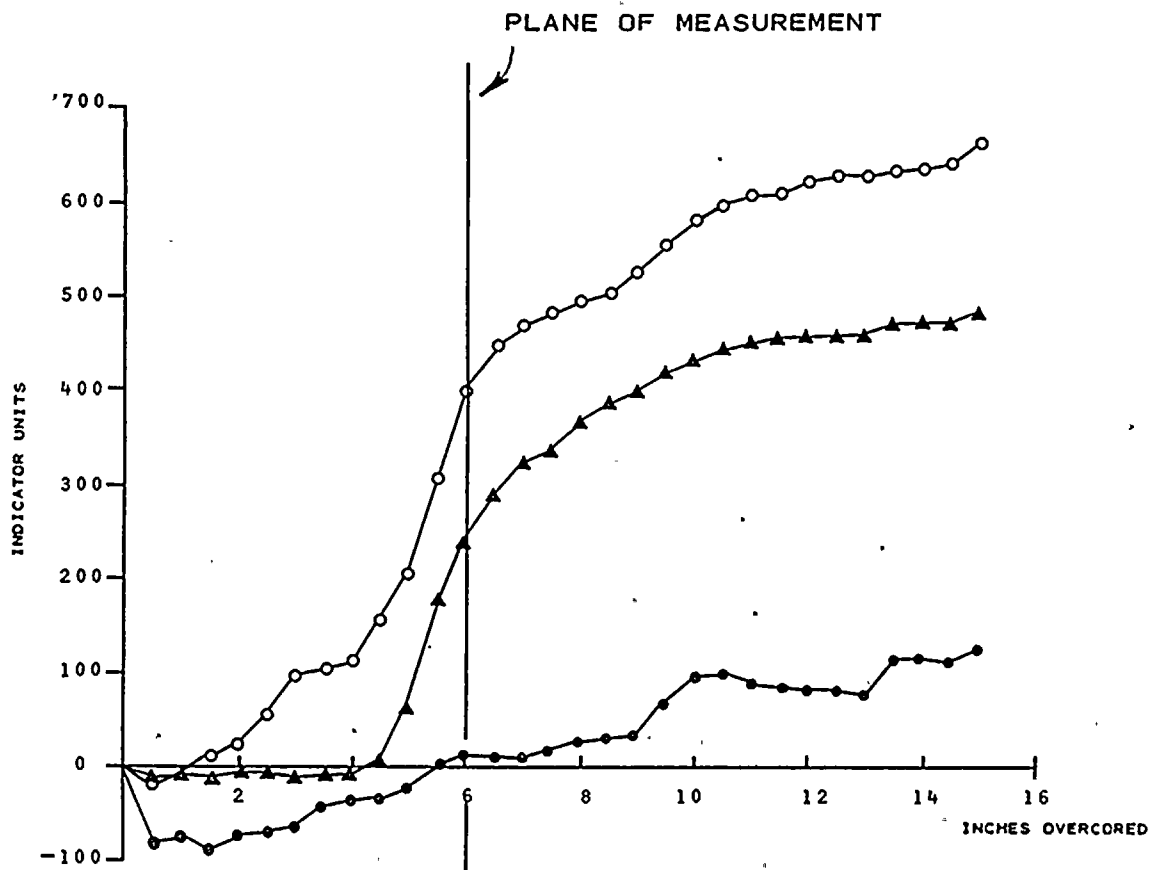
STRAIN RELIEF MEASUREMENTS
BORING RS - 3
TEST NO. 16
DEPTH 35'11 1/2"

NOTE: A POSITIVE INCREASE IN INDICATOR UNITS
INDICATES EXPANSION OF THE EX HOLE
DURING OVERCORING

ARROWS (↑) INDICATE TOTAL DEFORMATION
USED TO CALCULATE STRESS

PLATE E-74
DAWES & MOORE





KEY:

- ▲ AXIS I
- AXIS II
- AXIS III

ROCK TYPE: MEDIUM TO DARK GRAY ARGILLACEOUS SANDSTONE

STRAIN RELIEF MEASUREMENTS

BORING RS - 3

TEST NO. 17

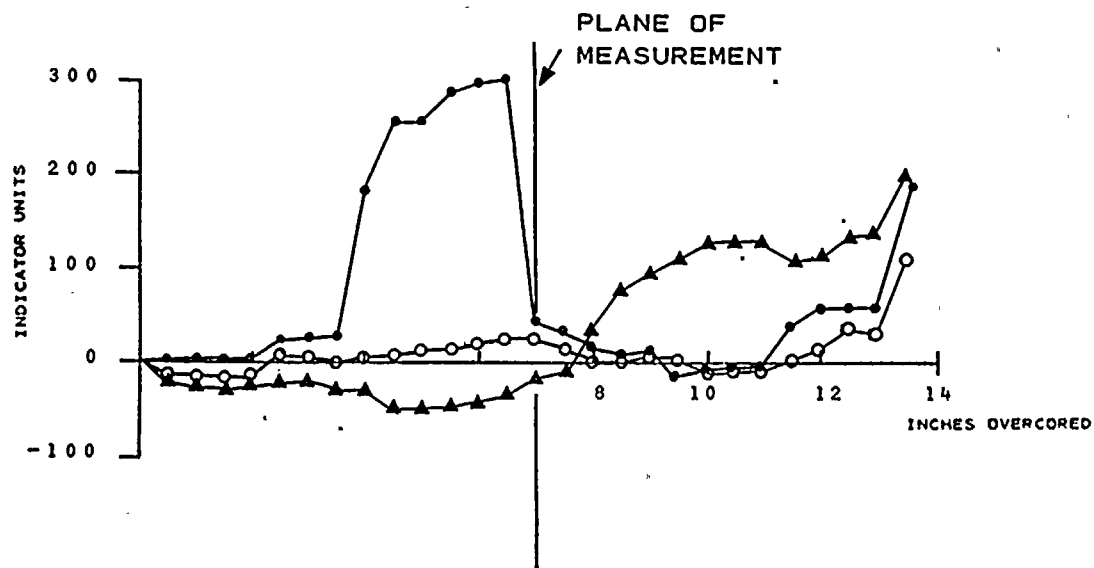
DEPTH 37' 1 1/2"

NOTE: A POSITIVE INCREASE IN INDICATOR UNITS INDICATES EXPANSION OF THE EX HOLE DURING OVERCORING

TEST RESULTS NOT INCLUDED IN THE OVERALL INTERPRETATION DUE TO THE IRREGULARITY OF THE RESULTS

PLATE E-75
DAMES & MOORE





KEY:

- ▲ AXIS I
- AXIS II
- AXIS III

ROCK TYPE: MEDIUM GRAY ARGILLACEOUS
SANDSTONE TO GRAYWACKE

STRAIN RELIEF MEASUREMENTS

BORING RS - 3

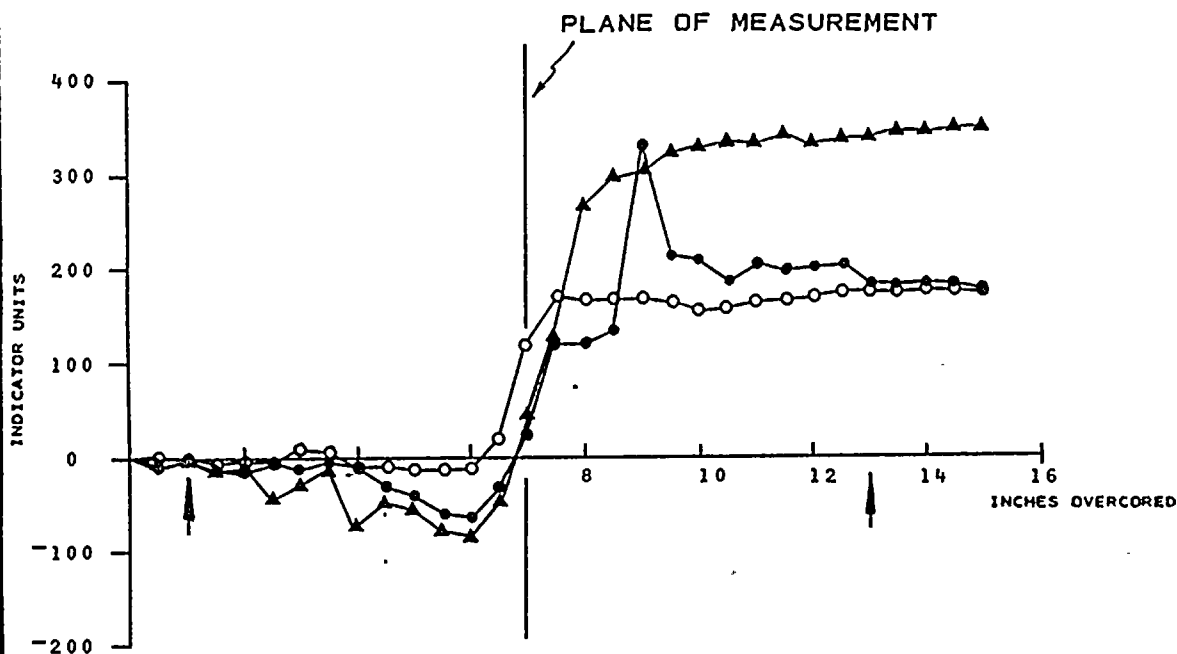
TEST NO. 18

DEPTH 38'5"

NOTE: A POSITIVE INCREASE IN INDICATOR UNITS
INDICATES EXPANSION OF THE EX HOLE
DURING OVERCORING
TEST RESULTS NOT INCLUDED IN THE OVERALL
INTERPRETATION DUE TO THE IRREGULARITY
OF THE RESULTS

PLATE E-76
DAMES & MOORE





KEY:

▲ AXIS I $\Delta R_1 = 340 - (-2) = 342$
 ○ AXIS II $\Delta R_2 = 172 - 0 = 172$
 ● AXIS III $\Delta R_3 = 181 - 0 = 181$

$K_1 = 0.98 \mu\text{IN.}$ $U_1 = 0.98 \times 342 = 335$
 $K_2 = 1.00 \mu\text{IN.}$ $U_2 = 1.00 \times 172 = 172$
 $K_3 = 0.98 \mu\text{IN.}$ $U_3 = 0.98 \times 181 = 177$

ROCK TYPE: MEDIUM TO DARK GRAY ARGILLACEOUS SANDSTONE

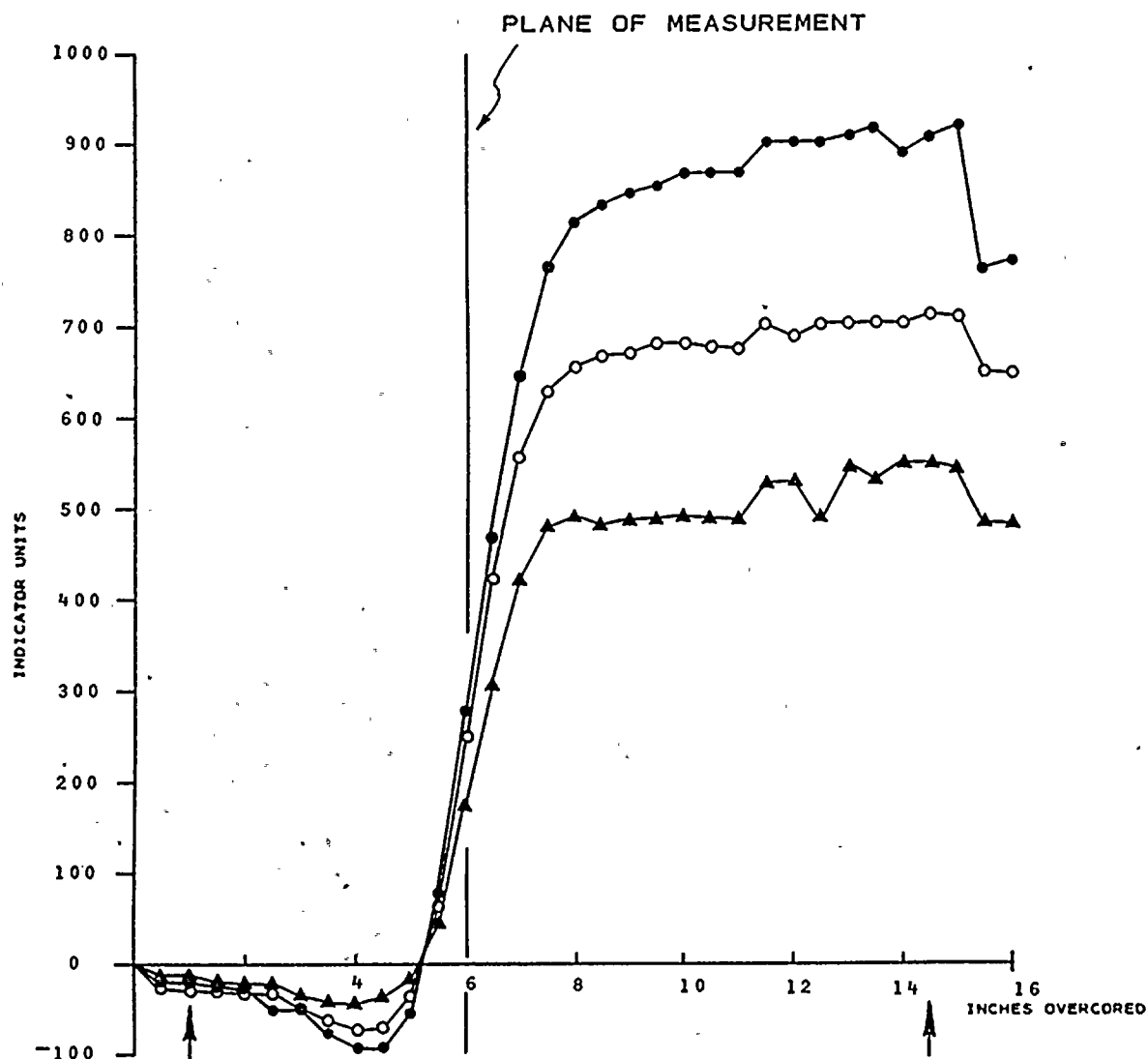
STRAIN RELIEF MEASUREMENTS
 BORING NO. RS - 3
 TEST NO. 19
 DEPTH 39'7"

NOTE: A POSITIVE INCREASE IN INDICATOR UNITS
 INDICATES EXPANSION OF THE EX HOLE
 DURING OVERCORING

ARROWS (↑) INDICATE TOTAL DEFORMATION
 USED TO CALCULATE STRESS

PLATE E-77
 DAMES & MOORE





KEY:

▲ AXIS I $\Delta R_1 = 556 - (-15) = 571$
 ○ AXIS II $\Delta R_2 = 715 - (-29) = 744$
 • AXIS III $\Delta R_3 = 908 - (-23) = 931$

$K_1 = 1.01 \mu\text{IN.}$ $U_1 = 1.01 \times 571 = 577$

$K_2 = 0.97 \mu\text{IN.}$ $U_2 = 0.97 \times 744 = 722$

$K_3 = 1.01 \mu\text{IN.}$ $U_3 = 1.01 \times 931 = 940$

ROCK TYPE: MEDIUM GRAY ARGILLACEOUS SANDSTONE

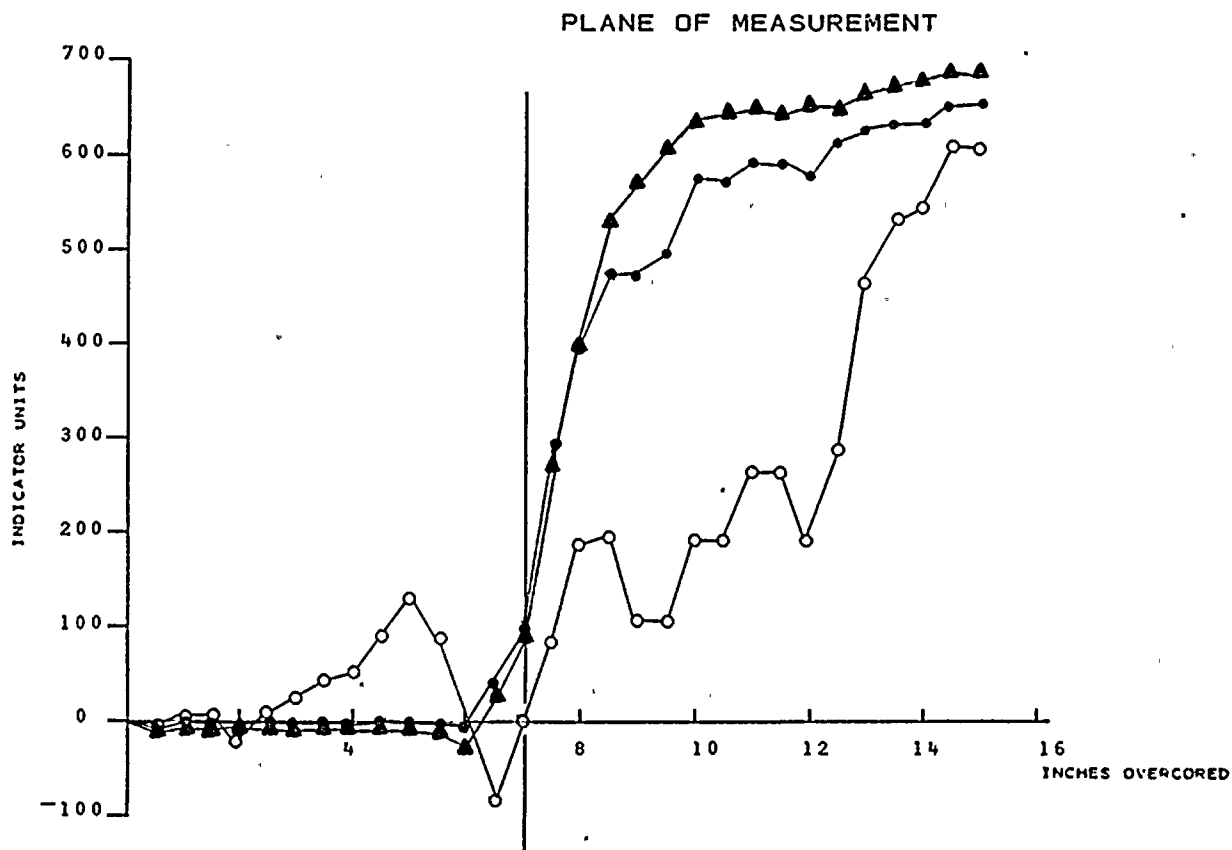
STRAIN RELIEF MEASUREMENTS
 BORING NO. RS - 3
 TEST NO. 24
 DEPTH 48'5"

NOTE: A POSITIVE INCREASE IN INDICATOR UNITS
INDICATES EXPANSION OF THE EX HOLE
DURING OVERCORING

ARROWS (↓) INDICATE TOTAL DEFORMATION
USED TO CALCULATE STRESS

PLATE E-78
 DAMES & MOORE





KEY:

AXIS I
AXIS II
AXIS III

STRAIN RELIEF MEASUREMENTS

BORING RS - 3

TEST NO. 27

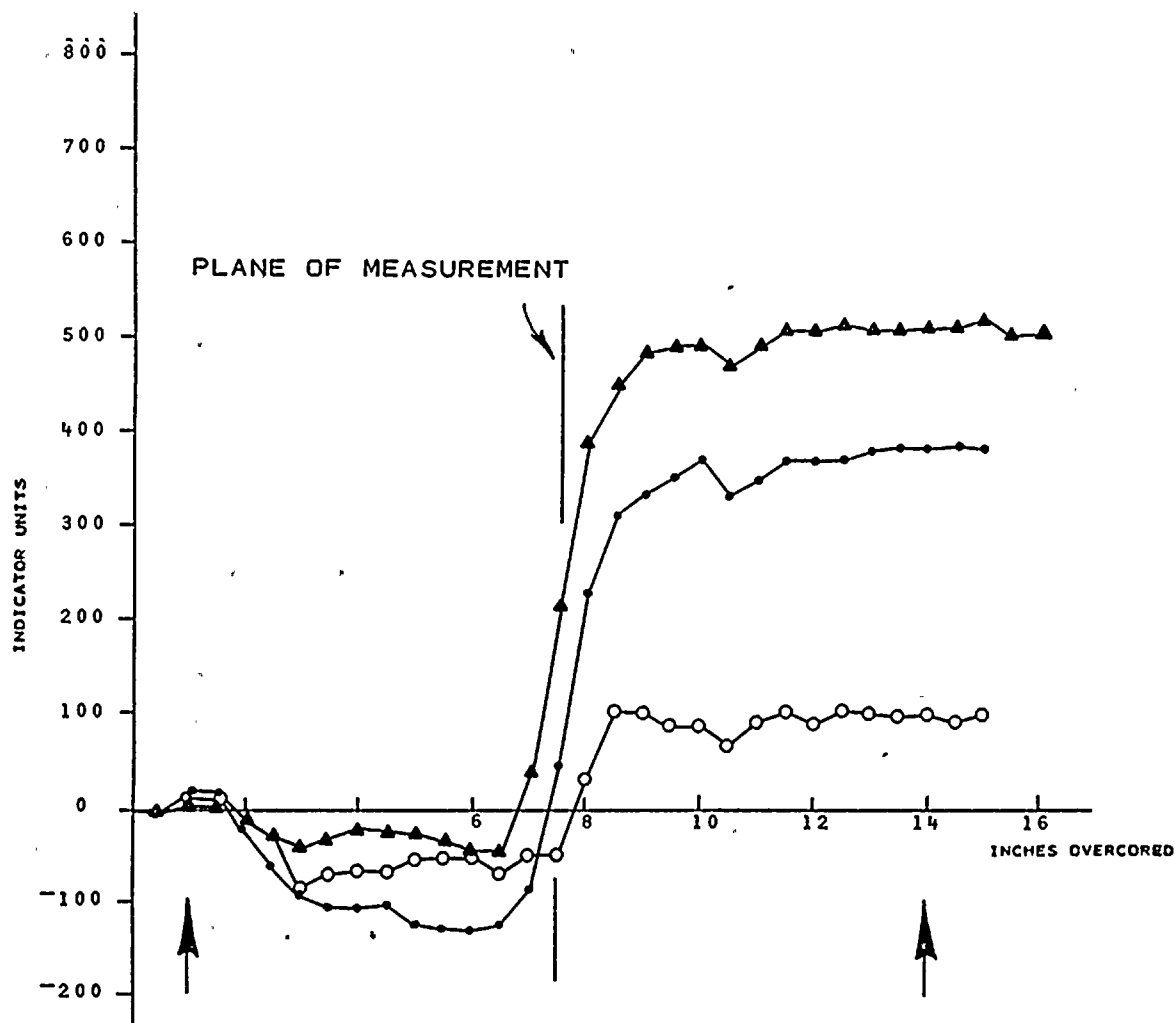
DEPTH 53' 1/2"

NOTE: A POSITIVE INCREASE IN INDICATOR UNITS
INDICATES EXPANSION OF THE EX HOLE
DURING OVERCORING

TEST RESULTS NOT INCLUDED IN THE OVERALL
INTERPRETATION DUE TO THE IRREGULARITY
OF THE RESULTS

PLATE E-79
DAMES & MOORE





KEY:

- ▲ AXIS I
- AXIS II
- AXIS III

$$\Delta R_1 = 517 - 0 = 517$$

$$\Delta R_2 = 102 - 7 = 95$$

$$\Delta R_3 = 381 - 16 = 365$$

$$K_1 = 1.01 \mu\text{IN.}$$

$$U_1 = 1.01 \times 517 = 522$$

$$K_2 = 0.97 \mu\text{IN.}$$

$$U_2 = 0.97 \times 95 = 92$$

$$K_3 = 1.01 \mu\text{IN.}$$

$$U_3 = 1.01 \times 365 = 369$$

ROCK TYPE: MEDIUM GRAY ARGILLACEOUS SANDSTONE
WITH OCCASIONAL SILICEOUS SANDSTONE AND
SHALE INTERBEDS

STRAIN RELIEF MEASUREMENTS

BORING RS - 3

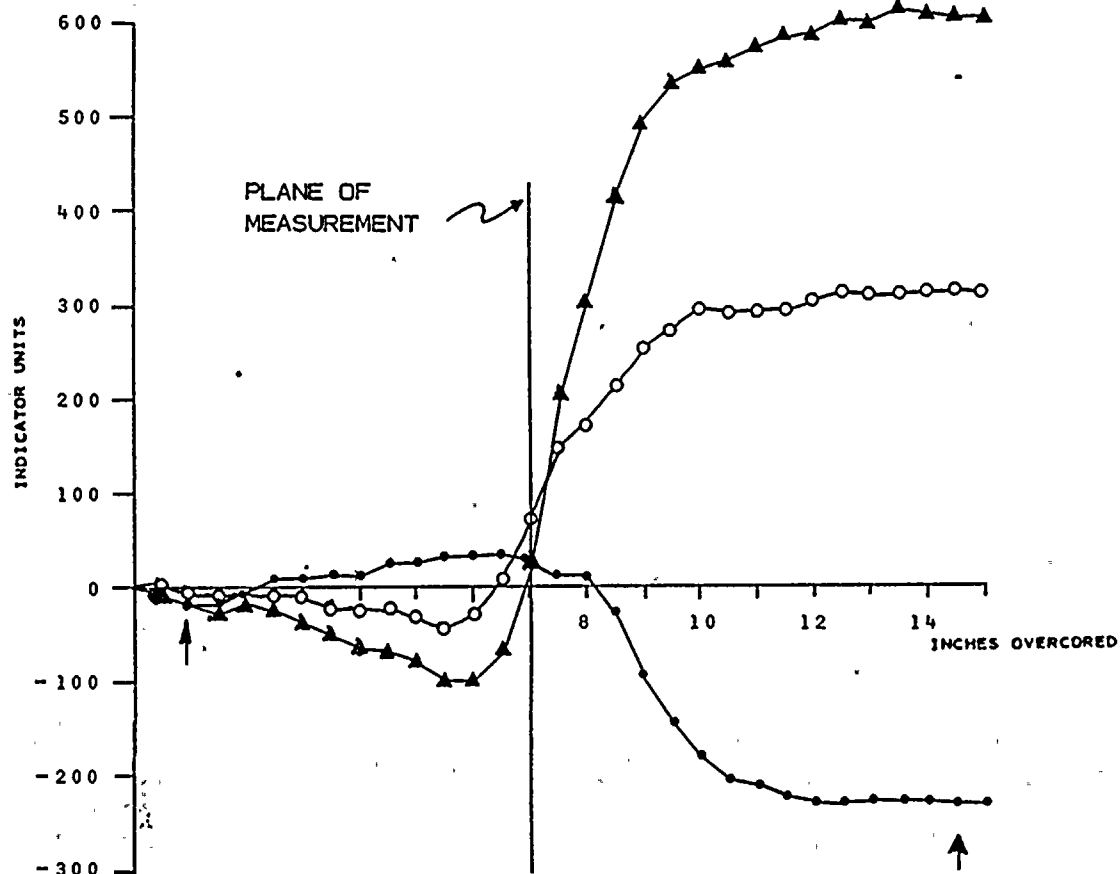
TEST NO. 28

DEPTH 54'4"

NOTE: A POSITIVE INCREASE IN INDICATOR UNITS
INDICATES EXPANSION OF THE EX HOLE
DURING OVERCORING

ARROWS (A) INDICATE TOTAL DEFORMATION
USED TO CALCULATE STRESS

PLATE E-80
DAMES & MOORE



KEY:

- ▲ AXIS I
- AXIS II
- AXIS III

$$\begin{aligned}\Delta R_1 &= 602 - (-18) = 620 \\ \Delta R_2 &= 317 - (-12) = 329 \\ \Delta R_3 &= -230 - (-19) = -211\end{aligned}$$

$$\begin{aligned}K_1 &= 1.06 \mu\text{IN.} \\ K_2 &= 1.09 \mu\text{IN.} \\ K_3 &= 1.08 \mu\text{IN.}\end{aligned}$$

$$\begin{aligned}U_1 &= 1.06 \times 620 = 657 \\ U_2 &= 1.09 \times 329 = 359 \\ U_3 &= 1.08 \times -211 = -228\end{aligned}$$

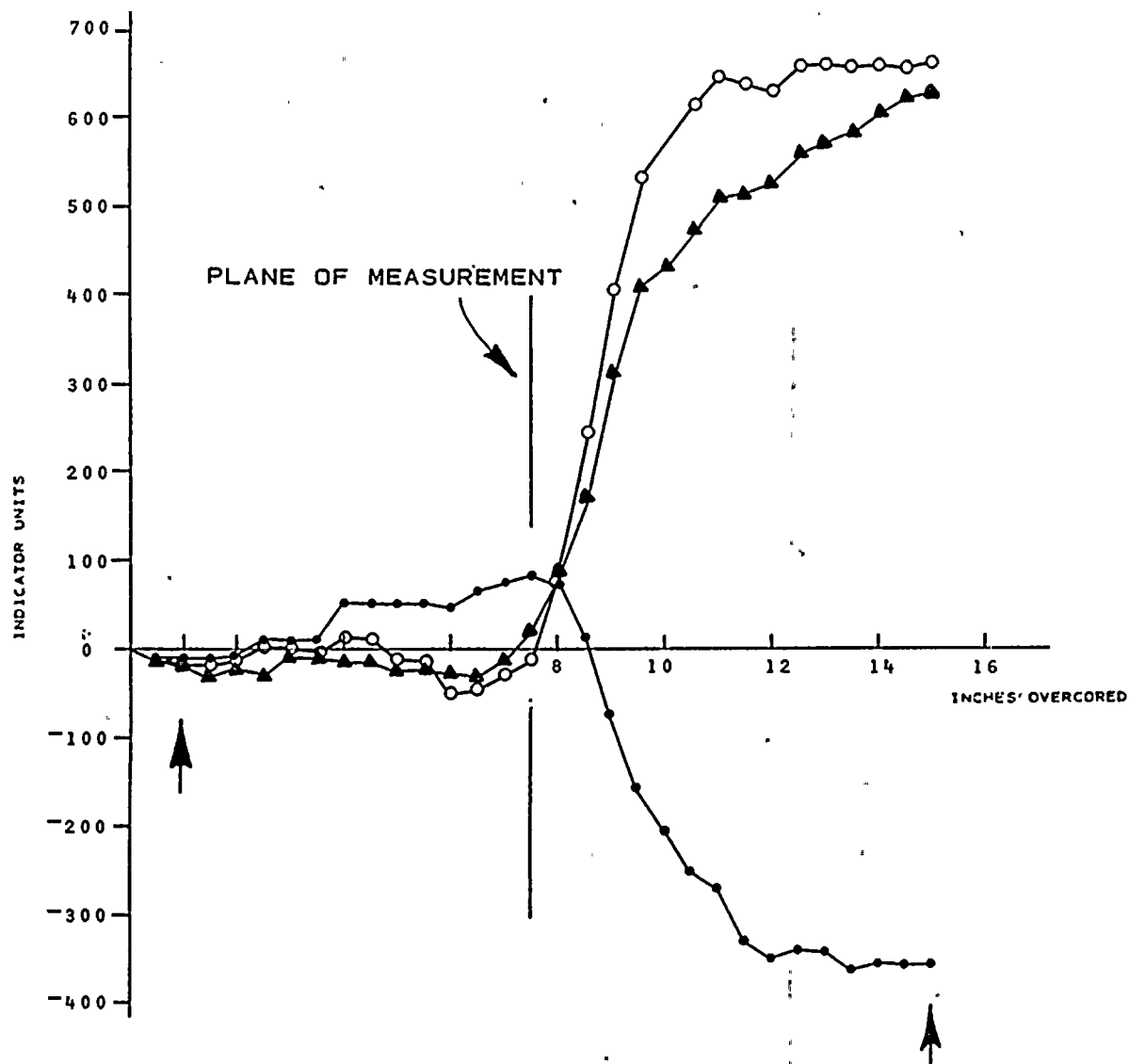
ROCK TYPE: MEDIUM GRAY ARGILLACEOUS SANDSTONE
WITH SILICEOUS SANDSTONE INTERBEDS

STRAIN RELIEF MEASUREMENTS

BORING RS - 3
TEST NO. 35
DEPTH 67'2"

NOTE: A POSITIVE INCREASE IN INDICATOR UNITS
INDICATES EXPANSION OF THE EX HOLE
DURING OVERCORING

ARROWS (↑) INDICATE TOTAL DEFORMATION
USED TO CALCULATE STRESS



KEY:

- ▲ AXIS I
- AXIS II
- AXIS III

$$\begin{aligned}\Delta R_1 &= 629 - (-19) = 648 \\ \Delta R_2 &= .663 - (-12) = 675 \\ \Delta R_3 &= -356 - (-12) = -344\end{aligned}$$

$$K_1 = 1.06 \mu\text{IN.}$$

$$U_1 = 1.06 \times 648 = 687$$

$$K_2 = 1.09 \mu\text{IN.}$$

$$U_2 = 1.09 \times 675 = 736$$

$$K_3 = 1.08 \mu\text{IN.}$$

$$U_3 = 1.08 \times -344 = -372$$

ROCK TYPE: MEDIUM GRAY ARGILLACEOUS SANDSTONE

STRAIN RELIEF MEASUREMENTS

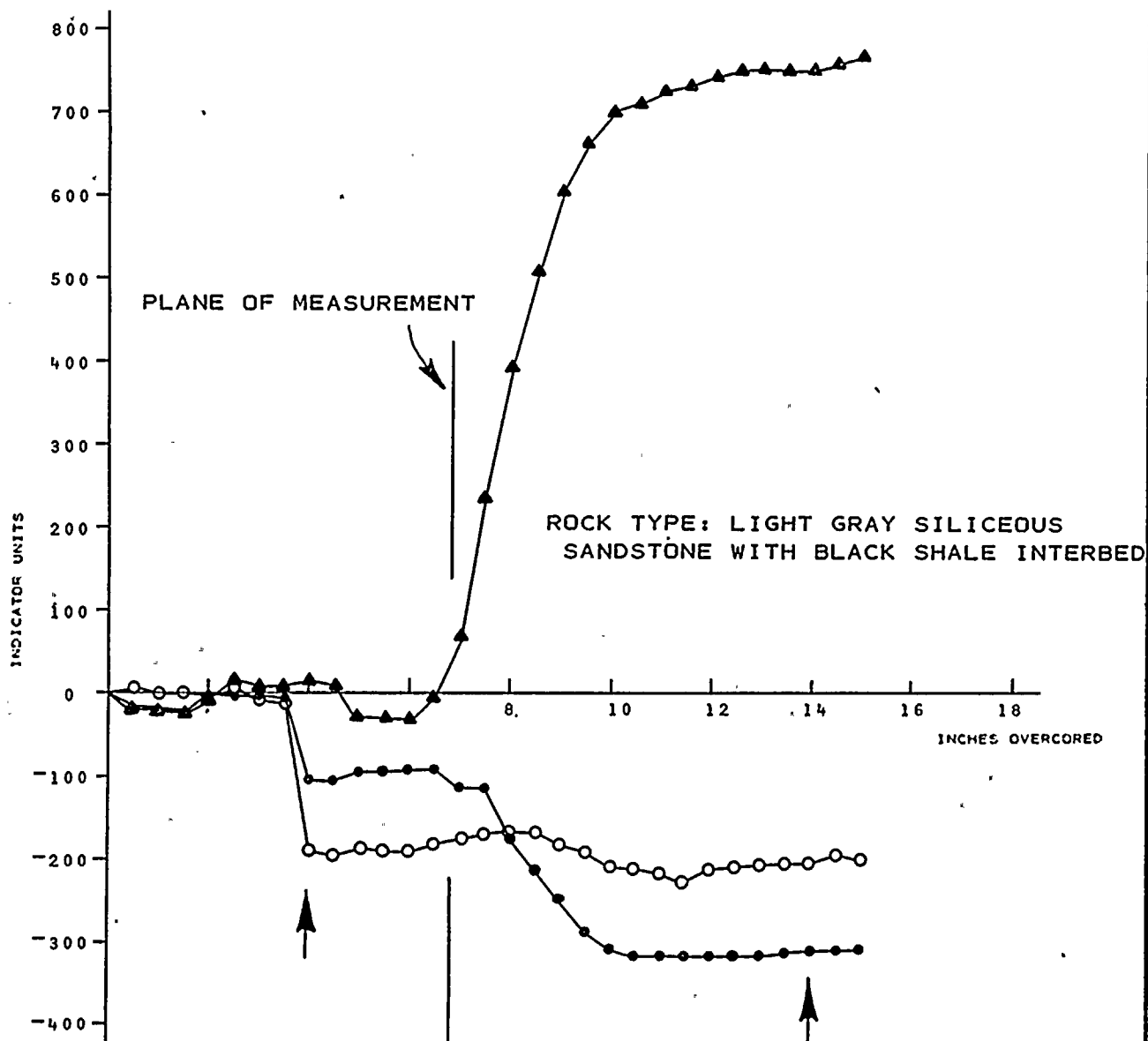
BORING RS - 3

TEST NO. 36

DEPTH 68' 5 1/2"

NOTE: A POSITIVE INCREASE IN INDICATOR UNITS
INDICATES EXPANSION OF THE EX HOLE
DURING OVERCORING

ARROWS (±) INDICATE TOTAL DEFORMATION
USED TO CALCULATE STRESS



KEY:

- ▲ AXIS I
- AXIS II
- AXIS III

$$\Delta R_1 = 755 - (-17) = 738$$

$$\Delta R_2 = -206 - (-188) = -19$$

$$\Delta R_3 = -317 - (-107) = -210$$

$$K_1 = 1.06 \mu\text{IN.}$$

$$U_1 = 1.06 \times 738 = 782$$

$$K_2 = 1.09 \mu\text{IN.}$$

$$U_2 = 1.09 \times -19 = -21$$

$$K_3 = 1.08 \mu\text{IN.}$$

$$U_3 = 1.08 \times -210 = -227$$

STRAIN RELIEF MEASUREMENTS

BORING NO. RS - 3

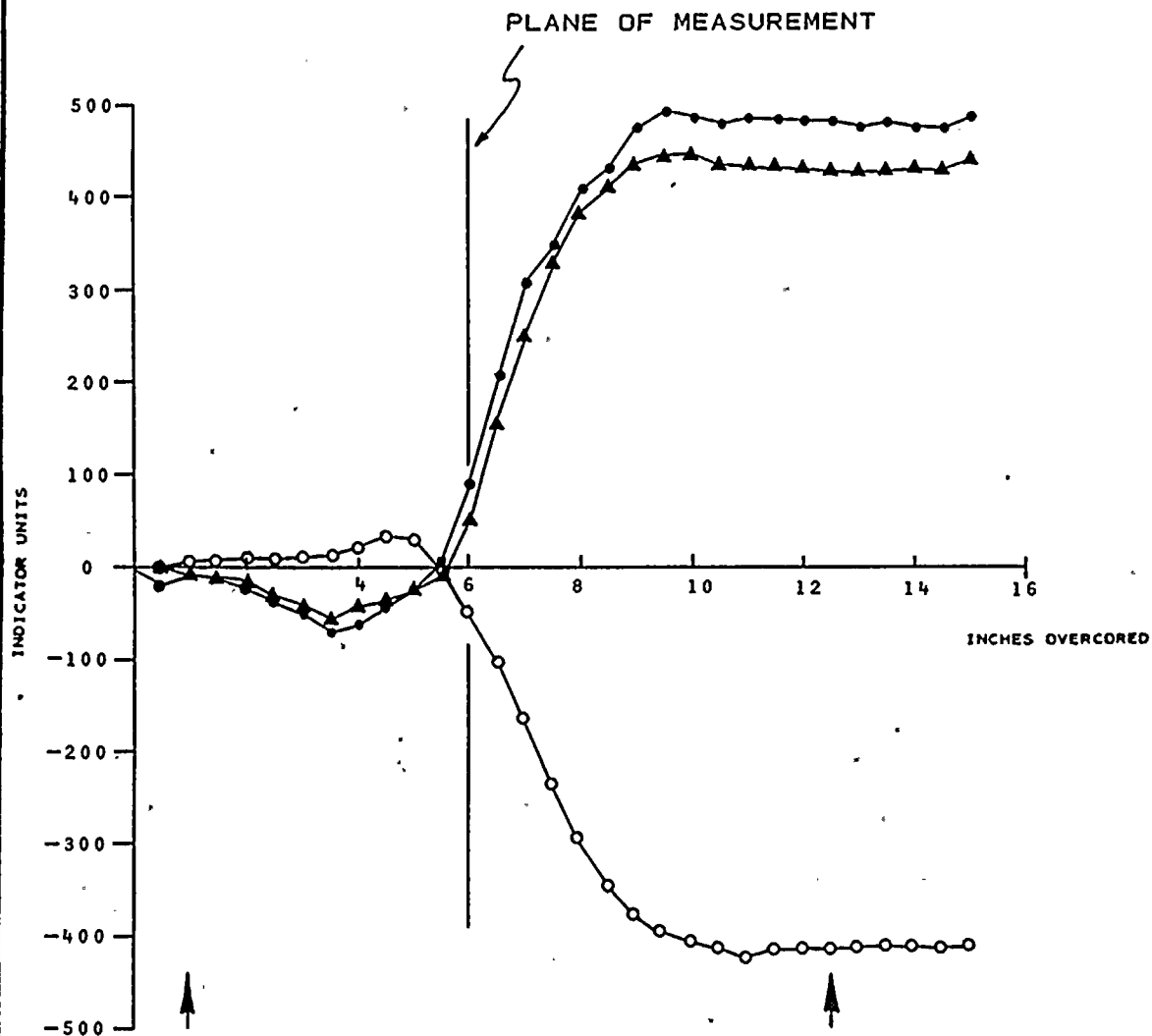
TEST NO. 37

DEPTH 69'7 3/4"

NOTE: A POSITIVE INCREASE IN INDICATOR UNITS INDICATES EXPANSION OF THE EX HOLE DURING OVERCORING

ARROWS (†) INDICATE TOTAL DEFORMATION USED TO CALCULATE STRESS





KEY:

- ▲ AXIS I
- AXIS II
- AXIS III

$$\begin{aligned}\Delta R_1 &= 430 - (-9) = 439 \\ \Delta R_2 &= -414 - 6 = -420 \\ \Delta R_3 &= 483 - (-12) = 495\end{aligned}$$

$$K_1 = 0.85 \mu\text{IN.}$$

$$U_1 = 0.85 \times 439 = 373$$

$$K_2 = 0.87 \mu\text{IN.}$$

$$U_2 = 0.87 \times -420 = -365$$

$$K_3 = 0.87 \mu\text{IN.}$$

$$U_3 = 0.87 \times 495 = 431$$

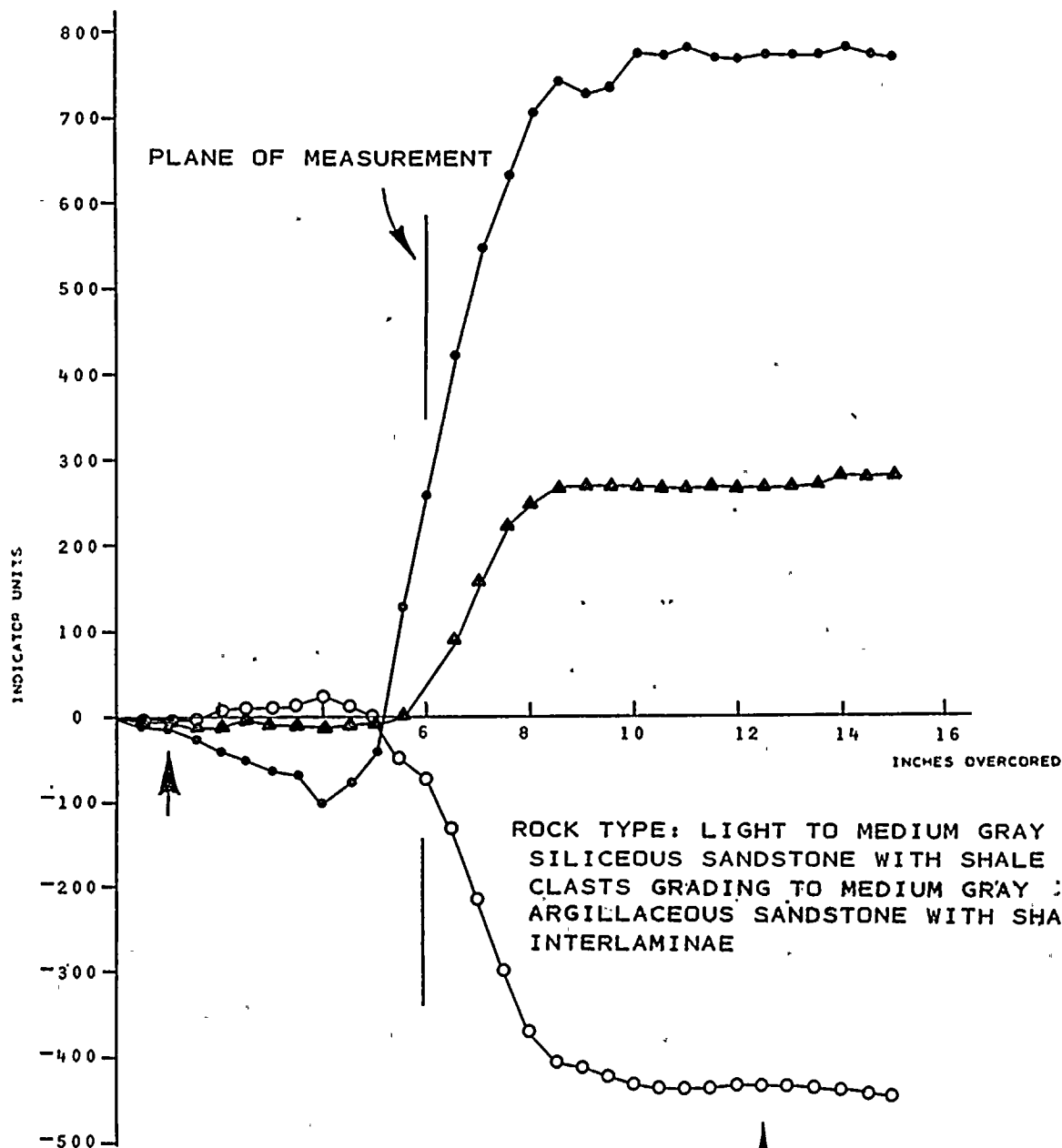
ROCK TYPE: LIGHT GRAY SILICEOUS SANDSTONE TO MEDIUM
GRAY ARGILLACEOUS SANDSTONE

STRAIN RELIEF MEASUREMENTS
BORING RS - 3
TEST NO. 38
DEPTH 70'10"

NOTE: A POSITIVE INCREASE IN INDICATOR UNITS
INDICATES EXPANSION OF THE EX HOLE
DURING OVERCORING

ARROWS (↑) INDICATE TOTAL DEFORMATION
USED TO CALCULATE STRESS





KEY:

- ▲ AXIS I
- AXIS II
- AXIS III

$$\Delta R_1 = 274 - (-9) = 283$$

$$\Delta R_2 = -438 - (-3) = -435$$

$$\Delta R_3 = 777 - (-17) = 794$$

$$K_1 = 0.85 \mu\text{IN.}$$

$$U_1 = 0.85 \times 283 = 241$$

$$K_2 = 0.87 \mu\text{IN.}$$

$$U_2 = 0.87 \times -435 = -378$$

$$K_3 = 0.87 \mu\text{IN.}$$

$$U_3 = 0.87 \times 794 = 691$$

STRAIN RELIEF MEASUREMENTS

BORING NO. RS - 3

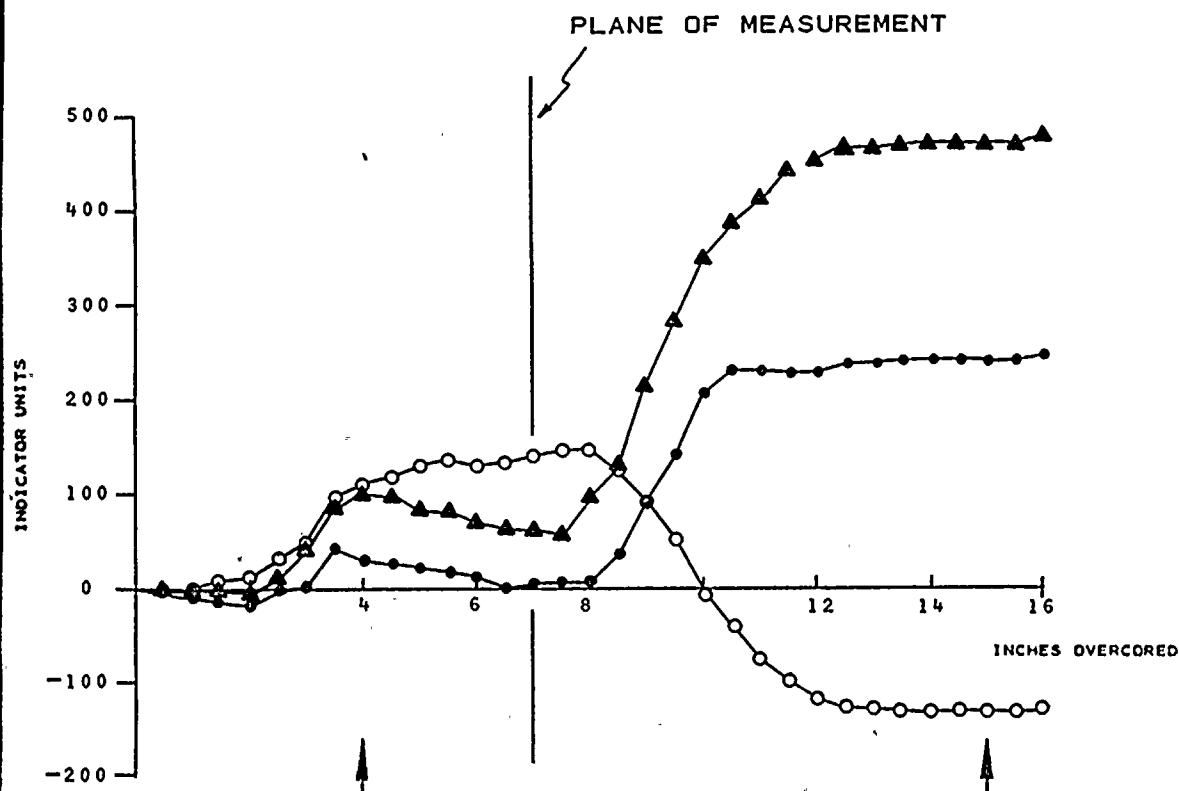
TEST NO. 39

DEPTH 72'0"

NOTE: A POSITIVE INCREASE IN INDICATOR UNITS INDICATES EXPANSION OF THE EX HOLE DURING OVERCORING

ARROWS (A) INDICATE TOTAL DEFORMATION USED TO CALCULATE STRESS





KEY:

- ▲ AXIS I
- AXIS II
- AXIS III

$$\begin{aligned}\Delta R_1 &= 478 - 100 = 378 \\ \Delta R_2 &= -130 - 105 = -235 \\ \Delta R_3 &= 243 - 30 = 213\end{aligned}$$

$$\begin{aligned}K_1 &= 0.85 \mu\text{IN.} & U_1 &= 0.85 \times 378 = 321 \\ K_2 &= 0.87 \mu\text{IN.} & U_2 &= 0.87 \times -235 = -204 \\ K_3 &= 0.87 \mu\text{IN.} & U_3 &= 0.87 \times 213 = 185\end{aligned}$$

ROCK TYPE: LIGHT TO MEDIUM GRAY SILICEOUS SANDSTONE WITH MEDIUM GRAY ARGILLACEOUS SANDSTONE INTERBED

STRAIN RELIEF MEASUREMENTS

BORING NO. RS - 3

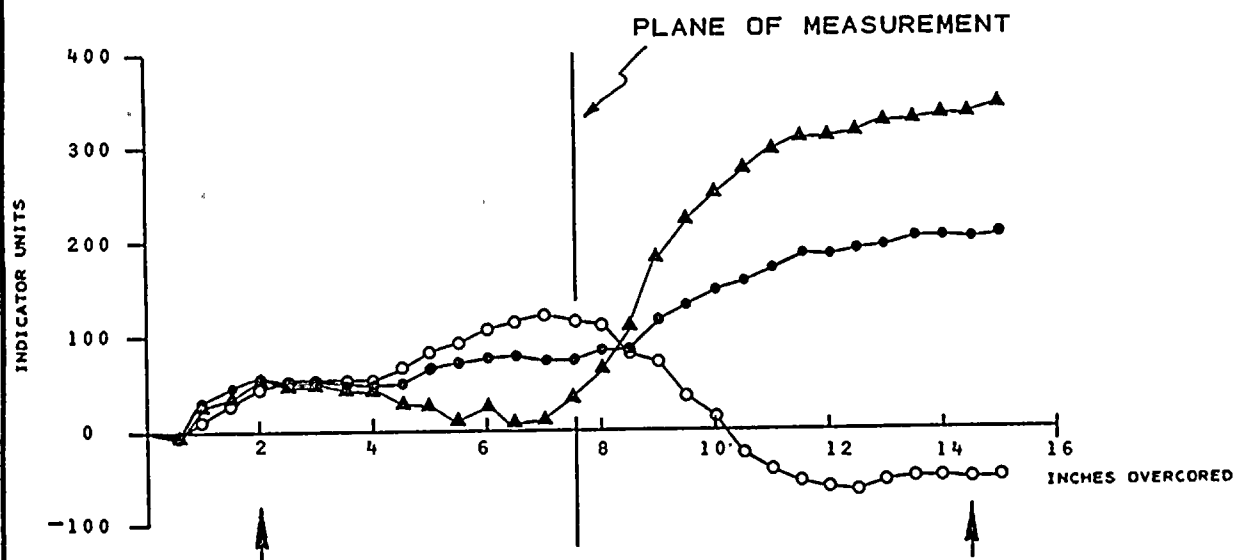
TEST NO. 41

DEPTH 74'6"

NOTE: A POSITIVE INCREASE IN INDICATOR UNITS INDICATES EXPANSION OF THE SX HOLE DURING OVERCORING

ARROWS (↑) INDICATE TOTAL DEFORMATION USED TO CALCULATE STRESS





KEY:

▲ AXIS I $\Delta R_1 = 338 - 55 = 283$
 ○ AXIS II $\Delta R_2 = -54 - 46 = -100$
 • AXIS III $\Delta R_3 = 202 - 57 = 145$

$K_1 = 0.85 \mu\text{IN.} \quad U_1 = 0.85 \times 283 = 241$
 $K_2 = 0.87 \mu\text{IN.} \quad U_2 = 0.87 \times -100 = -87$
 $K_3 = 0.87 \mu\text{IN.} \quad U_3 = 0.87 \times 145 = 126$

ROCK TYPE: MEDIUM TO LIGHT GRAY SILICEOUS SANDSTONE,
SLIGHTLY ARGILLACEOUS SANDSTONE INTERBEDS

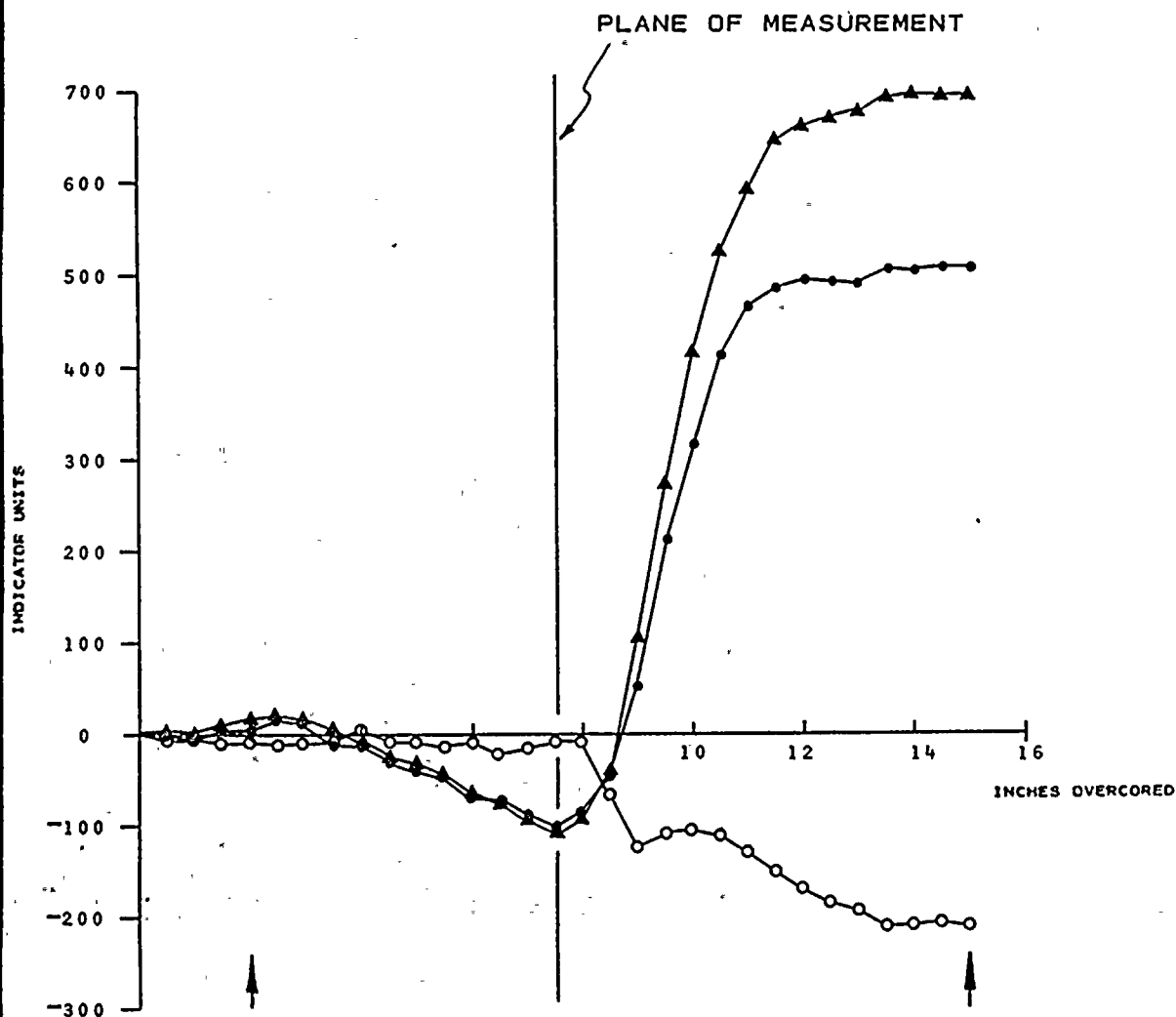
STRAIN RELIEF MEASUREMENTS
 BORING RS - 3
 TEST NO. 42
 DEPTH 75' 10 1/2"

NOTE: A POSITIVE INCREASE IN INDICATOR UNITS
INDICATES EXPANSION OF THE EX HOLE
DURING OVERCORING

ARROWS (↑) INDICATE TOTAL DEFORMATION
USED TO CALCULATE STRESS

PLATE E-87
 DAMES & MOORE





KEY:

▲ AXIS I $\Delta R_1 = 688 - 17 = 671$
 ○ AXIS II $\Delta R_2 = -207 - (-9) = -198$
 • AXIS III $\Delta R_3 = 505 - 3 = 502$

$K_1 = 0.85 \mu\text{IN.}$ $U_1 = 0.85 \times 671 = 570$
 $K_2 = 0.87 \mu\text{IN.}$ $U_2 = 0.87 \times -198 = -172$
 $K_3 = 0.87 \mu\text{IN.}$ $U_3 = 0.87 \times 502 = 437$

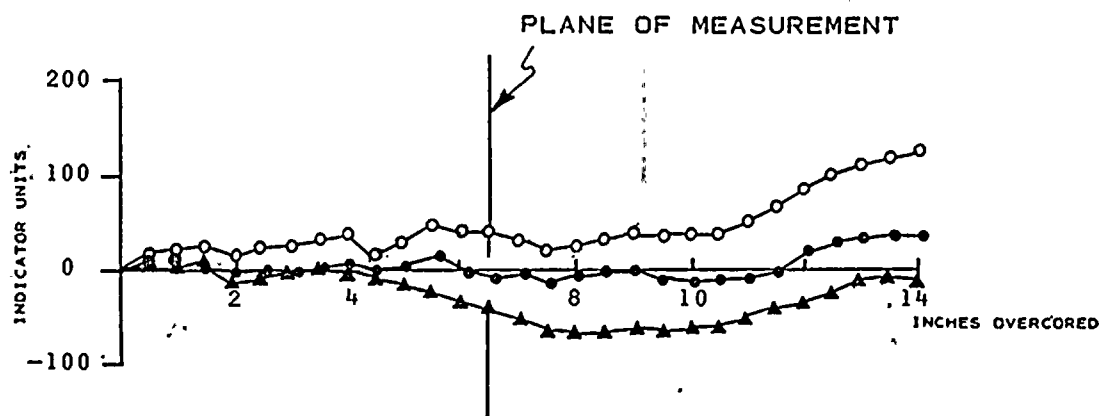
ROCK TYPE: MEDIUM GRAY ARGILLACEOUS SANDSTONE, OCCASIONAL
LIGHT GRAY SILICEOUS SANDSTONE INTERBEDS

STRAIN RELIEF MEASUREMENTS
 BORING NO. RS - 3
 TEST NO. 43
 DEPTH 77'1 1/2"

NOTE: A POSITIVE INCREASE IN INDICATOR UNITS
INDICATES EXPANSION OF THE EX HOLE
DURING OVERCORING

ARROWS (↑) INDICATE TOTAL DEFORMATION
USED TO CALCULATE STRESS





KEY:

- ▲ AXIS I
- AXIS II
- AXIS III

ROCK TYPE: LIGHT GRAY SILICEOUS
SANDSTONE

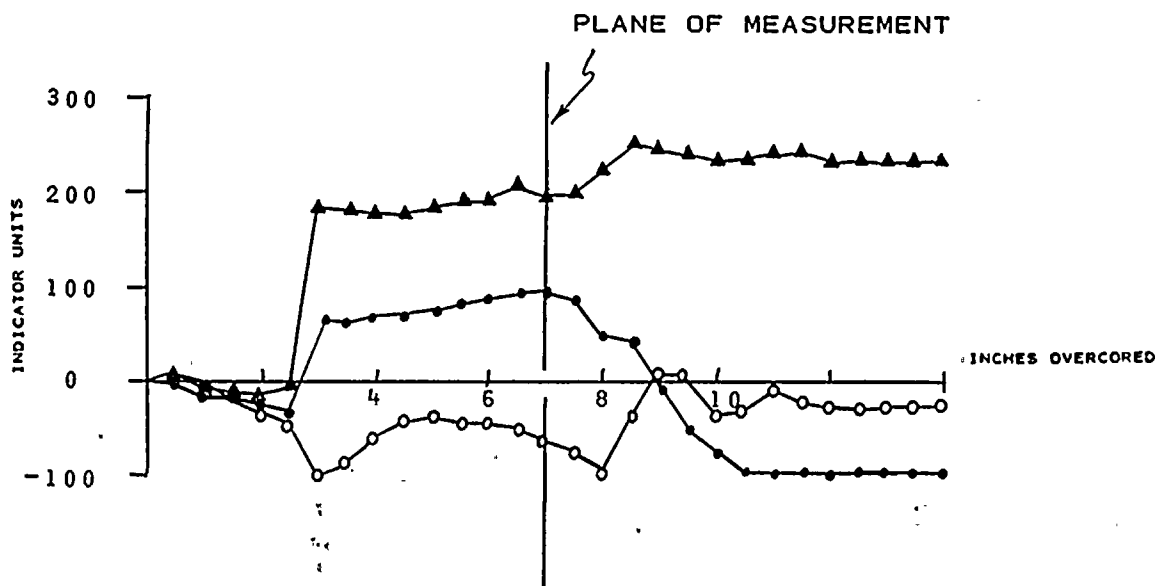
STRAIN RELIEF MEASUREMENTS
BORING RS - 4
TEST NO. 1
DEPTH 22'2"

NOTE: A POSITIVE INCREASE IN INDICATOR UNITS
INDICATES EXPANSION OF THE EX HOLE
DURING OVERCORING

TEST RESULTS NOT INCLUDED IN THE OVERALL
INTERPRETATION DUE TO THE IRREGULARITY
OF THE RESULTS

PLATE E-89
DAMES & MOORE





KEY;

- ▲ AXIS I
- AXIS II
- AXIS III

ROCK TYPE: LIGHT GRAY SILICEOUS
SANDSTONE

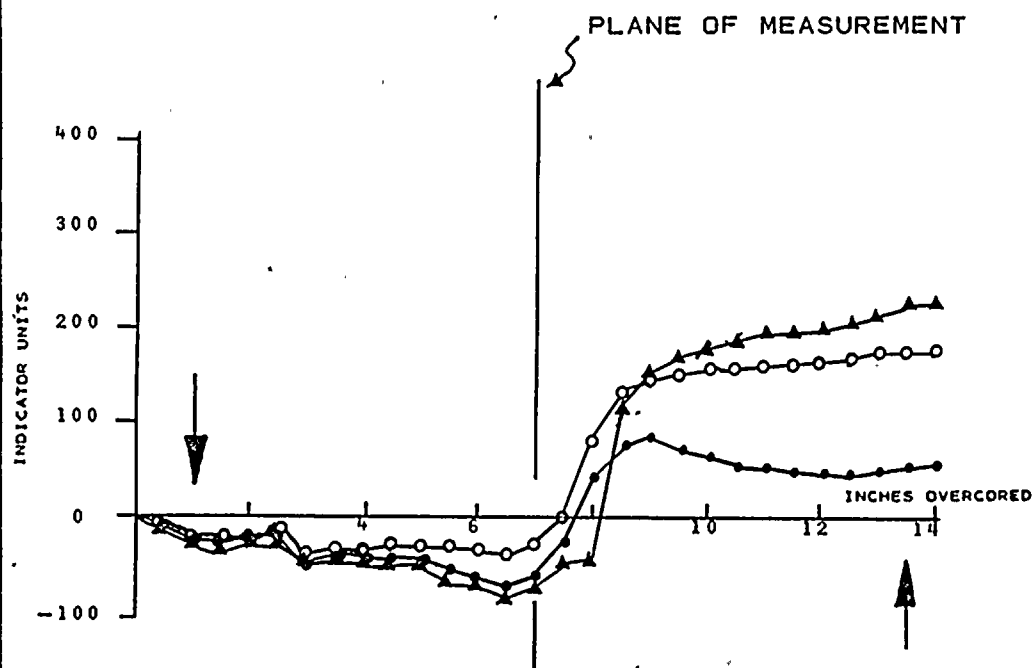
STRAIN RELIEF MEASUREMENTS
BORING RS - 4
TEST NO. 2
DEPTH 23'4"

NOTE: A POSITIVE INCREASE IN INDICATOR UNITS
INDICATES EXPANSION OF THE EX HOLE
DURING OVERCORING

TEST RESULTS NOT INCLUDED IN THE OVERALL
INTERPRETATION DUE TO THE IRREGULARITY
OF THE RESULTS

PLATE E-90
DAMES & MOORE





KEY;

▲ AXIS I	$\Delta R_1 = 228 - (-30) = 258$
○ AXIS II	$\Delta R_2 = 175 - (-32) = 207$
● AXIS III	$\Delta R_3 = 52 - (-23) = 75$

$K_1 = 1.02 \mu\text{IN.}$	$U_1 = 1.02 \times 258 = 263$
$K_2 = .99 \mu\text{IN.}$	$U_2 = .99 \times 207 = 205$
$K_3 = 1.00 \mu\text{IN.}$	$U_3 = 1.00 \times 75 = 75$

ROCK TYPE: MEDIUM GRAY, ARGILLACEOUS
SANDSTONE TO LIGHT GRAY
SILICEOUS SANDSTONE

STRAIN RELIEF MEASUREMENTS

BORING RS - 4

TEST NO. 3

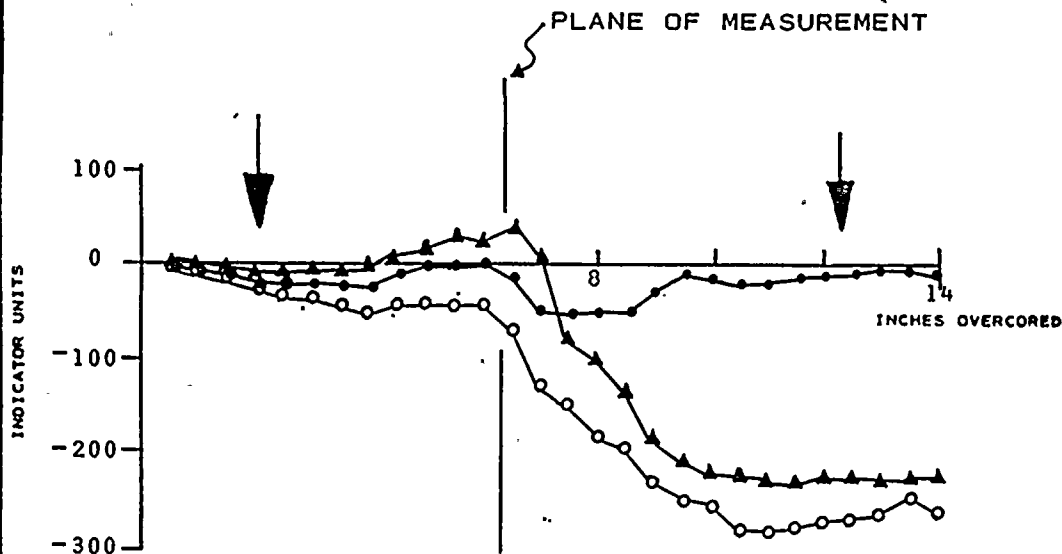
DEPTH 24'6"

NOTE: A POSITIVE INCREASE IN INDICATOR UNITS
INDICATES EXPANSION OF THE EX HOLE
DURING OVERCORING

ARROWS (↓) INDICATE TOTAL DEFORMATION
USED TO CALCULATE STRESS

PLATE E-91
DAMES & MOORE





KEY:

- ▲ AXIS I
- AXIS II
- AXIS III

$$\begin{aligned}\Delta R_1 &= -230 - (-7) = -223 \\ \Delta R_2 &= -272 - (-8) = -264 \\ \Delta R_3 &= -10 - (-10) = 0\end{aligned}$$

$$K_1 = 1.02 \mu\text{IN.}$$

$$U_1 = 1.02 \times -223 = -228$$

$$K_2 = 0.99 \mu\text{IN.}$$

$$U_2 = 0.99 \times -264 = -261$$

$$K_3 = 1.03 \mu\text{IN.}$$

$$U_3 = 1.03 \times 0 = 0$$

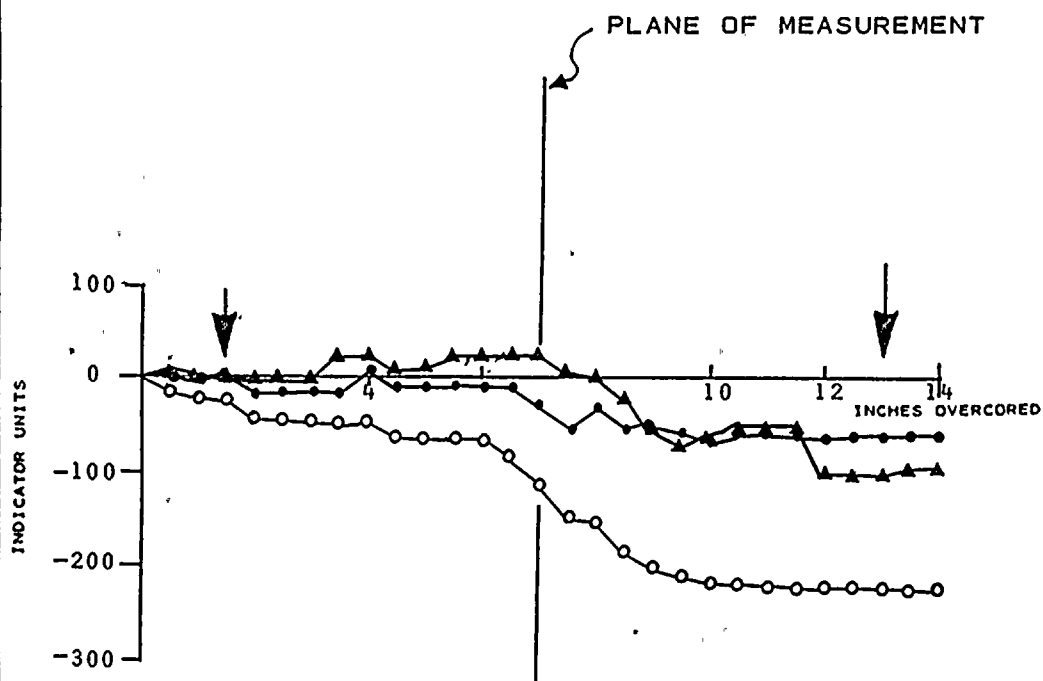
ROCK TYPE: LIGHT GRAY SILICEOUS SANDSTONE

STRAIN RELIEF MEASUREMENTS
BORING RS - 4
TEST NO. 4
DEPTH 27'1 1/2"

NOTE: A POSITIVE INCREASE IN INDICATOR UNITS
INDICATES EXPANSION OF THE EX HOLE
DURING OVERCORING

ARROWS (f) INDICATE TOTAL DEFORMATION
USED TO CALCULATE STRESS





KEY:

▲ AXIS I	$\Delta R_1 = -109 - (-2) = -107$
○ AXIS II	$\Delta R_2 = -226 - (-26) = -200$
● AXIS III	$\Delta R_3 = -65 - 0 = -65$

$K_1 = 1.04 \mu\text{IN.}$	$U_1 = 1.04 \times -107 = -111$
$K_2 = 1.00 \mu\text{IN.}$	$U_2 = 1.00 \times -200 = -200$
$K_3 = 1.03 \mu\text{IN.}$	$U_3 = 1.03 \times -65 = -67$

ROCK TYPE: LIGHT GRAY SILICEOUS SANDSTONE

STRAIN RELIEF MEASUREMENTS

BORING RS - 4

TEST NO. 5

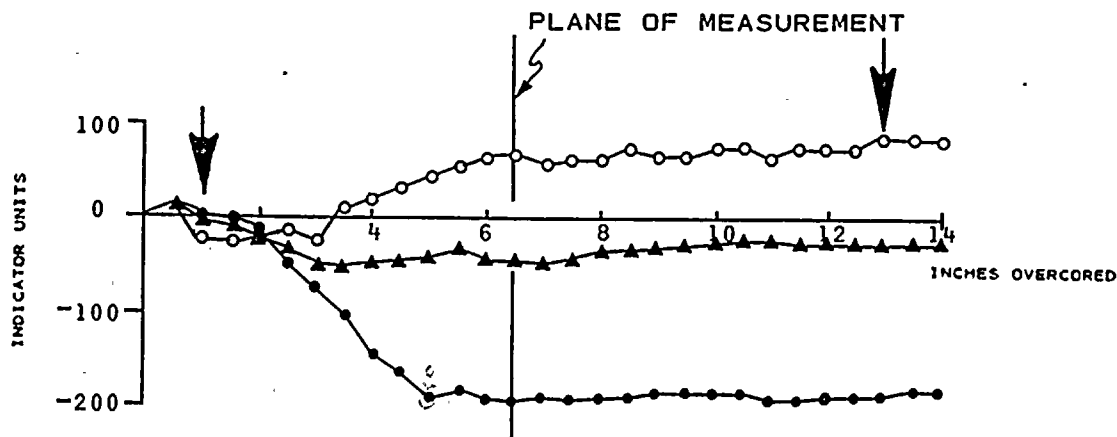
DEPTH 28'6"

NOTE: A POSITIVE INCREASE IN INDICATOR UNITS
INDICATES EXPANSION OF THE EX HOLE
DURING OVERCORING

ARROWS (†) INDICATE TOTAL DEFORMATION
USED TO CALCULATE STRESS

PLATE E-93
DAMES & MOORE





KEY:

▲ AXIS I
○ AXIS II
● AXIS III

$$\begin{aligned}\Delta R_1 &= -28 - (-6) = -22 \\ \Delta R_2 &= 84 - (-24) = 108 \\ \Delta R_3 &= -187 - (-5) = -182\end{aligned}$$

$$\begin{aligned}K_1 &= 1.04 \mu\text{IN.} \\ K_2 &= 1.00 \mu\text{IN.} \\ K_3 &= 1.03 \mu\text{IN.}\end{aligned}$$

$$\begin{aligned}U_1 &= 1.04 \times -22 = -23 \\ U_2 &= 1.00 \times 108 = 108 \\ U_3 &= 1.03 \times -182 = -188\end{aligned}$$

ROCK TYPE: LIGHT GRAY SILICEOUS SANDSTONE

STRAIN RELIEF MEASUREMENTS

BORING RS - 4

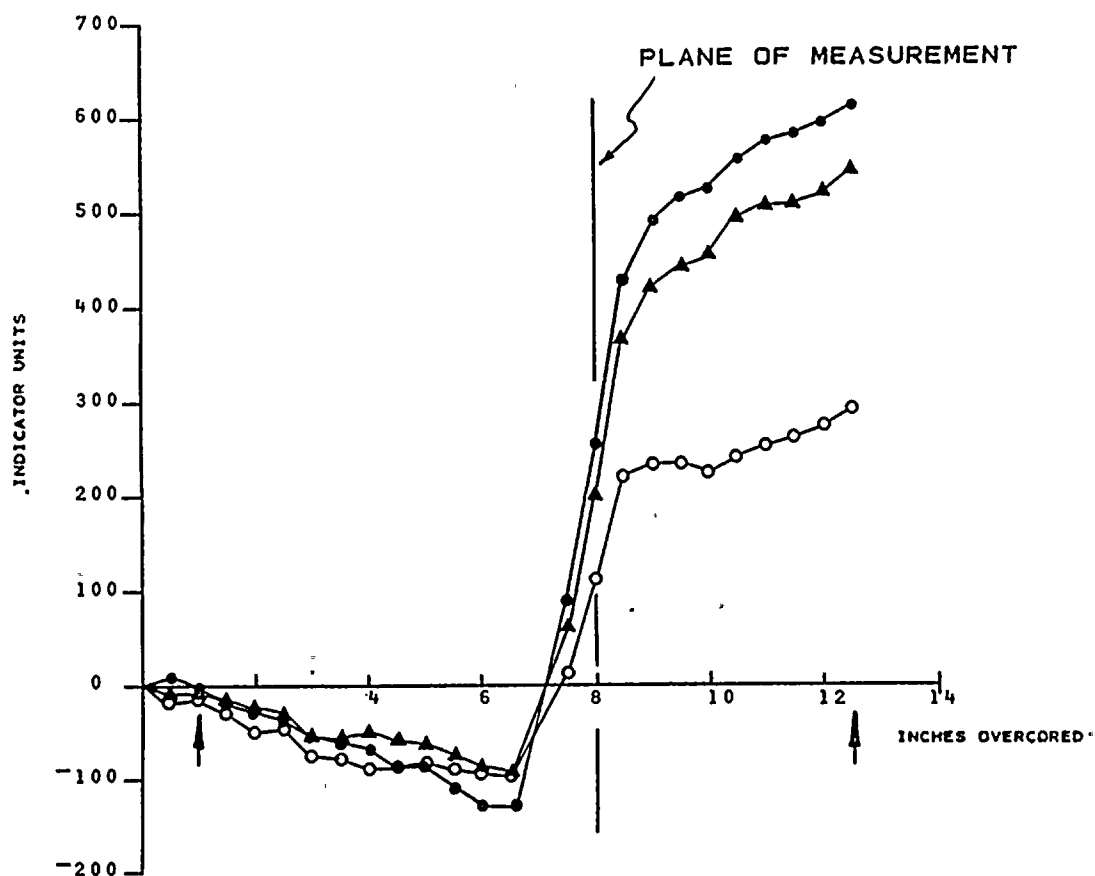
TEST NO. 6

DEPTH 30'11 1/2"

NOTE: A POSITIVE INCREASE IN INDICATOR UNITS INDICATES EXPANSION OF THE EX HOLE DURING OVERCORING

ARROWS (↓) INDICATE TOTAL DEFORMATION USED TO CALCULATE STRESS





KEY:

▲ AXIS I $\Delta R_1 = 543 - (-8) = 551$
 ○ AXIS II $\Delta R_2 = 291 - (-14) = 305$
 • AXIS III $\Delta R_3 = 616 - (-17) = 633$

$K_1 = 1.04 \mu\text{IN.}$ $U_1 = 1.04 \times 551 = 573$
 $K_2 = 1.00 \mu\text{IN.}$ $U_2 = 1.00 \times 305 = 305$
 $K_3 = 1.03 \mu\text{IN.}$ $U_3 = 1.03 \times 633 = 652$

ROCK TYPE: BLACK SHALE TO GRAYWACKE TO SILICEOUS SANDSTONE

STRAIN RELIEF MEASUREMENTS

BORING NO. RS-4

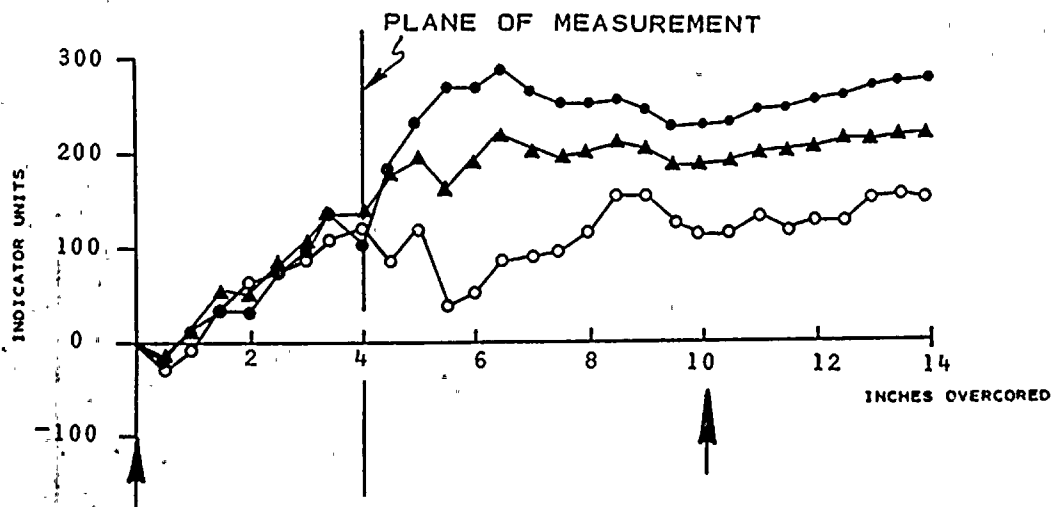
TEST NO. 7

DEPTH 36' 1 1/2"

NOTE: A POSITIVE INCREASE IN INDICATOR UNITS INDICATES EXPANSION OF THE EX HOLE DURING OVERCORING

ARROWS (↑) INDICATE TOTAL DEFORMATION USED TO CALCULATE STRESS





KEY:

▲ AXIS I	$R_1 = 181 - 0 = 181$
○ AXIS II	$R_2 = 114 - 0 = 114$
● AXIS III	$R_3 = 231 - 0 = 231$

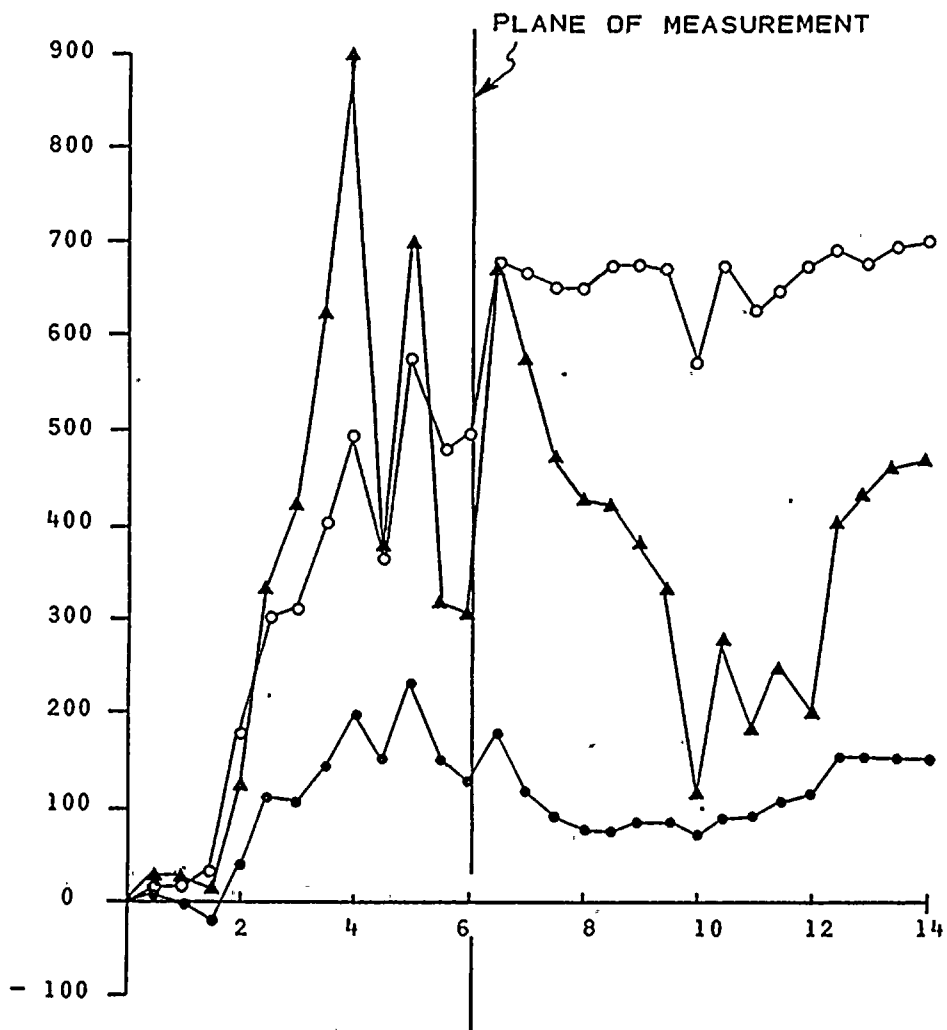
$K_1 = 1.02 \mu\text{IN.}$	$U_1 = 1.02 \times 181 = 185$
$K_2 = 1.00 \mu\text{IN.}$	$U_2 = 1.00 \times 114 = 114$
$K_3 = 1.02 \mu\text{IN.}$	$U_3 = 1.02 \times 231 = 236$

ROCK TYPE: LIGHT GRAY SILICEOUS SANDSTONE,
OCCASIONAL SHALE CLASTS

STRAIN RELIEF MEASUREMENTS
BORING RS - 4
TEST NO. 8
DEPTH 39'3"

NOTE: A POSITIVE INCREASE IN INDICATOR UNITS
INDICATES EXPANSION OF THE EX HOLE
DURING OVERCORING

ARROWS (↓) INDICATE TOTAL DEFORMATION
USED TO CALCULATE STRESS



KEY:

- ▲ AXIS I
- AXIS II
- AXIS III

ROCK TYPE: DARK TO MEDIUM GRAY ARGILLACEOUS
SANDSTONE GRADING TO LIGHT GRAY
SILICEOUS SANDSTONE

STRAIN RELIEF MEASUREMENTS

BORING RS - 4

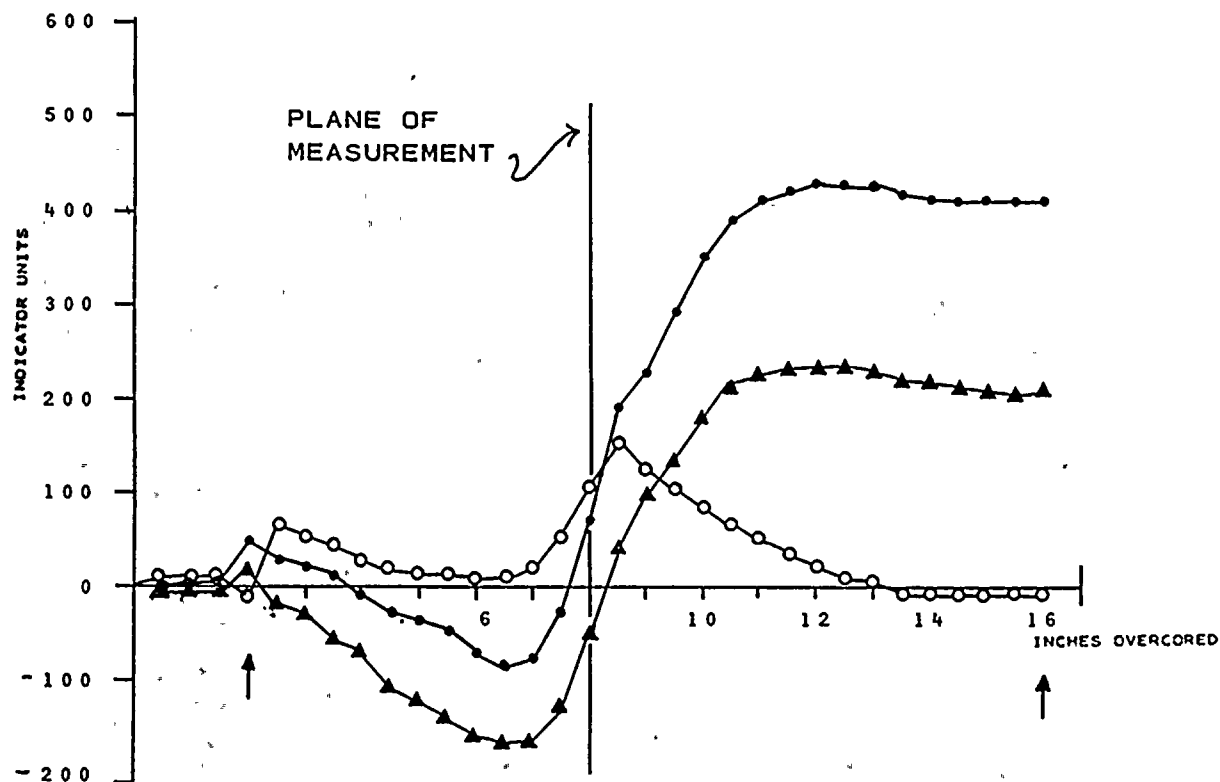
TEST NO. 9

DEPTH 54'6"

NOTE: A POSITIVE INCREASE IN INDICATOR UNITS
INDICATES EXPANSION OF THE EX HOLE
DURING OVERCORING

TEST RESULTS NOT INCLUDED IN THE OVERALL
INTERPRETATION DUE TO THE IRREGULARITY
OF THE RESULTS

PLATE E-97
DAMES & MOORE



KEY:

▲ AXIS I
○ AXIS II
● AXIS III

$\Delta R_1 = 206 - 18 = 188$
 $\Delta R_2 = -6 - (-8) = 2$
 $\Delta R_3 = 412 - 44 = 368$

$K_1 = 0.85 \mu\text{IN.}$ $U_1 = 0.85(188) = 160$
 $K_2 = 0.87 \mu\text{IN.}$ $U_2 = 0.87(2) = 2$
 $K_3 = 0.87 \mu\text{IN.}$ $U_3 = 0.87(368) = 320$

ROCK TYPE: MEDIUM GRAY ARGILLACEOUS
SANDSTONE (GRAYWACKE)

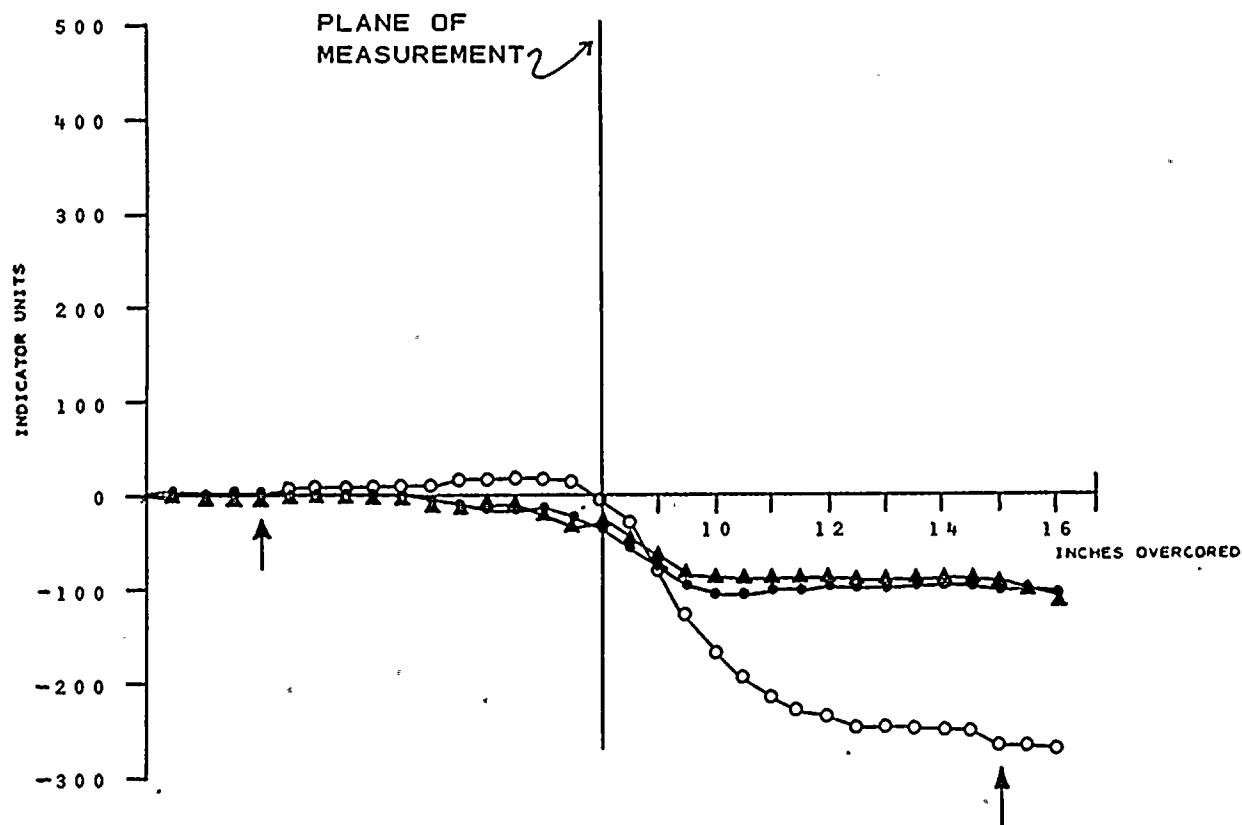
STRAIN RELIEF MEASUREMENTS
BORING RS - 4
TEST NO. 11
DEPTH 58'8"

NOTE: A POSITIVE INCREASE IN INDICATOR UNITS
INDICATES EXPANSION OF THE EX HOLE
DURING OVERCORING

ARROWS (↑) INDICATE TOTAL DEFORMATION
USED TO CALCULATE STRESS

PLATE E-98
DAMES & MOORE





KEY:

- ▲ AXIS I
- AXIS II
- AXIS III

$$\begin{aligned}\Delta R_1 &= -96 - (-2) = -94 \\ \Delta R_2 &= -262 - 0 = -262 \\ \Delta R_3 &= -100 - 2 = -102\end{aligned}$$

$$\begin{aligned}K_1 &= 0.85 \mu\text{IN.} \\ K_2 &= 0.87 \mu\text{IN.} \\ K_3 &= 0.87 \mu\text{IN.}\end{aligned}$$

$$\begin{aligned}U_1 &= 0.85(-94) = -80 \\ U_2 &= 0.87(-262) = -228 \\ U_3 &= 0.87(-102) = -89\end{aligned}$$

ROCK TYPE: MEDIUM GRAY GRAYWACKE

STRAIN RELIEF MEASUREMENTS

BORING RS - 4

TEST NO. 12

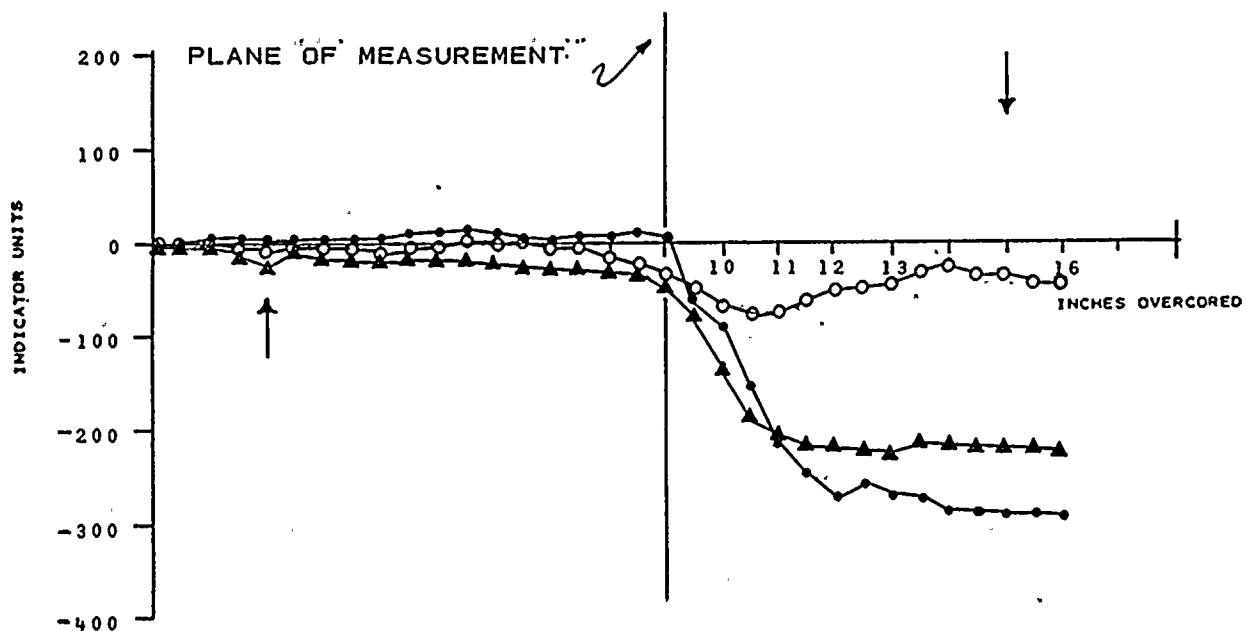
DEPTH 60'7"

NOTE: A POSITIVE INCREASE IN INDICATOR UNITS INDICATES EXPANSION OF THE EX HOLE DURING OVERCORING

ARROWS (↑) INDICATE TOTAL DEFORMATION USED TO CALCULATE STRESS

PLATE E-99
DAMES & MOORE





KEY:

- ▲ AXIS I
- AXIS II
- AXIS III

$$\begin{aligned}\Delta R_1 &= -218 - (-22) = -196 \\ \Delta R_2 &= -32 - (-4) = -28 \\ \Delta R_3 &= -288 - 0 = -288\end{aligned}$$

$$K_1 = 0.85 \text{ MIN.}$$

$$U_1 = 0.85 \times -196 = -167$$

$$K_2 = 0.87 \text{ MIN.}$$

$$U_2 = 0.87 \times -28 = -24$$

$$K_3 = 0.87 \text{ MIN.}$$

$$U_3 = 0.87 \times -288 = -251$$

ROCK TYPE: MEDIUM TO LIGHT GRAY ARGILLACEOUS SANDSTONE,
OCCASIONAL SILICEOUS SANDSTONE INTERBEDS

STRAIN RELIEF MEASUREMENTS

BORING RS - 4

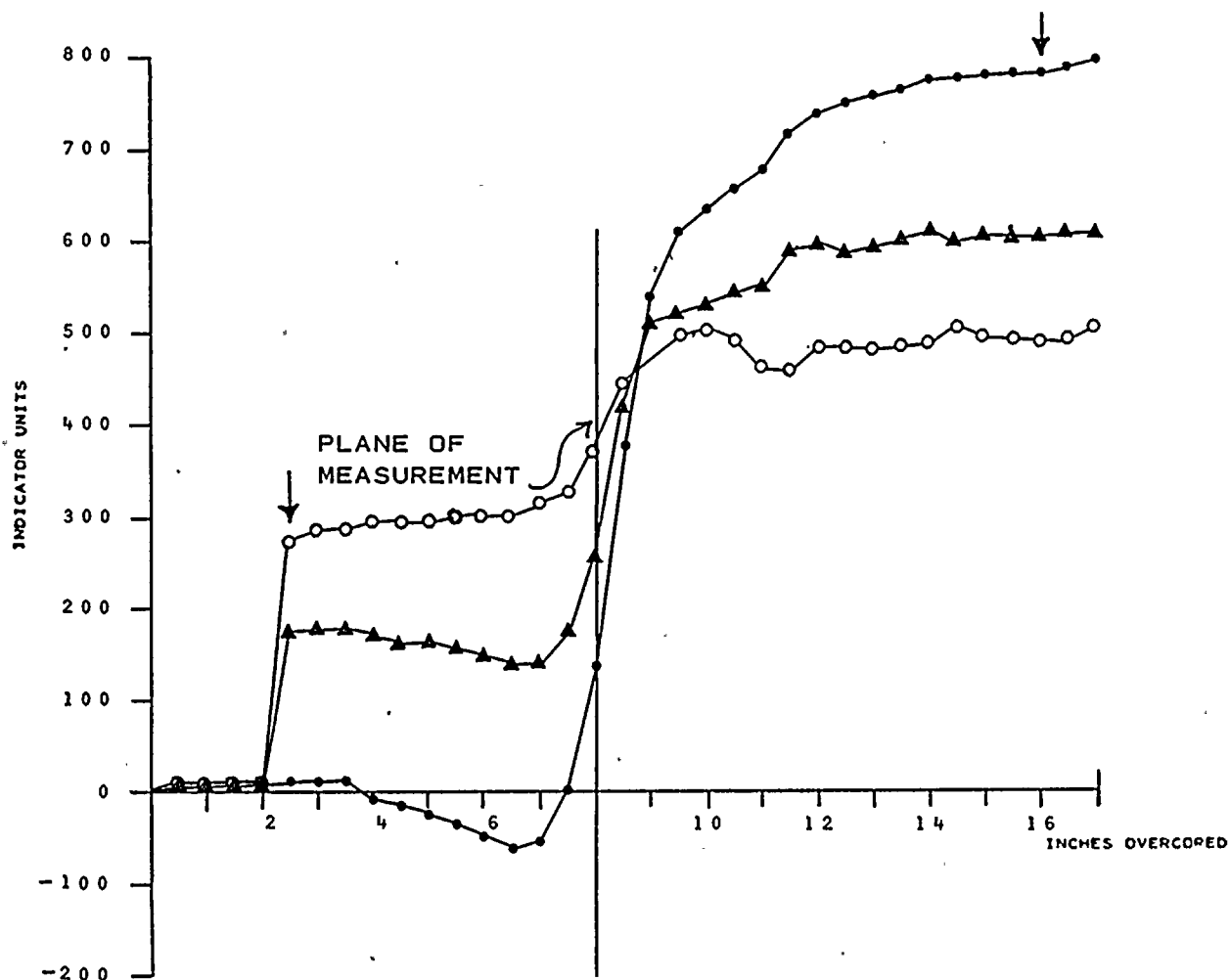
TEST NO. 13

DEPTH 62'0"

NOTE: A POSITIVE INCREASE IN INDICATOR UNITS
INDICATES EXPANSION OF THE EX HOLE
DURING OVERCORING

ARROWS (?) INDICATE TOTAL DEFORMATION
USED TO CALCULATE STRESS





KEY:

- ▲ AXIS I
- AXIS II
- AXIS III

$$\begin{aligned}\Delta R_1 &= 600 - 176 = 424 \\ \Delta R_2 &= 488 - 270 = 218 \\ \Delta R_3 &= 778 - 6 = 772\end{aligned}$$

$$\begin{aligned}K_1 &= 0.91 \mu\text{IN.} \\ K_2 &= 0.87 \mu\text{IN.} \\ K_3 &= 0.89 \mu\text{IN.}\end{aligned}$$

$$\begin{aligned}U_1 &= 0.91 \times 424 = 386 \\ U_2 &= 0.87 \times 218 = 190 \\ U_3 &= 0.89 \times 772 = 687\end{aligned}$$

ROCK TYPE: MEDIUM GRAY ARGILLACEOUS SANDSTONE WITH LIGHT GRAY SILICEOUS SANDSTONE AND SHALEY INTERBEDS

STRAIN RELIEF MEASUREMENTS

BORING RS - 4

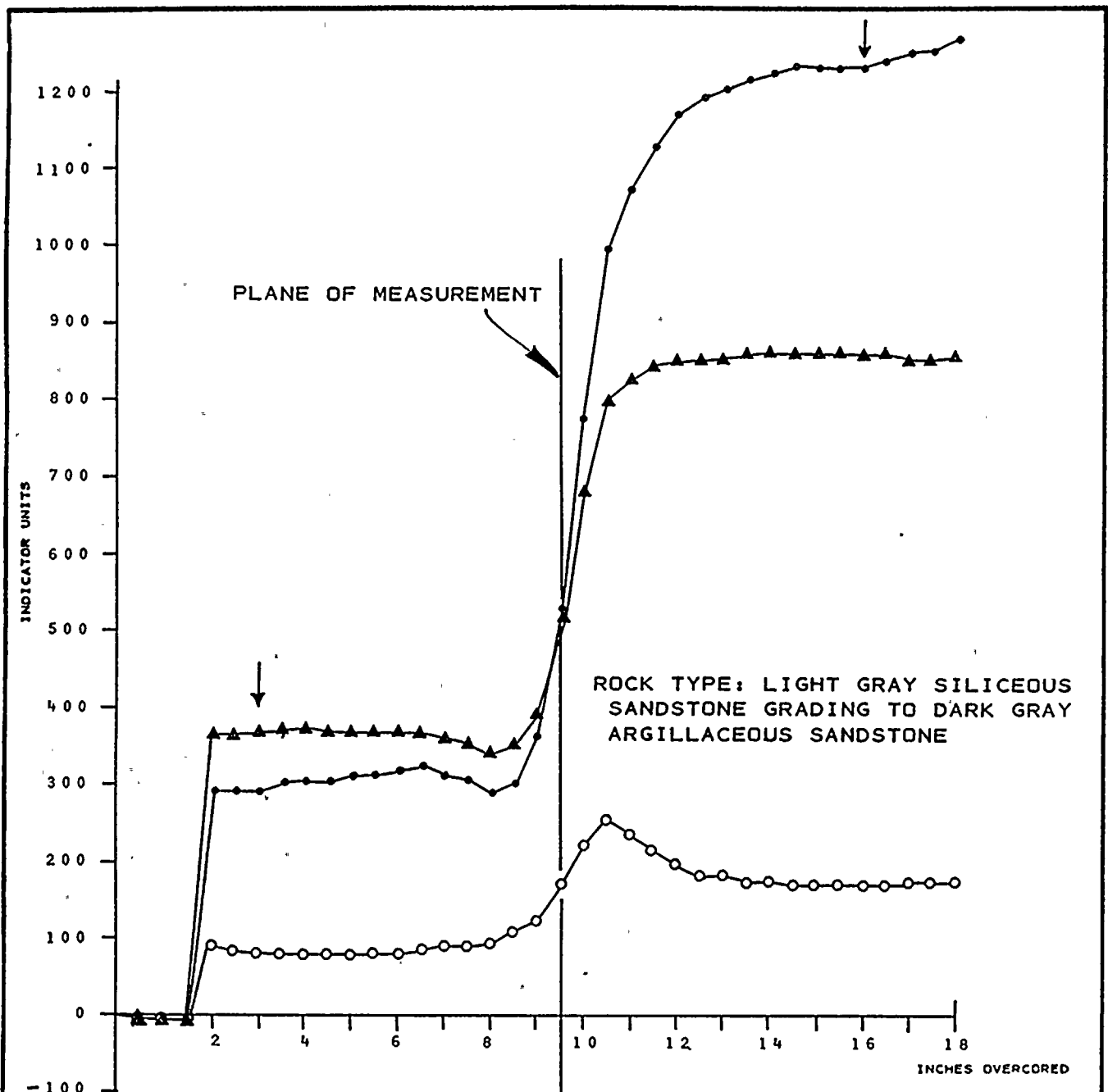
TEST NO. 14

DEPTH 63'8"

NOTE: A POSITIVE INCREASE IN INDICATOR UNITS INDICATES EXPANSION OF THE EX HOLE DURING OVERCORING

ARROWS (↓) INDICATE TOTAL DEFORMATION USED TO CALCULATE STRESS





KEY:

▲ AXIS I

○ AXIS II

● AXIS III

$$\Delta R_1 = 860 - 366 = 494$$

$$\Delta R_2 = 172 - 80 = 92$$

$$\Delta R_3 = 1234 - 290 = 944$$

$$K_1 = 0.91 \mu\text{IN.}$$

$$K_2 = 0.87 \mu\text{IN.}$$

$$K_3 = 0.89 \mu\text{IN.}$$

$$U_1 = 0.91(494) = 450$$

$$U_2 = 0.87(92) = 80$$

$$U_3 = 0.89(944) = 840$$

STRAIN RELIEF MEASUREMENTS

BORING RS - 4

TEST NO. 15

DEPTH 65'9 1/2"

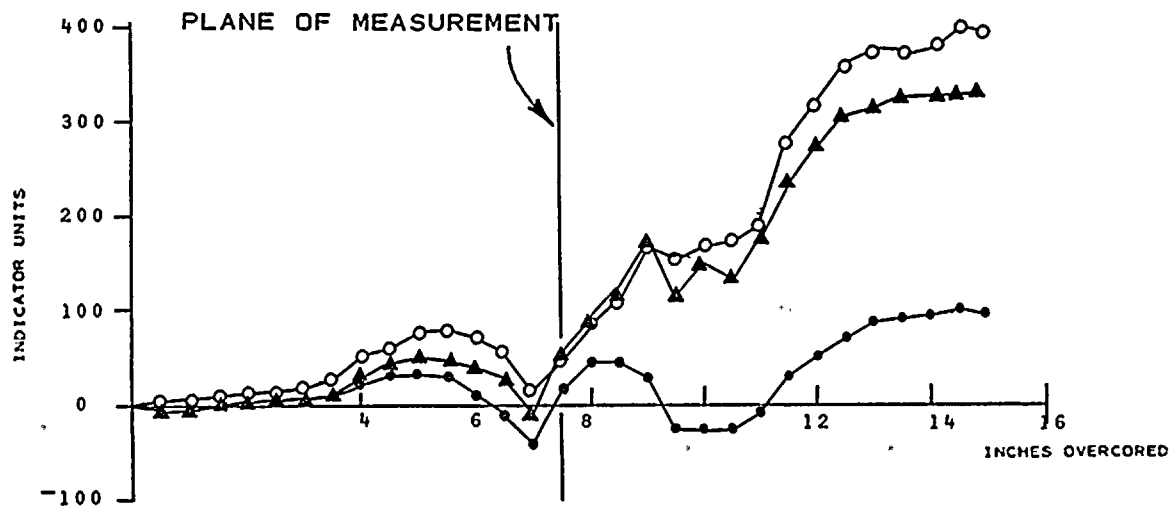
NOTE: AXIS II UNCERTAIN

NOTE: A POSITIVE INCREASE IN INDICATOR UNITS INDICATES EXPANSION OF THE EX HOLE DURING OVERCORING

ARROWS (f) INDICATE TOTAL DEFORMATION USED TO CALCULATE STRESS

PLATE E-102
DAMES & MOORE





KEY:

- ▲ AXIS I
- AXIS II
- ◐ AXIS III

ROCK TYPE: LIGHT GRAY SILICEOUS SANDSTONE,
OCCASIONAL MEDIUM TO DARK GRAY
ARGILLACEOUS SANDSTONE INTERBEDS

STRAIN RELIEF MEASUREMENTS

BORING NO. RS - 4

TEST NO. 16

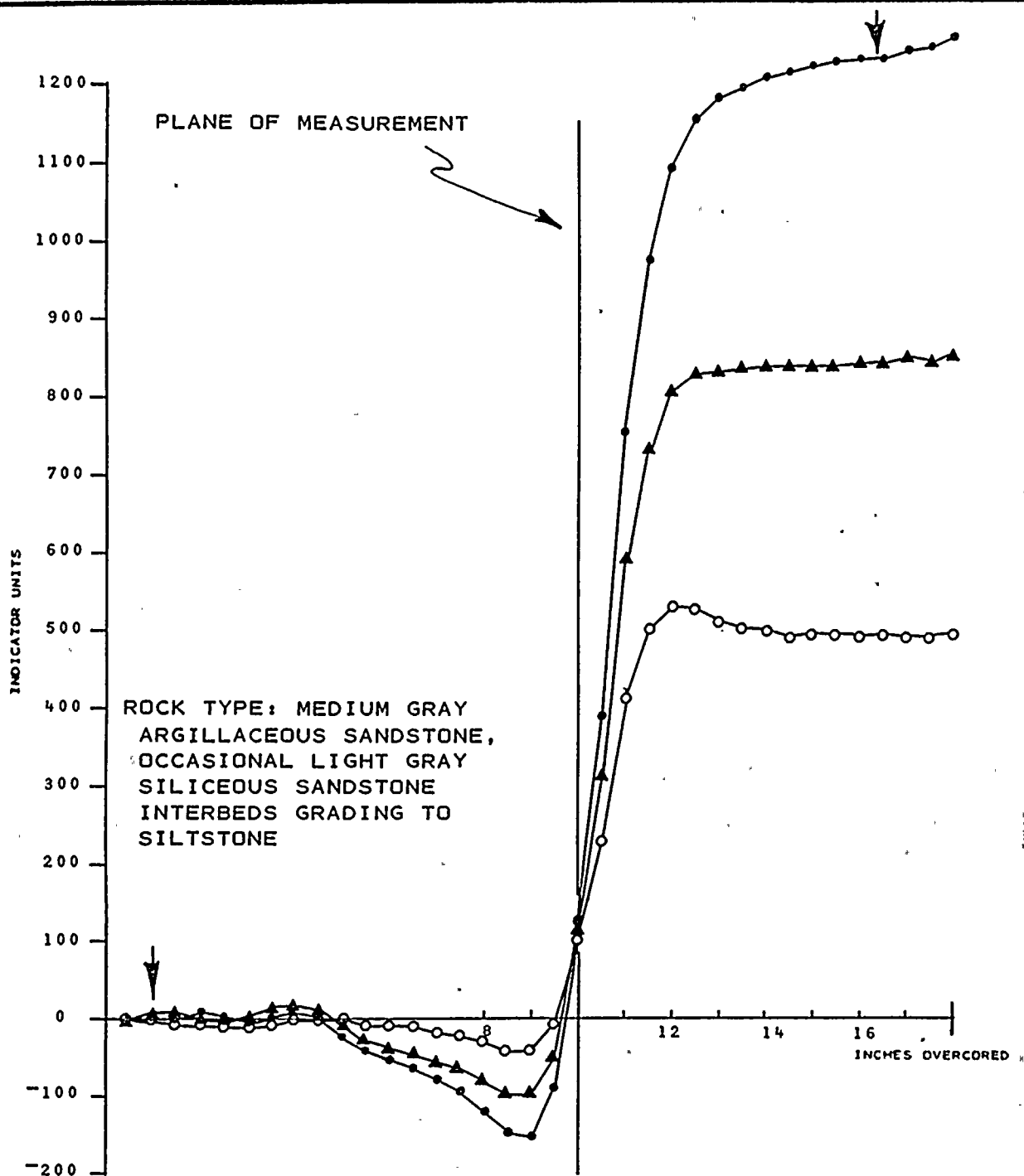
DEPTH 67'1 1/2"

NOTE: A POSITIVE INCREASE IN INDICATOR UNITS
INDICATES EXPANSION OF THE EX HOLE
DURING OVERCORING

TEST RESULTS NOT INCLUDED IN THE OVERALL
INTERPRETATION DUE TO THE IRREGULARITY
OF THE RESULTS

PLATE E-103
DAMES & MOORE





KEY:

- ▲ AXIS I
- AXIS II
- AXIS III

$$\Delta R_1 = 840 - (-4) = 844$$

$$\Delta R_2 = 492 - (-4) = 496$$

$$\Delta R_3 = 1234 - 0 = 1234$$

$$K_1 = 0.91 \mu\text{IN.}$$

$$U_1 = 0.91 \times 844 = 768$$

$$K_2 = 0.87 \mu\text{IN.}$$

$$U_2 = 0.87 \times 496 = 432$$

$$K_3 = 0.89 \mu\text{IN.}$$

$$U_3 = 0.89 \times 1234 = 1098$$

STRAIN RELIEF MEASUREMENTS

BORING NO. RS - 4

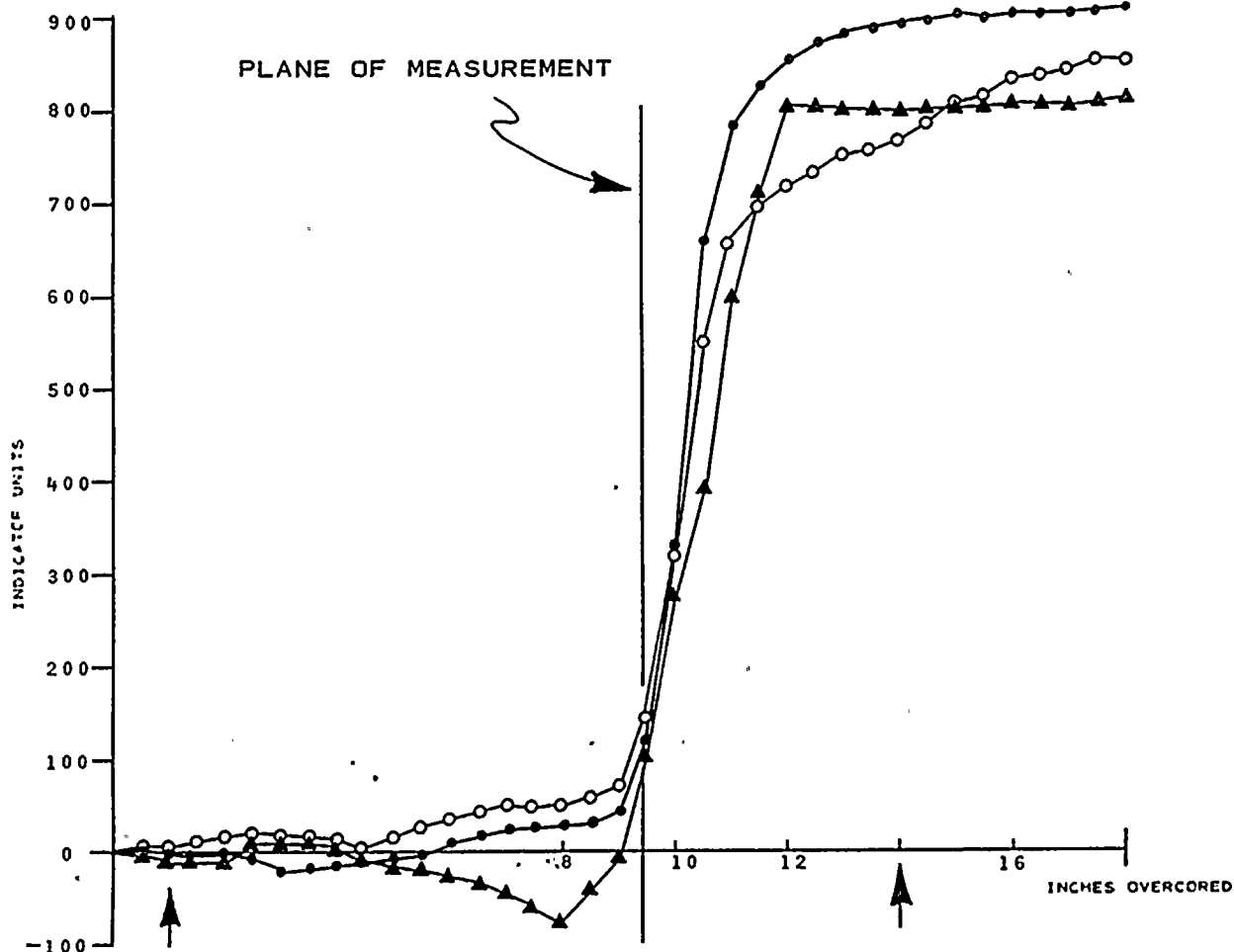
TEST NO. 17

DEPTH 68'7"

NOTE: A POSITIVE INCREASE IN INDICATOR UNITS INDICATES EXPANSION OF THE EX HOLE DURING OVERCoring

ARROWS (↓) INDICATE TOTAL DEFORMATION USED TO CALCULATE STRESS

PLATE E-104
DAMES & MOORE



KEY:

▲ AXIS I	$\Delta R_1 = 798 - (-2) = 800$
○ AXIS II	$\Delta R_2 = 767 - 7 = 760$
● AXIS III	$\Delta R_3 = 890 - (-3) = 893$

$K_1 = 0.95 \mu\text{IN.}$	$U_1 = 0.95 \times 800 = 760$
$K_2 = 1.00 \mu\text{IN.}$	$U_2 = 1.00 \times 760 = 760$
$K_3 = 0.94 \mu\text{IN.}$	$U_3 = 0.94 \times 893 = 839$

ROCK TYPE: INTERBEDDED MEDIUM TO DARK GRAY ARGILLACEOUS SANDSTONE AND LIGHT GRAY SILICEOUS SANDSTONE, OCCASIONAL SHALE LAMINATIONS

STRAIN RELIEF MEASUREMENTS

BORING RS - 4

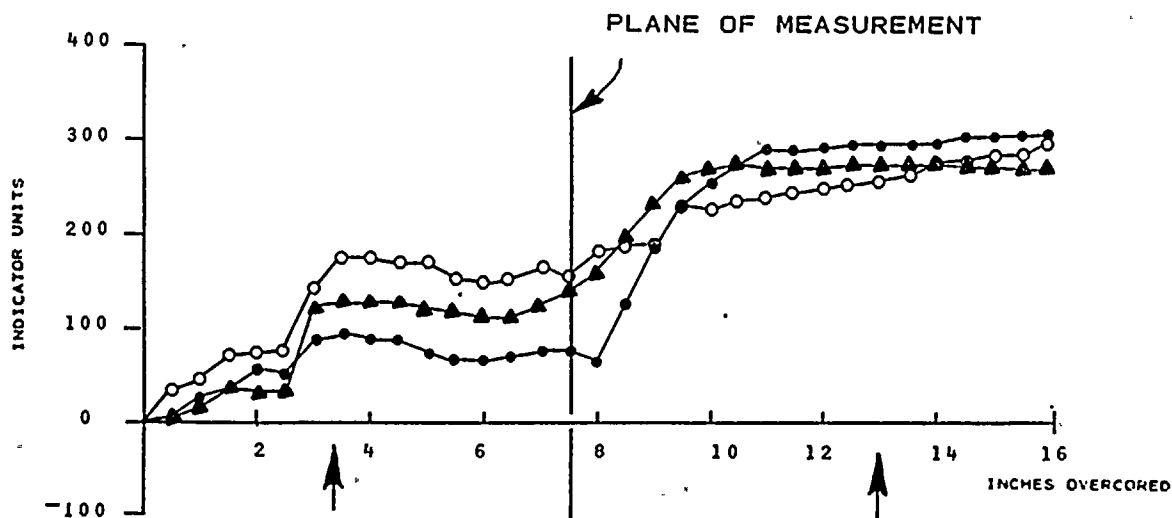
TEST NO. 19

DEPTH 71'3"

NOTE: A POSITIVE INCREASE IN INDICATOR UNITS INDICATES EXPANSION OF THE EX HOLE DURING OVERCORING

ARROWS (f) INDICATE TOTAL DEFORMATION USED TO CALCULATE STRESS





KEY:

▲ AXIS I	$\Delta R_1 = 276 - 132 = 144$
○ AXIS II	$\Delta R_2 = 257 - 174 = 83$
● AXIS III	$\Delta R_3 = 75 - 63 = 12$

$K_1 = 0.95 \mu\text{IN.}$	$U_1 = 0.95 \times 144 = 137$
$K_2 = 0.94 \mu\text{IN.}$	$U_2 = 0.94 \times 83 = 78$
$K_3 = 0.91 \mu\text{IN.}$	$U_3 = 0.91 \times 12 = 11$

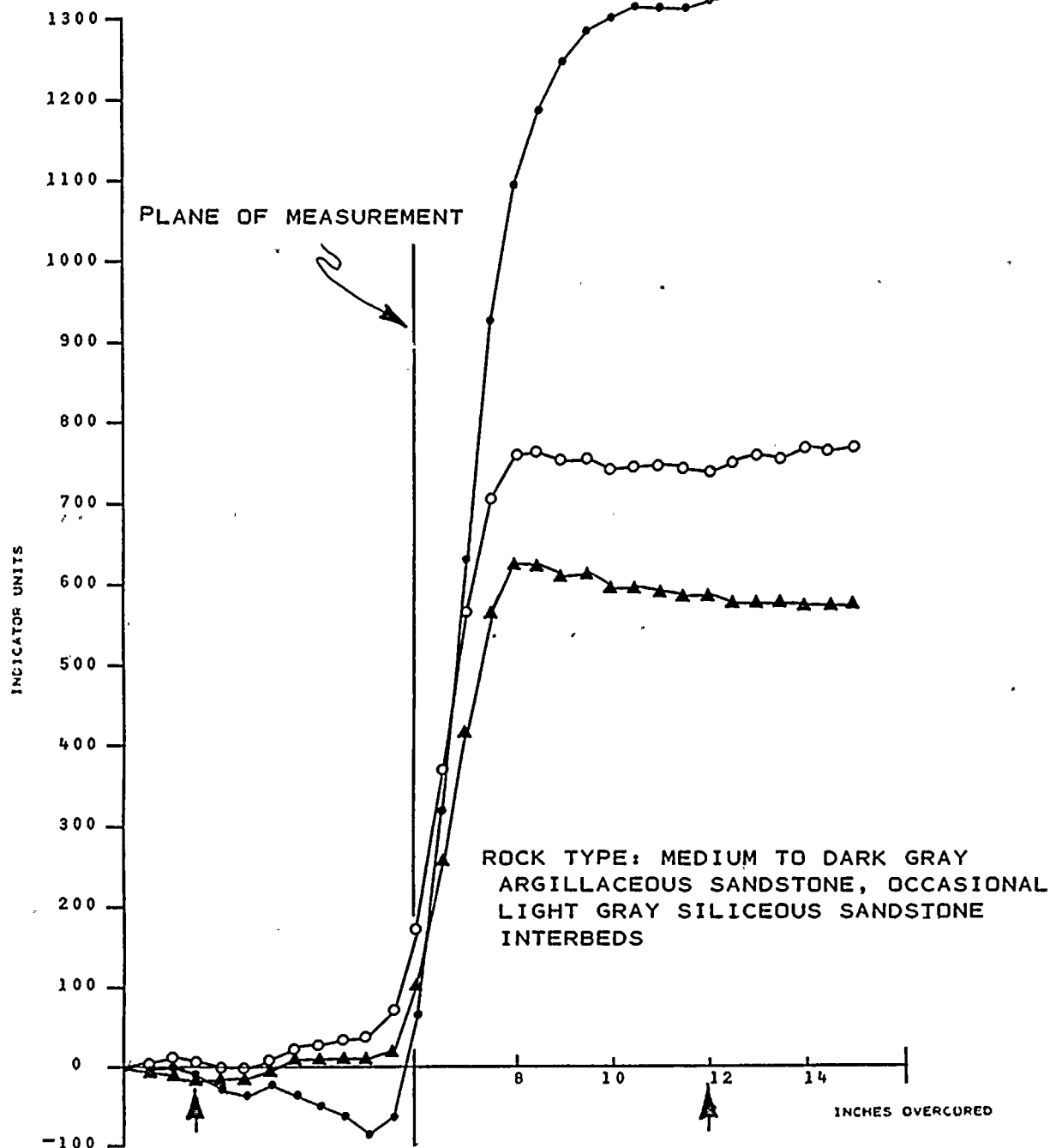
ROCK TYPE: LIGHT GRAY SILICEOUS SANDSTONE

STRAIN RELIEF MEASUREMENTS
 BORING RS - 4
 TEST NO. 24
 DEPTH 80' 10 1/2"

NOTE: A POSITIVE INCREASE IN INDICATOR UNITS
 INDICATES EXPANSION OF THE EX HOLE
 DURING OVERCORING

ARROWS (↑) INDICATE TOTAL DEFORMATION
 USED TO CALCULATE STRESS

PLATE E-106
 DAMES & MOORE



KEY:

- ▲ AXIS I
- AXIS II
- AXIS III

$$\Delta R_1 = 582 - (-15) = 597$$

$$\Delta R_2 = 739 - 2 = 737$$

$$\Delta R_3 = 1322 - (-11) = 1333$$

$$K_1 = 0.95 \mu\text{IN.}$$

$$U_1 = 0.95 \times 597 = 567$$

$$K_2 = 0.94 \mu\text{IN.}$$

$$U_2 = 0.94 \times 737 = 693$$

$$K_3 = 0.91 \mu\text{IN.}$$

$$U_3 = 0.91 \times 1333 = 1213$$

STRAIN RELIEF MEASUREMENTS

BORING NO. RS - 4

TEST NO. 25

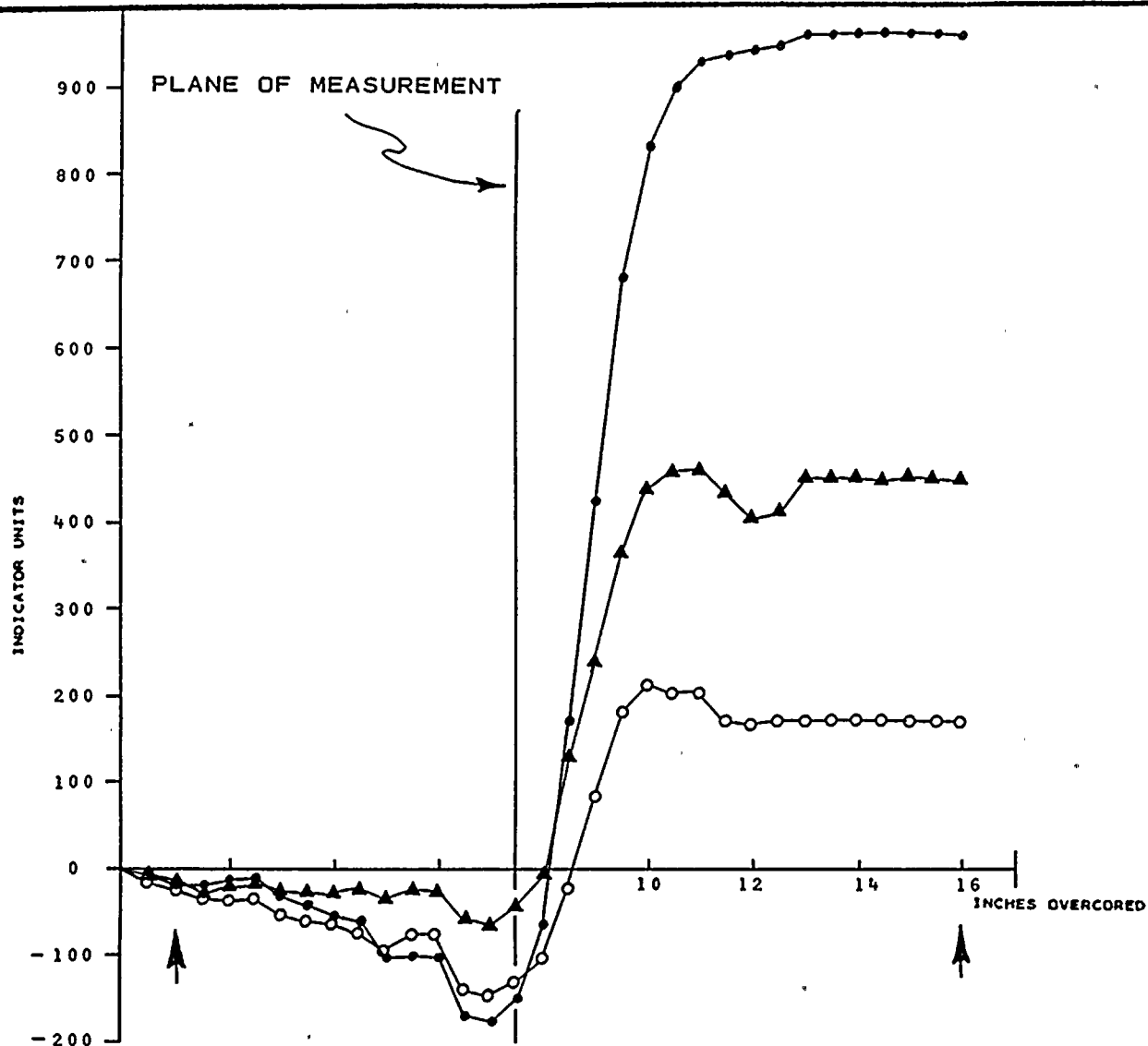
DEPTH 82' 1 1/2"

NOTE: A POSITIVE INCREASE IN INDICATOR UNITS INDICATES EXPANSION OF THE EX HOLE DURING OVERCURING

ARROWS (↓) INDICATE TOTAL DEFORMATION USED TO CALCULATE STRESS

PLATE E-107
DAMES & MOORE





KEY:

▲ AXIS I	$\Delta R_1 = 450 - (-15) = 465$
○ AXIS II	$\Delta R_2 = 169 - (-25) = 194$
● AXIS III	$\Delta R_3 = 981 - (-15) = 996$

$K_1 = 1.01 \mu\text{IN.}$	$U_1 = 1.01 \times 465 = 470$
$K_2 = 0.96 \mu\text{IN.}$	$U_2 = 0.96 \times 194 = 186$
$K_3 = 0.96 \mu\text{IN.}$	$U_3 = 0.96 \times 996 = 956$

ROCK TYPE: MEDIUM TO DARK GRAY ARGILLACEOUS SANDSTONE
WITH SHALE INTERBEDS

STRAIN RELIEF MEASUREMENTS

BORING RS - 4

TEST NO. 27

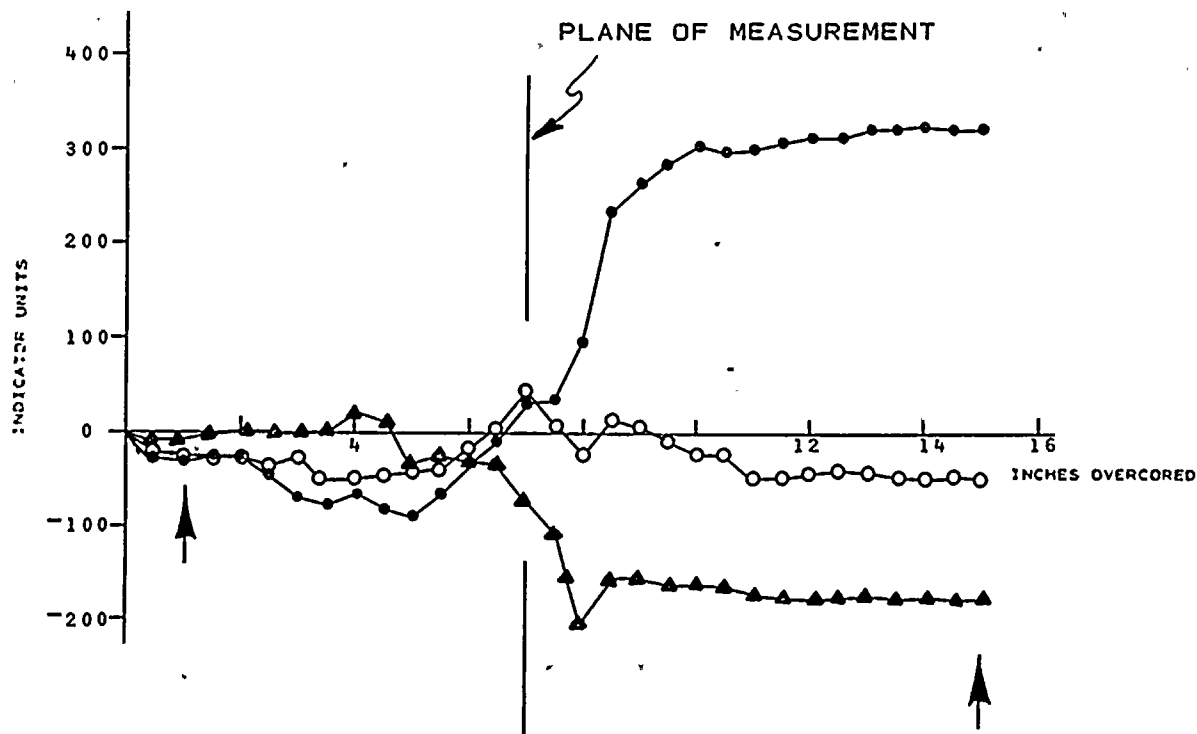
DEPTH 83'11"

NOTE: A POSITIVE INCREASE IN INDICATOR UNITS
INDICATES EXPANSION OF THE EX HOLE
DURING OVERCORING

ARROWS (↓) INDICATE TOTAL DEFORMATION
USED TO CALCULATE STRESS

PLATE E-108
DAMES & MOORE





KEY:

▲ AXIS I	$\Delta R_1 = -180 - (-15) = -165$
○ AXIS II	$\Delta R_2 = -48 - (-21) = -69$
● AXIS III	$\Delta R_3 = 320 - (-33) = 353$

$K_1 = 1.01 \mu\text{IN.}$	$U_1 = 1.01 \times -165 = -167$
$K_2 = 0.96 \mu\text{IN.}$	$U_2 = 0.96 \times -69 = -66$
$K_3 = 0.96 \mu\text{IN.}$	$U_3 = 0.96 \times 353 = 339$

ROCK TYPE: DARK GRAY SILTSTONE TO ARGILLACEOUS
SANDSTONE WITH LIGHT TO MEDIUM GRAY
SILICEOUS SANDSTONE INTERBEDS

STRAIN RELIEF MEASUREMENTS

BORING NO. RS - 4

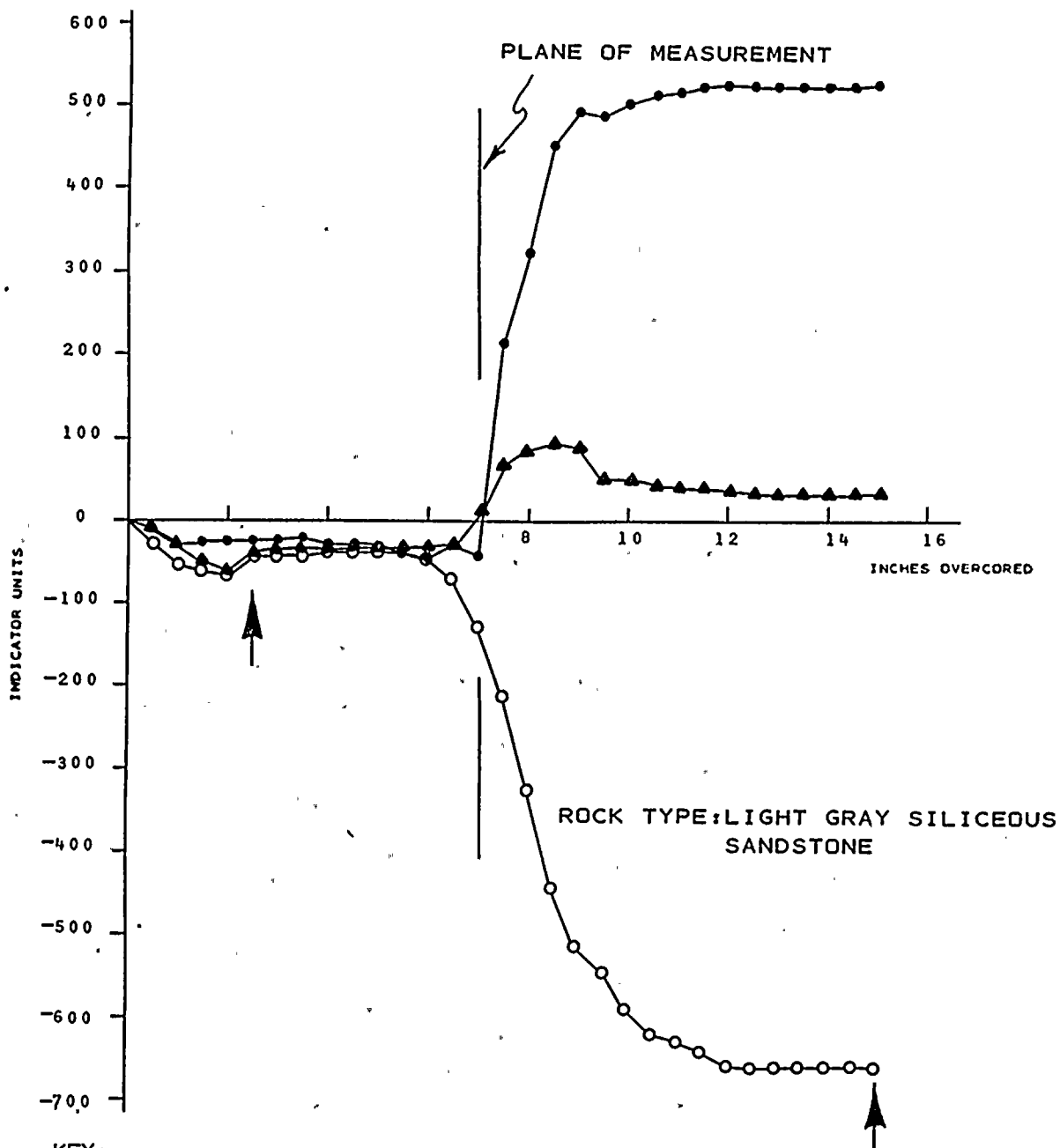
TEST NO. 28

DEPTH 35'3"

NOTE: A POSITIVE INCREASE IN INDICATOR UNITS
INDICATES EXPANSION OF THE EX HOLE
DURING OVERCORING

ARROWS (↔) INDICATE TOTAL DEFORMATION
USED TO CALCULATE STRESS





KEY:

- ▲ AXIS I
- AXIS II
- AXIS III

$$\begin{aligned}\Delta R_1 &= 32 - (-40) = 72 \\ \Delta R_2 &= -659 - (-42) = -617 \\ \Delta R_3 &= 524 - (-25) = 549\end{aligned}$$

$$K_1 = 1.03 \mu\text{IN.}$$

$$U_1 = 1.03 \times 72 = 74$$

$$K_2 = 0.98 \mu\text{IN.}$$

$$U_2 = 0.98 \times -617 = -605$$

$$K_3 = 1.00 \mu\text{IN.}$$

$$U_3 = 1.00 \times 549 = 549$$

STRAIN RELIEF MEASUREMENTS

BORING NO. RS - 4

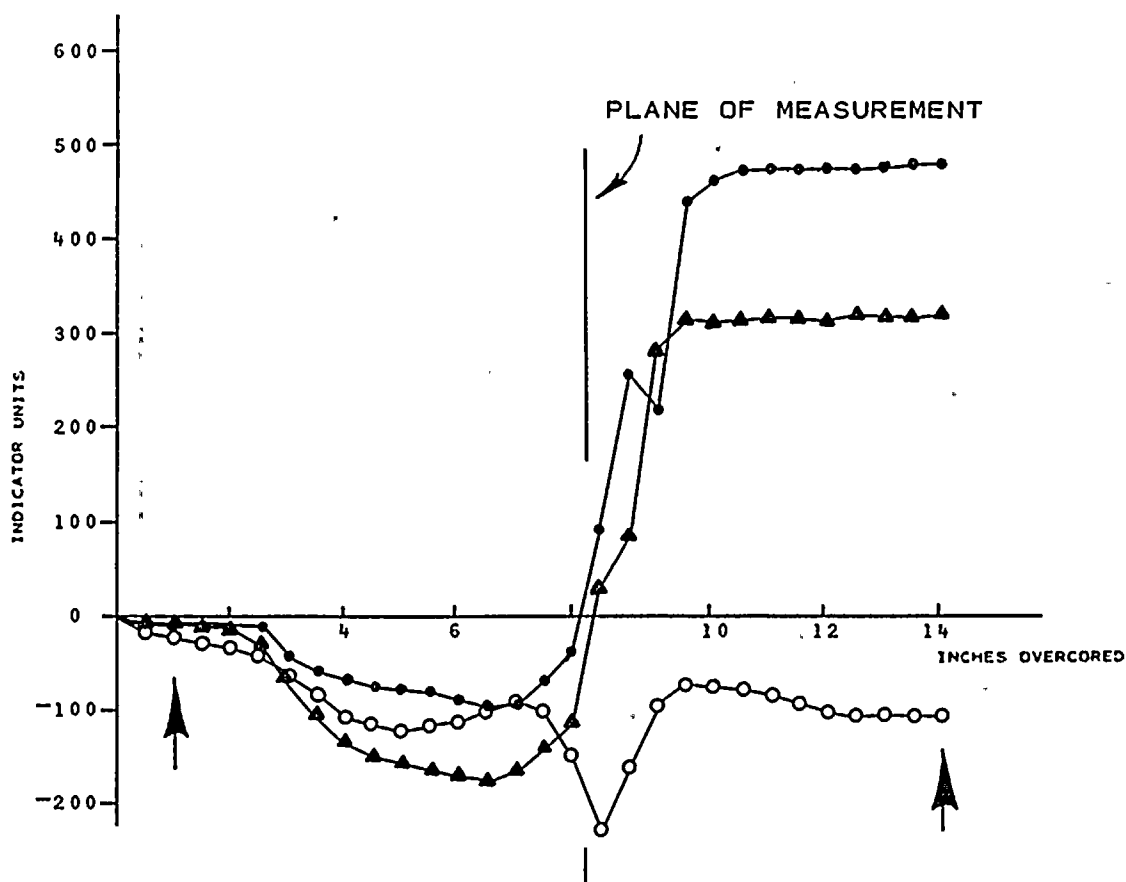
TEST NO. 33

DEPTH 91'6"

NOTE: A POSITIVE INCREASE IN INDICATOR UNITS INDICATES EXPANSION OF THE EX HOLE, DURING OVERCUTTING

ARROWS (↓) INDICATE TOTAL DEFORMATION USED TO CALCULATE STRESS





KEY:

- ▲ AXIS I
- AXIS II
- ◆ AXIS III

$$\Delta R_1 = 318 - (-13) = 331$$

$$\Delta R_2 = -109 - (-22) = -87$$

$$\Delta R_3 = 479 - (-9) = 488$$

$$K_1 = 1.03 \mu\text{IN.} \quad U_1 = 1.03 \times 331 = 341$$

$$K_2 = 0.94 \mu\text{IN.} \quad U_2 = 0.94 \times -87 = -82$$

$$K_3 = 1.05 \mu\text{IN.} \quad U_3 = 1.05 \times 488 = 512$$

ROCK TYPE: INTERBEDDED ARGILLACEOUS SANDSTONE, 'LIGHT GRAY
SILICEOUS SANDSTONE AND BLACK SHALE

STRAIN RELIEF MEASUREMENTS

BORING NO. RS - 4

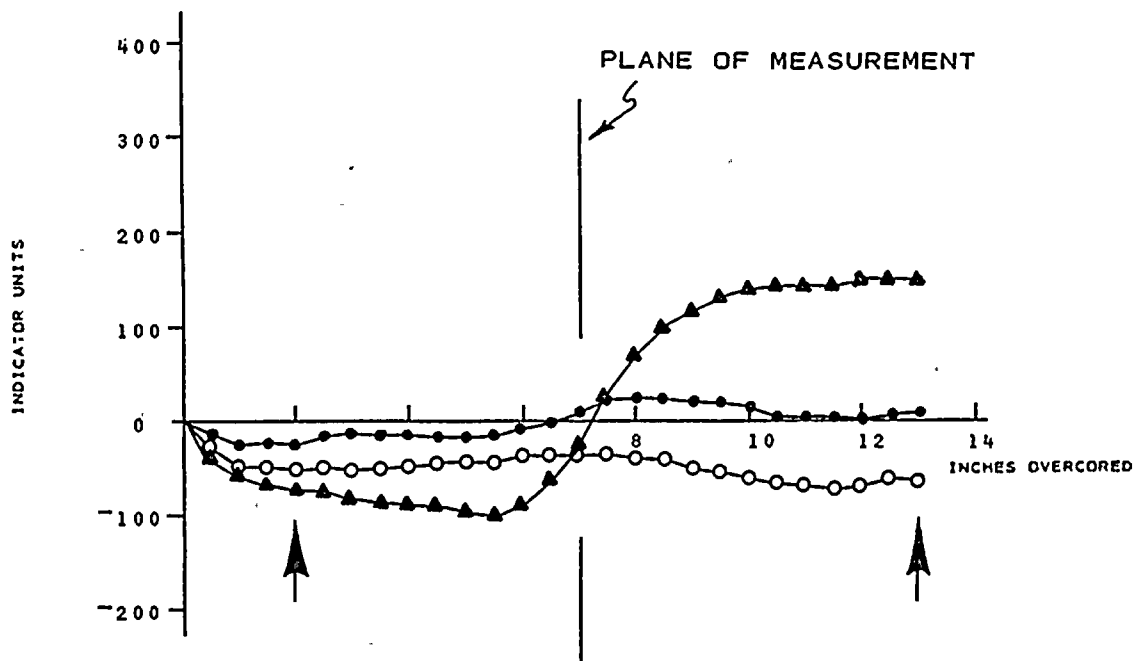
TEST NO. 49

DEPTH 115' 9 3/4"

NOTE: A POSITIVE INCREASE IN INDICATOR UNITS
INDICATES EXPANSION OF THE EX HOLE
DURING OVERCORING

ARROWS (↔) INDICATE TOTAL DEFORMATION
USED TO CALCULATE STRESS





KEY:

▲ AXIS I	$\Delta R_1 = 148 - (-73) = 221$
○ AXIS II	$\Delta R_2 = -60 - (-54) = -8$
● AXIS III	$\Delta R_3 = 8 - (-24) = 32$

$K_1 = 1.03 \mu\text{IN.}$	$U_1 = 1.03 \times 221 = 228$
$K_2 = 0.94 \mu\text{IN.}$	$U_2 = 0.94 \times -8 = -8$
$K_3 = 1.05 \mu\text{IN.}$	$U_3 = 1.05 \times 32 = 34$

ROCK TYPE: LIGHT GRAY SILICEOUS SANDSTONE

STRAIN RELIEF MEASUREMENTS

BORING NO. RS - 4

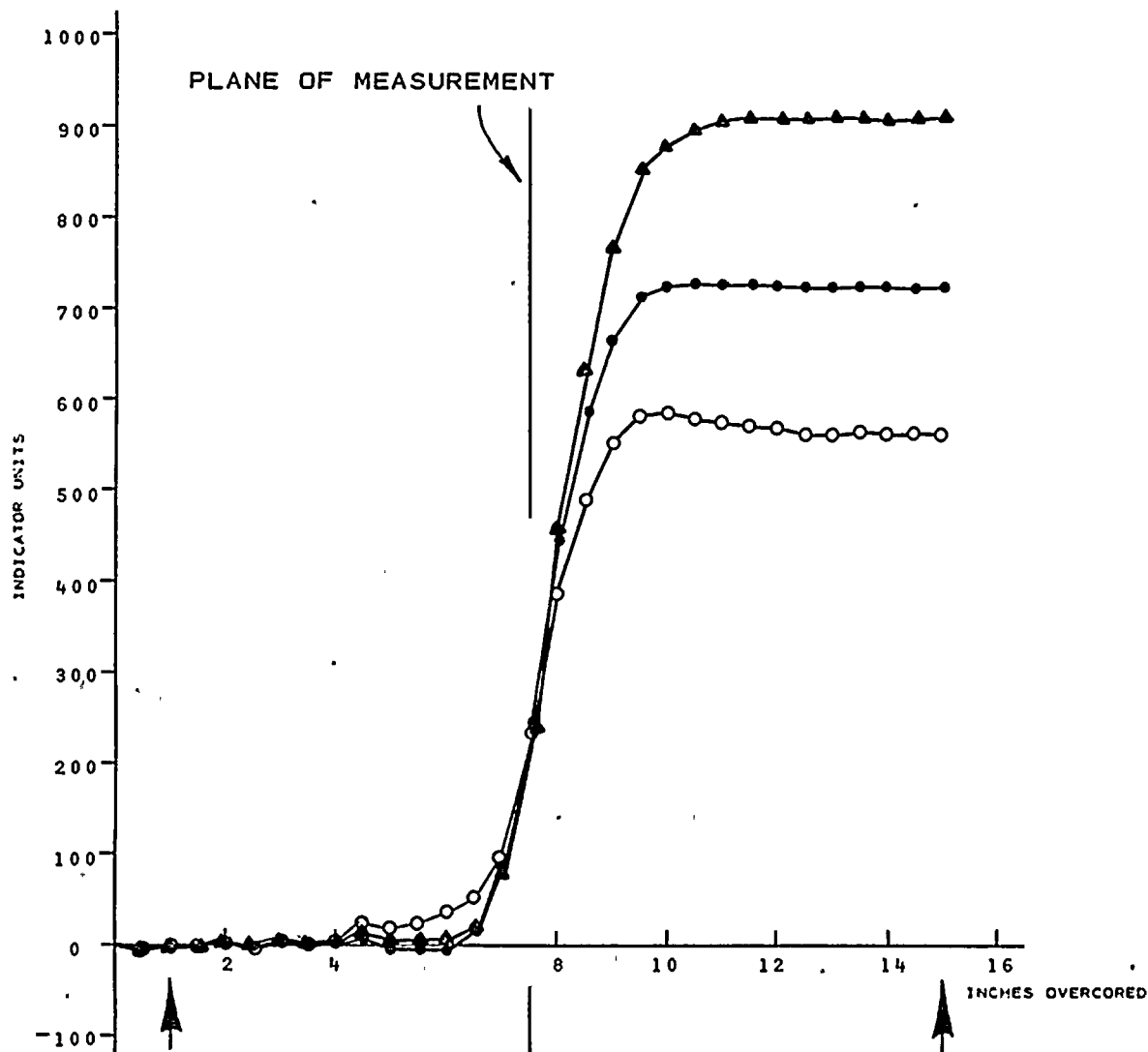
TEST NO. 50

DEPTH 116' 10 1/2"

NOTE: A POSITIVE INCREASE IN INDICATOR UNITS INDICATES EXPANSION OF THE EX HOLE DURING OVERCORING

ARROWS (4) INDICATE TOTAL DEFORMATION USED TO CALCULATE STRESS





KEY:

- ▲ AXIS I
- AXIS II
- AXIS III

$$\begin{aligned}\Delta R_1 &= 905 - (-3) = 908 \\ \Delta R_2 &= 560 - (-1) = 561 \\ \Delta R_3 &= 720 - (-3) = 723\end{aligned}$$

$$\begin{aligned}K_1 &= 1.03 \mu\text{IN.} & U_1 &= 1.03 \times 908 = 935 \\ K_2 &= 0.94 \mu\text{IN.} & U_2 &= 0.94 \times 561 = 527 \\ K_3 &= 1.05 \mu\text{IN.} & U_3 &= 1.05 \times 723 = 759\end{aligned}$$

ROCK TYPE: LIGHT GRAY SILICEOUS SANDSTONE TO DARK GRAY ARGILLACEOUS SANDSTONE

STRAIN RELIEF MEASUREMENTS

BORING RS - 4

TEST NO. 51

DEPTH 119'9"

NOTE: A POSITIVE INCREASE IN INDICATOR UNITS INDICATES EXPANSION OF THE EX HOLE DURING OVERCORING

ARROWS (↑) INDICATE TOTAL DEFORMATION USED TO CALCULATE STRESS



ASSESSMENT OF THE
RADWASTE STRUCTURE
AT
NINE MILE POINT
NUCLEAR STATION

BY

Neville J. Price, D.Sc. Ph.D. B.Sc.



INTRODUCTION

In this assessment of the Radwaste SStructure I have tried to keep to the spirit of the letter addressed to Mr. Markham by Mr. Klein. It has not proved possible to answer each of the points as expressed in this letter because the topic is complex and the questions are interrelated. The only point to which I do not apply myself is Item g). "Can further movement along the fault be impeded or prevent". My reasons for not doing so will become apparent.



AGE OF RADWASTE STRUCTURE

In a preliminary meeting the external consultants suggested the possibility, even probability, that the structure in question developed during the Palaeozoic. This is a viewpoint completely contrary to that expressed by the staff of Dames & Moore who hold that the structure occurred, in a near surface environment, in relatively recent times and that a significant proportion of the movement has taken place within the last 10,000 years.

On this issue I concur absolutely with the viewpoint held by the staff of Dames & Moore.

The Radwaste Structure has a general geometry which is similar to structures, found elsewhere, that have developed in sediments (directly comparable with those exposed at NMP) but which undoubtedly formed at depths of several kilometers. Hence, there is a superficial case for considering the Radwaste Structure to have formed at considerable depths.

Let us play Devils Advocate and make the assumption that the Radwaste Structure was formed at depth. In order that the brittle deformation and void spaces (which are such conspicuous features of the Radwaste Structure) could have developed, it would be necessary to postulate that the effective vertical confining pressure was close to zero. That is, the fluid pressure (P) would have been almost equal to the total vertical



pressure (S_z) (here we introduce the symbol $\lambda [= P/S_z] \approx 1.0$) Such conditions are known to develop in the crust. However, not only must the fluid pressure be high but there must also be sufficient quantities of fluid available, in order to fill and support the void spaces. When such conditions actually exist in structures elsewhere in the world, and when the P.T. and chemistry of the fluids is suitable, hydrothermal minerals develop in the voids to form veins and vugs. Vein material (e.g. calcite) [which yields high temperatures data from homogenisation temp tests on bubble inclusions] has not developed in the void spaces. Yet it is known that conditions in these sediments were conducive to the deposition of hydrothermal calcite in fractures etc. during Palaeozoic times.

Thus, the absence of calcite veins etc. which yield high homogenisation temperatures mitigates against the concept that the Radwaste Structure formed at depth during the Palaeozoic times.

Let us now consider the physical properties of the brecciated materials in the Radwaste Structure. This material is a dense, silty clay. One can extract it from the fault zone and deform it between ones fingers. It is ductile and relatively uncompacted. Such material would certainly be produced in a deep structure which formed when $\lambda=1.0$. However, high fluid pressures are transient. It has been argued [N.M.P. Report, Appendix III-L] that when the normal faults (on site) were initiated the fluid pressure was about 6000 lb in² at a



time when the vertical pressure S_z was 12,500 bm^2 i.e. $\lambda=0.48$. Thus, if the Radwaste breccia formed at depth, when $\lambda=1.0$, it would subsequently have experienced very considerable compaction and would have been transformed into moderately competent material which could not be deformed by digital pressure.

When one turns to the alternative proposal [i.e. that the Radwaste Structure is one which developed under near-surface condition and that significant movement has occurred during the last 10,000 years] the available evidence slots nicely into place.

- 1) The confining pressure under near surface conditions is low - so that void spaces present no problem.
 - 2) The rocks are "cold" - so brittle behaviour is to be expected.
 - 3) What calcite is formed in association with the Radwaste Structure is the result of "low temperature" mineralization.
 - 4) Post-glacial lacustrine deposits are included into and deformed by the structure. [In this context one may note that the generation of void spaces in the structures will result in the induction (sucking-in) of clay laden water. One would not merely need to rely on the "washing in" of material by migrating ground water]
- and finally
- 5) The breccia has been subjected to little vertical load and therefore has had no opportunity to compact.



The Dames & Moore conclusions are beyond reasonable doubt and must be accepted. One must assume that the structure formed in the recent past and that the whole 7 foot of displacement developed in a near surface environment.

We are here concerned with safety problems of monumental proportions. The onus of proof rests with anyone who advocates that the Radwaste Structure is of Palaeozoic age. I suggest that this is a task or a challenge which no competent geologist would be prepared to accept.

Geometry and Extent of Radwaste Structure

In Figure 1 A-C, I have attempted to indicate the geometries in plan and section. It is emphasised that the geometries are presented in an extremely simplistic manner. For example, in Figure 1C the "Ramp" in the profile through the structure is represented as a simple linear feature; whereas, we know that in the Radwaste Trench the ramp geometry is complex. Never-the-less, these figures enable one to indicate the magnitude of the problems of interpretation which face us. The facts available to us regarding the geometry available to us are: -

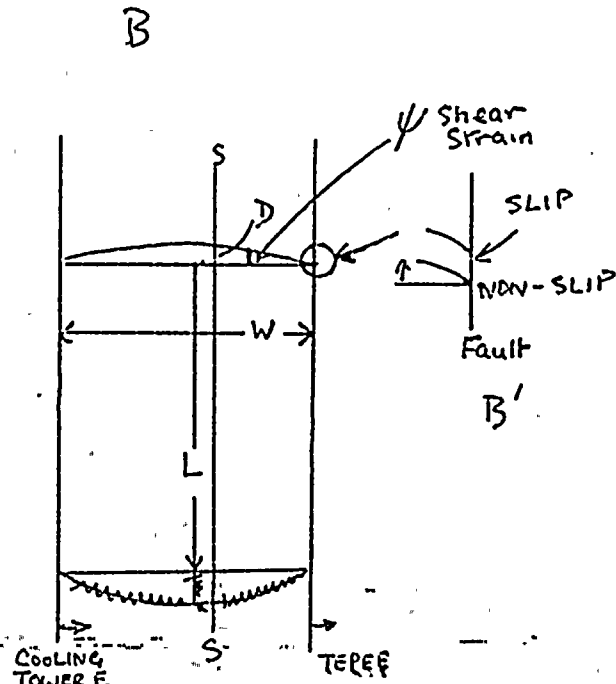
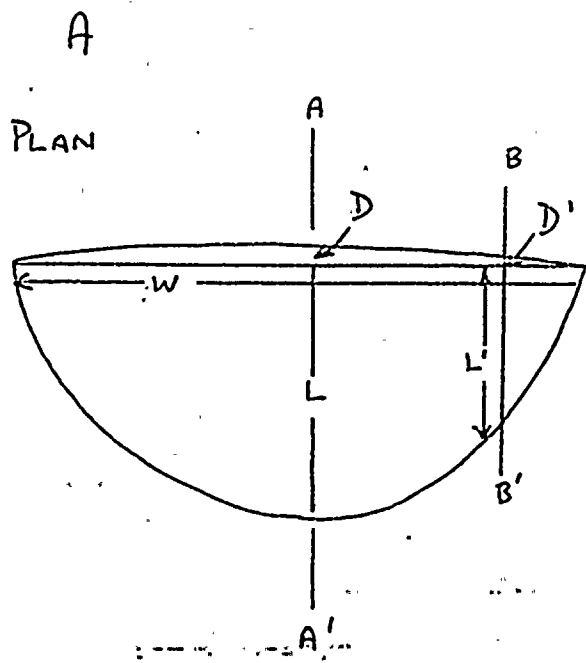
- 1) the displacement D (or D' in Figure 1A)
- 2) the uplift U (or U')
- 3) the general direction of transport and
- 4) an average value for θ_R .

Otherwise our ignorance of the structures geometry is complete.

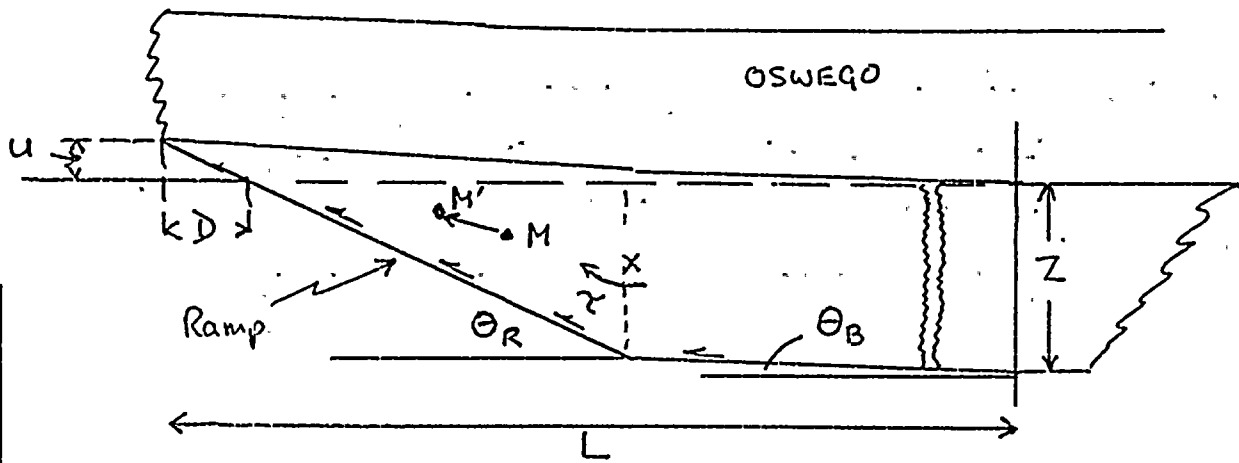
In plan, the structure could have the outline indicated in Figure 1A. If so, where does the section through the Radwaste Trench



REVISIONS
 BY _____ DATE _____ TO EO _____
 BY _____ DATE _____ TO EO _____



SECTION C



BY _____ DATE _____
 CHECKED BY _____
 COPY TO EO _____

occur on this plan? It would indeed be surprising if the section coincided with the maximum dimension of L (along AA'). The Radwaste section could be along BB' - or anywhere else in the structure. A second possibility is that the Radwaste structure is confined between the Cooling Tower and Teepee faults as indicated in Figure 2B. For this situation the fault boundaries may have behaved as non-slip planes, or planes along which the Radwaste Structure detached itself and exhibited some degree of slip (see Figure 1B'). The fault boundary conditions influence the mode of dissipation of the energy that gave rise to the Radwaste Structure. If lateral slip took place energy would be absorbed by frictional sliding. Alternatively if horizontal slip did not take place on these fault boundaries energy would be absorbed in developing a shear strain (γ) [One may infer that shear strain energy would also be stored in the rocks if the plan of the Radwaste Structure is as represented in Figure 1A]. This non-slip situation has the greater danger potential, as far as the engineering structures are concerned. In assessing the Radwaste structure it is obviously important to establish the dip and extent of the ramp (Figure 1C) and to determine whether the ramp turns into bedding plane slip (and if so at what depth Z this occurs). If Z and θ_R are known it is possible to estimate the stresses needed to overcome friction and move the rock mass (M) on the ramp [Energy is also absorbed in initiating fractures, buckling, overcoming the resistance of the steps on the ramp and in the hysteresis of flexuring of the beds as they transfer, near line X in Figure 1C from bedding slip to ramp-slip. The energy consumed by these elements in these brackets, are not



easily assessed and will be ignored].

Thus, we can set up an approximate stress equation of

$$S_I - [S_\psi + S_{\text{slip}} - S_E] = S_R$$

where S_I = The initial stress state that resulted

in the development of the Radwaste Structure.

S_ψ = The stresses used to induce the shear strains ψ

S_{slip} = The stresses needed to overcome slip and
cause mass transfer

S_E = The stress available to cause elastic recovery
and give rise to displacements D and U

S_R = The residual ground stresses still obtaining.

Some constraints can be placed on the probable maximum value of S_I . Reasonable estimates can be put forward for the residual stresses S_R . If a specific model is chosen and values of Z , W etc. are assumed, then it is possible to estimate the stresses S_{slip} and S_ψ needed to induce slip and shear strain in any model per unit lengths L_u . Thus, S_E can be estimated for some length L which is compatible with the other stresses and dimensions. When this exercise is completed we are in a position to estimate future monuments etc. which could be or may be induced by the residual stresses (S_R) - FOR ONE SPECIFIC MODEL.

The first question then, is which model to choose?

Choice of Model

If one assumed the Radwaste Structure had a plan comparable

with that in Figure 1A - it immediately becomes apparent that, because one has no knowledge of the position of the Radwaste section in this plan, one cannot put any constraints on the size of the structure. This would lead to open ended estimates and exploration. Fortunately, there are reasons, other than convenience, which leads one to consider the second model, represented in Figure 1B, in which the Radwaste Structure is contained in two faults.

I argued in NMP Report, Appendix III that the cross-flexures associated with the development of normal faulting could give rise to high stress values approximately parallel to the trend of the normal faults. These stresses it was suggested could have given rise to the structures observed in the Heater Bay excavations.

The magnitude of structure which could be inferred from the analysis, presented in Appendix III, was small i.e. displacements of inches and fracture extent measured in a few tens of feet. At the time I conducted this analysis the existence of the Demster complex was unknown. Hence, the conclusions reached in the earlier analysis needs to be revised.

From the distribution of stratum contours presented by the N.Y. State E&G Corporation [Figure s.5-16] it is obvious that, during its development, the Demster Structure caused flexuring of the Oswego Sandstone and adjacent units. As one



would expect, this effect decreases with distance from the Demster Structure. At a distance of 5 miles its influence is likely to be limited to bringing about an increase in the NW-SE stresses and causing a relatively small degree of augmentation of existing minor structural flexures. It is suggested, therefore, that the predicted gentle flexure or roll in the vicinity of the Heater Bay increased in amplitude and wavelength because of the influence of the Demster Structure. In so doing, the extent of the zone of high stresses, also predicted in the previous analysis, became sufficiently extensive that, when the strata was uplifted to near surface environments, they eventually gave rise to the Radwaste Structure.

The original deflexions caused by movement on the normal fault changed at the fault plane. It is likely that when these original deflexions were augmented, the fault planes continued to represent boundaries to the lateral development of the flexure. Hence, the plan represented in Figure 1B is the model which most probably represents the extent of the Radwaste Structure.

It has been noted that the boundary conditions which are likely to cause greatest danger to Engineering structures is that in which strike-slip movement along the inclined fault planes is completely inhibited - with the consequence that horizontal shear strains of considerable magnitudes may develop in the

rocks in the hanging wall of the Radwaste Structure. Because we are concerned with safety we are obliged to consider the worst possible condition. At first sight this would appear to exist when both boundaries are fixed along the fault planes. As we shall see, if slip occurs on one plane and not on the other this could possibly represent a situation of even greater potential danger.

Initial Stress S_I

One could write at length on the pros and cons of any suggested magnitude of stress S_I . Hence, I will follow the conclusion presented in the previous analysis (Appendix III) and take the differential stress at failure to be 23,000 lb in². It has been argued, hence and elsewhere, that the Radwaste Structure developed under near surface conditions. That is the confining pressure was very small: so one can take the magnitude of stress S_I (acting N60°E) to be 23,000 lb in².

Residual Stresses (S_R)

The stresses (in the N60°E direction) which currently exist in the near surface rocks and which probably exist at modest depths can be taken to have an average value of 2000 lb in².

Stresses Required to Induce Sliding (S_{slip}) and Shear Strain ($S\psi$)

As noted earlier, to estimate these quantities (i.e. S_{slip} and $S\psi$) it is necessary to attribute specific values to W , Z , θ_{ramp} (θ_B we can put at zero) and L . In our model the slip is contained between the faults so $W=2,600$ ft. Let us assume $Z=100$ ft and that

$\theta_{\text{ramp}} = 20^\circ$. The value of L must be chosen to be compatible with all other parameters. This value can be obtained analytically or by trial and error. In the time available I chose the latter cause of action and arrived at a value $L = 2100$ ft.

$S_{\text{(slip)}}$

By taking values of $\mu = 0.4$ for sliding friction on bedding and using $\mu = 1.0$ as a fudge factor for sliding on the ramp - thereby accommodating some of the effects of ramp roughness - one obtains a value that $S_{\text{(slip)}} \approx 850 \text{ lb in}^2$.

Stress (S_ψ) Required to Induce Shear Stress ψ

To calculate this quantity I have assumed point loading which gives rise to a chevron like distribution of shear stress (see Figure 2). More correctly one should use the correct deflexion model (also indicated on Figure 2). However, lack of time and reference facilities prevented me from doing so. Using this point loaded, chevron shear strain model and taking the average shear strain to be 0.0027 (i.e. 3.5 ft/1300 ft) and the shear modulus $G = 1.75 \times 10^6 \text{ lbs in}^2$; then $S_\psi \approx 9400 \text{ lb in}^2$. This value would be smaller using the correct strain model, but it will suffice for our purposes.

Stress (P_E) Available to Cause Elastic Recovery and Displacement (D)

All the quantities, except one, for the stress equation

$$S_I - [S_\psi + S_{\text{slip}} + S_E] = S_R$$

have been found. Consequently, $S_E =$



$$S_I - S_\psi - S_{\text{slip}} - S_R = 23,000 - 9400 - 850 - 2000 = 11,750 \text{ lb in}^2$$

If we take $L = 2100 \text{ ft}$, $S_E = 11,750 \text{ lb in}^2$ and $E = 3.5 \times 10^6 \text{ in}^2$: then the predicted displacement (D_{pr}) = 7.05 ft. Thus, the predicted displacement is well within the likely error band for the displacement D estimated from the field data.

Using the Model to Predict Future Movements on Radwaste Structure

One may infer from the above argument that high stresses continue to obtain in the site rocks. This we already knew, of course. The total magnitude of the stresses contain two components (this is a point I deliberately skated over when considering the value of the residual stresses). They are 1) the "residual stresses" which are still available to cause movement on the Radwaste Structure and 2) the stresses associated with the shear strains induced by previous movements on the Radwaste Structure (these will not contribute to further movement on the geological structure - but, of course, would have considerable effect upon Engineering Structures - a point to which I will return).

What movements could be induced by the residual stresses in the future? If we take $S_R = 1000 \text{ lb. in}^2$ and note that the stress (S_{slip}) needed to induce further movement is 850 lb in^2 then only 150 lb in^2 remains available to induce further shear strain and by further elastic recovery to give rise to a further increment of displacement. For the values of L , E , etc. previously used we are dealing with further increments of displacement of less than 1.0 inch.



Fig 2

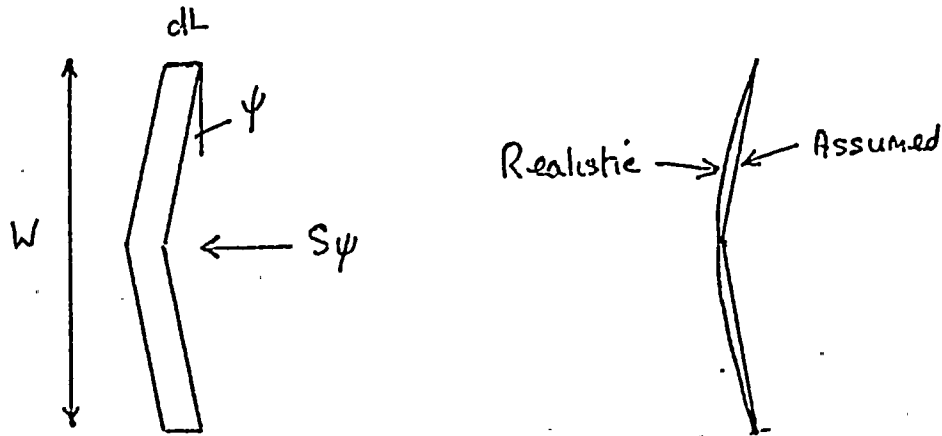
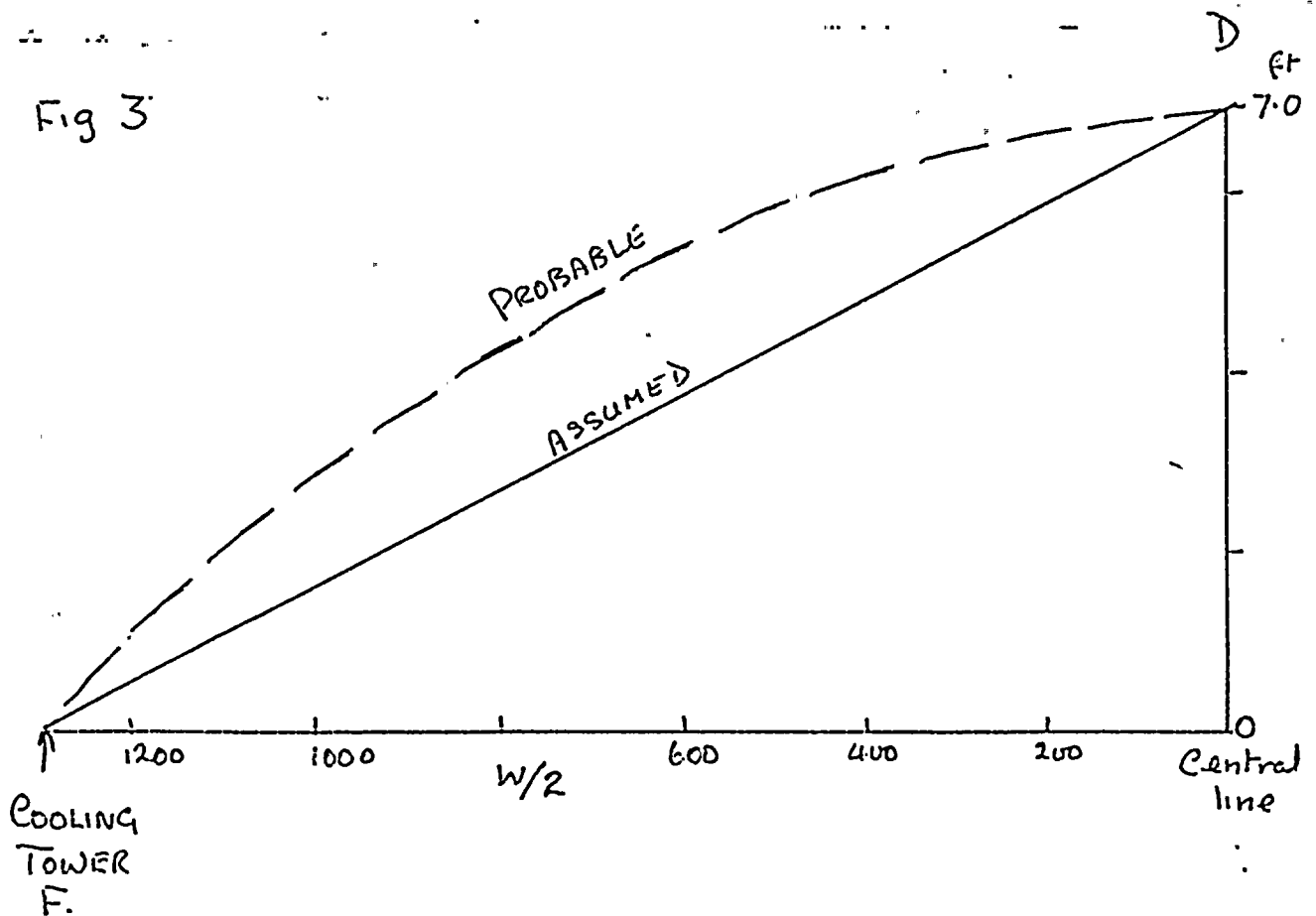


Fig 3



This displacement refers only to this model and only for the values of stresses used. A whole spectrum of values could and should be used in calculations to delineate the possible range of movements which could be expected on the Radwaste Structure. Moreover this exercise should be repeated for other models with other boundary conditions. Only then could one predict probable tolerances of movement on the Radwaste Structure.

The corollary to this is that a limited programme of ground exploration should be carried out so that geological constraints may be placed on which model is applicable: and greater precision of prediction attained.

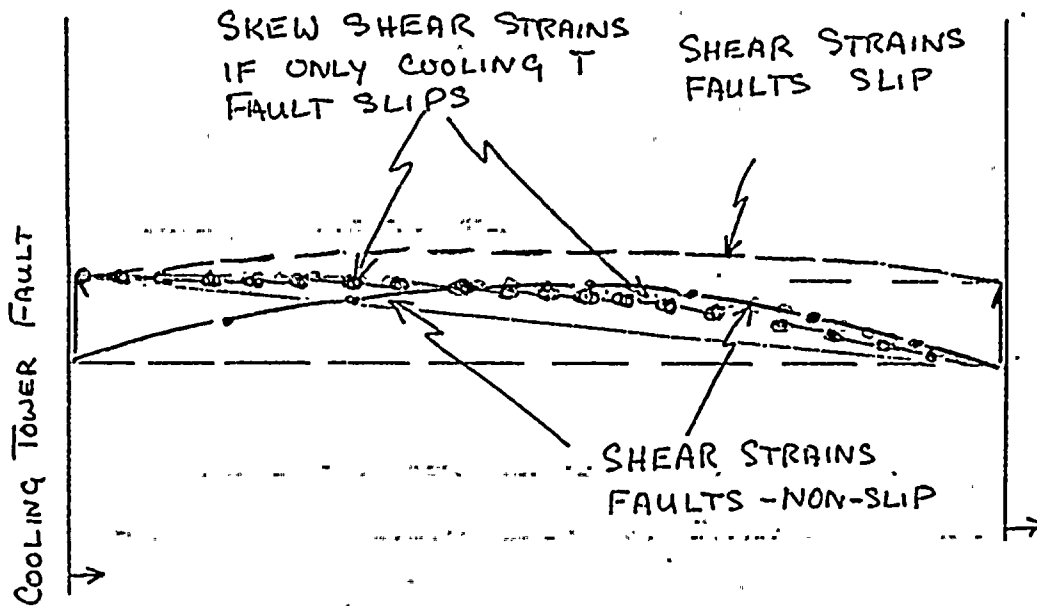
Modification of the Model

The stresses induced by shear strain invoked in the model are large. These were based on assumed average shear strains. The probable distribution of shear strain is curved, as indicated in Figure 3. (Unit 2 straddles the central line where the shear strains are at their smallest - but the engineering structure could experience shear strain recovery in a clockwise direction to the south and counter-clockwise to the north: which could cause compression on the E walls and tension on the W walls).

The shear strain and hence the shear stresses on the boundary faults (for this model) are therefore very high. They are probably sufficient to cause strike-slip on the boundary faults - or perhaps only on the Cooling Tower Fault. The argument presented for the simple model with rigid boundaries should therefore

FIG. 4

REVISIONS
 BY _____ DATE _____ TO EO _____
 BY _____ DATE _____ TO EO _____



BY _____ DATE _____
 CHECKED BY _____
 COPY TO EO _____

be extended to include an element of slip on one or both fault boundaries. If slip has occurred on both boundaries the shear strain component can be reduced (but cannot possibly go to zero). If slip has occurred on only the Cooling Tower Fault the shear strain distribution will be skew (see Figure 4) and almost certainly will vary with depth. This relationship of skew shear may already have made itself manifest in the trend of fold axes in the Radwaste Trench.

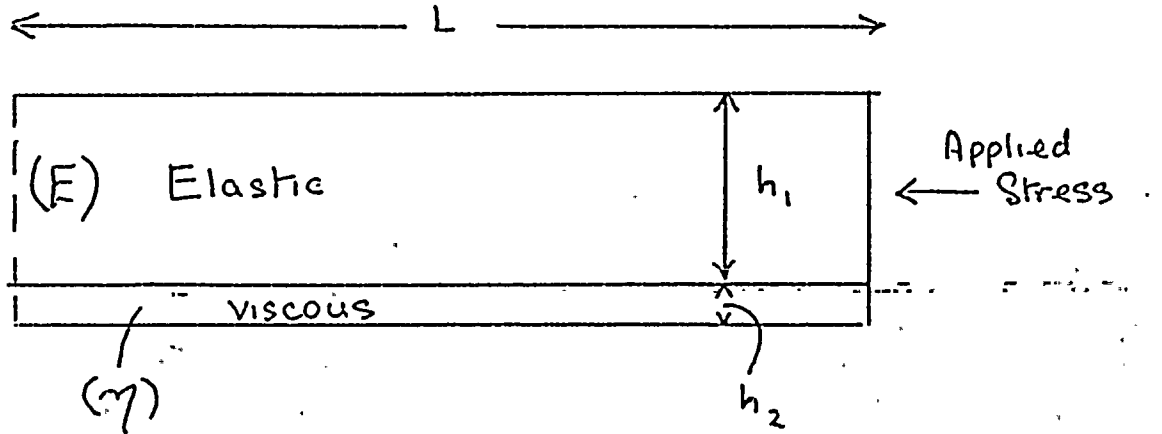
Once again one should emphasise that these shear strains induced by the Radwaste Structure are stable - until you dig a hole! Then your trouble begins. Stress measurements and displacement patterns around holes at selected points on site will help determine the magnitude of the engineering problems to be faced - as well as being crucial in indicating the model which best fits the Radwaste Structure - and this in turn will lead to more confident predictions regarding future movements on the Radwaste Structure.

Rates of Movement

Here, I assume, we are concerned with the rates of movement associated with any possible further displacements of the Radwaste Structure. In particular, will such displacements give rise to vibratory ground motion?

The formation of brittle fracture must be accompanied by some microseismic activity. Hence the fracturing of individual beds, as seen in the Radwaste Trench, must have caused microshocks. However, the energy involved would be extremely small and would have no significant effect.

Fig. 5



E = Youngs Modulus
 γ = Coef. of viscosity

REVISIONS
 BY _____ DATE _____ TO EO _____
 BY _____ DATE _____ TO EO _____

BY _____ DATE _____
 CHECKED BY _____
 COPY TO EO _____

The main structure - I believe - is now, and for most of its life has been, aseismic. My reason for believing so is as follows. The basal movement plane, as exposed in the Radwaste Trench contains about 5 inches of relatively soft breccia. If this breccia extends under most of the Radwaste Structure (and it probably does) then it will exert the influence of a "shock-absorber".

The mechanism has been predicted on theoretical grounds and has been seen to operate in physical models.

The physical and theoretical models comprise a thick elastic cover on a thin viscous substratum as indicated in Figure 5. It can be shown that if a pressure is suddenly applied at one end of the model the time (T) in seconds taken for the stress wave to traverse distance L is given by:

$$T = \frac{\eta}{E} \cdot \frac{L^2}{h_1 h_2}$$

Where E is Youngs Modulus in dynes/cm² and η is in poise: The other dimensions are as indicated in Figure 5 and must be expressed in cms. One has to guess the viscosity of the breccia. It is weak but probably has a value $\eta = 10^{12}$ poise. Youngs Modulus $E = 2.4 \times 10^{11}$ dynes/cm². The thickness of elastic block $Z = h_1 = 30$ metres or 3000 cm. Let us assume that average thickness of breccia (h_2) is 10 cms and L, of course, is approximately 700 metres. Then

$$\begin{aligned} T &= \frac{10^{12}}{2.4 \times 10^{11}} \times \frac{[7 \times 10^4]^2}{10 \times 3000} = \frac{49 \times 10^{20}}{7.2 \times 10^{14}} = 7 \times 10^6 \text{ Sec} \\ &= 80 \text{ days} \end{aligned}$$



If η is significantly higher than 10^{12} poise the de-stressing period could last for years.

This concept helps one understand the slow closure of pits and cuts already made on site. The closures are a delayed elastic reponse.

Conclusions

- 1) The Radwaste Structure is a high level but aseismic structure.
- 2) Analysis of models will permit the possible range of movement on the structure to be forecast.
- 3) Limited field investigations recommended with the objectives
 - a) finding 'Z' - depth to bedding slip
 - b) establishing nature of intercept of Radwaste Structure and Cooling Tower Fault and
 - c) survey of shear strain distribution in the site area.

Opinion

We lack basic knowledge regarding the geometry and other parameters relating to the Radwaste Structure. Consequently, the possibility of new movements cannot be ruled out. However, even if it moves, it is my opinion (I cannot go further than this without further calculations) that the displacements will be small (say less than 3 inches in the horizontal direction - and possibly 1-1.5" in the vertical direction). The damage has already been done. Previous movements on the Radwaste Structure has changed the site area with compressional and shear strains.

Prior to the on-set of construction, these strains were in meta-stable equilibrium. Excavations for the erection of engineering structures have disrupted this equilibrium situation. The shear strains are potentially the most destructive. To assess the engineering problems it is necessary that better documentation be obtained relating to the magnitude and distribution of these strains in the site area.

Walter J. Rao

5th November 1979



FURTHER THOUGHTS ON THE STABILITY OF THE

NINE MILE POINT SITE

by

Neville J. Price, D.Sc., Ph.D.

An Internal and CONFIDENTIAL
Report for DAMES & MOORE

Introduction

The stability of the Nine Mile Point Area resolves itself into a number of distinct but interrelated problems. These can be categorised as:-

- 1) The future stability of the region regarding movements in a general northerly direction.
- 2) The stability of the Rad-waste Structure regarding movements in a direction N70°W.
- 3) The magnitude of the metastable shear-strains in the Site area and movements associated with their release as a result of engineering construction, and
- 4) The possible influence of vibratory ground motion on the stability of the area.

We shall discuss the problems indicated in these categories in the following sections.

1. Regional N-S Stability

The site is bounded to the north by Lake Ontario, the floor of which is inclined to the north at an average dip of 0.3° (figure obtained from the Times Atlas). Consequently, a considerable thickness of the sediments of the region which, in the Site area dip to the south at about 0.7° , crop out in the lake floor. The lake floor, therefore, constitutes a free surface.

The post-glacial rebound continues; and it can be shown that this will induce shear strains which will, in the next 40 years, reduce the resistance to sliding on bedding in a general northerly direction by approximately 6 lb.in^2 . This process of tilt and induced shearing has been going on for several thousand years. Consequently, it is extremely likely that this process has produced a condition of metastability in the area. As a result, slip along bedding planes has almost certainly occurred in the recent past. I consider that slip would have



occurred on a number of select bedding planes (where the inherent slip resistance was minimal) as soon as the shear stresses on these planes reached the critical value. Such slip planes are probably several, or tens of, feet apart in the Transition and Pulaski beds; but are rare and impersistent in the Oswego. Movement on these select bedding planes would probably produce thin layers of gouge material with a lower resistance to shear failure. In the arguments which follow, a coefficient of friction of $\mu = 0.3$ ($\phi = 16.7^\circ$) is assigned to these layers. (I have no evidence to justify this figure).

Thus, starting with the assumption that the sediments in the Site area are metastable and that they contain several planes of easy slip; what effects can be expected in the Site area if the resistance to sliding (in a northerly direction) is everywhere reduced by about 6 lb.in^2 in the next 40 years?

The effects are threefold. a) Slip on deep planes of easy slip can result in the bulk transport of the Site in a general northerly direction. b) The stress drop attendant upon this slip results in extension of the beds, i.e. north-south tensile strains will develop in the Site rocks, and c) Lateral regional variations in the amount of slip can result in lateral shear strains being induced in the Site rocks.

I will now consider these three aspects and attempt to quantify the amount of slip and extension which are likely to be induced in the next 40 years and the amount of shear strain which may have already been induced.

Northerly Slip

The model used in the following arguments is the triangular wedge represented in Figure 1a. It has a length L and a vertical thickness at the rear boundary of Z . Shear resistance along the base is everywhere controlled by the shear resistance to sliding (Amonton's Law): so that

$$\tau = \sigma_n \mu$$

That is, the shear resistance decreases from zero at the apex of the wedge to a

maximum at the rear boundary. In calculating the stability, I find the horizontal force ($\sigma_H Z$) which is just capable of overcoming the shear force S_R where

$$S_R = \bar{\tau} \cdot L$$

and $\bar{\tau} = \frac{\rho g Z}{2}$

where ρ = effective density of rock.

Taking the water table as being immediately beneath the Quaternary clays, $\rho g = 1.6$ grams/cc.

The shear force on the base of the wedge results in a clock-wise turning moment. It is usual to counter this moment by considering a shear stress acting on the vertical boundary plane (Figure 1b). One could change the basal slip plane from Z to $Z' - Z''$ and the model would be basically unchanged. It can be inferred that the vertical shear force on this vertical boundary is $\bar{\tau} Z$.

Tim Harper has suggested that bedding-parallel shear stresses may exceed the limiting value set at the base for sliding. If such a possibility is conceded and the distribution of shear stress with depth is as indicated in Figure 1c, then one may infer that, if the shaded areas are equal, the vertical shear force is the same as that in Figure 1b and that the original model has not been seriously modified. If, however, one assumes that the distribution of shear stress with depth is as indicated in 1d, then the vertical shear force is greater than for 1b. Consequently, the stability of the original model has been upset and a much more sophisticated analysis is required to determine the boundary conditions. I will, therefore, only consider the simple basal slip model represented in Figure 1a (and 1b).

Consider slip on one specific layer which is situated at a depth of 170 feet beneath the southern limit of the Cooling Tower (2,500 feet from the lake shore). The horizontal stresses for stability at boundaries A and B (where B is 1 mile south of A) are σ_{H1} and σ_{H2} respectively. As can be seen from Figure 2, these average stresses are 968 and 1,519 lb.in² respectively.



It is emphasised that these stresses are averages. That is, they are stresses which one would expect to find at depths $Z/2$ (at 85' and 140'). In upper levels, the stresses are likely to be smaller and at deeper levels they will probably be larger. Also, they are magnitudes of stress which reflect, and are a compromise between, the 'high' stresses in sandstones and the 'low' stresses in shales.

The manner in which stress intensity varies with depth is not known with any precision. However, from OC-4 data, there is a trend for the horizontal stresses to increase by about 300-500 lb.in² per hundred feet increase in depth. Hence, the average stresses σ_{H1} and σ_{H2} would probably vary with depth, as indicated in Figures 3a and b.

In the Oswego sandstone (where the proportion of shale is small) the average figure probably represents the real rock stress required for stability. In the Transition beds and Pulaski series, the average stresses must be adjusted for rock type. This adjustment must take into account the proportion of different rock types and their respective elastic moduli. This is a point to which we shall return. We do not have sufficient data, I suspect, to determine whether such a deep plane is, in fact, metastable. However, I doubt whether the rock stresses are sufficiently high to cause slip.

Now consider sliding on a bedding plane which is at a depth of only 55 feet at the southern edge of the Cooling Tower. This situation is modelled somewhat more carefully in Figure 4. It will be seen, that the average horizontal stress for N-S metastability is 444 lb.in².

One may infer from the data for the Oswego taken from OC-4 that the average stress some 1,000 feet to the south could easily attain a value of 444 lb.in² and result in a metastable condition.

One can conclude, therefore, that the rocks beneath the Site pass from the metastable situation to a stable situation. This transition could occur at some depth between 55 feet and 170 feet. Also, at some distance to the south, the metastable wedge must eventually encounter stress conditions where they become stable.

Stress Drop

Let us now consider what stress drop would accompany a change in shear resistance of 6 lb.in^2 , by taking the model indicated in Figure 4. If the shear resistance on the basal slip plane is reduced from 8 lb.in^2 to 2 lb.in^2 , then the new metastable horizontal pressure is 111 lb.in^2 . Hence, the stress drop would be $(\sigma_d) = 333 \text{ lb.in}^2$.

The release of 333 lb.in^2 of compressive stress would result in a northerly extension of the rocks and thereby cause a displacement on the basal slip plane of the model. This displacement, on a relatively deep slip plane, could result in a northerly translation of the Site by 8 or 9 inches. This, however, would not be significant. What would be important is the accompanying extension of the actual Site rocks. The extension 'd' of the Site would be given by:-

$$d = \frac{L \times \sigma_{\text{drop}}}{E}$$

For a Site length "L" = 2,000 feet and $E = 3.5 \times 10^6 \text{ lb.in}^2$ (the value used previously),

$$d = \frac{2000 \times 12 \times 333}{3.5 \times 10^6} = 2.3 \text{ inches}$$

A 500' long building would extend by 0.6 inches. The value of E is critical.

Given an average stress drop σ_{drop} in sediments of high and low modulus E_1 and E_2 , the average modulus will be:-

$$E_{\text{av}} = \frac{aE_1 + bE_2}{a + b}$$

where a and b are the proportion of materials with moduli E_1 and E_2 . Thus, if $E_1 = 3.5 \times 10^6$ and $E_2 = 2 \times 10^6$ and $a = b$, then $E_{\text{av}} = 2.75 \times 10^6 \text{ lb.in}^2$, and the quoted strains would be correspondingly larger.

Lateral Regional Variations in Slip

If the metastable wedge reaches a distance of 7,500 feet south of the shore line, then the wedge would extend by about 8 to 9 inches in the next 140



years. The process of glacial rebound has been going on for thousands of years. One cannot state for what length of time the Site area has been undergoing N-S slip. However, during the Admiralty stage of lake drainage, conditions especially favourable to N-S slip existed. Slip which almost certainly occurred at this time probably contributed to the development of the Tepee and Cooling Tower buckles. Hence, one may infer that a general slip of several feet N-S has already occurred in the Site rocks.

One may infer from the slip-stability analysis presented here that the dip of the bedding planes is critical. The Demster structure has induced very considerable variation in the orientation of bedding in the area to the east of the Site. Consequently, the ease or difficulty of N-S slip will vary as this structure is approached. Indeed, at the structure itself (and here I am relying on memory), the orientation of the Oswego would completely inhibit northerly slip. Thus, relative to the Demster, the metastable Site rocks have moved N by several feet and so will have induced lateral, clockwise, shear strains which, on average, will be about 0.2×10^{-3} radians ($\approx 1/100^\circ$).

Any calculation regarding N-S movement of Site rocks in the next 40 years that neglects the component of stress release (which increases such lateral shear strains) will result in a small over-estimate of the N-S displacements and extensions which will develop by movement of the metastable rocks.

2. Stability of the Radwaste Structure

In the initial report on the Radwaste structure, I considered the question of its stability by evaluating the various stress levels involved in the structure's "Energy Budget", which I presented in the form:-

$$S_1 - (S_\psi + S_{\text{slip}} + S_E) = S_R$$

where S_1 = the initial stress state that resulted in the development of the Radwaste structure

S_ψ = the stresses used to induce the shear strains



S_{slip} = the stresses needed to overcome slip and cause mass transfer

S_E = the stresses available to cause elastic recovery and give rise to displacement (D) of the Radwaste structure

and S_R = the residual (or remnant) ground stresses still obtaining.

I evaluated the stresses for a model in which the Radwaste structure was contained between the Cooling Tower and Tepee Faults.

On reflection, I consider that this is still the best analytical approach to the stability problem: but now think that the various values of stress assigned to the symbols should be reappraised and that the model requires modification. Let us first consider the model.

Model Modifications

In the previous report, the Radwaste structure was represented as a ramp thrust joining at depth (Z) a single plane of bedding-slip. This structure was contained between the Cooling Tower and Tepee Faults and that strike-slip motion along these (60-75° dipping) fault boundaries to the Radwaste structure was inhibited. Indeed, in the calculations presented in the previous report it was assumed that slip was completely inhibited. However, when presenting a qualitative argument, it was indicated that strike-slip along these faults could have occurred.

I now wish to amend the model presented in the previous report in two respects. a) The Radwaste structure should be considered as a "Ramp" which joins not one, but two or more planes of bedding slip (see Figure 5a); and b) Strike-slip movement on the bounding Cooling Tower and Tepee Faults did occur. The details of these modifications affect the values of stress (S_1 etc.). I shall therefore consider these details and present arguments for reassessing the various stress values.

Values of Stress

Initial Stress (S_1)

In the previous report, I followed an even earlier assessment (Appendix III of the N.M.P. Report) and took the stress required to initiate failure as $23,000 \text{ lb.in}^2$. This value of stress is probably required to initiate the shear failures which define the Ramp part of the structure. Such high stresses would not, however, be required to give rise to sliding on bedding planes. Consequently, I now think that it is unrealistic and unnecessary to assume such a high value of S_1 . I now consider that the average stresses associated with the initiation and development of the whole structure (including the slip on bedding planes) was much smaller than $23,000 \text{ lb.in}^2$ - probably ^{than} less ~~less~~ half this amount (see Figure 5). Given time, and by making assumptions regarding the probable value of the regional stress S_{Reg} and the values of positive and negative radii of curvature etc., one could derive the distribution of values of stress in a vertical plane which trends $N60^\circ W$.

However, from Figure 5b, one can see that initiation of the Radwaste Ramp probably occurred at some modest depth (100 - 200 feet) and that movement on bedding planes enabled the relief of the horizontal stress to occur. It may be inferred, that the lower planes of bedding slip as they propagated to the SE would first encounter low lateral stresses (the result of -R associated with down-throw on the normal fault. See Appendix III of original N.M.P. Report). Hence, the planes of bedding slip nearer the surface would have the greatest lateral extent.

Thus, we tentatively conclude that the average lateral stresses at level Z_L in Figure 5 would be ~~somewhat less than~~ ^{less than} $11,500 \text{ lb.in}^2$. But at a higher level Z_U the average value of lateral stresses will be lower and closer to the magnitude of the regional stress S_{Reg} . These considerations are, to some extent,

academic. They have their value in estimating the lateral extent of the bedding slip planes. However, from elasticity theory and a knowledge of D, it is known that the planes are of considerable extent. Consequently, the stability of these planes is the question which really concerns us.

From the trench exposures, one may infer that bedding plane slip occurs in the Transition beds and that movement on this plane (or planes) may have attained a total slip of 30 inches. It is reasonable to expect that this slip plane extends in a SE direction beyond OC-4. Consequently, it is significant to consider the stability of the structure on this 40 feet deep, slip plane in the light of the magnitude of stresses determined in OC-4, a distance of about 1,400 feet from the 'outcrop' of the Radwaste structure.

The model used to estimate resistance to sliding on the 40 feet deep bedding plane is represented in Figure 6. One may note that the assumed 10' of Quaternary will contribute to the normal stress on the glide plane, but the horizontal stress will be significant only in the Oswego and Transition beds. From Figure 6, it can be seen that the resistance to sliding on a 40 feet deep, bedding plane plus the 'buttress' effect of the Ramp totals 467 lb.in². Let us now consider the resistance to sliding on the bounding normal faults.

Sliding on Normal Faults

It will be assumed that the shear resistance to movement is limited to the solid rock and that any resistance to shear offered by the Quaternary sediments will constitute a small safety factor. Because of the coefficient of friction of sandstone on sandstone, coupled with the roughness of the fault plane, it follows that we should not use $\mu = 0.3$ for these calculations. I shall choose $\mu = 0.5$ ($\phi = 26.5^\circ$): and this is probably a conservative figure.

To estimate the frictional shear resistance, we now require the average normal stress acting on the two faults. The average normal stresses can be estimated from the average horizontal stress acting perpendicular to the faults.



These horizontal stresses will be close in value to the stresses necessary for metastability. So, clearly, we can make two general statements.

- 1) The shear resistance will be far greater on the Cooling Tower fault than on the Tepee fault.
- 2) The shear resistance decreases on both these faults as one transverses from east to west.

These variations in shear resistance will have an obvious influence on the development of shear strains. However, first consider the average shear resistance of the two faults. This can be done by taking the mid-line (between OC-4 and the Radwaste "outcrop") which is perpendicular to the trend of the faults and calculating the horizontal stresses required for metastability. This line meets the trace of the Tepee structure where it intercepts the shore-line and the Cooling Tower fault at the western margin of the Cooling Tower itself. The normal stresses on the faults at these points are about 330 lb.in^2 and 200 lb.in^2 for the Cooling Tower and Tepee structures respectively. Hence, the shear forces along these two faults, resisting movement on the Radwaste structure, are 20×10^8 and 6×10^8 lbs. respectively. (The differences in magnitude of the forces reflect not only the differences in the normal stresses, but also the fact that the area of the Cooling Tower fault involved in the slipping is almost twice as large as that for the Tepee structure.)

To overcome these forces a component of stress of 180 lb.in^2 must act perpendicular to the Radwaste structure.

Thus, the horizontal stresses perpendicular to the Radwaste required to overcome slipping on the normal faults and the $40'$ bedding plane and also to overcome the Ramp effect need to be 647 lb.in^2 . To this figure a component of stress ($S\psi$) must be added, which causes horizontal shear strains (ψ) in the Radwaste structure. Assume, for the moment, that $S\psi = 100 \text{ lb.in}^2$. Then, the stability stress on the Radwaste structure at a distance of 1,400 feet (i.e. near OC-4) is about 750 lb.in^2 .

Now compare this figure with the stress data available for OC-4. The resolved components of stress for measuring stations 1-4 (for solid triangles only; i.e reliable data) are indicated in Table 1. The smooth change in trend of σ_1 between stations 1 and 4 and the abrupt change between stations 4 and 5 and 6, lead one to suggest that the slip plane lies between stations 4 and 5.

Table 1. Stresses perpendicular to Radwaste, from OC-4

Station	Depth (approx)	S_{Rw}	τ_{Rw}
1	14'	1025 lb.in ²	225 lb.in ²
2	24'	525 " "	360 " "
3	28'	870 " "	375 " "
4	35'	375 " "	75 " "
Mean values		698.75	258.75
		$\approx 700 \text{ lb.in}^2$	$\approx 260 \text{ lb.in}^2$

These stations are all in the Oswego; and, if the measurement points were not located too close to shale partings, the stresses are presumably representative. If the average horizontal stress is taken to be 700 lb.in², then one may infer that the portion of the Radwaste structure to the east of OC-4 is currently stable; with a safety factor of about 50 lb.in² before the metastable condition is reached.

The question now arises - will the structure remain stable throughout the next 40 years? The stability can be influenced by two main factors.

- 1) The shear resistance to sliding on the 40' bedding plane could be reduced by a highering of the water table. (This factor can be countered. Indeed, if the water table were lowered by 40', by pumping, this would greatly increase the stability of the Site area)
- 2) Glacial rebound is inducing shear strains in a general N-S plane and these, as has been noted, can reduce the resistance to bedding slip in the N-S direction by about 6 lb.in². This factor can have two effects on the Radwaste structure.



a) There will be a component of reduction in shear resistance in a direction perpendicular to the Radwaste structure induced by the N-S rotation. This effect can result in a reduction of the shear resistance perpendicular to the Radwaste structure by 2 lb.in^2 . This could result in a component of potential stress drop perpendicular to the Radwaste structure of 85 lb.in^2 .

b) The average, potential N-S stress drop in the vicinity of the Radwaste structure which is likely to take place in the next 40 years is of the order of 250 lb.in^2 . This stress drop will greatly reduce the shear resistance on the Cooling Tower and Tepee faults, so that these will contribute a further component of potential stress drop perpendicular to the Radwaste structure of approximately 140 lb.in^2 .

The total stress drop is, therefore, likely to be:-

$$\sigma_{\text{drop}} = 85 + 140 - 50 \text{ lb.in}^2 = 175 \text{ lb.in}^2,$$

(where, it will be remembered that the 50 lb.in^2 is the current safety factor).

(If the water table were lowered, by pumping, by 30 feet, this would increase bedding stability by 3.9 lb.in^2 (shear resistance) and prevent 80 lb.in^2 stress drop.)

A stress drop of 175 lb.in^2 would give rise to a displacement on the Radwaste for $L = 1,400$ feet of:-

$$d = \frac{175 \times 1400 \times 12}{3.5 \times 10^6} = 0.84 \text{ inches.}$$

{If, as the result of pumping, the stress drop is kept to 95 lb.in^2 ,

$$d = 0.46 \text{ inches.}}$$

These displacements would be approximately doubled if the Radwaste structure extended a further 1,400 feet to the east of OC-4.

The extent of the Radwaste structure will be related to the stress drop associated with its initiation; and this is speculative. However, the initiation of the shears in the Ramp which cut across beds must have given rise to a significant stress drop. Also, the decrease in stress, acting normal to the Cooling Tower and Tepee faults, which took place when the buckles and pop-ups



developed, must have been of the order of $2,500 \text{ lb.in}^2$. Such a reduction in normal stress would have permitted a stress drop perpendicular to the Radwaste structure of about $1,400 \text{ lb.in}^2$. Consequently, one can infer that the stress drop associated with the Radwaste structure (Ramp and bedding slip) could easily have exceeded $3,000 \text{ lb.in}^2$.

If the average stress drop was, in fact, $3,000 \text{ lb.in}^2$, the extent of the structure (L) would be 2,900 feet. Thus, one can conclude that the displacement in the next 40 years, on the 40' slip plane, is likely to be about 1.7 inches (or about 0.9 inches if the water table is lowered).

If movements occur on several planes of slip; the higher percentage of shale in the lower horizons would mean that the average E is lower than $3.5 \times 10^6 \text{ lb.in}^2$. Consequently, the total slip on the Radwaste may get as high as 3.0 inches.

Let us now turn to shear strains in the Site area.

3. Shear Strains

It has been noted, that a clock-wise shear strain has probably been induced by differential, northward slip of the Site area. However, in the upper layers of the Radwaste structure, it may be inferred that this sense of shear strain has been reversed. Because the normal stresses on the Teepee fault are lower than those on the Cooling Tower fault, the northern part of the Radwaste structure was able to move differentially, relative to the southern part of the structure. The average shear stress acting perpendicular to the trend of the Radwaste Ramp in OC-4 is about 260 lb.in^2 (see Table 1). These stresses could be associated with shear strains (ψ) of:-

$$\psi = \frac{260}{1750000} = 0.00015 \text{ radians} \\ \approx 0.001^\circ$$

The resistance to slip on the Teepee structure decreases to the west. Hence, the shear strains would increase as Unit 2 is approached. Even if there were a tenfold



increase in the shear strains, the value of ψ at Unit 2 would be only 0.01° . The relief of such a shear strain, as the result of engineering construction, would give rise to a shear displacement of about 1 inch in a 500' long engineering structure.

This shear strain angle would decrease with depth and even reverse its sense of shear. What precise difficulties this would present to engineering structures are not easy to envisage.

Seismic Risk

The important question regarding seismic risk to the Site constructions relates to the magnitude of a stress wave at the Site which has been generated by a distant seismic event.

If one considers that a volume of rock, radius 1.25 miles (2 km) exhibits a near-instantaneous stress drop of $1,000 \text{ lb.in}^2$ (70 bars). Then, using a reasonable value for the elastic modulus, the energy of the event will give rise to an earthquake of magnitude 6.0.

At a distance of 125 miles from the epicentre, the magnitude of the P-wave will be less than 1 lb.in^2 . (This conclusion is reached by taking the stress attenuation following a curve derived by Ahrens and O'Keefe in "Impact and Explosion Cratering", ed. Roddy et al., Pergamon)

A horizontal stress of 1 lb.in^2 is unlikely to be significant. If, as the result of refraction, the P-wave travels at 45° to the horizontal in the Site area, then the vertical component would be 0.7 lb.in^2 and this could reduce the shear resistance by 0.2 lb.in^2 . This lowering of shear resistance could possibly trigger a small stress drop. But the effect is not likely to be significant nor (for reasons discussed in my previous report) rapid.

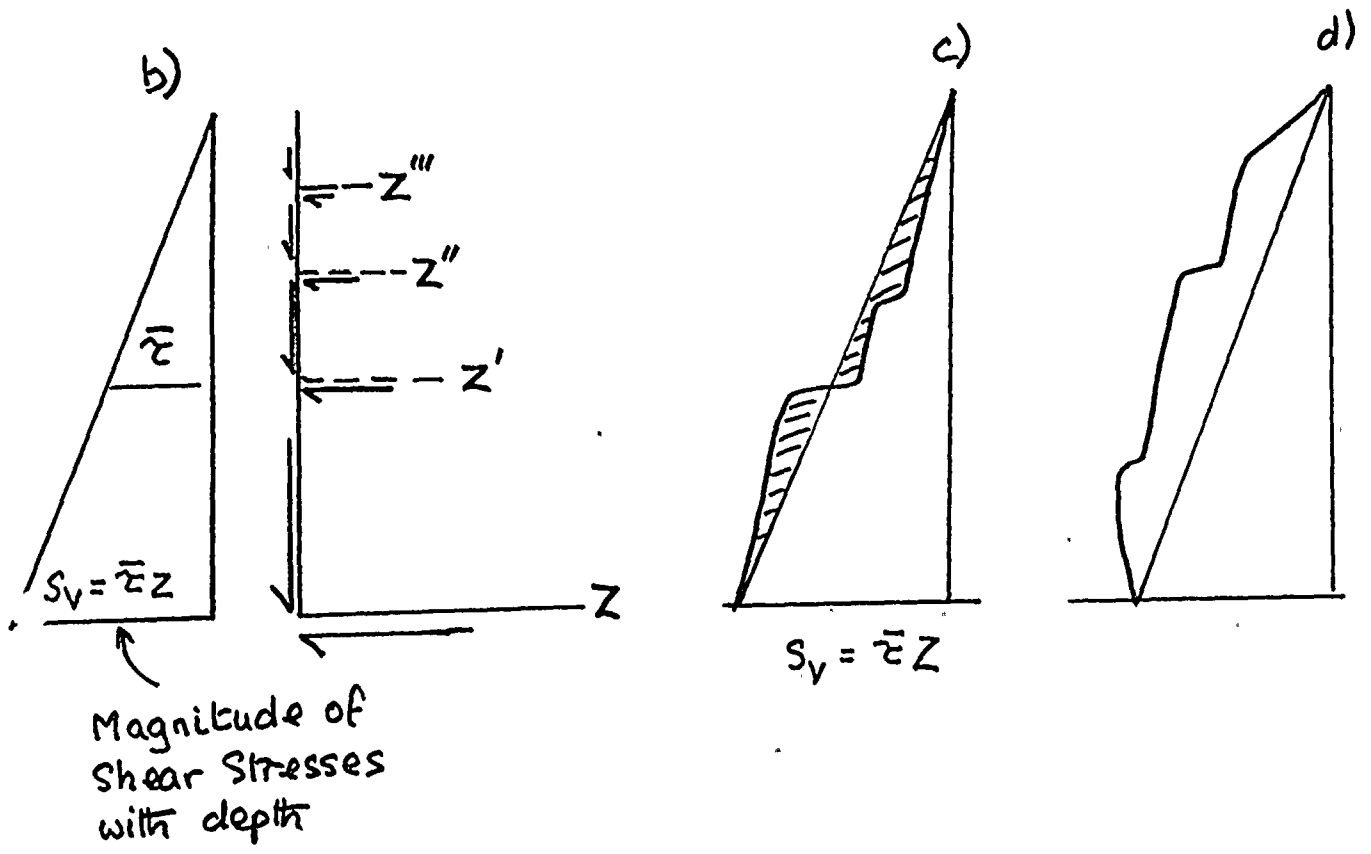
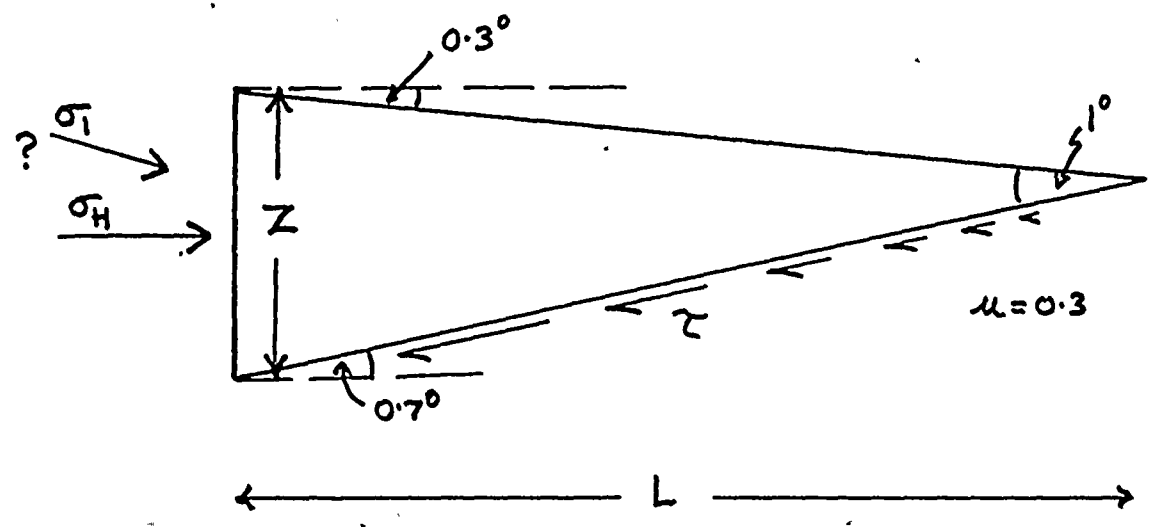
I have to pass the question back to you. Is there likely to be an earthquake of greater than magnitude 6.0 within 125 miles of the Site?

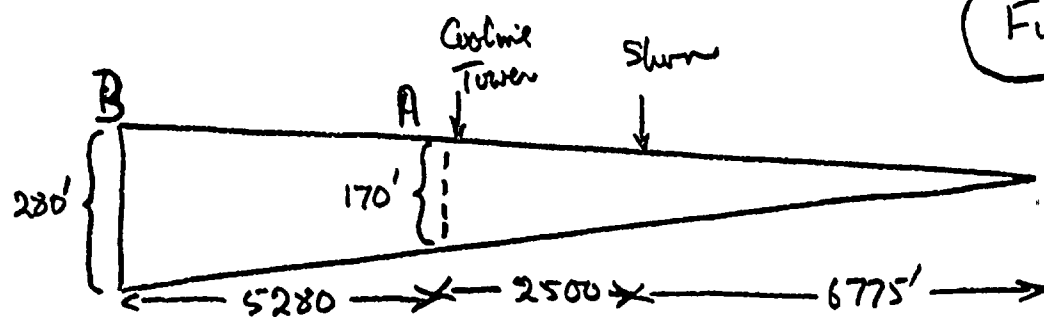
To assess the risk one needs to know the magnitude of 'shock', the stress drop and the 'sphere' of activity. Are such data available for the region?

3rd Dec 1979.

Neill J. Rice

Fig 1 a





$$\Rightarrow \sigma_{H_2}$$

$$\Rightarrow \sigma_{H_1}$$

$$\mu = 0.3$$

$$P = 1.6$$

Average σ_{H_1} if boundary is set at Cooling Tower [A]

$$\frac{Z}{2} = 85' \quad \bar{\sigma}_V = 59 \text{ lb m}^2$$

$$\bar{z} = \bar{\sigma}_V \cdot \mu = 59 \times 0.3 = 17.74$$

$$S_g = 17.74 \times 9275 \times 12. \text{ lbs.}$$

$$\sigma_{H_1} = \frac{17.74 \times 9275 \times 12}{170 \times 12} = 968 \text{ lb m}^2.$$

Average σ_{H_2} if boundary is set at B [Inlet to South]

$$\frac{Z}{2} = 140 \text{ ft.} \quad \bar{\sigma}_V = 97.4 \quad \bar{z} = 29.2$$

$$\sigma_{H_1} = \frac{29.2 \times 14555}{280} = 1519 \text{ lb m}^2.$$



Figure 3

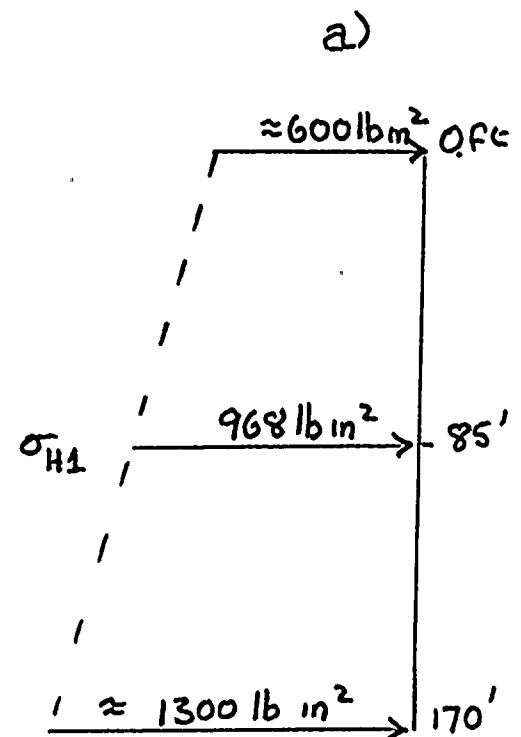
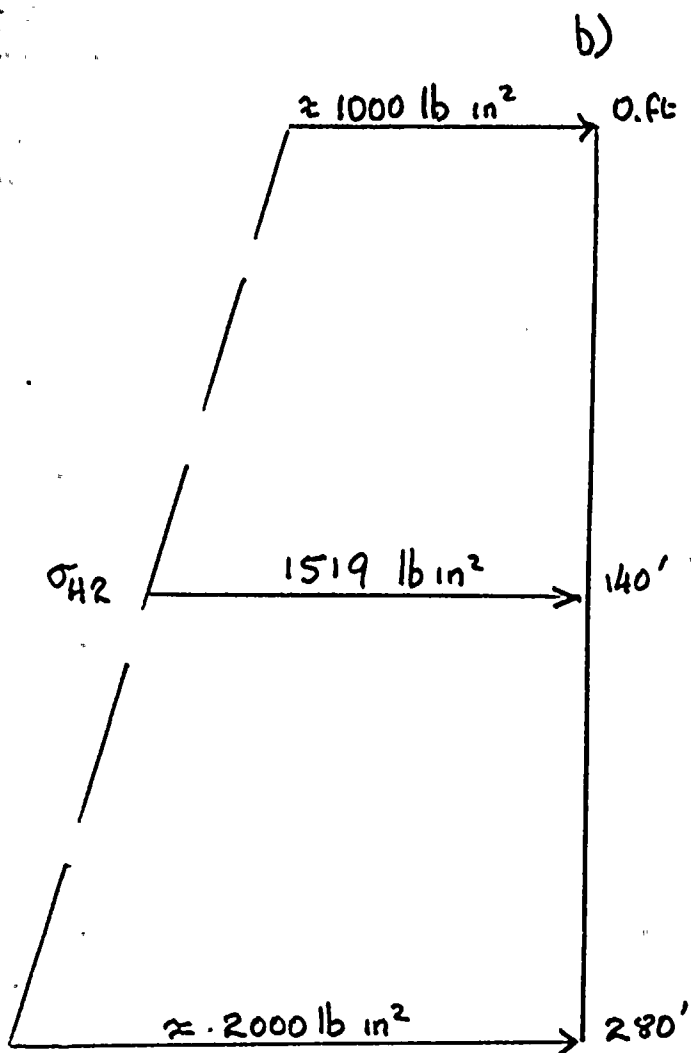
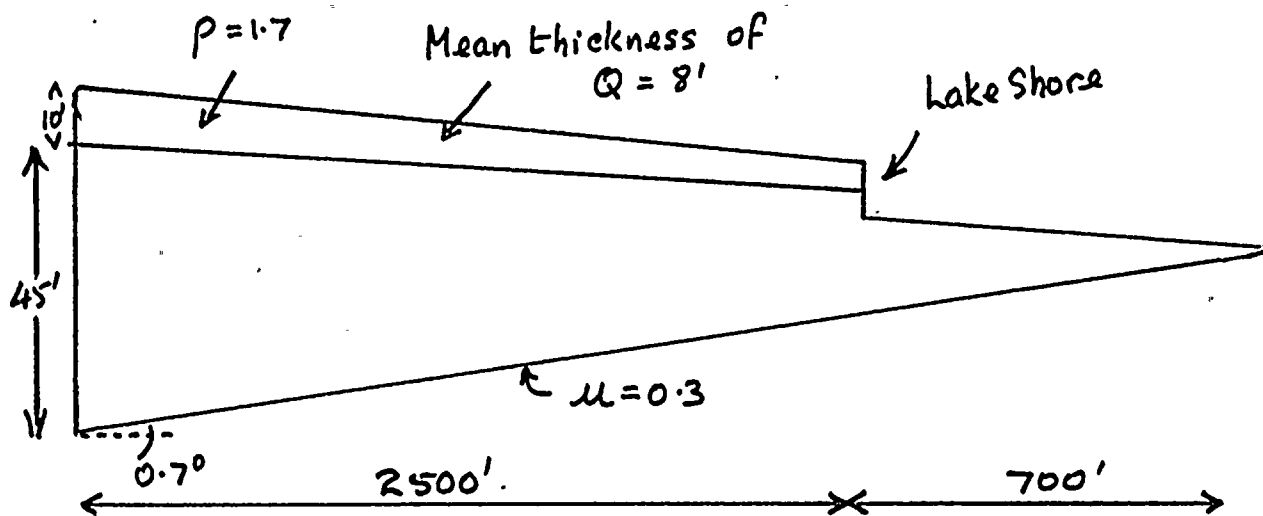




Fig 4



$$\sigma_{V_{Tot}} = \sigma_{V_Q} + \sigma_{V_{osw}}$$

For land block: Average $\sigma_V = 26.4 \text{ lb/in}^2$
 $\tau = \mu \sigma_n = 8 \text{ lb/in}^2$

$$T_r = 240000 \text{ lbs}$$

$$\sigma_H = \frac{240000}{45 \times 12} = 444 \text{ lb/in}^2$$

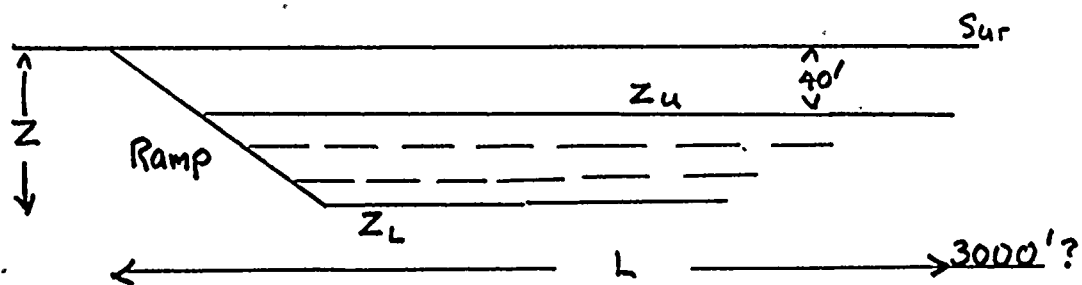
Off-shore wedge adds 11 lb/in^2 to σ_H [this we will neglect]

if τ goes from $8 \rightarrow 2 \text{ lb/in}^2$

σ_H' goes to 111 lb/in^2



Fig 5a



5b

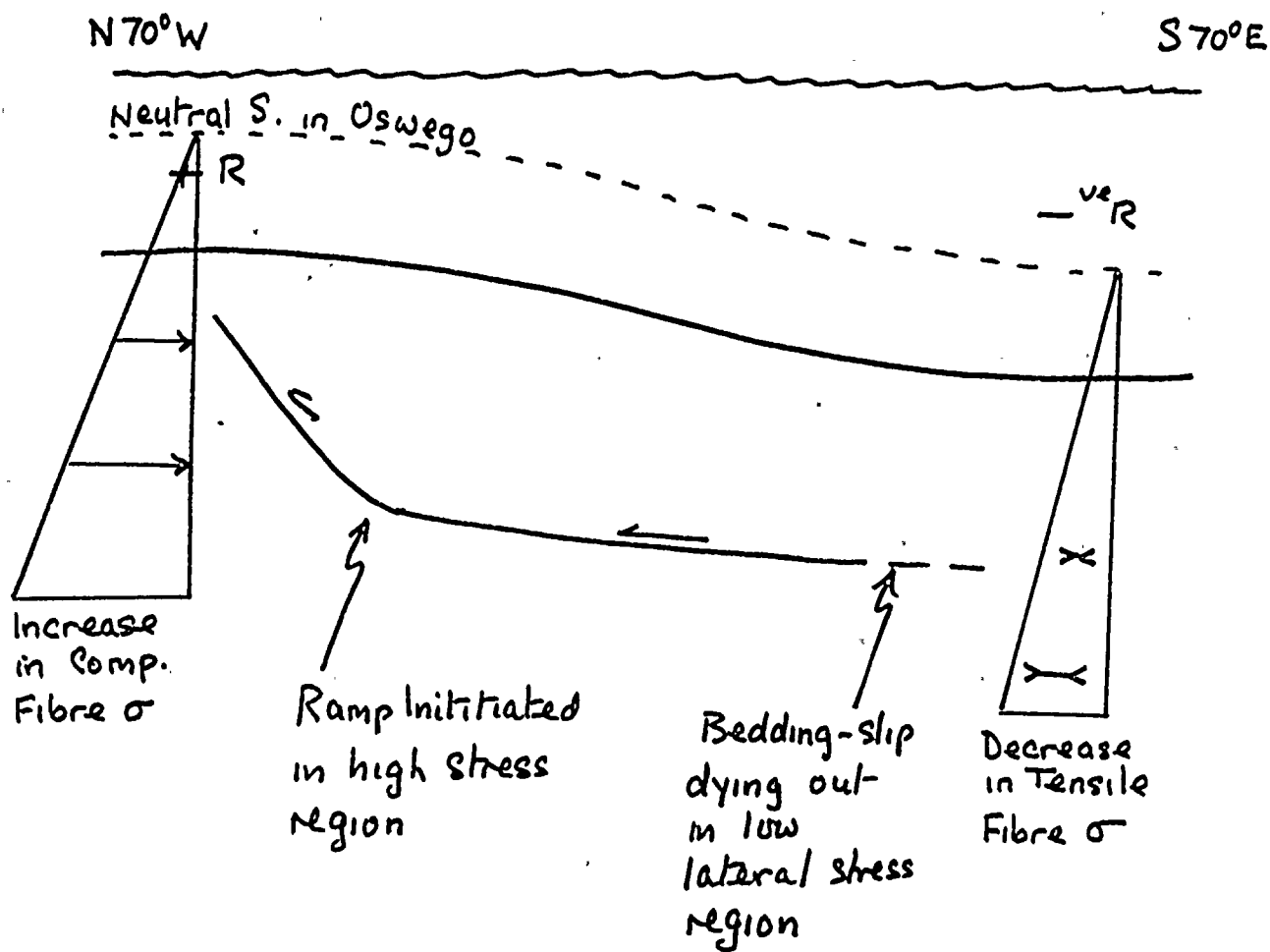
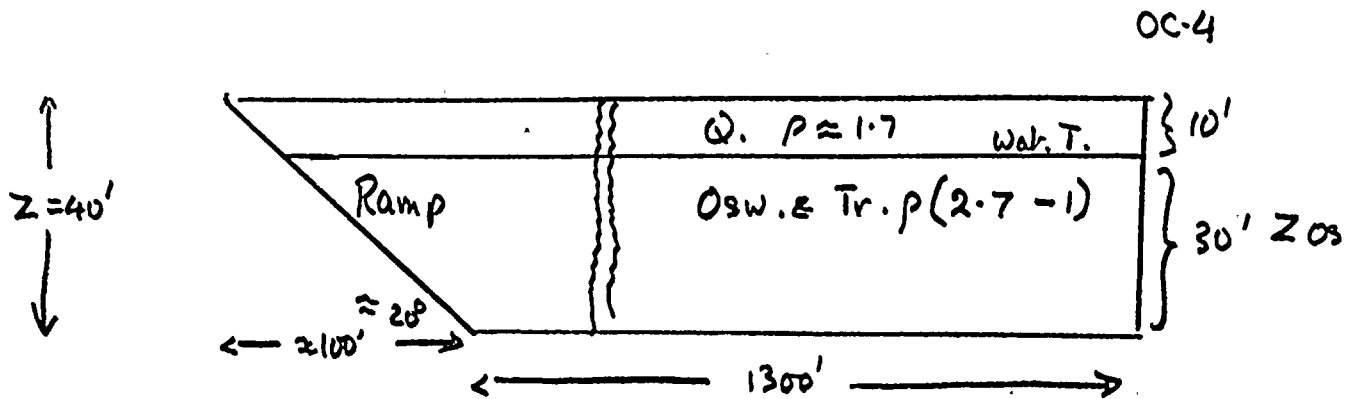


Fig 6.



Sliding on
b.p

$$S_v = 29.5 \text{ lb m}^2$$

$$\tau = 0.3 \times 29.5 = 8.9$$

$$\sigma_H = \frac{\tau L}{Z_{os}} = \frac{8.9 \times 1300}{30} = 385 \text{ lb m}^2$$

Ramp Contribution:-

The main contribution of resistance to movement on Ramp will be "roughness". Using a value of $\mu = 1.2$ (4x that on bedding): then

$$\left. \begin{aligned} \sigma_H &= \frac{18 \times 106}{30} \approx 64 \text{ lb m} \\ \text{Ramp wt contr} &\approx 18 \text{ lb m} \end{aligned} \right\} \underline{82 \text{ lb m}^2}$$

Combined b.p Sliding & Ramp Resistance

$$\underline{467 \text{ lb m}^2}$$



THIRD THOUGHTS ON THE STABILITY OF THE RAD-WASTE STRUCTURE

by

N.J.Price D.Sc., Ph.D.

Introduction

My two previous reports on the stability of the Rad-waste Structure have been concerned with conceptual models. The conclusions reached, using this approach are only valid provided the model parameters and the assumptions made are also valid. I will now review some of the stated and tacit assumptions and values used in the previous calculations and reappraise my earlier conclusions in the light of this review and the new data obtained from RS 2 and 3.

The question of whether or not there will be future movement on the Rad-waste Structure will be considered in two main parts. Firstly, I will consider the question of the general and intrinsic stability of the Structure as a whole. Secondly, I will estimate what movements may be induced locally, perhaps on some element of the Rad-waste Structure, as the result of excavation and construction of engineering structures. When dealing with this second aspect it is necessary to consider what movement may be expected from a) the release of elastically stored horizontal shear stresses, b) the release of elastically stored horizontal normal stresses and c) from the swelling of shales.

The last of these three aspects, relating to the swelling of shales has been studied by Drs. T.Harper and J.Szyrmanski. I feel that I cannot improve on their expertise and therefore will not comment on this aspect further: but will deal with the remaining aspects in the order set out above.

Intrinsic stability of the Rad-waste Structure

One of the most important items presented in my previous reports, relating to the future stability of the Radwaste Structure, was that bedding parallel shear stresses are developing in the site rocks as a result of 'rebound'. I previously estimated that in the next 40 years these shear stresses would increase by about 6 lb. in². This figure was based on the average rate of rebound. As may be inferred from Figure 2 of your draft report and as quoted on page 2 of that report, the contemporary rate of shear straining is approximately 0.04/1 mile/1 year (This would be better expressed as 0.025mm/1 km./per year, or 2.5×10^{-8} rads./per year). This rate is significantly slower than the average rate and would give rise, in the next 40 years, to a change in bedding parallel

shear stress of no more than 21 lb. in^2 (using, as previously, the value of shear modulus ' G ' = $1.75 \times 10^6 \text{ lb. in}^2$). Thus, the shear stress effect expressed in my previous report is over-emphasised by a factor of 3.0.

If the other parameters used in my previous analysis are, for the moment, assumed to be unchanged; then the reduction in the N-S normal stress which may take place in the next 40 years would be only a little more than 100 lb. in^2 . (rather than the 330 lb. in^2 , previously reported). Hence, the change in Site of length 2000 feet would be approximately $\frac{0.8}{1}$, while a 500 foot long building would extend by only 0.2 in.

It will be recalled that the secondary, but important effect of this N-S stress reduction related to the 'clamping stresses', exhibited by the Tepee and Cooling Tower faults on the Rad-waste Structure must also be accounted for. Because the N-S normal stresses are likely to decrease by only 100 lb. in^2 , the concomitant stress drop normal to the Rad-waste Ramp, as the result of this effect, is rather less than 50 lb. in^2 . The small contribution of the component of change in the bedding parallel shear stress (related to rebound) would permit the release of an additional component of horizontal stress (normal to the Ramp) of about 30 lb. in^2 . Thus, the combined effects of changes in bedding parallel shear stresses could, in the next 40 years, give rise to a stress drop, perpendicular to the Rad-waste Ramp of about $75\text{-}80 \text{ lb. in}^2$.

In my previous report I suggested that the Rad-waste block was not metastable for sliding in the $N70^\circ W$ direction and that consequently, the potential stress drop may be significantly less than 80 lb. in^2 ... probably about 30 lb. in^2 . If this stress drop occurred over a length of 3000 feet, movement on the Rad-waste would not exceed one inch. Even this movement could be obviated by lowering the water-table. (This is also true regarding the potential changes of water table level which may result from tilting)

Let me now consider another point. A tacit assumption I used in my previous report, when assessing the N-S stability of the Site during the next 40 years, was that there was a progressive increase in the N-S normal stress as one traverses south from the Lake. On reflection, there is reason to doubt the validity of this assumption based on a priori arguments. However, more to the point, the new stress data from RS2 and 3 demonstrate conclusively that this tacit assumption is not valid.

The new data show that the N-S normal stresses in RS 2 and 3 are lower than in OC 4 and also that the normal stress acting parallel to the two normal boundary faults are also lower in the RS 2 and 3 holes than in OC 4.

Two significant points result from these new data. Firstly, the "clamping stresses" on the normal faults are of small, or even negligible importance, so that changes in the bedding parallel shear stresses, in the next 40 years would also have a negligible influence on the over-all future



stability of the Rad-waste Structure. Secondly, the average horizontal stress acting N70°W is smaller than that assumed in my previous report, where, it will be recalled, the component of horizontal stress necessary to overcome the clamping stress was estimated to be about 180 lb. in². Hence, if the average value of stress in the N70°W direction is 180 lb. in² lower than the value, which was based on the data from OC-4, the Radwaste Structure is almost certainly stable.

The difference between the new data from RS 2 and 3 are so different from that from OC-4; a detailed analysis involving orientations ~~are~~^{is} not necessary. One need only look at the mean values of normal stress and mean horizontal differential stress, as given in Table 1.

TABLE 1	BOREHOLE	MEAN HOR. STR.	$\frac{1}{2}$. MEAN DIFF. STR. = τ_{xy}
	RS-3	95 lb. in ²	90 lb. in ²
	RS-2	100 lb. in ²	85 lb. in ²
	OC-4	625 lb. in ²	600 lb. in ²

From the new stress data one may infer that the normal stress acting perpendicular to the Radwaste Ramp is many hundreds of pounds per square inch lower than the value used in my previous report.

Moreover, even if one assumes, as I did previously, that a wedge, with its back wall at OC-4 were metastable, one can conclude that similar N-S oriented wedges with back walls set at RS-2 and RS-3 respectively are certainly not metastable. Even if changes in bedding parallel stresses induced during the next 40 years could produce N-S movement of the OC-4 wedge, the RS-2 and 3 wedges would remain stable to such movement. Because the component of bedding parallel shear stress, which may be induced by rebound in the next 40 years, in the N70°W direction is likely to be much smaller than that which would develop in the N-S direction: I conclude from the available data that the Radwaste Structure as a whole is unlikely to move as the result of bedding parallel shear stress changes which may take place in the next 40 years

Movements on elements of Radwaste Structure induced by Engineering Construction

Although the Radwaste Structure is intrinsically stable, the excavations associated with engineering construction will release a portion of the stored elastic energy in the site rocks, with the result that some movement on elements of the Radwaste Structure will almost certainly take place. As indicated earlier, movement can be considered under three headings: the effects of normal stress release, shear stress release and swelling.



Movements resulting from the release of stored normal stresses

The average normal stresses in RS-2 and 3 are about 100 lb. in^2 . Providing that these magnitudes of stress are representative of the stresses obtaining throughout the site rocks in the vicinity of the construction, then one can infer that the average movements which will result from the release of all or part of these normal stresses will not be large. Thus, if a 500 ft diameter excavation reduced the average normal stress by 50% over a distance equal to the diameter of the excavation (i.e. 500 ft), then assuming the average value of E (including both sandstone, siltstone and shale) is $2 \times 10^6 \text{ lb. in}^2$, ~~then~~ movements of the walls of the excavation are not on average likely to exceed 0.15 inches. However, it should be noted that this is an average. Some of the stresses determined in the RS boreholes are tensile. One would expect the excavation to open in response to the release of these stresses. At levels where the stored stresses are compressive, the excavation will tend to close. At some horizons (e.g. at about 40 ft in RS-2) the compressive stresses are as high as 600 lb. in^2 . If all these stresses were relieved over a distance of 500 feet (a most unlikely event) the movement at this level would be approximately 0.9 ins (using the specific horizon modulus of $4 \times 10^6 \text{ lb. in}^2$). Hence, from the data available to me, it is unlikely that movements resulting from the release of normal stresses will reach 1.0 inch.

Movements resulting from the release of stored horizontal shear stresses

The emplacement of the Radwaste structure may have locally induced relatively high shear strains in the Site Rocks, particularly adjacent to and in the Ramp. However, ~~the bulk~~^{most} of such shear strains are permanent and are of no importance as far as movement in the vicinity of excavations is concerned. Here we need only deal with the stored elastic horizontal shear strains, or stresses. One may see from Table 1 that in RS-2 and 3, the average horizontal shear stresses (i.e. half the differential stress in the horizontal plane) is less than 100 lb. in^2 . If all these shear stresses were released by the excavation and taking the shear modulus as $1.75 \times 10^6 \text{ lb. in}^2$, the resulting angle-shear displacement would be about 6×10^{-5} radians. For an excavation of 500 ft. this would result in an insignificant differential movement of the excavation wall. Hence, provided the stresses as determined in RS-2 and 3 are representative of the site rocks in the vicinity of the excavations, shear stresses in these rocks will not give rise to severe engineering problems.



Movements resulting from rock swell

As stated earlier, the two people who are best qualified to comment on this topic are Drs Harper and Szyrmanski. It is my opinion however that this is the aspect of rock behaviour which is unlikely to represent an engineering problem. I can envisage no conditions which would enable me, or probably anyone else, to guarantee that movement resulting from rock swell will be less than one inch.

CONCLUSIONS

- 1) The data obtained from the RS holes are extremely valuable and permit conclusions to be reached regarding the stability of the Radwaste Structure. Were these data not available, opinions regarding the structures stability would of necessity remain conjectural.
- 2) Provided the magnitudes of stresses measured in RS-2 and 3 are representative of stresses in rocks adjacent to constructions areas (I have no information relating to RS-4); then the Radwaste Structure as a geological entity is stable and will not move in the next 40 years.
- 3) Small movements are likely to take place on elements of the Radwaste Structure as the result of excavations which locally release stored stresses. However, subject to the proviso made in conclusion 2), neither the stored normal nor the stored shear stresses should, on release, give rise to rock movements which constitute a hazard to engineering structures.
- 4) Rock swell probably constitutes a significant engineering problem. However, movements resulting from this mechanism will be slow. Monitoring would obviously be essential.

W. J. Price



538 E. Fairmont Drive
Tempe, AZ 85282

March 10, 1980

Mr. John J. Markham
Geologist, Dames & Moore
2996 Belgium Road
Baldwinsville, NY 13207

Dear Mr. Markham:

The following is a letter report initiated at the request of Mr. William Swiger of Stone & Webster and later by Mr. James T. Dette of Dames & Moore that I consider the effect of permafrost with subsequent growth of ground ice in the formation of small asymmetric folds (buckles, teepees) associated with small faults in sedimentary bedrock at Nine Mile Point Nuclear Station - Unit 2, Scriba, New York. The report is based on discussions with geologist working on the site and a brief site investigation.

Introduction

Geologists of Dames & Moore and Stone & Webster have been studying the bedrock and overlying unconsolidated sediments at the Nine Mile Point site for several years for three power sites. My field inspection of the site was about 2 hours in the morning of February 29, 1980. The Nine Mile Point Nuclear Station - Unit 2 is on the shore of Lake Ontario at Nine Mile Point, Scriba township, Oswego County, New York.

Geology

General statement

My understanding of the geology is dependent upon thorough briefings given by geologists of Dames & Moore and Stone & Webster and a brief field site investigation. Discussions with Stone & Webster geologists took place on the afternoon of February 28, 1980 in Boston, MA and on the site on the morning of February 29, 1980. Discussions in detail with geologists of Dames & Moore occurred Friday afternoon at the site. In the morning of Friday, 29th, there was a field site visit in which we examined the geology in the Drainage Ditch, the North Radwaste Trench, the Screen Well Area, North Electric Cable "Tunnel" and the Cooling Tower Excavation. In addition, it was possible to examine black and white and color photographs as well as many field sketches and preliminary diagrams of geologic exposures.



Unconsolidated sediments

The area lies in the Erie-Ontario Lowland and has been overridden by glacier ice several times. Unconsolidated sediments included till of late Wisconsinan age. Unpublished data provided by site geologists indicate perhaps two tills, a dense basal till and the overlying upper till, interpreted to be an ablation till. Overlying the tills are various glaciofluvial deposits characteristic of stagnating glaciers, and thawing ground, including glacial ice blocks. Also present are laminated clay-silts thought to be lake clays of former Lake Iroquois. Field inspection and the numerous diagrams indicate that the unconsolidated sediments (soils) overlying the bedrock are characteristically minutely deformed with slumps, drapes, faults, minor folds. Such are characteristic of glacial sediments throughout the world. These minor structures are ubiquitous in the unconsolidated sediments.

Bedrock

The consolidated rocks at the site are of the Oswego Formation of upper Ordovician age. The rocks consist of tabular, thin to medium beds of light gray to greenish-gray, fine-grain sandstone interlaid with thin beds of gray siltstone and dark gray shale. In the site area the top bed is a rather massive gray sandstone 3 to 5 feet thick. The beds dip very gently to the south or southwest less than 1 degree. Existing exposures permitted observation of bedrock faces as much as 30 to more than 50 feet high.

Small faults in the bedrock of the Nine Mile Point area have been studied: Barge Slip Fault, Radwaste Fault, Drainage Ditch Fault (an extension of fault in the Fitzpatrick excavation) and the Cooling Tower Fault. The later two are of interest in this investigation. The Drainage Ditch Fault and Cooling Tower Fault are approximately parallel to each other and strike about north 77 degrees west and dip around 75 degrees north. They are reverse or thrust faults with the hanging wall moving up relative to the footwall. Stratigraphic displacement ranges from a few inches to a few feet. The gouge zone is less than an inch to several inches thick and filled with sandy or clay gouge depending upon the particular bed involved in the displacement.

The beds adjacent to the fault on both sides are displaced upward, upturned along the fault. The deformation of the edges of the rock strata range from a few degrees to locally almost vertical. Generally it is a gentle arch that may have an actual displacement of a few inches to a few feet. The arching is reflected away from the fault from a distance of 1 to as much as 10 feet. These folds have been referred to as buckles or teepees and are asymmetric. For the most part it appears that the steeper limb is on the footwall side of the fault. It is reported that the buckling extends to a depth of 80 to as much as 200 feet where it dies out. The upwarping follows the fault and therefore is a linear feature that extends at least 1500 feet. The buckling is definitely associated with the thrust faults.

The origin and age of the buckles, teepees or the broken fold is of interest to this report. The buckling could be directly associated with the fault in origin and time or, the buckling could have occurred along the fault at some time after the initial faulting. Suggestions made for post-fault buckling range from the initiation by tectonic movement to disturbance by glacier ice and origin by growth of ground ice in permafrost.



Frozen ground and growth of ice in relation to the bedrock folds

General statement

According to a telephone conversation with Mr. William Swiger on February 19, 1980, I was asked to determine whether ice wedging (growth of ground ice) could have formed the folds (buckles, teepees) present along the Drainage Ditch Fault and the Cooling Tower Fault. This is an innovative idea, and indeed, the growth of ground ice has caused great disturbance to the sediments adjacent to massive bodies of ice in the Quaternary sediments in Alaska, Northern Canada, and Siberia. (Upon returning from the discussions and site investigations I received a letter from Mr. James T. Dette explaining that I was being requested to evaluate the possibility of ice wedging being the cause of recent movement on the Drainage Ditch Fault and the Cooling Tower Fault).

Permafrost

In considering the growth of ground ice as the cause of buckling, one must establish the presence of permafrost because the features in bedrock are too deep to have formed by ice growth in seasonally frozen ground, even though seasonally frozen ground forms annually at the site today. Although no permafrost is present today at the site, permafrost was present widespread in the northern part of the United States during Pleistocene time. The presence of ice-wedge casts and pingo scars support the idea that permafrost was present, most firmly in the late (and early) Wisconsinan time in northeastern United States. Permafrost was present near the edge of the late (and early) Wisconsinan ice fronts at the maximum stand, and it also formed in front of the ice sheet as it withdrew. Permafrost was not thought to exist widespread underneath the ice sheet in the temperate latitudes. At the site, Lake Iroquois formed with the withdrawal of the glacier, and no permafrost formed until the lake was less than 4 feet deep or absent. The lake is reported to have left 13,500 years ago; therefore, permafrost formed in the area after that date. Around 10,000 years ago, with the amelioration of the climate, permafrost disappeared.

Permafrost at the site may either be post-Wisconsinan in age or it may have formed before the advance of the early Wisconsinan ice or after the withdrawal of the early Wisconsinan ice sheet. In other words, there are many times when permafrost and subsequent ice growth at the Nuclear Power Plant Site could have formed within the last 2 million years, the latest being from 13,500 to 10,000 years.

Types of ice in the ground

Permafrost is a natural-occurring material that has a temperature colder than 0°C continuously for two or more years. This layer of frozen ground is designated exclusively on the basis of temperature. Parts or all of its moisture may be unfrozen, depending upon the chemical composition of the water or the depression of the freezing point by capillary forces. Most permafrost is consolidated by ice; permafrost with no water, and thus no ice is termed dry permafrost. The ice content of permafrost is probably the most important feature of permafrost affecting land-use. Ice in perennially frozen ground exists in various sizes and shapes and has definite distribution characteristics.



A simple classification of the forms of ground ice groups the ice into five main types: pore ice, foliated or ice wedge ice, pingo ice, segregated or Taber ice, and buried ice.

Pore ice is defined as ice which fills or partially fills the pore spaces in the ground. It forms by freezing pore water in place with no addition of water. This ice exists both in seasonally frozen ground and perennially frozen ground. The ground contains no more water in the solid state than the ground can hold if the water were in the liquid state. There is no ice heaving with this ice and therefore it cannot be considered in the formation of the bedrock buckle.

Foliated ground ice or wedge ice is the term given to large masses of ice which grow in thermal contraction cracks in permafrost. It is the most conspicuous and controversial type of ground ice in permafrost and the large ice wedges or masses are characterized by a parallel or sub-parallel foliated structures. Foliated ice masses occur as wedge-shaped, vertical or inclined sheets or dykes one quarter of an inch to 10 feet wide and 10-30 feet high as seen in transverse cross-section. Some masses, when seen on the face of frozen cliffs, may appear as horizontal bodies. Ice wedges grow in thermal contraction cracks about $\frac{1}{2}$ inch wide and 6 to 10 feet deep which form in the frozen ground during a cold winter. In early spring, water from the melting snow runs down these tension cracks and freezes, producing a vertical vein of ice that penetrates permafrost. When the permafrost warms and re-expands during the following summer, horizontal compression results in the upturning of frozen sediments along the wedge by plastic deformation. During the next winter, renewed thermal tension re-opens the vertical cemented crack, which may be a zone of weakness. Over the years, a vertical wedge-shaped mass of ice is produced and the adjacent sediments are severely buckled and even turned to a vertical position adjacent to the massive ice wedge. For the ground to crack in permafrost in the cold winter, the mean annual air temperature of the region should be about -6°C to -8°C and the temperature at the top of the permafrost should be around -15°C . The ground that cracks is generally ice rich.

Although the deformation of formerly horizontal frozen sediments adjacent to ice wedges is about the same magnitude in horizontal distance as the buckles in the bedrock at the site, the bedrock buckles were not formed by the growth of ice wedges. To form bedrock buckles as seen at the site would require enormous ice wedges as much as 5 feet across and upon disappearance of these ice wedges, there would be formed large ice wedge casts. There are no such ice wedge casts present at the site.

Also, ice wedges generally form symmetrical buckles or symmetrical folding on each side of the wedge, and the bedrock buckle at the site are asymmetrical. In addition, the buckles extend far too deeply for the growth of an ice wedge. The large ice wedges that have been reported from Alaska and Siberia are as much as 30 feet deep and may have formed as the sediment accumulated. Another point is that even though the bedrock was saturated with water, it would not contain nearly the amount of water as ice content that the frozen unconsolidated sediments have to permit an expansion and contraction of the ground (in this case the bedrock) between summer and winter to allow wide contraction cracks to form. A final point is that ice wedges have been very rarely reported from bedrock. Those that are known to exist in bedrock formed in a rather crushed bedrock with many silt and clay size particles with high ice content.

Pingo ice is a second type of massive ground ice in permafrost that causes severe disturbance to the surrounding sediments, even bedrock. Pingos are isolated steep-sided hills that are unique to permafrost areas. They are generally circular to oval in ground plan and range from 10 to more than 100 feet in height and from 50 to 1000 feet in diameter. They are composed of a core of massive ice which is overlain by a few feet of silt, sand or peat, or even bedrock. These mounds commonly have craters on their tops which are occupied by ponds.

Pingos form when large, massive layers of ice grow near the surface of permafrost. There are two distinct types of pingos, the closed system and the open system. The closed system type forms in nearly level areas when unfrozen groundwater migrates under pressure to a site where the permafrost is heaved up to form a mound. These are the larger of two types of pingos and occur in areas of continuous permafrost, the tundra areas. The tundra areas are one of most rigorous climate and the mean annual air temperature is generally colder than -6°C . The open system type is generally smaller and forms on sloping ground where water beneath, or within, the permafrost penetrates the permafrost under high hydraulic pressure and, along with the crystallization pressure, heaves the overlying material to form a mound. The later type of pingos are far the most common in the subarctic.

When pingos grow they arch the sediments or bedrock on the sides of the ice core from a few degrees to as much as 45 degrees. When the ice core melts, the summit sediments or rocks collapse into the pit along with fine-grained material and a circular or oval pit surrounded by a low ridge remains as a pingo scar. Such pingo scars are common in temperate latitudes today, such as Illinois, Belgium, Ireland, where permafrost no longer exists. They are also present in the subarctic and arctic indicating the former presence of pingos.

Although some pingos have turned up bedrock strata similar to the buckles and teepees reported at the Nuclear Power Site, the pingo feature is generally one of much larger magnitude. Because of this and other points it is felt that the bedrock folds at the Nuclear Power Site are not related to the growth of pingo ice. If they were pingos, the scar would be generally oval or circular, not linear, and there definitely would be a scar depression or filling of some sort, which is not present at the site. Also, the short period that permafrost existed in late Wisconsinan time at the site probably was during an interval of not the most rigorous climate, therefore, not favorable for the growth of closed system pingos. It was definitely not favorable for the growth of open system pingos because for the lack of hilly terrain. Finally, pingos in bedrock are extremely rare, although they have been reported from northern Greenland. Therefore, all evidence points the fact that pingo ice growth is not responsible for the small asymmetric arches in bedrock seen on a linear trend at the Nuclear Power Plant Site.

Segregated or Taber ice is the most common type of ground ice. It is described as ice films, seams, lenses, pods or layers generally a fraction of an inch to an inch or two thick that grow in the ground by drawing in of water as the ground freezes. These small ice segregations are not spectacular, and yet they are one of the most extensive types of ground ice. Ground does expand upon freezing because of the growth of ice. Great ground distortion happens as freezing occurs in fine-grained material (silt or clay). Water is drawn to

the freezing ice crystal, and ice lenses or other types of ice segregations of clear ice form. Geologists and engineers have proven that the expansion in volume of the soil upon freezing cannot be due alone to the expansion of water originally contained in the soil voids because as much as 60-140% expansion in ground volume is recorded due to freezing. This means that extra water has to be drawn in.

The present concept of frost heaving perhaps owes its origin to a North American geologist named Taber; therefore, the term Taber ice is sometimes used for this type of ice segregation. Maximum force that can be developed during growth of ice crystals in a confined space is 29,100 lbs per square inch. During the process of freezing soil moisture, additional water is drawn to the points of freezing from the adjacent unfrozen ground. The basic physical phenomenon permitting expansion in ground volume upon freezing is due to the fact that some water in the ground remains liquid, although subjected to temperatures below 0°C. There are several hypothesis as to why the liquid water remains liquid even though colder than 0°C and why it migrates to the growing ice crystals. It is not necessary to review these concepts here. It is only necessary to note that the amount of ice finally concentrated in the ground and the size, shape and position of the ice segregation depend upon many physical factors. The most important are air temperature and texture and moisture content of the ground.

Texture of the ground means the size of the soil particles and their distribution. It is the size of the particle of grain, and the size distribution of the grains that control the pore size. In small pores or voids, such as those in silt or clay, some water remains liquid at temperatures considerably below 0°C. In sand and gravel, and openings in bedrock, the voids are so large that most of the water freezes near or at 0°C, and no channels are left open to supply a growing ice segregation. Lean clay (low plasticity) and silt contain pore sizes that are ideal for the passage of liquid water while they are freezing; fat or heavy clay (high plasticity) have all or most of the water so tightly held in the absorbed layer that no free water can be added. In summary, silt or silty clay soil in its natural state is the most favorable medium for growth of ice segregations upon freezing. This concept is born out by extensive field and laboratory investigations.

The amount of ice which forms in the ground upon freezing depends upon the moisture originally in the ground and the amount of water that can be drawn to the freezing centers from the unfrozen ground. Poorly drained areas underlain with fine-grain sediment are therefore ideally suited for the growth of ice segregation and subsequent frost heaving.

In summary, probably the most favorable condition for the growth of ice segregation and the resultant frost heaving is the slow freezing of moist nonhomogeneous organic silt or silty clay.

When we compare the conditions for the growth of ice segregations in the bedrock at the site we see that it is not altogether favorable. Although the water table today is high, and could have been high in Pleistocene time, and there does exist some shale and clay seams, the conditions are relatively unfavorable for ice segregations. There are no layers of silt, and the clay seams and shales are not ideal for capillary transmission of water and the growth of ground ice. Ice indeed would form in the bedding planes and in the

many joints, but conditions are unfavorable for continually drawing in of water.

It is necessary to have a reason for the localization of growth ice to form buckles. The only possible reason is to use the fault with its gouge as a conduit for the water. The gouge is not necessarily silty but sandy, and in many places, clayey. Ice would undoubtedly grow in the gouge, but it would have no reason to grow in the joints of bedding adjacent to the gouge except for ice fill without ability to continue to bring more water to a particular area. Great amounts of segregated ice which are known throughout the world occur in perennially frozen (formerly unconsolidated) sediments and not in bedrock. It would be well to consider exposures of perennially frozen bedrock.

Exposures of perennially frozen ground, both natural and artificial, throughout the world are almost entirely in unconsolidated sediments (soil) ranging from very coarse to very fine. Exposures of perennially frozen bedrock (permafrost) are rare. They are known in mines and some exposures made in the construction of dams in the far north. Most mining exposures are in crystalline rock and descriptions of such exposures reveal no large masses of ice nor buckling of the bedrock by ice. Last summer I was fortunate to examine permafrost in Svalbard (Spitsbergen) in coal mines in horizontal sandstones and shales. The ground ice was very rare, and what did exist was in small seams filling joints and bedding planes and not typical ice segregations. Even though the bedrock was cut by faults, there were no distortion or buckling of the rock, either away from or near the faults, by ice in these bedrock exposures. The frozen bedrock with a small amount of ice in seams and joints was exposed from the surface to depths of 1000 feet.

In summary, it appears that the growth of ice segregations (Taber ice) causing frost heaving (ice wedging) would be unlikely to produce any of the bedrock buckles present at the Nuclear Power Site.

The fifth type of ice, buried ice, is related to various types of glacial ice or lake ice that may have become buried by sediments and continually existed in permafrost for a long time. It is a miscellaneous category and does not apply to our particular problem.

It is interesting to note that although the bedrock may not have been disturbed by perennially frozen ground, the overlying 10 feet of unconsolidated sediment (soils), in addition to being highly disturbed by slumping, settling, and otherwise being moved about either during deposition or after deposition by the melting of glacial ice, was also undoubtedly alternately frozen and thawed many many times during the last 10,000 years. Seasonally freezing and thawing plus, natural slumping, folding, draping in glacial sediments does produce an enumerable minor structures that are common in such sediments throughout the world and seem to be well represented in the various exposures made at the site. I think it would be most difficult to demonstrate that these structures were related to underground movements of the bedrock.

Conclusion

It is my opinion after having seen the site, discussing the geology with geologists, reading reports, and examining photographs of exposures that the

perennially frozen ground with simultaneous growth or subsequent growth of ground ice did not cause the asymmetric folds (buckles, teepees) that are exposed in the bedrock in a linear trend along faults and reported to extend to a depth of 200 feet. After studying ground ice for many years in various parts of the arctic and subarctic in North America, Europe, Asia and in Antarctica, I believe that none of the five main types of ice in permafrost created the bedrock buckles. Pore ice does not distort the ground. Foliated ice and pingo ice would leave well developed ice wedge casts, pingo scars, and other features. Such are not present. Foliated ice and pingo ice do not distort rock to depths of 200 feet. Ice segregations would not grow as required to distort the rock because lack of unconsolidated silt and silty clay layers. Buried ice was not present. The growth of ground ice is extremely important in land-use planning and engineering geology, but it generally reflects disturbances in the unconsolidated sediments and not in the bedrock.

Thank you very much for allowing me to consider the possible effect of growth of ground ice in the bedrock in relation to foundation problems in the area, and I would be most pleased to add additional information if necessary.

Sincerely yours,


Troy L. Péwé
Professor of Geology

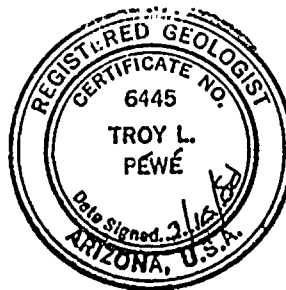
Registered Geologist,
State of Arizona No. 6445

Registered Geologist,
State of California No. 2834

Registered Engineering Geologist,
State of California No. 832

TLP:phh

cc: J. T. Dette
W. Swiger





POTENTIAL FOR DIFFERENTIAL MOVEMENT ALONG RADWASTE STRUCTURE
NINE MILE POINT, NEW YORK
OVER THE NEXT 50 YEARS

by

Charles Fairhurst
Consultant
May 23, 1980

Introduction

The Radwaste Structure is a low-angle (to the horizontal) thrust fault feature exposed in a shallow excavation on the proposed site for Unit 2 of the Nuclear Power Plant at Nine Mile Point, in Upper New York State on the southern shore of Lake Ontario. The exposure reveals that horizontal translational movement approaching 7 ft. has occurred along the structure. Since the structure is in close proximity to the emergency cooling water tunnel for the Unit 2 plant, and intersects the reactor excavation, it is obviously important to assess the potential for displacement to occur along the structure during the operating life of the nuclear plant; approximately 50 years.

Acting as a member of an advisory panel convened by Dames and Moore, geotechnical consultants to the plant owner, Niagara Mohawk Power Commission, I have carefully studied the reports prepared by Dames and Moore, and papers and comments by Stone and Webster, the plant designers. I have also visited the site, inspected the Radwaste exposure, and discussed geotechnical questions concerning it with Dames and Moore personnel. As a result of these deliberations I have formed the opinions presented below concerning the general problem posed by the Radwaste structure.

The program of geotechnical investigation and analysis conducted by Dames and Moore is very thorough and competent. It provides a very good, logical



basis on which to examine the stability of the Radwaste structure. The most recent report, a 21 page document* with 23 plates and an Appendix** is a succinct statement of Dames and Moore's current views on the genesis of the Radwaste structure and displacements along it, and serves as a very useful basis on which to present my own views on the structure. Rather than repeat the points made in the Dames and Moore report (D & M report), I shall refer to the specific sections as appropriate in the comments below.

1. Mechanics of Formation of the Radwaste Structure

Recent exploratory drilling (Plate 16, D & M report) indicates that the Radwaste structure is probably the uppermost of two or more similar structures, each increasing in scale with depth. The structures seem to be clearly the result of high normal stresses acting essentially parallel to the surface. The faulting, bedding plane slip, etc., seen in the Radwaste trench suggest that the nearby erosional valley in the Oswego sandstone could have provided the local stress concentration that produced the structure (i.e., as described in page 10, D & M report). A less plausible, but possible, interpretation is that the shear-slip occurred through the Oswego sandstone directly to the surface and that the valley formed subsequently as an easily erodable path for glacial action. The apparent lack of shearing in the lower portion of the Oswego, above the structure tends to weaken this explanation.

The existence of a deeper structure suggests a deeper erosional valley further westward, i.e., in the floor of Lake Ontario. It is also possible that the lower structures were a consequence of the Radwaste structure, in that slip along the latter reduced the normal stresses above it and caused stress concentration below it, this leading to bedding-plane slip below. This

* No title is given for the report.

** Displacements of the Wall of A Cue in Horizontally Bedded Rock due to Joint Shear and Sliding under Relief of High Horizontal Ground Stress (by J. A. Franklin), 11 p.

process will continue progressively until the principal stress orientation is sufficiently inclined (i.e., normal stress high enough) to the bedding planes to prevent further slip.

The lower structure is also of interest in that it is to be expected that the (essentially horizontal) normal stress below the lower planes of bedding plane slip should be significantly higher than above those planes, and would tend to indicate the magnitude of the original near-surface normal stress (σ_n in D & M report, e.g., Plates 24, 25). Since the lower structure lies entirely below the plant site displacements along it, if they occur, are unlikely to cause differential displacement of one part of the plant foundation with respect to another.

The change in observed lateral translation along the Radwaste structure (D & M report, p. 11) can probably be ascribed to a combination of 'unaccounted for' intrastratal bedding slip and relative translation due to swelling.

The dipping nature of the overall displacement zone suggests that further displacement is less likely than suggested by Dr. Price's assumed single horizontal plane of sliding.

The inclined shear zone and associated, apparently contemporaneous, dilation strongly suggests that the structure developed under low normal pressure, i.e., near surface conditions. If it is argued that dilation developed later than the initial shear zone, then it must be accepted that the dilatation (which requires low normal stress, i.e., near surface conditions), indicates recent (i.e., post glacial) movement along the structure, subsequent to earlier formation.



2. Age of Radwaste Structure

I feel unqualified to judge the validity of the two views, that the structure is ancient (millions of years old) or 'modern' (12,000 years 'young'). However, it appears difficult to reconcile the near-surface environment considered necessary for formation of the structure, with the 3 km depth of burial that existed in Palaeozoic and early Mesozoic times (see Plate 1, D & M report). It seems, from Plate 1, that the depth of burial may have been minimal for the past 1 million or so years.

3. Stability of Radwaste Structure

It is quite certain that the Radwaste structure developed due to high lateral (i.e., essentially parallel to the bedding planes) stresses (i.e., the strain energy stored in the rock, referred to in D & M report; see e.g., p. 16). The boundary conditions suggested in the D & M report, pp. 16-17, seem appropriate--recent stress determinations suggest that the normal stresses (σ_{n2}) along the boundaries $\beta 1$ and $\beta 2$ (Cooling Tower Fault and Drainage Ditch Fault) are almost negligible, so that the shear resistance along them, dS_1 and dS_2 (D & M report, p. 17) will be also small.

Displacement along the structure will reduce the applied stress (σ_n) until the driving force (F_n) and resisting force (F_r) [shear resistance along bedding planes and against 'steps' in the inclined shear path] just balance and displacement ceases--simply in accordance with Newton's law of motion:

$$(F_n - F_r) = m a$$

where m is the mass of the sliding structure (rock above the sliding surface), 'a' is the acceleration (d^2u/dt^2 where u = displacement, t = time) of that mass. Obviously if the displacement (u) stops, then $a = 0$, and $F_n = F_r$.



If F_n increases and/or F_p decreases, then additional displacement will occur. Thus, the question of the stability of the Radwaste structure may be simply divided into two parts:

- i) will F_n increase
- ii) will F_p decrease

If either happens then movement will occur.

4. Changes in Driving Force F_n

The force (F_n) or stress (σ_n) causing westward movement (of the upper Radwaste mass) could arise from several sources:

- i) remanent lateral compression due to orogenic processes. This could be, in essence, an overall pre-compression upon which processes such as ii) would be superimposed.
- ii) differential uplift due to a combination of long-term tectonic uplift and glacial rebound (see D & M, Plate 20).

The force (or stress) could undergo reduction, or even reversal due to 'downwarping' during periods of glacial advance (e.g., as in Plate 20). Depending on the rate of development and duration of downwarping (and the viscous characteristics of the bedding planes) this could result in tensile stresses being generated in the rock adjacent to the bedding planes.

Some estimate of the magnitude and rate of development of (ii) may be obtained from cores of vertical crustal movements in the region (D & M report, Plate 2), which indicates a differential uplift rate of the order of $-(-2 \pm 1)$ mm/25 miles (contour interval) per year, or 0.04 mm/mile/yr. This corresponds approximately to:

$$\frac{0.04}{5280 \times 12 \times 25.4} \text{ mm/mm/yr} = 2.5 \times 10^{-8} \text{ rads/yr}$$



If we assume an overall shear modulus of the rock formations of 1×10^6 p.s.i. then the shear stress produced by differential uplift is of the order of

$$2.5 \times 10^{-2} = 0.02 \text{ p.s.i./yr}$$

or 1 p.s.i. in 50 years.

Thus, it would appear that uplift should have no effect on displacement of the Radwaste structure over the lifetime of the plant.

5. Changes in Resisting Force (F_r)

The resisting force is predominantly the shear resistance of the bedding planes involved in the 'slip base' of the Radwaste structure. Apart from long-term creep causing a progressive slow displacement, the other main possibility of reduction in the effective strength of the bedding planes and slip surfaces is due to a rise in the water table. According to Plate 6 (D & H report), the rise in the level of Lake Ontario has been very gradual, corresponding to approximately 50 ft. in 8,300 years or 4 inches in 50 years (see also p. 3 of D & H report). 4 inches head of water corresponds to an uplift pressure of 0.15 p.s.i. Again, it would seem that this is a negligible amount.

Thus, it would appear that changes in the stresses over the next 50 years, other than those resulting from the interaction between the applied tectonic stresses, (i) above, and the shear strength of the beds, should be negligible. We will, then, turn attention to the existing situation.

6. Stress Determinations

Overcoring measurements (some still underway) in the vicinity of the Radwaste structure indicate that the stresses are low close to the surface at the 'front' of the structure, increasing 'markedly' below the 'slip-plane

region', and again increasing with distance from the 'front' of the structure. It appears further that the stresses normal to the Cooling Tower and Drainage Ditch (bounding) Faults are quite low such that these fault surfaces probably do not severely inhibit slip of the Radwaste structure.

The above arguments suggest that it is reasonable to consider bedding-plane displacement along the Radwaste structure to be the result of a constant tectonic stress σ_n and a time-dependent (decreasing) shear resistance along the bedding plane-slip surface.

In such a case the displacement (δ) may be expected to increase exponentially until a fixed value is reached. At this point the (decreasing) applied force F_n will balance the resisting force F_r . Little is known about the very long-term shear strength of rocks or rock surfaces but it seems reasonable to assume that the long-term value of F_r , say $(F_r)_\infty$ is greater than 0. ["If not," it has been argued, "how could we have mountains?" (assuming, of course, that mountain uplift is not compensating for the long-term creep towards a plane)].

The exponential growth of the displacement may be expressed as:

$$\delta_{\max} - \delta_t = \delta_{\max} e^{-\alpha t}$$

where δ_{\max} is the final displacement [when $(F_n)_t = (F_r)_\infty$]

δ_t is the displacement at time t

α is the decay constant

t is the time from start of displacement.

If we assume, for example, that half of the total (final) displacement occurs in time $t = 1$, then $\alpha = 0.7$ or

$$\frac{\delta_t}{\delta_{\max}} = 1 - e^{-0.7t}$$

Thus after time $10t$

$$\frac{\delta_t}{\delta_{\max}} = 1 - 0.000912 = 99.91 \times 10^{-2}$$

or, 99.9% of all the movement that will ultimately develop will have occurred in 10 times the period required for the first 50% of the movement.

If this model is valid for the Radwaste structure, this would suggest, for example, that if 50% of the movement occurred in the first 1,000 years (I have no basis for this number except that, in creep tests on rocks most of the movement occurs relatively very quickly) then, after 10,000 years, 99.9% of all the movement would have taken place. Thus, if 100 inches displacement has occurred in 10,000+ years, then all but 1/10 inch of possible movement has been dissipated from that driving force.

7. General Comment

The above considerations tend to suggest that movement on the Radwaste structure will be negligibly small over the next 50 years. It should be borne in mind, however, that numerous assumptions have been made in order to proceed with the computations, and that other factors have been neglected. For example, stress determinations do show sizeable (1,000 - 2,000 p.s.i.) normal stresses in the near surface rocks, away from the front (i.e., Radwaste trench) of the structure. Also, the normal pressure across the bedding planes (i.e., preventing sliding) is equal only to the weight/unit area of the overlying column of rock (i.e., at 40 ft = 40 p.s.i.). The cohesive strength of bedding planes along which sliding has occurred is essentially nil. Thus, if water under pressure approaching that sufficient to "float" the overlying rock (i.e., 40 p.s.i. at 40 ft depth) were introduced into the bedding plane, release of the normal stress in the rock would occur and promote displacement along the bedding plane.

It has been noted (D & M report, p. 7) that the laboratory (short-term) measured shear strengths of bedding planes in the Radwaste region are very close to the shear stresses observed to be acting along those planes in the field. This is consistent with the view that the system is just in equilibrium ($F_n = F_r \neq 0$), "metastable equilibrium". A more sensitive comparison of the potential for further slipping along a bedding plane would be to determine the slip as a function of fluid pressure applied along the bedding plane. Such a test, carefully performed with control "outlet" boreholes around a central input pressurized borehole, would be a direct test that circumvents a number of arguable hypotheses.

Still another approach to assess the tendency for movement would be to overcore drill holes that have been grouted, in order to determine whether there has been any offset in the grouted column. I understand that there are some holes that have been grouted for almost 10 years. This is a long enough period to make some estimates of the probable behaviour over 50 years.

One obvious method of assessing whether movement has taken place recently is to examine structures (e.g., in Unit 1) built on the same rock formations--to check for any signs of damage (e.g., cracking) due to ground movement. I understand that this has been done both by Stone and Webster, and by Dames and Moore personnel. I do not have exact details of what has been observed.

8. Need for Numerical Modelling

The above discussion has been directed towards a preliminary assessment of the potential for further movement along the Radwaste structure. Although there are several unknowns (e.g., age of Radwaste structure), it does appear that there should be a negligible amount of movement (i.e., less than the

1 inch/50 years limit considered desirable). if the assumptions are correct. However, considerable effort has been made to map the Radwaste feature in detail, and to make stress and inclinometer measurements. Dames and Moore have made qualitative and some quantitative interpretations of the data obtained in these investigations. As yet, however, the data have not been incorporated into a comprehensive numerical model, so that rationally derived estimates can be made of the probable maximum values of future displacement. I feel that the model will confirm my intuition, based on arguments outlined above, that there will be no movement of consequence. However, I would be much more confident if an analysis incorporating all (or most) of the actually observed data were conducted.

As mentioned in my earlier letter, I recommended that this modelling effort be undertaken by Dr. Peter A. Cundall. I do this because Dr. Cundall has developed the 'discrete element analysis' procedure incorporating computer inter-active graphics. This procedure is far more appropriate (and relatively economical) than any other of which I am aware for the particular type of problem represented by the Radwaste structure.

I have taken the liberty of asking Dr. Cundall to give me his opinion of the problem and whether it could be adequately modelled. His preliminary comments are attached.

C. Fairhurst
May 1980



MODELLING OF RADWASTE STRUCTURE

by

Peter A. Cundall

The main features of the North Radwaste Fault and its associated structures have been described in detail in the document entitled, "Geologic Evaluation, North Radwaste Fault, Nine Mile Point Nuclear Station - Unit 2" by Dames & Moore, Job 04702-022-19, dated November 13, 1979. I shall not repeat that information, but will concentrate on the possibilities for numerical modelling.

It seems to me that the geological mechanisms put forward in the report are plausible. In particular, the evidence so far to hand does not preclude the possibility of future movement on the fault. It should be a cause for concern that seven feet of movement has occurred in the recent geological past, and that the system may be in limiting equilibrium.

I propose that a series of numerical experiments be performed in order to explore the conditions under which the noted geological mechanism can occur. Only the limited data shown in Table 1(a) are available; any numerical model must, at the very least, match or use these data. However there are a number of unknowns [see Table 1(b)], for which values must be assumed. It is hoped that the observed behaviour will be found to occur only for a limited range of the unknown parameters. If this is the case, the simulation of the system may be extended into future time, to predict likely movements during the life of the power plant. The prediction will probably consist of a range of values for displacement, depending on the input assumptions.

It would be interesting if the numerical modelling demonstrated that bedding-plane kinking, of the kind observed, always unloads the strata past

the point of limiting equilibrium, so that shear stresses on bedding planes drop well below shear strengths. Such unloading will occur almost certainly if the kinking takes place rapidly, but it is not clear whether viscosity in the rock will inhibit the unloading by slowing down movement. The numerical model should answer the question. If unloading does occur under all conditions, a good case could be made for expecting little future movement.

Even though some data are unknown, a computer model can provide new information, as the preceding example has shown. The model can also suggest critical field tests that would enable a choice to be made between two conflicting hypotheses. A further use for the model is to evaluate any remedial measures that are proposed.

TABLE 1(a)

INFORMATION THAT IS AVAILABLE, OR PARTIALLY AVAILABLE,
AND MUST BE MATCHED IN ANY MODEL

- o observed vertical and horizontal displacements across fault, and observed final geometry
- o maximum time for displacement to occur
- o present measured stresses
- o swelling properties of intact rock
- o short-term elastic rock moduli, densities and joint properties
- o known changes in water table
- o known regional shear straining
- o known orientation of bedding-planes



TABLE 1(b)

UNKNOWNIS (FREE PARAMETERS)

- initial stress-drop
- distance normal to strike at which stress applies
- viscosity of bedding planes and rock
- other properties involving time: e.g., joint friction
- lateral boundaries (is the movement confined between 2 faults?)
- long-term elastic/plastic properties of rock
- effective bedding-plane spacing

NOTES ON THE RADWASTE FAULT STRUCTURE, NINE MILE POINT
NO. 2 GENERATING STATION, NIAGARA MOHAWK POWER CORP.

Richard H. Jahns and Shailer S. Philbrick

These notes derive from (a) detailed reviews of notes, reports, and documentation prepared or provided by Dames & Moore and Stone & Webster geologists and by Troy L. Pewe of Arizona State University, (b) personal inspections of the Radwaste Trench and the bedrock exposures it provides, (c) several conferences with Dames & Moore and Stone & Webster personnel, and (d) personal knowledge of other occurrences in the eastern and southwestern United States where bedrock structures comparable to the Radwaste Fault are present. It should be added that some of the currently available reports and findings represent investigations post-dating our own visits to the Nine Mile Point Site.

As exposed in the excavation from which it is named, the Radwaste Fault is a well-defined zone of rupture, dislocation, and displacement in stratified rocks of Paleozoic age. It strikes approximately north-south and dips eastward at low angles; average dip in the trench exposures is near 15 degrees. The sense of slip is essentially east-west, with relatively westward movement on the hanging wall. Dip slip of 4.0 ft and 6.8 ft has been determined at two places, and it is evident that some associated slip has been accommodated along bedding surfaces adjacent to the fault.

Exploration in the area centering about the Radwaste Trench indicates that the fault is part of a family of subparallel breaks, each of which evidently flattens eastward into one or more zones of bedding-surface slip. As indicated by Dames & Moore geologists, expressions of the fault structure diminish eastward from the trench, and eastward from the easterly margin of a small buried bedrock valley with which the breaks are spatially associated. All the breaks evidently are confined to the shallow subsurface.

The radwaste Fault Structure has been carefully explored and analyzed, in greatest overall detail by Dames & Moore geologists. Their principal conclusions, which we regard as demonstrable and defensible, can be summarized as follows:

1. The faulting reflects relief of strain energy that has been stored in the bedrock. In the total context of regional geologic history, it can be concluded that no increase in the amount of stored strain energy will occur during the coming centuries.



2. The faulting reflects lengthening of a local crustal block in the near-surface environment, and it probably was at least in part localized by the presence of a small valley cut into the bedrock.
3. Loading and unloading of the subject ground, as associated with episodes of Pleistocene glaciation and deglaciation, could well have been significant factors in prompting movements along one or more of the fault breaks.
4. The faulting is late Cenozoic in age.
5. The faulting is not related to current tectonic processes that could introduce additional amounts of strain energy into the affected ground.

The Radwaste Structure, with characteristic low dip, downdip flattening and diminishing of displacement, occurrence in a near-surface environment, and daylighting in a domain of largely de-stressed rocks, represents a large and widespread family of structural features ordinarily referred to as "exfoliation products". Such surfaces of rupture and displacement reflect the expansion and movement of rock masses toward the nearest free surfaces, most commonly the ground surface. The stress field is highly anisotropic, and rock failure occurs along gently-dipping surfaces wherever pre-existing breaks are not available in the proper orientations for relief of the strain that is present. The strain energy in rocks that once were deeply buried typically derives in part from earlier tectonic input and in part from erosional unloading of the rocks (the "residual" component).

Breaks of the Radwaste Structure, along with associated zones of bedding-surface movement, are dilatational features that have accompanied extension of the overlying rock masses. These masses, in their present condition, have been progressively destressed both upward toward the ground surface and up-dip along the Radwaste Structure. Recent in situ stress determinations in the area bespeak this progressive relationship, and they are compatible with development of the Radwaste faulting by down-dip propagation from original daylight lines.

Toward assessing the possibility of future movements along the Radwaste Structure in the power plant area, it is necessary to consider the age of the movements that have occurred in the past. On this score, Dames & Moore geologists suggest that "a majority of the displacements" probably occurred during Holocene time. This view is based mainly upon:

1. Deformation of clayey silts that occur within the zone of rupturing. These silts probably were

associated with glacial Lake Iroquois, and they have been dated as approximately 11,000 years of age.

2. Presence of calcite mineralization within the fault zone. The calcite has been deformed, and some of it has been dated as about 14,000 years old.
3. Presence of significant levels of strain energy in the rocks at the present time.

In contrast, the clayey silts noted above are regarded by Stone & Webster geologists as younger than the deformation expressed in the bedrock of the fault zone. This view is shared by Pewe, who ascribes deformation of the silts to syndepositional processes such as slumping, differential settling, and liquefaction. We also are inclined to the view that the silts post-date essentially all of the bedrock deformation, although we have not had opportunity to view all of the evidence on the ground. The relationships that we have seen, however, can be readily explained as syndepositional. It can be added that we do not regard the occurrence of layered silts with steep dips as necessarily an indication of tilting or other deformation, as such silts commonly are plated, layer by layer, on steeply inclined and even vertical surfaces. Late-glacial lacustrine silts have been observed, for example, as steeply inclined coatings on the sides of ice-rafted boulders, without associated faulting or other deformation, at many localities in the northeastern United States (e.g., Connecticut Valley, Champlain Valley).

The evidence provided by some dated calcite mineralization strongly suggests that some movement has occurred along the Radwaste Structure, or parts of it, during Holocene and/or latest Pleistocene time. This movement need not have been more than a small fraction of the total displacement, but we have not seen enough of the pertinent evidence to hold a firm opinion concerning the nature and timing of the inferred movement.

That the bedrock along and near the Radwaste Structure still contains strain energy is well documented, and indeed is to be expected in the light of known geologic history of the region. The energy levels unquestionably are low as compared with what they once were, thanks in part to relief through movements along the Radwaste Structure.

Our conclusions concerning age and activity of the Radwaste Structure in the power plant area are as follows:

1. The structure was initially developed in pre-Holocene time, and probably in pre-Pleistocene



time. That at least most of its movement occurred in pre-Holocene time is indicated by the partial infilling of structurally-formed openings by silts that are about 11,000 years old.

2. Initial formation of the structure probably was abrupt, with displacements at a given place relatively large at first and attenuating with time.
3. Movements along the structure probably occurred during Pleistocene time, as prompted by episodes of glacial loading and unloading.
4. Post-Pleistocene (Holocene) movements have been small if they have occurred at all. It cannot be demonstrated that no Holocene movements have occurred, as no reference features (e.g., dated infilling sediments) extend entirely across the zones of disturbance.
5. Future movements along the structure are not likely to occur. Further relief of the limited amounts of strain now in the rocks will be distributed in the affected ground as dilation and small movements along fractures and bedding surfaces. The Radwaste Structure is so nearly dead at present levels of exposure that its participation in such future movements would amount to no more than a small fraction of an inch.
6. The Radwaste Structure is not seismotectonic in the defined sense of that form.

Toward generating further perspective on ages of deformation, the role of the Radwaste Structure, and the possibility of further movement along this structure, we offer the following comments concerning similar and comparable features that have been studied in New England and adjacent parts of the north-eastern United States.

Exposed at several localities in Maine, Vermont, New Hampshire, Massachusetts, and New York are low-angle thrust-like faults that are similar in all important respects to the Radwaste Structure. They occur in many kinds of competent rocks, generally within 300 ft of the present ground surface, and the ones that have been studied in detail are well exposed in granite quarries. Their relationships can be summarized as follows:

1. They range from knife-edge breaks to zones of closely-spaced anastomosing breaks as much as a few inches across. The brittle rocks are typically ruptured and slickensided in detail.



2. The zones die out into massive rock as traced down their undulatory dip, generally in distances of tens to a few hundreds of feet.
3. They represent thrust-like translation, with net slip (where determinable) rarely greater than about 5 ft.
4. The rock in many of the zones is weathered, in all cases to an extent far greater than the effects of Holocene weathering.
5. All the zones definitely antedate the development of sheet structure in the host rocks. They also antedate development of most of the microfractures that represent rift in these rocks.

The thrust-like breaks and zones of breaks are best interpreted as relief features with respect to strain energy in the host rocks, and on this score they evidently represent a combination of ancient tectonic input and differential stresses attendant upon erosional unloading. They can be regarded as late Tertiary or early to middle Quaternary in age.

The sheet structure in these rocks can be dated relative to episodes of glaciation, as its orientation reflects local topography. Gross modifications of this topography typically lead to reorientation of sheets as they continue to develop.

Post-Wisconsinan sheets are thin and few; not more than three of these exfoliation features are present in most places, and at some localities there are none. Most of the sheet structure seen in natural and quarry exposures is plainly pre-Wisconsinan, and much of it may date back to early glacial times and possibly into pre-glacial times. It is significant that all this sheet structure post-dates development and essentially all movement on the thrust-like features noted above.

Like the Radwaste Structure, the thrust-like features were formed long ago, and certainly in pre-Wisconsinan times. Once formed, they seem quickly to have run most of their respective courses. Indeed, subsequent relief of strain energy in the rocks evidently was accommodated by more intimately distributed movements in the affected rocks, chiefly along sheet and other fractures (or small cross-fractures and bedding surfaces in the Radwaste situation).

Because there is a similarity in form and genesis between the faults in the bottoms of some of the valleys in the upper Ohio River basin and the Radwaste structure, we shall consider the Ohio River basin valley faults.

In 1959, H.F. Ferguson and Philbrick reported to the Engineering Geology Division of the Geological Society of America that in the bedrock foundations of 18 flood control and navigation dams in the upper Ohio River basin constructed since 1934 they had encountered faults in 11 of those foundations. A generalized description follows. "Most occur as low angle thrust faults with a displacement of 2 feet or less. Soft gouge or breccia zones are found up to 18 inches thick but are seldom recovered by coring (diamond drill) if more than 1 inch thick. There is no general orientation (compass) of the strike of the faults and no apparent relationship to regional structures."

Ferguson (1967) continued the examination of these phenomena during other construction operations in valley bottoms in the same district. He states, "The valley bottoms have been subject to compression forces produced by that zone of the valley walls that has fractured and expanded horizontally. This horizontal movement together with the load of this mass, produces forces (similar to s1 above) that cause a wedge failure of the valley walls and bottom in the form of arching, thrust faulting, or shear breaks in the rocks. These areas of release of stress have been in the center of the valley with valleys of uniform topography. (But some have been nearer the base of the valley walls) The depth of the compressional breaks in the valley vary with the competency of the rock with the more massive rocks such as limestone or sandstone having deeper areas of disturbance than the weaker non-competent rocks such as clay shales or indurated clays." But basically these faults are shallow.

Philbrick reviewed these phenomena by telephone on 22 March 1980 when Ferguson expressed his belief that these phenomena were even more widely distributed than he had believed in 1967. An on 29 March Philbrick discussed this by telephone with Robert H. Nesbitt, formerly chief geologist of the Corps of Engineers, who reported his familiarity with these phenomena in Alabama, as well.

In summary the valley bottom faults develop as a result of the vertical load of valley walls, thrusting outward, as s1, with a shallow thickness of rock in the valley bottom, s3, resulting from eorision of the valley being insufficient to resist the thrust of s1 and failure occurring as a low angle thrust fault, a compressional failure. The Radwaste fault is similar in appearance and form to the valley bottom faults. The mechanics of the two fault systems is similar, but the genesis is different, although the reduction of s3 to the point of failure is caused in both cases by erosion and removal of rock, in the valleys mainly by stream erosion and at Nine Mile Point by glacial erosion.

Several of the dams included in the 11 beneath which faults were found, as stated in the 1959 paper (Ferguson and Philbrick, 1959), were equipped with crest gates supported on piers on adjacent monoliths, which monoliths were free to move being tied to each other across the monolith joints with nothing stronger than sheet copper waterstops. The fault gouge had been removed beneath monoliths where the faults were shallow and the concrete founded on the footwall. As the faults dipped cross stream beneath the valley, depth to the footwall was too great to permit all the monoliths to be founded in the footwall. Thus, the last monolith on the foot wall was contiguous to the first monolith founded on the hanging wall. The difference in elevation between the adjacent foundations was several feet with the monolith in the hanging wall having as much as a foot of gouge in its foundation rock.

The lack of differential settlement or motion of the hanging wall with respect to the footwall is demonstrated by the fact that there is reported to have been no necessity for adjustment of the gates or gate machinery supported on piers founded on separate monoliths over a period of nearly 40 years.

On May 20, 1980, Philbrick reexamined the Radwaste fault in the trench where it has been exposed all winter and again noted its similarity to the valley bottom faults. The similarity of the gouge and broken rock in a nearly horizontal fault in the Cooling Tower excavation to the in the foundation of the locks at New Cumberland Locks on the Ohio River is convincing of the parallelism of the structural development of the two foundations, each in nearly horizontally bedded, sandy and shaly sedimentary rocks. New Cumberland Locks have been in operation for over 20 years with apparently no distress in the gates.

It is apparent that motion on the valley bottom thrust faults has ceased, even though some of them are post-Wisconsinan.

It would seem reasonable to believe that the motion on the Radwaste structure has ceased since its origin and development closely parallels the cause and development of the valley bottom faults.

REFERENCES

Ferguson, H.F. and Philbrick, S.S., 1959, "Faulting in Engineering Structures Located in the Allegheny Plateau", abst., Bull. Geol. Soc. Amer., v. 70, p. 1601-1602.

Ferguson, H.F., 1967, "Valley Stress Release in the Allegheny Plateau", Engineering Geology, v. 4, p. 63-71.

